Investigating the anti-cancer effects of a-solanine on glioblastoma cell-lines for in-vitro evaluation against the chemotherapeutic standard-of-care

A dissertation presented to the Faculty of Medicine and Surgery in part fulfilment of the requirements of the degree of Master of Science in Biochemistry at the University of Malta

Supervisor: Professor Byron Baron BSc.(Bio.&Chem.)(Hons)(Melit.),Ph.D.(Melit.)

Andrea Cuschieri BSc.(Hons)(Melit.)

2023

L-Università ta' Malta

University of Malta Library – Electronic Thesis & Dissertations (ETD) Repository

The copyright of this thesis/dissertation belongs to the author. The author's rights in respect of this work are as defined by the Copyright Act (Chapter 415) of the Laws of Malta or as modified by any successive legislation.

Users may access this full-text thesis/dissertation and can make use of the information contained in accordance with the Copyright Act provided that the author must be properly acknowledged. Further distribution or reproduction in any format is prohibited without the prior permission of the copyright holder.





The research work disclosed in this publication is partially funded by the Endeavour II Scholarship Scheme. The project may be co-funded by the ESF+ 2021-2027





The research work disclosed in this publication was primarily funded by the ENDEAVOUR II Scholarships Scheme, awarded by the Government of Malta part-financed by the European Social Fund, and partially funded by the Kunsill Studenti Universitarji Research Grant.

GOVERNMENT OF MALTA

MINISTRY FOR EDUCATION, SPORT, YOUTH, RESEARCH AND INNOVATION

MINISTRY FOR THE ECONOMY, EUROPEAN FUNDS AND LANDS

PARLIAMENTARY SECRETARIAT FOR EUROPEAN FUNDS

ENDEAVOUR SCHOLARSHIPS SCHEME

KSU

Dedication

I would like to express my deep gratitude and dedicate this thesis to both the esteemed Faculty Board of the Faculty of Medicine and Surgery and my beloved family, whose invaluable contributions were integral to the successful completion of this project. To the members of the Faculty Board, I extend my heartfelt appreciation for placing their trust in me to pursue a Master of Science degree, graciously allowing me to temporarily suspend my studies from the Doctor of Medicine and Surgery course. This experience has not only honed my soft skills and critical thinking but also enriched my clinical learning, which I am committed to applying diligently.

Furthermore, I want to extend my heartfelt thanks to my family for their unwavering support throughout my sometimes-unconventional pursuits. Without your unwavering support, my post-graduate studies and overall education would not have been possible.

Lastly, I would like to express my deepest appreciation to my better half, Desireé. Alongside my family, you are my pillar of support, and I am forever indebted to your kindness, understanding, and unwavering commitment to helping me achieve my goals. Your presence and encouragement have been instrumental in my journey, and I am eternally grateful for your love and support.

Acknowledgments

I am immensely grateful to the Endeavour II Scholarship Scheme and Kunsill Studenti Universitarji for granting the essential funding that enabled me to undertake and successfully complete this study. This project has not only equipped me with crucial technical and soft skills but has also been instrumental in my professional growth.

I would like to express my whole-hearted appreciation to my supervisor, Professor Byron Baron, whose unwavering support, invaluable guidance, and unparalleled expertise have been pivotal to the successful completion of this research endeavour. Professor Baron's dedication to unravelling the molecular intricacies of life and adhering rigorously to the research process has deepened my passion for scientific inquiry and reinforced my belief in evidence-based medicine.

Furthermore, I would like to convey my sincere gratitude to Dr. Analise Cassar, whose assistance was instrumental in acquainting me with and conducting the flow cytometry experiments outlined in this study. Additionally, I would like to acknowledge Dr. Christian Zammit and Dr. Jean-Paul Ebejer for their valuable contributions through their expert insights on fluorescent imaging and bioinformatics, respectively.

Moreover, I extend my thanks to Mr. Isaac Micallef, Ms. Kimberly Fenech, and Dr. Vanessa Zammit, students of Professor Baron, who were always available to provide assistance during technical challenges and helped familiarize me with the various laboratory equipment necessary for my study. I am also thankful to my colleagues, staff, and fellow researchers at the Department of Clinical Pharmacology and Therapeutics for their support in providing or facilitating the acquisition of the required equipment and materials for my investigation.

I am profoundly grateful to each and every individual mentioned above for their unwavering support and indispensable contributions to the success of this study. Their collective efforts have enriched my research experience and propelled me towards further growth and development in my scientific journey.

Abstract

Despite optimal treatment, glioblastoma multiforme (GBM) has an abysmal associated prognosis of approximately 15 months. Published literature has increasingly demonstrated the potential of phytochemicals as putative agents against cancer. α-solanine, a glycoalkaloid derived from plants belonging to the genus *Solanum*, has emerged as a promising anti-cancer molecule. Here, the efficacy of α-solanine versus temozolomide (TMZ) against U87MG, U251 and T98G GBM cell lines *in-vitro* was investigated. Viability, migration, and invasion assays were conducted to assess α-solanine's anti-cancer potential in comparison to TMZ. Moreover, the effect of α-solanine on cell death was investigated on a cellular level through fluorescent imaging and flow cytometry, and on a molecular level through rt-PCR and proteome profiling assays. The GBM cell lines used in the study were confirmed to be $IDH_{wildtype}$ according to the WHO 2021 CNST classification. α-solanine induced potent cytotoxic on all GBM lines, with IC_{50} ranging between 19.66 µM – 22.87 µM, while also demonstrating significantly inhibiting GBM cell migration, in comparison to TMZ treatment. Fluorescent imaging and flow-cytometry demonstrated increased occurrence of autophagic cell death, however this finding was not statistically different between α-solanine and control treatments. Rt-qPCR and anti-body array profiling demonstrated upregulation of both apoptotic and autophagy proteins. The upregulation of BECN1 at both RNA and protein levels suggests its key role in α-solanine-induced cell death. Additionally, α-solanine may be an inducer of mitophagy through the upregulation of BNIP3L. Further investigations are required to consolidate α-solanine's effects on GBM cells, and the specific mechanisms of cell death it induces. Results presented in this study contribute

to the search for novel and effective treatments for GBM. Further work should strive to increase the number biological replicates for the experiments conducted to and carry out alternative methods to strengthen this study's findings. Moreover, in-vivo experiments and testing using patient-derived GBM tissue to better evaluate the clinical potential of α-solanine.

Keywords

Glioblastoma multiforme; in-vitro; $IDH_{wildtype}$; α-solanine; cell death; BECN1

Table of Contents

DEDICATION ..... **V**

ACKNOWLEDGMENTS ..... **VI**

ABSTRACT ..... **VIII**

TABLE OF CONTENTS ..... **X**

TABLE OF FIGURES ..... **XX**

TABLE OF TABLES ..... **XLIV**

TABLE OF OUTPUTS ..... **XLIX**

TABLE OF EQUATIONS ..... **CV**

LIST OF ABBREVIATIONS ..... **CVI**

CHAPTER 1 ..... INTRODUCTION 1

1.1. AIM 3

1.2. OBJECTIVES 3

CHAPTER 2 ..... LITERATURE REVIEW 4

2.1. GLIOBLASTOMA MULTIFORME 4

2.1.1. Epidemiology of Glioblastoma Multiforme 4

2.1.2. Classification of Glioblastoma Multiforme 5

2.1.3. An overview of Glioblastoma Multiforme molecular biology 8

2.1.3.1. Major genetic alterations in Glioblastoma Multiforme in the context of the World Health Organisation 2021 Central Nervous System Tumour Classification 8

2.1.3.2. Glioblastoma Multiforme metabolism: glycolysis and the Warburg effect 10

2.1.3.3. Glioblastoma Multiforme oncogenic Receptor Tyrosine Kinase signalling 11

2.1.3.3.1. PI3K-Akt-mTOR signalling 12

2.1.3.3.2. Ras-Raf-ERK1/2 signalling 14

2.1.3.4. Glioblastoma Multiforme cell death signalling pathways 15
2.1.3.4.1. Apoptosis 15
2.1.3.4.1.1. Intrinsic apoptotic pathway 16
2.1.3.4.1.2. Extrinsic pathway 17
2.1.3.4.1.3. Glioblastoma multiforme and apoptosis 18
2.1.3.4.2. Autophagy 19
2.1.3.4.2.1. Autophagy in Glioblastoma Multiforme 21
2.1.3.5. Role of oxidative and Endoplasmic Reticulum stress in Glioblastoma Multiforme molecular biology 22
2.1.3.5.1. Oxidative stress 22
2.1.3.5.2. Endoplasmic reticulum stress 24
2.1.3.6. Hypoxia and angiogenesis in glioblastoma multiforme molecular biology 25
2.1.3.7. Cross talk in glioblastoma multiforme molecular signalling 26
2.1.3.7.1. Dynamic relationship between apoptosis and autophagy 27
2.1.3.7.2. Interplay between cell death and RTK-PI3K-Akt-mTOR signalling 28
2.1.3.7.3. EGFR and PKM2, ROS 29
2.1.3.7.4. HIF-1α, oxidative stress, EGFR and cell death signalling cross talk 30
2.1.3.7.5. Hypoxia, ER stress and cell death signalling 31
2.1.3.8. Glioblastoma multiforme molecular characteristics which confer therapeutic resistance 32
2.1.4. Current Glioblastoma Multiforme standard-of-care 33
2.1.5. Natural molecules as putative drugs against Glioblastoma Multiforme in-vitro 36
2.2. A-SOLANINE 44
2.2.1. Ethnopharmacological sources of α-solanine 44
2.2.2. Chemical properties and biosynthesis of α-Solanine 45
2.2.3. Pharmacology of α-Solanine 47
2.2.3.1. Pharmacokinetics 47
2.2.3.2. Pharmacodynamics 48
2.2.3.2.1. Effect on serum and liver enzymes 48
2.2.3.2.2. *Effect on physiological parameters and histopathology* 49
2.2.3.2.3. Effect on gene transcription 51

2.2.3.2.4. *Toxicokinetics* 51

2.2.3.2.5. Teratogenicity studies 52

2.3. **α**-SOLANINE'S ANTI-CANCER PROPERTIES 53

*2.3.1. **α**-solanine as an anti-cancer agent in-vitro 53*

2.3.1.1. **α**-solanine decreases cancer cell viability 53

2.3.1.2. **α**-solanine induces marked morphological changes 55

2.3.1.3. **α**-solanine unequivocally generates ROS 56

2.3.1.4. **α**-solanine supresses growth signalling 57

2.3.1.5. **α**-solanine suppresses metastatic potential 58

2.3.1.6. **α**-solanine produces cell-death through apoptosis and autophagy 59

2.3.1.7. **α**-solanine increases cytosolic calcium ion concentration 61

2.3.1.8. **α**-solanine inhibits angiogenesis 61

2.3.1.9. **α**-solanine as adjuvant chemotherapy 62

*2.3.2. **α**-solanine as an anti-cancer agent in-vivo 62*

CHAPTER 3 ..... METHODS 64

3.1. OVERVIEW 64

3.2. MATERIALS AND EQUIPMENT 65

3.3. MICROSCOPY 66

3.4. CELL CULTURE AND MAINTENANCE TECHNIQUES 67

3.4.1. Medium Preparation 68

3.4.2. Cell thawing 69

3.4.3. Cell culture maintenance 70

3.4.4. Medium change 71

3.4.5. Cell splitting 71

3.4.6. Resuspension 72

3.4.7. Preparation of cell pellets 73

3.4.8. Cell counting 73

3.4.9. Cryopreservation 74

3.5. CELL VIABILITY ASSAY 75
3.5.1. Presto blue® assay 75
3.6. SCRATCH MIGRATION ASSAY 76
3.7. TRANS-WELL INVASION ASSAY 77
3.8. DNA TECHNIQUES 77
3.8.1. Primer design 78
3.8.1.1. Bioinformatic primer validation and optimisation 79
3.8.2. Ribonucleic acid extraction 80
3.8.3. Spectrophotometry 81
3.8.4. Reverse transcription 81
3.8.5. End-point polymerase chain reaction 82
3.8.6. Gel electrophoresis 83
3.8.7. Sanger sequencing 85
3.8.8. Real-time quantitative polymerase chain reaction 85
3.9. FLUORESCENT MICROSCOPY 86
3.10. FLOW CYTOMETRY 87
3.10.1. Gating strategy and final analysis 89
3.11. PROTEIN TECHNIQUES 90
3.11.1. Cell lysis and protein extraction 90
3.11.2. Bradford assay 91
3.11.3. Antibody array profiling 92
3.11.4. Construction of a protein-protein interaction network 94
3.12. DATA TREATMENT 95
3.12.1. Normalisation of cell viability data 95
3.12.2. Extracting IC_{50} data and linear regression to obtain 95
3.12.3. Data extraction and analysis from scratch migration assay 95
3.12.4. Data extraction and analysis from polymerase chain reaction product gel electrophoresis for RNA primer validation 96

3.12.5. Obtaining fold change data from real-time quantitative polymerase chain reaction data 97

3.12.6. Generation and transformation of corrected total cell fluorescence data from fluorescent imaging 97

3.12.7. Data extraction and transformation from flow-cytometry plots 98

3.12.8. Data extraction and analysis from antibody array profiling 98

3.13. STATISTICAL ANALYSIS 99

CHAPTER 4 ..... RESULTS 101

4.1. ALL CELL LINES ARE GBM $IDH_{WILDTYPE}$ 101

4.2. GLIOBLASTOMA CELLS ARE MORE SENSITIVE TO A-SOLANINE THAN TO TEMOZOLOMIDE 101

4.3. A-SOLANINE INDUCES MORPHOLOGICAL CHANGES ACROSS ALL CELL LINES AFTER 24-HOURS. 103

4.4. A-SOLANINE AND TEMOZOLOMIDE TREATMENT ALTER GBM CELL MIGRATION 104

4.4.1. α-solanine and temozolomide treatment on GBM cell migration varies with time and between cell lines 105

4.4.2. α-Solanine inhibits cell migration more than temozolomide treatment 107

4.4.3. Rate of relative cell migration does not differ between cell lines with α-solanine treatment. 107

4.5. GLIOBLASTOMA MULTIFORME CELL INVASION DOES NOT DIFFER BETWEEN TEMOZOLOMIDE AND A-SOLANINE TREATMENT. 108

4.6. AUTOPHAGY STAINING INTENSITY WAS GREATER ACROSS ALL TREATMENT CONDITIONS. 109

4.7. FLOW CYTOMETRY 111

4.7.1. Necrosis and autophagy were the predominant forms of cell death induced across all treatment conditions. 114

4.7.2. Necrosis and autophagy were enhanced, although no significant differences were observed between the treatment conditions investigated. 114

4.7.3. Induced cell death and the effect of treatment on cell death varied between cell lines 116

4.8. A-SOLANINE INDUCED INCREASED EXPRESSION OF BAX, BECN1, ATG4B AND PKM2 GENES..... 118

4.9. BOTH APOPTOTIC AND AUTOPHAGIC PROTEINS WERE UPREGULATED FOLLOWING A-SOLANINE TREATMENT 119

4.10. PROTEIN-PROTEIN INTERACTION ANALYSIS DEMONSTRATED INTERPLAY BETWEEN PROTEINS INVOLVED IN AUTOPHAGY AND CASPASE INDEPENDENT APOPTOSIS. 121

CHAPTER 5 ..... DISCUSSION 124

5.1. A-SOLANINE VEHICLE TROUBLESHOOTING 125

5.2. A-SOLANINE HAS THE POTENTIAL TO BE A PUTATIVE AGENT AGAINST GLIOBLASTOMA MULTIFORME WHILE EXHIBITING COMPARABLE EFFECTIVENESS TO OTHER TYPES OF CANCERS 126

5.3. A-SOLANINE MAY BE SUPERIOR TO TEMOZOLOMIDE AGAINST GLIOBLASTOMA MULTIFORME *IN-VITRO* 128

5.4. FLUORESCENT MICROSCOPY AND AND FLOW CYTOMETRY ASSAYS PROVIDED AMBIGIOUS CONCLUSIONS REGARDING MODE OF CELL DEATH INDUCED BY A-SOLANINE 130

5.5. EXPERIMENTS INVESTIGATING THE EFFECT OF A-SOLANINE TREATMENT ON MOLECULAR CELL DEATH CHANGES SUGGEST DYSREGULATION OF KEY PROTEINS 133

5.6. LIMITATIONS, AND AREAS FOR IMPROVEMENT 136

CHAPTER 6 ..... CONCLUSIONS AND RECOMMENDATIONS 138

CHAPTER 7 ..... REFERENCES 140

CHAPTER 8 ..... APPENDIX I: ETHICAL APPROVAL 186

CHAPTER 9 ..... APPENDIX II: SYSTEMATIC LITERATURE SEARCHING 187

9.1. GENERAL SYSTEMATIC LITERATURE SEARCH METHOD 187

9.1.1. Study identification and selection 187

9.2. SYSTEMATIC LITERATURE SEARCH RESULTS 191

9.2.1. Systematic literature search results for section 2.1.1. 191

9.2.2. Systematic literature search results for section 2.1.2. 192

9.2.3. Systematic literature search results for section 2.1.3. 193

9.2.4. Systematic literature search results for section 2.1.4. 195

9.2.5. Systematic literature search results for section 2.1.5. 197

9.2.6. Systematic literature search results for section 2.2.1. 199

9.2.7. Systematic literature search results for section 2.2.2. (part 1) 201

9.2.8. Systematic literature search results for section 2.2.2. (part 2) 201

9.2.9. Systematic literature search results for section 2.2.3. 202

9.2.10. Systematic literature search results for section 2.3. 203

9.3. REFERENCES 205

CHAPTER 10 ..... APPENDIX III: VIABILITY ASSAY OPTIMISATION 258

10.1. HYPOTHESISING GLIOBLASTOMA MULTIFORME CELLS ARE SENSITIVE TO DIMETHYL-SULFOXIDE 258

10.2. INVESTIGATING THE SUITABILITY OF DIMETHYL-SULFOXIDE AS A VEHICLE FOR A-SOLANINE SOLANINE 258

CHAPTER 11 ..... APPENDIX IV: RNA PRIMER SEARCH BIOINFORMATIC AND EXPERIMENTAL VALIDATION 262

11.1. SEARCH AND VALIDATION OF PRIMERS DESIGNED AGAINST HUMAN AUTOPHAGY RELATED 4B CYSTEINE PEPTIDASE GENE 262

11.2. SEARCH AND VALIDATION OF PRIMERS DESIGNED AGAINST HUMAN BCL-2 ASSOCIATED X PROTEIN GENE 264

11.3. SEARCH AND VALIDATION OF PRIMERS DESIGNED AGAINST HUMAN BECLIN-1 GENE 270

11.4. SEARCH AND VALIDATION OF PRIMERS DESIGNED AGAINST HUMAN CASPASE-3 GENE 273

11.5. SEARCH AND VALIDATION OF PRIMERS DESIGNED AGAINST HUMAN PYRUVATE KINASE ISOZYME-2 GENE 277

11.6. SEARCH AND VALIDATION OF PRIMERS DESIGNED AGAINST HUMAN VASCULAR ENDOTHELIAL GROWTH FACTOR GENE 280

11.7. SEARCH AND VALIDATION OF PRIMERS DESIGNED AGAINST HUMAN ACTIVATING TRANSCRIPTION FACTOR 6 A GENE 283

11.8. SEARCH AND VALIDATION OF PRIMERS DESIGNED AGAINST HUMAN ISOCITRATE DEHYDROGENASE-1 GENE 288

11.9. ISOCITRATE-DEHYDROGENASE PRIMER OPTIMISATION AND EXPERIMENTAL VALIDATION 291

11.10. RIBONUCLEIC ACID PRIMER EXPERIMENTAL VALIDATION 292

11.11. REFERENCES 294

CHAPTER 12 ..... APPENDIX V RAW DATA 305

12.1. ISOCITRATE DEHYDROGENASE 1 SEQUENCING DATA 305

12.2. PRESTO BLUE® CELL VIABILITY ASSAY DATA 306

12.3. SCRATCH MIGRATION ASSAY DATA 308

12.4. TRANS-WELL INVASION ASSAY DATA 310

12.5. REAL-TIME QUANTITATIVE POLYMERASE CHAIN REACTION DATA 312

12.5.1. Real-time quantitative polymerase chain reaction data for U87MG cells 312

12.5.2. Real-time quantitative polymerase chain reaction data for U251 cells 313

12.5.3. Real-time quantitative polymerase chain reaction data for U87MG cells 314

12.6. FLUORESCENT INTENSITY DATA 315

12.6.1. Images obtained from fluorescent staining experiments 315

12.6.1.1. U87MG, U251 and T98G cell staining against apoptotic cell death 315

12.6.1.1.1. Bright field imaging 315

12.6.1.1.2. Propidium iodide staining 329

12.6.1.1.3. Annexin-V-fluorescein isothiocyanate staining. 343

12.6.1.1.4. Merged images demonstrating dual Annexin-V-fluorescein isothiocyanate/ propidium iodide staining. 357

12.6.1.2. U87MG, U251 and T98G cell staining against autophagic cell death 371

12.6.1.2.1. Bright field imaging 371

12.6.1.2.2. Monodansylcadaverine staining. 385

12.6.2. Corrected total cell fluorescence data 399

12.7. FLOW CYTOMETRY FINAL ANALYSIS DATA 402

12.7.1. U87MG cell flow cytometric analysis pseudo-colour plots 402

12.7.2. U251 cell flow cytometric analysis pseudo-colour plots 414

12.7.3. T98G cell flow cytometric analysis pseudo-colour plots 426

12.7.4. Flow cytometry data extracted from final analysis pseudo-colour plots 438

12.8. ANTIBODY ARRAY DATA 441

12.9. PRESTO BLUE® CELL VIABILITY ASSAY OPTIMISATION DATA 444

CHAPTER 13 ..... APPENDIX VI: STATISTICAL ANALYSIS 446

13.1. STATISTICAL ANALYSIS OF PRESTO BLUE® CELL VIABILITY ASSAYS 446

13.1.1. Statistical analysis of Presto blue® cell viability data regarding U87MG, U251 and T98G cells following 72 hours treatment with different concentrations of α-temozolomide. 446

13.1.2. Statistical analysis of Presto blue® cell viability data regarding U87MG, U251 and T98G cells following 72 hours treatment with different concentrations of α-solanine..... 451

13.1.3. Generation of IC_{50} α-solanine using AATC BioQuest® IC_{50} calculator..... 456

13.1.4. Logistic linear regression of α-solanine and temozolomide cell viability data to determine IC_{75} α-solanine using GraphPad® linear regression calculator. 457

13.2. STATISTICAL ANALYSIS OF SCRATCH MIGRATION ASSAYS..... 461

13.2.1. Statistical analysis of relative scratch assay wound closure (%) data for U87MG versus U251 versus T98G cells treated with 1200.00 µM temozolomide or 6.25 µM α-solanine per duration of incubation. 461

13.2.2. Statistical analysis of relative scratch assay wound closure (%) data glioblastoma cell lines treated with 1200.00 µM temozolomide or 6.25 µM α-solanine for 24-hours versus 48 hours versus 72 hours duration of incubation, per cell line 468

13.2.3. Statistical analysis comparing relative scratch assay wound closure (%) data of glioblastoma cell lines treated with 1200.00 µM temozolomide versus 6.25 µM α-solanine at 24-hours, 48 hours or 72 hours duration of incubation. 475

13.2.4. Statistical analysis of relative rate of scratch assay wound closure (%) data of glioblastoma cell lines treated with 1200.00 µM temozolomide versus 6.25 µM α-solanine..... 484

13.3. STATISTICAL ANALYSIS OF TRANS-WELL INVASION ASSAYS 490

13.4. STATISTICAL ANALYSIS OF REAL-TIME QUANTITATIVE POLYMERASE CHAIN REACTION EXPERIMENTS 492

13.5. STATISTICAL ANALYSIS OF FLUORESCENT IMAGING EXPERIMENTS 501

13.5.1. Assessing changes in different staining corrected total cell fluorescence per treatment condition. 501

13.5.2. Assessing the effect of different treatment conditionson stain specific corrected total cell fluorescence. 505

13.6. STATISTICAL ANALYSIS OF FLOW-CYTOMETRY EXPERIMENTS 508

13.6.1. Assessing mode of cell death between cell lines per treatment condition..... 508

13.6.2. Assessing differences in the occurrence of different cell death types investigated per cell line and treatment condition. 524

13.6.3. Comparing the effect of treatment conditions on cell death investigated per cell line 537

13.6.4. Assessing the overall changes in the different forms of cell death under the treatment conditions investigation..... 551

13.7. STATISTICAL ANALYSIS OF ANTIBODY ARRAY EXPERIMENTS 561

13.8. STATISTICAL ANALYSIS OF PRESTO BLUE® CELL VIABILITY ASSAY OPTIMISATION 654

CHAPTER 14 PUBLISHED AND SUBMITTED MANUSCRIPTS; CONFERENCE PRESENTATIONS AND SCIENCE COMMUNICATION ARTICLES 662

Table of figures

Figure 2.1.: Biosynthesis of α-solanine. Generated using MarvinSketch version 19.21.7. 46

Figure 3.1.: Overview of the experiments conducted throughout this project. Created in Biorender.com 64

Figure 4.1.: Isocitrate dehydrogenase-1 sanger sequencing demonstrating the locus of R132. 101

Figure 4.2.: Viability of U87MG, U251 and T98G cells following 72 hours treatment with different concentrations of temozolomide. 102

Figure 4.3.: Viability of U87MG, U251 and T98G cells following 72 hours treatment with different concentrations of a-solanine. 102

Figure 4.4.: U87MG, U251 and T98G cell morphology under control, temozolomide and a-solanine treatment conditions. U87MG, U251 and T98G cell morphology under [A] negative control; [B] positive control; [C] 1200.00 μM temozolomide (TMZ); [D] 6.25 μM a-solanine treatment conditions for 24-hours. Magnification: X100; scale bar: 50 μM. 104

Figure 4.5.: U87MG, U251 and T98G cell migration under control, temozolomide and a-solanine treatment conditions. Selected images representing [A] U87MG; [B] U251 and [C] T98G cell morphology under negative control (vehicle); 1200.00 μM temozolomide (TMZ) and 6.25 μM a-solanine conditions at 0-, 24-, 48- and 72- hours of incubation. Magnification: X40; scale bar: 50 μM. 106

Figure 4.6.: Comparison of relative wound closure between individual time-points per cell line and treatment condition. Comparison between 24-, 48-, and 72-hour incubation with [A] 1200.00 μM temozolomide (TMZ) and [B] 6.25 μM a-solanine in U87MG, U251 and T98G cells. 106

Figure 4.7.: Comparison of relative wound closure cell-line per time-point and treatment condition. Comparison between U87MG, U251 and T98G cells after incubating for 24-, 48-, and 72 hours with [A] 1200.00 μM temozolomide (TMZ) and [B] 6.25 μM a-solanine. 106

Figure 4.8.: Comparing the effect of temozolomide and a-solanine treatment at each time-point investigating on U87MG, U251 and T98G cells. Effect of 1200.00 μM temozolomide (TMZ) and 6.25 μM a-solanine on [A] U87MG, [B] U251 and [C] T98G cell at each time point investigated..... **Error! Bookmark not defined.**

Figure 4.9.: Relative rate of U87MG, U251 and T98G cell migration under temozolomide and a-solanine treatment. [A] Between cell line and [B] between treatment comparison of the effect of 1200.00 μM

temozolomide (TMZ) and 6.25 μM a-solanine treatment on relative rate of U87MG, U251 and T98G cell migration. 108
Figure 4.10.: Comparing the cell-line specific effect of 72-hour a-solanine and temozolomide treatment. 108
Figure 4.11.: Comparing the effect of 72-hour a-solanine and temozolomide treatment between glioblastoma cell lines 109
Figure 4.12.: Comparing changes corrected total cell fluorescence following different treatment conditions. Comparing changes in propidium iodide (PI), annexin-V-fluorescein isothiocyanate (Annexin-V-FITC) or monodansylcadaverine (MDC) corrected total cell fluorescence following treatment with 6.25 μM a-solanine, 1200.00 μM temozolomide or culture (negative control) conditions in glioblastoma cells. 110
Figure 4.13.: Effect of treatment on corrected total cell fluorescence. Comparing the effect of 6.25 μM a-solanine, 1200.00 μM temozolomide or culture (negative control) treatment conditions on propidium iodide (PI), annexin-V-fluorescein isothiocyanate (Annexin-V-FITC) or monodansylcadaverine (MDC) corrected total cell fluorescence in glioblastoma multiforme cells. 110
Figure 4.14.:Identifying flow-cytometry gating cut-off values for final analysis. Distinguishing of flow-cytometric cut-off values was achieved by plotting histograms of positive (5.00 mM H2O2) and negative (culture) control conditions and identifying where on the x-axis the two conditions intersect. Cell detected greater than the cut-off values were considered as staining positive for the respective dye. [Blue – culture (negative) control conditions; green/red/yellow - 5.00 mM H_2O_2 (positive) control conditions]. 111
Figure 4.15.: Annexin-V-fluoroscein isothiocyanate flow and propidium iodide flow cytometry analysis. Pseudo-colour plots demonstrating final flow cytometric analysis of U87MG, U251 and T98G cells stained with Annexin-V-fluoroscein isothiocyanate flow (Annexin-V-FITC) and propidium iodide (PI) treated with negative control (culture), positive control (5.00 mM H_20_2), 6.25 μM a-solanine or 1200.00 μM temozolomide for 24-hours. 112
Figure 4.16.: Monodansylcadaverine flow cytometry analysis. Pseudo-colour plots demonstrating final flow cytometric analysis of U87MG, U251 and T98G cells stained with monodansylcadaverine (MDC) treated with negative control (culture), positive control (5.00 mM H_20_2), 6.25 μM a-solanine or 1200.00 μM temozolomide for 24-hours. 113

FIGURE 4.17.: COMPARING THE EFFECT OF TREATMENT OVERALL DETECTED CELL DEATH. [A] COMPARING OVERALL EARLY APOPTOSIS, LATE APOPTOSIS, NECROSIS, AND AUTOPHAGY PER TREATMENT CONDITION AND [B] COMPARING NEGATIVE CONTROL (CULTURE CONDITIONS) POSITIVE CONTROL (5.00 MM H_20_2); 6.25 µM A-SOLANINE; AND 1200.00 µM TEMOZOLOMIDE TREATMENT PER CELL DEATH..... 114

FIGURE 4.18.: COMPARING CELL DEATH OBSERVED THROUGH FLOW-CYTOMETRY PER CELL LINE AND TREATMENT CONDITION. COMPARISON OF DETECTED GLIOBLASTOMA MULTIFORME CELLS UNDERGOING EARLY APOPTOSIS, LATE APOPTOSIS, NECROSIS, OR AUTOPHAGY UNDER [A] NEGATIVE CONTROL (CULTURE CONDITIONS); [B] POSITIVE CONTROL (5.00 MM H_20_2); [C] 6.25 µM A-SOLANINE; AND [D] 1200.00 µM TEMOZOLOMIDE TREATMENT FOR 24-HOURS IN U87MG, U251 AND T98G CELLS..... 115

FIGURE 4.19.: COMPARING THE EFFECT OF TREATMENT ON CELL DEATH THROUGH FLOW-CYTOMETRY PER CELL LINE. COMPARING THE EFFECT OF NEGATIVE CONTROL (CULTURE CONDITIONS); POSITIVE CONTROL (5.00 MM H_20_2); 6.25 µM A-SOLANINE; AND 1200.00 µM TEMOZOLOMIDE TREATMENT FOR 24-HOURS ON [A] EARLY APOPTOSIS; [B] LATE APOPTOSIS; [C] NECROSIS AND [D] AUTOPHAGY, IN U87MG, U251 AND T98G CELLS 116

FIGURE 4.20.: COMPARING THE EFFECT OF TREATMENT ON CELL DEATH THROUGH FLOW-CYTOMETRY BETWEEN CELL LINES. COMPARING THE EFFECT OF NEGATIVE CONTROL (CULTURE CONDITIONS); POSITIVE CONTROL (5.00 MM H_20_2); 6.25 µM A-SOLANINE; AND 1200.00 µM TEMOZOLOMIDE TREATMENT FOR 24-HOURS ON [A] EARLY APOPTOSIS; [B] LATE APOPTOSIS; [C] NECROSIS AND [D] AUTOPHAGY, BETWEEN U87MG, U251 AND T98G CELLS..... 117

FIGURE 4.21.: COMPARING CELL DEATH OBSERVED THROUGH FLOW-CYTOMETRY PER TREATMENT CONDITION BETWEEN CELL LINES. COMPARISON OF DETECTED GLIOBLASTOMA MULTIFORME CELLS UNDERGOING EARLY APOPTOSIS, LATE APOPTOSIS, NECROSIS, OR AUTOPHAGY UNDER [A] NEGATIVE CONTROL (CULTURE CONDITIONS); [B] POSITIVE CONTROL [5.00 MM H_20_2]; [C] 6.25 µM A-SOLANINE; AND [D] 1200.00 µM TEMOZOLOMIDE TREATMENT FOR 24-HOURS BETWEEN U87MG, U251 AND T98G CELLS. .....**ERROR! BOOKMARK NOT DEFINED.**

FIGURE 4.22.: EFFECT OF TEMOZOLOMIDE, SOLANINE AND POSITIVE CONTROL TREATMENT ON THE EXPRESSION OF PRE-SELECTED GENES. GRAPHS DEMONSTRATING THE EFFECT OF 1200.00 µM TEMOZOLOMIDE VERSUS 6.25 µM A-SOLANINE VERSUS 5.00 MM H_2O_2 ON [A] BAX; [B] CASP-3; [C] BECN1; [D] ATG4B; [E] ATF6; [F] PKM2 AND [G] VEGFA GENE EXPRESSION. 118

FIGURE 4.23.: REFERENCE FOR THE PROTEINS TESTED USING ANTIBODY ARRAYS. 119

FIGURE 4.24.: APOPTOSIS ANTIBODY ARRAY RESULTS..... 120

FIGURE 4.25.: AUTOPHAGY ANTIBODY ARRAY RESULTS..... 120

FIGURE 4.26.: INITIAL PROTEIN -PROTEIN INTERACTION NETWORK 122
FIGURE 4.27.: FINALISED PROTEIN-PROTEIN INTERACTION NETWORK. 123
FIGURE 5.1.: PROPOSED MODE OF ACTION OF A-SOLANINE ON THE APOPTOSIS-AUTOPHAGY AXIS 136
FIGURE 9.1.: PREFERRED REPORTING ITEMS FOR SYSTEMATIC REVIEWS AND META-ANALYSES 2020 FLOW DIAGRAM FOR SYSTEMATIC LITERATURE REGARDING SECTION 2.1.1.. ADAPTED FROM PAGE ET AL., 2021. 192
FIGURE 9.2.: PREFERRED REPORTING ITEMS FOR SYSTEMATIC REVIEWS AND META-ANALYSES 2020 FLOW DIAGRAM FOR SYSTEMATIC LITERATURE SEARCH FOR SECTION 2.1.2.. ADAPTED FROM PAGE ET AL., 2021. 193
FIGURE 9.3.: PREFERRED REPORTING ITEMS FOR SYSTEMATIC REVIEWS AND META-ANALYSES 2020 FLOW DIAGRAM FOR SYSTEMATIC LITERATURE SEARCH FOR SECTION 2.1.3.. ADAPTED FROM PAGE ET AL., 2021. 195
FIGURE 9.4.: PREFERRED REPORTING ITEMS FOR SYSTEMATIC REVIEWS AND META-ANALYSES 2020 FLOW DIAGRAM FOR SYSTEMATIC LITERATURE SEARCH FOR SECTION 2.1.4.. ADAPTED FROM PAGE ET AL., 2021. 196
FIGURE 9.5.: PREFERRED REPORTING ITEMS FOR SYSTEMATIC REVIEWS AND META-ANALYSES 2020 FLOW DIAGRAM FOR SYSTEMATIC LITERATURE SEARCH FOR SECTION 2.1.4.. ADAPTED FROM PAGE ET AL., 2021. 199
FIGURE 9.6.: PREFERRED REPORTING ITEMS FOR SYSTEMATIC REVIEWS AND META-ANALYSES 2020 FLOW DIAGRAM FOR SYSTEMATIC LITERATURE SEARCH FOR SECTION 2.2.1.. ADAPTED FROM PAGE ET AL., 2021. 200
FIGURE 9.7.: PREFERRED REPORTING ITEMS FOR SYSTEMATIC REVIEWS AND META-ANALYSES 2020 FLOW DIAGRAM FOR SYSTEMATIC LITERATURE SEARCH FOR SECTION 2.1.4.. ADAPTED FROM PAGE ET AL., 2021. 202
FIGURE 9.8.: PREFERRED REPORTING ITEMS FOR SYSTEMATIC REVIEWS AND META-ANALYSES 2020 FLOW DIAGRAM FOR SYSTEMATIC LITERATURE SEARCH FOR SECTION 2.2.3.. ADAPTED FROM PAGE ET AL., 2021. 203
FIGURE 9.9.: PREFERRED REPORTING ITEMS FOR SYSTEMATIC REVIEWS AND META-ANALYSES 2020 FLOW DIAGRAM FOR SYSTEMATIC LITERATURE SEARCH FOR SECTION 2.1.4.. ADAPTED FROM PAGE ET AL., 2021. 204
FIGURE 10.1.: U87MG VIABILITY AFTER 72 HOURS TREATED WITH 1.00 % DMSO VERSUS 10.00 % DMSO. 259
FIGURE 10.2.: U87MG VIABILITY AFTER 72 HOURS TREATED WITH 5.00 µM A-SOLANINE IN DMSO VERSUS 50.00 µM A-SOLANINE IN DMSO. 259
FIGURE 10.3.: U87MG VIABILITY AFTER 72 HOURS TREATED WITH WITH 5.00 µM A-SOLANINE IN DMEM/F12 MEDIUM VERSUS 50.00 µM A-SOLANINE IN DMEM/F12 MEDIUM. 260
FIGURE 10.4.: U87MG VIABILITY AFTER 72 HOURS TREATED WITH 1.00% DMSO VERSUS 5.00 µM A-SOLANINE IN DMSO. 260

FIGURE 10.5.: U87MG VIABILITY AFTER 72 HOURS TREATED WITH 10.00% DMSO VERSUS 50.00 μM A-SOLANINE IN DMSO. 261
FIGURE 10.6.: U87MG VIABILITY AFTER 72 HOURS WITH 5.00 μM A-SOLANINE IN DMSO VERSUS 5.00 μM A-SOLANINE IN DMEM/F12 MEDIUM. 261
FIGURE 10.7.: U87MG VIABILITY AFTER 72 HOURS WITH 50.00 μM A-SOLANINE IN DMSO VERSUS 50.00 μM A-SOLANINE IN DMEM/F12 MEDIUM. 261
FIGURE 11.1.: DEOXYRIBONUCLEIC ACID BINDING ASSAY OPTIMISE AND VALIDATE THE ISOCITRATE DEHYDROGENASE PRIMERS. POLYMERASE CHAIN REACTION (PCR_ GEL OBTAINED UNDER 61 ^{O}C ANNEALING TEMPERATURE CONDITIONS DEMONSTRATED THE STRONGEST BAND (RED ARROWS) AROUND 1200BP WITH MINIMAL ACCESSORY BANDS (BLUE ARROWS). 291
FIGURE 11.2.: LOGISTIC REGRESSION TO ESTIMATE THE SIZE OF THE ISOCITRATE DEHYDROGENASE POLYMERASE CHAIN REACTION PRODUCT OBTAINED. [A] LOGISTIC REGRESSION, AND [B] DETERMINATION OF ESTIMATED PRODUCT SIZE (BP) FOR THE ISOCITRATE DEHYDROGENASE (IDH) GENE POLYMERASE CHAIN REACTION (PCR) PRODUCT OBTAINED UNDER OPTIMAL CONDITIONS 292
FIGURE 11.3.: DEOXYRIBONUCLEIC ACID-BINDING ASSAY TO VALIDATE PRIMER SPECIFICITY. LANE 0: LADDER/ MARKER; LANES 1– 7: PCR PRODUCTS OBTAINED USING PRIMERS DESIGNED TO TARGET THE GENES ATG4B, BAX, BECN1, CASPASE-3, PKM2, VEGFA, ATF6A, RESPECTIVELY. 293
FIGURE 11.4.: LOGISTIC REGRESSION TO ESTIMATE THE SIZE OF THE POLYMERASE CHAIN REACTION PRODUCTS OBTAINED. [A] LOGISTIC REGRESSION, AND [B] DETERMINATION OF ESTIMATED PRODUCT SIZE (BP) FOR THE ATG4B, BAX, BECN1, CASPASE-3, PKM2, VEGFA AND ATF6A, GENE POLYMERASE CHAIN REACTION (PCR) PRODUCTS OBTAINED UNDER OPTIMAL CONDITIONS. 293
FIGURE 12.1.: U87MG, U251 AND T98G ISOCITRATE DEHYDROGENASE-1 GENE SANGER SEQUENCING ALIGNED AGAINST THE CANONICAL GENE SEQUENCE. 305
FIGURE 12.2.: BRIGHT FIELD VIEW OF U87MG CELLS UNDER CULTURE (NEGATIVE CONTROL) CONDITIONS INCUBATED FOR 24HOURS. REPLICATE: 1; MAGNIFICATION: X100. 315
FIGURE 12.3.: BRIGHT FIELD VIEW OF U87MG CELLS UNDER CULTURE (NEGATIVE CONTROL) CONDITIONS INCUBATED FOR 24 -HOURS. REPLICATE: 2; MAGNIFICATION: X100. 316
FIGURE 12.4.: BRIGHT FIELD VIEW OF U87MG CELLS UNDER CULTURE (NEGATIVE CONTROL) CONDITIONS INCUBATED FOR 24HOURS. REPLICATE: 3; MAGNIFICATION: X100. 316

FIGURE 12.5.: BRIGHT FIELD VIEW OF U251 CELLS UNDER CULTURE (NEGATIVE CONTROL) CONDITIONS INCUBATED FOR 24 - HOURS. REPLICATE: 1; MAGNIFICATION: X100. 317
FIGURE 12.6.: BRIGHT FIELD VIEW OF U251 CELLS UNDER CULTURE (NEGATIVE CONTROL) CONDITIONS INCUBATED FOR 24 - HOURS. REPLICATE: 2; MAGNIFICATION: X100. 317
FIGURE 12.7.: BRIGHT FIELD VIEW OF U251 CELLS UNDER CULTURE (NEGATIVE CONTROL) CONDITIONS INCUBATED FOR 24 - HOURS. REPLICATE: 3; MAGNIFICATION: X100. 318
FIGURE 12.8.: BRIGHT FIELD VIEW OF T98G CELLS UNDER CULTURE (NEGATIVE CONTROL) CONDITIONS INCUBATED FOR 24- HOURS. REPLICATE: 1; MAGNIFICATION: X100. 318
FIGURE 12.9.:BRIGHT FIELD VIEW OF T98G CELLS UNDER CULTURE (NEGATIVE CONTROL) CONDITIONS INCUBATED FOR 24- HOURS. REPLICATE: 2; MAGNIFICATION: X100. 319
FIGURE 12.10.: BRIGHT FIELD VIEW OF T98G CELLS UNDER CULTURE (NEGATIVE CONTROL) CONDITIONS INCUBATED FOR 24- HOURS. REPLICATE: 3; MAGNIFICATION: X100. 319
FIGURE 12.11.: BRIGHT FIELD VIEW OF U87MG CELLS TREATED WITH 6.25 µM A-SOLANINE AND INCUBATED FOR 24- HOURS. REPLICATE: 1; MAGNIFICATION: X100. 320
FIGURE 12.12.: BRIGHT FIELD VIEW OF U87MG CELLS TREATED WITH 6.25 µM A-SOLANINE AND INCUBATED FOR 24- HOURS. REPLICATE: 2; MAGNIFICATION: X100. 320
FIGURE 12.13.: BRIGHT FIELD VIEW OF U87MG CELLS TREATED WITH 6.25 µM A-SOLANINE AND INCUBATED FOR 24- HOURS. REPLICATE: 3; MAGNIFICATION: X100. 321
FIGURE 12.14.: BRIGHT FIELD VIEW OF U251 CELLS TREATED WITH 6.25 µM A-SOLANINE AND INCUBATED FOR 24-HOURS. REPLICATE: 1; MAGNIFICATION: X100. 321
FIGURE 12.15.: BRIGHT FIELD VIEW OF U251 CELLS TREATED WITH 6.25 µM A-SOLANINE AND INCUBATED FOR 24-HOURS. REPLICATE: 2; MAGNIFICATION: X100. 322
FIGURE 12.16.: BRIGHT FIELD VIEW OF U251 CELLS TREATED WITH 6.25 µM A-SOLANINE AND INCUBATED FOR 24-HOURS. REPLICATE: 3; MAGNIFICATION: X100. 322
FIGURE 12.17.: BRIGHT FIELD VIEW OF T98G CELLS TREATED WITH 6.25 µM A-SOLANINE AND INCUBATED FOR 24-HOURS. REPLICATE: 1; MAGNIFICATION: X100. 323
FIGURE 12.18.:BRIGHT FIELD VIEW OF T98G CELLS TREATED WITH 6.25 µM A-SOLANINE AND INCUBATED FOR 24-HOURS. REPLICATE: 2; MAGNIFICATION: X100. 323

FIGURE 12.19.: BRIGHT FIELD VIEW OF T98G CELLS TREATED WITH 6.25 μM A-SOLANINE AND INCUBATED FOR 24-HOURS. REPLICATE: 3; MAGNIFICATION: X100. 324
FIGURE 12.20.: BRIGHT FIELD VIEW OF U87MG CELLS TREATED WITH 1200.00 μM TEMOZOLOMIDE AND INCUBATED FOR 24-HOURS. REPLICATE: 1; MAGNIFICATION: X100. 324
FIGURE 12.21.: BRIGHT FIELD VIEW OF U87MG CELLS TREATED WITH 1200.00 μM TEMOZOLOMIDE AND INCUBATED FOR 24-HOURS. REPLICATE: 2; MAGNIFICATION: X100. 325
FIGURE 12.22.: BRIGHT FIELD VIEW OF U87MG CELLS TREATED WITH 1200.00 μM TEMOZOLOMIDE AND INCUBATED FOR 24-HOURS. REPLICATE: 3; MAGNIFICATION: X100. 325
FIGURE 12.23.: BRIGHT FIELD VIEW OF U251 CELLS TREATED WITH 1200.00 μM TEMOZOLOMIDE AND INCUBATED FOR 24-HOURS. REPLICATE: 1; MAGNIFICATION: X100. 326
FIGURE 12.24.: BRIGHT FIELD VIEW OF U251 CELLS TREATED WITH 1200.00 μM TEMOZOLOMIDE AND INCUBATED FOR 24-HOURS. REPLICATE: 1; MAGNIFICATION: X100. 326
FIGURE 12.25.: BRIGHT FIELD VIEW OF U251 CELLS TREATED WITH 1200.00 μM TEMOZOLOMIDE AND INCUBATED FOR 24-HOURS. REPLICATE: 1; MAGNIFICATION: X100. 327
FIGURE 12.26.: BRIGHT FIELD VIEW OF T98G CELLS TREATED WITH 1200.00 μM TEMOZOLOMIDE AND INCUBATED FOR 24-HOURS. REPLICATE: 1; MAGNIFICATION: X100. 327
FIGURE 12.27.:BRIGHT FIELD VIEW OF T98G CELLS TREATED WITH 1200.00 μM TEMOZOLOMIDE AND INCUBATED FOR 24-HOURS. REPLICATE: 2; MAGNIFICATION: X100. 328
FIGURE 12.28.: BRIGHT FIELD VIEW OF T98G CELLS TREATED WITH 1200.00 μM TEMOZOLOMIDE AND INCUBATED FOR 24-HOURS. REPLICATE: 3; MAGNIFICATION: X100. 328
FIGURE 12.29.: U87MG CELLS UNDER CULTURE (NEGATIVE CONTROL) CONDITIONS INCUBATED FOR 24-HOURS AND STAINED WITH PROPIDIUM IODIDE. REPLICATE: 1; MAGNIFICATION: X100. 329
FIGURE 12.30.:U87MG CELLS UNDER CULTURE (NEGATIVE CONTROL) CONDITIONS INCUBATED FOR 24-HOURS AND STAINED WITH PROPIDIUM IODIDE. REPLICATE: 2; MAGNIFICATION: X100. 330
FIGURE 12.31.: U87MG CELLS UNDER CULTURE (NEGATIVE CONTROL) CONDITIONS INCUBATED FOR 24-HOURS AND STAINED WITH PROPIDIUM IODIDE. REPLICATE: 3; MAGNIFICATION: X100. 330
FIGURE 12.32.: U251 CELLS UNDER CULTURE (NEGATIVE CONTROL) CONDITIONS INCUBATED FOR 24-HOURS AND STAINED WITH PROPIDIUM IODIDE. REPLICATE: 1; MAGNIFICATION: X100. 331

FIGURE 12.33.: U251 CELLS UNDER CULTURE (NEGATIVE CONTROL) CONDITIONS INCUBATED FOR 24-HOURS AND STAINED WITH PROPIDIUM IODIDE. REPLICATE: 2; MAGNIFICATION: X100. 331
FIGURE 12.34.: U251 CELLS UNDER CULTURE (NEGATIVE CONTROL) CONDITIONS INCUBATED FOR 24-HOURS AND STAINED WITH PROPIDIUM IODIDE. REPLICATE: 3; MAGNIFICATION: X100. 332
FIGURE 12.35.: T98G CELLS UNDER CULTURE (NEGATIVE CONTROL) CONDITIONS INCUBATED FOR 24-HOURS AND STAINED WITH PROPIDIUM IODIDE. REPLICATE: 1; MAGNIFICATION: X100. 332
FIGURE 12.36.: T98G CELLS UNDER CULTURE (NEGATIVE CONTROL) CONDITIONS INCUBATED FOR 24-HOURS AND STAINED WITH PROPIDIUM IODIDE. REPLICATE: 2; MAGNIFICATION: X100. 333
FIGURE 12.37.: T98G CELLS UNDER CULTURE (NEGATIVE CONTROL) CONDITIONS INCUBATED FOR 24-HOURS AND STAINED WITH PROPIDIUM IODIDE. REPLICATE: 3; MAGNIFICATION: X100. 333
FIGURE 12.38.:U87MG CELLS TREATED WITH 6.25 μM A-SOLANINE AND INCUBATED FOR 24-HOURS AND STAINED WITH PROPIDIUM IODIDE. REPLICATE: 1; MAGNIFICATION: X100. 334
FIGURE 12.39.: U87MG CELLS TREATED WITH 6.25 μM A-SOLANINE AND INCUBATED FOR 24-HOURS AND STAINED WITH PROPIDIUM IODIDE. REPLICATE: 2; MAGNIFICATION: X100. 334
FIGURE 12.40.: U87MG CELLS TREATED WITH 6.25 μM A-SOLANINE AND INCUBATED FOR 24-HOURS DUAL STAINED WITH PROPIDIUM IODIDE. REPLICATE: 3; MAGNIFICATION: X100. 335
FIGURE 12.41.: U251 CELLS TREATED WITH 6.25 μM A-SOLANINE AND INCUBATED FOR 24-HOURS AND STAINED WITH PROPIDIUM IODIDE. REPLICATE: 1; MAGNIFICATION: X100. 335
FIGURE 12.42.: U251 CELLS TREATED WITH 6.25 μM A-SOLANINE AND INCUBATED FOR 24-HOURS AND STAINED WITH PROPIDIUM IODIDE. REPLICATE: 2; MAGNIFICATION: X100. 336
FIGURE 12.43.: U251 CELLS TREATED WITH 6.25 μM A-SOLANINE AND INCUBATED FOR 24-HOURS AND STAINED WITH PROPIDIUM IODIDE. REPLICATE: 3; MAGNIFICATION: X100. 336
FIGURE 12.44.: T98G CELLS TREATED WITH 6.25 μM A-SOLANINE AND INCUBATED FOR 24-HOURS AND STAINED WITH PROPIDIUM IODIDE. REPLICATE: 1; MAGNIFICATION: X100. 337
FIGURE 12.45.: T98G CELLS TREATED WITH 6.25 μM A-SOLANINE AND INCUBATED FOR 24-HOURS AND STAINED WITH PROPIDIUM IODIDE. REPLICATE: 2; MAGNIFICATION: X100. 337
FIGURE 12.46.: T98G CELLS TREATED WITH 6.25 μM A-SOLANINE AND INCUBATED FOR 24-HOURS AND STAINED WITH PROPIDIUM IODIDE. REPLICATE: 3; MAGNIFICATION: X100. 338

FIGURE 12.47.: U87MG CELLS TREATED WITH 1200.00 μM TEMOZOLOMIDE AND INCUBATED FOR 24-HOURS AND STAINED WITH PROPIDIUM IODIDE. REPLICATE: 1; MAGNIFICATION: X100..... 338
FIGURE 12.48.: U87MG CELLS TREATED WITH 1200.00 μM TEMOZOLOMIDE AND INCUBATED FOR 24-HOURS AND STAINED WITH PROPIDIUM IODIDE. REPLICATE: 2; MAGNIFICATION: X100..... 339
FIGURE 12.49.: U87MG CELLS TREATED WITH 1200.00 μM TEMOZOLOMIDE AND INCUBATED FOR 24-HOURS AND STAINED WITH PROPIDIUM IODIDE. REPLICATE: 3; MAGNIFICATION: X100..... 339
FIGURE 12.50.: U251 CELLS TREATED WITH 1200.00 μM TEMOZOLOMIDE AND INCUBATED FOR 24-HOURS AND STAINED WITH PROPIDIUM IODIDE. REPLICATE: 1; MAGNIFICATION: X100 340
FIGURE 12.51.:U251 CELLS TREATED WITH 1200.00 μM TEMOZOLOMIDE AND INCUBATED FOR 24-HOURS AND STAINED WITH PROPIDIUM IODIDE. REPLICATE: 2; MAGNIFICATION: X100 340
FIGURE 12.52.: U251 CELLS TREATED WITH 1200.00 μM TEMOZOLOMIDE AND INCUBATED FOR 24-HOURS AND STAINED WITH PROPIDIUM IODIDE. REPLICATE: 3; MAGNIFICATION: X100. 341
FIGURE 12.53.: T98G CELLS TREATED WITH 1200.00 μM TEMOZOLOMIDE AND INCUBATED FOR 24-HOURS AND STAINED WITH PROPIDIUM IODIDE. REPLICATE: 1; MAGNIFICATION: X100. 341
FIGURE 12.54.: T98G CELLS TREATED WITH 1200.00 μM TEMOZOLOMIDE AND INCUBATED FOR 24-HOURS AND STAINED WITH PROPIDIUM IODIDE. REPLICATE: 2; MAGNIFICATION: X100 342
FIGURE 12.55.: T98G CELLS TREATED WITH 1200.00 μM TEMOZOLOMIDE AND INCUBATED FOR 24-HOURS AND STAINED WITH PROPIDIUM IODIDE. REPLICATE: 3; MAGNIFICATION: X100 342
FIGURE 12.56.: U87MG CELLS UNDER CULTURE (NEGATIVE CONTROL) CONDITIONS INCUBATED FOR 24-HOURS AND STAINED WITH ANNEXIN-V-FLUORESCEIN ISOTHIOCYANATE. REPLICATE: 1; MAGNIFICATION: X100. 343
FIGURE 12.57.: U87MG CELLS UNDER CULTURE (NEGATIVE CONTROL) CONDITIONS INCUBATED FOR 24-HOURS AND STAINED WITH ANNEXIN-V-FLUORESCEIN ISOTHIOCYANATE. REPLICATE: 2; MAGNIFICATION: X100. 344
FIGURE 12.58.: U87MG CELLS UNDER CULTURE (NEGATIVE CONTROL) CONDITIONS INCUBATED FOR 24-HOURS AND STAINED WITH ANNEXIN-V-FLUORESCEIN ISOTHIOCYANATE. REPLICATE: 3; MAGNIFICATION: X100. 344
FIGURE 12.59.: U251 CELLS UNDER CULTURE (NEGATIVE CONTROL) CONDITIONS INCUBATED FOR 24-HOURS AND STAINED WITH ANNEXIN-V-FLUORESCEIN ISOTHIOCYANATE. REPLICATE: 1; MAGNIFICATION: X100. 345
FIGURE 12.60.: U251 CELLS UNDER CULTURE (NEGATIVE CONTROL) CONDITIONS INCUBATED FOR 24-HOURS AND STAINED WITH ANNEXIN-V-FLUORESCEIN ISOTHIOCYANATE. REPLICATE: 2; MAGNIFICATION: X100. 345

FIGURE 12.61.: U251 CELLS UNDER CULTURE (NEGATIVE CONTROL) CONDITIONS INCUBATED FOR 24-HOURS AND STAINED WITH ANNEXIN-V-FLUORESCEIN ISOTHIOCYANATE. REPLICATE: 3; MAGNIFICATION: X100. 346

FIGURE 12.62.: T98G CELLS UNDER CULTURE (NEGATIVE CONTROL) CONDITIONS INCUBATED FOR 24-HOURS AND STAINED WITH ANNEXIN-V-FLUORESCEIN ISOTHIOCYANATE. REPLICATE: 1; MAGNIFICATION: X100. 346

FIGURE 12.63.: T98G CELLS UNDER CULTURE (NEGATIVE CONTROL) CONDITIONS INCUBATED FOR 24-HOURS AND STAINED WITH ANNEXIN-V-FLUORESCEIN ISOTHIOCYANATE. REPLICATE: 2; MAGNIFICATION: X100. 347

FIGURE 12.64.: T98G CELLS UNDER CULTURE (NEGATIVE CONTROL) CONDITIONS INCUBATED FOR 24-HOURS AND STAINED WITH ANNEXIN-V-FLUORESCEIN ISOTHIOCYANATE. REPLICATE: 3; MAGNIFICATION: X100. 347

FIGURE 12.65.: U87MG CELLS TREATED WITH 6.25 μM A-SOLANINE AND INCUBATED FOR 24-HOURS AND STAINED WITH ANNEXIN-V-FLUORESCEIN ISOTHIOCYANATE. REPLICATE: 1; MAGNIFICATION: X100. 348

FIGURE 12.66.: U87MG CELLS TREATED WITH 6.25 μM A-SOLANINE AND INCUBATED FOR 24-HOURS AND STAINED WITH ANNEXIN-V-FLUORESCEIN ISOTHIOCYANATE. REPLICATE: 2; MAGNIFICATION: X100. 348

FIGURE 12.67.: U87MG CELLS TREATED WITH 6.25 μM A-SOLANINE AND INCUBATED FOR 24-HOURS AND STAINED WITH ANNEXIN-V-FLUORESCEIN ISOTHIOCYANATE. REPLICATE: 3; MAGNIFICATION: X100. 349

FIGURE 12.68.: U251 CELLS TREATED WITH 6.25 μM A-SOLANINE AND INCUBATED FOR 24-HOURS AND STAINED WITH ANNEXIN-V-FLUORESCEIN ISOTHIOCYANATE. REPLICATE: 1; MAGNIFICATION: X100. 349

FIGURE 12.69.: U251 CELLS TREATED WITH 6.25 μM A-SOLANINE AND INCUBATED FOR 24-HOURS AND STAINED WITH ANNEXIN-V-FLUORESCEIN ISOTHIOCYANATE. REPLICATE: 2; MAGNIFICATION: X100. 350

FIGURE 12.70.: U251 CELLS TREATED WITH 6.25 μM A-SOLANINE AND INCUBATED FOR 24-HOURS AND STAINED WITH ANNEXIN-V-FLUORESCEIN ISOTHIOCYANATE. REPLICATE: 3; MAGNIFICATION: X100. 350

FIGURE 12.71.: T98G CELLS TREATED WITH 6.25 μM A-SOLANINE AND INCUBATED FOR 24-HOURS AND STAINED WITH ANNEXIN-V-FLUORESCEIN ISOTHIOCYANATE. REPLICATE: 1; MAGNIFICATION: X100. 351

FIGURE 12.72.: T98G CELLS TREATED WITH 6.25 μM A-SOLANINE AND INCUBATED FOR 24-HOURS AND STAINED WITH ANNEXIN-V-FLUORESCEIN ISOTHIOCYANATE. REPLICATE: 2; MAGNIFICATION: X100. 351

FIGURE 12.73.: T98G CELLS TREATED WITH 6.25 μM A-SOLANINE AND INCUBATED FOR 24-HOURS AND STAINED WITH ANNEXIN-V-FLUORESCEIN ISOTHIOCYANATE. REPLICATE: 3; MAGNIFICATION: X100. 352

FIGURE 12.74.: U87MG CELLS TREATED WITH 1200.00 μM TEMOZOLOMIDE AND INCUBATED FOR 24-HOURS AND STAINED WITH ANNEXIN-V-FLUORESCEIN ISOTHIOCYANATE. REPLICATE: 1; MAGNIFICATION: X100. 352

FIGURE 12.75.: U87MG CELLS TREATED WITH 1200.00 μM TEMOZOLOMIDE AND INCUBATED FOR 24-HOURS AND STAINED WITH ANNEXIN-V-FLUORESCEIN ISOTHIOCYANATE. REPLICATE: 2; MAGNIFICATION: X100. 353
FIGURE 12.76.: U87MG CELLS TREATED WITH 1200.00 μM TEMOZOLOMIDE AND INCUBATED FOR 24-HOURS AND STAINED WITH ANNEXIN-V-FLUORESCEIN ISOTHIOCYANATE. REPLICATE: 3; MAGNIFICATION: X100. 353
FIGURE 12.77.: U251 CELLS TREATED WITH 1200.00 μM TEMOZOLOMIDE AND INCUBATED FOR 24-HOURS AND STAINED WITH ANNEXIN-V-FLUORESCEIN ISOTHIOCYANATE. REPLICATE: 1; MAGNIFICATION: X100. 354
FIGURE 12.78.: U251 CELLS TREATED WITH 1200.00 μM TEMOZOLOMIDE AND INCUBATED FOR 24-HOURS AND STAINED WITH ANNEXIN-V-FLUORESCEIN ISOTHIOCYANATE. REPLICATE: 1; MAGNIFICATION: X100. 354
FIGURE 12.79.: U251 CELLS TREATED WITH 1200.00 μM TEMOZOLOMIDE AND INCUBATED FOR 24-HOURS AND STAINED WITH ANNEXIN-V-FLUORESCEIN ISOTHIOCYANATE. REPLICATE: 1; MAGNIFICATION: X100. 355
FIGURE 12.80.: T98G CELLS TREATED WITH 1200.00 μM TEMOZOLOMIDE AND INCUBATED FOR 24-HOURS AND STAINED WITH ANNEXIN-V-FLUORESCEIN ISOTHIOCYANATE. REPLICATE: 1; MAGNIFICATION: X100. 355
FIGURE 12.81.: T98G CELLS TREATED WITH 1200.00 μM TEMOZOLOMIDE AND INCUBATED FOR 24-HOURS AND STAINED WITH ANNEXIN-V-FLUORESCEIN ISOTHIOCYANATE. REPLICATE: 2; MAGNIFICATION: X100. 356
FIGURE 12.82.: T98G CELLS TREATED WITH 1200.00 μM TEMOZOLOMIDE AND INCUBATED FOR 24-HOURS AND STAINED WITH ANNEXIN-V-FLUORESCEIN ISOTHIOCYANATE. REPLICATE: 3; MAGNIFICATION: X100. 356
FIGURE 12.83.: U87MG CELLS UNDER CULTURE (NEGATIVE CONTROL) CONDITIONS INCUBATED FOR 24-HOURS AND DUAL STAINED WITH ANNEXIN-V-FLUORESCEIN ISOTHIOCYANATE AND PROPIDIUM IODIDE. REPLICATE: 1; MAGNIFICATION: X100. 357
FIGURE 12.84.:U87MG CELLS UNDER CULTURE (NEGATIVE CONTROL) CONDITIONS INCUBATED FOR 24-HOURS AND DUAL STAINED WITH ANNEXIN-V-FLUORESCEIN ISOTHIOCYANATE AND PROPIDIUM IODIDE. REPLICATE: 2; MAGNIFICATION: X100. 358
FIGURE 12.85.: U87MG CELLS UNDER CULTURE (NEGATIVE CONTROL) CONDITIONS INCUBATED FOR 24-HOURS AND DUAL STAINED WITH ANNEXIN-V-FLUORESCEIN ISOTHIOCYANATE AND PROPIDIUM IODIDE. REPLICATE: 3; MAGNIFICATION: X100. 358
FIGURE 12.86.: U251 CELLS UNDER CULTURE (NEGATIVE CONTROL) CONDITIONS INCUBATED FOR 24-HOURS AND DUAL STAINED WITH ANNEXIN-V-FLUORESCEIN ISOTHIOCYANATE AND PROPIDIUM IODIDE. REPLICATE: 1; MAGNIFICATION: X100. 359

FIGURE 12.87.: U251 CELLS UNDER CULTURE (NEGATIVE CONTROL) CONDITIONS INCUBATED FOR 24-HOURS AND DUAL STAINED WITH ANNEXIN-V-FLUORESCEIN ISOTHIOCYANATE AND PROPIDIUM IODIDE. REPLICATE: 2; MAGNIFICATION: X100. 359
FIGURE 12.88.: U251 CELLS UNDER CULTURE (NEGATIVE CONTROL) CONDITIONS INCUBATED FOR 24-HOURS AND DUAL STAINED WITH ANNEXIN-V-FLUORESCEIN ISOTHIOCYANATE AND PROPIDIUM IODIDE. REPLICATE: 3; MAGNIFICATION: X100. 360
FIGURE 12.89.: T98G CELLS UNDER CULTURE (NEGATIVE CONTROL) CONDITIONS INCUBATED FOR 24-HOURS AND DUAL STAINED WITH ANNEXIN-V-FLUORESCEIN ISOTHIOCYANATE AND PROPIDIUM IODIDE. REPLICATE: 1; MAGNIFICATION: X100. 360
FIGURE 12.90.: T98G CELLS UNDER CULTURE (NEGATIVE CONTROL) CONDITIONS INCUBATED FOR 24-HOURS AND DUAL STAINED WITH ANNEXIN-V-FLUORESCEIN ISOTHIOCYANATE AND PROPIDIUM IODIDE. REPLICATE: 2; MAGNIFICATION: X100. 361
FIGURE 12.91.: T98G CELLS UNDER CULTURE (NEGATIVE CONTROL) CONDITIONS INCUBATED FOR 24-HOURS AND DUAL STAINED WITH ANNEXIN-V-FLUORESCEIN ISOTHIOCYANATE AND PROPIDIUM IODIDE. REPLICATE: 3; MAGNIFICATION: X100. 361
FIGURE 12.92.: U87MG CELLS TREATED WITH 6.25 μM A-SOLANINE AND INCUBATED FOR 24-HOURS AND DUAL STAINED WITH ANNEXIN-V-FLUORESCEIN ISOTHIOCYANATE AND PROPIDIUM IODIDE. REPLICATE: 1; MAGNIFICATION: X100.362
FIGURE 12.93.: U87MG CELLS TREATED WITH 6.25 μM A-SOLANINE AND INCUBATED FOR 24-HOURS AND DUAL STAINED WITH ANNEXIN-V-FLUORESCEIN ISOTHIOCYANATE AND PROPIDIUM IODIDE. REPLICATE: 2; MAGNIFICATION: X100.362
FIGURE 12.94.: U87MG CELLS TREATED WITH 6.25 μM A-SOLANINE AND INCUBATED FOR 24-HOURS AND DUAL STAINED WITH ANNEXIN-V-FLUORESCEIN ISOTHIOCYANATE AND PROPIDIUM IODIDE. REPLICATE: 3; MAGNIFICATION: X100.363
FIGURE 12.95.: U251 CELLS TREATED WITH 6.25 μM A-SOLANINE AND INCUBATED FOR 24-HOURS AND DUAL STAINED WITH ANNEXIN-V-FLUORESCEIN ISOTHIOCYANATE AND PROPIDIUM IODIDE. REPLICATE: 1; MAGNIFICATION: X100.363
FIGURE 12.96.: U251 CELLS TREATED WITH 6.25 μM A-SOLANINE AND INCUBATED FOR 24-HOURS AND DUAL STAINED WITH ANNEXIN-V-FLUORESCEIN ISOTHIOCYANATE AND PROPIDIUM IODIDE. REPLICATE: 2; MAGNIFICATION: X100.364
FIGURE 12.97.: U251 CELLS TREATED WITH 6.25 μM A-SOLANINE AND INCUBATED FOR 24-HOURS AND DUAL STAINED WITH ANNEXIN-V-FLUORESCEIN ISOTHIOCYANATE AND PROPIDIUM IODIDE. REPLICATE: 3; MAGNIFICATION: X100.364
FIGURE 12.98.: T98G CELLS TREATED WITH 6.25 μM A-SOLANINE AND INCUBATED FOR 24-HOURS AND DUAL STAINED WITH ANNEXIN-V-FLUORESCEIN ISOTHIOCYANATE AND PROPIDIUM IODIDE. REPLICATE: 1; MAGNIFICATION: X100.365

FIGURE 12.99.: T98G CELLS TREATED WITH 6.25 μM A-SOLANINE AND INCUBATED FOR 24-HOURS AND DUAL STAINED WITH ANNEXIN-V-FLUORESCEIN ISOTHIOCYANATE AND PROPIDIUM IODIDE. REPLICATE: 2; MAGNIFICATION: X100.365
FIGURE 12.100.: T98G CELLS TREATED WITH 6.25 μM A-SOLANINE AND INCUBATED FOR 24-HOURS AND DUAL STAINED WITH ANNEXIN-V-FLUORESCEIN ISOTHIOCYANATE AND PROPIDIUM IODIDE. REPLICATE: 3; MAGNIFICATION: X100.366
FIGURE 12.101.: U87MG CELLS TREATED WITH 1200.00 μM TEMOZOLOMIDE AND INCUBATED FOR 24-HOURS AND DUAL STAINED WITH ANNEXIN-V-FLUORESCEIN ISOTHIOCYANATE AND PROPIDIUM IODIDE. REPLICATE: 1; MAGNIFICATION: X100. 366
FIGURE 12.102.: U87MG CELLS TREATED WITH 1200.00 μM TEMOZOLOMIDE AND INCUBATED FOR 24-HOURS AND DUAL STAINED WITH ANNEXIN-V-FLUORESCEIN ISOTHIOCYANATE AND PROPIDIUM IODIDE. REPLICATE: 2; MAGNIFICATION: X100. 367
FIGURE 12.103.: U87MG CELLS TREATED WITH 1200.00 μM TEMOZOLOMIDE AND INCUBATED FOR 24-HOURS AND DUAL STAINED WITH ANNEXIN-V-FLUORESCEIN ISOTHIOCYANATE AND PROPIDIUM IODIDE. REPLICATE: 3; MAGNIFICATION: X100. 367
FIGURE 12.104.: U251 CELLS TREATED WITH 1200.00 μM TEMOZOLOMIDE AND INCUBATED FOR 24-HOURS AND DUAL STAINED WITH ANNEXIN-V-FLUORESCEIN ISOTHIOCYANATE AND PROPIDIUM IODIDE. REPLICATE: 1; MAGNIFICATION: X100. 368
FIGURE 12.105.: U251 CELLS TREATED WITH 1200.00 μM TEMOZOLOMIDE AND INCUBATED FOR 24-HOURS AND DUAL STAINED WITH ANNEXIN-V-FLUORESCEIN ISOTHIOCYANATE AND PROPIDIUM IODIDE. REPLICATE: 2; MAGNIFICATION: X100. 368
FIGURE 12.106.: U251 CELLS TREATED WITH 1200.00 μM TEMOZOLOMIDE AND INCUBATED FOR 24-HOURS AND DUAL STAINED WITH ANNEXIN-V-FLUORESCEIN ISOTHIOCYANATE AND PROPIDIUM IODIDE. REPLICATE: 3; MAGNIFICATION: X100. 369
FIGURE 12.107.: T98G CELLS TREATED WITH 1200.00 μM TEMOZOLOMIDE AND INCUBATED FOR 24-HOURS AND DUAL STAINED WITH ANNEXIN-V-FLUORESCEIN ISOTHIOCYANATE AND PROPIDIUM IODIDE. REPLICATE: 1; MAGNIFICATION: X100. 369
FIGURE 12.108.: T98G CELLS TREATED WITH 1200.00 μM TEMOZOLOMIDE AND INCUBATED FOR 24-HOURS AND DUAL STAINED WITH ANNEXIN-V-FLUORESCEIN ISOTHIOCYANATE AND PROPIDIUM IODIDE. REPLICATE: 2; MAGNIFICATION: X100. 370

FIGURE 12.109.: T98G CELLS TREATED WITH 1200.00 μM TEMOZOLOMIDE AND INCUBATED FOR 24-HOURS AND DUAL STAINED WITH ANNEXIN-V-FLUORESCEIN ISOTHIOCYANATE AND PROPIDIUM IODIDE. REPLICATE: 3; MAGNIFICATION: X100. 370

FIGURE 12.110.: BRIGHT FIELD VIEW OF U87MG CELLS UNDER CULTURE (NEGATIVE CONTROL) CONDITIONS INCUBATED FOR 24-HOURS. REPLICATE: 1; MAGNIFICATION: X100. 371

FIGURE 12.111.: BRIGHT FIELD VIEW OF U87MG CELLS UNDER CULTURE (NEGATIVE CONTROL) CONDITIONS INCUBATED FOR 24-HOURS. REPLICATE: 2; MAGNIFICATION: X100. 372

FIGURE 12.112.: BRIGHT FIELD VIEW OF U87MG CELLS UNDER CULTURE (NEGATIVE CONTROL) CONDITIONS INCUBATED FOR 24-HOURS. REPLICATE: 3; MAGNIFICATION: X100. 372

FIGURE 12.113.: BRIGHT FIELD VIEW OF U251 CELLS UNDER CULTURE (NEGATIVE CONTROL) CONDITIONS INCUBATED FOR 24HOURS. REPLICATE: 1; MAGNIFICATION: X100. 373

FIGURE 12.114.: BRIGHT FIELD VIEW OF U251 CELLS UNDER CULTURE (NEGATIVE CONTROL) CONDITIONS INCUBATED FOR 24HOURS. REPLICATE: 2; MAGNIFICATION: X100. 373

FIGURE 12.115.: BRIGHT FIELD VIEW OF U251 CELLS UNDER CULTURE (NEGATIVE CONTROL) CONDITIONS INCUBATED FOR 24HOURS. REPLICATE: 3; MAGNIFICATION: X100. 374

FIGURE 12.116.: BRIGHT FIELD VIEW OF T98G CELLS UNDER CULTURE (NEGATIVE CONTROL) CONDITIONS INCUBATED FOR 24HOURS. REPLICATE: 1; MAGNIFICATION: X100. 374

FIGURE 12.117.: BRIGHT FIELD VIEW OF T98G CELLS UNDER CULTURE (NEGATIVE CONTROL) CONDITIONS INCUBATED FOR 24HOURS. REPLICATE: 2; MAGNIFICATION: X100. 375

FIGURE 12.118.: BRIGHT FIELD VIEW OF T98G CELLS UNDER CULTURE (NEGATIVE CONTROL) CONDITIONS INCUBATED FOR 24HOURS. REPLICATE: 3; MAGNIFICATION: X100. 375

FIGURE 12.119.: BRIGHT FIELD VIEW OF U87MG CELLS TREATED WITH 6.25 μM A-SOLANINE AND INCUBATED FOR 24-HOURS. REPLICATE: 1; MAGNIFICATION: X100. 376

FIGURE 12.120.: BRIGHT FIELD VIEW OF U87MG CELLS TREATED WITH 6.25 μM A-SOLANINE AND INCUBATED FOR 24-HOURS. REPLICATE: 2; MAGNIFICATION: X100. 376

FIGURE 12.121.: BRIGHT FIELD VIEW OF U87MG CELLS TREATED WITH 6.25 μM A-SOLANINE AND INCUBATED FOR 24-HOURS. REPLICATE: 3; MAGNIFICATION: X100. 377

FIGURE 12.122.: BRIGHT FIELD VIEW OF U251 CELLS TREATED WITH 6.25 μM A-SOLANINE AND INCUBATED FOR 24-HOURS. REPLICATE: 1; MAGNIFICATION: X100. 377

FIGURE 12.123.: BRIGHT FIELD VIEW OF U251 CELLS TREATED WITH 6.25 μM A-SOLANINE AND INCUBATED FOR 24-HOURS. REPLICATE: 2; MAGNIFICATION: X100. 378
FIGURE 12.124.: BRIGHT FIELD VIEW OF U251 CELLS TREATED WITH 6.25 μM A-SOLANINE AND INCUBATED FOR 24-HOURS. REPLICATE: 3; MAGNIFICATION: X100. 378
FIGURE 12.125.: BRIGHT FIELD VIEW OF T98G CELLS TREATED WITH 6.25 μM A-SOLANINE AND INCUBATED FOR 24-HOURS. REPLICATE: 1; MAGNIFICATION: X100. 379
FIGURE 12.126.: BRIGHT FIELD VIEW OF T98G CELLS TREATED WITH 6.25 μM A-SOLANINE AND INCUBATED FOR 24-HOURS. REPLICATE: 2; MAGNIFICATION: X100. 379
FIGURE 12.127.: BRIGHT FIELD VIEW OF T98G CELLS TREATED WITH 6.25 μM A-SOLANINE AND INCUBATED FOR 24-HOURS. REPLICATE: 3; MAGNIFICATION: X100. 380
FIGURE 12.128.: BRIGHT FIELD VIEW OF U87MG CELLS TREATED WITH 1200.00 μM TEMOZOLOMIDE AND INCUBATED FOR 24-HOURS. REPLICATE: 1; MAGNIFICATION: X100. 380
FIGURE 12.129.: BRIGHT FIELD VIEW OF U87MG CELLS TREATED WITH 1200.00 μM TEMOZOLOMIDE AND INCUBATED FOR 24-HOURS. REPLICATE: 2; MAGNIFICATION: X100. 381
FIGURE 12.130.: BRIGHT FIELD VIEW OF U87MG CELLS TREATED WITH 1200.00 μM TEMOZOLOMIDE AND INCUBATED FOR 24-HOURS. REPLICATE: 3; MAGNIFICATION: X100. 381
FIGURE 12.131.: BRIGHT FIELD VIEW OF U251 CELLS TREATED WITH 1200.00 μM TEMOZOLOMIDE AND INCUBATED FOR 24-HOURS. REPLICATE: 1; MAGNIFICATION: X100. 382
FIGURE 12.132.: BRIGHT FIELD VIEW OF U251 CELLS TREATED WITH 1200.00 μM TEMOZOLOMIDE AND INCUBATED FOR 24-HOURS. REPLICATE: 2; MAGNIFICATION: X100. 382
FIGURE 12.133.: BRIGHT FIELD VIEW OF U251 CELLS TREATED WITH 1200.00 μM TEMOZOLOMIDE AND INCUBATED FOR 24-HOURS. REPLICATE: 3; MAGNIFICATION: X100. 383
FIGURE 12.134.: BRIGHT FIELD VIEW OF T98G CELLS TREATED WITH 1200.00 μM TEMOZOLOMIDE AND INCUBATED FOR 24-HOURS. REPLICATE: 1; MAGNIFICATION: X100. 383
FIGURE 12.135.: BRIGHT FIELD VIEW OF T98G CELLS TREATED WITH 1200.00 μM TEMOZOLOMIDE AND INCUBATED FOR 24-HOURS. REPLICATE: 2; MAGNIFICATION: X100. 384
FIGURE 12.136.: BRIGHT FIELD VIEW OF T98G CELLS TREATED WITH 1200.00 μM TEMOZOLOMIDE AND INCUBATED FOR 24-HOURS. REPLICATE: 3; MAGNIFICATION: X100. 384

FIGURE 12.137.: U87MG CELLS UNDER CULTURE (NEGATIVE CONTROL) CONDITIONS INCUBATED FOR 24-HOURS AND STAINED WITH MONODANSYLCADAVERINE. REPLICATE: 1; MAGNIFICATION: X100. 385
FIGURE 12.138.: U87MG CELLS UNDER CULTURE (NEGATIVE CONTROL) CONDITIONS INCUBATED FOR 24-HOURS AND STAINED WITH MONODANSYLCADAVERINE. REPLICATE: 2; MAGNIFICATION: X100. 386
FIGURE 12.139.: U87MG CELLS UNDER CULTURE (NEGATIVE CONTROL) CONDITIONS INCUBATED FOR 24-HOURS AND STAINED WITH MONODANSYLCADAVERINE. REPLICATE: 3; MAGNIFICATION: X100. 386
FIGURE 12.140.: U251 CELLS UNDER CULTURE (NEGATIVE CONTROL) CONDITIONS INCUBATED FOR 24-HOURS AND STAINED WITH MONODANSYLCADAVERINE. REPLICATE: 1; MAGNIFICATION: X100. 387
FIGURE 12.141.: U251 CELLS UNDER CULTURE (NEGATIVE CONTROL) CONDITIONS INCUBATED FOR 24-HOURS AND STAINED WITH MONODANSYLCADAVERINE. REPLICATE: 2; MAGNIFICATION: X100. 387
FIGURE 12.142.: U251 CELLS UNDER CULTURE (NEGATIVE CONTROL) CONDITIONS INCUBATED FOR 24-HOURS AND STAINED WITH MONODANSYLCADAVERINE. REPLICATE: 3; MAGNIFICATION: X100. 388
FIGURE 12.143.: T98G CELLS UNDER CULTURE (NEGATIVE CONTROL) CONDITIONS INCUBATED FOR 24-HOURS AND STAINED WITH MONODANSYLCADAVERINE. REPLICATE: 1; MAGNIFICATION: X100. 388
FIGURE 12.144.: T98G CELLS UNDER CULTURE (NEGATIVE CONTROL) CONDITIONS INCUBATED FOR 24-HOURS AND STAINED WITH MONODANSYLCADAVERINE. REPLICATE: 2; MAGNIFICATION: X100. 389
FIGURE 12.145.: T98G CELLS UNDER CULTURE (NEGATIVE CONTROL) CONDITIONS INCUBATED FOR 24-HOURS AND STAINED WITH MONODANSYLCADAVERINE. REPLICATE: 3; MAGNIFICATION: X100. 389
FIGURE 12.146.: U87MG CELLS TREATED WITH 6.25 μM A-SOLANINE AND INCUBATED FOR 24-HOURS AND STAINED WITH MONODANSYLCADAVERINE. REPLICATE: 1; MAGNIFICATION: X100. 390
FIGURE 12.147.: U87MG CELLS TREATED WITH 6.25 μM A-SOLANINE AND INCUBATED FOR 24-HOURS AND STAINED WITH MONODANSYLCADAVERINE. REPLICATE: 2; MAGNIFICATION: X100. 390
FIGURE 12.148.: U87MG CELLS TREATED WITH 6.25 μM A-SOLANINE AND INCUBATED FOR 24-HOURS AND STAINED WITH MONODANSYLCADAVERINE. REPLICATE: 3; MAGNIFICATION: X100. 391
FIGURE 12.149.: U251 CELLS TREATED WITH 6.25 μM A-SOLANINE AND INCUBATED FOR 24-HOURS AND STAINED WITH MONODANSYLCADAVERINE. REPLICATE1; MAGNIFICATION: X100. 391
FIGURE 12.150.: U251 CELLS TREATED WITH 6.25 μM A-SOLANINE AND INCUBATED FOR 24-HOURS AND STAINED WITH MONODANSYLCADAVERINE. REPLICATE: 2; MAGNIFICATION: X100. 392

FIGURE 12.151.: U251 CELLS TREATED WITH 6.25 μM A-SOLANINE AND INCUBATED FOR 24-HOURS AND STAINED WITH MONODANSYLCADAVERINE. REPLICATE: 3; MAGNIFICATION: X100. 392
FIGURE 12.152.: T98G CELLS TREATED WITH 6.25 μM A-SOLANINE AND INCUBATED FOR 24-HOURS AND STAINED WITH MONODANSYLCADAVERINE. REPLICATE: 1; MAGNIFICATION: X100. 393
FIGURE 12.153.: T98G CELLS TREATED WITH 6.25 μM A-SOLANINE AND INCUBATED FOR 24-HOURS AND STAINED WITH MONODANSYLCADAVERINE. REPLICATE: 2; MAGNIFICATION: X100. 393
FIGURE 12.154.: T98G CELLS TREATED WITH 6.25 μM A-SOLANINE AND INCUBATED FOR 24-HOURS AND STAINED WITH MONODANSYLCADAVERINE. REPLICATE: 3; MAGNIFICATION: X100. 394
FIGURE 12.155.: U87MG CELLS TREATED WITH 1200.00 μM TEMOZOLOMIDE AND INCUBATED FOR 24-HOURS AND STAINED WITH MONODANSYLCADAVERINE. REPLICATE: 1; MAGNIFICATION: X100. 394
FIGURE 12.156.: U87MG CELLS TREATED WITH 1200.00 μM TEMOZOLOMIDE AND INCUBATED FOR 24-HOURS AND STAINED WITH MONODANYSLCADAVERINE. REPLICATE: 2; MAGNIFICATION: X100. 395
FIGURE 12.157.: U87MG CELLS TREATED WITH 1200.00 μM TEMOZOLOMIDE AND INCUBATED FOR 24-HOURS AND STAINED WITH MONODANSYLCADAVERINE. REPLICATE: 3; MAGNIFICATION: X100. 395
FIGURE 12.158.: U251 CELLS TREATED WITH 1200.00 μM TEMOZOLOMIDE AND INCUBATED FOR 24-HOURS AND STAINED WITH MONODANSYLCADAVERINE. REPLICATE: 1; MAGNIFICATION: X100. 396
FIGURE 12.159.: U251 CELLS TREATED WITH 1200.00 μM TEMOZOLOMIDE AND INCUBATED FOR 24-HOURS AND STAINED WITH MONODANSYLCADAVERINE. REPLICATE: 2; MAGNIFICATION: X100. 396
FIGURE 12.160.: U251 CELLS TREATED WITH 1200.00 μM TEMOZOLOMIDE AND INCUBATED FOR 24-HOURS AND STAINED WITH MONODANSYLCADAVERINE. REPLICATE: 3; MAGNIFICATION: X100. 397
FIGURE 12.161.: T98G CELLS TREATED WITH 1200.00 μM TEMOZOLOMIDE AND INCUBATED FOR 24-HOURS AND STAINED WITH MONODANSYLCADAVERINE. REPLICATE: 1; MAGNIFICATION: X100. 397
FIGURE 12.162.: T98G CELLS TREATED WITH 1200.00 μM TEMOZOLOMIDE AND INCUBATED FOR 24-HOURS AND STAINED WITH MONODANSYLCADAVERINE. REPLICATE: 2; MAGNIFICATION: X100. 398
FIGURE 12.163.: T98G CELLS TREATED WITH 1200.00 μM TEMOZOLOMIDE AND INCUBATED FOR 24-HOURS AND STAINED WITH MONODANSYLCADAVERINE. REPLICATE: 3; MAGNIFICATION: X100. 398
FIGURE 12.164.: FLOW CYTOMETRY FINAL ANALYSIS FOR U87MG CELLS TREATED WITH CULTURE (NEGATIVE CONTROL) CONDITIONS FOR 24-HOURS AND DUAL STAINED WITH ANNEXIN-V-FLUORESCEIN ISOTHIOCYANATE AND PROPIDIUM IODIDE, REPLICATE 1. 402

FIGURE 12.165.: FLOW CYTOMETRY FINAL ANALYSIS FOR U87MG CELLS TREATED WITH CULTURE (NEGATIVE CONTROL) CONDITIONS FOR 24-HOURS AND DUAL STAINED WITH ANNEXIN-V-FLUORESCEIN ISOTHIOCYANATE AND PROPIDIUM IODIDE, REPLICATE 2. 402

FIGURE 12.166.: FLOW CYTOMETRY FINAL ANALYSIS FOR U87MG CELLS TREATED WITH CULTURE (NEGATIVE CONTROL) CONDITIONS FOR 24-HOURS AND DUAL STAINED WITH ANNEXIN-V-FLUORESCEIN ISOTHIOCYANATE AND PROPIDIUM IODIDE, REPLICATE 3. 403

FIGURE 12.167.: FLOW CYTOMETRY FINAL ANALYSIS FOR U87MG CELLS TREATED WITH 5.00 MM H_20_2 (POSITIVE CONTROL) CONDITIONS FOR 24-HOURS AND DUAL STAINED WITH ANNEXIN-V-FLUORESCEIN ISOTHIOCYANATE AND PROPIDIUM IODIDE, REPLICATE 1. 403

FIGURE 12.168.: FLOW CYTOMETRY FINAL ANALYSIS FOR U87MG CELLS TREATED WITH 5.00 MM H_20_2 (POSITIVE CONTROL) CONDITIONS FOR 24-HOURS AND DUAL STAINED WITH ANNEXIN-V-FLUORESCEIN ISOTHIOCYANATE AND PROPIDIUM IODIDE, REPLICATE 2. 404

FIGURE 12.169.: FLOW CYTOMETRY FINAL ANALYSIS FOR U87MG CELLS TREATED WITH 5.00 MM H_20_2 (POSITIVE CONTROL) CONDITIONS FOR 24-HOURS AND DUAL STAINED WITH ANNEXIN-V-FLUORESCEIN ISOTHIOCYANATE AND PROPIDIUM IODIDE, REPLICATE 3. 404

FIGURE 12.170.: FLOW CYTOMETRY FINAL ANALYSIS FOR U87MG CELLS TREATED WITH 6.25 μM A-SOLANINE FOR 24-HOURS AND DUAL STAINED WITH ANNEXIN-V-FLUORESCEIN ISOTHIOCYANATE AND PROPIDIUM IODIDE, REPLICATE 1. 405

FIGURE 12.171.: FLOW CYTOMETRY FINAL ANALYSIS FOR U87MG CELLS TREATED WITH 6.25 μM A-SOLANINE FOR 24-HOURS AND DUAL STAINED WITH ANNEXIN-V-FLUORESCEIN ISOTHIOCYANATE AND PROPIDIUM IODIDE, REPLICATE 2. 405

FIGURE 12.172.: FLOW CYTOMETRY FINAL ANALYSIS FOR U87MG CELLS TREATED WITH 6.25 μM A-SOLANINE FOR 24-HOURS AND DUAL STAINED WITH ANNEXIN-V-FLUORESCEIN ISOTHIOCYANATE AND PROPIDIUM IODIDE, REPLICATE 3. 406

FIGURE 12.173.: FLOW CYTOMETRY FINAL ANALYSIS FOR U87MG CELLS TREATED WITH 1200.00 μM TEMOZOLOMIDE FOR 24-HOURS AND DUAL STAINED WITH ANNEXIN-V-FLUORESCEIN ISOTHIOCYANATE AND PROPIDIUM IODIDE, REPLICATE 1. 406

Figure 12.174.: Flow cytometry final analysis for U87MG cells treated with 1200.00 μM temozolomide for 24-hours and dual stained with Annexin-V-fluorescein isothiocyanate and propidium iodide, replicate 2. 407
Figure 12.175.: Flow cytometry final analysis for U87MG cells treated with 1200.00 μM temozolomide for 24-hours and dual stained with Annexin-V-fluorescein isothiocyanate and propidium iodide, replicate 3. 407
Figure 12.176.: Flow cytometry final analysis for U87MG cells treated with culture (negative control) conditions for 24-hours and dual stained with monodansylcadaverine, replicate 1. 408
Figure 12.177.: Flow cytometry final analysis for U87MG cells treated with culture (negative control) conditions for 24-hours and dual stained with monodansylcadaverine, replicate 2. 408
Figure 12.178.: Flow cytometry final analysis for U87MG cells treated with culture (negative control) conditions for 24-hours and dual stained with monodansylcadaverine, replicate 3. 409
Figure 12.179.: Flow cytometry final analysis for U87MG cells treated with 5.00 mM H_20_2 (positive control) conditions for 24-hours and dual stained with monodansylcadaverine, replicate 1. 409
Figure 12.180.: Flow cytometry final analysis for U87MG cells treated with 5.00 mM H_20_2 (positive control) conditions for 24-hours and dual stained with monodansylcadaverine, replicate 2. 410
Figure 12.181.: Flow cytometry final analysis for U87MG cells treated with 5.00 mM H_20_2 (positive control) conditions for 24-hours and dual stained with monodansylcadaverine, replicate 3. 410
Figure 12.182.: Flow cytometry final analysis for U87MG cells treated with 6.25 μM a-solanine for 24-hours and dual stained with monodansylcadaverine, replicate 1. 411
Figure 12.183.: Flow cytometry final analysis for U87MG cells treated with 6.25 μM a-solanine for 24-hours and dual stained with monodansylcadaverine, replicate 2. 411
Figure 12.184.: Flow cytometry final analysis for U87MG cells treated with 6.25 μM a-solanine for 24-hours and dual stained with monodansylcadaverine, replicate 3. 412
Figure 12.185.: Flow cytometry final analysis for U87MG cells treated with 1200.00 μM temozolomide for 24-hours and dual stained with monodansylcadaverine, replicate 1. 412
Figure 12.186.: Flow cytometry final analysis for U87MG cells treated with 1200.00 μM temozolomide for 24-hours and dual stained with monodansylcadaverine, replicate 2. 413

Figure 12.187.: Flow cytometry final analysis for U87MG cells treated with 1200.00 μM temozolomide for 24-hours and dual stained with monodansylcadaverine, replicate 3. 413
Figure 12.188.: Flow cytometry final analysis for U251 cells treated with culture (negative control) conditions for 24-hours and dual stained with Annexin-V-fluorescein isothiocyanate and propidium iodide, replicate 1. 414
Figure 12.189.: Flow cytometry final analysis for U251 cells treated with culture (negative control) conditions for 24-hours and dual stained with Annexin-V-fluorescein isothiocyanate and propidium iodide, replicate 2. 414
Figure 12.190.: Flow cytometry final analysis for U251 cells treated with culture (negative control) conditions for 24-hours and dual stained with Annexin-V-fluorescein isothiocyanate and propidium iodide, replicate 3. 415
Figure 12.191.: Flow cytometry final analysis for U251 cells treated with 5.00 mM H_20_2 (positive control) conditions for 24-hours and dual stained with Annexin-V-fluorescein isothiocyanate and propidium iodide, replicate 1. 415
Figure 12.192.: Flow cytometry final analysis for U251 cells treated with 5.00 mM H_20_2 (positive control) conditions for 24-hours and dual stained with Annexin-V-fluorescein isothiocyanate and propidium iodide, replicate 2. 416
Figure 12.193.: Flow cytometry final analysis for U251 cells treated with 5.00 mM H_20_2 (positive control) conditions for 24-hours and dual stained with Annexin-V-fluorescein isothiocyanate and propidium iodide, replicate 3. 416
Figure 12.194.: Flow cytometry final analysis for U251 cells treated with 6.25 μM a-solanine for 24-hours and dual stained with Annexin-V-fluorescein isothiocyanate and propidium iodide, replicate 1. 417
Figure 12.195.: Flow cytometry final analysis for U251 cells treated with 6.25 μM a-solanine for 24-hours and dual stained with Annexin-V-fluorescein isothiocyanate and propidium iodide, replicate 2. 417
Figure 12.196.: Flow cytometry final analysis for U251 cells treated with 6.25 μM a-solanine for 24-hours and dual stained with Annexin-V-fluorescein isothiocyanate and propidium iodide, replicate 3. 418
Figure 12.197.: Flow cytometry final analysis for U251 cells treated with 1200.00 μM temozolomide for 24-hours and dual stained with Annexin-V-fluorescein isothiocyanate and propidium iodide, replicate 1. 418

Figure 12.198.: Flow cytometry final analysis for U251 cells treated with 1200.00 μM temozolomide for 24-hours and dual stained with Annexin-V-fluorescein isothiocyanate and propidium iodide, replicate 2. 419
Figure 12.199.: Flow cytometry final analysis for U251 cells treated with 1200.00 μM temozolomide for 24-hours and dual stained with Annexin-V-fluorescein isothiocyanate and propidium iodide, replicate 3. 419
Figure 12.200.: Flow cytometry final analysis for U251 cells treated with culture (negative control) conditions for 24-hours and dual stained with monodansylcadaverine, replicate 1. 420
Figure 12.201.: Flow cytometry final analysis for U251 cells treated with culture (negative control) conditions for 24-hours and dual stained with monodansylcadaverine, replicate 2. 420
Figure 12.202.: Flow cytometry final analysis for U251 cells treated with culture (negative control) conditions for 24-hours and dual stained with monodansylcadaverine, replicate 3. 421
Figure 12.203.: Flow cytometry final analysis for U251 cells treated with 5.00 mM H_20_2 (positive control) conditions for 24-hours and dual stained with monodansylcadaverine, replicate 1. 421
Figure 12.204.: Flow cytometry final analysis for U251 cells treated with 5.00 mM H_20_2 (positive control) conditions for 24-hours and dual stained with monodansylcadaverine, replicate 2. 422
Figure 12.205.: Flow cytometry final analysis for U251 cells treated with 5.00 mM H_20_2 (positive control) conditions for 24-hours and dual stained with monodansylcadaverine, replicate 3. 422
Figure 12.206.: Flow cytometry final analysis for U251 cells treated with 6.25 μM a-solanine for 24-hours and dual stained with monodansylcadaverine, replicate 1. 423
Figure 12.207.: Flow cytometry final analysis for U251 cells treated with 6.25 μM a-solanine for 24-hours and dual stained with monodansylcadaverine, replicate 2. 423
Figure 12.208.: Flow cytometry final analysis for U251 cells treated with 6.25 μM a-solanine for 24-hours and dual stained with monodansylcadaverine, replicate 3. 424
Figure 12.209.: Flow cytometry final analysis for U251 cells treated with 1200.00 μM temozolomide for 24-hours and dual stained with monodansylcadaverine, replicate 1. 424
Figure 12.210.: Flow cytometry final analysis for U251 cells treated with 1200.00 μM temozolomide for 24-hours and dual stained with monodansylcadaverine, replicate 2. 425

FIGURE 12.211.: FLOW CYTOMETRY FINAL ANALYSIS FOR U251 CELLS TREATED WITH 1200.00 μM TEMOZOLOMIDE FOR 24-HOURS AND DUAL STAINED WITH MONODANSYLCADAVERINE, REPLICATE 3. 425
FIGURE 12.212.: FLOW CYTOMETRY FINAL ANALYSIS FOR T98G CELLS TREATED WITH CULTURE (NEGATIVE CONTROL) CONDITIONS FOR 24-HOURS AND DUAL STAINED WITH ANNEXIN-V-FLUORESCEIN ISOTHIOCYANATE AND PROPIDIUM IODIDE, REPLICATE 1. 426
FIGURE 12.213.: FLOW CYTOMETRY FINAL ANALYSIS FOR T98G CELLS TREATED WITH CULTURE (NEGATIVE CONTROL) CONDITIONS FOR 24-HOURS AND DUAL STAINED WITH ANNEXIN-V-FLUORESCEIN ISOTHIOCYANATE AND PROPIDIUM IODIDE, REPLICATE 2. 426
FIGURE 12.214.: FLOW CYTOMETRY FINAL ANALYSIS FOR T98G CELLS TREATED WITH CULTURE (NEGATIVE CONTROL) CONDITIONS FOR 24-HOURS AND DUAL STAINED WITH ANNEXIN-V-FLUORESCEIN ISOTHIOCYANATE AND PROPIDIUM IODIDE, REPLICATE 3. 427
FIGURE 12.215.: FLOW CYTOMETRY FINAL ANALYSIS FOR T98G CELLS TREATED WITH 5.00 MM H_20_2 (POSITIVE CONTROL) CONDITIONS FOR 24-HOURS AND DUAL STAINED WITH ANNEXIN-V-FLUORESCEIN ISOTHIOCYANATE AND PROPIDIUM IODIDE, REPLICATE 1. 427
FIGURE 12.216.: FLOW CYTOMETRY FINAL ANALYSIS FOR T98G CELLS TREATED WITH 5.00 MM H_20_2 (POSITIVE CONTROL) CONDITIONS FOR 24-HOURS AND DUAL STAINED WITH ANNEXIN-V-FLUORESCEIN ISOTHIOCYANATE AND PROPIDIUM IODIDE, REPLICATE 2. 428
FIGURE 12.217.: FLOW CYTOMETRY FINAL ANALYSIS FOR T98G CELLS TREATED WITH 5.00 MM H_20_2 (POSITIVE CONTROL) CONDITIONS FOR 24-HOURS AND DUAL STAINED WITH ANNEXIN-V-FLUORESCEIN ISOTHIOCYANATE AND PROPIDIUM IODIDE, REPLICATE 3. 428
FIGURE 12.218.: FLOW CYTOMETRY FINAL ANALYSIS FOR T98G CELLS TREATED WITH 6.25 μM A-SOLANINE FOR 24-HOURS AND DUAL STAINED WITH ANNEXIN-V-FLUORESCEIN ISOTHIOCYANATE AND PROPIDIUM IODIDE, REPLICATE 1. 429
FIGURE 12.219.: FLOW CYTOMETRY FINAL ANALYSIS FOR T98G CELLS TREATED WITH 6.25 μM A-SOLANINE FOR 24-HOURS AND DUAL STAINED WITH ANNEXIN-V-FLUORESCEIN ISOTHIOCYANATE AND PROPIDIUM IODIDE, REPLICATE 2. 429
FIGURE 12.220.: FLOW CYTOMETRY FINAL ANALYSIS FOR T98G CELLS TREATED WITH 6.25 μM A-SOLANINE FOR 24-HOURS AND DUAL STAINED WITH ANNEXIN-V-FLUORESCEIN ISOTHIOCYANATE AND PROPIDIUM IODIDE, REPLICATE 3. 430
FIGURE 12.221.: FLOW CYTOMETRY FINAL ANALYSIS FOR T98G CELLS TREATED WITH 1200.00 μM TEMOZOLOMIDE FOR 24-HOURS AND DUAL STAINED WITH ANNEXIN-V-FLUORESCEIN ISOTHIOCYANATE AND PROPIDIUM IODIDE, REPLICATE 1. 430

FIGURE 12.222.: FLOW CYTOMETRY FINAL ANALYSIS FOR T98G CELLS TREATED WITH 1200.00 μM TEMOZOLOMIDE FOR 24-HOURS AND DUAL STAINED WITH ANNEXIN-V-FLUORESCEIN ISOTHIOCYANATE AND PROPIDIUM IODIDE, REPLICATE 2. 431

FIGURE 12.223.: FLOW CYTOMETRY FINAL ANALYSIS FOR T98G CELLS TREATED WITH 1200.00 μM TEMOZOLOMIDE FOR 24-HOURS AND DUAL STAINED WITH ANNEXIN-V-FLUORESCEIN ISOTHIOCYANATE AND PROPIDIUM IODIDE, REPLICATE 3. 431

FIGURE 12.224.: FLOW CYTOMETRY FINAL ANALYSIS FOR T98G CELLS TREATED WITH CULTURE (NEGATIVE CONTROL) CONDITIONS FOR 24-HOURS AND DUAL STAINED WITH MONODANSYLCADAVERINE, REPLICATE 1. 432

FIGURE 12.225.: FLOW CYTOMETRY FINAL ANALYSIS FOR T98G CELLS TREATED WITH CULTURE (NEGATIVE CONTROL) CONDITIONS FOR 24-HOURS AND DUAL STAINED WITH MONODANSYLCADAVERINE, REPLICATE 2. 432

FIGURE 12.226.: FLOW CYTOMETRY FINAL ANALYSIS FOR T98G CELLS TREATED WITH CULTURE (NEGATIVE CONTROL) CONDITIONS FOR 24-HOURS AND DUAL STAINED WITH MONODANSYLCADAVERINE, REPLICATE 3. 433

FIGURE 12.227.: FLOW CYTOMETRY FINAL ANALYSIS FOR T98G CELLS TREATED WITH 5.00 MM H_20_2 (POSITIVE CONTROL) CONDITIONS FOR 24-HOURS AND DUAL STAINED WITH MONODANSYLCADAVERINE, REPLICATE 1. 433

FIGURE 12.228.: FLOW CYTOMETRY FINAL ANALYSIS FOR T98G CELLS TREATED WITH 5.00 MM H_20_2 (POSITIVE CONTROL) CONDITIONS FOR 24-HOURS AND DUAL STAINED WITH MONODANSYLCADAVERINE, REPLICATE 2. 434

FIGURE 12.229.: FLOW CYTOMETRY FINAL ANALYSIS FOR T98G CELLS TREATED WITH 5.00 MM H_20_2 (POSITIVE CONTROL) CONDITIONS FOR 24-HOURS AND DUAL STAINED WITH MONODANSYLCADAVERINE, REPLICATE 3. 434

FIGURE 12.230.: FLOW CYTOMETRY FINAL ANALYSIS FOR T98G CELLS TREATED WITH 6.25 μM A-SOLANINE FOR 24-HOURS AND DUAL STAINED WITH MONODANSYLCADAVERINE, REPLICATE 1. 435

FIGURE 12.231.: FLOW CYTOMETRY FINAL ANALYSIS FOR T98G CELLS TREATED WITH 6.25 μM A-SOLANINE FOR 24-HOURS AND DUAL STAINED WITH MONODANSYLCADAVERINE, REPLICATE 2. 435

FIGURE 12.232.: FLOW CYTOMETRY FINAL ANALYSIS FOR T98G CELLS TREATED WITH 6.25 μM A-SOLANINE FOR 24-HOURS AND DUAL STAINED WITH MONODANSYLCADAVERINE, REPLICATE 3. 436

FIGURE 12.233.: FLOW CYTOMETRY FINAL ANALYSIS FOR T98G CELLS TREATED WITH 1200.00 μM TEMOZOLOMIDE FOR 24-HOURS AND DUAL STAINED WITH MONODANSYLCADAVERINE, REPLICATE 1. 436

FIGURE 12.234.: FLOW CYTOMETRY FINAL ANALYSIS FOR T98G CELLS TREATED WITH 1200.00 μM TEMOZOLOMIDE FOR 24-HOURS AND DUAL STAINED WITH MONODANSYLCADAVERINE, REPLICATE 2. 437

FIGURE 12.235.: FLOW CYTOMETRY FINAL ANALYSIS FOR T98G CELLS TREATED WITH 1200.00 μM TEMOZOLOMIDE FOR 24-HOURS AND DUAL STAINED WITH MONODANSYLCADAVERINE, REPLICATE 3..... 437

Table of Tables

TABLE 2.1: CHEMOTHERAPEUTIC AGENTS CURRENTLY INDICATED AGAINST GLIOBLASTOMA MULTIFORME.....35

TABLE 2.2.: NATURAL EXTRACTS INVESTIGATED AGAINST GLIOBLASTOMA MULTIFORME IN-VITRO. STUDIES WERE IDENTIFIED THROUGH SYSTEMATIC LITERATURE REVIEW (CHAPTER 9). ADAPTED FROM CUSCHIERI & BARON (2023)..... 37

TABLE 2.3.: NATURAL EXTRACTS INVESTIGATED AGAINST GLIOBLASTOMA MULTIFORME IN-VITRO. STUDIES WERE IDENTIFIED THROUGH SYSTEMATIC LITERATURE REVIEW (CHAPTER 9). ADAPTED FROM CUSCHIERI & BARON (2023). 40

TABLE 2.4.: SOURCES, METHODS, AND CONCENTRATION OF A-SOLANINE EXTRACTED FROM POTATO PRODUCTS. STUDIES WERE IDENTIFIED THROUGH SYSTEMATIC LITERATURE REVIEW (CHAPTER 9)..... 45

TABLE 2.5.: IN-VITRO STUDIES INVESTIGATING THE CYTOTOXICITY OF A– SOLANINE AGAINST CANCER CELL-LINES. STUDIES WERE IDENTIFIED THROUGH SYSTEMATIC LITERATURE REVIEW (CHAPTER 9)..... 54

TABLE 2.6.: COMPARISON BETWEEN ∝-SOLANINE IC_{50} AT 24 AND 48 HOURS OF INCUBATION..... 55

TABLE 3.1.: MATERIALS AND EQUIPMENT USED THROUGHOUT THE PROJECT..... 65

TABLE 3.2.: DESIGNED PRIMER PAIRS..... 79

TABLE 3.3.: REVERSE TRANSCRIPTION THERMOCYCLER SETTINGS 82

TABLE 3.4.: THERMAL CYCLER SETTINGS FOR END-POINT PCR..... 83

TABLE 3.5.: PREPARATION OF ELECTROPHORESIS GEL 83

TABLE 3.6.: REAL-TIME QUANTITATIVE POLYMERASE CHAIN REACTION MIXTURE PREPERATION 85

TABLE 3.7.: ROTOR-GENE Q SETTINGS FOR REAL-TIME QUANTITATIVE POLYMERASE CHAIN REACTION. 86

TABLE 3.8.: PREPARATION OF REACTION COMPONENTS FOR ANTIBODY ARRAY ASSAYS. 92

TABLE 4.1.: A-SOLANINE IC_{50} DATA..... 103

TABLE 4.2.: A-SOLANINE AND TEMOZOLOMIDE WORKING CONCENTRATIONS 103

TABLE 4.3.: DIFFERENTIALLY EXPRESSED PROTEINS FOLLOWING 24 HOUR TREATMENT WITH 6.25 μM A-SOLANINE. 121

TABLE 9.1.: SYSTEMATIC SEARCHING INCLUSION CRITERIA AND DATABASE SPECIFIC SEARCH TERMS..... 188

TABLE 11.1.: HUMAN AUTOPHAGY RELATED 4B CYSTEINE PEPTIDASE CANONICAL GENE SEQUENCE. CANONICAL GENE SEQUENCE WAS RETRIEVED FROM THE CONSENSUS CODING SEQUENCE PROJECT DATABASE [BLUE – EXONS, BLACK - INTRONS]. 262

TABLE 11.2.: POTENTIAL RNA PRIMER-PAIRS AGAINST THE HUMAN AUTOPHAGY RELATED 4B CYSTEINE PEPTIDASE GENE. POTENTIAL PRIMER PAIRS WERE IDENTIFIED THROUGH HAPHAZARD LITERATURE REVIEW. 262

TABLE 11.3.: SELECTED TENTATIVE RNA PRIMER PAIR AGAINST THE HUMAN AUTOPHAGY RELATED 4B CYSTEINE PEPTIDASE GENE. 263

TABLE 11.4.: PRIMER-BLAST SEARCH PARAMETERS AND OTHER DETAILS FOR THE SELECTED HUMAN AUTOPHAGY RELATED 4B CYSTEINE PEPTIDASE RNA PRIMER PAIR. 263

TABLE 11.5.: HUMAN BCL-2 ASSOCIATED X PROTEIN CANONICAL GENE SEQUENCE. CANONICAL GENE SEQUENCE WAS RETRIEVED FROM THE CONSENSUS CODING SEQUENCE PROJECT DATABASE [BLUE – EXONS, BLACK - INTRONS]. 264

TABLE 11.6.: POTENTIAL RNA PRIMER-PAIRS AGAINST THE HUMAN BCL-2 ASSOCIATED X PROTEIN CANONICAL GENE. POTENTIAL PRIMER PAIRS WERE IDENTIFIED THROUGH HAPHAZARD LITERATURE REVIEW. 265

TABLE 11.7.: SELECTED TENTATIVE RNA PRIMER PAIR AGAINST THE HUMAN BCL-2 ASSOCIATED X PROTEIN GENE. 266

TABLE 11.8.: PRIMER-BLAST SEARCH PARAMETERS AND OTHER DETAILS FOR THE SELECTED HUMAN BCL-2 ASSOCIATED X PROTEIN RNA PRIMER PAIR. 266

TABLE 11.9.: HUMAN BECLIN-1 CANONICAL GENE SEQUENCE. CANONICAL GENE SEQUENCE WAS RETRIEVED FROM THE CONSENSUS CODING SEQUENCE PROJECT DATABASE [BLUE – EXONS, BLACK - INTRONS]. 270

TABLE 11.10.: POTENTIAL RNA PRIMER-PAIRS AGAINST THE HUMAN BECLIN-1 GENE. POTENTIAL PRIMER PAIRS WERE IDENTIFIED THROUGH HAPHAZARD LITERATURE REVIEW. 270

TABLE 11.11.: SELECTED TENTATIVE RNA PRIMER PAIR AGAINST THE HUMAN BECLIN-1 GENE. 271

TABLE 11.12.:PRIMER-BLAST SEARCH PARAMETERS AND OTHER DETAILS FOR THE SELECTED HUMAN BECLIN-1 RNA PRIMER PAIR. 271

TABLE 11.13.: HUMAN CASPASE-3 CANONICAL GENE SEQUENCE. CANONICAL GENE SEQUENCE WAS RETRIEVED FROM THE CONSENSUS CODING SEQUENCE PROJECT DATABASE [BLUE – EXONS, BLACK - INTRONS]. 273

TABLE 11.14.: POTENTIAL RNA PRIMER-PAIRS AGAINST THE HUMAN CASPASE-3 GENE. POTENTIAL PRIMER PAIRS WERE IDENTIFIED THROUGH HAPHAZARD LITERATURE REVIEW. 274

TABLE 11.15.: SELECTED TENTATIVE RNA PRIMER PAIR AGAINST THE HUMAN CASPASE-3 GENE. 275

TABLE 11.16.: PRIMER-BLAST SEARCH PARAMETERS AND OTHER DETAILS FOR THE SELECTED HUMAN CASPASE-3 PEPTIDASE RNA PRIMER PAIR. 275

TABLE 11.17.: HUMAN PYRUVATE KINASE ISOZYME-2 GENE SEQUENCE. CANONICAL GENE SEQUENCE WAS RETRIEVED FROM THE CONSENSUS CODING SEQUENCE PROJECT DATABASE [BLUE – EXONS, BLACK - INTRONS]. 277

TABLE 11.18.: POTENTIAL RNA PRIMER-PAIRS AGAINST THE HUMAN PYRUVATE KINASE ISOZYME-2. POTENTIAL PRIMER PAIRS WERE IDENTIFIED THROUGH HAPHAZARD LITERATURE REVIEW. 278

TABLE 11.19.: SELECTED TENTATIVE RNA PRIMER PAIR AGAINST THE HUMAN PYRUVATE KINASE ISOZYME-2 GENE. 278

TABLE 11.20.: PRIMER-BLAST SEARCH PARAMETERS AND OTHER DETAILS FOR THE SELECTED HUMAN PYRUVATE KINASE ISOZYME-2 RNA PRIMER PAIR. 278

TABLE 11.21.: HUMAN VASCULAR ENDOTHELIAL GROWTH FACTOR A CANONICAL GENE SEQUENCE. CANONICAL GENE SEQUENCE WAS RETRIEVED FROM THE CONSENSUS CODING SEQUENCE PROJECT DATABASE [BLUE – EXONS, BLACK - INTRONS]. 280

TABLE 11.22.: POTENTIAL RNA PRIMER-PAIRS AGAINST THE VASCULAR ENDOTHELIAL GROWTH FACTOR A GENE. POTENTIAL PRIMER PAIRS WERE IDENTIFIED THROUGH HAPHAZARD LITERATURE REVIEW. 281

TABLE 11.23.: SELECTED TENTATIVE RNA PRIMER PAIR AGAINST THE HUMAN VASCULAR ENDOTHELIAL GROWTH FACTOR A GENE. 281

TABLE 11.24.: PRIMER-BLAST SEARCH PARAMETERS AND OTHER DETAILS FOR THE SELECTED HUMAN VASCULAR ENDOTHELIAL GROWTH FACTOR RNA PRIMER PAIR. 281

TABLE 11.25.: HUMAN ACTIVATING TRANSCRIPTION FACTOR 6 A CANONICAL GENE SEQUENCE. CANONICAL GENE SEQUENCE WAS RETRIEVED FROM THE CONSENSUS CODING SEQUENCE PROJECT DATABASE [BLUE – EXONS, BLACK - INTRONS]. 283

TABLE 11.26.: POTENTIAL RNA PRIMER-PAIRS AGAINST THE HUMAN ACTIVATING TRANSCRIPTION FACTOR 6 A GENE. POTENTIAL PRIMER PAIRS WERE IDENTIFIED THROUGH HAPHAZARD LITERATURE REVIEW. 284

TABLE 11.27.: SELECTED TENTATIVE RNA PRIMER PAIR AGAINST THE HUMAN VASCULAR ENDOTHELIAL GROWTH FACTOR A GENE. 284

TABLE 11.28.: PRIMER-BLAST SEARCH PARAMETERS AND OTHER DETAILS FOR THE SELECTED THE HUMAN ACTIVATING TRANSCRIPTION FACTOR 6 A RNA PRIMER PAIR. 285

TABLE 11.29.: HUMAN ISOCITRATE DEHYDROGENASE-1 CANONICAL GENE SEQUENCE. CANONICAL GENE SEQUENCE WAS RETRIEVED FROM THE CONSENSUS CODING SEQUENCE PROJECT DATABASE [BLUE – EXONS, BLACK - INTRONS]. 288

TABLE 11.30.: SELECTED TENTATIVE RNA PRIMER PAIR AGAINST THE HUMAN ISOCITRATE DEHYDROGENASE-1 GENE. PRIMER PAIR WERE IDENTIFIED USING PRIME3® SOFTWARE. 289

TABLE 11.31.: PRIMER-BLAST SEARCH PARAMETERS AND OTHER DETAILS FOR THE SELECTED HUMAN AUTOPHAGY RELATED 4B CYSTEINE PEPTIDASE RNA PRIMER PAIR. 289

TABLE 12.1.: PRESTO BLUE® CELL VIABILITY ASSAY DATA FOR U87MG CELLS CELLS TREATED WITH A-SOLANINE AND TEMOZOLOMIDE FOR 72 HOURS. 306

TABLE 12.2.: PRESTO BLUE® CELL VIABILITY ASSAY DATA FOR U251 CELLS TREATED WITH A-SOLANINE AND TEMOZOLOMIDE FOR 72 HOURS. 306

TABLE 12.3.: PRESTO BLUE® CELL VIABILITY ASSAY DATA FOR T98G CELLS TREATED WITH A-SOLANINE AND TEMOZOLOMIDE FOR 72 HOURS. 307

TABLE 12.4.: SCRATCH MIGRATION ASSAY DATA FOR U87MG CELLS TREATED WITH TEMOZOLOMIDE OR A-SOLANINE FOR 24, 48 AND 72 HOURS. 308

TABLE 12.5.: SCRATCH MIGRATION ASSAY DATA FOR U251 CELLS TREATED WITH TEMOZOLOMIDE OR A-SOLANINE FOR 24, 48 AND 72 HOURS. 309

TABLE 12.6.: SCRATCH MIGRATION ASSAY DATA FOR T98G CELLS TREATED WITH TEMOZOLOMIDE OR A-SOLANINE FOR 24, 48 AND 72 HOURS. 309

TABLE 12.7.: TRANS-WELL INVASION ASSAY DATA FOR U87MG, U251 AND T98G CELLS TREATED WITH A-SOLANINE FOR 72 HOURS. 310

TABLE 12.8.: TRANS-WELL INVASION ASSAY DATA FOR U87MG, U251 AND T98G CELLS TREATED WITH TEMOZOLOMIDE FOR 72 HOURS. 310

TABLE 12.9.: TRANS-WELL INVASION ASSAY DATA FOR U87MG, U251 AND T98G CELLS TREATED WITH H_2O_2 FOR 72 HOURS. 311

TABLE 12.10.: TRANS-WELL INVASION ASSAY DATA FOR U87MG, U251 AND T98G CELLS TREATED WITH NEGATIVE CONTROL FOR 72 HOURS. 311

TABLE 12.11.: REAL-TIME POLYMERASE CHAIN REACTION DATA FOR U87MG CELLS. BAX, BECN1, CASP3, PKM2, VEGFA, ATF6 AND ATG4B REAL-TIME QUANTITATIVE POLYMERASE CHAIN REACTION DATA (RT-QPCR)IN U87MG CELLS UNDER 6.25 µM A-SOLANINE, 1200.00 µM TEMOZOLOMIDE, 5MM H_2O_2 AND CULTURE (NEGATIVE CONTROL) CONDITIONS FOR 24-HOURS. 312

TABLE 12.12.: REAL-TIME POLYMERASE CHAIN REACTION DATA FOR U87MG CELLS. BAX, BECN1, CASP3, PKM2, VEGFA, ATF6 AND ATG4B REAL-TIME QUANTITATIVE POLYMERASE CHAIN REACTION DATA (RT-QPCR) IN U87MG CELLS UNDER 6.25 µM A-SOLANINE, 1200.00 µM TEMOZOLOMIDE, 5MM H_2O_2 AND CULTURE (NEGATIVE CONTROL) CONDITIONS FOR 24-HOURS. 313

TABLE 12.13.: REAL-TIME POLYMERASE CHAIN REACTION DATA FOR U87MG CELLS. BAX, BECN1, CASP3, PKM2, VEGFA, ATF6 AND ATG4B REAL-TIME QUANTITATIVE POLYMERASE CHAIN REACTION DATA (RT-QPCR) IN U87MG CELLS

under 6.25 μM α-solanine, 1200.00 μM temozolomide, 5mM H_2O_2 and culture (negative control) conditions for 24-hours. 314
Table 12.14.: U87MG fluorescent intensity data 399
Table 12.15.: U251 fluorescent intensity data 400
Table 12.16.: T98G fluorescent intensity data 401
Table 12.17.: U87MG flow cytometry data 438
Table 12.18.: U251 flow cytometry data 439
Table 12.19.: T98G flow cytometry data 439
Table 12.20.: Antibody array data for glioblastoma cells treated with 6.25 μM ∝-solanine. 441
Table 12.21.: Antibody array data for glioblastoma cells treated with negative control (culture) conditions. 443
Table 12.22.: Presto blue® cell viability assay optimisation data..... 444

Table of Outputs

Output 11.1.: Primer-BLAST output for other potential products on unintended templates for the selected human Autophagy Related 4B Cysteine Peptidase RNA primer pair. 263

Output 11.2.: Primer-BLAST output for other potential products on unintended templates for the selected human Bcl-2 associated X protein RNA primer pair. 266

Output 11.3.: Primer-BLAST output for other potential products on unintended templates for the selected human beclin-1 RNA primer pair. 272

Output 11.4.: Primer-BLAST output for other potential products on unintended templates for the selected human caspase-3 RNA primer pair. 276

Output 11.5.: Primer-BLAST output for other potential products on unintended templates for the selected human pyruvate kinase isozyme-2 RNA primer pair. 279

Output 11.6.: Primer-BLAST output for other potential products on unintended templates for the selected human vascular endothelial growth factor A RNA primer pair. 282

Output 11.7.: Primer-BLAST output for other potential products on unintended templates for the selected activating transcription factor 6 A RNA primer pair. 285

Output 11.8.: Primer-BLAST output for other potential products on unintended templates for the selected human isocitrate dehydrogenase-1 gene RNA primer pair. 290

Output 13.1.: Descriptive statistics and normality (Shapiro-Wilk) assumption checking for U87MG, U251 and T98G cell-lines treated with 800.00 μM temozolomide for 72 hours. 446

Output 13.2.: Equality of Variance (Levene's) assumption checking for U87MG, U251 and T98G cell-lines treated with 800.00 μM temozolomide for 72 hours 446

Output 13.3.: One-way ANOVA testing for U87MG versus U251 versus T98G cells treated cell-lines treated with 800.00 temozolomide μM a-solanine for 72 hours. 446

Output 13.4.: One-way ANOVA post-hoc analysis for U87MG versus U251 versus T98G cells treated cell-lines treated with 800.00 μM a-solanine for 72 hours. 447

Output 13.5.: Descriptive statistics and normality (Shapiro-Wilk) assumption checking for U87MG, U251 and T98G cell-lines treated with 1200.00 μM temozolomide for 72 hours. 447

Output 13.6.: Equality of Variance (Levene's) assumption checking for U87MG, U251 and T98G cell-lines treated with 1200.00 μM temozolomide for 72 hours..... 447
Output 13.7.: One-way ANOVA testing for U87MG versus U251 versus T98G cells treated cell-lines treated with 1200.00 temozolomide μM a-solanine for 72 hours. 448
Output 13.8.: Descriptive statistics and normality (Shapiro-Wilk) assumption checking for U87MG, U251 and T98G cell-lines treated with 1600.00 μM temozolomide for 72 hours. 448
Output 13.9.: Equality of Variance (Levene's) assumption checking for U87MG, U251 and T98G cell-lines treated with 1600.00 μM temozolomide for 72 hours..... 448
Output 13.10.: Kruskal-Wallis testing for U87MG versus U251 versus T98G cells treated cell-lines treated with 1600.00 temozolomide μM a-solanine for 72 hours. 448
Output 13.11.: Descriptive statistics and normality (Shapiro-Wilk) assumption checking for U87MG, U251 and T98G cell-lines treated with 2000.00 μM temozolomide for 72 hours. 449
Output 13.12.: Equality of Variance (Levene's) assumption checking for U87MG, U251 and T98G cell-lines treated with 2000.00 μM temozolomide for 72 hours..... 449
Output 13.13.: One-way ANOVA testing for U87MG versus U251 versus T98G cells treated cell-lines treated with 2000.00 temozolomide μM a-solanine for 72 hours..... 449
Output 13.14.: One-way ANOVA post-hoc analysis for U87MG versus U251 versus T98G cells treated cell-lines treated with 2000.00 μM a-solanine for 72 hours. 449
Output 13.15.: Descriptive statistics and normality (Shapiro-Wilk) assumption checking for U87MG, U251 and T98G cell-lines treated with 2400.00 μM temozolomide for 72 hours. 450
Output 13.16.: Equality of Variance (Levene's) assumption checking for U87MG, U251 and T98G cell-lines treated with 2400.00 μM temozolomide for 72 hours..... 450
Output 13.17.: One-way ANOVA testing for U87MG versus U251 versus T98G cells treated cell-lines treated with 2400.00 temozolomide μM a-solanine for 72 hours..... 450
Output 13.18.: One-way ANOVA post-hoc analysis for U87MG versus U251 versus T98G cells treated cell-lines treated with 2400.00 μM a-solanine for 72 hours. 451
Output 13.19.: Descriptive statistics and normality (Shapiro-Wilk) assumption checking for U87MG, U251 and T98G cell-lines treated with 5.00 μM a-solanine for 72 hours..... 451

OUTPUT 13.20.: EQUALITY OF VARIANCE (LEVENE'S) ASSUMPTION CHECKING FOR U87MG, U251 AND T98G CELL-LINES TREATED WITH 5.00 μM A-SOLANINE FOR 72 HOURS. 452
OUTPUT 13.21.: ONE-WAY ANOVA TESTING FOR U87MG VERSUS U251 VERSUS T98G CELLS TREATED CELL-LINES TREATED WITH 5.00 μM A-SOLANINE FOR 72 HOURS. 452
OUTPUT 13.22.: DESCRIPTIVE STATISTICS AND NORMALITY (SHAPIRO-WILK) ASSUMPTION CHECKING FOR U87MG, U251 AND T98G CELL-LINES TREATED WITH 25.00 μM A-SOLANINE FOR 72 HOURS..... 452
OUTPUT 13.23.: EQUALITY OF VARIANCE (LEVENE'S) ASSUMPTION CHECKING FOR U87MG, U251 AND T98G CELL-LINES TREATED WITH 25.00 μM A-SOLANINE FOR 72 HOURS. 452
OUTPUT 13.24.: KRUSKAL-WALLIS TESTING FOR U87MG VERSUS U251 VERSUS T98G CELLS TREATED CELL-LINES TREATED WITH 25.00 μM A-SOLANINE FOR 72 HOURS..... 453
OUTPUT 13.25.: KURSKAL-WALLIS POST-HOC ANALYSIS FOR U87MG VERSUS U251 VERSUS T98G CELLS TREATED CELL-LINES TREATED WITH 25.00 μM A-SOLANINE FOR 72 HOURS. 453
OUTPUT 13.26.: DESCRIPTIVE STATISTICS AND NORMALITY (SHAPIRO-WILK) ASSUMPTION CHECKING FOR U87MG, U251 AND T98G CELL-LINES TREATED WITH 50.00 μM A-SOLANINE FOR 72 HOURS..... 453
OUTPUT 13.27.: EQUALITY OF VARIANCE (LEVENE'S) ASSUMPTION CHECKING FOR U87MG, U251 AND T98G CELL-LINES TREATED WITH 50.00 μM A-SOLANINE FOR 72 HOURS. 453
OUTPUT 13.28.: ONE-WAY ANOVA TESTING FOR U87MG VERSUS U251 VERSUS T98G CELLS TREATED CELL-LINES TREATED WITH 50.00 μM A-SOLANINE FOR 72 HOURS. 454
OUTPUT 13.29.: ONE-WAY ANOVA POST-HOC ANALYSIS FOR U87MG VERSUS U251 VERSUS T98G CELLS TREATED CELL-LINES TREATED WITH 50.00 μM A-SOLANINE FOR 72 HOURS. 454
OUTPUT 13.30.: DESCRIPTIVE STATISTICS AND NORMALITY (SHAPIRO-WILK) ASSUMPTION CHECKING FOR U87MG, U251 AND T98G CELL-LINES TREATED WITH 75.00 μM A-SOLANINE FOR 72 HOURS..... 454
OUTPUT 13.31.: EQUALITY OF VARIANCE (LEVENE'S) ASSUMPTION CHECKING FOR U87MG, U251 AND T98G CELL-LINES TREATED WITH 75.00 μM A-SOLANINE FOR 72 HOURS. 455
OUTPUT 13.32.: ONE-WAY ANOVA TESTING FOR U87MG VERSUS U251 VERSUS T98G CELLS TREATED CELL-LINES TREATED WITH 75.00 μM A-SOLANINE FOR 72 HOURS. 455
OUTPUT 13.33.: ONE-WAY ANOVA POST-HOC ANALYSIS FOR U87MG VERSUS U251 VERSUS T98G CELLS TREATED CELL-LINES TREATED WITH 75.00 μM A-SOLANINE FOR 72 HOURS. 455
OUTPUT 13.34.: U87MG IC_{50} A-SOLANINE 456

OUTPUT 13.35.: U251 IC_{50} A-SOLANINE 456
OUTPUT 13.36.: T98G IC_{50} A-SOLANINE 456
OUTPUT 13.37.: U87MG A-SOLANINE CELL VIABILITY DATA LINEAR REGRESSION 457
OUTPUT 13.38.: U251 A-SOLANINE CELL VIABILITY DATA LINEAR REGRESSION. 458
OUTPUT 13.39.: T98G A-SOLANINE CELL VIABILITY DATA LINEAR REGRESSION. 458
OUTPUT 13.40.: U87MG TEMOZOLOMIDE CELL VIABILITY DATA LINEAR REGRESSION 459
OUTPUT 13.41.: U251 TEMOZOLOMIDE CELL VIABILITY DATA LINEAR REGRESSION 459
OUTPUT 13.42.: T98G TEMOZOLOMIDE CELL VIABILITY DATA LINEAR REGRESSION 460
OUTPUT 13.43.: DESCRIPTIVE STATISTICS AND NORMALITY (SHAPIRO-WILK) ASSUMPTION CHECKING OF U87MG VERSUS U251M VERSUS T98G CELLS TREATED WITH 1200.00 μM TEMOZOLOMIDE FOR 24-HOURS. 461
OUTPUT 13.44.: EQUALITY OF VARIANCE (LEVENE'S) ASSUMPTION CHECKING OF U87MG VERSUS U251M VERSUS T98G CELLS TREATED WITH 1200.00 μM TEMOZOLOMIDE FOR 24-HOURS. 461
OUTPUT 13.45.: ONE-WAY ANOVA TESTING FOR U87MG VERSUS U251 VERSUS T98G CELLS TREATED CELL-LINES TREATED WITH 1200.00 μM TEMOZOLOMIDE FOR 24-HOURS. 461
OUTPUT 13.46.: ONE-WAY ANOVA POST-HOC ANALYSIS FOR U87MG VERSUS U251 VERSUS T98G CELLS TREATED CELL-LINES TREATED WITH 1200.00 μM TEMOZOLOMIDE FOR 24-HOURS. 462
OUTPUT 13.47.:DESCRIPTIVE STATISTICS AND NORMALITY (SHAPIRO-WILK) ASSUMPTION CHECKING OF U87MG VERSUS U251M VERSUS T98G CELLS TREATED WITH 1200.00 μM TEMOZOLOMIDE FOR 48 HOURS. 462
OUTPUT 13.48.: EQUALITY OF VARIANCE (LEVENE'S) ASSUMPTION CHECKING OF U87MG VERSUS U251M VERSUS T98G CELLS TREATED WITH 1200.00 μM TEMOZOLOMIDE FOR 48 HOURS. 462
OUTPUT 13.49.: KRUSKAL-WALLIS TESTING FOR U87MG VERSUS U251 VERSUS T98G CELLS TREATED CELL-LINES TREATED WITH 1200.00 μM TEMOZOLOMIDE FOR 48 HOURS. 462
OUTPUT 13.50.: KRUSKAL-WALLIS POST-HOC ANALYSIS FOR U87MG VERSUS U251 VERSUS T98G CELLS TREATED CELL-LINES TREATED WITH 1200.00 μM TEMOZOLOMIDE FOR 48 HOURS. 463
OUTPUT 13.51.: DESCRIPTIVE STATISTICS AND NORMALITY (SHAPIRO-WILK) ASSUMPTION CHECKING OF U87MG VERSUS U251M VERSUS T98G CELLS TREATED WITH 1200.00 μM TEMOZOLOMIDE FOR 72 HOURS. 463
OUTPUT 13.52.: EQUALITY OF VARIANCE (LEVENE'S) ASSUMPTION CHECKING OF U87MG VERSUS U251M VERSUS T98G CELLS TREATED WITH 1200.00 μM TEMOZOLOMIDE FOR 72 HOURS. 463

Output 13.53.: One-way ANOVA testing for U87MG versus U251 versus T98G cells treated cell-lines treated with 1200.00 μM temozolomide for 72 hours..... 464
Output 13.54.: Descriptive statistics and normality (Shapiro-Wilk) assumption checking of U87MG versus U251M versus T98G cells treated with 6.25 μM a-solanine for 24-hours. 464
Output 13.55.: Equality of Variance (Levene's) assumption checking of U87MG versus U251M versus T98G cells treated with 6.25 μM a-solanine for 24-hours..... 464
Output 13.56.: One-way ANOVA testing for U87MG versus U251 versus T98G cells treated cell-lines treated with 6.25 μM a-solanine for 24-hours..... 464
Output 13.57.: One-way ANOVA post-hoc analysis for U87MG versus U251 versus T98G cells treated cell-lines treated with 6.25 μM a-solanine for 24-hours..... 465
Output 13.58.: Descriptive statistics and normality (Shapiro-Wilk) assumption checking of U87MG versus U251M versus T98G cells treated with 6.25 μM a-solanine for 48 hours..... 465
Output 13.59.: Equality of Variance (Levene's) assumption checking of U87MG versus U251M versus T98G cells treated with 6.25 μM a-solanine for 48 hours. 465
Output 13.60.: One-way ANOVA testing for U87MG versus U251 versus T98G cells treated cell-lines treated with 6.25 μM a-solanine for 48 hours. 466
Output 13.61.: Descriptive statistics and normality (Shapiro-Wilk) assumption checking of U87MG versus U251M versus T98G cells treated with 6.25 μM a-solanine for 72 hours..... 466
Output 13.62.: Equality of Variance (Levene's) assumption checking of U87MG versus U251M versus T98G cells treated with 6.25 μM a-solanine for 72 hours. 466
Output 13.63.: One-way ANOVA testing for U87MG versus U251 versus T98G cells treated cell-lines treated with 6.25 μM a-solanine for 72 hours. 467
Output 13.64.: One-way ANOVA post-hoc analysis for U87MG versus U251 versus T98G cells treated cell-lines treated with 6.25 μM a-solanine for 72 hours. 467
Output 13.65.: Descriptive statistics and normality (Shapiro-Wilk) assumption checking of U251 cells incubated for 24-hours versus 48 hours versus 72 hours treated with 1200.00 μM temozolomide. 468
Output 13.66.: Equality of Variance (Levene's) assumption checking of U251 cells incubated for 24-hours versus 48 hours versus 72 hours treated with 1200.00 μM temozolomide. 468

OUTPUT 13.67.: ONE-WAY ANOVA TESTING FOR OF U251 CELLS INCUBATED FOR 24-HOURS VERSUS 48 HOURS VERSUS 72 HOURS TREATED WITH 1200.00 μM TEMOZOLOMIDE. 468
OUTPUT 13.68.: ONE-WAY ANOVA POST-HOC ANALYSIS FOR U251 CELLS INCUBATED FOR 24-HOURS VERSUS 48 HOURS VERSUS 72 HOURS TREATED WITH 1200.00 μM TEMOZOLOMIDE. 469
OUTPUT 13.69.: DESCRIPTIVE STATISTICS AND NORMALITY (SHAPIRO-WILK) ASSUMPTION CHECKING OF T98G CELLS INCUBATED FOR 24-HOURS VERSUS 48 HOURS VERSUS 72 HOURS TREATED WITH 1200.00 μM TEMOZOLOMIDE. 469
OUTPUT 13.70.: EQUALITY OF VARIANCE (LEVENE'S) ASSUMPTION CHECKING OF T98G CELLS INCUBATED FOR 24-HOURS VERSUS 48 HOURS VERSUS 72 HOURS TREATED WITH 1200.00 μM TEMOZOLOMIDE. 469
OUTPUT 13.71.: KRUSKAL-WALLIS TESTING FOR OF T98G CELLS INCUBATED FOR 24-HOURS VERSUS 48 HOURS VERSUS 72 HOURS TREATED WITH 1200.00 μM TEMOZOLOMIDE. 470
OUTPUT 13.72.: DESCRIPTIVE STATISTICS AND NORMALITY (SHAPIRO-WILK) ASSUMPTION CHECKING OF U87MG CELLS INCUBATED FOR 24-HOURS VERSUS 48 HOURS VERSUS 72 HOURS TREATED WITH 1200.00 μM TEMOZOLOMIDE. 470
OUTPUT 13.73.: EQUALITY OF VARIANCE (LEVENE'S) ASSUMPTION CHECKING OF U87MG CELLS INCUBATED FOR 24-HOURS VERSUS 48 HOURS VERSUS 72 HOURS TREATED WITH 1200.00 μM TEMOZOLOMIDE. 470
OUTPUT 13.74.: KRUSKAL-WALLIS TESTING FOR OF U87MG CELLS INCUBATED FOR 24-HOURS VERSUS 48 HOURS VERSUS 72 HOURS TREATED WITH 1200.00 μM TEMOZOLOMIDE. 470
OUTPUT 13.75.: KRUSKAL-WALLIS POST-HOC ANALYSIS FOR U87MG CELLS INCUBATED FOR 24-HOURS VERSUS 48 HOURS VERSUS 72 HOURS TREATED WITH 1200.00 μM TEMOZOLOMIDE. 471
OUTPUT 13.76.: DESCRIPTIVE STATISTICS AND NORMALITY (SHAPIRO-WILK) ASSUMPTION CHECKING OF U251 CELLS INCUBATED FOR 24-HOURS VERSUS 48 HOURS VERSUS 72 HOURS TREATED WITH 6.25 μM A-SOLANINE. 471
OUTPUT 13.77.: EQUALITY OF VARIANCE (LEVENE'S) ASSUMPTION CHECKING OF U251 CELLS INCUBATED FOR 24-HOURS VERSUS 48 HOURS VERSUS 72 HOURS TREATED WITH 6.25 μM A-SOLANINE. 471
OUTPUT 13.78.: ONE-WAY ANOVA TESTING FOR OF U251 CELLS INCUBATED FOR 24-HOURS VERSUS 48 HOURS VERSUS 72 HOURS TREATED WITH 6.25 μM A-SOLANINE. 471
OUTPUT 13.79.: ONE-WAY ANOVA POST-HOC ANALYSIS FOR U251 CELLS INCUBATED FOR 24-HOURS VERSUS 48 HOURS VERSUS 72 HOURS TREATED WITH 6.25 μM A-SOLANINE..... 472
OUTPUT 13.80.: DESCRIPTIVE STATISTICS AND NORMALITY (SHAPIRO-WILK) ASSUMPTION CHECKING OF T98G CELLS INCUBATED FOR 24-HOURS VERSUS 48 HOURS VERSUS 72 HOURS TREATED WITH 6.25 μM A-SOLANINE. 472

Output 13.81.: Equality of Variance (Levene's) assumption checking of T98G cells incubated for 24-hours versus 48 hours versus 72 hours treated with 6.25 μM a-solanine. 472
Output 13.82.: One-way ANOVA testing for of T98G cells incubated for 24-hours versus 48 hours versus 72 hours treated with 6.25 μM a-solanine. 473
Output 13.83.: One-way ANOVA post-hoc analysis for T98G cells incubated for 24-hours versus 48 hours versus 72 hours treated with 6.25 μM a-solanine..... 473
Output 13.84.: Descriptive statistics and normality (Shapiro-Wilk) assumption checking of U87MG cells incubated for 24-hours versus 48 hours versus 72 hours treated with 6.25 μM a-solanine. 473
Output 13.85.: Equality of Variance (Levene's) assumption checking of U87MG cells incubated for 24-hours versus 48 hours versus 72 hours treated with 6.25 μM a-solanine. 474
Output 13.86.: One-way ANOVA testing for of U87MG cells incubated for 24-hours versus 48 hours versus 72 hours treated with 6.25 μM a-solanine. 474
Output 13.87.: One-way ANOVA post-hoc analysis for U87MG cells incubated for 24-hours versus 48 hours versus 72 hours treated with 6.25 μM a-solanine..... 474
Output 13.88.: Descriptive statistics of U87MG cells treated with 1200.00 μM temozolomide versus with 6.25 μM a-solanine incubated for 24-hours. 475
Output 13.89.: Normality (Shapiro-Wilk) and Equality of Variance (Levene's) assumption checks for pairwise sample testing for U87MG cells treated with 1200.00 μM temozolomide versus with 6.25 μM a-solanine incubated for 24-hours. 475
Output 13.90.: Independent sample T-testing for U87MG cells treated with 1200.00 μM temozolomide versus with 6.25 μM a-solanine incubated for 24-hours..... 476
Output 13.91.: Descriptive statistics of U251 cells treated with 1200.00 μM temozolomide versus with 6.25 μM a-solanine incubated for 24-hours. 476
Output 13.92.: Normality (Shapiro-Wilk) and Equality of Variance (Levene's) assumption checks for pairwise sample testing for U251 cells treated with 1200.00 μM temozolomide versus with 6.25 μM a-solanine incubated for 24-hours..... 476
Output 13.93.: Independent sample T-testing for U251 cells treated with 1200.00 μM temozolomide versus with 6.25 μM a-solanine incubated for 24-hours. 477

Output 13.94.: Descriptive statistics of T98G cells treated with 1200.00 μM temozolomide versus with 6.25 μM a-solanine incubated for 24-hours. 477
Output 13.95.: Normality (Shapiro-Wilk) and Equality of Variance (Levene's) assumption checks for pairwise sample testing for T98G cells treated with 1200.00 μM temozolomide versus with 6.25 μM a-solanine incubated for 24-hours. 477
Output 13.96.: Welch T-testing for T98G cells treated with 1200.00 μM temozolomide versus with 6.25 μM a-solanine incubated for 24-hours. 478
Output 13.97.: Descriptive statistics of U87MG cells treated with 1200.00 μM temozolomide versus with 6.25 μM a-solanine incubated for 48 hours. 478
Output 13.98.: Normality (Shapiro-Wilk) and Equality of Variance (Levene's) assumption checks for pairwise sample testing for U87MG cells treated with 1200.00 μM temozolomide versus with 6.25 μM a-solanine incubated for 48 hours. 478
Output 13.99.: Welch T-testing for U87MG cells treated with 1200.00 μM temozolomide versus with 6.25 μM a-solanine incubated for 48 hours. 479
Output 13.100.: Descriptive statistics of U251 cells treated with 1200.00 μM temozolomide versus with 6.25 μM a-solanine incubated for 48 hours. 479
Output 13.101.: Normality (Shapiro-Wilk) and Equality of Variance (Levene's) assumption checks for pairwise sample testing for U251 cells treated with 1200.00 μM temozolomide versus with 6.25 μM a-solanine incubated for 48 hours. 479
Output 13.102.: Independent sample T-testing for U251 cells treated with 1200.00 μM temozolomide versus with 6.25 μM a-solanine incubated for 48 hours. 480
Output 13.103.: Descriptive statistics of T98G cells treated with 1200.00 μM temozolomide versus with 6.25 μM a-solanine incubated for 48 hours. 480
Output 13.104.: Normality (Shapiro-Wilk) and Equality of Variance (Levene's) assumption checks for pairwise sample testing for T98G cells treated with 1200.00 μM temozolomide versus with 6.25 μM a-solanine incubated for 48 hours. 480
Output 13.105.: Independent sample T-testing for T98G cells treated with 1200.00 μM temozolomide versus with 6.25 μM a-solanine incubated for 48 hours. 481

Output 13.106.: Descriptive statistics of U87MG cells treated with 1200.00 μM temozolomide versus with 6.25 μM a-solanine incubated for 72 hours. 481
Output 13.107.: Normality (Shapiro-Wilk) and Equality of Variance (Levene's) assumption checks for pairwise sample testing for U87MG cells treated with 1200.00 μM temozolomide versus with 6.25 μM a-solanine incubated for 72 hours. 481
Output 13.108.: Independent sample T-testing for U87MG cells treated with 1200.00 μM temozolomide versus with 6.25 μM a-solanine incubated for 72 hours. 482
Output 13.109.: Descriptive statistics of U251 cells treated with 1200.00 μM temozolomide versus with 6.25 μM a-solanine incubated for 72 hours. 482
Output 13.110.: Normality (Shapiro-Wilk) and Equality of Variance (Levene's) assumption checks for pairwise sample testing for U251 cells treated with 1200.00 μM temozolomide versus with 6.25 μM a-solanine incubated for 72 hours. 482
Output 13.111.: Independent sample T-testing for U251 cells treated with 1200.00 μM temozolomide versus with 6.25 μM a-solanine incubated for 72 hours. 483
Output 13.112.: Descriptive statistics of T98G cells treated with 1200.00 μM temozolomide versus with 6.25 μM a-solanine incubated for 72 hours. 483
Output 13.113.: Normality (Shapiro-Wilk) and Equality of Variance (Levene's) assumption checks for pairwise sample testing for T98G cells treated with 1200.00 μM temozolomide versus with 6.25 μM a-solanine incubated for 72 hours. 483
Output 13.114.: Welch T-testing for T98G cells treated with 1200.00 μM temozolomide versus with 6.25 μM a-solanine incubated for 72 hours. 484
Output 13.115.: Descriptive statistics of relative rate of migration of U87MG cells treated with 1200.00 μM temozolomide versus with 6.25 μM a-solanine. 484
Output 13.116.: Normality (Shapiro-Wilk) and Equality of Variance (Levene's) assumption checks for pairwise sample testing for relative rate of migration of U87MG cells treated with 1200.00 μM temozolomide versus with 6.25 μM a-solanine. 485
Output 13.117.: Independent sample T-testing for relative rate of migration of U87MG cells treated with 1200.00 μM temozolomide versus with 6.25 μM a-solanine. 485

OUTPUT 13.118.: DESCRIPTIVE STATISTICS OF RELATIVE RATE OF MIGRATION OF U251 CELLS TREATED WITH 1200.00 μM TEMOZOLOMIDE VERSUS WITH 6.25 μM A-SOLANINE. 486
OUTPUT 13.119.: NORMALITY (SHAPIRO-WILK) AND EQUALITY OF VARIANCE (LEVENE'S) ASSUMPTION CHECKS FOR PAIRWISE SAMPLE TESTING FOR RELATIVE RATE OF MIGRATION OF U251 CELLS TREATED WITH 1200.00 μM TEMOZOLOMIDE VERSUS WITH 6.25 μM A-SOLANINE. 486
OUTPUT 13.120.: INDEPENDENT SAMPLE T-TESTING FOR RELATIVE RATE OF MIGRATION OF U251 CELLS TREATED WITH 1200.00 μM TEMOZOLOMIDE VERSUS WITH 6.25 μM A-SOLANINE. 486
OUTPUT 13.121.: DESCRIPTIVE STATISTICS OF RELATIVE RATE OF MIGRATION OF T98G CELLS TREATED WITH 1200.00 μM TEMOZOLOMIDE VERSUS WITH 6.25 μM A-SOLANINE. 487
OUTPUT 13.122.: NORMALITY (SHAPIRO-WILK) AND EQUALITY OF VARIANCE (LEVENE'S) ASSUMPTION CHECKS FOR PAIRWISE SAMPLE TESTING FOR RELATIVE RATE OF MIGRATION OF T98G CELLS TREATED WITH 1200.00 μM TEMOZOLOMIDE VERSUS WITH 6.25 μM A-SOLANINE. 487
OUTPUT 13.123.: INDEPENDENT SAMPLE T-TESTING FOR RELATIVE RATE OF MIGRATION OF T98G CELLS TREATED WITH 1200.00 μM TEMOZOLOMIDE VERSUS WITH 6.25 μM A-SOLANINE. 488
OUTPUT 13.124.: DESCRIPTIVE STATISTICS AND NORMALITY (SHAPIRO-WILK) ASSUMPTION CHECKING OF RELATIVE RATE OF MIGRATION OF U87MG VERSUS U251 VERSUS T98G CELLS TREATED WITH 1200.00 μM TEMOZOLOMIDE..... 488
OUTPUT 13.125.: EQUALITY OF VARIANCE (LEVENE'S) ASSUMPTION CHECKS FOR ONE-WAY ANOVA TESTING OF RELATIVE RATE OF MIGRATION OF U87MG VERSUS U251 VERSUS T98G CELLS TREATED WITH 1200.00 μM TEMOZOLOMIDE. 488
OUTPUT 13.126.: KRUSKAL-WALLIS TESTING FOR RELATIVE RATE OF MIGRATION OF U87MG VERSUS U251 VERSUS T98G CELLS TREATED WITH 1200.00 μM TEMOZOLOMIDE. 488
OUTPUT 13.127.: ONE-WAY ANOVA POST-HOC ANALYSIS FOR RELATIVE RATE OF MIGRATION OF U87MG VERSUS U251 VERSUS T98G CELLS TREATED WITH 1200.00 μM TEMOZOLOMIDE. 489
OUTPUT 13.128.: DESCRIPTIVE STATISTICS AND NORMALITY (SHAPIRO-WILK) ASSUMPTION CHECKING OF RELATIVE RATE OF MIGRATION OF U87MG VERSUS U251 VERSUS T98G CELLS TREATED WITH 6.25 μM A-SOLANINE. 489
OUTPUT 13.129.: EQUALITY OF VARIANCE (LEVENE'S) ASSUMPTION CHECKS FOR ONE-WAY ANOVA TESTING OF RELATIVE RATE OF MIGRATION OF U87MG VERSUS U251 VERSUS T98G CELLS TREATED WITH 6.25 μM A-SOLANINE..... 489
OUTPUT 13.130.: KRUSKAL-WALLIS TESTING FOR RELATIVE RATE OF MIGRATION OF U87MG VERSUS U251 VERSUS T98G CELLS TREATED WITH 6.25 μM A-SOLANINE. 490

Output 13.131.: Chi-square analysis for trans-well invasion assay data of U87MG cells treated with a-solanine versus temozolomide for 72 hours. 490

Output 13.132.: Chi-square analysis for trans-well invasion assay data of U251 cells treated with a-solanine versus Temozolomide for 72 hours. 490

Output 13.133.: Chi-square analysis for trans-well invasion assay data of T98G cells treated with a-solanine versus Temozolomide for 72 hours. 491

Output 13.134.:Chi-square analysis for trans-well invasion assay data of U87MG versus U251 versus T98G cells treated with a-solanine for 72 hours. 491

Output 13.135.: Chi-square analysis for trans-well invasion assay data of U87MG versus U251 versus T98G cells treated with temozolomide for 72 hours. 491

Output 13.136.: Descriptive statistics and normality (Shapiro-Wilk) assumption checking of real time quantitative polymerase chain reaction data of fold change in expression of the Bax gene in glioblastoma multiforme cells treated with 1200.00 μM temozolomide versus 6.25 μM a-solanine versus 5.00 mM H_2O_2 incubated for 24-hours. 492

Output 13.137.: Equality of Variance (Levene's) assumption checks for one-way ANOVA testing of real time quantitative polymerase chain reaction data of fold change in expression of the Bax gene in glioblastoma multiforme cells treated with 1200.00 μM temozolomide versus 6.25 μM a-solanine versus 5.00 mM H_2O_2 incubated for 24-hours. 492

Output 13.138.: Kruskal-Wallis testing for relative rate real time quantitative polymerase chain reaction data of fold change in expression of the Bax gene in glioblastoma multiforme cells treated with 1200.00 μM temozolomide versus 6.25 μM a-solanine versus 5.00 mM H_2O_2 incubated for 24-hours. 493

Output 13.139.: Kruskal-Wallis post-hoc analysis for relative rate real time quantitative polymerase chain reaction data of fold change in expression of the Bax gene in glioblastoma multiforme cells treated with 1200.00 μM temozolomide versus 6.25 μM a-solanine versus 5.00 mM H_2O_2 incubated for 24-hours. 493

Output 13.140.: Descriptive statistics and normality (Shapiro-Wilk) assumption checking of real time quantitative polymerase chain reaction data of fold change in expression of the BECN1 gene in

glioblastoma multiforme cells treated with 1200.00 μM temozolomide versus 6.25 μM a-solanine versus 5.00 mM H_2O_2 incubated for 24-hours. 493

Output 13.141.: Equality of Variance (Levene's) assumption checks for one-way ANOVA testing of real time quantitative polymerase chain reaction data of fold change in expression of the BECN1 gene in glioblastoma multiforme cells treated with 1200.00 μM temozolomide versus 6.25 μM a-solanine versus 5.00 mM H_2O_2 incubated for 24-hours. 494

Output 13.142.: One-way ANOVA testing for relative rate real time quantitative polymerase chain reaction data of fold change in expression of the BECN1 gene in glioblastoma multiforme cells treated with 1200.00 μM temozolomide versus 6.25 μM a-solanine versus 5.00 mM H_2O_2 incubated for 24-hours. 494

Output 13.143.: One-way ANOVA post-hoc analysis for relative rate real time quantitative polymerase chain reaction data of fold change in expression of the BECN1 gene in glioblastoma multiforme cells treated with 1200.00 μM temozolomide versus 6.25 μM a-solanine versus 5.00 mM H_2O_2 incubated for 24-hours..... 494

Output 13.144.: Descriptive statistics and normality (Shapiro-Wilk) assumption checking of real time quantitative polymerase chain reaction data of fold change in expression of the Casp-3 gene in glioblastoma multiforme cells treated with 1200.00 μM temozolomide versus 6.25 μM a-solanine versus 5.00 mM H_2O_2 incubated for 24-hours. 495

Output 13.145.: Equality of Variance (Levene's) assumption checks for one-way ANOVA testing of real time quantitative polymerase chain reaction data of fold change in expression of the Casp-3 gene in glioblastoma multiforme cells treated with 1200.00 μM temozolomide versus 6.25 μM a-solanine versus 5.00 mM H_2O_2 incubated for 24-hours. 495

Output 13.146.: Kruskal-Wallis testing for relative rate real time quantitative polymerase chain reaction data of fold change in expression of the Casp-3 gene in glioblastoma multiforme cells treated with 1200.00 μM temozolomide versus 6.25 μM a-solanine versus 5.00 mM H_2O_2 incubated for 24-hours. 496

Output 13.147.: Descriptive statistics and normality (Shapiro-Wilk) assumption checking of real time quantitative polymerase chain reaction data of fold change in expression of the PKM2 gene in

glioblastoma multiforme cells treated with 1200.00 μM temozolomide versus 6.25 μM a-solanine versus 5.00 mM H_2O_2 incubated for 24-hours. 496

Output 13.148.: Equality of Variance (Levene's) assumption checks for one-way ANOVA testing of real time quantitative polymerase chain reaction data of fold change in expression of the PKM2 gene in glioblastoma multiforme cells treated with 1200.00 μM temozolomide versus 6.25 μM a-solanine versus 5.00 mM H_2O_2 incubated for 24-hours. 496

Output 13.149.: Kruskal-Wallis testing for relative rate real time quantitative polymerase chain reaction data of fold change in expression of the PKM2 gene in glioblastoma multiforme cells treated with 1200.00 μM temozolomide versus 6.25 μM a-solanine versus 5.00 mM H_2O_2 incubated for 24-hours. 497

Output 13.150.: Kruskal-Wallis post-hoc analysis for relative rate real time quantitative polymerase chain reaction data of fold change in expression of the PKM2 gene in glioblastoma multiforme cells treated with 1200.00 μM temozolomide versus 6.25 μM a-solanine versus 5.00 mM H_2O_2 incubated for 24-hours. 497

Output 13.151.: Descriptive statistics and normality (Shapiro-Wilk) assumption checking of real time quantitative polymerase chain reaction data of fold change in expression of the VEGFA gene in glioblastoma multiforme cells treated with 1200.00 μM temozolomide versus 6.25 μM a-solanine versus 5.00 mM H_2O_2 incubated for 24-hours. 497

Output 13.152.: Equality of Variance (Levene's) assumption checks for one-way ANOVA testing of real time quantitative polymerase chain reaction data of fold change in expression of the VEGFA gene in glioblastoma multiforme cells treated with 1200.00 μM temozolomide versus 6.25 μM a-solanine versus 5.00 mM H_2O_2 incubated for 24-hours. 498

Output 13.153.: Kruskal-Wallis testing for relative rate real time quantitative polymerase chain reaction data of fold change in expression of the VEGFA gene in glioblastoma multiforme cells treated with 1200.00 μM temozolomide versus 6.25 μM a-solanine versus 5.00 mM H_2O_2 incubated for 24-hours. 498

Output 13.154.: Descriptive statistics and normality (Shapiro-Wilk) assumption checking of real time quantitative polymerase chain reaction data of fold change in expression of the ATF6 gene in

glioblastoma multiforme cells treated with 1200.00 μM temozolomide versus 6.25 μM a-solanine versus 5.00 mM H_2O_2 incubated for 24-hours. 498

Output 13.155.: Equality of Variance (Levene's) assumption checks for one-way ANOVA testing of real time quantitative polymerase chain reaction data of fold change in expression of the ATF6 gene in glioblastoma multiforme cells treated with 1200.00 μM temozolomide versus 6.25 μM a-solanine versus 5.00 mM H_2O_2 incubated for 24-hours. 499

Output 13.156.: Kruskal-Wallis testing for relative rate real time quantitative polymerase chain reaction data of fold change in expression of the ATF6 gene in glioblastoma multiforme cells treated with 1200.00 μM temozolomide versus 6.25 μM a-solanine versus 5.00 mM H_2O_2 incubated for 24-hours. 499

Output 13.157.: Descriptive statistics and normality (Shapiro-Wilk) assumption checking of real time quantitative polymerase chain reaction data of fold change in expression of the ATG4B gene in glioblastoma multiforme cells treated with 1200.00 μM temozolomide versus 6.25 μM a-solanine versus 5.00 mM H_2O_2 incubated for 24-hours. 499

Output 13.158.: Equality of Variance (Levene's) assumption checks for one-way ANOVA testing of real time quantitative polymerase chain reaction data of fold change in expression of the ATG4B gene in glioblastoma multiforme cells treated with 1200.00 μM temozolomide versus 6.25 μM a-solanine versus 5.00 mM H_2O_2 incubated for 24-hours. 500

Output 13.159.: Kruskal-Wallis testing for relative rate real time quantitative polymerase chain reaction data of fold change in expression of the ATG4B gene in glioblastoma multiforme cells treated with 1200.00 μM temozolomide versus 6.25 μM a-solanine versus 5.00 mM H_2O_2 incubated for 24-hours. 500

Output 13.160.: One-way ANOVA post-hoc analysis for relative rate real time quantitative polymerase chain reaction data of fold change in expression of the ATG4B gene in glioblastoma multiforme cells treated with 1200.00 μM temozolomide versus 6.25 μM a-solanine versus 5.00 mM H_2O_2 incubated for 24-hours 500

Output 13.161.: Descriptive statistics and normality (Shapiro-Wilk) assumption checking of corrected total cell fluorescence data on glioblastoma cells stained with Annexin-V-fluorescein isothiocyanate,

propidium iodide or monodansylcadaverine treated with 6.25 μM a-solanine incubated for 24-hours. 501

Output 13.162.: Equality of Variance (Levene's) assumption checks for one-way ANOVA testing of corrected total cell fluorescence data on glioblastoma cells stained with Annexin-V-fluorescein isothiocyanate, propidium iodide or monodansylcadaverine treated with 6.25 μM a-solanine incubated for 24-hours. 501

Output 13.163.: Kruskal-Wallis testing for corrected total cell fluorescence data on glioblastoma cells stained with Annexin-V-fluorescein isothiocyanate, propidium iodide or monodansylcadaverine treated with 6.25 μM a-solanine incubated for 24-hours. 502

Output 13.164.: Kurskal-Wallis post-hoc analysis for corrected total cell fluorescence data on glioblastoma cells stained with Annexin-V-fluorescein isothiocyanate, propidium iodide or monodansylcadaverine treated with 6.25 μM a-solanine incubated for 24-hours. 502

Output 13.165.: Descriptive statistics and normality (Shapiro-Wilk) assumption checking of corrected total cell fluorescence data on glioblastoma cells stained with Annexin-V-fluorescein isothiocyanate, propidium iodide or monodansylcadaverine treated with 1200.00 μM temozolomide incubated for 24-hours. 502

Output 13.166.: Equality of Variance (Levene's) assumption checks for one-way ANOVA testing of corrected total cell fluorescence data on glioblastoma cells stained with Annexin-V-fluorescein isothiocyanate, propidium iodide or monodansylcadaverine treated with 1200.00 μM temozolomide incubated for 24-hours. 503

Output 13.167.: Kruskal-Wallis testing for corrected total cell fluorescence data on glioblastoma cells stained with Annexin-V-fluorescein isothiocyanate, propidium iodide or monodansylcadaverine treated with 1200.00 μM temozolomide incubated for 24-hours. 503

Output 13.168.: Kurskal-Wallis post-hoc analysis for corrected total cell fluorescence data on glioblastoma cells stained with Annexin-V-fluorescein isothiocyanate, propidium iodide or monodansylcadaverine and treated with 1200.00 μM temozolomide incubated for 24-hours. 503

Output 13.169.: Descriptive statistics and normality (Shapiro-Wilk) assumption checking of corrected total cell fluorescence data on glioblastoma cells stained with Annexin-V-fluorescein isothiocyanate,

propidium iodide or monodansylcadaverine and treated with culture (negative control) conditions incubated for 24-hours. 504
Output 13.170.: Equality of Variance (Levene's) assumption checks for one-way ANOVA testing of corrected total cell fluorescence data on glioblastoma cells stained with Annexin-V-fluorescein isothiocyanate, propidium iodide or monodansylcadaverine and treated with culture (negative control) conditions incubated for 24-hours. 504
Output 13.171.: Kruskal-Wallis testing for corrected total cell fluorescence data on glioblastoma cells stained with Annexin-V-fluorescein isothiocyanate, propidium iodide or monodansylcadaverine and treated with culture (negative control) conditions incubated for 24-hours. 504
Output 13.172.: Kurskal-Wallis post-hoc analysis for corrected total cell fluorescence data on glioblastoma cells stained with Annexin-V-fluorescein isothiocyanate, propidium iodide or monodansylcadaverine treated with culture (negative control) conditions incubated for 24-hours. 505
Output 13.173.: Descriptive statistics and normality (Shapiro-Wilk) assumption checking of corrected total cell fluorescence data on glioblastoma cells stained with propidium iodide treated with 1200.00 μM temozolomide, 6.25 μM a-solanine versus culture (negative control) conditions incubated for 24-hours. 505
Output 13.174.: Equality of Variance (Levene's) assumption checks for one-way ANOVA testing of corrected total cell fluorescence data on glioblastoma cells stained with propidium iodide treated with 1200.00 μM temozolomide, 6.25 μM a-solanine versus culture (negative control) conditions incubated for 24-hours. 505
Output 13.175.: Kruskal-Wallis testing for corrected total cell fluorescence data on glioblastoma cells stained with propidium iodide treated with 1200.00 μM temozolomide, 6.25 μM a-solanine versus culture (negative control) conditions incubated for 24-hours. 506
Output 13.176.: Descriptive statistics and normality (Shapiro-Wilk) assumption checking of corrected total cell fluorescence data on glioblastoma cells stained with annexin-V conjugated fluorescein isothiocyanate treated with 1200.00 μM temozolomide, 6.25 μM a-solanine versus culture (negative control) conditions incubated for 24-hours. 506

OUTPUT 13.177: EQUALITY OF VARIANCE (LEVENE'S) ASSUMPTION CHECKS FOR ONE-WAY ANOVA TESTING OF CORRECTED TOTAL CELL FLUORESCENCE DATA ON GLIOBLASTOMA CELLS STAINED WITH ANNEXIN-V CONJUGATED FLUORESCEIN ISOTHIOCYANATE TREATED WITH 1200.00 μM TEMOZOLOMIDE, 6.25 μM A-SOLANINE VERSUS CULTURE (NEGATIVE CONTROL) CONDITIONS INCUBATED FOR 24-HOURS. 506

OUTPUT 13.178.: KRUSKAL-WALLIS TESTING FOR CORRECTED TOTAL CELL FLUORESCENCE DATA ON GLIOBLASTOMA CELLS STAINED WITH ANNEXIN-V CONJUGATED FLUORESCEIN ISOTHIOCYANATE TREATED WITH 1200.00 μM TEMOZOLOMIDE, 6.25 μM A-SOLANINE VERSUS CULTURE (NEGATIVE CONTROL) CONDITIONS INCUBATED FOR 24-HOURS. 507

OUTPUT 13.179.: DESCRIPTIVE STATISTICS AND NORMALITY (SHAPIRO-WILK) ASSUMPTION CHECKING OF CORRECTED TOTAL CELL FLUORESCENCE DATA ON GLIOBLASTOMA CELLS STAINED WITH MONODANSYLCADAVERINE TREATED WITH 1200.00 μM TEMOZOLOMIDE, 6.25 μM A-SOLANINE VERSUS CULTURE (NEGATIVE CONTROL) CONDITIONS INCUBATED FOR 24-HOURS. 507

OUTPUT 13.180.: EQUALITY OF VARIANCE (LEVENE'S) ASSUMPTION CHECKS FOR ONE-WAY ANOVA TESTING OF CORRECTED TOTAL CELL FLUORESCENCE DATA ON GLIOBLASTOMA CELLS STAINED WITH MONODANSYLCADAVERINE TREATED WITH 1200.00 μM TEMOZOLOMIDE, 6.25 μM A-SOLANINE VERSUS CULTURE (NEGATIVE CONTROL) CONDITIONS INCUBATED FOR 24-HOURS. 507

OUTPUT 13.181.: KRUSKAL-WALLIS TESTING FOR CORRECTED TOTAL CELL FLUORESCENCE DATA ON GLIOBLASTOMA CELLS STAINED WITH MONODANSYLCADAVERINE TREATED WITH 1200.00 μM TEMOZOLOMIDE, 6.25 μM A-SOLANINE VERSUS CULTURE (NEGATIVE CONTROL) CONDITIONS INCUBATED FOR 24-HOURS. 508

OUTPUT 13.182.: DESCRIPTIVE STATISTICS AND NORMALITY (SHAPIRO-WILK) ASSUMPTION CHECKING OF DATA REPRESENTING THE OCCURRENCE OF EARLY APOPTOSIS IN U87MG VERSUS U251 VERSUS T98G CELLS TREATED WITH 5.00 MM H_2O_2 FOR 24-HOURS. 508

OUTPUT 13.183.: EQUALITY OF VARIANCE (LEVENE'S) ASSUMPTION CHECKS OF OF DATA REPRESENTING THE OCCURRENCE OF EARLY APOPTOSIS IN U87MG VERSUS U251 VERSUS T98G CELLS TREATED WITH 5.00 MM H_2O_2 FOR 24-HOURS. 508

OUTPUT 13.184.: KRUSKAL-WALLIS TESTING OF DATA REPRESENTING THE OCCURRENCE OF EARLY APOPTOSIS IN U87MG VERSUS U251 VERSUS T98G CELLS TREATED WITH 5.00 MM H2O2 FOR 24-HOURS. 509

OUTPUT 13.185.: K*RUS*KAL-WALLIS POST-HOC ANALYSIS OF DATA REPRESENTING THE OCCURRENCE OF EARLY APOPTOSIS IN U87MG VERSUS U251 VERSUS T98G CELLS TREATED WITH 5.00 MM H_2O_2 FOR 24-HOURS. 509

OUTPUT 13.186.: DESCRIPTIVE STATISTICS AND NORMALITY (SHAPIRO-WILK) ASSUMPTION CHECKING OF DATA REPRESENTING THE OCCURRENCE OF LATE APOPTOSIS IN U87MG VERSUS U251 VERSUS T98G CELLS TREATED WITH 5.00 MM H_2O_2 FOR 24-HOURS..... 509
OUTPUT 13.187.: EQUALITY OF VARIANCE (LEVENE'S) ASSUMPTION CHECKS OF OF DATA REPRESENTING THE OCCURRENCE OF LATE APOPTOSIS IN U87MG VERSUS U251 VERSUS T98G CELLS TREATED WITH 5.00 MM H_2O_2 FOR 24-HOURS. 509
OUTPUT 13.188.: KRUSKAL-WALLIS TESTING OF DATA REPRESENTING THE OCCURRENCE OF LATE APOPTOSIS IN U87MG VERSUS U251 VERSUS T98G CELLS TREATED WITH 5.00 MM H_2O_2 FOR 24-HOURS. 510
OUTPUT 13.189.: DESCRIPTIVE STATISTICS AND NORMALITY (SHAPIRO-WILK) ASSUMPTION CHECKING OF DATA REPRESENTING THE OCCURRENCE OF NECROSIS IN U87MG VERSUS U251 VERSUS T98G CELLS TREATED WITH 5.00 MM H_2O_2 FOR 24-HOURS. 510
OUTPUT 13.190.: EQUALITY OF VARIANCE (LEVENE'S) ASSUMPTION CHECKS OF OF DATA REPRESENTING THE OCCURRENCE OF NECROSIS IN U87MG VERSUS U251 VERSUS T98G CELLS TREATED WITH 5.00 MM H_2O_2 FOR 24-HOURS. 510
OUTPUT 13.191.: KRUSKAL-WALLIS TESTING OF DATA REPRESENTING THE OCCURRENCE OF NECROSIS IN U87MG VERSUS U251 VERSUS T98G CELLS TREATED WITH 5.00 MM H_2O_2 FOR 24-HOURS. 510
OUTPUT 13.192.: KURSKAL-WALLIS POST-HOC ANALYSIS OF DATA REPRESENTING THE OCCURRENCE OF NECROSIS IN U87MG VERSUS U251 VERSUS T98G CELLS TREATED WITH 5.00 MM H_2O_2 FOR 24-HOURS. 511
OUTPUT 13.193.: DESCRIPTIVE STATISTICS AND NORMALITY (SHAPIRO-WILK) ASSUMPTION CHECKING OF DATA REPRESENTING THE OCCURRENCE OF AUTOPHAGY IN U87MG VERSUS U251 VERSUS T98G CELLS TREATED WITH 5.00 MM H_2O_2 FOR 24-HOURS. 511
OUTPUT 13.194.: EQUALITY OF VARIANCE (LEVENE'S) ASSUMPTION CHECKS FOR DATA REPRESENTING THE OCCURRENCE OF AUTOPHAGY IN U87MG VERSUS U251 VERSUS T98G CELLS TREATED WITH 5.00 MM H_2O_2 FOR 24-HOURS. 511
OUTPUT 13.195.: ONE-WAY ANOVA TESTING OF DATA REPRESENTING THE OCCURRENCE OF AUTOPHAGY IN U87MG VERSUS U251 VERSUS T98G CELLS TREATED WITH 5.00 MM H_2O_2 FOR 24-HOURS. 511
OUTPUT 13.196.: ONE-WAY ANOVA POST-HOC ANALYSIS OF DATA REPRESENTING THE OCCURRENCE OF AUTOPHAGY IN U87MG VERSUS U251 VERSUS T98G CELLS TREATED WITH 5.00 MM H_2O_2 FOR 24-HOURS. 512
OUTPUT 13.197.: DESCRIPTIVE STATISTICS AND NORMALITY (SHAPIRO-WILK) ASSUMPTION CHECKING OF DATA REPRESENTING THE OCCURRENCE OF EARLY APOPTOSIS IN U87MG VERSUS U251 VERSUS T98G CELLS TREATED WITH 6.25 μM A-SOLANINE FOR 24-HOURS. 512

Output 13.198.: Equality of Variance (Levene's) assumption checks of of data representing the occurrence of early apoptosis in U87MG versus U251 versus T98G cells treated with 6.25 μM a-solanine for 24-hours. 512
Output 13.199.: One-way ANOVA testing of data representing the occurrence of early apoptosis in U87MG versus U251 versus T98G cells treated with 6.25 μM a-solanine or 24-hours. 512
Output 13.200.: One-way ANOVA post-hoc analysis of data representing the occurrence of early apoptosis in U87MG versus U251 versus T98G cells treated with 6.25 μM a-solanine for 24-hours. 513
Output 13.201.: Descriptive statistics and normality (Shapiro-Wilk) assumption checking of data representing the occurrence of late apoptosis in U87MG versus U251 versus T98G cells treated with 6.25 μM a-solanine for 24-hours. 513
Output 13.202.: Equality of Variance (Levene's) assumption checks of of data representing the occurrence of late apoptosis in U87MG versus U251 versus T98G cells treated with 6.25 μM a-solanine for 24-hours. 513
Output 13.203.: One-way ANOVA testing of data representing the occurrence of late apoptosis in U87MG versus U251 versus T98G cells treated with 6.25 μM a-solanine for 24-hours. 513
Output 13.204.: One-way ANOVA post-hoc analysis of data representing the occurrence of late apoptosis in U87MG versus U251 versus T98G cells treated with 6.25 μM a-solanine for 24-hours. 514
Output 13.205.: Descriptive statistics and normality (Shapiro-Wilk) assumption checking of data representing the occurrence of necrosis in U87MG versus U251 versus T98G cells treated with 6.25 μM a-solanine for 24-hours. 514
Output 13.206.:Equality of Variance (Levene's) assumption checks of of data representing the occurrence of necrosis in U87MG versus U251 versus T98G cells treated with 6.25 μM a-solanine for 24-hours.. 514
Output 13.207.: One-way ANOVA testing of data representing the occurrence of necrosis in U87MG versus U251 versus T98G cells treated with 6.25 μM a-solanine for 24-hours. 514
Output 13.208.: One-way ANOVA post-hoc analysis of data representing the occurrence of necrosis in U87MG versus U251 versus T98G cells treated with 6.25 μM a-solanine for 24-hours. 515
Output 13.209.: Descriptive statistics and normality (Shapiro-Wilk) assumption checking of data representing the occurrence of autophagy in U87MG versus U251 versus T98G cells treated with 6.25 μM a-solanine for 24-hours. 515

Output 13.210.:Equality of Variance (Levene's) assumption checks of of data representing the occurrence of autophagy in U87MG versus U251 versus T98G cells treated with 6.25 μM a-solanine for 24-hours. 515
Output 13.211.: One-way ANOVA testing of data representing the occurrence of autophagy in U87MG versus U251 versus T98G cells treated with 6.25 μM a-solanine for 24-hours. 515
Output 13.212.: Descriptive statistics and normality (Shapiro-Wilk) assumption checking of data representing the occurrence of early apoptosis in U87MG versus U251 versus T98G cells treated with culture (negative control) conditions for 24-hours. 516
Output 13.213.: Equality of Variance (Levene's) assumption checks of of data representing the occurrence of early apoptosis in U87MG versus U251 versus T98G cells treated with culture (negative control) conditions for 24-hours. 516
Output 13.214.: One-way ANOVA testing of data representing the occurrence of early apoptosis in U87MG versus U251 versus T98G cells treated with culture (negative control) conditions for 24-hours. .. 516
Output 13.215.: One-way ANOVA post-hoc analysis of data representing the occurrence of early apoptosis in U87MG versus U251 versus T98G cells treated with culture (negative control) conditions for 24-hours. 517
Output 13.216.: Descriptive statistics and normality (Shapiro-Wilk) assumption checking of data representing the occurrence of late apoptosis in U87MG versus U251 versus T98G cells treated with culture (negative control) conditions for 24-hours. 517
Output 13.217.: Equality of Variance (Levene's) assumption checks of of data representing the occurrence of late apoptosis in U87MG versus U251 versus T98G cells treated with culture (negative control) conditions for 24-hours. 517
Output 13.218.:One-way ANOVA testing of data representing the occurrence of late apoptosis in U87MG versus U251 versus T98G cells treated with culture (negative control) conditions for 24-hours. .. 517
Output 13.219.: One-way ANOVA post-hoc analysis of data representing the occurrence of late apoptosis in U87MG versus U251 versus T98G cells treated with culture (negative control) conditions for 24-hours. 518

Output 13.220.: Descriptive statistics and normality (Shapiro-Wilk) assumption checking of data representing the occurrence of necrosis in U87MG versus U251 versus T98G cells treated with culture (negative control) conditions for 24-hours. 518
Output 13.221.: Equality of Variance (Levene's) assumption checks of of data representing the occurrence of necrosis in U87MG versus U251 versus T98G cells treated with culture (negative control) conditions for 24-hours..... 518
Output 13.222.: One-way ANOVA testing of data representing the occurrence of necrosis in U87MG versus U251 versus T98G cells treated with culture (negative control) conditions for 24-hours..... 518
Output 13.223.: One-Way ANOVA post-hoc analysis of data representing the occurrence of necrosis in U87MG versus U251 versus T98G cells treated with culture (negative control) conditions for 24-hours..... 519
Output 13.224.: Descriptive statistics and normality (Shapiro-Wilk) assumption checking of data representing the occurrence of autophagy in U87MG versus U251 versus T98G cells treated with culture (negative control) conditions for 24-hours. 519
Output 13.225.: Equality of Variance (Levene's) assumption checks of of data representing the occurrence of autophagy in U87MG versus U251 versus T98G cells treated with culture (negative control) conditions for 24-hours. 519
Output 13.226.: Kruskal-Wallis testing of data representing the occurrence of autophagy in U87MG versus U251 versus T98G cells treated with culture (negative control) conditions for 24-hours..... 519
Output 13.227.: Kurskal-Wallis post-hoc analysis of data representing the occurrence of autophagy in U87MG versus U251 versus T98G cells treated with culture (negative control) conditions for 24-hours..... 520
Output 13.228.: Descriptive statistics and normality (Shapiro-Wilk) assumption checking of data representing the occurrence of early apoptosis in U87MG versus U251 versus T98G cells treated with 1200.00 μM temozolomide for 24-hours. 520
Output 13.229.: Equality of Variance (Levene's) assumption checks of of data representing the occurrence of early apoptosis in U87MG versus U251 versus T98G cells treated with 1200.00 μM temozolomide for 24-hours. 520

Output 13.230.: Kruskal-Wallis testing of data representing the occurrence of early apoptosis in U87MG versus U251 versus T98G cells treated with 1200.00 μM temozolomide or 24-hours. 520
Output 13.231.: Kurskal-Wallis post-hoc analysis of data representing the occurrence of early apoptosis in U87MG versus U251 versus T98G cells treated with 1200.00 μM temozolomide for 24-hours. 521
Output 13.232.: Descriptive statistics and normality (Shapiro-Wilk) assumption checking of data representing the occurrence of late apoptosis in U87MG versus U251 versus T98G cells treated with 1200.00 μM temozolomide for 24-hours. 521
Output 13.233.: Equality of Variance (Levene's) assumption checks of data representing the occurrence of late apoptosis in U87MG versus U251 versus T98G cells treated with 1200.00 μM temozolomide for 24-hours. 521
Output 13.234.: Kruskal-Wallis testing of data representing the occurrence of late apoptosis in U87MG versus U251 versus T98G cells treated with 1200.00 μM temozolomide for 24-hours. 521
Output 13.235.: Kruskal-Wallis post-hoc analysis of data representing the occurrence of late apoptosis in U87MG versus U251 versus T98G cells treated with 1200.00 μM temozolomide for 24-hours. 522
Output 13.236.: Descriptive statistics and normality (Shapiro-Wilk) assumption checking of data representing the occurrence of necrosis in U87MG versus U251 versus T98G cells treated with 1200.00 μM temozolomide for 24-hours. 522
Output 13.237.: Equality of Variance (Levene's) assumption checks of of data representing the occurrence of necrosis in U87MG versus U251 versus T98G cells treated with 1200.00 μM temozolomide for 24-hours. 522
Output 13.238.: One-way ANOVA testing of data representing the occurrence of necrosis in U87MG versus U251 versus T98G cells treated with 1200.00 μM temozolomide for 24-hours. 523
Output 13.239.: One-way ANOVA post-hoc analysis of data representing the occurrence of necrosis in U87MG versus U251 versus T98G cells treated with 1200.00 μM temozolomide for 24-hours. 523
Output 13.240.: Descriptive statistics and normality (Shapiro-Wilk) assumption checking of data representing the occurrence of autophagy in U87MG versus U251 versus T98G cells treated with 1200.00 μM temozolomide for 24-hours. 523

Output 13.241.: Equality of Variance (Levene's) assumption checks of of data representing the occurrence of autophagy in U87MG versus U251 versus T98G cells treated with 1200.00 μM temozolomide for 24-hours. 523
Output 13.242.: One-way ANOVA testing of data representing the occurrence of autophagy in U87MG versus U251 versus T98G cells treated with 1200.00 μM temozolomide for 24-hours. 524
Output 13.243.: One-way ANOVA post-hoc analysis of data representing the occurrence of autophagy in U87MG versus U251 versus T98G cells treated with 1200.00 μM temozolomide for 24-hours. 524
Output 13.244.: Descriptive statistics and normality (Shapiro-Wilk) assumption checking of data representing the occurrence of early apoptosis versus late apoptosis versus necrosis versus autophagy in U87MG cells treated with 5.00 mM H_2O_2 for 24-hours. 524
Output 13.245.: Equality of Variance (Levene's) assumption checks of data representing the occurrence of early apoptosis versus late apoptosis versus necrosis versus autophagy in U87MG cells treated with 5.00 mM H_2O_2 for 24-hours..... 524
Output 13.246.: Kruskal-Wallis testing of data representing the occurrence of early apoptosis versus late apoptosis versus necrosis versus autophagy in U87MG cells treated with 5.00 mM H_2O_2 for 24-hours. 525
Output 13.247.: Kurskal-Wallis post-hoc analysis of data representing the occurrence of early apoptosis versus late apoptosis versus necrosis versus autophagy in U87MG cells treated with 5.00 mM H_2O_2 for 24-hours..... 525
Output 13.248.: Descriptive statistics and normality (Shapiro-Wilk) assumption checking of data representing the occurrence of early apoptosis versus late apoptosis versus necrosis versus autophagy in U251 cells treated with 5.00 mM H_2O_2 for 24-hours. 525
Output 13.249.: Equality of Variance (Levene's) assumption checks of data representing the occurrence of early apoptosis versus late apoptosis versus necrosis versus autophagy in U251 cells treated with 5.00 mM H_2O_2 for 24-hours. 526
Output 13.250.: Kruskal-Wallis testing of data representing the occurrence of early apoptosis versus late apoptosis versus necrosis versus autophagy in U251 cells treated with 5.00 mM H_2O_2 for 24-hours. 526

OUTPUT 13.251.: KRUSKAL-WALLIS POST-HOC ANALYSIS OF DATA REPRESENTING THE OCCURRENCE OF EARLY APOPTOSIS VERSUS LATE APOPTOSIS VERSUS NECROSIS VERSUS AUTOPHAGY IN U251 CELLS TREATED WITH 5.00 MM H_2O_2 FOR 24-HOURS. 526

OUTPUT 13.252.: DESCRIPTIVE STATISTICS AND NORMALITY (SHAPIRO-WILK) ASSUMPTION CHECKING OF DATA REPRESENTING THE OCCURRENCE OF EARLY APOPTOSIS VERSUS LATE APOPTOSIS VERSUS NECROSIS VERSUS AUTOPHAGY IN T98G CELLS TREATED WITH 5.00 MM H_2O_2 FOR 24-HOURS. 526

OUTPUT 13.253.: EQUALITY OF VARIANCE (LEVENE'S) ASSUMPTION CHECKS OF DATA REPRESENTING THE OCCURRENCE OF EARLY APOPTOSIS VERSUS LATE APOPTOSIS VERSUS NECROSIS VERSUS AUTOPHAGY IN T98G CELLS TREATED WITH 5.00 MM H_2O_2 FOR 24-HOURS. 527

OUTPUT 13.254.: ONE-WAY ANOVA TESTING OF DATA REPRESENTING THE OCCURRENCE OF EARLY APOPTOSIS VERSUS LATE APOPTOSIS VERSUS NECROSIS VERSUS AUTOPHAGY IN T98G CELLS TREATED WITH 5.00 MM H_2O_2 FOR 24-HOURS. 527

OUTPUT 13.255.: ONE-WAY ANOVA POST-HOC ANALYSIS OF DATA REPRESENTING THE OCCURRENCE OF EARLY APOPTOSIS VERSUS LATE APOPTOSIS VERSUS NECROSIS VERSUS AUTOPHAGY IN T98G CELLS TREATED WITH 5.00 MM H_2O_2 FOR 24-HOURS. 527

OUTPUT 13.256.: DESCRIPTIVE STATISTICS AND NORMALITY (SHAPIRO-WILK) ASSUMPTION CHECKING OF DATA REPRESENTING THE OCCURRENCE OF EARLY APOPTOSIS VERSUS LATE APOPTOSIS VERSUS NECROSIS VERSUS AUTOPHAGY IN U87MG CELLS TREATED WITH 6.25 μM A-SOLANINE FOR 24-HOURS. 527

OUTPUT 13.257.: EQUALITY OF VARIANCE (LEVENE'S) ASSUMPTION CHECKS OF DATA REPRESENTING THE OCCURRENCE OF EARLY APOPTOSIS VERSUS LATE APOPTOSIS VERSUS NECROSIS VERSUS AUTOPHAGY IN U87MG CELLS TREATED WITH 6.25 μM A-SOLANINE FOR 24-HOURS. 528

OUTPUT 13.258.: ONE-WAY ANOVA TESTING OF DATA REPRESENTING THE OCCURRENCE OF EARLY APOPTOSIS VERSUS LATE APOPTOSIS VERSUS NECROSIS VERSUS AUTOPHAGY IN U87MG CELLS TREATED WITH 6.25 μM A-SOLANINE FOR 24-HOURS. 528

OUTPUT 13.259.:ONE-WAY ANOVA POST-HOC ANALYSIS OF DATA REPRESENTING THE OCCURRENCE OF EARLY APOPTOSIS VERSUS LATE APOPTOSIS VERSUS NECROSIS VERSUS AUTOPHAGY IN U87MG CELLS TREATED WITH 6.25 μM A-SOLANINE FOR 24-HOURS. 528

Output 13.260.: Descriptive statistics and normality (Shapiro-Wilk) assumption checking of data representing the occurrence of early apoptosis versus late apoptosis versus necrosis versus autophagy in U251 cells treated with 6.25 μM a-solanine for 24-hours. 528
Output 13.261.: Equality of Variance (Levene's) assumption checks of data representing the occurrence of early apoptosis versus late apoptosis versus necrosis versus autophagy in U251 cells treated with 6.25 μM a-solanine for 24-hours. 529
Output 13.262.: One-way ANOVA testing of data representing the occurrence of early apoptosis versus late apoptosis versus necrosis versus autophagy in U251 cells treated with 6.25 μM a-solanine for 24-hours. 529
Output 13.263.: One-way ANOVA post-hoc analysis of data representing the occurrence of early apoptosis versus late apoptosis versus necrosis versus autophagy in U251 cells treated with 6.25 μM a-solanine for 24-hours 529
Output 13.264.: Descriptive statistics and normality (Shapiro-Wilk) assumption checking of data representing the occurrence of early apoptosis versus late apoptosis versus necrosis versus autophagy in T98G cells treated with 6.25 μM a-solanine for 24-hours. 529
Output 13.265.: Equality of Variance (Levene's) assumption checks of data representing the occurrence of early apoptosis versus late apoptosis versus necrosis versus autophagy in T98G cells treated with 6.25 μM a-solanine for 24-hours. 530
Output 13.266.: Kruskal-Wallis testing of data representing the occurrence of early apoptosis versus late apoptosis versus necrosis versus autophagy in T98G cells treated with 6.25 μM a-solanine for 24-hours. 530
Output 13.267.: Kruskal-Wallis post-hoc analysis of data representing the occurrence of early apoptosis versus late apoptosis versus necrosis versus autophagy in T98G cells treated with 6.25 μM a-solanine for 24-hours 530
Output 13.268.: Descriptive statistics and normality (Shapiro-Wilk) assumption checking of data representing the occurrence of early apoptosis versus late apoptosis versus necrosis versus autophagy in U87MG cells treated with culture (negative control) conditions for 24-hours. 531

OUTPUT 13.269.: EQUALITY OF VARIANCE (LEVENE'S) ASSUMPTION CHECKS OF DATA REPRESENTING THE OCCURRENCE OF EARLY APOPTOSIS VERSUS LATE APOPTOSIS VERSUS NECROSIS VERSUS AUTOPHAGY IN U87MG CELLS TREATED WITH CULTURE (NEGATIVE CONTROL) CONDITIONS FOR 24-HOURS. 531

OUTPUT 13.270.: KRUSKAL-WALLIS TESTING OF DATA REPRESENTING THE OCCURRENCE OF EARLY APOPTOSIS VERSUS LATE APOPTOSIS VERSUS NECROSIS VERSUS AUTOPHAGY IN U87MG CELLS TREATED WITH CULTURE (NEGATIVE CONTROL) CONDITIONS FOR 24-HOURS..... 531

OUTPUT 13.271.: *KRUSKAL*-WALLIS POST-HOC ANALYSIS OF DATA REPRESENTING THE OCCURRENCE OF EARLY APOPTOSIS VERSUS LATE APOPTOSIS VERSUS NECROSIS VERSUS AUTOPHAGY IN U87MG CELLS TREATED WITH CULTURE (NEGATIVE CONTROL) CONDITIONS FOR 24-HOURS. 531

OUTPUT 13.272.: DESCRIPTIVE STATISTICS AND NORMALITY (SHAPIRO-WILK) ASSUMPTION CHECKING OF DATA REPRESENTING THE OCCURRENCE OF EARLY APOPTOSIS VERSUS LATE APOPTOSIS VERSUS NECROSIS VERSUS AUTOPHAGY IN U251 CELLS TREATED WITH CULTURE (NEGATIVE CONTROL) CONDITIONS FOR 24-HOURS. 532

OUTPUT 13.273.: EQUALITY OF VARIANCE (LEVENE'S) ASSUMPTION CHECKS OF DATA REPRESENTING THE OCCURRENCE OF EARLY APOPTOSIS VERSUS LATE APOPTOSIS VERSUS NECROSIS VERSUS AUTOPHAGY IN U251 CELLS TREATED WITH CULTURE (NEGATIVE CONTROL) CONDITIONS FOR 24-HOURS. 532

OUTPUT 13.274.: KRUSKAL-WALLIS TESTING OF DATA REPRESENTING THE OCCURRENCE OF EARLY APOPTOSIS VERSUS LATE APOPTOSIS VERSUS NECROSIS VERSUS AUTOPHAGY IN U251 CELLS TREATED WITH CULTURE (NEGATIVE CONTROL) CONDITIONS FOR 24-HOURS. 532

OUTPUT 13.275.: KRUSKAL-WALLIS POST-HOC ANALYSIS OF DATA REPRESENTING THE OCCURRENCE OF EARLY APOPTOSIS VERSUS LATE APOPTOSIS VERSUS NECROSIS VERSUS AUTOPHAGY IN U251 CELLS TREATED WITH CULTURE (NEGATIVE CONTROL) CONDITIONS FOR 24-HOURS..... 532

OUTPUT 13.276.: DESCRIPTIVE STATISTICS AND NORMALITY (SHAPIRO-WILK) ASSUMPTION CHECKING OF DATA REPRESENTING THE OCCURRENCE OF EARLY APOPTOSIS VERSUS LATE APOPTOSIS VERSUS NECROSIS VERSUS AUTOPHAGY IN T98G CELLS TREATED WITH CULTURE (NEGATIVE CONTROL) CONDITIONS FOR 24-HOURS. 533

OUTPUT 13.277.: EQUALITY OF VARIANCE (LEVENE'S) ASSUMPTION CHECKS OF DATA REPRESENTING THE OCCURRENCE OF EARLY APOPTOSIS VERSUS LATE APOPTOSIS VERSUS NECROSIS VERSUS AUTOPHAGY IN T98G CELLS TREATED WITH CULTURE (NEGATIVE CONTROL) CONDITIONS FOR 24-HOURS. 533

Output 13.278.: One-way ANOVA testing of data representing the occurrence of early apoptosis versus late apoptosis versus necrosis versus autophagy in T98G cells treated with culture (negative control) conditions for 24-hours. 533
Output 13.279.: One-way ANOVA post-hoc analysis of data representing the occurrence of early apoptosis versus late apoptosis versus necrosis versus autophagy in T98G cells treated with culture (negative control) conditions for 24-hours. 533
Output 13.280.: Descriptive statistics and normality (Shapiro-Wilk) assumption checking of data representing the occurrence of early apoptosis versus late apoptosis versus necrosis versus autophagy in U87MG cells treated with 1200.00 μM temozolomide for 24-hours. 534
Output 13.281.: Equality of Variance (Levene's) assumption checks of data representing the occurrence of early apoptosis versus late apoptosis versus necrosis versus autophagy in U87MG cells treated with 1200.00 μM temozolomide for 24-hours. 534
Output 13.282.: Kruskal-Wallis testing of data representing the occurrence of early apoptosis versus late apoptosis versus necrosis versus autophagy in U87MG cells treated with 1200.00 μM temozolomide for 24-hours 534
Output 13.283.: Kurskal-Wallis post-hoc analysis of data representing the occurrence of early apoptosis versus late apoptosis versus necrosis versus autophagy in U87MG cells treated with 1200.00 μM temozolomide for 24-hours. 535
Output 13.284.: Descriptive statistics and normality (Shapiro-Wilk) assumption checking of data representing the occurrence of early apoptosis versus late apoptosis versus necrosis versus autophagy in U251 cells treated with 1200.00 μM temozolomide for 24-hours. 535
Output 13.285.: Equality of Variance (Levene's) assumption checks of data representing the occurrence of early apoptosis versus late apoptosis versus necrosis versus autophagy in U251 cells treated with 1200.00 μM temozolomide for 24-hours. 535
Output 13.286.: Kruskal-Wallis testing of data representing the occurrence of early apoptosis versus late apoptosis versus necrosis versus autophagy in U251 cells treated with 1200.00 μM temozolomide for 24-hours. 535

OUTPUT 13.287.: KRUSKAL-WALLIS POST-HOC ANALYSIS OF DATA REPRESENTING THE OCCURRENCE OF EARLY APOPTOSIS VERSUS LATE APOPTOSIS VERSUS NECROSIS VERSUS AUTOPHAGY IN U251 CELLS TREATED WITH 1200.00 μM TEMOZOLOMIDE FOR 24-HOURS. 536

OUTPUT 13.288.: DESCRIPTIVE STATISTICS AND NORMALITY (SHAPIRO-WILK) ASSUMPTION CHECKING OF DATA REPRESENTING THE OCCURRENCE OF EARLY APOPTOSIS VERSUS LATE APOPTOSIS VERSUS NECROSIS VERSUS AUTOPHAGY IN T98G CELLS TREATED WITH 1200.00 μM TEMOZOLOMIDE FOR 24-HOURS. 536

OUTPUT 13.289.: EQUALITY OF VARIANCE (LEVENE'S) ASSUMPTION CHECKS OF DATA REPRESENTING THE OCCURRENCE OF EARLY APOPTOSIS VERSUS LATE APOPTOSIS VERSUS NECROSIS VERSUS AUTOPHAGY IN T98G CELLS TREATED WITH 1200.00 μM TEMOZOLOMIDE FOR 24-HOURS. 536

OUTPUT 13.290.: KRUSKAL-WALLIS TESTING OF DATA REPRESENTING THE OCCURRENCE OF EARLY APOPTOSIS VERSUS LATE APOPTOSIS VERSUS NECROSIS VERSUS AUTOPHAGY IN T98G CELLS TREATED WITH 1200.00 μM TEMOZOLOMIDE FOR 24-HOURS. 536

OUTPUT 13.291.: *KRUSKAL*-WALLIS POST-HOC ANALYSIS OF DATA REPRESENTING THE OCCURRENCE OF EARLY APOPTOSIS VERSUS LATE APOPTOSIS VERSUS NECROSIS VERSUS AUTOPHAGY IN T98G CELLS TREATED WITH 1200.00 μM TEMOZOLOMIDE FOR 24-HOURS. 537

OUTPUT 13.292.: DESCRIPTIVE STATISTICS AND NORMALITY (SHAPIRO-WILK) ASSUMPTION CHECKING OF DATA REPRESENTING THE OCCURRENCE OF EARLY APOPTOSIS IN U87MG CELLS TREATED WITH 6.25 μM A-SOLANINE VERSUS 5.00 MM H_2O_2 VERSUS CULTURE (NEGATIVE CONTROL) CONDITIONS VERSUS 1200.00 μM TEMOZOLOMIDE FOR 24-HOURS. 537

OUTPUT 13.293.: EQUALITY OF VARIANCE (LEVENE'S) ASSUMPTION CHECKS OF DATA REPRESENTING THE OCCURRENCE OF EARLY APOPTOSIS IN U87MG CELLS TREATED WITH 6.25 μM A-SOLANINE VERSUS 5.00 MM H_2O_2 VERSUS CULTURE (NEGATIVE CONTROL) CONDITIONS VERSUS 1200.00 μM TEMOZOLOMIDE FOR 24-HOURS. 538

OUTPUT 13.294.: KRUSKAL-WALLIS TESTING OF DATA REPRESENTING THE OCCURRENCE OF EARLY APOPTOSIS IN U87MG CELLS TREATED WITH 6.25 μM A-SOLANINE VERSUS 5.00 MM H_2O_2 VERSUS CULTURE (NEGATIVE CONTROL) CONDITIONS VERSUS 1200.00 μM TEMOZOLOMIDE FOR 24-HOURS. 538

OUTPUT 13.295.: KRUSKAL-WALLIS POST-HOC ANALYSIS OF DATA REPRESENTING THE OCCURRENCE OF DATA REPRESENTING THE OCCURRENCE OF EARLY APOPTOSIS IN U87MG CELLS TREATED WITH 6.25 μM A-SOLANINE VERSUS 5.00 MM H_2O_2 VERSUS CULTURE (NEGATIVE CONTROL) CONDITIONS VERSUS 1200.00 μM TEMOZOLOMIDE FOR 24-HOURS. 538

OUTPUT 13.296.: DESCRIPTIVE STATISTICS AND NORMALITY (SHAPIRO-WILK) ASSUMPTION CHECKING OF DATA REPRESENTING THE OCCURRENCE OF LATE APOPTOSIS IN U87MG CELLS TREATED WITH 6.25 μM A-SOLANINE VERSUS 5.00 MM H_2O_2 VERSUS CULTURE (NEGATIVE CONTROL) CONDITIONS VERSUS 1200.00 μM TEMOZOLOMIDE FOR 24-HOURS. 538

OUTPUT 13.297.: EQUALITY OF VARIANCE (LEVENE'S) ASSUMPTION CHECKS OF DATA REPRESENTING THE OCCURRENCE OF LATE APOPTOSIS IN U87MG CELLS TREATED WITH 6.25 μM A-SOLANINE VERSUS 5.00 MM H_2O_2 VERSUS CULTURE (NEGATIVE CONTROL) CONDITIONS VERSUS 1200.00 μM TEMOZOLOMIDE FOR 24-HOURS. 539

OUTPUT 13.298.: KRUSKAL-WALLIS TESTING OF DATA REPRESENTING THE OCCURRENCE OF LATE APOPTOSIS IN U87MG CELLS TREATED WITH 6.25 μM A-SOLANINE VERSUS 5.00 MM H_2O_2 VERSUS CULTURE (NEGATIVE CONTROL) CONDITIONS VERSUS 1200.00 μM TEMOZOLOMIDE FOR 24-HOURS. 539

OUTPUT 13.299.: KRUSKAL-WALLIS POST-HOC ANALYSIS OF DATA REPRESENTING THE OCCURRENCE OF DATA REPRESENTING THE OCCURRENCE OF LATE APOPTOSIS IN U87MG CELLS TREATED WITH 6.25 μM A-SOLANINE VERSUS 5.00 MM H_2O_2 VERSUS CULTURE (NEGATIVE CONTROL) CONDITIONS VERSUS 1200.00 μM TEMOZOLOMIDE FOR 24-HOURS. 539

OUTPUT 13.300.:DESCRIPTIVE STATISTICS AND NORMALITY (SHAPIRO-WILK) ASSUMPTION CHECKING OF DATA REPRESENTING THE OCCURRENCE OF NECROSIS IN U87MG CELLS TREATED WITH 6.25 μM A-SOLANINE VERSUS 5.00 MM H_2O_2 VERSUS CULTURE (NEGATIVE CONTROL) CONDITIONS VERSUS 1200.00 μM TEMOZOLOMIDE FOR 24-HOURS. 540

OUTPUT 13.301.: EQUALITY OF VARIANCE (LEVENE'S) ASSUMPTION CHECKS OF DATA REPRESENTING THE OCCURRENCE OF NECROSIS IN U87MG CELLS TREATED WITH 6.25 μM A-SOLANINE VERSUS 5.00 MM H_2O_2 VERSUS CULTURE (NEGATIVE CONTROL) CONDITIONS VERSUS 1200.00 μM TEMOZOLOMIDE FOR 24-HOURS. 540

OUTPUT 13.302.: ONE-WAY ANOVA TESTING OF DATA REPRESENTING THE OCCURRENCE OF NECROSIS IN U87MG CELLS TREATED WITH 6.25 μM A-SOLANINE VERSUS 5.00 MM H_2O_2 VERSUS CULTURE (NEGATIVE CONTROL) CONDITIONS VERSUS 1200.00 μM TEMOZOLOMIDE FOR 24-HOURS. 541

OUTPUT 13.303.: ONE-WAY ANOVA POST-HOC ANALYSIS OF DATA REPRESENTING THE OCCURRENCE OF DATA REPRESENTING THE OCCURRENCE OF NECROSIS IN U87MG CELLS TREATED WITH 6.25 μM A-SOLANINE VERSUS 5.00 MM H_2O_2 VERSUS CULTURE (NEGATIVE CONTROL) CONDITIONS VERSUS 1200.00 μM TEMOZOLOMIDE FOR 24-HOURS. 541

OUTPUT 13.304.: DESCRIPTIVE STATISTICS AND NORMALITY (SHAPIRO-WILK) ASSUMPTION CHECKING OF DATA REPRESENTING THE OCCURRENCE OF AUTOPHAGY IN U87MG CELLS TREATED WITH 6.25 μM A-SOLANINE VERSUS 5.00 MM H_2O_2 VERSUS CULTURE (NEGATIVE CONTROL) CONDITIONS VERSUS 1200.00 μM TEMOZOLOMIDE FOR 24-HOURS. 541

OUTPUT 13.305.: EQUALITY OF VARIANCE (LEVENE'S) ASSUMPTION CHECKS OF DATA REPRESENTING THE OCCURRENCE OF AUTOPHAGY IN U87MG CELLS TREATED WITH 6.25 μM A-SOLANINE VERSUS 5.00 MM H_2O_2 VERSUS CULTURE (NEGATIVE CONTROL) CONDITIONS VERSUS 1200.00 μM TEMOZOLOMIDE FOR 24-HOURS. 542

OUTPUT 13.306.: ONE-WAY ANOVA TESTING OF DATA REPRESENTING THE OCCURRENCE OF AUTOPHAGY IN U87MG CELLS TREATED WITH 6.25 μM A-SOLANINE VERSUS 5.00 MM H_2O_2 VERSUS CULTURE (NEGATIVE CONTROL) CONDITIONS VERSUS 1200.00 μM TEMOZOLOMIDE FOR 24-HOURS 542

OUTPUT 13.307.: ONE-WAY ANOVA POST-HOC ANALYSIS OF DATA REPRESENTING THE OCCURRENCE OF DATA REPRESENTING THE OCCURRENCE OF AUTOPHAGY IN U87MG CELLS TREATED WITH 6.25 μM A-SOLANINE VERSUS 5.00 MM H_2O_2 VERSUS CULTURE (NEGATIVE CONTROL) CONDITIONS VERSUS 1200.00 μM TEMOZOLOMIDE FOR 24-HOURS. 542

OUTPUT 13.308.: DESCRIPTIVE STATISTICS AND NORMALITY (SHAPIRO-WILK) ASSUMPTION CHECKING OF DATA REPRESENTING THE OCCURRENCE OF EARLY APOPTOSIS IN U251 CELLS TREATED WITH 6.25 μM A-SOLANINE VERSUS 5.00 MM H_2O_2 VERSUS CULTURE (NEGATIVE CONTROL) CONDITIONS 1200.00 μM VERSUS TEMOZOLOMIDE FOR 24-HOURS. 542

OUTPUT 13.309.: EQUALITY OF VARIANCE (LEVENE'S) ASSUMPTION CHECKS OF DATA REPRESENTING THE OCCURRENCE OF EARLY APOPTOSIS IN U251 CELLS TREATED WITH 6.25 μM A-SOLANINE VERSUS 5.00 MM H_2O_2 VERSUS CULTURE (NEGATIVE CONTROL) CONDITIONS VERSUS 1200.00 μM TEMOZOLOMIDE FOR 24-HOURS. 543

OUTPUT 13.310.:KRUSKAL-WALLIS TESTING OF DATA REPRESENTING THE OCCURRENCE OF EARLY APOPTOSIS IN U251 CELLS TREATED WITH 6.25 μM A-SOLANINE VERSUS 5.00 MM H_2O_2 VERSUS CULTURE (NEGATIVE CONTROL) CONDITIONS VERSUS 1200.00 μM TEMOZOLOMIDE FOR 24-HOURS 543

OUTPUT 13.311.: DESCRIPTIVE STATISTICS AND NORMALITY (SHAPIRO-WILK) ASSUMPTION CHECKING OF DATA REPRESENTING THE OCCURRENCE OF LATE APOPTOSIS IN U251 CELLS TREATED WITH 6.25 μM A-SOLANINE VERSUS 5.00 MM H_2O_2 VERSUS CULTURE (NEGATIVE CONTROL) CONDITIONS VERSUS 1200.00 μM TEMOZOLOMIDE FOR 24-HOURS. 543

Output 13.312.: Equality of Variance (Levene's) assumption checks of data representing the occurrence of late apoptosis in U251 cells treated with 6.25 μM a-solanine versus 5.00 mM H_2O_2 versus culture (negative control) conditions versus 1200.00 μM temozolomide for 24-hours. 544

Output 13.313.: One-way ANOVA testing of data representing the occurrence of late apoptosis in U251 cells treated with 6.25 μM a-solanine versus 5.00 mM H_2O_2 versus culture (negative control) conditions versus 1200.00 μM temozolomide for 24-hours. 544

Output 13.314.: Descriptive statistics and normality (Shapiro-Wilk) assumption checking of data representing the occurrence of necrosis in U251 cells treated with 6.25 μM a-solanine versus 5.00 mM H_2O_2 versus culture (negative control) conditions versus 1200.00 μM temozolomide for 24-hours. 544

Output 13.315.: Equality of Variance (Levene's) assumption checks of data representing the occurrence of necrosis in U251 cells treated with 6.25 μM a-solanine versus 5.00 mM H_2O_2 versus culture (negative control) conditions versus 1200.00 μM temozolomide for 24-hours. 545

Output 13.316.: One-way ANOVA testing of data representing the occurrence of necrosis in U251 cells treated with 6.25 μM a-solanine versus 5.00 mM H_2O_2 versus culture (negative control) conditions versus 1200.00 μM temozolomide for 24-hours 545

Output 13.317.: One-way ANOVA post-hoc analysis of data representing the occurrence of data representing the occurrence of necrosis in U251 cells treated with 6.25 μM a-solanine versus 5.00 mM H_2O_2 versus culture (negative control) conditions versus 1200.00 μM temozolomide for 24-hours. 545

Output 13.318.: Descriptive statistics and normality (Shapiro-Wilk) assumption checking of data representing the occurrence of autophagy in U251 cells treated with 6.25 μM a-solanine versus 5.00 mM H_2O_2 versus culture (negative control) conditions versus 1200.00 μM temozolomide for 24-hours. 546

Output 13.319.: Equality of Variance (Levene's) assumption checks of data representing the occurrence of autophagy in U251 cells treated with 6.25 μM a-solanine versus 5.00 mM H_2O_2 versus culture (negative control) conditions versus 1200.00 μM temozolomide for 24-hours. 546

OUTPUT 13.320.: ONE-WAY ANOVA TESTING OF DATA REPRESENTING THE OCCURRENCE OF AUTOPHAGY IN U251 CELLS TREATED WITH 6.25 μM A-SOLANINE VERSUS 5.00 MM H_2O_2 VERSUS CULTURE (NEGATIVE CONTROL) CONDITIONS VERSUS 1200.00 μM TEMOZOLOMIDE FOR 24-HOURS..... 547

OUTPUT 13.321.: ONE-WAY ANOVA POST-HOC ANALYSIS OF DATA REPRESENTING THE OCCURRENCE OF DATA REPRESENTING THE OCCURRENCE OF AUTOPHAGY IN U251 CELLS TREATED WITH 6.25 μM A-SOLANINE VERSUS 5.00 MM H_2O_2 VERSUS CULTURE (NEGATIVE CONTROL) CONDITIONS VERSUS 1200.00 μM TEMOZOLOMIDE FOR 24-HOURS..... 547

OUTPUT 13.322.: DESCRIPTIVE STATISTICS AND NORMALITY (SHAPIRO-WILK) ASSUMPTION CHECKING OF DATA REPRESENTING THE OCCURRENCE OF EARLY APOPTOSIS IN T98G CELLS TREATED WITH 6.25 μM A-SOLANINE VERSUS 5.00 MM H_2O_2 VERSUS CULTURE (NEGATIVE CONTROL) CONDITIONS VERSUS 1200.00 μM TEMOZOLOMIDE FOR 24-HOURS..... 547

OUTPUT 13.323.: EQUALITY OF VARIANCE (LEVENE'S) ASSUMPTION CHECKS OF DATA REPRESENTING THE OCCURRENCE OF EARLY APOPTOSIS IN T98G CELLS TREATED WITH 6.25 μM A-SOLANINE VERSUS 5.00 MM H_2O_2 VERSUS CULTURE (NEGATIVE CONTROL) CONDITIONS VERSUS 1200.00 μM TEMOZOLOMIDE FOR 24-HOURS..... 548

OUTPUT 13.324.: ONE-WAY ANOVA OF DATA REPRESENTING THE OCCURRENCE OF EARLY APOPTOSIS IN T98G CELLS TREATED WITH 6.25 μM A-SOLANINE VERSUS 5.00 MM H_2O_2 VERSUS CULTURE (NEGATIVE CONTROL) CONDITIONS VERSUS 1200.00 μM TEMOZOLOMIDE FOR 24-HOURS..... 548

OUTPUT 13.325.: ONE-WAY ANOVA POST-HOC ANALYSIS OF DATA REPRESENTING THE OCCURRENCE OF DATA REPRESENTING THE OCCURRENCE OF EARLY APOPTOSIS IN T98G CELLS TREATED WITH 6.25 μM A-SOLANINE VERSUS 5.00 MM H_2O_2 VERSUS CULTURE (NEGATIVE CONTROL) CONDITIONS VERSUS 1200.00 μM TEMOZOLOMIDE FOR 24-HOURS..... 548

OUTPUT 13.326.: DESCRIPTIVE STATISTICS AND NORMALITY (SHAPIRO-WILK) ASSUMPTION CHECKING OF DATA REPRESENTING THE OCCURRENCE OF LATE APOPTOSIS IN T98G CELLS TREATED WITH 6.25 μM A-SOLANINE VERSUS 5.00 MM H_2O_2 VERSUS CULTURE (NEGATIVE CONTROL) CONDITIONS VERSUS 1200.00 μM TEMOZOLOMIDE FOR 24-HOURS..... 548

OUTPUT 13.327.: EQUALITY OF VARIANCE (LEVENE'S) ASSUMPTION CHECKS OF DATA REPRESENTING THE OCCURRENCE OF LATE APOPTOSIS IN T98G CELLS TREATED WITH 6.25 μM A-SOLANINE VERSUS 5.00 MM H_2O_2 VERSUS CULTURE (NEGATIVE CONTROL) CONDITIONS VERSUS 1200.00 μM TEMOZOLOMIDE FOR 24-HOURS..... 549

Output 13.328.: Kruskal-Wallis testing of data representing the occurrence of late apoptosis in T98G cells treated with 6.25 μM a-solanine versus 5.00 mM H_2O_2 versus culture (negative control) conditions versus 1200.00 μM temozolomide for 24-hours..... 549

Output 13.329.: Descriptive statistics and normality (Shapiro-Wilk) assumption checking of data representing the occurrence of necrosis in T98G cells treated with 6.25 μM a-solanine versus 5.00 mM H_2O_2 versus culture (negative control) conditions versus 1200.00 μM temozolomide for 24-hours..... 549

Output 13.330.: Equality of Variance (Levene's) assumption checks of data representing the occurrence of necrosis in T98G cells treated with 6.25 μM a-solanine versus 5.00 mM H_2O_2 versus culture (negative control) conditions versus 1200.00 μM temozolomide for 24-hours..... 550

Output 13.331.: Kruskal-Wallis testing of data representing the occurrence of necrosis in T98G cells treated with 6.25 μM a-solanine versus 5.00 mM H_2O_2 versus culture (negative control) conditions versus 1200.00 μM temozolomide for 24-hours..... 550

Output 13.332.: Descriptive statistics and normality (Shapiro-Wilk) assumption checking of data representing the occurrence of autophagy in T98G cells treated with 6.25 μM a-solanine versus 5.00 mM H_2O_2 versus culture (negative control) conditions versus 1200.00 μM temozolomide for 24-hours..... 550

Output 13.333.: Equality of Variance (Levene's) assumption checks of data representing the occurrence of autophagy in T98G cells treated with 6.25 μM a-solanine versus 5.00 mM H_2O_2 versus culture (negative control) conditions versus 1200.00 μM temozolomide for 24-hours..... 551

Output 13.334.: Kruskal-Wallis testing of data representing the occurrence of autophagy in T98G cells treated with 6.25 μM a-solanine versus 5.00 mM H_2O_2 versus culture (negative control) conditions versus 1200.00 μM temozolomide for 24-hours..... 551

Output 13.335.: Descriptive statistics and normality (Shapiro-Wilk) assumption checking of data representing the overall occurrence of early apoptosis versus late apoptosis versus necrosis versus autophagy in glioblastoma multiforme cells treated with 5.00 mM H_2O_2 for 24-hours. 551

Output 13.336.: Equality of Variance (Levene's) assumption checks of data representing the overall occurrence of early apoptosis versus late apoptosis versus necrosis versus autophagy in glioblastoma multiforme cells treated with 5.00 mM H_2O_2 for 24-hours..... 552

Output 13.337.: Kruskal-Wallis testing of data representing the overall occurrence of early apoptosis versus late apoptosis versus necrosis versus autophagy in glioblastoma multiforme cells treated with 5.00 mM H_2O_2 for 24-hours..... 552

Output 13.338.: Kruskal-Wallis post-hoc analysis of data representing the overall occurrence of early apoptosis versus late apoptosis versus necrosis versus autophagy in glioblastoma multiforme cells treated with 5.00 mM H_2O_2 for 24-hours. 552

Output 13.339.: Descriptive statistics and normality (Shapiro-Wilk) assumption checking of data representing the overall occurrence of early apoptosis versus late apoptosis versus necrosis versus autophagy in glioblastoma multiforme cells treated with 6.25 μM a-solanine for 24-hours..... 553

Output 13.340.: Equality of Variance (Levene's) assumption checks of data representing the overall occurrence of early apoptosis versus late apoptosis versus necrosis versus autophagy in glioblastoma multiforme cells treated with 6.25 μM a-solanine for 24-hours. 553

Output 13.341.: Kruskal-Wallis testing of data representing the overall occurrence of early apoptosis versus late apoptosis versus necrosis versus autophagy in glioblastoma multiforme cells treated with 6.25 μM a-solanine for 24-hours. 553

Output 13.342.: *Kruskal*-Wallis post-hoc analysis of data representing the overall occurrence of early apoptosis versus late apoptosis versus necrosis versus autophagy in glioblastoma multiforme cells treated with 6.25 μM a-solanine for 24-hours..... 554

Output 13.343.: Descriptive statistics and normality (Shapiro-Wilk) assumption checking of data representing the overall occurrence of early apoptosis versus late apoptosis versus necrosis versus autophagy in glioblastoma multiforme cells treated with 1200.00 μM temozolomide for 24-hours. 554

Output 13.344.: Equality of Variance (Levene's) assumption checks of data representing the overall occurrence of early apoptosis versus late apoptosis versus necrosis versus autophagy in glioblastoma multiforme cells treated with 1200.00 μM temozolomide for 24-hours. 554

Output 13.345.: One-way ANOVA testing of data representing the overall occurrence of early apoptosis versus late apoptosis versus necrosis versus autophagy in glioblastoma multiforme cells treated with 1200.00 μM temozolomide for 24-hours. 555

OUTPUT 13.346.: ONE-WAY ANOVA POST-HOC ANALYSIS OF DATA REPRESENTING THE OVERALL OCCURRENCE OF EARLY APOPTOSIS VERSUS LATE APOPTOSIS VERSUS NECROSIS VERSUS AUTOPHAGY IN GLIOBLASTOMA MULTIFORME CELLS TREATED WITH 1200.00 μM TEMOZOLOMIDE FOR 24-HOURS. 555

OUTPUT 13.347.: DESCRIPTIVE STATISTICS AND NORMALITY (SHAPIRO-WILK) ASSUMPTION CHECKING OF DATA REPRESENTING THE OVERALL OCCURRENCE OF EARLY APOPTOSIS VERSUS LATE APOPTOSIS VERSUS NECROSIS VERSUS AUTOPHAGY IN GLIOBLASTOMA MULTIFORME CELLS TREATED WITH CULTURE (NEGATIVE CONTROL) CONDITIONS FOR 24-HOURS. 555

OUTPUT 13.348.: EQUALITY OF VARIANCE (LEVENE'S) ASSUMPTION CHECKS OF DATA REPRESENTING THE OVERALL OCCURRENCE OF EARLY APOPTOSIS VERSUS LATE APOPTOSIS VERSUS NECROSIS VERSUS AUTOPHAGY IN GLIOBLASTOMA MULTIFORME CELLS TREATED WITH CULTURE (NEGATIVE CONTROL) CONDITIONS FOR 24-HOURS. 556

OUTPUT 13.349.: KRUSKAL-WALLIS TESTING OF DATA REPRESENTING THE OVERALL OCCURRENCE OF EARLY APOPTOSIS VERSUS LATE APOPTOSIS VERSUS NECROSIS VERSUS AUTOPHAGY IN GLIOBLASTOMA MULTIFORME CELLS TREATED WITH CULTURE (NEGATIVE CONTROL) CONDITIONS FOR 24-HOURS. 556

OUTPUT 13.350.: KRUSKAL-WALLIS POST-HOC ANALYSIS OF DATA REPRESENTING THE OVERALL OCCURRENCE OF EARLY APOPTOSIS VERSUS LATE APOPTOSIS VERSUS NECROSIS VERSUS AUTOPHAGY IN GLIOBLASTOMA MULTIFORME CELLS TREATED WITH CULTURE (NEGATIVE CONTROL) CONDITIONS FOR 24-HOURS. 556

OUTPUT 13.351.: DESCRIPTIVE STATISTICS AND NORMALITY (SHAPIRO-WILK) ASSUMPTION CHECKING OF DATA REPRESENTING THE OVERALL OCCURRENCE OF EARLY APOPTOSIS IN GLIOBLASTOMA MULTIFORME CELLS TREATED WITH 6.25 μM A-SOLANINE VERSUS 5.00 MM H_2O_2 VERSUS CULTURE (NEGATIVE CONTROL) CONDITIONS VERSUS 1200.00 μM TEMOZOLOMIDE FOR 24-HOURS. 557

OUTPUT 13.352.: EQUALITY OF VARIANCE (LEVENE'S) ASSUMPTION CHECKS OF DATA REPRESENTING THE OVERALL OCCURRENCE OF EARLY APOPTOSIS IN GLIOBLASTOMA MULTIFORME CELLS TREATED WITH 6.25 μM A-SOLANINE VERSUS 5.00 MM H_2O_2 VERSUS CULTURE (NEGATIVE CONTROL) CONDITIONS VERSUS 1200.00 μM TEMOZOLOMIDE FOR 24-HOURS..... 557

OUTPUT 13.353.: ONE-WAY ANOVA TESTING OF DATA REPRESENTING THE OVERALL OCCURRENCE OF EARLY APOPTOSIS IN GLIOBLASTOMA MULTIFORME CELLS TREATED WITH 6.25 μM A-SOLANINE VERSUS 5.00 MM H_2O_2 VERSUS CULTURE (NEGATIVE CONTROL) CONDITIONS VERSUS 1200.00 μM TEMOZOLOMIDE FOR 24-HOURS. 557

OUTPUT 13.354.: DESCRIPTIVE STATISTICS AND NORMALITY (SHAPIRO-WILK) ASSUMPTION CHECKING OF DATA REPRESENTING THE OVERALL OCCURRENCE OF LATE APOPTOSIS IN GLIOBLASTOMA MULTIFORME CELLS TREATED WITH

6.25 μM A-SOLANINE VERSUS 5.00 MM H_2O_2 VERSUS CULTURE (NEGATIVE CONTROL) CONDITIONS VERSUS 1200.00 μM TEMOZOLOMIDE FOR 24-HOURS. 558

OUTPUT 13.355.: EQUALITY OF VARIANCE (LEVENE'S) ASSUMPTION CHECKS OF DATA REPRESENTING THE OVERALL OCCURRENCE OF LATE APOPTOSIS IN GLIOBLASTOMA MULTIFORME CELLS TREATED WITH 6.25 μM A-SOLANINE VERSUS 5.00 MM H_2O_2 VERSUS CULTURE (NEGATIVE CONTROL) CONDITIONS VERSUS 1200.00 μM TEMOZOLOMIDE FOR 24-HOURS. 558

OUTPUT 13.356.: KRUSKAL-WALLIS TESTING OF DATA REPRESENTING THE OVERALL OCCURRENCE OF LATE APOPTOSIS IN GLIOBLASTOMA MULTIFORME CELLS TREATED WITH 6.25 μM A-SOLANINE VERSUS 5.00 MM H_2O_2 VERSUS CULTURE (NEGATIVE CONTROL) CONDITIONS VERSUS 1200.00 μM TEMOZOLOMIDE FOR 24-HOURS. 558

OUTPUT 13.357.: DESCRIPTIVE STATISTICS AND NORMALITY (SHAPIRO-WILK) ASSUMPTION CHECKING OF DATA REPRESENTING THE OVERALL OCCURRENCE OF NECROSIS IN GLIOBLASTOMA MULTIFORME CELLS TREATED WITH 6.25 μM A-SOLANINE VERSUS 5.00 MM H_2O_2 VERSUS CULTURE (NEGATIVE CONTROL) CONDITIONS VERSUS 1200.00 μM TEMOZOLOMIDE FOR 24-HOURS. 559

OUTPUT 13.358.: EQUALITY OF VARIANCE (LEVENE'S) ASSUMPTION CHECKS OF DATA REPRESENTING THE OVERALL OCCURRENCE OF NECROSIS IN GLIOBLASTOMA MULTIFORME CELLS TREATED WITH 6.25 μM A-SOLANINE VERSUS 5.00 MM H_2O_2 VERSUS CULTURE (NEGATIVE CONTROL) CONDITIONS VERSUS 1200.00 μM TEMOZOLOMIDE FOR 24-HOURS. 559

OUTPUT 13.359.: KRUSKAL-WALLIS TESTING OF DATA REPRESENTING THE OVERALL OCCURRENCE OF NECROSIS IN GLIOBLASTOMA MULTIFORME CELLS TREATED WITH 6.25 μM A-SOLANINE VERSUS 5.00 MM H_2O_2 VERSUS CULTURE (NEGATIVE CONTROL) CONDITIONS VERSUS 1200.00 μM TEMOZOLOMIDE FOR 24-HOURS. 559

OUTPUT 13.360.: DESCRIPTIVE STATISTICS AND NORMALITY (SHAPIRO-WILK) ASSUMPTION CHECKING OF DATA REPRESENTING THE OVERALL OCCURRENCE OF AUTOPHAGY IN GLIOBLASTOMA MULTIFORME CELLS TREATED WITH 6.25 μM A-SOLANINE VERSUS 5.00 MM H_2O_2 VERSUS CULTURE (NEGATIVE CONTROL) CONDITIONS VERSUS 1200.00 μM TEMOZOLOMIDE FOR 24-HOURS. 560

OUTPUT 13.361.: EQUALITY OF VARIANCE (LEVENE'S) ASSUMPTION CHECKS OF DATA REPRESENTING THE OVERALL OCCURRENCE OF AUTOPHAGY IN GLIOBLASTOMA MULTIFORME CELLS TREATED WITH 6.25 μM A-SOLANINE VERSUS 5.00 MM H_2O_2 VERSUS CULTURE (NEGATIVE CONTROL) CONDITIONS VERSUS 1200.00 μM TEMOZOLOMIDE FOR 24-HOURS. 560

Output 13.362.: Kruskal-Wallis testing of data representing the overall occurrence of autophagy in glioblastoma multiforme cells treated with 6.25 μM a-solanine versus 5.00 mM H_2O_2 versus culture (negative control) conditions versus 1200.00 μM temozolomide for 24-hours. 560

Output 13.363.: Descriptive statistics for Bad protein corrected mean grey area data for glioblastoma multiforme cells treated with 6.25 μM a-solanine versus negative control (culture) treatment..... 561

Output 13.364.: Normality (Shapiro-Wilk) and Equality of Variance (Levene's) assumption checks for pairwise sample testing for Bad protein corrected mean grey area data for glioblastoma multiforme cells treated with 6.25 μM a-solanine versus negative control (culture) treatment. 561

Output 13.365.:Output 13.366.: Welch testing for Bad protein corrected mean grey area data for glioblastoma multiforme cells treated with 6.25 μM a-solanine versus negative control (culture) treatment. 562

Output 13.367.: Descriptive statistics for Bax protein corrected mean grey area data for glioblastoma multiforme cells treated with 6.25 μM a-solanine versus negative control (culture) treatment..... 562

Output 13.368.: Normality (Shapiro-Wilk) and Equality of Variance (Levene's) assumption checks for pairwise sample testing for Bax protein corrected mean grey area data for glioblastoma multiforme cells treated with 6.25 μM a-solanine versus negative control (culture) treatment. 562

Output 13.369.: Independent sample T-testing for Bax protein corrected mean grey area data for glioblastoma multiforme cells treated with 6.25 μM a-solanine versus negative control (culture) treatment. 563

Output 13.370.: Descriptive statistics for Bcl-2 protein corrected mean grey area data for glioblastoma multiforme cells treated with 6.25 μM a-solanine versus negative control (culture) treatment..... 563

Output 13.371.: Normality (Shapiro-Wilk) and Equality of Variance (Levene's) assumption checks for pairwise sample testing for Bcl-2 protein corrected mean grey area data for glioblastoma multiforme cells treated with 6.25 μM a-solanine versus negative control (culture) treatment. 564

Output 13.372.: Independent sample T-testing for Bcl-2 protein corrected mean grey area data for glioblastoma multiforme cells treated with 6.25 μM a-solanine versus negative control (culture) treatment. 564

Output 13.373.: Descriptive statistics for Bcl-w protein corrected mean grey area data for glioblastoma multiforme cells treated with 6.25 μM a-solanine versus negative control (culture) treatment..... 565

Output 13.374.: Normality (Shapiro-Wilk) and Equality of Variance (Levene's) assumption checks for pairwise sample testing for Bcl-w protein corrected mean grey area data for glioblastoma multiforme cells treated with 6.25 μM a-solanine versus negative control (culture) treatment. 565
Output 13.375.: Independent sample T-testing for Bcl-w protein corrected mean grey area data for glioblastoma multiforme cells treated with 6.25 μM a-solanine versus negative control (culture) treatment. 565
Output 13.376.: Descriptive statistics for Bid protein corrected mean grey area data for glioblastoma multiforme cells treated with 6.25 μM a-solanine versus negative control (culture) treatment..... 566
Output 13.377.: Normality (Shapiro-Wilk) and Equality of Variance (Levene's) assumption checks for pairwise sample testing for Bid protein corrected mean grey area data for glioblastoma multiforme cells treated with 6.25 μM a-solanine versus negative control (culture) treatment. 566
Output 13.378.: Independent sample T-testing for Bid protein corrected mean grey area data for glioblastoma multiforme cells treated with 6.25 μM a-solanine versus negative control (culture) treatment. 567
Output 13.379.: Descriptive statistics for Bim protein corrected mean grey area data for glioblastoma multiforme cells treated with 6.25 μM a-solanine versus negative control (culture) treatment..... 567
Output 13.380.: Normality (Shapiro-Wilk) and Equality of Variance (Levene's) assumption checks for pairwise sample testing for Bim protein corrected mean grey area data for glioblastoma multiforme cells treated with 6.25 μM a-solanine versus negative control (culture) treatment. 568
Output 13.381.: Independent sample T-testing for Bim protein corrected mean grey area data for glioblastoma multiforme cells treated with 6.25 μM a-solanine versus negative control (culture) treatment. 568
Output 13.382.: Descriptive statistics for Casp-3 protein corrected mean grey area data for glioblastoma multiforme cells treated with 6.25 μM a-solanine versus negative control (culture) treatment..... 569
Output 13.383.: Normality (Shapiro-Wilk) and Equality of Variance (Levene's) assumption checks for pairwise sample testing for Casp-3 protein corrected mean grey area data for glioblastoma multiforme cells treated with 6.25 μM a-solanine versus negative control (culture) treatment..... 569

Output 13.384.: Independent sample T-testing for Casp-3 protein corrected mean grey area data for glioblastoma multiforme cells treated with 6.25 μM a-solanine versus negative control (culture) treatment. 570
Output 13.385.: Descriptive statistics for Casp-8 protein corrected mean grey area data for glioblastoma multiforme cells treated with 6.25 μM a-solanine versus negative control (culture) treatment..... 570
Output 13.386.: Normality (Shapiro-Wilk) and Equality of Variance (Levene's) assumption checks for pairwise sample testing for Casp-8 protein corrected mean grey area data for glioblastoma multiforme cells treated with 6.25 μM a-solanine versus negative control (culture) treatment..... 571
Output 13.387.: Independent sample T-testing for Casp-8 protein corrected mean grey area data for glioblastoma multiforme cells treated with 6.25 μM a-solanine versus negative control (culture) treatment. 571
Output 13.388.: Descriptive statistics for CD40 protein corrected mean grey area data for glioblastoma multiforme cells treated with 6.25 μM a-solanine versus negative control (culture) treatment..... 572
Output 13.389.: Normality (Shapiro-Wilk) and Equality of Variance (Levene's) assumption checks for pairwise sample testing for CD40 protein corrected mean grey area data for glioblastoma multiforme cells treated with 6.25 μM a-solanine versus negative control (culture) treatment. 572
Output 13.390.: Welch testing for CD40 protein corrected mean grey area data for glioblastoma multiforme cells treated with 6.25 μM a-solanine versus negative control (culture) treatment..... 573
Output 13.391.: Descriptive statistics for CD40 ligand protein corrected mean grey area data for glioblastoma multiforme cells treated with 6.25 μM a-solanine versus negative control (culture) treatment. 573
Output 13.392.: Normality (Shapiro-Wilk) and Equality of Variance (Levene's) assumption checks for pairwise sample testing for CD40 ligand protein corrected mean grey area data for glioblastoma multiforme cells treated with 6.25 μM a-solanine versus negative control (culture) treatment..... 574
Output 13.393.: Welch testing for CD40 ligand protein corrected mean grey area data for glioblastoma multiforme cells treated with 6.25 μM a-solanine versus negative control (culture) treatment..... 574
Output 13.394.: Descriptive statistics for cIAP-2 protein corrected mean grey area data for glioblastoma multiforme cells treated with 6.25 μM a-solanine versus negative control (culture) treatment..... 575

Output 13.395.: Normality (Shapiro-Wilk) and Equality of Variance (Levene's) assumption checks for pairwise sample testing for cIAP-2 protein corrected mean grey area data for glioblastoma multiforme cells treated with 6.25 μM a-solanine versus negative control (culture) treatment..... 575
Output 13.396.: Independent sample T-testing for cIAP-2 protein corrected mean grey area data for glioblastoma multiforme cells treated with 6.25 μM a-solanine versus negative control (culture) treatment. 576
Output 13.397.: Descriptive statistics for Cyt-C protein corrected mean grey area data for glioblastoma multiforme cells treated with 6.25 μM a-solanine versus negative control (culture) treatment..... 576
Output 13.398.: Normality (Shapiro-Wilk) and Equality of Variance (Levene's) assumption checks for pairwise sample testing for Cyt-C protein corrected mean grey area data for glioblastoma multiforme cells treated with 6.25 μM a-solanine versus negative control (culture) treatment. 577
Output 13.399.: Independent sample T-testing for Cyt-C protein corrected mean grey area data for glioblastoma multiforme cells treated with 6.25 μM a-solanine versus negative control (culture) treatment. 577
Output 13.400.: Descriptive statistics for TNFRSF21 protein corrected mean grey area data for glioblastoma multiforme cells treated with 6.25 μM a-solanine versus negative control (culture) treatment. 578
Output 13.401.: Normality (Shapiro-Wilk) and Equality of Variance (Levene's) assumption checks for pairwise sample testing for TNFRSF21 protein corrected mean grey area data for glioblastoma multiforme cells treated with 6.25 μM a-solanine versus negative control (culture) treatment..... 578
Output 13.402.: Independent sample T-testing for TNFRSF21 protein corrected mean grey area data for glioblastoma multiforme cells treated with 6.25 μM a-solanine versus negative control (culture) treatment. 579
Output 13.403.: Descriptive statistics for Fas protein corrected mean grey area data for glioblastoma multiforme cells treated with 6.25 μM a-solanine versus negative control (culture) treatment..... 579
Output 13.404.: Normality (Shapiro-Wilk) and Equality of Variance (Levene's) assumption checks for pairwise sample testing for Fas protein corrected mean grey area data for glioblastoma multiforme cells treated with 6.25 μM a-solanine versus negative control (culture) treatment. 580

Output 13.405.: Independent sample T-testing for Fas protein corrected mean grey area data for glioblastoma multiforme cells treated with 6.25 μM a-solanine versus negative control (culture) treatment. 580
Descriptive statistics for Fas ligand protein corrected mean grey area data for glioblastoma multiformOutput 13.406.:e cells treated with 6.25 μM a-solanine versus negative control (culture) treatment. 581
Output 13.407.: Normality (Shapiro-Wilk) and Equality of Variance (Levene's) assumption checks for pairwise sample testing for Fas ligand protein corrected mean grey area data for glioblastoma multiforme cells treated with 6.25 μM a-solanine versus negative control (culture) treatment..... 581
Output 13.408.: Independent sample T-testing for Fas ligand protein corrected mean grey area data for glioblastoma multiforme cells treated with 6.25 μM a-solanine versus negative control (culture) treatment. 582
Output 13.409.: Descriptive statistics for HSP27 protein corrected mean grey area data for glioblastoma multiforme cells treated with 6.25 μM a-solanine versus negative control (culture) treatment..... 582
Output 13.410.: Normality (Shapiro-Wilk) and Equality of Variance (Levene's) assumption checks for pairwise sample testing for HSP27 protein corrected mean grey area data for glioblastoma multiforme cells treated with 6.25 μM a-solanine versus negative control (culture) treatment..... 583
Output 13.411.: Welch testing for HSP27 protein corrected mean grey area data for glioblastoma multiforme cells treated with 6.25 μM a-solanine versus negative control (culture) treatment..... 583
Output 13.412.: Descriptive statistics for HSP60 protein corrected mean grey area data for glioblastoma multiforme cells treated with 6.25 μM a-solanine versus negative control (culture) treatment..... 584
Output 13.413.: Normality (Shapiro-Wilk) and Equality of Variance (Levene's) assumption checks for pairwise sample testing for HSP60 protein corrected mean grey area data for glioblastoma multiforme cells treated with 6.25 μM a-solanine versus negative control (culture) treatment..... 584
Output 13.414.: Independent sample T-testing for HSP60 protein corrected mean grey area data for glioblastoma multiforme cells treated with 6.25 μM a-solanine versus negative control (culture) treatment. 585
Output 13.415.: Descriptive statistics for HSP70 protein corrected mean grey area data for glioblastoma multiforme cells treated with 6.25 μM a-solanine versus negative control (culture) treatment..... 585

Output 13.416.: Normality (Shapiro-Wilk) and Equality of Variance (Levene's) assumption checks for pairwise sample testing for HSP70 protein corrected mean grey area data for glioblastoma multiforme cells treated with 6.25 μM a-solanine versus negative control (culture) treatment..... 586
Output 13.417.: Independent sample T-testing for HSP70 protein corrected mean grey area data for glioblastoma multiforme cells treated with 6.25 μM a-solanine versus negative control (culture) treatment. 586
Output 13.418.: Descriptive statistics for HTRA2 protein corrected mean grey area data for glioblastoma multiforme cells treated with 6.25 μM a-solanine versus negative control (culture) treatment..... 587
Output 13.419.: Normality (Shapiro-Wilk) and Equality of Variance (Levene's) assumption checks for pairwise sample testing for HTRA2 protein corrected mean grey area data for glioblastoma multiforme cells treated with 6.25 μM a-solanine versus negative control (culture) treatment..... 587
Output 13.420.: Independent sample T-testing for HTRA2 protein corrected mean grey area data for glioblastoma multiforme cells treated with 6.25 μM a-solanine versus negative control (culture) treatment. 588
Output 13.421.: Descriptive statistics for IGF-1 protein corrected mean grey area data for glioblastoma multiforme cells treated with 6.25 μM a-solanine versus negative control (culture) treatment..... 588
Output 13.422.: Normality (Shapiro-Wilk) and Equality of Variance (Levene's) assumption checks for pairwise sample testing for IGF-1 protein corrected mean grey area data for glioblastoma multiforme cells treated with 6.25 μM a-solanine versus negative control (culture) treatment. 589
Output 13.423.: Independent sample T-testing for IGF-1 protein corrected mean grey area data for glioblastoma multiforme cells treated with 6.25 μM a-solanine versus negative control (culture) treatment. 589
Output 13.424.: Descriptive statistics for IGF-2 protein corrected mean grey area data for glioblastoma multiforme cells treated with 6.25 μM a-solanine versus negative control (culture) treatment..... 590
Output 13.425.: Normality (Shapiro-Wilk) and Equality of Variance (Levene's) assumption checks for pairwise sample testing for IGF-2 protein corrected mean grey area data for glioblastoma multiforme cells treated with 6.25 μM a-solanine versus negative control (culture) treatment. 590

Output 13.426.: Independent sample T-testing for IGF-2 protein corrected mean grey area data for glioblastoma multiforme cells treated with 6.25 μM a-solanine versus negative control (culture) treatment. 591
Output 13.427.: Descriptive statistics for IGFBP-1 protein corrected mean grey area data for glioblastoma multiforme cells treated with 6.25 μM a-solanine versus negative control (culture) treatment..... 591
Output 13.428.: Normality (Shapiro-Wilk) and Equality of Variance (Levene's) assumption checks for pairwise sample testing for IGFBP-1 protein corrected mean grey area data for glioblastoma multiforme cells treated with 6.25 μM a-solanine versus negative control (culture) treatment..... 592
Output 13.429.: Independent sample T-testing for IGFBP-1 protein corrected mean grey area data for glioblastoma multiforme cells treated with 6.25 μM a-solanine versus negative control (culture) treatment. 592
Output 13.430.: Descriptive statistics for IGFBP-2 protein corrected mean grey area data for glioblastoma multiforme cells treated with 6.25 μM a-solanine versus negative control (culture) treatment..... 593
Output 13.431.: Normality (Shapiro-Wilk) and Equality of Variance (Levene's) assumption checks for pairwise sample testing for IGFBP-2 protein corrected mean grey area data for glioblastoma multiforme cells treated with 6.25 μM a-solanine versus negative control (culture) treatment..... 593
Output 13.432.: Independent sample T-testing for IGFBP-2 protein corrected mean grey area data for glioblastoma multiforme cells treated with 6.25 μM a-solanine versus negative control (culture) treatment. 594
Output 13.433.: Descriptive statistics for IGFBP-3 protein corrected mean grey area data for glioblastoma multiforme cells treated with 6.25 μM a-solanine versus negative control (culture) treatment..... 594
Output 13.434.: Normality (Shapiro-Wilk) and Equality of Variance (Levene's) assumption checks for pairwise sample testing for IGFBP-3 protein corrected mean grey area data for glioblastoma multiforme cells treated with 6.25 μM a-solanine versus negative control (culture) treatment..... 595
Output 13.435.: Independent sample T-testing for IGFBP-3 protein corrected mean grey area data for glioblastoma multiforme cells treated with 6.25 μM a-solanine versus negative control (culture) treatment. 595
Output 13.436.: Descriptive statistics for IGFBP-4 protein corrected mean grey area data for glioblastoma multiforme cells treated with 6.25 μM a-solanine versus negative control (culture) treatment..... 596

Output 13.437.: Normality (Shapiro-Wilk) and Equality of Variance (Levene's) assumption checks for pairwise sample testing for IGFBP-4 protein corrected mean grey area data for glioblastoma multiforme cells treated with 6.25 μM a-solanine versus negative control (culture) treatment..... 596
Output 13.438.: Independent sample T-testing for IGFBP-4 protein corrected mean grey area data for glioblastoma multiforme cells treated with 6.25 μM a-solanine versus negative control (culture) treatment. 597
Output 13.439.: Descriptive statistics for IGFBP-5 protein corrected mean grey area data for glioblastoma multiforme cells treated with 6.25 μM a-solanine versus negative control (culture) treatment..... 597
Output 13.440.: Normality (Shapiro-Wilk) and Equality of Variance (Levene's) assumption checks for pairwise sample testing for IGFBP-5 protein corrected mean grey area data for glioblastoma multiforme cells treated with 6.25 μM a-solanine versus negative control (culture) treatment..... 598
Output 13.441.: Independent sample T-testing for IGFBP-5 protein corrected mean grey area data for glioblastoma multiforme cells treated with 6.25 μM a-solanine versus negative control (culture) treatment. 598
Output 13.442.: Descriptive statistics for IGFBP-6 protein corrected mean grey area data for glioblastoma multiforme cells treated with 6.25 μM a-solanine versus negative control (culture) treatment..... 599
Output 13.443.: Normality (Shapiro-Wilk) and Equality of Variance (Levene's) assumption checks for pairwise sample testing for IGFBP-6 protein corrected mean grey area data for glioblastoma multiforme cells treated with 6.25 μM a-solanine versus negative control (culture) treatment..... 599
Output 13.444.: Independent sample T-testing for IGFBP-6 protein corrected mean grey area data for glioblastoma multiforme cells treated with 6.25 μM a-solanine versus negative control (culture) treatment. 600
Output 13.445.: Descriptive statistics for IGF-1R protein corrected mean grey area data for glioblastoma multiforme cells treated with 6.25 μM a-solanine versus negative control (culture) treatment..... 600
Output 13.446.: Normality (Shapiro-Wilk) and Equality of Variance (Levene's) assumption checks for pairwise sample testing for IGF-1R protein corrected mean grey area data for glioblastoma multiforme cells treated with 6.25 μM a-solanine versus negative control (culture) treatment..... 601

Output 13.447.: Independent sample T-testing for IGF-1R protein corrected mean grey area data for glioblastoma multiforme cells treated with 6.25 μM a-solanine versus negative control (culture) treatment. 601

Output 13.448.: Descriptive statistics for livin protein corrected mean grey area data for glioblastoma multiforme cells treated with 6.25 μM a-solanine versus negative control (culture) treatment..... 602

Output 13.449.: Normality (Shapiro-Wilk) and Equality of Variance (Levene's) assumption checks for pairwise sample testing for livin protein corrected mean grey area data for glioblastoma multiforme cells treated with 6.25 μM a-solanine versus negative control (culture) treatment. 602

Output 13.450.: Welch testing for livin protein corrected mean grey area data for glioblastoma multiforme cells treated with 6.25 μM a-solanine versus negative control (culture) treatment. 603

Output 13.451.:Descriptive statistics for p21 protein corrected mean grey area data for glioblastoma multiforme cells treated with 6.25 μM a-solanine versus negative control (culture) treatment..... 603

Output 13.452.: Normality (Shapiro-Wilk) and Equality of Variance (Levene's) assumption checks for pairwise sample testing for p21 protein corrected mean grey area data for glioblastoma multiforme cells treated with 6.25 μM a-solanine versus negative control (culture) treatment. 604

Output 13.453.: Independent sample T-testing for p21 protein corrected mean grey area data for glioblastoma multiforme cells treated with 6.25 μM a-solanine versus negative control (culture) treatment. 604

Output 13.454.: Descriptive statistics for p27 protein corrected mean grey area data for glioblastoma multiforme cells treated with 6.25 μM a-solanine versus negative control (culture) treatment..... 605

Output 13.455.: Normality (Shapiro-Wilk) and Equality of Variance (Levene's) assumption checks for pairwise sample testing for p27 protein corrected mean grey area data for glioblastoma multiforme cells treated with 6.25 μM a-solanine versus negative control (culture) treatment. 605

Output 13.456.: Independent sample T-testing for p27 protein corrected mean grey area data for glioblastoma multiforme cells treated with 6.25 μM a-solanine versus negative control (culture) treatment. 606

Output 13.457.: Descriptive statistics for p53 protein corrected mean grey area data for glioblastoma multiforme cells treated with 6.25 μM a-solanine versus negative control (culture) treatment..... 606

Output 13.458.: Normality (Shapiro-Wilk) and Equality of Variance (Levene's) assumption checks for pairwise sample testing for p53 protein corrected mean grey area data for glioblastoma multiforme cells treated with 6.25 μM a-solanine versus negative control (culture) treatment. 607
Output 13.459.: Independent sample T-testing for p5 protein corrected mean grey area data for glioblastoma multiforme cells treated with 6.25 μM a-solanine versus negative control (culture) treatment. 607
Output 13.460.: Descriptive statistics for SMAC protein corrected mean grey area data for glioblastoma multiforme cells treated with 6.25 μM a-solanine versus negative control (culture) treatment..... 608
Output 13.461.: Normality (Shapiro-Wilk) and Equality of Variance (Levene's) assumption checks for pairwise sample testing for SMAC protein corrected mean grey area data for glioblastoma multiforme cells treated with 6.25 μM a-solanine versus negative control (culture) treatment. 608
Output 13.462.: Independent sample T-testing for SMAC protein corrected mean grey area data for glioblastoma multiforme cells treated with 6.25 μM a-solanine versus negative control (culture) treatment. 609
Output 13.463.: Descriptive statistics for survivin protein corrected mean grey area data for glioblastoma multiforme cells treated with 6.25 μM a-solanine versus negative control (culture) treatment..... 609
Output 13.464.: Normality (Shapiro-Wilk) and Equality of Variance (Levene's) assumption checks for pairwise sample testing for survivin protein corrected mean grey area data for glioblastoma multiforme cells treated with 6.25 μM a-solanine versus negative control (culture) treatment..... 610
Output 13.465.: Independent sample T-testing for survivin protein corrected mean grey area data for glioblastoma multiforme cells treated with 6.25 μM a-solanine versus negative control (culture) treatment. 610
Output 13.466.: Descriptive statistics for TNF-RI protein corrected mean grey area data for glioblastoma multiforme cells treated with 6.25 μM a-solanine versus negative control (culture) treatment..... 611
Output 13.467.: Normality (Shapiro-Wilk) and Equality of Variance (Levene's) assumption checks for pairwise sample testing for TNF-RI protein corrected mean grey area data for glioblastoma multiforme cells treated with 6.25 μM a-solanine versus negative control (culture) treatment..... 611

Output 13.468.: Independent sample T-testing for TNF-RI protein corrected mean grey area data for glioblastoma multiforme cells treated with 6.25 μM a-solanine versus negative control (culture) treatment. 612
Output 13.469.: Descriptive statistics for TNF-RII protein corrected mean grey area data for glioblastoma multiforme cells treated with 6.25 μM a-solanine versus negative control (culture) treatment..... 612
Output 13.470.: Normality (Shapiro-Wilk) and Equality of Variance (Levene's) assumption checks for pairwise sample testing for TNF-RII protein corrected mean grey area data for glioblastoma multiforme cells treated with 6.25 μM a-solanine versus negative control (culture) treatment..... 613
Output 13.471.: Independent sample T-testing for TNF-RII protein corrected mean grey area data for glioblastoma multiforme cells treated with 6.25 μM a-solanine versus negative control (culture) treatment. 613
Output 13.472.: Descriptive statistics for TNF-a protein corrected mean grey area data for glioblastoma multiforme cells treated with 6.25 μM a-solanine versus negative control (culture) treatment..... 614
Output 13.473.: Normality (Shapiro-Wilk) and Equality of Variance (Levene's) assumption checks for pairwise sample testing for TNF-a protein corrected mean grey area data for glioblastoma multiforme cells treated with 6.25 μM a-solanine versus negative control (culture) treatment. 614
Output 13.474.: Independent sample T-testing for TNF-a protein corrected mean grey area data for glioblastoma multiforme cells treated with 6.25 μM a-solanine versus negative control (culture) treatment. 615
Output 13.475.: Descriptive statistics for TNF-B protein corrected mean grey area data for glioblastoma multiforme cells treated with 6.25 μM a-solanine versus negative control (culture) treatment..... 615
Output 13.476.: Normality (Shapiro-Wilk) and Equality of Variance (Levene's) assumption checks for pairwise sample testing for TNF-B protein corrected mean grey area data for glioblastoma multiforme cells treated with 6.25 μM a-solanine versus negative control (culture) treatment. 616
Output 13.477.: Independent sample T-testing for TNF-B protein corrected mean grey area data for glioblastoma multiforme cells treated with 6.25 μM a-solanine versus negative control (culture) treatment. 616
Output 13.478.: Descriptive statistics for TRAIL R1 protein corrected mean grey area data for glioblastoma multiforme cells treated with 6.25 μM a-solanine versus negative control (culture) treatment..... 617

Output 13.479.: Normality (Shapiro-Wilk) and Equality of Variance (Levene's) assumption checks for pairwise sample testing for TRAIL R1 protein corrected mean grey area data for glioblastoma multiforme cells treated with 6.25 μM a-solanine versus negative control (culture) treatment..... 617
Output 13.480.: Independent sample T-testing for TRAIL R1 protein corrected mean grey area data for glioblastoma multiforme cells treated with 6.25 μM a-solanine versus negative control (culture) treatment. 618
Output 13.481.: Descriptive statistics for TRAIL R2 protein corrected mean grey area data for glioblastoma multiforme cells treated with 6.25 μM a-solanine versus negative control (culture) treatment..... 618
Output 13.482.: Normality (Shapiro-Wilk) and Equality of Variance (Levene's) assumption checks for pairwise sample testing for TRAIL R2 protein corrected mean grey area data for glioblastoma multiforme cells treated with 6.25 μM a-solanine versus negative control (culture) treatment..... 619
Output 13.483.: Independent sample T-testing for TRAIL R2 protein corrected mean grey area data for glioblastoma multiforme cells treated with 6.25 μM a-solanine versus negative control (culture) treatment. 619
Output 13.484.: Descriptive statistics for TRAIL R3 protein corrected mean grey area data for glioblastoma multiforme cells treated with 6.25 μM a-solanine versus negative control (culture) treatment..... 620
Output 13.485.: Normality (Shapiro-Wilk) and Equality of Variance (Levene's) assumption checks for pairwise sample testing for TRAIL R3 protein corrected mean grey area data for glioblastoma multiforme cells treated with 6.25 μM a-solanine versus negative control (culture) treatment..... 620
Output 13.486.: Independent sample T-testing for TRAIL R3 protein corrected mean grey area data for glioblastoma multiforme cells treated with 6.25 μM a-solanine versus negative control (culture) treatment. 621
Output 13.487.: Descriptive statistics for TRAIL R4 protein corrected mean grey area data for glioblastoma multiforme cells treated with 6.25 μM a-solanine versus negative control (culture) treatment..... 621
Output 13.488.: Normality (Shapiro-Wilk) and Equality of Variance (Levene's) assumption checks for pairwise sample testing for TRAIL R4 protein corrected mean grey area data for glioblastoma multiforme cells treated with 6.25 μM a-solanine versus negative control (culture) treatment..... 622

Output 13.489.: Independent sample T-testing for TRAIL R4 protein corrected mean grey area data for glioblastoma multiforme cells treated with 6.25 μM a-solanine versus negative control (culture) treatment. 622
Output 13.490.: Descriptive statistics for XIAP protein corrected mean grey area data for glioblastoma multiforme cells treated with 6.25 μM a-solanine versus negative control (culture) treatment..... 623
Output 13.491.: Normality (Shapiro-Wilk) and Equality of Variance (Levene's) assumption checks for pairwise sample testing for XIAP protein corrected mean grey area data for glioblastoma multiforme cells treated with 6.25 μM a-solanine versus negative control (culture) treatment. 623
Output 13.492.: Independent sample T-testing for XIAP protein corrected mean grey area data for glioblastoma multiforme cells treated with 6.25 μM a-solanine versus negative control (culture) treatment. 624
Output 13.493.: Descriptive statistics for ATG3 protein corrected mean grey area data for glioblastoma multiforme cells treated with 6.25 μM a-solanine versus negative control (culture) treatment..... 624
Output 13.494.: Normality (Shapiro-Wilk) and Equality of Variance (Levene's) assumption checks for pairwise sample testing for ATG3 protein corrected mean grey area data for glioblastoma multiforme cells treated with 6.25 μM a-solanine versus negative control (culture) treatment. 625
Output 13.495.: Independent sample T-testing for ATG3 protein corrected mean grey area data for glioblastoma multiforme cells treated with 6.25 μM a-solanine versus negative control (culture) treatment. 625
Output 13.496.: Descriptive statistics for ATG4A protein corrected mean grey area data for glioblastoma multiforme cells treated with 6.25 μM a-solanine versus negative control (culture) treatment..... 626
Output 13.497.: Normality (Shapiro-Wilk) and Equality of Variance (Levene's) assumption checks for pairwise sample testing for ATG4A protein corrected mean grey area data for glioblastoma multiforme cells treated with 6.25 μM a-solanine versus negative control (culture) treatment..... 626
Output 13.498.: Welch testing for ATG4A protein corrected mean grey area data for glioblastoma multiforme cells treated with 6.25 μM a-solanine versus negative control (culture) treatment..... 627
Output 13.499.: Descriptive statistics for ATG4B protein corrected mean grey area data for glioblastoma multiforme cells treated with 6.25 μM a-solanine versus negative control (culture) treatment..... 627

OUTPUT 13.500.: NORMALITY (SHAPIRO-WILK) AND EQUALITY OF VARIANCE (LEVENE'S) ASSUMPTION CHECKS FOR PAIRWISE SAMPLE TESTING FOR ATG4B PROTEIN CORRECTED MEAN GREY AREA DATA FOR GLIOBLASTOMA MULTIFORME CELLS TREATED WITH 6.25 μM A-SOLANINE VERSUS NEGATIVE CONTROL (CULTURE) TREATMENT..... 628

OUTPUT 13.501.: INDEPENDENT SAMPLE T-TESTING FOR ATG4B PROTEIN CORRECTED MEAN GREY AREA DATA FOR GLIOBLASTOMA MULTIFORME CELLS TREATED WITH 6.25 μM A-SOLANINE VERSUS NEGATIVE CONTROL (CULTURE) TREATMENT. 628

OUTPUT 13.502.: DESCRIPTIVE STATISTICS FOR ATG5 PROTEIN CORRECTED MEAN GREY AREA DATA FOR GLIOBLASTOMA MULTIFORME CELLS TREATED WITH 6.25 μM A-SOLANINE VERSUS NEGATIVE CONTROL (CULTURE) TREATMENT..... 629

OUTPUT 13.503.: NORMALITY (SHAPIRO-WILK) AND EQUALITY OF VARIANCE (LEVENE'S) ASSUMPTION CHECKS FOR PAIRWISE SAMPLE TESTING FOR ATG5 PROTEIN CORRECTED MEAN GREY AREA DATA FOR GLIOBLASTOMA MULTIFORME CELLS TREATED WITH 6.25 μM A-SOLANINE VERSUS NEGATIVE CONTROL (CULTURE) TREATMENT. 629

OUTPUT 13.504.: INDEPENDENT SAMPLE T-TESTING FOR ATG5 PROTEIN CORRECTED MEAN GREY AREA DATA FOR GLIOBLASTOMA MULTIFORME CELLS TREATED WITH 6.25 μM A-SOLANINE VERSUS NEGATIVE CONTROL (CULTURE) TREATMENT. 630

OUTPUT 13.505.: DESCRIPTIVE STATISTICS FOR ATG7 PROTEIN CORRECTED MEAN GREY AREA DATA FOR GLIOBLASTOMA MULTIFORME CELLS TREATED WITH 6.25 μM A-SOLANINE VERSUS NEGATIVE CONTROL (CULTURE) TREATMENT..... 630

OUTPUT 13.506.: NORMALITY (SHAPIRO-WILK) AND EQUALITY OF VARIANCE (LEVENE'S) ASSUMPTION CHECKS FOR PAIRWISE SAMPLE TESTING FOR ATG7PROTEIN CORRECTED MEAN GREY AREA DATA FOR GLIOBLASTOMA MULTIFORME CELLS TREATED WITH 6.25 μM A-SOLANINE VERSUS NEGATIVE CONTROL (CULTURE) TREATMENT. 631

OUTPUT 13.507.: INDEPENDENT SAMPLE T-TESTING FOR ATG7 PROTEIN CORRECTED MEAN GREY AREA DATA FOR GLIOBLASTOMA MULTIFORME CELLS TREATED WITH 6.25 μM A-SOLANINE VERSUS NEGATIVE CONTROL (CULTURE) TREATMENT. 631

OUTPUT 13.508.: DESCRIPTIVE STATISTICS FOR ATG10 PROTEIN CORRECTED MEAN GREY AREA DATA FOR GLIOBLASTOMA MULTIFORME CELLS TREATED WITH 6.25 μM A-SOLANINE VERSUS NEGATIVE CONTROL (CULTURE) TREATMENT..... 632

OUTPUT 13.509.: NORMALITY (SHAPIRO-WILK) AND EQUALITY OF VARIANCE (LEVENE'S) ASSUMPTION CHECKS FOR PAIRWISE SAMPLE TESTING FOR ATG10 PROTEIN CORRECTED MEAN GREY AREA DATA FOR GLIOBLASTOMA MULTIFORME CELLS TREATED WITH 6.25 μM A-SOLANINE VERSUS NEGATIVE CONTROL (CULTURE) TREATMENT..... 632

Output 13.510.: Independent sample T-testing for ATG10 protein corrected mean grey area data for glioblastoma multiforme cells treated with 6.25 μM a-solanine versus negative control (culture) treatment. 633
Output 13.511.: Descriptive statistics for ATG12 protein corrected mean grey area data for glioblastoma multiforme cells treated with 6.25 μM a-solanine versus negative control (culture) treatment..... 633
Output 13.512.: Normality (Shapiro-Wilk) and Equality of Variance (Levene's) assumption checks for pairwise sample testing for ATG12 protein corrected mean grey area data for glioblastoma multiforme cells treated with 6.25 μM a-solanine versus negative control (culture) treatment..... 634
Output 13.513.: Independent sample T-testing for ATG12 protein corrected mean grey area data for glioblastoma multiforme cells treated with 6.25 μM a-solanine versus negative control (culture) treatment. 634
Output 13.514.: Descriptive statistics for ATG13 protein corrected mean grey area data for glioblastoma multiforme cells treated with 6.25 μM a-solanine versus negative control (culture) treatment..... 635
Output 13.515.: Normality (Shapiro-Wilk) and Equality of Variance (Levene's) assumption checks for pairwise sample testing for ATG13 protein corrected mean grey area data for glioblastoma multiforme cells treated with 6.25 μM a-solanine versus negative control (culture) treatment..... 635
Output 13.516.: Independent sample T-testing for ATG13 protein corrected mean grey area data for glioblastoma multiforme cells treated with 6.25 μM a-solanine versus negative control (culture) treatment. 636
Output 13.517.: Descriptive statistics for BECN1 protein corrected mean grey area data for glioblastoma multiforme cells treated with 6.25 μM a-solanine versus negative control (culture) treatment..... 636
Output 13.518.: Normality (Shapiro-Wilk) and Equality of Variance (Levene's) assumption checks for pairwise sample testing for BECN1 protein corrected mean grey area data for glioblastoma multiforme cells treated with 6.25 μM a-solanine versus negative control (culture) treatment..... 637
Output 13.519.: Independent sample T-testing for BECN1 protein corrected mean grey area data for glioblastoma multiforme cells treated with 6.25 μM a-solanine versus negative control (culture) treatment. 637
Output 13.520.: Descriptive statistics for BNIP3L protein corrected mean grey area data for glioblastoma multiforme cells treated with 6.25 μM a-solanine versus negative control (culture) treatment..... 638

Output 13.521.: Normality (Shapiro-Wilk) and Equality of Variance (Levene's) assumption checks for pairwise sample testing for BNIP3L protein corrected mean grey area data for glioblastoma multiforme cells treated with 6.25 μM a-solanine versus negative control (culture) treatment..... 638
Output 13.522.: Independent sample T-testing for BNIP3L protein corrected mean grey area data for glioblastoma multiforme cells treated with 6.25 μM a-solanine versus negative control (culture) treatment. 639
Output 13.523.: Descriptive statistics for DDR2 protein corrected mean grey area data for glioblastoma multiforme cells treated with 6.25 μM a-solanine versus negative control (culture) treatment..... 639
Output 13.524.: Normality (Shapiro-Wilk) and Equality of Variance (Levene's) assumption checks for pairwise sample testing for DDR2 protein corrected mean grey area data for glioblastoma multiforme cells treated with 6.25 μM a-solanine versus negative control (culture) treatment. 640
Output 13.525.: Independent sample T-testing for DDR2 protein corrected mean grey area data for glioblastoma multiforme cells treated with 6.25 μM a-solanine versus negative control (culture) treatment. 640
Output 13.526.: Descriptive statistics for GABARAP protein corrected mean grey area data for glioblastoma multiforme cells treated with 6.25 μM a-solanine versus negative control (culture) treatment..... 641
Output 13.527.: Normality (Shapiro-Wilk) and Equality of Variance (Levene's) assumption checks for pairwise sample testing for GABARAP protein corrected mean grey area data for glioblastoma multiforme cells treated with 6.25 μM a-solanine versus negative control (culture) treatment..... 641
Output 13.528.: Independent sample T-testing for GABARAP protein corrected mean grey area data for glioblastoma multiforme cells treated with 6.25 μM a-solanine versus negative control (culture) treatment. 642
Output 13.529.: Descriptive statistics for LAMP1 protein corrected mean grey area data for glioblastoma multiforme cells treated with 6.25 μM a-solanine versus negative control (culture) treatment..... 642
Output 13.530.: Normality (Shapiro-Wilk) and Equality of Variance (Levene's) assumption checks for pairwise sample testing for LAMP1 protein corrected mean grey area data for glioblastoma multiforme cells treated with 6.25 μM a-solanine versus negative control (culture) treatment..... 643

Output 13.531.: Independent sample T-testing for LAMP1 protein corrected mean grey area data for glioblastoma multiforme cells treated with 6.25 μM a-solanine versus negative control (culture) treatment. 643
Output 13.532.: Descriptive statistics for LC3 protein corrected mean grey area data for glioblastoma multiforme cells treated with 6.25 μM a-solanine versus negative control (culture) treatment..... 644
Output 13.533.: Normality (Shapiro-Wilk) and Equality of Variance (Levene's) assumption checks for pairwise sample testing for LC3A protein corrected mean grey area data for glioblastoma multiforme cells treated with 6.25 μM a-solanine versus negative control (culture) treatment. 644
Output 13.534.: Independent sample T-testing for LC3A protein corrected mean grey area data for glioblastoma multiforme cells treated with 6.25 μM a-solanine versus negative control (culture) treatment. 645
Output 13.535.: Descriptive statistics for LC3B protein corrected mean grey area data for glioblastoma multiforme cells treated with 6.25 μM a-solanine versus negative control (culture) treatment..... 645
Output 13.536.: Normality (Shapiro-Wilk) and Equality of Variance (Levene's) assumption checks for pairwise sample testing for LC3B protein corrected mean grey area data for glioblastoma multiforme cells treated with 6.25 μM a-solanine versus negative control (culture) treatment. 646
Output 13.537.: Independent sample T-testing for LC3B protein corrected mean grey area data for glioblastoma multiforme cells treated with 6.25 μM a-solanine versus negative control (culture) treatment. 646
Output 13.538.: Descriptive statistics for NBS1 protein corrected mean grey area data for glioblastoma multiforme cells treated with 6.25 μM a-solanine versus negative control (culture) treatment..... 647
Output 13.539.: Normality (Shapiro-Wilk) and Equality of Variance (Levene's) assumption checks for pairwise sample testing for NBS1 protein corrected mean grey area data for glioblastoma multiforme cells treated with 6.25 μM a-solanine versus negative control (culture) treatment. 647
Output 13.540.: Independent sample T-testing for NBS1 protein corrected mean grey area data for glioblastoma multiforme cells treated with 6.25 μM a-solanine versus negative control (culture) treatment. 648
Output 13.541.: Descriptive statistics for p62 protein corrected mean grey area data for glioblastoma multiforme cells treated with 6.25 μM a-solanine versus negative control (culture) treatment..... 648

Output 13.542.: Normality (Shapiro-Wilk) and Equality of Variance (Levene's) assumption checks for pairwise sample testing for p62 protein corrected mean grey area data for glioblastoma multiforme cells treated with 6.25 μM a-solanine versus negative control (culture) treatment. 649
Output 13.543.: Independent sample T-testing for p62 protein corrected mean grey area data for glioblastoma multiforme cells treated with 6.25 μM a-solanine versus negative control (culture) treatment. 649
Output 13.544.: Descriptive statistics for Rheb protein corrected mean grey area data for glioblastoma multiforme cells treated with 6.25 μM a-solanine versus negative control (culture) treatment..... 650
Output 13.545.: Normality (Shapiro-Wilk) and Equality of Variance (Levene's) assumption checks for pairwise sample testing for Rheb protein corrected mean grey area data for glioblastoma multiforme cells treated with 6.25 μM a-solanine versus negative control (culture) treatment. 650
Output 13.546.: Independent sample T-testing for Rheb protein corrected mean grey area data for glioblastoma multiforme cells treated with 6.25 μM a-solanine versus negative control (culture) treatment. 651
Output 13.547.: Descriptive statistics for MSK1 protein corrected mean grey area data for glioblastoma multiforme cells treated with 6.25 μM a-solanine versus negative control (culture) treatment..... 651
Output 13.548.: Normality (Shapiro-Wilk) and Equality of Variance (Levene's) assumption checks for pairwise sample testing for MSK1 protein corrected mean grey area data for glioblastoma multiforme cells treated with 6.25 μM a-solanine versus negative control (culture) treatment. 652
Output 13.549.: Independent sample T-testing for MSK1 protein corrected mean grey area data for glioblastoma multiforme cells treated with 6.25 μM a-solanine versus negative control (culture) treatment. 652
Output 13.550.: Descriptive statistics for alpha-synuclein protein corrected mean grey area data for glioblastoma multiforme cells treated with 6.25 μM a-solanine versus negative control (culture) treatment. 653
Output 13.551.: Normality (Shapiro-Wilk) and Equality of Variance (Levene's) assumption checks for pairwise sample testing for alpha-synuclein protein corrected mean grey area data for glioblastoma multiforme cells treated with 6.25 μM a-solanine versus negative control (culture) treatment..... 653

Output 13.552.: Independent sample T-testing for alpha-synuclein protein corrected mean grey area data for glioblastoma multiforme cells treated with 6.25 μM a-solanine versus negative control (culture) treatment. 653
Output 13.553.: Descriptive statistics for U87MG cells treated with 1.00 % DMSO versus 10.00 % DMSO at 72 hours. 654
Output 13.554.: Normality (Shapiro-Wilk) and Equality of Variance (Levene's) assumption checks for pairwise sample testing for U87MG cells treated with 1.00 % DMSO versus 10.00 % DMSO at 72 hours. 654
Output 13.555.: Independent sample T-testing for U87MG cells treated with 1.00 % DMSO versus 10.00 % DMSO at 72 hours. 655
Output 13.556.: Descriptive statistics for U87MG cells treated with with 5.00 μM a-solanine versus 50.00 μM a-solanine dissolved in DMSO at 72 hours. 655
Output 13.557.: Normality (Shapiro-Wilk) and Equality of Variance (Levene's) assumption checks for pairwise sample testing for U87MG cells treated with 5.00 μM a-solanine versus 50.00 μM a-solanine dissolved in DMSO at 72 hours. 655
Output 13.558.: Welch testing for U87MG cells treated with with 5.00 μM a-solanine versus 50.00 μM a-solanine dissolved in DMSO at 72 hours. 656
Output 13.559.: Descriptive statistics for U87MG cells treated with with 5.00 μM a-solanine versus 50.00 μM a-solanine dissolved in DMEM/F12 medium at 72 hours. 656
Output 13.560.: Normality (Shapiro-Wilk) and Equality of Variance (Levene's) assumption checks for pairwise sample testing for U87MG cells treated with 5.00 μM a-solanine versus 50.00 μM a-solanine dissolved in DMEM/F12 medium at 72 hours 656
Output 13.561.: Independent sample T-testing for U87MG cells treated with 5.00 μM a-solanine versus 50.00 μM a-solanine dissolved in DMEM/F12 medium for 72 hours. 657
Output 13.562.: Descriptive statistics for U87MG cells treated with 1.00 % DMSO versus 5.00 a-solanine dissolved in DMSO for 72 hours. 657
Output 13.563.: Normality (Shapiro-Wilk) and Equality of Variance (Levene's) assumption checks for pairwise sample testing for U87MG cells treated with 1.00 % DMSO versus 5.00 μM a-solanine dissolved in DMSO for 72 hours. 657

Output 13.564.: Independent sample T-testing for U87MG cells treated with 1.00 % DMSO versus 5.00 μM a-solanine dissolved in DMSO for 72 hours. 658
Output 13.565.: Descriptive statistics for U87MG cells treated with 10.00 % DMSO versus 50.00 μM a-solanine dissolved in DMSO for 72 hours. 658
Output 13.566.: Normality (Shapiro-Wilk) and Equality of Variance (Levene's) assumption checks for pairwise sample testing for U87MG cells treated with 10.00 % DMSO versus 50.00 μM a-solanine dissolved in DMSO for 72 hours. 658
Output 13.567.: Independent sample T-testing for U87MG cells treated with 10.00 % DMSO versus 50.00 μM a-solanine dissolved in DMSO for 72 hours..... 659
Output 13.568.: Descriptive statistics for U87MG cells treated with 5.00 μM a-solanine dissolved in DMSO versus 5.00 μM a-solanine dissolved in DMEM/F12 medium for 72 hours 659
Output 13.569.: Normality (Shapiro-Wilk) and Equality of Variance (Levene's) assumption checks for pairwise sample testing for U87MG cells treated with 5.00 μM a-solanine dissolved in DMSO versus 5.00 μM a-solanine dissolved in DMEM/F12 medium for 72 hours. 659
Output 13.570.: Independent sample T-testing for U87MG cells treated with 5.00 μM a-solanine dissolved in DMSO versus 5.00 μM a-solanine dissolved in DMEM/F12 medium for 72 hours. 660
Output 13.571.: Descriptive statistics for U87MG cells treated with 50 μM a-solanine dissolved in DMSO versus 50 μM a-solanine dissolved in DMEM/F12 medium for 72 hours. 660
Output 13.572.: Normality (Shapiro-Wilk) and Equality of Variance (Levene's) assumption checks for pairwise sample testing for U87MG cells treated with 50.00 μM a-solanine dissolved in DMSO versus 50.00 μM a-solanine dissolved in DMEM/F12 medium for 72 hours. 660
Output 13.573.: Independent sample T-testing for U87MG cells treated with 05 μM a-solanine dissolved in DMSO versus 50 μM a-solanine dissolved in DMEM/F12 medium for 72 hours. 661

Table of Equations

EQUATION 1.: CALCULATING CELL VIABILITY..... 95

EQUATION 2.: CALCULATING THE RELATIVE WOUND CLOSURE. 96

EQUATION 3.: CALCULATING THE RATE OF RELATIVE WOUND CLOSURE..... 96

EQUATION 4.: CALCULATING THE RETARDATION FACTOR. 96

EQUATION 5.: CALCULATING ΔCt. 97

EQUATION 6.: CALCULATING $\boldsymbol{\Delta\Delta Ct}$. 97

EQUATION 7.: CALCULATING THE CORRECTED TOTAL CELL FLUORESCENCEACKNOWLEDGMENTS. 98

EQUATION 8.: TRANSFORMATION OF FLOW CYTOMETRY PERCENTAGE DETECTED CELLS 98

EQUATION 9.: CALCULATING PROTEIN FOLD CHANGE..... 99

List of abbreviations

α-KG	α-ketoglutarate
Akt	Serine/Threonine Protein Kinase
AMBRA-1	BECN1 regulated autophagy-1
ARE	Antioxidant response Element
ATF6	Activating Transcription Factor 6
Atg	Autophagy-Regulating Protease
ATP	Adenosine Triphosphate
ATRX	α -Thalassemia/Mental Retardation Syndrome X-linked
AUC	Area Under the Curve
Bak	Bcl-2 Killer
Bax	Bcl-2 Associated X
Bcl-2	B-cell lymphoma 2
Bcl-xL	B-cell Lymphoma Extra Large
BECN-1	Beclin-1
Bif-1	Bax-Interacting Factor-1
BSA	Bovine Serum Albumin
BuChe	Butyrylcholinesterase
CCDS	Consensus Coding Sequence
cDNA	Complementary Deoxyribonucleic Acid
CMAX	Peak serum Concentration
CNST	Central Nervous System Tumours
CTCF	Corrected Total Cell Fluorescence

D2HG	(D)2-hydroxyglutarate
DDR	Deoxyribonucleic acid damage respone
DDT	Dithiothreitol
DISC	Death Inducing-Signalling-Complex
DMEM/F12	Dulbecco's Modified Eagle Medium/Nutrient Mixture F-12 HAM
DMSO	Dimethyl Sulfoxide
DNA	Deoxyribonucleic acid
ECM	Endothelial Extra-Cellular Matrix ECM
EDTA	Etheylenediaminetetraacetic acid
EGFR	Epidermal growth factor receptor
ER	Endoplasmic Reticulum
ERK1/2	Extracellular Signal Regulated Kinase
ETC	Electron Transport Chain
FA	Fatty Acids
FITC	Fluorescein Isothiocyanate
FoV	Field of View
FSH	Forward Scatter
GBM	Glioblastoma Multiforme
GC	Guanine-Cytosine
GLUT1	Glucose Transporter 1
GTP	Guanosine Triphosphate
HIF1-α	Hypoxia Inducible Factor 1- α
HRM	High Resolution Melt
IDH	Isocitrate Dehydrogenase

Intdeg	Integrated Density
IRE1	Inositol-requiring enzyme 1
LC3	Light Chain 3
LD50	Concentration required to achieve half the lethal dose
LDHA	Lactate Dehydrogenase
MAP1	Microtubule-Associated protein 1
MAPK	Mitogen-Activated Protein Kinase
MDC	Monodansylcadaverine
MDM2	Mouse Double Minute 2 MDM2
MR	Metabolic Remodelling (
mTOR	Mammalian Target of Rapamycin
mTORC1	mTOR Complex I
NEC	Not-Elsewhere-Classified
NF1	Neurofibromin 1
NOS	Not-Otherwise-Specified
Nrf2	Nuclear Factor Erythroid related factor 2
OMM	Outer Mitochondrial Membrane
PBS	Phosphate buffered saline
PCR	Polymerase Chain Reaction
Pe	Phosphatidylethanolamine
PERK	Protein Kinase R-like Endoplasmic Reticulum Kinase
PFS	Progression-Free Survival
PGA	Potato Glycoalkaloid
PI	Propidium Iodide

PI3K	Phosphoinositide-3 Kinase
PIN1	Peptidylprolyl cis/trans isomerase NIMA-interacting 1
PIP2	Phosphatidylinositol 4,5-Bisphosphate
PIP3	Phosphatidylinositol 3,4,5-Triphosphate
PKD1/2	Phospoinositise-Dependent Protein Kinase Isozymes 1 and 2
PKM2	Pyruvate Kinase isoenzyme M2 isoform
PPI	Protein-Protein interaction
PTEN	Phosphatase and Tensin Homologue Deleted on Chromosome 10
Raf	Serine/Threonine Kinase Rapidly Accelerate Fibrosarcoma
Rf	Retardation Factor
RNA	Ribonucleic acid
ROS	Reactive Oxygen Species
RTKs	Receptor tyrosine kinases
SGOT	Serum Glutamic Oxalacetic Transaminase
SGPT	Serum Glutamic Pyruvic Acid Transaminase
SSC	Side Scatter
T1/2	Half-life
TAE	Tris-Acetate-EDTA
TCA	Tricarboxylic acid cycle
TERT	Telomerase reverse transcriptase promoter
Tm	Melting Temperature
TMAX	Time taken to achieve CMAX
TMZ	Temozolomide
TP53	Tumour Protein 53

UGTs	Uridine Diphosphate-dependent Glycosyltransferase
ULK1/2	Unc-51-Like Kinase 1/2
UPR	Unfolded protein Reponse
UV	Ultraviolet
VEGF	Vascular Endothelial Growth Factor
VEGF	Vascular Endothelial Growth Factor
Vps34	Vacuolar Protein Sortin 34
WHO	World Health Organisation

Chapter 1 Introduction

Glioblastoma multiforme (GBM) is the most commonly occurring malignant brain tumour, representing approximately 50.00 % of all primary malignant central nervous system tumours (CNSTs) (Miller et al., 2021). GBM is classified as a grade-IV glioma, the highest grade afforded by the World Health Organisation (WHO) classification for tumours of glial origin (Louis *et al.,* 2021).

Routine treatment of GBM involves maximum surgical resection (MSR) of the tumour. Administration of adjuvant temozolomide (TMZ), an alkylating chemotherapeutic agent, following MSR has been established as the first line chemotherapeutic treatment for histologically confirmed GBM (Stupp et al., 2005). Despite optimal treatment the prognosis of GBM is still abysmal, with the median survival being estimated at 15 months (Fisher & Adamson, 2021).

Thus, GBM is not only a major health care burden, but also a socio-economic burden that requires costly treatment which has minimal improvement in patient prognosis (Fisher & Adamson, 2021; Stummer et al., 2012). This emphasises the necessity and urgency to identify novel and cost-effective putative therapeutic strategies for treating GBM (Pearson & Regad, 2017).

Recent research on alternative anti-cancer therapeutic approaches has focused on bioactive compounds derived from natural sources such as plants and microorganisms (Colapietro et al., 2020; Liang et al., 2017). A growing body of literature has recently demonstrated the effectiveness of ∝-solanine, a glycoalkaloid which can be derived from *Solanum* plants, as a putative chemotherapeutic anti-cancer drug (Hassan *et al*., 2020 Luo *et al*., 2021).

∝-solanine's anti-cancer potential has been extensively studied against several different cancers and this phytochemical is thought to inhibit cancer cell growth, proliferation and metastasis primarily by modulating Akt/MTOR and Ras/Rak/ERK pathways as well as MMP expression. Moreover ∝-solanine has been documented to induce both apoptotic and autophagic death, however the exact mode of cell death induced by ∝-solanine is still disputed (Arslan & Yerer, 2018; Friedman et al., 2005; Gao et al., 2020; Gao et al., 2006; Gouhar et al., 2022; Hasanain et al., 2015; Ji & Gao, 2012; Krisnamurti et al., 2022; Lee et al., 2004; Lin et al., 2020; Lu et al., 2010; Lv et al., 2014; Meng et al., 2016; Mohsenikia et al., 2013, 2016; Pan et al., 2016; Shen et al., 2014; Sun et al., 2014; Wang et al., 2016; Yuanyuan Wang et al., 2016; Wen et al., 2016; Yamashoji & Matsuda, 2013; Yan et al., 2020; Jinhui Yang et al., 2019; Zhang et al., 2016; Zheng et al., 2020; Zou et al., 2021).

The effectiveness of ∝-solanine as a cytotoxic agent against GBM in comparison to TMZ has not been investigated. Moreover, current evidence demonstrating the cytotoxic effect of ∝-solanine against GBM may require further scrutiny due to limitations and inconsistencies in the available published literature (Guo et al., 2019). Furthermore, given the increasing incidence and poor prognosis of GBM, investigating the anti-cancer potential of ∝-solanine against this malignant tumour is appropriate and important to confirm or rule-out whether ∝-solanine can be a considered as a putative drug for treating GBM, while striving to better understand the mode of action of this phytochemical.

1.1. Aim

To investigate the effectiveness of ∝-Solanine as an anti-cancer agent on commercially available GBM cell lines in comparison to the current chemotherapeutic standard-of-care *in-vitro* (TMZ).

1.2. Objectives

- To investigate the effectiveness of ∝-solanine on GBM cell viability, migration, and invasion in-comparison to TMZ.
- To evaluate to presence of stimulated cell death by ∝-solanine on a cellular level through fluorescent imaging and flow cytometric techniques.
- To assess any dysregulation in cell death signalling induced ∝-solanine on a molecular level using real time quantitative polymerase chain reaction (rt-qPCR) and protein techniques.
- To assess the effect of ∝-solanine treatment on the expression of proteins which take part in the regulation of apoptosis and autophagy using antibody arrays.
- To increase knowledge on the current understanding on the precise mode of cell death induced by ∝-solanine by identify dysregulated cell death pathways through protein-protein (PPI) network analysis.

Chapter 2 Literature review

2.1. Glioblastoma multiforme

2.1.1. Epidemiology of Glioblastoma Multiforme

CNSTs account for a disproportionally high global morbidity, mortality and associated socioeconomic burden due to their substantial cost of complex treatment regimes and malignant potential (El Hage et al., 2021). GBM accounts for the majority of primary CNST, representing approximately 50 % of all malignant and 14 % of the overall CNSTs (Miller et al., 2021).

Miller *et al.* (2021) estimated the overall incidence of GBM to be 3.23 per 100,000 population. Age-adjusted incidence rates stratified by sex follow similar trends with GBM being more prevalent in males across all ages (5.60 vs 3.50 per 100,000 population). GBM is primarily diagnosed in adults $\geq$ 65 years of age, however, this has been reported to vary between studies (Grochans et al., 2022). Irrespective of age, the median survival associated with GBM is less than 15 months in optimally treated patients, with $\leq$ 1.00 % surviving beyong 10 years following diagnosis (Tykocki & Eltayeb, 2018).

Recent literature suggests that the annual incidence of GBM is on the rise, with an increase from 3.27 to 7.34 per 100,000 population in men and 2.00 to 4.45 per 100,000 population in women between 1995 and 2017 in England (Wanis et al., 2021). This trend has also been noted in Malta, with an increase in the overall incidence from 0.73 to 4.49 per 100,000 population between 2007 and 2017 (Grech et al., 2020). This may be attributed to ageing populations and procurement of improved imaging

technology (Grech et al., 2020), while being propelled by changing socioeconomic and regional circumstances (Engberg et al., 2022; Miller et al., 2021).

Notwithstanding, the increasing incidence and abysmal prognosis act to increase GBM's already high burden of disease. Consequentially, this necessitates an urgent global effort to study novel drugs to increase GBM patient survival.

2.1.2. Classification of Glioblastoma Multiforme

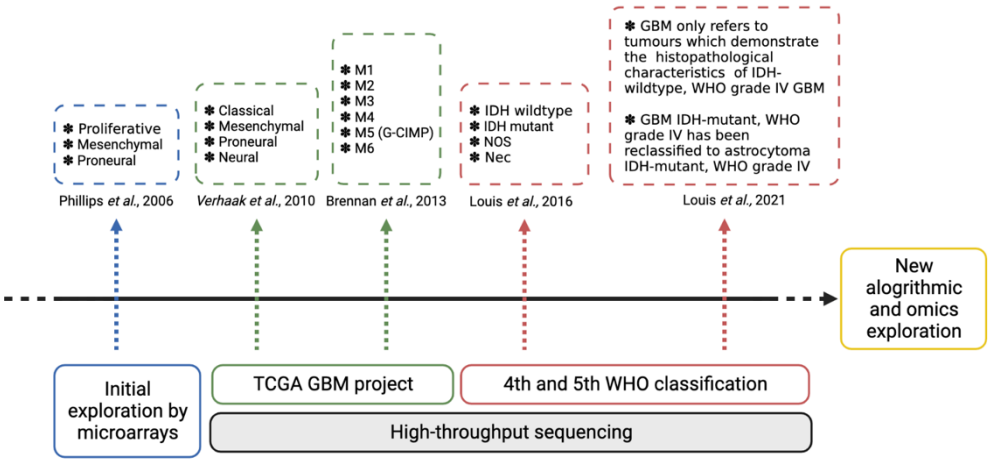
The World Health Organization (WHO) categorization for CNSTs has become the globally accepted benchmark for the identification and classification of gliomas, which afforded GBM the highest status possible (grade-IV), due to its poor prognosis and aggressiveness (Lee et al., 2018). GBM has been classified as primary or secondary depending on presenting clinicopathologic features. Primary GBM arises as grade WHO IV *de-novo*, without evidence of preceding lower grades. Secondary GBM evolves from grade II or III astrocytoma which progressively increase in size and aggressiveness until grade-IV transformation occurs (Ohgaki & Kleihues, 2013). Nevertheless, the mechanisms governing GBM are still unclear, with significant intra- and inter-tumoural heterogeneity engendering histopathological ambiguity complicating the establishment precise classification systems (Lee et al., 2018).

Since the turn of the 21st century, great strides have been made towards gaining insights into GBM molecular biology, begetting several classification systems (Figure 2.1) (Zhang et al., 2020). Initial exploration by microarrays classified GBM into proliferative, mesenchymal and proneural subgroups based on diffeent transcriptional signatures between the sub-types (Phillips et al., 2006). High-throughput sequencing

updated Phillips *et al.* (2006)'s classification system by categorising the previously proneuroal subtype into distinct neural and classical groups (Verhaak et al., 2010). Brennan *et al.* (2013) further stratifyied of GBM sub-types based on different methylation signatures.

Further work with high throughput sequencing identified variable IDH expression between GBM subtypes. This formed the basis of the fourth WHO classification system for gliomas, wherein four neoplasms have been discerned. GBM IDH-wildtype is the most prevalent GBM sub-type, occurring *de-novo.* GBM IDH-mutant generally encompasses secondary GBM, while GBM not-otherwise-specified (NOS) relates to instances where the presence of IDH mutations could not be ascertained due to insufficient histological or molecular samples for testing purposes. The fourth category not-elsewhere-classified (NEC), details cases wherein the necessary biomedical testing has been done; however, the results do not match any of the other categories listed by the WHO 2016 classification system. Such circumstances can arise when there are inconsistencies or deviations among the histological, genetic, and clinical characteristics of the tumor.

In 2021, WHO significantly updated its classification of CNSTs and categorised GBM under 'adult-type diffuse gliomas'. Most noticeably GBM IDH_{mutant} WHO grade-IV has been reclassified to astrocytoma-IDH_{mutant}, WHO grade-IV. GBM should now solely refer to GBM IDH-wildtype. Moreover, a grade III IDH-wildtype glioma may now be upgraded to glioblastoma with advanced molecular testing (Louis et al., 2021), and gliomas can only be denoted as GBM if they occur as IDH-*wildtype* grade-IV *de-novo.*



Phillips *et al.* (2006)	Proneural		Proliferative		Mesenchymal
Verhaak *et al.* (2006)	Proneural		Neural	Classical	Mesenchymal
Brennan *et al.* (2013)	M5 (G-CIMP)	M6	N.A.	M3, M4	M1, M2
Louis *et al.* (2016)	GBM IDH-mutant, WHO Grade IV		GBM IDH-wildtype, WHO Grade IV		
Louis *et al.* (2021)	Astrocytoma IDH-mutant, WHO Grade IV		GBM IDH-wildtype, WHO Grade IV		

Figure 2.1.: Frameworks for classifying glioblastoma multiforme. The development of several classification systems for glioblastoma multiforme (GBM) has resulted from advances in molecular biology, with initial microarray analysis identifying three subgroups: proliferative, mesenchymal, and proneural (Phillips et al., 2006). This classification has since been updated by high-throughput sequencing, which has separated the proliferative subgroup into neural and classical groups (Verhaak et al., 2010). Based on methylation signatures, this classification system was further stratified into subtypes (Brennan et al., 2013). The fourth World Health Organization (WHO) classification system for gliomas is based on variable isocitrate dehydrogenase (IDH) expression and distinguishes four neoplasms: GBM IDH-wildtype, GBM IDH-mutant, GBM not-otherwise-specified, and GBM not-elsewhere-classified (Louis et al., 2016). The World Health Organization updated its classification of central nervous system tumors in 2021, reclassifying GBM IDH-mutant as astrocytoma-IDH-mutant and reserving the term GBM only for IDH-wildtype grade IV de-novo tumors (Louis et al., 2021). Obtained from Cuschieri & Baron (2023).

Despite the major conceptual advancement, the WHO 2021 CNST classification may act as a double-edged sword. The new classification should decrease heterogeneity in prognosis and treatment delivered against grade-IV tumours, while it will inevitably result in delays in intiating therapy on account of the time required to scrutinize over tumours' correct classification (Horbinski et al., 2022). A paradigm shift must occur in GBM epidemiological research since approximately 10 % of all patients with GBM are

now considered to have WHO grade IV astrocytoma on account of GBH IDH-mutated WHO grade IV tumours' reclassification. Moreover, the new classification framework will act to clarify reporting of pre-clinical studies, while also casting doubt onto the validitity of preivous research on GBM which does disclose the IDH-status of cells of tissues being used. Hence, future research should ensure to disclose the IDH status of the cells and/or tissues used to ensure comparability and generalisability of results, especially when considering the disease's intra- and inter-tumour heterogeneity (Cuschieri & Baron, 2023).

2.1.3. An overview of Glioblastoma Multiforme molecular biology

2.1.3.1. Major genetic alterations in Glioblastoma Multiforme in the context of the World Health Organisation 2021 Central Nervous System Tumour Classification

Wildtype-IDH is the has been recognised as the defining molecular characteristic of GBM by the WHO 2021 classification of CNSTs (Louis et al., 2021), since IDH-wildtype tumours are clinical distinct from other gliomas expressing IDH-mutations (Molinaro et al., 2019). *Wildtype* IDH protein canonically catalyses the decarboxylation of isocitrate to produce α-ketoglutarate (α-KG). In GBM, expression of *wildtype*-IDH confers resistance to cell death and tumour progression, by upregulating the production of fatty acids (FAs) and reactive oxygen species (ROS) scavenging (Lunt & Vander Heiden, 2011). Under hypoxic conditions, a shift from oxidative phosphorylation to glycolysis occurs. GBM cells rely on glutamine-dependent reductive carboxylation by IDH for lipid biosynthesis, since glucose intake is primarily utilized for the production of adenosine

triphosphate (ATP) (Alzial et al., 2022). GBM IDH-*wildtype* also commonly display amplification and mutation of mouse double minute 2 (MDM2) homolog, epidermal growth factor receptor (EGFR) upregulation or mutation and mutations in, telomerase reverse transcriptase (TERT) promoter. Gain of chromosome 7 and loss of heterozygosity in q10 (chromosome 10) are also frequently present in GBM (Masui et al., 2016).

Conversely, *mutant* IDH1 metabolises α-KG to the oncometabolite (D)2-hydroxyglutarate (D2HG), which upon accumulation inhibits αKG-dependent dioxygenases leading to epigenetic changes (Figueroa et al., 2010; Sasaki et al., 2012; Turcan et al., 2012), hypoxia inducible factor 1- α (HIF1α) stabilization (Zhao et al., 2009), and alterations in cellular differentiation status (C. Lu et al., 2012). *Mutant*-IDH1 also triggers a metabolic remodelling towards oxidative phosphorylation (van Noorden et al., 2021). IDH1/2 mutation also decreases intracellular antioxidant agents, which together making tumour cells more susceptible to radiation and chemotherapy (Inoue et al., 2016; Lu et al., 2017; Núñez et al., 2019; Wang et al., 2015), thus giving IDH-*mutant* tumours better prognosis in comparison to IDH-*wildtype* tumours (Alzial et al., 2022). IDH-*mutant* gliomas are known to intrinsically express O6-methylguanine-DNA methyltransferase promoter methylation (MGMT) (75%) and tumour protein 53 (TP53) mutations, together with functional loss (mutation or deletion) of α - Thalassemia/Mental Retardation Syndrome X-linked (ATRX) (Masui et al., 2016; Velázquez Vega & Brat, 2017).

Both *mutant* and *wildtype* IDH enzymes respectively constitute cornerstones of tumour aggressiveness and dynamic metabolic plasticity, allowing tumour cells to cope

with multifactorial cellular stress (El Khayari et al., 2022). Notwithstanding, most of the research assessing the molecular biology and response to therapy of GBM has been conducted without specifying the IDH status of the cells and tissues used. Thus, this literature review will discuss studies which use nomenclature pertaining to WHO 2016 classification of CNSTs and readers should keep in mind that any generalisations made henceforth are applicable to grade IV gliomas, but the specifics pertaining to GBM $IDH_{wildtype}$, WHO grade IV may not be specified.

2.1.3.2. Glioblastoma Multiforme metabolism: glycolysis and the Warburg effect

GBM cells demonstrate deregulation of numerous metabolic pathways (El Khayari et al., 2022). Acquired mutations or hypoxic conditions promote metabolic remodelling (MR) by directing metabolism in GBM cells towards glycolysis (Guntuku et al., 2016). This phenomenon is known as the Warburg effect, and like the majority of cancers, is a hallmark of GBM (Vander Heiden et al., 2009). The shift toward glycolysis ensures the availability energy required for proliferation, invasion, and adaptation (Agnihotri & Zadeh, 2016), and has been associated with poorer prognosis (Schwartzentruber et al., 2012; Toyonaga et al., 2017).

With the strong shift towards glycolysis, efforts have been made to better understand the expression of several key glycolytic enzymes. In particular pyruvate kinase (PK) is crucial for glycolysis as it mediates the ultimate step of the glycolytic metabolic pathway to produce pyruvate and generate ATP (Porporato et al., 2011).

Although it is not typically found in the normal adult brain (Kefas et al., 2010), the M2 isoform of pyruvate kinase (PKM2) is highly expressed in GBM cells (Mukherjee et al., 2013), primarily due to the switching from PKM1 to PKM2 isoforms (Desai et al., 2014). PKM2 expression results in increased glycolytic turnover, maintenance of mitochondrial activity and regulation of tumour growth (Gilbert et al., 2014; Heddleston et al., 2009; Mukherjee et al., 2013; Sutendra & Michelakis, 2013). In addition, HIF1-α directly targets PKM2 to enhance tumour progression (Bensinger & Christofk, 2012), by suppression of mitochondrial function through decreased ROS production (Christofk et al., 2008; Mukherjee et al., 2013; Sutendra & Michelakis, 2013). This induces a positive feedback loop which amplifies the expression of HIF1-α (Bensinger & Christofk, 2012), and thus PKM2 is a crucial driver of the Warbug effect (Ruiz-Rodado et al., 2020).

2.1.3.3. Glioblastoma Multiforme oncogenic Receptor Tyrosine Kinase signalling

Receptor tyrosine kinases (RTKs) are a group of transmembrane receptors that share a similar structure, consisting of three primary domains: (1) an extracellular ligand-binding domain, (2) a hydrophobic transmembrane domain, and (3) an intracellular tyrosine kinase domain. Binding of the ligand leads to receptor dimerization, followed by autophosphorylation of the tyrosine kinase domain, initiating downstream signaling primarily through the PI3K-AKT-mTOR and Ras-MAPK-ERK pathways. These signaling cascades play crucial roles in cell proliferation, invasion, and angiogenesis.Thus, they can be considered as oncogenic and act as putative targets for the development of novel therapies (Pearson & Regad, 2017). Here, the main pathways downstream to RTK signalling, primarily downstream to the EGFR, are discussed since

there pastways the foremost RKT signalling cascades inovled in GBM oncogenesis (Figure 2.2).

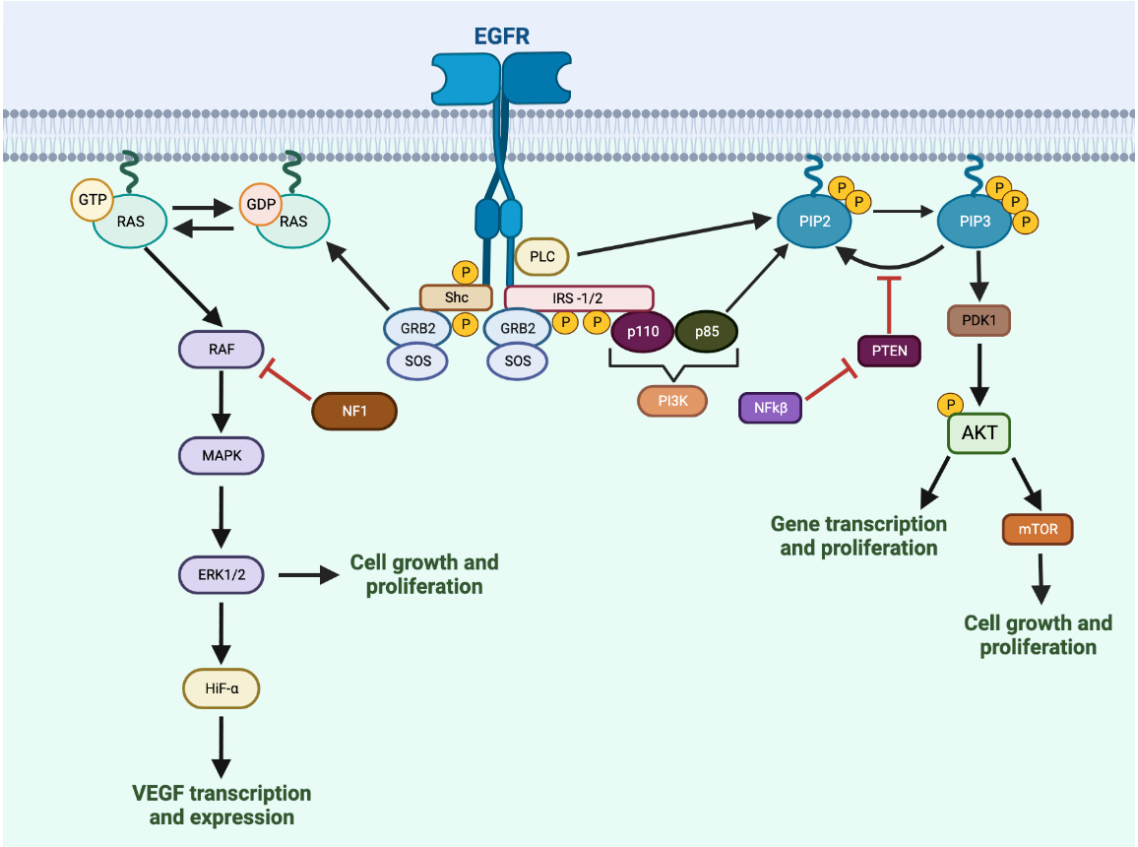


Figure 2.2.: Receptor tyrosine kinase signalling in frequently deregulated in glioblastoma multiforme. The most frequently altered RTK signaling pathways in glioblastoma multiforme (GBM) are the PI3K-Akt-mTOR and Ras-Raf-ERK1/2 pathways (Li et al., 2016; Nørøxe et al., 2016). The PI3K-Akt-mTOR signaling pathway controls cell migration, invasion, and apoptosis. RTK phosphorylation activates the pathway, which produces PIP3 and mediates Akt activation. PTEN is the pathway's negative regulator. ActiveAkt can both activate mTOR and inhibit pro-apoptotic proteins (Li et al., 2016; Majewska & Szeliga, 2017; Sami & Karsy, 2013). Ras-Raf-ERK1/2 signaling controls cell proliferation, migration, and survival. Raf activation is regulated by NF1, which acts as a negative regulator of the pathway (Carrasco-García et al., 2014; Sanchez-Ortiz et al., 2014) [AKT -serine/threonine protein kinase; EGFR – epidermal growth factor receptor; ERK1/2 - extracellular signal regulated kinase; GTPase - guanosine triphosphate; MAPK - mitogen-activated protein kinase; mTOR - mammalian target of rapamycin; NF1 - neurofibromin 1; PI3K - phosphoinositide-3 kinase; PIP2 - phosphatidylinositol 4,5-bisphosphate; PIP3 - phosphatidylinositol 3,4,5-triphosphate; PKD1/2 - phospoinositise-dependent protein kinase isozymes 1 and 2; PTEN - phosphatase and tensin homologue; Raf - rapidly accelerate fibrosarcoma; VEGF - vascular endothelial growth factor]. Obtained from Cuschieri & Baron (2023).

2.1.3.3.1. PI3K-Akt-mTOR signalling

The primary role of the PI3K-Akt-mTOR pathway is to regulate cell invasion and migration. However, this pathway also contributes to the regulation of apoptosis.

Phosphorylation of receptor tyrosine kinases (RTKs) activates phosphoinositide-3 kinase (PI3K), which in turn phosphorylates phosphatidylinositol 4,5-bisphosphate (PIP2) to generate phosphatidylinositol 3,4,5-triphosphate (PIP3). This leads to the activation of serine/threonine protein kinase (Akt) by promoting its localization to the inner plasma membrane. Akt activation involves phosphorylation at threonine 308 by phosphoinositide-dependent protein kinase isozyme 1 (PKD1) and at serine 473 by phosphoinositide-dependent protein kinase isozyme 2 (PKD2). The signaling of Akt is regulated by the tumor suppressor phosphatase and tensin homologue deleted on chromosome 10 (PTEN), which is located on chromosome 10. PTEN catalyzes the dephosphorylation of PIP3, serving as a negative regulator of PI3K/Akt/mTOR signaling.Active Akt can phosphorylate a myrad of downstream signalling molecules. Noteably, Akt activates mammalian target of rapamycin (mTOR) which integrates numerous updream signalls into effector actions by activating transcription factors invovled in cell growth and proliferation. Moreover, Akt also acts as a negative regulator of apoptosis by directly inhibiting pro-apoptoic proteins, or their transcription (Carrasco-García et al., 2014; Majewska & Szeliga, 2017; Mao et al., 2012; Pearson & Regad, 2017).

Constitutative activation of the PI3K-Akt-mTOR signalling cascades is crucial for GBM proliferation. This pathway is disregulated in approximately 70 % of GBMs, either via loss or PTEN function or EGFR amplification (Zhi et al., 2009). EGFR overexpression occurs in about 35 % of tumours, and its amplification results in upregulation of the PI3K pathway. In addition, a ligand-independent mutant EGFvIII is present in roughly 40 % of GBM tumours (Huang et al., 2007), and 40 % of tumours also present with loss of

function PTEN mutations (Wang et al., 1997), together acting to upregulate PI3K-Akt-mTOR signalling leading to uncontrolled cell growth.

2.1.3.3.2. Ras-Raf-ERK1/2 signalling

Ras-Raf-ERK1-2 signaling is initiated by RTK signaling to control cellular processes such as proliferation, migration, and survival. RTKs drive the phosphorylation of Rat sarcoma virus (Ras) proteins, small guanosine triphosphate (GTP)ases bound to the inner cell membrane. The formation GTP-Ras activates the serine/threonine kinase rapidly accelerate fibrosarcoma (Raf) leading to to mitogen-activated protein kinase (MAPK) cascade activation and eventual downstream extracellular signal regulated kinase (ERK1/2) phosyphorlation (Carrasco-García et al., 2014; Majewska & Szeliga, 2017; Mao et al., 2012; Pearson & Regad, 2017). The activation of Raf is regulated by the tumour suppressor neurofibromin 1 (NF1) as this protein inhibits the dephosphorylation of GTP-RAS (Sanchez-Ortiz et al., 2014), thus acting as a negative regulator of the Ras-Raf-ERK1/2 pathway. ERK1/2 activates a number of downstream substrates and may also translocate to the nucleus to modulate the activity of numerous transcription factors which together regulate cell proliferation, metabolism and survival. ERK1/2 also functions to phosphorylate HIF-1α, which in-itself promotes tumorigenesis and activation of vascular endothelial growth factor (VEGF) (Carrasco-García et al., 2014; Majewska & Szeliga, 2017; Mao et al., 2012; Pearson & Regad, 2017).

Mutations affecting the Ras-Raf-ERK1/2 pathway occur in roughly 2 % of GBM tumours. However, elevated RAS activity is frequently observed, underscoring the significance of this pathway in the oncogenesis of GBM. (Cancer Genome Atlas Research

Network, 2008; Holland et al., 2000). Additionally 18 % of GBM patients demonstrate mutated or deleted NF1 (Brennan et al., 2013; Cancer Genome Atlas Research Network, 2008). This permits constitutiave activation of this pathway further promoting unregulated oncogenesis.

2.1.3.4. Glioblastoma Multiforme cell death signalling pathways

Cancer transformation is a multifaceted process in which a sequence of events, typically initiated within a single cell, leads to the development of a detectable tumor. Various aspects of cancer transformation influence the progression and aggressiveness of cancer cells. Genomic instability and disrupted DNA damage response (DDR) can result in mutations that contribute to cancer transformation (Ou & Schumacher, 2018). When the level of DNA damage surpasses the capacity of cancer cells to repair, such as in response to anticancer drugs, cells are directed towards programmed cell death pathways, primarily apoptosis (Lin et al., 2017). However, cancer cells can also engage other cell death pathways, such as autophagy, as a response to the accumulation of harmful cellular components. The precise triggers and role of autophagy in cancer cells remain unclear, as conflicting reports suggest both tumor-promoting and tumor-suppressive roles for this pathway (Zhang et al., 2018).

2.1.3.4.1. Apoptosis

Apoptosis is a crucial homeostatic mechanism which balances corporal development, maintence and cell death. Apoptosis is activated when cells become damaged and intracellular mechanisms fail to repair the damage. This process can be

achieved through two prinicpal molecular pathways which both result in the proteolytic activation of caspases (Figure 2.3) (Trejo-Solís et al., 2018).

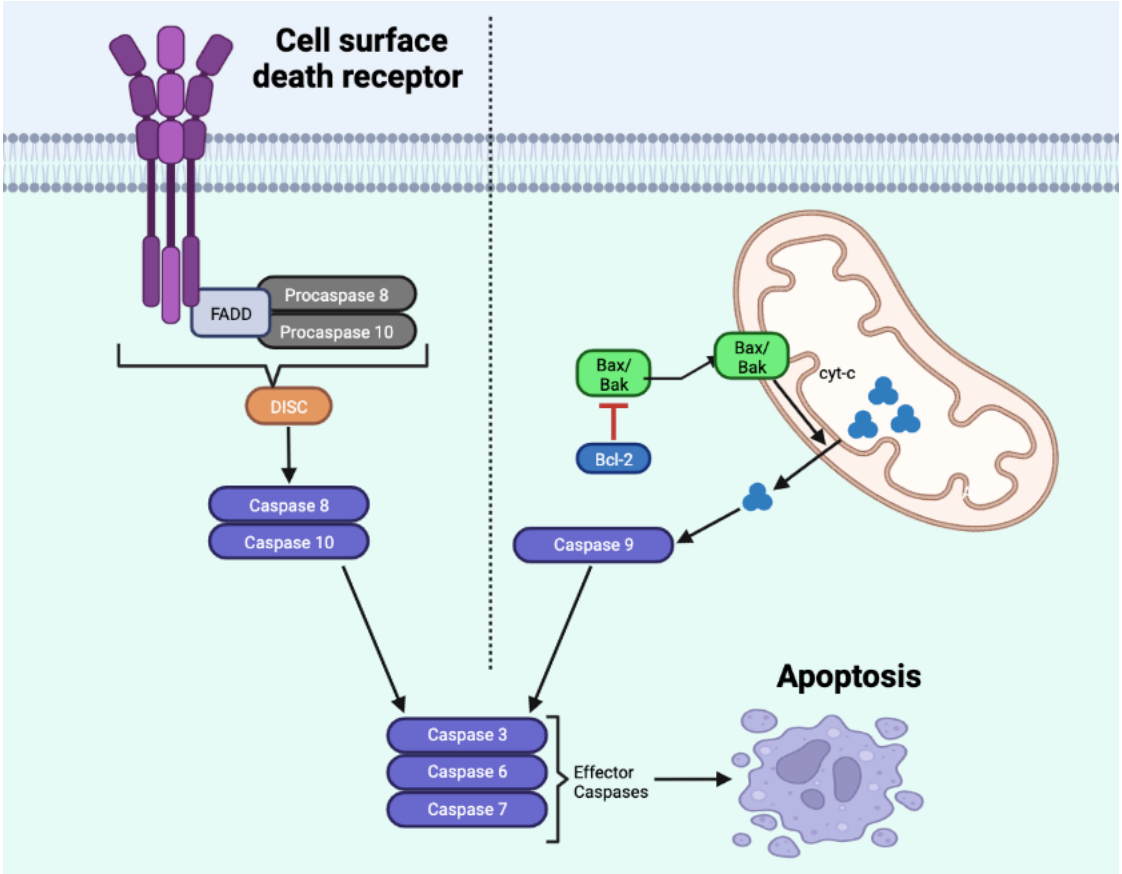


Figure 2.3.: Mechanisms of apoptotic cell death. [A] The docking of extracellular pro-apoptotic ligands on cell surface death receptors initiates the extrinsic apoptotic pathway, resulting in the formation of a death-inducing signalling complex (DISC). The DISC dimerizes procaspases, resulting in the active form of the proteins and triggering apoptosis. Procaspase-8 cleaves to caspase-8, which activates effector caspases until cell death occurs (Pawlowska et al., 2018; Trejo-Solís et al., 2018). [B] The intrinsic apoptotic pathway, which is independent of death receptors, is activated by severe cell stress. B cell lymphoma 2 (Bcl-2) family proteins that promote or inhibit cell death can be found on the inner mitochondrial membrane. Bcl-2 can either promote cell death by promoting the release of other pro-apoptotic proteins like cytochrome-C (Cyt-c), or it can prevent cell death by inhibiting cyt-c release via the pro-apoptotic proteins Bcl-2 associated X (Bax) and Bcl-2 killer (Bak) (Hockenbery, 2010). Cyt-c then associates with procaspase-9 to form an apoptosome, which activates effector caspases to initiate apoptosis (Valdés-Rives et al., 2017). Cyt-c release also disrupts the electron transport chain (ETC) and increases reactive oxygen species (ROS) synthesis (Moroni et al., 2001). Obtained from Cuschieri & Baron (2023).

2.1.3.4.1.1. Intrinsic apoptotic pathway

The mitochondrial or intrinsic apoptotic pathway is triggered from within the cell as a response to severe cellular stress, independent of death receptors. Severe cellular

stress leads to the activation of pro-apoptotic B-cell lymphoma 2 (Bcl-2) family proteins, which play a role in regulating cell death. Bcl-2 can either promote apoptosis by causing outer mitochondrial membrane (OMM) permeabilization, leading to the release of other pro-apoptotic proteins from the mitochondria to the cytosol, or it can counteract apoptotic death by preventing the release of cytochrome c (cyt-c) through pro-apoptotic proteins such as Bcl-2-associated X (Bax) and Bcl-2 killer (Bak), which regulate OMM permeability (Hockenbery, 2010; Wu et al., 2014).

Cytosolic cyt-c forms a complex called the apoptosome with apoptotic protease activating factor-1 (Apaf-1) and initiator procaspase-9. The procaspase-9 is cleaved, resulting in the activation of caspase-9, which dissociates from the apoptosome and further activates effector caspases, including caspases-3, -6, and -7, ultimately leading to the execution of apoptosis. Effector caspases activate nucleases, specific proteins that terminate metabolic functions, reorganize the cytoskeleton, and sever connections with neighboring cells (Valdés-Rives et al., 2017). The presence of cyt-c in the cytosol also disrupts the electron transport chain (ETC), reducing energy production and increasing the generation of reactive oxygen species (ROS) (Moroni et al., 2001).

2.1.3.4.1.2. Extrinsic pathway

The extrinsic apoptotic pathway is initiated by the binding of proapoptotic ligands to death receptors on the cell surface, leading to the formation of a complex known as the death-inducing signaling complex (DISC). This complex determines

procaspase autoactivation by dimerisation to yield active proteins, ensuring the onset of apoptosis (Pawlowska et al., 2018; Trejo-Solís et al., 2018) .

2.1.3.4.1.3. Glioblastoma multiforme and apoptosis

GBM cells demonstrate intrinsic deregugulation of apoptosis (Valdés-Rives et al., 2017), which may confer resistance against treatment due to upregulatgion in anti-apoptotitc proteins and downregulationof pro-apoptic proteins, favouring survival (Krakstad & Chekenya, 2010). Elevated levels of anti-apoptotic proteins Bcl-2 or B-cell lymphoma extra-large (Bcl-xL) in GBM have been linked to increased invasion, migration, and resistance to apoptosis (Stegh et al., 2007). Likewise, GBM cases that exhibit resistance to apoptosis often show upregulation of Bcl-2 or Bcl-xL and downregulation of pro-apoptotic proteins Bax and Bak, which have been associated with unfavorable clinical outcomes (Ruano et al., 2008; Steinbach & Weller, 2004; Strik et al., 1999; Tyagi et al., 2002). Consequently, increased expression of Bax is likely to confer a survival advantage, while upregulation of Bcl-2 is linked to a worse prognosis, as it inhibits the release of cyt-c and the formation of the apoptosome (Trejo-Solís et al., 2018).

Differential caspase expression has also been oberved in GBMpatient dervised tissues and cell lines. Increased expression of procaspase-3 was correlated with increased sensitivity to chemotherapy and increased progression-free survival (PFS) (Murphy et al., 2013). Similarly, dysregulation of pro-apaoptoic genes procaspase-8 and-7 noted in patient derived tissue suggested dysregulation in the formation of DICS, and thus decreased caspase activity resulting in reduced apoptosis (Blahovcova et al., 2015).

2.1.3.4.2. Autophagy

Autophagy is a catabolic cellular process that allows cells to adjust to stressful conditions by recycling proteins and undergoing the degradation of unnecessary or detrimental components through lysosomal digestion (Trejo-Solís et al., 2018). This process is also cytoprotective as it contributes to the removal of misfolded proteins facilitating regulation of growth, metabolism and survival (Ryter et al., 2013). Autophagic mechanism are characterised into three main types; (1) macroautophagy; microautophagy; and (3) chaperone-mediated autophagy (Trejo-Solís et al., 2018). Here, macroautophagy, henceforth referred to as autophagy, will be discussed.

Autophagy is a complex cascade of phosphatases, kinases and GTPases. At the onset of this cascade, organelles or proteins destined for destruction are surrounded by an autophagosome, which once mature fuses with a lysosome to enable hydrolyic enzymes to disgest the contents of these vacuoles (Trejo-Solís et al., 2018). This process has been described to be devided into five main processes (Figure 2.4), with Beclin-1 (BECN-1) and autophagy-regulating protease (Atg4) being key regulators of this process (Maruyama & Noda, 2017; Wirawan et al., 2010).

Initiation of autophagy is triggered by conditions of cell stress. This results in the inactivation of mTOR complex I (mTORC1) (an inhibitor of this pathway) leading to the phosphorylation of mATG13 and FIP200 by the Unc-51-Like kinase1/2 (ULK1/ULK2) to induce the formation of the autophagasome (Jung et al., 2009; Kim et al., 2011). In nucleation of the autophagosome, cytosolic components are recuirted to from omegasomes (phagophore assembly sites) (Law et al., 2017; Polson et al., 2010).

Vacuolar protein sortin 34 (Vps34) is activated consequent to protein complex formation consisting of BECN1, Atg15 and p150 (Morris et al., 2015). BECN1 acts as a gating regulator of autophagy. When bound to activating molecule in BECN1 regulated autophagy-1 (AMBRA-1) and Bax-interacting factor-1 (Bif-1) BECN1 upregulates autophagy, while binding to Bcl-2 inhibits autophagy (Cao & Klionsky, 2007; Russell et al., 2013).

The maturation of the autophagosome involves two key steps that are regulated by two ubiquitin-like protein conjugation systems: Atg8-phosphatidylethanolamine (PE) and Atg5-Atg12-Atg16. The initial compartments of the autophagosome expand, facilitated by the binding of Atg12 to Atg5 and subsequent conjugation with Atg16. Once the expansion of the autophagosome is complete, the protein complex Atg5-Atg12-Atg16 dissociates, initiating the second step of maturation. In this step, the microtubule-associated protein 1 light-chain 3 complex (MAP1-LC3 or Atg8) is released, forming the cytosolic isoform LC3-I. The cleavage of LC3 by Atg4B is a key regulatory event in autophagosome formation and serves as a marker for the induction of autophagy (Yang et al., 2015). Subsequently, Atg7 and Atg3 conjugate LC3-I to PE, forming LC3-II, which remains within the autophagosome until it is degraded (Wild et al., 2014). Once mature, the autophagosome is transported to lysosomes, where the membranes of the two organelles fuse, and hydrolases are released into the autophagolysosome to degrade and recycle cellular components (Monastyrska et al., 2009).

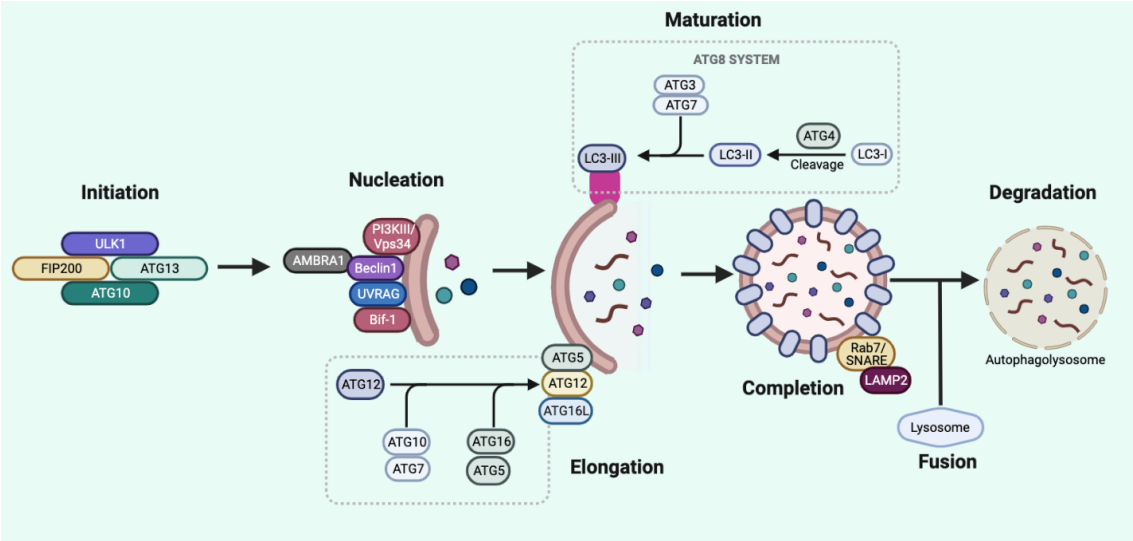


Figure 2.4.: Formation of the autophagasome. Autophagosome formation can be triggered by a variety of stimuli and necessitates the inhibition of mTOR1, which inhibits autophagy (Trejo-Solís et al., 2018). Unc-51-Like Kinase 1/2 (ULK1/ULK2) activation phosphorylates mATG13 and FIP200, resulting in autophagosome formation. BECN1, an autophagy gating regulator, binds to various proteins to either promote or inhibit autophagy. The PI3KC3 protein is the master regulator of autophagy, with two complexes controlling its function. Atg8-PE and Atg5-Atg12-Atg16 protein systems are involved in two stages of autophagosome maturation. LC3/Atg8 is cleaved to form LC3-I, which is then conjugated with PE by Atg7 and Atg3 to form LC3-II, signaling the initiation of autophagy. Lastly, To degrade and recycle cellular components, autophagosomes fuse with lysosomes (Cao & Klionsky, 2007; Jung et al., 2009; Kim et al., 2011; Law et al., 2017; Monastyrska et al., 2009; Morris et al., 2015; Polson et al., 2010; Russell et al., 2013; Wild et al., 2014; Yu et al., 2019). Obtained from Cuschieri & Baron (2023).

2.1.3.4.2.1. Autophagy in Glioblastoma Multiforme

In GBM autophagy can be induced by internal, such as mTOR activation, and external stimuli. The foremost external stimuli driving autophagy in GBM are hypoxia and anti-cancer therapy. Hypoxia iduces a state of starvation and autophagy is activated by BECN1 phosphorylation via the HIF-1α -BECN1 signaling pathway, to increase energy availability by degredation of superfluous cellular compenents (Chu et al., 2012). In fact, baseline autophagy has been observed to be increased in hypoxic areas of GBM tumours (Bronisz et al., 2020), with overexpression cytosolic BECN1. This indicates autophagy's necessary adaptive role for the survival of GBM (Denton et al., 2012; Park et al., 2017). Similarly, in response to chemotherapy, upregulated autophagy has been associated

with a worse progrnosis coupled with more agressive clinical behaviour of GBM tumours, demonstrating autophagy's survival advantage. This highlights how autophagy can be a mechanism by which cancers evade therapy, leading to protumoural adaptive reponse (Galavotti et al., 2013; Li et al., 2019; Tamrakar et al., 2019; Wen et al., 2019; Zhao et al., 2015). Notwithstanding, it should be noted that numerous studies highlight the anti-tumoural function of autophagy by demonstrating the excessive activation of the autophagic leading to mass autophagic vacuolization without of the condensation of chromatin. The role of mass autophagy activation in response to therapy is still a subject of controversy, as it remains uncertain whether it contributes to cell death or if it represents a last-ditch effort for cellular survival. (Bustos et al., 2020; Lim et al., 2021; Morselli et al., 2009; Yun & Lee, 2018).

2.1.3.5. Role of oxidative and Endoplasmic Reticulum stress in Glioblastoma Multiforme molecular biology

2.1.3.5.1. Oxidative stress

Oxidative stress denotes the imbalance between ROS, generalised as oxygen carry molecules which have reactive properties such radicals (eg superoxide and hydroxyl) and non-radicals (eg peroxide), and the capacity to repair consequent oxidative damage or scavenge reactive intermediates (Olivier et al., 2020). The precise effect of ROS in cancer cells is still uncertain with two main paradigms polarising the debate (Olivier et al., 2020). The "threshold concept for cancer therapy" concept dictates that as ROS levels increase, the ratio between antioxidants and ROS is maintained until equilibrium is reached, after which reduction of antioxidants or

increases in ROS production will result in cell death or increased sensitivity to therapy (Kong et al., 2000).

The second paradigm suggest that when both healthy and tumour cells are subject to ROS producing exogenous agents, the ROS levels within tumour cells will increase more rapidly in comparison to healthy cells to induce cell death (Wang & Yi, 2008). The elevated production in ROS within cancer cells will trigger oncogenesis by dysregulating DNA repair mechanisms begetting an accumulation of DNA damage, together with protein and lipid damage (Kong et al., 2000). Thus, the initiation of cell death consequent to oxidative stress in cancer cells is a possible survival mechanism initiated when antioxidant machinery is unable to reduce intracellular ROS levels (Kong et al., 2000).

In GBM, ROS activate numerous transcription factors, mainly HIF-1α and nuclear factor erythroid 2-related factor 2 (Nrf2) (Liu et al., 2022). Upon detection of oxidative stress, Nrf2 dissociated from its inhibitor to translocate to the nucleus to interact with anti-oxidant response elements (AREs) to regulate the expression of anti-oxidant genes (Reuter et al., 2010). Nrf2 mediates regulatory HIF-1α signalling in response to oxidative stress. HIF-1 alpha is upregulated in tumours with high Nrf2 activity, since Nrf2 binds to the ARE responsible for the transcription of HIF-1α (Lacher et al., 2018). The effect of hypoxia and downstream signalling of HIF-1α in response oxidative stress is further discussed in Section 2.1.3.7.4.

2.1.3.5.2. Endoplasmic reticulum stress

The endoplasmic reticulum (ER) functions to synthesize lipids and proteins (Aoyama-Ishiwatari & Hirabayashi, 2021). When unfolded proteins accumulate in the endoplasmic reticulum (ER) and reactive oxygen species (ROS) are present, ER stress is induced, leading to the activation of the unfolded protein response (UPR). The primary function of the UPR is to facilitate proper protein folding and restore ER homeostasis. (Gonzalez-Gronow et al., 2021). ER stress can also be generated via exogenous stress and the build-up of deleterious metabolites, noteably ROS, which affect the production of proteins and lipids. ER stress can induce the expression of glucose regulatory and other ER molecular chaperones to protect cell proliferation (Gonzalez-Gronow et al., 2021). Under continual ER stress inositol-requiring enzyme 1 (IRE1) protein kinase R-like endoplasmic reticulum kinase (PERK), and activating transcription factor 6 (ATF6) signaling pathways are initiated to result in the downstream autophagic pathways (Kavitha et al., 2015; D. Zhang et al., 2017), with ATF6 being recognised as a marker for endoplasmic reticulum stress (Dadey et al., 2016; Prell et al., 2019). Hence, persistent activation of the unfolded protein response (UPR) due to cellular stress might play a protective role in the oncogenesis of glioblastoma (GBM) by promoting cell death and preventing the accumulation of misfolded proteins (Shi et al., 2021). Conversely, inducing ER stress through external agents could lead to widespread cell death, making it a promising therapeutic target against GBM (Kim & Kim, 2018).

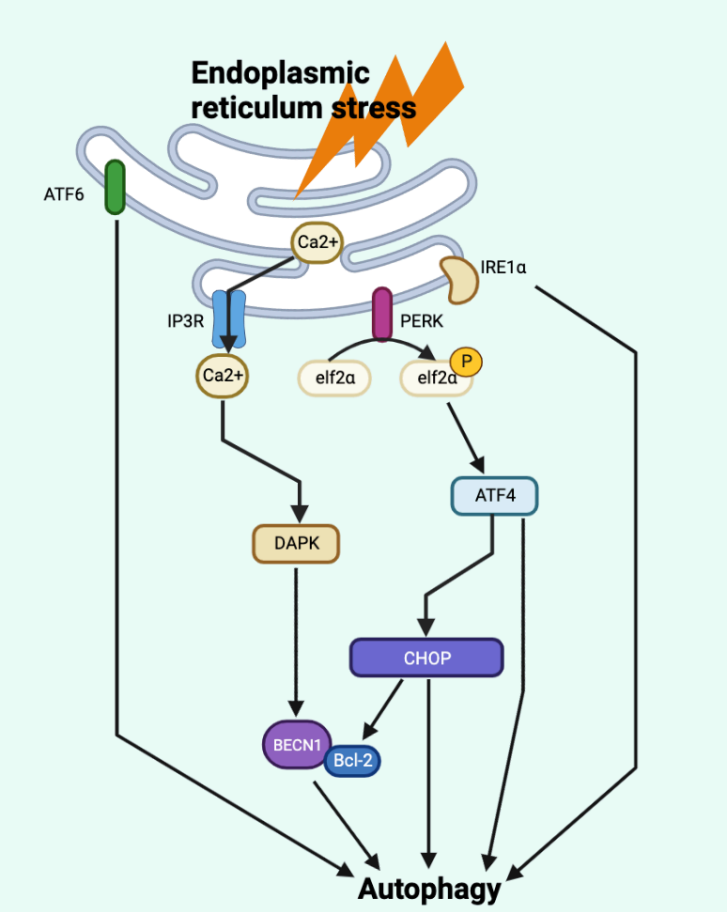


Figure 2.5.: Endoplasmic reticulum stress resulting in autophagy. Endoplasmic reticulum (ER) stress can also induce autophagy and, as a result, affect cell fate (Yadav et al., 2014). Under continuous ER stress, signaling pathways such as protein kinase Rlike endoplasmic reticulum kinase (PERK), inositolrequiring enzyme 1 (IRE1), and activating transcription factor 6 (ATF6) are activated to transduce the downstream autophagic pathways [Bcl-2 - B-cell lymphoma 2 (Bcl-2); Chop - C/EBP homologous protein; Dapk - Death-associated protein kinase; elf2α - eukaryotic translation initiation factor-2α; Ip3r - Inositol 1,4,5-trisphosphate receptor] (Kavitha et al., 2015; Zhang et al., 2017) Adapted from Cuschieri & Baron (2023).

2.1.3.6. Hypoxia and angiogenesis in glioblastoma multiforme molecular biology

A characteristic feature of GBM is intra-tumoural hypoxic regions and assoicated necrosis (Papale et al., 2020). To withstand such harsh conditions, GBM cells trigger physiological angiogenesis to guarante the necessary supply of oxygen and nutrients (Balandeh et al., 2021). The induction of angiogensis is directly regulated by the balancing of anti- and pro- angiogenic factors. Hypoxia triggers the stabilization of the pro-angiogenic transcription factor HIF-1α, leading to the expression of various proteins and the secretion of other pro-angiogenic growth factors (Fitsialos et al., 2008; Stacker

et al., 2001; Wise et al., 2011). Among these factors, vascular endothelial growth factor (VEGF) plays a crucial role. VEGF binds to its receptor, contributing to the degradation of the extracellular matrix (ECM) and basement membranes of endothelial cells. This process leads to the remodeling of ECM components, facilitating the generation of a new matrix that supports stromal cells and enhances the migration and proliferation of endothelial cells, ultimately resulting in the formation of capillary tube structures (Lakka & Rao, 2008). As newly formed endothelial vessels mature, they become surrounded by a more stable vascular basement membrane, synthesized by mural cells, leading to the establishment of stable blood vessels (Hong et al., 2014). Therefore, the induction of angiogenesis by hypoxic conditions enables GBM to withstand adverse conditions.

2.1.3.7. Cross talk in glioblastoma multiforme molecular signalling

Cancer cell molecular biology is highly complex, with significant crosstalk between signalling cascades which are often reported to be distinct (Hon et al., 2021). Here, the interplay between EGFR and cell death signalling in GBM is discussed (Figure 2.6).

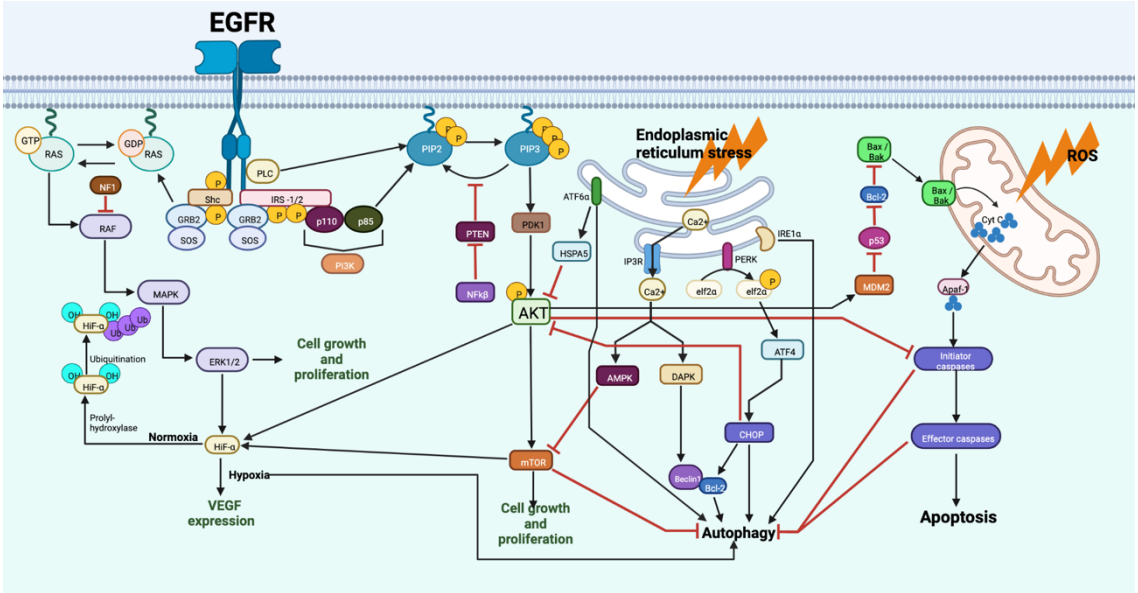


Figure 2.6.: Crosstalk between epidermal growth factor receptor and cell death signalling. Autophagy and apoptosis have common upstream contributing regulator signalling cascades. Primarily, PI3K-Akt-mTOR and Ras-Raf-ERK signalling significantly regulate cell proliferation and invasions. Consequently, this epidermal growth factor receptor (EGFR) signalling pathways are intertwined with both apoptotic and autophagic cell death to direct cell proliferation or death [Akt – serine/threonine protien kinase; AMPK – inositol triphosphate receptor AMP-activated protein kinase; Apaf-1 – apoptotic protease activating factor-1; ATF6 – activating transcript factor 6 Bak – Bcl-2 killer; Bax – Bcl-2 associated X; Bcl-2 – B-cell lymphoma; BECN1 – beclin-1; CHOP – C/EBP homologous protein; Cyc-c – cytochrome-C; DAPK – dominant-negative and constitutively active death-associated protein kinase; Elf-2 α – eukaryotic translation initiation factor-2α; ERK1/2 – extracellular signal regulated kinase 1/2; HIF-1α – hypoxia inducible factor 1; HSPA5 – heat shock protein family A (Hsp70) member 5; IRE1 – inositol-requring enzyme 1; MAPK – mitogen-activated protein kinase ; mTOR – mammalian target of rapamycin; NF-κB – nuclear factor kappa B; NF1 – neurofibromin-1; PDK1 – protein kinase isozyme 1; PERK – protein kinase R-like endoplasmic reticulum kinase; PI3K – phosphoinositide-3 kinase; PIP2 – phosphatidlyinositol 4,5-bisphosphate; PIP3 – phosphatidylinositol 3,4,5-triphosphate; PLC – phospholipase C; PTEN – phosphatase and tensin homologue deleted on chromosome ten; Raf – rapidly accelerate fibrosarcoma; Ras – rat sarcoma virus; VEGF – vascular endothelial growth factor] (Trejo-Solís et al., 2018). Adapted from Cuschieri & Baron (2023).

2.1.3.7.1. Dynamic relationship between apoptosis and autophagy

Apoptosis and autophagy are intricately intertwined, with the inducition of either cell death pathway being initiated by the inhibition of the other. Significant overlap regarding the regulatory machinery between both apoptosis and autophagy exits, with both cell death pathways having common upstream contirbuting signalling pathways (namely EGFR-PI3K-Akt-mTOR) and common regulatory proteins (such as Bcl-2 family proteins and BECN-1) (Trejo-Solís et al., 2018).

The BECN1/Bcl-2 complex exerts inhibitory effects on autophagy in nutrient-rich conditions by preventing the interaction of BECN1 with the PI3K complex, which is responsible for autophagosome formation (Gump & Thorburn, 2011; Mathew et al., 2009). However, during starvation, the interaction between BECN1 and Bcl-2 is induced, promoting autophagic death. This complex is regulated by pro-apoptotic proteins that bind to Bcl-2, favoring apoptosis (Luo & Rubinsztein, 2010; Maiuri et al., 2007). Additionally, caspase-3-mediated degradation of BECN1 inhibits autophagy (Rubinstein et al., 2011). Therefore, the regulation of BECN1 by apoptotic components determines

the inhibition or activation of the autophagic process, depending on intra- and extracellular factors (Mukhopadhyay et al., 2014). Initiator and effector caspases further inhibit autophagy by degrading Atg3, Atg5, and BECN1, thereby inducing apoptosis and preventing the assembly of autophagy machinery (Ojha et al., 2015). The fragmentation of BECN1 (Ojha et al., 2015) has been reported to translocate to the mitochondria and promote the release of pro-apoptotic factors into the cytosol, amplifying the apoptotic response (Zhu et al., 2010).

Similarly, Atg proteins have been implicated in the regulation of apoptosis. Atg5 serves as a signaling mediator between autophagy and apoptosis, as it regulates autophagosome formation through its interaction with Atg12, and it increases susceptibility to apoptotic stimuli when autophagy is inhibited (Yousefi et al., 2006). Additionally, Atg5 associates with Bcl-xL, inhibiting its anti-apoptotic function (Levin-Salomon et al., 2014). Atg12 induces mitochondrial apoptosis by inhibiting Bcl-2, which leads to the activation of Bax, permeabilization of the outer mitochondrial membrane (OMM), release of cytochrome c, and subsequent activation of effector caspases (Rubinstein et al., 2011).

2.1.3.7.2. Interplay between cell death and RTK-PI3K-Akt-mTOR signalling

Autophagic regulation by RTK-PI3K-Akt-mTOR signalling is poorly understood (Fan & Weiss, 2012), with the majority of literature originating from observing autophagy following amdinsitration of Akt/mTOR dual inhibitors. Protoncogene MDM2 is upregulated by Akt, which results in downstream inhibition of Bad, inhibiting the inductiong of apoptosis (Datta et al., 1997). Excessive activation of the PI3K-Akt-mTOR pathway hinders autophagy, whereas suppression of this pathway promotes autophagy.

The mTORC1 complex plays a critical role in governing the autophagic process. During periods of ample nutrients, mTORC1 becomes activated and impedes autophagy. However, under conditions of starvation or low energy, AMP-activated protein kinase (AMPK) is activated, leading to the inactivation of mTORC1 and subsequent initiation of autophagy (Xia et al., 2020).

2.1.3.7.3. EGFR and PKM2, ROS

EGFR signalling acts to upregulate the expression of PKM2 (Yang et al., 2012). In addition, via the Ras-Raf-ERK1/2 pathway, EGFR signalling induces ERK2 to phosphorylate PKM2 facilitating its binding with peptidylprolyl cis/trans isomerase NIMA-interacting 1 (PIN1), prompting the translocation of PKM2 to the nucleus. This increases glucose transporter 1 (GLUT1) and lactate dehydrogenase A (LDHA) expression shifting metabolism towards aerobic glycolysis promoting the Warburg effect (Yang et al., 2012). PKM2 expression is associated with the production of ROS (Kurihara-Shimomura et al., 2018; Li et al., 2016; Taniguchi et al., 2016); however, the exact nature of this association is still undetermined.

According to Qi et al. (2017), increased levels of PKM2 have been associated with reduced production of reactive oxygen species (ROS). However, a study by Shuvalov et al. (2020) reported that overexpression of PKM2 led to elevated mitochondrial membrane potential, resulting in an increase in ROS production. Notwithstanding, substantial evidence indicates that ROS has a negative effect on PKM2 (Brandi et al., 2016; Liang et al., 2019; Wang et al., 2019; Yu et al., 2019; Zhang et al., 2019). RNA expression of PKM2 is not inhibited by ROS, and the decreased expression is attributed

to PKM2 degradation (Duraipandy et al., 2018). The interplay between ROS and PKM2 may also sensitise cells to ROS (Duraipandy et al., 2018), by inducing the mitochondrial PKM2 translocation where it interacts with and phosphorylates Bcl-2 resulting in inhibition ROS-induced apoptosis (Liang et al., 2017).

2.1.3.7.4. HIF-1α, oxidative stress, EGFR and cell death signalling cross talk

HIF-1α is a central protein with important roles in regulating metabolism to ensure that the biosynthetic demands are met (Lo Dico et al., 2018). Under conditions of abundant oxygen supply, the activation of oncogenic signaling pathways, including the PI3K-Akt and MAPK-ERK pathways, leads to an increase in the expression of HIF-1α at the transcriptional level. This upregulation of HIF-1α promotes enhanced glucose utilization (Rankin & Giaccia, 2008). The loss of PTEN in GBM has also been demonstrated to enhance HIF-1α transcription by the unregulated activation of PI3K-Akt-mTOR pathway (Muh et al., 2014). Similarly, overexpression of EGFR or the presence of EGFRvIII also results in constitutive Ras-Raf-Erk1/2 signalling, which additionally upregulates HIF-1α expression (Velpula et al., 2013). In hypoxic conditions, GBM cells undergo a metabolic shift from oxygen-dependent efficient ATP production through mitochondrial oxidative phosphorylation to a less efficient process known as cytoplasmic glycolysis (Shen et al., 2015).Under such circumstances HIF-1α reduces mitochondrial respiration to inhibit aberrant ROS leakage from the ETC, safe guarding tumour survival by preventing ROS production. In the presence of ROS, HIF-1α protects cells from oxidative damage by inducing pyruvate dehydrogenase kinase 1 (PDK1) (Velpula et al., 2013). PKM2 controls HIF-1α activity by increasing its interaction to

hypoxia response elements (HREs), leading to the upregulation of HIF-1α target gene expression. HIF-1α activation also leads to an upregulation of anti-apoptotic members of the Bcl-2 family, thereby inhibiting cell apoptosis (Wang et al., 2016).

2.1.3.7.5. Hypoxia, ER stress and cell death signalling

Hypoxia can stimulate an adaptive response to promote cell proliferation and survival, as well as angiogenesis (Shi et al., 2021). Hypoxia may directly, or through the production of ROS, lead to ER stress which upregulates numerous proteins. In particular, the upregulation of ATF6 results in the inhibition of C/EBP homologous protein (CHOP) which subsequently acts to inhibit Bcl-2 family proteins and the translocation of the Bax to mitochondria. This in turn induces the intrinsic apoptotic pathway and autophagy (Shuvalov et al., 2020).

Moreover, hypoxia directs GBM cells towards aerobic glycolysis resulting in a decrease in cytosolic pH due to the increased production of lactate. Such acidic stress may not only contirbute to apoptosis as a consequence to ER stress (Berghauser Pont et al., 2015; Vasilatos et al., 2013), but also initiate apoptosis directly by caspase activation (W.-J. Huang et al., 2011). It should be noted that acid stress has also been observed to upregulate VEGF expression as an pro-angiogenic survival mehcanism (Redjal et al., 2016; W. Zhang et al., 2014).

2.1.3.8. Glioblastoma multiforme molecular characteristics which confer therapeutic resistance

Like other cancers, GBM has a plethora of different pathways which can be activated or silenced to induce therapeutic resistance. Namely, GBM cells demonstrate significant heterogeneity and hypermutation leading to therapeutic resistance (Wang et al., 2016; Yuhao Wang et al., 2019).

GBM exhibits intratumoural, intertumoral, molecular and functional heterogeneity (Patel et al., 2014; G. Wang et al., 2016), and an increase in tumour heterogeneity was associated with a decrease in patients' survival (Medema et al., 2013; Wang et al., 2016). Like other cancers, heterogeneity in GBM can be explained by tumour stem cells and clonal evolution theory. GBM stem cells (GSC) are intratumorally cells capable of increased proliferation and differentiation and are account for the beginning and maintenance of tumours following treatment (Marjanovic et al., 2013).

The theory of clonal evolution suggests that successive mutations give rise to clonal expansions, which thrive under specific stress conditions such as acidosis, hypoxia, and treatment. Epigenomic alterations can also confer advantageous characteristics to tumor subpopulations, facilitating the rapid development of clonal outgrowths (Marjanovic et al., 2013).

Furthermore, within the same tumour, multiple subtypes of GBM exist, each characterized by distinct molecular profiles, and exhibiting varying clinical responses (Sottoriva et al., 2013).Different subpopulations may demonstrated varying degrees of dysregulated RKT signalling may activated numerous downstream pathways which confer crucial role in therapeutic resistance and GBM recurrence (Cheng & Guo, 2019; Cruickshanks et al., 2017; F. Liu & Mischel, 2018), making extremely difficult to selected

targeted therapy (Dymova et al., 2021). Furthermore, cells within the same tumour demonstrate differential expression of genes leading to varied intratumorally oncogenic signalling, stress response mechanisms and proliferation (Bao et al., 2006).

Hypermutation is a common feature of GBM, and it is assumed that this phenomenon arises due to *de-novo* pathways assigned to constitutive defects in DNA polymerase and pathways involving mismatch repair (MMR) genes. These pathways often occur after treatment with alkylating agents (Daniel et al., 2019), however the emergence of hypermutations may also occur due to GSCs (Dymova et al., 2021). Whether or not hypermutation poses a better or worse clinical outcome is still debated, however mouse models demonstrate a decrease in tumour growth with an increasing mutational burden (McFarland et al., 2017), making cells less aggressive and more amendable to additional treatment (Dymova et al., 2021).

2.1.4. Current Glioblastoma Multiforme standard-of-care

The current standard-of-care approach against for GBM IDH-*wildtype* WHO grade IV involves maximal safe resection (MSR). Resection is generally followed by concomitant chemoradiotherapy, consisting of TMZ and radiotherapy with subsequent maintenance administration of TMZ (Figure 2.7) (Stupp et al., 2005).

TMZ, an orally administered alkylating agent, exerts its effectiveness by inducing DNA alkylation/methylation, primarily targeting the O^6 position of guanine residues (Stupp et al., 2005). Re followed by chemoradiotherapy is also indicated for recurrent GBM (Figure 2.7), where chemotherapy may also consist of carmustine (BCNU) and lomustine bevacizumab (BVZ) (Table 2.1). BVZ inhibits the action of VEGF by binding to

its receptor on endothelial cells, reducing tumour angiogenesis (Pope et al., 2011). This approach towards treating GBM is dependent on patients' Karnofsky performance status (KPS), where supportive care is indicated for patients with a KPS < 60% (Weller et al., 2019).

Despite optimal treatment, median overall survival for GBM patients is still approximately 14.6 months (Fisher & Adamson, 2021; Stummer et al., 2012). This limited efficacy is caused by the development of intrinsic resistance to TMZ and/or drug-resistant phenotypes (G. Liu et al., 2006; Sakariassen et al., 2007). Intrinsic resistance arises when GBM inherently exhibits methylated guanine residues, while acquired resistance occurs due to activation of PI3K-Akt-mTOR pathway as a result of to DNA damage and tumour cell death (Ben Mabrouk et al., 2017; X. Li et al., 2016). Moreover, TMZ demonstrates indiscriminate cytotoxicity leading to considerable side effects, further hampering the drug's use against GBM (Silva et al., 2020). Thus, it is important continue striving towards developing new therapy with lower toxicity and increased efficacy to overcome GBM's chemotherapeutic resistance.

Table 2.1.: Chemotherapeutic agents currently indicated against Glioblastoma multiforme. Temozolomide (TMZ) is the current gold-standard chemotherapeutic agent for treating glioblastoma multiforme (GBM). Carmustine (BCNU); Lomustine (CCNU) and bevacizumab (BVZ) are currently indicated against recurrent GBM (Fisher & Adamson, 2021; Pope et al., 2011; Stupp et al., 2005; Weller et al., 2019) [OS – overall survival; PFS – progression free survival].

	Approved for	Mode of action	6-month PFS (OS in months)	Complications
Temozolomide (TMZ)	All GBM	• Nonspecific alkylating agent • Induces mismatch repair in DNA by methylating guanine at the O^6 position	53.90% (14.60 – 16.10)	• Haematologic toxicity (16 %) • thrombocytopenia (12 %) • neutropenia (7 %) • leukopenia (7 %)
Carmustine (BCNU)	Recurrent GBM	• Nonspecific alkylating agent. • Causes DNA and RNA crosslinking in dividing cells • Binds to, and modifies glutathione reductase	/ (11.75)	• Pulmonary toxicity (<30 %), ocular toxicity (>10 %) and bone marrow suppression (>10 %)
Lomustine (CCNU)	Recurrent GBM	• Nonspecific alkylating agent • Causes DNA and RNA crosslinking in dividing cells	/ (11.50)	• Haematologic toxicity (50 %)
Bevacizumab (BVZ)	Recurrent GBM	• Therapeutic antibody • Binds and inhibits VEGF protein	36% (9.30) in recurrent GBM	• Hypertension (6 – 11 %) • Thromboembolic events (3 – 12 %) • Gastrointestinal perforation (1.50 – 5.40 %) • Cerebral bleeding (2.00 – 5.30 %) • Proteinuria (2.70 – 11.40 %)

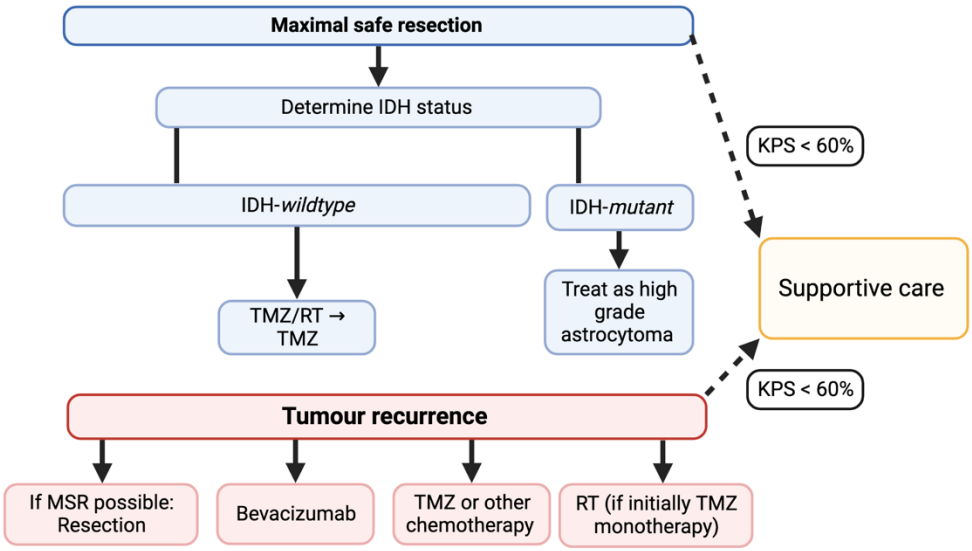


Figure 2.7.: Current treatment pathways against Glioblastoma Multiforme. Current treatment involves maximal safe resection (MSR) coupled with chemoradiotherapy. Treatment for resistant tumours involves MSR where possible and chemotherapy consisting of bevacizumab, lomousine and/or carmustine [IDH – isocitrate dehydrogenase; KPS – karnofsky performance score; RT – radiotherapy; TMZ – temozolomide] (Weller et al., 2019). Obtained from Cuschieri & Baron (2023).

2.1.5. Natural molecules as putative drugs against Glioblastoma Multiforme *in-vitro*

The continuous search for putative drugs against GBM has veered towards investigating natural compounds as both singular chemotherapeutic drugs or chemotherapeutic adjuvants. Phytochemicals and natural extracts provide a large variety of, biologically active, inexpensive and readily accessible molecules, with a some having known cytotoxic effects against GBM (Colapietro et al., 2020; Liang et al., 2017).

Studies identified through systematic review (Chapter 9) suggest that extracts demonstrate a wide range of non-specific cytotoxicity against GBM (Table 2.2). Moreover, the bioactive precise molecule(s) within the extract which produce anti-cancer effects are unspecified. Singular molecules derived from natural sources have showed increased potency against GBM cells *in-vitro* (Table 2.3). Moreover, studies were also were able to elucidate specific mechanisms by which the phytochemicals

carry out their cytotoxic effects (Chaicharoenaudomrung et al., 2018; Hatziagapiou et al., 2022; Li et al., 2013; Tang et al., 2020; Wang et al., 2016).

Several phytochemicals evaluated for their effectiveness against GBM have shown notable drawbacks, including limited water solubility (Pejin et al., 2021), significant toxicity with prolonged storage in adipose tissue (Hatziagapiou et al., 2022), and the requirement for co-administration with other drugs (Chaicharoenaudomrung et al., 2018). The most commonly studied class of phytochemicals assessed against GBM were alkaloids. (Bezerra et al., 2015; Li et al., 2019; Munari et al., 2014). Many researchers consider alkaloids among one of the most important drugs in human history. Historically, these chemicals were determined to be exclusively harmful. Yet, alkaloids are being tested putative anti-cancer agents (Matsuura & Fett-Neto, 2015), warranting further research to unequivocally elucidate the cytotoxic effects of alkaloid compounds against GBM.

Table 2.2.: Natural extracts investigated against glioblastoma multiforme in-vitro. Studies were identified through systematic literature review (Chapter 9). Adapted from Cuschieri & Baron (2023).

Extract	Cell lines	IC_{50} (µg/ml)			Mode of action	Reference
		24 hrs	48 hrs	72 hrs		
Rhazya stricta and *Zingiber officinale* crude alkaloid	U251	200.00	135.00	80.00	• Induction of apoptosis by the intrinsic pathway • Increases expression of p53, p21 and NOXA	(Elkady et al., 2014)
Rhazya stricta and *Zingiber officinale* flavonoid	U251	150.00	115.00	75.00		
Solanum lycocarpum fruit	MO59J	18.26	/	/	/	(Munari et al., 2014)
	U343MG	20.04	/	/		
	U251	23.58	/	/		

Brazilian red propolis	SF295	34.27	/	/	• Interferes with mitosis by inducing apoptosis • Repairs damage caused by oxygen free radicals	(de Mendonça et al., 2015)
Abutilon indicum	U87MG	/	/	42.20	/	(Khan et al., 2015)
Cedrus atlantica	DBTRG-05MG	46.59	44.59	/	• Triggers G0/G1 cell cycle arrest and apoptosis • Produces reactive oxygen species and induces DNA damage • Regulates p53/p21 and CDK4/cyclin D1 protein expression • Decreased Akt/mTOR signalling	(H. Gu et al., 2016)
	G5T/VGH	39.20	41.33	/		
	GBM8401	49.71	43.28	/		
	GBM8901	40.55	41.71	/		
Hexaplex trunculus hypobran-chial gland	U87MG	/	22.00	/	/	(Ben Mabrouk et al., 2017)
Danshenn	LN-229	50.00	/	/	/	(Di Cesare Mannelli et al., 2018)

Clerodendrum volubile	U87MG	/	120.00	/	• Attenuation of redox imbalance inactivating G0/G1 phase • DNA depopulation in the G0/G1 and G2/M phases • Cell cycle arrest at S phase leading to apoptosis	(Erukainure et al., 2018)
Prunus spinosa L.	LN-229 U87 T98G	5250.00 9780.00 5550.00	/ / /	/ / /	/	(Karakas et al., 2019)
Fagara tessmannii bark	U87MG	/	/	17.34	• Enhanced reactive oxygen species production • Apoptosis mediated through the intrinsic pathway • Mitochondrial membrane potential alteration	(Mbaveng et al., 2019)
Salvia officinalis l. *Rosmarinus officinalis l.*	42-GBMA	52.27 63.59	/ /	/ /	/	(Choukairi et al., 2020)
Dendrobium transparens *Papilio-nanthe uniflora*	U251	75.84 2585.88	/ /	/ /	/	(Joshi et al., 2020)

Pholidota articulata	U251	3170.55	/	/	/	(Joshi et al., 2020)
Vanda cristata		163.66	/	/		
Araliopsis soyauxii bark	U87MG	/	/	18.67	• Mitochondrial membrane potential alteration • Enhanced reactive oxygen species production • Apoptosis mediated through the intrinsic pathway	(Mbaveng et al., 2021)
Araliopsis soyauxii root		/	/	35.42		
Araliopsis soyauxii leaf		/	/	33.22		
Hexane extract of seaweed Caulerpa lentillifera	A172	22.47	/	/	/	(Sangpairoj, 2021)
Herba anthrisci cerefolii extract	A172	/	765.21	/	/	(Stojkovic et al., 2022)

Table 2.3.: Natural extracts investigated against glioblastoma multiforme in-vitro. Studies were identified through systematic literature review (Chapter 9). Adapted from Cuschieri & Baron (2023).

Phyto-chemical	Cell line	IC_{50} (µg/ml) 24 hrs	48 hrs	72 hrs	Mode of action	Reference
Honokiol	DBTRG-05MG	/	/	30.00	• Triggers sub-G0 arrest leading to apoptosis	(K.-H. Chang et al., 2013)

Saponin 1	U251	7.40	/	/	• Decrease in Bcl-2/Bax ratio, initiated apoptosis by activating casp-3 and casp-9	(J. Li et al., 2013)
	U87MG	8.60	/	/		
Solamargine	MO59J	9.59	/	/	/	(Munari et al., 2014)
	U343MG	16.30	/	/		
	U251	8.09	/	/		
Solasonine	MO59J	21.72	/	/	/	
	U343MG	23.09	/	/		
	U251	26.21	/	/		
Gossypol	U87MG	/	340695.89	/	/	(Keshmiri-Neghab et al., 2014)
Piplartine	SF295	0.80	/	/	/	(Bezerra et al., 2015)
Deoxypodo-phyllotoxin (DPT)	SF126	/	/	5.56	• Triggers G2/M arrest	(Guerram et al., 2015)
	U87MG	/	/	6.00		
Olivetoric acid	U87MG	/	17.55	/	• Autophagy • Oxidative DNA damage	(Emsen et al., 2016)
Physodic acid		/	410.72	/		
Psoromic acid		/	56.22	/		
Kukoamine A.	U251	73.40	/	/	• Triggers G0/G1 arrest • Upregulation of Bax and casp-3, downregulation of Bcl-2	(Q. Wang et al., 2016)
	WJ1	22.10	/	/		
Gastrodin	DBTRG-05MG	7157.00	/	/	• Oxidative stress-associated apoptosis • P53 activation	(W.-Z. Liang et al., 2017)

Dihydro-tanshinone	T98G U87MG	/ /	/ /	509.58 417.46	/	(Kumar et al., 2017)
Cordycepin	U251	43967.00	/	/	• Upregulates p53, Bax, casp-3 and casp-9 and downregulates Bcl-2 • Induced generation of reactive oxygen species and SOD, GPX and catalase	(Chaicharoen-audomrung et al., 2018)
Tanshinone IIA Crypto-tashinone	LN-229	14185.26 15383.16	/ /	/ /	/	(Di Cesare Mannelli et al., 2018)
Bacoside A	U87MG	83.01	/	/	• Triggers sub-G0 arrest • Induced early apoptosis	(Aithal & Rajeswari, 2019)
Nuciferine	U87MG U251	/ /	21355.68 17693.02	/ /	• Triggers G2/M arrest • Inhibited proliferation, mobility, stemness, angiogenesis and epithelial-to-mesenchymal transition	(Z. Li et al., 2019)
Naringin	U87MG	/	8766.17	/	/	(Aroui et al., 2020)
Cedrol	DBTRG-05MG	26395.32	22570.56	23838.06	• Produces reactive oxygen species resulting in autophagy and apoptotic cell death	(K.-F. Chang et al., 2020)

Ascorbic acid	42-GBMA	20.61	/	/	/	(Choukairi et al., 2020)
PBI-05204	U87MG	/	/	4.90	• Induction of apoptosis and suppressed expression of Akt and mTOR	(Colapietro et al., 2020)
	U251	/	/	7.30		
	T98G	/	/	8.45		
Withaferin A	U87MG	/	2169.49	/	• Triggers G2/M arrest • Initiates intrinsic apoptosis by endoplasmic reticulum stress through the ATF4-ATF4-CHOP axis	(Tang et al., 2020)
	U251	/	644.73	/		
Matteucinol	U251	/	/	26.57	/	(Silva et al., 2020)
Gallotannin	DBTRG-05MG	/	/	22.50 µg/ml	/	(Kamarudin et al., 2021)
Chalcone	U87MG	4061.07	3438.37	3736.26	• Triggers G2/M arrest	(Mendanha et al., 2021)
Zerumbone	U87MG	32739.50	/	/	• Decreased expression of MMP-2 and MMP-9 • Inhibits Akt and ERK1/2 signalling	(Jalili-Nik et al., 2021)
Crocin	A172	3100.00	2190.00	1720.00	• Apoptosis by upregulation of Bax	(Hatzia-gapiou et al., 2022)
Dimethyl-crocetin	A172				• Apoptosis by upregulation of Bax and downregulation of Bcl-2	
p-coumaric acid	U87MG	/	82.08	/	• Triggers G2/M arrest • Increase in p53	(Oliva et al., 2022)

2.2. α-Solanine

Glycoalkaloids (SGAs) are steroidal glycosides which occur naturally in plants belonging to the *Solanum* genus. The most abundant and prototypical SGA is α-Solanine, has increasingly been demonstrated to have potent cytotoxic effects against cancer cells (Mendel Friedman, 2004).

2.2.1. Ethnopharmacological sources of α-solanine

Continuous availability of natural compounds is regarded as the foremost limitation for developing the lead structure for therapeutic use (Omayio et al., 2016). Notwithstanding, α-solanine is found readily available in potatoes (*Solanum tuberosum*) ensuring is continuous availability. The highest concentrations of α-solanine have been documented potato tubers and green peel, yet α-solanine can occur in any part of the plant acting to protect these plants from predators and pathogens (Spochacz et al., 2018). Potatoes are the main staple crop, ensuring food security for human beings all over the world. Large volumes (70,000 – 140,000 tons per annum) of potato peels are generated which are either sold at low cost or produced as waste (Hossain et al., 2014). α-solanine may be extracted from potato waste using numerous methods (Table 2.4). Thus, this molecule produced sustainably from bi-products of commercial food production (Fallows & Wheelock, 1982), and since potato production has a low environmental impact (0.97 kg CO_2-eq/FU) (Parajuli e*t al*., 2021), ∝-solanine can be sourced ethically.

Table 2.4.: Sources, methods, and concentration of α-solanine extracted from potato products. Studies were identified through systematic literature review (Chapter 9).

Reference	Potato product used	Method	Concentration of α-solanine extracted
(Kondamudi et al., 2017)	Idaho grown tubers	Microwave assisted extraction	6.50 mg/kg
	Mashed potato flakes		15.00 – 28.00 mg/kg
(Hossain, Rawson, et al., 2015)	Potato peel	Pressurised liquid extraction	597.00 µg/g
(Kondamudi et al., 2017)	Potato peel	Ultrasound assisted extraction	4.20 mg/100g
(Hossain et al., 2014)	Potato peel		273.00 µg/g
	Potato peel		180.00 µg/g
(Hossain, Aguiló-Aguayo, et al., 2015)	Potato peel	Solid liquid extraction	69.00 µg/g

2.2.2. Chemical properties and biosynthesis of α-Solanine

α-Solanine is a nitrogen-containing organic heterocyclic base. It is composed of a sugar moiety and an aglycone. The aglycone unit is the hydrophobic and nonpolar part of the molecule, with a steroidal structure to which the carbohydrate moieties are attached at the 3-OH position. The sugar unit is polar and water-soluble, consisting of three monosaccharide molecules: D-glucose, D-galactose, and L-rhamnose (Mendel Friedman, 2004; Nepal & Stine, 2019).

α-Solanine is produced in abundance as a secondary by *Solanum* plants under conditions of stress to deter their consumption by pests (Omayio et al., 2016). Like all SGAs, α-solanine is two main structural components; an aglycone unit composed of nitrogen containing steroid derived from cholesterol, and an oligosaccharide. The aglycone unit is produced from cholesterol via potato glycoalkaloid (PGA) biosynthesis by first producing the metabolic intermediate (*22S,25S*)-spirosol-5-enβ-ol. This molecule then undergoes E,F-ring rearrangement to produce solanidine. The aglycone

unit is then glycosylated at C-3 with a solatriose moiety consisting of glucose, galactose and rhamnose via uridine diphosphate-dependent glycosyltransferases (UGTs), to produce α-solanine (Baur et al., 2021; Nakayasu et al., 2017; Okamoto et al., 2020). The timing of glycosylation of the aglycone unit is still disputed, with some authors claiming that this step occurs earlier in the biosynthetic cascade, prior to the formation of solanidine, as represented in Figure 2.8 (Akiyama et al., 2021).

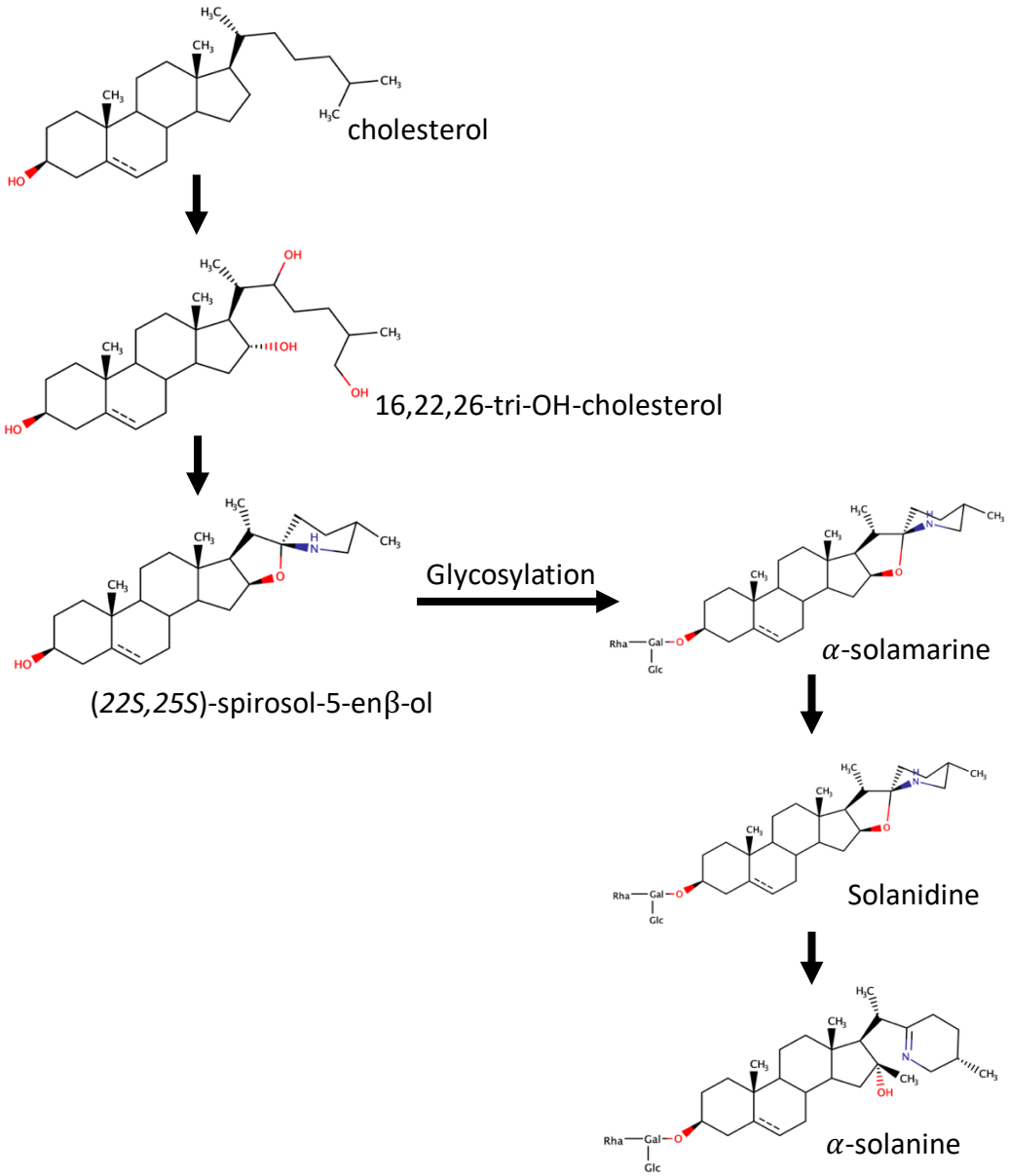


Figure 2.1.: Biosynthesis of α-solanine. Generated using MarvinSketch version 19.21.7.

2.2.3. Pharmacology of *α-Solanine*

A precise understanding regarding the pharmacology of α-solanine is limited. Hereto, salient studies identified through a systematic literature search (Chapter 9) are reviewed to obtain a generalised understanding regarding the pharmacokinetic and pharmacodynamic properties of α-solanine. Yet, included studies do not detail the age and weight of recruited human or animal participants, limiting observations made.

2.2.3.1. Pharmacokinetics

Research consistently demonstrates that the pharmacokinetic characteristics of α-solanine rely on the method of administration and reveal species-specific responses. Oral administration of tritiated α-solanine (5.00 mg/kg body weight) in adult male Fischer rats demonstrated rapid excretion of the molecule. Peak concentrations of accumulation occurred around 12 hours after administration for all tissues. α-solanine accumulated abundantly in the kidneys, liver and spleen, and to a lesser extent in adipose, heart, brain and blood. Within 24-hours, 78 % of the drug was excreted, most within the faeces. 4 days after administration, 94 % of the original dose was exerted, 84 % by faecal excretion and 10 % by urinary excretion. Intraperitoneal (i.p.) administration of α-solanine demonstrated increased accumulation of the molecule in the kidneys, liver and spleen in a dose-dependent manner (up to 35.00 mg/g body weight). This indicates rats' impaired ability to catabolise parenterally administered α-solanine or inefficient excretion of the molecule at higher doses. The rapid excretion of α-solanine reflects its poor absorption by the gastrointestinal tract (Norred et al., 1976). Additionally, 65.00 % tritium excreted via the faecal route following oral administration was identified as solanidine, suggesting biotransformation of the molecule by the digestive tract (Nishie

et al., 1971), more specifically the presence first pass effect, postulated to occur in the stomach where α-solanine is hydrolysed its less toxic aglycone unit, solanidine (Norred et al., 1976).

In humans, a peak serum concentration (C_{MAX}) of 7.66 ng/mL 5.1 hours (T_{MAX}) after ingesting a meal consisting of 0.4 mg/kg body weight α-solanine. The half-life ($t_{1/2}$) of α-solanine was estimated at 10.71 hours (Hellenäs et al., 1992). Biotransformation of α-solanine was also noted, with solanidine being detected after oral administration of α-solanine (Hellenäs et al., 1992). Mensinga et al. (2004) reported that C_{MAX} was at T_{MAX} > 6 hours when administering a dose of 0.70 mgTGA/ kg body weight, which increased in a dose-dependent manner. A definitive $t_{1/2}$ was not estimated, however was reported to vary considerably (5.00 – 42.00 hours). Correlation analysis demonstrated minimal intraindividual C_{MAX} and area under the curve (AUC) variation, while inter-individual differences were considerable, elucidating subject-specific susceptibility to adverse systemic effects at administration of higher doses (Mensinga et al., 2005).

2.2.3.2. Pharmacodynamics

2.2.3.2.1. Effect on serum and liver enzymes

Sprague-Dawley rats administered with α-solanine i.p. demonstrated statistically significant increased serum glutamic oxalacetic transaminase (SGOT) and serum glutamic pyruvic acid transaminase (SGPT) expression. SGOT and SGPT upregulation was also noted in mice fed α-solanine, albeit statistically insignificant. In addition, cholinesterase activity, cytochrome P450 and liver benzphetamine n-

demethylase activity were also significantly decrease following i.p. administration, as opposed to oral administration (Dalvi, 1985). Oral administration of α-solanine at a dose of 33.3 mg/kg body weight in Syrian golden hamsters significantly increased aspartate amino transferase and phosphatase compared to controls. Similarly, the same dose oral α-solanine increased plasma butyrylcholinesterase (BuChe) in a dose independent manner. The effect of i.p. administration on aspartate amino transferase and phosphatase and BuChe levels was not explored (Langkilde et al., 2009). Together, these studies further elucidate the biotransformation of ingested α-solanine and systemic accumulation of i.p. administered α-solanine.

2.2.3.2.2. *Effect on physiological parameters and histopathology*

In Syrian golden hamsters, a maximum dose of 33.3 mg/kg body weight did not produce body and organ weight changes, except for a decrease in weight in the left adrenal gland. A statistically significant dose-dependent increase in white blood cell, red blood cell, haematocrit, haemoglobin, albumin, urea and protein levels was observed (Langkilde et al., 2009). These findings are conflicted by results obtained by the same research group who demonstrated a statistically significant decrease in liver weight and adrenal grand weight in female golden Syrian hamsters (Langkilde et al., 2008). Similarly, in rabbits a decrease in haematological parameters were observed (Mendel Friedman, 2006), while a decrease in body and liver weights decreased relative to controls in adult female swiss-webster mice (Friedman et al., 1996). Such conflicting report do not concretely define the effect of α-solanine on basal physiology, despite elucidating

hepatotoxicity (Friedman et al., 1996; Langkilde et al., 2008), warranting further investigation.

Langkilde et al. (2008) (2009) similarly investigated the histopathological effects of α-solanine in Syrian golden hamsters. Significant dose response effect on the intestines and stomach was noted. At highest doses (100.00 mg/kg body weight), the animals suffered from dilated small intestines often filled with foamy fluids coupled with hyperemia of the stomach and small intestines. Large, dilated vacuoles were observed in the tips of intestinal villi. Changes in liver texture was noted in a few animals, but this finding was not supported by histological evidence (Langkilde et al., 2008). Macroscopic evaluation of the adrenal glands and kidneys did not reveal any dose-related changes (Langkilde et al., 2009). Langkilde et al. (2008) (2009) concluded that histopathological findings were not consistent across hamster and did not directly relate with the administration of α-solanine. Their findings coincide with previously reported findings, which demonstrated that statistically significant minor haematological and blood chemistry changes were not internally consistent both within individual the treatment groups, across treatment groups and sex in Wistar rats feed potato isolates containing known concentrations of α-solanine (Lynch et al., 2012). Moreover, Lynch et al. (2012) demonstrated that observed changes in haematological parameters were not correlated with histopathological findings. No studies investigating the effect of α-solanine on human basal physiology were identified.

2.2.3.2.3. Effect on gene transcription

Only one study was identified which investigated the effect *of* α-solanine administration on gene expression. Langkilde et al. (2009) observed downregulated gene expression, in epithelial cells obtained from Syrian golden hamsters dosed with 33.30 mg/kg body weight α-solanine. Hierarchal clustering demonstrated clear separation of gene expression profiles of treated and control groups. Moreover, Langkilde et al. (2009) identified genes associated with oxidative phosphorylation, tricarboxylic acid cycle (TCA), as well as lipid and carbohydrate metabolism.

Toxicokinetics

α-solanine administered i.p. is more potent than orally administration of the molecule in both mice (LD_{50} i.p. 42.00 mg/kg body weight vs > 1000.00 mg/kg body weight) (Nishie et al., 1971) and rats (LD_{50} i.p. 75.00 mg/kg body weight vs 590.00 mg/kg body weight) (Gull et al., 1970). Another study conducted on mice identified obtained a similar LD_{50} i.p. (67.00 mg/kg body weight). The i.p. LD_{50} in rhesus monkeys was reported to be <40.00 mg/kg body weight (Chaube & Swinyard, 1976).

In humans, administration α-solanine at doses of 2.00 – 5.00 mg TGA/kg body weight may be toxic, while 3.00 – 6.00 mgTGA/kg body may be potentially fatal (C. Morris & Lee, 1984). In another study conducted on healthy volunteers, α-solanine caused light to severe nausea and diarrhoea, however, no correlation was present between the severity or duration of clinical toxicity and the concentration of α-solanine in blood samples. Volunteers were aware of the experimental conditions and thus the

symptoms reported may be attributed to the placebo effect (Hellenäs et al., 1992). Moreover, reports have documented acute potato glycoalkaloid toxicity in humans, yet they could not attribute the observed effects to α-solanine (Internationally Peer Reviewed Chemical Saftey information, n.d.).

2.2.3.2.5. Teratogenicity studies

In pregnant Wistar rats gavaged with 0.30 – 3.00 mg/kg body weight between days 6 – 15 of gestation sacrificed on day 22, only one foetus demonstrated craniorachischisis and exophthalmos (1/117) from the group receiving the highest dose and another with malformed limbs (1/108) from the group receiving the lowest dose. No maternal toxicity was observed (Ruddick et al., 1974). Renwick et al. (1984) investigated the teratogenicity of α-solanine in pregnant Syrian golden hamsters gavaged 200.00 mg/ kg body weight. However, a high incidence of neural tube defects (NTD) (11 – 13 %) and exencephaly (5 – 12 %) was observed, without any apparent toxicity in the dams (Renwick et al., 1984). Direct administration of α-solanine (doses ranging from 0.13 – 0.26 mg/egg) in White Leghorn chick embryos resulted in a high incidence of embryo mortality (20 – 27 %) and foetal anomalies such as cranioschisis and cardiac septal defects (Jelínek et al., 1976; Mun et al., 1975). Other reports have demonstrated the teratogenicity of potato glycoalkaloids in marmosets, however results obtained were not directly attributed to α-solanine (Poswillo et al., 1972, 1973a, 1973b).

Despite reports suggesting teratogenicity *α-solanine* in humans (Nevin & Merrett, 1975; Renwick, 1972; Renwick et al., 1974) and efforts to elucidate α-solanine's teratogenic mode of action (Cuschieri & Calleja-Agius, 2020; Gal, 1973), no empirical evidence has been synthesised which unequivocally demonstrates α-solanine's human teratogenicity (Chaube & Swinyard, 1976). Yet, a recent epidemiological study still supports the notion that prevalence of NTD may be associated with maternal potato consumption (Ni et al., 2018).

2.3. α-solanine's anti-cancer properties

2.3.1. α-solanine as an anti-cancer agent *in-vitro*

2.3.1.1. *α*-solanine decreases cancer cell viability

∝-Solanine's anti-cancer potential has been investigated in a myriad of cell lines (Table 2.5), as identified through systematic review (Chapter 9). However, the IC_{50} of α-solanine was only determined in 9 human cancer cell lines (Arslan & Yerer, 2018; Gouhar et al., 2022; Hasanain et al., 2015; Mohsenikia et al., 2013; Yan et al., 2020; Zheng et al., 2020). (Table 2.6).

Table 2.5.: In-vitro studies investigating the cytotoxicity of α– solanine against cancer cell-lines. Studies were identified through systematic literature review (Chapter 9).

Reference	Cell line	Cancer type
(Karaboğa Arslan & Yerer, 2018)	RL95-2	Human oestrogen receptor positive endometrial cancer
(Mendel Friedman et al., 2005)	HepG2	Human hepatocellular carcinoma
	AGS	Human gastric adenocarcinoma
	KATOIII	Human gastric carcinoma
(Gao et al., 2006)	HepG2	Human hepatocellular carcinoma
(Gouhar et al., 2022)	HepG2	Human hepatocellular carcinoma
(T. Gu et al., 2021)	JEG-3	Human choriocarcinoma
(Hasanain et al., 2015)	A549	Human lung carcinoma
	MCF-7	Human breast adenocarcinoma
	DU145	Human prostate carcinoma
	KB	Human mouth epidermal carcinoma
(Ji & Gao, 2012)	HepG2	Human hepatocellular carcinoma
	SGC-7901	Human papillomavirus-related endocervical adenocarcinoma
	LS-174T	Human colorectal adenocarcinoma
(K.-R. Lee et al., 2004)	HT29	Human colon adenocarcinoma
	HepG2	Human hepatocellular carcinoma
(L.-T. Lin et al., 2020)	HepG2	Human hepatocellular carcinoma
(M.-K. Lu et al., 2010)	A2058	Human amelanotic melanoma
	A375	Human malignant melanoma
(Lv et al., 2014)	PANC-1	Human pancreatic duct carcinoma
	SW1990	Human pancreatic adenocarcinoma
	MIA PaCa-2	Human pancreatic adenocarcinoma
(Meng et al., 2016)	HepG2	Human hepatocellular carcinoma
(Mohsenikia et al., 2013)	4T1	Mouse mammary gland cells mimicking human stage IV breast cancer
(Mohsenikia et al., 2016)	4T1	Mouse mammary gland cells mimicking human stage IV breast cancer
(Pan et al., 2016)	DU145	Human prostate carcinoma
(K.-H. Shen et al., 2014)	PC-3	Human grade IV prostatic carcinoma
(Sun et al., 2014)	SW1990	Human pancreatic adenocarcinoma
	PANC-1	Human pancreatic duct carcinoma
(Yuanyuan Wang et al., 2016)	EC9706	Human oesophageal squamous cell carcinoma
	KYSE30	Human squamous cell oesophageal carcinoma
(L. Wang et al., 2016)	EC9706	Human oesophageal squamous cell carcinoma
	ECA109	Human oesophageal squamous cell carcinoma
(Z. Wen et al., 2016)	PANC-1	Human hepatocellular carcinoma

(Yamashoji & Matsuda, 2013)	C6	Rat glioma
(Yan et al., 2020)	RKO	Human colon carcinoma
(J. Yang et al., 2019)	PC-3	Human grade IV prostatic carcinoma
	DU145	Human prostate carcinoma
(F. Zhang et al., 2016)	A549	Human lung carcinoma
	H1299	Human non-small cell lung carcinoma
(Zheng et al., 2020)	AML-196	Human acute myeloid leukaemia

Table 2.6.: Comparison between ∝-solanine IC_{50} at 24 and 48 hours of incubation.

Duration of incubation	Reference	Cell line	IC_{50} (µM)
24 hours	(Karaboğa Arslan & Yerer, 2018)	RL95-2	26.27
	(Hasanain et al., 2015)	DU145	32.18
	(Zheng et al., 2020)	AML-196	10.00
	(Mohsenikia et al., 2013)	4T1	34.0(
48 hours	(Mohsenikia et al., 2013)	4T1	17.0(
	(Hasanain et al., 2015)	DU145	9.63
		A549	9.37
		KB	11.99
		MCF-7	11.63
	(K.-R. Lee et al., 2004)	HepG2	16.67
		HT29	20.32
	(Yan et al., 2020)	RKO	20.84

2.3.1.2. α-solanine induces marked morphological changes

∝-solanine treatment induced marked morphological changes in different cancer cell lines, as evidenced through fluorescent and scanning electron microscopy. Acridine orange/ethidium bromide (AO/EB) and 4',6-diamidino-2-phenylindole (DAPI) staining demonstrated irregular with concentrated and marginalised chromatin (Gao et al., 2006; Zheng et al., 2020). Apoptotic bodies were also observed, which appeared in

a dose-dependent manner (Gao et al., 2006; Hasanain et al., 2015; Zheng et al., 2020). Hasanain *et al.* (2015) also noted the formation of autophagosomes in various stages of maturation, coupled with ER swelling and disruption of mitochondrial ultrastructure in A549 cells. Similarly, reduced mitochondrial membrane potential was also observed in HepG2 cells (Gao et al., 2006; Gouhar et al., 2022; Ji & Gao, 2012). These findings indicate that ∝-solanine causes widespread cell death, possibly through the activation of both apoptosis and autophagy, however further clarification is required to determine whether a primary cell-death cascade is initiated by ∝-solanine treatment

2.3.1.3. α-solanine unequivocally generates ROS

α-solanine unequivocally generates ROS in tumour cells *in-vitro* (Gouhar et al., 2022; Hasanain et al., 2015; Meng et al., 2016; Pan et al., 2016; Yan et al., 2020). In HepG2 cells α-solanine administration resulted in the decrease of cytoplasmic malondialdehyde (MDA), glutathione (GSH), superoxide dismutase (SOD) and catalase levels in a dose dependent manner, indicating the presence of elevated cellular oxidative stress (Gouhar et al., 2022). Moreover, co-incubation of α-solanine with N-acetly-L-cystein (NAC), a ROS scavenger, antagonises the effects of α-solanine compared to sole administration of α-solanine on the same cells (Hasanain et al., 2015; Pan et al., 2016; Yan et al., 2020). Using A549 cells, Hasanain *et al*. (2015) postulated that ROS production occurs consequent to mitochondrial pore opening, induced by apoptosis since an increase in MitoSOX red (dye selective for mitochondrial superoxide) fluorescence was observed (Hasanain et al., 2015).

Albeit, Meng *et al.* (2016) suggested ROS production following α-solanine treatment, occurs in various cellular locations by a myriad of mechanisms. In DU145

cells co-incubation of α-solanine with NAC increased Bax and decreased Bcl-2 levels, while similarly reducing caspase-3, caspase-8 and caspase-9 expression in RKO cells. This may indicate that ROS production is contributed to the onset of apoptosis, confounding the hypothesis put forward by Hasanain and colleagues. It is important to highlight that the majority of natural derivative produce oxidative stress (NavaneethaKrishnan et al., 2019). Hence, this property is not specific to α-solanine and research should strive to understand the unique mechanisms with which α-solanine exerts its cytotoxic effects.

2.3.1.4. α-solanine supresses growth signalling

α-solanine demonstrates a significant dose-dependent decrease in of tumour cell growth *in-vitro*, across a host of cancer cell lines (Arslan & Yerer, 2018; Hasanain et al., 2015; Lu et al., 2010; Lv et al., 2014; Shen et al., 2014; Sun et al., 2014; Yan et al., 2020), likely by suppressing EGFR Akt/mTOR and G-protein coupled receptor (GPCR) Ras/Ra/ERK1/2 growth signalling. Downregulated Akt phosphorylation was observed in RL95-2 ER-positive (Arslan & Yerer, 2018), A549 (Hasanain et al., 2015), A2058 (Lu et al., 2010), A375 (Lu et al., 2010), PANC-1 (Lv et al., 2014; Shen et al., 2014; Sun et al., 2014) and SW1990 cells. PI3K suppression was only investigated and observed in PC-3 cells by Shen and colleagues. Downstream to Akt, mTOR was also observed to be downregulated in A549 and PC-3 cells (Hasanain et al., 2015; K.-H. Shen et al., 2014). Moreover, α-solanine upregulated RNA and protein expression of nuclear factor- κB (NF-κB). This acts to promote PI3K/Akt/mTOR signalling since NF-κB is a negative regulator of PTEN, which itself suppresses PI3K/Akt/mTOR signalling by inhibiting PI3K signalling (Gouhar et al., 2022). This corroborates evidence which suggest that α-solanine's suppressive effect on PI3K/Akt/mTOR signalling occurs by directly inhibiting

Akt phosphorylation (Arslan & Yerer, 2018; Hasanain et al., 2015). Moreover, this finding explains the decreased PI3K expression in PANC-1 cells noted by Shen *et al.* (2014). Under $CoCl_2$ hypoxia mimicking-conditions, α-solanine inhibited ERK1/2 but not Akt expression in PANC-1 cells (Wen et al., 2016). Under normoxic conditions, ERK1/2 expression was suppressed in PC-3 (Shen et al., 2014), A549 (Hasanain et al., 2015), and RL95-2 ER-positive cells (Arslan & Yerer, 2018), but not A2058 (Lu et al., 2010), A375 (Lu et al., 2010). Downregulation of Akt/mTOR andERK1/2 signalling may thus be responsible for decrease tumour cell growth following α-solanine treatment.

The effect of growth signalling suppression on other pathways has been suggested, with Hasanain et al. (2015) and Shen et al. (2014) suggesting a pro-autophagic role and anti-migratory role respectively, but further evidence is required to reinforce these claims. Moreover, down-regulation of intra-cellular growth signalling cascades may be consequent to the initiation of cell death signally, due to the intricate and dynamic relation between proliferative and cell death signalling (Section 2.1.3.7.).

2.3.1.5. α-solanine suppresses metastatic potential

Both migration and invasion were markedly suppressed following α-solanine treatment, in a host of different cancer cell lines. Wound healing and scratch assays demonstrated a significant dose-dependent reduction in JEG-3 (Gu et al., 2021), A2058 (Lu et al., 2010), A375 (Lu et al., 2010), RKO (Yan et al., 2020), EC9706, ECA109 (Wang et al., 2016), PANC-1 (Lv et al., 2014; Z. Wen et al., 2016), SW1990 (Lv et al., 2014), MIA PaCa-2 (Lv et al., 2014), and HCT-116 cell migration (Yan et al., 2020), while dose-independent suppression in A549 and H12999 motility cells was observed (Zhang et al., 2016). Yet Shen *et al*. (2014)'s demonstrated suggest that α-solanine does not inhibit

PC-3 migration. Invasion was similarly suppressed in JEG-3 (Gu et al., 2021), PANC-1, SW1990 and MIA PaCa-2 (Lv et al., 2014), RKO (Yan et al., 2020), A2058 (Lu et al., 2010), A375 (Lu et al., 2010), EC9706 (Wang et al., 2016), ECA109 (Wang et al., 2016), HCT-116 (Yan et al., 2020), A549 and H1299 cells (Zhang et al., 2016). The decrease in metastatic potential across different cell lines may be attributed to decreased matrix metallopeptidase (MMP)-2/MMP-9 expression, both at an RNA and protein level (Gu et al., 2021; Lin et al., 2020; Lu et al., 2010; Lv et al., 2014; Wang et al., 2016).

2.3.1.6. α-solanine produces cell-death through apoptosis and autophagy

Numerous studies have demonstrated α-solanine's ability to induce cell death through apoptosis. Annexin V fluorescein isothiocyanate (FITC) / propidium iodide (PI) flow cytometry demonstrated the dose-dependent induction of apoptosis in JEG-3 (Gu et al., 2021), HepG2 (Ji & Gao, 2012), Panc-1 (Sun et al., 2014), SW1990 (Sun et al., 2014), EC9706 (L. Wang et al., 2016), RKO (Yan et al., 2020), DU145 (Pan et al., 2016), A549 (Hasanain et al., 2015), and AML-196 cells (Zheng et al., 2020). In JEG-3, Panc-1, SW1990, EC9706 and AML-196 cells. Similarly, protein expression of pro-apoptotic Bax was upregulated while anti-apoptotic Bcl-2 was downregulated, both in a dose-dependent manner (Gu et al., 2021; Pan et al., 2016; Sun et al., 2014; Wang et al., 2016; Zheng et al., 2020). Using western blotting, Sun *et al.* (2014) and Hasanain *et al.* (2015) observed increased cytosolic cyt-C in α-solanine treated cells in comparison to controls, elucidating the occurrence of mitochondrial mediated apoptosis. Although Yan *et al.* (2020) also observed casp-8 to be upregulated in RKO cells, which may demonstrate a possible role of the extrinsic apoptosis in α-solanine induced apoptotic cell death (Pawlowska et al., 2018; Trejo-Solís et al., 2018), no other studies have documented

upregulation in caspase-8 or the activation of cell surface death receptors and formation of DISC following α-solanine treatment. Meanwhile numerous studies have documented upregulation of caspase-9 and caspase-3 downstream to cyt-c release in α-solanine treated cells (Ji & Gao, 2012; Sun et al., 2014; Wang et al., 2016; Yan et al., 2020), further consolidating the notion that α-solanine likely induces apoptosis via the intrinsic pathway.

Cell death mediated by autophagy following α-solanine treatment is poorly substantiated in comparison to evidence accumulated which indicate cytotoxicity through apoptosis. In C6 rat glioma cells incubation with α-solanine demonstrated a weak increase in LDH release, suggesting cell autophagy (Yamashoji & Matsuda, 2013). Extensive investigation by Hasanain *et al*. (2015) in A459 cells elucidate the induction of autophagy mediated by ER-stress, consequent to oxidative stress. This is evidenced by upregulation of autophagic proteins ATF6, ATF4, GADD153 coupled with ER lumen swelling as revealed by immunoblotting and scanning electron microscopy, following with treatment α-solanine as opposed to α-solanine in cells pre-treated with NAC (Hasanain et al., 2015). Downstream, western blotting demonstrated time-dependent upregulation of LC3-II, lysosomal associated membrane protein-2 (LAMP2), BECN1 and ATG5, verifying the occurrence of autophagy after α-solanine treatment. Interestingly, LC3-II upregulation occurred prior to casp-3 upregulation (after 24 and 48 hours incubation respectively) (Hasanain et al., 2015), suggesting that autophagy occurs prior to apoptotic cell death. This finding further obfuscates the hypothesis that ER-stress is induced following ROS release from opening of mitochondrial pores during apoptosis. Notwithstanding, apoptosis and autophagy are likely to act synergistically to produce α-

solanine cytotoxicity, yet further studies are required to fully understand α-solanine cell death signalling.

2.3.1.7. α-solanine increases cytosolic calcium ion concentration

Fluorescent imaging evidenced a dose dependent increase in cytosolic calcium ion concentration ($[Ca^{2+}]_i$) in HepG2 (Gao et al., 2006; Ji & Gao, 2012) and A549 cells (Hasanain et al., 2015), following α-solanine treatment. Hasanain *et al.* (2015) suggested that α-solanine induces Ca^{2+} efflux from within ER stores into the cytosol, since parallel findings were observed when A549 cells were treated with Thapsigargin, a non-competitive inhibitor of the ER-Ca^{2+}-ATPase. Gao *et al.* (2006) observed an corresponding increase in apoptotic bodies and $[Ca^{2+}]$i, which was most concentrated around regions were mitochondrial membrane potential was distributed. These findings may potentially suggest a synergistic role between the ER and mitochondrion to produce simultaneous apoptosis-and autophagy in response to α-solanine. This warrants further research to elucidate the role of ER-mitochondrion microdomain in α-solanine cytotoxicity.

2.3.1.8. α-solanine inhibits angiogenesis

Limited studies investigating on α-solanine's effect on blood vessel formation indicate an anti-angiogenic role. Under cobalt chloride ($CoCl_2$) hypoxia-mimicking conditions, HIF-1α and VEGF RNA and protein expression in PANC-1 cells were markedly downregulated (Lv et al., 2014; Wen et al., 2016). α-solanine similarly suppressed PANC-1's tube formation of human umbilical vein endothelial cells (HUVEC) (Lv et al., 2014). Inhibition of VEGF expression occurred in a dose-dependent manner, with Lv *et*

al. (2014) concluding that the primary anti-angiogenic action of α-solanine is restraining VEGF expression.

2.3.1.9. α-solanine as adjuvant chemotherapy

Steroidal glycoalkaloids have been suggested as potential adjuvant chemotherapeutic agents (Mendel Friedman, 2015). α-solanine reduced the X-ray radiation required to achieve IC_{50} in DU145 and PC-3 cells, EC9706 and KYSE30 cells (Wang et al., 2016), and A549 and H1299 cells (Zhang et al., 2016). Similarly, α-solanine sensitised A549 and H1299 cells to cisplatin (Zhang et al., 2016). Notwithstanding, studies providing empirical evidence regarding α-solanine's potential as an adjuvant chemotherapeutic agent are limited, warranting further research to consolidate available data and extend such investigations to cell lines of different cancer types.

2.3.2. α-solanine as an anti-cancer agent *in-vivo*

In-vivo evidence demonstrating α-solanine's anti-cancer properties was accumulated through xenographt mouse models. -solanine treatment significantly decreased tumour weight and size in JEG-3 (Gu et al., 2021), PANC-1 (Lv et al., 2014), 4T1 (Mohsenikia et al., 2016), DU145 (Pan et al., 2016), and SW1990 xenographts (Sun et al., 2014), while improving survival rates in comparison to control groups (Mohsenikia et al., 2016). Immunochemistry demonstrated an increased expression of Bax protein and decreased expression of Bcl-2 protein noted in JEG-3 and 4TI xenographts consolidate *in-vitro* findings which elucidate apoptosis as a principle cytotoxic action of α-solanine (Gu et al., 2021; Mohsenikia et al., 2013; Sun et al., 2014). Similarly, MMP-2

and MMP-9 expression were downregulated in PANC-1 cells (Lv et al., 2014). This confers the with absence of metastasis exhibited by 4T1 xenographts treated with α-solanine's, in comparison to the marked metastasis observed in control groups (Mohsenikia et al., 2013). VEGF expression in PANC-1 xenographts was also downregulated, further demonstrating α-solanine's anti-angiogenic properties. Inter-study comparison was difficult to achieve since the route of administration and dose of α-solanine administered *in-vivo* was either incongruent between studies or not clearly stated. Notwithstanding, preliminary evidence indicates that α-solanine is a potent anti-cancer agent *in-vivo.*

Chapter 3 Methods

3.1. Overview

Cell culture and maintenance was conducted throughout the project to ensure the necessary provision of cells, and by extension genomic and protein material, for the experiments conducted throughout this project. IDH gene sanger sequencing was conducted at the start of the project to assess the WHO classification of the cell lines used in this project. The anti-cancer properties of α-solanine were assessed through Presto Blue®, scratch-migration and trans well-invasion assays. Consequently, the effect of α-solanine on the apoptosis-autophagy axis was determined on a cellular and molecular level. Fluorescent imaging and flow cytometry were employed to examine the occurrence of apoptosis and autophagy at the cellular level. At the molecular level, RNA and protein experiments were performed to evaluate the impact of α-solanine treatment on the expression of specific genes and proteins involved in apoptosis and autophagy. These assays were carried out under various conditions, including TMZ, positive control, and negative control. Data analysis and statistical treatment was conducted as necessary.

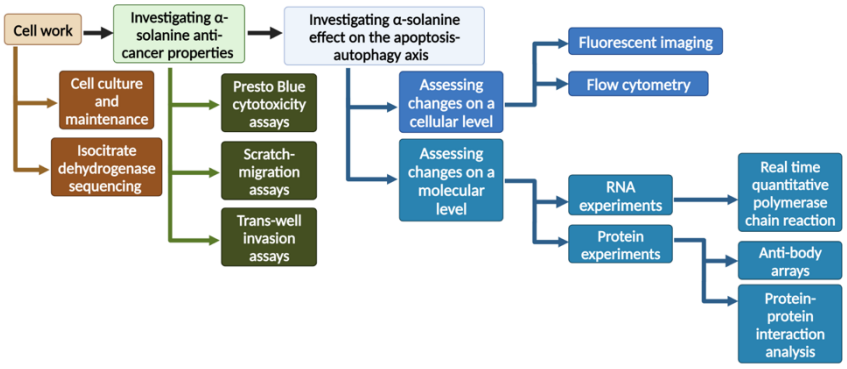


Figure 3.1.: Overview of the experiments conducted throughout this project. Cell work was conducted throughout the project. IDH sequencing was conducted at the beginning of the project to confirm that the cells being used are GBM. The anti-cancer properties of α-solanine were determined through 1) presto blue cytotoxicity; 2) scratch migration and 3) trans-well invasion assays. The effect of α-solanine on the apoptosis-autophagy axis was determined on a cellular level through fluorescent imaging and flow cytometry; and on a molecular level using Rt-qPCR and anti-body array protein profiling. Created in Biorender.com

3.2. Materials and equipment

Table 3.1.: Materials and equipment used throughout the project.

Item	Supplier	Item number
>98.5 ethylenediamine tetra acetic acid (EDTA) powder	Sigma Aldrich	A3578
>98% Bovine Serum Albumin (BSA) powder	Sigma Aldrich	A7906
>99.9% Dimethyl sulfoxide (DMSO)	Fluka® analytical	51779
1000bp DNA marker	Solis BioDyne	07-12-000S
10X Trypsin-EDTA stock solution	Sigma Aldrich	T4174
24-well plates NunclonTM Delta Surface	ThermoScientific	142485
3,3′,5,5′-tetramethylbenzidine (TMB) solution (high sensitivity)	Abcam	Ab171523
96-microwell plates (Nuc-Immunn TM)	Thermo fisher scientific	M9410
Alpha-solanine	Santa Cruz Biotech	sc-252340A
Analytical balance (0.1 mg)	RADWAG	AS/220X
Annexin V/PI staining kit	Santa Cruz Biotech	sc-4252 AK
Autophagy Assay kit	Sigma Aldrich	MAK138-1KT
BD FACS flow tubes	BD bioscience	663028
BD FACSCalibur™ Flow Cytometer	BD bioscience	N./A.
Benchtop refrigerated centrifuge	Eppendorf®	5810R
BioPhotometer Plus UV/VIS photometer (spectrophotometer)	Eppendorf®	952000006
Block heater (heating block)	Grant	QBD2
Casein Sodium salt from Bovine Milk	Sigma Aldrich	C8654
Class II Laminar Flow Hood	SafeFAST Elite-212	N/A
Consort mini-Electrophoresis Power Supply	Sigma Aldrich	E143
Dulbecco's Modified Eagle Medium /Nutrient Mixture F-12 HAM (DMEM/F12) powder	Sigma Aldrich	D0547
Eclipse Ti-2U Inverted microscope	Nikon	N/A
Fetal Bovine Serume (FBS)	Sigma Aldrich	F7524
GeneJET RNA Purification kit	ThermoscientificK0731	
H202	Sigma Aldrich	7722-84-1
Human Apoptosis Array C1 8 sample kit	RayBioTech	AAH-APO-1-8
Human Autophagy Array C1 8 sample kit	RayBioTech	AAH-ATG-1-8
Incubator	(Memmert INCO 2)	ICO50
IRDye® 680 RD Goat Anti-Rabbit IgG secondary antibody	Li-Cor® Biosciences	926-68071
IRDye® 800 CW RD Goat Anti-Mouse IgG secondary antibody	Li-Cor® Biosciences	926-32210

iScript reverse transcription supermix kit for RT-qPCR	Bio-Rad	5000205
IX50 Inverted Phase Contrast Microscope	Olympus IX50	N/A
Mitras LB 940 Multimode microplate reader	Berthold	38099
Odyssey® infrared imaging system	Li-Cor® Biosciences	N/A
Penicillin/Streptomycin (PenStrep)	Sigma Aldrich	P0781
Phosphate Buffered Saline	Sigma Aldrich	P3813
Precision balance (0.01 g)	RADWAG	PS10100.R2
PrestoBlueTM Cell Viability Reagent	Invitrogen	A13261
Quantitect SYBR Green PCR master mix (),	Qiagen	204143
Quick start™ bradford Protein Assay	Bio-Rad	5000205
RNA primers	IDT Europe	N/A
RNeasy® mini Kit	Qiagen	74104, 74106
Rotor-Gene Q	Qiagen	N/A
Scratch assay inserts	ibidi	80209
sterile Filter Upper Cup	VWR®	514-0337
Stuart Scientific Gyro Rocker	Rocker shaker	Z316520
T98G cells	CLS (Cell line services)	305030
Temozolomide	Cayman Chemical company	14163
Thermal cycler	Eppendorf 5333 Master cycler	
Thermo Fisher Scientific	Orion 3 star pH benchtop	B37009
Trans-well inserts with a pore size of 8.00 µm	cellQART®	932 80 12
U251 cells	CLS (Cell line services)	300385
U87MG cells	U87MG	ATCC HTB-14
UVette® (Cuvette)	Eppendorf®	Z618683
Vacuum pump	Integra Bioscience	158 320
Vortex machine	Whirli Mixer	SGP-202-010J

3.3. Microscopy

The cells were examined using an inverted Phase Contrast Microscope following procedures such as medium changes, splitting, resuspension, and cell counting. The microscope stage was configured to accommodate the 96-microwell plates, T-25 flask, or haemocytometer, positioned above the aperture and below the objective lens. Using the fine and coarse adjustment knobs, a crisp and sharp image of the cells could be seen

through the eyepiece. This microscope employed magnifications of x100 and x200 (x10 eyepiece and x10 or x20 lens).

An Inverted Eclipse Ti-2U microscope was used to observe and take images of cells at cells x40, x100 and x200 magnification (x10 eyepiece and x4, x10 or x20 lens). Photographs were taken using the following parameters for the program (NIS element): manual exposure (mode), medium contrast, 1280 x 960 resolution (Focus), and 2560x1920 Quality capture. The PH3 condenser lens was selected in the microscope's condenser turret. During the live cell viewing, images were captured, and the auto white balance feature was utilized to eliminate any background colour present in the medium.

3.4. Cell culture and maintenance techniques

All cell culture procedures were carried out in a sterile environment. Sterility was maintained by performing all steps within a Class II Laminar Flow cabinet. The laminar flow hood underwent daily exposure to 3 hours of ultraviolet (UV) radiation and was activated for a minimum of 30 minutes prior to each use. To ensure cleanliness, the surfaces of the laminar flow hood were regularly disinfected by spraying and wiping with 70.00% ethanol before and after each procedure. All materials placed inside the laminar flow hood were treated with 70.00% ethanol spray, and gloves were consistently worn throughout the process. Between each procedure, gloves were sprayed with 70.00 % to maintain sterility and prevent cross contamination. Gilson® micropipettes were used to carry out micro-pipetting, while disposable sterile serological pipettes (2.00 mL, 5.00 mL, 10.00 mL) and an automated electrical pipette filler were used for macro-pipetting.

3.4.1. Medium Preparation

U87MG, U251 and T98G cells were grown in Dulbecco's Modified Eagle Medium/Nutrient Mixture F-12 HAM (DMEM/F12) since it is routinely used for the successful development of a wide variety of cell lines, include glial like cells (ThermoFisher Scientific, n.d.). Twelve grams of DMEM/F12 and 1.20 g of sodium bicarbonate ($NaHCO_3$) powder were weighed using a high precision analytical balance (0.05 mg) (A200S Analytical balance; Sartorius Analytical®) to prepare 1.00 L of DMEM/F12.

The measured powders were transferred into a glass beaker with a volume of 2.00 L. To this, 1.00 L of distilled water at room temperature, sterilized beforehand, was added. The mixture was thoroughly stirred using a magnetic stirrer until complete dissolution was achieved. The pH of the solution was adjusted to the desired working pH of 7.40 using a phenol red indicator. Once fully dissolved, the solution was passed through a sterile Filter Upper Cup equipped with a polyethersulfone membrane measuring 50.00 mm in asymmetric diameter and containing 0.45 µm pores. The filtrate was collected in a receiver with a capacity of 150.00 mL, connected to a 500.00 mL media bottle via a vacuum pump. The media bottle was appropriately labelled with the preparation date and the name of the medium, and then stored in a dark refrigerator set at a temperature of 4.00 ^{o}C for a maximum period of 12 months.

To facilitate cell culture procedures such as cell thawing, media changes, cell splitting, and resuspension, a weekly supply of 50.00 mL of complete growth medium was prepared prior to using the DMEM/F12 medium. The complete medium formulation consisted of 2.50 mL (5%) of human serum, 0.50 mL (1%) of penicillin/streptomycin, 0.50 mL (1%) of amphotericin, and 0.25 µL of heparin and 0.20

mg/mL of platelet lysate. These components were combined in a 50.00 mL Falcon flask, and the volume was adjusted with the prepared DMEM/F12 medium. The flask was appropriately labelled as complete DMEM/F12 medium, indicating the date of production and initialled. The complete medium was then stored in in a dark fridge set at 4.00 ^{o}C for up to a week.

3.4.2. Cell thawing

Cryovials containing 1.00 mL of U87MG, U251, and T98G cells were retrieved from the cryostorage container located in the -80.00 ^{o}C freezer. They were then placed in a plastic beaker filled with lukewarm water (~25.00 ^{o}C) for approximately 3 minutes. The cell suspensions within the cryovials (1.00 mL each) were subsequently transferred to separate 15.00 mL centrifuge tubes, which were properly labelled as U87MG, U251, and T98G. To each centrifuge tube, 4.00 mL of complete DMEM/F12 medium was rapidly added using different sterile pipette tips for each sample. This was done to dilute the dimethyl sulfoxide (DMSO) present in the cryovials. The contents of each centrifuge tube were aspirated and dispensed using appropriate pipettes to ensure thorough mixing. The sealed centrifuge tubes were then centrifuged at 1200.00 RPM for 5 minutes. After centrifugation, the presence of a cell pellet and supernatant was confirmed for each centrifuge tube. The supernatant was carefully removed into a dedicated waste container within the laminar flow hood under aseptic conditions. Each tube was gently flicked to dislodge the cell pellet. Next, 4.00 mL of complete DMEM/F12 medium was added to each centrifuge tube to resuspend the cells in fresh growth medium. The contents of each centrifuge tube were transferred separately into three

pre-labelled T-25 culture flasks, indicating the date of thawing, cell type, and user's initials. The flasks were horizontally placed in an incubator set to 37 °C, 5% CO_2, and >95% humidity. These incubation conditions were used throughout the project. In cases where the T-25 flasks did not have an integrated filter cap, the cap was slightly loosened to facilitate gaseous exchange.

3.4.3. Cell culture maintenance

Cultured cells were monitored periodically (every 2 – 3 days) using an inverted light microscope, to visually assess morphology (indication of cells' health), confluency (cell density), adherence and to ensure that no contamination occurred within the culture flasks. Any contaminiation was noted by the presence of turbidity in the culture medium coupled with the identification of extraneous living microorganisms, such as fungi (characterised as white spots) or bacteria (characterised as fast moving specs). Changes in the phenol red indicator present within the culture medium to shades of orange or yellow indicated a decrease in pH, suggestive of increased cellular metabolism indicating the need of changing the spend medium with fresh complete DMEM/F12 growth medium. When conducting microscopy to monitor the status of cells, the confluency and level of dead cells and debris were noted. Once cell confluency reached ~80.00 % (determined as having ~80.00 % of the bottom surface of the T-25 flask covered by cells), the cells were split from one flask into two (1:2) or three flasks (1:3) depending on cell confluency present.

3.4.4. Medium change

The media within the T-25 flasks were changed every 3 – 4 days, depending on the respective cell turnover rate as indicated by changes in the colour of phenol red indicator. Four millilitres of spend medium in the T-25 flasks were aspirated out using 5.00 mL disposable sterile serological pipette and automated electrical pipette filler, ensuring to not scrape off any of the adherent cells. The spent medium was used to wash the bottom surface of the T-25 flask from 3 times to remove any debris and was consequently discarded. To each T-25 flask, 4.00 mL of fresh complete DMEM/12 medium was added. The cells were subsequently observed using an inverted light microscope to ensure the removal of any floating debris and dead cells. The T-25 flasks were then placed in the incubator and allowed to incubate until the next scheduled cell check.

3.4.5. Cell splitting

The spent cell culture medium was removed from the T-25 flasks as outlined in Section 3.4.4. However, rather than being discarded, the spent medium from each respective T-25 flask were placed in 15.00 mL centrifuge tubes, labelled with the name of the cell line. One millilitres of etheylenediaminetetraacetic acid (EDTA)/phosphate buffered saline (PBS) solution were added to each respective T-25 flask to detach the cells. If several clumped cells were noted under microscopy, 1.00 mL of trypsin/EDTA were added instead. The T-25 flasks were then incubated for 5 minutes, after which the T-25 flasks were examined under the inversted light microscope to ensure cell detachment. The T-25 flasks were also tapped gently to help dislodge the cells. The T-

25 flask contents were transferred to their corresponding 15.00 mL centrifuge tubes to deactivate the EDTA/PBS or trypsin/EDTA using a sterile 2.00 mL disposable serological pipette and an automated electrical pipette filler. A separate pipette was used for each flask. Once transferred, the 15.00 mL centrifuge tubes were subjected to centrifugation at 1200 RPM for 5 minutes to obtain cell pellets. The supernatant from each centrifuge tube was appropriately discarded within the laminar flow hood. The cell pellets were then resuspended by adding complete DMEM/F12 medium to each centrifuge tube. For a 1:2 split, 8.00 mL of complete DMEM/F12 medium was added, while for a 1:3 split, 12.00 mL of complete DMEM/F12 medium was added to the centrifuge tube.

During subculturing, a new T-25 flask and the flask previously containing the respective cells were utilized. Both flasks were labelled with the date of subculture. However, if the flasks had been used for more than two weeks, a new T-25 flask was substituted. The medium containing the cells within the centrifuge tubes was divided accordingly and transferred into the corresponding T-25 flasks, with 4.00 mL of medium per flask. After transferring all the contents, the T-25 flasks were capped again and appropriately labelled. The flasks were then observed under an inverted light microscope to ensure an even distribution of cells and subsequently placed in the incubator.

3.4.6. Resuspension

The resuspension procedure followed the same protocol as cell splitting (Section 3.4.5.). However, instead of transferring the detached cells into multiple T-25 flasks, the cells were returned to their respective original flasks. Trypsin/EDTA was not used for cell

detachment during resuspension, as the purpose was to disrupt multi-layered colonies or remove debris and weakly adherent cells. Therefore, EDTA/PBS was employed for this procedure.

3.4.7. Preparation of cell pellets

The spent medium was collected from the T-25 culture flasks, and the cells were washed with DMEM/F12 to ensure the removal of any remaining culture medium, as it could potentially hinder cell lysis. To detach the cells from the T-25 culture flasks, they were incubated with EDTA/PBS for 5 minutes. Subsequently, 2.00 mL of complete DMEM/F12 medium was added to the T-25 culture flask to neutralize the EDTA/PBS solution. The contents of the T-25 flasks were transferred to a centrifuge tube and centrifuged at 250 G for 5 minutes. The resulting supernatant was discarded, and the cell pellet was resuspended in 1.00 mL of PBS. The cells were centrifuged again at 250 RPM for 5 minutes, and the supernatant was discarded. The prepared cell pellet was stored in a freezer set at -20 ^{o}C until use.

3.4.8. Cell counting

Cell counting was an essential aspect of the project to ensure the appropriate cell numbers were used in each experiment. The collection of U87MG, U251, and T98G cells followed the procedure described in Section 3.4.7., utilizing 2.00 mL of trypsin/EDTA. After collection, the cell pellet was resuspended in 1.00 mL of DMEM/F12. A 50.00 µL aliquot of the resuspended pellet was transferred to a 1.50 mL microcentrifuge tube. This 50.00 µL aliquot was further diluted in a 1:10 ratio with

DMEM/F12 (without PBS). Manual cell counting was performed using a sterilized haemocytometer.

To begin the counting process, a coverslip was placed over the centre of the haemocytometer slide, which was then positioned on a flat surface. The diluted samples were carefully dispensed into the haemocytometer chamber at the edges of the coverslip, employing a micropipette and sterile disposable tip at a 45-degree angle. The haemocytometer slide was then placed on the stage of an inverted light microscope. Each counting chamber was observed at a magnification of 100x. Cells present in all 16 boxes within the 4 by 4 grid were counted, including those touching the left and top boundary lines of the grid.

The number of cells counted in each chamber was recorded, and the average cell count in the solution was calculated by multiplying the obtained mean cell count by 10^4 to estimate the cell density in 1.00 mL. This value was further multiplied by 10 to account for the 1:10 dilution performed earlier (abcam, n.d.). As a result, an estimation of the number of cells present within the suspension (consisting of the cell pellet dissolved in 1.00 mL) was obtained.

3.4.9. Cryopreservation

Cryopreservation (freezing of cells) was carried out to replenish cell stocks. The cells with the best morphology and confluency were usually frozen. 100 µL DMSO were added to each respective cryovial, which were labelled with the date of freezing, user, name of cell line and any other important details. The procedure outlined in Section 3.4.7. to obtain a cell pellet was carried out. However, each respective cell pellet was

resuspended in 900.00 µL FBS which were added to the corresponding cryovial. The contents of the cryovials were carefully mixed by gentle manual shaking to ensure a homogeneous solution. Subsequently, the cryovials were placed in a cryobox and stored in the -80°C freezer for a maximum period of 6 months. If the cells were not expected to be used within the next 6 months, the cryovials would be transferred to a liquid nitrogen cryopreservation tank after spending 48 hours in the -80°C freezer.

3.5. Cell viability assay

The viability of U87MG, U251 and T98G cells against different concentrations of α-solanine, TMZ, negative control (100% DMEM/F12), positive control (5.00 mM H_2O_2), determined using Presto Blue® assays. Optimisation of the Presto Blue® assay was conducted as noted in Chapter 10.

3.5.1. Presto blue® assay

Microwells of a 96-microwell plate were seeded at approximately 1 x 10^4 cells per 100 µl, adjusted accordingly to ensure that each well has a volume of 100.00 µl. According to the estimated cell count, the volume to be transferred to each well of the 96 microwell plate from resuspended cell pellet present in the 1.00 mL DMEM/F12 was determined by simple proportion and added to the corresponding microwell. Any remaining volume was topped up with DMEM/F12 (no serum), until each microwell had a final volume of 100 µl. After seeding the microwells, cell confluency and morphology was assessed using the inverted light microscope. The drugs being used were added to their respective well before the cells became adherent to the bottom of the microwell. This was done to remove 'weaker' cells which were weakly adherent to the T-25 flask.

Different concentrations of α-Solanine, TMZ, positive (5.00 mM H_2O_2) and negative (culture conditions) controls were added to the respective wells. Individual aliquots from each stock solution of respective drug/control were used to prevent cross contamination. Different volumes were taken from the aliquots to add the required concentration of drug/control to the respective microwells, and the plate was incubated for 72 hours. Consequently 10.00 µl of Presto Blue® were added to all the microwells. Once the Presto Blue® reagent was added, the 96-microwell plate was replaced in the incubator. Four viability readings were conducted at intervals of 30 minutes over a period of 2 hours using the Mithras LB 940 multimode microplate reader equipped with a 490 nm filter. The MicroWin 2000 software was utilized to control the microplate reader and record the readings. During each reading, the cover of the 96-microwell plate was removed. Following each reading, the 96-microwell plate was promptly returned to the incubator until the next reading was scheduled. The viability assays were performed in biological triplicate, and readings taken 2 hours after adding the Presto Blue® reagent were considered for analysis. Working concentrations of α-solanine and TMZ for all consequent experiments was determined using data generated from the viability assays.

3.6. Scratch migration assay

87MG, U251, and T98G cells were seeded in scratch assay inserts placed in twenty-four-well plates. The cells were allowed to grow until they reached 80 % confluency, which was considered suitable for conducting the scratch assay. Using fine tip forceps, the inserts were gently removed from the micro-wells. The culture medium

was then replaced with fresh medium and the cells were treated with either vehicle, 6.25 µM α-solanine, 1200.00 µM TMZ, or 5.00 µM H_20_2. Images of the vertical scratch were captured using the Nikon Eclipse Ti Inverted microscope, and the cells were incubated overnight. Subsequent images were taken at 24, 48, and 72 hours to assess the impact of the drugs on the migration rate. The images were captured from the same field of view at each time point. The scratch migration assay experiments were performed in biological triplicate.

3.7. Trans-well invasion assay

Trans-well inserts with a pore size of 8.00 µm were used for this experiment, inserted in microwells of a 24 microwell plate. U87MG, U251 and T98G at a confluency of $5x10^4$ cells were seeded in individual inserts. The wells were filled with 1.00 mL of media followed by the addition of the negative (culture conditions) control, 6.25 µM α-solanine, 1200.00 µM TMZ or 5 µM H_20_2. The cells were incubated for a period of three days, and images of five fields of view (FoV) per microwell were captured using the Nikon Eclipse Ti Inverted microscope. The number of cells which invaded through the microwells were recorded. Trans-well invasion assay experiments were conducted in biological triplicate.

3.8. DNA techniques

Numerous experimental techniques involving the extraction, preparation, and analysis of genetic material from U87MG, U251 and T98G cells were performed to analyse the differential expression of select genes under cellular conditions induced by

administration of α-solanine, TMZ and controls. In addition, the mutation status of IDH gene of the cell lines used was investigated to confirm whether the cells can be classified as GBM, opposed to high grade glioma.

3.8.1. Primer design

The primers required throughout the duration of this study were designed in-house, validated bioinformatically (Chapter 11) prior to purchase from IDT Europe. After purchase the primers were then also validated experimentally (Chapter 11). The canonical nucleotide gene sequences for the target human genes were identified using UniProt (UniProt, n.d.) and retrieved from Consensus Coding Sequence (CCDS) databases (NCBI, n.d.). Potential primers were identified by a haphazard literature search in PubMed and Google Scholar databases. In instances where no potential primers could be identified through haphazard literature review, Prime3 software version 4.1.0 was used to identify potential primer pairs (Untergasser et al., 2012).

Potential primer pairs designed to qualitatively assess the presence or absence of gene expression must; 1) produce a polymerase chain reaction (PCR) product between 200 and 250 bases (+/- 10 bases) in length; and 2) produce a product which spans multiple exons (Van Holm et al., 2021). Primer pairs designed for Sanger sequencing of whole genes were ensured to span the entirety of the target gene. Tentative primer pairs and their respective resultant product length were tabulated.

3.8.1.1. Bioinformatic primer validation and optimisation

Primer pairs which met the above mentioned inclusion criteria were optimized using OligoCalc software Version 3.27 (Kibbe, 2007) to meet ensure that; 1) Primer length was between 20 – 25 bases ; 2) the presence of a guanine-cytosine (GC) clamp on the 3' end of the forward and reverse primers; 3) respectively have a melting temperature (T_m) of 50°C – 55°C degrees (+/- 3 ^{o}C); 4) have a T_m within 5°C of one another; 5) ensured not the have complementary sequences to prevent the formation of primer dimers, and; 6) GC content between 40 % - 60 % (Bustin et al., 2020). Optimized primers were assessed for: 1) potential hairpin formation; 2) 3' complementarity, and; 3) potential self-annealing sites (Table 3.1). Finalised primer pairs (Table 3.1.) were then validated by aligning against intended canonical gene sequences using Primer-BLAST® and any alignments against unintended templates were noted (Ye et al., 2012) (Chapter 11).

Table 3.2.: Designed primer pairs.

Gene	Primer (5' → 3')	T_M [basic] (^{o}C)	GC content (%)	Potential hairpin formation	3' Compleme-ntarity	Potential self-annealing sites
ATG4B	F: GGTGTGGACATGATCTTGCC	53.80	55.00	None	None	None
	R: CTCCACGTATCGAAGACAGC	53.80	55.00	None	None	None
Bax	F: GGACAGTAACATGGAGCTGC	53.80	55.00	None	None	None
	R: GAGGAAGTCCAATGTCCAGC	53.80	55.00	None	None	None
BECN-1	F: GAGTTTCAAGATCCTGGACC	51.80	50.00	None	None	None
	R: CTCCCCAATCAGAGTGAAGC	53.80	55.00	None	None	None
Casp-3	F: GAGAACACTGAAAACTCAGTGG	53.00	45.00	None	None	None
	R: GAATGTTTCCCTGAGGTTTGC'	52.40	48.00	None	None	None
PKM2	F: ACAGCCAAAGGGGACTATCC	53.80	55.00	None	None	None
	R: CTTGGTGAGGACGATTATGG	51.80	50.00	None	None	None
VEGFA	F: TGTCTTGGGTGCATTGGAGC	53.80	55.00	None	None	None
	R: GGCACACAGGATGGCTTGAA	53.80	55.00	None	None	None
ATF6A	F: GCTTTACATTCCTCCACCTCC	54.40	52.00	None	None	None
	R: ATCAGCTGAGAATTTGAGCCC	52.40	48.00	None	None	None
IDH1	F: AATCAGTGGCGGTTCTGTGG	53.80	55.00	None	None	None
	R: CAAGTAGTCAGAACGTTGC	48.90	47.00	None	None	None

3.8.2. Ribonucleic acid extraction

The GeneJET RNA Purification Kit was used for ribonucleic acid (RNA) extraction. A cell lysate from each cell line being used was prepared to extract RNA from the collected cell samples. Respective cell pellets for each cell line were removed from the -20.00 ^{o}C storage, thawed, and prepared for lysis. To the cell pellet, 600.00 µl of lysis buffer supplemented with dithiothreitol (DDT) were added, and the suspension was vortexed for 10 seconds to ensure thorough mixing. If any debris was observed, the suspension was centrifuged at 1,400.00 RPM for 5 minutes to homogenize it. Next, 700 microliters of the resulting lysate were transferred to a GeneJet RNA purification column, which was placed in a collection tube. The RNA column was then centrifuged at 12,000.00 RPM for 1 minute. The flow-through and collection tube were discarded, and the GeneJet RNA purification column was transferred to a fresh collection tube.

To wash the RNA column, 700.00 µl of wash buffer 1 supplemented with 70.00% ethanol were added. The RNA column was centrifuged at 12,000.00 RPM for 1 minute, and the resulting flow-through was discarded. The purification column was placed back in the same collection tube. Next, 250.00 µl of wash buffer 2 were added to the GeneJet RNA purification column, which was then centrifuged at maximum speed for 1 minute. The collection tube containing the flow-through was discarded, and the purification column was transferred to a labelled sterile 1.50 mL RNase-free microcentrifuge tube.

To elute the RNA, 100 microliters of nuclease-free water were added to the centre of the GeneJet RNA purification column membrane. The column was centrifuged at 12,000 RPM for 1 minute, and the eluted RNA was collected. This step was repeated with an additional 100.00 µl of nuclease-free water for maximum yield. The purification column was then discarded, and the concentration of the purified RNA was determined

using spectrophotometry. The purified RNA could be used immediately or stored in a dark freezer at -20.00 ^{o}C.

3.8.3. Spectrophotometry

RNA concentration obtained from cell lysates was measured using a spectrophotometer. The spectrophotometer's absorbance was set at 280 nm. Blank readings (98 µL sterile deionised water) were used to calibrate the spectrophotometer. A 1:50 dilution of the extracted RNA was prepared by diluting 2.00 µl of extract RNA in 98.00 µl of sterile deionised water, which was measured three times against the blank sample, and an average of the three readings was noted.

3.8.4. Reverse transcription

Reverse transcription of RNA to produce complementary deoxyribonucleic acid (cDNA) was carried out using the iScript reverse transcription supermix kit for rt-qPCR. The RNA samples (Section 3.8.2) were thawed on ice, while the components of the reverse transcription kit were thawed at room temperature (15.00-25.00 ^{o}C). After thawing, each component of the reverse transcription kit, they were mixed by flicking them and briefly centrifuging for 1 minute at 250 RPM to ensure that all contents of the respective tubes were collected at the bottom. First, any contaminating genomic DNA was removed from the purified RNA sample by adding 2.00 µl of x 7 gDNA Wipeout Buffer for every 1.00 µg of RNA, on ice. RNase-free water was added to the solution to titter up to 14.00 µl. The reaction components were linearly scaled up according to the amount of RNA being used, to have a final gDNA Wipeout buffer concentration of x 1.

The gDNA elimination reaction mixture was then incubated at 42.00 ^{o}C for 2 minutes, after which it was immediately placed on ice. Consequently, the reverse transcription mixture was prepared on ice by mixing 4.00 µl of iScript reverse transcriptase supermix to 8.00 µl of RNA. The mixture was titered with RNase free water to have a final volume of 20.00 µl. The components were mixed and returned on ice. If more than one reaction was being conducted, the reaction components were linearly scaled-up as done previously. The reverse transcription mix was incubated in the thermocycler set with the programme outlined in Table 3.3. Once the reverse transcription reaction was complete, the reaction tube was retrieved and placed on ice or stored in a fridge set at -20 ^{o}C until use.

Table 3.3.: Reverse transcription thermocycler settings

Process	Duration (min)	Temperature (^{o}C)
Priming	5	25
Reverse transcription	20	46
Reverse transcription inactivation	1	96

3.8.5. End-point polymerase chain reaction

End point PCR was carried out to generate gene products for ATG4B, Bax, BECN-1, Casp-3, PKM2, VEGFA, ATF6 and IDH genes. The PCR reaction mixture (9.00 µLPCR master mix, 0.25 µL of 10.00 µM forward and reverse primers, respectively, and 0.50 µL of template cDNA) was prepared for each sample according to in 0.50 mL microcentrifuge tubes. A 1:10 dilution of the in-house designed primers (x10) was prepared by adding 1.00 µl of primer to 9.00 µl of sterile deionised water, prior to their addition to the PCR reaction mixture. The reaction mixture was placed in the Eppendorf

5333 Master cycler Thermal cycler, and it was programmed according to Table 3.4. The amplified gene products were visualised via agarose gel electrophoresis (Section3.8.6.)

Table 3.4.: Thermal cycler settings for end-point PCR.

Step	Time	Temperature (°C)	Number of cycles
Initial Denaturation	5 minutes	94	1
Denaturation	50 seconds	94	
Annealing	1 minute	50 (ATG4B, Bax, BECN-1, Casp-3, PKM2, VEGFA, ATF6) 61 (IDH)	35
Extension	2 minutes	72	
Final extension	10 minutes	72	1

3.8.6. Gel electrophoresis

Visualisation through gel electrophoresis was performed on all PCR prodcuts to experimentally validate PCR conditions on the self-designed primers (Chapter 11). Tris-acetate-EDTA (TAE) buffer was utilized, both to produce the gel and use as a running buffer. Fifty millilitres of 1.00 % electrophoresis gel was prepared by first diluting the stock x 50 TAE buffer which was prepared according to Table 3.4.. Half a gram of high gelling temperature agorase were weighed in a 250.00 mL conical flask, and 50.00 mL of x 1 TAE buffer were added and the flask was swirled to ensure complete mixing of the suspension. The suspension was microwaved for 50 s, swirled and heated again as neccessary until all the agarose was dissolved.

Table 3.5.: Preparation of electrophoresis gel

Component	Amount (g)
Tris Base	242.00
Glacial Acetic Acid	57.10
EDTA (pH 8)	18.60

While the agarose was dissolving, the sides of the casting tray were sealed using plastic dams. Once fully dissolved, the flask was cooled in room temperature water for 5 minutes until a the flask was cool enough to handle (around 60 ^{o}C). A volume of 1.00 µl of 2.00 mg/mL ethidium bromide (1:5 dilution of the stock solution) were added to the flask which was then swirled to ensure complete mixing. The prepared liquid gel was poured into the casting tray at a slow pace, ensuring the removal of any air bubbles by gently pushing them aside with a clean disposable pipette tip. The comb was then inserted into the gel, and the entire setup was left undisturbed for 30 minutes to allow the gel to solidify. Once the gel had set, the plastic dams was carefully removed, and the casting tray containing the gel was placed into the electrophoretic tank.

Ten microliters of sample and 1kb DNA ladder as marker were loaded onto the gel. The electrophoretic tank lid was closed, and the power supply was switched on to run the gel at 300.00 mA and 1 00 V for 45 minutes. Progression of the gel was monitored with reference to the marker dye, and after 45 minutes the bromophenol blue had migrated around 75 % the length of the gel. Once complete, the power supply was switched off and unplugged prior to removing the gel. The gel was placed into a 254 nm wavelength UV-light box transilluminator and the resultant bands of the PCR products were recorded digitally.

3.8.7. Sanger sequencing

Sanger sequencing against the IDH gene using cDNA prepared form U87MG, U251 and T98G cells was conducted. Sanger sequencing was performed by MLS BioDNA Ltd.

3.8.8. Real-time quantitative polymerase chain reaction

U87MG, U251, and T98G cells were grown in a 96-well plate and then exposed to different treatments, including 6.25 µM α-solanine, 1200.00 µM TMZ, or control substances. Following a 24-hour incubation period, the medium was carefully aspirated, and the cells were harvested for further analysis. RNA was extracted and reverse transcription was performed. The primers, cDNA and two times quantitect SYBR Green PCR master mix, were thawed (being previously stored -20 ^{o}C), in a beaker with room temperature water. Each solution tube was mixed gently, and the reaction mix was prepared according to Table 3.6. up to a total reaction mix volume of 10.00 µL; for each reaction of a given gene. The tubes containing the reaction mix were vortexed briefly to mix the contents. For every rt-qPCR analysis one No Template Control (NTC) mix was prepared for each gene. The PCR tubes were then placed in the Rotor-Gene Q (Qiagen, Netherlands) which was programmed according to Table 3.7. rt-qPCR experiments were conducted in biological duplicates.

Table 3.6.: Real-time quantitative polymerase chain reaction mixture preparation

Reaction mixture component	Volume (µL)
SYBR Green PCR master mix (providing 2.5.00 mM of Mg^{2+})	5.00
RNase-free water	3.00
Forward primers	0.50
Reverse primers	0.50
cDNA	1.00

Table 3.7.: Rotor-Gene Q settings for real-time quantitative polymerase chain reaction.

rt-qPCR step	Duration	Temperature (°C)	Number of cycles
Initial denaturation	15 min	94	1
Denaturation	15 s	94	40
Annealing	20 s	50	40
Elongation	20 s	71	40
High resolution melt (HRM)		55 – 90; increasing at increments of 1 ◦C/min	1

3.9. Fluorescent microscopy

To assess apoptosis, an Annexin V/PI staining kit was employed. U87MG, U251, and T98G cells were cultured in the microwells of a 96-well plate until they reached a density of 0.5-1.0 x 105 cells. Subsequently, the cells were treated with either 6.25 µM α-solanine, 1200.00 µM TMZ, or control substances. After 24 hours, all assay reagents were equilibrated to room temperature while being shielded from light (previously stored at 4°C), and the culture medium was removed. The cells were washed once with PBS and then with 100 µL of 1x Assay Buffer per well. Next, 100 µL of 1x Assay Buffer, 0.5 µL (0.1 µg) of Annexin V-FITC, and 10 µL of propidium iodide PI were added to each well. The cells were incubated for 15 minutes at room temperature in the dark and subsequently washed twice with PBS. Finally, the stained cells were examined under an inverted microscope equipped with a fluorescent mercury lamp, using appropriate green and red filters to visualize Annexin V-FITC and PI staining, respectively.

To assess autophagy, an Autophagy Assay kit containing monodansylcadaverine (MDC), a specific stain for autophagosomes, was utilized. U87MG, U251, and T98G cells were cultured in the microwells of a 96-well plate until reaching a density of 1.0 x 104 cells. The cells were then treated with either 6.25 µM α-solanine, 1200.00 µM TMZ, or control substances. After 24 hours, the assay reagents were thawed (previously stored

at -20°C). The culture medium was removed, and the cells were washed once with 100 µL of wash buffer per well. Subsequently, 100 µL of autophagosome detection reagent was added to each well, and the cells were incubated for one hour. Following incubation, the autophagosome detection reagent was removed, and the cells were washed 3-4 times by gently adding 100 µL of wash buffer per well. Finally, the cells were examined under an inverted microscope equipped with a fluorescent mercury lamp, using an appropriate blue filter to visualize the excitation of the autophagosome detection reagent at 518 nm for accurate visualization. All fluorescent microscopy images were captured using x100 magnification, manual exposure at 8.00 s and 1.2x gain, and fluorescent imaging assays were conducted in biological triplicate.

3.10. Flow cytometry

Flow cytometry to measure the occurrence of apoptosis or autophagy was conducted.

The same Annexin V/PI staining kit used for fluorescent microscopy was used to stain against the occurrence of apoptosis. U87MG, U251 and T98G cells were grown in microwells of a 96-well plate up to a density of density of 0.5-1.0 x 10^5.

Following the treatment with either 6.25 µM α-solanine, 1200.00 µM TMZ, or controls, all assay reagents were equilibrated to room temperature while being shielded from light (previously stored at 4°C). The cells were detached using trypsin/EDTA and transferred along with the medium to appropriately labelled microcentrifuge tubes. After centrifuging for 5 minutes at 400 RPM, the supernatant was discarded, and the cells were resuspended in 100 µL of 1x Assay Buffer per microtube. Then, 0.5 µL (0.1 µg)

of Annexin V- FITC and 10.00 µL of PI were added to each tube. The cells were incubated for 15 minutes at room temperature in the dark, followed by another centrifugation step at 400 RPM for 5 minutes. The supernatant was removed, and the cells were resuspended in 100 µL of 1x Assay Buffer per microtube.

The same autophagy kit used in the fluorescent imaging experiments was used to stain for flow cytometry. U87MG, U251 and T98G cells were grown in microwells of a 96-well plate up to a density of density of 1.0×10^4. The cells were then treated with either 6.25 µM α-solanine, 1200.00 µM TMZ, or controls. After 24-hours the assay reagents were thawed (previously being stored at – 20 ^{o}C). The cells were detached using trypsin/EDTA and transferred to appropriately labelled microcentrifuge tubes. After centrifugation for 5 minutes at 400 G, the supernatant was carefully removed, and the cells were resuspended in 100 µL of autophagosome detection reagent per well. The cells were then incubated for one hour. Following the incubation period, the cells were detached again using trypsin/EDTA and centrifuged for 5 minutes at 400 G. The supernatant was discarded, and the cell pellet was resuspended in 100 µL of wash buffer per microcentrifuge tube.

The microcentrifuge tubes were put on ice and kept in the dark to prevent photobleaching. Stained cells were transferred into separate BD FACS flow tubes and the samples were analysed using a flow cytometer (FACS Calibur). Cells stained against apoptosis were excited at 485 nm and 560 nm and their emission spectra detected at 535 nm and 595 for Annexin V and PI respectively. Cells stained against autophagy were excited at 333 nm and their emission spectra detected at 518 nm. All flow cytometry experiments were conducted in technical triplicate.

3.10.1. Gating strategy and final analysis

A forward scatter (FSH-A) versus time plot was used to assess the detection of cells with time, and any anomalies were removed. GBM cell populations were gated based on forward scatter height (FSH-H) and forward scatter width (FSH-W) characteristics. Doublet detection events were excluded using a FSH-H and FSC-A plot. Any remaining aggregate events were excluded using a side scatter heigh (SSC-H) and side scatter width (SSC-W) plot. Debris were identified and excluded using a FSC-A and SSC-A plot

The gate for PI staining was identified by assessing the intersection of histograms on a count YL1-A::PI plot representative of GBM cells treated with culture (negative control) and 5.00 mM H_2O_2 (positive control) conditions. The gate for Annexin V-FITC staining was identified by assessing the intersection of histograms on a count BLA-1::FITC plot representative of GBM cells treated with culture (negative control) and 5.00 mM H_2O_2 (positive control) conditions. The gate for MDC staining was assessed by identifying the intersection of histograms on a count BLA-1::FITC plot representative of GBM cells treated with culture (negative control) and 5.00 mM H_2O_2 (positive control) conditions.

Final analysis for PI and Annexin V-FITC detection was conducted using a YL1-A::PI BLA-1::FITC plot, by considering the following (Wlodkowic et al., 2011):

- Lower inner quadrant: Viable cells [Annexin V-FITC$^-$/PI$^-$]
- Lower outer quadrant: Cells undergoing early apoptosis [Annexin V-FITC$^+$/PI$^-$]
- Upper outer quadrant: Cells undergoing late apoptosis [Annexin V-FITC$^+$/PI$^+$]
- Upper inner quadrant: Necrotic cells [Annexin V-FITC$^-$/PI$^+$]

Analysis of early and late apoptosis was conducted to elucidate the effect of treatment on the progression of apoptosis (Bracuhle et al., 2014). Final analysis was for MDC staining was conducted using a FSC-H BLA-1::FITC plot, since the detection of the emission spectra of MDC is comparable to that of FITC. Biexponential scale transformation was used throughout gating and final analysis to improve visualisation of data (FlowJo 2023).

3.11. Protein techniques

Protein extraction and quantification, through Bradford assays, was conducted using U87MG, U251 and T98G cells. The extracted protein was then used to assess changes in apoptotic and autophagic proteins following treatment through the use of antibody arrays.

3.11.1. Cell lysis and protein extraction

The cells were washed briefly with phosphate-buffered saline (PBS) and the PBS was subsequently removed. The cells were then solubilized in lysis buffer, which was provided with the antibody array kits, at a concentration of $1x10^7$ cells/mL. To ensure proper resuspension, the cells were aspirated and released using a pipette. The cell lysates were placed on a rocker shaker and refrigerated at 4°C for 30 minutes for thorough mixing. After incubation, the cell lysates were retrieved using a 20-gauge needle to ensure complete cell lysis. The collected lysates were then centrifuged for 5 minutes at 14,000 G. The resultant supernatant was collected and transferred into a

fresh, clean microcentrifuge tube. Quantitation of the extract ed protein samples was conducted using a Bradford Assay.

3.11.2. Bradford assay

Resultant protein concentrations from cell extracts were quantified by Bradford assay which involves the generation of a standard calibration curve for bovine serum albumin (BSA) using different dilutions of the extracted protein. One times Bradford reagent was brought to room temperature and allowed to acclimatise for 5 minutes. Then, 200.00 µL of x1 Bradford reagent were diluted in 800.00 µL of sterile deionised water. The 2.00mg/mL BSA solution was utilised to prepare three concentrations for the standard calibration curve: 0 µg/µL, 2 µg/µL and 4 µg/µL diluted in 0 µL, 1 µL and 2 µL of the previously prepared BSA solution in 2 µL, 1 µL and 0 µL of sterile deionised water, respectively.

To prepare the cell lysate solutions for spectrophotometry, a 1:50 dilution was made by pipetting 2.00 µL of each extracted protein sample into 0.50 mL microcentrifuge tubes. Next, 98.00 µL of diluted Bradford reagent was added to each sample. In addition, a blank sample for spectrophotometry was prepared by combining 2.00 µL of lysis buffer with 98.00 µL of diluted Bradford reagent. After preparing the samples, they were allowed to acclimate to room temperature for 10 minutes. Following the acclimation period, the samples were retrieved, briefly vortexed, and transferred into plastic cuvettes. The spectrophotometer was then blanked, and triplicate readings of the absorbance were taken for each BSA dilution and sample. The absorbance measurements were recorded at a wavelength of 595 nm, and the average

absorbance values were calculated. The resultant spectrophotometry absorbance values were then utilized to plot a standard calibration curve by plotting the BSA concentrations on the x-axis versus the absorbance values on the y-axis. A best fitting line graph was constructed with an intercept of 0. The protein concentrations for each protein sample were calculated using linear regression.

3.11.3. Antibody array profiling

Antibody arrays were used to assess the differential expression of apoptotic and autophagic proteins. All reagents and samples were thawed to room temperature and prepared according to Table 3.8. The biotinylated antibody cocktail and HRP-streptavidin concentrate solutions were briefly centrifuges at 1000g for 1 minute before use.

Table 3.8.: Preparation of reaction components for antibody array assays.

Reaction component	Preparation
Protein sample	Original lysate concentration of 2.00 g/ml diluted 10-fold
Antibody arrays **Blocking buffer**	No preparation
Biotinylated antibody cocktail	150.00 µl of blocking buffer were pipetted into each vial respectively. For each vial, the blocking buffer and biotinylated antibody cocktail was mixed gently and transferred to a prepared tube containing 1.80 ml of blocking buffer
1,000X HRP-streptavidin concentrate	The HRP-Streptavidin concentrated was diluted 1,000-fold using blocking buffer, and was subsequently mixed gently with a pipette
20X wash buffer I concentrate **20X wash buffer II concentrate**	The wash buffers were diluted 20-fold with distilled water
Protease inhibitor cocktail	60.00 µl of 1X cell lysis buffer were aliquoted into a tube
2X cell lysis buffer concentrate	The cell lysis buffer concentrate was diluted 2-fold with distilled water. 20.00 µl of the prepared protease cocktail inhibitor were pipetted into 1.98 ml of 1x cell lysis buffer.
Detection buffer C **Detection buffer D** **8-well incubation tray with lid**	No preparation

The antibody arrays were removed from their packaging and individually placed (print side up) into a well of the incubation tray. 2.00 ml of blocking buffer were pipetted into each well, and the membranes were incubated for 30 minutes at room temperature, and subsequently aspirated. 1.00 ml of diluted sample were pipetted into each well and incubated for 1.5 hours at room temperature. The samples were then aspirated from each well.

Two millilitres of 1X wash buffer 1 were pipetted into each well and incubated for 5 minutes at room temperature. The wash buffer 1 wash was repeated two more times for a total of 3 washes using fresh buffer and aspirating out the buffer completely after each wash. Two millilitres of 1X wash buffer 2 were pipetted into each well and incubated for 5 minutes at room temperature. The wash buffer 1 wash was repeated once more for a total of 2 washes using fresh buffer and aspirating out the buffer completely after each wash.

One millilitre of the prepared biotinylated antibody cocktail was pipetted into each well and incubated for 1.5 hours at room temperature, and subsequently aspirated. The afore-described washes with wash buffers 1 and 2 were repeated. millilitres of diluted HRP-streptavidin were pipetted into each well and incubated for 2 hours at room temperature, and subsequently aspirated. The afore-described washes with wash buffers I and II were repeated.

The membranes were then retrieved from the last washing step and were incubated with anti-rabbit and anti-mouse IgG secondary antibodies. Five millilitres of each diluted anti-rabbit and anti-mouse antibodies (a 1:10000 dilution of secondary antibodies in 5.00% caseinate TBS) were added to each membrane and incubated for an hour at room temperature. The secondary antibody solution was then discarded, and

the membranes were washed with wash buffer I and II as for 3 times. The dot blots were then detected using the Odyssey infrared imaging system, by placing them facing down on the scanner with the software being set at 800 nm with an intensity of 2.

All incubations were conducted under gentle rocking using a rocker shaker (approximately 0.5 – 1 cycle per second, while ensuring even incubations and that no bubbles appeared on or between membranes.

3.11.4. Construction of a protein-protein interaction network

Using UniProt, GeneCards, and Search Tool for the retrieval of interacting gene/proteins databases (String v10.5) the top 5 predicted direct protein-protein interactions, which have an apoptotic or autophagic biological function, for the proteins assayed in the apoptosis and autophagy antibody array kits used in Section 3.11.3. were identified. The interactions used in this study were obtained from reliable sources, including high-throughput experiments and curated databases, ensuring a high level of confidence. To construct the protein-protein interaction (PPI) network associated with the apoptosis-autophagic axis, the Cystoscape software (version 3.9.1) was employed (Shannon et al., 2003). Cystoscape is a software environment specifically designed for integrating models of biomolecular interaction networks. The constructed PPI network was presented as a perfuse force directed layout. The PPI network was then pruned to only demonstrate significantly differentially expressed proteins identified through antibody array assays (Section 3.12.8.). Significantly upregulated or down regulated proteins were presented by colouring 'nodes' in the form of a heat map.

3.12. Data treatment

3.12.1. Normalisation of cell viability data

Percentage cell viability using data obtained at the 2-hour timepoint following addition of the Presto blue® reagent using the Mithras LB 940 multimode microplate reader was calculated using Equation 1.

$$\%\, Viability = \frac{Treatment\ absorbance\ - mean\ negative\ control\ abaorbance}{mean\ positive\ control\ absorbance - mean\ negative\ control\ absorbance} \times 100$$

Equation 1.: Calculating cell viability.

3.12.2. Extracting IC_{50} data and linear regression to obtain

α-Solanine IC_{50} was determined using the AAT Bioquest, Inc. Quest Graph™ IC50 Calculator (AAT Bioquest, Inc., n.d.) (Section 13.1.3). GraphPad™ linear regression calculator (Section 13.1.4.) was utilised to determine the cell viability at work concentration of α-solanine and TMZ used throughout this project.

3.12.3. Data extraction and analysis from scratch migration assay

Percentage relative would closure was calculating using Equation 2, using data extracted using ImageJ (Fuji) wound healing add-on (Suarez-Arnedo et al., 2020), were A refers to wound area at the start of the assay while B refers to the wound area 72-hours following the start of assay. The percentage relative wound closure was then calculated by multiplying relative wound closure by 100. The rate of relative of wound closure for each treatment condition per cell line was calculated using Equation 3.

$$Relative\ wound\ closure = \frac{Treatment\ wound\ area\ (B) - Treatment\ Wound\ area\ (A)}{Negative\ control\ mean\ wound\ area\ (B) - \ Negative\ control\ mean\ wound\ area\ (A)}$$

Equation 2.: Calculating the relative wound closure.

$$Rate\ of\ relative\ wound\ closure = \frac{Relative\ wound\ closure\ (72\ hours) - \ relative\ wound\ closure\ (24\ hours)}{72 - 24}$$

Equation 3.: Calculating the rate of relative wound closure

3.12.4. Data extraction and analysis from polymerase chain reaction product gel electrophoresis for RNA primer validation

This sizes of the gel electrophoretic bands obtained were deduced semi-quantitatively using ImageJ software version 1.53t (Schneider et al., 2012). Triplicate measurements of the ladder migration distance and bands in relation to the migration front were recorded. The measurements were averaged, and the retardation factor (Rf) (in bp) were determined using Equation 4. The logarithmic expression of the weight of the discernible ladder bands were plotted (on the Y-axis) against the Rf value (on the X-axis) using Microsoft excel version 16.67. Through linear regression, the logarithmic molecular weight of the bands obtained were determined, which were normalised by finding the corresponding antilog to obtain the size (bp).

$$\mathrm{Rf} = \frac{\text{band migration distance}}{\text{migration front distance}}$$

Equation 4.: Calculating the retardation factor.

3.12.5. Obtaining fold change data from real-time quantitative polymerase chain reaction data

Rt-qPCR data was analysed by using the ΔΔ Ct method. Ct values relative to each gene were used to calculate ethe average Ct value by taking a reading of the two Ct values generated from each gene belonging to each treatment. The RPLP0 housekeeping gene was used since this was the most stable throughout the rt-qPCR experiments. Delta Ct values were calculated by normalisation of Ct target gene to the Ct of the reference gene, according to Equation 5, for each gene being investigated. Then, ΔΔ Ct values for each gene were calculated as according to Equation 6. The ΔΔCt calculation was repeated for each treatment condition using the ΔCt treatment and ΔCt control values for the same gene. Then, using the ΔΔCt the fold difference in gene expression was determined by calculating 2 to the power of the negative ΔΔCt ($2^{-\Delta\Delta Ct}$). for each sample and treatment condition.

$$\Delta\text{Ct} = \text{average target gene Ct} - \text{average housekeeping gene Ct}$$

Equation 5.: Calculating ΔCt.

$$\Delta\Delta\text{Ct} = \text{target gene } \Delta\text{Ct [treatment]} - \text{target gene } \Delta\text{Ct [negative control]}$$

Equation 6.: Calculating $\Delta\Delta Ct$.

3.12.6. Generation and transformation of corrected total cell fluorescence data from fluorescent imaging

Using ImageJ, images of fluorescent staining were first converted to grey scale. Then, the area, mean grey value and integrated density (Intdeg), and mean background grey value data were extracted for individual cells which were visible under using fluorescent

microscopy, per image. The number of cells per image was not considered as part of the analysis. The corrected total cell fluorescence (CTCF) for each image was calculated using Equation 7. For optimal graphical representation of the data, CTCF data was logarithmically transformed (log(CTCF)).

$$\mathrm{CTCF} = \bar{\mathrm{x}}\,[\mathrm{Intdeg} - (\mathrm{Area\ of\ selected\ cell} \times \mathrm{mean\ background\ fluorescence})]$$

Equation 7.: Calculating the corrected total cell fluorescenceAcknowledgments.

3.12.7. Data extraction and transformation from flow-cytometry plots

The number and percentage of cells in each quadrant of the YL1-A::PI BLA-1::FITC plot to assess the occurrence of early apoptosis, late apoptosis and necrosis as well as the number and percentage of MDC^{+} cells to assess the occurrence of autophagy. Percentage data was transformed using Equation 8 (where p refers to the percentage data obtained from flow cytometry plots) to ameliorate magnitude differences between samples, reduce the influence of outlier events and to decrease the vast dynamic range which makes visualising flow cytometric data difficult (Finak et al., 2010; Folcarelli et al., 2020).

$$\ln\left[\frac{p}{100-p}\right]$$

Equation 8.: Transformation of flow cytometry percentage detected cells

3.12.8. Data extraction and analysis from antibody array profiling

Fold change and protein-ratio *p*-value were used to assess whether proteins were significantly differentially expressed between treatment and control conditions,

with a fold change value of ≤0.7 / 1.5≤ (+/- 0.05) being set at the cut-off value for down-regulation and upregulation respectively. ImageJ was used to extract mean grey value from high resolution images of each of the antibody-array membranes. Mean grey value data was corrected by subtracting it from 255 (the maximum value for white pixels). Fold change was calculated using Equation 9, where Y is the observed treatment mean signal intensity and X is the negative control (culture conditions) mean signal intensity. The protein ratio *p*-values were then calculating using two-way pair-ways testing (Section 3.31).

$$Fold\ change = \frac{Y}{X}$$

Equation 9.: Calculating protein fold change.

3.13. Statistical analysis

Descriptive and inferential statistics were conducted throughout this project were appropriate to summarise data and confirm whether changes between cell lines, durations of incubation and treatment conditions were significant. Jasp version 0.15 was used to conduct all parametric inferential statistical testing. Chi square testing and graphical representation of data was conducted using Excel version 16.73. Normality (Shapiro-Wilk) and equal variance (Levene) testing was conducted prior to conducting inferential statistical testing. Standard error was deduced while obtaining descriptive statistics.

For inferential parametric testing consisting of two groups pair-wise statistical testing was conducted. If between group data was normally disturbed and homogeneity of variance was present, Student's T-testing was used. If a Shapiro-Wilk testing p-value

of ≤ 0.05 was obtained, Mann Whitney U-testing was conducted. If a Levene's testing p-value of ≤ 0.05 was obtained Welch testing was conducted. For inferential testing consisting of three or more groups, ANOVA statistical testing was conducted, assuming normality and equality of variance between groups. If Shapiro-Wilk and/ or Levene's testing testing p-value of ≤ 0.05 was obtained, Kruskal-Wallis testing was conducted. Where appropriate post-hoc testing was conducted and represented in Chapter 13. Non-parametric testing was conducted using Chi square testing.

Three levels of $\propto$-value were determined for better graphical representation: (*) $0.05 \geq$ p-value > 0.01; (**) $0.01 \geq$ p-value > 0.001; (***) p-value ≤ 0.001.

Chapter 4 Results

4.1. All cell lines are GBM $IDH_{wildtype}$

The IDH-1 gene is most frequently mutated at R132 (Alzial et al., 2022). End-point PCR and subsequent sanger sequencing performed for the IDH-1 gene for U87MG, U251 and T98G cell lines demonstrated the absence of mutations at R132 (Figure 4.1.). No additional mutations were noted (Section 12.1.). Hence, the cell lines used in this project can be classified as WHO grade IV GBM $IDH_{wildtype}$.

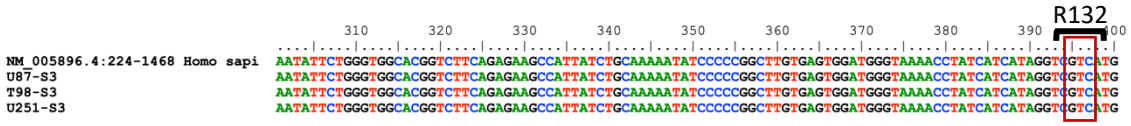


Figure 4.1.: Isocitrate dehydrogenase-1 sanger sequencing demonstrating the locus of R132. The Isocitrate dehydrogenase-1 (IDH1) gene is most frequently mutated at R132. Sanger sequencing of U87MG, T98G and U251 IDH1 genes demonstrated the presence of IDH wildtype when compared to the canonical IDH1 gene sequence.

4.2. Glioblastoma cells are more sensitive to α-solanine than to Temozolomide

The viability of U87MG, U251 and T98G cells against different concentrations of α-solanine and TMZ was investigated. Figure 4.2. indicates that all 3 cell lines demonstrated resistance against TMZ treatment, with T98G cells being the most resistant. α-solanine had a significant dose-dependent cytotoxic effect on U87MG, U252 and T98G cells (Figure 4.3.).

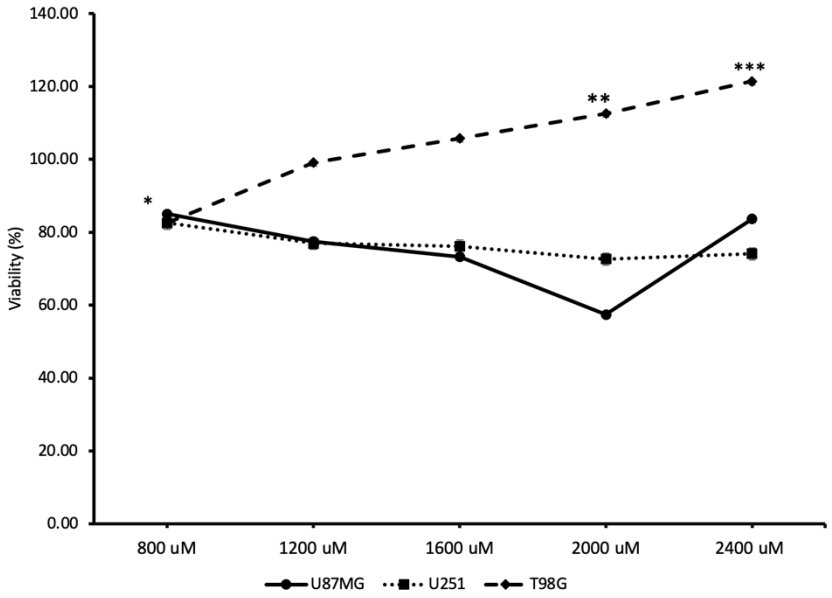


Figure 4.2.: Viability of U87MG, U251 and T98G cells following 72 hours treatment with different concentrations of temozolomide. Graph demonstrating normalised % viability data on the Y-axis and concentration of temozolomide (TMZ) on the X-axis per cell line investigated. Statistically significant different between cell lines was noted at TMZ concentrations of 800 µM (F[2,6]: 10.307; p = 0.011), 2000 µM (F[2,6]: 23.278; p = 0.001) and 2400 µM (F[2,6]: 117.956; p < 0.001).

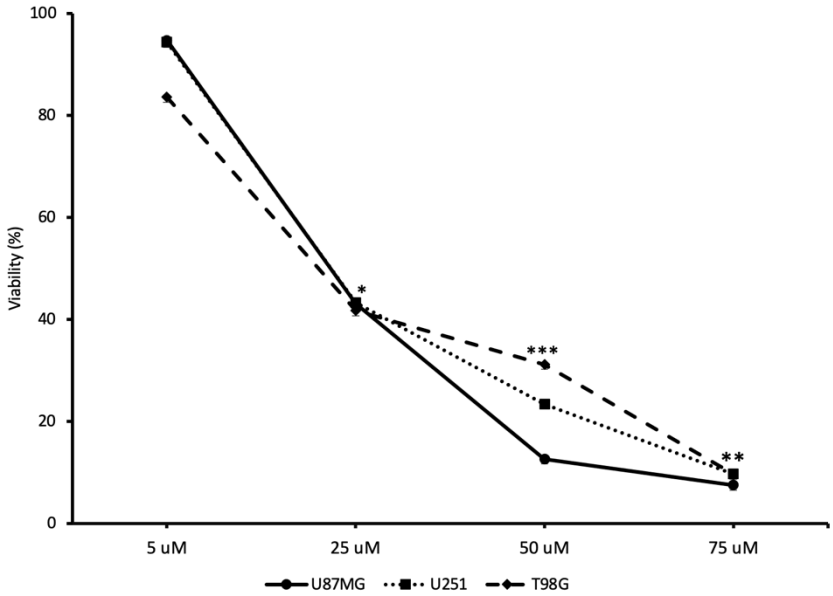


Figure 4.3.: Viability of U87MG, U251 and T98G cells following 72 hours treatment with different concentrations of α-solanine. Graph demonstrating normalised % viability data on the Y-axis and concentration of α-solanine on the X-axis per cell line investigated. Statistically significant different between cell lines was noted at TMZ concentrations of 25 µM (H[2]: 6.489; p = 0.039), 50 µM (F[2,6]: 30.616; p < 0.001) and 75 µM (F[2,6]: 12.419; p = 0.007).

α-solanine IC_{50} data for each cell line was generated, and are represented in Table 4.1.. TMZ treatment did not achieve IC_{50} experimentally and this data could not be extrapolated graphically due to the resistance against TMZ which occured. Suitable working concentrations representing concentrations closely representing IC_{25} for both α-solanine and TMZ treatment (Table 4.2.).

Table 4.1.: α-Solanine IC_{50} data. Table demonstrating IC_{50} α-solanine data for each cell line investigated as obtained through logistic regression of presto-blue viability (%) concentration graph.

Cell line	IC_{50} (μM)
U87MG	22.87
U251	19.66
T98G	21.32

Table 4.2.: α-Solanine and temozolomide working concentrations. Working concentrations of α-Solanine and temozolomide (TMZ) were determined through logistic regression of presto-blue viability (%) concentration graph of each respective drug. Concentrations close to IC_{25} were utilised to ensure the a sufficient cell pellet remained following treatment.

Treatment condition	U87MG	U251	T98G	Average IC_{25} concentration (μM)	Final working concentration (μM)
α-solanine IC_{25} (μM)	9.63	10.47	4.37	8.16	6.25
TMZ IC_{25} (μM)	1665.49	1876.06	315.05	1285.53	1200.00

4.3. α-Solanine induces morphological changes across all cell lines after 24-hours.

Under normal culture (negative control) conditions, all three GBM cell lines exhibited stellate morphology, typical of glial cells. U87MG cells did not achieve the same culturing confluency as U251 and T98G cells (Figure 4.4. [A]). 5.00 mM H_2O_2 (positive control) treatment markedly changed GBM cell morphology, with all three cell lines losing their gross morphological characteristics with resultant characteristic necrotic appearance (Figure 4.4. [B]). Treatment with 1200.00 μM TMZ and 6.25 μM α-solanine respectively produced similar changes in GBM cell morphology, which suggested presence of cell stress (Figure 4.4. [C,D]).

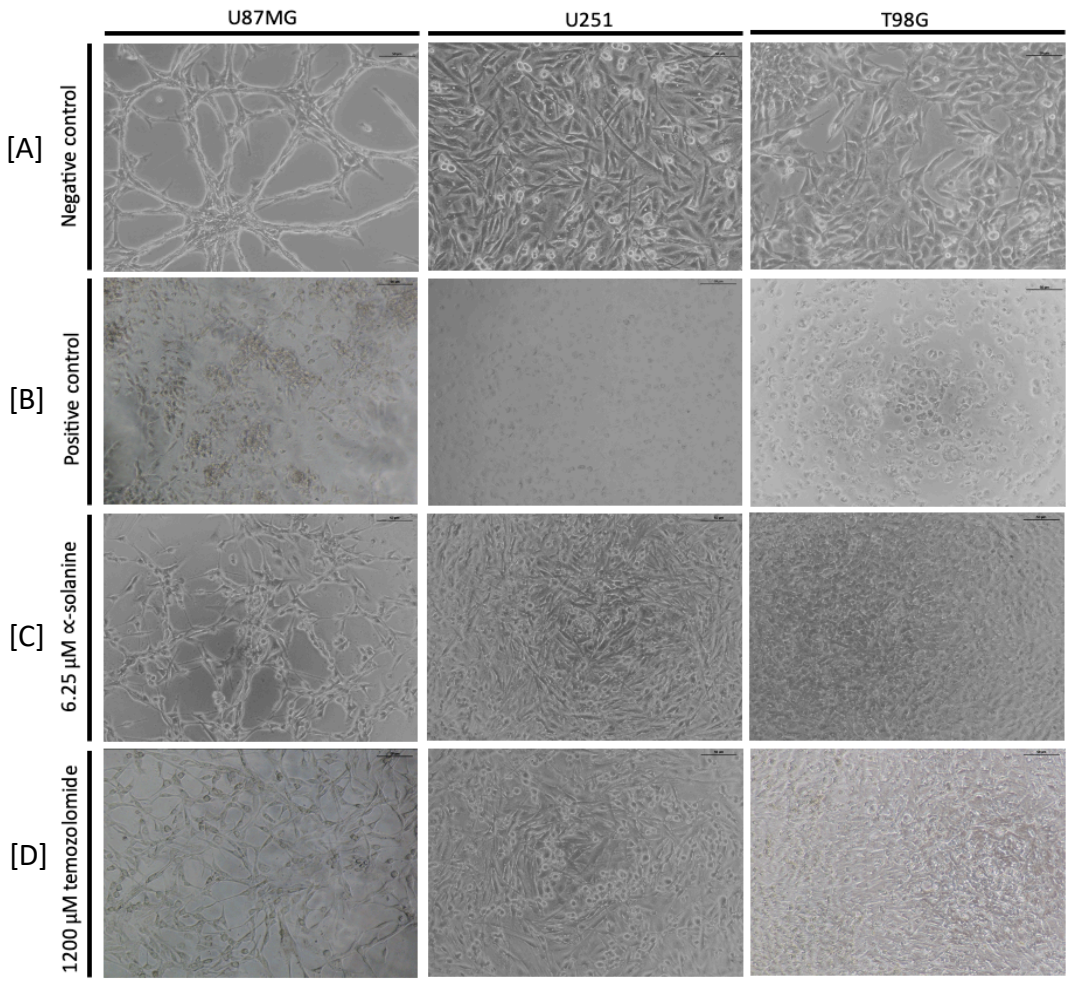


Figure 4.4.: U87MG, U251 and T98G cell morphology under control, temozolomide and α-solanine treatment conditions. U87MG, U251 and T98G cell morphology under [A] negative control; [B] positive control; [C] 1200.00 µM temozolomide (TMZ); [D] 6.25 µM α-solanine treatment conditions for 24-hours. Magnification: X100; scale bar: 50 µm.

4.4. α-solanine and temozolomide treatment alter GBM cell migration

The effect of 24-hour, 48-hour and 72-hour negative control, 1200.00 µM TMZ and 6.25 µM α-solanine treatment on U87MG, U251 and T98G cell migration was investigated using scratch migration assays.

4.4.1. α-solanine and temozolomide treatment on GBM cell migration varies with time and between cell lines

Visual inspection of serial imaging demonstrates a decrease in wound area across time, across all cell lines and treatment conditions (Figure 4.5.). The difference in wound closure across time was statistically significant between all cell lines, stratified by treatment conditions, except for T98G cells treated with 1200.00 µM TMZ (Figure 4.6.). Moreover, relative wound closure also varied between cell lines across the different time points, except for 72-hour treatment with 1200.00 µM TMZ.

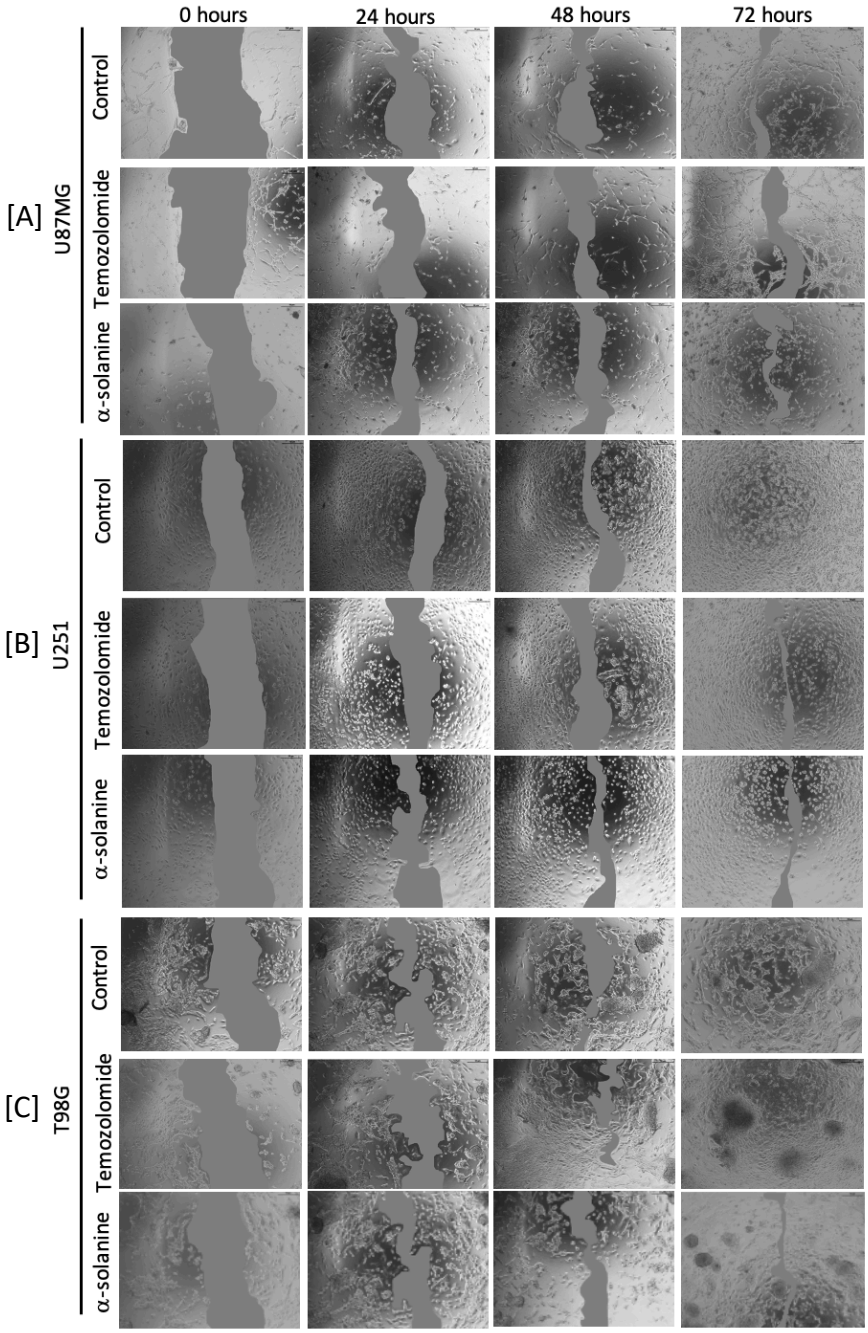


Figure 4.5.: U87MG, U251 and T98G cell migration under control, temozolomide and α-solanine treatment conditions. Selected images representing [A] U87MG; [B] U251 and [C] T98G cell morphology under negative control (vehicle); 1200.00 µM temozolomide (TMZ) and 6.25 µM α-solanine conditions at 0-, 24-, 48- and 72- hours of incubation. Magnification: X40; scale bar: 50 µm.

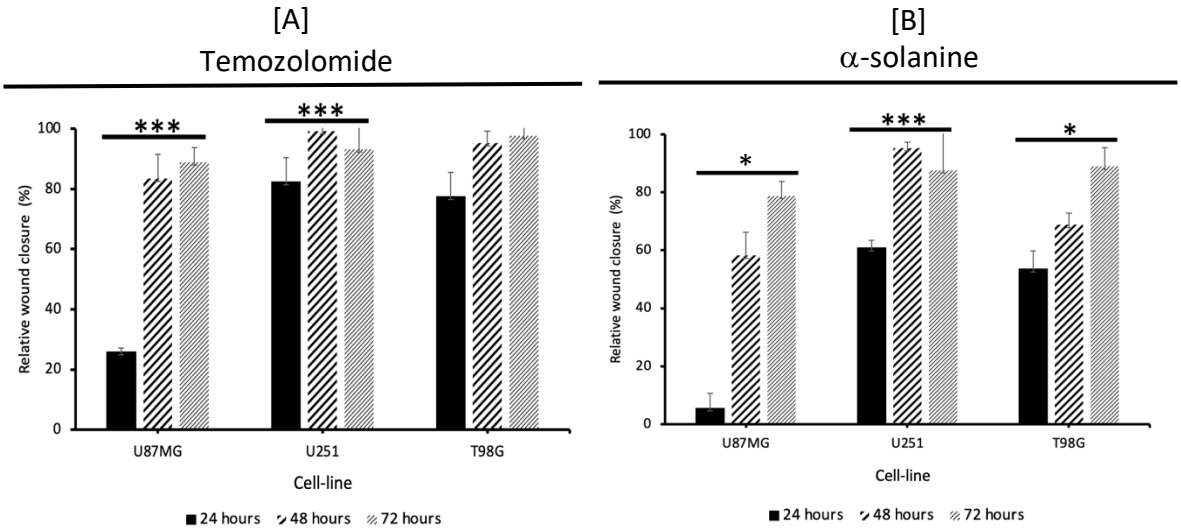


Figure 4.6.: Comparison of relative wound closure between individual time-points per cell line and treatment condition. Graph representing relative wound closure (%) on the Y-axis and duration of incubation per cell line on the X-axis. Comparison between 24-, 48-, and 72-hour incubation U87MG, U251 and T98G cells with [A] 1200.00 µM temozolomide (TMZ) with significant difference in the relative rate of wound closure (%) between time points in U87MG (H[2]: 6.489; p = 0.039) and U251 (F[2,6]: 117.971; p < 0.001) cells; and [B] 6.25 µM α-solanine with significant difference in the relative rate of wound closure (%) between time points in U87MG (F[1,4]: 44.510; p = 0.003), U251 (F[2,6]: 29.102; p < 0.001) and T98G (F[2,6]: 6.447; p = 0.032) cells.

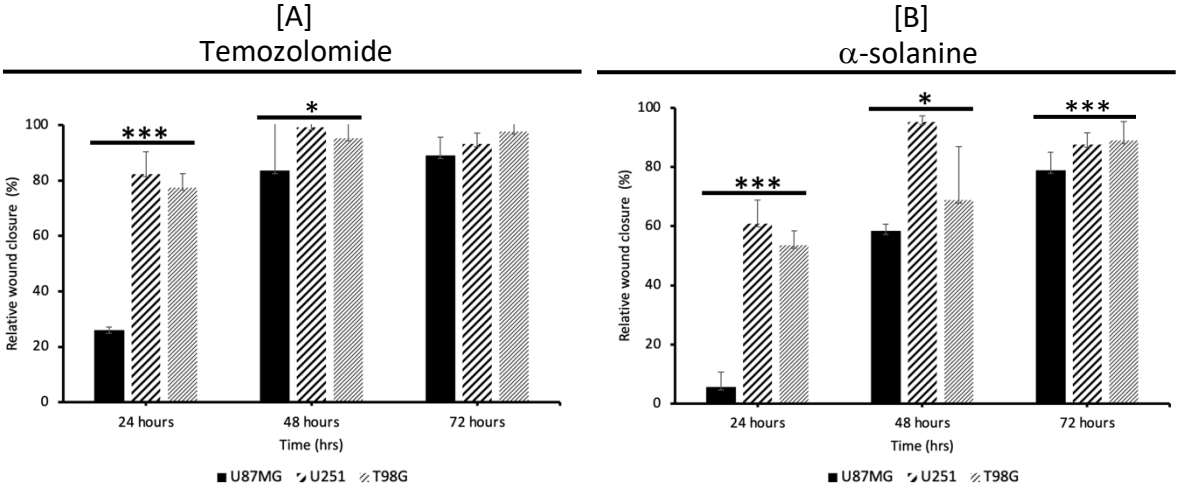


Figure 4.7.: Comparison of relative wound closure cell-line per time-point and treatment condition. Graph representing relative wound closure (%) on the Y-axis and cell line per duration of incubation on the X-axis. Comparison between U87MG, U251 and T98G cells after incubating for 24-, 48-, and 72 hours with [A] 1200.00 µM temozolomide (TMZ) with significance difference in relative wound closure (%) between cell lines noted at 24-hour (F[2,6]: 260.063; p < 0.001) and 48-hour (H[2]: 5.956; p = 0.051) duration of incubation and [B] 6.25 µM α-solanine with significant difference in relative wound closure (%) between cell lines at 24-hour (F[2,6]: 58.750; p < 0.001), 48-hour (F[2,6]: 4.889; p = 0.05) and 72-hour (F[2,6]: 76.247; p < 0.001) duration of incubation.

4.4.2. α-Solanine inhibits cell migration more than temozolomide treatment

α-Solanine treatment decreased relative wound closure across all cell lines at each time point investigated. However, relative wound closure across all cell lines was observed to be significantly reduced After 24-hour incubation with 6.25 µM α-solanine in-comparision to 1200.00 µM TMZ treatment. Moreover, this observation was also noted in U87MG after 72-hours of treatment and U251 cells after 48-hours of treatment (Figure 4.8.).

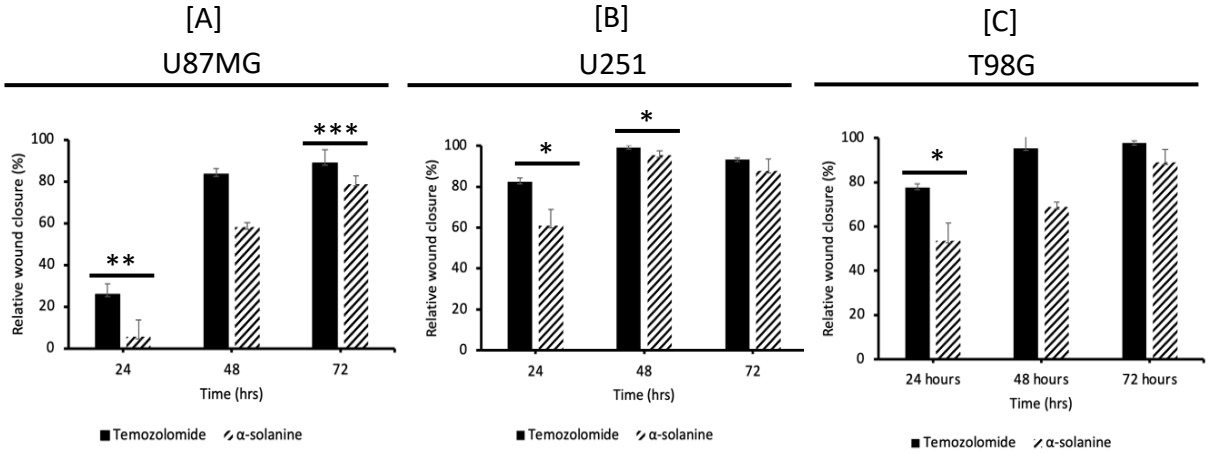


Figure 4.8.: Comparing the effect of temozolomide and α-solanine treatment at each time-point investigating on U87MG, U251 and T98G cells. Graph representing relative wound closure (%) on the Y-axis and treatment per duration of incubation on the X-axis. Effect of 1200.00 µM temozolomide (TMZ) and 6.25 µM α-solanine on [A] U87MG, with significant difference in relative wound closure (%) between TMZ and α-solanine at 24-hour (T[4]: 6.672; p = 0.003) and 72-hour (T[4]: 11.353; p < 0.001) duration of incubation; [B] U251 with significant difference in relative wound closure (%) between TMZ and α-solanine at 24-hour (T[4]: 4.518; p = 0.011) and 48-hour (T[4]: 2.866; p = 0.046) duration of incubation; and [C] T98G cell with significant difference in relative wound closure (%) between TMZ and α-solanine at 24-hour (W[2.191]: 4.750; p = 0.035) duration of incubation.

4.4.3. Rate of relative cell migration does not differ between cell lines with α-solanine treatment.

The rate of relative cell migration differed between cell lines under 1200.00 µM TMZ treatment, but not and 6.25 µM α-solanine treatment (Figure 4.9.[A]). α-solanine significantly decreased the rate of U87MG cell migration comparison to TMZ treatment,

however this observation was not extended to the relative rate of U251 and T98G cell migration (Figure 4.9.[B]).

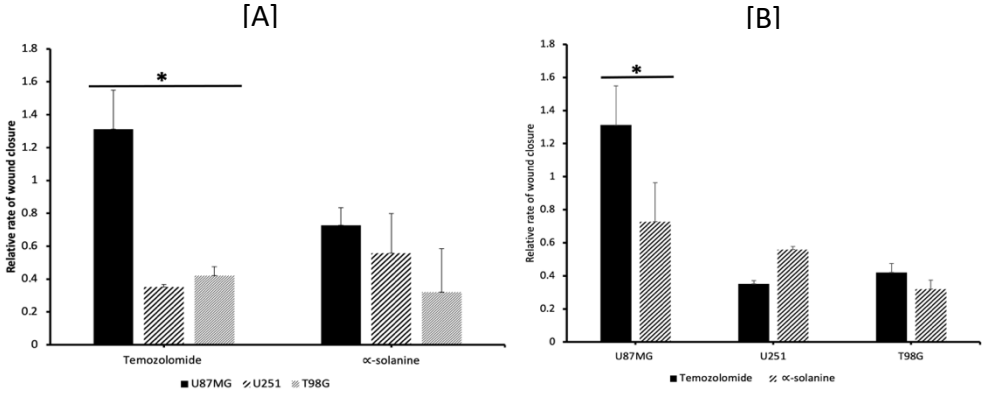


Figure 4.9.: Relative rate of U87MG, U251 and T98G cell migration under temozolomide and α-solanine treatment. Graph representing relative rate of wound closure on the Y-axis and [A] cell line per treatment or [B] treatment per cell line on the X-axis. [A] Between cell line with significant difference between cell lines treated with 1200.00 µM temozolomide (TMZ) (H[2]: 6.489; p = 0.039) and [B] between treatment comparison of the effect of 1200.00 µM TMZ and 6.25 µM α-solanine treatment with significant difference noted in U87MG cells (T[4]: 3.907; p = 0.017).

4.5. Glioblastoma multiforme cell invasion does not differ between temozolomide and α-solanine treatment.

Trans-well invasion assays were conducted to investigate the effect of α-solanine treatment in comparison to temozolomide (TMZ), on GBM cell invasion. No statistically significant differences between α-solanine and temozolomide (TMZ) treatments in individual cell lines (Figure 4.10.), and between cell-lines when stratified by treatment condition (Figure 4.11.), were observed.

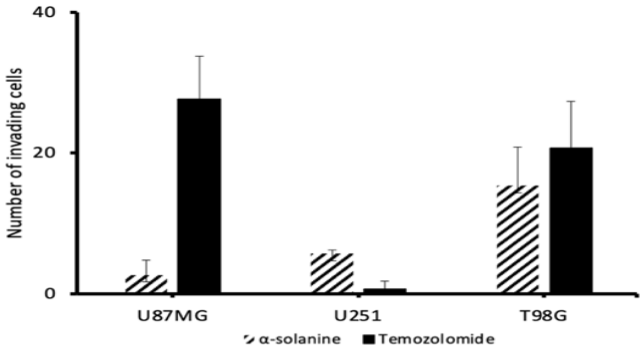


Figure 4.10.: Comparing the cell-line specific effect of 72-hour α-solanine and temozolomide treatment. Graph representing number of invading cell on the Y-axis and treatment per cell line on the X-axis.

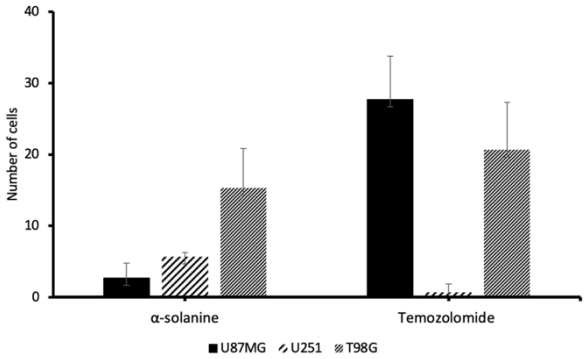


Figure 4.11.: Comparing the effect of 72-hour α-solanine and temozolomide treatment between glioblastoma cell lines. Graph representing number of invading cell on the Y-axis and cell line per treatment on the X-axis.

4.6. Autophagy staining intensity was greater across all treatment conditions.

The occurrence of apoptotic or autophagic cell death in U87MG, U251 and T98G cells treated for 24-hours with 1200.00 µM temozolomide, 6.25 µM α-solanine or culture (negative control) conditions was assessed using Annexin-V-FITC and PI, and MDC against apoptosis or autophagy respectively. MDC corrected total cell fluorescence (MDC) was higher in-comparison to Annexin-V-FITC and PI staining respectively (Figure 4.13.). Notwithstanding, MDC CTCF was not statistically significant under a particular treatment condition. α-solanine treatment increased PI and Annexin-V-FITC CTCF levels in comparison to TMZ and negative control treatment conditions, but this observation was not statistically significant (Figure 4.14.). The effect of 5.00 mM H_2O_2 (positive control) on Annexin-V-FITC, PI and MDC CTCF could not be elucidated since upon staining the cells detached from the T-25 flasks and were lost during washing. Moreover, not all cell-lines produced results upon fluorescent imaging after staining (Section 12.6.), hence inter-cell-line changes regarding Annexin-V-FITC, PI and MDC CTCF following the different treatment conditions could not be assessed. Images for Annexin-V-FITC/PI and MDC staining under each treatment condition investigated are presented in Section 12.6.

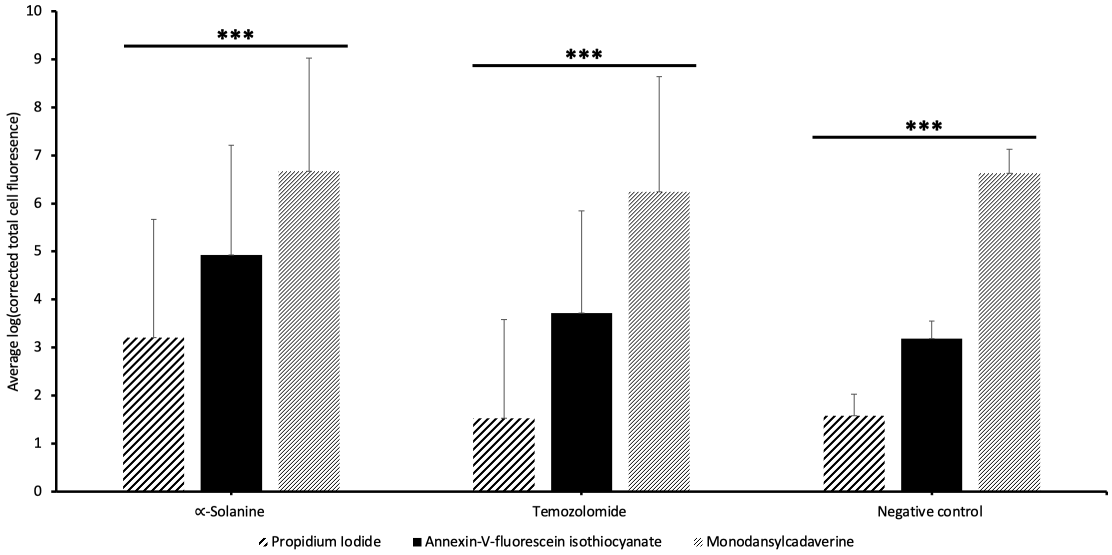


Figure 4.12.: Comparing changes corrected total cell fluorescence following different treatment conditions. Graph demonstrating average log corrected total cell fluorescence on the Y-axis and stain stratified per treatment on the X-axis. Comparing changes in propidium iodide (PI), annexin-V-fluorescein isothiocyanate (Annexin-V-FITC) or monodansylcadaverine (MDC) corrected total cell fluorescence following treatment with 6.25 µM α-solanine, 1200.00 µM temozolomide (TMZ) or culture (negative control) conditions demonstrated significant deference between stains in glioblastoma cells cultured with α-solanine (H[2]: 16.057; p < 0.001), TMZ (H[2]: 19.190; p < 0.001) and negative control (H[2]: 18.787; p < 0.001) conditions.

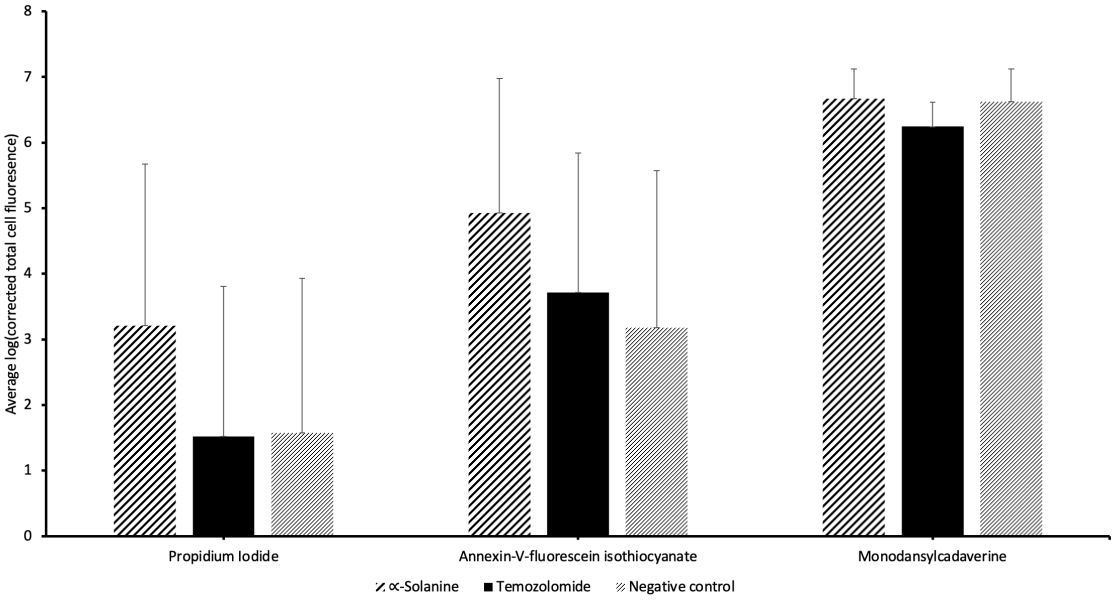


Figure 4.13.: Effect of treatment on corrected total cell fluorescence. Graph representing the average log corrected total cell fluorescence on the Y-axis and treatment stratified per dye on the X-axis. Comparing the effect of 6.25 µM α-solanine, 1200.00 µM temozolomide or culture (negative control) treatment conditions on propidium iodide (PI), annexin-V-fluorescein isothiocyanate (Annexin-V-FITC) or monodansylcadaverine (MDC) corrected total cell fluorescence in glioblastoma multiforme cells.

4.7. Flow cytometry

Flow-cytometry was conducted on U87MG, U251 and T98G cell each treated with 6.25 µM α-solanine, 1200.00 µM temozolomide, 5.00 mM H_20_2 (positive control) or culture conditions (negative control). Staining for each cell line under each treatment condition with Annexin-FITC, PI or MCD was conducted. Gating of samples was conducted to identify suitable cut-off points to detect cells which stained positive for the respective stains (Figure 4.15). All replicates for each cell line, stain and treatment condition are demonstrated in Section 12.7., exemplified by selected replicates in Figures 4.15. and 4.16.

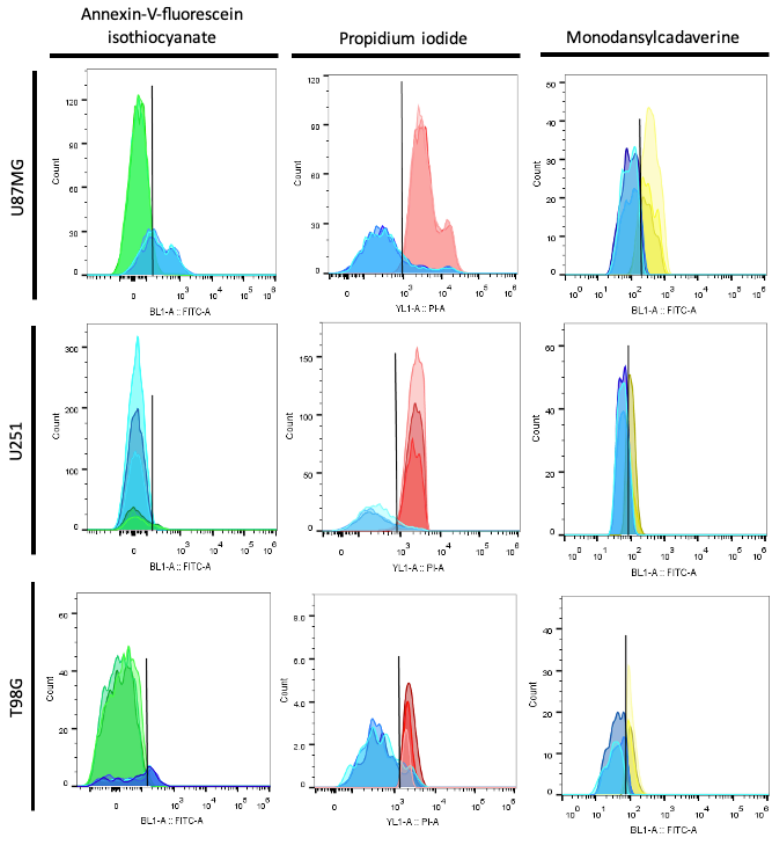


Figure 4.14.:Identifying flow-cytometry gating cut-off values for final analysis. Distinguishing of flow-cytometric cut-off values was achieved by plotting histograms of positive (5.00 mM H2O2) and negative (culture) control conditions and identifying where on the x-axis the two conditions intersect. Cell detected greater than the cut-off values were considered as staining positive for the respective dye. [Blue – culture (negative) control conditions; green/red/yellow - 5.00 mM H_2O_2 (positive) control conditions].

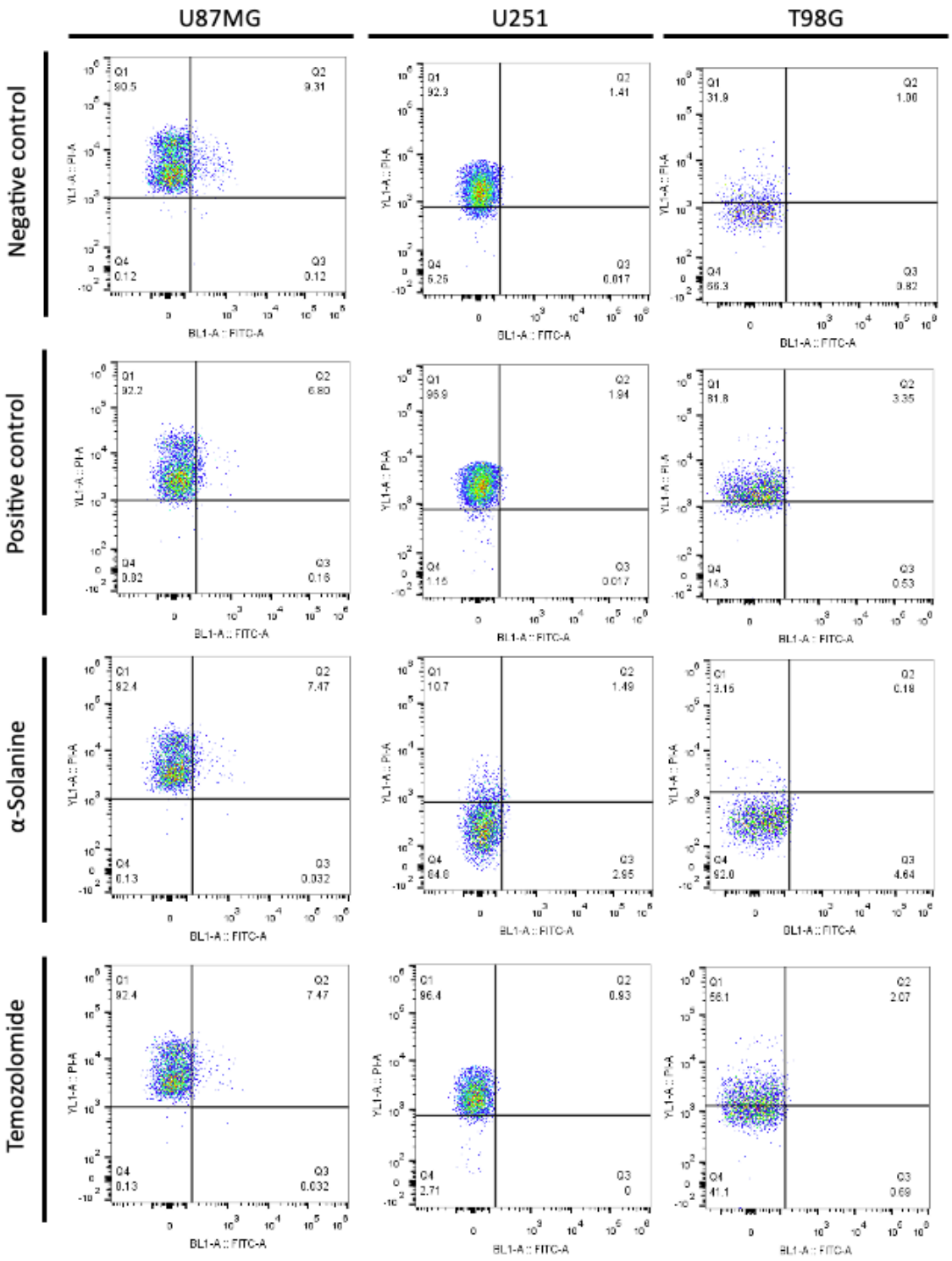


Figure 4.15.: Annexin-V-fluoroscein isothiocyanate flow and propidium iodide flow cytometry analysis. Pseudo-colour plots demonstrating final flow cytometric analysis of U87MG, U251 and T98G cells stained with Annexin-V-fluoroscein isothiocyanate flow (Annexin-V-FITC) and propidium iodide (PI) treated with negative control (culture), positive control (5.00 mM H_20_2), 6.25 µM α-solanine or 1200.00 µM temozolomide for 24-hours.

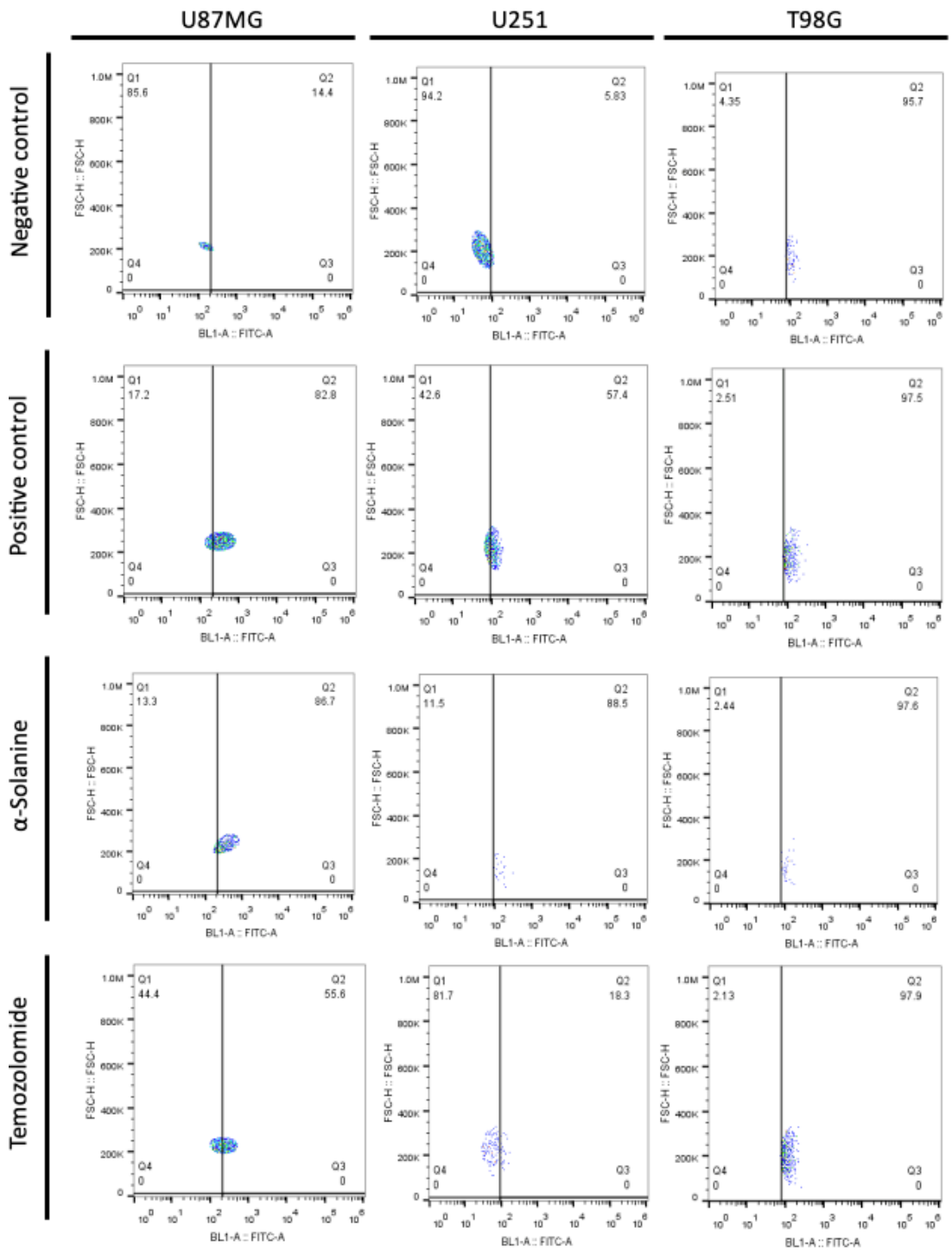


Figure 4.16.: Monodansylcadaverine flow cytometry analysis. Pseudo-colour plots demonstrating final flow cytometric analysis of U87MG, U251 and T98G cells stained with monodansylcadaverine (MDC) treated with negative control (culture), positive control (5.00 mM H_20_2), 6.25 µM α-solanine or 1200.00 µM temozolomide for 24-hours.

4.7.1. Necrosis and autophagy were the predominant forms of cell death induced across all treatment conditions.

Necrosis and autophagy were predominantly induced across all treatment conditions investigated. However, upon closer analysis it may be observed that following α-solanine treatment autophagy was the primary mode of cell death induced, while positive control, negative control and TMZ treatment resulted in necrotic cell death (Figure 4.17.).

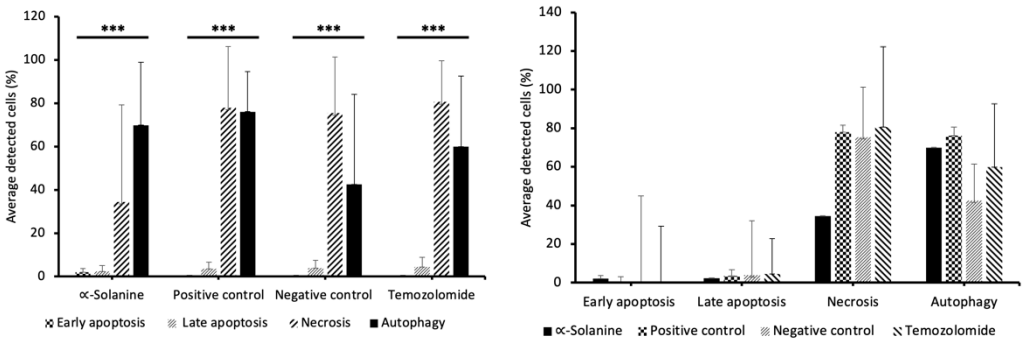


Figure 4.17.: Comparing the effect of treatment overall detected cell death. Graphs demonstrating average detected cell (%) and [left] stage of cell death per treatment condition; and [right] treatment condition per stage of cell death. [Left] Comparing overall early apoptosis, late apoptosis, necrosis, and autophagy per treatment condition with significant difference between stage of cell death detected in glioblastoma cells treated with α-solanine (H[3]: 20.714; p < 0.001), positive control (H[3]: 29.094; p < 0.001), negative control (H[3]: 28.393; P < 0.001) and temozolomide (F[3,32]: 59.506; P < 0.001); and [right] comparing negative control (culture conditions) positive control (5.00 mM H_20_2); 6.25 µM α-solanine; and 1200.00 µM temozolomide treatment per cell death.

4.7.2. Necrosis and autophagy were enhanced, although no significant differences were observed between the treatment conditions investigated.

Comparing the detected levels of the investigated modes of cell death per cell line and treatment condition demonstrated increased necrosis and autophagy across all treatment. It was observed that necrosis was predominant in U87MG and U251 cells (except for U251 cells treated with α-solanine) while autophagy was predominant in T98G cells across all treatment conditions (Figure 4.18.). Upon comparing the effect of

different treatment conditions per mode of cell death and cell line temozolomide treatment significantly increased the occurrence of early apoptosis in comparison to other treatment in U87MG cells, while α-solanine predominantly inducted the occurrence of early apoptosis in U251 and T98G cells, however this observation was only significant in T98G cells. α-solanine significantly increased induced necrosis in U87MG cells; and autophagy in U87MG and U251 cells in-comparison to negative control and temozolomide treatment but not positive control treatment (Figure 4.19.)

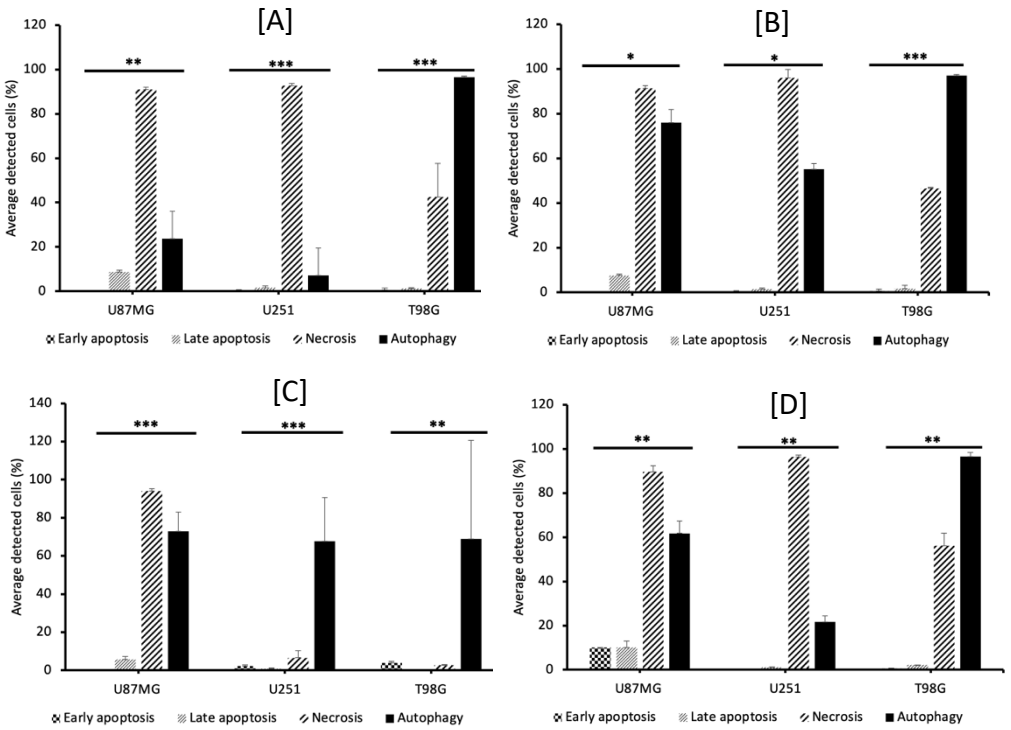


Figure 4.18.: Comparing cell death observed through flow-cytometry per cell line and treatment condition. Graphs representing average detected cell (%) on the Y-axis and stage of cell death per cell line. Comparison of detected glioblastoma multiforme cells undergoing early apoptosis, late apoptosis, necrosis, or autophagy under [A] negative control (culture conditions) with significant difference between stage of cell death noted in U87MG (H[3]: 10.385; p = 0.016), U251 (F[3,8]: 261.082; p < 0.001) and T98G (H[3]: 10.421; p = 0.015) cells; [B] positive control (5.00 mM H_20_2) with significant difference between stage of cell death noted in U87MG (H[3]: 9.452; p = 0.024), U251 (H[3]: 9.409; p = 0.024) and T98G (F[3,7]: 40.024; p < 0.001) cells; [C] 6.25 µM α-solanine with significant difference between stage of cell death noted in U87MG (F[3,8]: 210.407; p < 0.001), U251 (H[3,8]: 34.263; p < 0.001) and T98G (F[3,8]: 6.253; p = 0.017) cells; and [D] 1200.00 µM temozolomide treatment with significant difference between stage of cell death noted in U87MG (H[3]: 10.421; p = 0.015), U251 (H[3]: 10.421; p = 0.015) and T98G (H[3]: 10.385; p = 0.016) cell; for 24-hours.

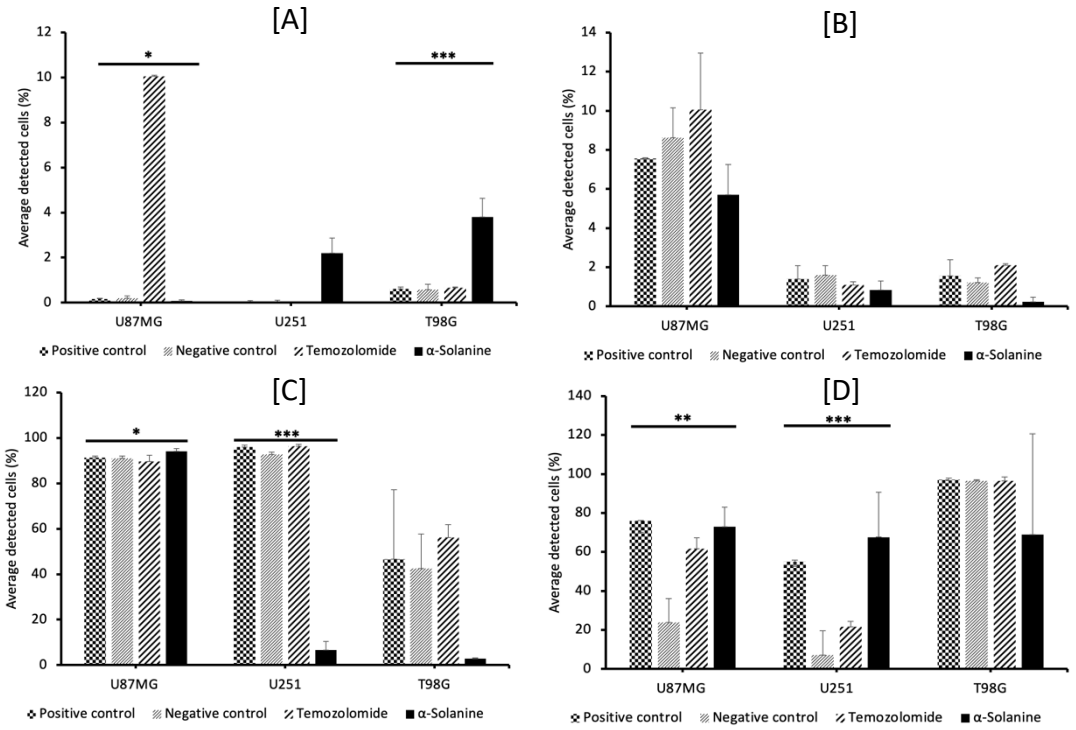


Figure 4.19.: Comparing the effect of treatment on cell death through flow-cytometry per cell line. Graphs comparing average detected cells (%) on the Y-axis and treatment per cell line on the X-axis. Comparing the effect of negative control (culture conditions); positive control (5.00 mM H_2O_2); 6.25 µM α-solanine; and 1200.00 µM temozolomide treatment for 24-hours on [A] early apoptosis with significant difference between treatments in U87MG (H[3]: 8.124; p = 0.044) and T98G (F[3,8]: 40.528; p < 0.001) cells; [B] late apoptosis ; [C] necrosis with significant difference between treatments in U87MG (F[3,8]4.838; p = 0.033) and U251 (F[3,8]: 19.979; p < 0.001) cells and [D] autophagy with significant difference between treatments in U87MG (F[3,8]: 13.459; p = 0.002) and U251 (F[3,8]: 19.979; p < 0.001) cells.

4.7.3. Induced cell death and the effect of treatment on cell death varied between cell lines

T98G cells demonstrated greater occurrence of early apoptosis across all treatment conditions, except for temozolomide treatment where U87MG predominantly underwent early apoptosis. U87MG cells predominantly underwent late apoptosis under all treatment conditions, while T98G cells were the least to under-go necrosis but most likely to undergo autophagy under positive control, negative control and temozolomide treatment. Autophagy induced by α-solanine did not vary between

cell lines (Figure 4.21.). Negative control conditions significantly induced the occurrence of necrosis in U87MG cells. Positive control conditions result in increased necrosis in U87MG and U251 cells and increased autophagy in T98G cells.

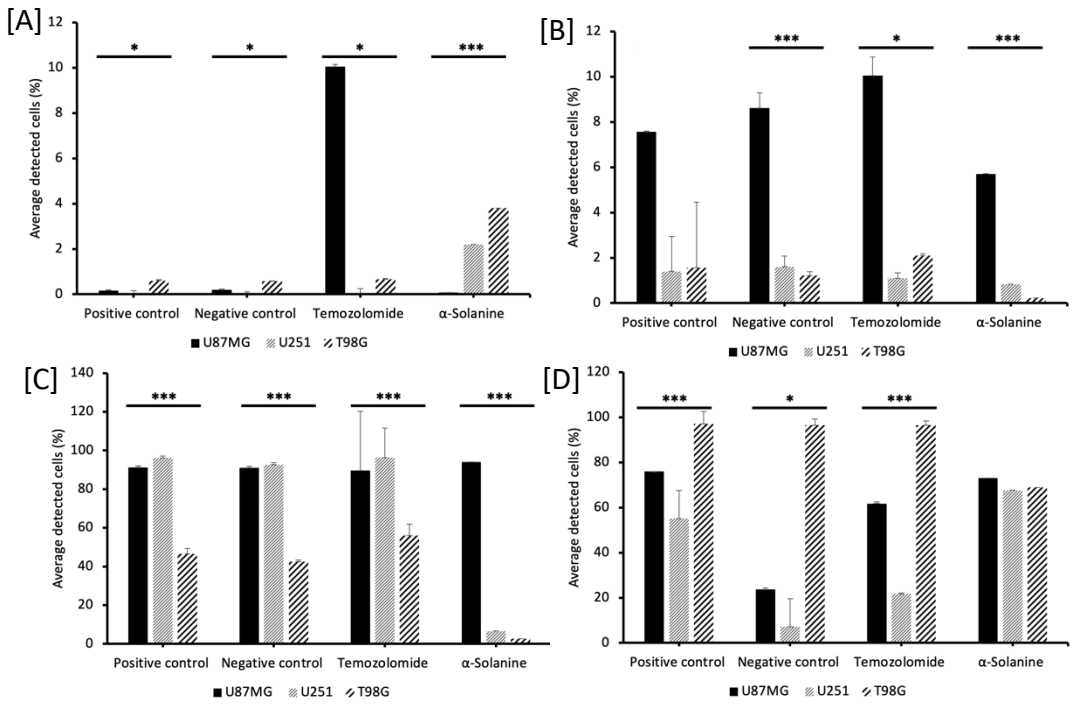


Figure 4.20.: Comparing the effect of treatment on cell death through flow-cytometry between cell lines. Graphs demonstrating the average detected cells (%) versus cell line stratified by treatment condition. Comparing the effect of negative control (culture conditions); positive control (5.00 mM H_20_2); 6.25 µM α-solanine; and 1200.00 µM temozolomide (TMZ) treatment for 24-hours on [A] early apoptosis with significant difference being noted between cell lines under positive control (H[2]: 7.261; p = 0.027), negative control (F[2,6]: 10.160; p = 0.012), TMZ (H[2]: 7.322; p = 0.026) AND α-solanine (F[2,6]: 65.825; p < 0.001), treatment; [B] late apoptosis with significant difference being noted between cell lines under negative control (F[2,6]: 37.518; p < 0.001), TMZ (H[2: 7.200; p = 0.027) AND α-solanine (F[2,6]: 235,709; p < 0.001), treatment; [C] necrosis with significant difference being noted between cell lines under positive control (H[2]: 7.200; p = 0.027), negative control (F[2,6]: 26.921; p = 0.001), TMZ (F[2,6]: 115.080; p < 0.001) AND α-solanine (F[2,6]: 235.709; p < 0.001), treatment; and [D] autophagy with significant difference being noted between cell lines under positive control (F[2,6]: 167.429; p < 0.001), negative control (H[2]: 7.261; p = 0.027) and TMZ (F[2,6]: 135.661; p < 0.001) treatment.

4.8. α-solanine induced increased expression of Bax, BECN1, ATG4B and PKM2 genes.

rt-qPCR was conducted to assess the effect of 1200.00 µM temozolomide versus 6.25 µM α-solanine versus 5.00 mM H_2O_2 (positive control) on Bax, Casp-3, BECN1, ATG4B, ATF6, PKM2, VEGFA gene expression. Due to the limited number of biological repeats conducted differences in gene expression between cell lines and within treatments could not be assessed. α-solanine treatment significantly increased the expression of Bax, BECN1 and ATG4B genes (Figure 4.12.).

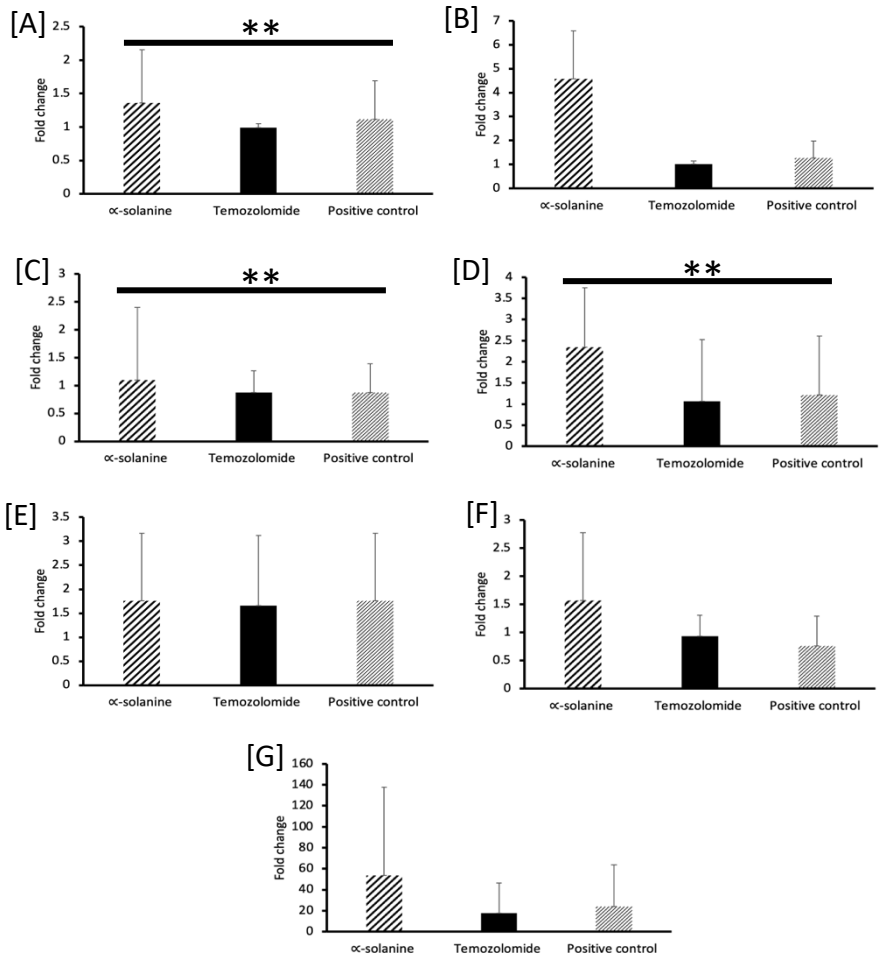


Figure 4.21: Effect of temozolomide, solanine and positive control treatment on the expression of pre-selected genes. Graphs demonstrating **gene fold change on the Y-axis and treatment condition on the X-axis. Comparision of** ***the effect of 1200.00 µM temozolomide versus 6.25 µM α-solanine versus 5.00 mM H2O2 on [A] Bax; [B] Casp-3; [C] BECN1; [D] ATG4B; [E] ATF6; [F] PKM2 and [G] VEGFA gene expression.*** **Stastistically significant difference in fold change between treatment was noted for Bax (H[2]: 11.380; p = 0.003), BECN1 (F[2,15]: 54.277; p < 0.001) and ATG4B (H[2]: 11.474; p = 0.003) genes.**

4.9. Both apoptotic and autophagic proteins were upregulated following α-solanine treatment

Antibody arrays were used to investigate the effect of 24 hour 6.25 µM α-solanine treatment in comparison to negative control (culture) conditions on the expression levels of proteins involved in apoptosis and autophagy. Figure 4.23. demonstrated the location on the membranes of and proteins investigated.

Apoptosis				Autophagy	
Location	Target	Location	Target	Location	Target
A1, A2	Positive reference	A5, A6	IGFBP-1	A1, A2	Positive reference
B1, B2	Positive reference	B5, B6	IGFBP-2	B1, B2	Positive reference
C1, C2	Negative reference	C5, C6	IGFBP-3	C1, C2	Negative reference
D1, D2	Negative reference	D5, D6	IGFBP-4	D1, D2	Negative reference
E1, E2	BLANK	E5, E6	IGFBP-5	E1, E2	ATG3
F1, F2	BLANK	F5, F6	IGFBP-6	F1, F2	ATG4A
G1, G2	Bad	G5, G6	IGF-1R	G1, G2	ATG4B
H1, H1	Bax	H5, H6	livin	H1, H1	ATG5
I1, I2	Bcl-2	I5, I6	p21	A3, A4	Negative reference
J1, J2	Bcl-w	J5, J6	p27	B3, A4	Negative reference
K1, K2	Bid	K5, K6	p53	C3, C4	ATG7
L1, L2	Bim	L5, L6	SMAC	D3, D4	ATG10
M1, M2	Casp-3	M5, M6	Survivin	E3, E4	ATG12
N1, M3	Casp-8	N5, N6	TNF RI	F3, F4	ATG13
A3, A4	CD40	A7, A8	TNF RII	G3, G4	BECN1
B3, A4	CD40 ligand	B7, B8	TNF alpha	H3, H4	BNIP3L
C3, C4	cIAP-2	C7, C8	TNF beta	A5, A6	DDR2
D3, D4	Cyt-C	D7, D8	TRAIL R1	B5, B6	GABARAP
E3, E4	TNFRSF21	E7, E8	TRAIL R2	C5, C6	LAMP1
F3, F4	Fas	F7, F8	TRAIL R3	D5, D6	LC3A
G3, G4	Fas ligand	G7, G8	TRAIL R 4	E5, E6	LC3B
H3, H4	Blank	H7, H8	XIAP	F5, F6	NBS1
I3, I4	HSP27	I7, I8	BLANK	G5, G6	P62
J3, J4	HSP60	J7, J8	BLANK	H5, H6	Negative reference
K3, K4	HSP70	K7, K8	Negative reference	A7, A8	Rheb
L3, L4	HTRA2	L7, L8	Negative reference	B7, B8	MSK1
M3, M4	IGF-1	M7, M8	Negative reference	C7, C8	Alpha-synuclein
N3, N4	IGF-2	N7, N8	Positive reference	D7, D8	Negative reference
				E7, E8	Negative reference
				F7, F8	Negative reference
				G7, G8	Negative reference
				H7, H8	Positive reference

Figure 4.22: Reference for the proteins tested using antibody arrays. Figure depicting the position of the anti-bodies on the dot-blots utilised to assess the expression of apoptosis and autophagic proteins following treatment. Loci obtained from manufacturer's (RayBiotech) brochure.

Resultant dot blots following membrane incubation with secondary antibodies demonstrated positive reference spots appearing dark and blank and negative reference spots appearing the same colour as the background signal, indicating reliability of results obtained (Figure 4.24.; Figure 4.25.). Of the 63 investigated proteins, only 18 satisfied the predetermined criteria to be considered as differentially expressed (Table 4.3.).

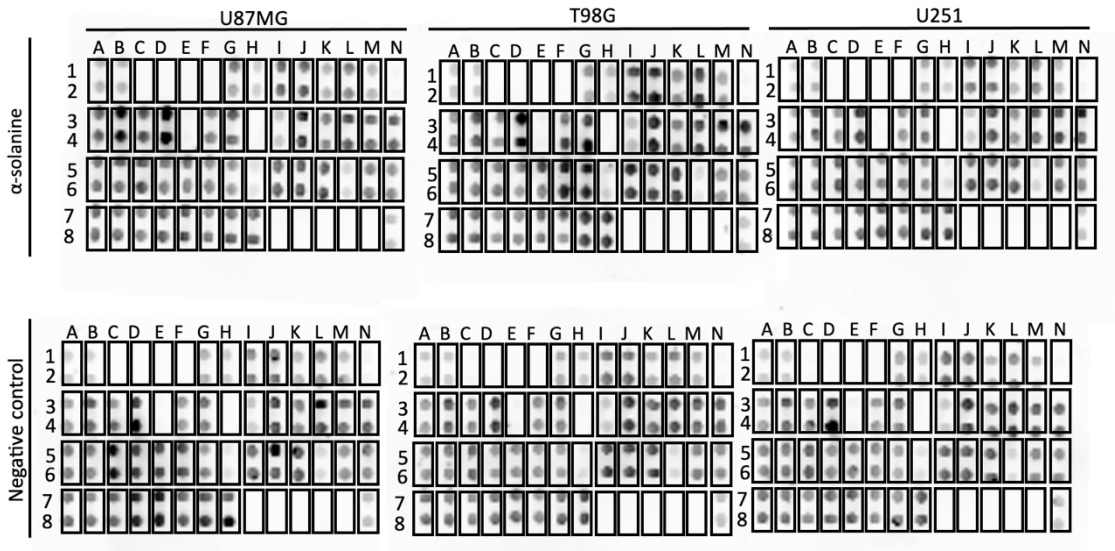


Figure 4.21.: Apoptosis antibody array results

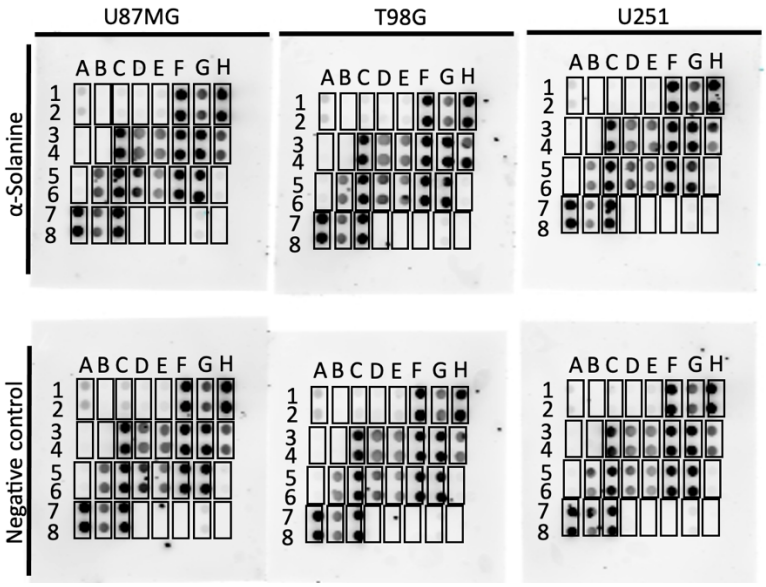


Figure 4.23.: Autophagy antibody array results. Dot blots obtained after incubating membranes containing anti-bodies against apoptotic and autophagic proteins with proteins from U87MG, T98G or U251 cells treated with either 6.25 µM α-solanine or negative control.

Table 4.3.: Differentially expressed proteins following 24 hour treatment with 6.25 µM α-solanine. Bad (W[5.905]; p = 0.022), Bcl-2 (T[10]: -6.517; p < 0.001), Bcl-w (T[10]: -9.720; p < 0.001), Bid (T[10]: -6.576; p < 0.001), Bim (W[5.171]; p = 0.021), TNFRSF5 (W[5.591]: -3.058; p = 0.024), TNSF5 (T[-3.398]: 5.110; p = 0.019), cIAP-2 (T[10]: -3.316; p = 0.011), Cyt-c (T[10]: -2.654; p = 0.024), Fas (T[10]: -3.072; p = 0.012), Fas ligand (T[10]: -2.729; p = 0.021), IGF-2 (T[10]: -2.777; p = 0.020), IGF-1R (T[10]: -2.240; p = 0.049), ATG4A (W[6.158]: -21.933; p < 0.001), ATG4B (T[10]: -9.606; p < 0.001), BECN1 (T[10]: -27.369; p < 0.001), BNIP3L (T[10]: -10.111; p < 0.001), and LC3A (T[10]: -4.913; p < 0.001) were significantly overexpressed under 6.25 µM α-solanine in comparison to negative control conditions.

Protein	Fold Change	Pair-wise sample testing
Bad	1.50	0.02
Bcl-2	1.54	<0.001
Bcl-w	1.47	<0.001
Bid	1.64	<0.001
Bim	1.74	0.02
TNFRSF5	1.57	0.02
TNFSF5	1.57	0.02
cIAP-2	1.48	0.01
Cyt-C	1.46	0.02
Fas	1.67	0.03
Fas ligand	1.73	0.04
IGF-2	1.47	0.03
IGF-1R	1.71	0.07
ATG4A	1.47	<0.001
ATG4B	1.46	<0.001
BECN1	1.46	<0.001
BNIP3L	1.54	<0.001
LC3A	1.46	<0.001

4.10. Protein-protein interaction analysis demonstrated interplay between proteins involved in autophagy and caspase independent apoptosis.

Initial PPI construction resulted in a network consisted of 367 interactions between the proteins investigated by the antibody-array experiments and their foremost direct protein targets which take part in apoptotic or autophagic cell death (Figure 4.26.) . Pruning of the initial PPI network to only include differentially expressed proteins resulted the PPI network demonstrated in Figure 4.27. Protein fold change was presented in the colouring of the PPI network nodes in form of a heat-map, with darker colours demonstrating larger fold change data. PPI network analysis demonstrated that

assayed proteins which were differentially expressed and interact with each-other may be involved in the induction of autophagy and caspase independent apoptosis.

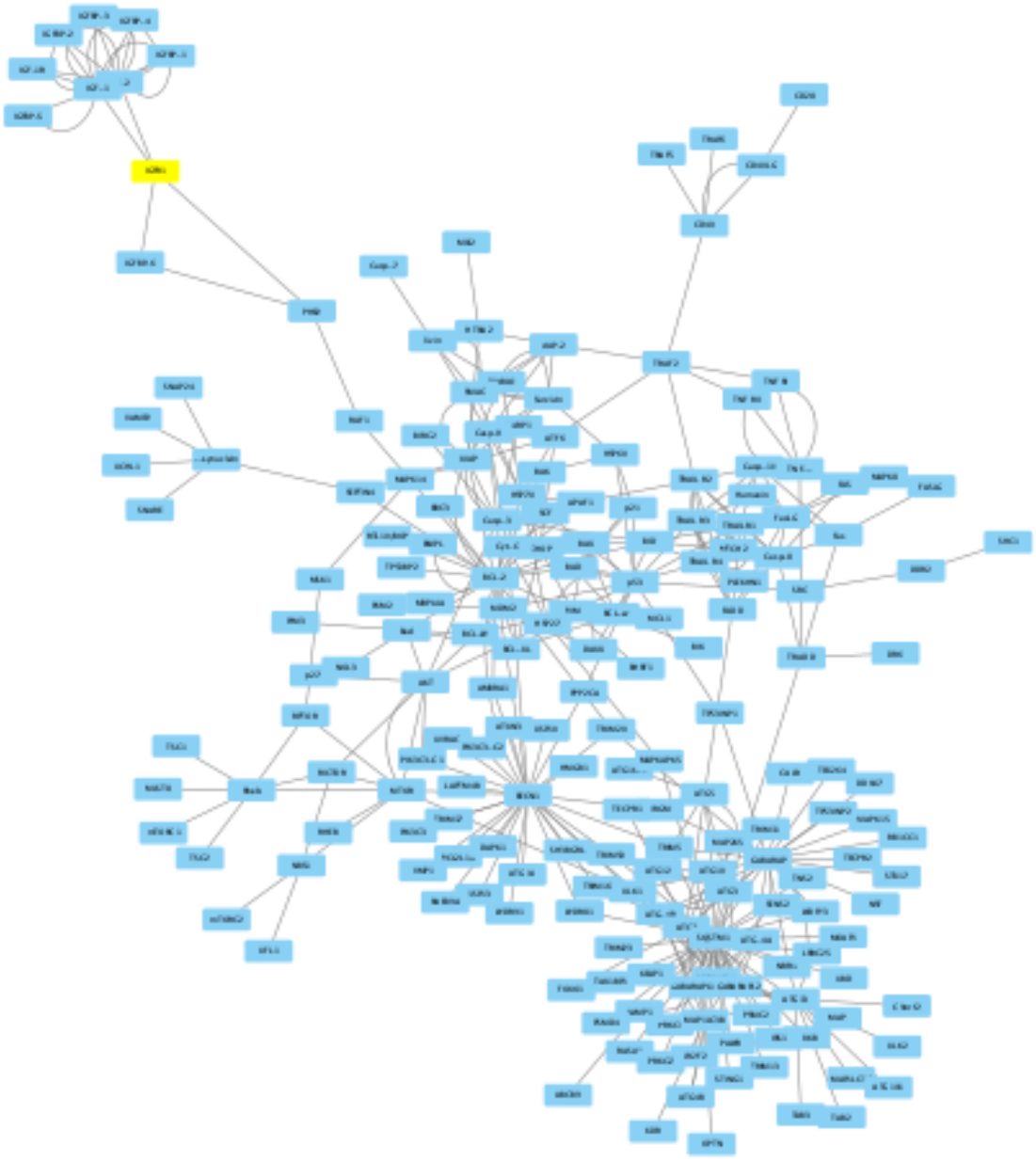


Figure 4.24.: Initial protein -protein interaction network. Protein-protein interaction network (PPIN) generated using cytoscape representing the top 5 interactions of the 63 proteins arrayed using the anti-body proteome profiling kits used.

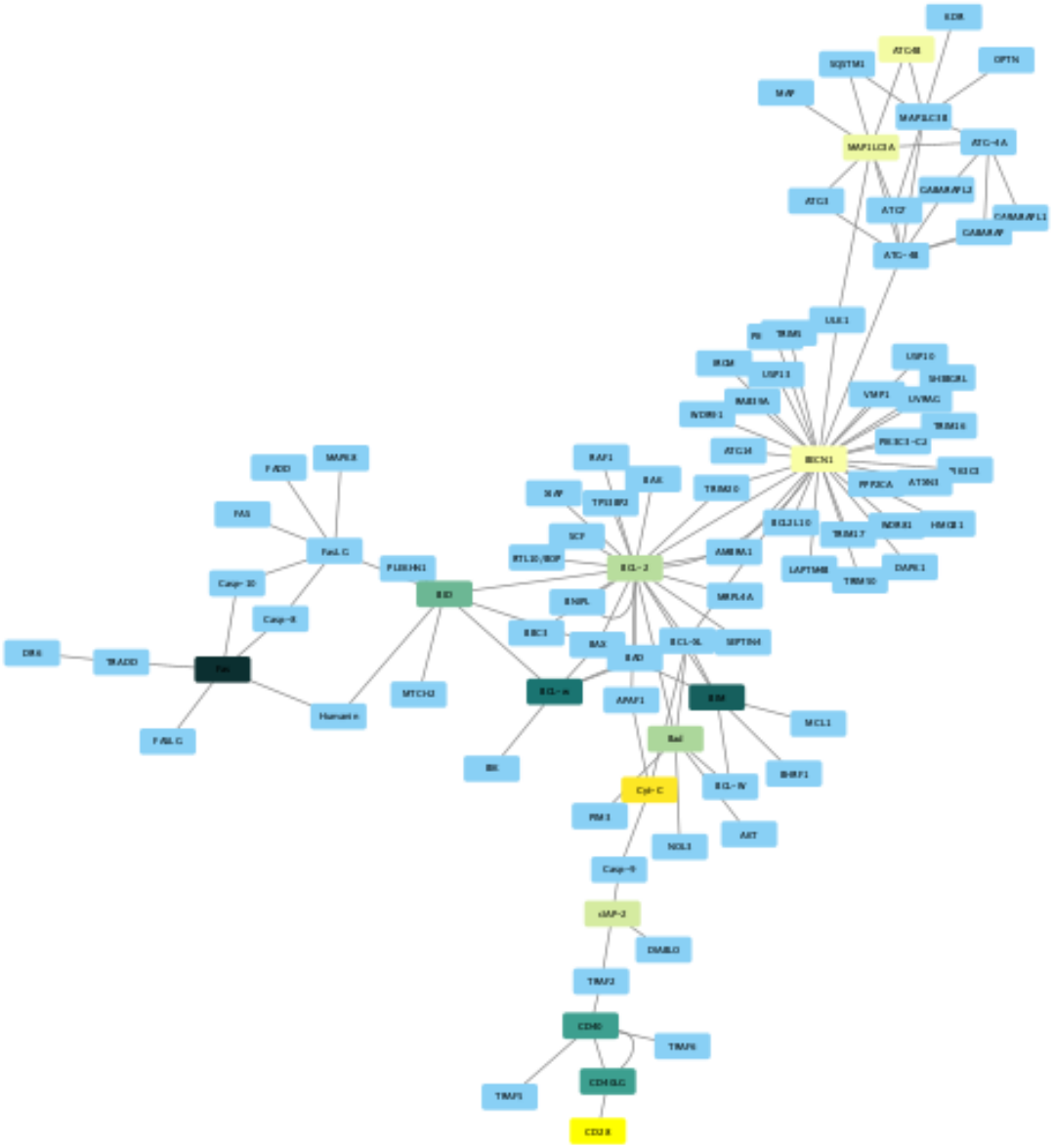


Figure 4.25.: Finalised protein-protein interaction network. Protein-protein interaction network (PPIN) which has been pruned to only demonstrate significantly overexpressed proteins under α-solanine in comparison to negative control conditions.

Chapter 5 Discussion

Following the post-Stupp treatment regimen era for treating GBM (Sheikh et al., 2020), and the advent of the WHO CNST 2021 being implemented across the board (Louis et al., 2021; Stoyanov et al., 2022), global efforts are being made to identify putative therapeutic agents which demonstrate superiority over TMZ against WHO grade IV $IDH_{wildtype}$ GBM. Phytochemicals have emerged as a promising, accessible, and abundant source of chemicals which may have potential chemotherapeutic significance against GBM (Salim et al., 2018). α-solanine, a glycoalkaloid dervided from *Solanum* plants such as potaotes and tomatoes (Friedman, 2015), has emerged as a promising anti-cancer agent against a multitude of different neoplasms (Luo et al., 2021) . The only study to assess the efficacy of α-solanine against TMZ-sensitive GBM cells *in-vitro* (U87MG and U251) was conducted using α-solanine dissolved in DMSO, prior to the WHO 2021 CNST classification (Guo et al., 2019). Our study has demonstrated that U87MG and U251 cells are extremely sensitive to DMSO (Chapter 10), hence conclusions made by Guo *et al.,* (2021) may not be reliable.

In this study, we conducted the first assessment of α-solanine's cytotoxicity and its effects on the migration and invasion properties of GBM (glioblastoma) cells. We examined both TMZ-sensitive and -resistant cell lines, and compared the efficacy of α-solanine with that of TMZ. H_2O_2 was used as a positive control, since current literature evidences that α-solanine primarily produces its cytotxic effects by generating ROS. Culture conditions (DMEM/F12) was used both as vehicle for α-solanine and TMZ as well as the negative control. Moreover, this project strived to increase the current understanding of α-solanine’s effect on the apoptosis-autophagy

axis on both a cellular and molecular level, by employing expeirmental and bioinformatic techniques.

In-light of the WHO 2021 CNST classification, the IDH gene of all three GBM cell-lines used throughout this project was sequenced since suppliers only specify that the cell lines used throughout this project were high-grade astrocytoma even through it is widely accepted that these cell lines may be considered as GBM. WHO grade IV $IDH_{wildtype}$ status was confirmed, and thus this study provides insight on α-solanine's effect on true GBM.

5.1. α-solanine vehicle troubleshooting

During the initial phases of this study, DMSO was used as a vehicle for α-solanine, since it is a commonly used vehicle for organic molecules. However, unexpected results were obtained after conducting PrestoBlue® viability assys on U87MG cells. Despite varying concentrations of α-solanine, minimal cell viability was observed in spite of increasing concentration, which contradicted published literature examining the cytotoxic effects of α-solanine on different cancer cell lines. This led to the hypothesis that GBM cells may exhibit sensitivty to DMSO.

To test this hypothesis, the viability of U87MG cells was evaluated using the lowest (5.00 µM α-solanine) and highest (50.00 µM α-solanine) concentrations of α-solanine in DMSO from the previous PrestoBlue® experiment, along with equivalent concentrations of DMSO as a control. Additionally, since some studies reported using α-solanine dissolved in aqueous solutions, the viability of U87MG cells treated with

equivalent concentrations of α-solanine dissolved in DMEM/F12 medium was also investigated.

The results showed no significant difference in U87MG cell viability between 1.00 % and 10.00 % DMSO, as well as between 5.00 µM α-solanine in DMSO and 50.00 µM α-solanine in DMSO. This suggests that the cytotoxic effect observed with α-solanine in DMSO was likely attributed to the vehicle (DMSO) itself rather than the effect of α-solanine. In contrast, α-solanine dissolved in DMEM/F12 medium yielded expected results, consistent with findings reported in published literature.

The obtained findings indicated that DMSO may not be suitable as a vehicle for α-solanine when studying its cytotoxic effects on GBM cells. Conversely, using α-solanine dissolved in DMEM/F12 medium appeared to be a more reliable approach to obtain accurate results, thus DMEM/12 medium was used as the vehicle for α-solanine throughout the project.

5.2. α-solanine has the potential to be a putative agent against glioblastoma multiforme while exhibiting comparable effectiveness to other types of cancers

Literature has demonstrated that α-solanine may potentially be an effective cytotoxic agent against numerous cancers, with documented 24-hour and 48-hour IC_{50} ranging between 10.00 µM – 32.18 µM and 9.65 µM – 20.84 µM respectively (Hasanain et al., 2015; Karaboğa Arslan & Yerer, 2018; K.-R. Lee et al., 2004; Mohsenikia et al., 2013, 2016; Yan et al., 2020; Zheng et al., 2020). Yet published evidence against its efficacy against GBM is ambigious. In this study the effect of α-solanine treatment was assessed against both TMZ-sensitive (U87MG and U251 cell lines) and TMZ-resistant

GBM (T98G cell line), with the experimentally obtained IC_{50} being congruent with that reported in published literature, ranging from 19.66 μM – 22.87 μM. Yet, it is worth noting that in this project cell viability assays were conducted after 72-hours as opposed to 24- and 48-hours reported in published literature assessing the viability of different cancer following α-solanine treatment. Seventy-two hour incubation with α-solanine was conducting instead of 24-hour or 48-hour since the GBM cells used in this study have long doubling times (Reichert et al., 2002). Through logistic regression of cell viability data obtained, the working concentration (IC_{25}) of α-solanine was deduced and used throughout the remainder of the project. IC_{25} was used since to ensure that any observed effects could not be attributed α-solanine's cytotoxic properties. Moreover, 24 hours duration was used for the remainder of the project since this enabled the collection of sufficient cell pellet.

The effect of α-solanine on GBM cell metastatic properties were also assessed. Migration of GBM cells was decreased in a time dependent manner, however the effect of different doses on the GBM cell migration was not assessed. Our findings are congruent with published literature which demonstrated that α-solanine decreases choriocarcinoma, lung, heptatocellular colorectal, pancreatic, hepatocellular and oesophageal caricnoma cell migration (Gu et al., 2021; Lu et al., 2010; Lv et al., 2014; Shen et al., 2014; Wang et al., 2016; Yan et al., 2020; Zhang et al., 2016). In our study, the effect of α-solanine on GBM invasion in comparision to negative control was not elucidated, as anomalous data was obtained for U87MG, U251 and T98G cell invasion under negative control treatment conditions. Published literature suggests that α-solanine decreases cell invasion in comparision to control conditions employed in the individual studies (Gu et al., 2021; Lu et al., 2010; Lv et al., 2014; Shen et al., 2014; Wang

et al., 2016; Yan et al., 2020; Zhang et al., 2016). Howeover, these studies utilise Matrigel invasion assays, in contrast to the trans-well invasion assays employed in this project. In matrigel invasion assays, cells are cultured on a layer of matrigel/ on a matrigel coated trans-well while starving cells of serum in the upper chamber of the assay to promote chemotaxic invasion (Justus et al., 2014). Moreover, statistical analysis of cancer cell invasion was assessed using one-way ANOVA and Dunnett's poc hoc testing, even though the number of invaded cells (count) data was presented, which is non-parametric. Such methodological disrepancies and lack of negative control data limited effective comparision between findings presented in this study and published literature.

Thus, α-solanine may be an efficatious cytotoxic agent against GBM *in-vitro*. Furthermore α-solanine has exhibited successful outcomes in reducing the migration of GBM cell *in*-vitro. However, while the phytochemical's effects on viability and migration are encouraging, its effect on invasion requires further work to elcuidate the effects of α-solanine versus control conditions.

5.3. α-solanine may be superior to temozolomide against glioblastoma multiforme *in-vitro*

The efficacy of α-solanine against TMZ treatment was assessed during this study. TMZ treatment IC_{50} against all three cell lines used in this project was not achieved. T98G cells demosntrated greater resistantce to TMZ, which was expected since this cell line is known to be inherently resistant to TMZ. Yet, U87MG and U251 cells have been documented to also develop resistance to TMZ, which may explain the viability results obtained in this study (S. Y. Lee, 2016).

α-Solanine treatment was more potentet than TMZ treatment, however TMZ IC_{50} was not achieved experimentally in this study, even though concentrations up to 2400.00 μM were assessed against GBM cell viability. This constraint impeded the ability to perform inferential statistical comparisons between the treatment of α-solanine and TMZ. The inability of TMZ treatment of reach that IC_{50} threshold even at concentrations exceeding 100 times the concentration achieved by α-solanine implies that the α-solanine compound exhibits greater potency than TMZ against GBM cells in an *in-vitro* setting.

This suggested superiority over TMZ against GBM may be extended to the drugs' potential in reducing GBM cell migration *in-vitro*. α-Solanine treatment demonstrated greater inhibition of relative wound closure across all cells lines after 24-hours of treatment. In TMZ-sensitive cells treatment further inhibited relative migration at 48-hour (U251) and 72-hour (U87MG) durations of incubation. However, no statistical difference between α-solanine and TMZ treatment was noted in T98G cells at 48- and 72- times, despite α-Solanine treatment exhibiting decreased T98G relative migration. Furthermore, GBM cell invasion was not statistically different between TMZ and α-solanine. Based on the evidence generated in this study, it can be suggested that α-solanine exhibits comparable effectiveness to TMZ in reducing GBM cell invasion. However, it is important to note that this should not be considered a definitive conclusion, but rather a rationale for further investigations to fully understand any potential distinctions between the effects of these two molecules on GBM cell invasion.

5.4. Fluorescent microscopy and and flow cytometry assays provided ambigious conclusions regarding mode of cell death induced by α-solanine

The present study aimed to investigate apoptotic and autophagic cell death in U87MG, U251, and T98G cells under TMZ and α-solanine treatment conditions. Fluorescent imaging and flow cytometric analyses were utilized to assess the occurrence of apoptosis (using Annexin-V-FITC and PI staining) and autophagy (using MDC staining).

Fluorescent imaging results indicated higher CTCF for MDC compared to Annexin-V-FITC and PI staining, although no statistically significant differences were observed when comparing between treatment conditions. Lack of fluoresence across all cells lines limited the comprehensive assessment of changes in Annexin-V-FITC, PI, and MDC CTCF following the different treatment conditions.

Flow cytometry was conducted on all three cell lines used in this project cells treated with α-solanine, TMZ, H_2O_2 (positive control), or culture conditions (negative control), to reinforce conclusions drawn during fluorescent imaging and observe the occurrence of early apoptosis, late apoptosis and necrosis. Samples were again stained with Annexin-V-FITC, PI, or MDC and gating was performed to identify cells staining positive for each marker. Necrosis and autophagy were predominantly induced across all treatment conditions. Notably, α-solanine treatment primarily induced autophagic cell death, while positive control, negative control, and TMZ treatments resulted in necrotic cell death.

Comparative analysis of cell death modes revealed increased necrosis and autophagy across all treatment conditions. Necrosis was predominantly observed in U87MG and U251 cells (except for U251 cells treated with α-solanine, whereas autophagy was more prevalent in T98G cells. TMZ treatment significantly increased

early apoptosis in U87MG cells compared to other treatments, while α-solanine predominantly induced early apoptosis in U251 and T98G cells, with significant effects observed only in T98G cells. α-solanine treatment significantly increased induced necrosis in U87MG cells and autophagy in U87MG and U251 cells compared to negative control and TMZ treatments, but not the positive control.

Notably, T98G cells exhibited a higher occurrence of early apoptosis across all treatment conditions, except for temozolomide treatment, where U87MG cells predominantly underwent early apoptosis. U87MG cells primarily underwent late apoptosis under all treatment conditions, while T98G cells exhibited the least susceptibility to necrosis but were more likely to undergo autophagy under positive control, negative control, and temozolomide treatment. Autophagy induced by α-solanine did not vary significantly between cell lines.

Negative control conditions significantly induced necrosis in U87MG cells, while positive control conditions led to increased necrosis in U87MG and U251 cells and increased autophagy in T98G cells. Similar trends were observed under α-solanine treatment, and to a lesser extent, temozolomide treatment.

The similarity in the results obtained from treatment conditions and negative control conditions poses limitations on the conclusions on a cellular level regarding the occurrence of apoptosis and autophagy that can be drawn from the study. The fact that negative control conditions induced necrosis in U87MG cells, while positive control conditions induced necrosis in U87MG and U251 cells, and autophagy in T98G cells, raises concerns regarding the specificity of the observed effects. These findings suggest that the observed cellular responses may not be solely attributed to α-solanine treatment, but could be influenced by factors unrelated to the experimental

interventions. It is also possible that the necrosis observed was an artifact, as visual inspection of GBM cells under negative control conditions appeared normal.

The lack of a distinct difference between the treatment conditions and the negative control condition undermines the ability to make definitive conclusions about the effectiveness or specific mode of action of α-solanine and temozolomide in inducing cell death. It indicates that the observed effects may be attributed to non-specific or inherent cellular responses rather than the direct actions of the treatments.

To establish a clear understanding of the effects of α-solanine and temozolomide on necrosis and autophagy, it is essential to compare the results with a negative control condition that does not induce significant cellular responses. The similarity between the treatment and negative control conditions raises questions about the specificity and reliability of the observed outcomes. Increasing the number of biological repeates, and further investigation employing different techniques (such as Hoescht staining against apoptosis and LC3-II and LAMP-1 immunohistochemistry) are necessary to validate and accurately interpret the effects of α-solanine on apoptosis, necrosis and autophagy in the studied GBM cell lines.

This study was the first to assess the occurrence of both apoptosis and autophagy and empoly the use of MDC staining in cancer cells treated with α-solanine. Despite inconclusive evidence on the occurrence of apoptosis and auophagy incuded by α-solanine treatment, findings presented in this study are on-par with published literature. Gu et al (2021), Gao et al (2012), Ji et al (2008), Meng et al (2016) Wang et al (2016a, 2016b) and Yang et al (2019) all evidence the occurence of apoptosis following α-solanine treatment (Gu et al., 2021; Ji & Gao, 2012; Yang et al., 2019) . However the

percentage of Annexin V-FITC^{+}/PI^{-}, Annexin V-FITC^{+}/PI^{+} cells detected following were often minimal (< 10.00 %), similar to findings presented in this study.

Despite noted limitations, the increased levels of autophagy in-comparision to apoptosis recorded in this study support conclusions made by Hasanain *et al.* (2015), who demonstrated in detail that α-solanine induces autophagy, likely by inducing ROS mediated ER stress. Upregulation of ER stress markers, formation of the autophagasome and its fusion with the lysosome were recorded through immunohistochemistry experiments and confirmed using PCR and western blot techniques (Hasanain et al., 2015). Parallel observations between the findings presented in this study and those recorded by Hasanain et al. (2015) strengthens the notion that α-solanine may predominantly induce autophagy rather than apoptosis.

5.5. Experiments investigating the effect of α-solanine treatment on molecular cell death changes suggest dysregulation of key proteins

Following evidence obtained on a cellular level regarding the mode of cell death induced by α-solanine, experiments to assess changes induced by α-solanine treatment on a molecular treatment were conducted to better understand how α-solanine induced cell death. Moreover, apoptosis and autophagy are intertwined, often sharing key regulatory proteins, necessitating in-depth analysis of the specific proteins governing apoptosis and autophgy (Boya et al., 2013; Noguchi et al., 2020; Thorburn, 2008).

Select genes were assayed using rt-qPCR to determine whether α-solanine dysregulated their expression levels. Noteably, Bax, BECN1 and ATG4B were

significantly upregulated in comparision to TMZ and positive control treatment, as demonstrated by post-hoc testing. Effector Casp-3, ER stress marker ATF6 expression levels, pro-angiogenic VEGFA and PKM2 expression levels were also investigated, however these were not signifcantly upregulated. The upregulation of the aforementioned genes support the hypothesis that α-solanine does not induce solely apoptosis or autophagy.

It is important to note that the number of genes investigated in this study was limited, representing a partial snapshot of the molecular response of GBM cells to α-solanine treatment. To complement the rt-qPCR analysis and gain a broader understanding of the molecular changes induced by α-solanine, proteome profiling of proteins involved in apoptosis and autophagy was conducted, since this approach enabled the identification and quantification of a larger set of proteins associated with the apoptotic and autophagic cellular response. Through employing rigorous threshold values Bad, Bcl-2, Bcl-w, Bid, Bim, CD40, CD40 ligand, ciAP-2, Cyt-C, Fas, Fas ligand, IGF-2, IGF-1R, ATG4A, ATG4B, BECN1, BNIP3L and LC3A proteins were observed to be upregulated. These results are supported by Hasanain et al. (2015) who demonstrated the upregulation of proteins invovled in autophagosome formation. Yet, numerous studies documented Bax upregulation and Bcl-2 down-regulation (Gao et al., 2020; Gouhar et al., 2022; Gu et al., 2021; Meng et al., 2016; Pan et al., 2016; Sun et al., 2014; Zhang et al., 2016). Rt-qPCR experiment supports bax upregulation, however proteome profiling demonstrated the opposite effect of Bax downregulation and Bcl-2 upregulation, further suggesting that α-solanine treatment directs cancer cell death through autophagy. Yet, it should be noted that Bid and Bim, which were noted to be upregulated, are known to upregulate Bax espression (Roufayel et al., 2022), which may

explain the observed rt-qPCR results. Since BECN1 gene upregulation was also observed at a protein level, this may suggest that increased expression of BECN1 is a significant molecular effect of α-solanine treatment.

Notwithstanding, the interaction between apoptotic and autophagic proteins is dynamic and very complex. A PPI network was constructed to visualise the interactions between the proteins noted to be upregulated through proteome profiling. The interactions between BENC1/Bcl-2; Bcl-2/Bim; Bcl-2/Bid and Fas/Bid emerged and promising targets dysregulated by α-solanine. Fas ligand and Fas receptor upregulation results in downstream Bid activation which subsequently acts to inhibit Bcl-2 and promote mitochondrial membrane permeabilization. Bcl-2 inhibition promotes BECN1 activation resulting in autophagy, consolidated by upregulating ATG4 and LC3A. Furthermore, thus study has identified that α-solanine induces BNIP3L upregulation which mediates mitophagy to ensure the removal of dysfunctional mitochondria and reduce oxidative damage (Figure 5.1). The upregulation of both BECN1 and Bcl-2 may reflect a dissociation of BECN1 from Bcl-2 in the BECN1/Bcl-2 complex. α-solanine thus has the potential to modulate cell death pathways, resulting in a complex cellular response involving apoptosis, autophagy as well as mitophagy.

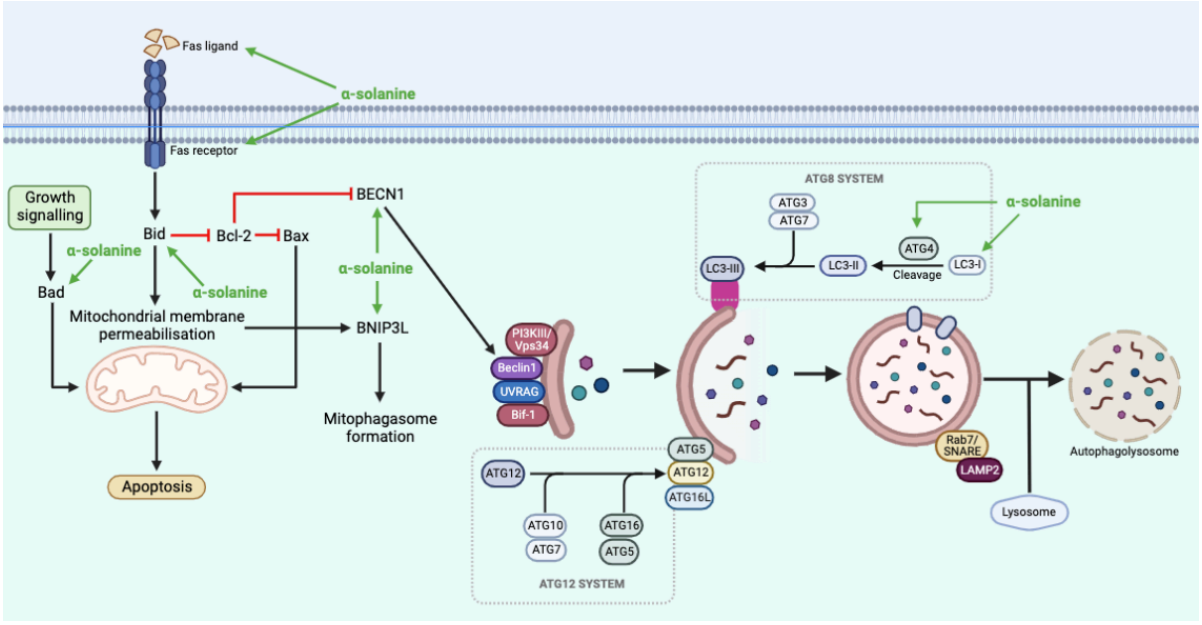


Figure 5.1.: Proposed mode of action of α-solanine on the apoptosis-autophagy axis. BECN1 appears to be central to cell death induced by α-solanine treatment since its upregulation was noted both at an RNA level and protein level using rt-qPCR and anti-body array profiling, respectively.

Determining the mode of action of α -solanine has considerable clinical importance. Understanding whether α -solanine induces apoptosis or autophagy would provide insights into its potential therapeutic applications. If it triggers apoptosis, it could be explored as a treatment to cause regulated cell death, while inducing autophagy may be beneficial for conditions where cellular recycling is necessary (Lim et al, 2021). Knowing the mode of action is crucial for assessing its safety and potential toxicity. If a-solanine induces apoptosis in healthy cells, it could be harmful, and if it leads to detrimental autophagy, it may cause adverse effects (Gu et al., 2021). However, the effect of α -solanine on healthy cells has yet to be determined. Moreover, knowing the precise mode of action could facilitate the development of combination therapies by identifying drugs that target similar cellular pathways (Luo et al., 2021).

5.6. Limitations, and areas for improvement

The viability assays conducted in this study were carried out for 72 hours, while the published literature assessing the viability of different cancers following α-solanine

treatment used 24-hour and 48-hour time durations. Moreover conducting 24-hour viability assays would result in higher concentrations of drugs which would made it very difficult to collect cell samples. This difference in time duration limits the direct comparison of the results through meta-analysis and interpretation of the efficacy of α-solanine on GBM. Furthermore, The study did not achieve the IC_{50} (of TMZ treatment against all three GBM cell lines. This constraint prevented inferential statistical comparisons between α-solanine and TMZ treatments, limiting the evaluation of their relative efficacy.

A significant limitation incurred was anomalous negative control data for cell invasion, which limited the comparison between the findings and published literature. Moreover additional repeats of trans-well invasion assay under negative control conditions could not be conducted due to financial and time constraints. The similarity between treatment conditions and negative control conditions in inducing necrosis and autophagy raises concerns about the specificity of the observed effects was another significant limitation. The study did not establish a clear distinction between the effects of α-solanine and non-specific or inherent cellular responses. However, results obtained are on par with and consolidate findings of published literature. Yet, considerable mean standard deviation obtained in specific assays and inconclusive evidence regarding the occurrence of apoptosis and autophagy induced by α-solanine treatment limits generalisation of this study's findings.

Chapter 6 Conclusions and Recommendations

Overall, this study provides insights into the potential of α-solanine as a therapeutic agent against GBM, and contributed further information on the current understanding of α-solanine induced cell death. This study explored the potential of α-solanine as a therapeutic agent against GBM in comparison to TMZ. The cytotoxicity of α-solanine and its impact on GBM metastatic properties such as migration and invasion, in comparison to TMZ treatment was investigated. H_2O_2 as a positive control because previous studies suggest that α-solanine exerts its cytotoxic effects by generating reactive oxygen species (ROS). Culture conditions (DMEM/F12) served as a vehicle for both α-solanine and TMZ, as well as the negative control. The study also focused on understanding the apoptosis-autophagy axis at both cellular and molecular levels using experimental and bioinformatic techniques. To align with the WHO 2021 CNST classification, $IDH_{wildtype}$ status of the GBM cell lines used throughout the study was confirmed.

α-Solanine exhibited cytotoxic effects on both TMZ-sensitive and TMZ-resistant GBM cell lines, with the obtained IC_{50} values consistent with those reported in the literature. Additionally, α-solanine showed potential in reducing GBM cell migration, although further investigation is required to assess its effect on invasion due to anomalous data. Results obtained suggest that α-solanine may be superior to TMZ in terms of cytotoxic potency against GBM cells. Although TMZ IC_{50} was not achieved in this study, α-solanine exhibited greater potency even at concentrations exceeding 100 times that of TMZ. Furthermore, α-solanine showed comparable effectiveness to TMZ in reducing GBM cell migration.

Assays conducted to investigate changes on RNA and protein levels

demonstrated upregulation of both apoptotic and autophagy proteins. BECN1 was upregulated at both an RNA and protein level, suggesting that BECN1 is a key protein in α-solanine induced cell death. Moreover this study highlighted the upregulation of BNIP3L following α-solanine treatment, suggesting that α-solanine also induces mitophagy.

Additional investigation is needed to overcome the limitations identified and fully elucidate the effects of α-solanine on GBM cell invasion and the specific mechanisms of cell death induced by the compound. These findings contribute to the ongoing efforts to identify novel and effective treatments for GBM. Future work should be conducted to consolidate the findings presented in this study by adding biological replicates and confirm conclusions made by employing different methods. Subsequent *in-vivo* experiments as well as further in-vitro testing using patient-derived GBM tissue is warranted to better elucidate the potential clinical applicability of α-solanine.

Chapter 7 References

abcam. (n.d.). *Counting cells using a hemocytometer*. Abcam. Retrieved December 8, 2022, from https://www.abcam.com/protocols/counting-cells-using-a-haemocytometer

Agnihotri, S., & Zadeh, G. (2016). Metabolic reprogramming in glioblastoma: the influence of cancer metabolism on epigenetics and unanswered questions. *Neuro-Oncology*, *18*(2), 160–172. https://doi.org/10.1093/neuonc/nov125

Akiyama, R., Watanabe, B., Nakayasu, M., Lee, H. J., Kato, J., Umemoto, N., Muranaka, T., Saito, K., Sugimoto, Y., & Mizutani, M. (2021). The biosynthetic pathway of potato solanidanes diverged from that of spirosolanes due to evolution of a dioxygenase. *Nature Communications*, *12*(1), 1300. https://doi.org/10.1038/s41467-021-21546-0

Alzial, G., Renoult, O., Paris, F., Gratas, C., Clavreul, A., & Pecqueur, C. (2022). Wild-type isocitrate dehydrogenase under the spotlight in glioblastoma. *Oncogene*, *41*(5), 613–621. https://doi.org/10.1038/s41388-021-02056-1

Aoyama-Ishiwatari, S., & Hirabayashi, Y. (2021). Endoplasmic Reticulum-Mitochondria Contact Sites-Emerging Intracellular Signaling Hubs. *Frontiers in Cell and Developmental Biology*, *9*, 653828. https://doi.org/10.3389/fcell.2021.653828

Balandeh, E., Mohammadshafie, K., Mahmoudi, Y., Hossein Pourhanifeh, M., Rajabi, A., Bahabadi, Z. R., Mohammadi, A. H., Rahimian, N., Hamblin, M. R., & Mirzaei, H. (2021). Roles of Non-coding RNAs and Angiogenesis in Glioblastoma. *Frontiers in Cell and Developmental Biology*, *9*, 716462. https://doi.org/10.3389/fcell.2021.716462

Bao, S., Wu, Q., McLendon, R. E., Hao, Y., Shi, Q., Hjelmeland, A. B., Dewhirst, M. W., Bigner, D. D., & Rich, J. N. (2006). Glioma stem cells promote radioresistance by

preferential activation of the DNA damage response. *Nature*, *444*(7120), 756–760. https://doi.org/10.1038/nature05236

Baur, S., Frank, O., Hausladen, H., Hückelhoven, R., Hofmann, T., Eisenreich, W., & Dawid, C. (2021). Biosynthesis of α-solanine and α-chaconine in potato leaves (Solanum tuberosum L.) - A 13CO2 study. *Food Chemistry*, *365*, 130461. https://doi.org/10.1016/j.foodchem.2021.130461

Ben Mabrouk, H., Nejia, S., Maram, M., Naziha, M., & Soufia, C.-E. (2017). A New Protein Extract Inhibitor from Hypobranchial Purple Gland of Hexaplex trunculus, a Mediterranean Mollusk, Impairs the Motility of Human Glioblastoma U87 and the HeLa Cell Line of Cervical Carcinoma Cells. *Nutrition and Cancer*, *69*(7), 1028–1035. https://doi.org/10.1080/01635581.2017.1359315

Bensinger, S. J., & Christofk, H. R. (2012). New aspects of the Warburg effect in cancer cell biology. *Seminars in Cell & Developmental Biology*, *23*(4), 352–361. https://doi.org/10.1016/j.semcdb.2012.02.003

Berghauser Pont, L. M. E., Kleijn, A., Kloezeman, J. J., van den Bossche, W., Kaufmann, J. K., de Vrij, J., Leenstra, S., Dirven, C. M. F., & Lamfers, M. L. M. (2015). The HDAC Inhibitors Scriptaid and LBH589 Combined with the Oncolytic Virus Delta24-RGD Exert Enhanced Anti-Tumor Efficacy in Patient-Derived Glioblastoma Cells. *Plos One*, *10*(5), e0127058. https://doi.org/10.1371/journal.pone.0127058

Bezerra, D. P., Ferreira, P. M. P., Machado, C. M. L., de Aquino, N. C., Silveira, E. R., Chammas, R., & Pessoa, C. (2015). Antitumour efficacy of Piper tuberculatum and piplartine based on the hollow fiber assay. *Planta Medica*, *81*(1), 15–19. https://doi.org/10.1055/s-0034-1383363

Blahovcova, E., Richterova, R., Kolarovszki, B., Dobrota, D., Racay, P., & Hatok, J. (2015). Apoptosis-related gene expression in tumor tissue samples obtained from patients diagnosed with glioblastoma multiforme. *International Journal of Molecular Medicine*, *36*(6), 1677–1684. https://doi.org/10.3892/ijmm.2015.2369

Boya, P., Reggiori, F., & Codogno, P. (2013). Emerging regulation and functions of autophagy. *Nature Cell Biology*, *15*(7), 713–720. https://doi.org/10.1038/ncb2788

Brauchle, E., Thude, S., Brucker, S. Y., & Schenke-Layland, K. (2014). Cell death stages in single apoptotic and necrotic cells monitored by Raman microspectroscopy. *Scientific reports*, *4*, 4698. https://doi.org/10.1038/srep04698

Brandi, J., Cecconi, D., Cordani, M., Torrens-Mas, M., Pacchiana, R., Dalla Pozza, E., Butera, G., Manfredi, M., Marengo, E., Oliver, J., Roca, P., Dando, I., & Donadelli, M. (2016). The antioxidant uncoupling protein 2 stimulates hnRNPA2/B1, GLUT1 and PKM2 expression and sensitizes pancreas cancer cells to glycolysis inhibition. *Free Radical Biology & Medicine*, *101*, 305–316. https://doi.org/10.1016/j.freeradbiomed.2016.10.499

Brennan, C. W., Verhaak, R. G. W., McKenna, A., Campos, B., Noushmehr, H., Salama, S. R., Zheng, S., Chakravarty, D., Sanborn, J. Z., Berman, S. H., Beroukhim, R., Bernard, B., Wu, C.-J., Genovese, G., Shmulevich, I., Barnholtz-Sloan, J., Zou, L., Vegesna, R., Shukla, S. A., … TCGA Research Network. (2013). The somatic genomic landscape of glioblastoma. *Cell*, *155*(2), 462–477. https://doi.org/10.1016/j.cell.2013.09.034

Bronisz, A., Salińska, E., Chiocca, E. A., & Godlewski, J. (2020). Hypoxic Roadmap of Glioblastoma-Learning about Directions and Distances in the Brain Tumor Environment. *Cancers*, *12*(5). https://doi.org/10.3390/cancers12051213

Bustin, S. A., Mueller, R., & Nolan, T. (2020). Parameters for successful PCR primer design. *Methods in Molecular Biology*, *2065*, 5–22. https://doi.org/10.1007/978-1-4939-9833-3_2

Bustos, S. O., Antunes, F., Rangel, M. C., & Chammas, R. (2020). Emerging Autophagy Functions Shape the Tumor Microenvironment and Play a Role in Cancer Progression - Implications for Cancer Therapy. *Frontiers in Oncology*, *10*, 606436. https://doi.org/10.3389/fonc.2020.606436

Cancer Genome Atlas Research Network. (2008). Comprehensive genomic characterization defines human glioblastoma genes and core pathways. *Nature*, *455*(7216), 1061–1068. https://doi.org/10.1038/nature07385

Cao, Y., & Klionsky, D. J. (2007). Physiological functions of Atg6/Beclin 1: a unique autophagy-related protein. *Cell Research*, *17*(10), 839–849. https://doi.org/10.1038/cr.2007.78

Carrasco-García, E., Saceda, M., & Martínez-Lacaci, I. (2014). Role of receptor tyrosine kinases and their ligands in glioblastoma. *Cells*, *3*(2), 199–235. https://doi.org/10.3390/cells3020199

Chaicharoenaudomrung, N., Jaroonwitchawan, T., & Noisa, P. (2018). Cordycepin induces apoptotic cell death of human brain cancer through the modulation of autophagy. *Toxicology in Vitro*, *46*, 113–121. https://doi.org/10.1016/j.tiv.2017.10.002

Chaube, S., & Swinyard, C. A. (1976). Teratological and toxicological studies of alkaloidal and phenolic compounds from Solanum Tuberosum L. *Toxicology and Applied Pharmacology*, *36*(2), 227–237. https://doi.org/10.1016/0041-008X(76)90002-8

Cheng, F., & Guo, D. (2019). MET in glioma: signaling pathways and targeted therapies. *Journal of Experimental & Clinical Cancer Research*, *38*(1), 270. https://doi.org/10.1186/s13046-019-1269-x

Christofk, H. R., Vander Heiden, M. G., Harris, M. H., Ramanathan, A., Gerszten, R. E., Wei, R., Fleming, M. D., Schreiber, S. L., & Cantley, L. C. (2008). The M2 splice isoform of pyruvate kinase is important for cancer metabolism and tumour growth. *Nature*, *452*(7184), 230–233. https://doi.org/10.1038/nature06734

Chu, P.-M., Chen, L.-H., Chen, M.-T., Ma, H.-I., Su, T.-L., Hsieh, P.-C., Chien, C.-S., Jiang, B.-H., Chen, Y.-C., Lin, Y.-H., Shih, Y.-H., Tu, P.-H., & Chiou, S.-H. (2012). Targeting autophagy enhances BO-1051-induced apoptosis in human malignant glioma cells. *Cancer Chemotherapy and Pharmacology*, *69*(3), 621–633. https://doi.org/10.1007/s00280-011-1747-0

Colapietro, A., Yang, P., Rossetti, A., Mancini, A., Vitale, F., Martellucci, S., Conway, T. L., Chakraborty, S., Marampon, F., Mattei, V., Gravina, G. L., Biordi, A. L., Wei, D., Newman, R. A., & Festuccia, C. (2020). The Botanical Drug PBI-05204, a Supercritical CO2 Extract of Nerium Oleander, Inhibits Growth of Human Glioblastoma, Reduces Akt/mTOR Activities, and Modulates GSC Cell-Renewal Properties. *Frontiers in Pharmacology*, *11*, 552428. https://doi.org/10.3389/fphar.2020.552428

Cruickshanks, N., Zhang, Y., Yuan, F., Pahuski, M., Gibert, M., & Abounader, R. (2017). Role and therapeutic targeting of the HGF/MET pathway in glioblastoma. *Cancers*, *9*(7). https://doi.org/10.3390/cancers9070087

Cuschieri, A., & Baron, B. (2023). Glioblastoma Multiforme: Molecular Biology and Updated Systematic Review on Natural Extract and Phytochemical Efficacy In-vitro.

Journal of Complementary and Alternative Medical Research, *21*(1), 24–51. https://doi.org/10.9734/jocamr/2023/v21i1427

Cuschieri, A., & Calleja-Agius, J. (2020). Wnt/PCP signalling cascade disruption by JNK inhibition as a potential mechanism underlying the teratogenic effects of potato glycoalkaloids. *Molecular Biology Reports*, *47*(11), 9235–9238. https://doi.org/10.1007/s11033-020-05921-6

Dadey, D. Y. A., Kapoor, V., Khudanyan, A., Urano, F., Kim, A. H., Thotala, D., & Hallahan, D. E. (2016). The ATF6 pathway of the ER stress response contributes to enhanced viability in glioblastoma. *Oncotarget*, *7*(2), 2080–2092. https://doi.org/10.18632/oncotarget.6712

Dalvi, R. R. (1985). Comparative assessment of the effect of solanine administered orally and intraperitoneally on hepatic dysfunction in male rats. *Nippon Juigaku Zasshi. The Japanese Journal of Veterinary Science*, *47*(4), 657–659. https://doi.org/10.1292/jvms1939.47.657

Daniel, P., Sabri, S., Chaddad, A., Meehan, B., Jean-Claude, B., Rak, J., & Abdulkarim, B. S. (2019). Temozolomide induced hypermutation in glioma: evolutionary mechanisms and therapeutic opportunities. *Frontiers in Oncology*, *9*, 41. https://doi.org/10.3389/fonc.2019.00041

Datta, S. R., Dudek, H., Tao, X., Masters, S., Fu, H., Gotoh, Y., & Greenberg, M. E. (1997). Akt phosphorylation of BAD couples survival signals to the cell-intrinsic death machinery. *Cell*, *91*(2), 231–241. https://doi.org/10.1016/s0092-8674(00)80405-5

Denton, D., Nicolson, S., & Kumar, S. (2012). Cell death by autophagy: facts and apparent artefacts. *Cell Death and Differentiation*, *19*(1), 87–95. https://doi.org/10.1038/cdd.2011.146

Desai, S., Ding, M., Wang, B., Lu, Z., Zhao, Q., Shaw, K., Yung, W. K. A., Weinstein, J. N., Tan, M., & Yao, J. (2014). Tissue-specific isoform switch and DNA hypomethylation of the pyruvate kinase PKM gene in human cancers. *Oncotarget*, *5*(18), 8202–8210. https://doi.org/10.18632/oncotarget.1159

Duraipandy, N., Dharunya, G., Lakra, R., Korapatti, P. S., & Syamala Kiran, M. (2018). Fabrication of plumbagin on silver nanoframework for tunable redox modulation: Implications for therapeutic angiogenesis. *Journal of Cellular Physiology*, *234*(8), 13110–13127. https://doi.org/10.1002/jcp.27981

Dymova, M. A., Kuligina, E. V., & Richter, V. A. (2021). Molecular mechanisms of drug resistance in glioblastoma. *International Journal of Molecular Sciences*, *22*(12). https://doi.org/10.3390/ijms22126385

El Hage, S., Kawtharani, M., Nabha, S., El Masri, J., & Saad, M. (2021). Distribution of Primary Brain Tumor Subtypes in Lebanon: A Multicenter Eleven-Year Study of 695 Patients. *Cureus*, *13*(9), e17918. https://doi.org/10.7759/cureus.17918

El Khayari, A., Bouchmaa, N., Taib, B., Wei, Z., Zeng, A., & El Fatimy, R. (2022). Metabolic rewiring in glioblastoma cancer: EGFR, IDH and beyond. *Frontiers in Oncology*, *12*, 901951. https://doi.org/10.3389/fonc.2022.901951

Engberg, H., Steding-Jessen, M., Øster, I., Jensen, J. W., Hansen, S., Laursen, R. J., Lukacova, S., & Møller, H. (2022). Regional and socio-economic variation in survival after glioblastoma in Denmark, 2013-2018. *Danish Medical Journal*, *69*(3).

Fan, Q.-W., & Weiss, W. A. (2012). Inhibition of PI3K-Akt-mTOR signaling in glioblastoma by mTORC1/2 inhibitors. *Methods in Molecular Biology*, *821*, 349–359. https://doi.org/10.1007/978-1-61779-430-8_22

FlowJo. (2023). *Biexponential Transformation Instructions*. FlowJo.

[https://docs.flowjo.com/flowjo/graphs-and-gating/gw-transform-overview/gw-transform-procedure/#:~:text=Biexponential%20scaling%20helps%20visualize%20data,view%20of%20flow%20cytometry%20data.]

Figueroa, M. E., Abdel-Wahab, O., Lu, C., Ward, P. S., Patel, J., Shih, A., Li, Y., Bhagwat, N., Vasanthakumar, A., Fernandez, H. F., Tallman, M. S., Sun, Z., Wolniak, K., Peeters, J. K., Liu, W., Choe, S. E., Fantin, V. R., Paietta, E., Löwenberg, B., … Melnick, A. (2010). Leukemic IDH1 and IDH2 mutations result in a hypermethylation phenotype, disrupt TET2 function, and impair hematopoietic differentiation. *Cancer Cell*, *18*(6), 553–567. https://doi.org/10.1016/j.ccr.2010.11.015

Fisher, J. P., & Adamson, D. C. (2021). Current FDA-Approved Therapies for High-Grade Malignant Gliomas. *Biomedicines*, *9*(3). https://doi.org/10.3390/biomedicines9030324

Finak, G., Perez, JM., Weng, A. *et al.* Optimizing transformations for automated, high throughput analysis of flow cytometry data. *BMC Bioinformatics* **11**, 546 (2010). https://doi.org/10.1186/1471-2105-11-546

Fitsialos, G., Bourget, I., Augier, S., Ginouvès, A., Rezzonico, R., Odorisio, T., Cianfarani, F., Virolle, T., Pouysségur, J., Meneguzzi, G., Berra, E., Ponzio, G., & Buscà, R. (2008). HIF1 transcription factor regulates laminin-332 expression and keratinocyte migration. *Journal of Cell Science*, *121*(Pt 18), 2992–3001. https://doi.org/10.1242/jcs.029256

Folcarelli, R., Tinnevelt, G. H., Hilvering, B., Wouters, K., van Staveren, S., Postma, G. J., Vrisekoop, N., Buydens, L. M. C., Koenderman, L., & Jansen, J. J. (2020). Multi-set

Pre-processing of Multicolor Flow Cytometry Data. *Scientific reports*, *10*(1), 9716. https://doi.org/10.1038/s41598-020-66195-3

Friedman, M, Henika, P. R., & Mackey, B. E. (1996). Feeding of potato, tomato and eggplant alkaloids affects food consumption and body and liver weights in mice. *The Journal of Nutrition*, *126*(4), 989–999. https://doi.org/10.1093/jn/126.4.989

Friedman, Mendel. (2004). Analysis of biologically active compounds in potatoes (Solanum tuberosum), tomatoes (Lycopersicon esculentum), and jimson weed (Datura stramonium) seeds. *Journal of Chromatography. A*, *1054*(1–2), 143–155. https://doi.org/10.1016/j.chroma.2004.04.049

Friedman, Mendel. (2006). Potato glycoalkaloids and metabolites: roles in the plant and in the diet. *Journal of Agricultural and Food Chemistry*, *54*(23), 8655–8681. https://doi.org/10.1021/jf061471t

Friedman, Mendel. (2015). Chemistry and anticarcinogenic mechanisms of glycoalkaloids produced by eggplants, potatoes, and tomatoes. *Journal of Agricultural and Food Chemistry*, *63*(13), 3323–3337. https://doi.org/10.1021/acs.jafc.5b00818

Gal, I. (1973). Possible mechanisms of human teratogenesis by imperfect potato. *Humangenetik*, *19*(3), 311–314. https://doi.org/10.1007/BF00278408

Galavotti, S., Bartesaghi, S., Faccenda, D., Shaked-Rabi, M., Sanzone, S., McEvoy, A., Dinsdale, D., Condorelli, F., Brandner, S., Campanella, M., Grose, R., Jones, C., & Salomoni, P. (2013). The autophagy-associated factors DRAM1 and p62 regulate cell migration and invasion in glioblastoma stem cells. *Oncogene*, *32*(6), 699–712. https://doi.org/10.1038/onc.2012.111

Gao, S.-Y., Wang, Q.-J., & Ji, Y.-B. (2006). Effect of solanine on the membrane potential of mitochondria in HepG2 cells and [Ca2+]i in the cells. *World J Gastroenterol*, *12*(21), 3359–3367.

Gilbert, M. R., Dignam, J. J., Armstrong, T. S., Wefel, J. S., Blumenthal, D. T., Vogelbaum, M. A., Colman, H., Chakravarti, A., Pugh, S., Won, M., Jeraj, R., Brown, P. D., Jaeckle, K. A., Schiff, D., Stieber, V. W., Brachman, D. G., Werner-Wasik, M., Tremont-Lukats, I. W., Sulman, E. P., … Mehta, M. P. (2014). A randomized trial of bevacizumab for newly diagnosed glioblastoma. *The New England Journal of Medicine*, *370*(8), 699–708. https://doi.org/10.1056/NEJMoa1308573

Gonzalez-Gronow, M., Gopal, U., Austin, R. C., & Pizzo, S. V. (2021). Glucose-regulated protein (GRP78) is an important cell surface receptor for viral invasion, cancers, and neurological disorders. *IUBMB Life*, *73*(6), 843–854. https://doi.org/10.1002/iub.2502

Gouhar, S. A., Abo-Elfadl, M. T., Gamal-Eldeen, A. M., & El-Daly, S. M. (2022). Involvement of miRNAs in response to oxidative stress induced by the steroidal glycoalkaloid α-solanine in hepatocellular carcinoma cells. *Environmental Toxicology*, *37*(2), 212–223. https://doi.org/10.1002/tox.23390

Grech, N., Dalli, T., Mizzi, S., Meilak, L., Calleja, N., & Zrinzo, A. (2020). Rising Incidence of Glioblastoma Multiforme in a Well-Defined Population. *Cureus*, *12*(5), e8195. https://doi.org/10.7759/cureus.8195

Grochans, S., Cybulska, A. M., Simińska, D., Korbecki, J., Kojder, K., Chlubek, D., & Baranowska-Bosiacka, I. (2022). Epidemiology of Glioblastoma Multiforme-Literature Review. *Cancers*, *14*(10). https://doi.org/10.3390/cancers14102412

Gu, T., Yuan, W., Li, C., Chen, Z., Wen, Y., Zheng, Q., Yang, Q., Xiong, X., & Yuan, A. (2021). α-Solanine Inhibits Proliferation, Invasion, and Migration, and Induces Apoptosis in Human Choriocarcinoma JEG-3 Cells In Vitro and In Vivo. *Toxins*, *13*(3). https://doi.org/10.3390/toxins13030210

Gull, D. D., Isenberg, F. M., & Bryan, H. H. (1970). Alkaloid toxicology of Solanum tuberosum . *Hort. Sicence*, *5*, 316.

Gump, J. M., & Thorburn, A. (2011). Autophagy and apoptosis: what is the connection? *Trends in Cell Biology*, *21*(7), 387–392. https://doi.org/10.1016/j.tcb.2011.03.007

Guntuku, L., Naidu, V. G. M., & Yerra, V. G. (2016). Mitochondrial dysfunction in gliomas: pharmacotherapeutic potential of natural compounds. *Current Neuropharmacology*, *14*(6), 567–583. https://doi.org/10.2174/1570159x14666160121115641

Hasanain, M., Bhattacharjee, A., Pandey, P., Ashraf, R., Singh, N., Sharma, S., Vishwakarma, A. L., Datta, D., Mitra, K., & Sarkar, J. (2015). α-Solanine induces ROS-mediated autophagy through activation of endoplasmic reticulum stress and inhibition of Akt/mTOR pathway. *Cell Death & Disease*, *6*, e1860. https://doi.org/10.1038/cddis.2015.219

Hatziagapiou, K., Nikola, O., Marka, S., Koniari, E., Kakouri, E., Zografaki, M.-E., Mavrikou, S. S., Kanakis, C., Flemetakis, E., Chrousos, G. P., Kintzios, S., Lambrou, G. I., Kanaka-Gantenbein, C., & Tarantilis, P. A. (2022). An in vitro study of saffron carotenoids: the effect of crocin extracts and dimethylcrocetin on cancer cell lines. *Antioxidants (Basel, Switzerland)*, *11*(6). https://doi.org/10.3390/antiox11061074

Heddleston, J. M., Li, Z., McLendon, R. E., Hjelmeland, A. B., & Rich, J. N. (2009). The hypoxic microenvironment maintains glioblastoma stem cells and promotes reprogramming towards a cancer stem cell phenotype. *Cell Cycle*, *8*(20), 3274–3284. https://doi.org/10.4161/cc.8.20.9701

Hellenäs, K. E., Nyman, A., Slanina, P., Lööf, L., & Gabrielsson, J. (1992). Determination of potato glycoalkaloids and their aglycone in blood serum by high-performance liquid chromatography. *Journal of Chromatography B: Biomedical Sciences and Applications*, *573*(1), 69–78. https://doi.org/10.1016/0378-4347(92)80476-7

Hockenbery, D. M. (2010). Targeting mitochondria for cancer therapy. *Environmental and Molecular Mutagenesis*, *51*(5), 476–489. https://doi.org/10.1002/em.20552

Holland, E. C., Celestino, J., Dai, C., Schaefer, L., Sawaya, R. E., & Fuller, G. N. (2000). Combined activation of Ras and Akt in neural progenitors induces glioblastoma formation in mice. *Nature Genetics*, *25*(1), 55–57. https://doi.org/10.1038/75596

Hon, K. W., Zainal Abidin, S. A., Othman, I., & Naidu, R. (2021). The crosstalk between signaling pathways and cancer metabolism in colorectal cancer. *Frontiers in Pharmacology*, *12*, 768861. https://doi.org/10.3389/fphar.2021.768861

Hong, H., Chen, F., Zhang, Y., & Cai, W. (2014). New radiotracers for imaging of vascular targets in angiogenesis-related diseases. *Advanced Drug Delivery Reviews*, *76*, 2–20. https://doi.org/10.1016/j.addr.2014.07.011

Horbinski, C., Berger, T., Packer, R. J., & Wen, P. Y. (2022). Clinical implications of the 2021 edition of the WHO classification of central nervous system tumours. *Nature Reviews. Neurology*, *18*(9), 515–529. https://doi.org/10.1038/s41582-022-00679-w

Hossain, M. B., Tiwari, B. K., Gangopadhyay, N., O'Donnell, C. P., Brunton, N. P., & Rai, D. K. (2014). Ultrasonic extraction of steroidal alkaloids from potato peel waste. *Ultrasonics Sonochemistry*, *21*(4), 1470–1476. https://doi.org/10.1016/j.ultsonch.2014.01.023

Huang, P. H., Cavenee, W. K., Furnari, F. B., & White, F. M. (2007). Uncovering therapeutic targets for glioblastoma: a systems biology approach. *Cell Cycle*, *6*(22), 2750–2754. https://doi.org/10.4161/cc.6.22.4922

Huang, W.-J., Lin, C.-W., Lee, C.-Y., Chi, L.-L., Chao, Y.-C., Wang, H.-N., Chiou, B.-L., Chen, T.-J., Huang, C.-Y., & Chen, C.-N. (2011). NBM-HD-3, a novel histone deacetylase inhibitor with anticancer activity through modulation of PTEN and AKT in brain cancer cells. *Journal of Ethnopharmacology*, *136*(1), 156–167. https://doi.org/10.1016/j.jep.2011.04.034

Inoue, S., Li, W. Y., Tseng, A., Beerman, I., Elia, A. J., Bendall, S. C., Lemonnier, F., Kron, K. J., Cescon, D. W., Hao, Z., Lind, E. F., Takayama, N., Planello, A. C., Shen, S. Y., Shih, A. H., Larsen, D. M., Li, Q., Snow, B. E., Wakeham, A., … Mak, T. W. (2016). Mutant IDH1 downregulates ATM and alters DNA repair and sensitivity to DNA damage independent of TET2. *Cancer Cell*, *30*(2), 337–348. https://doi.org/10.1016/j.ccell.2016.05.018

Internationally Peer Reviewed Chemical Saftey information (INCHEM). (n.d.). *Solanine and Chaconine* . INCHEM - Internaitonally Peer Reviewed Chemical Saftey Information. Retrieved November 8, 2022, from https://inchem.org/documents/jecfa/jecmono/v30je19.htm

Jelínek, R., Kyzlink, V., & Blatiný, C. (1976). An evaluation of the embryotoxic effects of blighted potatoes on chicken embryos. *Teratology*, *14*(3), 335–342. https://doi.org/10.1002/tera.1420140309

Ji, Y., & Gao, S. (2012). Antihepatocarcinoma Effect of Solanine and Its Mechanisms. *Chinese Herbal Medicines*, *4*(2), 126–135.

Jung, C. H., Jun, C. B., Ro, S.-H., Kim, Y.-M., Otto, N. M., Cao, J., Kundu, M., & Kim, D.-H. (2009). ULK-Atg13-FIP200 complexes mediate mTOR signaling to the autophagy machinery. *Molecular Biology of the Cell*, *20*(7), 1992–2003. https://doi.org/10.1091/mbc.E08-12-1249

Justus, C. R., Leffler, N., Ruiz-Echevarria, M., & Yang, L. V. (2014). In vitro cell migration and invasion assays. *Journal of Visualized Experiments*, *88*. https://doi.org/10.3791/51046

Karaboğa Arslan, A. K., & Yerer, M. B. (2018). α-Chaconine and α-Solanine Inhibit RL95-2 Endometrium Cancer Cell Proliferation by Reducing Expression of Akt (Ser473) and ERα (Ser167). *Nutrients*, *10*(6). https://doi.org/10.3390/nu10060672

Kavitha, C. V., Jain, A. K., Agarwal, C., Pierce, A., Keating, A., Huber, K. M., Serkova, N. J., Wempe, M. F., Agarwal, R., & Deep, G. (2015). Asiatic acid induces endoplasmic reticulum stress and apoptotic death in glioblastoma multiforme cells both in vitro and in vivo. *Molecular Carcinogenesis*, *54*(11), 1417–1429. https://doi.org/10.1002/mc.22220

Kawauchi, D., Ohno, M., Miyakita, Y., Takahashi, M., Yanagisawa, S., Omura, T., Yoshida, A., Kubo, Y., Igaki, H., Ichimura, K., & Narita, Y. (2022). Early diagnosis and surgical intervention within 3 weeks from symptom onset are associated with prolonged

survival of patients with glioblastoma. *Neurosurgery*, *91*(5), 741–748. https://doi.org/10.1227/neu.0000000000002096

Kefas, B., Comeau, L., Erdle, N., Montgomery, E., Amos, S., & Purow, B. (2010). Pyruvate kinase M2 is a target of the tumor-suppressive microRNA-326 and regulates the survival of glioma cells. *Neuro-Oncology*, *12*(11), 1102–1112. https://doi.org/10.1093/neuonc/noq080

Kibbe, W. A. (2007). OligoCalc: an online oligonucleotide properties calculator. *Nucleic Acids Research*, *35*(Web Server issue), W43-6. https://doi.org/10.1093/nar/gkm234

Kim, C., & Kim, B. (2018). Anti-Cancer Natural Products and Their Bioactive Compounds Inducing ER Stress-Mediated Apoptosis: A Review. *Nutrients*, *10*(8). https://doi.org/10.3390/nu10081021

Kim, J., Kundu, M., Viollet, B., & Guan, K.-L. (2011). AMPK and mTOR regulate autophagy through direct phosphorylation of Ulk1. *Nature Cell Biology*, *13*(2), 132–141. https://doi.org/10.1038/ncb2152

Kong, Q., Beel, J. A., & Lillehei, K. O. (2000). A threshold concept for cancer therapy. *Medical Hypotheses*, *55*(1), 29–35. https://doi.org/10.1054/mehy.1999.0982

Krakstad, C., & Chekenya, M. (2010). Survival signalling and apoptosis resistance in glioblastomas: opportunities for targeted therapeutics. *Molecular Cancer*, *9*, 135. https://doi.org/10.1186/1476-4598-9-135

Kurihara-Shimomura, M., Sasahira, T., Nakashima, C., Kuniyasu, H., Shimomura, H., & Kirita, T. (2018). The multifarious functions of pyruvate kinase M2 in oral cancer cells. *International Journal of Molecular Sciences*, *19*(10). https://doi.org/10.3390/ijms19102907

Lacher, S. E., Levings, D. C., Freeman, S., & Slattery, M. (2018). Identification of a functional antioxidant response element at the HIF1A locus. *Redox Biology*, *19*, 401–411. https://doi.org/10.1016/j.redox.2018.08.014

Lakka, S. S., & Rao, J. S. (2008). Antiangiogenic therapy in brain tumors. *Expert Review of Neurotherapeutics*, *8*(10), 1457–1473. https://doi.org/10.1586/14737175.8.10.1457

Langkilde, S., Mandimika, T., Schrøder, M., Meyer, O., Slob, W., Peijnenburg, A., & Poulsen, M. (2009). A 28-day repeat dose toxicity study of steroidal glycoalkaloids, alpha-solanine and alpha-chaconine in the Syrian Golden hamster. *Food and Chemical Toxicology*, *47*(6), 1099–1108. https://doi.org/10.1016/j.fct.2009.01.045

Langkilde, S., Schrøder, M., Stewart, D., Meyer, O., Conner, S., Davies, H., & Poulsen, M. (2008). Acute toxicity of high doses of the glycoalkaloids, alpha-solanine and alpha-chaconine, in the Syrian Golden hamster. *Journal of Agricultural and Food Chemistry*, *56*(18), 8753–8760. https://doi.org/10.1021/jf8012794

Law, F., Seo, J. H., Wang, Z., DeLeon, J. L., Bolis, Y., Brown, A., Zong, W.-X., Du, G., & Rocheleau, C. E. (2017). The VPS34 PI3K negatively regulates RAB-5 during endosome maturation. *Journal of Cell Science*, *130*(12), 2007–2017. https://doi.org/10.1242/jcs.194746

Lee, E., Yong, R. L., Paddison, P., & Zhu, J. (2018). Comparison of glioblastoma (GBM) molecular classification methods. *Seminars in Cancer Biology*, *53*, 201–211. https://doi.org/10.1016/j.semcancer.2018.07.006

Levin-Salomon, V., Bialik, S., & Kimchi, A. (2014). DAP-kinase and autophagy. *Apoptosis: An International Journal on Programmed Cell Death*, *19*(2), 346–356. https://doi.org/10.1007/s10495-013-0918-3

Li, H., Li, J., Zhang, G., Da, Q., Chen, L., Yu, S., Zhou, Q., Weng, Z., Xin, Z., Shi, L., Ma, L., Huang, A., Qi, S., & Lu, Y. (2019). HMGB1-Induced p62 Overexpression Promotes Snail-Mediated Epithelial-Mesenchymal Transition in Glioblastoma Cells via the Degradation of GSK-3β. *Theranostics*, *9*(7), 1909–1922. https://doi.org/10.7150/thno.30578

Li, J., Tang, H., Zhang, Y., Tang, C., Li, B., Wang, Y., Gao, Z., Luo, P., Yin, A., Wang, X., Cheng, G., & Fei, Z. (2013). Saponin 1 induces apoptosis and suppresses NF-κB-mediated survival signaling in glioblastoma multiforme (GBM). *Plos One*, *8*(11), e81258. https://doi.org/10.1371/journal.pone.0081258

Li, Q., Qi, X., & Jia, W. (2016). 3,3',5-triiodothyroxine inhibits apoptosis and oxidative stress by the PKM2/PKM1 ratio during oxygen-glucose deprivation/reperfusion AC16 and HCM-a cells: T3 inhibits apoptosis and oxidative stress by PKM2/PKM1 ratio. *Biochemical and Biophysical Research Communications*, *475*(1), 51–56. https://doi.org/10.1016/j.bbrc.2016.05.030

Li, X., Wu, C., Chen, N., Gu, H., Yen, A., Cao, L., Wang, E., & Wang, L. (2016). PI3K/Akt/mTOR signaling pathway and targeted therapy for glioblastoma. *Oncotarget*, *7*(22), 33440–33450. https://doi.org/10.18632/oncotarget.7961

Li, Z., Chen, Y., An, T., Liu, P., Zhu, J., Yang, H., Zhang, W., Dong, T., Jiang, J., Zhang, Y., Jiang, M., & Yang, X. (2019). Nuciferine inhibits the progression of glioblastoma by suppressing the SOX2-AKT/STAT3-Slug signaling pathway. *Journal of Experimental & Clinical Cancer Research*, *38*(1), 139. https://doi.org/10.1186/s13046-019-1134-y

Liang, J., Cao, R., Wang, X., Zhang, Y., Wang, P., Gao, H., Li, C., Yang, F., Zeng, R., Wei, P., Li, D., Li, W., & Yang, W. (2017). Mitochondrial PKM2 regulates oxidative stress-

induced apoptosis by stabilizing Bcl2. *Cell Research*, *27*(3), 329–351. https://doi.org/10.1038/cr.2016.159

Liang, W., Zhang, Y., Song, L., & Li, Z. (2019). 2,3'4,4',5-Pentachlorobiphenyl induces hepatocellular carcinoma cell proliferation through pyruvate kinase M2-dependent glycolysis. *Toxicology Letters*, *313*, 108–119. https://doi.org/10.1016/j.toxlet.2019.06.006

Liang, W.-Z., Jan, C.-R., & Hsu, S.-S. (2017). Cytotoxic effects of gastrodin extracted from the rhizome of Gastrodia elata Blume in glioblastoma cells, but not in normal astrocytes, via the induction of oxidative stress-associated apoptosis that involved cell cycle arrest and p53 activation. *Food and Chemical Toxicology*, *107*(Pt A), 280–292. https://doi.org/10.1016/j.fct.2017.07.013

Lim, S. M., Mohamad Hanif, E. A., & Chin, S.-F. (2021). Is targeting autophagy mechanism in cancer a good approach? The possible double-edge sword effect. *Cell & Bioscience*, *11*(1), 56. https://doi.org/10.1186/s13578-021-00570-z

Lin, A. B., McNeely, S. C., & Beckmann, R. P. (2017). Achieving Precision Death with Cell-Cycle Inhibitors that Target DNA Replication and Repair. *Clinical Cancer Research*, *23*(13), 3232–3240. https://doi.org/10.1158/1078-0432.CCR-16-0083

Lin, L.-T., Choong, C.-Y., & Tai, C.-J. (2020). Solanine attenuated hepatocarcinoma migration and invasion induced by acetylcholine. *Integrative Cancer Therapies*, *19*, 1534735420909895. https://doi.org/10.1177/1534735420909895

Liu, F., & Mischel, P. S. (2018). Targeting epidermal growth factor receptor co-dependent signaling pathways in glioblastoma. *Wiley Interdisciplinary Reviews. Systems Biology and Medicine*, *10*(1). https://doi.org/10.1002/wsbm.1398

Liu, G., Black, K. L., & Yu, J. S. (2006). Sensitization of malignant glioma to chemotherapy through dendritic cell vaccination. *Expert Review of Vaccines*, *5*(2), 233–247. https://doi.org/10.1586/14760584.5.2.233

Liu, S., Dong, L., Shi, W., Zheng, Z., Liu, Z., Meng, L., Xin, Y., & Jiang, X. (2022). Potential targets and treatments affect oxidative stress in gliomas: An overview of molecular mechanisms. *Frontiers in Pharmacology*, *13*, 921070. https://doi.org/10.3389/fphar.2022.921070

Lo Dico, A., Martelli, C., Diceglie, C., Lucignani, G., & Ottobrini, L. (2018). Hypoxia-Inducible Factor-1α Activity as a Switch for Glioblastoma Responsiveness to Temozolomide. *Frontiers in Oncology*, *8*, 249. https://doi.org/10.3389/fonc.2018.00249

Louis, D. N., Perry, A., Reifenberger, G., von DeimLing, A., Figarella-Branger, D., Cavenee, W. K., Ohgaki, H., Wiestler, O. D., Kleihues, P., & Ellison, D. W. (2016). The 2016 World Health Organization Classification of Tumors of the Central Nervous System: a summary. *Acta Neuropathologica*, *131*(6), 803–820. https://doi.org/10.1007/s00401-016-1545-1

Louis, D. N., Perry, A., Wesseling, P., Brat, D. J., Cree, I. A., Figarella-Branger, D., Hawkins, C., Ng, H. K., Pfister, S. M., Reifenberger, G., Soffietti, R., von DeimLing, A., & Ellison, D. W. (2021). The 2021 WHO Classification of Tumors of the Central Nervous System: a summary. *Neuro-Oncology*, *23*(8), 1231–1251. https://doi.org/10.1093/neuonc/noab106

Lu, C., Ward, P. S., Kapoor, G. S., Rohle, D., Turcan, S., Abdel-Wahab, O., Edwards, C. R., Khanin, R., Figueroa, M. E., Melnick, A., Wellen, K. E., O'Rourke, D. M., Berger, S. L., Chan, T. A., Levine, R. L., Mellinghoff, I. K., & Thompson, C. B. (2012). IDH mutation

impairs histone demethylation and results in a block to cell differentiation. *Nature*, *483*(7390), 474–478. https://doi.org/10.1038/nature10860

Lu, M.-K., Shih, Y.-W., Chang Chien, T.-T., Fang, L.-H., Huang, H.-C., & Chen, P.-S. (2010). α-Solanine inhibits human melanoma cell migration and invasion by reducing matrix metalloproteinase-2/9 activities. *Biological & Pharmaceutical Bulletin*, *33*(10), 1685–1691. https://doi.org/10.1248/bpb.33.1685

Lu, Y., Kwintkiewicz, J., Liu, Y., Tech, K., Frady, L. N., Su, Y.-T., Bautista, W., Moon, S. I., MacDonald, J., Ewend, M. G., Gilbert, M. R., Yang, C., & Wu, J. (2017). Chemosensitivity of IDH1-Mutated Gliomas Due to an Impairment in PARP1-Mediated DNA Repair. *Cancer Research*, *77*(7), 1709–1718. https://doi.org/10.1158/0008-5472.CAN-16-2773

Lunt, S. Y., & Vander Heiden, M. G. (2011). Aerobic glycolysis: meeting the metabolic requirements of cell proliferation. *Annual Review of Cell and Developmental Biology*, *27*, 441–464. https://doi.org/10.1146/annurev-cellbio-092910-154237

Luo, S., & Rubinsztein, D. C. (2010). Apoptosis blocks Beclin 1-dependent autophagosome synthesis: an effect rescued by Bcl-xL. *Cell Death and Differentiation*, *17*(2), 268–277. https://doi.org/10.1038/cdd.2009.121

Lv, C., Kong, H., Dong, G., Liu, L., Tong, K., Sun, H., Chen, B., Zhang, C., & Zhou, M. (2014). Antitumor efficacy of α-solanine against pancreatic cancer in vitro and in vivo. *Plos One*, *9*(2), e87868. https://doi.org/10.1371/journal.pone.0087868

Lynch, B., Simon, R. R., van Otterdijk, F. M., Emmen, H. H., Giuseppin, M. L. F., & Kemme-Kroonsberg, C. (2012). Subchronic toxicity evaluation of potato protein isolates. *Food and Chemical Toxicology*, *50*(2), 373–384. https://doi.org/10.1016/j.fct.2011.09.039

Maiuri, M. C., Le Toumelin, G., Criollo, A., Rain, J.-C., Gautier, F., Juin, P., Tasdemir, E., Pierron, G., Troulinaki, K., Tavernarakis, N., Hickman, J. A., Geneste, O., & Kroemer, G. (2007). Functional and physical interaction between Bcl-X(L) and a BH3-like domain in Beclin-1. *The EMBO Journal*, *26*(10), 2527–2539. https://doi.org/10.1038/sj.emboj.7601689

Majewska, E., & Szeliga, M. (2017). Akt/gsk3β signaling in glioblastoma. *Neurochemical Research*, *42*(3), 918–924. https://doi.org/10.1007/s11064-016-2044-4

Mao, H., Lebrun, D. G., Yang, J., Zhu, V. F., & Li, M. (2012). Deregulated signaling pathways in glioblastoma multiforme: molecular mechanisms and therapeutic targets. *Cancer Investigation*, *30*(1), 48–56. https://doi.org/10.3109/07357907.2011.630050

Marjanovic, N. D., Weinberg, R. A., & Chaffer, C. L. (2013). Cell plasticity and heterogeneity in cancer. *Clinical Chemistry*, *59*(1), 168–179. https://doi.org/10.1373/clinchem.2012.184655

Maruyama, T., & Noda, N. N. (2017). Autophagy-regulating protease Atg4: structure, function, regulation and inhibition. *The Journal of Antibiotics*, *71*(1), 72–78. https://doi.org/10.1038/ja.2017.104

Masui, K., Mischel, P. S., & Reifenberger, G. (2016). Molecular classification of gliomas. *Handbook of Clinical Neurology*, *134*, 97–120. https://doi.org/10.1016/B978-0-12-802997-8.00006-2

Mathew, R., Karp, C. M., Beaudoin, B., Vuong, N., Chen, G., Chen, H.-Y., Bray, K., Reddy, A., Bhanot, G., Gelinas, C., Dipaola, R. S., Karantza-Wadsworth, V., & White, E. (2009). Autophagy suppresses tumorigenesis through elimination of p62. *Cell*, *137*(6), 1062–1075. https://doi.org/10.1016/j.cell.2009.03.048

Matsuura, H. N., & Fett-Neto, A. G. (2015). Plant alkaloids: main features, toxicity, and mechanisms of action. In P. Gopalakrishnakone, C. R. Carlini, & R. Ligabue-Braun (Eds.), *Plant Toxins* (pp. 1–15). Springer Netherlands. https://doi.org/10.1007/978-94-007-6728-7_2-1

McFarland, C. D., Yaglom, J. A., Wojtkowiak, J. W., Scott, J. G., Morse, D. L., Sherman, M. Y., & Mirny, L. A. (2017). The damaging effect of passenger mutations on cancer progression. *Cancer Research*, *77*(18), 4763–4772. https://doi.org/10.1158/0008-5472.CAN-15-3283-T

Medema, J. P. (2013). Cancer stem cells: the challenges ahead. *Nature Cell Biology*, *15*(4), 338–344. https://doi.org/10.1038/ncb2717

Meng, X.-Q., Zhang, W., Zhang, F., Yin, S.-Y., Xie, H.-Y., Zhou, L., & Zheng, S.-S. (2016). Solanine-induced reactive oxygen species inhibit the growth of human hepatocellular carcinoma HepG2 cells. *Oncology Letters*, *11*(3), 2145–2151. https://doi.org/10.3892/ol.2016.4167

Mensinga, T. T., Sips, A. J. A. M., Rompelberg, C. J. M., van Twillert, K., Meulenbelt, J., van den Top, H. J., & van Egmond, H. P. (2005). Potato glycoalkaloids and adverse effects in humans: an ascending dose study. *Regulatory Toxicology and Pharmacology*, *41*(1), 66–72. https://doi.org/10.1016/j.yrtph.2004.09.004

Miller, K. D., Ostrom, Q. T., Kruchko, C., Patil, N., Tihan, T., Cioffi, G., Fuchs, H. E., Waite, K. A., Jemal, A., Siegel, R. L., & Barnholtz-Sloan, J. S. (2021). Brain and other central nervous system tumor statistics, 2021. *CA: A Cancer Journal for Clinicians*, *71*(5), 381–406. https://doi.org/10.3322/caac.21693

Mohsenikia, M., Alizadeh, A. M., Khodayari, S., Khodayari, H., Kouhpayeh, S. A., Karimi, A., Zamani, M., Azizian, S., & Mohagheghi, M. A. (2013). The protective and

therapeutic effects of alpha-solanine on mice breast cancer. *European Journal of Pharmacology*, *718*(1–3), 1–9. https://doi.org/10.1016/j.ejphar.2013.09.015

Mohsenikia, M., Farhangi, B., Alizadeh, A. M., Khodayari, H., Khodayari, S., Khori, V., Arjmand Abbassi, Y., Vesovic, M., Soleymani, A., & Najafi, F. (2016). Therapeutic effects of dendrosomal solanine on a metastatic breast tumor. *Life Sciences*, *148*, 260–267. https://doi.org/10.1016/j.lfs.2016.02.008

Molinaro, A. M., Taylor, J. W., Wiencke, J. K., & Wrensch, M. R. (2019). Genetic and molecular epidemiology of adult diffuse glioma. *Nature Reviews. Neurology*, *15*(7), 405–417. https://doi.org/10.1038/s41582-019-0220-2

Monastyrska, I., Rieter, E., Klionsky, D. J., & Reggiori, F. (2009). Multiple roles of the cytoskeleton in autophagy. *Biological Reviews of the Cambridge Philosophical Society*, *84*(3), 431–448. https://doi.org/10.1111/j.1469-185X.2009.00082.x

Moroni, M. C., Hickman, E. S., Lazzerini Denchi, E., Caprara, G., Colli, E., Cecconi, F., Müller, H., & Helin, K. (2001). Apaf-1 is a transcriptional target for E2F and p53. *Nature Cell Biology*, *3*(6), 552–558. https://doi.org/10.1038/35078527

Morris, C., & Lee, T. H. (1984). The toxicity and teratogenicity of Solanaceae glycoalkaloids, particularly those of the potato (Solanum tuberosum): a review. *Food Technology in Australia*.

Morris, D. H., Yip, C. K., Shi, Y., Chait, B. T., & Wang, Q. J. (2015). Beclin 1-vps34 complex architecture: understanding the nuts and bolts of therapeutic targets. *Frontiers in Biology*, *10*(5), 398–426. https://doi.org/10.1007/s11515-015-1374-y

Morselli, E., Galluzzi, L., Kepp, O., Vicencio, J.-M., Criollo, A., Maiuri, M. C., & Kroemer, G. (2009). Anti- and pro-tumor functions of autophagy. *Biochimica et Biophysica Acta*, *1793*(9), 1524–1532. https://doi.org/10.1016/j.bbamcr.2009.01.006

Muh, C. R., Joshi, S., Singh, A. R., Kesari, S., Durden, D. L., & Makale, M. T. (2014). PTEN status mediates 2ME2 anti-tumor efficacy in preclinical glioblastoma models: role of HIF1α suppression. *Journal of Neuro-Oncology*, *116*(1), 89–97. https://doi.org/10.1007/s11060-013-1283-3

Mukherjee, J., Phillips, J. J., Zheng, S., Wiencke, J., Ronen, S. M., & Pieper, R. O. (2013). Pyruvate kinase M2 expression, but not pyruvate kinase activity, is up-regulated in a grade-specific manner in human glioma. *Plos One*, *8*(2), e57610. https://doi.org/10.1371/journal.pone.0057610

Mukhopadhyay, S., Panda, P. K., Sinha, N., Das, D. N., & Bhutia, S. K. (2014). Autophagy and apoptosis: where do they meet? *Apoptosis: An International Journal on Programmed Cell Death*, *19*(4), 555–566. https://doi.org/10.1007/s10495-014-0967-2

Mun, A. M., Barden, E. S., Wilson, J. M., & Hogan, J. M. (1975). Teratogenic effects in early chick embryos of solanine and glycoalkaloids from potatoes infected with late-blight, Phytophthora infestans. *Teratology*, *11*(1), 73–78. https://doi.org/10.1002/tera.1420110109

Munari, C. C., de Oliveira, P. F., Campos, J. C. L., Martins, S. de P. L., Da Costa, J. C., Bastos, J. K., & Tavares, D. C. (2014). Antiproliferative activity of Solanum lycocarpum alkaloidic extract and their constituents, solamargine and solasonine, in tumor cell lines. *Journal of Natural Medicines*, *68*(1), 236–241. https://doi.org/10.1007/s11418-013-0757-0

Murphy, Á. C., Weyhenmeyer, B., Schmid, J., Kilbride, S. M., Rehm, M., Huber, H. J., Senft, C., Weissenberger, J., Seifert, V., Dunst, M., Mittelbronn, M., Kögel, D., Prehn, J. H. M., & Murphy, B. M. (2013). Activation of executioner caspases is a predictor of

progression-free survival in glioblastoma patients: a systems medicine approach. *Cell Death & Disease*, *4*, e629. https://doi.org/10.1038/cddis.2013.157

Nakayasu, M., Umemoto, N., Ohyama, K., Fujimoto, Y., Lee, H. J., Watanabe, B., Muranaka, T., Saito, K., Sugimoto, Y., & Mizutani, M. (2017). A Dioxygenase Catalyzes Steroid 16α-Hydroxylation in Steroidal Glycoalkaloid Biosynthesis. *Plant Physiology*, *175*(1), 120–133. https://doi.org/10.1104/pp.17.00501

NavaneethaKrishnan, S., Rosales, J. L., & Lee, K.-Y. (2019). ROS-Mediated Cancer Cell Killing through Dietary Phytochemicals. *Oxidative Medicine and Cellular Longevity*, *2019*, 9051542. https://doi.org/10.1155/2019/9051542

NCBI. (n.d.). *Consensus Coding Sequence Database* . CCDS Database. Retrieved October 10, 2022, from https://www.ncbi.nlm.nih.gov/projects/CCDS/CcdsBrowse.cgi

Nepal, B., & J. Stine, K. (2019). Glycoalkaloids: Structure, Properties, and Interactions with Model Membrane Systems. *Processes*, *7*(8), 513. https://doi.org/10.3390/pr7080513

Nevin, N. C., & Merrett, J. D. (1975). Potato avoidance during pregnancy in women with a previous infant with either anencephaly and/or spina bifida. *British Journal of Preventive & Social Medicine*, *29*(2), 111–115. https://doi.org/10.1136/jech.29.2.111

Ni, W., Tian, T., Zhang, L., Li, Z., Wang, L., & Ren, A. (2018). Maternal periconceptional consumption of sprouted potato and risks of neural tube defects and orofacial clefts. *Nutrition Journal*, *17*(1), 112. https://doi.org/10.1186/s12937-018-0420-4

Nishie, K., Gumbmann, M. R., & Keyl, A. C. (1971). Pharmacology of solanine. *Toxicology and Applied Pharmacology*, *19*(1), 81–92. https://doi.org/10.1016/0041-008X(71)90192-X

Noguchi, M., Hirata, N., Tanaka, T., Suizu, F., Nakajima, H., & Chiorini, J. A. (2020). Autophagy as a modulator of cell death machinery. *Cell Death & Disease*, *11*(7), 517. https://doi.org/10.1038/s41419-020-2724-5

Nørøxe, D. S., Poulsen, H. S., & Lassen, U. (2016). Hallmarks of glioblastoma: a systematic review. *ESMO Open*, *1*(6), e000144. https://doi.org/10.1136/esmoopen-2016-000144

Norred, W. P., Nishie, K., & Osman, S. F. (1976). Excretion, distribution and metabolic fate of 3H-alpha-chaconine. *Research Communications in Chemical Pathology and Pharmacology*, *13*(2), 161–171.

Núñez, F. J., Mendez, F. M., Kadiyala, P., Alghamri, M. S., Savelieff, M. G., Garcia-Fabiani, M. B., Haase, S., Koschmann, C., Calinescu, A.-A., Kamran, N., Saxena, M., Patel, R., Carney, S., Guo, M. Z., Edwards, M., Ljungman, M., Qin, T., Sartor, M. A., Tagett, R., … Castro, M. G. (2019). IDH1-R132H acts as a tumor suppressor in glioma via epigenetic up-regulation of the DNA damage response. *Science Translational Medicine*, *11*(479). https://doi.org/10.1126/scitranslmed.aaq1427

Ohgaki, H., & Kleihues, P. (2013). The definition of primary and secondary glioblastoma. *Clinical Cancer Research*, *19*(4), 764–772. https://doi.org/10.1158/1078-0432.CCR-12-3002

Ojha, R., Ishaq, M., & Singh, S. K. (2015). Caspase-mediated crosstalk between autophagy and apoptosis: Mutual adjustment or matter of dominance. *Journal of*

Cancer Research and Therapeutics, *11*(3), 514–524. https://doi.org/10.4103/0973-1482.163695

Okamoto, H., Ducreux, L. J. M., Allwood, J. W., Hedley, P. E., Wright, A., Gururajan, V., Terry, M. J., & Taylor, M. A. (2020). Light Regulation of Chlorophyll and Glycoalkaloid Biosynthesis During Tuber Greening of Potato S. tuberosum. *Frontiers in Plant Science*, *11*, 753. https://doi.org/10.3389/fpls.2020.00753

Olivier, C., Oliver, L., Lalier, L., & Vallette, F. M. (2020). Drug resistance in glioblastoma: the two faces of oxidative stress. *Frontiers in Molecular Biosciences*, *7*, 620677. https://doi.org/10.3389/fmolb.2020.620677

Omayio, D., Abong, G., & Okoth, M. (2016). A review of Occurrence of Glycoalkaloids in Potato and potato products. *Current Research in Nutrition and Food Science Journal*, *4*(3), 195–202. https://doi.org/10.12944/CRNFSJ.4.3.05

Ou, H.-L., & Schumacher, B. (2018). DNA damage responses and p53 in the aging process. *Blood*, *131*(5), 488–495. https://doi.org/10.1182/blood-2017-07-746396

Pan, B., Zhong, W., Deng, Z., Lai, C., Chu, J., Jiao, G., Liu, J., & Zhou, Q. (2016). Inhibition of prostate cancer growth by solanine requires the suppression of cell cycle proteins and the activation of ROS/P38 signaling pathway. *Cancer Medicine*, *5*(11), 3214–3222. https://doi.org/10.1002/cam4.916

Papale, M., Buccarelli, M., Mollinari, C., Russo, M. A., Pallini, R., Ricci-Vitiani, L., & Tafani, M. (2020). Hypoxia, inflammation and necrosis as determinants of glioblastoma cancer stem cells progression. *International Journal of Molecular Sciences*, *21*(8). https://doi.org/10.3390/ijms21082660

Park, S.-Y., Sun, E.-G., Lee, Y., Kim, M.-S., Kim, J. H., Kim, W.-J., & Jung, J.-Y. (2017). Autophagy induction plays a protective role against hypoxic stress in human

dental pulp cells. *Journal of Cellular Biochemistry*, *119*(2), 1992–2002. https://doi.org/10.1002/jcb.26360

Patel, A. P., Tirosh, I., Trombetta, J. J., Shalek, A. K., Gillespie, S. M., Wakimoto, H., Cahill, D. P., Nahed, B. V., Curry, W. T., Martuza, R. L., Louis, D. N., Rozenblatt-Rosen, O., Suvà, M. L., Regev, A., & Bernstein, B. E. (2014). Single-cell RNA-seq highlights intratumoral heterogeneity in primary glioblastoma. *Science*, *344*(6190), 1396–1401. https://doi.org/10.1126/science.1254257

Pawlowska, E., Szczepanska, J., Szatkowska, M., & Blasiak, J. (2018). An Interplay between Senescence, Apoptosis and Autophagy in Glioblastoma Multiforme-Role in Pathogenesis and Therapeutic Perspective. *International Journal of Molecular Sciences*, *19*(3). https://doi.org/10.3390/ijms19030889

Pearson, J. R. D., & Regad, T. (2017). Targeting cellular pathways in glioblastoma multiforme. *Signal Transduction and Targeted Therapy*, *2*, 17040. https://doi.org/10.1038/sigtrans.2017.40

Pejin, B., Simonovic, M., Talevska, A., Glumac, M., Jakimov, D., & Kojic, V. (2021). A neglected natural source for targeting glioblastoma. *Natural Product Research*, *35*(11), 1856–1860. https://doi.org/10.1080/14786419.2019.1638386

Phillips, H. S., Kharbanda, S., Chen, R., Forrest, W. F., Soriano, R. H., Wu, T. D., Misra, A., Nigro, J. M., Colman, H., Soroceanu, L., Williams, P. M., Modrusan, Z., Feuerstein, B. G., & Aldape, K. (2006). Molecular subclasses of high-grade glioma predict prognosis, delineate a pattern of disease progression, and resemble stages in neurogenesis. *Cancer Cell*, *9*(3), 157–173. https://doi.org/10.1016/j.ccr.2006.02.019

Polson, H. E. J., de Lartigue, J., Rigden, D. J., Reedijk, M., Urbé, S., Clague, M. J., & Tooze, S. A. (2010). Mammalian Atg18 (WIPI2) localizes to omegasome-anchored

phagophores and positively regulates LC3 lipidation. *Autophagy*, *6*(4), 506–522. https://doi.org/10.4161/auto.6.4.11863

Pope, W. B., Xia, Q., Paton, V. E., Das, A., Hambleton, J., Kim, H. J., Huo, J., Brown, M. S., Goldin, J., & Cloughesy, T. (2011). Patterns of progression in patients with recurrent glioblastoma treated with bevacizumab. *Neurology*, *76*(5), 432–437. https://doi.org/10.1212/WNL.0b013e31820a0a8a

Porporato, P. E., Dhup, S., Dadhich, R. K., Copetti, T., & Sonveaux, P. (2011). Anticancer targets in the glycolytic metabolism of tumors: a comprehensive review. *Frontiers in Pharmacology*, *2*, 49. https://doi.org/10.3389/fphar.2011.00049

Poswillo, D. E., Sopher, D., & Mitchell, S. (1972). Experimental induction of foetal malformation with “blighted” potato: a preliminary report. *Nature*, *239*(5373), 462–464. https://doi.org/10.1038/239462a0

Poswillo, D. E., Sopher, D., Mitchell, S. J., Coxon, D. T., Curtis, R. F., & Price, K. R. (1973a). Further investigations into the teratogenic potential of imperfect potatoes. *Nature*, *244*(5415), 367–368. https://doi.org/10.1038/244367a0

Poswillo, D. E., Sopher, D., Mitchell, S. J., Coxon, D. T., Curtis, R. F., & Price, K. R. (1973b). Investigations into the teratogenic potential of imperfect potatoes. *Teratology*, *8*(3), 339–347. https://doi.org/10.1002/tera.1420080317

Prell, T., Stubendorff, B., Le, T. T., Gaur, N., Tadić, V., Rödiger, A., Witte, O. W., & Grosskreutz, J. (2019). Reaction to endoplasmic reticulum stress via ATF6 in amyotrophic lateral sclerosis deteriorates with aging. *Frontiers in Aging Neuroscience*, *11*, 5. https://doi.org/10.3389/fnagi.2019.00005

Qi, W., Keenan, H. A., Li, Q., Ishikado, A., Kannt, A., Sadowski, T., Yorek, M. A., Wu, I.-H., Lockhart, S., Coppey, L. J., Pfenninger, A., Liew, C. W., Qiang, G., Burkart, A.

M., Hastings, S., Pober, D., Cahill, C., Niewczas, M. A., Israelsen, W. J., … King, G. L. (2017). Pyruvate kinase M2 activation may protect against the progression of diabetic glomerular pathology and mitochondrial dysfunction. *Nature Medicine*, *23*(6), 753–762. https://doi.org/10.1038/nm.4328

Rankin, E. B., & Giaccia, A. J. (2008). The role of hypoxia-inducible factors in tumorigenesis. *Cell Death and Differentiation*, *15*(4), 678–685. https://doi.org/10.1038/cdd.2008.21

Redjal, N., Reinshagen, C., Le, A., Walcott, B. P., McDonnell, E., Dietrich, J., & Nahed, B. V. (2016). Valproic acid, compared to other antiepileptic drugs, is associated with improved overall and progression-free survival in glioblastoma but worse outcome in grade II/III gliomas treated with temozolomide. *Journal of Neuro-Oncology*, *127*(3), 505–514. https://doi.org/10.1007/s11060-016-2054-8

Reichert, M., Steinbach, J. P., Supra, P., & Weller, M. (2002). Modulation of growth and radiochemosensitivity of human malignant glioma cells by acidosis. *Cancer*, *95*(5), 1113–1119. https://doi.org/10.1002/cncr.10767

Renwick, J. H. (1972). Hypothesis: anencephaly and spina bifida are usually preventable by avoidance of a specific but unidentified substance present in certain potato tubers. *British Journal of Preventive & Social Medicine*, *26*(2), 67–88. https://doi.org/10.1136/jech.26.2.67

Renwick, J. H., Claringbold, W. D., Earthy, M. E., Few, J. D., & McLean, A. C. (1984). Neural-tube defects produced in Syrian hamsters by potato glycoalkaloids. *Teratology*, *30*(3), 371–381. https://doi.org/10.1002/tera.1420300309

Renwick, J. H., Possamai, A. M., & Munday, M. R. (1974). Potatoes and spina bifida. *Proceedings of the Royal Society of Medicine*, *67*(5), 360–364.

Reuter, S., Gupta, S. C., Chaturvedi, M. M., & Aggarwal, B. B. (2010). Oxidative stress, inflammation, and cancer: how are they linked? *Free Radical Biology & Medicine*, *49*(11), 1603–1616. https://doi.org/10.1016/j.freeradbiomed.2010.09.006

Roufayel, R., Younes, K., Al-Sabi, A., & Murshid, N. (2022). BH3-Only Proteins Noxa and Puma Are Key Regulators of Induced Apoptosis. *Life (Basel, Switzerland)*, *12*(2). https://doi.org/10.3390/life12020256

Ruano, Y., Mollejo, M., Camacho, F. I., Rodríguez de Lope, A., Fiaño, C., Ribalta, T., Martínez, P., Hernández-Moneo, J.-L., & Meléndez, B. (2008). Identification of survival-related genes of the phosphatidylinositol 3'-kinase signaling pathway in glioblastoma multiforme. *Cancer*, *112*(7), 1575–1584. https://doi.org/10.1002/cncr.23338

Rubinstein, A. D., Eisenstein, M., Ber, Y., Bialik, S., & Kimchi, A. (2011). The autophagy protein Atg12 associates with antiapoptotic Bcl-2 family members to promote mitochondrial apoptosis. *Molecular Cell*, *44*(5), 698–709. https://doi.org/10.1016/j.molcel.2011.10.014

Ruddick, J. A., Harwig, J., & Scott, P. M. (1974). Nonteratogenicity in rats of blighted potatoes and compounds contained in them. *Teratology*, *9*(2), 165–168. https://doi.org/10.1002/tera.1420090207

Ruiz-Rodado, V., Seki, T., Dowdy, T., Lita, A., Zhang, M., Han, S., Yang, C., Cherukuri, M. K., Gilbert, M. R., & Larion, M. (2020). Metabolic landscape of a genetically engineered mouse model of IDH1 mutant glioma. *Cancers*, *12*(6). https://doi.org/10.3390/cancers12061633

Russell, R. C., Tian, Y., Yuan, H., Park, H. W., Chang, Y.-Y., Kim, J., Kim, H., Neufeld, T. P., Dillin, A., & Guan, K.-L. (2013). ULK1 induces autophagy by phosphorylating Beclin-

1 and activating VPS34 lipid kinase. *Nature Cell Biology*, *15*(7), 741–750. https://doi.org/10.1038/ncb2757

Ryter, S. W., Cloonan, S. M., & Choi, A. M. K. (2013). Autophagy: a critical regulator of cellular metabolism and homeostasis. *Molecules and Cells*, *36*(1), 7–16. https://doi.org/10.1007/s10059-013-0140-8

Sakariassen, P. Ø., Immervoll, H., & Chekenya, M. (2007). Cancer stem cells as mediators of treatment resistance in brain tumors: status and controversies. *Neoplasia*, *9*(11), 882–892. https://doi.org/10.1593/neo.07658

Salim, S., Snape, T., Welsby, P., & Welsby, G. (2018). Phytochemicals - an alternative therapy for glioblastoma? *Neuro-Oncology*, *20*(suppl_1), i5–i5. https://doi.org/10.1093/neuonc/nox237.021

Sami, A., & Karsy, M. (2013). Targeting the PI3K/AKT/mTOR signaling pathway in glioblastoma: novel therapeutic agents and advances in understanding. *Tumour Biology*, *34*(4), 1991–2002. https://doi.org/10.1007/s13277-013-0800-5

Sanchez-Ortiz, E., Cho, W., Nazarenko, I., Mo, W., Chen, J., & Parada, L. F. (2014). NF1 regulation of RAS/ERK signaling is required for appropriate granule neuron progenitor expansion and migration in cerebellar development. *Genes & Development*, *28*(21), 2407–2420. https://doi.org/10.1101/gad.246603.114

Sasaki, M., Knobbe, C. B., Munger, J. C., Lind, E. F., Brenner, D., Brüstle, A., Harris, I. S., Holmes, R., Wakeham, A., Haight, J., You-Ten, A., Li, W. Y., Schalm, S., Su, S. M., Virtanen, C., Reifenberger, G., Ohashi, P. S., Barber, D. L., Figueroa, M. E., … Mak, T. W. (2012). IDH1(R132H) mutation increases murine haematopoietic progenitors and alters epigenetics. *Nature*, *488*(7413), 656–659. https://doi.org/10.1038/nature11323

Schneider, C. A., Rasband, W. S., & Eliceiri, K. W. (2012). NIH Image to ImageJ: 25 years of image analysis. *Nature Methods*, *9*(7), 671–675. https://doi.org/10.1038/nmeth.2089

Schwartzentruber, J., Korshunov, A., Liu, X.-Y., Jones, D. T. W., Pfaff, E., Jacob, K., Sturm, D., Fontebasso, A. M., Quang, D.-A. K., Tönjes, M., Hovestadt, V., Albrecht, S., Kool, M., Nantel, A., Konermann, C., Lindroth, A., Jäger, N., Rausch, T., Ryzhova, M., … Jabado, N. (2012). Driver mutations in histone H3.3 and chromatin remodelling genes in paediatric glioblastoma. *Nature*, *482*(7384), 226–231. https://doi.org/10.1038/nature10833

Shannon, P., Markiel, A., Ozier, O., Baliga, N. S., Wang, J. T., Ramage, D., Amin, N., Schwikowski, B., & Ideker, T. (2003). Cytoscape: a software environment for integrated models of biomolecular interaction networks. *Genome research*, *13*(11), 2498–2504. https://doi.org/10.1101/gr.1239303.

Sheikh, S., Radivoyevitch, T., Barnholtz-Sloan, J. S., & Vogelbaum, M. (2020). Long-term trends in glioblastoma survival: implications for historical control groups in clinical trials. *Neuro-Oncology Practice*, *7*(2), 158–163. https://doi.org/10.1093/nop/npz046

Shen, H., Hau, E., Joshi, S., Dilda, P. J., & McDonald, K. L. (2015). Sensitization of glioblastoma cells to irradiation by modulating the glucose metabolism. *Molecular Cancer Therapeutics*, *14*(8), 1794–1804. https://doi.org/10.1158/1535-7163.MCT-15-0247

Shen, K.-H., Liao, A. C.-H., Hung, J.-H., Lee, W.-J., Hu, K.-C., Lin, P.-T., Liao, R.-F., & Chen, P.-S. (2014). α-Solanine inhibits invasion of human prostate cancer cell by

suppressing epithelial-mesenchymal transition and MMPs expression. *Molecules (Basel, Switzerland)*, *19*(8), 11896–11914. https://doi.org/10.3390/molecules190811896

Shi, P., Zhang, Z., Xu, J., Zhang, L., & Cui, H. (2021). Endoplasmic reticulum stress-induced cell death as a potential mechanism for targeted therapy in glioblastoma (Review). *International Journal of Oncology*, *59*(2). https://doi.org/10.3892/ijo.2021.5240

Shuvalov, O., Kizenko, A., Petukhov, A., Fedorova, O., Daks, A., Bottrill, A., Snezhkina, A. V., Kudryavtseva, A. V., & Barlev, N. (2020). SEMG1/2 augment energy metabolism of tumor cells. *Cell Death & Disease*, *11*(12), 1047. https://doi.org/10.1038/s41419-020-03251-w

Silva, A. G., Silva, V. A. O., Oliveira, R. J. S., de Rezende, A. R., Chagas, R. C. R., Pimenta, L. P. S., Romão, W., Santos, H. B., Thomé, R. G., Reis, R. M., & de Azambuja Ribeiro, R. I. M. (2020). Matteucinol, isolated from Miconia chamissois, induces apoptosis in human glioblastoma lines via the intrinsic pathway and inhibits angiogenesis and tumor growth in vivo. *Investigational New Drugs*, *38*(4), 1044–1055. https://doi.org/10.1007/s10637-019-00878-1

Sottoriva, A., Spiteri, I., Piccirillo, S. G. M., Touloumis, A., Collins, V. P., Marioni, J. C., Curtis, C., Watts, C., & Tavaré, S. (2013). Intratumor heterogeneity in human glioblastoma reflects cancer evolutionary dynamics. *Proceedings of the National Academy of Sciences of the United States of America*, *110*(10), 4009–4014. https://doi.org/10.1073/pnas.1219747110

Spochacz, M., Chowański, S., Walkowiak-Nowicka, K., Szymczak, M., & Adamski, Z. (2018). Plant-Derived Substances Used Against Beetles-Pests of Stored Crops and

Food-and Their Mode of Action: A Review. *Comprehensive Reviews in Food Science and Food Safety*, *17*(5), 1339–1366. https://doi.org/10.1111/1541-4337.12377

Stacker, S. A., Caesar, C., Baldwin, M. E., Thornton, G. E., Williams, R. A., Prevo, R., Jackson, D. G., Nishikawa, S., Kubo, H., & Achen, M. G. (2001). VEGF-D promotes the metastatic spread of tumor cells via the lymphatics. *Nature Medicine*, *7*(2), 186–191. https://doi.org/10.1038/84635

Stegh, A. H., Kim, H., Bachoo, R. M., Forloney, K. L., Zhang, J., Schulze, H., Park, K., Hannon, G. J., Yuan, J., Louis, D. N., DePinho, R. A., & Chin, L. (2007). Bcl2L12 inhibits post-mitochondrial apoptosis signaling in glioblastoma. *Genes & Development*, *21*(1), 98–111. https://doi.org/10.1101/gad.1480007

Steinbach, J. P., & Weller, M. (2004). Apoptosis in gliomas: molecular mechanisms and therapeutic implications. *Journal of Neuro-Oncology*, *70*(2), 247–256. https://doi.org/10.1007/s11060-004-2753-4

Strik, H., Deininger, M., Streffer, J., Grote, E., Wickboldt, J., Dichgans, J., Weller, M., & Meyermann, R. (1999). BCL-2 family protein expression in initial and recurrent glioblastomas: modulation by radiochemotherapy. *Journal of Neurology, Neurosurgery, and Psychiatry*, *67*(6), 763–768. https://doi.org/10.1136/jnnp.67.6.763

Stoyanov, G. S., Lyutfi, E., Georgieva, R., Georgiev, R., Dzhenkov, D. L., Petkova, L., Ivanov, B. D., Kaprelyan, A., & Ghenev, P. (2022). Reclassification of glioblastoma multiforme according to the 2021 world health organization classification of central nervous system tumors: A single institution report and practical significance. *Cureus*, *14*(2), e21822. https://doi.org/10.7759/cureus.21822

Stummer, W., Meinel, T., Ewelt, C., Martus, P., Jakobs, O., Felsberg, J., & Reifenberger, G. (2012). Prospective cohort study of radiotherapy with concomitant and

adjuvant temozolomide chemotherapy for glioblastoma patients with no or minimal residual enhancing tumor load after surgery. *Journal of Neuro-Oncology*, *108*(1), 89–97. https://doi.org/10.1007/s11060-012-0798-3

Stupp, R., Mason, W. P., van den Bent, M. J., Weller, M., Fisher, B., Taphoorn, M. J. B., Belanger, K., Brandes, A. A., Marosi, C., Bogdahn, U., Curschmann, J., Janzer, R. C., Ludwin, S. K., Gorlia, T., Allgeier, A., Lacombe, D., Cairncross, J. G., Eisenhauer, E., Mirimanoff, R. O., … National Cancer Institute of Canada Clinical Trials Group. (2005). Radiotherapy plus concomitant and adjuvant temozolomide for glioblastoma. *The New England Journal of Medicine*, *352*(10), 987–996. https://doi.org/10.1056/NEJMoa043330

Sun, H., Lv, C., Yang, L., Wang, Y., Zhang, Q., Yu, S., Kong, H., Wang, M., Xie, J., Zhang, C., & Zhou, M. (2014). Solanine induces mitochondria-mediated apoptosis in human pancreatic cancer cells. *BioMed Research International*, *2014*, 805926. https://doi.org/10.1155/2014/805926

Sutendra, G., & Michelakis, E. D. (2013). Pyruvate dehydrogenase kinase as a novel therapeutic target in oncology. *Frontiers in Oncology*, *3*, 38. https://doi.org/10.3389/fonc.2013.00038

Tamrakar, S., Yashiro, M., Kawashima, T., Uda, T., Terakawa, Y., Kuwae, Y., Ohsawa, M., & Ohata, K. (2019). Clinicopathological Significance of Autophagy-related Proteins and its Association With Genetic Alterations in Gliomas. *Anticancer Research*, *39*(3), 1233–1242. https://doi.org/10.21873/anticanres.13233

Tang, Q., Ren, L., Liu, J., Li, W., Zheng, X., Wang, J., & Du, G. (2020). Withaferin A triggers G2/M arrest and intrinsic apoptosis in glioblastoma cells via ATF4-ATF3-CHOP axis. *Cell Proliferation*, *53*(1), e12706. https://doi.org/10.1111/cpr.12706

Taniguchi, K., Sakai, M., Sugito, N., Kumazaki, M., Shinohara, H., Yamada, N., Nakayama, T., Ueda, H., Nakagawa, Y., Ito, Y., Futamura, M., Uno, B., Otsuki, Y., Yoshida, K., Uchiyama, K., & Akao, Y. (2016). PTBP1-associated microRNA-1 and -133b suppress the Warburg effect in colorectal tumors. *Oncotarget*, *7*(14), 18940–18952. https://doi.org/10.18632/oncotarget.8005

ThermoFisher Scientific. (n.d.). *DMEM/F-12, powder, HEPES*. ThermoFisher Scientific. Retrieved December 7, 2022, from https://www.thermofisher.com/order/catalog/product/12400024?SID=srch-hj-12400024

Thorburn, A. (2008). Apoptosis and autophagy: regulatory connections between two supposedly different processes. *Apoptosis: An International Journal on Programmed Cell Death*, *13*(1), 1–9. https://doi.org/10.1007/s10495-007-0154-9

Toyonaga, T., Yamaguchi, S., Hirata, K., Kobayashi, K., Manabe, O., Watanabe, S., Terasaka, S., Kobayashi, H., Hattori, N., Shiga, T., Kuge, Y., Tanaka, S., Ito, Y. M., & Tamaki, N. (2017). Hypoxic glucose metabolism in glioblastoma as a potential prognostic factor. *European Journal of Nuclear Medicine and Molecular Imaging*, *44*(4), 611–619. https://doi.org/10.1007/s00259-016-3541-z

Trejo-Solís, C., Serrano-Garcia, N., Escamilla-Ramírez, Á., Castillo-Rodríguez, R. A., Jimenez-Farfan, D., Palencia, G., Calvillo, M., Alvarez-Lemus, M. A., Flores-Nájera, A., Cruz-Salgado, A., & Sotelo, J. (2018). Autophagic and apoptotic pathways as targets for chemotherapy in glioblastoma. *International Journal of Molecular Sciences*, *19*(12). https://doi.org/10.3390/ijms19123773

Turcan, S., Rohle, D., Goenka, A., Walsh, L. A., Fang, F., Yilmaz, E., Campos, C., Fabius, A. W. M., Lu, C., Ward, P. S., Thompson, C. B., Kaufman, A., Guryanova, O., Levine, R., Heguy, A., Viale, A., Morris, L. G. T., Huse, J. T., Mellinghoff, I. K., & Chan, T. A. (2012). IDH1 mutation is sufficient to establish the glioma hypermethylator phenotype. *Nature*, *483*(7390), 479–483. https://doi.org/10.1038/nature10866

Tyagi, D., Sharma, B. S., Gupta, S. K., Kaul, D., Vasishta, R. K., & Khosla, V. K. (2002). Expression of Bcl2 proto-oncogene in primary tumors of the central nervous system. *Neurology India*, *50*(3), 290–294.

Tykocki, T., & Eltayeb, M. (2018). Ten-year survival in glioblastoma. A systematic review. *Journal of Clinical Neuroscience*, *54*, 7–13. https://doi.org/10.1016/j.jocn.2018.05.002

UniProt. (n.d.). *UniProt*. UniProt. Retrieved October 10, 2022, from https://www.uniprot.org/

Untergasser, A., Cutcutache, I., Koressaar, T., Ye, J., Faircloth, B. C., Remm, M., & Rozen, S. G. (2012). Primer3--new capabilities and interfaces. *Nucleic Acids Research*, *40*(15), e115. https://doi.org/10.1093/nar/gks596

Valdés-Rives, S. A., Casique-Aguirre, D., Germán-Castelán, L., Velasco-Velázquez, M. A., & González-Arenas, A. (2017). Apoptotic signaling pathways in glioblastoma and therapeutic implications. *BioMed Research International*, *2017*, 7403747. https://doi.org/10.1155/2017/7403747

Van Holm, W., Ghesquière, J., Boon, N., Verspecht, T., Bernaerts, K., Zayed, N., Chatzigiannidou, I., & Teughels, W. (2021). A viability quantitative PCR dilemma: are longer amplicons better? *Applied and Environmental Microbiology*, *87*(5), e0265320. https://doi.org/10.1128/AEM.02653-20

van Noorden, C. J. F., Hira, V. V. V., van Dijck, A. J., Novak, M., Breznik, B., & Molenaar, R. J. (2021). Energy Metabolism in IDH1 Wild-Type and IDH1-Mutated Glioblastoma Stem Cells: A Novel Target for Therapy? *Cells*, *10*(3). https://doi.org/10.3390/cells10030705

Vander Heiden, M. G., Cantley, L. C., & Thompson, C. B. (2009). Understanding the Warburg effect: the metabolic requirements of cell proliferation. *Science*, *324*(5930), 1029–1033. https://doi.org/10.1126/science.1160809

Vasilatos, S. N., Katz, T. A., Oesterreich, S., Wan, Y., Davidson, N. E., & Huang, Y. (2013). Crosstalk between lysine-specific demethylase 1 (LSD1) and histone deacetylases mediates antineoplastic efficacy of HDAC inhibitors in human breast cancer cells. *Carcinogenesis*, *34*(6), 1196–1207. https://doi.org/10.1093/carcin/bgt033

Velázquez Vega, J. E., & Brat, D. J. (2017). Molecular-Genetic Classification of Gliomas and Its Practical Application to Diagnostic Neuropathology. In H. Duffau (Ed.), *Diffuse Low-Grade Gliomas in Adults* (pp. 73–100). Springer International Publishing. https://doi.org/10.1007/978-3-319-55466-2_4

Velpula, K. K., Bhasin, A., Asuthkar, S., & Tsung, A. J. (2013). Combined targeting of PDK1 and EGFR triggers regression of glioblastoma by reversing the Warburg effect. *Cancer Research*, *73*(24), 7277–7289. https://doi.org/10.1158/0008-5472.CAN-13-1868

Verhaak, R. G. W., Hoadley, K. A., Purdom, E., Wang, V., Qi, Y., Wilkerson, M. D., Miller, C. R., Ding, L., Golub, T., Mesirov, J. P., Alexe, G., Lawrence, M., O'Kelly, M., Tamayo, P., Weir, B. A., Gabriel, S., Winckler, W., Gupta, S., Jakkula, L., … Cancer Genome Atlas Research Network. (2010). Integrated genomic analysis identifies clinically relevant subtypes of glioblastoma characterized by abnormalities in PDGFRA, IDH1, EGFR, and NF1. *Cancer Cell*, *17*(1), 98–110. https://doi.org/10.1016/j.ccr.2009.12.020

Wang, G., Wang, J.-J., Fu, X.-L., Guang, R., & To, S.-S. T. (2016). Advances in the targeting of HIF-1α and future therapeutic strategies for glioblastoma multiforme (Review). *Oncology Reports*, *37*(2), 657–670. https://doi.org/10.3892/or.2016.5309

Wang, J., & Yi, J. (2008). Cancer cell killing via ROS: to increase or decrease, that is the question. *Cancer Biology & Therapy*, *7*(12), 1875–1884. https://doi.org/10.4161/cbt.7.12.7067

Wang, L., Sun, Q.-Q., Zhang, S.-J., Du, Y.-W., Wang, Y.-Y., Zang, W.-Q., Chen, X.-N., & Zhao, G.-Q. (2016). Inhibitory effect of α-solanine on esophageal carcinoma in vitro. *Experimental and Therapeutic Medicine*, *12*(3), 1525–1530. https://doi.org/10.3892/etm.2016.3500

Wang, P., Wu, J., Ma, S., Zhang, L., Yao, J., Hoadley, K. A., Wilkerson, M. D., Perou, C. M., Guan, K.-L., Ye, D., & Xiong, Y. (2015). Oncometabolite D-2-Hydroxyglutarate Inhibits ALKBH DNA Repair Enzymes and Sensitizes IDH Mutant Cells to Alkylating Agents. *Cell Reports*, *13*(11), 2353–2361. https://doi.org/10.1016/j.celrep.2015.11.029

Wang, Q., Li, H., Sun, Z., Dong, L., Gao, L., Liu, C., & Wang, X. (2016). Kukoamine A inhibits human glioblastoma cell growth and migration through apoptosis induction and epithelial-mesenchymal transition attenuation. *Scientific Reports*, *6*, 36543. https://doi.org/10.1038/srep36543

Wang, S. I., Puc, J., Li, J., Bruce, J. N., Cairns, P., Sidransky, D., & Parsons, R. (1997). Somatic mutations of PTEN in glioblastoma multiforme. *Cancer Research*, *57*(19), 4183–4186.

Wang, Yuanyuan, Wu, J., Guo, W., Sun, Q., Chen, X., Zang, W., Dong, Z., & Zhao, G. (2016). α-Solanine Modulates the Radiosensitivity of Esophageal Cancer Cells by

Inducing MicroRNA 138 Expression. *Cellular Physiology and Biochemistry*, *39*(3), 996–1010. https://doi.org/10.1159/000447807

Wang, Yuhao, Hays, E., Rama, M., & Bonavida, B. (2019). Cell-mediated immune resistance in cancer. *Cancer Drug Resistance*. https://doi.org/10.20517/cdr.2019.98

Wang, Z., Yin, J., Li, M., Shen, J., Xiao, Z., Zhao, Y., Huang, C., Zhang, H., Zhang, Z., Cho, C. H., & Wu, X. (2019). Combination of shikonin with paclitaxel overcomes multidrug resistance in human ovarian carcinoma cells in a P-gp-independent manner through enhanced ROS generation. *Chinese Medicine*, *14*, 7. https://doi.org/10.1186/s13020-019-0231-3

Wanis, H. A., Møller, H., Ashkan, K., & Davies, E. A. (2021). The incidence of major subtypes of primary brain tumors in adults in England 1995-2017. *Neuro-Oncology*, *23*(8), 1371–1382. https://doi.org/10.1093/neuonc/noab076

Weller, M., Le Rhun, E., Preusser, M., Tonn, J.-C., & Roth, P. (2019). How we treat glioblastoma. *ESMO Open*, *4*(Suppl 2), e000520. https://doi.org/10.1136/esmoopen-2019-000520

Wen, Z., Huang, C., Xu, Y., Xiao, Y., Tang, L., Dai, J., Sun, H., Chen, B., & Zhou, M. (2016). α-Solanine inhibits vascular endothelial growth factor expression by down-regulating the ERK1/2-HIF-1α and STAT3 signaling pathways. *European Journal of Pharmacology*, *771*, 93–98. https://doi.org/10.1016/j.ejphar.2015.12.020

Wen, Z.-P., Zeng, W.-J., Chen, Y.-H., Li, H., Wang, J.-Y., Cheng, Q., Yu, J., Zhou, H.-H., Liu, Z.-Z., Xiao, J., & Chen, X.-P. (2019). Knockdown ATG4C inhibits gliomas progression and promotes temozolomide chemosensitivity by suppressing autophagic flux. *Journal of Experimental & Clinical Cancer Research*, *38*(1), 298. https://doi.org/10.1186/s13046-019-1287-8

Wild, P., McEwan, D. G., & Dikic, I. (2014). The LC3 interactome at a glance. *Journal of Cell Science*, *127*(Pt 1), 3–9. https://doi.org/10.1242/jcs.140426

Wirawan, E., Vande Walle, L., Kersse, K., Cornelis, S., Claerhout, S., Vanoverberghe, I., Roelandt, R., De Rycke, R., Verspurten, J., Declercq, W., Agostinis, P., Vanden Berghe, T., Lippens, S., & Vandenabeele, P. (2010). Caspase-mediated cleavage of Beclin-1 inactivates Beclin-1-induced autophagy and enhances apoptosis by promoting the release of proapoptotic factors from mitochondria. *Cell Death & Disease*, *1*(1), e18. https://doi.org/10.1038/cddis.2009.16

Wise, D. R., Ward, P. S., Shay, J. E. S., Cross, J. R., Gruber, J. J., Sachdeva, U. M., Platt, J. M., DeMatteo, R. G., Simon, M. C., & Thompson, C. B. (2011). Hypoxia promotes isocitrate dehydrogenase-dependent carboxylation of α-ketoglutarate to citrate to support cell growth and viability. *Proceedings of the National Academy of Sciences of the United States of America*, *108*(49), 19611–19616. https://doi.org/10.1073/pnas.1117773108

Wlodkowic, D., Telford, W., Skommer, J., & Darzynkiewicz, Z. (2011). Apoptosis and beyond: cytometry in studies of programmed cell death. *Methods in cell biology*, *103*, 55–98. https://doi.org/10.1016/B978-0-12-385493-3.00004-8

Wu, C.-S., Chen, G.-S., Lin, P.-Y., Pan, I.-H., Wang, S.-T., Lin, S. H., Yu, H.-S., & Lin, C.-C. (2014). Tazarotene induces apoptosis in human basal cell carcinoma via activation of caspase-8/t-Bid and the reactive oxygen species-dependent mitochondrial pathway. *DNA and Cell Biology*, *33*(10), 652–666. https://doi.org/10.1089/dna.2014.2366

Xia, Q., Xu, M., Zhang, P., Liu, L., Meng, X., & Dong, L. (2020). Therapeutic Potential of Autophagy in Glioblastoma Treatment With Phosphoinositide 3-

Kinase/Protein Kinase B/Mammalian Target of Rapamycin Signaling Pathway Inhibitors. *Frontiers in Oncology*, *10*, 572904. https://doi.org/10.3389/fonc.2020.572904

Yadav, R. K., Chae, S.-W., Kim, H.-R., & Chae, H. J. (2014). Endoplasmic reticulum stress and cancer. *Journal of Cancer Prevention*, *19*(2), 75–88. https://doi.org/10.15430/JCP.2014.19.2.75

Yamashoji, S., & Matsuda, T. (2013). Synergistic cytotoxicity induced by α-solanine and α-chaconine. *Food Chemistry*, *141*(2), 669–674. https://doi.org/10.1016/j.foodchem.2013.03.104

Yan, X., Li, M., Chen, L., Peng, X., Que, Z.-J., An, H.-M., Shen, K.-P., & Hu, B. (2020). α-Solanine inhibits growth and metastatic potential of human colorectal cancer cells. *Oncology Reports*, *43*(5), 1387–1396. https://doi.org/10.3892/or.2020.7519

Yang, W., Xia, Y., Cao, Y., Zheng, Y., Bu, W., Zhang, L., You, M. J., Koh, M. Y., Cote, G., Aldape, K., Li, Y., Verma, I. M., Chiao, P. J., & Lu, Z. (2012). EGFR-induced and PKCε monoubiquitylation-dependent NF-κB activation upregulates PKM2 expression and promotes tumorigenesis. *Molecular Cell*, *48*(5), 771–784. https://doi.org/10.1016/j.molcel.2012.09.028

Yang, W., Zheng, Y., Xia, Y., Ji, H., Chen, X., Guo, F., Lyssiotis, C. A., Aldape, K., Cantley, L. C., & Lu, Z. (2012). ERK1/2-dependent phosphorylation and nuclear translocation of PKM2 promotes the Warburg effect. *Nature Cell Biology*, *14*(12), 1295–1304. https://doi.org/10.1038/ncb2629

Yang, Z., Wilkie-Grantham, R. P., Yanagi, T., Shu, C.-W., Matsuzawa, S.-I., & Reed, J. C. (2015). ATG4B (Autophagin-1) phosphorylation modulates autophagy. *The Journal of Biological Chemistry*, *290*(44), 26549–26561. https://doi.org/10.1074/jbc.M115.658088

Ye, J., Coulouris, G., Zaretskaya, I., Cutcutache, I., Rozen, S., & Madden, T. L. (2012). Primer-BLAST: a tool to design target-specific primers for polymerase chain reaction. *BMC Bioinformatics*, *13*, 134. https://doi.org/10.1186/1471-2105-13-134

Yousefi, S., Perozzo, R., Schmid, I., Ziemiecki, A., Schaffner, T., Scapozza, L., Brunner, T., & Simon, H.-U. (2006). Calpain-mediated cleavage of Atg5 switches autophagy to apoptosis. *Nature Cell Biology*, *8*(10), 1124–1132. https://doi.org/10.1038/ncb1482

Yu, W., Yang, Z., Huang, R., Min, Z., & Ye, M. (2019). SIRT6 promotes the Warburg effect of papillary thyroid cancer cell BCPAP through reactive oxygen species. *OncoTargets and Therapy*, *12*, 2861–2868. https://doi.org/10.2147/OTT.S194256

Yun, C. W., & Lee, S. H. (2018). The roles of autophagy in cancer. *International Journal of Molecular Sciences*, *19*(11). https://doi.org/10.3390/ijms19113466

Zhang, D., Wang, F., Pang, Y., Ke, X.-X., Zhu, S., Zhao, E., Zhang, K., Chen, L., & Cui, H. (2017). Down-regulation of CHERP inhibits neuroblastoma cell proliferation and induces apoptosis through ER stress induction. *Oncotarget*, *8*(46), 80956–80970. https://doi.org/10.18632/oncotarget.20898

Zhang, F., Yang, R., Zhang, G., Cheng, R., Bai, Y., Zhao, H., Lu, X., Li, H., Chen, S., Li, J., Wu, S., Li, P., Chen, X., Sun, Q., & Zhao, G. (2016). Anticancer function of α-solanine in lung adenocarcinoma cells by inducing microRNA-138 expression. *Tumour Biology*, *37*(5), 6437–6446. https://doi.org/10.1007/s13277-015-4528-2

Zhang, J., Wang, G., Zhou, Y., Chen, Y., Ouyang, L., & Liu, B. (2018). Mechanisms of autophagy and relevant small-molecule compounds for targeted cancer therapy. *Cellular and Molecular Life Sciences*, *75*(10), 1803–1826. https://doi.org/10.1007/s00018-018-2759-2

Zhang, P., Xia, Q., Liu, L., Li, S., & Dong, L. (2020). Current opinion on molecular characterization for GBM classification in guiding clinical diagnosis, prognosis, and therapy. *Frontiers in Molecular Biosciences*, *7*, 562798. https://doi.org/10.3389/fmolb.2020.562798

Zhang, W., Lv, S., Liu, J., Zang, Z., Yin, J., An, N., Yang, H., & Song, Y. (2014). PCI-24781 down-regulates EZH2 expression and then promotes glioma apoptosis by suppressing the PIK3K/Akt/mTOR pathway. *Genetics and Molecular Biology*, *37*(4), 716–724. https://doi.org/10.1590/S1415-47572014005000011

Zhang, Y., Song, L., & Li, Z. (2019). Polychlorinated biphenyls promote cell survival through pyruvate kinase M2-dependent glycolysis in HeLa cells. *Toxicology Mechanisms and Methods*, *29*(6), 428–437. https://doi.org/10.1080/15376516.2019.1584658

Zhao, M., Xu, H., Zhang, B., Hong, B., Yan, W., & Zhang, J. (2015). Impact of nuclear factor erythroid-derived 2-like 2 and p62/sequestosome expression on prognosis of patients with gliomas. *Human Pathology*, *46*(6), 843–849. https://doi.org/10.1016/j.humpath.2015.02.009

Zhao, S., Lin, Y., Xu, W., Jiang, W., Zha, Z., Wang, P., Yu, W., Li, Z., Gong, L., Peng, Y., Ding, J., Lei, Q., Guan, K.-L., & Xiong, Y. (2009). Glioma-derived mutations in IDH1 dominantly inhibit IDH1 catalytic activity and induce HIF-1alpha. *Science*, *324*(5924), 261–265. https://doi.org/10.1126/science.1170944

Zheng, Y., Li, L., Gao, Q., Niu, B., & Wang, H. (2020). Solanine inhibits proliferation and promotes apoptosis of the human leukaemia cells by targeting the miR-16/Bcl-2 axis . *Journal of Haematology Oncology*, *25*(3), 1614–1618.

Zhi, Y.-H., Song, M.-M., Wang, P.-L., Zhang, T., & Yin, Z.-Y. (2009). Suppression of matrix metalloproteinase-2 via RNA interference inhibits pancreatic carcinoma cell invasiveness and adhesion. *World Journal of Gastroenterology*, *15*(9), 1072–1078. https://doi.org/10.3748/wjg.15.1072

Zhu, Y., Zhao, L., Liu, L., Gao, P., Tian, W., Wang, X., Jin, H., Xu, H., & Chen, Q. (2010). Beclin 1 cleavage by caspase-3 inactivates autophagy and promotes apoptosis. *Protein & Cell*, *1*(5), 468–477. https://doi.org/10.1007/s13238-010-0048-4

Chapter 8 Appendix I: Ethical approval

L-Università ta' Malta

Andrea Cuschieri <andrea.cuschieri.19@um.edu.mt>

The status of your REDP form (MED-2022-00115) has been updated to Acknowledged

1 message

form.urec@um.edu.mt <form.urec@um.edu.mt> 14 March 2023 at 11:06
To: andrea.cuschieri.19@um.edu.mt

Dear Andrea Cuschieri,

Please note that the status of your REDP form (MED-2022-00115) has been set to *Acknowledged*.

This status change was accompanied by the following explanation/justification: *Dear applicant, Your research ethics application has been received. As indicated in the Research Ethics Review Procedures, submissions which have no self-assessment issues are kept for record and audit purposes only, so research may commence. Kindly note that FREC will not issue any form of approval as the responsibility for the self-assessment part lies exclusively with the researcher. Regards, MED FREC*

You can keep track of your applications by visiting: https://www.um.edu.mt/research/ethics/redp-form/frontEnd/.

This email has been automatically generated by URECA. Please do not reply. If you wish to communicate with your F/REC please use the respective email address.

Chapter 9 Appendix II: Systematic literature searching

9.1. General systematic literature search method

Appropriate literature for chapter 1 was identified according to the Preferred Reporting Literature Searches in Systematic Reviews 2020 (PRISMA-S) guidelines (Rethlefsen et al., 2021).

9.1.1. Study identification and selection

PubMed, Google Scholar, Science Direct and Semantic Scholar databases were searched for relevant articles. Combinations of free text keywords and MESH terms (were appropriate), identified through a preliminary literature search, were used to develop database specific search strategy as outlined in **Table 9.1.**

Grey literature was not explored, since only articles published in reputable peer-reviewed journals were considered. A risk of bias assessment was not conducted since this systematic search was only conducted to identify relavant literature (Cornell University Library, 2022). Included studies were retried from the respective database and stored digitally in dedicated files.

Table 9.1.: Systematic searching inclusion criteria and database specific search terms.

Section	Inclusion criteria	Database	Search terms	Additional remarks
2.1.1.	1. Original studies or reviews; 2. Published between 2021 until week-34-2022; 3. Reporting relevant and updated GBM epidemiology; 4. Recorded GBM patient demographic characteristics	PubMed	((epidemiology[MeSH Terms] OR (epidemiology)) AND ((glioblastoma[MeSH Terms]) OR (glioblastoma multiforme[MeSH Terms]) OR (glioblastoma) OR (glioblastoma multiforme))	A publication not identified through the systematic search was included in this qualitative systematic review since this is the only study to document the epidemiology of GBM in the Maltese population (Grech et al., 2020).
		Google Scholar	allintitle: ("epidemiology") AND ("glioblastoma" OR "glioblastoma multiforme")	
		Science Direct	Title, abstract or author-specified keywords: ("epidemiology") AND ("glioblastoma" OR "glioblastoma multiforme")	
		Semantic scholar	Title: ("epidemiology") AND ("glioblastoma" OR "glioblastoma multiforme")	
2.1.2.	1. Original studies or reviews; 2. Published between 2017 until week-34-2022; 3. Discussing GBM classifications	PubMed	((classification[MeSH Terms] OR (classification)) AND ((glioblastoma[MeSH Terms]) OR (glioblastoma multiforme[MeSH Terms]) OR (glioblastoma) OR (glioblastoma multiforme))	This search was supplemented by snowball manual review of reference lists of retreived articles to ensure that the original publication outlining the latest GBM classification is found, if this was published prior to 2017.
		Google Scholar	allintitle: ("classification") AND ("glioblastoma" OR "glioblastoma multiforme")	
		Science Direct	Title, abstract or author-specified keywords: ("classification") AND ("glioblastoma" OR "glioblastoma multiforme")	
		Semantic scholar	Title: ("classification") AND ("glioblastoma" OR "glioblastoma multiforme")	
2.1.3.	1. Reviews; 2. Published between 2012 until week-35-2022; 3. Discussing cell signalling and/or molecular biology of GBM	PubMed	(((molecular biology[MeSH Terms]) OR (molecular biology)) OR ((signalling pathways[MeSH Terms]) OR (signalling pathways)) OR ((cell signalling [MeSH Terms])) OR (cell signalling)) OR (glioma biology)) AND ((glioblastoma[MeSH Terms]) OR (glioblastoma multiforme) OR (glioblastoma multiforme[MeSH Terms]))	/
		Google Scholar	allintitle: "glioblastoma" OR "glioblastoma multiforme" AND "cell signalling" OR "signalling pathway" OR "molecular biology" OR "glioma biology	

		Science Direct	Title, abstract or author-specified keywords: (“glioblastoma” OR “glioblastoma multiforme”) AND (“molecular biology” OR “cell signalling” OR “signalling pathway” OR “glioma biology	
		Semantic scholar	Title: ("molecular biology" OR "glioma biology" OR "cell signalling" OR "signalling pathway") AND ("glioblastoma" OR "glioblastoma multiforme")	
2.1.4.	1. Reviews; 2. Published between 2012 until week-38-2022; 3. Discussing the management and/or treatment for GBM	PubMed	((therapy) OR (treatment) OR (management)) ((glioblastoma[MeSH Terms]) OR (glioblastoma multiforme[MeSH Terms]) OR (glioblastoma) OR (glioblastoma multiforme))	
		Google Scholar	allintitle: ("therapy" OR "management" OR "treatment") ("glioblastoma" "glioblastoma multiforme")	
		Science Direct	Title, abstract or author-specified keywords: ("therapy OR "management" OR "treatment") AND ("glioblastoma" OR "glioblastoma multiforme")	
		Semantic scholar	Title: (“therapy” OR “management” OR “treatment”) AND (“glioblastoma” OR glioblastoma multiforme”)	
2.1.5.	1. Original studies; 2. Published between 2012 until week-36-2022; 3. Discussing the anti-cancer porperties of phytochemicals/ natural extracts against GBM	PubMed	(((phytochemical[MeSH Terms]) OR (phytochemical)) OR ((natural compound[MeSH Terms]) OR (natural compound)) OR ((extract[MeSH Terms])) OR (extract))) AND ((glioblastoma[MeSH Terms]) OR (glioblastoma multiforme) OR (glioblastoma multiforme[MeSH Terms]))	/
		Google Scholar	allintitle: "glioblastoma" OR "glioblastoma multiforme" AND "phytochemical” OR "natural compound" OR "extract" biology"	
		Science Direct	Title, abstract or author-specified keywords: (“glioblastoma” OR “glioblastoma multiforme”) AND (“phytochemical” OR “natural compound” OR extract”)	
		Semantic scholar	Title: ("phytochemical" OR "natural compound" OR	

			"extract") AND ("glioblastoma" OR "glioblastoma multiforme")	
2.2.1.	1. Original studies; 2. Published between 2012 until week37-2022; 3. Investigating the extraction of α-Solanine from plants	PubMed	((solanine[MeSH Terms]) OR (alpha-solanine) OR (α-Solanine)) AND ((extraction[MeSH Terms]) OR (extraction))	/
		Google Scholar	allintitle:("extraction") AND ("solanine" OR "alpha-solanine" OR "α-Solanine")	
		Science Direct	Title, abstract or author-specified keywords: ("extraction") AND ("solanine" OR "alpha-solanine" OR "α-Solanine")	
		Semantic scholar	Title: ("extraction") AND ("solanine" OR "alpha-solanine" OR "α-Solanine")	
2.2.2. (part 1)	1. Original studies or reviews; 2. Published between 2012 until week-35-2022; 3. Discussing the chemical properties of α-Solanine	PubMed	((solanine[MeSH Terms]) OR (alpha-solanine) OR (α-Solanine)) AND ((chemistry[MeSH Terms]) OR (chemistry) OR (chemical properties))	/
		Google Scholar	allintitle:("chemistry" OR "chemical properties") AND ("solanine" OR "alpha-solanine" OR "α-Solanine")	
		Science Direct	Title, abstract or author-specified keywords: ("chemistry" OR "chemical properties") AND ("solanine" OR "alpha-solanine" OR "α-Solanine")	
		Semantic scholar	Title: ("chemistry" OR "chemical properties") AND ("solanine" OR "alpha-solanine" OR "α-Solanine")	
2.2.2. (part 2)	1. Original studies or reviews; 2. Published between 2012 until week-35-2022; 3. Discussing the endogenous biosynthesis of α-Solanine in plants	PubMed	((solanine[MeSH Terms]) OR (alpha-solanine) OR (α-Solanine)) AND ((biosynthesis[MeSH Terms]) OR (biosynthesis))	/
		Google Scholar	allintitle:("biosynthesis") AND ("solanine" OR "alpha-solanine" OR "α-Solanine")	
		Science Direct	Title, abstract or author-specified keywords: ("biosynthesis") AND ("solanine" OR "alpha-solanine" OR "α-Solanine")	
		Semantic scholar	Title: ("biosynthesis") AND ("solanine" OR "alpha-solanine" OR "α-Solanine")	
2.2.3.	1. Original studies or reviews;	PubMed	((solanine[MeSH Terms]) OR (alpha-solanine) OR (α-Solanine)) AND	/

	2. Published between 2012 until week37-2022; 3. Investigated/ discussed the pharmacology and/or toxicology of α-Solanine		((pharmacology[MeSH Terms]) OR (pharmacology) OR (toxicology[MeSH Terms]) OR (toxicology))	
		Google Scholar	allintitle:("toxicology" OR "pharmacology") AND ("solanine" OR "alpha-solanine" OR "α-Solanine")	
		Science Direct	Title, abstract or author-specified keywords: (“toxicology” OR “pharmacology”) AND ("solanine" OR "alpha-solanine" OR "α-Solanine")	
		Semantic scholar	Title: ("toxicology" OR "pharmacology") AND ("solanine" OR "alpha-solanine" OR "α-Solanine")	
2.3.	1. In-vitro, in-vivo or in-silico studies; 2. Published until week-33-2022; 3. Investigated the anti-cancer effects of α-Solanine; 4. Reported extractable novel experimental outcomes	PubMed	((solanine[MeSH Terms]) OR (alpha-solanine) OR (solanine)) AND ((cancer[MeSH Terms]))	This search was supplemented by snowballing manual review of reference lists of retreived articles.
		Google Scholar	allintitle: ("alpha-Solanine" OR "Solanine" OR "α-Solanine") AND ("cancer")	
		Science Direct	Title, abstract or author-specified keywords: (“alpha-Solanine” OR “Solanine” OR “α-Solanine”) AND (“cancer”)	
		Semantic scholar	Title: ("alpha-Solanine" OR "Solanine" OR "α-Solanine") AND ("cancer")	

9.2. Systematic literature search results

9.2.1. Systematic literature search results for section 2.1.1.

258 tenative studies were identified, with 14 records being duplicates. 203 studies were excluded following title and abstract screening using the pre-defined inclusion and exclusion criteria. Thus, 41 reports were sought for retrieval and their full text was assessed in detail for eligibility. Among these, 2 could not be retreived. Of the 39 remaining studies, 27 studies were excluded as they did not meet our pre-defined inclusion criteria. resulting in a total of 12 studies being included (Alhalaseh et al., 2021; Cote & Ostrom, 2021; Efremov et al., 2021; El Hage et al., 2021; Engberg et al., 2022;

Grochans et al., 2022; H. Kang et al., 2021; Lam et al., 2018; D. Lin et al., 2021; Meel et al., 2021; Miller et al., 2021; Ståhl et al., 2022; Wanis et al., 2021) (**Figure 7.2.).**

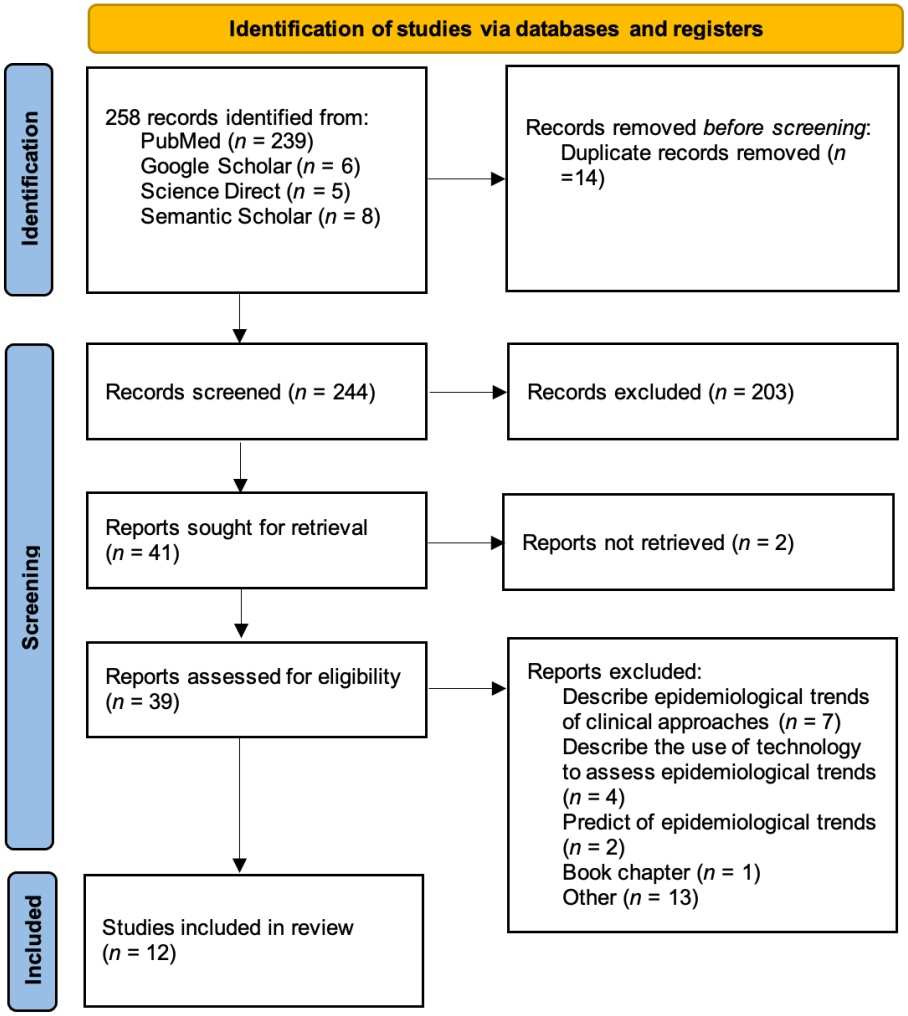


Figure 9.1.: Preferred Reporting Items for Systematic reviews and Meta-Analyses 2020 flow diagram for systematic literature regarding Section 2.1.1.. Adapted from Page et al., 2021.

9.2.2. Systematic literature search results for section 2.1.2.

767 tenative studies were identified, with 42 records being duplicates. 611 studies were excluded following title and abstract screening using the pre-defined inclusion and exclusion criteria. Thus, 113 reports were sought for retrieval and their full text was assessed in detail for eligibility. Among these, 5 could not be retreived. Of the 108 remaining studies, 102 studies were excluded as they did not meet our pre-defined inclusion criteria. Citation searching identified 7 additional studies, 3 of which were

duplicate rectors and 1 could not be retrieved. Of the two remaining studies, 1 studies was excluded, resulting in a total of 7 studies included being included (Gupta & Dwivedi, 2017; Komori, 2017; Lasorella & Iavarone, 2021; E. Lee et al., 2018; Stoyanov et al., 2022; van den Bent et al., 2017) (**Figure 7.3.).**

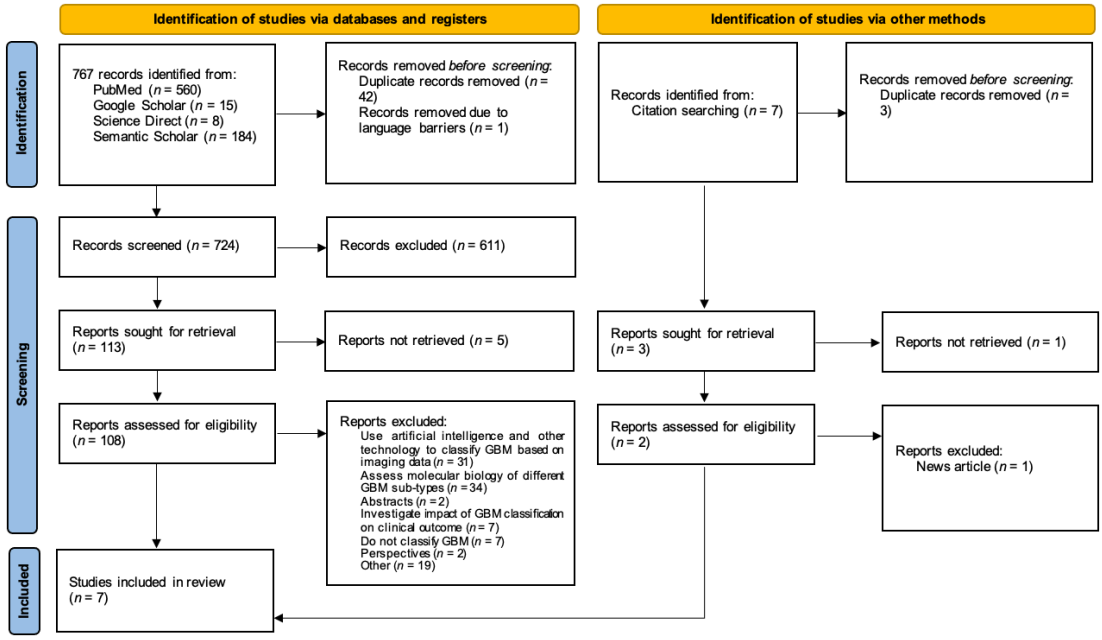


Figure 9.2.: Preferred Reporting Items for Systematic reviews and Meta-Analyses 2020 flow diagram for systematic literature search for Section 2.1.2.. Adapted from Page et al., 2021.

9.2.3. Systematic literature search results for section 2.1.3.

1,307 tenative studies were identified, with 91 records being duplicates. 1,042 studies were excluded following title and abstract screening using the pre-defined inclusion and exclusion criteria. Thus, 172 reports were sought for retrieval and their full text was assessed in detail for eligibility. Among these, 13 could not be retreived. Of the 159 remaining studies, 91 studies were excluded as they did not meet our pre-defined inclusion criteria. resulting in a total of 68 studies being included (Ahmed et al., 2021; Aldape et al., 2015; Alexandru et al., 2020; Atkins et al., 2013; Balandeh et al., 2021;

Bazzoni & Bentivegna, 2019; Buruiană et al., 2020; Campos et al., 2016; Carrasco-García et al., 2014; Cloughesy et al., 2014; B. P. Coelho et al., 2020; Colella et al., 2019; Crespo et al., 2015; do Carmo et al., 2013; Domènech et al., 2021; Duzgun et al., 2016; Dymova et al., 2021; El Khayari et al., 2022; Eskilsson et al., 2018; Gagliardi et al., 2014; Ghaffarian Zirak et al., 2022; Gray et al., 2014; Guelfi et al., 2016; Xuyang Guo et al., 2022; Iglesia et al., 2019; Jandrey et al., 2021; Jimenez-Pascual & Siebzehnrubl, 2019; Karsy et al., 2012; Lathia et al., 2015; J.-K. Lee et al., 2014; Y. Lee et al., 2016; X. Li et al., 2016; Litak et al., 2019; S.-Y. Liu et al., 2015; Majewska & Szeliga, 2017; Mao et al., 2012; Markouli et al., 2022; Matias et al., 2018; Miranda et al., 2017; Mosteiro et al., 2022; Nagy et al., 2015; Olivier et al., 2020; Ou et al., 2021; Pawlowska et al., 2018; Pearson & Regad, 2017; Pfeffer, 2016; Province et al., 2013; Qiu et al., 2017; Sami & Karsy, 2013; Sati & Parhar, 2021; P. Shi et al., 2021; Simpson & Gammoh, 2020; So et al., 2021; Soubannier & Stifani, 2017; Tilak et al., 2021; Tompa et al., 2018; Trejo-Solís et al., 2018; Tuncel & Kalkan, 2018; Urbantat et al., 2021; Uribe et al., 2022; Vakilian et al., 2017; Valdés-Rives et al., 2017; Velásquez et al., 2019; Veliz et al., 2015; Wallace et al., 2013; H. Wang et al., 2022; Wardak & Choe, 2013; Zuccarini et al., 2018) (**Figure 7.4.).**

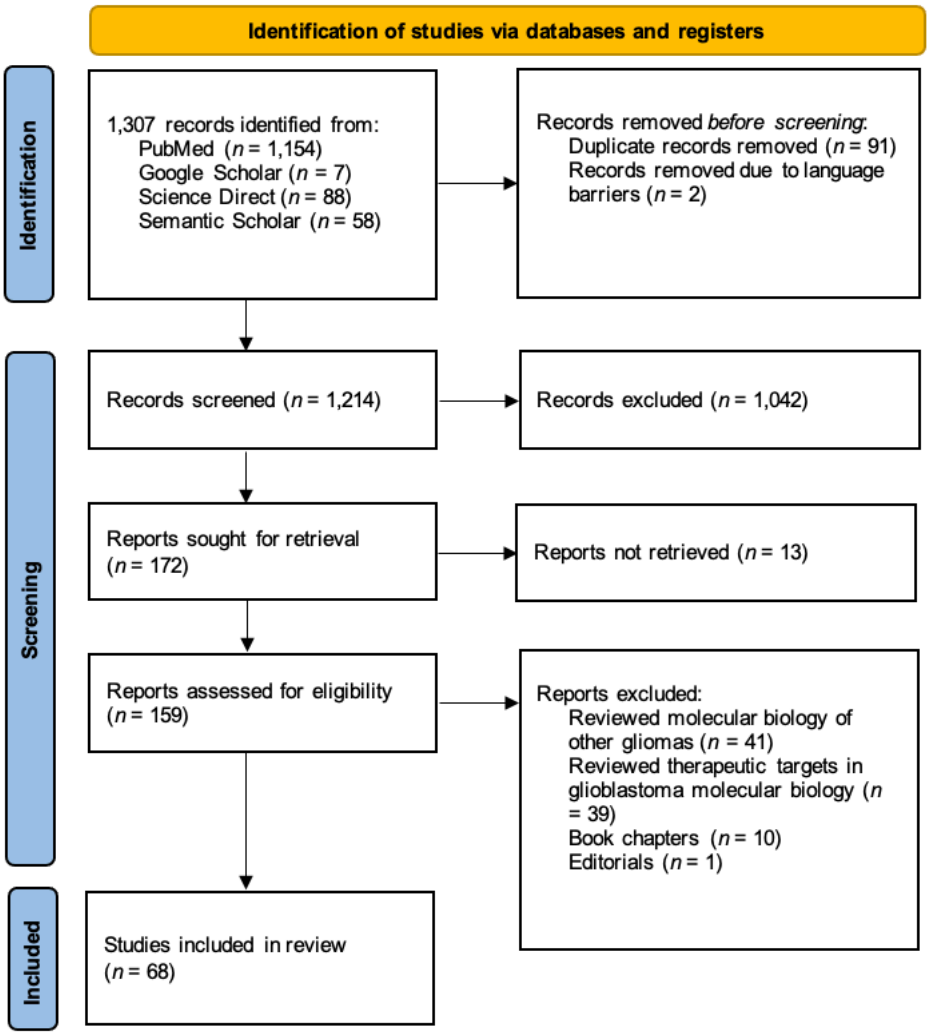


Figure 9.3.: Preferred Reporting Items for Systematic reviews and Meta-Analyses 2020 flow diagram for systematic literature search for Section 2.1.3.. Adapted from Page et al., 2021.

9.2.4. Systematic literature search results for section 2.1.4.

3,561 tenative studies were identified, with 268 records being duplicates. 3,121 studies were excluded following title and abstract screening using the pre-defined inclusion and exclusion criteria. Thus, 161 reports were sought for retrieval and their full text was assessed in detail for eligibility. Among these, 8 could not be retreived. Of the 153 remaining studies, 132 studies were excluded as they did not meet our pre-defined inclusion criteria, resulting in a total of 21 studies being included (Barbarite et al., 2017;

Batash et al., 2017; Cenciarini et al., 2019; Cramer & Chen, 2019; Xiaopeng Guo et al., 2022; Hasbum et al., 2021; Huang et al., 2020; Kim & Kim, 2020; Kuo et al., 2017; Le Rhun et al., 2019; Y. Li et al., 2021; Ma et al., 2021; McMahon et al., 2022; Minniti et al., 2021; Mungur et al., 2022; Ramalho et al., 2022; Roux et al., 2017; Sevastre et al., 2021; Tan et al., 2020; Touat et al., 2017; Guangwen Wang & Wang, 2022; Weller et al., 2019; Wick et al., 2018; Wick & Platten, 2018; Jun Yang et al., 2020; H. Zhang et al., 2019)(**Figure 7.5.).**

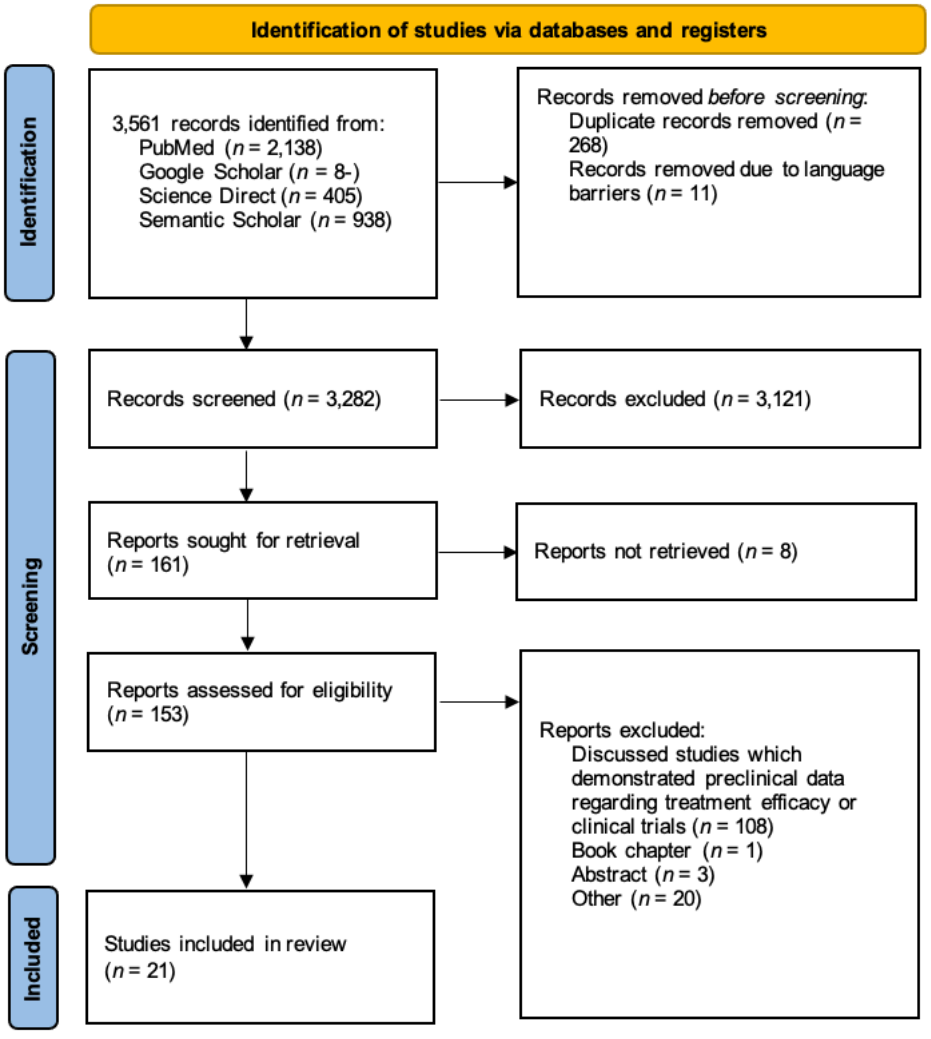


Figure 9.4.: Preferred Reporting Items for Systematic reviews and Meta-Analyses 2020 flow diagram for systematic literature search for Section 2.1.4.. Adapted from Page et al., 2021.

9.2.5. Systematic literature search results for section 2.1.5.

847 tenative studies were identified, with 31 records being duplicates. 504 studies were excluded following title and abstract screening using the pre-defined inclusion and exclusion criteria. Thus, 309 reports were sought for retrieval and their full text was assessed in detail for eligibility. Among these, 42 could not be retreived. Of the 267 remaining studies, 14 studies were excluded as they did not meet our pre-defined inclusion criteria, resulting in a total of 118 studies being included (Abubakar et al., 2015; Aghamohammadi et al., 2015; Aithal & Rajeswari, 2019; Alafnan et al., 2021; Alexandru et al., 2016; Amaral et al., 2019; Amirah Idris et al., 2019; Arcella et al., 2018; Aroui et al., 2020; Baradaran Rahimi et al., 2019; Ben Mabrouk et al., 2017; Bernardo et al., 2020; Bezerra et al., 2015; Bhuyan et al., 2017; Bona et al., 2020; Borawska et al., 2016; Chaicharoenaudomrung et al., 2018; K.-F. Chang et al., 2020, 2021; K.-H. Chang et al., 2013; C.-J. Chen et al., 2022; Y. Chen et al., 2020; Cho et al., 2017; Choukairi et al., 2020; Chung et al., 2021; Cimmino et al., 2016; P. L. C. Coelho et al., 2016; Colapietro, Mancini, et al., 2020; Colapietro, Yang, et al., 2020; Czarnik-Kwaśniak et al., 2019; Zhang'an Dai et al., 2021; Zhibo Dai et al., 2018; de Lima et al., 2022; de Mendonça et al., 2015; Dept. of Molecular Biology, Iraqi Center for Cancer and Medical Genetics Research, Baghdad, Iraq et al., 2018; Di Cesare Mannelli et al., 2018; Dörschmann et al., 2020; Elkady et al., 2014; Emsen et al., 2016; Erdogan & Eroglu, 2019; Franco et al., 2021; Gade et al., 2022; Garrido-Armas et al., 2018; Genovese et al., 2020; Gentile et al., 2015; Gu et al., 2016; Guerram et al., 2015; Ham et al., 2019; Hatziagapiou et al., 2022; Hilliard et al., 2017; Hsu et al., 2022; Hwang et al., 2019; Ibrahim et al., 2015; Izumi et al., 2020; Jalili-Nik et al., 2021; Jiao et al., 2015; Joshi et al., 2020; Kamarudin et al., 2021; C.-W. Kang et al., 2015; Kapoor et al., 2017; Karakas et al., 2019; Karkare et al., 2014; Keshmiri-

Neghab et al., 2014; Khaksar et al., 2022; Khan et al., 2015; Koc et al., 2018; Kowalczyk et al., 2019; V. Kumar et al., 2017; Kwanthongdee et al., 2019; Lampronti et al., 2020; J. Li et al., 2013; Zizhuo Li et al., 2019; Liang et al., 2017; Mbaveng et al., 2019, 2021; Mendanha et al., 2021; Mora et al., 2015; Moskwa et al., 2022; Munari et al., 2014; Murugesan et al., 2020; Mutlu et al., 2021; Mykhailenko et al., 2021; Oliva et al., 2022; Pang et al., 2022; Park et al., 2020; Peeri et al., 2021; Pejin et al., 2021; Ramachandran et al., 2015; Sangpairoj, 2021; Y. Shi et al., 2020; Shin et al., 2012; A. G. Silva et al., 2020; T. C. C. Silva et al., 2018; Soares et al., 2019; Stojković et al., 2021; Stojkovic et al., 2022; Su et al., 2017; Tang et al., 2020; Teixeira et al., 2018; Tezcan, Taskapilioglu, et al., 2017; Tezcan, Tunca, et al., 2017; Tovilovic-Kovacevic et al., 2018; Tsai et al., 2017; Gang Wang et al., 2015; J. Wang et al., 2016; Q. Wang et al., 2016; X. Wang et al., 2021; YanGang Wang et al., 2015; Z. Wang et al., 2020; Wong et al., 2018; Wright et al., 2022; Xiong et al., 2020; Xue et al., 2017; Yeh et al., 2020; Yuan et al., 2014; Zanotto-Filho et al., 2015; L. Zhang et al., 2014; Y. Zhang et al., 2014; Zhao et al., 2018; Y.-G. Zhu et al., 2021) (**Figure 7.6.).**

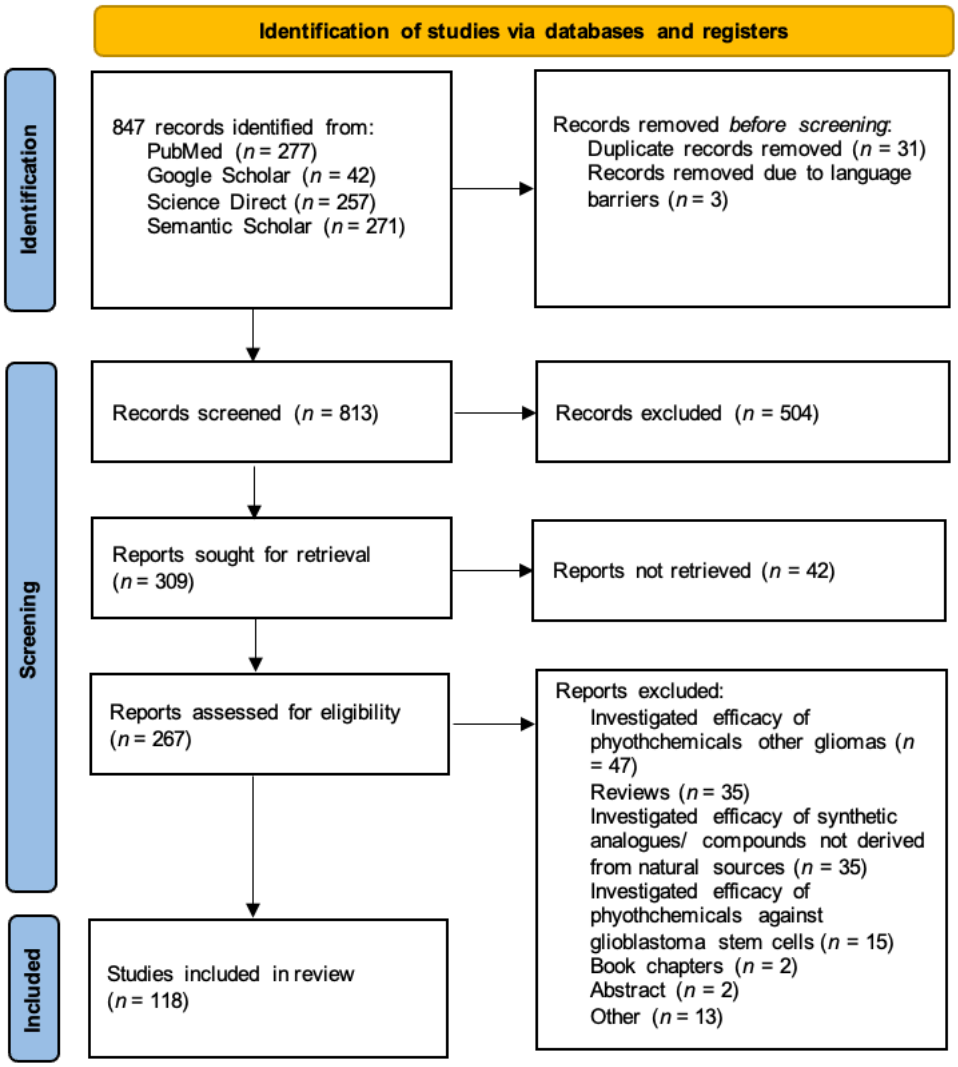


Figure 9.5.: Preferred Reporting Items for Systematic reviews and Meta-Analyses 2020 flow diagram for systematic literature search for Section 2.1.4.. Adapted from Page et al., 2021.

9.2.6. Systematic literature search results for section 2.2.1.

146 tenative studies were identified, with 19 records being duplicates. 89 studies were excluded following title and abstract screening using the pre-defined inclusion and exclusion criteria. Thus, 37 reports were sought for retrieval and their full text was assessed in detail for eligibility. Among these, 4 could not be retreived. Of the 33 remaining studies, 14 studies were excluded as they did not meet our pre-defined inclusion criteria, resulting in a total of 19 studies being included (Apel et al., 2020;

Attoumbré et al., 2012; Backleh et al., 2004; Baker et al., 1955; Distl et al., 2009; Hellenäs et al., 1992; Hellenás et al., 1997; Hossain et al., 2014, 2015; Houben & Brunt, 1994; Ismali et al., 2019; Kondamudi et al., 2017; Laus et al., 2017; Zhiwen Li et al., 2009; W. Liu et al., 2014; Mokgehle et al., 2022; Sánchez Maldonado et al., 2014; Wan et al., 2022; L. Zhu et al., 2020)(**Figure 7.7.).**

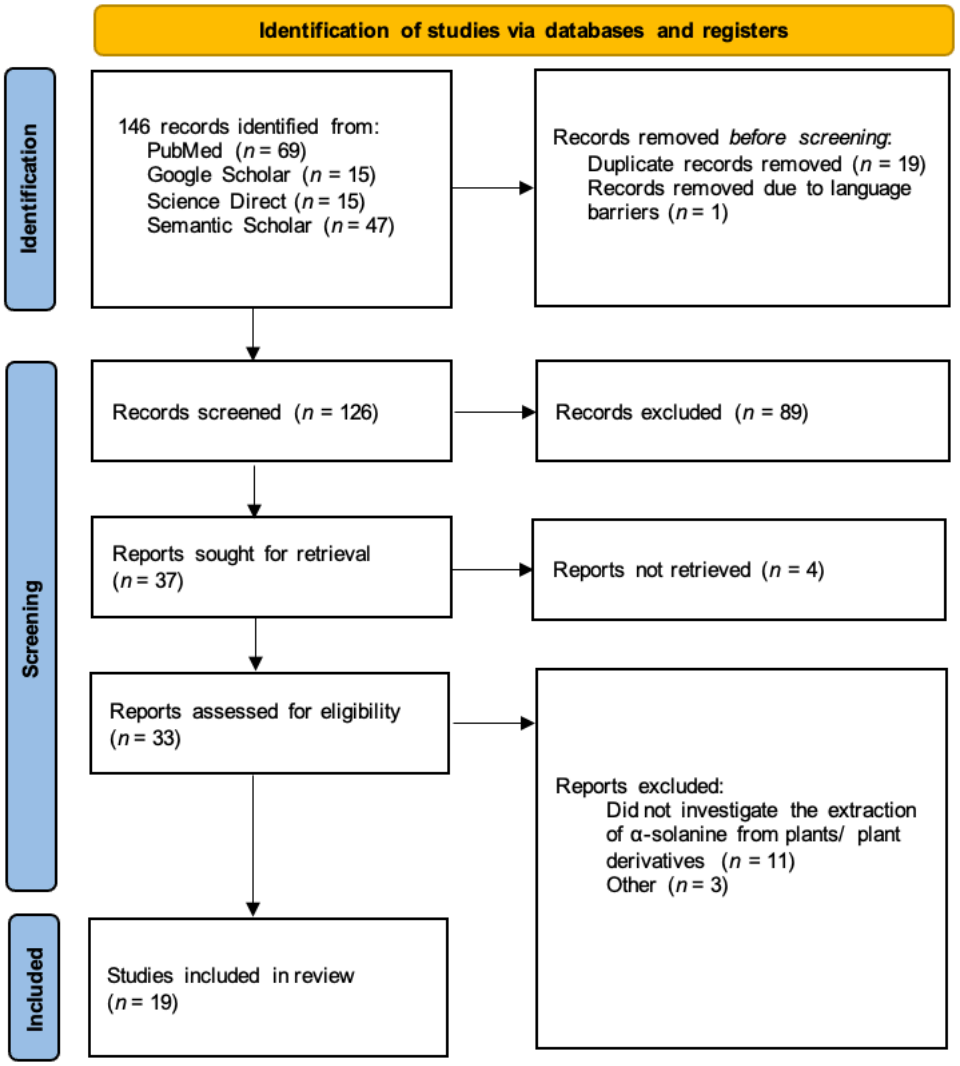


Figure 9.6.: Preferred Reporting Items for Systematic reviews and Meta-Analyses 2020 flow diagram for systematic literature search for Section 2.2.1.. Adapted from Page et al., 2021.

9.2.7. Systematic literature search results for section 2.2.2. (part 1)

No studies which met our pre-defined inclusion criteria were identified. In light of this, specalised websites and registries containing appropirate knowledge for the synthesis of Section 2.2.2. will also be utilized (National Library of Medicine, n.d.; Royal Society of Chemistry, n.d.; TMIC, n.d.).

9.2.8. Systematic literature search results for section 2.2.2. (part 2)

127 tenative studies were identified, with 1 records being duplicates. 97 studies were excluded following title and abstract screening using the pre-defined inclusion and exclusion criteria. Thus, 13 reports were sought for retrieval and their full text was assessed in detail for eligibility. Among these, 3 could not be retreived. Of the 10 remaining studies, 3 studies were excluded as they did not meet our pre-defined inclusion criteria, resulting in a total of 7 studies being included (Akiyama et al., 2021; Baur et al., 2021; Ginzberg et al., 2012; A. Kumar et al., 2017; Nakayasu et al., 2017; Okamoto et al., 2020; Umemoto et al., 2016) (**Figure 7.8.).**

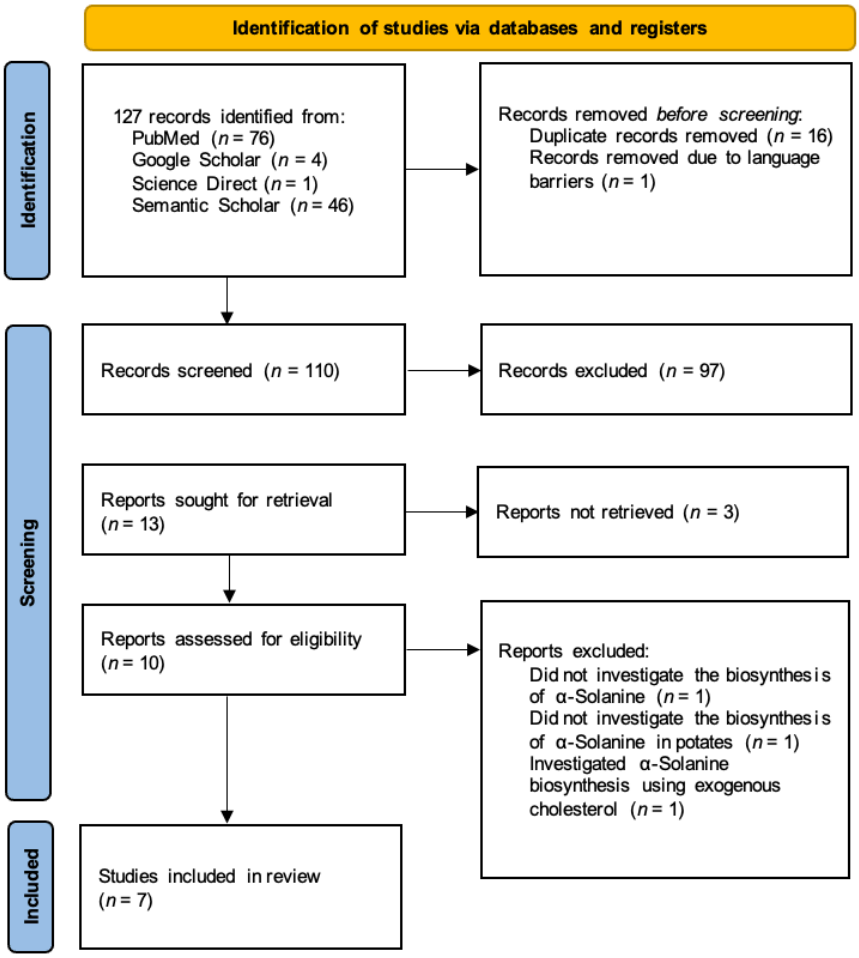


Figure 9.7.: Preferred Reporting Items for Systematic reviews and Meta-Analyses 2020 flow diagram for systematic literature search for Section 2.1.4.. Adapted from Page et al., 2021.

9.2.9. Systematic literature search results for section 2.2.3.

209 tenative studies were identified, with 5 records being duplicates. 149 studies were excluded following title and abstract screening using the pre-defined inclusion and exclusion criteria. Thus, 55 reports were sought for retrieval and their full text was assessed in detail for eligibility. Among these, 11 could not be retreived. Of the 44 remaining studies, 21 studies were excluded as they did not meet our pre-defined inclusion criteria, resulting in a total of 23 studies being included (Alexander et al., 1948; Barceloux, 2009; Carlier et al., 2015; Chaube & Swinyard, 1976; Crawford & Myhr, 1995; Dalvi, 1985; M Friedman et al., 1991, 1996; Mendel Friedman et al., 2003; Gaffield &

Keeler, 1996; Jelínek et al., 1976; Kline et al., 1961; Korpan et al., 2004; Langkilde et al., 2008, 2009, 2012; Lynch et al., 2012; Mensinga et al., 2005; Nara et al., 2019; Ni et al., 2018; Nishie et al., 1971; Patil et al., 1972; Slanina, 1990)(**Figure 7.9.).**

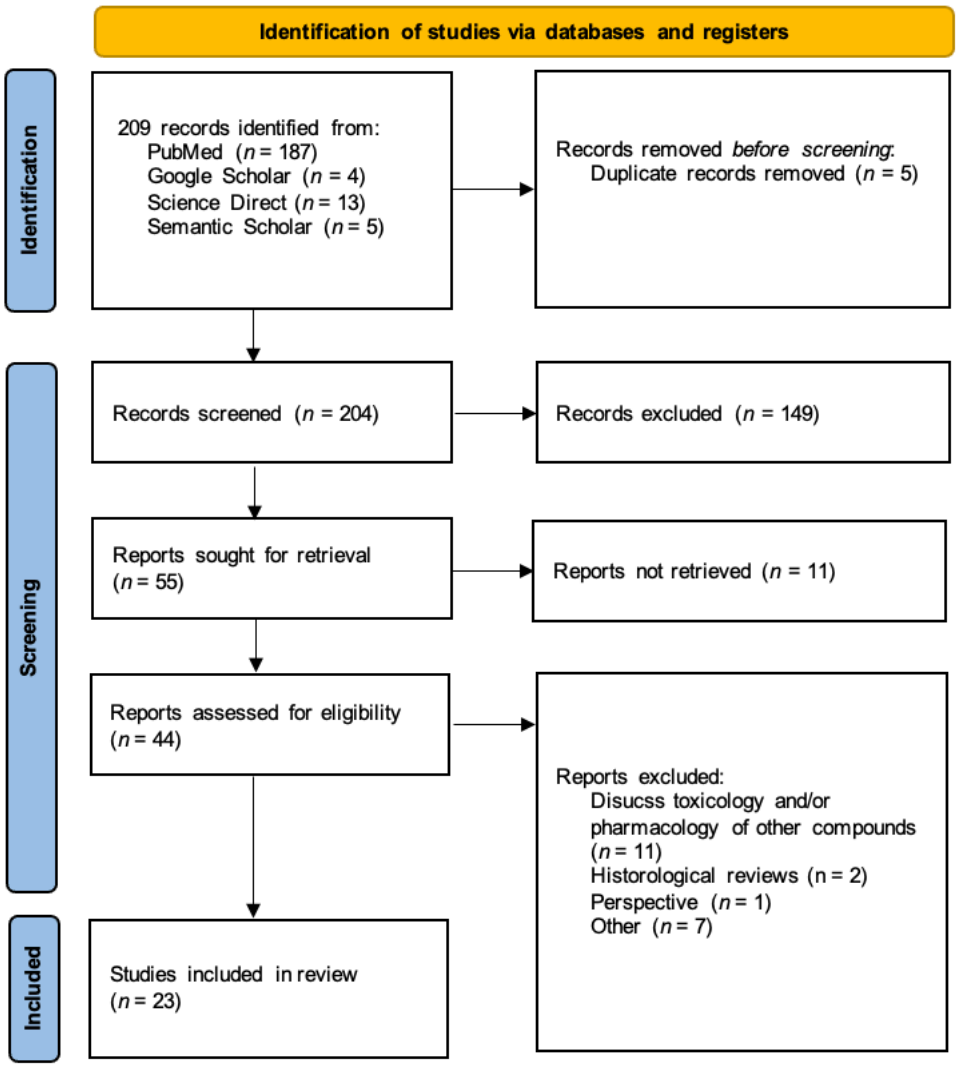


Figure 9.8.: Preferred Reporting Items for Systematic reviews and Meta-Analyses 2020 flow diagram for systematic literature search for Section 2.2.3.. Adapted from Page et al., 2021.

9.2.10. Systematic literature search results for section 2.3.

306 tenative studies were identified. 76 potential records were duplicates and 180 studies were excluded following title and abstract screening using the pre-defined inclusion and exclusion criteria. Thus, 47 reports were sought for retrieval and their full

text was assessed in detail for eligibility. Among these, 7 could not be retreived. Of the 40 remaining studies, 14 studies were excluded as they did not meet our pre-defined inclusion criteria. Citation-searching of the 27 included studies revealed an additional 2 potential studies, which met our inclusion criteria following in-depth assessment of their full text, resulting in a total of 28 studies included being included (Mendel Friedman et al., 2005; J. Gao et al., 2020; S.-Y. Gao et al., 2006; Gouhar et al., 2022; Hasanain et al., 2015; Ji & Gao, 2012; Karaboğa Arslan & Yerer, 2018; Krisnamurti et al., 2022; K.-R. Lee et al., 2004; L.-T. Lin et al., 2020; Lu et al., 2010; Lv et al., 2014; Meng et al., 2016; Mohsenikia et al., 2013, 2016; Pan et al., 2016; Shen et al., 2014; Sun et al., 2014; L. Wang et al., 2016; Yuanyuan Wang et al., 2016; Wen et al., 2016; Yamashoji & Matsuda, 2013; Yan et al., 2020; Jinhui Yang et al., 2019; F. Zhang et al., 2016; Zheng et al., 2020; Zou et al., 2021) **(Figure 7.10.).**

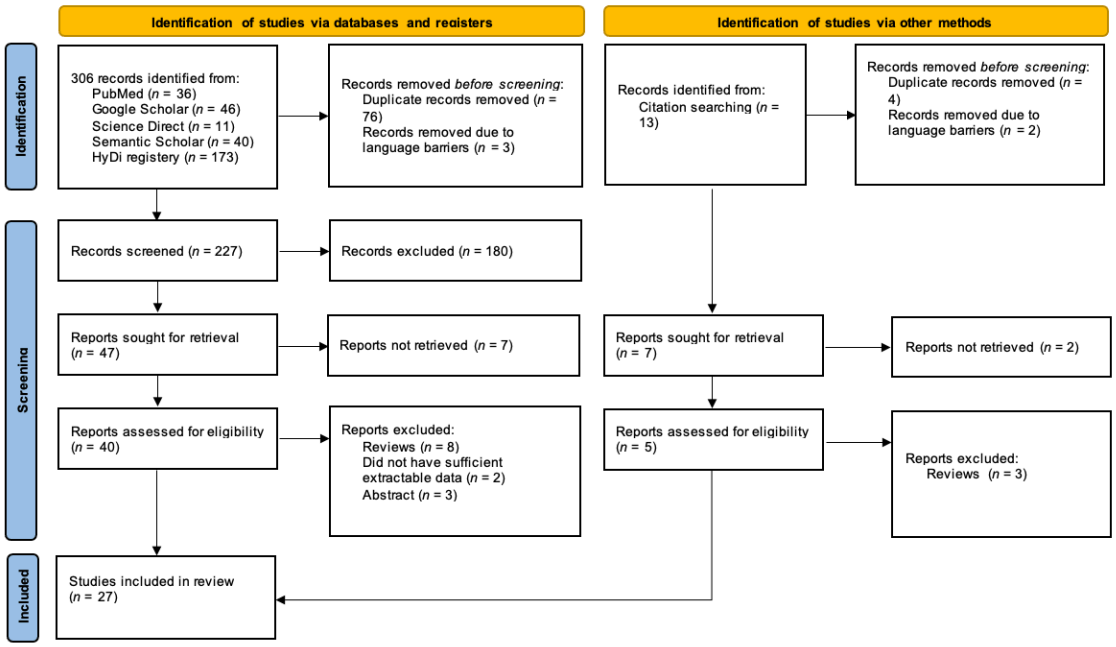


Figure 9.9.: Preferred Reporting Items for Systematic reviews and Meta-Analyses 2020 flow diagram for systematic literature search for Section 2.1.4.. Adapted from Page et al., 2021.

9.3. References

Abubakar, I. B., Lim, K.-H., & Loh, H.-S. (2015). Alkaloid extracts of Ficus species and palm oil-derived tocotrienols synergistically inhibit proliferation of human cancer cells. Natural Product Research, 29(22), 2137–2140. https://doi.org/10.1080/14786419.2014.991927

Aghamohammadi, A., Hosseinimehr, S. J., Ghasemi, A., Azadbakht, M., & Pourfallah, T. A. (2015). Radiosensitization Effects of a Zataria multiflora Extract on Human Glioblastoma Cells. Asian Pacific Journal of Cancer Prevention, 16(16), 7285–7290. https://doi.org/10.7314/APJCP.2015.16.16.7285

Ahmed, S. P., Castresana, J. S., & Shahi, M. H. (2021). Glioblastoma and MiRNAs. Cancers, 13(7). https://doi.org/10.3390/cancers13071581

Aithal, M. G. S., & Rajeswari, N. (2019). Bacoside A Induced Sub-G0 Arrest and Early Apoptosis in Human Glioblastoma Cell Line U-87 MG through Notch Signaling Pathway. Brain Tumor Research and Treatment, 7(1), 25–32. https://doi.org/10.14791/btrt.2019.7.e21

Akiyama, R., Watanabe, B., Nakayasu, M., Lee, H. J., Kato, J., Umemoto, N., Muranaka, T., Saito, K., Sugimoto, Y., & Mizutani, M. (2021). The biosynthetic pathway of potato solanidanes diverged from that of spirosolanes due to evolution of a dioxygenase. Nature Communications, 12(1), 1300. https://doi.org/10.1038/s41467-021-21546-0

Alafnan, A., Hussain, T., Alamri, A., Alshammari, F., Moin, A., & Krishna, K. L. (2021). Moringa Oleifera leaf extract exerts antiproliferative effects and induces mitochondria mediated apoptosis within rat glioblastoma (c6) cells. Pharmacognosy Magazine, 17(6), 240. https://doi.org/10.4103/pm.pm_145_21

Aldape, K., Zadeh, G., Mansouri, S., Reifenberger, G., & von Deimling, A. (2015). Glioblastoma: pathology, molecular mechanisms and markers. Acta Neuropathologica, 129(6), 829–848. https://doi.org/10.1007/s00401-015-1432-1

Alexander, R. F., Forbes, G. B., & Hawkins, E. S. (1948). A fatal case of solanine poisoning. British Medical Journal, 2(4575), 518. https://doi.org/10.1136/bmj.2.4575.518

Alexandru, O., Georgescu, A. M., Ene, L., Purcaru, S. O., Serban, F., Popescu, A., Brindusa, C., Tataranu, L. G., Ciubotaru, V., & Dricu, A. (2016). The effect of curcumin on low-passage glioblastoma cells in vitro. Journal of Cancer Research and Therapeutics, 12(2), 1025–1032. https://doi.org/10.4103/0973-1482.167609

Alexandru, O., Horescu, C., Sevastre, A.-S., Cioc, C. E., Baloi, C., Oprita, A., & Dricu, A. (2020). Receptor tyrosine kinase targeting in glioblastoma: performance, limitations and future approaches. Contemporary Oncology (Poznan, Poland), 24(1), 55–66. https://doi.org/10.5114/wo.2020.94726

Alhalaseh, Y. N., Abdulelah, Z. A., Abu-Shanab, A., Armouti, A. O., Amarin, J. Z., Mansour, R., Sultan, H., & Al-Hussaini, M. (2021). Glioblastoma in adolescents and young adults: An age-based comparative study from Jordan over a 17-year period. Cancer Epidemiology, 73, 101948. https://doi.org/10.1016/j.canep.2021.101948

Amaral, S. da C., Barbieri, S. F., Ruthes, A. C., Bark, J. M., Brochado Winnischofer, S. M., & Silveira, J. L. M. (2019). Cytotoxic effect of crude and purified pectins from Campomanesia xanthocarpa Berg on human glioblastoma cells. Carbohydrate Polymers, 224, 115140. https://doi.org/10.1016/j.carbpol.2019.115140

Amirah Idris, Izwandy Idris, & Wan Iryani Wan Ismail. (2019). The Effect of Diopatra claparedii Grube, 1878 Aqueous Extract on Chang Liver and Human Primary

Glioblastoma (U-87) Cell Lines. Universiti Malaysia Terengganu Journal of Undergraduate Research, 1(3), 56–67. https://doi.org/10.46754/umtjur.v1i3.79

Apel, C., Lyng, J. G., Papoutsis, K., Harrison, S. M., & Brunton, N. P. (2020). Screening the effect of different extraction methods (ultrasound-assisted extraction and solid–liquid extraction) on the recovery of glycoalkaloids from potato peels: Optimisation of the extraction conditions using chemometric tools. Food and Bioproducts Processing, 119, 277–286. https://doi.org/10.1016/j.fbp.2019.06.018

Arcella, A., Oliva, M. A., Staffieri, S., Sanchez, M., Madonna, M., Riozzi, B., Esposito, V., Giangaspero, F., & Frati, L. (2018). Effects of aloe emodin on U87MG glioblastoma cell growth: In vitro and in vivo study. Environmental Toxicology, 33(11), 1160–1167. https://doi.org/10.1002/tox.22622

Aroui, S., Fetoui, H., & Kenani, A. (2020). Natural dietary compound naringin inhibits glioblastoma cancer neoangiogenesis. BMC Pharmacology & Toxicology, 21(1), 46. https://doi.org/10.1186/s40360-020-00426-1

Atkins, R. J., Stylli, S. S., Luwor, R. B., Kaye, A. H., & Hovens, C. M. (2013). Glycogen synthase kinase-3β (GSK-3β) and its dysregulation in glioblastoma multiforme. Journal of Clinical Neuroscience, 20(9), 1185–1192. https://doi.org/10.1016/j.jocn.2013.02.003

Attoumbré, J., Lesur, D., Giordanengo, P., & Baltora-Rosset, S. (2012). Preparative separation of glycoalkaloids α-solanine and α-chaconine by centrifugal partition chromatography. Journal of Chromatography. B, Analytical Technologies in the Biomedical and Life Sciences, 908, 150–154. https://doi.org/10.1016/j.jchromb.2012.09.025

Backleh, M., Ekici, P., Leupold, G., Coelhan, M., & Parlar, H. (2004). Enrichment of the glycoalkaloids alpha-solanine and alpha-chaconine from potato juice by adsorptive bubble separation using a pH gradient. Journal of Separation Science, 27(12), 1042–1044. https://doi.org/10.1002/jssc.200301685

Baker, L. C., Lampitt, L. H., & Meredith, O. B. (1955). Solanine, glycoside of the potato. III. —An improved method of extraction and determination. Journal of the Science of Food and Agriculture, 6(4), 197–202. https://doi.org/10.1002/jsfa.2740060404

Balandeh, E., Mohammadshafie, K., Mahmoudi, Y., Hossein Pourhanifeh, M., Rajabi, A., Bahabadi, Z. R., Mohammadi, A. H., Rahimian, N., Hamblin, M. R., & Mirzaei, H. (2021). Roles of Non-coding RNAs and Angiogenesis in Glioblastoma. Frontiers in Cell and Developmental Biology, 9, 716462. https://doi.org/10.3389/fcell.2021.716462

Baradaran Rahimi, V., Mousavi, S. H., Haghighi, S., Soheili-Far, S., & Askari, V. R. (2019). Cytotoxicity and apoptogenic properties of the standardized extract of Portulaca oleracea on glioblastoma multiforme cancer cell line (U-87): a mechanistic study. EXCLI Journal, 18, 165–186. https://doi.org/10.17179/excli2019-1063

Barbarite, E., Sick, J. T., Berchmans, E., Bregy, A., Shah, A. H., Elsayyad, N., & Komotar, R. J. (2017). The role of brachytherapy in the treatment of glioblastoma multiforme. Neurosurgical Review, 40(2), 195–211. https://doi.org/10.1007/s10143-016-0727-6

Barceloux, D. G. (2009). Potatoes, tomatoes, and solanine toxicity (Solanum tuberosum L., Solanum lycopersicum L.). Disease-a-Month : DM, 55(6), 391–402. https://doi.org/10.1016/j.disamonth.2009.03.009

Batash, R., Asna, N., Schaffer, P., Francis, N., & Schaffer, M. (2017). Glioblastoma multiforme, diagnosis and treatment; recent literature review. Current Medicinal Chemistry, 24(27), 3002–3009. https://doi.org/10.2174/0929867324666170516123206

Baur, S., Frank, O., Hausladen, H., Hückelhoven, R., Hofmann, T., Eisenreich, W., & Dawid, C. (2021). Biosynthesis of α-solanine and α-chaconine in potato leaves (Solanum tuberosum L.) - A 13CO2 study. Food Chemistry, 365, 130461. https://doi.org/10.1016/j.foodchem.2021.130461

Bazzoni, R., & Bentivegna, A. (2019). Role of notch signaling pathway in glioblastoma pathogenesis. Cancers, 11(3). https://doi.org/10.3390/cancers11030292

Ben Mabrouk, H., Nejia, S., Maram, M., Naziha, M., & Soufia, C.-E. (2017). A New Protein Extract Inhibitor from Hypobranchial Purple Gland of Hexaplex trunculus, a Mediterranean Mollusk, Impairs the Motility of Human Glioblastoma U87 and the HeLa Cell Line of Cervical Carcinoma Cells. Nutrition and Cancer, 69(7), 1028–1035. https://doi.org/10.1080/01635581.2017.1359315

Bernardo, P. S., Guimarães, G. H. C., De Faria, F. C. C., Longo, G. M. D. C., Lopes, G. P. D. F., Netto, C. D., Costa, P. R. R., & Maia, R. C. (2020). LQB-118 compound inhibits migration and induces cell death in glioblastoma cells. Oncology Reports, 43(1), 346–357. https://doi.org/10.3892/or.2019.7402

Bezerra, D. P., Ferreira, P. M. P., Machado, C. M. L., de Aquino, N. C., Silveira, E. R., Chammas, R., & Pessoa, C. (2015). Antitumour efficacy of Piper tuberculatum and piplartine based on the hollow fiber assay. Planta Medica, 81(1), 15–19. https://doi.org/10.1055/s-0034-1383363

Bhuyan, D. J., Sakoff, J., Bond, D. R., Predebon, M., Vuong, Q. V., Chalmers, A. C., van Altena, I. A., Bowyer, M. C., & Scarlett, C. J. (2017). In vitro anticancer properties of

selected Eucalyptus species. In Vitro Cellular & Developmental Biology. Animal, 53(7), 604–615. https://doi.org/10.1007/s11626-017-0149-y

Bona, N. P., Pedra, N. S., Azambuja, J. H., Soares, M. S. P., Spohr, L., Gelsleichter, N. E., de M Meine, B., Sekine, F. G., Mendonça, L. T., de Oliveira, F. H., Braganhol, E., Spanevello, R. M., da Silveira, E. F., & Stefanello, F. M. (2020). Tannic acid elicits selective antitumoral activity in vitro and inhibits cancer cell growth in a preclinical model of glioblastoma multiforme. Metabolic Brain Disease, 35(2), 283–293. https://doi.org/10.1007/s11011-019-00519-9

Borawska, M. H., Naliwajko, S. K., Moskwa, J., Markiewicz-Żukowska, R., Puścion-Jakubik, A., & Soroczyńska, J. (2016). Anti-proliferative and anti-migration effects of Polish propolis combined with Hypericum perforatum L. on glioblastoma multiforme cell line U87MG. BMC Complementary and Alternative Medicine, 16, 367. https://doi.org/10.1186/s12906-016-1351-2

Buruiană, A., Florian, Ștefan I., Florian, A. I., Timiș, T.-L., Mihu, C. M., Miclăuș, M., Oșan, S., Hrapșa, I., Cataniciu, R. C., Farcaș, M., & Șușman, S. (2020). The Roles of miRNA in Glioblastoma Tumor Cell Communication: Diplomatic and Aggressive Negotiations. International Journal of Molecular Sciences, 21(6). https://doi.org/10.3390/ijms21061950

Campos, B., Olsen, L. R., Urup, T., & Poulsen, H. S. (2016). A comprehensive profile of recurrent glioblastoma. Oncogene, 35(45), 5819–5825. https://doi.org/10.1038/onc.2016.85

Carlier, J., Guitton, J., Romeuf, L., Bévalot, F., Boyer, B., Fanton, L., & Gaillard, Y. (2015). Screening approach by ultra-high performance liquid chromatography-tandem mass spectrometry for the blood quantification of thirty-four toxic principles of plant

origin. Application to forensic toxicology. Journal of Chromatography. B, Analytical Technologies in the Biomedical and Life Sciences, 975, 65–76. https://doi.org/10.1016/j.jchromb.2014.10.028

Carrasco-García, E., Saceda, M., & Martínez-Lacaci, I. (2014). Role of receptor tyrosine kinases and their ligands in glioblastoma. Cells, 3(2), 199–235. https://doi.org/10.3390/cells3020199

Cenciarini, M., Valentino, M., Belia, S., Sforna, L., Rosa, P., Ronchetti, S., D'Adamo, M. C., & Pessia, M. (2019). Dexamethasone in glioblastoma multiforme therapy: mechanisms and controversies. Frontiers in Molecular Neuroscience, 12, 65. https://doi.org/10.3389/fnmol.2019.00065

Chaicharoenaudomrung, N., Jaroonwitchawan, T., & Noisa, P. (2018). Cordycepin induces apoptotic cell death of human brain cancer through the modulation of autophagy. Toxicology in Vitro, 46, 113–121. https://doi.org/10.1016/j.tiv.2017.10.002

Chang, K.-F., Chang, J. T., Huang, X.-F., Huang, Y.-C., Li, C.-Y., Weng, J.-C., Hsiao, C.-Y., Hsu, H.-J., & Tsai, N.-M. (2021). Cedrus atlantica Extract Suppress Glioblastoma Growth through Promotion of Genotoxicity and Apoptosis: In Vitro and In Vivo Studies. International Journal of Medical Sciences, 18(11), 2417–2430. https://doi.org/10.7150/ijms.54468

Chang, K.-F., Huang, X.-F., Chang, J. T., Huang, Y.-C., Lo, W.-S., Hsiao, C.-Y., & Tsai, N.-M. (2020). Cedrol, a sesquiterpene alcohol, enhances the anticancer efficacy of temozolomide in attenuating drug resistance via regulation of the DNA damage response and MGMT expression. Journal of Natural Products, 83(10), 3021–3029. https://doi.org/10.1021/acs.jnatprod.0c00580

Chang, K.-H., Yan, M.-D., Yao, C.-J., Lin, P.-C., & Lai, G.-M. (2013). Honokiol-induced apoptosis and autophagy in glioblastoma multiforme cells. Oncology Letters, 6(5), 1435–1438. https://doi.org/10.3892/ol.2013.1548

Chaube, S., & Swinyard, C. A. (1976). Teratological and toxicological studies of alkaloidal and phenolic compounds from Solanum Tuberosum L. Toxicology and Applied Pharmacology, 36(2), 227–237. https://doi.org/10.1016/0041-008X(76)90002-8

Chen, C.-J., Shang, H.-S., Huang, Y.-L., Tien, N., Chen, Y.-L., Hsu, S.-Y., Wu, R. S.-C., Tang, C.-L., Lien, J.-C., Lee, M.-H., Lu, H.-F., & Hsia, T.-C. (2022). Bisdemethoxycurcumin suppresses human brain glioblastoma multiforme GBM 8401 cell migration and invasion via affecting NF-κB and MMP-2 and MMP-9 signaling pathway in vitro. Environmental Toxicology. https://doi.org/10.1002/tox.23604

Chen, Y., Niu, J., Li, L., Li, Z., Jiang, J., Zhu, M., Dong, T., Zhang, J., Shi, C., Xu, P., Lu, Y., Jiang, Y., Liu, P., & Chen, W. (2020). Polydatin executes anticancer effects against glioblastoma multiforme by inhibiting the EGFR-AKT/ERK1/2/STAT3-SOX2/Snail signaling pathway. Life Sciences, 258, 118158. https://doi.org/10.1016/j.lfs.2020.118158

Cho, C.-L., Lee, Y.-Z., Tseng, C.-N., Cho, J., Cheng, Y.-B., Wang, K.-W., Chen, H.-J., Chiou, S.-J., Chou, C.-H., & Hong, Y.-R. (2017). Hexane fraction of Pluchea indica root extract inhibits proliferation and induces autophagy in human glioblastoma cells. Biomedical Reports, 7(5), 416–422. https://doi.org/10.3892/br.2017.979

Choukairi, Z., Hazzaz, T., José, M. F., & Fechtali, T. (2020). The cytotoxic activity of Salvia officinalis L. and Rosmarinus officinalis L. Leaves extracts on human glioblastoma cell line and their antioxidant effect. Journal of Complementary & Integrative Medicine. https://doi.org/10.1515/jcim-2018-0189

Chung, H.-H., Hsieh, M.-J., Hsieh, Y.-S., Chen, P.-N., Ko, C.-P., Yu, N.-Y., Lin, C.-W., & Yang, S.-F. (2021). The Inhibitory Effects of Terminalia catappa L. Extract on the Migration and Invasion of Human Glioblastoma Multiforme Cells. Pharmaceuticals (Basel, Switzerland), 14(11). https://doi.org/10.3390/ph14111183

Cimmino, A., Mathieu, V., Evidente, M., Ferderin, M., Moreno Y Banuls, L., Masi, M., De Carvalho, A., Kiss, R., & Evidente, A. (2016). Glanduliferins A and B, two new glucosylated steroids from Impatiens glandulifera, with in vitro growth inhibitory activity in human cancer cells. Fitoterapia, 109, 138–145. https://doi.org/10.1016/j.fitote.2015.12.016

Cloughesy, T. F., Cavenee, W. K., & Mischel, P. S. (2014). Glioblastoma: from molecular pathology to targeted treatment. Annual Review of Pathology, 9(1), 1–25. https://doi.org/10.1146/annurev-pathol-011110-130324

Coelho, B. P., Fernandes, C. F. de L., Boccacino, J. M., Souza, M. C. da S., Melo-Escobar, M. I., Alves, R. N., Prado, M. B., Iglesia, R. P., Cangiano, G., Mazzaro, G. L. R., & Lopes, M. H. (2020). Multifaceted WNT Signaling at the Crossroads Between Epithelial-Mesenchymal Transition and Autophagy in Glioblastoma. Frontiers in Oncology, 10, 597743. https://doi.org/10.3389/fonc.2020.597743

Coelho, P. L. C., de Freitas, S. R. V.-B., Pitanga, B. P. S., da Silva, V. D. A., Oliveira, M. N., Grangeiro, M. S., Souza, C. dos S., El-Bachá, R. dos S., de Fátima Dias Costa, M., Barbosa, P. R., de Oliveira Nascimento, I. L., & Costa, S. L. (2016). Flavonoids from the Brazilian plant Croton betulaster inhibit the growth of human glioblastoma cells and induce apoptosis. Revista Brasileira de Farmacognosia, 26(1), 34–43. https://doi.org/10.1016/j.bjp.2015.05.013

Colapietro, A., Mancini, A., Vitale, F., Martellucci, S., Angelucci, A., Llorens, S., Mattei, V., Gravina, G. L., Alonso, G. L., & Festuccia, C. (2020). Crocetin Extracted from Saffron Shows Antitumor Effects in Models of Human Glioblastoma. International Journal of Molecular Sciences, 21(2). https://doi.org/10.3390/ijms21020423

Colapietro, A., Yang, P., Rossetti, A., Mancini, A., Vitale, F., Martellucci, S., Conway, T. L., Chakraborty, S., Marampon, F., Mattei, V., Gravina, G. L., Biordi, A. L., Wei, D., Newman, R. A., & Festuccia, C. (2020). The Botanical Drug PBI-05204, a Supercritical CO2 Extract of Nerium Oleander, Inhibits Growth of Human Glioblastoma, Reduces Akt/mTOR Activities, and Modulates GSC Cell-Renewal Properties. Frontiers in Pharmacology, 11, 552428. https://doi.org/10.3389/fphar.2020.552428

Colella, B., Faienza, F., & Di Bartolomeo, S. (2019). EMT regulation by autophagy: A new perspective in glioblastoma biology. Cancers, 11(3). https://doi.org/10.3390/cancers11030312

Cornell University Library. (2022, June 29). A Guide to Evidence Synthesis: 9. Risk of Bias Assessment . Cornell University Library. https://guides.library.cornell.edu/evidence-synthesis/bias

Cote, D. J., & Ostrom, Q. T. (2021). Epidemiology and etiology of glioblastoma. In J. J. Otero & A. P. Becker (Eds.), Precision molecular pathology of glioblastoma (pp. 3–19). Springer International Publishing. https://doi.org/10.1007/978-3-030-69170-7_1

Cramer, S. W., & Chen, C. C. (2019). Photodynamic therapy for the treatment of glioblastoma. Frontiers in Surgery, 6, 81. https://doi.org/10.3389/fsurg.2019.00081

Crawford, L., & Myhr, B. (1995). A preliminary assessment of the toxic and mutagenic potential of steroidal alkaloids in transgenic mice. Food and Chemical Toxicology, 33(3), 191–194. https://doi.org/10.1016/0278-6915(94)00135-B

Crespo, I., Vital, A. L., Gonzalez-Tablas, M., Patino, M. del C., Otero, A., Lopes, M. C., de Oliveira, C., Domingues, P., Orfao, A., & Tabernero, M. D. (2015). Molecular and genomic alterations in glioblastoma multiforme. The American Journal of Pathology, 185(7), 1820–1833. https://doi.org/10.1016/j.ajpath.2015.02.023

Czarnik-Kwaśniak, J., Kwaśniak, K., Kwasek, P., Świerzowska, E., Strojewska, A., & Tabarkiewicz, J. (2019). The Influence of Lycopene, [6]-Gingerol, and Silymarin on the Apoptosis on U-118MG Glioblastoma Cells In Vitro Model. Nutrients, 12(1). https://doi.org/10.3390/nu12010096

Dai, Zhang'an, Cai, L., Chen, Y., Wang, S., Zhang, Q., Wang, C., Tu, M., Zhu, Z., Li, Q., & Lu, X. (2021). Brusatol Inhibits Proliferation and Invasion of Glioblastoma by Down-Regulating the Expression of ECM1. Frontiers in Pharmacology, 12, 775680. https://doi.org/10.3389/fphar.2021.775680

Dai, Zhibo, Wang, L., Wang, X., Zhao, B., Zhao, W., Bhardwaj, S. S., Ye, J., Yin, Z., Zhang, J., & Zhao, S. (2018). Oxymatrine induces cell cycle arrest and apoptosis and suppresses the invasion of human glioblastoma cells through the EGFR/PI3K/Akt/mTOR signaling pathway and STAT3. Oncology Reports, 40(2), 867–876. https://doi.org/10.3892/or.2018.6512

Dalvi, R. R. (1985). Comparative assessment of the effect of solanine administered orally and intraperitoneally on hepatic dysfunction in male rats. Nippon Juigaku Zasshi. The Japanese Journal of Veterinary Science, 47(4), 657–659. https://doi.org/10.1292/jvms1939.47.657

de Lima, C. A., Cubero, M. C. Z., Franco, Y. E. M., Rodrigues, C. D. P., do Nascimento, J. R., Vendramini-Costa, D. B., Sciani, J. M., da Rocha, C. Q., & Longato, G. B. (2022). Antiproliferative Activity of Two Unusual Dimeric Flavonoids, Brachydin E and

Brachydin F, Isolated from Fridericia platyphylla (Cham.) L.G.Lohmann: In Vitro and Molecular Docking Evaluation. BioMed Research International, 2022, 3319203. https://doi.org/10.1155/2022/3319203

de Mendonça, I. C. G., Porto, I. C. C. de M., do Nascimento, T. G., de Souza, N. S., Oliveira, J. M. dos S., Arruda, R. E. dos S., Mousinho, K. C., dos Santos, A. F., Basílio-Júnior, I. D., Parolia, A., & Barreto, F. S. (2015). Brazilian red propolis: phytochemical screening, antioxidant activity and effect against cancer cells. BMC Complementary and Alternative Medicine, 15, 357. https://doi.org/10.1186/s12906-015-0888-9

Dept. of Molecular Biology, Iraqi Center for Cancer and Medical Genetics Research, Baghdad, Iraq, Abdulghany, Z., Mahmood, N., Dept. of Molecular Biology, Iraqi Center for Cancer and Medical Genetics Research, Baghdad, Iraq, Tawfeeq, A., Dept. of Molecular Biology, Iraqi Center for Cancer and Medical Genetics Research, Baghdad, Iraq, Yassen, N., & Dept. of Molecular Biology, Iraqi Center for Cancer and Medical Genetics Research, Baghdad, Iraq. (2018). Cyperus rotundus tubers extract inhibits stem cell markers expression in cervical and human glioblastoma cancer cell lines. Iraqi Journal of Medical Sciences, 16(2), 159–165. https://doi.org/10.22578/IJMS.16.2.7

Di Cesare Mannelli, L., Piccolo, M., Maione, F., Ferraro, M. G., Irace, C., De Feo, V., Ghelardini, C., & Mascolo, N. (2018). Tanshinones from Salvia miltiorrhiza Bunge revert chemotherapy-induced neuropathic pain and reduce glioblastoma cells malignancy. Biomedicine & Pharmacotherapy (Biomedecine & Pharmacotherapie), 105, 1042–1049. https://doi.org/10.1016/j.biopha.2018.06.047

Distl, M., Sibum, M., & Wink, M. (2009). Combination of On-Line Solid-Phase Extraction with LC-MS for the Determination of Potentially Hazardous Glycoalkaloids in

Potato Products. Potato Research, 52(1), 39–56. https://doi.org/10.1007/s11540-008-9106-1

do Carmo, A., Balça-Silva, J., Matias, D., & Lopes, M. C. (2013). PKC signaling in glioblastoma. Cancer Biology & Therapy, 14(4), 287–294. https://doi.org/10.4161/cbt.23615

Domènech, M., Hernández, A., Plaja, A., Martínez-Balibrea, E., & Balañà, C. (2021). Hypoxia: the cornerstone of glioblastoma. International Journal of Molecular Sciences, 22(22). https://doi.org/10.3390/ijms222212608

Dörschmann, P., Schmitt, C., Bittkau, K. S., Neupane, S., Synowitz, M., Roider, J., Alban, S., Held-Feindt, J., & Klettner, A. (2020). Evaluation of a Brown Seaweed Extract from Dictyosiphon foeniculaceus as a Potential Therapeutic Agent for the Treatment of Glioblastoma and Uveal Melanoma. Marine Drugs, 18(12). https://doi.org/10.3390/md18120625

Duzgun, Z., Eroglu, Z., & Biray Avci, C. (2016). Role of mTOR in glioblastoma. Gene, 575(2 Pt 1), 187–190. https://doi.org/10.1016/j.gene.2015.08.060

Dymova, M. A., Kuligina, E. V., & Richter, V. A. (2021). Molecular mechanisms of drug resistance in glioblastoma. International Journal of Molecular Sciences, 22(12). https://doi.org/10.3390/ijms22126385

Efremov, L., Abera, S. F., Bedir, A., Vordermark, D., & Medenwald, D. (2021). Patterns of glioblastoma treatment and survival over a 16-years period: pooled data from the German Cancer Registries. Journal of Cancer Research and Clinical Oncology, 147(11), 3381–3390. https://doi.org/10.1007/s00432-021-03596-5

El Hage, S., Kawtharani, M., Nabha, S., El Masri, J., & Saad, M. (2021). Distribution of Primary Brain Tumor Subtypes in Lebanon: A Multicenter Eleven-Year Study of 695 Patients. Cureus, 13(9), e17918. https://doi.org/10.7759/cureus.17918

El Khayari, A., Bouchmaa, N., Taib, B., Wei, Z., Zeng, A., & El Fatimy, R. (2022). Metabolic rewiring in glioblastoma cancer: EGFR, IDH and beyond. Frontiers in Oncology, 12, 901951. https://doi.org/10.3389/fonc.2022.901951

Elkady, A. I., Hussein, R. A. E. H., & Abu-Zinadah, O. A. (2014). Effects of crude extracts from medicinal herbs Rhazya stricta and Zingiber officinale on growth and proliferation of human brain cancer cell line in vitro. BioMed Research International, 2014, 260210. https://doi.org/10.1155/2014/260210

Emsen, B., Aslan, A., Togar, B., & Turkez, H. (2016). In vitro antitumor activities of the lichen compounds olivetoric, physodic and psoromic acid in rat neuron and glioblastoma cells. Pharmaceutical Biology, 54(9), 1748–1762. https://doi.org/10.3109/13880209.2015.1126620

Engberg, H., Steding-Jessen, M., Øster, I., Jensen, J. W., Hansen, S., Laursen, R. J., Lukacova, S., & Møller, H. (2022). Regional and socio-economic variation in survival after glioblastoma in Denmark, 2013-2018. Danish Medical Journal, 69(3).

Erdogan, K., & Eroglu, O. (2019). Investigation of the Effects of Momordica charantia Extract on Cell Survival and Migration in U87G Glioblastoma Cell Line. The 3rd International Conference on Natural Products for Cancer Prevention and Therapy, 18. https://doi.org/10.3390/proceedings2019040018

Eskilsson, E., Røsland, G. V., Solecki, G., Wang, Q., Harter, P. N., Graziani, G., Verhaak, R. G. W., Winkler, F., Bjerkvig, R., & Miletic, H. (2018). EGFR heterogeneity and

implications for therapeutic intervention in glioblastoma. Neuro-Oncology, 20(6), 743–752. https://doi.org/10.1093/neuonc/nox191

Franco, Y. E. M., de Lima, C. A., Rosa, M. N., Silva, V. A. O., Reis, R. M., Priolli, D. G., Carvalho, P. O., do Nascimento, J. R., da Rocha, C. Q., & Longato, G. B. (2021). Investigation of U-251 cell death triggered by flavonoid luteolin: towards a better understanding on its anticancer property against glioblastomas. Natural Product Research, 35(22), 4807–4813. https://doi.org/10.1080/14786419.2020.1727470

Friedman, M, Henika, P. R., & Mackey, B. E. (1996). Feeding of potato, tomato and eggplant alkaloids affects food consumption and body and liver weights in mice. The Journal of Nutrition, 126(4), 989–999. https://doi.org/10.1093/jn/126.4.989

Friedman, M, Rayburn, J. R., & Bantle, J. A. (1991). Developmental toxicology of potato alkaloids in the frog embryo teratogenesis assay--Xenopus (FETAX). Food and Chemical Toxicology, 29(8), 537–547. https://doi.org/10.1016/0278-6915(91)90046-A

Friedman, Mendel, Henika, P. R., & Mackey, B. E. (2003). Effect of feeding solanidine, solasodine and tomatidine to non-pregnant and pregnant mice. Food and Chemical Toxicology, 41(1), 61–71. https://doi.org/10.1016/S0278-6915(02)00205-3

Friedman, Mendel, Lee, K.-R., Kim, H.-J., Lee, I.-S., & Kozukue, N. (2005). Anticarcinogenic effects of glycoalkaloids from potatoes against human cervical, liver, lymphoma, and stomach cancer cells. Journal of Agricultural and Food Chemistry, 53(15), 6162–6169. https://doi.org/10.1021/jf050620p

Gade, I. S., Chadeneau, C., Richard, T. S., Atchade, A. D. T., Talla, E., Seite, P., Vannier, B., Guillard, J., Laurent, S., Henoumont, C., Nwabo, A. H. K., & Muller, J.-M. (2022). A new flavonoid glycoside from Tapinanthus sp. (Loranthaceae) and evaluation

of anticancer activity of extract and some isolated compounds. Natural Product Research, 36(16), 4085–4093. https://doi.org/10.1080/14786419.2021.1963243

Gaffield, W., & Keeler, R. F. (1996). Induction of terata in hamsters by solanidane alkaloids derived from Solanum tuberosum. Chemical Research in Toxicology, 9(2), 426–433. https://doi.org/10.1021/tx950091r

Gagliardi, F., Narayanan, A., Reni, M., Franzin, A., Mazza, E., Boari, N., Bailo, M., Zordan, P., & Mortini, P. (2014). The role of CXCR4 in highly malignant human gliomas biology: current knowledge and future directions. Glia, 62(7), 1015–1023. https://doi.org/10.1002/glia.22669

Gao, J., Ying, Y., Wang, J., & Cui, Y. (2020). Solanine inhibits immune escape mediated by hepatoma treg cells via the tgfβ/smad signaling pathway. BioMed Research International, 2020, 9749631. https://doi.org/10.1155/2020/9749631

Gao, S.-Y., Wang, Q.-J., & Ji, Y.-B. (2006). Effect of solanine on the membrane potential of mitochondria in HepG2 cells and [Ca2+]i in the cells. World J Gastroenterol, 12(21), 3359–3367.

Garrido-Armas, M., Corona, J. C., Escobar, M. L., Torres, L., Ordóñez-Romero, F., Hernández-Hernández, A., & Arenas-Huertero, F. (2018). Paraptosis in human glioblastoma cell line induced by curcumin. Toxicology in Vitro, 51, 63–73. https://doi.org/10.1016/j.tiv.2018.04.014

Genovese, C., Cambria, M. T., D'angeli, F., Addamo, A. P., Malfa, G. A., Siracusa, L., Pulvirenti, L., Anfuso, C. D., Lupo, G., & Salmeri, M. (2020). The double effect of walnut septum extract (Juglans regia L.) counteracts A172 glioblastoma cell survival and bacterial growth. International Journal of Oncology, 57(5), 1129–1144. https://doi.org/10.3892/ijo.2020.5130

Gentile, M. T., Ciniglia, C., Reccia, M. G., Volpicelli, F., Gatti, M., Thellung, S., Florio, T., Melone, M. A. B., & Colucci-D'Amato, L. (2015). Ruta graveolens L. induces death of glioblastoma cells and neural progenitors, but not of neurons, via ERK 1/2 and AKT activation. Plos One, 10(3), e0118864. https://doi.org/10.1371/journal.pone.0118864

Ghaffarian Zirak, R., Tajik, H., Asadi, J., Hashemian, P., & Javid, H. (2022). The role of micro rnas in regulating PI3K/AKT signaling pathways in glioblastoma. Iranian Journal of Pathology, 17(2), 122–136. https://doi.org/10.30699/IJP.2022.539029.2726

Ginzberg, I., Thippeswamy, M., Fogelman, E., Demirel, U., Mweetwa, A. M., Tokuhisa, J., & Veilleux, R. E. (2012). Induction of potato steroidal glycoalkaloid biosynthetic pathway by overexpression of cDNA encoding primary metabolism HMG-CoA reductase and squalene synthase. Planta, 235(6), 1341–1353. https://doi.org/10.1007/s00425-011-1578-6

Gouhar, S. A., Abo-Elfadl, M. T., Gamal-Eldeen, A. M., & El-Daly, S. M. (2022). Involvement of miRNAs in response to oxidative stress induced by the steroidal glycoalkaloid α-solanine in hepatocellular carcinoma cells. Environmental Toxicology, 37(2), 212–223. https://doi.org/10.1002/tox.23390

Gray, G. K., McFarland, B. C., Nozell, S. E., & Benveniste, E. N. (2014). NF-κB and STAT3 in glioblastoma: therapeutic targets coming of age. Expert Review of Neurotherapeutics, 14(11), 1293–1306. https://doi.org/10.1586/14737175.2014.964211

Grech, N., Dalli, T., Mizzi, S., Meilak, L., Calleja, N., & Zrinzo, A. (2020). Rising Incidence of Glioblastoma Multiforme in a Well-Defined Population. Cureus, 12(5), e8195. https://doi.org/10.7759/cureus.8195

Grochans, S., Cybulska, A. M., Simińska, D., Korbecki, J., Kojder, K., Chlubek, D., & Baranowska-Bosiacka, I. (2022). Epidemiology of Glioblastoma Multiforme-Literature Review. Cancers, 14(10). https://doi.org/10.3390/cancers14102412

Gu, H., Feng, J., Wang, H., Qian, Y., Yang, L., Chen, J., Jin, F., Shi, Y., Lu, S., & Liu, Y. (2016). Celastrus orbiculatus extract inhibits the migration and invasion of human glioblastoma cells in vitro. BMC Complementary and Alternative Medicine, 16(1), 387. https://doi.org/10.1186/s12906-016-1232-8

Guelfi, S., Duffau, H., Bauchet, L., Rothhut, B., & Hugnot, J.-P. (2016). Vascular Transdifferentiation in the CNS: A Focus on Neural and Glioblastoma Stem-Like Cells. Stem Cells International, 2016, 2759403. https://doi.org/10.1155/2016/2759403

Guerram, M., Jiang, Z.-Z., Sun, L., Zhu, X., & Zhang, L.-Y. (2015). Antineoplastic effects of deoxypodophyllotoxin, a potent cytotoxic agent of plant origin, on glioblastoma U-87 MG and SF126 cells. Pharmacological Reports, 67(2), 245–252. https://doi.org/10.1016/j.pharep.2014.10.003

Guo, Xiaopeng, Yang, X., Wu, J., Yang, H., Li, Y., Li, J., Liu, Q., Wu, C., Xing, H., Liu, P., Wang, Y., Hu, C., & Ma, W. (2022). Tumor-Treating Fields in Glioblastomas: Past, Present, and Future. Cancers, 14(15). https://doi.org/10.3390/cancers14153669

Guo, Xuyang, Zhou, S., Yang, Z., Li, Z.-A., Hu, W., Dai, L., Liang, W., & Wang, X. (2022). Cholesterol metabolism and its implication in glioblastoma therapy. Journal of Cancer, 13(6), 1745–1757. https://doi.org/10.7150/jca.63609

Gupta, A., & Dwivedi, T. (2017). A simplified overview of world health organization classification update of central nervous system tumors 2016. Journal of Neurosciences in Rural Practice, 8(4), 629–641. https://doi.org/10.4103/jnrp.jnrp_168_17

Ham, S. W., Kim, J.-K., Jeon, H.-Y., Kim, E.-J., Jin, X., Eun, K., Park, C. G., Lee, S. Y., Seo, S., Kim, J. Y., Choi, S.-H., Hong, N., Lee, Y. Y., & Kim, H. (2019). Korean Red ginseng extract inhibits glioblastoma propagation by blocking the Wnt signaling pathway. Journal of Ethnopharmacology, 236, 393–400. https://doi.org/10.1016/j.jep.2019.03.031

Hasanain, M., Bhattacharjee, A., Pandey, P., Ashraf, R., Singh, N., Sharma, S., Vishwakarma, A. L., Datta, D., Mitra, K., & Sarkar, J. (2015). α-Solanine induces ROS-mediated autophagy through activation of endoplasmic reticulum stress and inhibition of Akt/mTOR pathway. Cell Death & Disease, 6, e1860. https://doi.org/10.1038/cddis.2015.219

Hasbum, A., Quintanilla, J., Jr, J. A. A., Ding, M.-H., Levy, A., & Chew, S. A. (2021). Strategies to better treat glioblastoma: antiangiogenic agents and endothelial cell targeting agents. Future Medicinal Chemistry, 13(4), 393–418. https://doi.org/10.4155/fmc-2020-0289

Hassan, S. H., Gul, S., Zahra, H. S., Maryam, A., Shakir, H. A., Khan, M., & Irfan, M. (2021). Alpha solanine: A novel natural bioactive molecule with anticancer effects in multiple human malignancies. *Nutrition and Cancer*, *73*(9), 1541-1552.

Hatziagapiou, K., Nikola, O., Marka, S., Koniari, E., Kakouri, E., Zografaki, M.-E., Mavrikou, S. S., Kanakis, C., Flemetakis, E., Chrousos, G. P., Kintzios, S., Lambrou, G. I., Kanaka-Gantenbein, C., & Tarantilis, P. A. (2022). An in vitro study of saffron carotenoids: the effect of crocin extracts and dimethylcrocetin on cancer cell lines. Antioxidants (Basel, Switzerland), 11(6). https://doi.org/10.3390/antiox11061074.

Hellenäs, K. E., Nyman, A., Slanina, P., Lööf, L., & Gabrielsson, J. (1992). Determination of potato glycoalkaloids and their aglycone in blood serum by high-

performance liquid chromatography. Journal of Chromatography B: Biomedical Sciences and Applications, 573(1), 69–78. https://doi.org/10.1016/0378-4347(92)80476-7.

Hellenás, K.-E., Branzell, C., Collaborators:, Poutanen, H., Suortti, T., Kaario, R., Gjerstad, K. O., Brekke, T., Jensen, A. M., Larsen, K., Knuthsen, P., Halén, B., Olsson, K., Ingólfsdóttir;, I. K., & Pittet, A. (1997). Liquid Chromatographic Determination of the Glycoalkaloids α-Solanine and α-Chaconine in Potato Tubers: NMKL Interlaboratory Study. Journal of AOAC International, 80(3), 549–554. https://doi.org/10.1093/jaoac/80.3.549

Hilliard, T. S., Miklossy, G., Chock, C., Yue, P., Williams, P., & Turkson, J. (2017). 15α-methoxypuupehenol Induces Antitumor Effects In Vitro and In Vivo against Human Glioblastoma and Breast Cancer Models. Molecular Cancer Therapeutics, 16(4), 601–613. https://doi.org/10.1158/1535-7163.MCT-16-0291

Hossain, M. B., Rawson, A., Aguiló-Aguayo, I., Brunton, N. P., & Rai, D. K. (2015). Recovery of steroidal alkaloids from potato peels using pressurized liquid extraction. Molecules (Basel, Switzerland), 20(5), 8560–8573. https://doi.org/10.3390/molecules20058560

Hossain, M. B., Tiwari, B. K., Gangopadhyay, N., O'Donnell, C. P., Brunton, N. P., & Rai, D. K. (2014). Ultrasonic extraction of steroidal alkaloids from potato peel waste. Ultrasonics Sonochemistry, 21(4), 1470–1476. https://doi.org/10.1016/j.ultsonch.2014.01.023

Houben, R. J., & Brunt, K. (1994). Determination of glycoalkaloids in potato tubers by reversed-phase high-performance liquid chromatography. Journal of Chromatography A, 661(1–2), 169–174. https://doi.org/10.1016/0021-9673(94)85187-5

Hsu, S.-Y., Lee, S.-C., Liu, H.-C., Peng, S.-F., Chueh, F.-S., Lu, T.-J., Lee, H.-T., & Chou, Y.-C. (2022). Phenethyl Isothiocyanate Suppresses the Proinflammatory Cytokines in Human Glioblastoma Cells through the PI3K/Akt/NF-κB Signaling Pathway In Vitro. Oxidative Medicine and Cellular Longevity, 2022, 2108289. https://doi.org/10.1155/2022/2108289

Huang, B., Li, X., Li, Y., Zhang, J., Zong, Z., & Zhang, H. (2020). Current immunotherapies for glioblastoma multiforme. Frontiers in Immunology, 11, 603911. https://doi.org/10.3389/fimmu.2020.603911

Hwang, J. Y., Park, J. H., Kim, M. J., Kim, W. J., Ha, K.-T., Choi, B. T., Lee, S.-Y., & Shin, H. K. (2019). Isolinderalactone regulates the BCL-2/caspase-3/PARP pathway and suppresses tumor growth in a human glioblastoma multiforme xenograft mouse model. Cancer Letters, 443, 25–33. https://doi.org/10.1016/j.canlet.2018.11.027

Ibrahim, S. R. M., Mohamed, G. A., Shaala, L. A., Banuls, L. M. Y., Kiss, R., & Youssef, D. T. A. (2015). Calotroposides H-N, new cytotoxic oxypregnane oligoglycosides from the root bark of Calotropis procera. Steroids, 96, 63–72. https://doi.org/10.1016/j.steroids.2015.01.012

Iglesia, R. P., Fernandes, C. F. de L., Coelho, B. P., Prado, M. B., Melo Escobar, M. I., Almeida, G. H. D. R., & Lopes, M. H. (2019). Heat shock proteins in glioblastoma biology: where do we stand? International Journal of Molecular Sciences, 20(22). https://doi.org/10.3390/ijms20225794

Ismali, S. A., Abdullah, V. S., & Hussein Kamel, F. (2019). Extraction of α-solanine and α-chaconine from green potato tubers and evaluations of its antimicrobial activity . Plant Archives, 19(2), 4009–4014.

Izumi, C., Laure, H. J., Barbosa, N. G., Thomé, C. H., Ferreira, G. A., Sousa, J. P. B., Lopes, N. P., & Rosa, J. C. (2020). Sequesterpene Lactones Isolated from a Brazilian Cerrado Plant (Eremanthus spp.) as Anti-Proliferative Compounds, Characterized by Functional and Proteomic Analysis, are Candidates for New Therapeutics in Glioblastoma. International Journal of Molecular Sciences, 21(13). https://doi.org/10.3390/ijms21134713

Jalili-Nik, M., Afshari, A. R., Sabri, H., Bibak, B., Mollazadeh, H., & Sahebkar, A. (2021). Zerumbone, a ginger sesquiterpene, inhibits migration, invasion, and metastatic behavior of human malignant glioblastoma multiforme in vitro. BioFactors (Oxford, England), 47(5), 729–739. https://doi.org/10.1002/biof.1756

Jandrey, E. H. F., Bezerra, M., Inoue, L. T., Furnari, F. B., Camargo, A. A., & Costa, É. T. (2021). A key pathway to cancer resilience: the role of autophagy in glioblastomas. Frontiers in Oncology, 11, 652133. https://doi.org/10.3389/fonc.2021.652133

Jelínek, R., Kyzlink, V., & Blatiný, C. (1976). An evaluation of the embryotoxic effects of blighted potatoes on chicken embryos. Teratology, 14(3), 335–342. https://doi.org/10.1002/tera.1420140309

Ji, Y., & Gao, S. (2012). Antihepatocarcinoma Effect of Solanine and Its Mechanisms. Chinese Herbal Medicines, 4(2), 126–135.

Jiao, Y., Li, H., Liu, Y., Guo, A., Xu, X., Qu, X., Wang, S., Zhao, J., Li, Y., & Cao, Y. (2015). Resveratrol Inhibits the Invasion of Glioblastoma-Initiating Cells via Down-Regulation of the PI3K/Akt/NF-κB Signaling Pathway. Nutrients, 7(6), 4383–4402. https://doi.org/10.3390/nu7064383

Jimenez-Pascual, A., & Siebzehnrubl, F. A. (2019). Fibroblast growth factor receptor functions in glioblastoma. Cells, 8(7). https://doi.org/10.3390/cells8070715

Joshi, P. R., Paudel, M. R., Chand, M. B., Pradhan, S., Pant, K. K., Joshi, G. P., Bohara, M., Wagner, S. H., Pant, B., & Pant, B. (2020). Cytotoxic effect of selected wild orchids on two different human cancer cell lines. Heliyon, 6(5), e03991. https://doi.org/10.1016/j.heliyon.2020.e03991

Kamarudin, N. A., Nik Salleh, N. N. H., & Tan, S. C. (2021). Gallotannin-Enriched Fraction from Quercus infectoria Galls as an Antioxidant and Inhibitory Agent against Human Glioblastoma Multiforme. Plants, 10(12). https://doi.org/10.3390/plants10122581

Kang, C.-W., Park, M.-S., Kim, N.-H., Lee, J.-H., Oh, C.-W., Kim, H.-R., & Kim, G.-D. (2015). Hexane extract from Sargassum serratifolium inhibits the cell proliferation and metastatic ability of human glioblastoma U87MG cells. Oncology Reports, 34(5), 2602–2608. https://doi.org/10.3892/or.2015.4222

Kang, H., Song, S. W., Ha, J., Won, Y.-J., Park, C.-K., Yoo, H., & Jung, K.-W. (2021). A Nationwide, Population-Based Epidemiology Study of Primary Central Nervous System Tumors in Korea, 2007-2016: A Comparison with United States Data. Cancer Research and Treatment : Official Journal of Korean Cancer Association, 53(2), 355–366. https://doi.org/10.4143/crt.2020.847

Kapoor, H., Yadav, N., Chopra, M., Mahapatra, S. C., & Agrawal, V. (2017). Strong Anti-tumorous Potential of Nardostachys jatamansi Rhizome Extract on Glioblastoma and In Silico Analysis of its Molecular Drug Targets. Current Cancer Drug Targets, 17(1), 74–88. https://doi.org/10.2174/1570163813666161019143740

Karaboğa Arslan, A. K., & Yerer, M. B. (2018). α-Chaconine and α-Solanine Inhibit RL95-2 Endometrium Cancer Cell Proliferation by Reducing Expression of Akt (Ser473) and ERα (Ser167). Nutrients, 10(6). https://doi.org/10.3390/nu10060672

Karakas, N., Okur, M. E., Ozturk, I., Ayla, S., Karadag, A. E., & Polat, D. Ç. (2019). Antioxidant Activity of Blackthorn (Prunus spinosa L.) Fruit Extract and Cytotoxic Effects on Various Cancer Cell Lines. Medeniyet Medical Journal, 34(3), 297–304. https://doi.org/10.5222/MMJ.2019.87864

Karkare, S., Chhipa, R. R., Anderson, J., Liu, X., Henry, H., Gasilina, A., Nassar, N., Ghosh, J., Clark, J. P., Kumar, A., Pauletti, G. M., Ghosh, P. K., & Dasgupta, B. (2014). Direct inhibition of retinoblastoma phosphorylation by nimbolide causes cell-cycle arrest and suppresses glioblastoma growth. Clinical Cancer Research, 20(1), 199–212. https://doi.org/10.1158/1078-0432.CCR-13-0762

Karsy, M., Arslan, E., & Moy, F. (2012). Current progress on understanding micrornas in glioblastoma multiforme. Genes & Cancer, 3(1), 3–15. https://doi.org/10.1177/1947601912448068

Keshmiri-Neghab, H., Goliaei, B., & Nikoofar, A. (2014). Gossypol enhances radiation induced autophagy in glioblastoma multiforme. General Physiology and Biophysics, 33(4), 433–442. https://doi.org/10.4149/gpb_2014017

Khaksar, S., Kiarostami, K., & Alinaghi, S. (2022). The Effects of Methanol Extracts of Hyssopus officinalis on Model of Induced Glioblastoma Multiforme (GBM) in Rats. Journal of Molecular Neuroscience, 72(9), 2045–2066. https://doi.org/10.1007/s12031-022-02058-y

Khan, R. S., Senthi, M., Rao, P. C., Basha, A., Alvala, M., Tummuri, D., Masubuti, H., Fujimoto, Y., & Begum, A. S. (2015). Cytotoxic constituents of Abutilon indicum leaves against U87MG human glioblastoma cells. Natural Product Research, 29(11), 1069–1073. https://doi.org/10.1080/14786419.2014.976643

Kim, H. J., & Kim, D.-Y. (2020). Present and Future of Anti-Glioblastoma Therapies: A Deep Look into Molecular Dependencies/Features. Molecules (Basel, Switzerland), 25(20). https://doi.org/10.3390/molecules25204641

Kline, B. E., Von Elbe, H., Dahle, N. A., & Kupchan, S. M. (1961). Toxic effects of potato sprouts and of solanine fed to pregnant rats. Proceedings of the Society for Experimental Biology and Medicine. Society for Experimental Biology and Medicine, 107, 807–809. https://doi.org/10.3181/00379727-107-26762

Koc, K., Ozdemir, O., Ozdemir, A., Dogru, U., & Turkez, H. (2018). Antioxidant and anticancer activities of extract of Inula helenium (L.) in human U-87 MG glioblastoma cell line. Journal of Cancer Research and Therapeutics, 14(3), 658–661. https://doi.org/10.4103/0973-1482.187289

Komori, T. (2017). The 2016 WHO classification of tumours of the central nervous system: the major points of revision. Neurologia Medico-Chirurgica, 57(7), 301–311. https://doi.org/10.2176/nmc.ra.2017-0010

Kondamudi, N., Smith, J. K., & McDougal, O. M. (2017). Determination of glycoalkaloids in potatoes and potato products by microwave assisted extraction. American Journal of Potato Research, 94(2), 153–159. https://doi.org/10.1007/s12230-016-9558-9

Korpan, Y. I., Nazarenko, E. A., Skryshevskaya, I. V., Martelet, C., Jaffrezic-Renault, N., & El'skaya, A. V. (2004). Potato glycoalkaloids: true safety or false sense of security? Trends in Biotechnology, 22(3), 147–151. https://doi.org/10.1016/j.tibtech.2004.01.009

Kowalczyk, T., Sitarek, P., Skała, E., Toma, M., Wielanek, M., Pytel, D., Wieczfińska, J., Szemraj, J., & Śliwiński, T. (2019). Induction of apoptosis by in vitro and

in vivo plant extracts derived from Menyanthes trifoliata L. in human cancer cells. Cytotechnology, 71(1), 165–180. https://doi.org/10.1007/s10616-018-0274-9

Krisnamurti, G. C., Wulansari, S., & Tirto Sari, D. R. (2022). α-solanine and α-chaconine from Potato (Solanum tuberosum) for Endometrial Cancer Therapy: In silico Study . Proceeding International Conference on Religion, Science and Education, 1, 571–576.

Kumar, A., Fogelman, E., Weissberg, M., Tanami, Z., Veilleux, R. E., & Ginzberg, I. (2017). Lanosterol synthase-like is involved with differential accumulation of steroidal glycoalkaloids in potato. Planta, 246(6), 1189–1202. https://doi.org/10.1007/s00425-017-2763-z

Kumar, V., Radin, D., & Leonardi, D. (2017). Probing the oncolytic and chemosensitizing effects of dihydrotanshinone in an in vitro glioblastoma model. Anticancer Research, 37(11), 6025–6030. https://doi.org/10.21873/anticanres.12049

Kuo, Y.-C., Lee, C.-H., & Rajesh, R. (2017). Recent advances in the treatment of glioblastoma multiforme by inhibiting angiogenesis and using nanocarrier systems. Journal of the Taiwan Institute of Chemical Engineers, 77, 30–40. https://doi.org/10.1016/j.jtice.2017.04.034

Kwanthongdee, J., Sunrat, C., Munyoo, B., Tuchinda, P., Chabang, N., & Saengsawang, W. (2019). Phyllanthus taxodiifolius Beille suppresses microtubule dynamics and restricts glioblastoma aggressiveness. Biomedicine & Pharmacotherapy (Biomedecine & Pharmacotherapie), 112, 108645. https://doi.org/10.1016/j.biopha.2019.108645

Lam, S., Lin, Y., Zinn, P., Su, J., & Pan, I.-W. (2018). Patient and treatment factors associated with survival among pediatric glioblastoma patients: A Surveillance, Epidemiology, and End Results study. Journal of Clinical Neuroscience, 47, 285–293. https://doi.org/10.1016/j.jocn.2017.10.041

Lampronti, I., Simoni, D., Rondanin, R., Baruchello, R., Scapoli, C., Finotti, A., Borgatti, M., Tupini, C., & Gambari, R. (2020). Pro-apoptotic activity of novel synthetic isoxazole derivatives exhibiting inhibitory activity against tumor cell growth in vitro. Oncology Letters, 20(5), 151. https://doi.org/10.3892/ol.2020.12002

Langkilde, S., Mandimika, T., Schrøder, M., Meyer, O., Slob, W., Peijnenburg, A., & Poulsen, M. (2009). A 28-day repeat dose toxicity study of steroidal glycoalkaloids, alpha-solanine and alpha-chaconine in the Syrian Golden hamster. Food and Chemical Toxicology, 47(6), 1099–1108. https://doi.org/10.1016/j.fct.2009.01.045

Langkilde, S., Schrøder, M., Frank, T., Shepherd, L. V. T., Conner, S., Davies, H. V., Meyer, O., Danier, J., Rychlik, M., Belknap, W. R., McCue, K. F., Engel, K.-H., Stewart, D., Knudsen, I., & Poulsen, M. (2012). Compositional and toxicological analysis of a GM potato line with reduced α-solanine content--a 90-day feeding study in the Syrian Golden hamster. Regulatory Toxicology and Pharmacology, 64(1), 177–185. https://doi.org/10.1016/j.yrtph.2012.06.018

Langkilde, S., Schrøder, M., Stewart, D., Meyer, O., Conner, S., Davies, H., & Poulsen, M. (2008). Acute toxicity of high doses of the glycoalkaloids, alpha-solanine and alpha-chaconine, in the Syrian Golden hamster. Journal of Agricultural and Food Chemistry, 56(18), 8753–8760. https://doi.org/10.1021/jf8012794

Lasorella, A., & Iavarone, A. (2021). The making of the glioblastoma classification. British Journal of Cancer, 125(1), 4–6. https://doi.org/10.1038/s41416-021-01360-7

Lathia, J. D., Mack, S. C., Mulkearns-Hubert, E. E., Valentim, C. L. L., & Rich, J. N. (2015). Cancer stem cells in glioblastoma. Genes & Development, 29(12), 1203–1217. https://doi.org/10.1101/gad.261982.115

Laus, M. C., Klip, G., & Giuseppin, M. L. F. (2017). Improved Extraction and Sample Cleanup of Tri-glycoalkaloids α-Solanine and α-Chaconine in Non-denatured Potato Protein Isolates. Food Analytical Methods, 10(4), 845–853. https://doi.org/10.1007/s12161-016-0631-2

Le Rhun, E., Preusser, M., Roth, P., Reardon, D. A., van den Bent, M., Wen, P., Reifenberger, G., & Weller, M. (2019). Molecular targeted therapy of glioblastoma. Cancer Treatment Reviews, 80, 101896. https://doi.org/10.1016/j.ctrv.2019.101896

Lee, E., Yong, R. L., Paddison, P., & Zhu, J. (2018). Comparison of glioblastoma (GBM) molecular classification methods. Seminars in Cancer Biology, 53, 201–211. https://doi.org/10.1016/j.semcancer.2018.07.006

Lee, J.-K., Joo, K. M., Lee, J., Yoon, Y., & Nam, D.-H. (2014). Targeting the epithelial to mesenchymal transition in glioblastoma: the emerging role of MET signaling. OncoTargets and Therapy, 7, 1933–1944. https://doi.org/10.2147/OTT.S36582

Lee, K.-R., Kozukue, N., Han, J.-S., Park, J.-H., Chang, E.-Y., Baek, E.-J., Chang, J.-S., & Friedman, M. (2004). Glycoalkaloids and Metabolites Inhibit the Growth of Human Colon (HT29) and Liver (HepG2) Cancer Cells. Journal of Agricultural and Food Chemistry, 52, 2832–2839.

Lee, Y., Lee, J.-K., Ahn, S. H., Lee, J., & Nam, D.-H. (2016). WNT signaling in glioblastoma and therapeutic opportunities. Laboratory Investigation, 96(2), 137–150. https://doi.org/10.1038/labinvest.2015.140

Li, J., Tang, H., Zhang, Y., Tang, C., Li, B., Wang, Y., Gao, Z., Luo, P., Yin, A., Wang, X., Cheng, G., & Fei, Z. (2013). Saponin 1 induces apoptosis and suppresses NF-κB-mediated survival signaling in glioblastoma multiforme (GBM). Plos One, 8(11), e81258. https://doi.org/10.1371/journal.pone.0081258

Li, X., Wu, C., Chen, N., Gu, H., Yen, A., Cao, L., Wang, E., & Wang, L. (2016). PI3K/Akt/mTOR signaling pathway and targeted therapy for glioblastoma. Oncotarget, 7(22), 33440–33450. https://doi.org/10.18632/oncotarget.7961

Li, Y., Marcu, L. G., Hull, A., & Bezak, E. (2021). Radioimmunotherapy of glioblastoma multiforme - Current status and future prospects. Critical Reviews in Oncology/Hematology, 163, 103395. https://doi.org/10.1016/j.critrevonc.2021.103395

Li, Zhiwen, Zhou, B., Ding, Y., & Liu, X. (2009). Extraction and determination of a-solanine in eggplant fruits. Journal of Arts and Humanities, 11(01), 59–63. https://doi.org/10.37855/jah.2009.v11i01.12

Li, Zizhuo, Chen, Y., An, T., Liu, P., Zhu, J., Yang, H., Zhang, W., Dong, T., Jiang, J., Zhang, Y., Jiang, M., & Yang, X. (2019). Nuciferine inhibits the progression of glioblastoma by suppressing the SOX2-AKT/STAT3-Slug signaling pathway. Journal of Experimental & Clinical Cancer Research, 38(1), 139. https://doi.org/10.1186/s13046-019-1134-y

Liang, W.-Z., Jan, C.-R., & Hsu, S.-S. (2017). Cytotoxic effects of gastrodin extracted from the rhizome of Gastrodia elata Blume in glioblastoma cells, but not in normal astrocytes, via the induction of oxidative stress-associated apoptosis that involved cell cycle arrest and p53 activation. Food and Chemical Toxicology, 107(Pt A), 280–292. https://doi.org/10.1016/j.fct.2017.07.013

Lin, D., Wang, M., Chen, Y., Gong, J., Chen, L., Shi, X., Lan, F., Chen, Z., Xiong, T., Sun, H., & Wan, S. (2021). Trends in Intracranial Glioma Incidence and Mortality in the United States, 1975-2018. Frontiers in Oncology, 11, 748061. https://doi.org/10.3389/fonc.2021.748061

Lin, L.-T., Choong, C.-Y., & Tai, C.-J. (2020). Solanine attenuated hepatocarcinoma migration and invasion induced by acetylcholine. Integrative Cancer Therapies, 19, 1534735420909895. https://doi.org/10.1177/1534735420909895

Litak, J., Mazurek, M., Grochowski, C., Kamieniak, P., & Roliński, J. (2019). PD-L1/PD-1 Axis in Glioblastoma Multiforme. International Journal of Molecular Sciences, 20(21). https://doi.org/10.3390/ijms20215347

Liu, S.-Y., Chiang, M.-F., & Chen, Y.-J. (2015). Role of WW domain proteins WWOX in development, prognosis, and treatment response of glioma. Experimental Biology and Medicine, 240(3), 315–323. https://doi.org/10.1177/1535370214561588

Liu, W., Zhang, N., Li, B., Fan, S., Zhao, R., Li, L.-P., Wu, G.-H., & Zhao, Y. (2014). Determination of α-chaconine and α-solanine in commercial potato crisps by QuEChERS extraction and UPLC-MS/MS. Chemical Papers, 68(11). https://doi.org/10.2478/s11696-014-0617-8

Lu, M.-K., Shih, Y.-W., Chang Chein, T.-T., Fang, L.-H., Huang, H.-C., & Chen, P.-S. (2010). Alpha -Solanine Inhibits Human Melanoma Cell Migration and Invasion by Reducing Matrix Metalloproteinase-2/9 Activities. Biological and Pharmaceutical Bulletin, 22(10), 1685–1691.

Luo, S., Tian, G. J., Yu, F. X., & Wen, Z. D. (2021). A narrative review of the antitumor studies of solanine. *Translational Cancer Research*, *10*(3), 1578.

Lv, C., Kong, H., Dong, G., Liu, L., Tong, K., Sun, H., Chen, B., Zhang, C., & Zhou, M. (2014). Antitumor efficacy of α-solanine against pancreatic cancer in vitro and in vivo. Plos One, 9(2), e87868. https://doi.org/10.1371/journal.pone.0087868

Lynch, B., Simon, R. R., van Otterdijk, F. M., Emmen, H. H., Giuseppin, M. L. F., & Kemme-Kroonsberg, C. (2012). Subchronic toxicity evaluation of potato protein isolates. Food and Chemical Toxicology, 50(2), 373–384. https://doi.org/10.1016/j.fct.2011.09.039

Ma, R., Taphoorn, M. J. B., & Plaha, P. (2021). Advances in the management of glioblastoma. Journal of Neurology, Neurosurgery, and Psychiatry, 92(10), 1103–1111. https://doi.org/10.1136/jnnp-2020-325334

Majewska, E., & Szeliga, M. (2017). Akt/gsk3β signaling in glioblastoma. Neurochemical Research, 42(3), 918–924. https://doi.org/10.1007/s11064-016-2044-4

Mao, H., Lebrun, D. G., Yang, J., Zhu, V. F., & Li, M. (2012). Deregulated signaling pathways in glioblastoma multiforme: molecular mechanisms and therapeutic targets. Cancer Investigation, 30(1), 48–56. https://doi.org/10.3109/07357907.2011.630050

Markouli, M., Strepkos, D., Papavassiliou, K. A., Papavassiliou, A. G., & Piperi, C. (2022). Crosstalk of epigenetic and metabolic signaling underpinning glioblastoma pathogenesis. Cancers, 14(11). https://doi.org/10.3390/cancers14112655

Matias, D., Balça-Silva, J., da Graça, G. C., Wanjiru, C. M., Macharia, L. W., Nascimento, C. P., Roque, N. R., Coelho-Aguiar, J. M., Pereira, C. M., Dos Santos, M. F., Pessoa, L. S., Lima, F. R. S., Schanaider, A., Ferrer, V. P., Tania Cristina Leite de Sampaio e Spohr, & Moura-Neto, V. (2018). Microglia/Astrocytes-Glioblastoma Crosstalk: Crucial Molecular Mechanisms and Microenvironmental Factors. Frontiers in Cellular Neuroscience, 12, 235. https://doi.org/10.3389/fncel.2018.00235

Mbaveng, A. T., Damen, F., Çelik, İ., Tane, P., Kuete, V., & Efferth, T. (2019). Cytotoxicity of the crude extract and constituents of the bark of Fagara tessmannii towards multi-factorial drug resistant cancer cells. Journal of Ethnopharmacology, 235, 28–37. https://doi.org/10.1016/j.jep.2019.01.031

Mbaveng, A. T., Noulala, C. G. T., Samba, A. R. M., Tankeo, S. B., Fotso, G. W., Happi, E. N., Ngadjui, B. T., Beng, V. P., Kuete, V., & Efferth, T. (2021). Cytotoxicity of botanicals and isolated phytochemicals from Araliopsis soyauxii Engl. (Rutaceae) towards a panel of human cancer cells. Journal of Ethnopharmacology, 267, 113535. https://doi.org/10.1016/j.jep.2020.113535

McMahon, D. J., Gleeson, J. P., O'Reilly, S., & Bambury, R. M. (2022). Management of newly diagnosed glioblastoma multiforme: current state of the art and emerging therapeutic approaches. Medical Oncology, 39(9), 129. https://doi.org/10.1007/s12032-022-01708-w

Meel, M., Choudhary, N., Kumar, M., & Mathur, K. (2021). Epidemiological Profiling and Trends of Primary Intracranial Tumors: A Hospital-Based Brain Tumor Registry from a Tertiary Care Center. Journal of Neurosciences in Rural Practice, 12(1), 145–152. https://doi.org/10.1055/s-0040-1721622

Mendanha, D., Vieira de Castro, J., Moreira, J., Costa, B. M., Cidade, H., Pinto, M., Ferreira, H., & Neves, N. M. (2021). A New Chalcone Derivative with Promising Antiproliferative and Anti-Invasion Activities in Glioblastoma Cells. Molecules (Basel, Switzerland), 26(11). https://doi.org/10.3390/molecules26113383

Meng, X.-Q., Zhang, W., Zhang, F., Yin, S.-Y., Xie, H.-Y., Zhou, L., & Zheng, S.-S. (2016). Solanine-induced reactive oxygen species inhibit the growth of human

hepatocellular carcinoma HepG2 cells. Oncology Letters, 11(3), 2145–2151. https://doi.org/10.3892/ol.2016.4167

Mensinga, T. T., Sips, A. J. A. M., Rompelberg, C. J. M., van Twillert, K., Meulenbelt, J., van den Top, H. J., & van Egmond, H. P. (2005). Potato glycoalkaloids and adverse effects in humans: an ascending dose study. Regulatory Toxicology and Pharmacology, 41(1), 66–72. https://doi.org/10.1016/j.yrtph.2004.09.004

Miller, K. D., Ostrom, Q. T., Kruchko, C., Patil, N., Tihan, T., Cioffi, G., Fuchs, H. E., Waite, K. A., Jemal, A., Siegel, R. L., & Barnholtz-Sloan, J. S. (2021). Brain and other central nervous system tumor statistics, 2021. CA: A Cancer Journal for Clinicians, 71(5), 381–406. https://doi.org/10.3322/caac.21693

Minniti, G., Niyazi, M., Alongi, F., Navarria, P., & Belka, C. (2021). Current status and recent advances in reirradiation of glioblastoma. Radiation Oncology, 16(1), 36. https://doi.org/10.1186/s13014-021-01767-9

Miranda, A., Blanco-Prieto, M., Sousa, J., Pais, A., & Vitorino, C. (2017). Breaching barriers in glioblastoma. Part I: Molecular pathways and novel treatment approaches. International Journal of Pharmaceutics, 531(1), 372–388. https://doi.org/10.1016/j.ijpharm.2017.07.056

Mohsenikia, M., Alizadeh, A. M., Khodayari, S., Khodayari, H., Kouhpayeh, S. A., Karimi, A., Zamani, M., Azizian, S., & Mohagheghi, M. A. (2013). The protective and therapeutic effects of alpha-solanine on mice breast cancer. European Journal of Pharmacology, 718(1–3), 1–9. https://doi.org/10.1016/j.ejphar.2013.09.015

Mohsenikia, M., Farhangi, B., Alizadeh, A. M., Khodayari, H., Khodayari, S., Khori, V., Arjmand Abbassi, Y., Vesovic, M., Soleymani, A., & Najafi, F. (2016). Therapeutic

effects of dendrosomal solanine on a metastatic breast tumor. Life Sciences, 148, 260–267. https://doi.org/10.1016/j.lfs.2016.02.008

Mokgehle, T. M., Madala, N., Gitari, W. M., & Tavengwa, N. T. (2022). Effect of Microwave-Assisted Aqueous Two-Phase Extraction of α-Solanine from S. retroflexum and Analysis on UHPLC-qTOF-MS. Food Analytical Methods, 15(5), 1256–1268. https://doi.org/10.1007/s12161-021-02224-9

Mora, M. C., Bassa, L. M., Wong, K. E., Tirabassi, M. V., Arenas, R. B., & Schneider, S. S. (2015). Rhodiola crenulata inhibits Wnt/β-catenin signaling in glioblastoma. The Journal of Surgical Research, 197(2), 247–255. https://doi.org/10.1016/j.jss.2015.02.074

Moskwa, J., Naliwajko, S. K., Markiewicz-Żukowska, R., Gromkowska-Kępka, K. J., Soroczyńska, J., Puścion-Jakubik, A., Borawska, M. H., Isidorov, V., & Socha, K. (2022). Polish and New Zealand Propolis as Sources of Antioxidant Compounds Inhibit Glioblastoma (T98G, LN-18) Cell Lines and Astrocytoma Cells Derived from Patient. Antioxidants (Basel, Switzerland), 11(7). https://doi.org/10.3390/antiox11071305

Mosteiro, A., Pedrosa, L., Ferrés, A., Diao, D., Sierra, À., & González, J. J. (2022). The vascular microenvironment in glioblastoma: A comprehensive review. Biomedicines, 10(6). https://doi.org/10.3390/biomedicines10061285

Munari, C. C., de Oliveira, P. F., Campos, J. C. L., Martins, S. de P. L., Da Costa, J. C., Bastos, J. K., & Tavares, D. C. (2014). Antiproliferative activity of Solanum lycocarpum alkaloidic extract and their constituents, solamargine and solasonine, in tumor cell lines. Journal of Natural Medicines, 68(1), 236–241. https://doi.org/10.1007/s11418-013-0757-0

Mungur, R., Zheng, J., Wang, B., Chen, X., Zhan, R., & Tong, Y. (2022). Low-Intensity Focused Ultrasound Technique in Glioblastoma Multiforme Treatment. Frontiers in Oncology, 12, 903059. https://doi.org/10.3389/fonc.2022.903059

Murugesan, A., Holmstedt, S., Brown, K. C., Koivuporras, A., Macedo, A. S., Nguyen, N., Fonte, P., Rijo, P., Yli-Harja, O., Candeias, N. R., & Kandhavelu, M. (2020). Design and synthesis of novel quinic acid derivatives: in vitro cytotoxicity and anticancer effect on glioblastoma. Future Medicinal Chemistry, 12(21), 1891–1910. https://doi.org/10.4155/fmc-2020-0194

Mutlu, M., Tunca, B., Aksoy, S. A., Tekin, C., Cecener, G., & Egeli, U. (2021). Olea europaea leaf extract decreases tumour size by affecting the LncRNA expression status in glioblastoma 3D cell cultures. European Journal of Integrative Medicine, 45, 101345. https://doi.org/10.1016/j.eujim.2021.101345

Mykhailenko, O., Petrikaitė, V., Korinek, M., El-Shazly, M., Chen, B.-H., Yen, C.-H., Hsieh, C.-F., Bezruk, I., Dabrišiūtė, A., Ivanauskas, L., Georgiyants, V., & Hwang, T.-L. (2021). Bio-guided bioactive profiling and HPLC-DAD fingerprinting of Ukrainian saffron (Crocus sativus stigmas): moving from correlation toward causation. BMC Complementary Medicine and Therapies, 21(1), 203. https://doi.org/10.1186/s12906-021-03374-3

Nagy, A., Eder, K., Selak, M. A., & Kalman, B. (2015). Mitochondrial energy metabolism and apoptosis regulation in glioblastoma. Brain Research, 1595, 127–142. https://doi.org/10.1016/j.brainres.2014.10.062

Nakayasu, M., Umemoto, N., Ohyama, K., Fujimoto, Y., Lee, H. J., Watanabe, B., Muranaka, T., Saito, K., Sugimoto, Y., & Mizutani, M. (2017). A Dioxygenase Catalyzes

Steroid 16α-Hydroxylation in Steroidal Glycoalkaloid Biosynthesis. Plant Physiology, 175(1), 120–133. https://doi.org/10.1104/pp.17.00501

Nara, A., Saka, K., Yamada, C., Kodama, T., & Takagi, T. (2019). Forensic analysis using ultra-high-performance liquid chromatography-tandem mass spectrometry with solid-phase extraction of α-solanine and α-chaconine in whole blood. Forensic Toxicology, 37(1), 197–206. https://doi.org/10.1007/s11419-018-0452-7

National Library of Medicine. (n.d.). Solanine alpha . PubChem. Retrieved September 8, 2022, from https://pubchem.ncbi.nlm.nih.gov/compound/Solanine-alpha

Ni, W., Tian, T., Zhang, L., Li, Z., Wang, L., & Ren, A. (2018). Maternal periconceptional consumption of sprouted potato and risks of neural tube defects and orofacial clefts. Nutrition Journal, 17(1), 112. https://doi.org/10.1186/s12937-018-0420-4

Nishie, K., Gumbmann, M. R., & Keyl, A. C. (1971). Pharmacology of solanine. Toxicology and Applied Pharmacology, 19(1), 81–92. https://doi.org/10.1016/0041-008X(71)90192-X

Okamoto, H., Ducreux, L. J. M., Allwood, J. W., Hedley, P. E., Wright, A., Gururajan, V., Terry, M. J., & Taylor, M. A. (2020). Light Regulation of Chlorophyll and Glycoalkaloid Biosynthesis During Tuber Greening of Potato S. tuberosum. Frontiers in Plant Science, 11, 753. https://doi.org/10.3389/fpls.2020.00753

Oliva, M. A., Castaldo, S., Rotondo, R., Staffieri, S., Sanchez, M., & Arcella, A. (2022). Inhibiting effect of p-Coumaric acid on U87MG human glioblastoma cell growth. Journal of Chemotherapy, 34(3), 173–183. https://doi.org/10.1080/1120009X.2021.1953888

Olivier, C., Oliver, L., Lalier, L., & Vallette, F. M. (2020). Drug resistance in glioblastoma: the two faces of oxidative stress. Frontiers in Molecular Biosciences, 7, 620677. https://doi.org/10.3389/fmolb.2020.620677

Ou, A., Ott, M., Fang, D., & Heimberger, A. B. (2021). The role and therapeutic targeting of JAK/STAT signaling in glioblastoma. Cancers, 13(3). https://doi.org/10.3390/cancers13030437

Pan, B., Zhong, W., Deng, Z., Lai, C., Chu, J., Jiao, G., Liu, J., & Zhou, Q. (2016). Inhibition of prostate cancer growth by solanine requires the suppression of cell cycle proteins and the activation of ROS/P38 signaling pathway. Cancer Medicine, 5(11), 3214–3222. https://doi.org/10.1002/cam4.916

Pang, X., Huang, H., Wei, Y., & Leng, J. (2022). Ethanolic Leaf Extract of C. angustifolia Instigates ROS Mediated Apoptosis within Glioblastoma C6 Cells. Journal of Oleo Science, 71(9), 1375–1385. https://doi.org/10.5650/jos.ess22143

Park, S. Y., Cui, Z., Kim, B., Park, G., & Choi, Y.-W. (2020). Treatment with Gold Nanoparticles Using Cudrania tricuspidata Root Extract Induced Downregulation of MMP-2/-9 and PLD1 and Inhibited the Invasiveness of Human U87 Glioblastoma Cells. International Journal of Molecular Sciences, 21(4). https://doi.org/10.3390/ijms21041282

Patil, B. C., Sharma, R. P., Salunkhe, D. K., & Salunkhe, K. (1972). Evaluation of solanine toxicity. Food and Cosmetics Toxicology, 10(3), 395–398. https://doi.org/10.1016/S0015-6264(72)80258-X

Pawlowska, E., Szczepanska, J., Szatkowska, M., & Blasiak, J. (2018). An Interplay between Senescence, Apoptosis and Autophagy in Glioblastoma Multiforme-Role in

Pathogenesis and Therapeutic Perspective. International Journal of Molecular Sciences, 19(3). https://doi.org/10.3390/ijms19030889

Pearson, J. R. D., & Regad, T. (2017). Targeting cellular pathways in glioblastoma multiforme. Signal Transduction and Targeted Therapy, 2, 17040. https://doi.org/10.1038/sigtrans.2017.40

Peeri, H., Shalev, N., Vinayaka, A. C., Nizar, R., Kazimirsky, G., Namdar, D., Anil, S. M., Belausov, E., Brodie, C., & Koltai, H. (2021). Specific Compositions of Cannabis sativa Compounds Have Cytotoxic Activity and Inhibit Motility and Colony Formation of Human Glioblastoma Cells In Vitro. Cancers, 13(7). https://doi.org/10.3390/cancers13071720

Pejin, B., Simonovic, M., Talevska, A., Glumac, M., Jakimov, D., & Kojic, V. (2021). A neglected natural source for targeting glioblastoma. Natural Product Research, 35(11), 1856–1860. https://doi.org/10.1080/14786419.2019.1638386

Pfeffer, L. M. (2016). Dysregulated Signaling Pathways in Glioblastoma Cancer Stem-Like Cells: Potential Targets for Therapeutic Intervention. MOJ Cell Science & Report, 3(2). https://doi.org/10.15406/mojcsr.2016.03.00051

Province, P., E., C., Han, X., Louis, N., & Fathallah, H. (2013). Hypoxia, angiogenesis and mechanisms for invasion of malignant gliomas. In T. Lichtor (Ed.), Evolution of the molecular biology of brain tumors and the therapeutic implications. InTech. https://doi.org/10.5772/53298

Qiu, J., Shi, Z., & Jiang, J. (2017). Cyclooxygenase-2 in glioblastoma multiforme. Drug Discovery Today, 22(1), 148–156. https://doi.org/10.1016/j.drudis.2016.09.017

Ramachandran, C., Lollett, I. V., Escalon, E., Quirin, K.-W., & Melnick, S. J. (2015). Anticancer potential and mechanism of action of mango ginger (Curcuma amada Roxb.)

supercritical CO_2 extract in human glioblastoma cells. Journal of Evidence Based Complementary & Alternative Medicine, 20(2), 109–119. https://doi.org/10.1177/2156587214563731

Ramalho, M. J., Loureiro, J. A., Coelho, M. A. N., & Pereira, M. C. (2022). Transferrin Receptor-Targeted Nanocarriers: Overcoming Barriers to Treat Glioblastoma. Pharmaceutics, 14(2). https://doi.org/10.3390/pharmaceutics14020279

Rethlefsen, M. L., Kirtley, S., Waffenschmidt, S., Ayala, A. P., Moher, D., Page, M. J., Koffel, J. B., & PRISMA-S Group. (2021). PRISMA-S: an extension to the PRISMA Statement for Reporting Literature Searches in Systematic Reviews. Systematic Reviews, 10(1), 39. https://doi.org/10.1186/s13643-020-01542-z

Roux, A., Caire, F., Guyotat, J., Menei, P., Metellus, P., Pallud, J., & Neuro-Oncology Club of the French Neurosurgical Society. (2017). Carmustine wafer implantation for high-grade gliomas: Evidence-based safety efficacy and practical recommendations from the Neuro-oncology Club of the French Society of Neurosurgery. Neuro-Chirurgie, 63(6), 433–443. https://doi.org/10.1016/j.neuchi.2017.07.003

Royal Society of Chemistry. (n.d.). α-Solanine. ChemSpider. Retrieved September 8, 2022, from http://www.chemspider.com/Chemical-Structure.28033.html

Sami, A., & Karsy, M. (2013). Targeting the PI3K/AKT/mTOR signaling pathway in glioblastoma: novel therapeutic agents and advances in understanding. Tumour Biology, 34(4), 1991–2002. https://doi.org/10.1007/s13277-013-0800-5

Sánchez Maldonado, A. F., Mudge, E., Gänzle, M. G., & Schieber, A. (2014). Extraction and fractionation of phenolic acids and glycoalkaloids from potato peels using

acidified water/ethanol-based solvents. Food Research International, 65, 27–34. https://doi.org/10.1016/j.foodres.2014.06.018

Sangpairoj, K. (2021). Hexane Extract of Seaweed Caulerpa lentilliferaInhibits Cell Proliferation and Induces Apoptosis of Human Glioblastoma Cells. **กองบริหารการวิจัย**. https://doi.org/10.14456/scitechasia.2021.32

Sati, I. S. E. E., & Parhar, I. (2021). Micrornas regulate cell cycle and cell death pathways in glioblastoma. International Journal of Molecular Sciences, 22(24). https://doi.org/10.3390/ijms222413550

Sevastre, A.-S., Costachi, A., Tataranu, L. G., Brandusa, C., Artene, S. A., Stovicek, O., Alexandru, O., Danoiu, S., Sfredel, V., & Dricu, A. (2021). Glioblastoma pharmacotherapy: A multifaceted perspective of conventional and emerging treatments (Review). Experimental and Therapeutic Medicine, 22(6), 1408. https://doi.org/10.3892/etm.2021.10844

Shen, K.-H., Liao, A. C.-H., Hung, J.-H., Lee, W.-J., Hu, K.-C., Lin, P.-T., Liao, R.-F., & Chen, P.-S. (2014). α-Solanine inhibits invasion of human prostate cancer cell by suppressing epithelial-mesenchymal transition and MMPs expression. Molecules (Basel, Switzerland), 19(8), 11896–11914. https://doi.org/10.3390/molecules190811896

Shi, P., Zhang, Z., Xu, J., Zhang, L., & Cui, H. (2021). Endoplasmic reticulum stress-induced cell death as a potential mechanism for targeted therapy in glioblastoma (Review). International Journal of Oncology, 59(2). https://doi.org/10.3892/ijo.2021.5240

Shi, Y., Wang, X., Wang, N., Li, F.-F., You, Y.-L., & Wang, S.-Q. (2020). The effect of polysaccharides from Cibotium barometz on enhancing temozolomide-induced glutathione exhausted in human glioblastoma U87 cells, as revealed by 1H NMR

metabolomics analysis. International Journal of Biological Macromolecules, 156, 471–484. https://doi.org/10.1016/j.ijbiomac.2020.03.243

Shin, J. Y., Lee, J. M., Shin, H. S., Park, S. Y., Yang, J. E., Cho, S. K., & Yi, T.-H. (2012). Anti-Cancer Effect of Ginsenoside F2 against Glioblastoma Multiforme in Xenograft Model in SD Rats. Journal of Ginseng Research, 36(1), 86–92. https://doi.org/10.5142/jgr.2012.36.1.86

Silva, A. G., Silva, V. A. O., Oliveira, R. J. S., de Rezende, A. R., Chagas, R. C. R., Pimenta, L. P. S., Romão, W., Santos, H. B., Thomé, R. G., Reis, R. M., & de Azambuja Ribeiro, R. I. M. (2020). Matteucinol, isolated from Miconia chamissois, induces apoptosis in human glioblastoma lines via the intrinsic pathway and inhibits angiogenesis and tumor growth in vivo. Investigational New Drugs, 38(4), 1044–1055. https://doi.org/10.1007/s10637-019-00878-1

Silva, T. C. C., de Faria Lopes, G. P., de J Menezes-Filho, N., de Oliveira, D. M., Pereira, E., Pitanga, B. P. S., Dos Santos Costa, R., da Silva Velozo, E., Freire, S. M., Clarêncio, J., Borges, H. L., Rehen, S. K., Moura-Neto, V., & Costa, S. L. (2018). Specific Cytostatic and Cytotoxic Effect of Dihydrochelerythrine in Glioblastoma Cells: Role of NF-κB/β-catenin and STAT3/IL-6 Pathways. Anti-Cancer Agents in Medicinal Chemistry, 18(10), 1386–1393. https://doi.org/10.2174/1871520618666180412122101

Simpson, J. E., & Gammoh, N. (2020). The impact of autophagy during the development and survival of glioblastoma. Open Biology, 10(9), 200184. https://doi.org/10.1098/rsob.200184

Slanina, P. (1990). Solanine (glycoalkaloids) in potatoes: Toxicological evaluation. Food and Chemical Toxicology, 28(11), 759–761. https://doi.org/10.1016/0278-6915(90)90074-W

So, J.-S., Kim, H., & Han, K.-S. (2021). Mechanisms of invasion in glioblastoma: extracellular matrix, ca2+ signaling, and glutamate. Frontiers in Cellular Neuroscience, 15, 663092. https://doi.org/10.3389/fncel.2021.663092

Soares, J. M., Faria, B. M. D., Ascari, L. M., Souza, J. M. D., Soares, A. G., Cordeiro, Y., & Romão, L. F. (2019). Diosmin induces caspase-dependent apoptosis in human glioblastoma cells. Anais Da Academia Brasileira de Ciencias, 91(4), e20191031. https://doi.org/10.1590/0001-3765201920191031

Soubannier, V., & Stifani, S. (2017). NF-κB Signalling in Glioblastoma. Biomedicines, 5(2). https://doi.org/10.3390/biomedicines5020029

Ståhl, P., Henoch, I., Smits, A., Rydenhag, B., & Ozanne, A. (2022). Quality of life in patients with glioblastoma and their relatives. Acta Neurologica Scandinavica, 146(1), 82–91. https://doi.org/10.1111/ane.13625

Stojkovic, D., Drakulic, D., Dias, M. I., Zengin, G., Barros, L., Ivanov, M., Gašic, U., Rajcevic, N., Stevanovic, M., Ferreira, I. C. F. R., & Sokovic, M. (2022). Phlomis fruticosa L. exerts in vitro antineurodegenerative and antioxidant activities and induces prooxidant effect in glioblastoma cell line. EXCLI Journal, 21, 387–399. https://doi.org/10.17179/excli2021-4487

Stojković, D., Drakulić, D., Schwirtlich, M., Rajčević, N., Stevanović, M., Soković, M. D., & Gašić, U. (2021). Extract of Herba Anthrisci cerefolii: Chemical Profiling and Insights into Its Anti-Glioblastoma and Antimicrobial Mechanism of Actions. Pharmaceuticals (Basel, Switzerland), 14(1). https://doi.org/10.3390/ph14010055

Stoyanov, G. S., Lyutfi, E., Georgieva, R., Georgiev, R., Dzhenkov, D. L., Petkova, L., Ivanov, B. D., Kaprelyan, A., & Ghenev, P. (2022). Reclassification of glioblastoma multiforme according to the 2021 world health organization classification of central

nervous system tumors: A single institution report and practical significance. Cureus, 14(2), e21822. https://doi.org/10.7759/cureus.21822

Su, Y.-K., Shih, P.-H., Lee, W.-H., Bamodu, O. A., Wu, A. T. H., Huang, C.-C., Tzeng, Y.-M., Hsiao, M., Yeh, C.-T., & Lin, C.-M. (2017). Antrodia cinnamomea sensitizes radio-/chemo-therapy of cancer stem-like cells by modulating microRNA expression. Journal of Ethnopharmacology, 207, 47–56. https://doi.org/10.1016/j.jep.2017.06.004

Sun, H., Lv, C., Yang, L., Wang, Y., Zhang, Q., Yu, S., Kong, H., Wang, M., Xie, J., Zhang, C., & Zhou, M. (2014). Solanine induces mitochondria-mediated apoptosis in human pancreatic cancer cells. BioMed Research International, 2014, 805926. https://doi.org/10.1155/2014/805926

Tan, A. C., Ashley, D. M., López, G. Y., Malinzak, M., Friedman, H. S., & Khasraw, M. (2020). Management of glioblastoma: State of the art and future directions. CA: A Cancer Journal for Clinicians, 70(4), 299–312. https://doi.org/10.3322/caac.21613

Tang, Q., Ren, L., Liu, J., Li, W., Zheng, X., Wang, J., & Du, G. (2020). Withaferin A triggers G2/M arrest and intrinsic apoptosis in glioblastoma cells via ATF4-ATF3-CHOP axis. Cell Proliferation, 53(1), e12706. https://doi.org/10.1111/cpr.12706

Teixeira, M. V. S., Lima, J. Q., Pimenta, A. T. A., Silva, F. R. L. da, Oliveira, M. da C. F. de, Pereira, I. G., Costa-Junior, D. C., Ribeiro, P. R. V., Santiago, G. M. P., Lima, M. A. S., Braz-Filho, R., Bezerra, M. M., Montenegro, R. C., Rocha, D. D., Moraes, M. E. A. de, Medeiros, A. C. de, & Arriaga, A. M. C. (2018). New flavone and other compounds from Tephrosia egregia : assessing the cytotoxic effect on human tumor cell lines. Revista Brasileira de Farmacognosia, 28(3), 333–338. https://doi.org/10.1016/j.bjp.2018.03.008

Tezcan, G., Taskapilioglu, M. O., Tunca, B., Bekar, A., Demirci, H., Kocaeli, H., Aksoy, S. A., Egeli, U., Cecener, G., & Tolunay, S. (2017). Olea europaea leaf extract and bevacizumab synergistically exhibit beneficial efficacy upon human glioblastoma cancer stem cells through reducing angiogenesis and invasion in vitro. Biomedicine & Pharmacotherapy (Biomedecine & Pharmacotherapie), 90, 713–723. https://doi.org/10.1016/j.biopha.2017.04.022

Tezcan, G., Tunca, B., Demirci, H., Bekar, A., Taskapilioglu, M. O., Kocaeli, H., Egeli, U., Cecener, G., Tolunay, S., & Vatan, O. (2017). Olea europaea Leaf Extract Improves the Efficacy of Temozolomide Therapy by Inducing MGMT Methylation and Reducing P53 Expression in Glioblastoma. Nutrition and Cancer, 69(6), 873–880. https://doi.org/10.1080/01635581.2017.1339810

Tilak, M., Holborn, J., New, L. A., Lalonde, J., & Jones, N. (2021). Receptor tyrosine kinase signaling and targeting in glioblastoma multiforme. International Journal of Molecular Sciences, 22(4). https://doi.org/10.3390/ijms22041831

TMIC. (n.d.). alpha-Solanine . FoodB. Retrieved September 8, 2022, from https://foodb.ca/compounds/FDB012500

Tompa, M., Kalovits, F., Nagy, A., & Kalman, B. (2018). Contribution of the wnt pathway to defining biology of glioblastoma. Neuromolecular Medicine, 20(4), 437–451. https://doi.org/10.1007/s12017-018-8514-x

Touat, M., Idbaih, A., Sanson, M., & Ligon, K. L. (2017). Glioblastoma targeted therapy: updated approaches from recent biological insights. Annals of Oncology, 28(7), 1457–1472. https://doi.org/10.1093/annonc/mdx106

Tovilovic-Kovacevic, G., Krstic-Milosevic, D., Vinterhalter, B., Toljic, M., Perovic, V., Trajkovic, V., Harhaji-Trajkovic, L., & Zogovic, N. (2018). Xanthone-rich extract from

Gentiana dinarica transformed roots and its active component norswertianin induce autophagy and ROS-dependent differentiation of human glioblastoma cell line. Phytomedicine: International Journal of Phytotherapy and Phytopharmacology, 47, 151–160. https://doi.org/10.1016/j.phymed.2018.03.052

Trejo-Solís, C., Serrano-Garcia, N., Escamilla-Ramírez, Á., Castillo-Rodríguez, R. A., Jimenez-Farfan, D., Palencia, G., Calvillo, M., Alvarez-Lemus, M. A., Flores-Nájera, A., Cruz-Salgado, A., & Sotelo, J. (2018). Autophagic and apoptotic pathways as targets for chemotherapy in glioblastoma. International Journal of Molecular Sciences, 19(12). https://doi.org/10.3390/ijms19123773

Tsai, S.-F., Tao, M., Ho, L.-I., Chiou, T.-W., Lin, S.-Z., Su, H.-L., & Harn, H.-J. (2017). Isochaihulactone-induced DDIT3 causes ER stress-PERK independent apoptosis in glioblastoma multiforme cells. Oncotarget, 8(3), 4051–4061. https://doi.org/10.18632/oncotarget.13266

Tuncel, G., & Kalkan, R. (2018). Receptor tyrosine kinase-Ras-PI 3 kinase-Akt signaling network in glioblastoma multiforme. Medical Oncology, 35(9), 122. https://doi.org/10.1007/s12032-018-1185-5

Umemoto, N., Nakayasu, M., Ohyama, K., Yotsu-Yamashita, M., Mizutani, M., Seki, H., Saito, K., & Muranaka, T. (2016). Two cytochrome P450 monooxygenases catalyze early hydroxylation steps in the potato steroid glycoalkaloid biosynthetic pathway. Plant Physiology, 171(4), 2458–2467. https://doi.org/10.1104/pp.16.00137

Urbantat, R. M., Vajkoczy, P., & Brandenburg, S. (2021). Advances in chemokine signaling pathways as therapeutic targets in glioblastoma. Cancers, 13(12). https://doi.org/10.3390/cancers13122983

Uribe, D., Niechi, I., Rackov, G., Erices, J. I., San Martín, R., & Quezada, C. (2022). Adapt to persist: glioblastoma microenvironment and epigenetic regulation on cell plasticity. Biology, 11(2). https://doi.org/10.3390/biology11020313

Vakilian, A., Khorramdelazad, H., Heidari, P., Sheikh Rezaei, Z., & Hassanshahi, G. (2017). CCL2/CCR2 signaling pathway in glioblastoma multiforme. Neurochemistry International, 103, 1–7. https://doi.org/10.1016/j.neuint.2016.12.013

Valdés-Rives, S. A., Casique-Aguirre, D., Germán-Castelán, L., Velasco-Velázquez, M. A., & González-Arenas, A. (2017). Apoptotic signaling pathways in glioblastoma and therapeutic implications. BioMed Research International, 2017, 7403747. https://doi.org/10.1155/2017/7403747

van den Bent, M. J., Weller, M., Wen, P. Y., Kros, J. M., Aldape, K., & Chang, S. (2017). A clinical perspective on the 2016 WHO brain tumor classification and routine molecular diagnostics. Neuro-Oncology, 19(5), 614–624. https://doi.org/10.1093/neuonc/now277

Velásquez, C., Mansouri, S., Mora, C., Nassiri, F., Suppiah, S., Martino, J., Zadeh, G., & Fernández-Luna, J. L. (2019). Molecular and Clinical Insights into the Invasive Capacity of Glioblastoma Cells. Journal of Oncology, 2019, 1740763. https://doi.org/10.1155/2019/1740763

Veliz, I., Loo, Y., Castillo, O., Karachaliou, N., Nigro, O., & Rosell, R. (2015). Advances and challenges in the molecular biology and treatment of glioblastoma-is there any hope for the future? Annals of Translational Medicine, 3(1), 7. https://doi.org/10.3978/j.issn.2305-5839.2014.10.06

Wallace, G. C., Dixon-Mah, Y. N., Vandergrift, W. A., Ray, S. K., Haar, C. P., Mittendorf, A. M., Patel, S. J., Banik, N. L., Giglio, P., & Das, A. (2013). Targeting

oncogenic ALK and MET: a promising therapeutic strategy for glioblastoma. Metabolic Brain Disease, 28(3), 355–366. https://doi.org/10.1007/s11011-013-9401-7

Wan, L., Gao, H., Gao, H., Du, R., Wang, F., Wang, Y., & Chen, M. (2022). Selective extraction and determination of steroidal glycoalkaloids in potato tissues by electromembrane extraction combined with LC-MS/MS. Food Chemistry, 367, 130724. https://doi.org/10.1016/j.foodchem.2021.130724

Wang, Gang, Wang, J., Du, L., & Li, F. (2015). Effect and Mechanism of Total Flavonoids Extracted from Cotinus coggygria against Glioblastoma Cancer In Vitro and In Vivo. BioMed Research International, 2015, 856349. https://doi.org/10.1155/2015/856349

Wang, Guangwen, & Wang, W. (2022). Advanced cell therapies for glioblastoma. Frontiers in Immunology, 13, 904133. https://doi.org/10.3389/fimmu.2022.904133

Wang, H., Lai, Q., Wang, D., Pei, J., Tian, B., Gao, Y., Gao, Z., & Xu, X. (2022). Hedgehog signaling regulates the development and treatment of glioblastoma. Oncology Letters, 24(3), 294. https://doi.org/10.3892/ol.2022.13414

Wang, J., Qi, Q., Feng, Z., Zhang, X., Huang, B., Chen, A., Prestegarden, L., Li, X., & Wang, J. (2016). Berberine induces autophagy in glioblastoma by targeting the AMPK/mTOR/ULK1-pathway. Oncotarget, 7(41), 66944–66958. https://doi.org/10.18632/oncotarget.11396

Wang, L., Sun, Q.-Q., Zhang, S.-J., Du, Y.-W., Wang, Y.-Y., Zang, W.-Q., Chen, X.-N., & Zhao, G.-Q. (2016). Inhibitory effect of α-solanine on esophageal carcinoma in vitro. Experimental and Therapeutic Medicine, 12(3), 1525–1530. https://doi.org/10.3892/etm.2016.3500

Wang, Q., Li, H., Sun, Z., Dong, L., Gao, L., Liu, C., & Wang, X. (2016). Kukoamine A inhibits human glioblastoma cell growth and migration through apoptosis induction and epithelial-mesenchymal transition attenuation. Scientific Reports, 6, 36543. https://doi.org/10.1038/srep36543

Wang, X., Zou, S., Ren, T., Zhao, L.-J., Yu, L.-F., Li, X.-Y., Yan, X., & Zhang, L.-J. (2021). Alantolactone suppresses the metastatic phenotype and induces the apoptosis of glioblastoma cells by targeting LIMK kinase activity and activating the cofilin/G-actin signaling cascade. International Journal of Molecular Medicine, 47(5). https://doi.org/10.3892/ijmm.2021.4901

Wang, YanGang, Liu, W., He, X., & Fei, Z. (2015). Hispidulin enhances the anti-tumor effects of temozolomide in glioblastoma by activating AMPK. Cell Biochemistry and Biophysics, 71(2), 701–706. https://doi.org/10.1007/s12013-014-0252-6

Wang, Yuanyuan, Wu, J., Guo, W., Sun, Q., Chen, X., Zang, W., Dong, Z., & Zhao, G. (2016). α-Solanine Modulates the Radiosensitivity of Esophageal Cancer Cells by Inducing MicroRNA 138 Expression. Cellular Physiology and Biochemistry, 39(3), 996–1010. https://doi.org/10.1159/000447807

Wang, Z., Liu, F., Liao, W., Yu, L., Hu, Z., Li, M., & Xia, H. (2020). Curcumin suppresses glioblastoma cell proliferation by p-AKT/mTOR pathway and increases the PTEN expression. Archives of Biochemistry and Biophysics, 689, 108412. https://doi.org/10.1016/j.abb.2020.108412

Wanis, H. A., Møller, H., Ashkan, K., & Davies, E. A. (2021). The incidence of major subtypes of primary brain tumors in adults in England 1995-2017. Neuro-Oncology, 23(8), 1371–1382. https://doi.org/10.1093/neuonc/noab076

Wardak, Z., & Choe, K. S. (2013). Molecular pathways and potential therapeutic targets in glioblastoma multiforme. Expert Review of Anticancer Therapy, 13(11), 1307–1318. https://doi.org/10.1586/14737140.2013.852472

Weller, M., Le Rhun, E., Preusser, M., Tonn, J.-C., & Roth, P. (2019). How we treat glioblastoma. ESMO Open, 4(Suppl 2), e000520. https://doi.org/10.1136/esmoopen-2019-000520

Wen, Z., Huang, C., Xu, Y., Xiao, Y., Tang, L., Dai, J., Sun, H., Chen, B., & Zhou, M. (2016). α-Solanine inhibits vascular endothelial growth factor expression by down-regulating the ERK1/2-HIF-1α and STAT3 signaling pathways. European Journal of Pharmacology, 771, 93–98. https://doi.org/10.1016/j.ejphar.2015.12.020

Wick, W., Osswald, M., Wick, A., & Winkler, F. (2018). Treatment of glioblastoma in adults. Therapeutic Advances in Neurological Disorders, 11, 1756286418790452. https://doi.org/10.1177/1756286418790452

Wick, W., & Platten, M. (2018). Understanding and treating glioblastoma. Neurologic Clinics, 36(3), 485–499. https://doi.org/10.1016/j.ncl.2018.04.006

Wong, K. E., Mora, M. C., Sultana, N., Moriarty, K. P., Arenas, R. B., Yadava, N., Schneider, S. S., & Tirabassi, M. V. (2018). Evaluation of Rhodiola crenulata on growth and metabolism of NB-1691, an MYCN-amplified neuroblastoma cell line. Tumour Biology, 40(6), 1010428318779515. https://doi.org/10.1177/1010428318779515

Wright, A., Watanabe, R., & Koehler, J. W. (2022). European Mistletoe (Viscum album) Extract Is Cytotoxic to Canine High-Grade Astrocytoma Cells In Vitro and Has Additive Effects with Mebendazole. Veterinary Sciences, 9(1). https://doi.org/10.3390/vetsci9010031

Xiong, Y., Lai, X., Xiang, W., Zhou, J., Han, J., Li, H., Deng, H., Liu, L., Peng, J., & Chen, L. (2020). Galangin (GLN) Suppresses Proliferation, Migration, and Invasion of Human Glioblastoma Cells by Targeting Skp2-Induced Epithelial-Mesenchymal Transition (EMT). OncoTargets and Therapy, 13, 9235–9244. https://doi.org/10.2147/OTT.S264209

Xue, N., Zhou, Q., Ji, M., Jin, J., Lai, F., Chen, J., Zhang, M., Jia, J., Yang, H., Zhang, J., Li, W., Jiang, J., & Chen, X. (2017). Chlorogenic acid inhibits glioblastoma growth through repolarizating macrophage from M2 to M1 phenotype. Scientific Reports, 7, 39011. https://doi.org/10.1038/srep39011

Yamashoji, S., & Matsuda, T. (2013). Synergistic cytotoxicity induced by α-solanine and α-chaconine. Food Chemistry, 141(2), 669–674. https://doi.org/10.1016/j.foodchem.2013.03.104

Yan, X., Li, M., Chen, L., Peng, X., Que, Z.-J., An, H.-M., Shen, K.-P., & Hu, B. (2020). α-Solanine inhibits growth and metastatic potential of human colorectal cancer cells. Oncology Reports, 43(5), 1387–1396. https://doi.org/10.3892/or.2020.7519

Yang, Jinhui, Hao, T., Sun, J., Wei, P., & Zhang, H. (2019). Long noncoding RNA GAS5 modulates α-Solanine-induced radiosensitivity by negatively regulating miR-18a in human prostate cancer cells. Biomedicine & Pharmacotherapy (Biomedecine & Pharmacotherapie), 112, 108656. https://doi.org/10.1016/j.biopha.2019.108656

Yang, Jun, Shi, Z., Liu, R., Wu, Y., & Zhang, X. (2020). Combined-therapeutic strategies synergistically potentiate glioblastoma multiforme treatment via nanotechnology. Theranostics, 10(7), 3223–3239. https://doi.org/10.7150/thno.40298

Yeh, L.-T., Hsu, L.-S., Chung, Y.-H., & Chen, C.-J. (2020). Tectorigenin inhibits glioblastoma proliferation by G0/G1 cell cycle arrest. Medicina (Kaunas, Lithuania), 56(12). https://doi.org/10.3390/medicina56120681

Yuan, G., Yan, S.-F., Xue, H., Zhang, P., Sun, J.-T., & Li, G. (2014). Cucurbitacin I induces protective autophagy in glioblastoma in vitro and in vivo. The Journal of Biological Chemistry, 289(15), 10607–10619. https://doi.org/10.1074/jbc.M113.528760

Zanotto-Filho, A., Braganhol, E., Klafke, K., Figueiró, F., Terra, S. R., Paludo, F. J., Morrone, M., Bristot, I. J., Battastini, A. M., Forcelini, C. M., Bishop, A. J. R., Gelain, D. P., & Moreira, J. C. F. (2015). Autophagy inhibition improves the efficacy of curcumin/temozolomide combination therapy in glioblastomas. Cancer Letters, 358(2), 220–231. https://doi.org/10.1016/j.canlet.2014.12.044

Zhang, F., Yang, R., Zhang, G., Cheng, R., Bai, Y., Zhao, H., Lu, X., Li, H., Chen, S., Li, J., Wu, S., Li, P., Chen, X., Sun, Q., & Zhao, G. (2016). Anticancer function of α-solanine in lung adenocarcinoma cells by inducing microRNA-138 expression. Tumour Biology, 37(5), 6437–6446. https://doi.org/10.1007/s13277-015-4528-2

Zhang, H., Wang, R., Yu, Y., Liu, J., Luo, T., & Fan, F. (2019). Glioblastoma Treatment Modalities besides Surgery. Journal of Cancer, 10(20), 4793–4806. https://doi.org/10.7150/jca.32475

Zhang, L., Wang, H., Zhu, J., Xu, J., & Ding, K. (2014). Mollugin induces tumor cell apoptosis and autophagy via the PI3K/AKT/mTOR/p70S6K and ERK signaling pathways. Biochemical and Biophysical Research Communications, 450(1), 247–254. https://doi.org/10.1016/j.bbrc.2014.05.101

Zhang, Y., Xie, R.-F., Xiao, Q.-G., Li, R., Shen, X.-L., & Zhu, X.-G. (2014). Hedyotis diffusa Willd extract inhibits the growth of human glioblastoma cells by inducing mitochondrial apoptosis via AKT/ERK pathways. Journal of Ethnopharmacology, 158 Pt A, 404–411. https://doi.org/10.1016/j.jep.2014.10.017

Zhao, B., Shen, C., Zheng, Z., Wang, X., Zhao, W., Chen, X., Peng, F., Xue, L., Shu, M., Hou, X., Wang, K., Zhong, C., Sun, J., Wan, J., & Zhao, S. (2018). Peiminine inhibits glioblastoma in vitro and in vivo through cell cycle arrest and autophagic flux blocking. Cellular Physiology and Biochemistry, 51(4), 1566–1583. https://doi.org/10.1159/000495646

Zheng, Y., Li, L., Gao, Q., Niu, B., & Wang, H. (2020). Solanine inhibits proliferation and promotes apoptosis of the human leukaemia cells by targeting the miR-16/Bcl-2 axis . Journal of Haematology Oncology, 25(3), 1614–1618.

Zhu, L., Lu, Y., Sun, Z., Han, J., & Tan, Z. (2020). The application of an aqueous two-phase system combined with ultrasonic cell disruption extraction and HPLC in the simultaneous separation and analysis of solanine and Solanum nigrum polysaccharide from Solanum nigrum unripe fruit. Food Chemistry, 304, 125383. https://doi.org/10.1016/j.foodchem.2019.125383

Zhu, Y.-G., Lv, Y.-X., Guo, C.-Y., Xiao, Z.-M., Jiang, Q.-G., Kuang, H., Zhang, W.-H., & Hu, P. (2021). Harmine inhibits the proliferation and migration of glioblastoma cells via the FAK/AKT pathway. Life Sciences, 270, 119112. https://doi.org/10.1016/j.lfs.2021.119112

Zou, T., Si, Y., Hu, Y., Yang, L., Wei, J., Li, J., Zhao, Y., Shen, J., Li, M., Wu, X., Du, F., Chen, Y., Chen, M., Ye, Y., Xiao, Z., & Wu, Z. (2021). Alpha-Solanine Anti-Tumor Effects

in Non-Small Cell Lung Cancer Through Regulating the Glycolysis Pathway. Research Square. https://doi.org/10.21203/rs.3.rs-789534/v1

Zuccarini, M., Giuliani, P., Ziberi, S., Carluccio, M., Iorio, P. D., Caciagli, F., & Ciccarelli, R. (2018). The role of wnt signal in glioblastoma development and progression: A possible new pharmacological target for the therapy of this tumor. Genes, 9(2). https://doi.org/10.3390/genes9020105

Chapter 10 Appendix III: Viability assay optimisation

10.1. Hypothesising glioblastoma multiforme cells are sensitive to dimethyl-sulfoxide

α-solanine was initially disollved in DMSO, since this was the standard used by published literature. Presto blue® assays were intially conducted on U87MG cells using α-solanine dissolved in DMSO. However, the results obtained were not expected as very little viability was observed irrespective of the concentration of α-solanine used. Such findings contradicted published literature investigating α-solanine (dissolved in DMSO) against difference cancer cell lines. Thus, it was hypothesised that GBM cells lines, particularly U87MG cells, may be sensitive to DMSO. Thus the viability of U87MG cells against the lowest (5.00 μM α-solanine) and highest (50.00 μM α-solanine) concentrations of α-solanine in DMSO used in the previous Presto blue® experiment and equivalent concentrations of DMSO was conducted to test the aforementioned hypothesis. Some a few studies reported using solutions of α-solanine dissolved in aqueous solutions. Thus, the viability of U87MG cells against equivalent concentrations of α-solanine dissolved in DMEM/F12 medium was also investigated.

10.2. Investigating the suitability of dimethyl-sulfoxide as a vehicle for α-solanine solanine

U87MG viability did not differ significantly between 1.00 % versus 10.00% DMSO and 5.00 μM α-solanine in DMSO versus 50.00 μM α-solanine in DMSO (Figure xxx, appendix xxx, section xxxx). Moreover the viability of U87MG cells did not differ between DMSO and α-solanine in DMSO (Figure xxx, appendix xxx, section xxxx). Hence, the cytotoxic effect of α-solanine in DMSO was likely due to the vehicle (DMSO) rather than the effect of α-solanine. α-solanine dissolved in DMEM/F12 medium produced

expected results, similar to results documented by published literaute. However, the viability of U87MG cells treated with 50.00 μM α-solanine in DMSO was not statistically different from 50.00 μM α-solanine in DMEM/F12 medium.

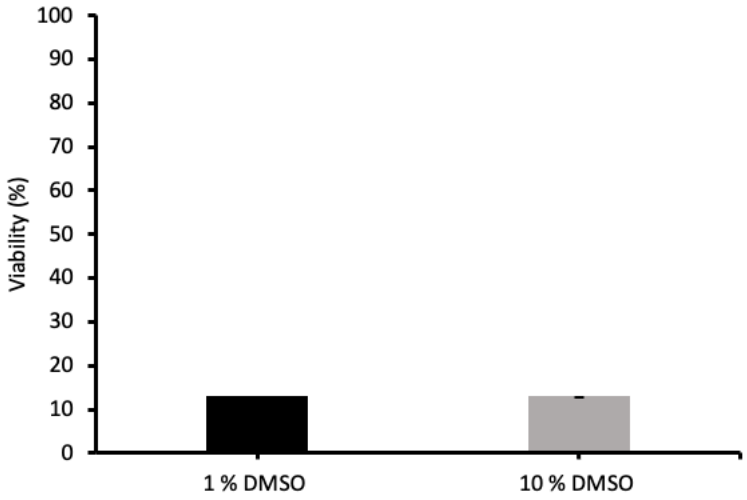


Figure 10.1.: U87MG viability after 72 hours treated with 1.00 % DMSO versus 10.00 % DMSO.

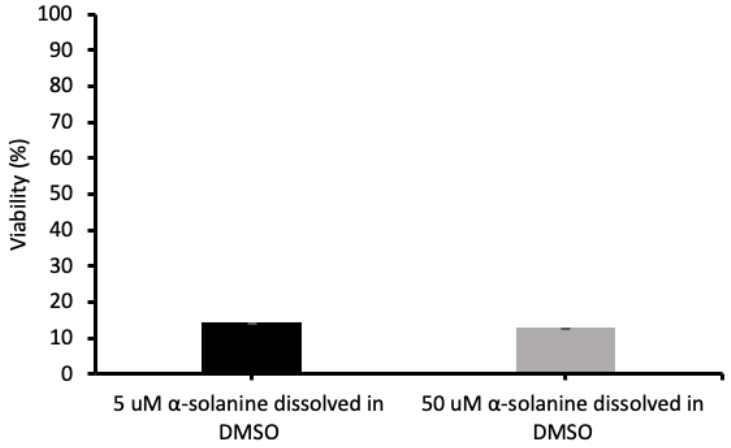


Figure 10.2.: U87MG viability after 72 hours treated with 5.00 μM α-solanine in DMSO versus 50.00 μM α-solanine in DMSO.

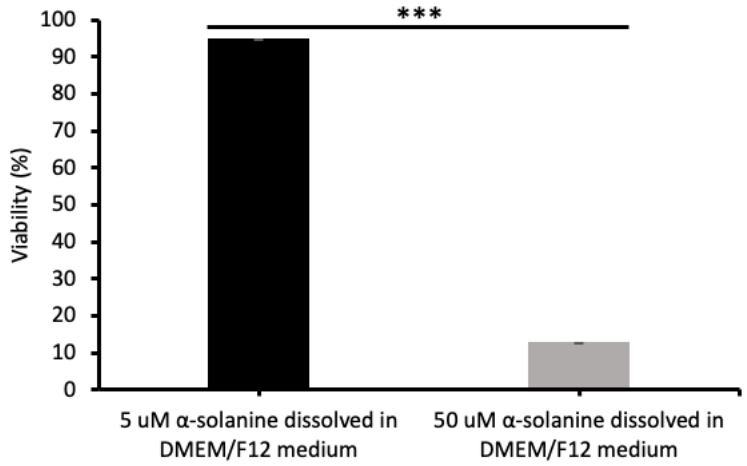


Figure 10.3.: U87MG viability after 72 hours treated with with 5.00 µM α-solanine in DMEM/F12 medium versus 50.00 µM α-solanine in DMEM/F12 medium.

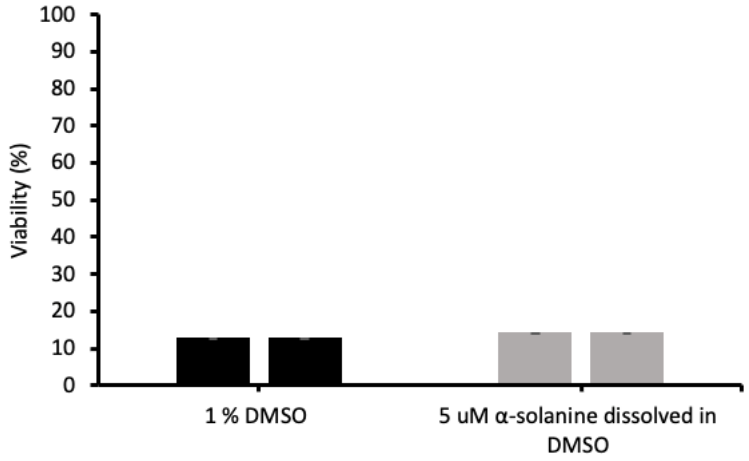


Figure 10.4.: U87MG viability after 72 hours treated with 1.00% DMSO versus 5.00 µM α-solanine in DMSO.

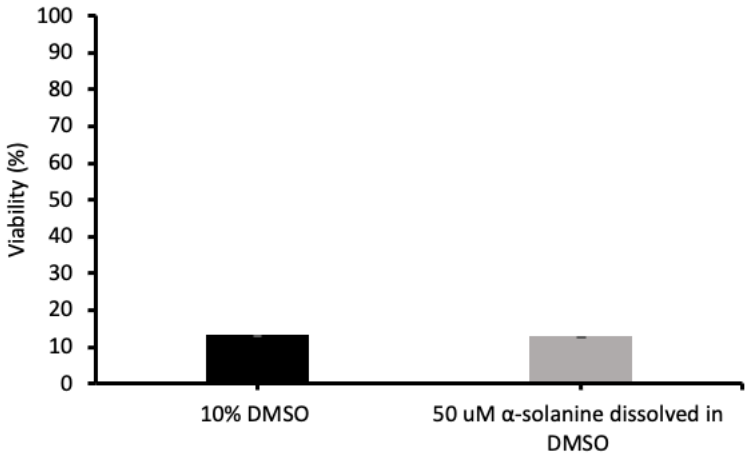


Figure 10.5.: U87MG viability after 72 hours treated with 10.00% DMSO versus 50.00 µM α-solanine in DMSO.

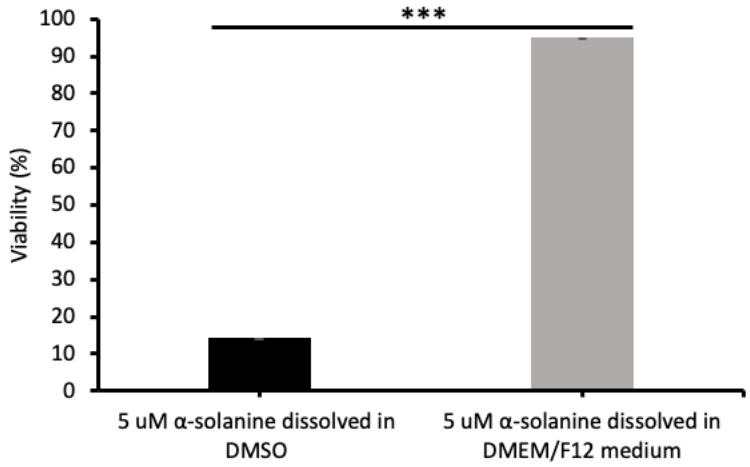


Figure 10.6.: U87MG viability after 72 hours with 5.00 µM α-solanine in DMSO versus 5.00 µM α-solanine in DMEM/F12 medium.

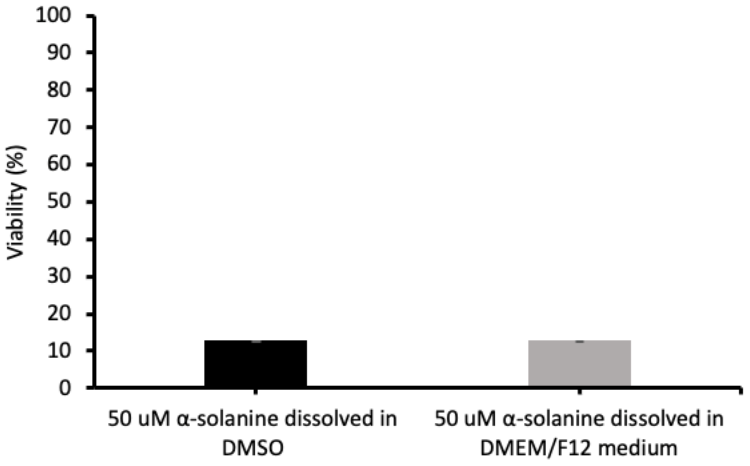


Figure 10.7.: U87MG viability after 72 hours with 50.00 µM α-solanine in DMSO versus 50.00 µM α-solanine in DMEM/F12 medium.

Chapter 11 Appendix IV: RNA primer search bioinformatic and experimental validation

11.1. Search and validation of primers designed against human autophagy related 4B cysteine peptidase gene

Table 11.1.: Human autophagy related 4B cysteine peptidase canonical gene sequence. Canonical gene sequence was retrieved from the Consensus coding sequence project database [blue – exons, black - introns].

Gene	Human Autophagy Related 4B Cysteine Peptidase (ATG4B)
Canonical gene sequence	ATGGACGCAGCTACTCTGACCTACGACACTCTCCGGTTTGCTGAGTTTAAGATTTTCCTG AGACCTCAGAGCCCGTTTGGATACTGGGTAGAAAATACAGCATTTTCACAGAAAAGGA CGAGATCTTGTCTGATGTGGCATCTAGACTTTGGTTTACATACAGGAAAAACTTTCCAG CCATTGGGGGGACAGGCCCCACCTCGGACACAGGCTGGGGCTGCATGCTGCGGTGTG GACATGATCTTGCCCAAGCCCTGGTGTGCCGGCACCTAGGCCGAGATTGGAGGTGGAC ACAAAGGAAGAGGCAGCCAGACAGCTACTTCAGCGTCCTCAACGCATTCATCGACAGG AAGGACAGTTACTACTCCATTCACCAGATAGCGCAAATGGGAGTTGGCGAAGGCAAGT CCATAGGCCAGTGGTACGGGCCCAACACTGTCGCCCAGGTCCTGAAGAAGCTTGCTGT CTTCGATACGTGGAGCTCCTTGGCGGTCCACATTGCAATGGACAACACTGTTGTGATGG AGGAAATCAGAAGGTTGTGCAGGACCAGCGTTCCCTGTGCAGGCGCCACTGCGTTTCC TGCAGATTCCGACCGGCACTGCAACGGATTCCCTGCCGGAGCTGAGGTCACCAACAGG CCGTCGCCATGGAGACCCCTGGTACTTCTCATTCCCCTGCGCCTGGGGCTCACGGACAT CAACGAGGCCTACGTGGAGACGCTGAAGCACTGCTTCATGATGCCCCAGTCCCTGGGC GTCATCGGAGGGAAGCCCAACAGCGCCCACTACTTCATCGGCTACGTTGGTGAGGAGC TCATCTACCTGGACCCCCACACCACGCAGCCAGCCGTGGAGCCCACTGATGGCTGCTTC ATCCCGGACGAGAGCTTCCACTGCCAGCACCCGCCGTGCCGCATGAGCATCGCGGAGC TTGACCCGTCCATCGCTGTGGGGTTTTTCTGTAAGACTGAAGATGACTTCAATGATTGG TGCCAGCAAGTCAAAAAGCTGTCTCTGCTTGGAGGTGCCCTGCCCATGTTTGAGCTGGT GGAGCTGCAGCCTTCACATCTGGCCTGCCCCGACGTCCTGAACCTGTCCCTAGATTCTT CTGATGTAGAGCGACTGGAAAGATTCTTCGACTCAGAAGATGAAGACTTTGAAATCCT GTCCCTTTGA

Table 11.2.: Potential RNA primer-pairs against the human autophagy related 4B cysteine peptidase gene. Potential primer pairs were identified through haphazard literature review.

	Forward primer (5' – 3')	Reverse primer (5' – 3')	Product size (bases)
Primers	TCGTTGATGTCCGTGAGCC	ATGGAGGAAATCAGAAGGTTGT	N.A.
Reference(s)	(Y. Xu et al., 2016)		
Primers	CCGCTCGAGGGCGCCGGCCGGA TCGATCG	CCCAAGCTTCCATCTTGCGGTACGGA CGT	N.A.
Reference(s)	(Peng et al., 2017)		
Primers	ATGGACGCAGCTACTCTGAC	TTTTCTACCCAGTATCCAAACGG	96
Reference(s)	(Wu et al., 2020)		
Primers	GGCAAGTCTATAGGCCAGTGGTA	GGCCCTGCATAACCTTCTGA	N.A.
Reference(s)	(Z. Li et al., 2018)		
Primers	GGTGTGGACAGATGATCTTTGC	CCAACTCCCATTTGCGCTATC	172

		(GATAGCGCAAATGGGAGTTGG)	
Reference(s)		(S. Chen et al., 2021)	
Primers	TACGACACTCTCCGGTTTGCT	CCAACTCCCATTTGCGCTATC	430
Reference(s)	(Guo et al., 2018)	(S. Chen et al., 2021)	
Primers	TACGACACTCTCCGGTTTGCT	GCAAAGATCATCTGTCCACACC	230
Reference(s)	(Guo et al., 2018)		
Primers	GGTGTGGACAGATGATCTTTGC	CCAACTCCCATTTGCGCTATC	181
Reference(s)	(Y. Sun et al., 2019)	(X. Zhang et al., 2020)	

Table 11.3.: Selected tentative RNA primer pair against the human Autophagy Related 4B Cysteine Peptidase gene.

Forward primer (5' – 3')	Reverse primer (5' – 3')	Product size (bases)
GGTGTGGACACATGATCTTGCC	CTCCACGTATCGAAGACAGC	254

Table 11.4.: Primer-BLAST search parameters and other details for the selected Human Autophagy Related 4B Cysteine Peptidase RNA primer pair.

Search parameter and other details	
Number of Blast hits analyzed	17889
Entrez query	/
Min total mismatches	2
Min 3' end mismatches	2
Defined 3' end region length	5
Mismatch threshold to ignore targets	6
Max target size	4000
Max number of Blast target sequences	50000
Blast E value	30000
Blast word size	7
Max candidate primer pairs	500
Min PCR product size	70
Max PCR product size	1000
Min Primer size	15
Opt Primer size	20
Max Primer size	25
Min Tm	57
Opt Tm	60
Max Tm	63
Max Tm difference	3
Repeat filter	AUTO
Low complexity filter	Yes

Output 11.1.: Primer-BLAST output for other potential products on unintended templates for the selected human Autophagy Related 4B Cysteine Peptidase RNA primer pair.

>XM_047443742.1 PREDICTED: Homo sapiens autophagy related 4B cysteine peptidase (ATG4B), transcript variant X6, RNA

product length = 256
Forward primer 1 GGTGTGGACAGATGATCTTTGC 22
Template 437 458
Reverse primer 1 CTCCACGTATCGAAGACAGC 20
Template 692 673

>XM_047443741.1 PREDICTED: Homo sapiens autophagy related 4B cysteine peptidase (ATG4B), transcript variant X5, RNA
product length = 256
Forward primer 1 GGTGTGGACAGATGATCTTTGC 22
Template 477 498
Reverse primer 1 CTCCACGTATCGAAGACAGC 20
Template 732 713

>XM_047443740.1 PREDICTED: Homo sapiens autophagy related 4B cysteine peptidase (ATG4B), transcript variant X4, RNA
product length = 256
Forward primer 1 GGTGTGGACAGATGATCTTTGC 22
Template 200 221
Reverse primer 1 CTCCACGTATCGAAGACAGC 20
Template 455 436

>XM_005246992.5 PREDICTED: Homo sapiens autophagy related 4B cysteine peptidase (ATG4B), transcript variant X1, RNA
product length = 256
Forward primer 1 GGTGTGGACAGATGATCTTTGC 22
Template 252 273
Reverse primer 1 CTCCACGTATCGAAGACAGC 20
Template 507 488

>NM_178326.3 Homo sapiens autophagy related 4B cysteine peptidase (ATG4B), transcript variant 2, RNA
product length = 256
Forward primer 1 GGTGTGGACAGATGATCTTTGC 22
Template 252 273
Reverse primer 1 CTCCACGTATCGAAGACAGC 20
Template 507 488

>NM_013325.5 Homo sapiens autophagy related 4B cysteine peptidase (ATG4B), transcript variant 1, RNA
product length = 256
Forward primer 1 GGTGTGGACAGATGATCTTTGC 22
Template 252 273
Reverse primer 1 CTCCACGTATCGAAGACAGC 20
Template 507 488

11.2. Search and validation of primers designed against human Bcl-2 associated X protein gene

Table 11.5.: Human Bcl-2 associated X protein canonical gene sequence. Canonical gene sequence was retrieved from the Consensus coding sequence project database [blue – exons, black - introns].

Gene	Human BCL-2 Associated X protein (Bax)

Canonical gene sequence	ATGGACGGGTCCGGGGAGCAGCCCAGAGGCGGGGGGCCCACCAGCTCTGAGCAG ATCATGAAGACAGGGGCCCTTTTGCTTCAGGGTTTCATCCAGGATCGAGCAGGGC GAATGGGGGGGGAGGCACCCGAGCTGGCCCTGGACCCGGTGCCTCAGGATGCGT CCACCAAGAAGCTGAGCGAGTGTCTCAAGCGCATCGGGGACGAACTGGACAGTAA CATGGAGCTGCAGAGGATGATTGCCGCCGTGGACACAGACTCCCCCCGAGAGGTC TTTTTCCGAGTGGCAGCTGACATGTTTTCTGACGGCAACTTCAACTGGGGCCGGGT TGTCGCCCTTTTCTACTTTGCCAGCAAACTGGTGCTCAAGGCCCTGTGCACCAAGGT GCCGGAACTGATCAGAACCATCATGGGCTGGACATTGGACTTCCTCCGGGAGCGG CTGTTGGGCTGGATCCAAGACCAGGGTGGTTGGGACGGCCTCCTCTCCTACTTTGG GACGCCCACGTGGCAGACCGTGACCATCTTTGTGGCGGGAGTGCTCACCGCCTCAC TCACCATCTGGAAGAAGATGGGCTGA

Table 11.6.: Potential RNA primer-pairs against the human Bcl-2 associated X protein canonical gene. Potential primer pairs were identified through haphazard literature review.

	Forward primer (5' – 3')	Reverse primer (5' – 3')	Product size (bases)
Primer	TCAGGATGCGTCCACCAAGAAG	TGTGTCCACGGCGGCAATCATC	103
Reference(s)	(OriGene Technologies, Inc., 2022a)		
Primer	ATGTTTTCTGACGGAACTTC	AGTCCAATGTCCAGCCCAT	N.A.
Reference(s)	(Laffon et al., 2001)		
Primer	ATGGACGGGTCCGGGGAG	TGTGTCCACGGCGGCAATCATC	255
Reference(s)	(Laffon et al., 2001)	(OriGene Technologies, Inc., 2022a)	
Primer	GCCTCTGGATCTTCACTTGG	GTCTGGGCATAAGTGCCAAT (ATTGGCACTTATGCCCAGAC)	N.A.
Reference(s)	(Yang et al., 2017)		
Primer	GCCCTTTTGCTTCAGGGTTT	TCC AAT GTC CAG CCC ATG AT	356
Reference(s)	(Mbazima et al., 2008)		
Primer	GCCCTTTTGCTTCAGGGTTT	TGTGTCCACGGCGGCAATCATC	186
Reference(s)	(Mbazima et al., 2008)	(OriGene Technologies, Inc., 2022a)	
Primer	TGGACGGGTCCGGG GAG	ATCCAGCCCAACAGCCGC	N.A.
Reference(s)	(Briton-Jones et al., 2006)		
Primer	GATGATTGCCGCCGTGGACACA	ATCCAGCCCAACAGCCGC	222
Reference(s)	(OriGene Technologies, Inc., 2022a)	(Briton-Jones et al., 2006)	
Primer	AACATGGAGCTGCAGAGGAT	5CAGTTGAAGTTGCCGTCAGA	104
Reference(s)	(Yamamoto et al., 2020)		

Primer	AACATGGAGCTGCAGAGGAT	AGTCCAATGTCCAGCCCAT	211
Reference(s)	(Yamamoto et al., 2020)	(Laffon et al., 2001)	

Table 11.7.: Selected tentative RNA primer pair against the human Bcl-2 associated X protein gene.

Forward primer (5' – 3')	Reverse primer (5' – 3')	Product size (bases)
GGACAGTAACATGGAGCTGC	GAGGAAGTCCAATGTCCAGC	255

Table 11.8.: Primer-BLAST search parameters and other details for the selected human Bcl-2 associated X protein RNA primer pair.

Search parameter and other details	
Number of Blast hits analyzed	23962
Entrez query	/
Min total mismatches	2
Min 3' end mismatches	2
Defined 3' end region length	5
Mismatch threshold to ignore targets	6
Max target size	4000
Max number of Blast target sequences	50000
Blast E value	30000
Blast word size	7
Max candidate primer pairs	500
Min PCR product size	70
Max PCR product size	1000
Min Primer size	15
Opt Primer size	20
Max Primer size	25
Min Tm	57
Opt Tm	60
Max Tm	63
Max Tm difference	3
Repeat filter	AUTO
Low complexity filter	Yes

Output 11.2.: Primer-BLAST output for other potential products on unintended templates for the selected human Bcl-2 associated X protein RNA primer pair.

>XM_047439168.1 PREDICTED: Homo sapiens BCL2 associated X, apoptosis regulator (BAX), transcript variant X1, RNA
product length = 223
Forward primer 1 GGACAGTAACATGGAGCTGC 20
Template 238 257
Reverse primer 1 GAGGAAGTCCAATGTCCAGC 20
Template 460 441

>NM_138764.5 Homo sapiens BCL2 associated X, apoptosis regulator (BAX), transcript variant sigma, RNA

product length = 223
Forward primer 1 GGACAGTAACATGGAGCTGC 20
Template 264 283
Reverse primer 1 GAGGAAGTCCAATGTCCAGC 20
Template 486 467

>NM_001291428.2 Homo sapiens BCL2 associated X, apoptosis regulator (BAX), transcript variant 1, RNA
product length = 223
Forward primer 1 GGACAGTAACATGGAGCTGC 20
Template 264 283
Reverse primer 1 GAGGAAGTCCAATGTCCAGC 20
Template 486 467

>NM_001291429.2 Homo sapiens BCL2 associated X, apoptosis regulator (BAX), transcript variant gamma, RNA
product length = 223
Forward primer 1 GGACAGTAACATGGAGCTGC 20
Template 212 231
Reverse primer 1 GAGGAAGTCCAATGTCCAGC 20
Template 434 415

>NM_004324.4 Homo sapiens BCL2 associated X, apoptosis regulator (BAX), transcript variant beta, RNA
product length = 223
Forward primer 1 GGACAGTAACATGGAGCTGC 20
Template 264 283
Reverse primer 1 GAGGAAGTCCAATGTCCAGC 20
Template 486 467

>NM_138761.4 Homo sapiens BCL2 associated X, apoptosis regulator (BAX), transcript variant alpha, RNA
product length = 223
Forward primer 1 GGACAGTAACATGGAGCTGC 20
Template 264 283
Reverse primer 1 GAGGAAGTCCAATGTCCAGC 20
Template 486 467

>XM_047419822.1 PREDICTED: Homo sapiens zinc finger protein 273 (ZNF273), transcript variant X26, RNA
product length = 3528
Forward primer 1 GGACAGTAACATGGAGCTGC 20
Template 1284 .....G.G....G....G 1303
Forward primer 1 GGACAGTAACATGGAGCTGC 20
Template 4811 A.C.T.A..A..... 4792

>XM_047419811.1 PREDICTED: Homo sapiens zinc finger protein 273 (ZNF273), transcript variant X15, RNA
product length = 3528
Forward primer 1 GGACAGTAACATGGAGCTGC 20
Template 1284 .....G.G....G....G 1303
Forward primer 1 GGACAGTAACATGGAGCTGC 20
Template 4811 A.C.T.A..A..... 4792

>XM_047419808.1 PREDICTED: Homo sapiens zinc finger protein 273 (ZNF273), transcript variant X12, RNA
product length = 3528
Forward primer 1 GGACAGTAACATGGAGCTGC 20
Template 1284 .....G.G....G....G 1303
Forward primer 1 GGACAGTAACATGGAGCTGC 20
Template 4811 A.C.T.A..A..... 4792

>XM_047419806.1 PREDICTED: Homo sapiens zinc finger protein 273 (ZNF273), transcript variant X10, RNA
product length = 3528

Forward primer 1 GGACAGTAACATGGAGCTGC 20
Template 1230 .....G.G....G....G 1249
Forward primer 1 GGACAGTAACATGGAGCTGC 20
Template 4757 A.C.T.A..A..... 4738

>XM_047419805.1 PREDICTED: Homo sapiens zinc finger protein 273 (ZNF273), transcript variant X9, RNA
product length = 3528
Forward primer 1 GGACAGTAACATGGAGCTGC 20
Template 1179 .....G.G....G....G 1198
Forward primer 1 GGACAGTAACATGGAGCTGC 20
Template 4706 A.C.T.A..A..... 4687

>XM_047419804.1 PREDICTED: Homo sapiens zinc finger protein 273 (ZNF273), transcript variant X8, RNA
product length = 3528
Forward primer 1 GGACAGTAACATGGAGCTGC 20
Template 2014 .....G.G....G....G 2033
Forward primer 1 GGACAGTAACATGGAGCTGC 20
Template 5541 A.C.T.A..A..... 5522

>XM_047419803.1 PREDICTED: Homo sapiens zinc finger protein 273 (ZNF273), transcript variant X7, RNA
product length = 3528
Forward primer 1 GGACAGTAACATGGAGCTGC 20
Template 2020 .....G.G....G....G 2039
Forward primer 1 GGACAGTAACATGGAGCTGC 20
Template 5547 A.C.T.A..A..... 5528

>XM_047419802.1 PREDICTED: Homo sapiens zinc finger protein 273 (ZNF273), transcript variant X6, RNA
product length = 3528
Forward primer 1 GGACAGTAACATGGAGCTGC 20
Template 1284 .....G.G....G....G 1303
Forward primer 1 GGACAGTAACATGGAGCTGC 20
Template 4811 A.C.T.A..A..... 4792

>XM_047419801.1 PREDICTED: Homo sapiens zinc finger protein 273 (ZNF273), transcript variant X5, RNA
product length = 3528
Forward primer 1 GGACAGTAACATGGAGCTGC 20
Template 1284 .....G.G....G....G 1303
Forward primer 1 GGACAGTAACATGGAGCTGC 20
Template 4811 A.C.T.A..A..... 4792

>XM_047419800.1 PREDICTED: Homo sapiens zinc finger protein 273 (ZNF273), transcript variant X4, RNA
product length = 3528
Forward primer 1 GGACAGTAACATGGAGCTGC 20
Template 2058 .....G.G....G....G 2077
Forward primer 1 GGACAGTAACATGGAGCTGC 20
Template 5585 A.C.T.A..A..... 5566

>XM_024446635.2 PREDICTED: Homo sapiens zinc finger protein 273 (ZNF273), transcript variant X3, RNA
product length = 3528
Forward primer 1 GGACAGTAACATGGAGCTGC 20
Template 1269 .....G.G....G....G 1288
Forward primer 1 GGACAGTAACATGGAGCTGC 20
Template 4796 A.C.T.A..A..... 4777

>NM_001083603.3 Homo sapiens patched 1 (PTCH1), transcript variant 1a', RNA
product length = 2514
Forward primer 1 GGACAGTAACATGGAGCTGC 20
Template 4632 TT.....AT..A.... 4613

Reverse primer 1 GAGGAAGTCCAATGTCCAGC 20
Template 2119 C.T.C.....C..... 2138
>NM_001083602.3 Homo sapiens patched 1 (PTCH1), transcript variant 1a, RNA
product length = 2514
Forward primer 1 GGACAGTAACATGGAGCTGC 20
Template 4786 TT.....AT..A.... 4767
Reverse primer 1 GAGGAAGTCCAATGTCCAGC 20
Template 2273 C.T.C.....C..... 2292
>NM_001354918.2 Homo sapiens patched 1 (PTCH1), transcript variant 8, RNA
product length = 2514
Forward primer 1 GGACAGTAACATGGAGCTGC 20
Template 5233 TT.....AT..A.... 5214
Reverse primer 1 GAGGAAGTCCAATGTCCAGC 20
Template 2720 C.T.C.....C..... 2739
>NM_000264.5 Homo sapiens patched 1 (PTCH1), transcript variant 1b, RNA
product length = 2514
Forward primer 1 GGACAGTAACATGGAGCTGC 20
Template 5389 TT.....AT..A.... 5370
Reverse primer 1 GAGGAAGTCCAATGTCCAGC 20
Template 2876 C.T.C.....C..... 2895
>NM_001083606.3 Homo sapiens patched 1 (PTCH1), transcript variant 1d, RNA
product length = 2514
Forward primer 1 GGACAGTAACATGGAGCTGC 20
Template 4482 TT.....AT..A.... 4463
Reverse primer 1 GAGGAAGTCCAATGTCCAGC 20
Template 1969 C.T.C.....C..... 1988
>NM_001083605.3 Homo sapiens patched 1 (PTCH1), transcript variant 1c', RNA
product length = 2514
Forward primer 1 GGACAGTAACATGGAGCTGC 20
Template 4373 TT.....AT..A.... 4354
Reverse primer 1 GAGGAAGTCCAATGTCCAGC 20
Template 1860 C.T.C.....C..... 1879
>NM_001083604.3 Homo sapiens patched 1 (PTCH1), transcript variant 1c, RNA
product length = 2514
Forward primer 1 GGACAGTAACATGGAGCTGC 20
Template 4390 TT.....AT..A.... 4371
Reverse primer 1 GAGGAAGTCCAATGTCCAGC 20
Template 1877 C.T.C.....C..... 1896
>NM_001083607.3 Homo sapiens patched 1 (PTCH1), transcript variant 1e, RNA
product length = 2514
Forward primer 1 GGACAGTAACATGGAGCTGC 20
Template 4546 TT.....AT..A.... 4527
Reverse primer 1 GAGGAAGTCCAATGTCCAGC 20
Template 2033 C.T.C.....C..... 2052
>XM_047436792.1 PREDICTED: Homo sapiens myosin XVB (MYO15B), transcript variant X16, RNA
product length = 656
Forward primer 1 GGACAGTAACATGGAGCTGC 20
Template 570 ...G..GG..C.....A 589
Reverse primer 1 GAGGAAGTCCAATGTCCAGC 20
Template 1225 .....GAG...C.....G 1206
>XM_047436790.1 PREDICTED: Homo sapiens myosin XVB (MYO15B), transcript variant X14, RNA
product length = 656
Forward primer 1 GGACAGTAACATGGAGCTGC 20
Template 653 ...G..GG..C.....A 672
Reverse primer 1 GAGGAAGTCCAATGTCCAGC 20

Template 1308 .....GAG...C.....G 1289

>XM_017025131.3 PREDICTED: Homo sapiens myosin XVB (MYO15B), transcript variant X13, RNA

product length = 656

Forward primer 1 GGACAGTAACATGGAGCTGC 20

Template 672 ...G..GG..C.....A 691

Reverse primer 1 GAGGAAGTCCAATGTCCAGC 20

Template 1327 .....GAG...C.....G 1308

11.3. Search and validation of primers designed against human beclin-1 gene

Table 11.9.: Human beclin-1 canonical gene sequence. Canonical gene sequence was retrieved from the Consensus coding sequence project database [blue – exons, black - introns].

Gene	Human Beclin-1 (BECN-1)
Canonical gene sequence	ATGGAAGGGTCTAAGACGTCCAACAACAGCACCATGCAGGTGAGCTTCGTGTGCCA GCGCTGCAGCCAGCCCCTGAAACTGGACACGAGTTTCAAGATCCTGGACCGTGTCAC CATCCAGGAACTCACAGCTCCATTACTTACCACAGCCCAGGCGAAACCAGGAGAGAC CCAGGAGGAAGAGACTAACTCAGGAGAGGAGCCATTTATTGAAACTCCTCGCCAGG ATGGTGTCTCTCGCAGATTCATCCCCCCAGCCAGGATGATGTCCACAGAAAGTGCCA ACAGCTTCACTCTGATTGGGGAGGCATCTGATGGCGGCACCATGGAGAACCTCAGCC GAAGACTGAAGGTCACTGGGGACCTTTTTGACATCATGTCGGGCCAGACAGATGTG GATCACCCACTCTGTGAGGAATGCACAGATACTCTTTTAGACCAGCTGGACACTCAGC TCAACGTCACTGAAAATGAGTGTCAGAACTACAAACGCTGTTTGGAGATCTTAGAGC AAATGAATGAGGATGACAGTGAACAGTTACAGATGGAGCTAAAGGAGCTGGCACTA GAGGAGGAGAGGCTGATCCAGGAGCTGGAAGACGTGGAAAAGAACCGCAAGATAG TGGCAGAAAATCTCGAGAAGGTCCAGGCTGAGGCTGAGAGACTGGATCAGGAGGA AGCTCAGTATCAGAGAGAATACAGTGAATTTAAACGACAGCAGCTGGAGCTGGATG ATGAGCTGAAGAGTGTTGAAAACCAGATGCGTTATGCCCAGACGCAGCTGGATAAG CTGAAGAAAACCAACGTCTTTAATGCAACCTTCCACATCTGGCACAGTGGACAGTTTG GCACAATCAATAACTTCAGGCTGGGTCGCCTGCCCAGTGTTCCCGTGGAATGGAATG AGATTAATGCTGCTTGGGGCCAGACTGTGTTGCTGCTCCATGCTCTGGCCAATAAGA TGGGTCTGAAATTTCAGAGATACCGACTTGTTCCTTACGGAAACCATTCATATCTGGA GTCTCTGACAGACAAATCTAAGGAGCTGCCGTTATACTGTTCTGGGGGGTTGCGGTT TTTCTGGGACAACAAGTTTGACCATGCAATGGTGGCTTTCCTGGACTGTGTGCAGCA GTTCAAAGAAGAGGTTGAGAAAGGCGAGACACGTTTTTGTCTTCCCTACAGGATGGA TGTGGAGAAAGGCAAGATTGAAGACACAGGAGGCAGTGGCGGCTCCTATTCCATCA AAACCCAGTTTAACTCTGAGGAGCAGTGGACAAAAGCTCTCAAGTTCATGCTGACGA ATCTTAAGTGGGGTCTTGCTTGGGTGTCCTCACAATTTTATAACAAATGA

Table 11.10.: Potential RNA primer-pairs against the human beclin-1 gene. Potential primer pairs were identified through haphazard literature review.

Primer pair	Forward primer (5' – 3')	Reverse primer (5' – 3')	Product size (bases)
Primer	CAAGATCCTGGACCGTGTCA	TGGCACTTTCTGTGG	N.A.
Reference(s)	(Miracco et al., 2007)		
Primer	ACCGTGTCACCATCCAGGAA	GAAGCTGTTGGCACTTTCTGT	N.A.
Reference(s)	(Morikawa et al., 2015)		

Primer	CCTTAACGAAAATTTCCTAT GTCTGTCTATTGG	GCATACCAATAGACAGACATAGGAA TATGC ATTTTCGTTAA	N.A.
Reference(s)	(H. Zhu et al., 2009)		
Primer	ACTGCCTCCTGTGTCTTCAA TCTT	AGCTGCCGTTATACTGTTCTG	N.A.
Reference(s)	(J. Wang et al., 2013)		
Primer	ACCGTGTCACCATCCAGGA A	GAAGCTGTTGGCACTTTCTGT	N.A.
Reference(s)	(Idikio, 2011)		
Primer	GGTTGCCGTTTTTCTGGGA C	TTGATGGAATAGGAGCCGCC	N.A.
Reference(s)	(N. Sun et al., 2019)		
Primer	GGCTGAGAGACTGGATCA GG	5CTGCGTCTGGGCATAACG	N.A.
Reference(s)	(W. Wang et al., 2013)		
Primer	AGTGGCGGCTCCTATTC	GGACACCCAAGCAAGAC	N.A.
Reference(s)	(L. Xu et al., 2021)		
Primer	GGTGTCTCTCGCAGATTCA TC	TCAGTCTTCGGCTGAGGTTCT	121
Reference(s)	(J. Zhu et al., 2018)		
Primer	CAAGATCCTGGACCGTGTC A	TCAGTCTTCGGCTGAGGTTCT	257
Reference(s)	(Miracco et al., 2007)	(J. Zhu et al., 2018)	
Primer	CAGCTGGACACTCAGCTCA A	TTTCCACGTCTTCCAGCTCC	169
Reference(s)	(N. Zhang et al., 2017)		
Primer	ACAACATGCCATCTATAGTT GCC	CCCACATTATCCAACTGTGCATC	N.A.
Reference(s)	(Guo et al., 2018)		

Table 11.11.: Selected tentative RNA primer pair against the human beclin-1 gene.

Forward primer (5’ – 3’)	Reverse primer (5’ – 3’)	Product size (bases)
GAGTTTCAAGATCCTGGACC	CTCCCCAARCAGAGTCAAGC	257

Table 11.12.:Primer-BLAST search parameters and other details for the selected Human beclin-1 RNA primer pair.

Search parameter and other details	
Number of Blast hits analyzed	27523
Entrez query	/
Min total mismatches	2
Min 3' end mismatches	2
Defined 3' end region length	5
Mismatch threshold to ignore targets	6
Max target size	4000
Max number of Blast target sequences	50000
Blast E value	30000
Blast word size	7
Max candidate primer pairs	500
Min PCR product size	70
Max PCR product size	1000

Min Primer size	15
Opt Primer size	20
Max Primer size	25
Min Tm	57
Opt Tm	60
Max Tm	63
Max Tm difference	3
Repeat filter	AUTO
Low complexity filter	Yes

Output 11.3.: Primer-BLAST output for other potential products on unintended templates for the selected human beclin-1 RNA primer pair.

>XM_017025264.3 PREDICTED: Homo sapiens beclin 1 (BECN1), transcript variant X4, RNA
product length = 220
Forward primer 1 GAGTTTCAAGATCCTGGACC 20
Template 239 258
Reverse primer 1 CTCCCCAATCAGAGTGAAGC 20
Template 458 439
>XM_005257760.5 PREDICTED: Homo sapiens beclin 1 (BECN1), transcript variant X3, RNA
product length = 220
Forward primer 1 GAGTTTCAAGATCCTGGACC 20
Template 217 236
Reverse primer 1 CTCCCCAATCAGAGTGAAGC 20
Template 436 417
>XM_017025263.3 PREDICTED: Homo sapiens beclin 1 (BECN1), transcript variant X2, RNA
product length = 220
Forward primer 1 GAGTTTCAAGATCCTGGACC 20
Template 239 258
Reverse primer 1 CTCCCCAATCAGAGTGAAGC 20
Template 458 439
>XM_005257759.4 PREDICTED: Homo sapiens beclin 1 (BECN1), transcript variant X1, RNA
product length = 220
Forward primer 1 GAGTTTCAAGATCCTGGACC 20
Template 217 236
Reverse primer 1 CTCCCCAATCAGAGTGAAGC 20
Template 436 417
>NM_003766.5 Homo sapiens beclin 1 (BECN1), transcript variant 1, RNA
product length = 220
Forward primer 1 GAGTTTCAAGATCCTGGACC 20
Template 239 258
Reverse primer 1 CTCCCCAATCAGAGTGAAGC 20
Template 458 439
>NM_001313998.2 Homo sapiens beclin 1 (BECN1), transcript variant 2, RNA
product length = 220
Forward primer 1 GAGTTTCAAGATCCTGGACC 20
Template 217 236
Reverse primer 1 CTCCCCAATCAGAGTGAAGC 20
Template 436 417
>NM_001313999.1 Homo sapiens beclin 1 (BECN1), transcript variant 3, RNA
product length = 220
Forward primer 1 GAGTTTCAAGATCCTGGACC 20
Template 89 108
Reverse primer 1 CTCCCCAATCAGAGTGAAGC 20

Template 308 289

>XM_017017209.2 PREDICTED: Homo sapiens neurexophilin and PC-esterase domain family member 2 (NXPE2), transcript variant X3, RNA

product length = 676

Reverse primer 1 CTCCCCAATCAGAGTGAAGC 20

Template 3636 .....AG.A..... 3617

Reverse primer 1 CTCCCCAATCAGAGTGAAGC 20

Template 2961 .....AG.A..... 2980

>XM_017017207.2 PREDICTED: Homo sapiens neurexophilin and PC-esterase domain family member 2 (NXPE2), transcript variant X2, RNA

product length = 676

Reverse primer 1 CTCCCCAATCAGAGTGAAGC 20

Template 3389 .....AG.A..... 3370

Reverse primer 1 CTCCCCAATCAGAGTGAAGC 20

Template 2714 .....AG.A..... 2733

>XM_006724329.4 PREDICTED: Homo sapiens ess-2 splicing factor homolog (ESS2), transcript variant X2, RNA

product length = 3089

Forward primer 1 GAGTTTCAAGATCCTGGACC 20

Template 1263 AGC...T.....G. 1282

Forward primer 1 GAGTTTCAAGATCCTGGACC 20

Template 4351 .GC.G.....A.C.... 4332

>XM_005261282.5 PREDICTED: Homo sapiens ess-2 splicing factor homolog (ESS2), transcript variant X1, RNA

product length = 3089

Forward primer 1 GAGTTTCAAGATCCTGGACC 20

Template 1040 AGC...T.....G. 1059

Forward primer 1 GAGTTTCAAGATCCTGGACC 20

Template 4128 .GC.G.....A.C.... 4109

>NM_022719.3 Homo sapiens ess-2 splicing factor homolog (ESS2), transcript variant 1, RNA

product length = 3089

Forward primer 1 GAGTTTCAAGATCCTGGACC 20

Template 1037 AGC...T.....G. 1056

Forward primer 1 GAGTTTCAAGATCCTGGACC 20

Template 4125 .GC.G.....A.C.... 4106

11.4. Search and validation of primers designed against human caspase-3 gene

Table 11.13.: Human caspase-3 canonical gene sequence. Canonical gene sequence was retrieved from the Consensus coding sequence project database [blue – exons, black - introns].

Gene	Human Caspase-3 (Casp-3)
Canonical gene sequence	ATGGAGAACACTGAAAACTCAGTGGATTCAAAATCCATTAAAAATTTGGAACCAAAGA TCATACATGGAAGCGAATCAATGGACTCTGGAATATCCCTGGACAACAGTTATAAAAT GGATTATCCTGAGATGGGTTTATGTATAATAATTAATAATAAGAATTTTCATAAAAGCA CTGGAATGACATCTCGGTCTGGTACAGATGTCGATGCAGCAAACCTCAGGGAAACATT CAGAAACTTGAAATATGAAGTCAGGAATAAAAATGATCTTACACGTGAAGAAATTGTG GAATTGATGCGTGATGTTTCTAAAGAAGATCACAGCAAAAGGAGCAGTTTTGTTTGTG TGCTTCTGAGCCATGGTGAAGAAGGAATAATTTTTGGAACAAATGGACCTGTTGACCT GAAAAAAATAACAAACTTTTTCAGAGGGGATCGTTGTAGAAGTCTAACTGGAAAACCC AAACTTTTCATTATTCAGGCCTGCCGTGGTACAGAACTGGACTGTGGCATTGAGACAGA CAGTGGTGTTGATGATGACATGGCGTGTCATAAAATACCAGTGGAGGCCGACTTCTTG TATGCATACTCCACAGCACCTGGTTATTATTCTTGGCGAAATTCAAAGGATGGCTCCTG GTTCATCCAGTCGCTTTGTGCCATGCTGAAACAGTATGCCGACAAGCTTGAATTTATGC

	ACATTCTTACCCGGGTTAACCGAAAGGTGGCAACAGAATTTGAGTCCTTTTCCTTTGAC GCTACTTTTCATGCAAAGAAACAGATTCCATGTATTGTTTCCATGCTCACAAAAGAACTC TATTTTTATCACTAA

Table 11.14.: Potential RNA primer-pairs against the human caspase-3 gene. Potential primer pairs were identified through haphazard literature review.

Primer pair	Forward primer (5' – 3')	Reverse primer (5' – 3')	Product size (bases)
Primer	GGAAGCGAATCAATGGACT CTGG	GCATCGACATCTGTACCAGAC C	N.A.
Reference(s)	(OriGene Technologies, Inc., 2022b)		
Primer	TTGCTGCATCGACATCTGTA	TGGATTATCCTGAGATG GTTT	N.A.
Reference(s)	(Park et al., 2018)		
Primer	GGCTCAGAAGCACACAAAC A	AGCACTGGAATGACATCTCG	N.A.
Reference(s)	(J. Chen et al., 2016)		
Primer	ATGGAGAACACTGAAAACT CAGTGGATT	CCACCAACCAACCATTTCTTT AGTG	N.A.
Reference(s)	(Dohmoto et al., 2001)		
Primer	TGAGCATGGAAACAATACA TGG	ATTCTTGGCGAAATTCAAAG G	N.A.
Reference(s)	(Jin et al., 2022)		
Primer	AAA*GGATCC*TTAATAAAGG TATCCATGGAGAACACT	AAA*GAATTC*TTAGTGATAAA AATAGAGTTCTTTTGTGAG	N.A.
Reference(s)	(Jänicke et al., 1998)		
Primer	AAA*GGATCC*AAAGATCAT ACATGGAAGCGAATCAAT	AAA*GAATTC*CATCACGCATCAA TTCCACAATTTCTT	N.A.
Reference(s)	(Jänicke et al., 1998)		
Primer	TGCGTGTGGAGTATTTGG ATG	TGGTACAGTCAGAGCCAACCTC	N.A.
Reference(s)	(Deng et al., 2019)		
Primer	TGTTTGTGTGCTTCTGAG CC	CACGCCATGTCATCATCAAC	N.A.
Reference(s)	(D.-H. Wang et al., 2012)		
Primer	TCGCTGCAAATCGCTGGT	CTGTGGAGAAGGCGTAGAGGA	N.A.
Reference(s)	(S. Li et al., 2019)		
Primer	AGCAAACCTCAGGGAAA CATT	CTCAGAAGCACACAAACAAAA CT	N.A.
Reference(s)	(Qian et al., 2018)		
Primer	TATGGTTTTGTGATGTTT GTCC	TAGATCCAGGGGCATTGTAG	N.A.
Reference(s)	(Baharara et al., 2015)		
Primer	TGACAGCCAGTGAGACTT GG	GACTCTAGACGGCATCCAGC	N.A.
Reference(s)	(Gibot et al., 2009)		
Primer	AGGACTCTAGACGGCATC CA	CAGTGAGACTTGGTGCAGTA	N.A.
Reference(s)	(Ali et al., 2018)		
Primer	GGTTAACCCGGGTAAGA ATGTGCA	CTCGGTCTGGTACAGATGTCGA TG	N.A.
Reference(s)	(L. S. Wang et al., 2000)		
Primer	CCGACTTCCTGTATGCTTA CTCTA	CATGACCCGTCCCTTGAA	N.A.

Reference(s)	(Mukherjee et al., 2013)		
Primer	CAGTGGAGGCCGACTTCTTG	TGGCACAAAGCGACTGGA	63
Reference(s)	(Ho et al., 2009)		
Primer	AATTCAAGGGACGGGTCATG	GCTTGTGCGCGTACAGTTTC	N.A.
Reference(s)	(Cao et al., 2007)		
Primer	AGCAAACCTCAGGGAAACATT	CACGCCATGTCATCATCAAC	339
Reference(s)	(Qian et al., 2018)	(Mitupatum et al., 2016)	
Primer	ATGGAGAACACTGAAAACTCAGTGGATT	AATGTTTCCCTGAGGTTTGCT	233
Reference(s)	(Dohmoto et al., 2001)	(Qian et al., 2018)	
Primer	AATTGCCTCCACACCTTCAC	TCACCAAGCTGCTCATCAAC	N.A.
Reference(s)	(Yang et al., 2017)		

Table 11.15.: Selected tentative RNA primer pair against the human caspase-3 gene.

Forward primer (5’ – 3’)	Reverse primer (5’ – 3’)	Product size (bases)
GAGAACACTGAAAACTCAGTGG	GAATGTTTCCCTGAGGTTTGC	233

Table 11.16.: Primer-BLAST search parameters and other details for the selected human caspase-3 Peptidase RNA primer pair.

Search parameter and other details	
Number of Blast hits analyzed	40980
Entrez query	/
Min total mismatches	2
Min 3' end mismatches	2
Defined 3' end region length	5
Mismatch threshold to ignore targets	6
Max target size	4000
Max number of Blast target sequences	50000
Blast E value	30000
Blast word size	7
Max candidate primer pairs	500
Min PCR product size	70
Max PCR product size	1000
Min Primer size	15
Opt Primer size	20
Max Primer size	25
Min Tm	57
Opt Tm	60
Max Tm	63
Max Tm difference	3
Repeat filter	AUTO
Low complexity filter	Yes

Output 11.4.: Primer-BLAST output for other potential products on unintended templates for the selected human caspase-3 RNA primer pair.

>XM_047416239.1 PREDICTED: Homo sapiens caspase 3 (CASP3), transcript variant X4, RNA
product length = 231
Forward primer 1 GAGAACACTGAAAACTCAGTGG 22
Template 431 452
Reverse primer 1 GAATGTTTCCCTGAGGTTTGC 21
Template 661 641
>XM_047416238.1 PREDICTED: Homo sapiens caspase 3 (CASP3), transcript variant X3, RNA
product length = 231
Forward primer 1 GAGAACACTGAAAACTCAGTGG 22
Template 488 509
Reverse primer 1 GAATGTTTCCCTGAGGTTTGC 21
Template 718 698
>XM_047416237.1 PREDICTED: Homo sapiens caspase 3 (CASP3), transcript variant X2, RNA
product length = 231
Forward primer 1 GAGAACACTGAAAACTCAGTGG 22
Template 469 490
Reverse primer 1 GAATGTTTCCCTGAGGTTTGC 21
Template 699 679
>XM_047416236.1 PREDICTED: Homo sapiens caspase 3 (CASP3), transcript variant X1, RNA
product length = 231
Forward primer 1 GAGAACACTGAAAACTCAGTGG 22
Template 526 547
Reverse primer 1 GAATGTTTCCCTGAGGTTTGC 21
Template 756 736
>NM_001354783.2 Homo sapiens caspase 3 (CASP3), transcript variant 9, RNA
product length = 231
Forward primer 1 GAGAACACTGAAAACTCAGTGG 22
Template 431 452
Reverse primer 1 GAATGTTTCCCTGAGGTTTGC 21
Template 661 641
>NM_032991.3 Homo sapiens caspase 3 (CASP3), transcript variant 2, RNA
product length = 231
Forward primer 1 GAGAACACTGAAAACTCAGTGG 22
Template 72 93
Reverse primer 1 GAATGTTTCCCTGAGGTTTGC 21
Template 302 282
>NM_001354779.2 Homo sapiens caspase 3 (CASP3), transcript variant 5, RNA
product length = 227
Forward primer 1 GAGAACACTGAAAACTCAGTGG 22
Template 72 93

Reverse primer 1 GAATGTTTCCCTGAGGTTTGC 21
Template 298 278

>NM_001354777.2 Homo sapiens caspase 3 (CASP3), transcript variant 3, RNA
product length = 231
Forward primer 1 GAGAACACTGAAAACTCAGTGG 22
Template 201 222

Reverse primer 1 GAATGTTTCCCTGAGGTTTGC 21
Template 431 411
>NM_001354780.2 Homo sapiens caspase 3 (CASP3), transcript variant 6, RNA
product length = 227
Forward primer 1 GAGAACACTGAAAACTCAGTGG 22

Template 239 260

Reverse primer 1 GAATGTTTCCCTGAGGTTTGC 21
Template 465 445
>NM_001354784.2 Homo sapiens caspase 3 (CASP3), transcript variant 10, RNA
product length = 227
Forward primer 1 GAGAACACTGAAAACTCAGTGG 22
Template 72 93

Reverse primer 1 GAATGTTTCCCTGAGGTTTGC 21
Template 298 278
>NM_001354781.2 Homo sapiens caspase 3 (CASP3), transcript variant 7, RNA
product length = 231
Forward primer 1 GAGAACACTGAAAACTCAGTGG 22
Template 72 93

Reverse primer 1 GAATGTTTCCCTGAGGTTTGC 21
Template 302 282
>NM_001354782.2 Homo sapiens caspase 3 (CASP3), transcript variant 8, RNA
product length = 231
Forward primer 1 GAGAACACTGAAAACTCAGTGG 22
Template 239 260
Reverse primer 1 GAATGTTTCCCTGAGGTTTGC 21
Template 469 449

>NM_004346.4 Homo sapiens caspase 3 (CASP3), transcript variant 1, RNA
product length = 231
Forward primer 1 GAGAACACTGAAAACTCAGTGG 22
Template 239 260
Reverse primer 1 GAATGTTTCCCTGAGGTTTGC 21
Template 469 449

11.5. Search and validation of primers designed against human pyruvate kinase isozyme-2 gene

Table 11.17.: Human pyruvate kinase isozyme-2 gene sequence. Canonical gene sequence was retrieved from the Consensus coding sequence project database [blue – exons, black - introns].

Gene	Human Pyruvate Kinase Isozyme 2 (PKM2)
Canonical gene sequence	ATGTCGAAGCCCCATAGTGAAGCCGGGACTGCCTTCATTCAGACCCAGCAGCTGCACG CAGCCATGGCTGACACATTCCTGGAGCACATGTGCCGCCTGGACATTGATTCACCACCC ATCACAGCCCGGAACACTGGCATCATCTGTACCATTGGCCCAGCTTCCCGATCAGTGGA GACGTTGAAGGAGATGATTAAGTCTGGAATGAATGTGGCTCGTCTGAACTTCTCTCAT GGAACTCATGAGTACCATGCGGAGACCATCAAGAATGTGCGCACAGCCACGGAAAGC TTTGCTTCTGACCCCATCCTCTACCGGCCCGTTGCTGTGGCTCTAGACACTAAAGGACCT GAGATCCGAACTGGGCTCATCAAGGGCAGCGGCACTGCAGAGGTGGAGCTGAAGAA GGGAGCCACTCTCAAAATCACGCTGGATAACGCCTACATGGAAAAGTGTGACGAGAAC ATCCTGTGGCTGGACTACAAGAACATCTGCAAGGTGGTGGAAGTGGGCAGCAAGATC TACGTGGATGATGGGCTTATTTCTCTCCAGGTGAAGCAGAAAGGTGCCGACTTCCTGG TGACGGAGGTGGAAAATGGTGGCTCCTTGGGCAGCAAGAAGGGTGTGAACCTTCCTG GGGCTGCTGTGGACTTGCCTGCTGTGTCGGAGAAGGACATCCAGGATCTGAAGTTTGG GGTCGAGCAGGATGTTGATATGGTGTTTGCGTCATTCATCCGCAAGGCATCTGATGTCC ATGAAGTTAGGAAGGTCCTGGGAGAGAAGGGAAAGAACATCAAGATTATCAGCAAAA

	TCGAGAATCATGAGGGGGTTCGGAGGTTTGATGAAATCCTGGAGGCCAGTGATGGGA TCATGGTGGCTCGTGGTGATCTAGGCATTGAGATTCCTGCAGAGAAGGTCTTCCTTGCT CAGAAGATGATGATTGGACGGTGCAACCGAGCTGGGAAGCCTGTCATCTGTGCTACTC AGATGCTGGAGAGCATGATCAAGAAGCCCCGCCCCACTCGGGCTGAAGGCAGTGATG TGGCCAATGCAGTCCTGGATGGAGCCGACTGCATCATGCTGTCTGGAGAAACAGCCAA AGGGGACTATCCTCTGGAGGCTGTGCGCATGCAGCACCTGATTGCCCGTGAGGCAGA GGCTGCCATCTACCACTTGCAATTATTTGAGGAACTCCGCCGCCTGGCGCCCATTACCA GCGACCCCACAGAAGCCACCGCCGTGGGTGCCGTGGAGGCCTCCTTCAAGTGCTGCAG TGGGGCCATAATCGTCCTCACCAAGTCTGGCAGGTCTGCTCACCAGGTGGCCAGATAC CGCCCACGTGCCCCCATCATTGCTGTGACCCGGAATCCCCAGACAGCTCGTCAGGCCCA CCTGTACCGTGGCATCTTCCCTGTGCTGTGCAAGGACCCAGTCCAGGAGGCCTG GGCTGAGGACGTGGACCTCCGGGTGAACTTTGCCATGAATGTTGGCAAGGCCCGAGG CTTCTTCAAGAAGGGAGATGTGGTCATTGTGCTGACCGGATGGCGCCCTGGCTCCGGC TTCACCAACACCATGCGTGTTGTTCCTGTGCCGTGA

Table 11.18.: Potential RNA primer-pairs against the human pyruvate kinase isozyme-2. Potential primer pairs were identified through haphazard literature review.

Primer pair	Forward primer (5’ – 3’)	Reverse primer (5’ – 3’)	Product size (bases)
Primer	ATGGCTGACACATTCCTG GAGC	CCTTCAACGTCTCCACTGATCG	N.A.
Reference(s)	(OriGene Technologies, Inc., 2022c)		
Primer	ATGTCGAAGCCCCATAGT GAA	TGGACATTGATTCACCACCCA	118
Reference(s)	(X. Zhang et al., 2020)		
Primer	ATGGCTGACACATTCCTG GAGC	TGGACATTGATTCACCACCC	187
Reference(s)	(OriGene Technologies, Inc., 2022c)	(X. Zhang et al., 2020)	
Primer	GAGGCCTCCTTCAAGTGC	CAGACTTGGTGAGGACGAT	N.A.
Reference(s)	(Mukherjee et al., 2013)		
Primer	CTATCCTCTGGAGGCTGT GC	GTGGGGTCGCTGGTAATG	N.A.
Reference(s)	(Morita et al., 2018)		
Primer	CAGCCAAAGGGGACTAT CCT	TTCCTCAAATAATTGCAAGTGG	N.A.
Reference(s)	(Morita et al., 2018)		
Primer	CAGCCAAAGGGGACTAT CCT	CAGACTTGGTGAGGACGAT	210
Reference(s)	Morita et al., 2018)	(Mukherjee et al., 2013)	

Table 11.19.: Selected tentative RNA primer pair against the human pyruvate kinase isozyme-2 gene.

Forward primer (5’ – 3’)	Reverse primer (5’ – 3’)	Product size (bases)
ACAGCCAAAGGGGACTATCC	CTTGGTGAGGACGATTATGG	210

Table 11.20.: Primer-BLAST search parameters and other details for the selected human pyruvate kinase isozyme-2 RNA primer pair.

Search parameter and other details	
Number of Blast hits analyzed	15010
Entrez query	/

Min total mismatches	2
Min 3' end mismatches	2
Defined 3' end region length	5
Mismatch threshold to ignore targets	6
Max target size	4000
Max number of Blast target sequences	50000
Blast E value	30000
Blast word size	7
Max candidate primer pairs	500
Min PCR product size	70
Max PCR product size	1000
Min Primer size	15
Opt Primer size	20
Max Primer size	25
Min Tm	57
Opt Tm	60
Max Tm	63
Max Tm difference	3
Repeat filter	AUTO
Low complexity filter	Yes

Output 11.5.: Primer-BLAST output for other potential products on unintended templates for the selected human pyruvate kinase isozyme-2 RNA primer pair.

>NM_001411081.1 Homo sapiens pyruvate kinase M1/2 (PKM), RNA
product length = 207
Forward primer 1 ACAGCCAAAGGGGACTATCC 20
Template 1518 1537
Reverse primer 1 CTTGGTGAGGACGATTATGG 20
Template 1724 1705
>XM_005254445.6 PREDICTED: Homo sapiens pyruvate kinase M1/2 (PKM), transcript variant X9, RNA
product length = 207
Forward primer 1 ACAGCCAAAGGGGACTATCC 20
Template 1248 1267
Reverse primer 1 CTTGGTGAGGACGATTATGG 20
Template 1454 1435
>XM_047432666.1 PREDICTED: Homo sapiens pyruvate kinase M1/2 (PKM), transcript variant X8, RNA
product length = 207
Forward primer 1 ACAGCCAAAGGGGACTATCC 20
Template 2560 2579
Reverse primer 1 CTTGGTGAGGACGATTATGG 20
Template 2766 2747
>XM_047432664.1 PREDICTED: Homo sapiens pyruvate kinase M1/2 (PKM), transcript variant X6, RNA
product length = 207
Forward primer 1 ACAGCCAAAGGGGACTATCC 20
Template 3413 3432
Reverse primer 1 CTTGGTGAGGACGATTATGG 20
Template 3619 3600
>XM_005254443.2 PREDICTED: Homo sapiens pyruvate kinase M1/2 (PKM), transcript variant X4, RNA
product length = 207

Forward primer 1 ACAGCCAAAGGGGACTATCC 20
Template 3530 3549
Reverse primer 1 CTTGGTGAGGACGATTATGG 20
Template 3736 3717
>XM_047432662.1 PREDICTED: Homo sapiens pyruvate kinase M1/2 (PKM), transcript variant X1, RNA
product length = 207
Forward primer 1 ACAGCCAAAGGGGACTATCC 20
Template 1345 1364
Reverse primer 1 CTTGGTGAGGACGATTATGG 20
Template 1551 1532
>NM_001206798.3 Homo sapiens pyruvate kinase M1/2 (PKM), transcript variant 6, RNA
product length = 207
Forward primer 1 ACAGCCAAAGGGGACTATCC 20
Template 1206 1225
Reverse primer 1 CTTGGTGAGGACGATTATGG 20
Template 1412 1393
>NM_001206797.3 Homo sapiens pyruvate kinase M1/2 (PKM), transcript variant 5, RNA
product length = 207
Forward primer 1 ACAGCCAAAGGGGACTATCC 20
Template 959 978
Reverse primer 1 CTTGGTGAGGACGATTATGG 20
Template 1165 1146
>NM_002654.6 Homo sapiens pyruvate kinase M1/2 (PKM), transcript variant 1, RNA
product length = 207
Forward primer 1 ACAGCCAAAGGGGACTATCC 20
Template 1181 1200
Reverse primer 1 CTTGGTGAGGACGATTATGG 20
Template 1387 1368
>XM_011521670.2 PREDICTED: Homo sapiens pyruvate kinase M1/2 (PKM), transcript variant X5, RNA
product length = 207
Forward primer 1 ACAGCCAAAGGGGACTATCC 20
Template 1401 1420
Reverse primer 1 CTTGGTGAGGACGATTATGG 20
Template 1607 1588

11.6. Search and validation of primers designed against human vascular endothelial growth factor gene

Table 11.21.: Human vascular endothelial growth factor A canonical gene sequence. Canonical gene sequence was retrieved from the Consensus coding sequence project database [blue – exons, black - introns].

Gene	Human Vascular Endothelial Growth Factor A (VEGFA)
Canonical gene sequence	ATGAACTTTCTGCTGTCTTGGGTGCATTGGAGCCTTGCCTTGCTGCTCTACCTCCACCATGCCAA GTGGTCCCAGGCTGCACCCATGGCAGAAGGAGGAGGGCAGAATCATCACGAAGTGGTGAAGT TCATGGATGTCTATCAGCGCAGCTACTGCCATCCAATCGAGACCCTGGTGGACATCTTCCAGGA GTACCCTGATGAGATCGAGTACATCTTCAAGCCATCGCGGGGGCTGCTGCAATGACGAGGGCC TGGAGTGTGTGCCCACTGAGGAGTCCAACATCACCATGCAGATTATGCGGATCAAACCTCACC AAGGCCAGCACATAGGAGAGATGAGCTTCCTACAGCACAACAAATGTGAATGCAGACCAAAG AAAGATAGAGCAAGACAAGAAAAAAAATCAGTTCGAGGAAAGGGAAAGGGGCAAAAACGAA

	AGCGCAAGAAATCCCGGTATAAGTCCTGGAGCGTGTACGTTGGTGCCCGCTGCTGTCTAATGC CCTGGAGCCTCCCTGGCCCCCATCCCTGTGGGCCTTGCTCAGAGCGGAGAAAGCATTTGTTTGT ACAAGATCCGCAGACGTGTAAATGTTCCTGCAAAAACACAGACTCGCGTTGCAAGGCGAGGCA GCTTGAGTTAAACGAACGTACTTGCAGATGTGACAAGCCGAGGCGGTGA

Table 11.22.: Potential RNA primer-pairs against the vascular endothelial growth factor A gene. Potential primer pairs were identified through haphazard literature review.

Primer pair	Forward primer (5’ – 3’)	Reverse primer (5’ – 3’)	Product size (bases)
Primer	5TGCAGATTATGCGGATCA AACC	TGCATTCACATTTGTTGTGCTGTAG	81
Reference(s)	(Chung et al., 2004)		
Primer	TTGCCTTGCTGCTCTACCTC CA	GATGGCAGTAGCTGCGCTGATA	N.A.
Reference(s)	(OriGene Technologies, Inc., 2022d)		
Primer	TTGCCTTGCTGCTCTACCTC CA	TGCATTCACATTTGTTGTGCTGTAG	355
Reference(s)	(OriGene Technologies, Inc., 2022d)	(Chung et al., 2004)	
Primer	GGGCAGAATCATCACGAAG T	ATCTGCATGGTGATGTTGGA	218
Reference(s)	(Clifford et al., 2008)		
Primer	GAGTACCCTGATGAGATCG AG	TCACCGCCTCGGCTTGT CACA	510
Reference(s)	(Abdel-Majid & Marshall, 2004)		
Primer	5GGAGAGATGAGCTTCCTA CAG	TCACCGCCTCGGCTTGT CACA	342
Reference(s)	(Abdel-Majid & Marshall, 2004)		
Primer	5’-ATGACGAGGGCCTGGAGT GTG-3’	5’-CCTATGTGCTGGCCTTGGTGAG-3’ (CTCACCAAGGCCAGCACATAGG)	N.A.
Reference(s)	(Zaravinos et al., 2008)		
Primer	5’-GCTACTGCCGTCCGATTGA GAC-3’	5’-GTGCTGGCTTTGGTGAGGTTTG-3’ (CAAACCTCACCAAAGCCAGCAC)	N.A.
Reference(s)	(Chiu et al., 2013)		
Primer	AGCCTTGCCTTGCTGCTCTA	GTGATGATTCTGCCCTCCTCCT	86
Reference(s)	(Vrtačnik et al., 2018)		
Primer	CAGAGGAGGAGGGCAGAA T	ATCGCATCAGGGGCACACAG	N.A.
Reference(s)	(Di Tommaso et al., 2013)		
Primer	AGCCTTGCCTTGCTGCTCTA	ATCGCATCAGGGGCACACAG	217
Reference(s)	(Vrtačnik et al., 2018)	(Di Tommaso et al., 2013)	

Table 11.23.: Selected tentative RNA primer pair against the human vascular endothelial growth factor A gene.

Forward primer (5’ – 3’)	Reverse primer (5’ – 3’)	Product size (bases)
TGTCTTGGGTGCATTGGAGC	GGCACACAGGATGGCTTGAA	217

Table 11.24.: Primer-BLAST search parameters and other details for the selected human vascular endothelial growth factor RNA primer pair.

Search parameter and other details

Number of Blast hits analyzed	15010
Entrez query	/
Min total mismatches	2
Min 3' end mismatches	2
Defined 3' end region length	5
Mismatch threshold to ignore targets	6
Max target size	4000
Max number of Blast target sequences	50000
Blast E value	30000
Blast word size	7
Max candidate primer pairs	500
Min PCR product size	70
Max PCR product size	1000
Min Primer size	15
Opt Primer size	20
Max Primer size	25
Min Tm	57
Opt Tm	60
Max Tm	63
Max Tm difference	3
Repeat filter	AUTO
Low complexity filter	Yes

Output 11.6.: Primer-BLAST output for other potential products on unintended templates for the selected human vascular endothelial growth factor A RNA primer pair.

>NM_001411081.1 Homo sapiens pyruvate kinase M1/2 (PKM), RNA
product length = 207
Forward primer 1 ACAGCCAAAGGGGACTATCC 20
Template 1518 1537
Reverse primer 1 CTTGGTGAGGACGATTATGG 20
Template 1724 1705

>XM_005254445.6 PREDICTED: Homo sapiens pyruvate kinase M1/2 (PKM), transcript variant X9, RNA
product length = 207
Forward primer 1 ACAGCCAAAGGGGACTATCC 20
Template 1248 1267
Reverse primer 1 CTTGGTGAGGACGATTATGG 20
Template 1454 1435

>XM_047432666.1 PREDICTED: Homo sapiens pyruvate kinase M1/2 (PKM), transcript variant X8, RNA
product length = 207
Forward primer 1 ACAGCCAAAGGGGACTATCC 20
Template 2560 2579
Reverse primer 1 CTTGGTGAGGACGATTATGG 20
Template 2766 2747

>XM_047432664.1 PREDICTED: Homo sapiens pyruvate kinase M1/2 (PKM), transcript variant X6, RNA
product length = 207
Forward primer 1 ACAGCCAAAGGGGACTATCC 20
Template 3413 3432
Reverse primer 1 CTTGGTGAGGACGATTATGG 20
Template 3619 3600

>XM_005254443.2 PREDICTED: Homo sapiens pyruvate kinase M1/2 (PKM), transcript variant X4, RNA
product length = 207
Forward primer 1 ACAGCCAAAGGGGACTATCC 20
Template 3530 3549
Reverse primer 1 CTTGGTGAGGACGATTATGG 20
Template 3736 3717
>XM_047432662.1 PREDICTED: Homo sapiens pyruvate kinase M1/2 (PKM), transcript variant X1, RNA
product length = 207
Forward primer 1 ACAGCCAAAGGGGACTATCC 20
Template 1345 1364
Reverse primer 1 CTTGGTGAGGACGATTATGG 20
Template 1551 1532
>NM_001206798.3 Homo sapiens pyruvate kinase M1/2 (PKM), transcript variant 6, RNA
product length = 207
Forward primer 1 ACAGCCAAAGGGGACTATCC 20
Template 1206 1225
Reverse primer 1 CTTGGTGAGGACGATTATGG 20
Template 1412 1393
>NM_001206797.3 Homo sapiens pyruvate kinase M1/2 (PKM), transcript variant 5, RNA
product length = 207
Forward primer 1 ACAGCCAAAGGGGACTATCC 20
Template 959 978
Reverse primer 1 CTTGGTGAGGACGATTATGG 20
Template 1165 1146
>NM_002654.6 Homo sapiens pyruvate kinase M1/2 (PKM), transcript variant 1, RNA
product length = 207
Forward primer 1 ACAGCCAAAGGGGACTATCC 20
Template 1181 1200
Reverse primer 1 CTTGGTGAGGACGATTATGG 20
Template 1387 1368
>XM_011521670.2 PREDICTED: Homo sapiens pyruvate kinase M1/2 (PKM), transcript variant X5, RNA
product length = 207
Forward primer 1 ACAGCCAAAGGGGACTATCC 20
Template 1401 1420
Reverse primer 1 CTTGGTGAGGACGATTATGG 20
Template 1607 1588

11.7. Search and validation of primers designed against human activating transcription factor 6 A gene

Table 11.25.: Human activating transcription factor 6 A canonical gene sequence. Canonical gene sequence was retrieved from the Consensus coding sequence project database [blue – exons, black - introns].

Gene	ATF6A
Canonical gene sequence	ATGGGGGAGCCGGCTGGGGTTGCCGGCACCATGGAGTCACCTTTTAGCCCGGGACTCT TTCACAGGCTGGATGAAGATTGGGATTCTGCTCTCTTTGCTGAACTCGGTTATTTCACA GACACTGATGAGCTGCAATTGGAAGCAGCAAATGAGACGTATGAAAACAATTTTGATA ATCTTGATTTTGATTTGGATTTGATGCCTTGGGAGTCAGACATTTGGGACATCAACAAC CAAATCTGTACAGTTAAAGATATTAAGGCAGAACCTCAGCCACTTTCTCCAGCCTCCTC

AAGTTATTCAGTCTCGTCTCCTCGGTCAGTGGACTCTTATTCTTCAACTCAGCATGTTCC
TGAGGAGTTGGATTTGTCTTCTAGTTCTCAGATGTCTCCCCTTTCCTTATATGGTGAAAA
CTCTAATAGTCTCTCTTCAGCGGAGCCACTGAAGGAAGATAAGCCTGTCACTGGTCCTA
GGAACAAGACTGAAAATGGACTGACTCCAAAGAAAAAAATTCAGGTGAATTCAAAACC
TTCAATTCAGCCCAAGCCTTTATTGCTTCCAGCAGCACCCAAGACTCAAACAAACTCCA
GTGTTCCAGCAAAAACCATCATTATTCAGACAGTACCAACGCTTATGCCATTGGCAAAG
CAGCAACCAATTATCAGTTTACAACCTGCACCCACTAAAGGCCAGACGGTTTTGCTGTC
TCAGCCTACTGTGGTACAACTTCAAGCACCTGGAGTTCTGCCCTCTGCTCAGCCAGTCCT
TGCTGTTGCTGGGGGAGTCACACAGCTCCCTAATCACGTGGTGAATGTGGTACCAGCC
CCTTCAGCGAATAGCCCAGTGAATGGAAAACTTTCCGTGACTAAACCTGTCCTACAAAG
TACCATGAGAAATGTCGGTTCAGATATTGCTGTGCTAAGGAGACAGCAACGTATGATA
AAAAATCGAGAATCCGCTTGTCAGTCTCGCAAGAAGAAGAAAGAATATATGCTAGGGT
TAGAGGCGAGATTAAAGGCTGCCCTCTCAGAAAACGAGCAACTGAAGAAAGAAAATG
GAACACTGAAGCGGCAGCTGGATGAAGTTGTGTCAGAGAACCAGAGGCTTAAAGTCC
CTAGTCCAAAGCGAAGAGTTGTCTGTGTGATGATAGTATTGGCATTTATAATACTGAAC
TATGGACCTATGAGCATGTTGGAACAGGATTCCAGGAGAATGAACCCTAGTGTGAGCC
CTGCAAATCAAAGGAGGCACCTTCTAGGATTTTCTGCTAAAGAGGCACAGGACACATC
AGATGGTATTATCCAGAAAAACAGCTACAGATATGATCATTCTGTTTCAAATGACAAAG
CCCTGATGGTGCTAACTGAAGAACCATTGCTTTACATTCCTCCACCTCCTTGTCAGCCCC
TAATTAACACAACAGAGTCTCTCAGGTTAAATCATGAACTTCGAGGATGGGTTCATAGA
CATGAAGTAGAAAGGACCAAGTCAAGAAGAATGACAAATAATCAACAGAAAACCCGT
ATTCTTCAGGGTGCTCTGGAACAGGGCTCAAATTCTCAGCTGATGGCTGTTCAATACAC
AGAAACCACTAGTAGTATCAGCAGGAACTCAGGGAGTGAGCTACAAGTGTATTATGCT
TCACCCAGAAGTTATCAAGACTTTTTTGAAGCCATCCGCAGAAGGGGAGACACATTTTA
TGTTGTGTCATTTCGAAGGGATCACCTGCTGTTACCAGCTACCACCCATAACAAGACCA
CAAGACCAAAAATGTCAATTGTGTTACCAGCAATAAACATAAATGAGAATGTGATCAAT
GGGCAGGACTACGAAGTGATGATGCAGATTGACTGTCAGGTGATGGACACCAGGATC
CTCCATATCAAAAGTTCGTCAGTTCCTCCTTACCTCCGAGATCAGCAGAGGAATCAAAC
CAACACCTTCTTTGGCTCCCCTCCCGCAGCCACAGAGGCAACCCACGTTGTCAGCACCA
TCCCTGAGTCATTACAATAG

Table 11.26.: Potential RNA primer-pairs against the human activating transcription factor 6 A gene. Potential primer pairs were identified through haphazard literature review.

Primer pair	Forward primer (5' – 3')	Reverse primer (5' – 3')	Product size (bases)
Primer	TCGGTCAGTGGACTCTTATT	CCAGTGACAGGCTTATCTTC	153
Reference(s)	(Tan et al., 2018)		
Primer	AAGTAGTTTGTCTTTACTAG GC	TGAGTGGGATCTGAGAATGT	N.A.
Reference(s)	(Kroeger et al., 2021)		
Primer	GCTTTACATTCCTCCACCTC CTTG	ATTTGAGCCCTGTTCCAGAGCAC	180
Reference(s)	(Chiang et al., 2017)		
Primer	GCTTTACATTCCTCCACCTC C	ATCAGCTGAGAATTTGAGCCC	192
Reference(s)	(Chiang et al., 2017)	Modified (Chiang et al., 2017)	

Table 11.27.: Selected tentative RNA primer pair against the human vascular endothelial growth factor A gene.

Forward primer (5' – 3')	Reverse primer (5' – 3')	Product size (bases)
GCTTTACATTCCTCCACCTCC	ATCAGCTGAGAATTTGAGCCC	192

Table 11.28.: Primer-BLAST search parameters and other details for the selected the human activating transcription factor 6 A RNA primer pair.

Search parameters and other details	
Number of Blast hits analyzed	49294
Entrez query	
Min total mismatches	2
Min 3' end mismatches	2
Defined 3' end region length	5
Mismatch threshold to ignore targets	6
Max target size	4000
Max number of Blast target sequences	50000
Blast E value	30000
Blast word size	7
Max candidate primer pairs	500
Min PCR product size	62
Max PCR product size	1000
Min Primer size	15
Opt Primer size	20
Max Primer size	25
Min Tm	57
Opt Tm	60
Max Tm	63
Max Tm difference	3
Repeat filter	AUTO
Low complexity filter	Yes

Output 11.7.: Primer-BLAST output for other potential products on unintended templates for the selected activating transcription factor 6 A RNA primer pair.

>NM_001410890.1 Homo sapiens activating transcription factor 6 (ATF6), transcript variant 2, RNA
product length = 192
Forward primer 1 GCTTTACATTCCTCCACCTCC 21
Template 1418 1438
Reverse primer 1 ATCAGCTGAGAATTTGAGCCC 21
Template 1609 1589

>XM_047449542.1 PREDICTED: Homo sapiens activating transcription factor 6 (ATF6), transcript variant X5, RNA
product length = 192
Forward primer 1 GCTTTACATTCCTCCACCTCC 21
Template 1418 1438
Reverse primer 1 ATCAGCTGAGAATTTGAGCCC 21
Template 1609 1589

>XM_011509310.3 PREDICTED: Homo sapiens activating transcription factor 6 (ATF6), transcript variant X4, RNA
product length = 192
Forward primer 1 GCTTTACATTCCTCCACCTCC 21
Template 1475 1495
Reverse primer 1 ATCAGCTGAGAATTTGAGCCC 21

Template 1666 1646

>NM_007348.4 Homo sapiens activating transcription factor 6 (ATF6), transcript variant 1, RNA
product length = 192
Forward primer 1 GCTTTACATTCCTCCACCTCC 21
Template 1418 1438
Reverse primer 1 ATCAGCTGAGAATTTGAGCCC 21
Template 1609 1589

>XM_011509309.1 PREDICTED: Homo sapiens activating transcription factor 6 (ATF6),
transcript variant X2, RNA
product length = 192
Forward primer 1 GCTTTACATTCCTCCACCTCC 21
Template 1475 1495
Reverse primer 1 ATCAGCTGAGAATTTGAGCCC 21
Template 1666 1646

>XM_011509308.1 PREDICTED: Homo sapiens activating transcription factor 6 (ATF6),
transcript variant X1, RNA
product length = 192
Forward primer 1 GCTTTACATTCCTCCACCTCC 21
Template 1475 1495
Reverse primer 1 ATCAGCTGAGAATTTGAGCCC 21
Template 1666 1646

>XM_017029358.3 PREDICTED: Homo sapiens connector enhancer of kinase suppressor of Ras
2 (CNKSR2), transcript variant X3, RNA
product length = 1527
Forward primer 1 GCTTTACATTCCTCCACCTCC 21
Template 1383 T..C.....C..T..... 1403
Forward primer 1 GCTTTACATTCCTCCACCTCC 21
Template 2909 ..C.CC.C.....T..... 2889

>XM_011545472.4 PREDICTED: Homo sapiens connector enhancer of kinase suppressor of Ras
2 (CNKSR2), transcript variant X2, RNA
product length = 1617
Forward primer 1 GCTTTACATTCCTCCACCTCC 21
Template 1383 T..C.....C..T..... 1403
Forward primer 1 GCTTTACATTCCTCCACCTCC 21
Template 2999 ..C.CC.C.....T..... 2979

>XM_011545471.4 PREDICTED: Homo sapiens connector enhancer of kinase suppressor of Ras
2 (CNKSR2), transcript variant X1, RNA
product length = 1527
Forward primer 1 GCTTTACATTCCTCCACCTCC 21
Template 1530 T..C.....C..T..... 1550
Forward primer 1 GCTTTACATTCCTCCACCTCC 21
Template 3056 ..C.CC.C.....T..... 3036

>NM_001330771.2 Homo sapiens connector enhancer of kinase suppressor of Ras 2 (CNKSR2),
transcript variant 6, RNA
product length = 1527
Forward primer 1 GCTTTACATTCCTCCACCTCC 21
Template 1383 T..C.....C..T..... 1403
Forward primer 1 GCTTTACATTCCTCCACCTCC 21
Template 2909 ..C.CC.C.....T..... 2889

>NM_001168649.3 Homo sapiens connector enhancer of kinase suppressor of Ras 2 (CNKSR2),
transcript variant 4, RNA
product length = 1617
Forward primer 1 GCTTTACATTCCTCCACCTCC 21
Template 1383 T..C.....C..T..... 1403
Forward primer 1 GCTTTACATTCCTCCACCTCC 21
Template 2999 ..C.CC.C.....T..... 2979

>NM_001168647.3 Homo sapiens connector enhancer of kinase suppressor of Ras 2 (CNKSR2), transcript variant 2, RNA
product length = 1527
Forward primer 1 GCTTTACATTCCTCCACCTCC 21
Template 1530 T..C.....C..T..... 1550
Forward primer 1 GCTTTACATTCCTCCACCTCC 21
Template 3056 ..C.CC.C.....T..... 3036

>NM_001330773.2 Homo sapiens connector enhancer of kinase suppressor of Ras 2 (CNKSR2), transcript variant 8, RNA
product length = 1527
Forward primer 1 GCTTTACATTCCTCCACCTCC 21
Template 1530 T..C.....C..T..... 1550
Forward primer 1 GCTTTACATTCCTCCACCTCC 21
Template 3056 ..C.CC.C.....T..... 3036

>NM_001330770.2 Homo sapiens connector enhancer of kinase suppressor of Ras 2 (CNKSR2), transcript variant 5, RNA
product length = 1617
Forward primer 1 GCTTTACATTCCTCCACCTCC 21
Template 1383 T..C.....C..T..... 1403
Forward primer 1 GCTTTACATTCCTCCACCTCC 21
Template 2999 ..C.CC.C.....T..... 2979

>NM_001168648.3 Homo sapiens connector enhancer of kinase suppressor of Ras 2 (CNKSR2), transcript variant 3, RNA
product length = 1617
Forward primer 1 GCTTTACATTCCTCCACCTCC 21
Template 1530 T..C.....C..T..... 1550
Forward primer 1 GCTTTACATTCCTCCACCTCC 21
Template 3146 ..C.CC.C.....T..... 3126

>NM_001330772.2 Homo sapiens connector enhancer of kinase suppressor of Ras 2 (CNKSR2), transcript variant 7, RNA
product length = 1527
Forward primer 1 GCTTTACATTCCTCCACCTCC 21
Template 1383 T..C.....C..T..... 1403
Forward primer 1 GCTTTACATTCCTCCACCTCC 21
Template 2909 ..C.CC.C.....T..... 2889

>NM_014927.5 Homo sapiens connector enhancer of kinase suppressor of Ras 2 (CNKSR2), transcript variant 1, RNA
product length = 1617
Forward primer 1 GCTTTACATTCCTCCACCTCC 21
Template 1530 T..C.....C..T..... 1550
Forward primer 1 GCTTTACATTCCTCCACCTCC 21
Template 3146 ..C.CC.C.....T..... 3126

>XM_047445427.1 PREDICTED: Homo sapiens keratin-associated protein 5-5-like (LOC124902215), transcript variant X4, RNA
product length = 3450
Forward primer 1 GCTTTACATTCCTCCACCTCC 21
Template 4876 C..G...C.A.....C.. 4856
Reverse primer 1 ATCAGCTGAGAATTTGAGCCC 21
Template 1427 CC.C....T....C..... 1447

>XM_047424314.1 PREDICTED: Homo sapiens keratin-associated protein 5-5-like (LOC124902215), transcript variant X3, RNA
product length = 3914
Forward primer 1 GCTTTACATTCCTCCACCTCC 21
Template 5340 C..G...C.A.....C.. 5320
Reverse primer 1 ATCAGCTGAGAATTTGAGCCC 21
Template 1427 CC.C....T....C..... 1447

>XM_047424313.1 PREDICTED: Homo sapiens keratin-associated protein 5-5-like (LOC124902215), transcript variant X2, RNA
product length = 3878
Forward primer 1 GCTTTACATTCCTCCACCTCC 21
Template 5304 C..G...C.A.....C.. 5284
Reverse primer 1 ATCAGCTGAGAATTTGAGCCC 21
Template 1427 CC.C....T....C..... 1447

>XM_047424311.1 PREDICTED: Homo sapiens keratin-associated protein 5-5-like (LOC124902215), transcript variant X1, RNA
product length = 3914
Forward primer 1 GCTTTACATTCCTCCACCTCC 21
Template 5340 C..G...C.A.....C.. 5320
Reverse primer 1 ATCAGCTGAGAATTTGAGCCC 21
Template 1427 CC.C....T....C..... 1447

>XM_006710585.4 PREDICTED: Homo sapiens ribosomal modification protein rimK like family member A (RIMKLA), transcript variant X2, RNA
product length = 3710
Reverse primer 1 ATCAGCTGAGAATTTGAGCCC 21
Template 10194 ...TCA.....C....A 10174
Reverse primer 1 ATCAGCTGAGAATTTGAGCCC 21
Template 6485 ..........CA.GA...T. 6505

>XM_047418484.1 PREDICTED: Homo sapiens ribosomal modification protein rimK like family member A (RIMKLA), transcript variant X1, RNA
product length = 3710
Reverse primer 1 ATCAGCTGAGAATTTGAGCCC 21
Template 10371 ...TCA.....C....A 10351
Reverse primer 1 ATCAGCTGAGAATTTGAGCCC 21
Template 6662 ..........CA.GA...T. 6682

>NM_173642.4 Homo sapiens ribosomal modification protein rimK like family member A (RIMKLA), RNA
product length = 3710
Reverse primer 1 ATCAGCTGAGAATTTGAGCCC 21
Template 10310 ...TCA.....C....A 10290
Reverse primer 1 ATCAGCTGAGAATTTGAGCCC 21
Template 6601 ..........CA.GA...T. 6621

>NM_001396057.1 Homo sapiens olfactory receptor family 56 subfamily B member 2 pseudogene (OR56B2P), RNA
product length = 1562
Forward primer 1 GCTTTACATTCCTCCACCTCC 21
Template 816 ..C...AG.A...G..... 836
Reverse primer 1 ATCAGCTGAGAATTTGAGCCC 21
Template 2377 .....G.TGA.....T... 2357

11.8. Search and validation of primers designed against human isocitrate dehydrogenase-1 gene

Table 11.29.: Human isocitrate dehydrogenase-1 canonical gene sequence. Canonical gene sequence was retrieved from the Consensus coding sequence project database [blue – exons, black - introns].

Gene	Isocitrate dehydrogenase (IDH)

Canonical gene sequence	ATGTCCAAAAAAATCAGTGGCGGTTCTGTGGTAGAGATGCAAGGAGATGAAATGACACGAAT CATTTGGGAATTGATTAAAGAGAAACTCATTTTTCCCTACGTGGAATTGGATCTACATAGCTAT GATTTAGGCATAGAGAATCGTGATGCCACCAACGACCAAGTCACCAAGGATGCTGCAGAAGCT ATAAAGAAGCATAATGTTGGCGTCAAATGTGCCACTATCACTCCTGATGAGAAGAGGGTTGAG GAGTTCAAGTTGAAACAAATGTGGAAATCACCAAATGGCACCATACGAAATATTCTGGGTGGC ACGGTCTTCAGAGAAGCCATTATCTGCAAAAATATCCCCCGGCTTGTGAGTGGATGGGTAAAA CCTATCATCATAGGTCGTCATGCTTATGGGGATCAATACAGAGCAACTGATTTTGTTGTTCCTG GGCCTGGAAAAGTAGAGATAACCTACACACCAAGTGACGGAACCCAAAAGGTGACATACCTG GTACATAACTTTGAAGAAGGTGGTGGTGTTGCCATGGGGATGTATAATCAAGATAAGTCAATT GAAGATTTTGCACACAGTTCCTTCCAAATGGCTCTGTCTAAGGGTTGGCCTTTGTATCTGAGCA CCAAAAACACTATTCTGAAGAAATATGATGGGCGTTTTAAAGACATCTTTCAGGAGATATATGA CAAGCAGTACAAGTCCCAGTTTGAAGCTCAAAAGATCTGGTATGAGCATAGGCTCATCGACGA CATGGTGGCCCAAGCTATGAAATCAGAGGGAGGCTTCATCTGGGCCTGTAAAAACTATGATGG TGACGTGCAGTCGGACTCTGTGGCCCAAGGGTATGGCTCTCTCGGCATGATGACCAGCGTGCT GGTTTGTCCAGATGGCAAGACAGTAGAAGCAGAGGCTGCCCACGGGACTGTAACCCGTCACTA CCGCATGTACCAGAAAGGACAGGAGACGTCCACCAATCCCATTGCTTCCATTTTTGCCTGGACC AGAGGGTTAGCCCACAGAGCAAAGCTTGATAACAATAAAGAGCTTGCCTTCTTTGCAAATGCTT TGGAAGAAGTCTCTATTGAGACAATTGAGGCTGGCTTCATGACCAAGGACTTGGCTGCTTGCA TTAAAGGTTTACCCAATGTGCAACGTTCTGACTACTTGAATACATTTGAGTTCATGGATAAACTT GGAGAAAACTTGAAGATCAAACTAGCTCAGGCCAAACTTTAA

Table 11.30.: Selected tentative RNA primer pair against the human isocitrate dehydrogenase-1 gene. Primer pair were identified using Prime3® software.

Forward primer (5' – 3')	Reverse primer (5' – 3')	Product size (bases)
AATCAGTGGCGGTTCTGTGG	CAAGTAGTCAGAACGTTGC	1,165

Table 11.31.: Primer-BLAST search parameters and other details for the selected human Autophagy Related 4B Cysteine Peptidase RNA primer pair.

Search parameter and other details	
Number of Blast hits analyzed	9867
Entrez query	
Min total mismatches	2
Min 3' end mismatches	2
Defined 3' end region length	5
Mismatch threshold to ignore targets	6
Max target size	4000
Max number of Blast target sequences	50000
Blast E value	30000
Blast word size	7
Max candidate primer pairs	500
Min PCR product size	59
Max PCR product size	1000
Min Primer size	15
Opt Primer size	20
Max Primer size	25
Min Tm	57
Opt Tm	60
Max Tm	63
Max Tm difference	3

Repeat filter	AUTO
Low complexity filter	Yes

Output 11.8.: Primer-BLAST output for other potential products on unintended templates for the selected human isocitrate dehydrogenase-1 gene RNA primer pair.

>NM_005896.4 Homo sapiens isocitrate dehydrogenase (NADP(+)) 1 (IDH1), transcript variant 1, RNA
product length = 1165
Forward primer 1 AATCAGTGGCGGTTCTGTGG 20
Template 235 254

Reverse primer 1 CAAGTAGTCAGAACGTTGC 19
Template 1399 1381

>NM_001282387.1 Homo sapiens isocitrate dehydrogenase (NADP(+)) 1 (IDH1), transcript variant 3, RNA
product length = 1165
Forward primer 1 AATCAGTGGCGGTTCTGTGG 20
Template 375 394
Reverse primer 1 CAAGTAGTCAGAACGTTGC 19
Template 1539 1521

>NM_001282386.1 Homo sapiens isocitrate dehydrogenase (NADP(+)) 1 (IDH1), transcript variant 2, RNA
product length = 1165
Forward primer 1 AATCAGTGGCGGTTCTGTGG 20
Template 218 237
Reverse primer 1 CAAGTAGTCAGAACGTTGC 19
Template 1382 1364

11.9. Isocitrate-dehydrogenase primer optimisation and experimental validation

Optimisation of the PCR assay for the application of the IDH gene was conducted to identify the optimal assay conditions. The in-house designed IDH primers were temperature was varied between runs to identify optimal assay conditions. An annealing temperature of 61 °C degrees was chosen as the optimum temperature, since under these conditions one strong band around 1200bp and minimal accessory/ residual bands, representing IDH gene and accessory/ residual PCR products respectively, were obtained (Figure 10.1.).

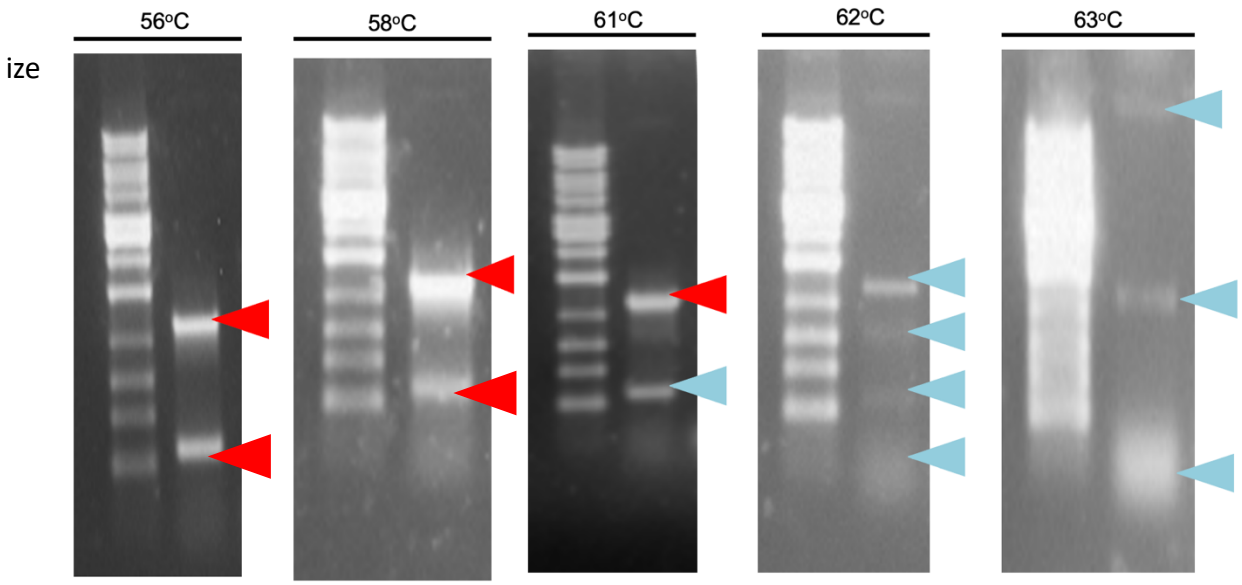
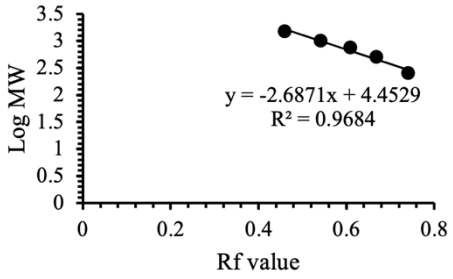


Figure 11.1.: Deoxyribonucleic acid binding assay optimise and validate the isocitrate dehydrogenase primers. Polymerase chain reaction (PCR_ gel obtained under 61 °C annealing temperature conditions demonstrated the strongest band (red arrows) around 1200bp with minimal accessory bands (blue arrows).

Logistic regression analysis based on the obtained R_f value of discernible ladder bands demonstrated an obtained product size of 1244.31bp, within acceptable limits in comparison to the theoretical product size.

[A]



[B]

Gene	Theoretical product size (bp)	R_f value	Estimated product size (bp)
IDH	1165.00	0.51	1244.31

Figure 11.2.: Logistic regression to estimate the size of the isocitrate dehydrogenase polymerase chain reaction product obtained. [A] Logistic regression, and [B] determination of estimated product size (bp) for the isocitrate dehydrogenase (IDH) gene polymerase chain reaction (PCR) product obtained under optimal conditions

11.10. Ribonucleic acid primer experimental validation

The in-house designed primers were assayed for specificity to their respective target genes using RNA extracted from U87MG cells. PCR products were produced and visualised (Section) (Figure xx). The logarithmic expression of the weight of the discernible ladder bands were plotted (on the Y-axis) against the R_f value (on the X-axis) using Microsoft excel version 16.67. Through regression, the logarithmic molecular size of the bands obtained was determined which were normalised by finding the corresponding antilog to obtain the size (bp) (Figure xxx). The theoretical PCR products' sizes, obtained from the respective canonical gene sequences (Appendix xx), were compared against the obtained PCR products' sizes.

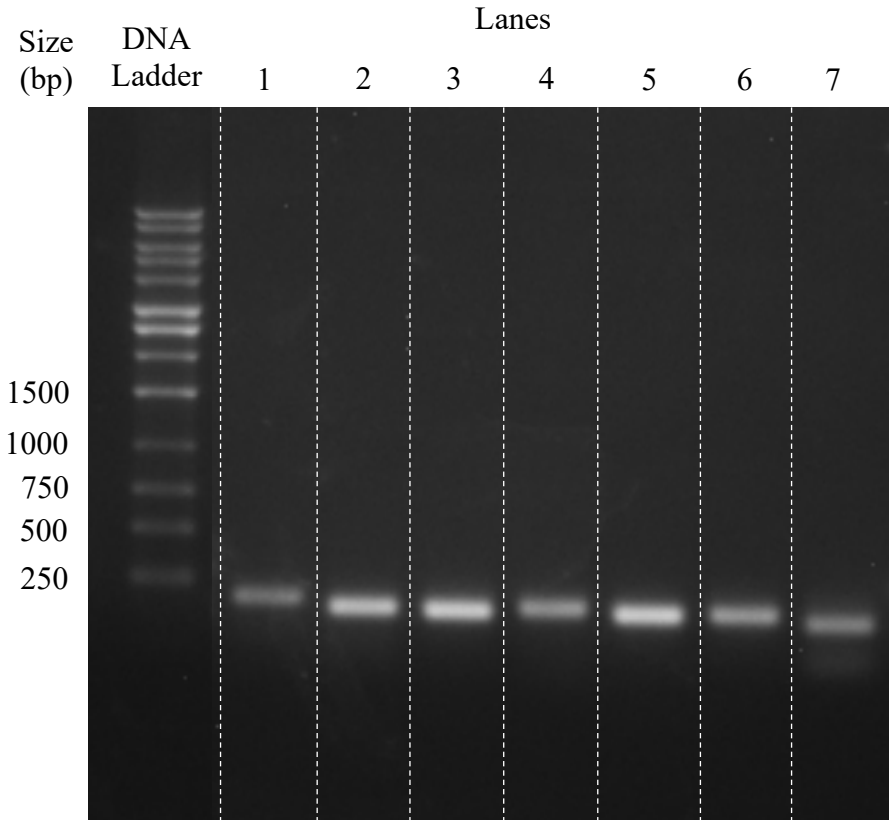
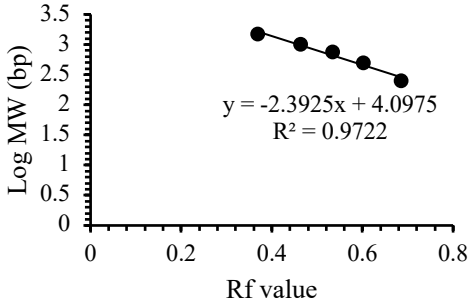


Figure 11.3.: Deoxyribonucleic acid-binding assay to validate primer specificity. Lane 0: Ladder/ Marker; lanes 1– 7: PCR products obtained using primers designed to target the genes ATG4b, Bax, BECN1, Caspase-3, PKM2, VEGFA, ATF6A, respectively.

[A]



[B]

Gene	Theoretical product size (bp)	R_f value	Estimated product size (bp)
ATG4b	253.00	0.7124584	247.14
Bax	223.00	0.7283521	226.42
BECN1	220.00	0.7296023	224.87
Casp-3	231.00	0.7302175	224.11
PKM2	207.00	0.7380057	214.69
VEGFA	223.00	0.7426792	209.24
ATF6A	192.00	0.7592305	191.00

Figure 11.4.: Logistic regression to estimate the size of the polymerase chain reaction products obtained. [A] Logistic regression, and [B] determination of estimated product size (bp) for the ATG4b, Bax, BECN1, Caspase-3, PKM2, VEGFA and ATF6A, gene polymerase chain reaction (PCR) products obtained under optimal conditions.

11.11. References

Abdel-Majid, R. M., & Marshall, J. S. (2004). Prostaglandin E2 induces degranulation-independent production of vascular endothelial growth factor by human mast cells. *Journal of Immunology*, *172*(2), 1227–1236. https://doi.org/10.4049/jimmunol.172.2.1227

Ali, D., Tripathi, A., Al Ali, H., Shahi, Y., Mishra, K. K., Alarifi, S., Alkahtane, A. A., & Manohardas, S. (2018). ROS-dependent Bax/Bcl2 and caspase 3 pathway-mediated apoptosis induced by zineb in human keratinocyte cells. *OncoTargets and Therapy*, *11*, 489–497. https://doi.org/10.2147/OTT.S140358

Baharara, J., Namvar, F., Ramezani, T., Mousavi, M., & Mohamad, R. (2015). Silver Nanoparticles Biosynthesized Using Achillea biebersteinii Flower Extract: Apoptosis Induction in MCF-7 Cells via Caspase Activation and Regulation of Bax and Bcl-2 Gene Expression. *Molecules (Basel, Switzerland)*, *20*(2), 2693–2706. https://doi.org/10.3390/molecules20022693

Briton-Jones, C., Lok, I. H., Po, A. L. S., Cheung, C. K., Chiu, T. T. Y., & Haines, C. (2006). Changes in the ratio of Bax and Bcl-2 RNA expression and their cellular localization throughout the ovulatory cycle in the human oviduct. *Journal of Assisted Reproduction and Genetics*, *23*(3), 149–156. https://doi.org/10.1007/s10815-005-9012-2

Cao, Y., Chen, L., Zhang, W., Liu, Y., Papaconstantinou, H. T., Bush, C. R., Townsend, C. M., Thompson, E. A., & Ko, T. C. (2007). Identification of apoptotic genes mediating TGF-beta/Smad3-induced cell death in intestinal epithelial cells using a genomic approach. *American Journal of Physiology. Gastrointestinal and Liver Physiology*, *292*(1), G28-38. https://doi.org/10.1152/ajpgi.00437.2005

Chen, J., Ran, R.-K., Chen, Y., Zhang, Z.-Z., Tao, N.-N., Ren, J.-H., Zhou, L., Tang, H., Chen, X., Chen, K., Li, W.-Y., & Huang, A.-L. (2016). SIRT6 overexpression potentiates apoptosis evasion in hepatocellular carcinoma via BCL2-associated X protein-dependent apoptotic pathway. *Clinical Cancer Research*. https://doi.org/10.1158/1078-0432.CCR-15-1638

Chen, S., Wu, H., Wang, Z., Jia, M., Guo, J., Jin, J., Li, X., Meng, D., Lin, L., He, A. R., Zhou, P., & Zhi, X. (2021). Loss of SPTBN1 suppresses autophagy via SETD7-mediated YAP methylation in hepatocellular carcinoma initiation and development. *Cellular and Molecular Gastroenterology and Hepatology*. https://doi.org/10.1016/j.jcmgh.2021.10.012

Chiang, W.-C., Chan, P., Wissinger, B., Vincent, A., Skorczyk-Werner, A., Krawczyński, M. R., Kaufman, R. J., Tsang, S. H., Héon, E., Kohl, S., & Lin, J. H. (2017). Achromatopsia mutations target sequential steps of ATF6 activation. *Proceedings of the National Academy of Sciences of the United States of America*, *114*(2), 400–405. https://doi.org/10.1073/pnas.1606387114

Chiu, C. L., Morgan, C. T., Lupton, S. J., & Lind, J. M. (2013). Parent of origin influences the cardiac expression of vascular endothelial growth factor (Vegfa). *BMC Medical Genetics*, *14*, 43. https://doi.org/10.1186/1471-2350-14-43

Chung, J.-Y., Song, Y., Wang, Y., Magness, R. R., & Zheng, J. (2004). Differential expression of vascular endothelial growth factor (VEGF), endocrine gland derived-VEGF, and VEGF receptors in human placentas from normal and preeclamptic pregnancies. *The Journal of Clinical Endocrinology and Metabolism*, *89*(5), 2484–2490. https://doi.org/10.1210/jc.2003-031580

Clifford, R. L., Deacon, K., & Knox, A. J. (2008). Novel regulation of vascular endothelial

growth factor-A (VEGF-A) by transforming growth factor (beta)1: requirement for Smads, (beta)-CATENIN, AND GSK3(beta). *The Journal of Biological Chemistry*, *283*(51), 35337–35353. https://doi.org/10.1074/jbc.M803342200

Deng, C., Li, J., Li, L., Sun, F., & Xie, J. (2019). Effects of hypoxia ischemia on caspase-3 expression and neuronal apoptosis in the brain of neonatal mice. *Experimental and Therapeutic Medicine*, *17*(6), 4517–4521. https://doi.org/10.3892/etm.2019.7487

Di Tommaso, S., Massari, S., Malvasi, A., Bozzetti, M. P., & Tinelli, A. (2013). Gene expression analysis reveals an angiogenic profile in uterine leiomyoma pseudocapsule. *Molecular Human Reproduction*, *19*(6), 380–387. https://doi.org/10.1093/molehr/gat007

Dohmoto, K., Hojo, S., Fujita, J., Yang, Y., Ueda, Y., Bandoh, S., Yamaji, Y., Ohtsuki, Y., Dobashi, N., Ishida, T., & Takahara, J. (2001). The role of caspase 3 in producing cytokeratin 19 fragment (CYFRA21-1) in human lung cancer cell lines. *International Journal of Cancer*, *91*(4), 468–473. https://doi.org/10.1002/1097-0215(200002)9999:9999<::aid-ijc1082>3.0.co;2-t

Gibot, L., Follet, J., Metges, J.-P., Auvray, P., Simon, B., Corcos, L., & Le Jossic-Corcos, C. (2009). Human caspase 7 is positively controlled by SREBP-1 and SREBP-2. *The Biochemical Journal*, *420*(3), 473–483. https://doi.org/10.1042/BJ20082057

Guo, J., Fang, W., Chen, X., Lin, Y., Hu, G., Wei, J., Zhang, X., Yang, C., & Li, J. (2018). Upstream stimulating factor 1 suppresses autophagy and hepatic lipid droplet catabolism by activating mTOR. *FEBS Letters*, *592*(16), 2725–2738. https://doi.org/10.1002/1873-3468.13203

Ho, Y.-T., Lu, C.-C., Yang, J.-S., Chiang, J.-H., Li, T.-C., Ip, S.-W., Hsia, T.-C., Liao, C.-L., Lin,

J.-G., Wood, W. G., & Chung, J.-G. (2009). Berberine induced apoptosis via promoting the expression of caspase-8, -9 and -3, apoptosis-inducing factor and endonuclease G in SCC-4 human tongue squamous carcinoma cancer cells. *Anticancer Research*, *29*(10), 4063–4070.

Idikio, H. A. (2011). Galectin-3 and Beclin1/Atg6 genes in human cancers: using cDNA tissue panel, qRT-PCR, and logistic regression model to identify cancer cell biomarkers. *Plos One*, *6*(10), e26150. https://doi.org/10.1371/journal.pone.0026150

Jänicke, R. U., Sprengart, M. L., Wati, M. R., & Porter, A. G. (1998). Caspase-3 is required for DNA fragmentation and morphological changes associated with apoptosis. *The Journal of Biological Chemistry*, *273*(16), 9357–9360. https://doi.org/10.1074/jbc.273.16.9357

Jin, J., Xu, C., Wu, S., Wu, Z., Wu, S., Sun, M., & Bao, W. (2022). m6a demethylase ALKBH5 restrains PEDV infection by regulating GAS6 expression in porcine alveolar macrophages. *International Journal of Molecular Sciences*, *23*(11). https://doi.org/10.3390/ijms23116191

Kibbe, W. A. (2007). OligoCalc: an online oligonucleotide properties calculator. *Nucleic Acids Research*, *35*(Web Server issue), W43-6. https://doi.org/10.1093/nar/gkm234

Kroeger, H., Grandjean, J. M. D., Chiang, W.-C. J., Bindels, D. D., Mastey, R., Okalova, J., Nguyen, A., Powers, E. T., Kelly, J. W., Grimsey, N. J., Michaelides, M., Carroll, J., Wiseman, R. L., & Lin, J. H. (2021). ATF6 is essential for human cone photoreceptor development. *Proceedings of the National Academy of Sciences of the United States of America*, *118*(39).

https://doi.org/10.1073/pnas.2103196118

Laffon, B., Pásaro, E., & Méndez, J. (2001). Effects of styrene-7,8-oxide over p53, p21, bcl-2 and bax expression in human lymphocyte cultures. *Mutagenesis*, *16*(2), 127–132. https://doi.org/10.1093/mutage/16.2.127

Li, S., Li, J., Peng, W., Hao, G., & Sun, J. (2019). Characterization of the responses of the caspase 2, 3, 6 and 8 genes to immune challenges and extracellular ATP stimulation in the Japanese flounder (Paralichthys olivaceus). *BMC Veterinary Research*, *15*(1), 20. https://doi.org/10.1186/s12917-018-1763-y

Li, Z., Wang, G., Feng, D., Zu, G., Li, Y., Shi, X., Zhao, Y., Jing, H., Ning, S., Le, W., Yao, J., & Tian, X. (2018). Targeting the miR-665-3p-ATG4B-autophagy axis relieves inflammation and apoptosis in intestinal ischemia/reperfusion. *Cell Death & Disease*, *9*(5), 483. https://doi.org/10.1038/s41419-018-0518-9

Liu, P.-F., Tsai, K.-L., Hsu, C.-J., Tsai, W.-L., Cheng, J.-S., Chang, H.-W., Shiau, C.-W., Goan, Y.-G., Tseng, H.-H., Wu, C.-H., Reed, J. C., Yang, L.-W., & Shu, C.-W. (2018). Drug Repurposing Screening Identifies Tioconazole as an ATG4 Inhibitor that Suppresses Autophagy and Sensitizes Cancer Cells to Chemotherapy. *Theranostics*, *8*(3), 830–845. https://doi.org/10.7150/thno.22012

Mbazima, V. G., Mokgotho, M. P., February, F., Rees, D. J. G., & Mampuru, L. J. M. (2008). Alteration of Bax-to-Bcl-2 ratio modulates the anticancer activity of methanolic extract of Commelina benghalensis (Commelinaceae) in Jurkat T cells. *African Journal of Biotechnology*, *7*(20).

Miracco, C., Cosci, E., Oliveri, G., Luzi, P., Pacenti, L., Monciatti, I., Mannucci, S., De Nisi, M. C., Toscano, M., Malagnino, V., Falzarano, S. M., Pirtoli, L., & Tosi, P. (2007). Protein and RNA expression of autophagy gene Beclin 1 in human brain tumours.

International Journal of Oncology, *30*(2), 429–436.

Mitupatum, T., Aree, K., Kittisenachai, S., Roytrakul, S., Puthong, S., Kangsadalampai, S., & Rojpibulstit, P. (2016). RNA Expression of Bax, Bcl-2, p53, Cathepsin B, Caspase-3 and Caspase-9 in the HepG2 Cell Line Following Induction by a Novel Monoclonal Ab Hep88 mAb: Cross-Talk for Paraptosis and Apoptosis. *Asian Pacific Journal of Cancer Prevention*, *17*(2), 703–712. https://doi.org/10.7314/APJCP.2016.17.2.703

Morikawa, A., Takeuchi, T., Kito, Y., Saigo, C., Sakuratani, T., Futamura, M., & Yoshida, K. (2015). Expression of beclin-1 in the microenvironment of invasive ductal carcinoma of the breast: correlation with prognosis and the cancer-stromal interaction. *Plos One*, *10*(5), e0125762. https://doi.org/10.1371/journal.pone.0125762

Morita, M., Sato, T., Nomura, M., Sakamoto, Y., Inoue, Y., Tanaka, R., Ito, S., Kurosawa, K., Yamaguchi, K., Sugiura, Y., Takizaki, H., Yamashita, Y., Katakura, R., Sato, I., Kawai, M., Okada, Y., Watanabe, H., Kondoh, G., Matsumoto, S., … Tanuma, N. (2018). PKM1 Confers Metabolic Advantages and Promotes Cell-Autonomous Tumor Cell Growth. *Cancer Cell*, *33*(3), 355–367.e7. https://doi.org/10.1016/j.ccell.2018.02.004

Mukherjee, J., Phillips, J. J., Zheng, S., Wiencke, J., Ronen, S. M., & Pieper, R. O. (2013). Pyruvate kinase M2 expression, but not pyruvate kinase activity, is up-regulated in a grade-specific manner in human glioma. *Plos One*, *8*(2), e57610. https://doi.org/10.1371/journal.pone.0057610

NCBI. (n.d.-a). *Consensus Coding Sequence Database* . CCDS Database. Retrieved October 10, 2022, from

https://www.ncbi.nlm.nih.gov/projects/CCDS/CcdsBrowse.cgi

NCBI. (n.d.-b). *Primer-BLAST*. Primer-BLAST. Retrieved October 10, 2022, from https://www.ncbi.nlm.nih.gov/tools/primer-blast/

OriGene Technologies, Inc. (2022a). *BAX Human qPCR Primer Pair (NM_004324)*. OriGene. https://www.origene.com/catalog/gene-expression/qpcr-primer-pairs/hp207656/bax-human-qpcr-primer-pair-nm_004324

OriGene Technologies, Inc. (2022b). *Caspase 3 (CASP3) Human qPCR Primer Pair (NM_004346)*. OriGene. https://www.origene.com/catalog/gene-expression/qpcr-primer-pairs/hp207674/caspase-3-casp3-human-qpcr-primer-pair-nm_004346

OriGene Technologies, Inc. (2022c). *PKM2 (PKM) Human qPCR Primer Pair (NM_002654)*. OriGene. https://www.origene.com/catalog/gene-expression/qpcr-primer-pairs/hp206306/pkm2-pkm-human-qpcr-primer-pair-nm_002654https://www.origene.com/catalog/gene-expression/qpcr-primer-pairs/hp206306/pkm2-pkm-human-qpcr-primer-pair-nm_002654

OriGene Technologies, Inc. (2022d). *VEGFA Human qPCR Primer Pair (NM_001025366)*. 0riGene. https://www.origene.com/catalog/gene-expression/qpcr-primer-pairs/hp202779/vegfa-human-qpcr-primer-pair-nm_001025366

Park, J. K., Doseff, A. I., & Schmittgen, T. D. (2018). MicroRNAs Targeting Caspase-3 and -7 in PANC-1 Cells. *International Journal of Molecular Sciences*, *19*(4). https://doi.org/10.3390/ijms19041206

Peng, W. X., Wan, Y. Y., Gong, A. H., Ge, L., Jin, J., Xu, M., & Wu, C. Y. (2017). Egr-1 regulates irradiation-induced autophagy through Atg4B to promote radioresistance in hepatocellular carcinoma cells. *Oncogenesis*, *6*(1), e292.

https://doi.org/10.1038/oncsis.2016.91

Qian, H., Huang, Q., Chen, Y.-X., Liu, Q., Fang, J.-X., & Ye, M.-W. (2018). Caspase-9 was involved in cell apoptosis in human dental pulp stem cells from deciduous teeth. *Molecular Medicine Reports*, *18*(1), 1067–1073. https://doi.org/10.3892/mmr.2018.9046

Shu, C.-W., Bee, Y.-S., Chen, J.-L., Tsen, C.-L., Tsai, W.-L., & Sheu, S.-J. (2021). Detection of Autophagy-Related Gene Expression by Conjunctival Impression Cytology in Age-Related Macular Degeneration. *Diagnostics (Basel)*, *11*(2). https://doi.org/10.3390/diagnostics11020296

Sun, N., Sun, P., Yao, M., Khan, A., Sun, Y., Fan, K., Yin, W., & Li, H. (2019). Autophagy involved in antiviral activity of sodium tanshinone IIA sulfonate against porcine reproductive and respiratory syndrome virus infection in vitro. *Antiviral Therapy*, *24*(1), 27–33. https://doi.org/10.3851/IMP3268

Sun, Y., Zheng, Q., Wang, Y., Pang, Z., Liu, J., Yin, Z., & Lou, Z. (2019). Activity-Based Protein Profiling Identifies ATG4B as a Key Host Factor for Enterovirus 71 Proliferation. *Journal of Virology*, *93*(24). https://doi.org/10.1128/JVI.01092-19

Tan, Z., Zhang, W., Sun, J., Fu, Z., Ke, X., Zheng, C., Zhang, Y., Li, P., Liu, Y., Hu, Q., Wang, H., & Zheng, Z. (2018). ZIKV infection activates the IRE1-XBP1 and ATF6 pathways of unfolded protein response in neural cells. *Journal of Neuroinflammation*, *15*(1), 275. https://doi.org/10.1186/s12974-018-1311-5

UniProt. (n.d.). *UniProt*. UniProt. Retrieved October 10, 2022, from https://www.uniprot.org/

Vrtačnik, P., Zupan, J., Mlakar, V., Kranjc, T., Marc, J., Kern, B., & Ostanek, B. (2018). Epigenetic enzymes influenced by oxidative stress and hypoxia mimetic in

osteoblasts are differentially expressed in patients with osteoporosis and osteoarthritis. *Scientific Reports*, *8*(1), 16215. https://doi.org/10.1038/s41598-018-34255-4

Wang, D.-H., Hu, J.-R., Wang, L.-Y., Hu, Y.-J., Tan, F.-Q., Zhou, H., Shao, J.-Z., & Yang, W.-X. (2012). The apoptotic function analysis of p53, Apaf1, Caspase3 and Caspase7 during the spermatogenesis of the Chinese fire-bellied newt Cynops orientalis. *Plos One*, *7*(6), e39920. https://doi.org/10.1371/journal.pone.0039920

Wang, J., Pan, X.-L., Ding, L.-J., Liu, D.-Y., Da-Peng Lei, & Jin, T. (2013). Aberrant expression of Beclin-1 and LC3 correlates with poor prognosis of human hypopharyngeal squamous cell carcinoma. *Plos One*, *8*(7), e69038. https://doi.org/10.1371/journal.pone.0069038

Wang, L. S., Liu, H. J., Xia, Z. B., Broxmeyer, H. E., & Lu, L. (2000). Expression and activation of caspase-3/CPP32 in CD34(+) cord blood cells is linked to apoptosis after growth factor withdrawal. *Experimental Hematology*, *28*(8), 907–915. https://doi.org/10.1016/s0301-472x(00)00485-9

Wang, W., Fan, H., Zhou, Y., Duan, P., Zhao, G., & Wu, G. (2013). Knockdown of autophagy-related gene BECLIN1 promotes cell growth and inhibits apoptosis in the A549 human lung cancer cell line. *Molecular Medicine Reports*, *7*(5), 1501–1505. https://doi.org/10.3892/mmr.2013.1379

Wu, M., Chen, B., Pan, X., & Su, J. (2020). Prognostic Value of Autophagy-related Proteins in Human Gastric Cancer. *Cancer Management and Research*, *12*, 13527–13540. https://doi.org/10.2147/CMAR.S278354

Xu, L., Deng, C., Zhang, Y., Zhao, L., Linghu, Y., & Yu, Y. (2021). Expression of Autophagy-Related Factors LC3A and Beclin 1 and Apoptosis-Related Factors Bcl-2 and BAX

in Osteoblasts Treated With Sodium Fluoride. *Frontiers in Physiology*, *12*, 603848. https://doi.org/10.3389/fphys.2021.603848

Xu, Y., Huang, X., Xie, J., Chen, Y., Fu, J., & Wang, L. (2016). Let-7I-Induced Atg4B Suppression is Essential for Autophagy of Placental Trophoblast in Preeclampsia. *Journal of Cellular Physiology*. https://doi.org/10.1002/jcp.25661

Yamamoto, Y., Ito, S., Okuda, K., & Kimura, K. (2020). Involvement of activin signal pathway in cyclic apoptosis of the oviductal isthmic epithelium in cows. *Theriogenology*, *153*, 143–150. https://doi.org/10.1016/j.theriogenology.2020.05.009

Yang, W., Guo, C., Fan, H., & Liu, F. (2017). Studying the RNA and protein expression pattern of apoptosis and autophagy-related genes in renal cell carcinoma. *International Journal of Clinical and Experimental Medicine*, *10*(10), 14593–14598.

Zaravinos, A., Soufla, G., Bizakis, J., & Spandidos, D. A. (2008). Expression analysis of VEGFA, FGF2, TGFbeta1, EGF and IGF1 in human nasal polyposis. *Oncology Reports*, *19*(2), 385–391.

Zhang, N., Wu, Y., Lyu, X., Li, B., Yan, X., Xiong, H., Li, X., Huang, G., Zeng, Y., Zhang, Y., Lian, J., Ni, Z., & He, F. (2017). HSF1 upregulates ATG4B expression and enhances epirubicin-induced protective autophagy in hepatocellular carcinoma cells. *Cancer Letters*. https://doi.org/10.1016/j.canlet.2017.08.039

Zhang, X., Dong, Y., Zhao, M., Ding, L., Yang, X., Jing, Y., Song, Y., Chen, S., Hu, Q., & Ni, Y. (2020). ITGB2-mediated metabolic switch in CAFs promotes OSCC proliferation by oxidation of NADH in mitochondrial oxidative phosphorylation system. *Theranostics*, *10*(26), 12044–12059.

https://doi.org/10.7150/thno.47901

Zhu, H., Wu, H., Liu, X., Li, B., Chen, Y., Ren, X., Liu, C.-G., & Yang, J.-M. (2009). Regulation of autophagy by a beclin 1-targeted microRNA, miR-30a, in cancer cells. *Autophagy*, *5*(6), 816–823. https://doi.org/10.4161/auto.9064

Zhu, J., Cai, Y., Xu, K., Ren, X., Sun, J., Lu, S., Chen, J., & Xu, P. (2018). Beclin1 overexpression suppresses tumor cell proliferation and survival via an autophagy-dependent pathway in human synovial sarcoma cells. *Oncology Reports*, *40*(4), 1927–1936. https://doi.org/10.3892/or.2018.6599

Chapter 12 Appendix V Raw data

12.1. Isocitrate dehydrogenase 1 sequencing data

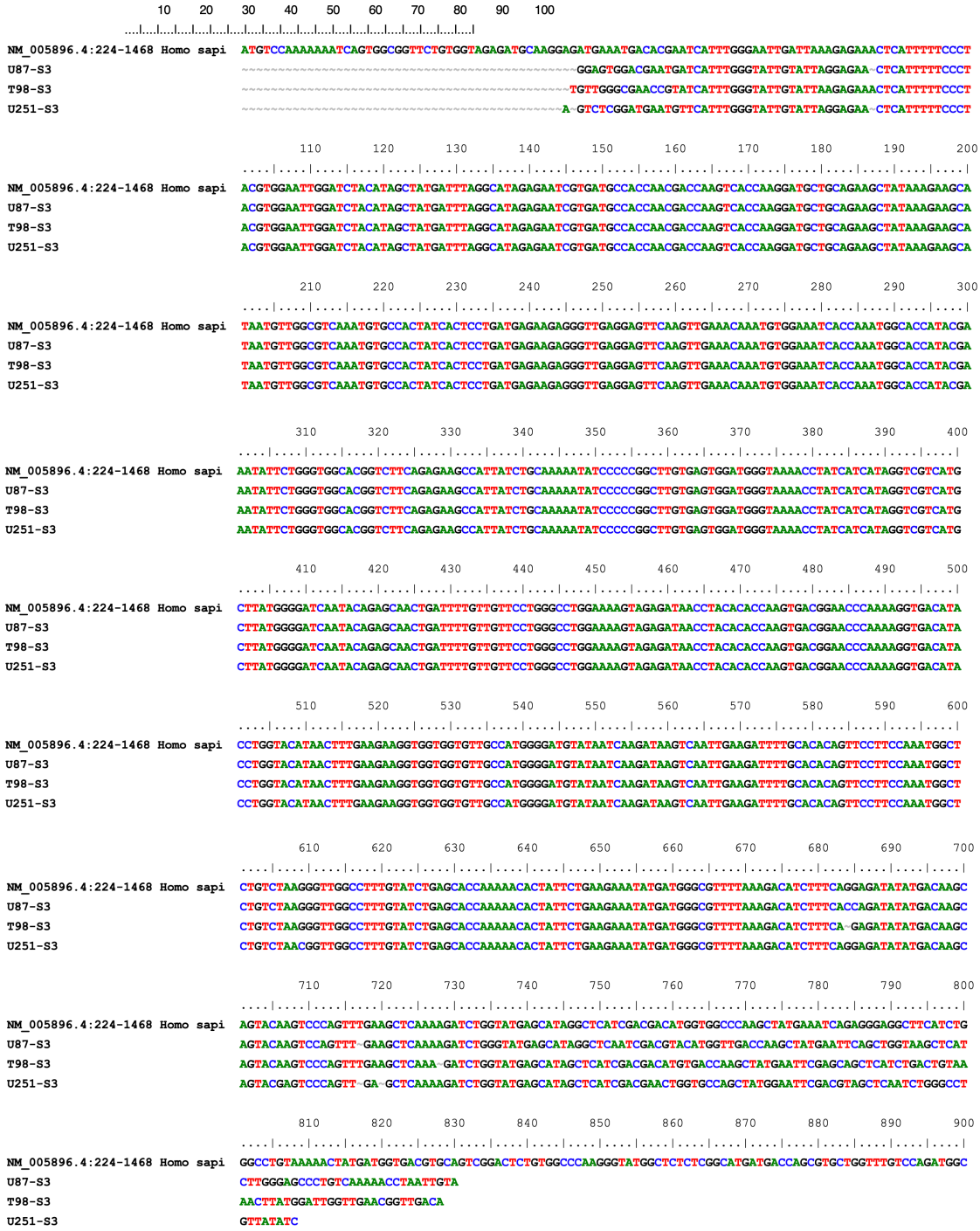


Figure 12.1.: U87MG, U251 and T98G isocitrate dehydrogenase-1 gene sanger sequencing aligned against the canonical gene sequence.

12.2. Presto blue® cell viability assay data

Table 12.1.: Presto blue® cell viability assay data for U87MG cells cells treated with α-solanine and temozolomide for 72 hours.

Cell-line	Condition	Drug	Replicate	Colourimetric reading	% overall viability
U87MG	α-solanine	5 uM	R1	0.672	94.729
			R2	0.645	
			R3	0.668	
		25 uM	R1	0.637	43.1
			R2	0.645	
			R3	0.693	
		50 uM	R1	0.459	12.678
			R2	0.472	
			R3	0.478	
		75 uM	R1	0.438	7.55
			R2	0.455	
			R3	0.480	
	Temozolmide	800 uM	R1	0.642	85.04274
			R2	0.635	
			R3	0.640	
		1200 uM	R1	0.622	77.49288
			R2	0.624	
			R3	0.618	
		1600 uM	R1	0.609	73.21937
			R2	0.614	
			R3	0.611	
		2000 uM	R1	0.578	57.40741
			R2	0.566	
			R3	0.579	
		2400 uM	R1	0.487	83.72093
			R2	0.493	
			R3	0.496	

Table 12.2.: Presto blue® cell viability assay data for U251 cells treated with α-solanine and temozolomide for 72 hours.

Cell-line	Condition	Drug	Replicate	Colourimetric reading	% viability
U251	α-solanine	5 uM	R1	0.69	94.35
			R2	0.679	
			R3	0.676	

		25 uM	R1	0.544	43.27
			R2	0.559	
			R3	0.551	
		50 uM	R1	0.57	23.447
			R2	0.553	
			R3	0.533	
		75 uM	R1	0.494	9.713
			R2	0.5	
			R3	0.508	
	Temozolmide	**800 uM**	R1	0.6	82.56
			R2	0.611	
			R3	0.621	
		1200 uM	R1	0.612	76.95473
			R2	0.621	
			R3	0.634	
		1600 uM	R1	0.658	76.138
			R2	0.641	
			R3	0.646	
		2000 uM	R1	0.626	72.63374
			R2	0.628	
			R3	0.592	
		2400 uM	R1	0.603	74.07407
			R2	0.609	
			R3	0.641	

Table 12.3.: Presto blue® cell viability assay data for T98G cells treated with α-solanine and temozolomide for 72 hours.

Cell-line	Condition	Drug	Replicate	Colourimetric reading	% viability
T98G	**α-solanine**	**5 uM**	R1	0.659	83.57
			R2	0.626	
			R3	0.702	
		25 uM	R1	0.572	41.77
			R2	0.554	
			R3	0.57	
		50 uM	R1	0.537	31.22
			R2	0.561	

			R3	0.567	
		75 uM	R1	0.508	9.671
			R2	0.526	
			R3	0.506	
	Temozolmide	800 uM	R1	0.600	82.56071
			R2	0.611	
			R3	0.621	
		1200 uM	R1	0.627	99.117
			R2	0.633	
			R3	0.647	
		1600 uM	R1	0.643	105.7395
			R2	0.651	
			R3	0.643	
		2000 uM	R1	0.655	112.5828
			R2	0.643	
			R3	0.670	
		2400 uM	R1	0.655	112.5828
			R2	0.670	
			R3	0.683	

12.3. Scratch migration assay data

Table 12.4.: Scratch migration assay data for U87MG cells treated with Temozolomide or α-solanine for 24, 48 and 72 hours.

Cell-line	Duration of incubation	Drug	Replicate	Initial wound size (pixels)	Final wound size (pixels)	Wound closure relative to control (%)
U87MG	24-hours	Temozolomide	R1	998279.00	826674.00	27.58
			R2	1050801.00	854280.00	30.00
			R3	1028866.00	899865.00	20.11
		α-solanine	R1	995298.00	42342.00	6.82
			R2	1010729.00	28596.00	4.54
			R3	980178.00	32051.00	5.25
	48 hours	Temozolomide	R1	998279.00	717851.00	81.06
			R2	1050801.00	747091.00	83.40
			R3	1027226.00	720619.00	86.13
		α-solanine	R1	999275.00	725933.00	78.93
			R2	1010729.00	828327.00	52.08
			R3	980178.00	832121.00	43.59
	72 hours	Temozolomide	R1	342700.00	75156.00	88.06

			R2	339014.00	89298.00	83.08
			R3	309720.00	47452.00	95.51
		α-solanine	R1	960507.00	320110.00	71.15
			R2	981957.00	234568.00	81.23
			R3	983182.00	208926.00	84.04

Table 12.5.: Scratch migration assay data for U251 cells treated with Temozolomide or α-solanine for 24, 48 and 72 hours.

Cell-line	Duration of incubation	Drug	Replicate	Initial wound size (pixels)	Final wound size (pixels)	Wound closure relative to control (%)
U251	24-hours	Temozolomide	R1	753274.00	171764.00	83.32
			R2	967761.00	249736.00	80.08
			R3	795650.00	179529.00	83.57
		α-solanine	R1	509907.00	189024.00	67.92
			R2	520407.00	268730.00	52.20
			R3	231333.00	97325.00	62.52
	48 hours	Temozolomide	R1	718698.00	16006.00	99.89
			R2	795650.00	32347.00	98.02
			R3	749049.00	18146.00	99.69
		α-solanine	R1	599316.00	26702.00	97.62
			R2	509907.00	43363.00	93.48
			R3	691007.00	49427.00	94.86
	72 hours	Temozolomide	R1	769244.00	56377.00	93.72
			R2	795650.00	69800.00	92.26
			R3	749049.00	54360.00	93.79
		α-solanine	R1	930124.00	178078.00	81.77
			R2	509907.00	65936.00	88.06
			R3	520407.00	40655.00	93.23

Table 12.6.: Scratch migration assay data for T98G cells treated with Temozolomide or α-solanine for 24, 48 and 72 hours.

Cell-line	Duration of incubation	Drug	Replicate	Initial wound size (pixels)	Final wound size (pixels)	Wound closure relative to control (%)
T98G	24-hours	Temozolomide	R1	735150.00	179075.00	75.64
			R2	584203.00	131327.00	77.52
			R3	663639.00	136841.00	79.38
		α-solanine	R1	288376.00	122345.00	57.58

			R2	498959.00	203318.00	59.25
			R3	360156.00	202898.00	43.67
	48 hours	Temozolomide	R1	735150.00	81283.00	99.06
			R2	511975.00	110740.00	87.28
			R3	294422.00	31270.00	99.54
		α-solanine	R1	676783.00	144302.00	87.63
			R2	626325.00	247133.00	67.43
			R3	360156.00	193582.00	51.51
	72 hours	Temozolomide	R1	735150.00	21073.00	97.80
			R2	584203.00	11745.00	98.66
			R3	294422.00	11745.00	96.67
		α-solanine	R1	676783.00	56327.00	92.31
			R2	626325.00	46691.00	93.18
			R3	498959.00	94852.00	81.55

12.4. Trans-well invasion assay data

Table 12.7.: Trans-well invasion assay data for U87MG, U251 and T98G cells treated with α-solanine for 72 hours.

	Solanine								
	U87MG			U251			T98G		
FOV	R1	R2	R3	R1	R2	R3	R1	R2	R3
Upper left	0.00	3.00	0.00	0.00	0.00	0.00	7.00	4.00	4.00
Upper right	0.00	0.00	0.00	1.00	0.00	3.00	6.00	3.00	3.00
Middle	1.00	1.00	1.00	2.00	4.00	3.00	3.00	4.00	2.00
Bottom left	1.00	0.00	0.00	2.00	2.00	0.00	0.00	2.00	1.00
Bottom right	0.00	1.00	0.00	0.00	0.00	0.00	5.00	2.00	0.00
Total	2.00	5.00	1.00	5.00	6.00	6.00	21.00	15.00	10.00
Average	2.67			5.67			15.33		
Average overall	7.89								

Table 12.8.: Trans-well invasion assay data for U87MG, U251 and T98G cells treated with temozolomide for 72 hours.

	Temozolomide								
	U87MG			U251			T98G		
FOV	R1	R2	R3	R1	R2	R3	R1	R2	R3
Upper left	7.00	12.00	15.00	0.00	0.00	0.00	9.00	2.00	3.00
Upper right	6.00	3.00	2.00	0.00	0.00	0.00	0.00	3.00	2.00
Middle	1.00	1.00	0.00	0.00	0.00	0.00	0.00	0.00	1.00

Bottom left	8.00	2.00	3.00	0.00	0.00	0.00	7.00	7.00	6.00
Bottom right	7.00	15.00	1.00	0.00	0.00	2.00	9.00	12.00	1.00
Total	29.00	33.00	21.00	0.00	0.00	2.00	25.00	24.00	13.00
Average	27.67			0.67			20.67		
Average overall	16.33								

Table 12.9.: Trans-well invasion assay data for U87MG, U251 and T98G cells treated with H_2O_2 for 72 hours.

	H2O2								
	U87MG			**U251**			**T98G**		
FOV	R1	R2	R3	R1	R2	R3	R1	R2	R3
Upper left	0.00	0.00	0.00	0.00	0.00	0.00	8.00	3.00	0.00
Upper right	0.00	0.00	0.00	0.00	0.00	0.00	2.00	2.00	1.00
Middle	0.00	0.00	0.00	0.00	0.00	0.00	9.00	7.00	7.00
Bottom left	0.00	0.00	0.00	0.00	0.00	0.00	3.00	4.00	3.00
Bottom right	1.00	0.00	0.00	2.00	0.00	0.00	2.00	1.00	2.00
Total	1.00	0.00	0.00	2.00	0.00	0.00	24.00	17.00	13.00
Average	0.33			0.67			18.00		
Average overall	6.33								

Table 12.10.: Trans-well invasion assay data for U87MG, U251 and T98G cells treated with negative control for 72 hours.

	DMEM/F12 medium								
	U87MG			**U251**			**T98G**		
FOV	R1	R2	R3	R1	R2	R3	R1	R2	R3
Upper left	2.00	0.00	/	0.00	1.00	/	2.00	1.00	0.00
Upper right	0.00	1.00	/	0.00	0.00	/	2.00	0.00	1.00
Middle	0.00	0.00	/	0.00	0.00	/	3.00	0.00	4.00
Bottom left	3.00	0.00	/	0.00	0.00	/	1.00	0.00	0.00
Bottom right	1.00	7.00	/	0.00	0.00	/	1.00	0.00	0.00
Total	6.00	8.00	/	0.00	1.00	/	9.00	1.00	5.00
Average	7.00			0.50			5.00		
Average overall	4.17								

12.5. Real-time quantitative polymerase chain reaction data

12.5.1. Real-time quantitative polymerase chain reaction data for U87MG cells

Table 12.11.: Real-time polymerase chain reaction data for U87MG cells. Bax, Becn1, Casp3, PKM2, VEGFA, ATF6 and ATG4B real-time quantitative polymerase chain reaction data (rt-qPCR)in U87MG cells under 6.25 µM α-solanine, 1200.00 µM temozolomide, 5mM H_2O_2 and culture (negative control) conditions for 24-hours.

Cell Line	Gene	Reading 1	Reading 2	Fold change
U87MG α-solanine	Bax	24.93	25.1	2.09
	Becn1	25.31	25.11	2.58
	Casp3	34.92	36.28	6.77
	PKM2	19.07	19.77	2.68
	VEGFA	20.79	20.58	8.82
	ATF6	26.24	26.76	2.24
	ATG4B	32.98	33.34	4.92
	RPLP0	21.78	21.88	/
U87MG TMZ	Bax	22.65	22.24	1.06
	Becn1	22.74	22.53	1.31
	Casp3	35.19	34.3	1.04
	PKM2	16.89	16.93	1.30
	VEGFA	19.53	19.59	1.64
	ATF6	24.22	24	1.00
	ATG4B	31.47	31.36	1.40
	RPLP0	18.08	18.47	/
U87MG H2O2	Bax	21.83	21.93	1.75
	Becn1	22.47	22.82	1.45
	Casp3	37.36	34.65	0.49
	PKM2	17.04	17.18	1.26
	VEGFA	19.9	19.81	1.49
	ATF6	23.96	24	1.22
	ATG4B	31.01	31.11	2.01
	RPLP0	18.86	18.01	/
U87MG negative control	Bax	22.63	22.31	/
	Becn1	23.19	22.75	/
	Casp3	35.11	34.39	/
	PKM2	17.25	17.21	/
	VEGFA	20.09	20.34	/
	ATF6	23.94	24.17	/
	ATG4B	32.3	31.4	/
	RPLP0	18.1	18.34	/

12.5.2. Real-time quantitative polymerase chain reaction data for U251 cells

Table 12.12.: Real-time polymerase chain reaction data for U87MG cells. Bax, Becn1, Casp3, PKM2, VEGFA, ATF6 and ATG4B real-time quantitative polymerase chain reaction data (rt-qPCR) in U87MG cells under 6.25 µM α-solanine, 1200.00 µM temozolomide, 5mM H_2O_2 and culture (negative control) conditions for 24-hours.

U251 α-solanine	Bax	25.2	25.29	0.52
	Becn1	26.24	26.23	0.18
	Casp3	36.65	36.77	2.87
	PKM2	19.49	19.36	0.28
	VEGFA	24.03	23.94	0.83
	ATF6	27.52	27.44	0.18
	ATG4B	33.77	34.12	0.53
	RPLP0	23.69	23.64	/
U251 TMZ	Bax	20.83	20.77	0.96
	Becn1	20.95	21.08	0.57
	Casp3	34.63	35.06	0.89
	PKM2	14.81	14.98	0.55
	VEGFA	21.07	21.24	0.50
	ATF6	21.95	22.19	0.65
	ATG4B	29.73	29.93	0.79
	RPLP0	17.81	18.68	/
U251 H2O2	Bax	21.78	21.35	0.63
	Becn1	21.51	21.43	0.46
	Casp3	34.37	33.61	1.80
	PKM2	16.59	16.39	0.21
	VEGFA	22.17	21.9	0.30
	ATF6	22.35	21.89	0.70
	ATG4B	30.72	30.81	0.46
	RPLP0	17.19	17.2	/
U251 negative control	Bax	20.79	20.59	/
	Becn1	20.38	19.92	/
	Casp3	34.93	34.31	/
	PKM2	14.1	13.88	/
	VEGFA	19.94	20.27	/
	ATF6	21.05	21.75	/
	ATG4B	29.81	29.05	/
	RPLP0	16.1	16.37	/

12.5.3. Real-time quantitative polymerase chain reaction data for U87MG cells

Table 12.13.: Real-time polymerase chain reaction data for U87MG cells. Bax, Becn1, Casp3, PKM2, VEGFA, ATF6 and ATG4B real-time quantitative polymerase chain reaction data (rt-qPCR) in U87MG cells under 6.25 µM α-solanine, 1200.00 µM temozolomide, 5mM H_2O_2 and culture (negative control) conditions for 24-hours.

T98G α-solanine	Bax	23.2	23.04	1.47
	Becn1	24.74	25.25	0.54
	Casp3	37.03	37.02	4.08
	PKM2	17.34	17.47	1.76
	VEGFA	30.89	30.9	150.64
	ATF6	31.65	31.56	2.86
	ATG4B	32.99	32.67	1.58
	RPLP0	22.24	22.23	/
T98G TMZ	Bax	20.32	20.09	0.95
	Becn1	21.21	20.71	0.75
	Casp3	35.69	34.97	1.13
	PKM2	14.86	14.58	0.96
	VEGFA	28.84	28.98	50.74
	ATF6	27.2	28.46	3.33
	ATG4B	29.95	29.88	1.01
	RPLP0	17.23	17.64	/
T98G H2O2	Bax	20.55	20.1	0.97
	Becn1	21.31	21.11	0.70
	Casp3	35.5	34.58	1.54
	PKM2	15.22	15.02	0.82
	VEGFA	28.58	28.63	70.03
	ATF6	28.14	27.82	3.35
	ATG4B	29.76	30.01	1.16
	RPLP0	17.53	17.83	/
T98G negative control	Bax	20.21	19.93	/
	Becn1	20.58	20.4	/
	Casp3	35.17	35.73	/
	PKM2	14.6	14.62	/
	VEGFA	32.36	36.68	/
	ATF6	28.67	30.35	/
	ATG4B	29.97	29.79	/
	RPLP0	17.86	17.64	/

12.6. Fluorescent intensity data

12.6.1. Images obtained from fluorescent staining experiments

12.6.1.1. U87MG, U251 and T98G cell staining against apoptotic cell death

12.6.1.1.1. Bright field imaging

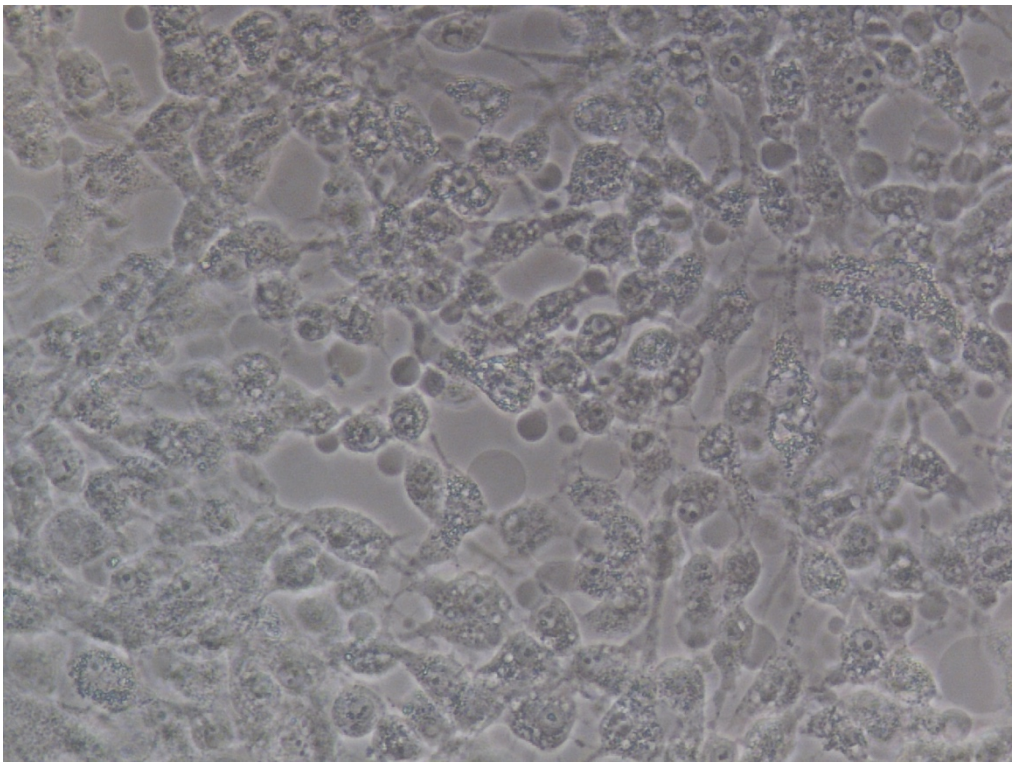


Figure 12.2.: Bright field view of U87MG cells under culture (negative control) conditions incubated for 24hours. Replicate: 1; magnification: x100.

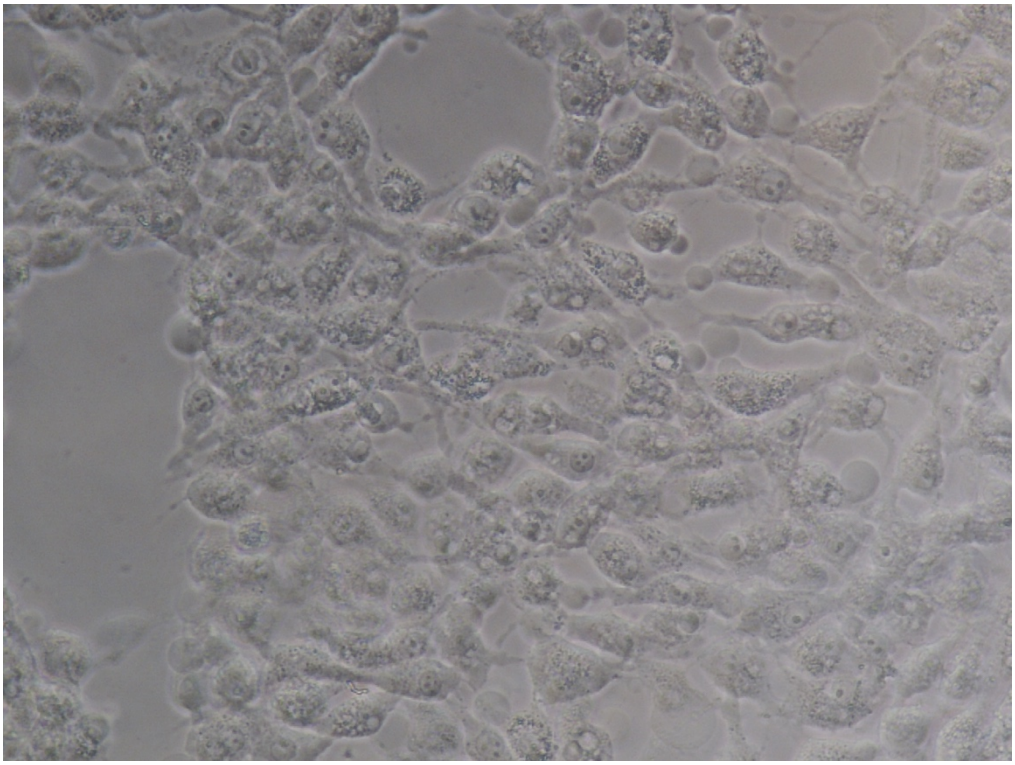


Figure 12.3.: Bright field view of U87MG cells under culture (negative control) conditions incubated for 24 -hours. Replicate: 2; magnification: x100.

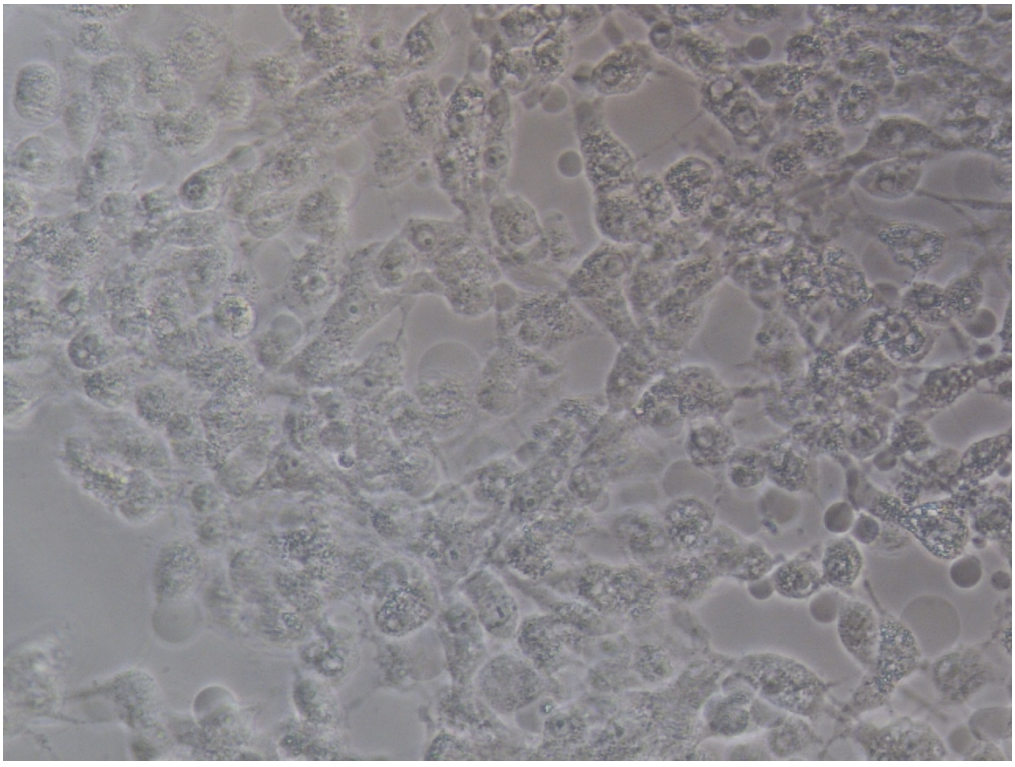


Figure 12.4.: Bright field view of U87MG cells under culture (negative control) conditions incubated for 24hours. Replicate: 3; magnification: x100.

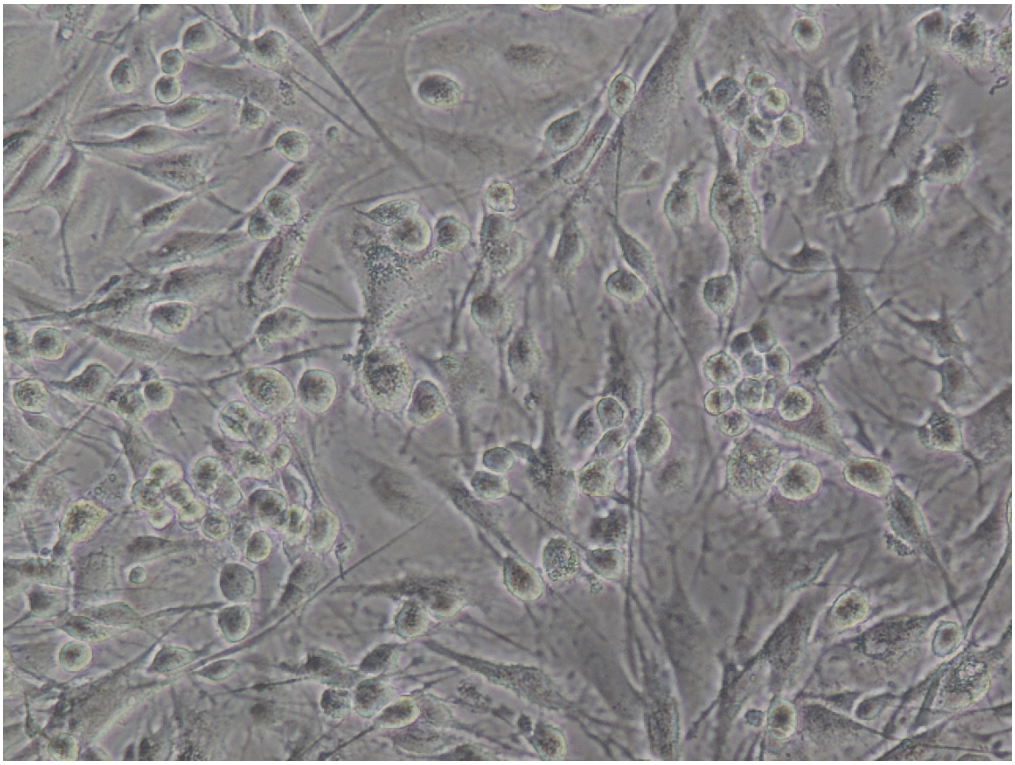


Figure 12.5.: Bright field view of U251 cells under culture (negative control) conditions incubated for 24 -hours. Replicate: 1; magnification: x100.

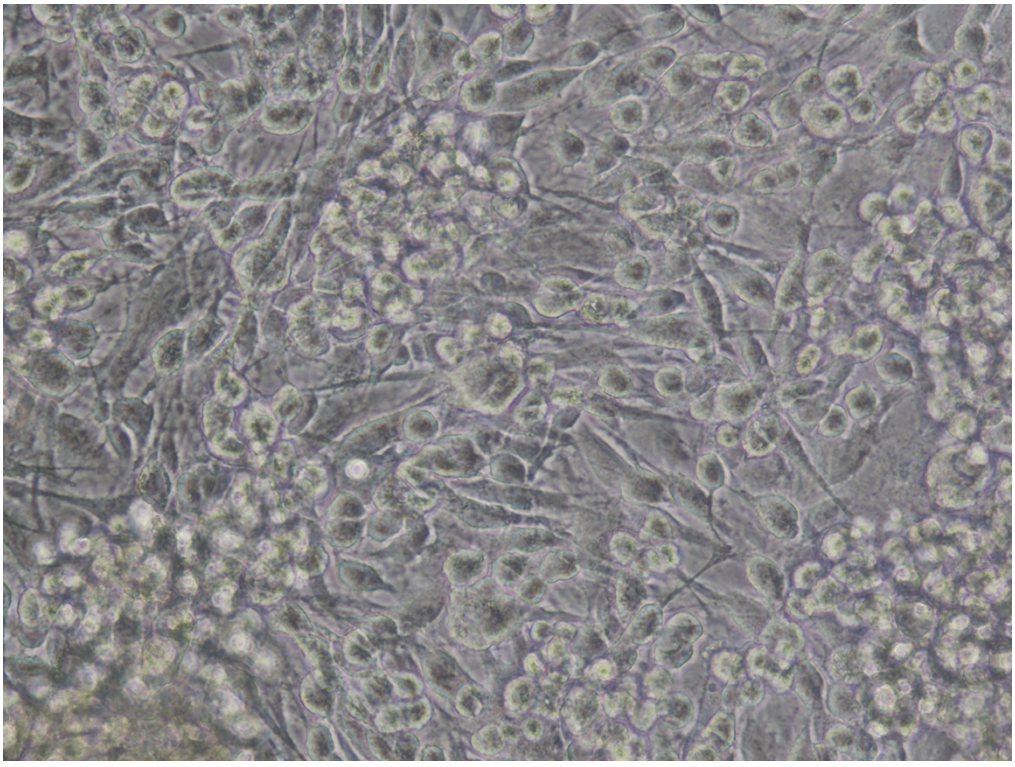


Figure 12.6.: Bright field view of U251 cells under culture (negative control) conditions incubated for 24 -hours. Replicate: 2; magnification: x100.

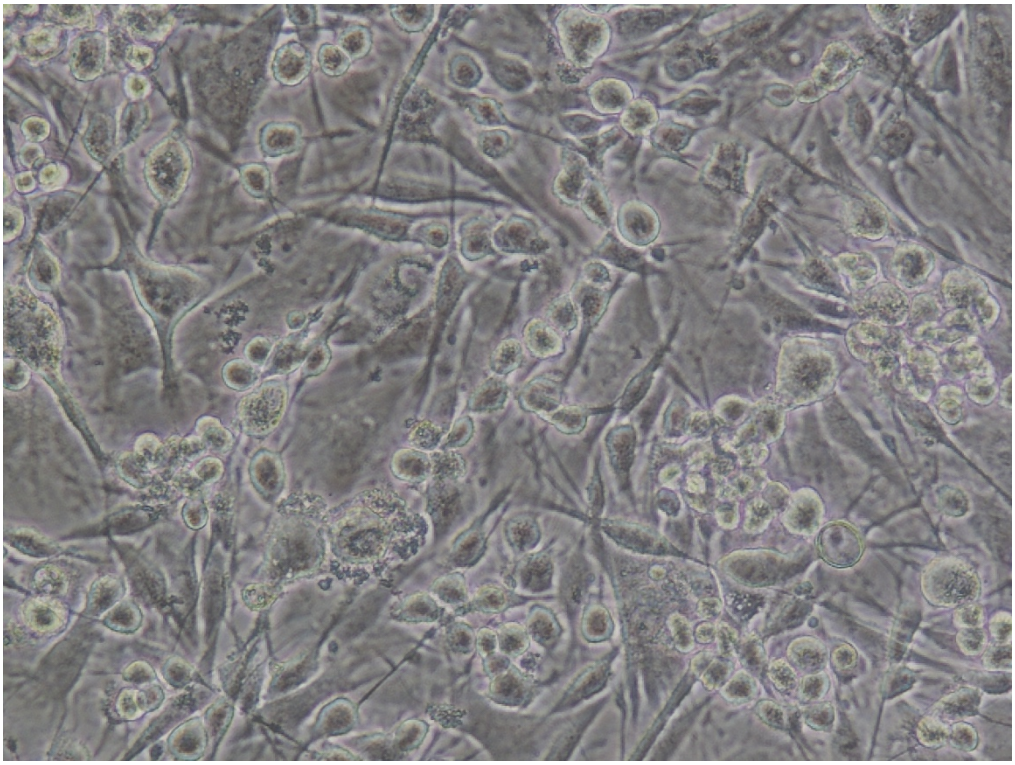


Figure 12.7.: Bright field view of U251 cells under culture (negative control) conditions incubated for 24 -hours. Replicate: 3; magnification: x100.

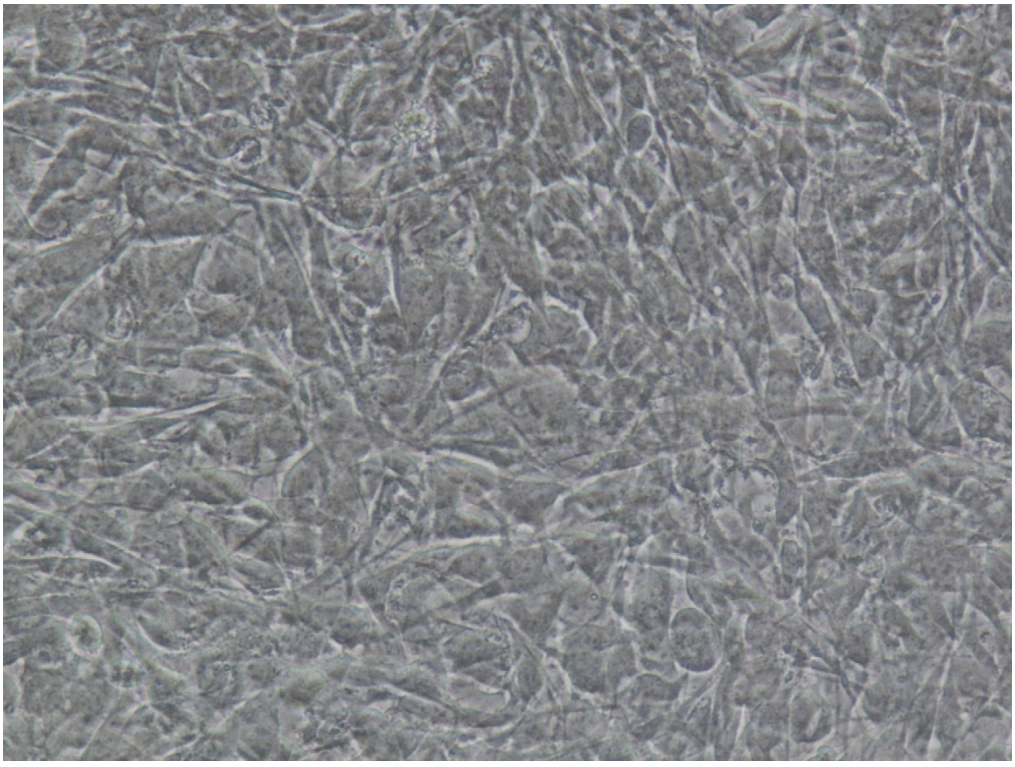


Figure 12.8.: Bright field view of T98G cells under culture (negative control) conditions incubated for 24-hours. Replicate: 1; magnification: x100.

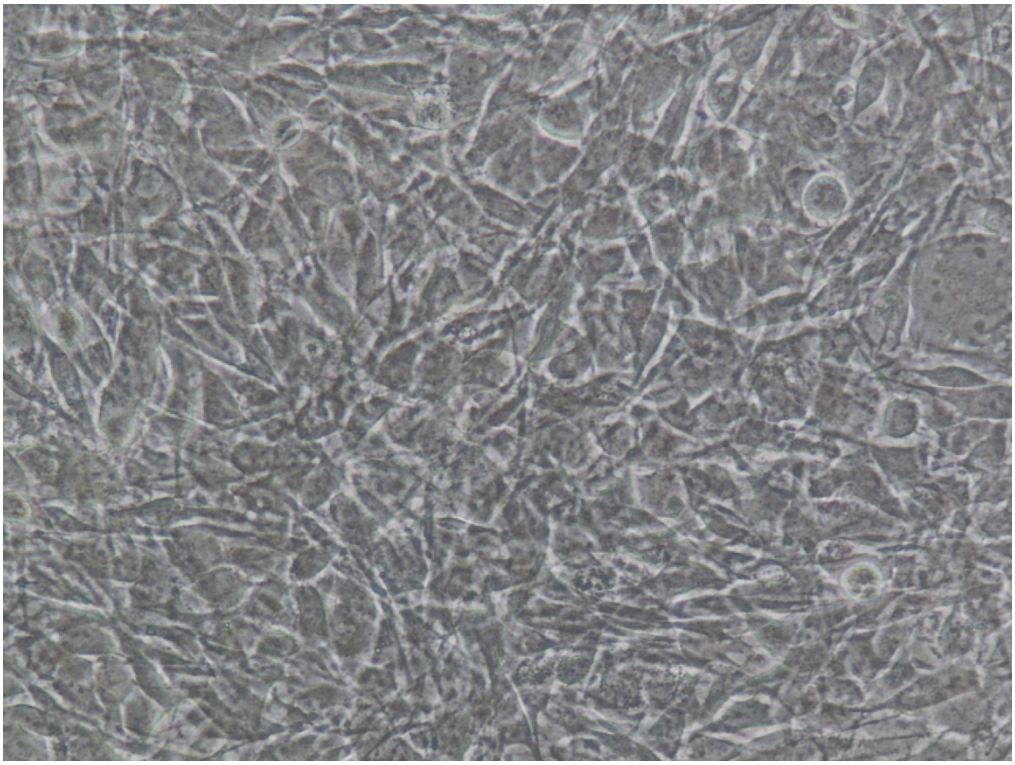


Figure 12.9.:Bright field view of T98G cells under culture (negative control) conditions incubated for 24-hours. Replicate: 2; magnification: x100.

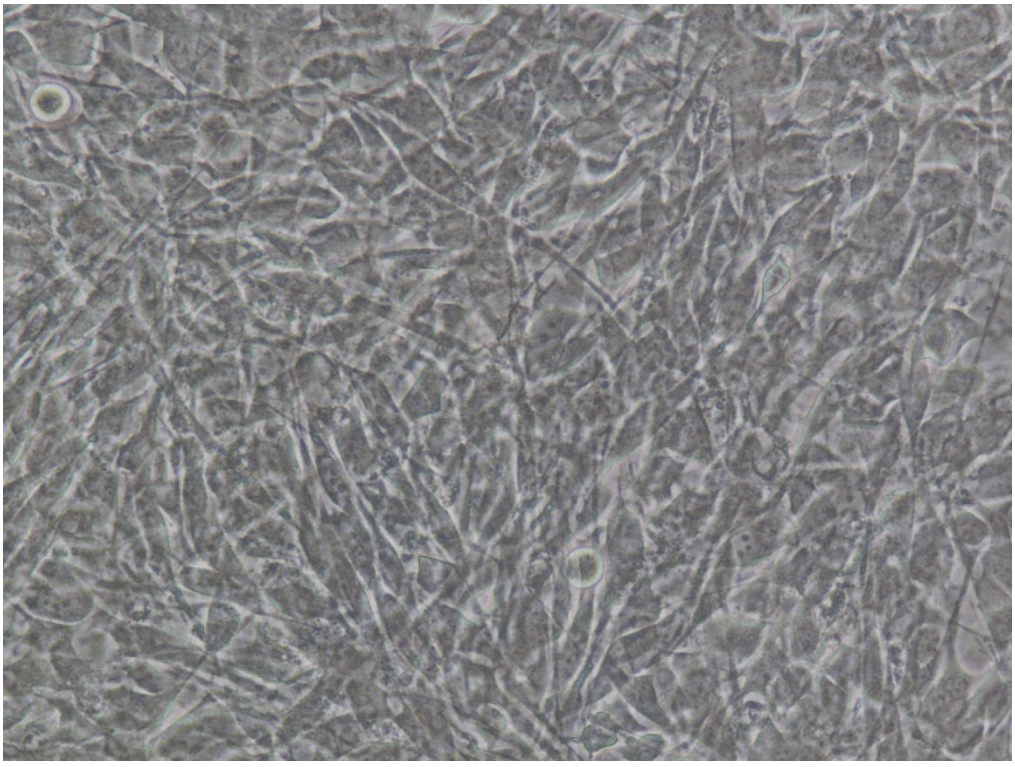


Figure 12.10.: Bright field view of T98G cells under culture (negative control) conditions incubated for 24-hours. Replicate: 3; magnification: x100.

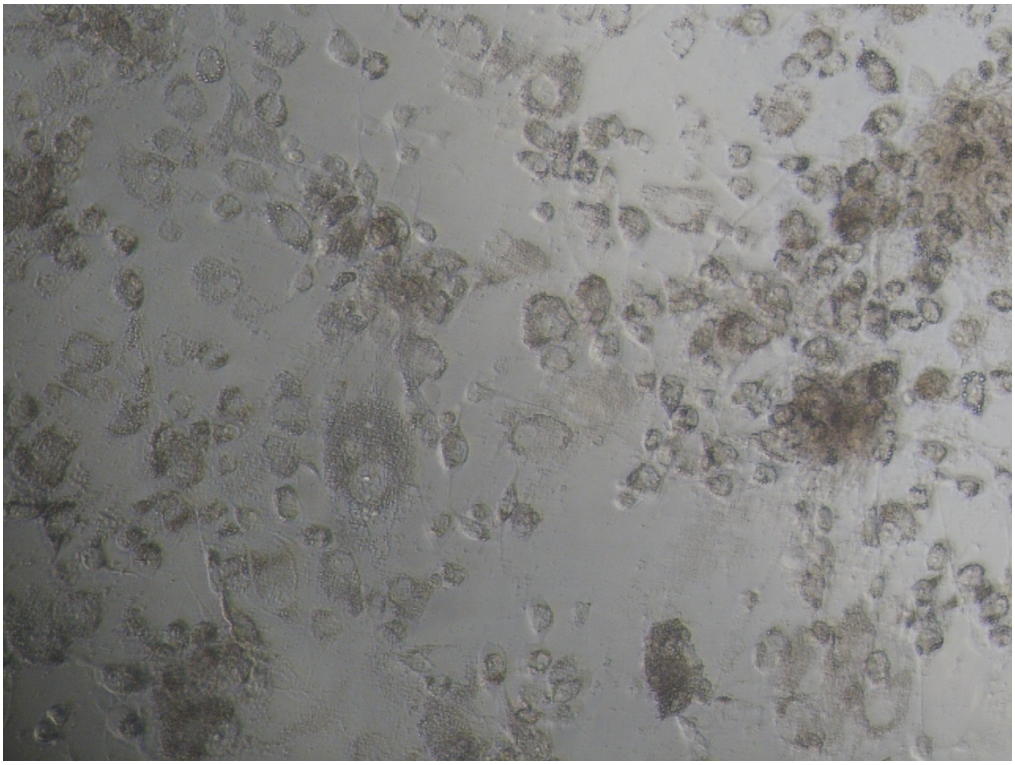


Figure 12.11.: Bright field view of U87MG cells treated with 6.25 µM α-solanine and incubated for 24-hours. Replicate: 1; magnification: x100.

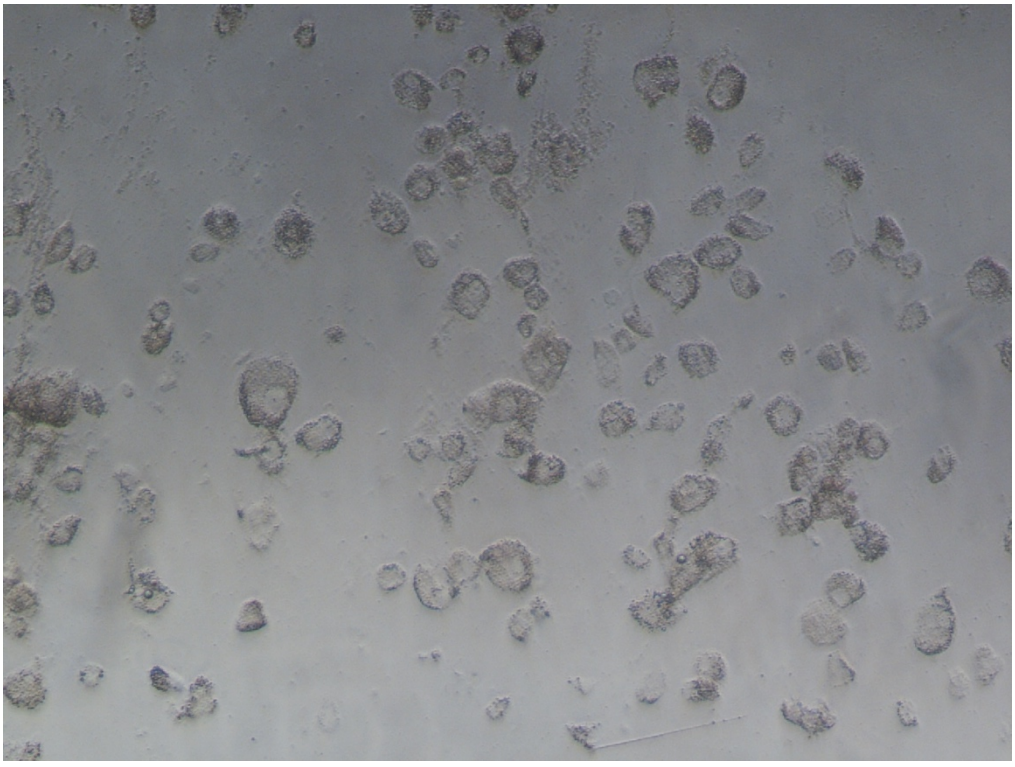


Figure 12.12.: Bright field view of U87MG cells treated with 6.25 µM α-solanine and incubated for 24-hours. Replicate: 2; magnification: x100.

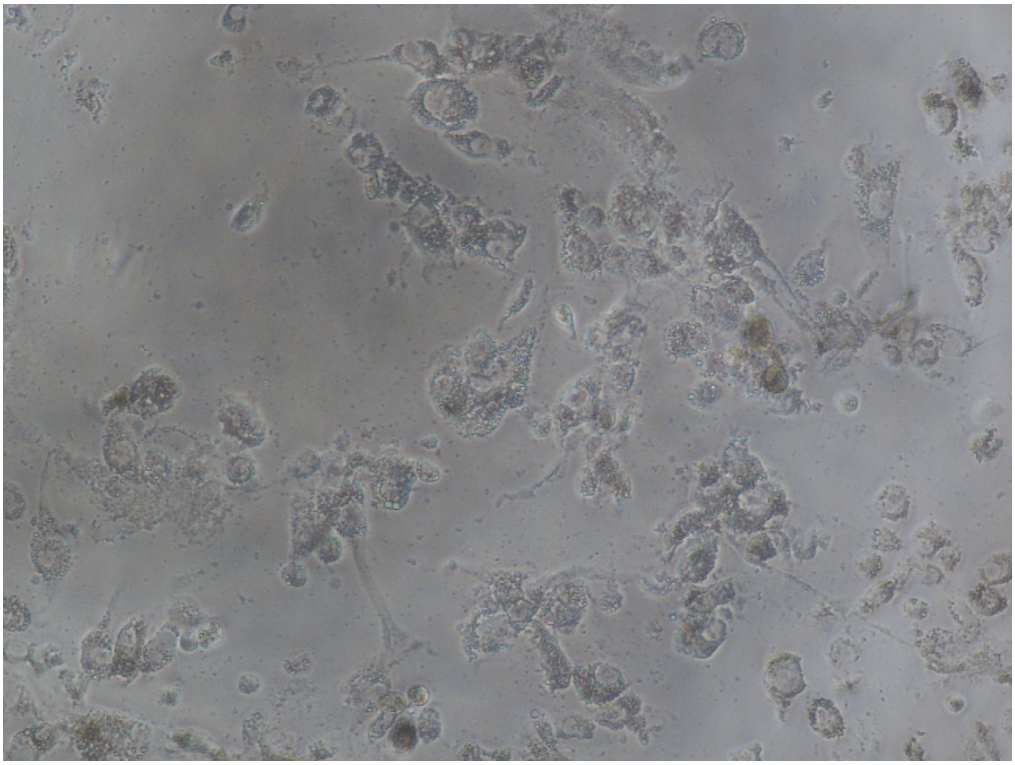


Figure 12.13.: Bright field view of U87MG cells treated with 6.25 µM α-solanine and incubated for 24-hours. Replicate: 3; magnification: x100.

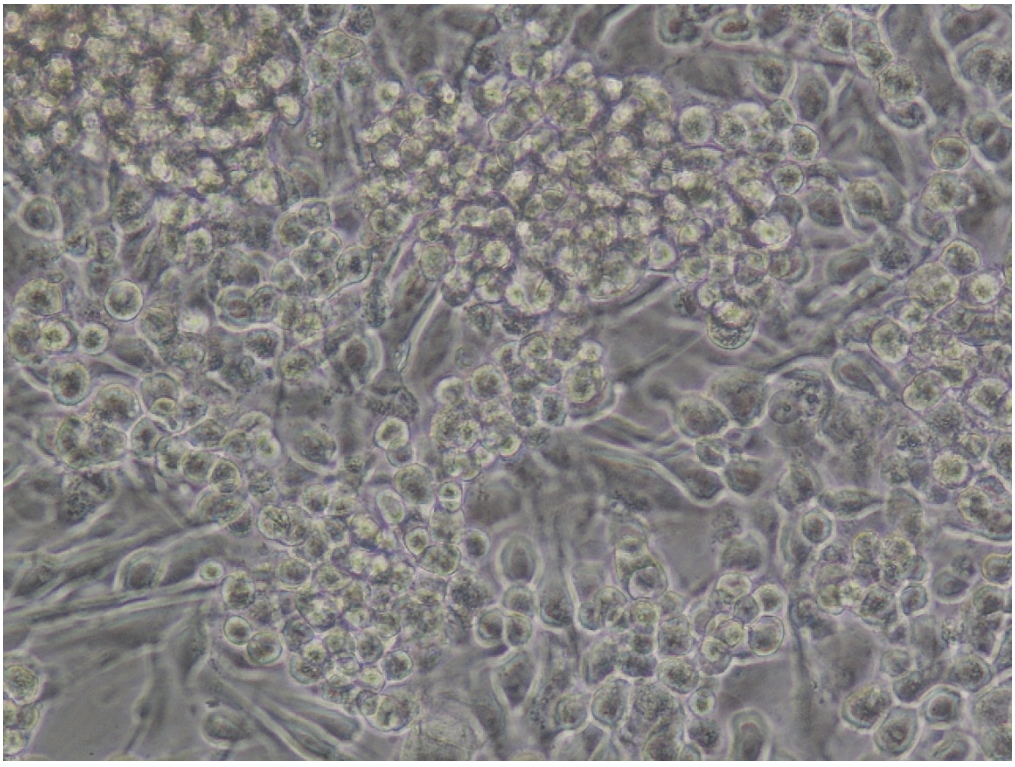


Figure 12.14.: Bright field view of U251 cells treated with 6.25 µM α-solanine and incubated for 24-hours. Replicate: 1; magnification: x100.

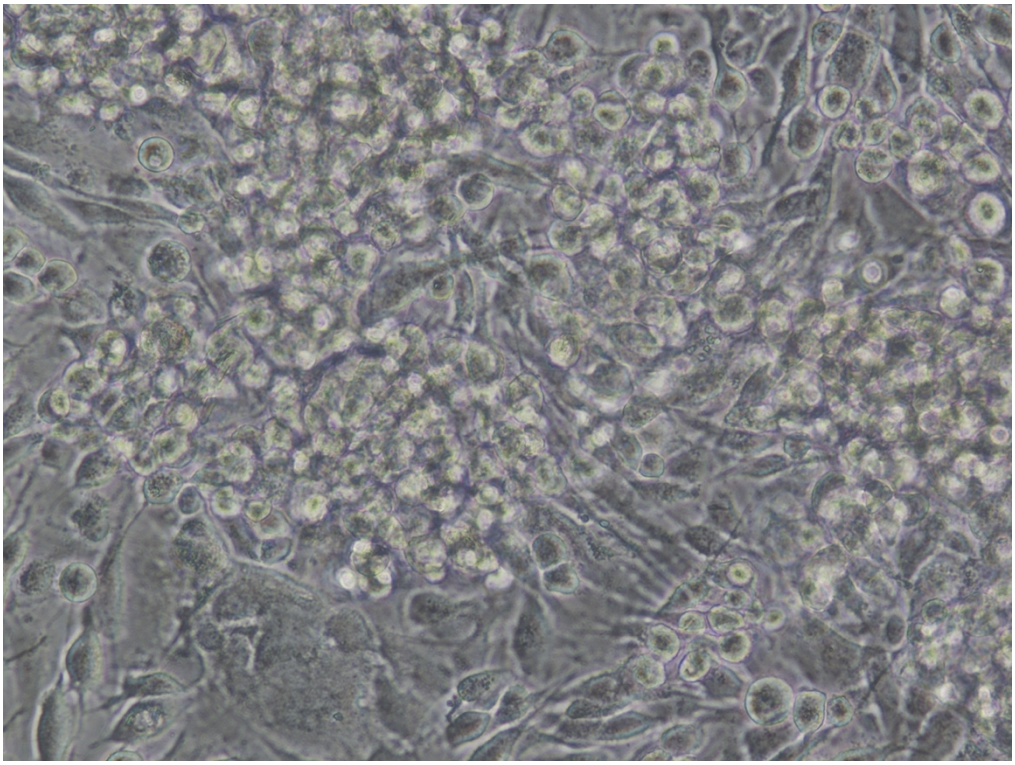


Figure 12.15.: Bright field view of U251 cells treated with 6.25 µM α-solanine and incubated for 24-hours. Replicate: 2; magnification: x100.

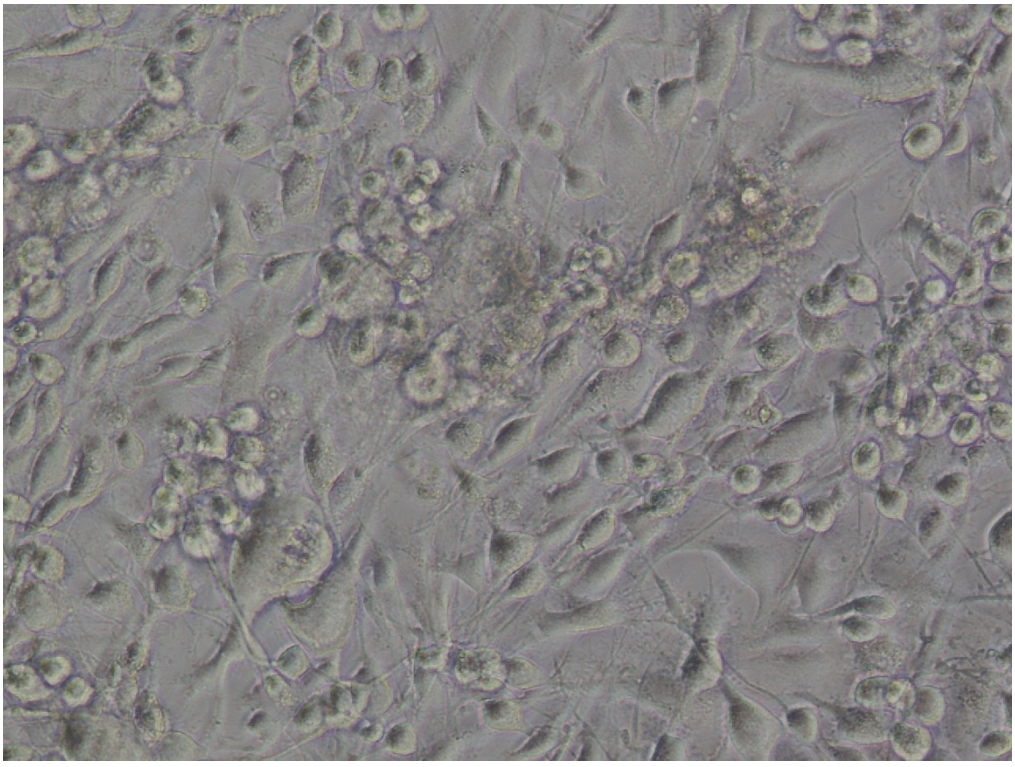


Figure 12.16.: Bright field view of U251 cells treated with 6.25 µM α-solanine and incubated for 24-hours. Replicate: 3; magnification: x100.

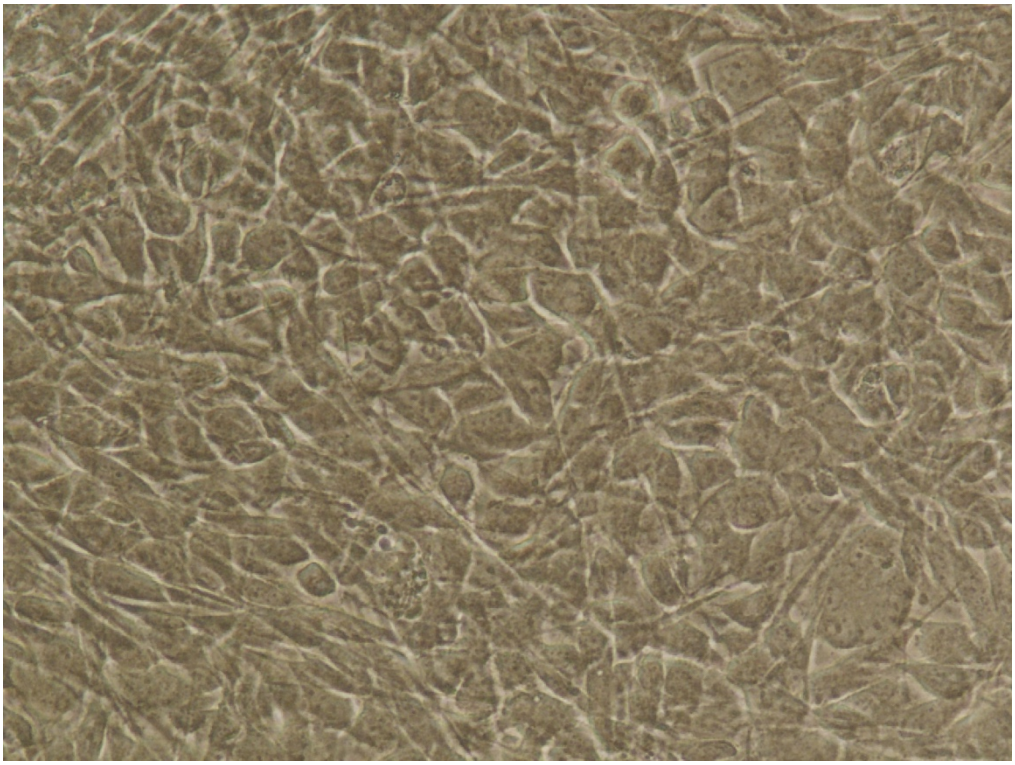


Figure 12.17.: Bright field view of T98G cells treated with 6.25 µM α-solanine and incubated for 24-hours. Replicate: 1; magnification: x100.

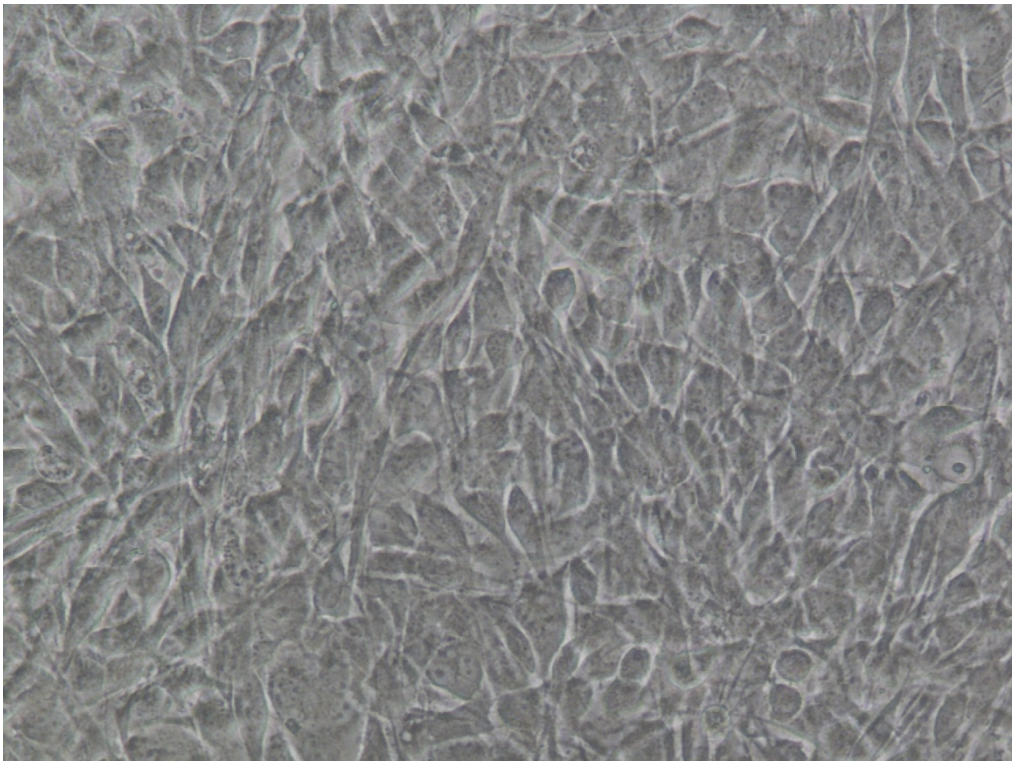


Figure 12.18.:Bright field view of T98G cells treated with 6.25 µM α-solanine and incubated for 24-hours. Replicate: 2; magnification: x100.

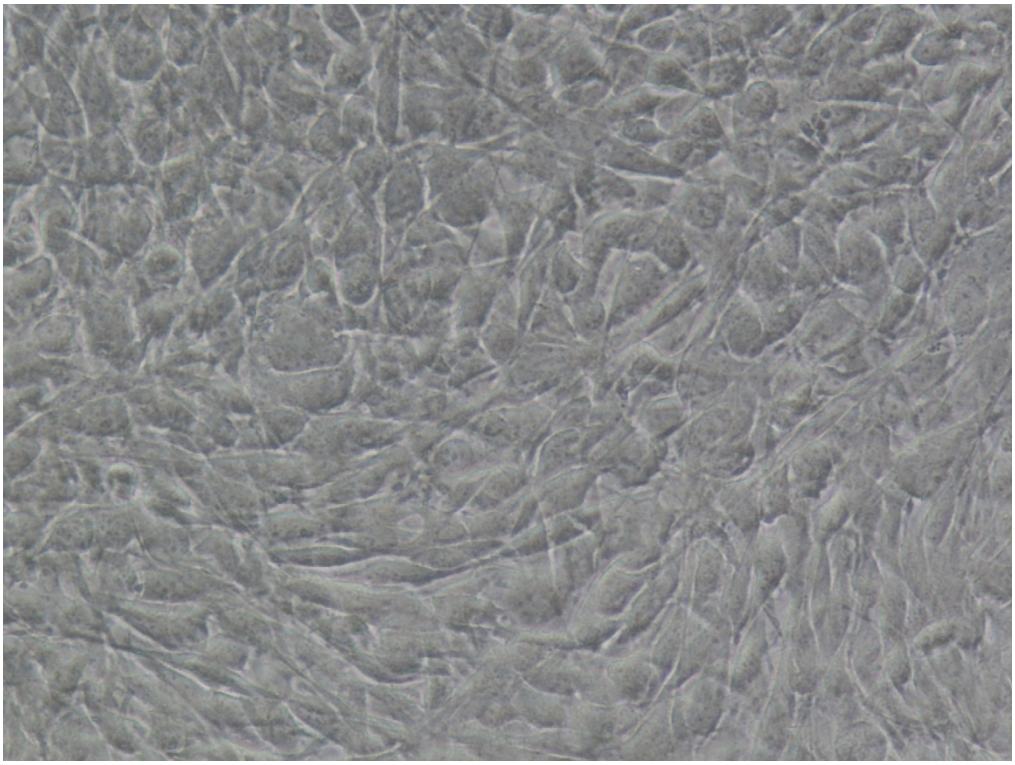


Figure 12.19.: Bright field view of T98G cells treated with 6.25 µM α-solanine and incubated for 24-hours. Replicate: 3; magnification: x100.

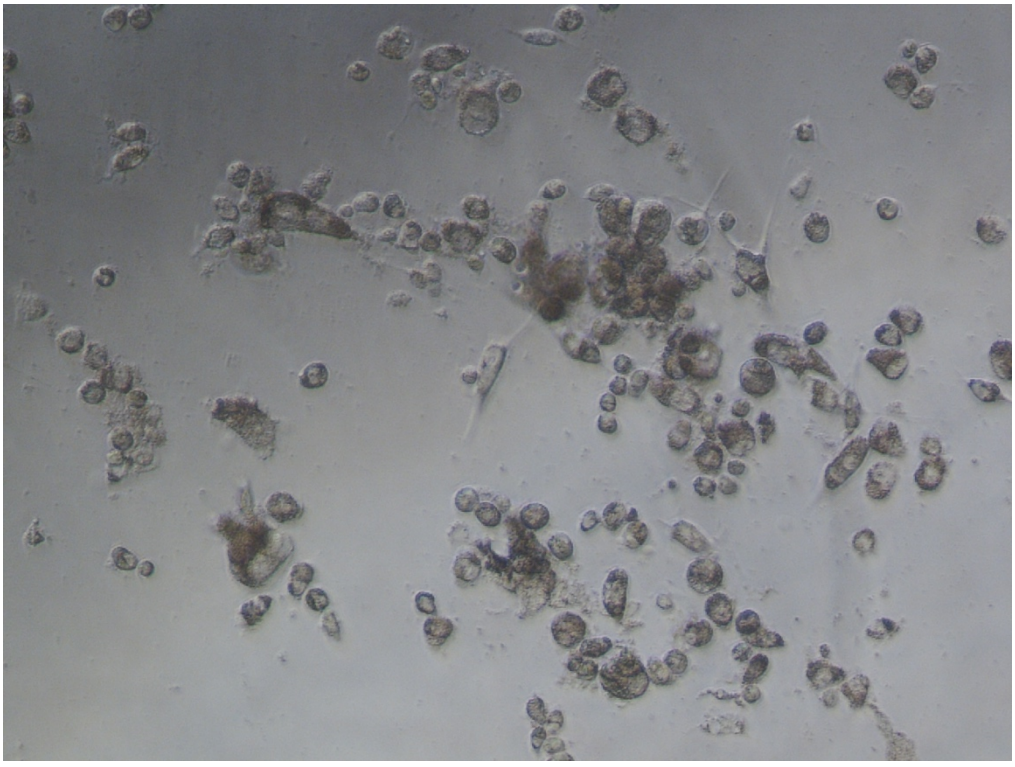


Figure 12.20.: Bright field view of U87MG cells treated with 1200.00 µM temozolomide and incubated for 24-hours. Replicate: 1; magnification: x100.

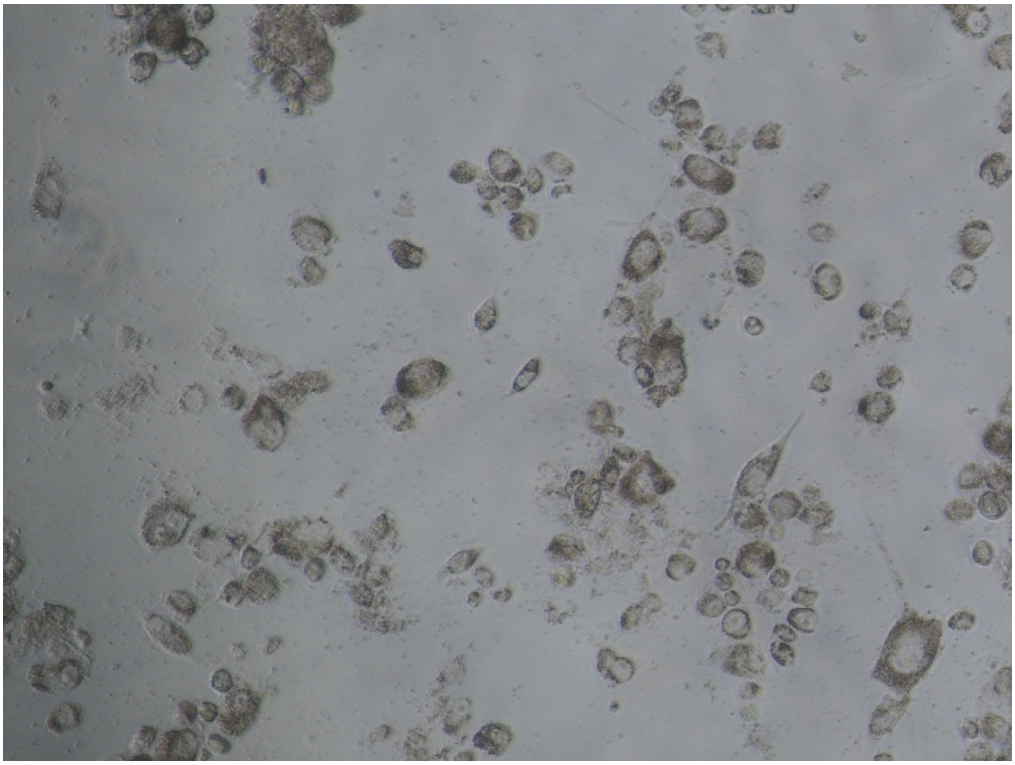


Figure 12.21.: Bright field view of U87MG cells treated with 1200.00 µM temozolomide and incubated for 24-hours. Replicate: 2; magnification: x100.

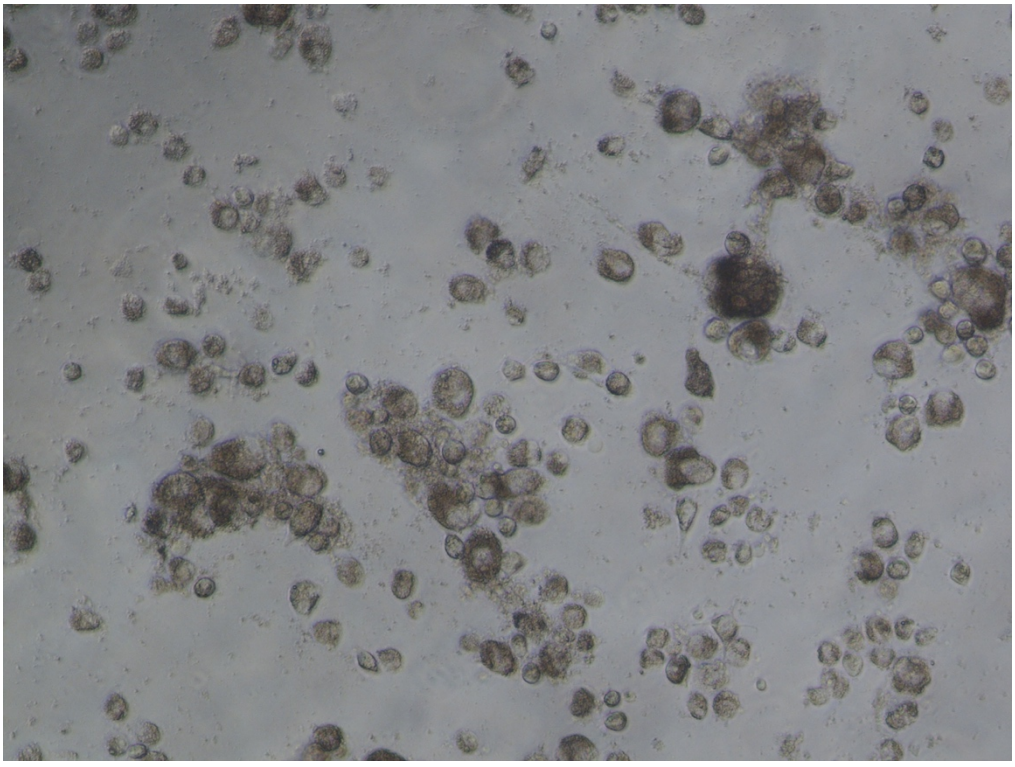


Figure 12.22.: Bright field view of U87MG cells treated with 1200.00 µM temozolomide and incubated for 24-hours. Replicate: 3; magnification: x100.

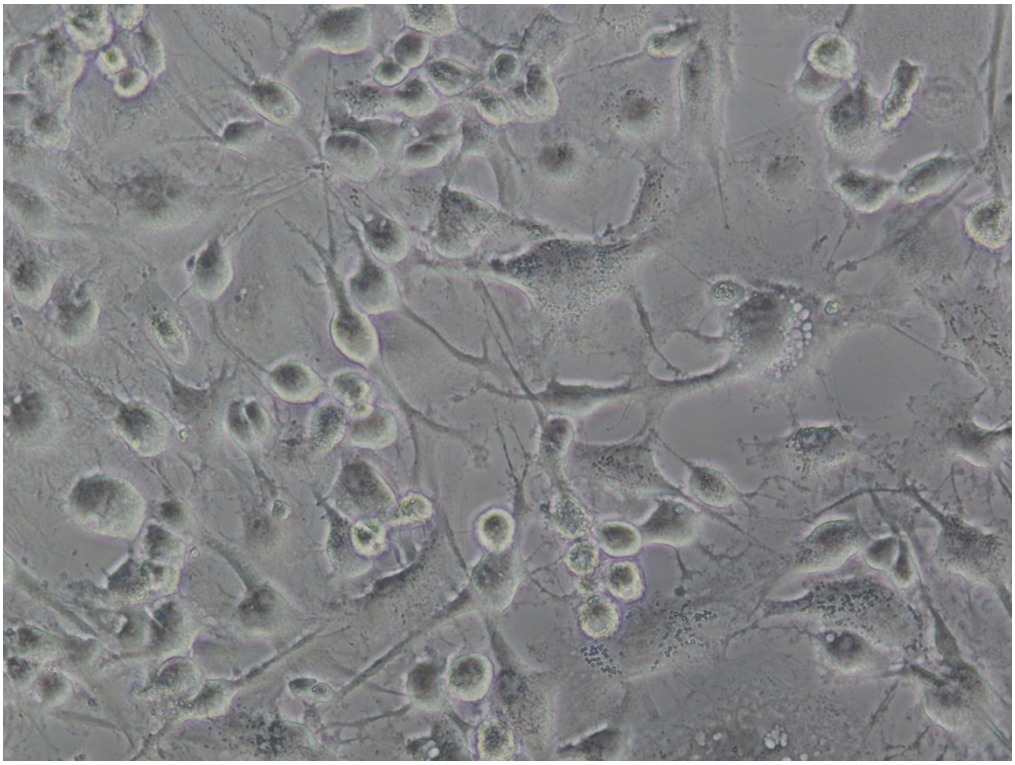


Figure 12.23.: Bright field view of U251 cells treated with 1200.00 µM temozolomide and incubated for 24-hours. Replicate: 1; magnification: x100.

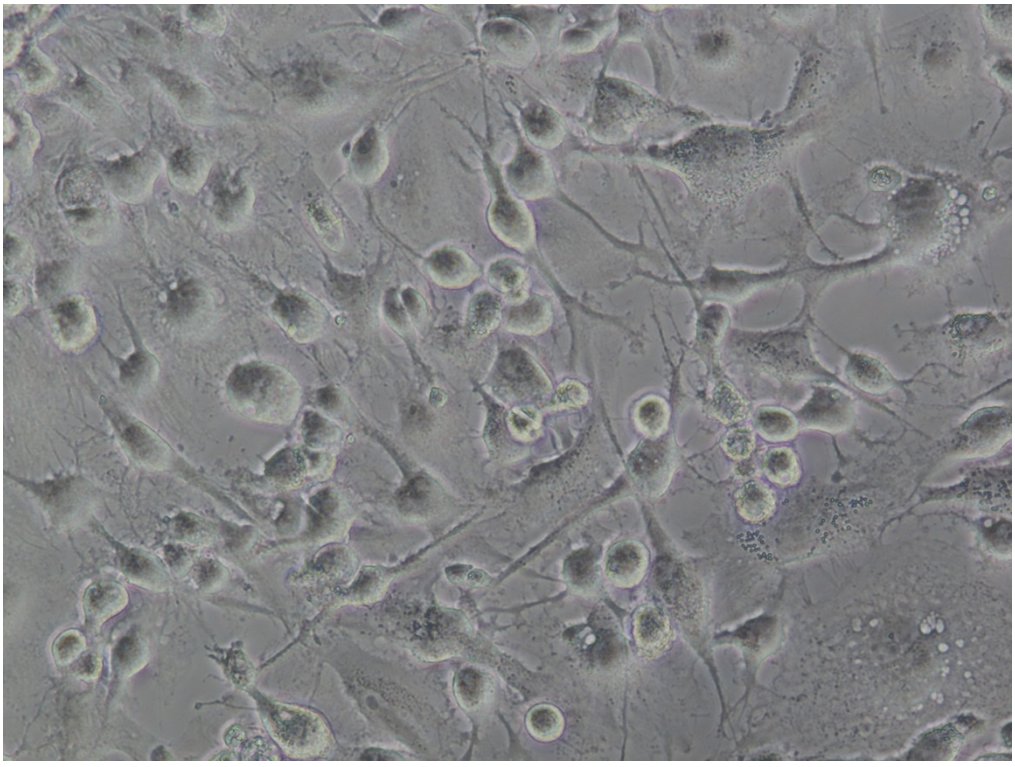


Figure 12.24.: Bright field view of U251 cells treated with 1200.00 µM temozolomide and incubated for 24-hours. Replicate: 1; magnification: x100.

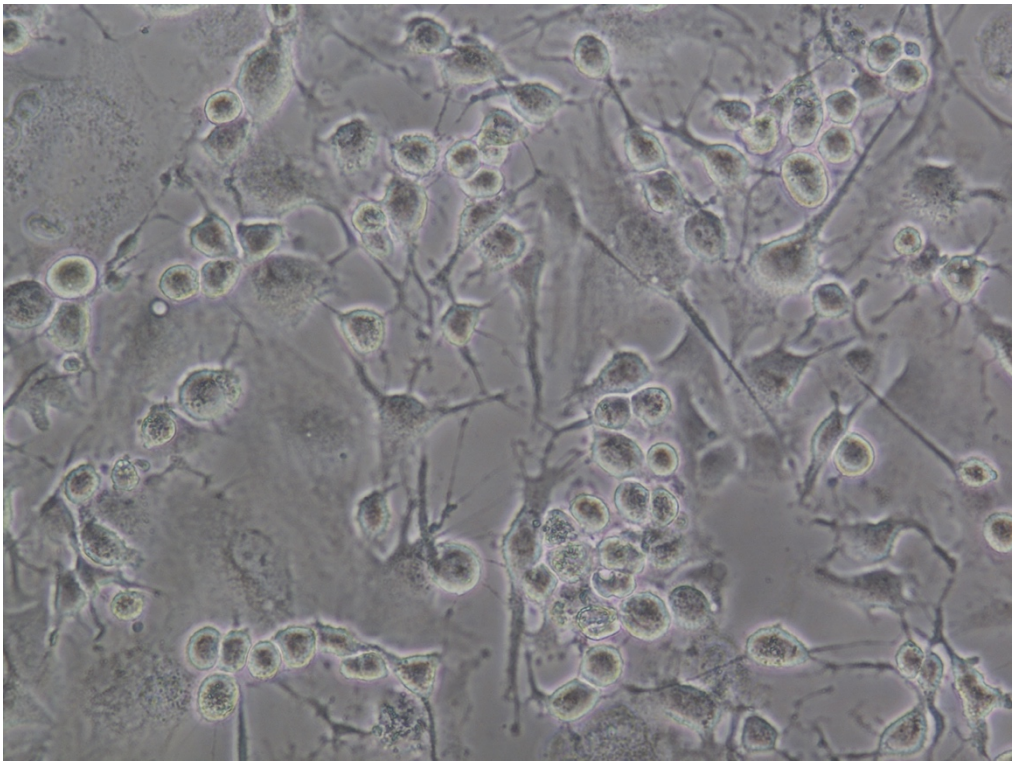


Figure 12.25.: Bright field view of U251 cells treated with 1200.00 µM temozolomide and incubated for 24-hours. Replicate: 1; magnification: x100.

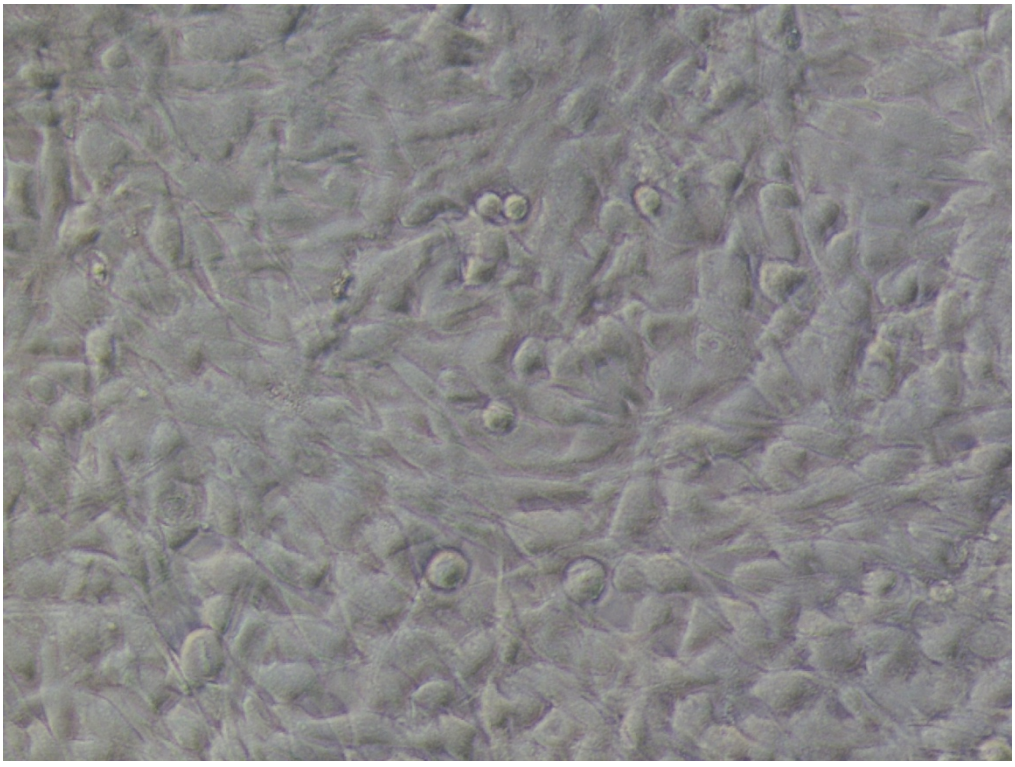


Figure 12.26.: Bright field view of T98G cells treated with 1200.00 µM temozolomide and incubated for 24-hours. Replicate: 1; magnification: x100.

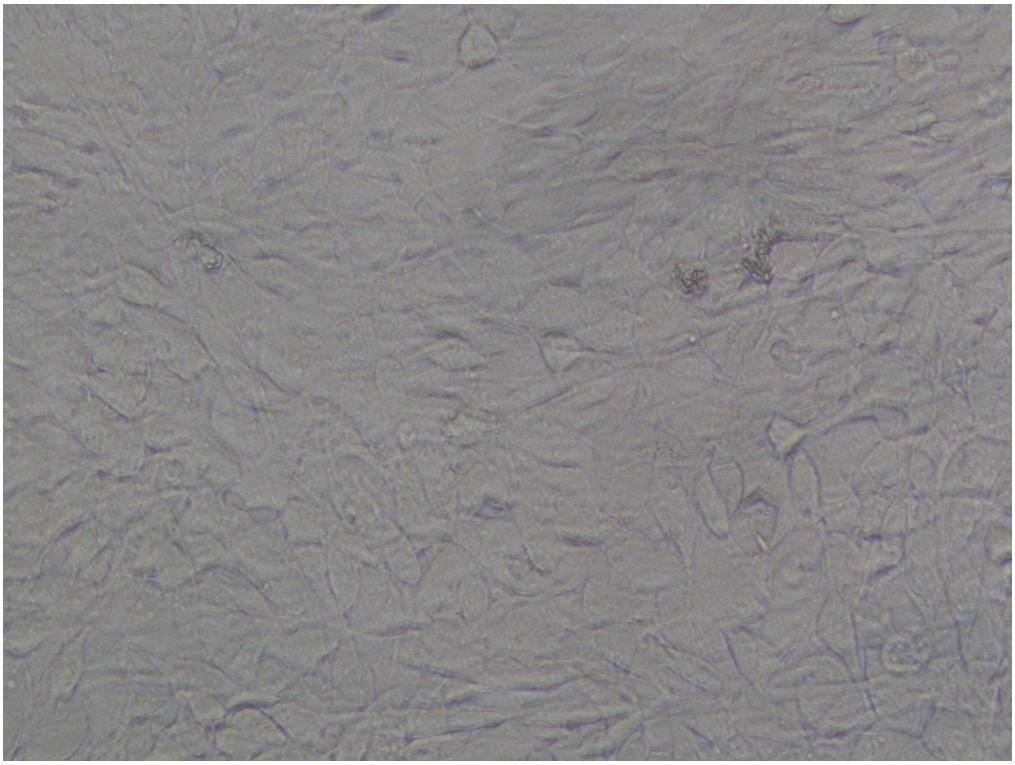


Figure 12.27.:Bright field view of T98G cells treated with 1200.00 µM temozolomide and incubated for 24-hours. Replicate: 2; magnification: x100.

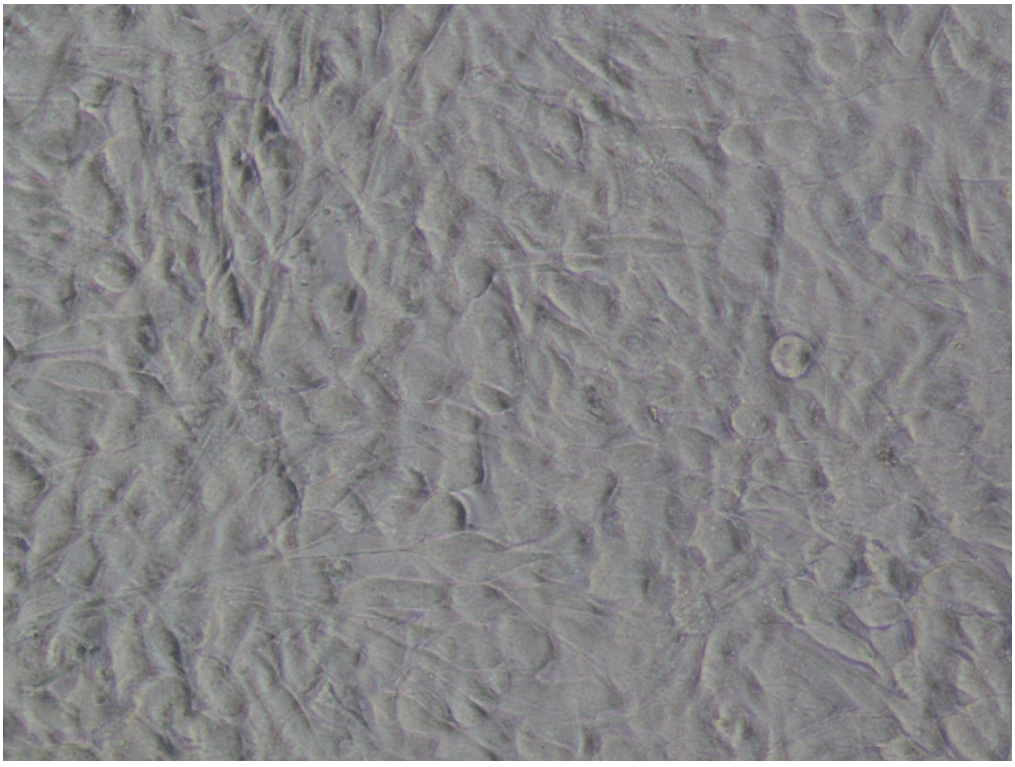


Figure 12.28.: Bright field view of T98G cells treated with 1200.00 µM temozolomide and incubated for 24-hours. Replicate: 3; magnification: x100.

12.6.1.1.2. Propidium iodide staining



Figure 12.29.: U87MG cells under culture (negative control) conditions incubated for 24-hours and stained with propidium iodide. Replicate: 1; magnification: x100.



Figure 12.30.:U87MG cells under culture (negative control) conditions incubated for 24-hours and stained with propidium iodide. Replicate: 2; magnification: x100.

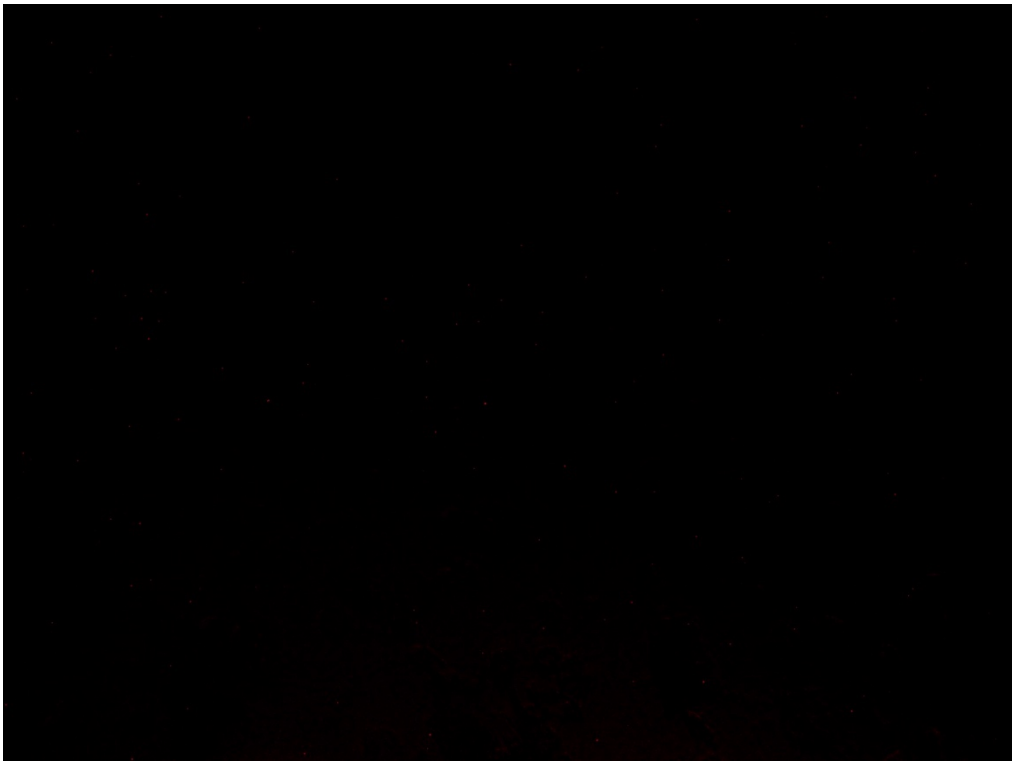


Figure 12.31.: U87MG cells under culture (negative control) conditions incubated for 24-hours and stained with propidium iodide. Replicate: 3; magnification: x100.



Figure 12.32.: U251 cells under culture (negative control) conditions incubated for 24-hours and stained with propidium iodide. Replicate: 1; magnification: x100.



Figure 12.33.: U251 cells under culture (negative control) conditions incubated for 24-hours and stained with propidium iodide. Replicate: 2; magnification: x100.



Figure 12.34.: U251 cells under culture (negative control) conditions incubated for 24-hours and stained with propidium iodide. Replicate: 3; magnification: x100.

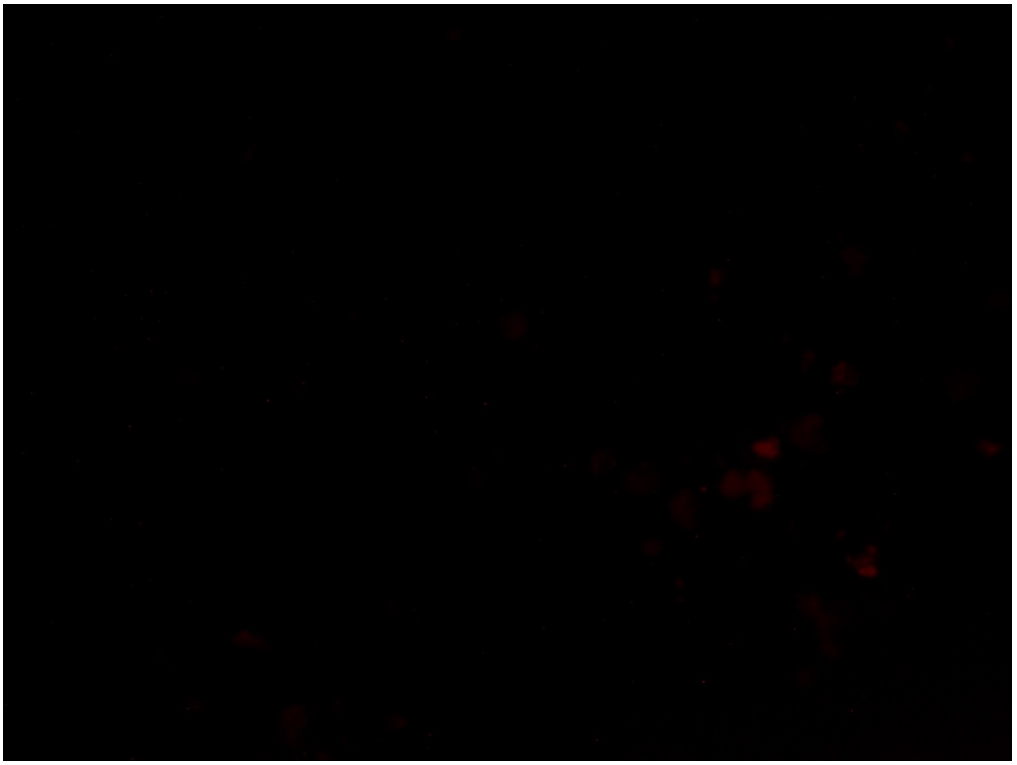


Figure 12.35.: T98G cells under culture (negative control) conditions incubated for 24-hours and stained with propidium iodide. Replicate: 1; magnification: x100.

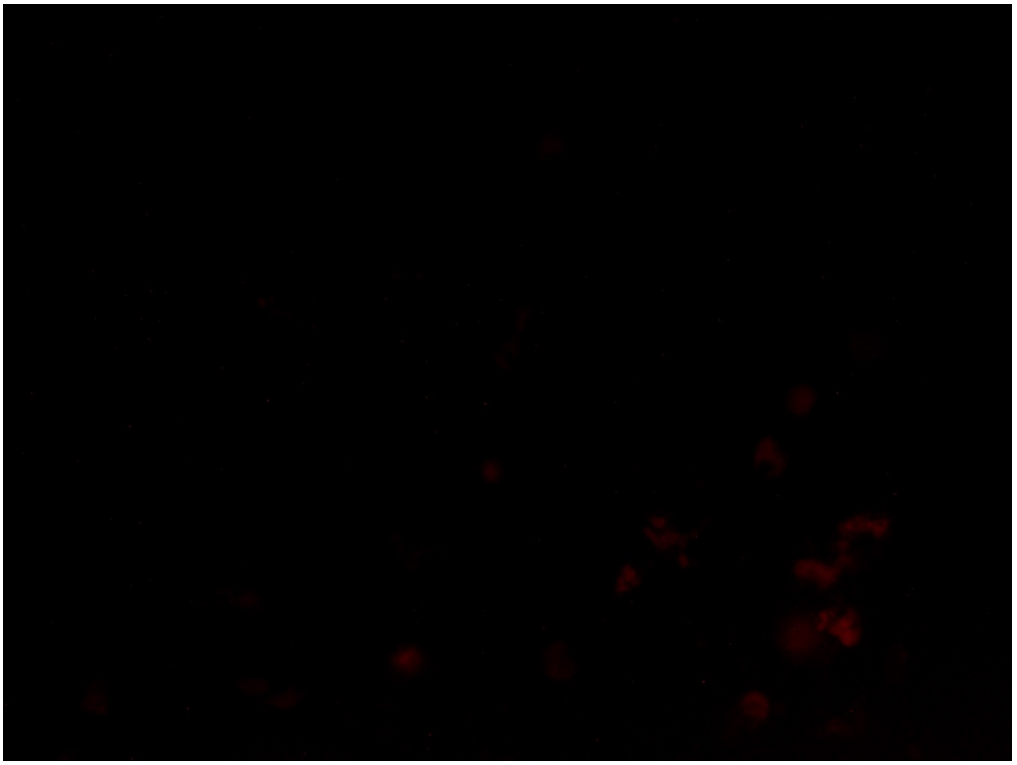


Figure 12.36.: T98G cells under culture (negative control) conditions incubated for 24-hours and stained with propidium iodide. Replicate: 2; magnification: x100.

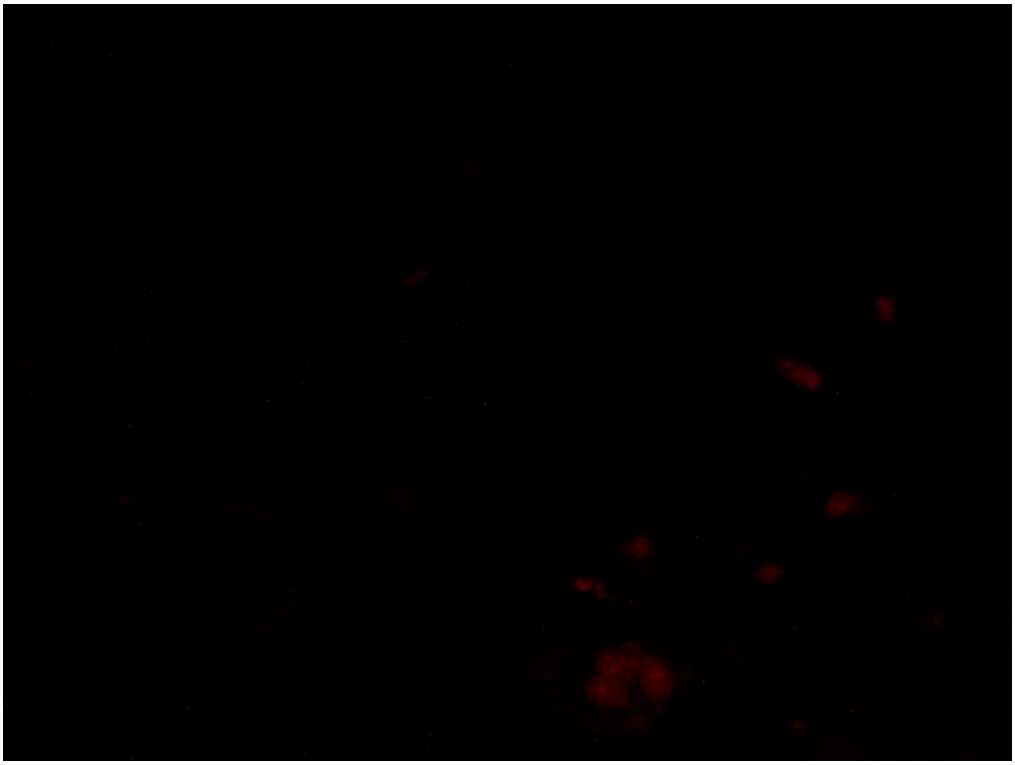


Figure 12.37.: T98G cells under culture (negative control) conditions incubated for 24-hours and stained with propidium iodide. Replicate: 3; magnification: x100.



Figure 12.38.:U87MG cells treated with 6.25 µM α-solanine and incubated for 24-hours and stained with propidium iodide. Replicate: 1; magnification: x100.



Figure 12.39.: U87MG cells treated with 6.25 µM α-solanine and incubated for 24-hours and stained with propidium iodide. Replicate: 2; magnification: x100.

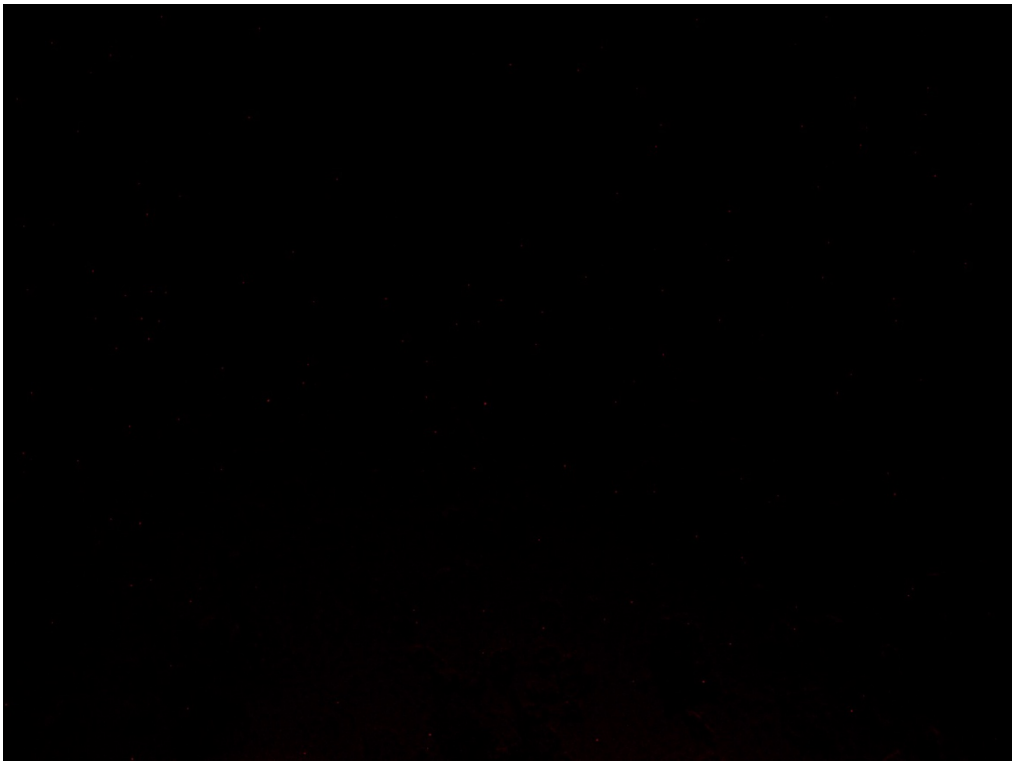


Figure 12.40.: U87MG cells treated with 6.25 µM α-solanine and incubated for 24-hours dual stained with propidium iodide. Replicate: 3; magnification: x100.

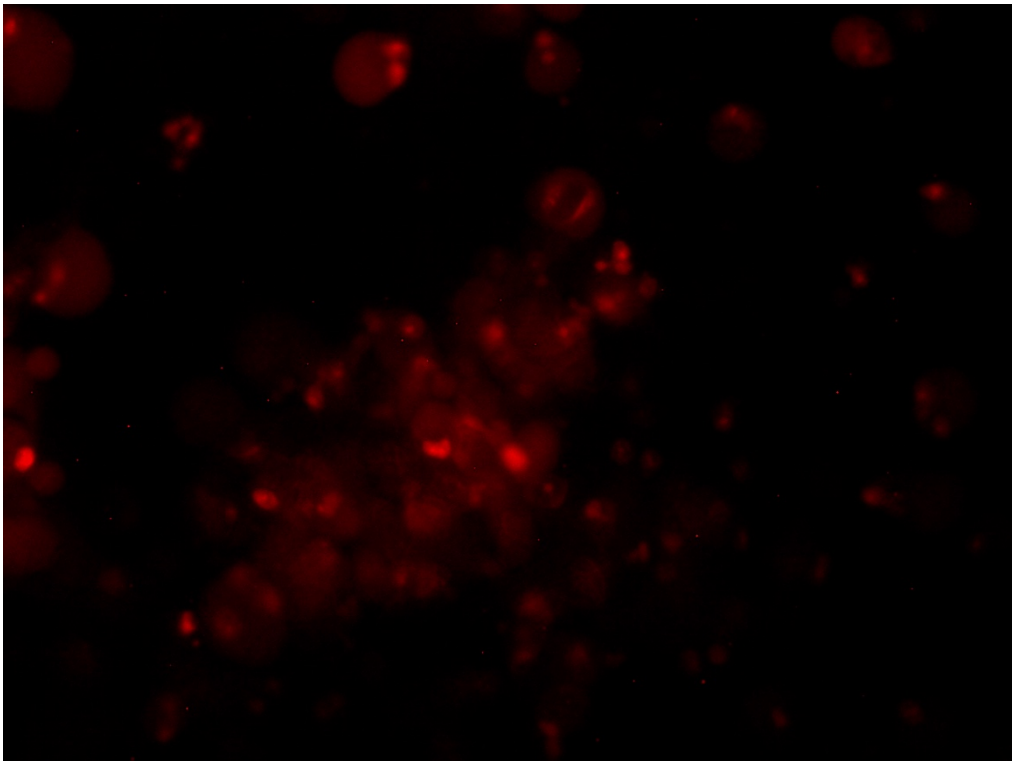


Figure 12.41.: U251 cells treated with 6.25 µM α-solanine and incubated for 24-hours and stained with propidium iodide. Replicate: 1; magnification: x100.

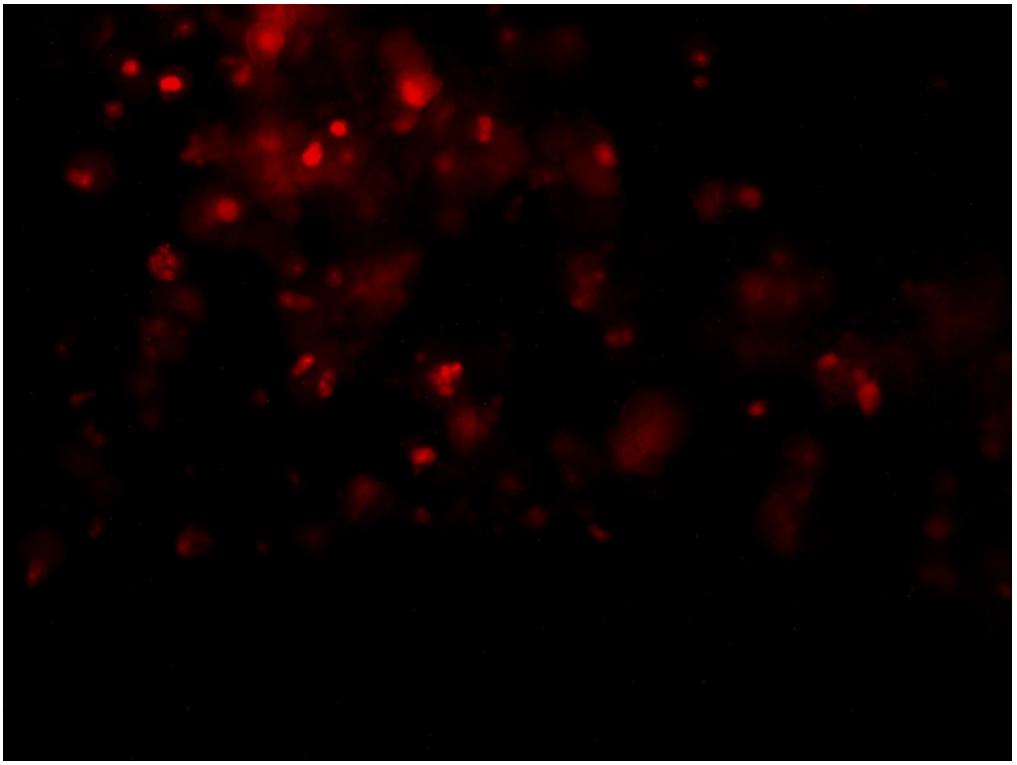


Figure 12.42.: U251 cells treated with 6.25 µM α-solanine and incubated for 24-hours and stained with propidium iodide. Replicate: 2; magnification: x100.

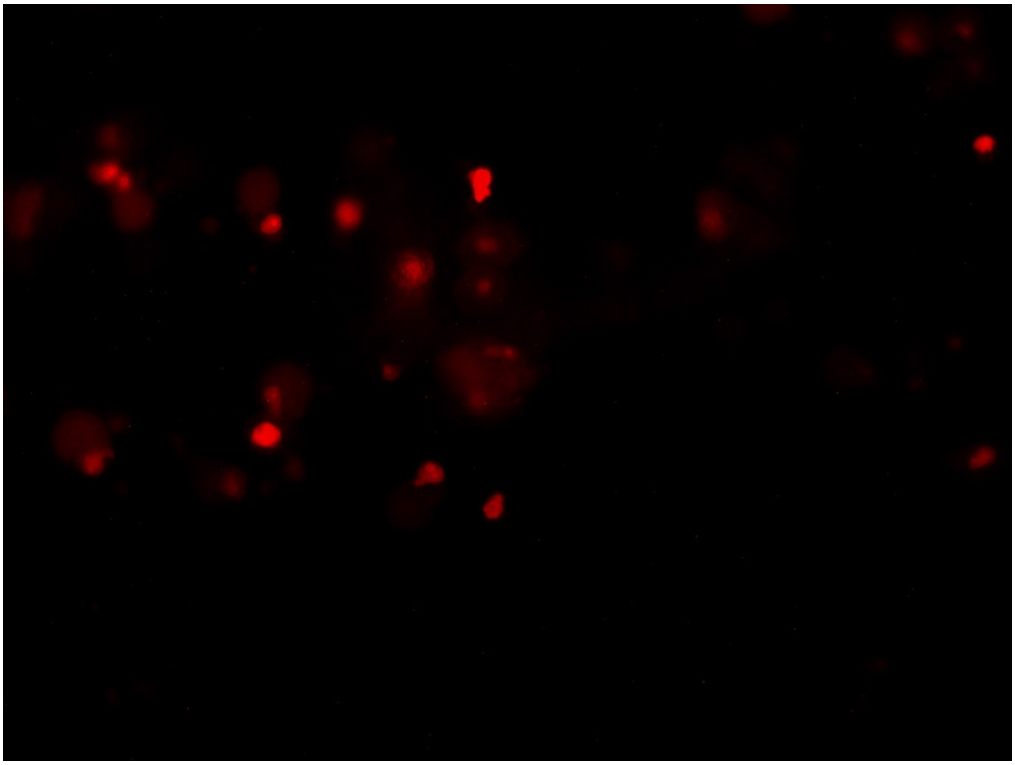


Figure 12.43.: U251 cells treated with 6.25 µM α-solanine and incubated for 24-hours and stained with propidium iodide. Replicate: 3; magnification: x100.

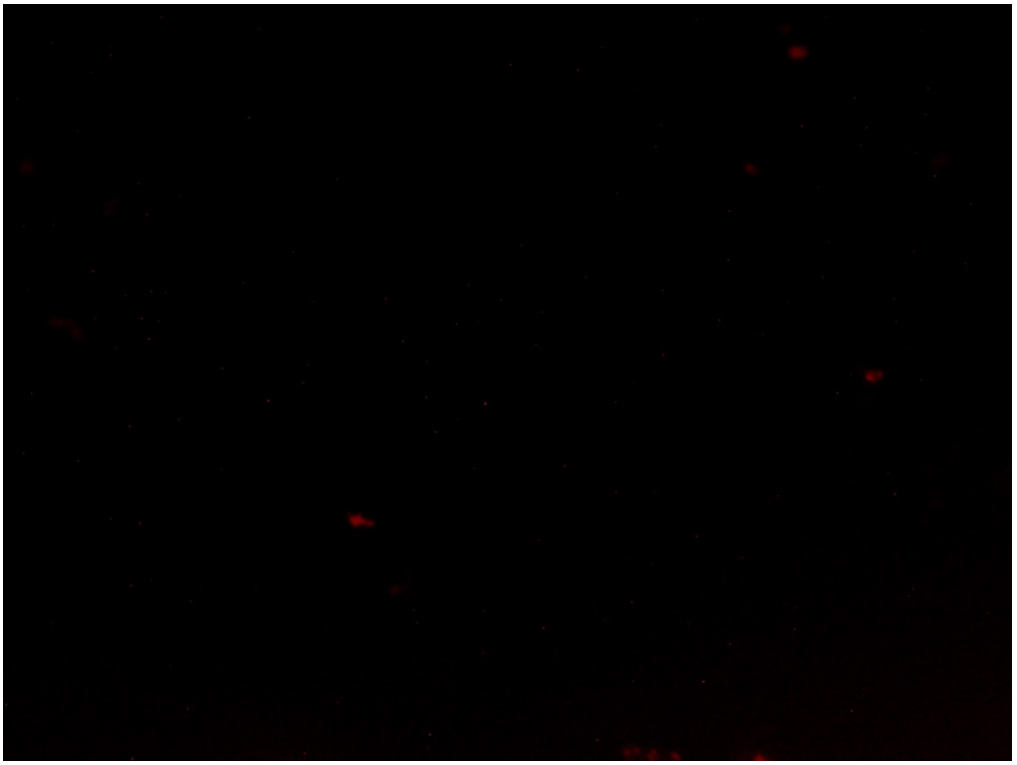


Figure 12.44.: T98G cells treated with 6.25 µM α-solanine and incubated for 24-hours and stained with propidium iodide. Replicate: 1; magnification: x100.

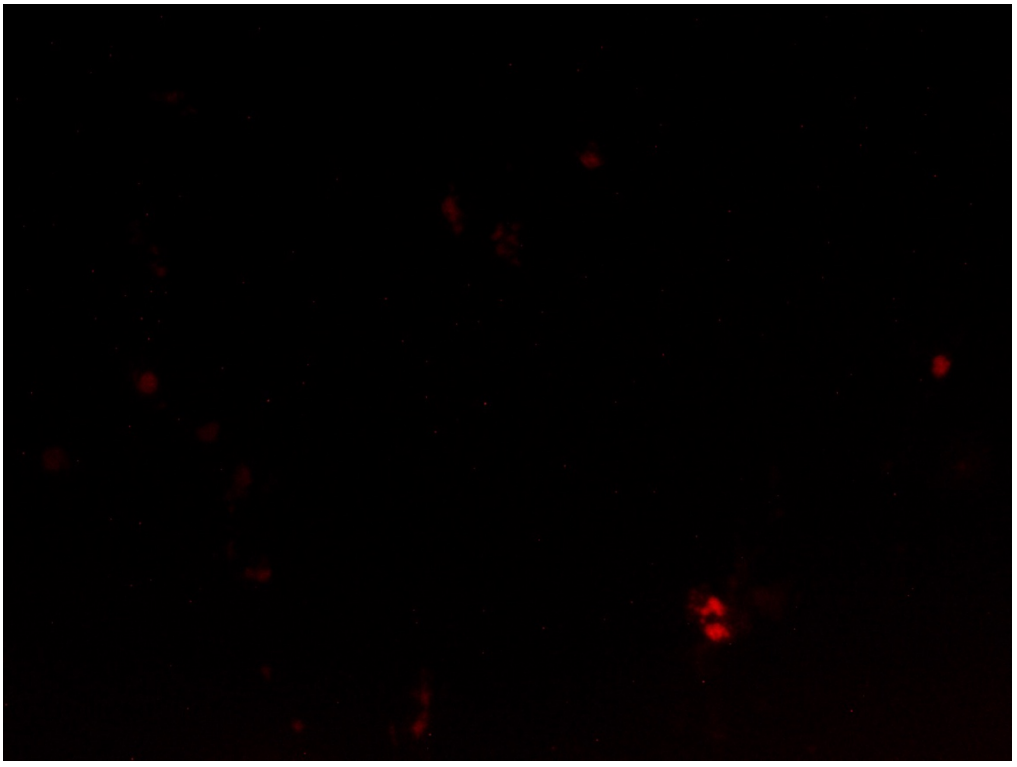


Figure 12.45.: T98G cells treated with 6.25 µM α-solanine and incubated for 24-hours and stained with propidium iodide. Replicate: 2; magnification: x100.



Figure 12.46.: T98G cells treated with 6.25 µM α-solanine and incubated for 24-hours and stained with propidium iodide. Replicate: 3; magnification: x100.



Figure 12.47.: U87MG cells treated with 1200.00 µM temozolomide and incubated for 24-hours and stained with propidium iodide. Replicate: 1; magnification: x100

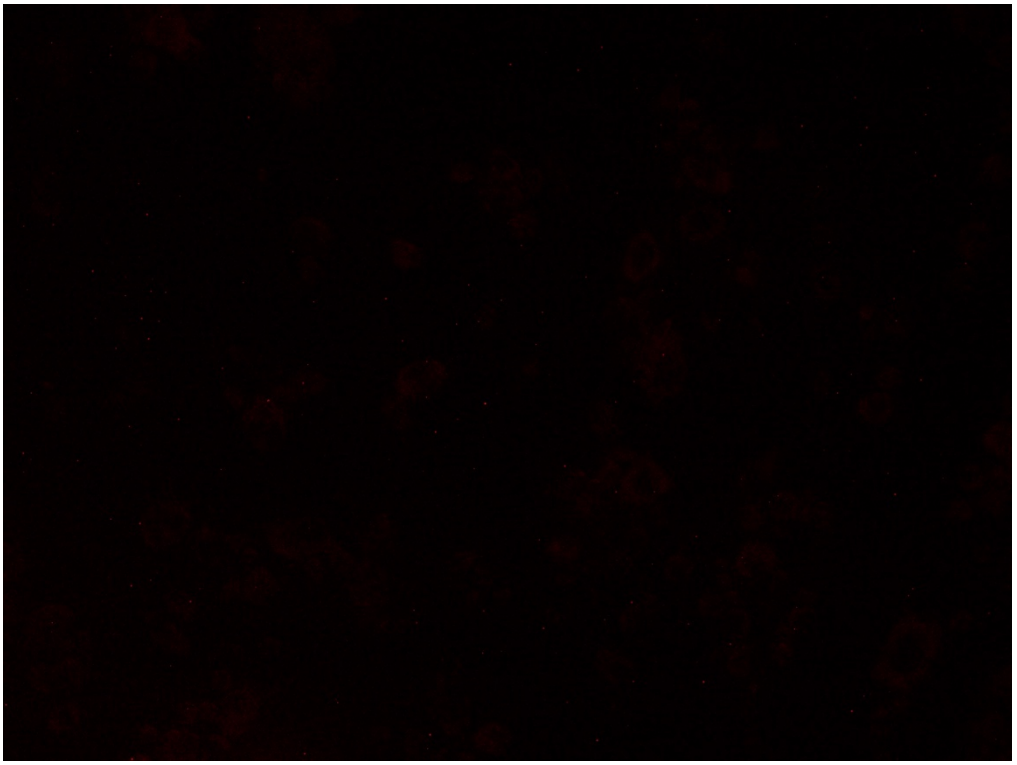


Figure 12.48.: U87MG cells treated with 1200.00 µM temozolomide and incubated for 24-hours and stained with propidium iodide. Replicate: 2; magnification: x100



Figure 12.49.: U87MG cells treated with 1200.00 µM temozolomide and incubated for 24-hours and stained with propidium iodide. Replicate: 3; magnification: x100

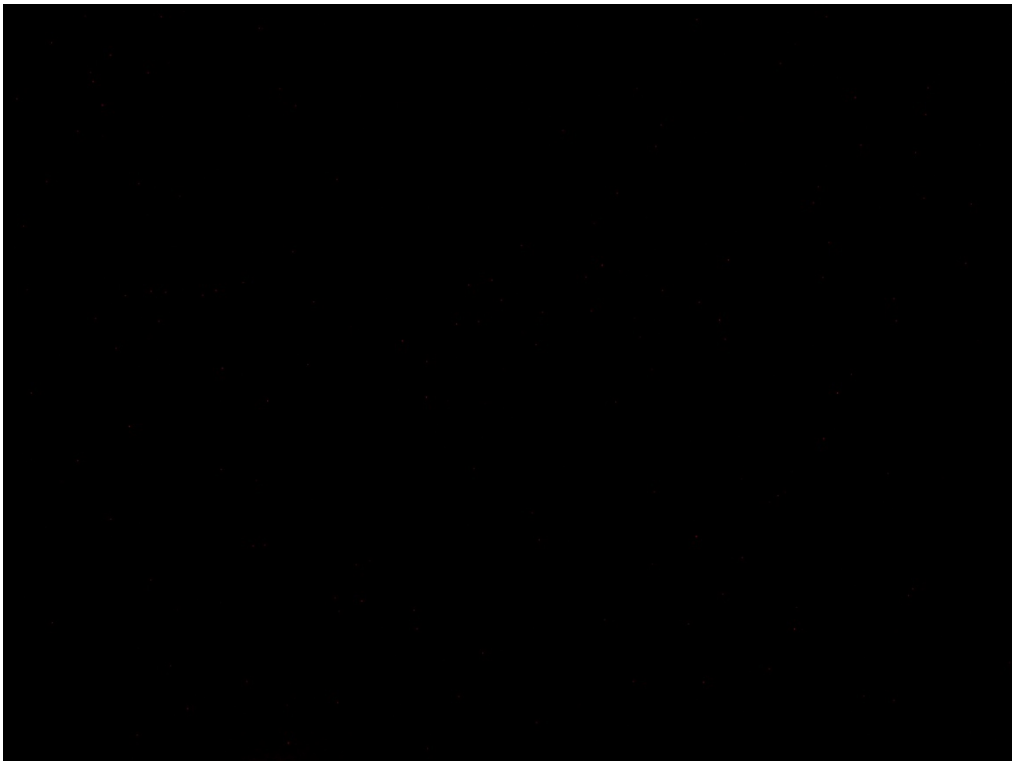


Figure 12.50.: U251 cells treated with 1200.00 µM temozolomide and incubated for 24-hours and stained with propidium iodide. Replicate: 1; magnification: x100



Figure 12.51.:U251 cells treated with 1200.00 µM temozolomide and incubated for 24-hours and stained with propidium iodide. Replicate: 2; magnification: x100

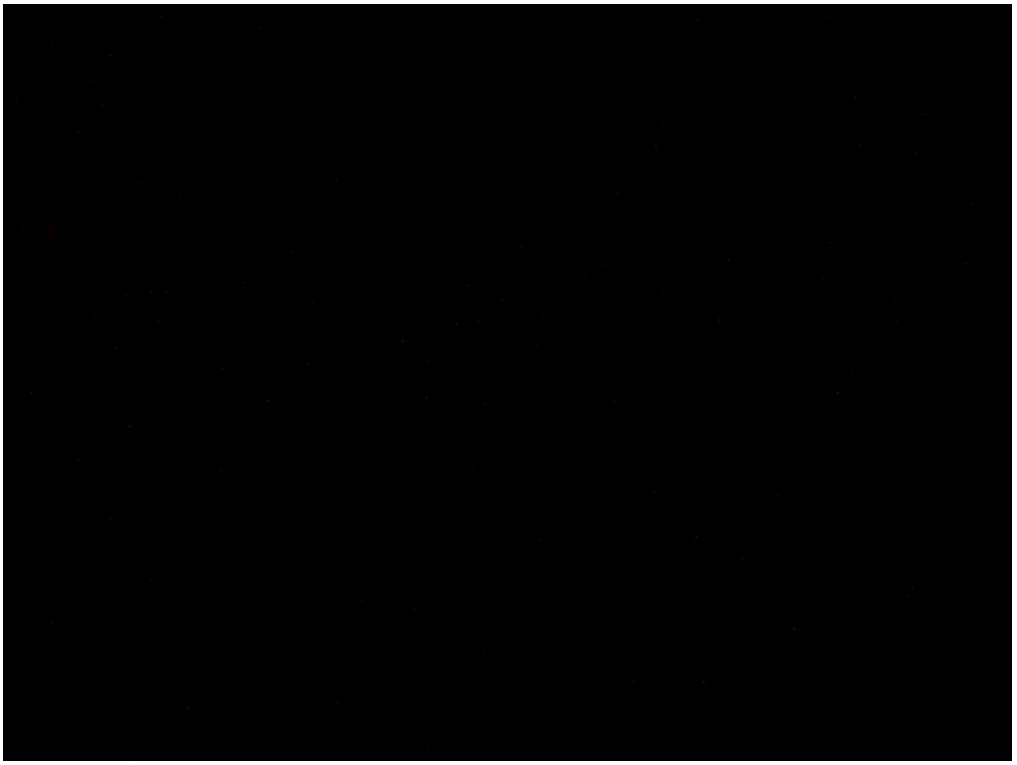


Figure 12.52.: U251 cells treated with 1200.00 µM temozolomide and incubated for 24-hours and stained with propidium iodide. Replicate: 3; magnification: x100.



Figure 12.53.: T98G cells treated with 1200.00 µM temozolomide and incubated for 24-hours and stained with propidium iodide. Replicate: 1; magnification: x100.

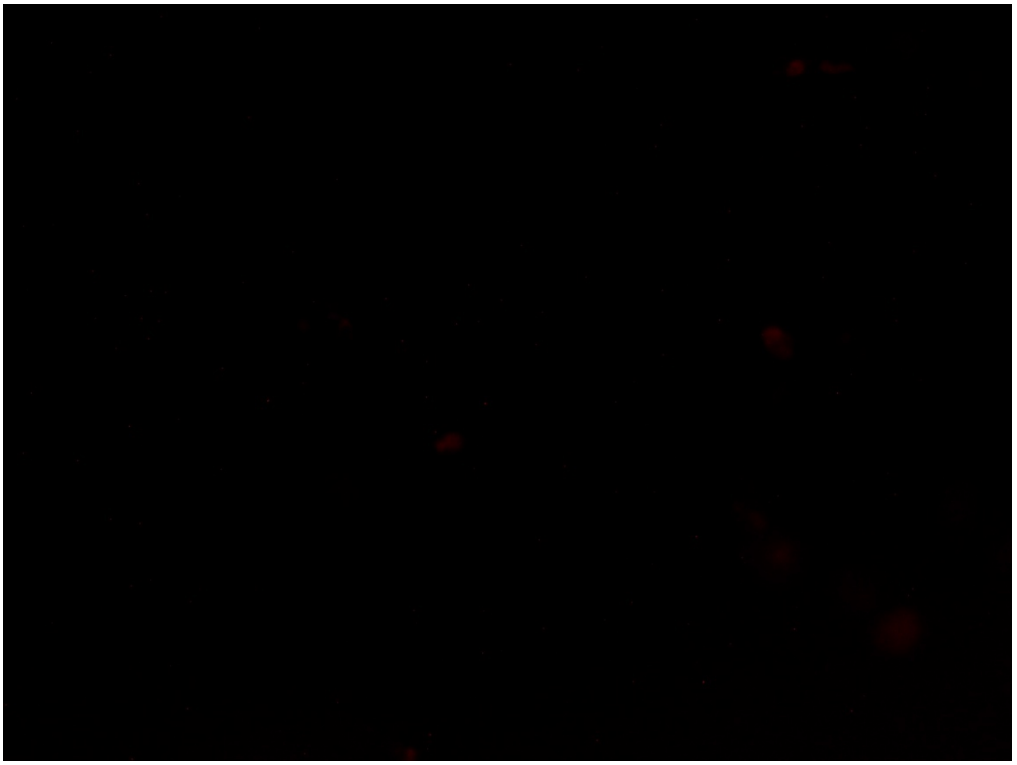


Figure 12.54.: T98G cells treated with 1200.00 µM temozolomide and incubated for 24-hours and stained with propidium iodide. Replicate: 2; magnification: x100

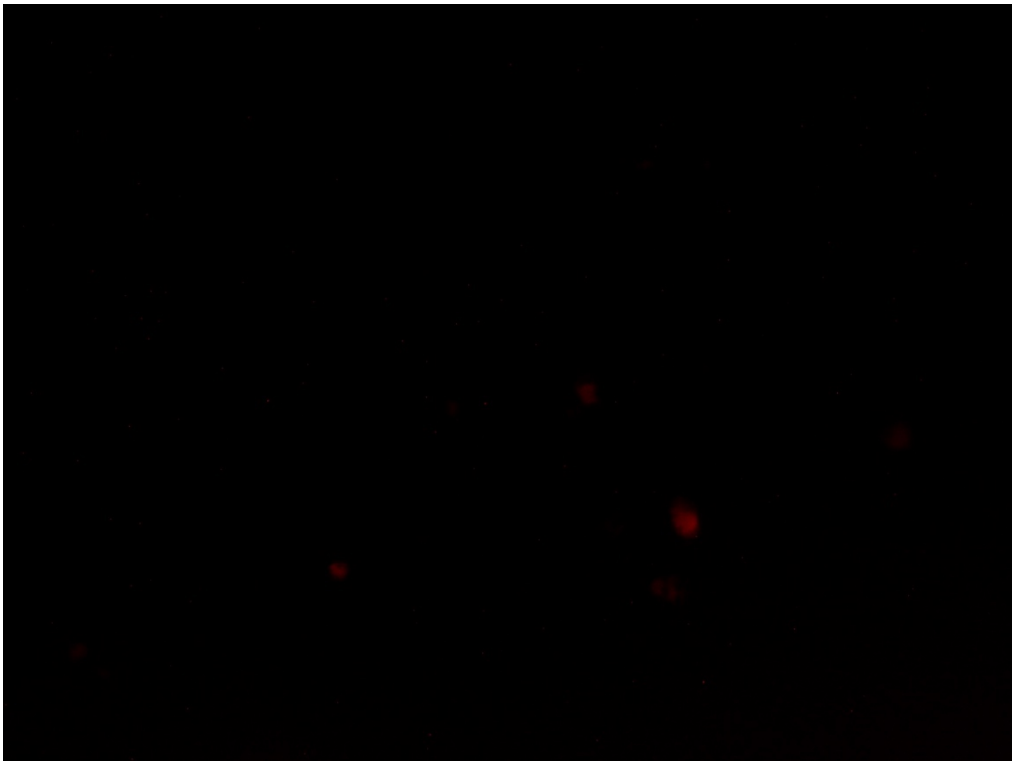


Figure 12.55.: T98G cells treated with 1200.00 µM temozolomide and incubated for 24-hours and stained with propidium iodide. Replicate: 3; magnification: x100

12.6.1.1.3. Annexin-V-fluorescein isothiocyanate staining.

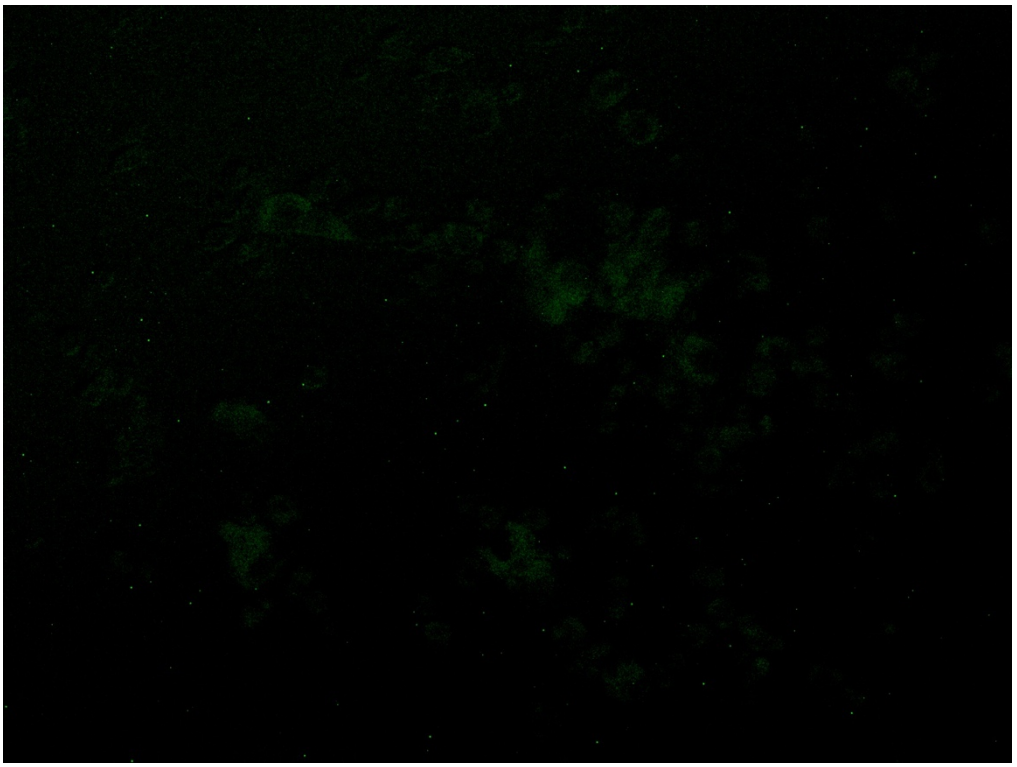


Figure 12.56.: U87MG cells under culture (negative control) conditions incubated for 24-hours and stained with annexin-V-fluorescein isothiocyanate. Replicate: 1; magnification: x100.

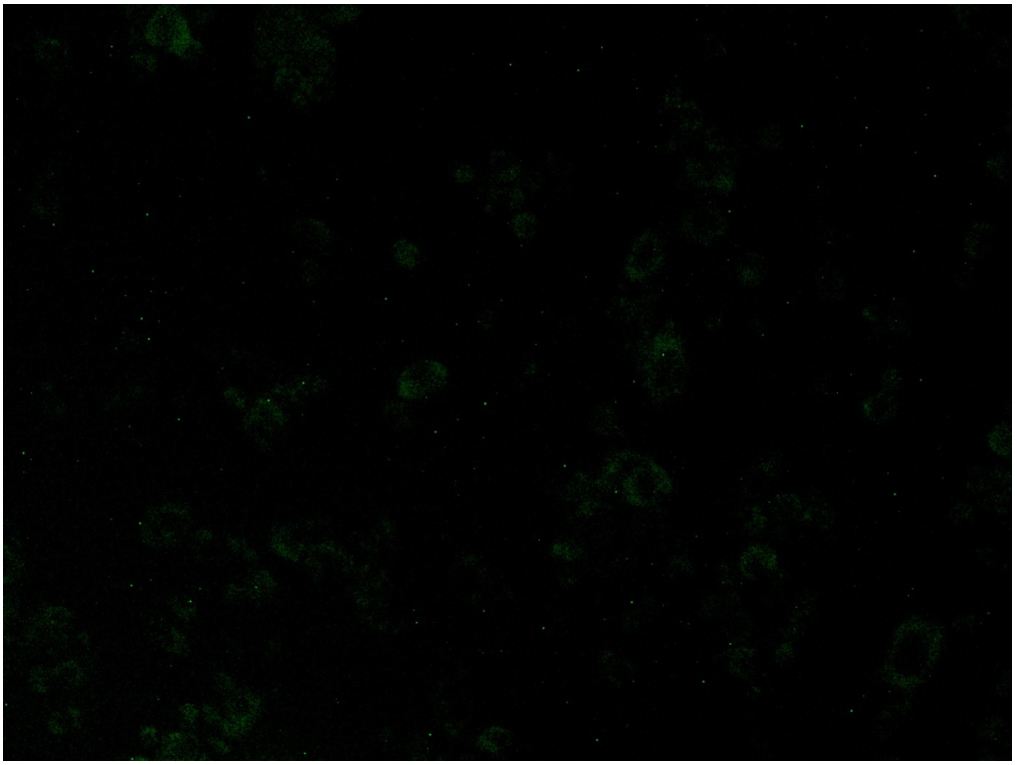


Figure 12.57.: U87MG cells under culture (negative control) conditions incubated for 24-hours and stained with annexin-V-fluorescein isothiocyanate. Replicate: 2; magnification: x100.

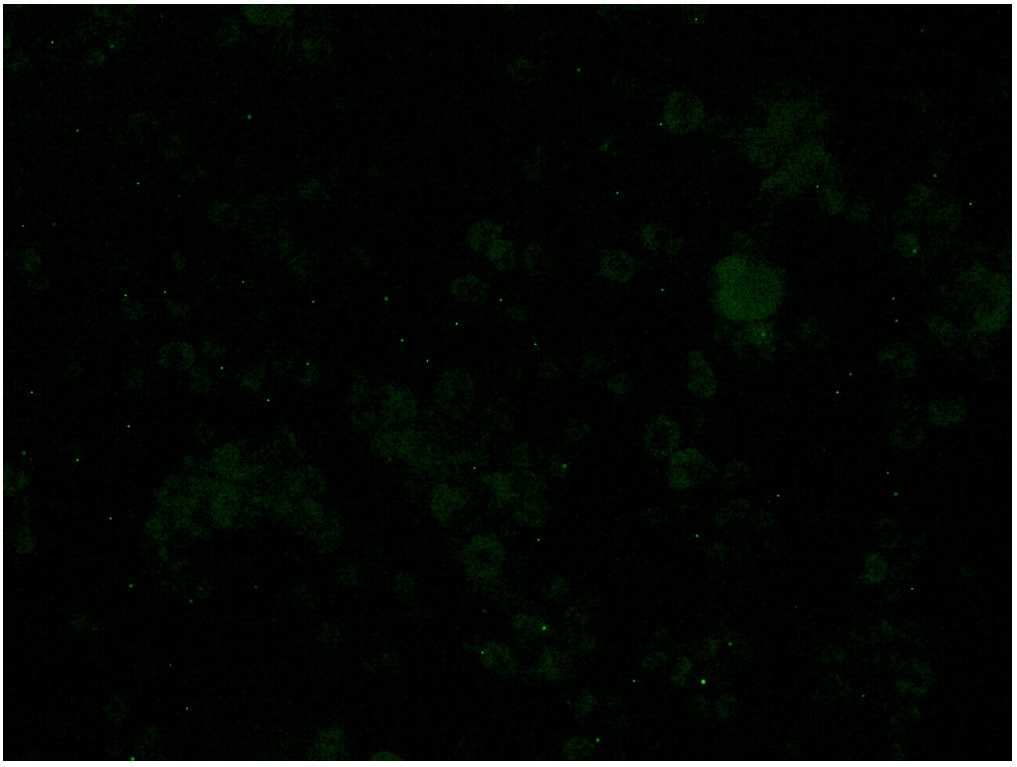


Figure 12.58.: U87MG cells under culture (negative control) conditions incubated for 24-hours and stained with annexin-V-fluorescein isothiocyanate. Replicate: 3; magnification: x100.



Figure 12.59.: U251 cells under culture (negative control) conditions incubated for 24-hours and stained with annexin-V-fluorescein isothiocyanate. Replicate: 1; magnification: x100.



Figure 12.60.: U251 cells under culture (negative control) conditions incubated for 24-hours and stained with annexin-V-fluorescein isothiocyanate. Replicate: 2; magnification: x100.



Figure 12.61.: U251 cells under culture (negative control) conditions incubated for 24-hours and stained with annexin-V-fluorescein isothiocyanate. Replicate: 3; magnification: x100.



Figure 12.62.: T98G cells under culture (negative control) conditions incubated for 24-hours and stained with annexin-V-fluorescein isothiocyanate. Replicate: 1; magnification: x100.



Figure 12.63.: T98G cells under culture (negative control) conditions incubated for 24-hours and stained with annexin-V-fluorescein isothiocyanate. Replicate: 2; magnification: x100.



Figure 12.64.: T98G cells under culture (negative control) conditions incubated for 24-hours and stained with annexin-V-fluorescein isothiocyanate. Replicate: 3; magnification: x100.

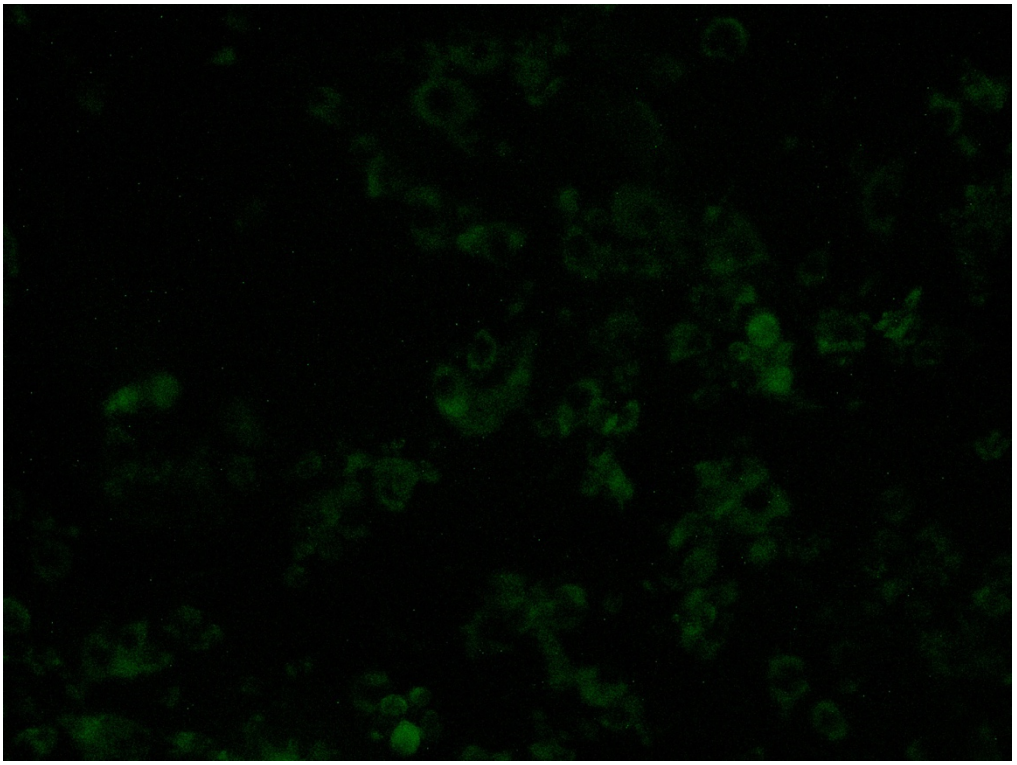


Figure 12.65.: U87MG cells treated with 6.25 µM α-solanine and incubated for 24-hours and stained with annexin-V-fluorescein isothiocyanate. Replicate: 1; magnification: x100.

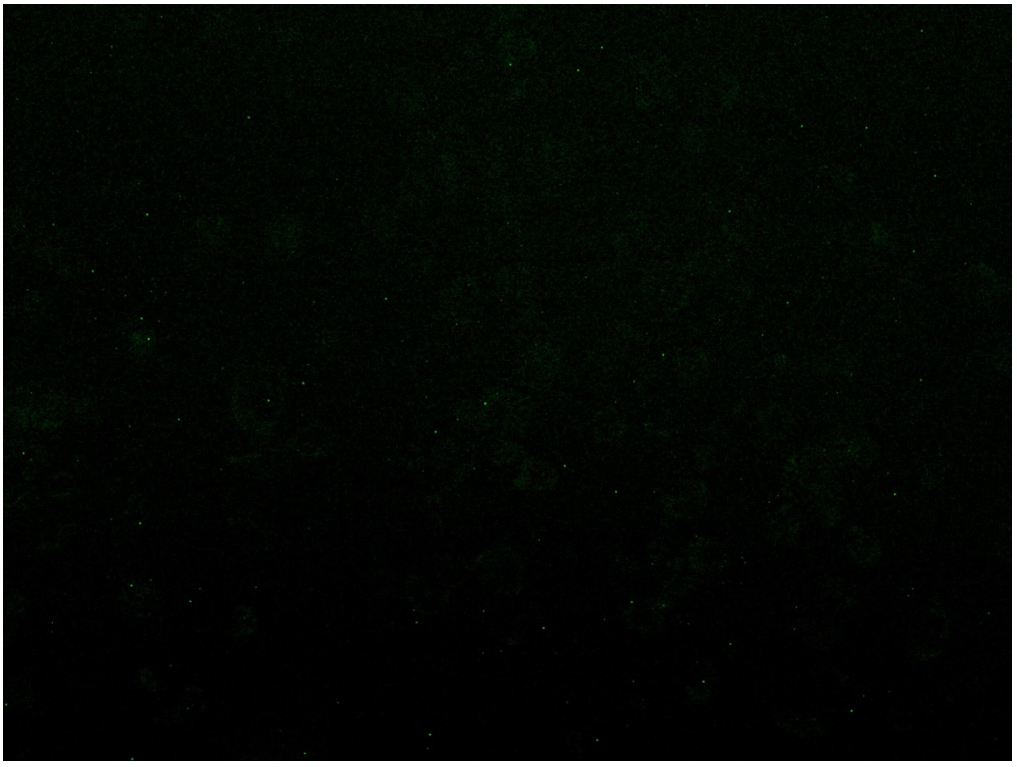


Figure 12.66.: U87MG cells treated with 6.25 µM α-solanine and incubated for 24-hours and stained with annexin-V-fluorescein isothiocyanate. Replicate: 2; magnification: x100.

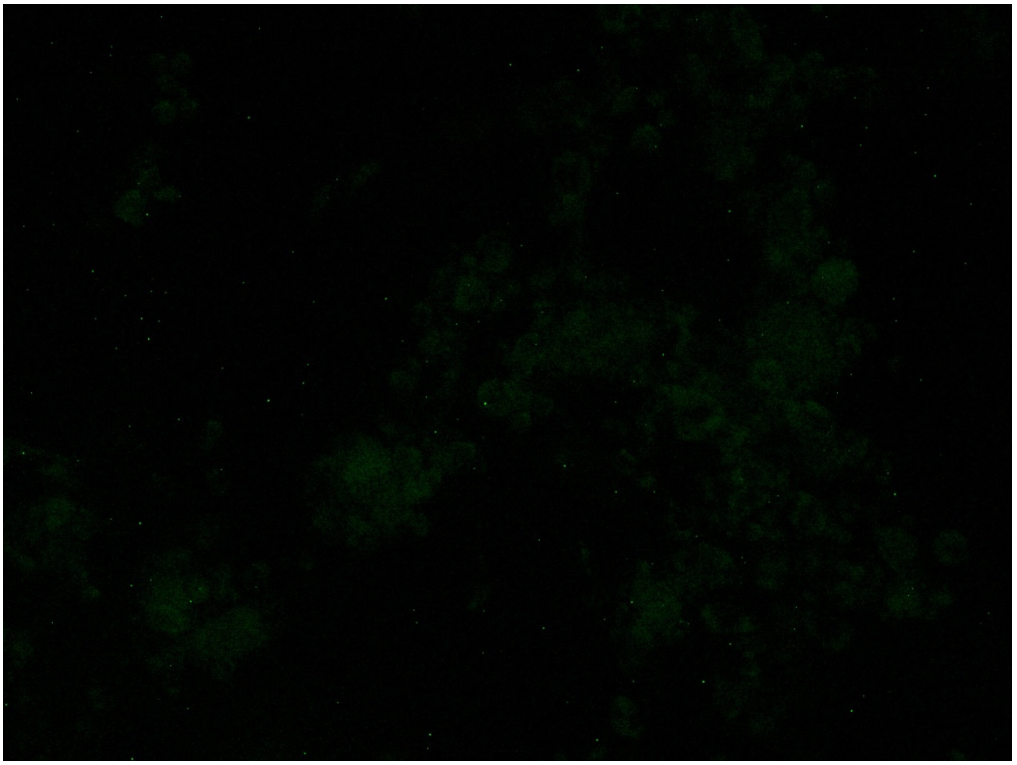


Figure 12.67.: U87MG cells treated with 6.25 µM α-solanine and incubated for 24-hours and stained with annexin-V-fluorescein isothiocyanate. Replicate: 3; magnification: x100.

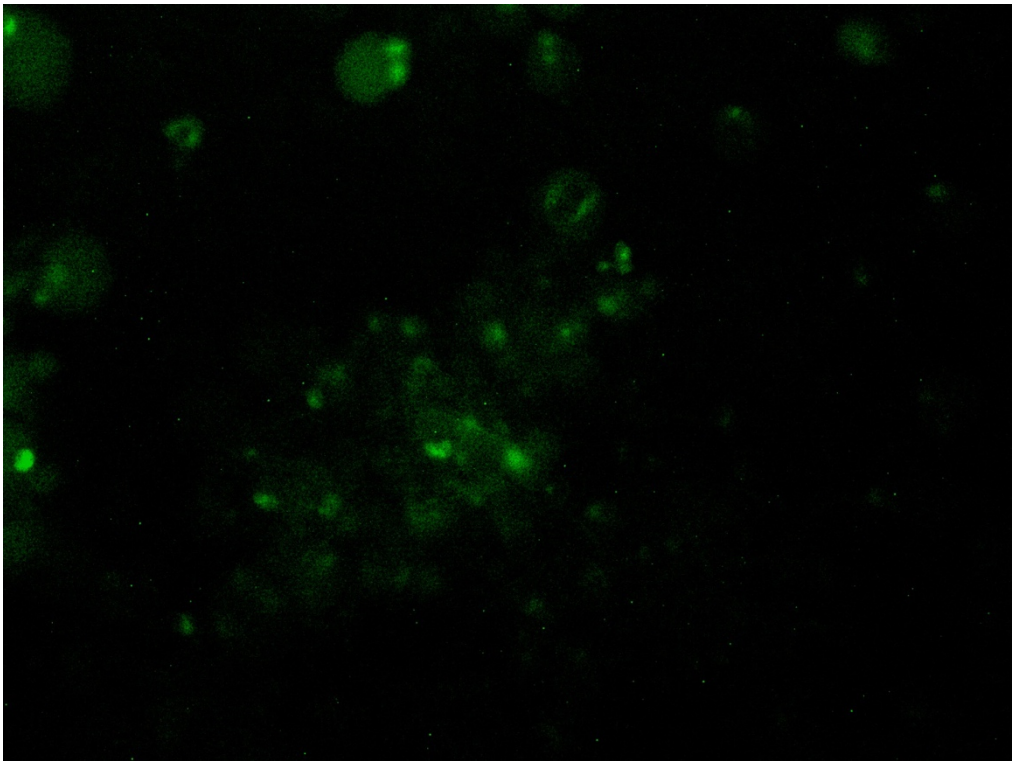


Figure 12.68.: U251 cells treated with 6.25 µM α-solanine and incubated for 24-hours and stained with annexin-V-fluorescein isothiocyanate. Replicate: 1; magnification: x100.

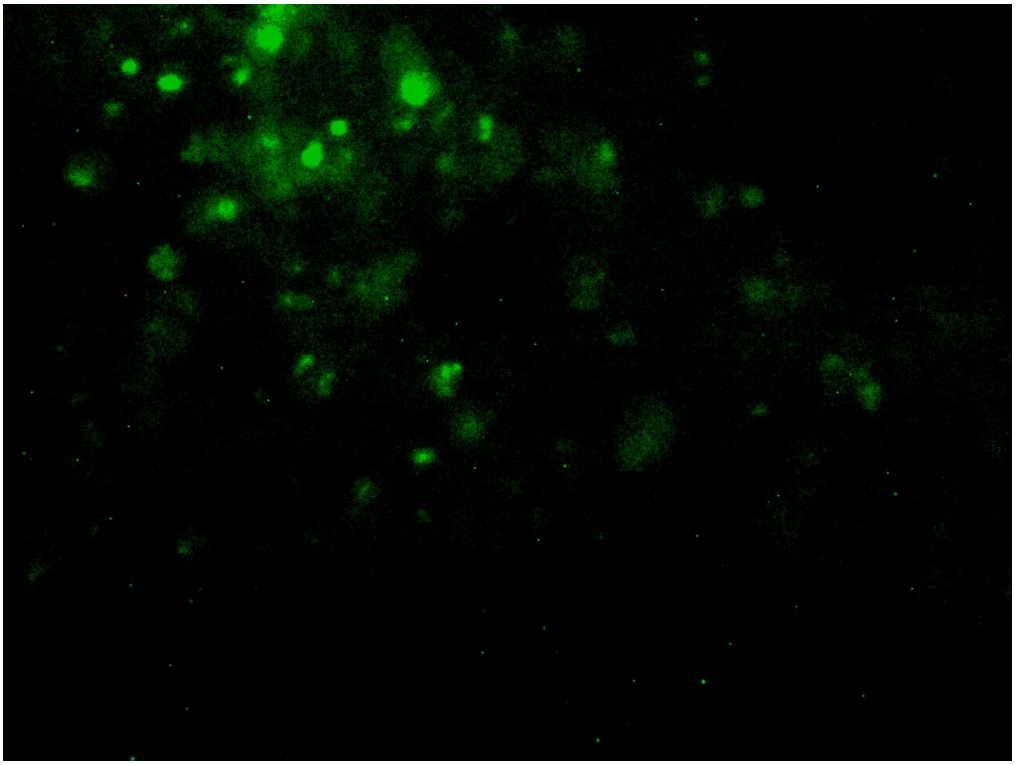


Figure 12.69.: U251 cells treated with 6.25 µM α-solanine and incubated for 24-hours and stained with annexin-V-fluorescein isothiocyanate. Replicate: 2; magnification: x100.

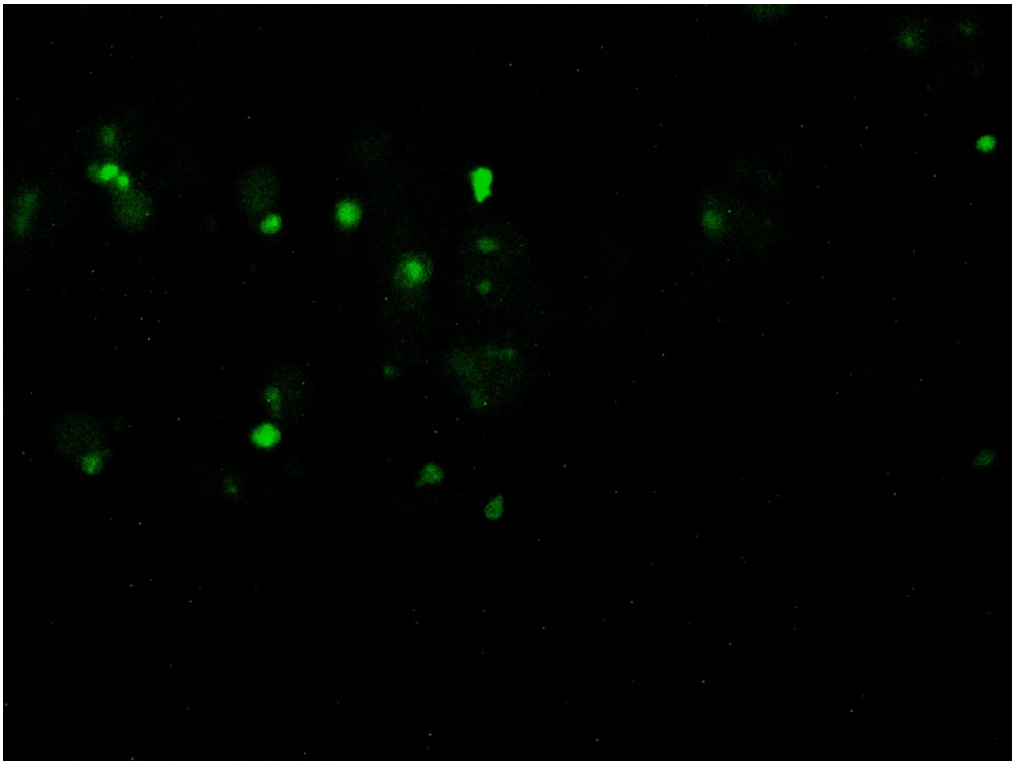


Figure 12.70.: U251 cells treated with 6.25 µM α-solanine and incubated for 24-hours and stained with annexin-V-fluorescein isothiocyanate. Replicate: 3; magnification: x100.



Figure 12.71.: T98G cells treated with 6.25 µM α-solanine and incubated for 24-hours and stained with annexin-V-fluorescein isothiocyanate. Replicate: 1; magnification: x100.

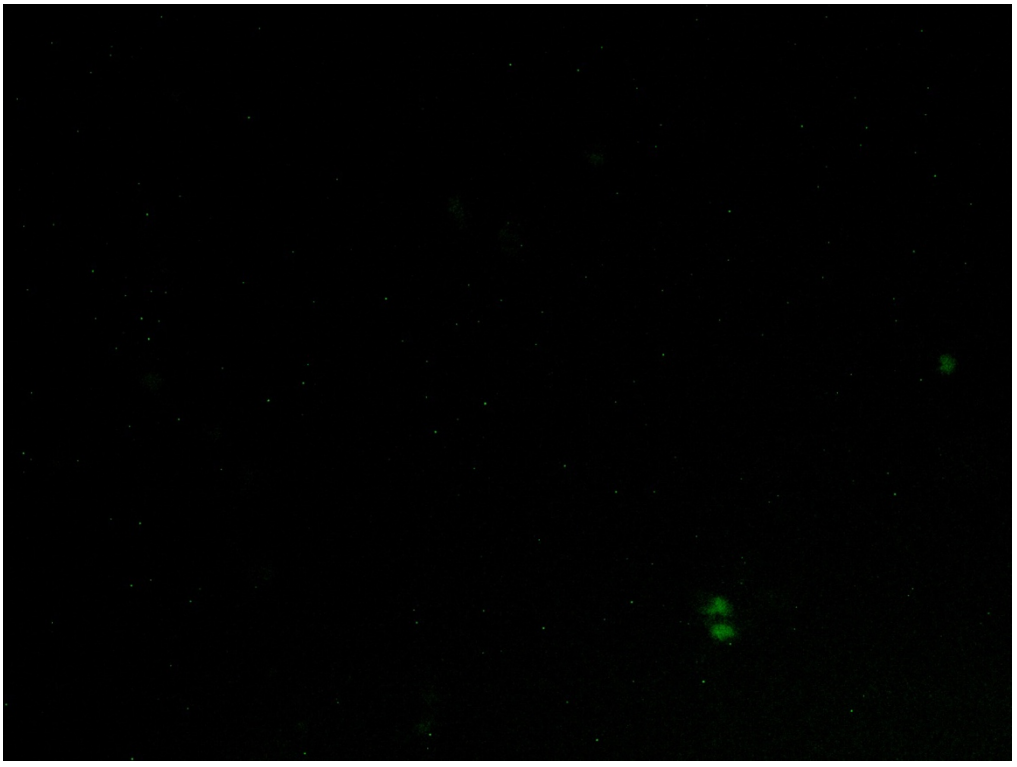


Figure 12.72.: T98G cells treated with 6.25 µM α-solanine and incubated for 24-hours and stained with annexin-V-fluorescein isothiocyanate. Replicate: 2; magnification: x100.



Figure 12.73.: T98G cells treated with 6.25 µM α-solanine and incubated for 24-hours and stained with annexin-V-fluorescein isothiocyanate. Replicate: 3; magnification: x100.

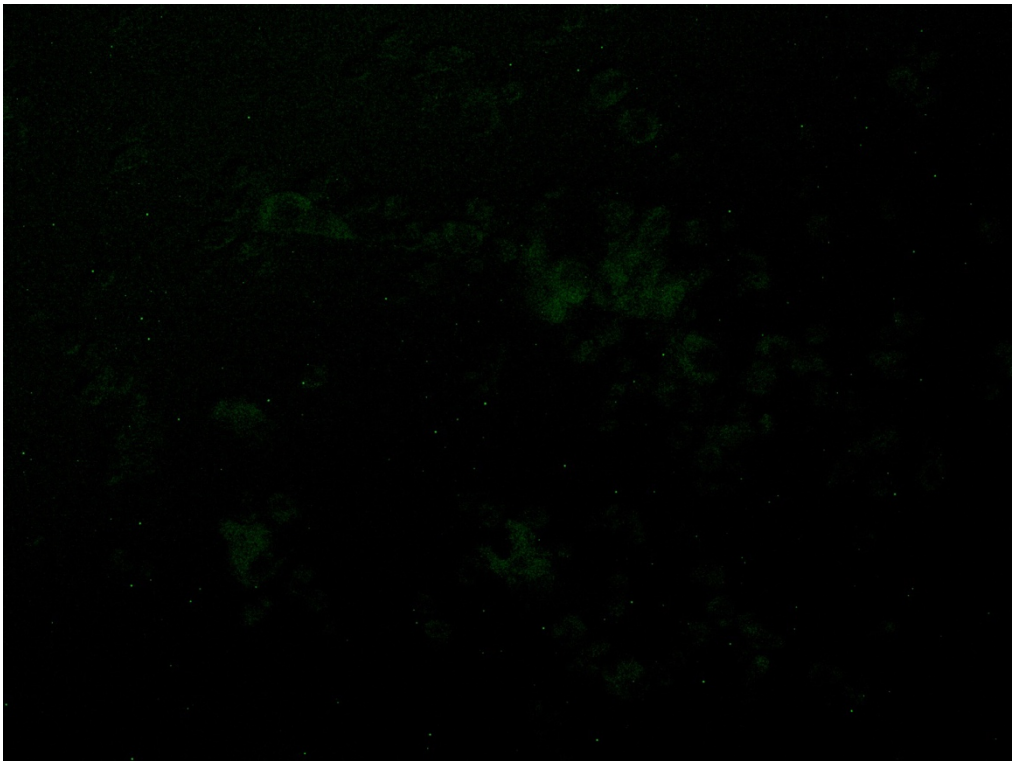


Figure 12.74.: U87MG cells treated with 1200.00 µM temozolomide and incubated for 24-hours and stained with annexin-V-fluorescein isothiocyanate. Replicate: 1; magnification: x100.

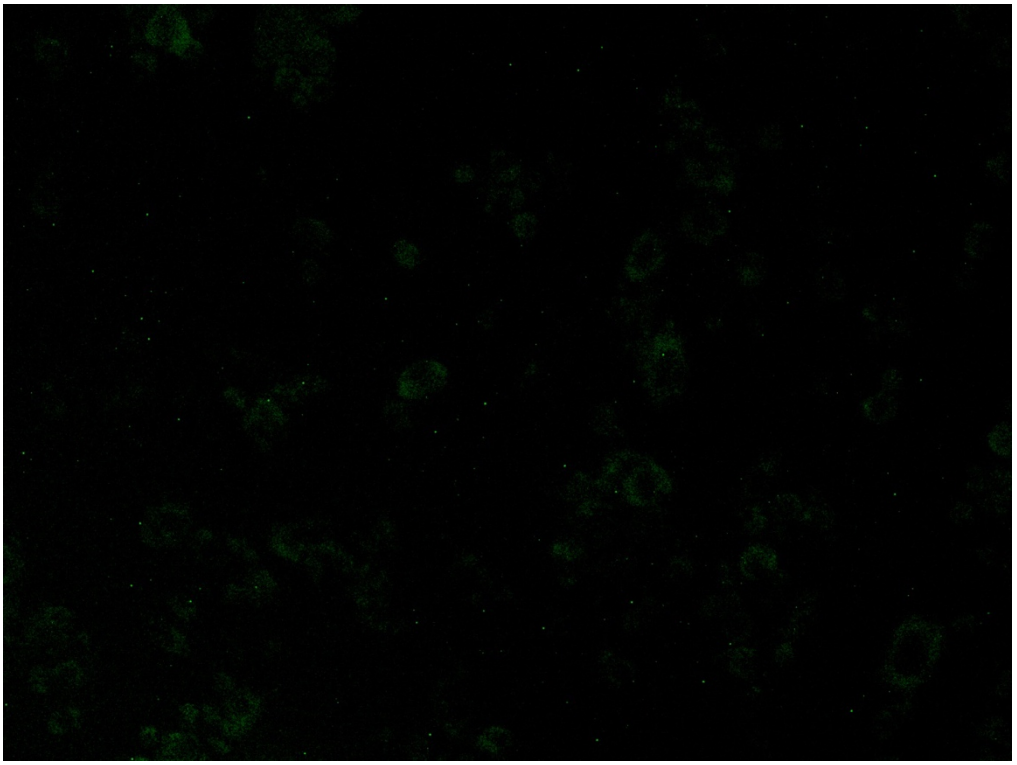


Figure 12.75.: U87MG cells treated with 1200.00 µM temozolomide and incubated for 24-hours and stained with annexin-V-fluorescein isothiocyanate. Replicate: 2; magnification: x100.

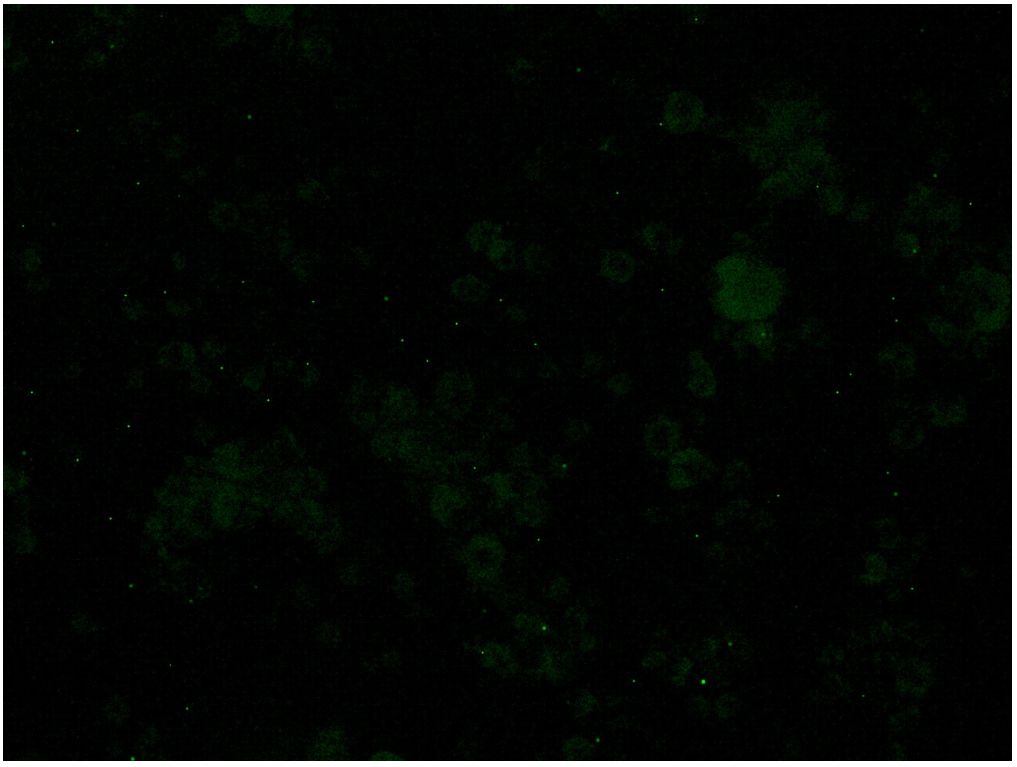


Figure 12.76.: U87MG cells treated with 1200.00 µM temozolomide and incubated for 24-hours and stained with annexin-V-fluorescein isothiocyanate. Replicate: 3; magnification: x100.



Figure 12.77.: U251 cells treated with 1200.00 µM temozolomide and incubated for 24-hours and stained with annexin-V-fluorescein isothiocyanate. Replicate: 1; magnification: x100.



Figure 12.78.: U251 cells treated with 1200.00 µM temozolomide and incubated for 24-hours and stained with annexin-V-fluorescein isothiocyanate. Replicate: 1; magnification: x100.



Figure 12.79.: U251 cells treated with 1200.00 µM temozolomide and incubated for 24-hours and stained with annexin-V-fluorescein isothiocyanate. Replicate: 1; magnification: x100.



Figure 12.80.: T98G cells treated with 1200.00 µM temozolomide and incubated for 24-hours and stained with annexin-V-fluorescein isothiocyanate. Replicate: 1; magnification: x100.



Figure 12.81.: T98G cells treated with 1200.00 µM temozolomide and incubated for 24-hours and stained with annexin-V-fluorescein isothiocyanate. Replicate: 2; magnification: x100.

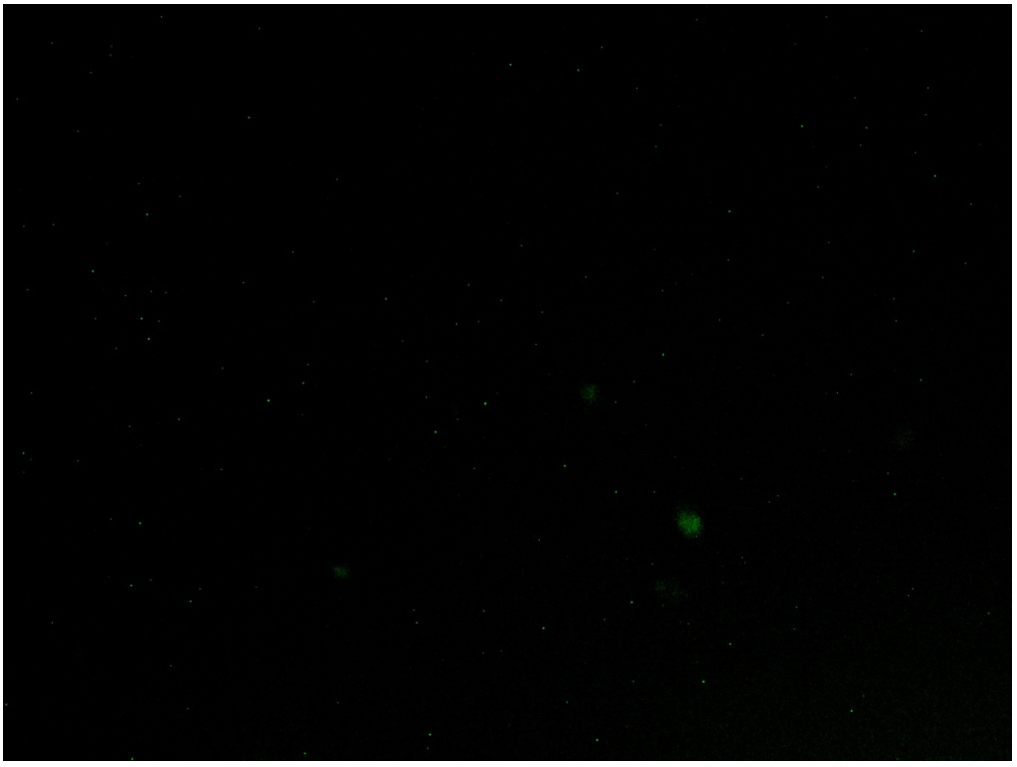


Figure 12.82.: T98G cells treated with 1200.00 µM temozolomide and incubated for 24-hours and stained with annexin-V-fluorescein isothiocyanate. Replicate: 3; magnification: x100.

12.6.1.1.4. Merged images demonstrating dual Annexin-V-fluorescein isothiocyanate/ propidium iodide staining.



Figure 12.83.: U87MG cells under culture (negative control) conditions incubated for 24-hours and dual stained with Annexin-V-fluorescein isothiocyanate and propidium iodide. Replicate: 1; magnification: x100.

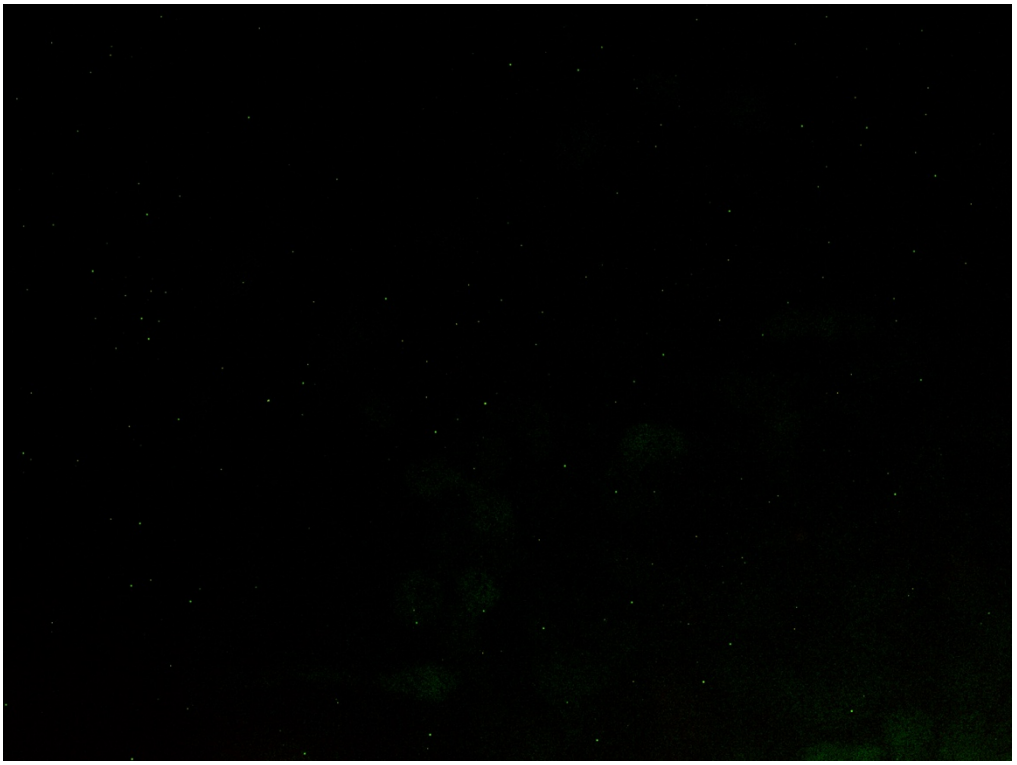


Figure 12.84.:U87MG cells under culture (negative control) conditions incubated for 24-hours and dual stained with Annexin-V-fluorescein isothiocyanate and propidium iodide. Replicate: 2; magnification: x100.



Figure 12.85.: U87MG cells under culture (negative control) conditions incubated for 24-hours and dual stained with Annexin-V-fluorescein isothiocyanate and propidium iodide. Replicate: 3; magnification: x100.



Figure 12.86.: U251 cells under culture (negative control) conditions incubated for 24-hours and dual stained with Annexin-V-fluorescein isothiocyanate and propidium iodide. Replicate: 1; magnification: x100.



Figure 12.87.: U251 cells under culture (negative control) conditions incubated for 24-hours and dual stained with Annexin-V-fluorescein isothiocyanate and propidium iodide. Replicate: 2; magnification: x100.



Figure 12.88.: U251 cells under culture (negative control) conditions incubated for 24-hours and dual stained with Annexin-V-fluorescein isothiocyanate and propidium iodide. Replicate: 3; magnification: x100.



Figure 12.89.: T98G cells under culture (negative control) conditions incubated for 24-hours and dual stained with Annexin-V-fluorescein isothiocyanate and propidium iodide. Replicate: 1; magnification: x100.

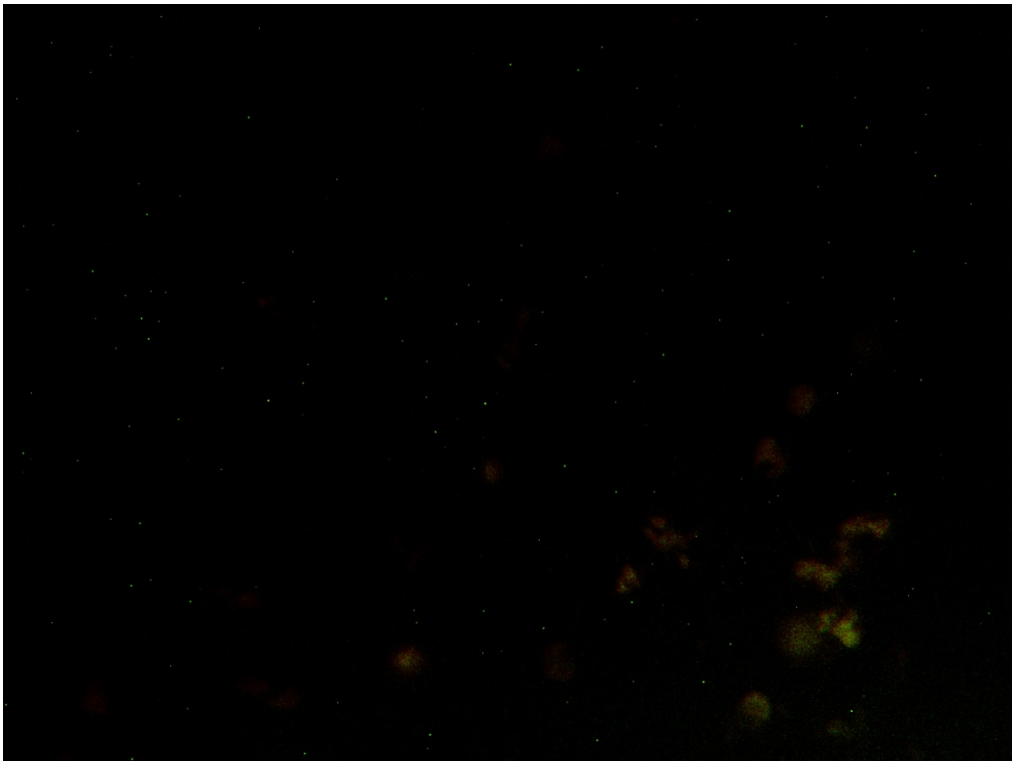


Figure 12.90.: T98G cells under culture (negative control) conditions incubated for 24-hours and dual stained with Annexin-V-fluorescein isothiocyanate and propidium iodide. Replicate: 2; magnification: x100.

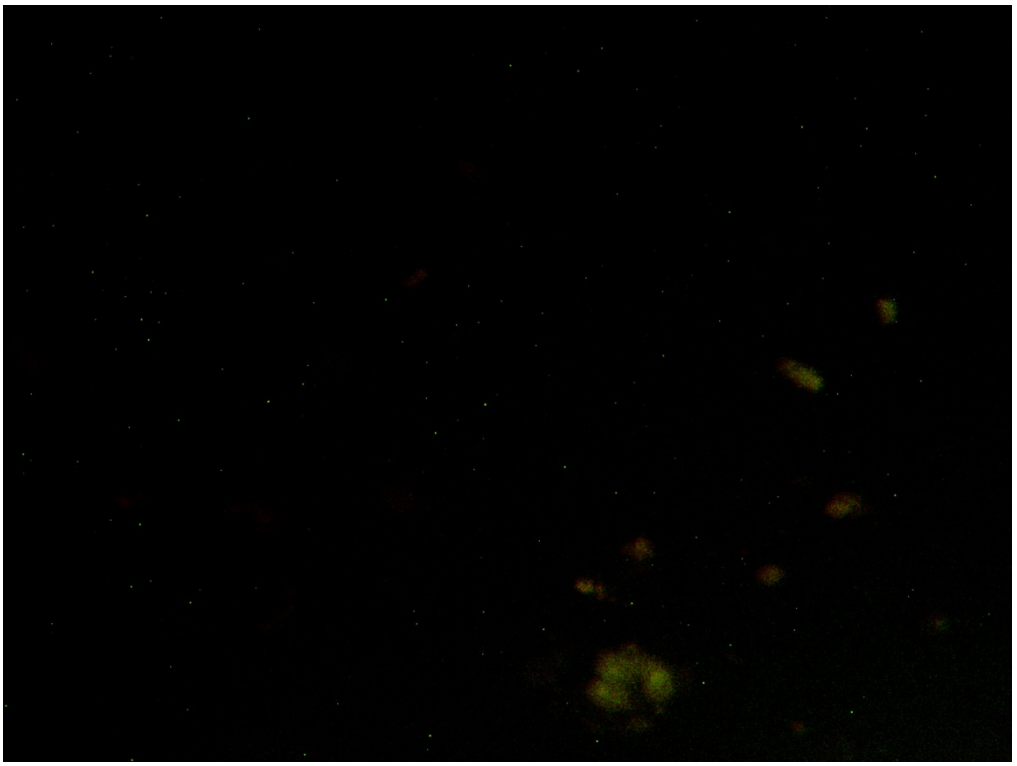


Figure 12.91.: T98G cells under culture (negative control) conditions incubated for 24-hours and dual stained with Annexin-V-fluorescein isothiocyanate and propidium iodide. Replicate: 3; magnification: x100.

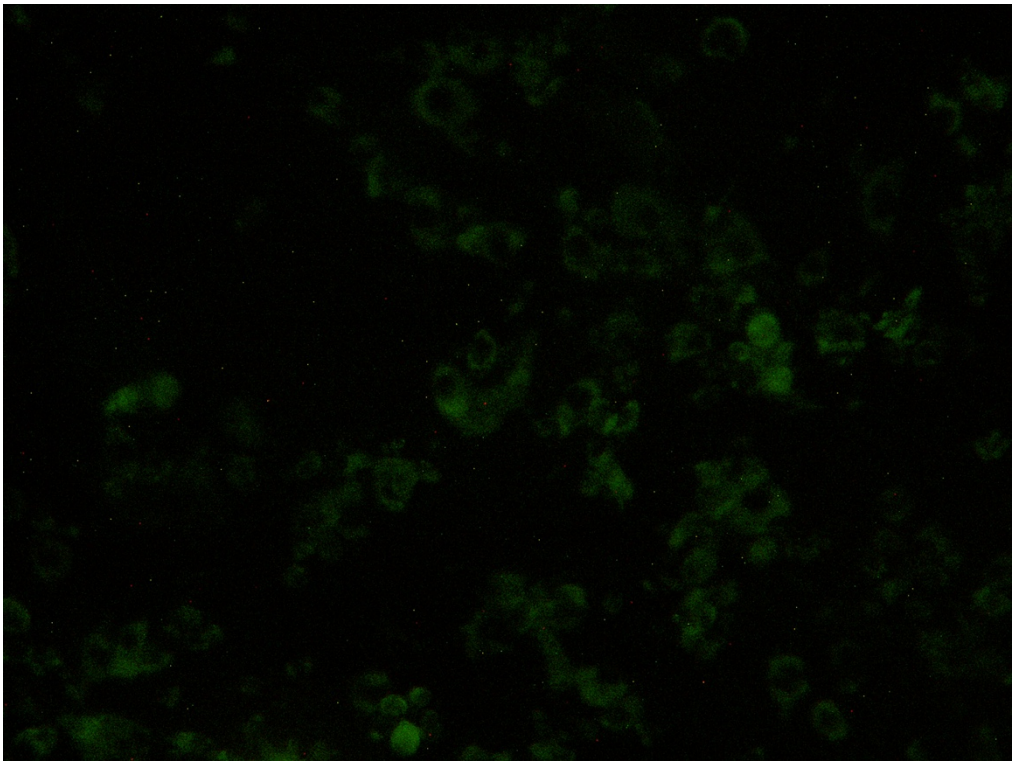


Figure 12.92.: U87MG cells treated with 6.25 µM α-solanine and incubated for 24-hours and dual stained with Annexin-V-fluorescein isothiocyanate and propidium iodide. Replicate: 1; magnification: x100.

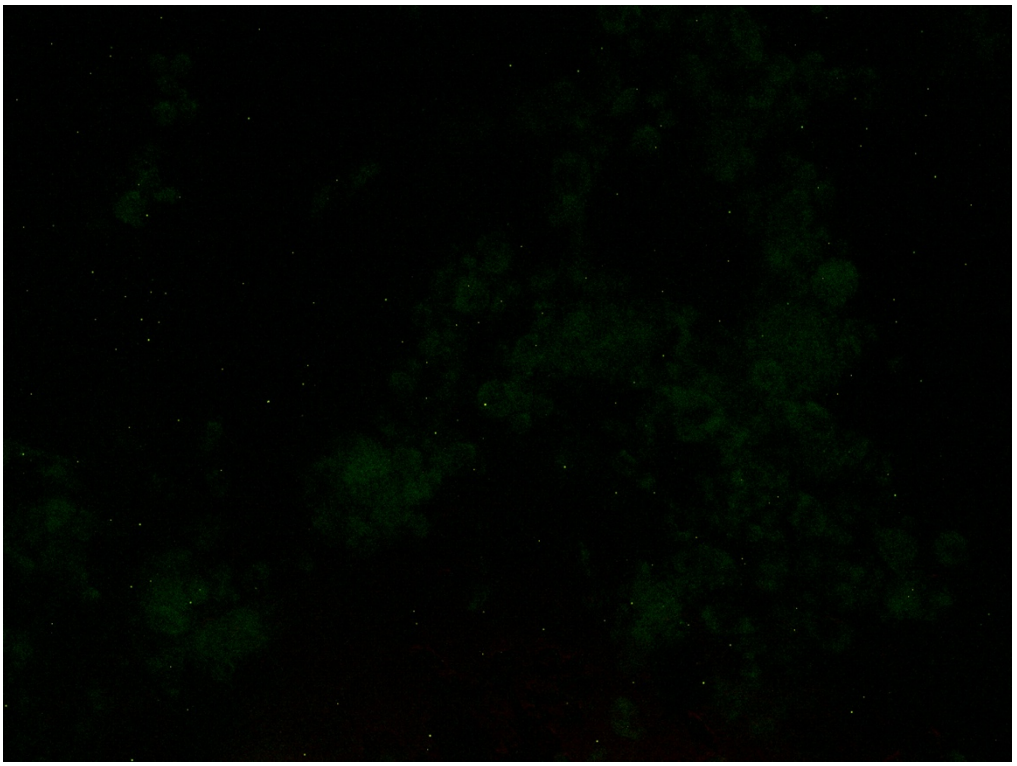


Figure 12.93.: U87MG cells treated with 6.25 µM α-solanine and incubated for 24-hours and dual stained with Annexin-V-fluorescein isothiocyanate and propidium iodide. Replicate: 2; magnification: x100.

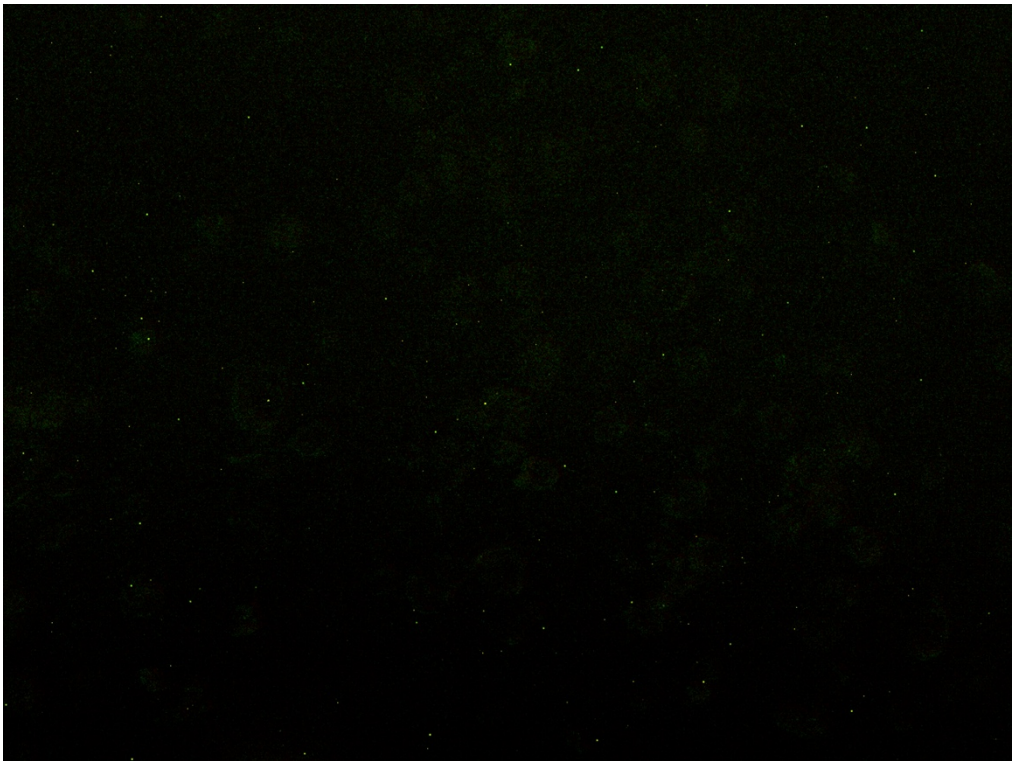


Figure 12.94.: U87MG cells treated with 6.25 µM α-solanine and incubated for 24-hours and dual stained with Annexin-V-fluorescein isothiocyanate and propidium iodide. Replicate: 3; magnification: x100.

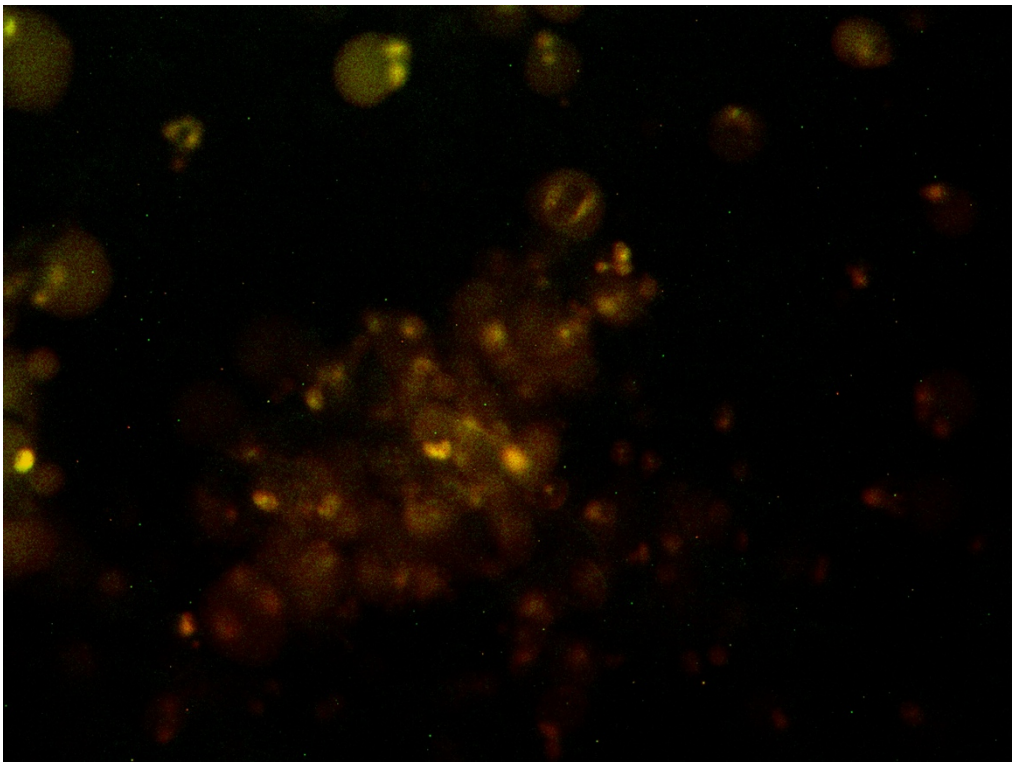


Figure 12.95.: U251 cells treated with 6.25 µM α-solanine and incubated for 24-hours and dual stained with Annexin-V-fluorescein isothiocyanate and propidium iodide. Replicate: 1; magnification: x100.

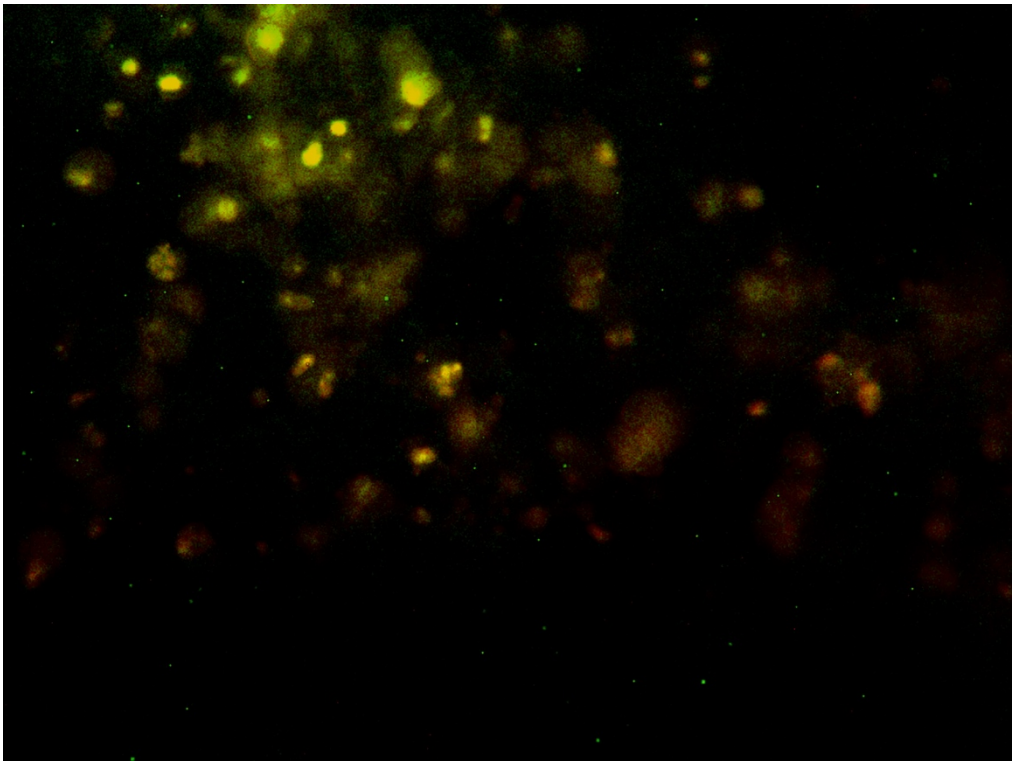


Figure 12.96.: U251 cells treated with 6.25 µM α-solanine and incubated for 24-hours and dual stained with Annexin-V-fluorescein isothiocyanate and propidium iodide. Replicate: 2; magnification: x100.

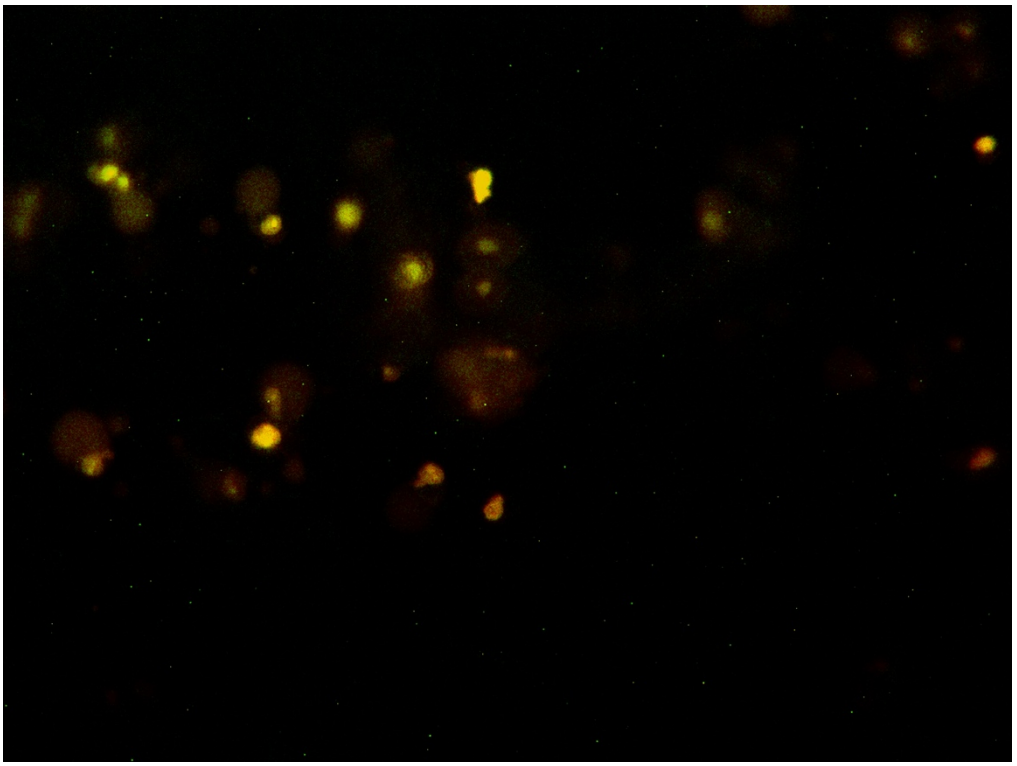


Figure 12.97.: U251 cells treated with 6.25 µM α-solanine and incubated for 24-hours and dual stained with Annexin-V-fluorescein isothiocyanate and propidium iodide. Replicate: 3; magnification: x100.



Figure 12.98.: T98G cells treated with 6.25 µM α-solanine and incubated for 24-hours and dual stained with Annexin-V-fluorescein isothiocyanate and propidium iodide. Replicate: 1; magnification: x100.

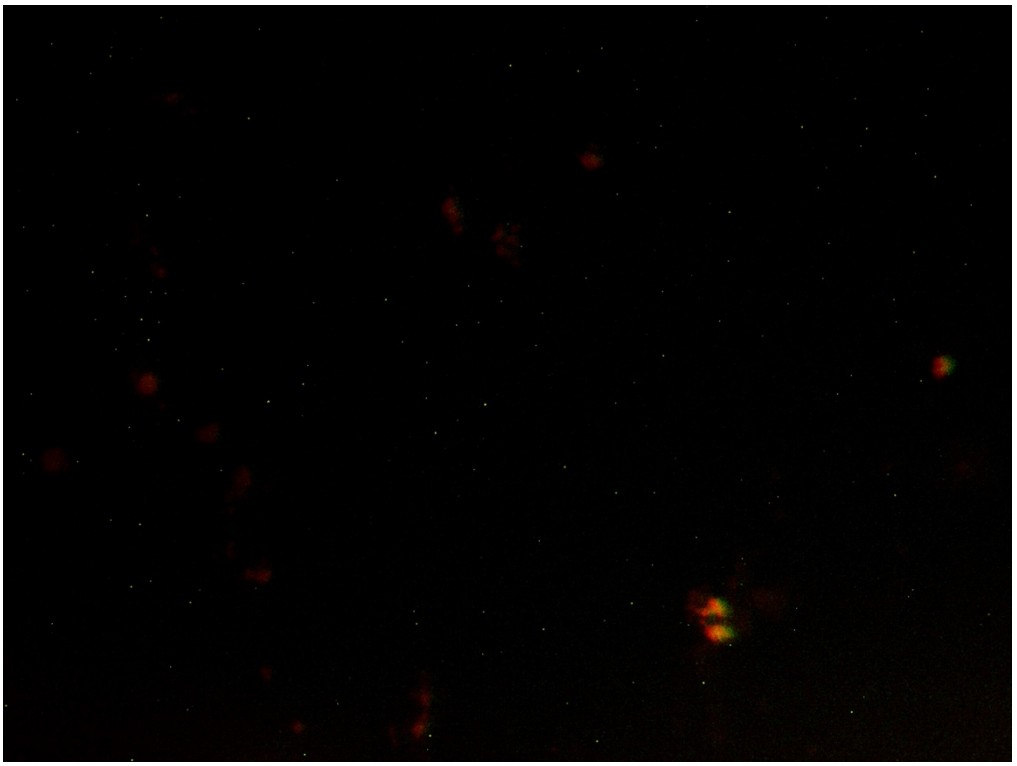


Figure 12.99.: T98G cells treated with 6.25 µM α-solanine and incubated for 24-hours and dual stained with Annexin-V-fluorescein isothiocyanate and propidium iodide. Replicate: 2; magnification: x100.



Figure 12.100.: T98G cells treated with 6.25 µM α-solanine and incubated for 24-hours and dual stained with Annexin-V-fluorescein isothiocyanate and propidium iodide. Replicate: 3; magnification: x100.

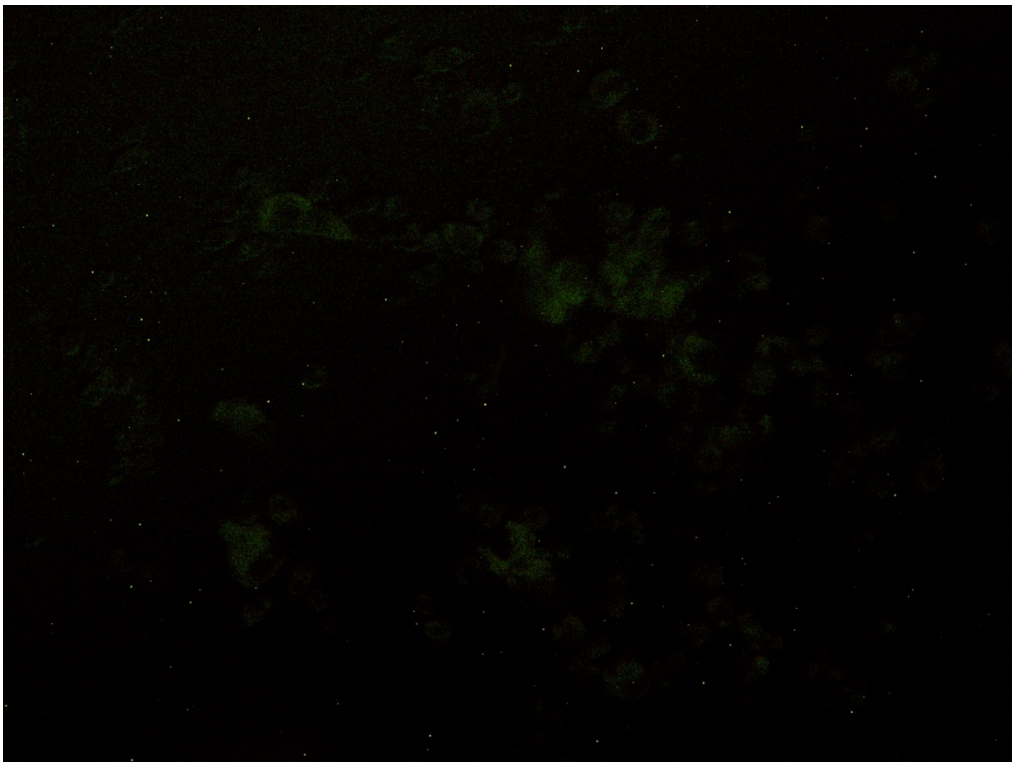


Figure 12.101.: U87MG cells treated with 1200.00 µM temozolomide and incubated for 24-hours and dual stained with Annexin-V-fluorescein isothiocyanate and propidium iodide. Replicate: 1; magnification: x100.

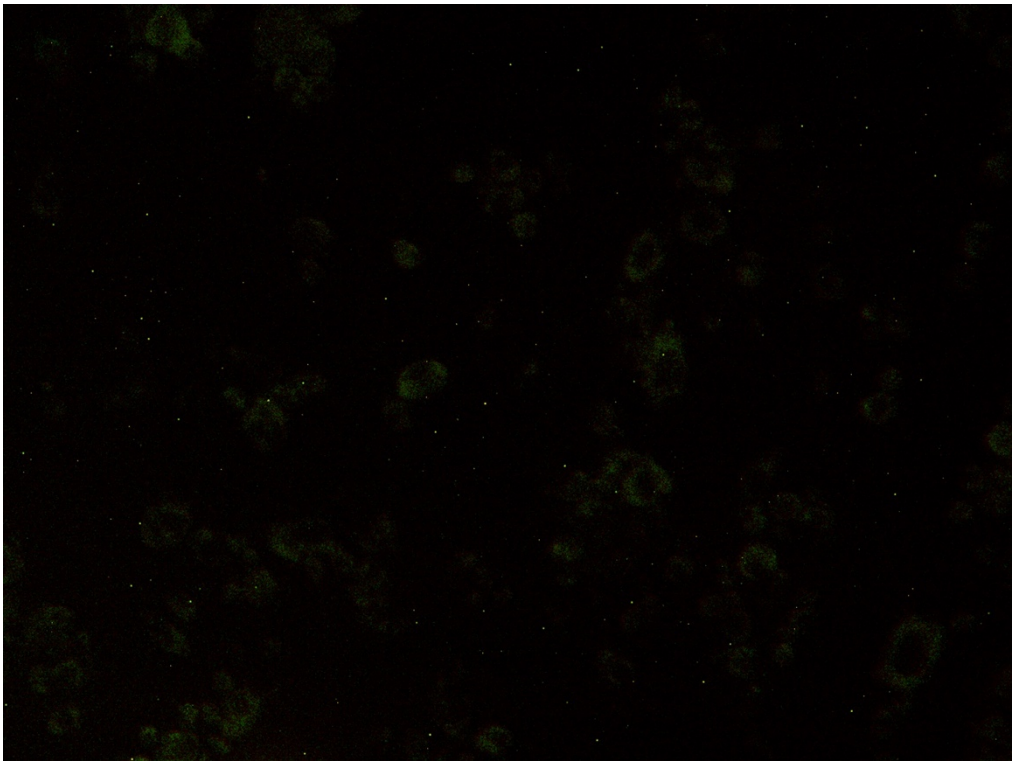


Figure 12.102.: U87MG cells treated with 1200.00 µM temozolomide and incubated for 24-hours and dual stained with Annexin-V-fluorescein isothiocyanate and propidium iodide. Replicate: 2; magnification: x100.

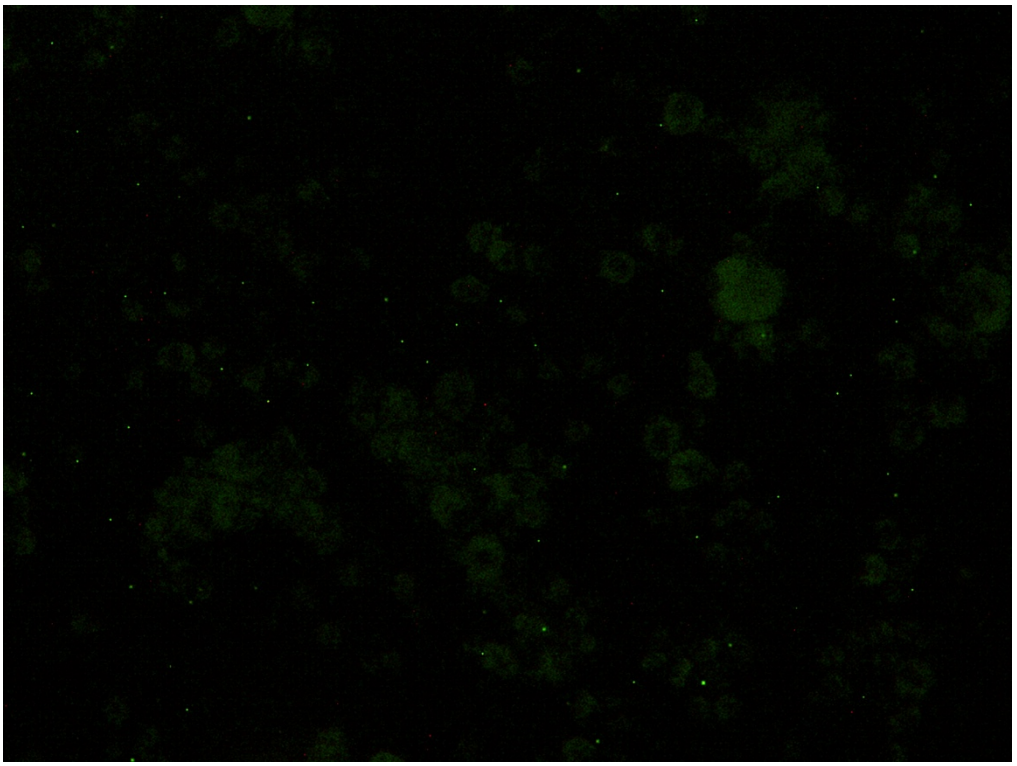


Figure 12.103.: U87MG cells treated with 1200.00 µM temozolomide and incubated for 24-hours and dual stained with Annexin-V-fluorescein isothiocyanate and propidium iodide. Replicate: 3; magnification: x100.

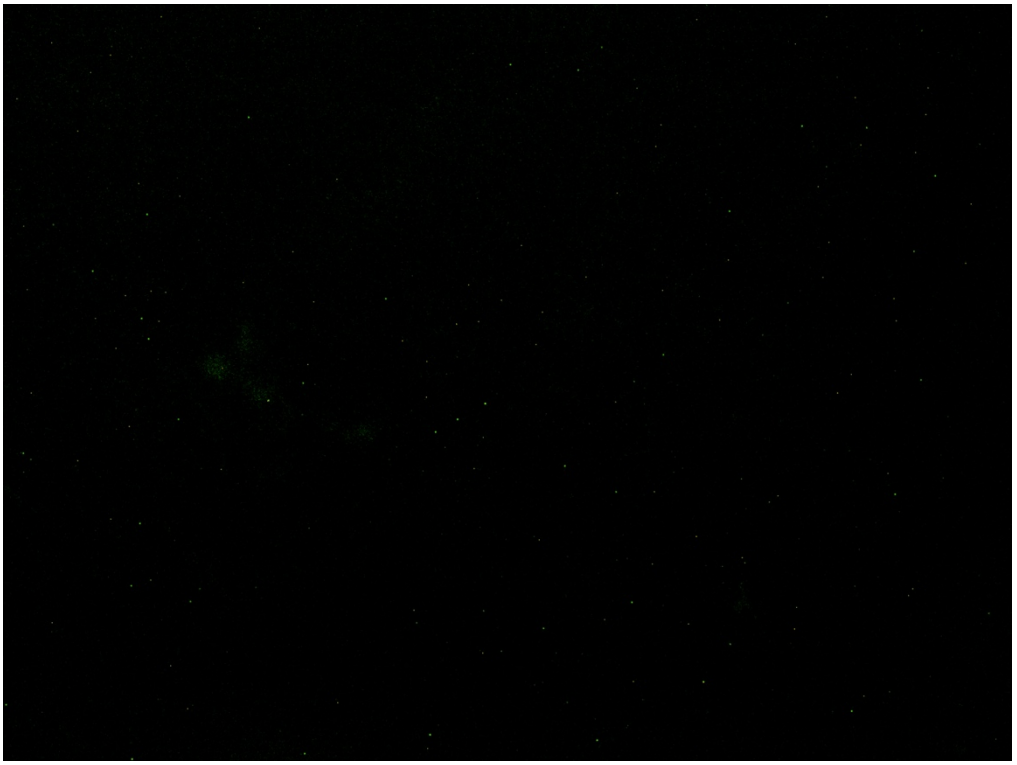


Figure 12.104.: U251 cells treated with 1200.00 µM temozolomide and incubated for 24-hours and dual stained with Annexin-V-fluorescein isothiocyanate and propidium iodide. Replicate: 1; magnification: x100.



Figure 12.105.: U251 cells treated with 1200.00 µM temozolomide and incubated for 24-hours and dual stained with Annexin-V-fluorescein isothiocyanate and propidium iodide. Replicate: 2; magnification: x100.



Figure 12.106.: U251 cells treated with 1200.00 µM temozolomide and incubated for 24-hours and dual stained with Annexin-V-fluorescein isothiocyanate and propidium iodide. Replicate: 3; magnification: x100.



Figure 12.107.: T98G cells treated with 1200.00 µM temozolomide and incubated for 24-hours and dual stained with Annexin-V-fluorescein isothiocyanate and propidium iodide. Replicate: 1; magnification: x100.



Figure 12.108.: T98G cells treated with 1200.00 µM temozolomide and incubated for 24-hours and dual stained with Annexin-V-fluorescein isothiocyanate and propidium iodide. Replicate: 2; magnification: x100.



Figure 12.109.: T98G cells treated with 1200.00 µM temozolomide and incubated for 24-hours and dual stained with Annexin-V-fluorescein isothiocyanate and propidium iodide. Replicate: 3; magnification: x100.

12.6.1.2. U87MG, U251 and T98G cell staining against autophagic cell death

12.6.1.2.1. Bright field imaging

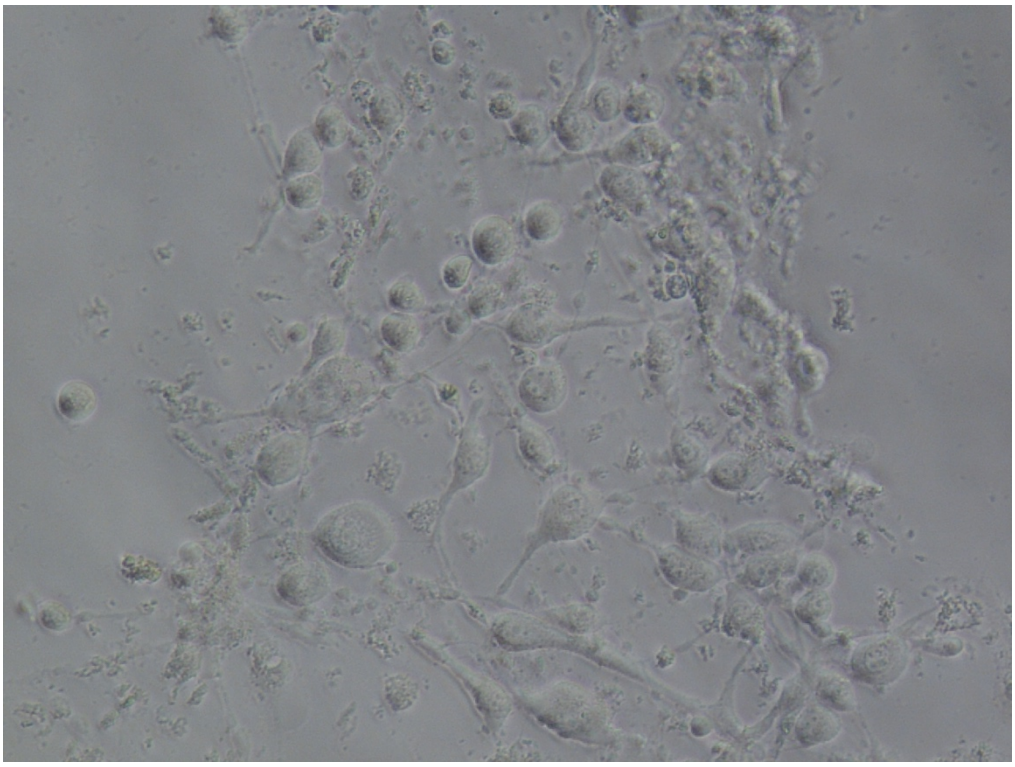


Figure 12.110.: Bright field view of U87MG cells under culture (negative control) conditions incubated for 24-hours. Replicate: 1; magnification: x100.

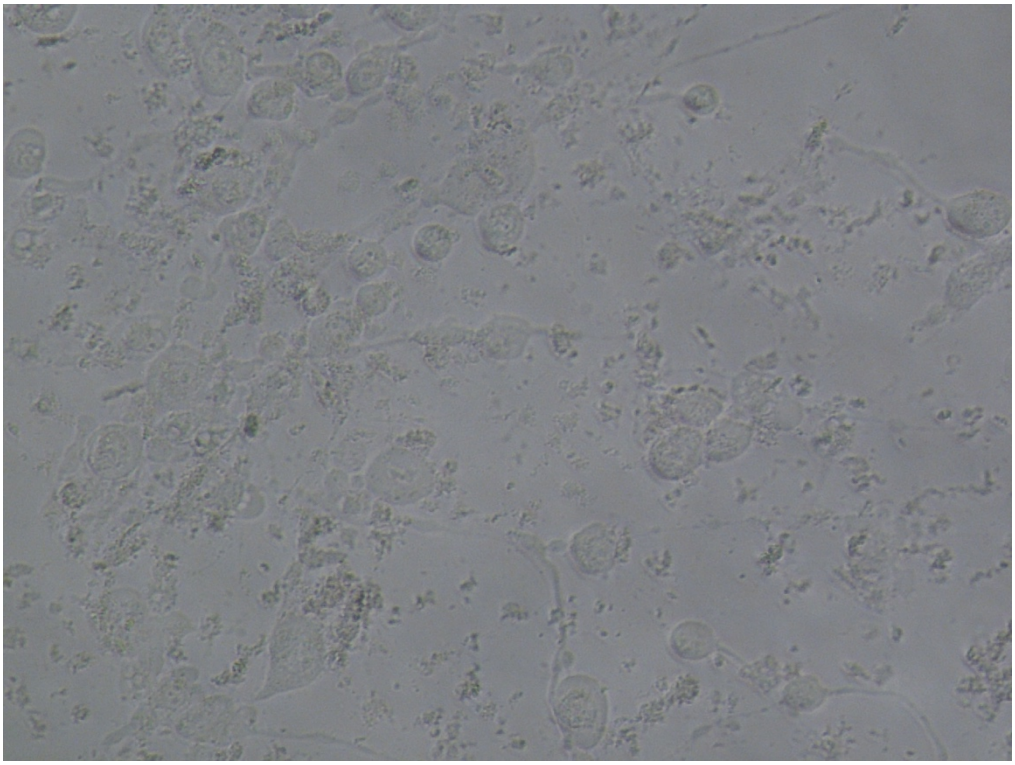


Figure 12.111.: Bright field view of U87MG cells under culture (negative control) conditions incubated for 24-hours. Replicate: 2; magnification: x100.

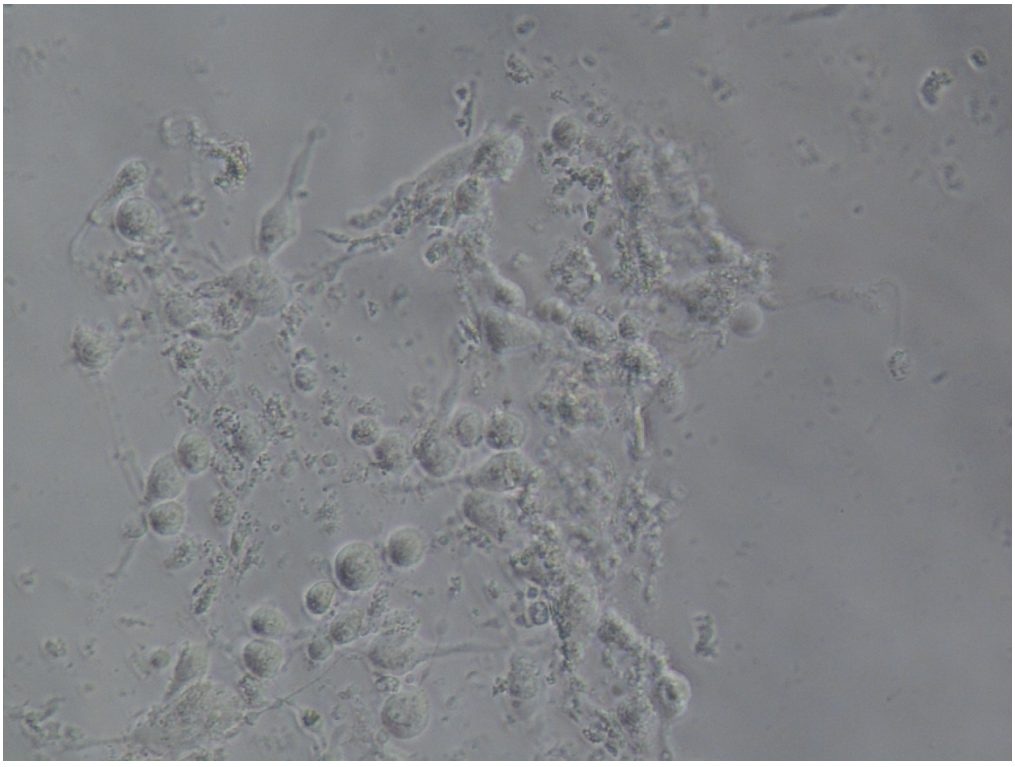


Figure 12.112.: Bright field view of U87MG cells under culture (negative control) conditions incubated for 24-hours. Replicate: 3; magnification: x100.

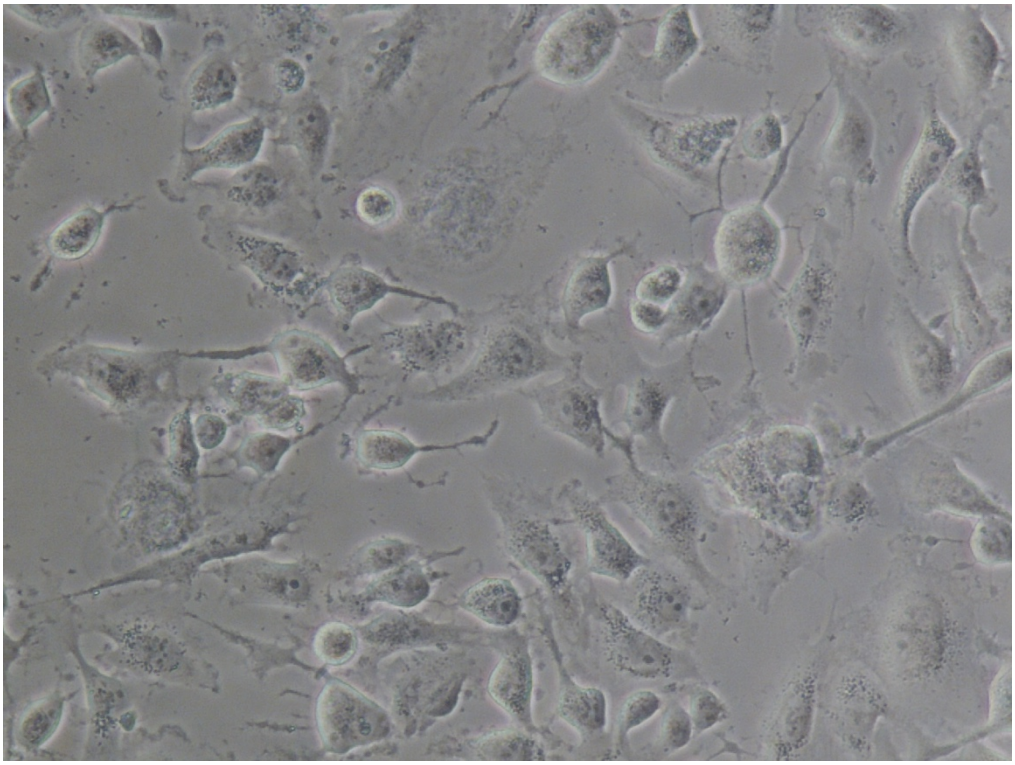


Figure 12.113.: Bright field view of U251 cells under culture (negative control) conditions incubated for 24hours. Replicate: 1; magnification: x100.

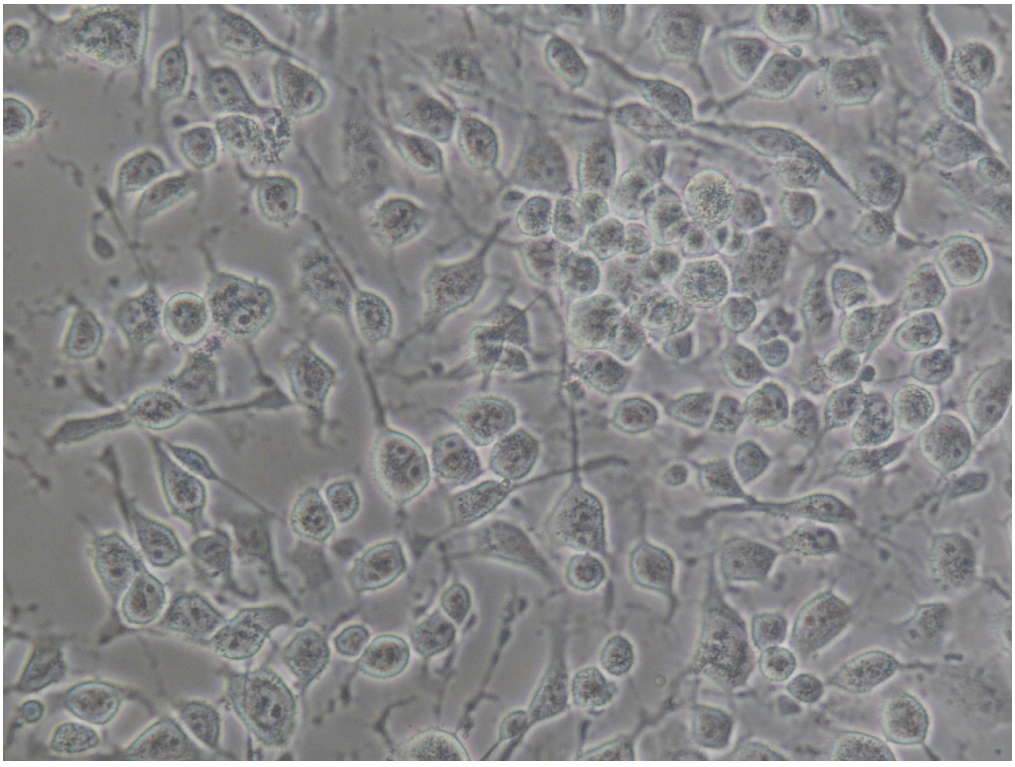


Figure 12.114.: Bright field view of U251 cells under culture (negative control) conditions incubated for 24hours. Replicate: 2; magnification: x100.

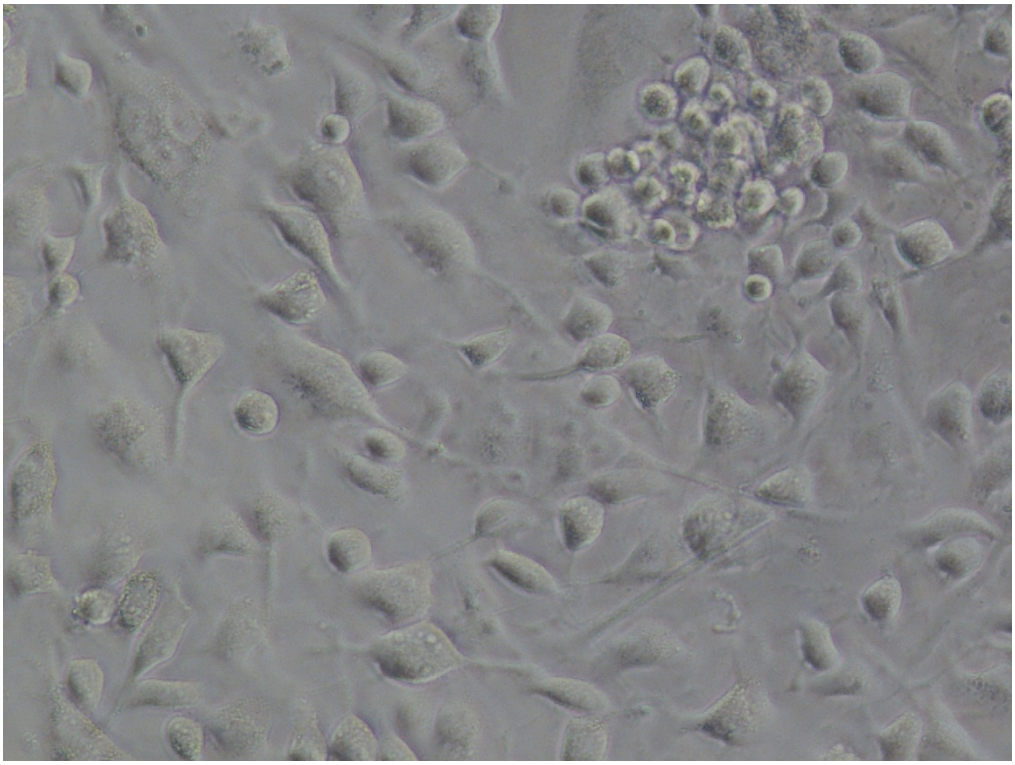


Figure 12.115.: Bright field view of U251 cells under culture (negative control) conditions incubated for 24hours. Replicate: 3; magnification: x100.

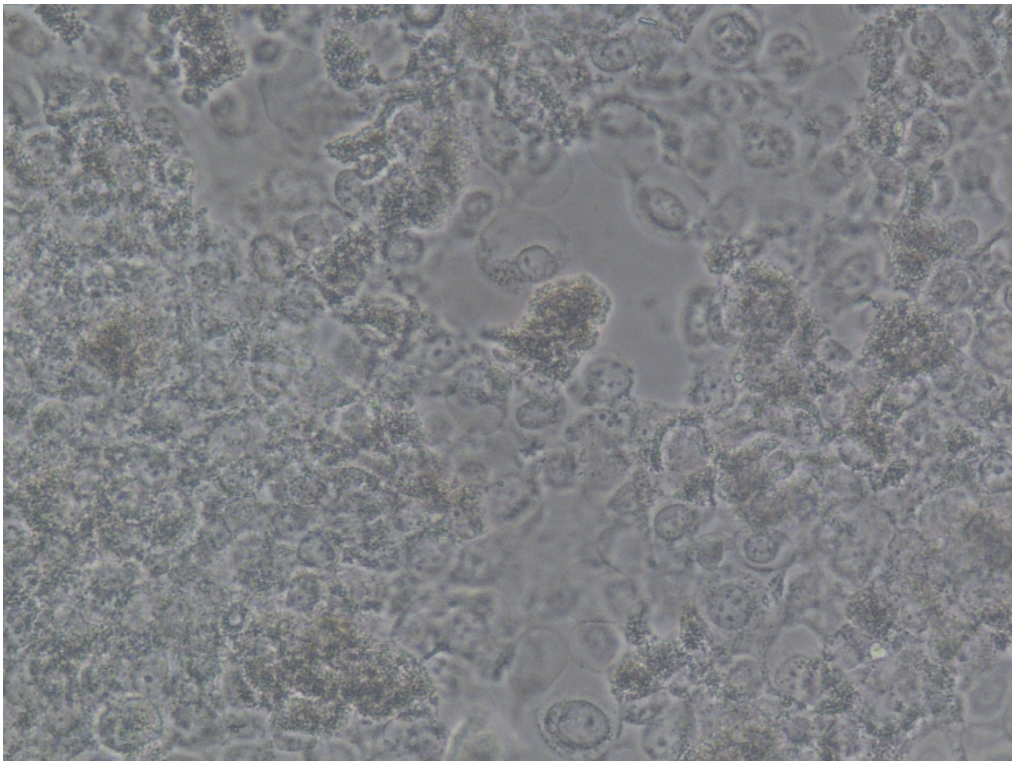


Figure 12.116.: Bright field view of T98G cells under culture (negative control) conditions incubated for 24hours. Replicate: 1; magnification: x100.

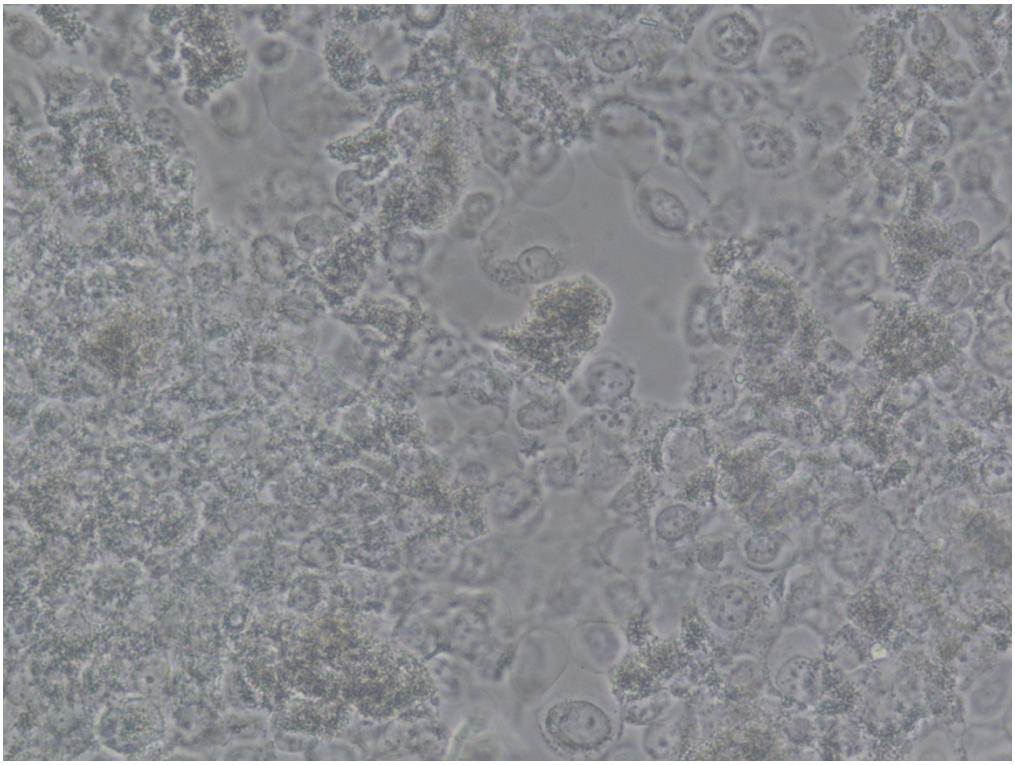


Figure 12.117.: Bright field view of T98G cells under culture (negative control) conditions incubated for 24hours. Replicate: 2; magnification: x100.

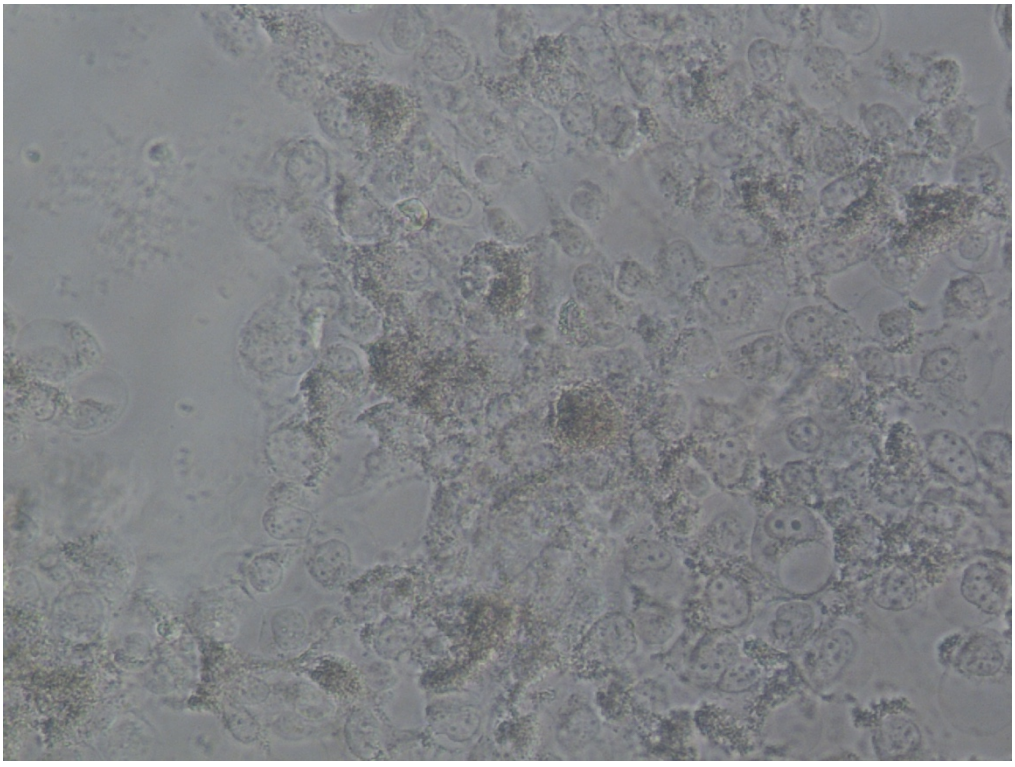


Figure 12.118.: Bright field view of T98G cells under culture (negative control) conditions incubated for 24hours. Replicate: 3; magnification: x100.

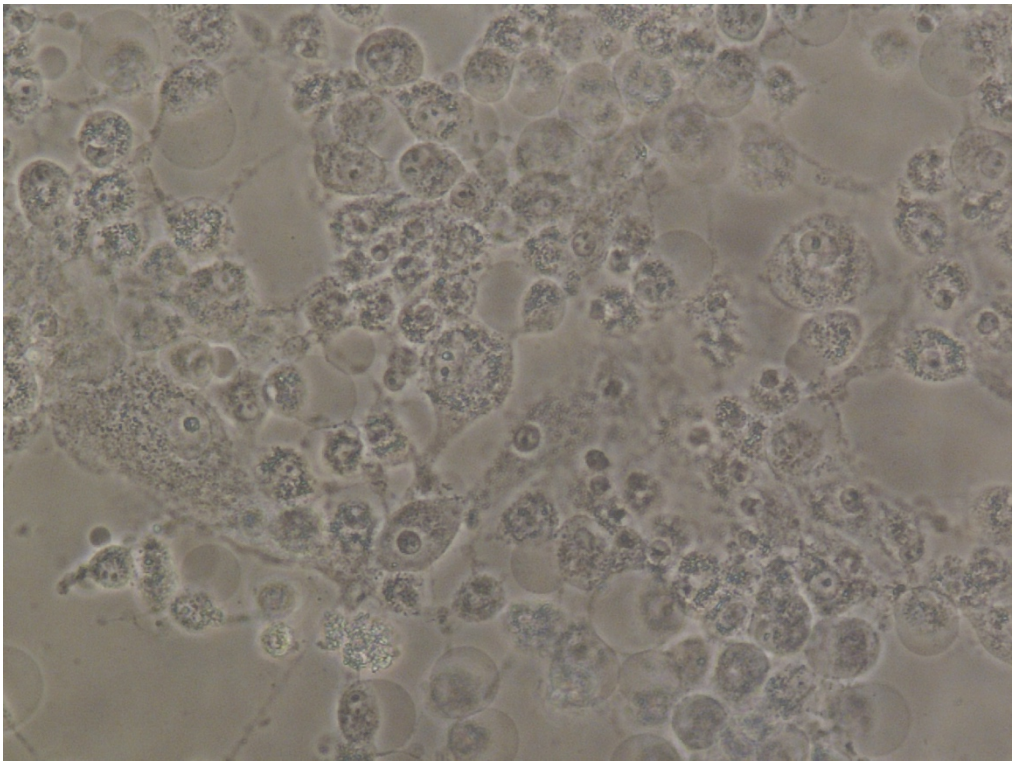


Figure 12.119.: Bright field view of U87MG cells treated with 6.25 µM α-solanine and incubated for 24-hours. Replicate: 1; magnification: x100.

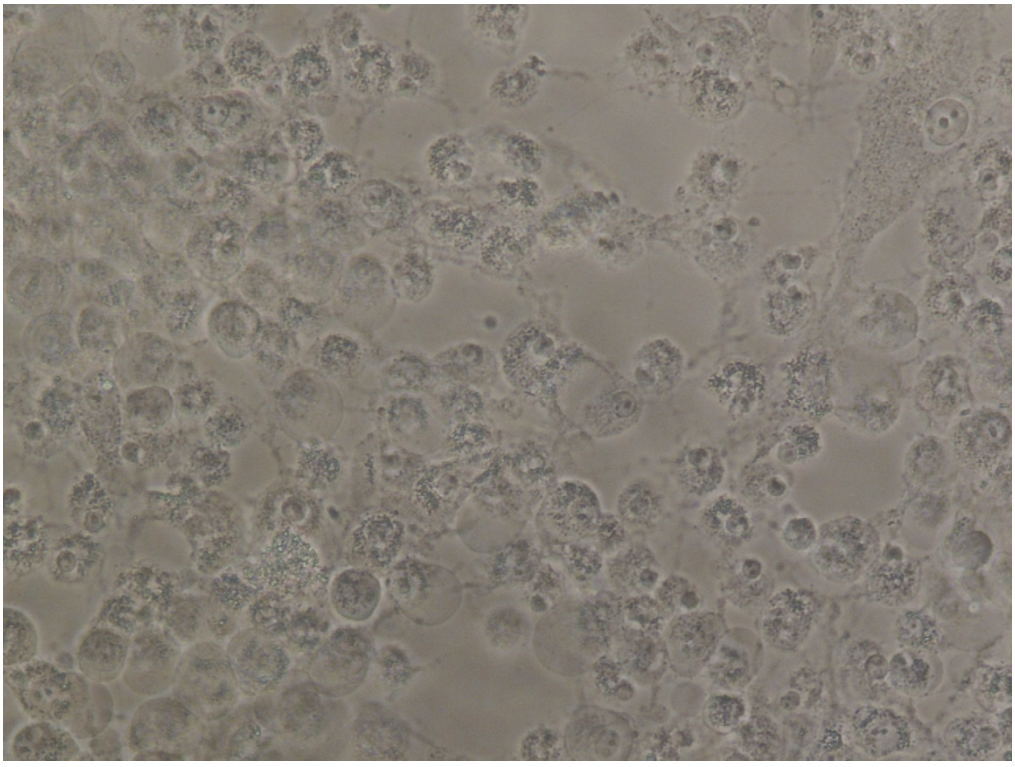


Figure 12.120.: Bright field view of U87MG cells treated with 6.25 µM α-solanine and incubated for 24-hours. Replicate: 2; magnification: x100.

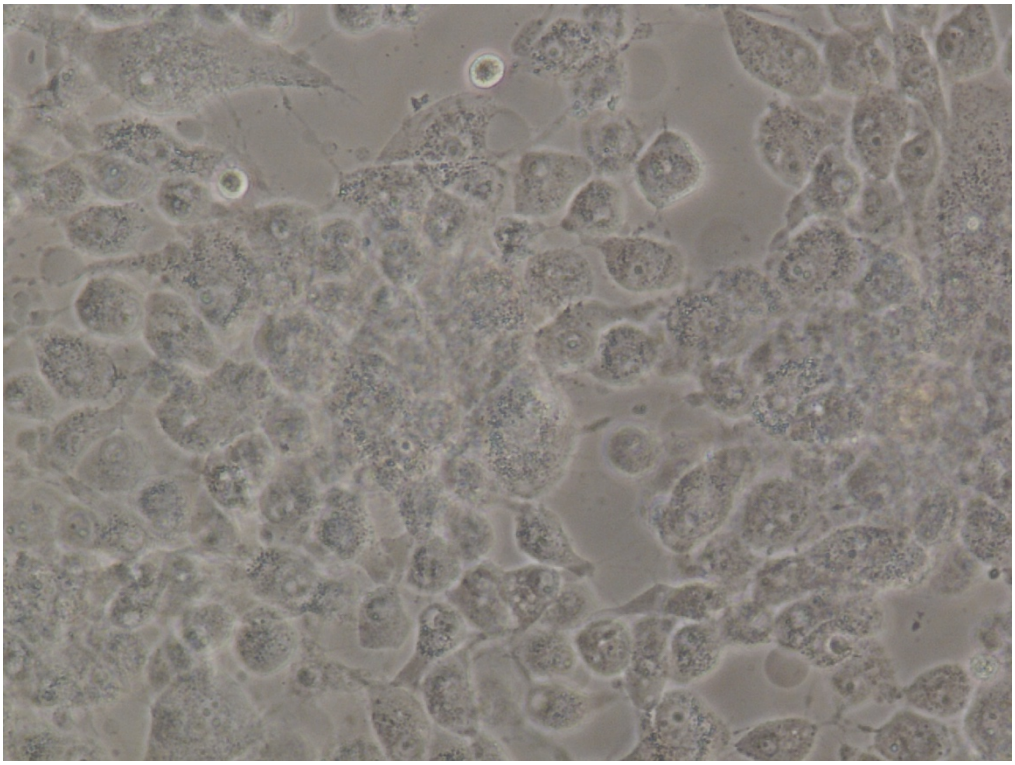


Figure 12.121.: Bright field view of U87MG cells treated with 6.25 µM α-solanine and incubated for 24-hours. Replicate: 3; magnification: x100.

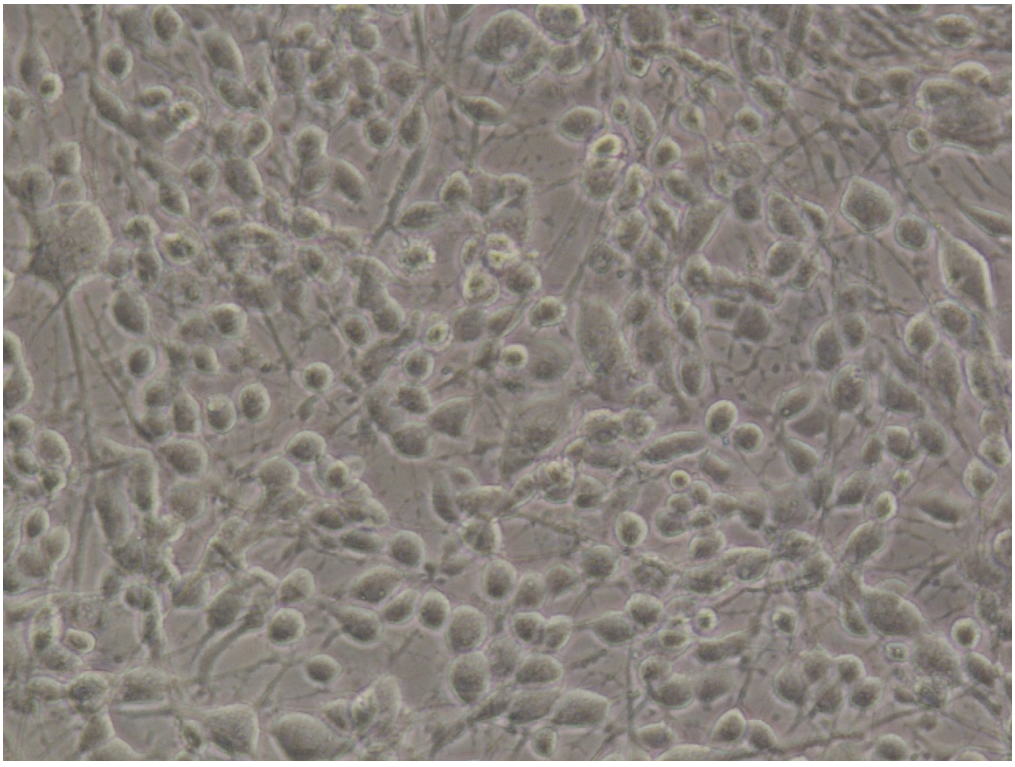


Figure 12.122.: Bright field view of U251 cells treated with 6.25 µM α-solanine and incubated for 24-hours. Replicate: 1; magnification: x100.

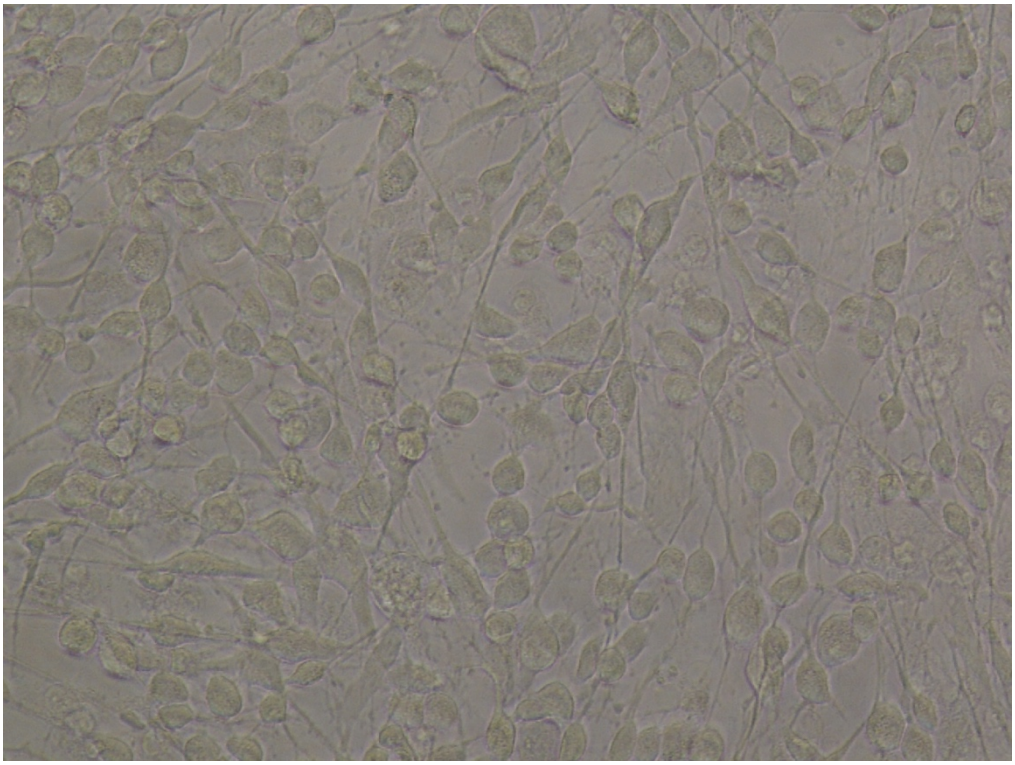


Figure 12.123.: Bright field view of U251 cells treated with 6.25 µM α-solanine and incubated for 24-hours. Replicate: 2; magnification: x100.

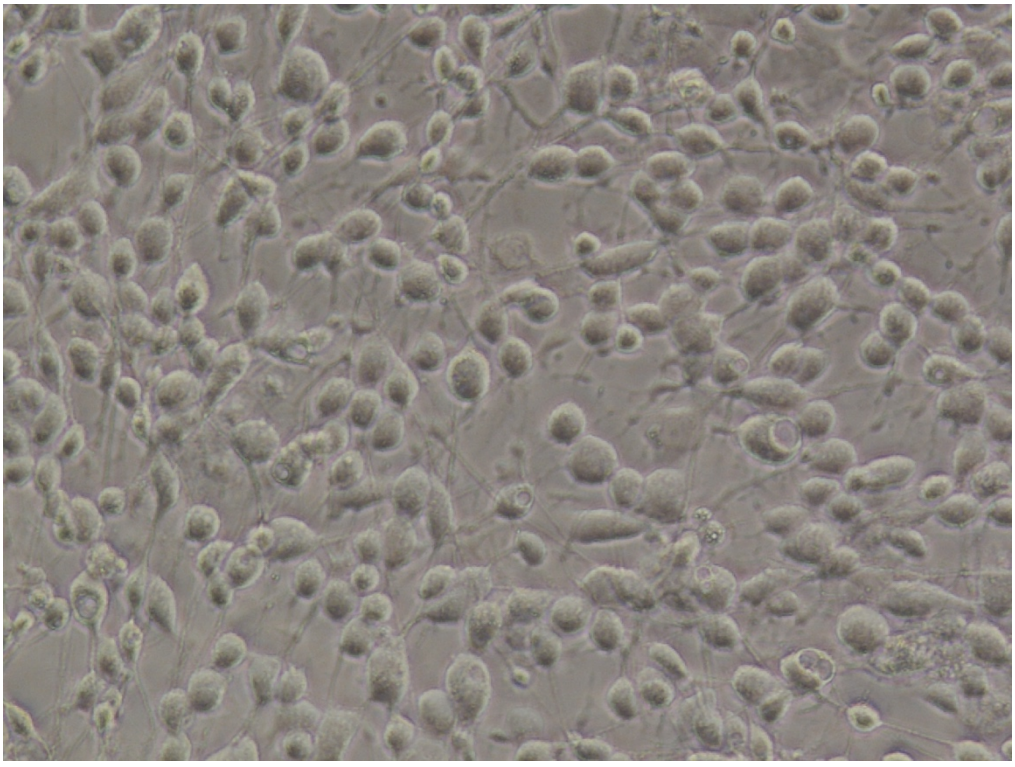


Figure 12.124.: Bright field view of U251 cells treated with 6.25 µM α-solanine and incubated for 24-hours. Replicate: 3; magnification: x100.

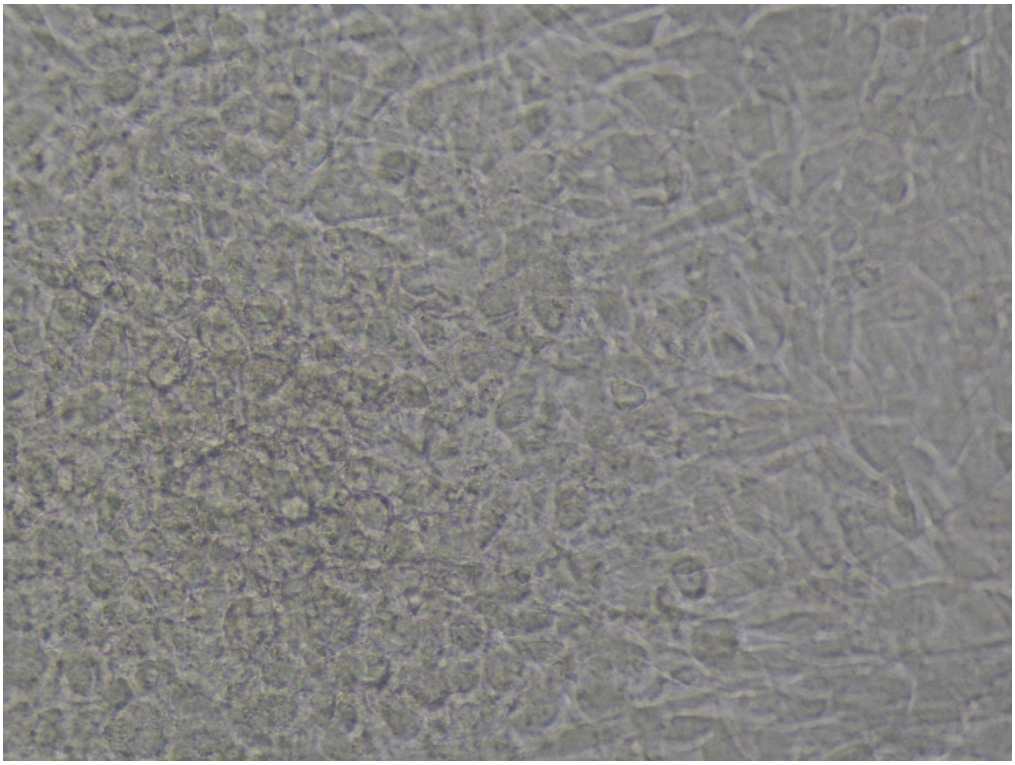


Figure 12.125.: Bright field view of T98G cells treated with 6.25 µM α-solanine and incubated for 24-hours. Replicate: 1; magnification: x100.

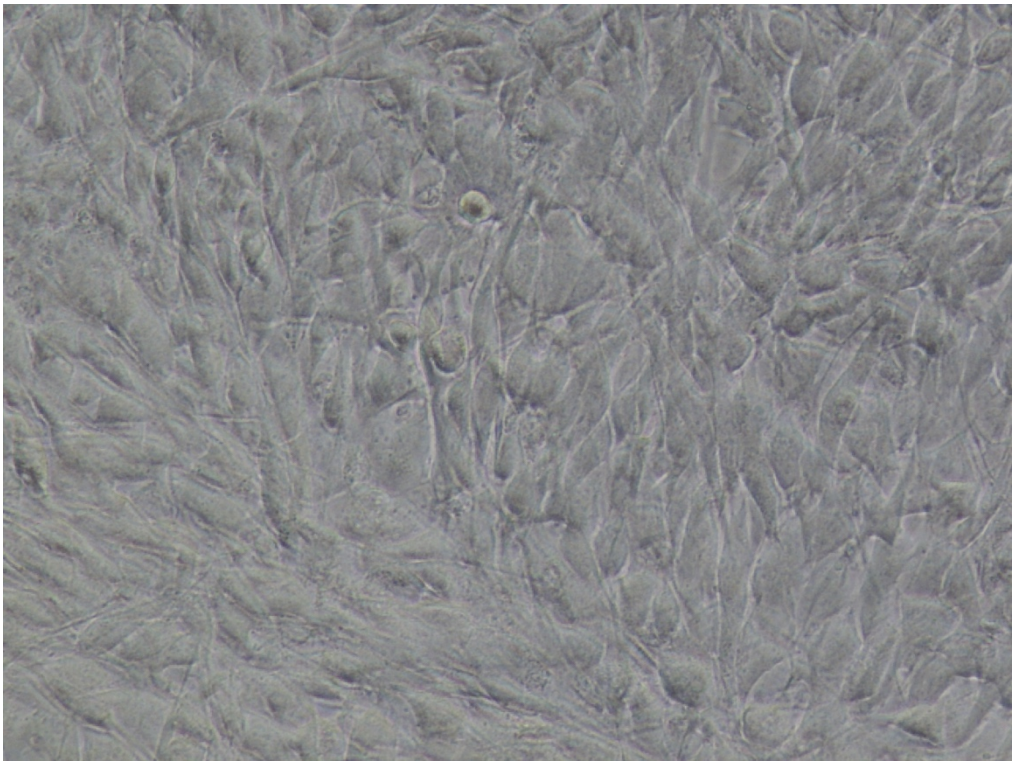


Figure 12.126.: Bright field view of T98G cells treated with 6.25 µM α-solanine and incubated for 24-hours. Replicate: 2; magnification: x100.

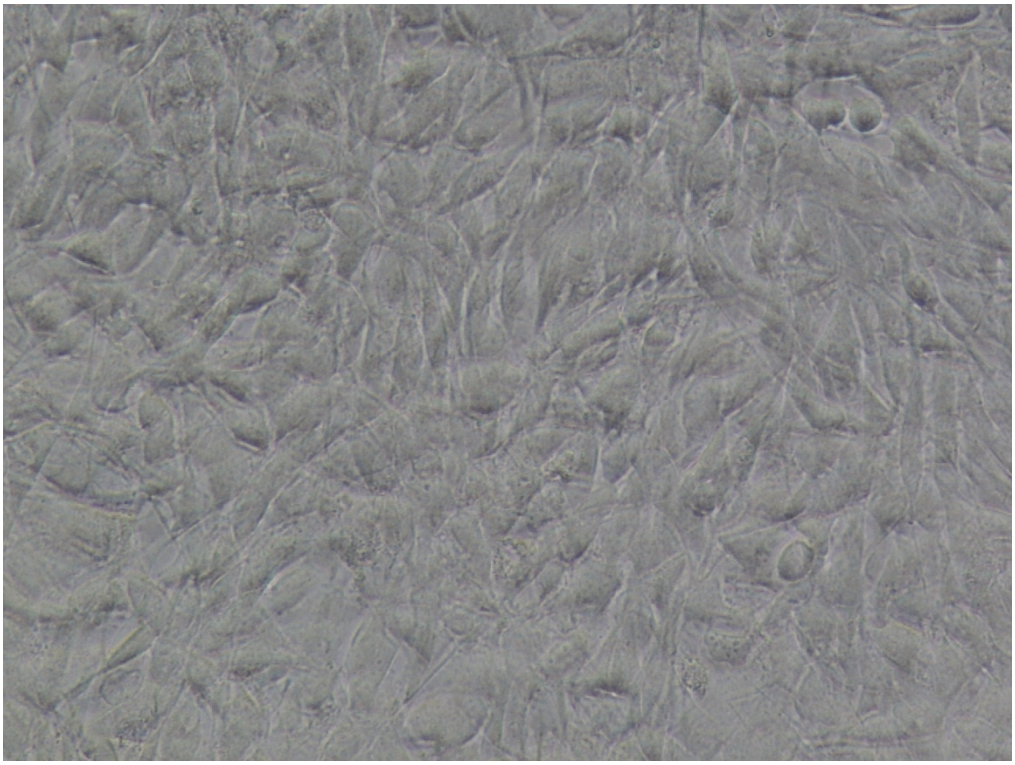


Figure 12.127.: Bright field view of T98G cells treated with 6.25 µM α-solanine and incubated for 24-hours. Replicate: 3; magnification: x100.

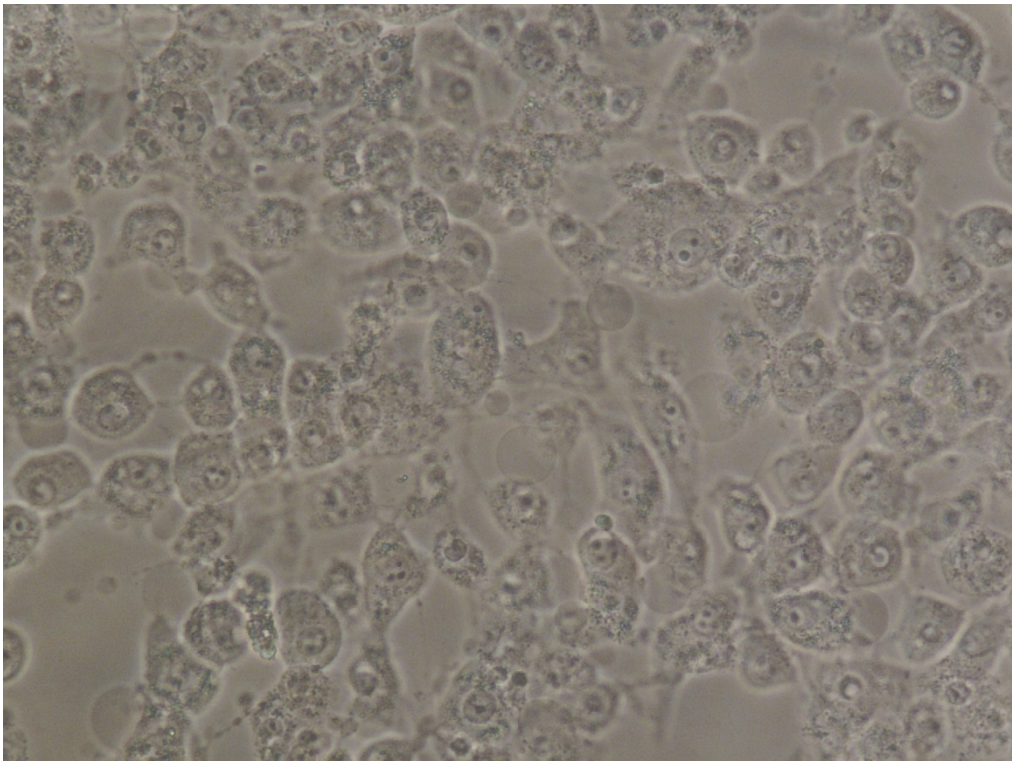


Figure 12.128.: Bright field view of U87MG cells treated with 1200.00 µM temozolomide and incubated for 24-hours. Replicate: 1; magnification: x100.

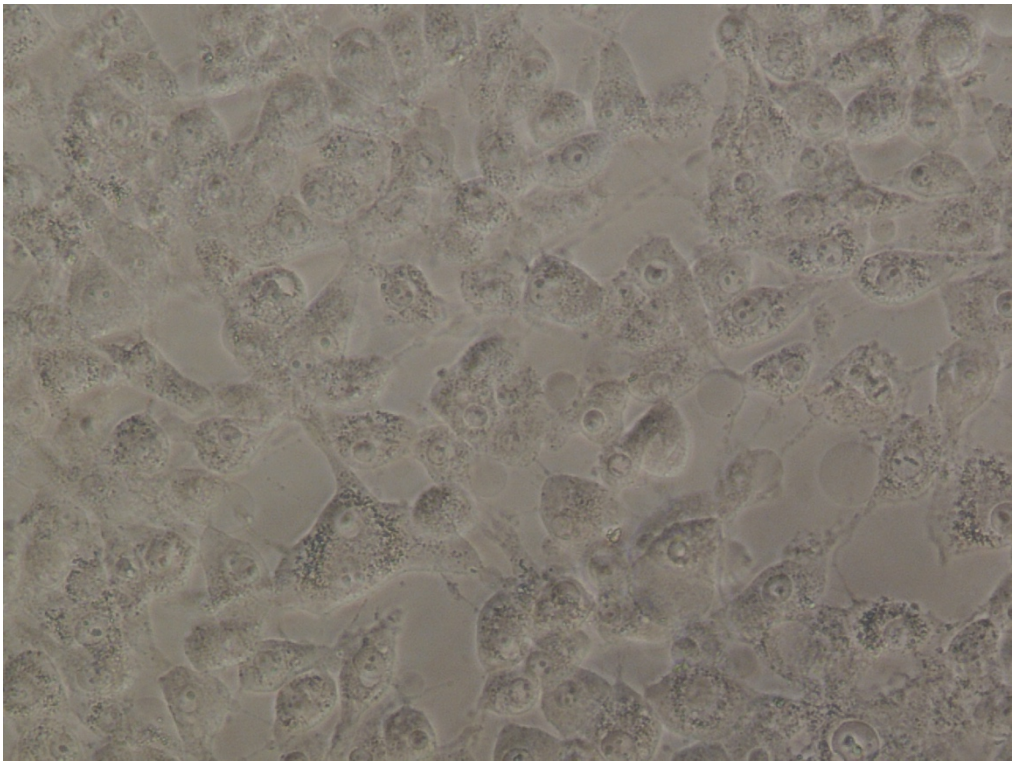


Figure 12.129.: Bright field view of U87MG cells treated with 1200.00 µM temozolomide and incubated for 24-hours. Replicate: 2; magnification: x100.

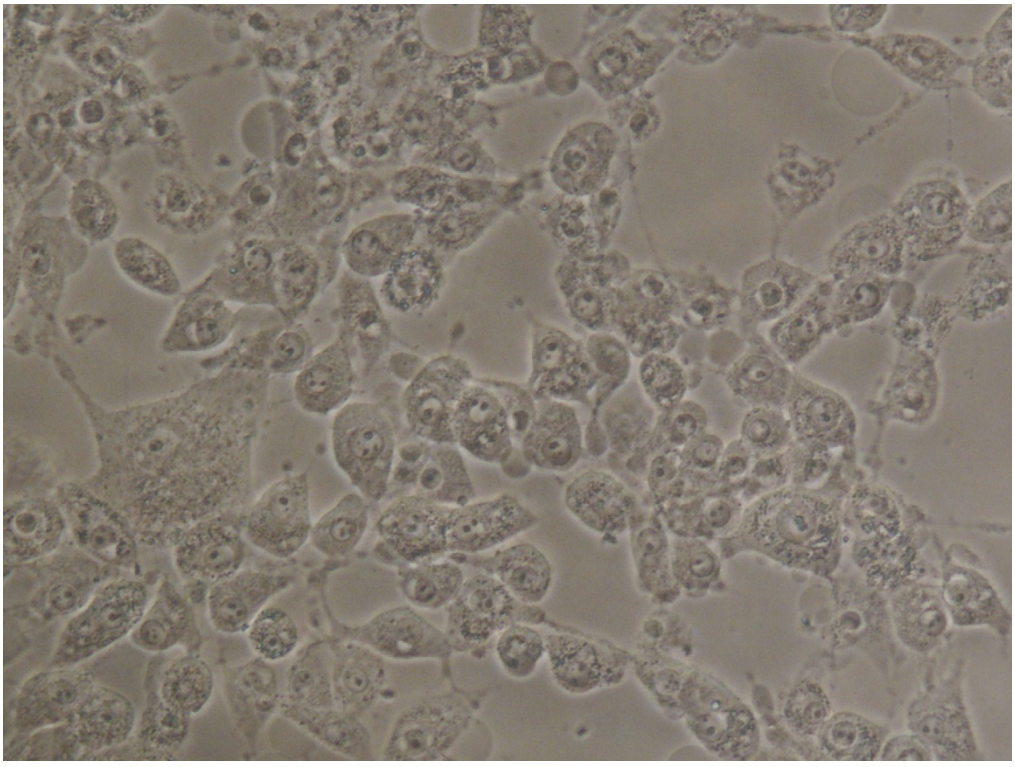


Figure 12.130.: Bright field view of U87MG cells treated with 1200.00 µM temozolomide and incubated for 24-hours. Replicate: 3; magnification: x100.

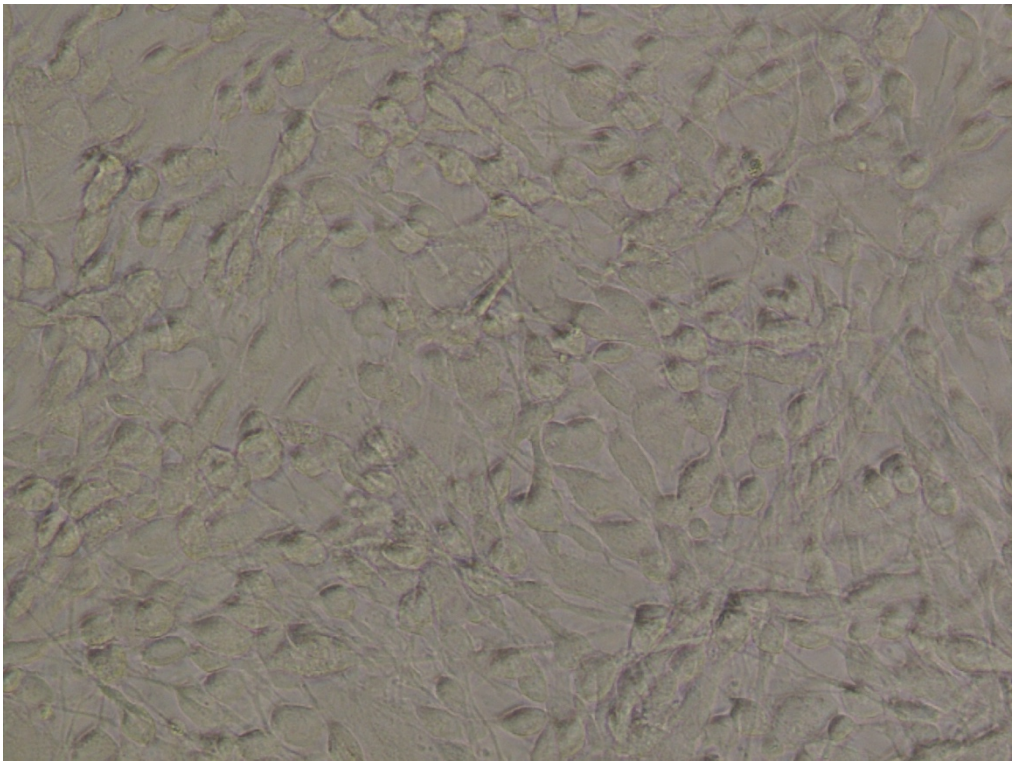


Figure 12.131.: Bright field view of U251 cells treated with 1200.00 µM temozolomide and incubated for 24-hours. Replicate: 1; magnification: x100.

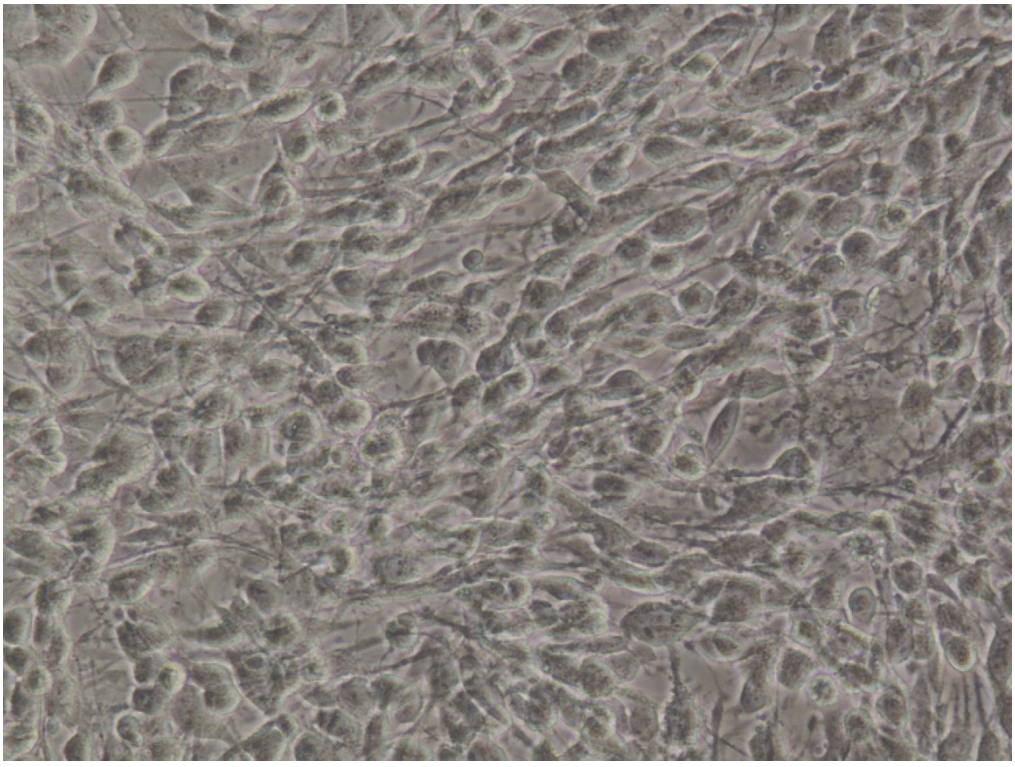


Figure 12.132.: Bright field view of U251 cells treated with 1200.00 µM temozolomide and incubated for 24-hours. Replicate: 2; magnification: x100.

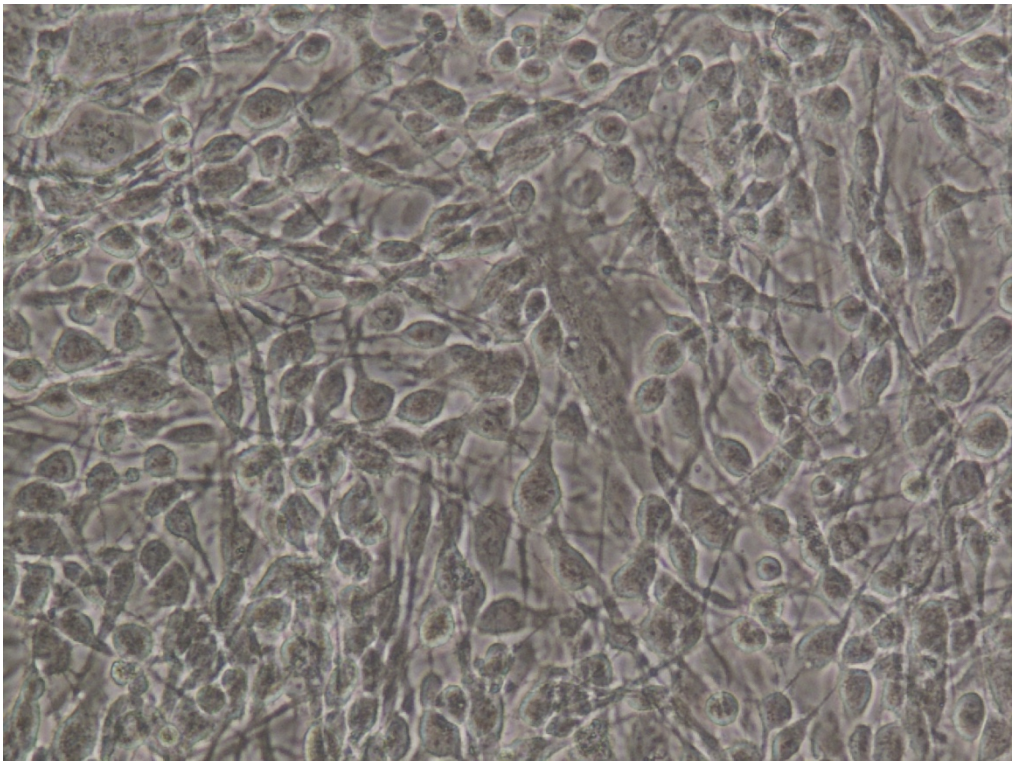


Figure 12.133.: Bright field view of U251 cells treated with 1200.00 µM temozolomide and incubated for 24-hours. Replicate: 3; magnification: x100.

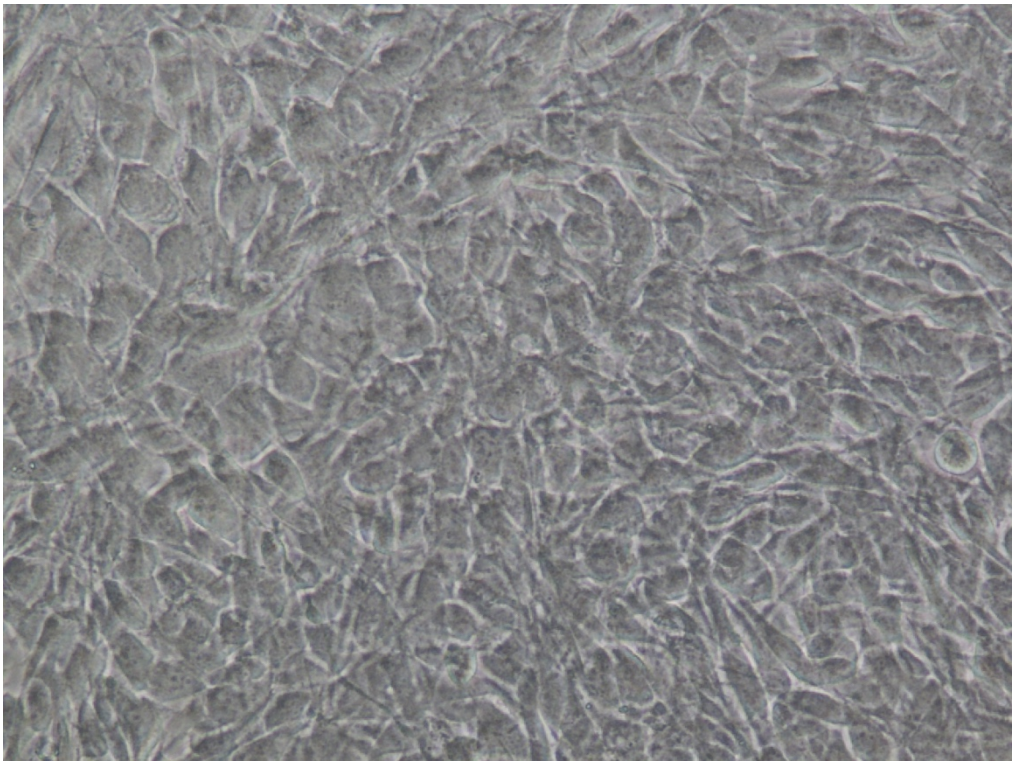


Figure 12.134.: Bright field view of T98G cells treated with 1200.00 µM temozolomide and incubated for 24-hours. Replicate: 1; magnification: x100.

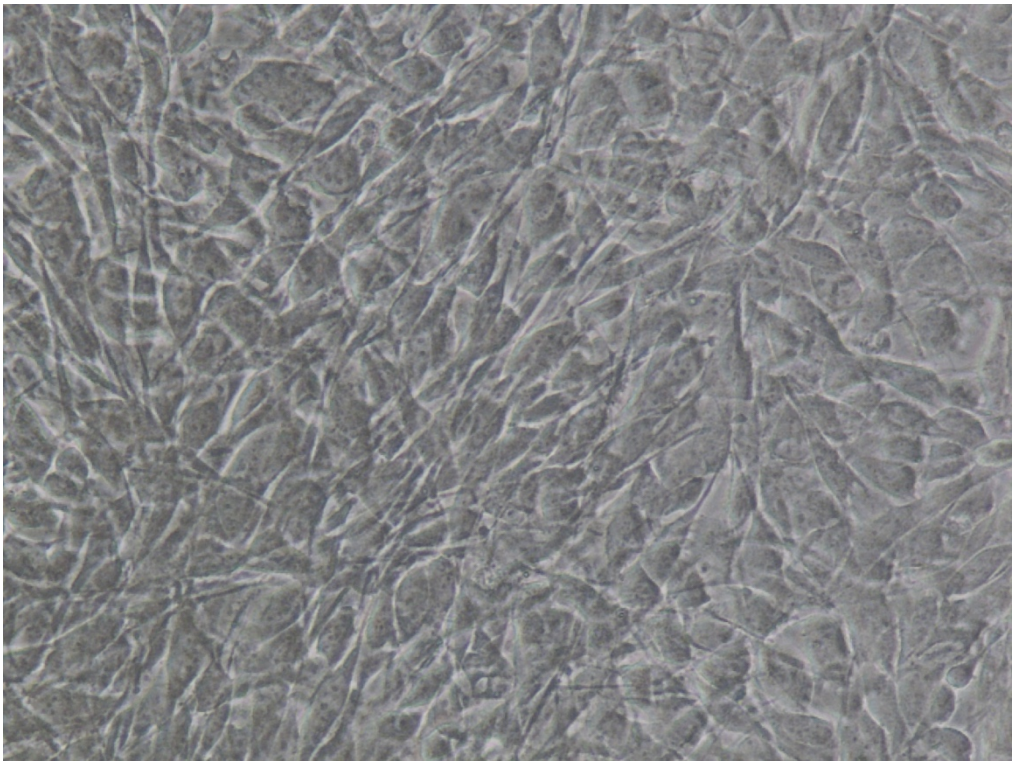


Figure 12.135.: Bright field view of T98G cells treated with 1200.00 µM temozolomide and incubated for 24-hours. Replicate: 2; magnification: x100.

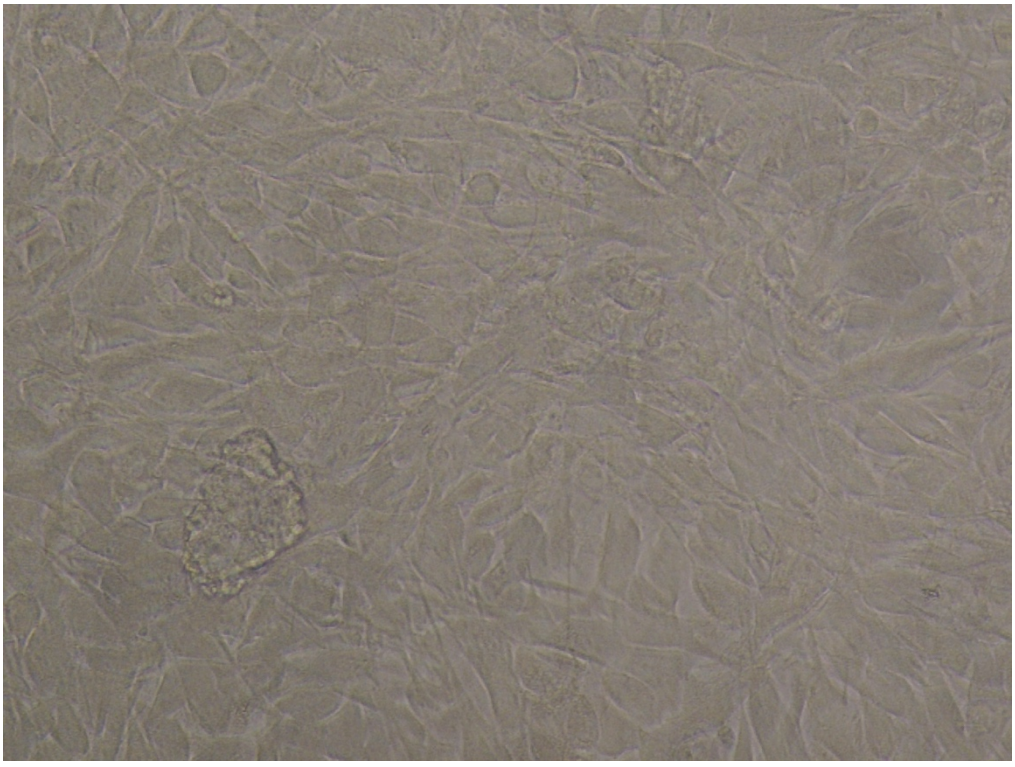


Figure 12.136.: Bright field view of T98G cells treated with 1200.00 µM temozolomide and incubated for 24-hours. Replicate: 3; magnification: x100.

12.6.1.2.2. Monodansylcadaverine staining.



Figure 12.137.: U87MG cells under culture (negative control) conditions incubated for 24-hours and stained with monodansylcadaverine. Replicate: 1; magnification: x100.



Figure 12.138.: U87MG cells under culture (negative control) conditions incubated for 24-hours and stained with monodansylcadaverine. Replicate: 2; magnification: x100.

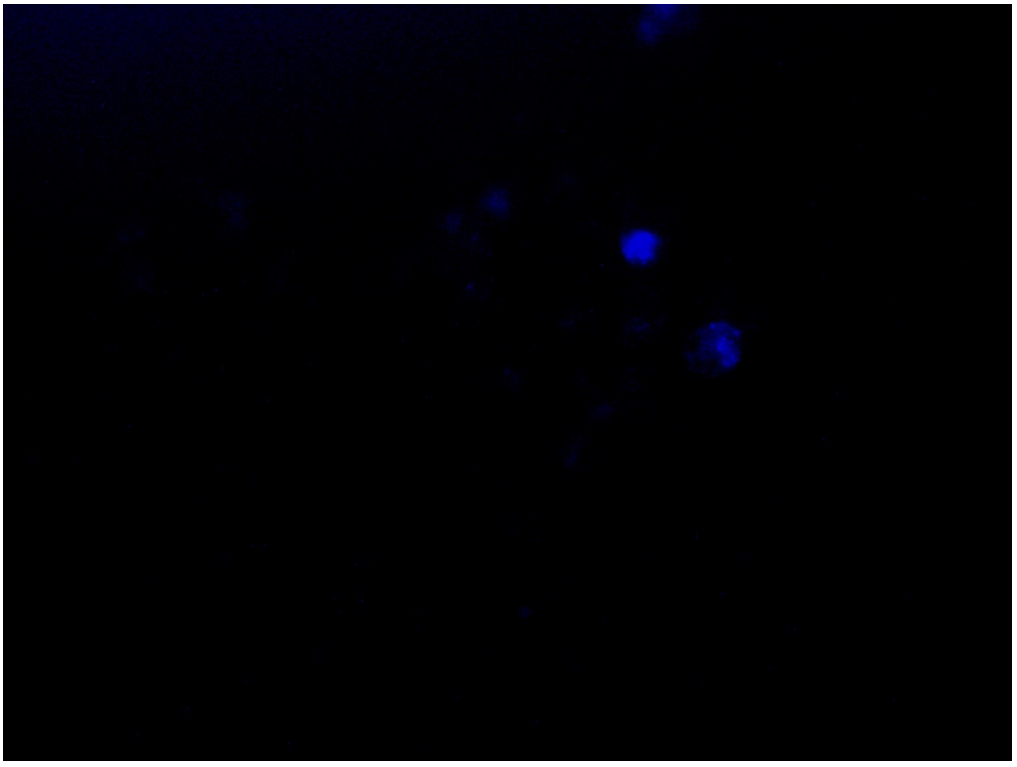


Figure 12.139.: U87MG cells under culture (negative control) conditions incubated for 24-hours and stained with monodansylcadaverine. Replicate: 3; magnification: x100.

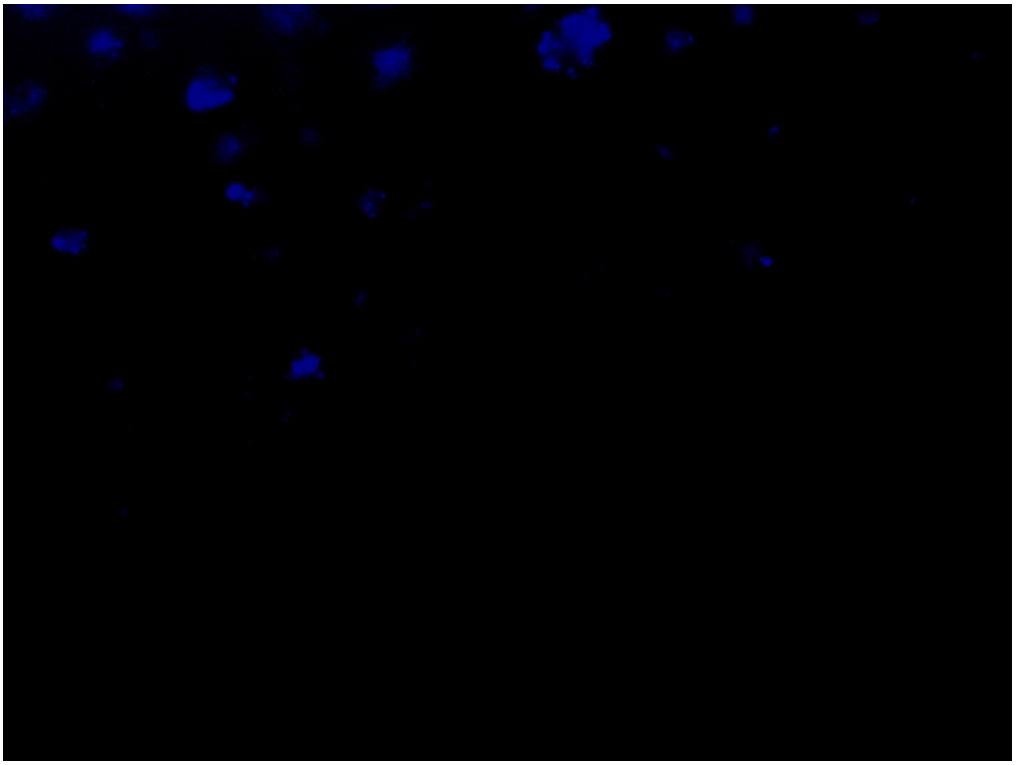


Figure 12.140.: U251 cells under culture (negative control) conditions incubated for 24-hours and stained with monodansylcadaverine. Replicate: 1; magnification: x100.

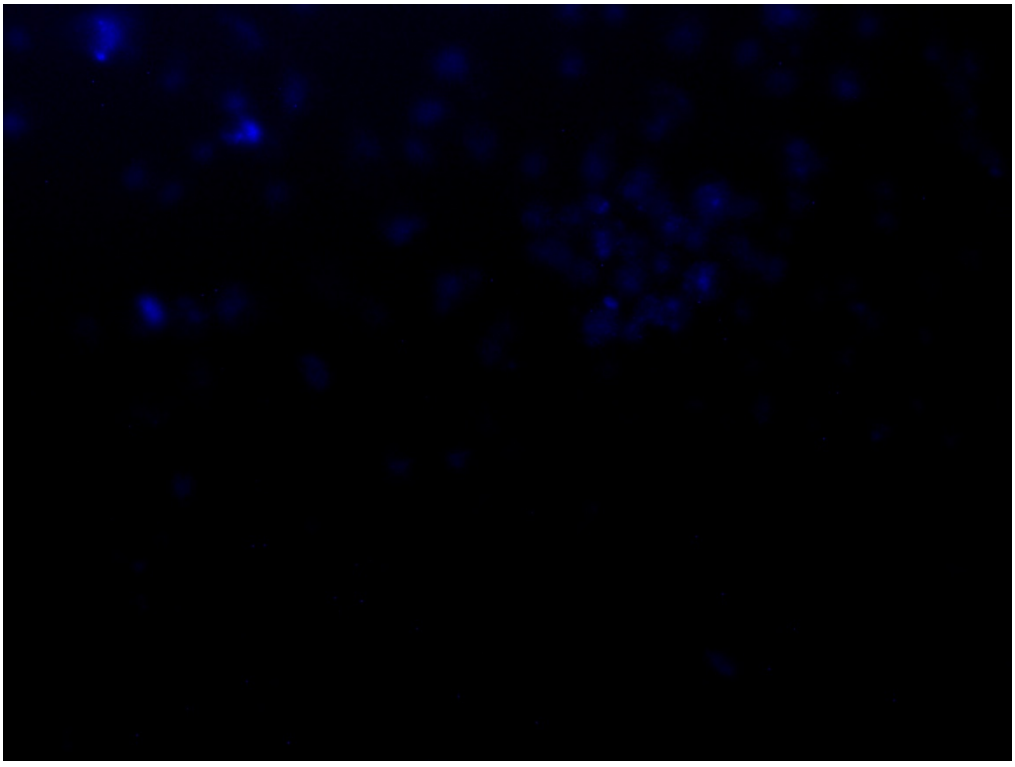


Figure 12.141.: U251 cells under culture (negative control) conditions incubated for 24-hours and stained with monodansylcadaverine. Replicate: 2; magnification: x100.

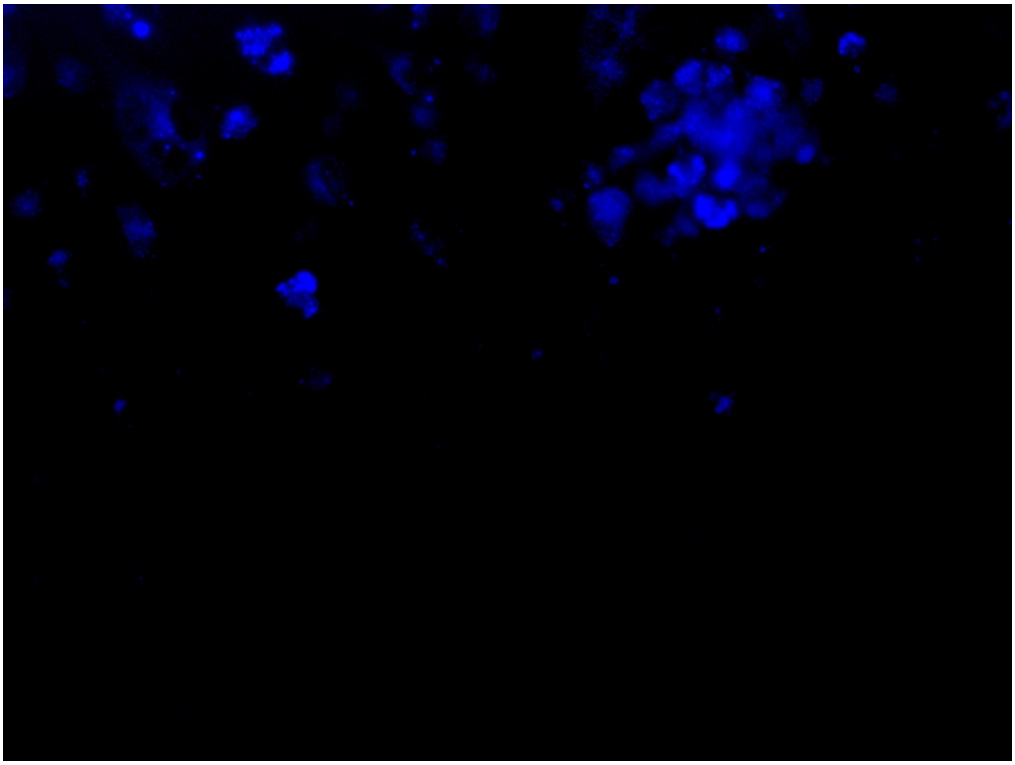


Figure 12.142.: U251 cells under culture (negative control) conditions incubated for 24-hours and stained with monodansylcadaverine. Replicate: 3; magnification: x100.

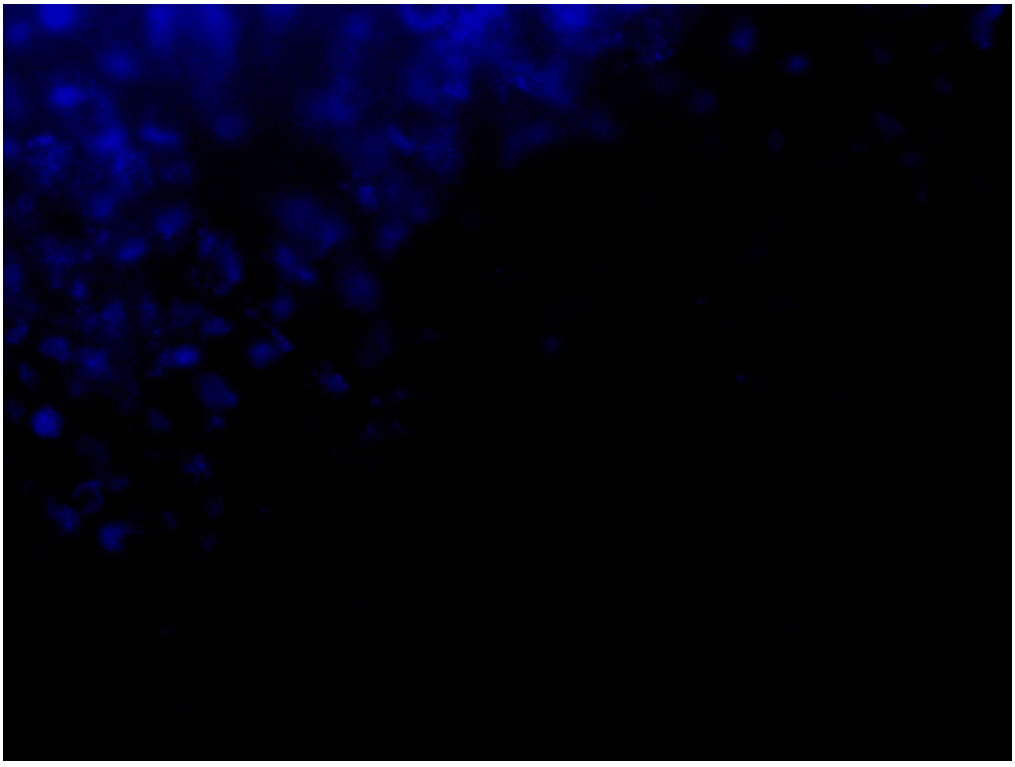


Figure 12.143.: T98G cells under culture (negative control) conditions incubated for 24-hours and stained with monodansylcadaverine. Replicate: 1; magnification: x100.

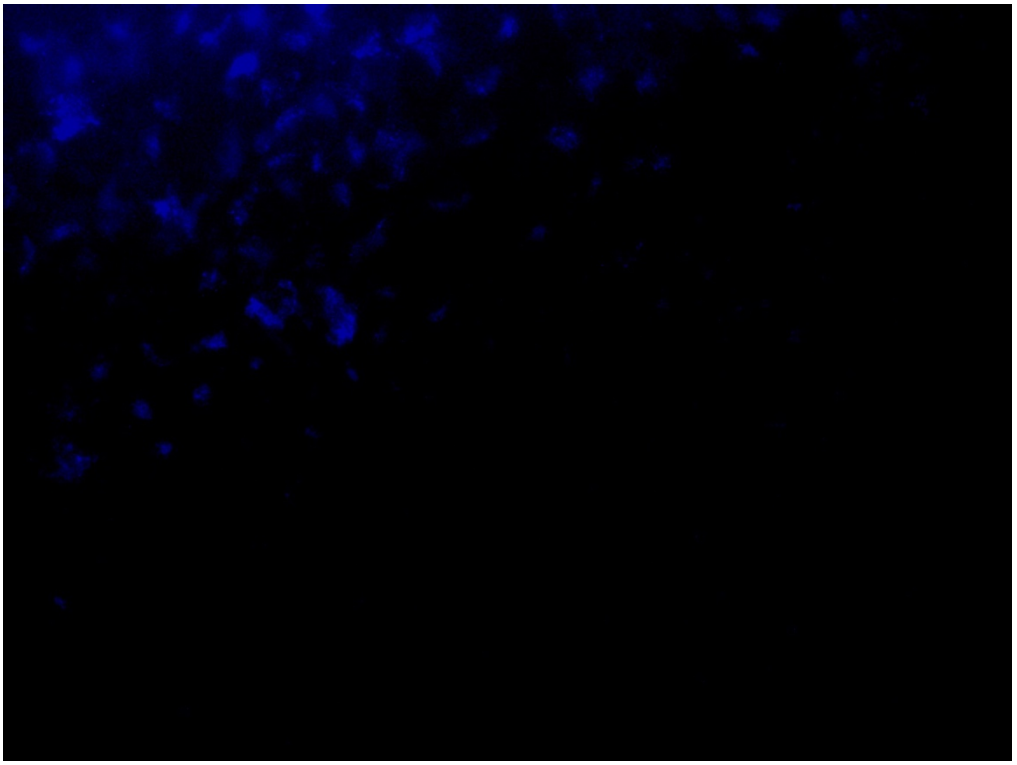


Figure 12.144.: T98G cells under culture (negative control) conditions incubated for 24-hours and stained with monodansylcadaverine. Replicate: 2; magnification: x100.

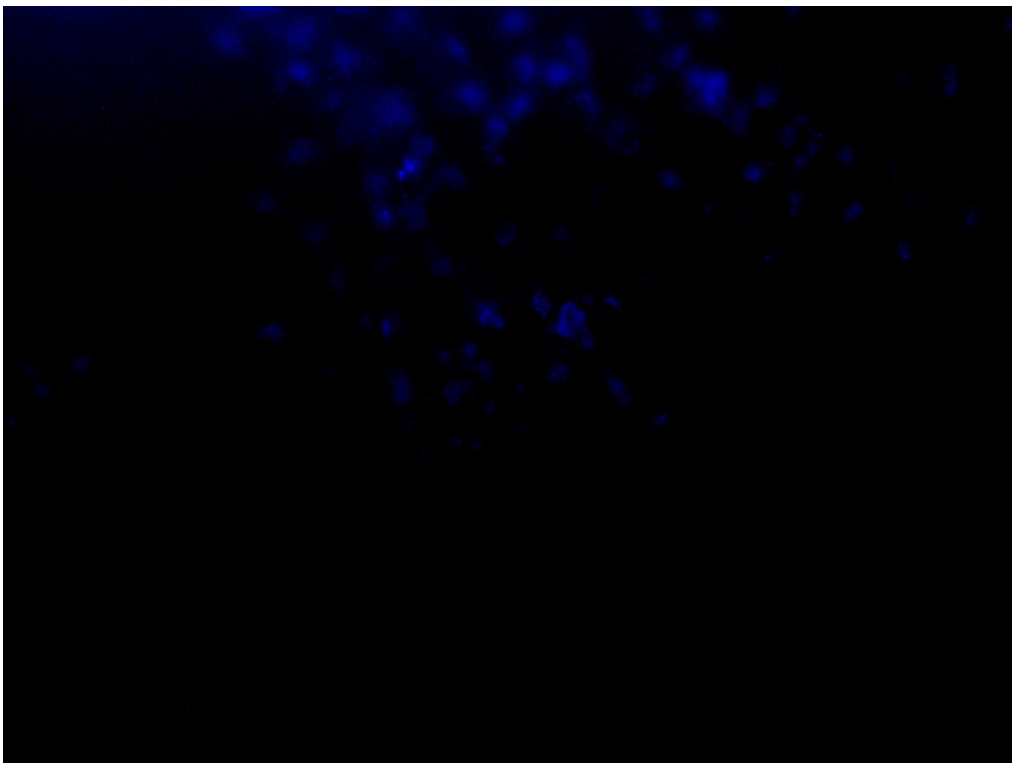


Figure 12.145.: T98G cells under culture (negative control) conditions incubated for 24-hours and stained with monodansylcadaverine. Replicate: 3; magnification: x100.



Figure 12.146.: U87MG cells treated with 6.25 µM α-solanine and incubated for 24-hours and stained with monodansylcadaverine. Replicate: 1; magnification: x100.



Figure 12.147.: U87MG cells treated with 6.25 µM α-solanine and incubated for 24-hours and stained with monodansylcadaverine. Replicate: 2; magnification: x100.

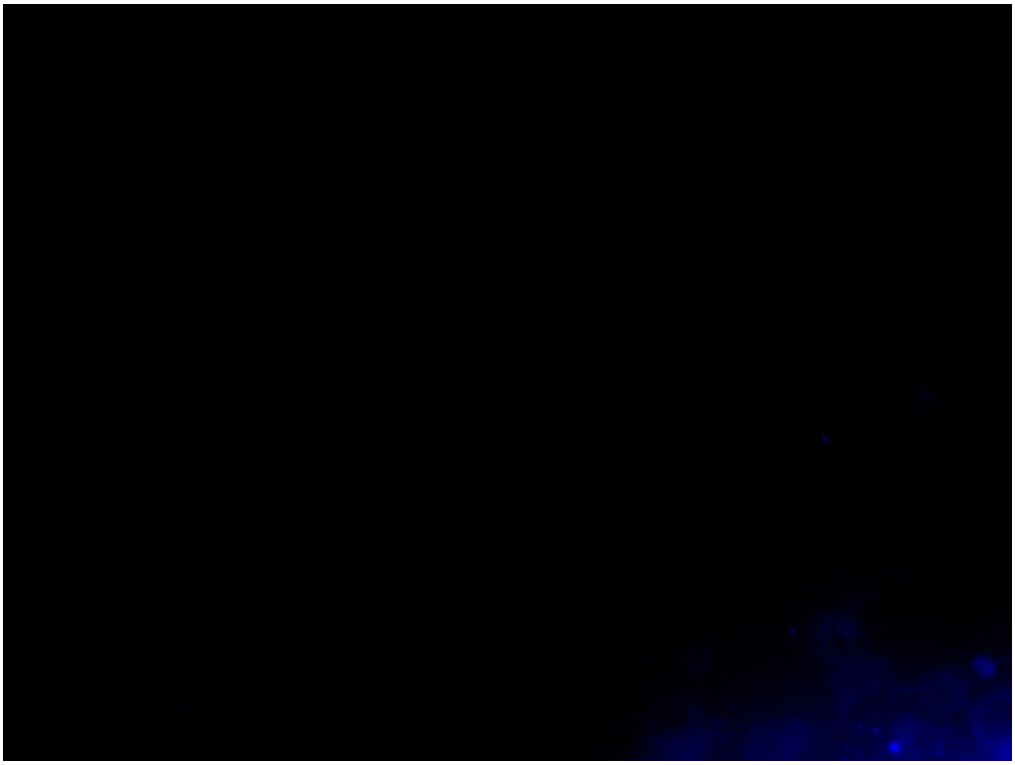


Figure 12.148.: U87MG cells treated with 6.25 µM α-solanine and incubated for 24-hours and stained with monodansylcadaverine. Replicate: 3; magnification: x100.

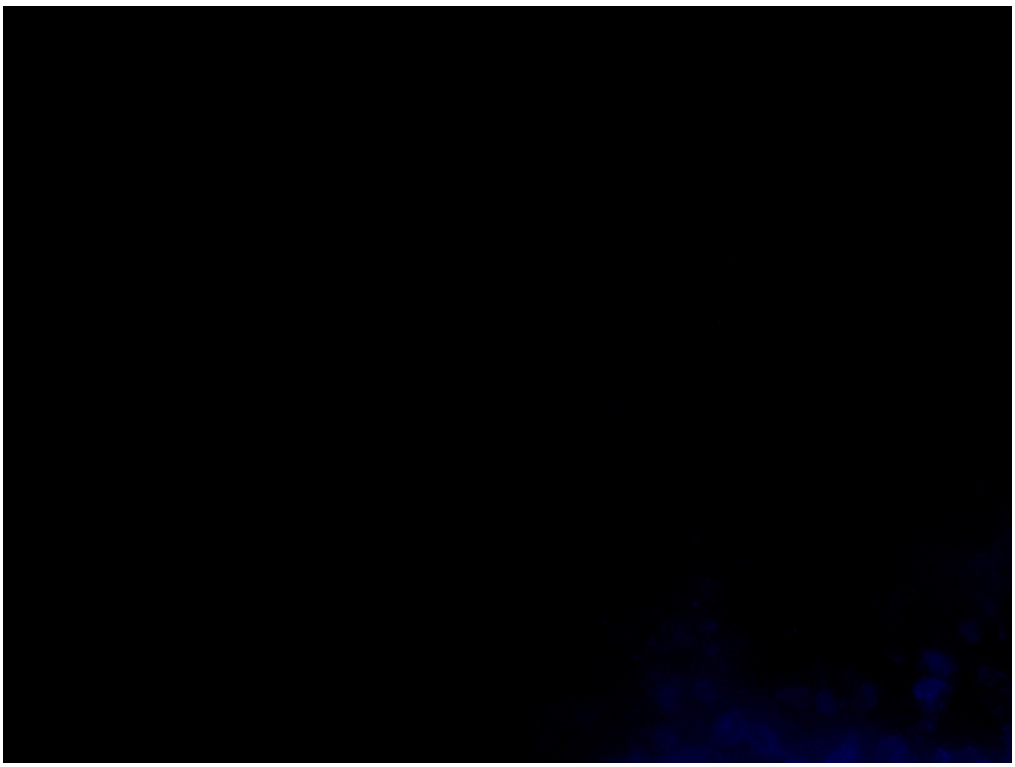


Figure 12.149.: U251 cells treated with 6.25 µM α-solanine and incubated for 24-hours and stained with monodansylcadaverine. Replicate1; magnification: x100.



Figure 12.150.: U251 cells treated with 6.25 µM α-solanine and incubated for 24-hours and stained with monodansylcadaverine. Replicate: 2; magnification: x100.

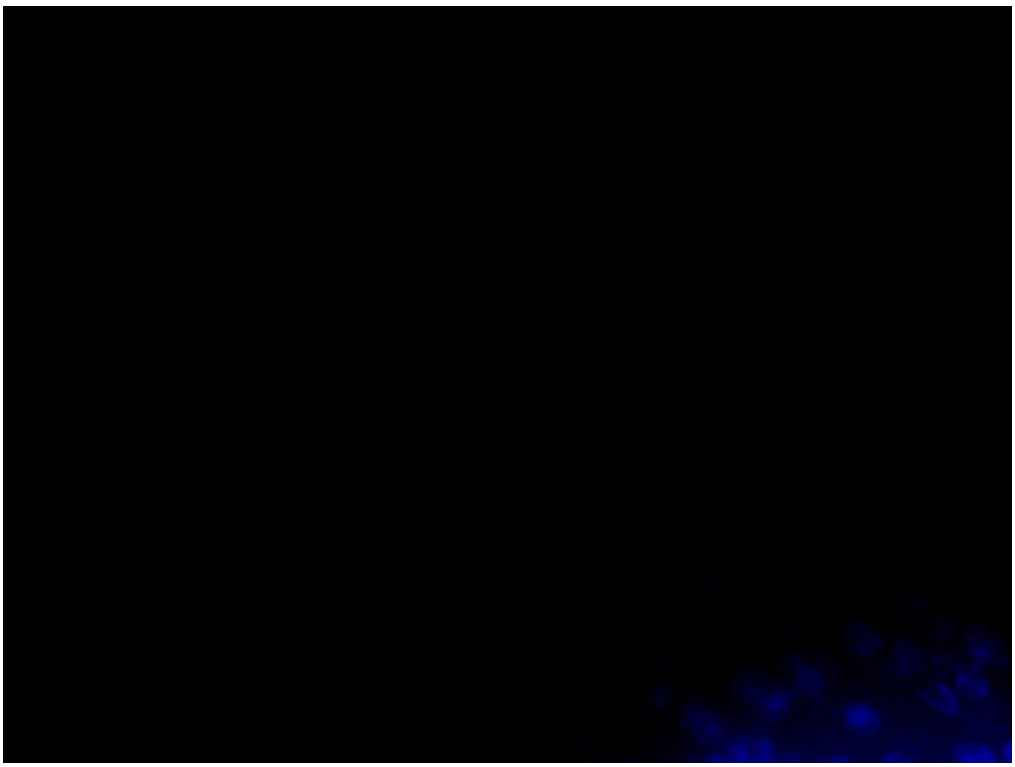


Figure 12.151.: U251 cells treated with 6.25 µM α-solanine and incubated for 24-hours and stained with monodansylcadaverine. Replicate: 3; magnification: x100.



Figure 12.152.: T98G cells treated with 6.25 µM α-solanine and incubated for 24-hours and stained with monodansylcadaverine. Replicate: 1; magnification: x100.



Figure 12.153.: T98G cells treated with 6.25 µM α-solanine and incubated for 24-hours and stained with monodansylcadaverine. Replicate: 2; magnification: x100.



Figure 12.154.: T98G cells treated with 6.25 µM α-solanine and incubated for 24-hours and stained with monodansylcadaverine. Replicate: 3; magnification: x100.



Figure 12.155.: U87MG cells treated with 1200.00 µM temozolomide and incubated for 24-hours and stained with monodansylcadaverine. Replicate: 1; magnification: x100.



Figure 12.156.: U87MG cells treated with 1200.00 µM temozolomide and incubated for 24-hours and stained with monodanyslcadaverine. Replicate: 2; magnification: x100.



Figure 12.157.: U87MG cells treated with 1200.00 µM temozolomide and incubated for 24-hours and stained with monodansylcadaverine. Replicate: 3; magnification: x100.



Figure 12.158.: U251 cells treated with 1200.00 µM temozolomide and incubated for 24-hours and stained with monodansylcadaverine. Replicate: 1; magnification: x100.

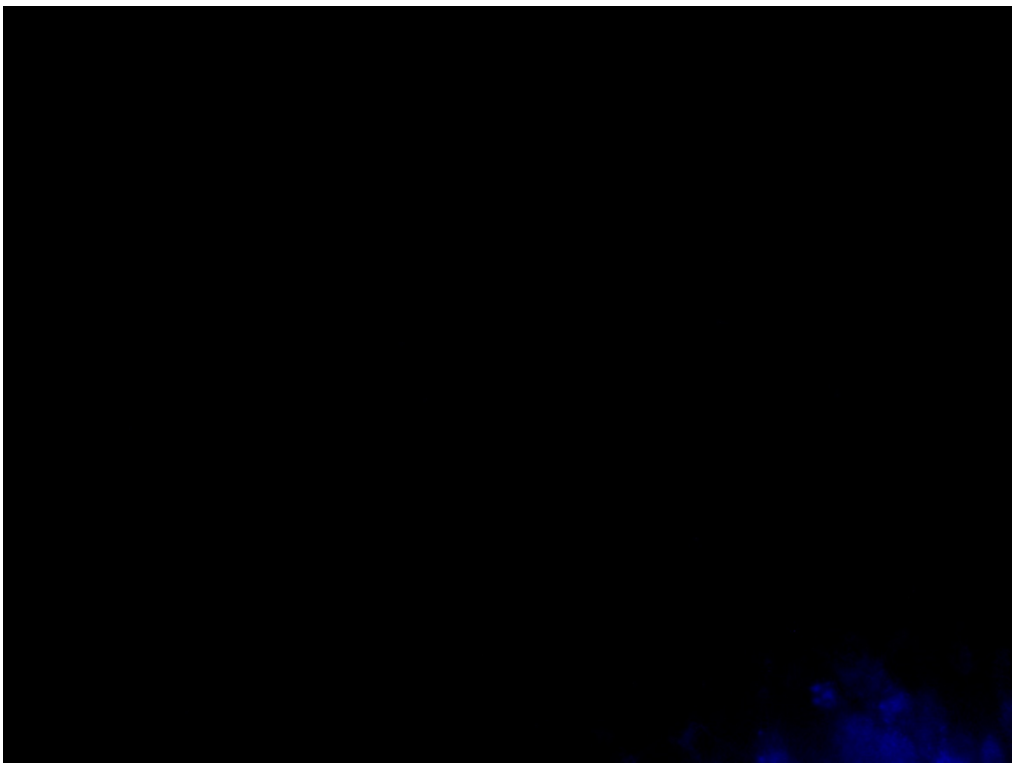


Figure 12.159.: U251 cells treated with 1200.00 µM temozolomide and incubated for 24-hours and stained with monodansylcadaverine. Replicate: 2; magnification: x100.



Figure 12.160.: U251 cells treated with 1200.00 µM temozolomide and incubated for 24-hours and stained with monodansylcadaverine. Replicate: 3; magnification: x100.

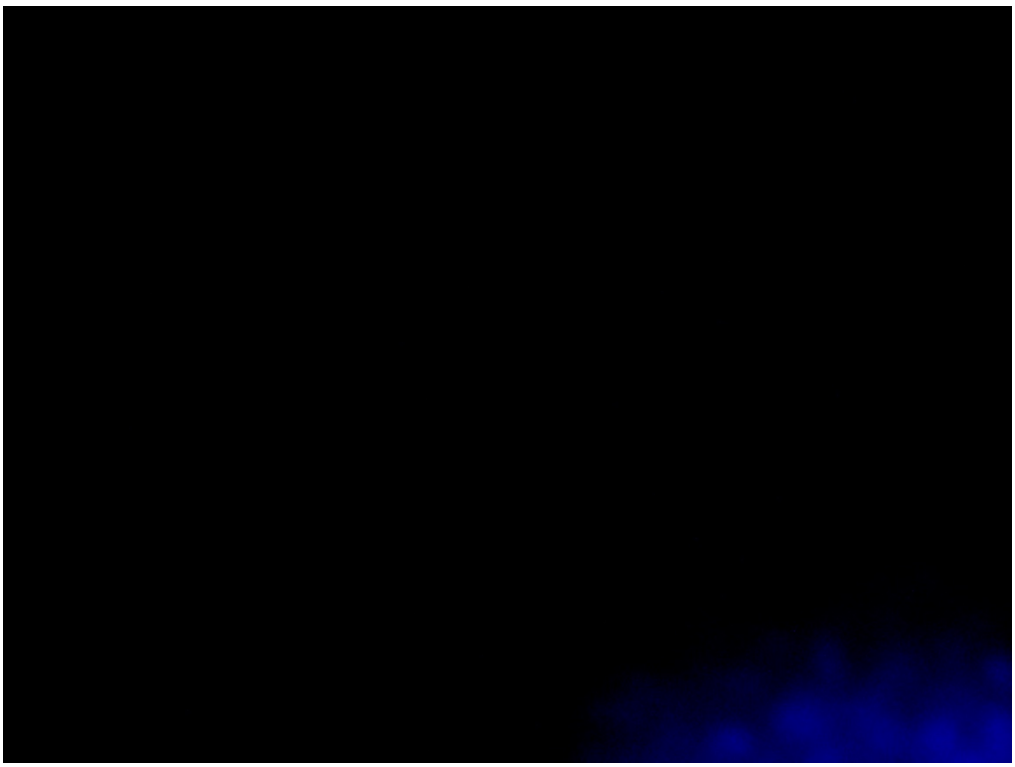


Figure 12.161.: T98G cells treated with 1200.00 µM temozolomide and incubated for 24-hours and stained with monodansylcadaverine. Replicate: 1; magnification: x100.



Figure 12.162.: T98G cells treated with 1200.00 µM temozolomide and incubated for 24-hours and stained with monodansylcadaverine. Replicate: 2; magnification: x100.



Figure 12.163.: T98G cells treated with 1200.00 µM temozolomide and incubated for 24-hours and stained with monodansylcadaverine. Replicate: 3; magnification: x100.

12.6.2. Corrected total cell fluorescence data

Table 12.14.: U87MG fluorescent intensity data

Cell line	Treatment condition	Stain	Replicate	Average corrected total cell fluorescence
U87MG	Negative control	Propidium Iodide	R1	0.00
			R2	0.00
			R3	0.00
		Annexin V-Fluorescein isothiocyanate	R1	132724.87
			R2	39102.32
			R3	82673.87
	∝-solanine	Propidium Iodide	R1	0.00
			R2	0.00
			R3	0.00
		Annexin V-Fluorescein isothiocyanate	R1	1758601.62
			R2	6480932.95
			R3	2828288.36
	Temozolomide	Propidium Iodide	R1	0.00
			R2	0.00
			R3	0.00
		Annexin V-Fluorescein isothiocyanate	R1	145430.64
			R2	142071.50
			R3	131658.92
	Negative control	Monodansylcadaverine	R1	1063158.98
			R2	1079787.23
			R3	2669353.25
	∝-solanine		R1	4668933.72
			R2	3134101.67
			R3	3386091.36
	Temozolomide		R1	952995.59
			R2	2185749.28
			R3	652867.14

Table 12.15.: U251 fluorescent intensity data

Cell line	Treatment condition	Stain	Replicate	Average corrected total cell fluorescence
U251	Negative control	Propidium Iodinde	R1	0.00
			R2	0.00
			R3	0.00
		Annexin V-Fluorescein isothiocyanate	R1	0.00
			R2	0.00
			R3	0.00
	∝-solanine	Propidium Iodinde	R1	180594.47
			R2	148648.58
			R3	408756.65
		Annexin V-Fluorescein isothiocyanate	R1	108002.29
			R2	516535.67
			R3	277904.10
	Temozolomide	Propidium Iodinde	R1	0.00
			R2	0.00
			R3	0.00
		Annexin V-Fluorescein isothiocyanate	R1	0.00
			R2	0.00
			R3	37079.27
	Negative control	Monodansylcadaverine	R1	3787424.27
			R2	9636098.78
			R3	9969896.57
	∝-solanine		R1	8906421.81
			R2	36527740.96
			R3	9958758.70
	Temozolomide		R1	907693.89
			R2	1931539.97
			R3	674119.94

Table 12.16.: T98G fluorescent intensity data

Cell line	Treatment condition	Stain	Replicate	Average corrected total cell fluorescence
T98G	Negative control	Propidium Iodide	R1	38983.05
			R2	53563.79
			R3	69073.50
		Annexin V-Fluorescein isothiocyanate	R1	32475.84
			R2	37705.33
			R3	80133.10
	∝-solanine	Propidium Iodide	R1	21796.49
			R2	48523.06
			R3	6417.44
		Annexin V-Fluorescein isothiocyanate	R1	8451.90
			R2	50023.94
			R3	0.00
	Temozolomide	Propidium Iodide	R1	45217.10
			R2	23080.28
			R3	47017.64
		Annexin V-Fluorescein isothiocyanate	R1	40012.25
			R2	33442.16
			R3	20098.06
	Negative control	Monodansylcadaverine	R1	21436114.63
			R2	13116755.64
			R3	1371652.47
	∝-solanine		R1	8906421.81
			R2	36527740.96
			R3	9958758.70
	Temozolomide		R1	6263867.20
			R2	3387561.30
			R3	4667144.11

12.7. Flow cytometry final analysis data

12.7.1. U87MG cell flow cytometric analysis pseudo-colour plots

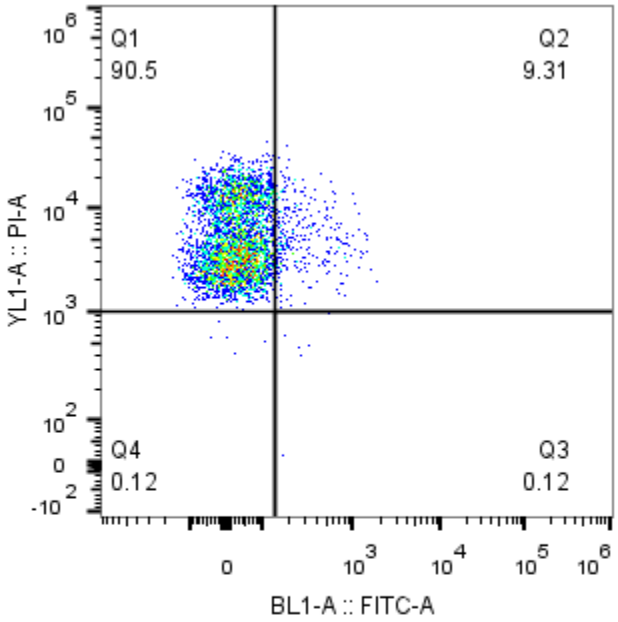


Figure 12.164.: Flow cytometry final analysis for U87MG cells treated with culture (negative control) conditions for 24-hours and dual stained with Annexin-V-fluorescein isothiocyanate and propidium iodide, replicate 1.

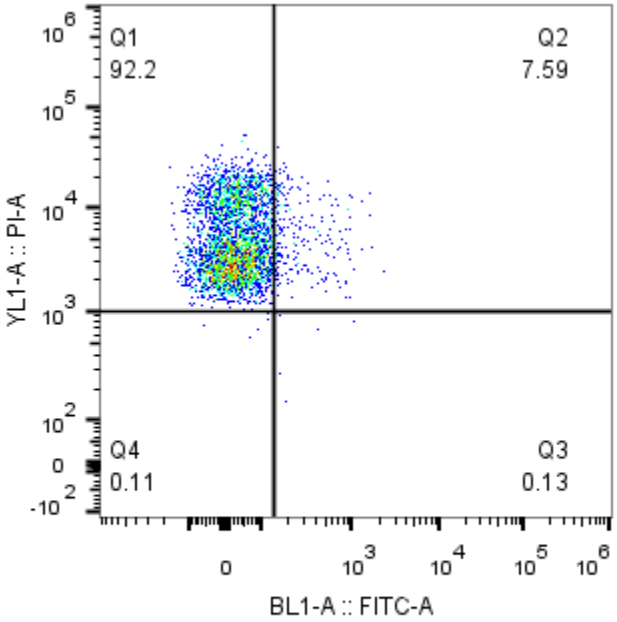


Figure 12.165.: Flow cytometry final analysis for U87MG cells treated with culture (negative control) conditions for 24-hours and dual stained with Annexin-V-fluorescein isothiocyanate and propidium iodide, replicate 2.

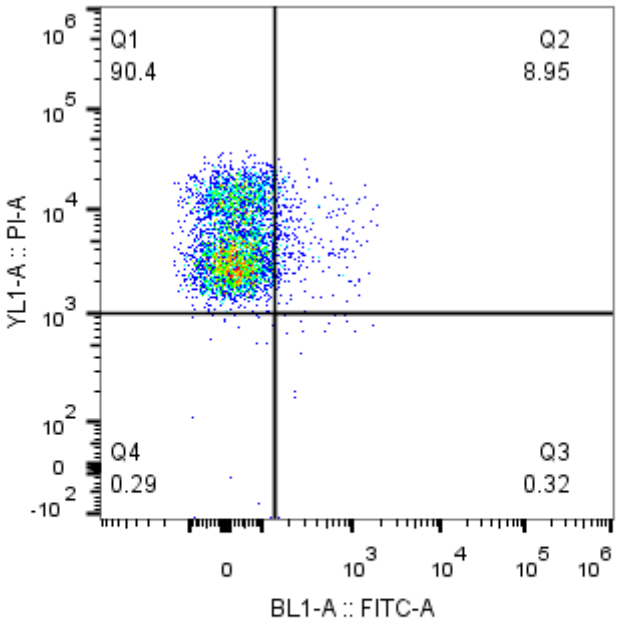


Figure 12.166.: Flow cytometry final analysis for U87MG cells treated with culture (negative control) conditions for 24-hours and dual stained with Annexin-V-fluorescein isothiocyanate and propidium iodide, replicate 3.

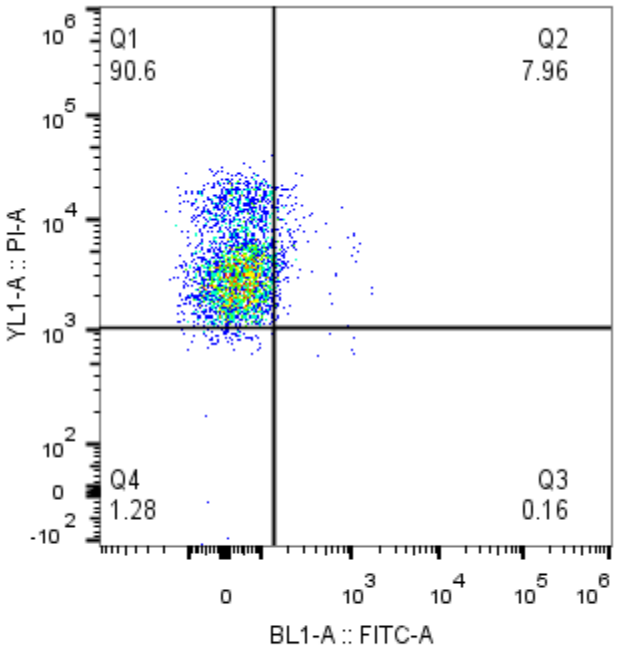


Figure 12.167.: Flow cytometry final analysis for U87MG cells treated with 5.00 mM H_20_2 (positive control) conditions for 24-hours and dual stained with Annexin-V-fluorescein isothiocyanate and propidium iodide, replicate 1.

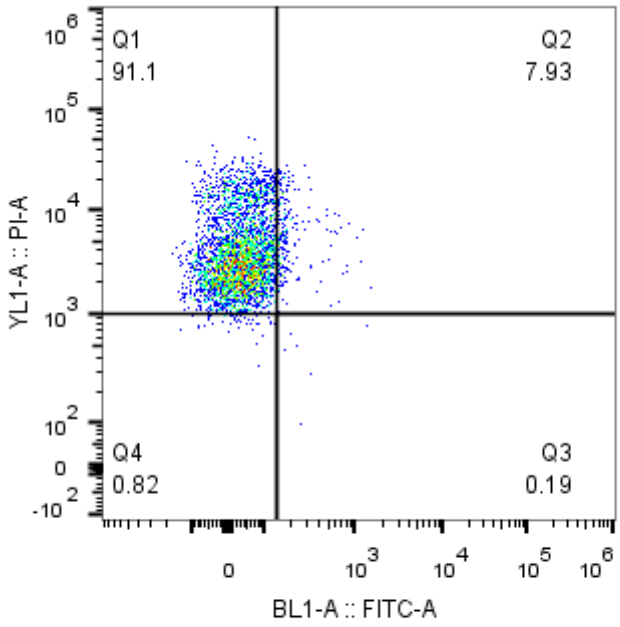


Figure 12.168.: Flow cytometry final analysis for U87MG cells treated with 5.00 mM H_20_2 (positive control) conditions for 24-hours and dual stained with Annexin-V-fluorescein isothiocyanate and propidium iodide, replicate 2.

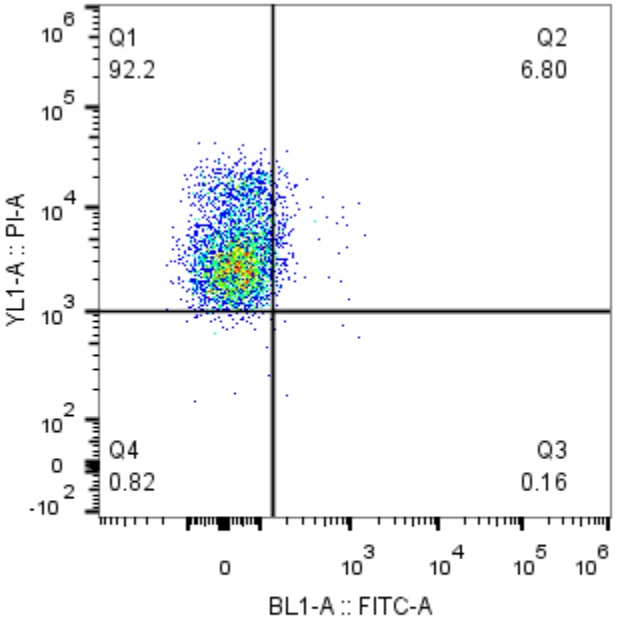


Figure 12.169.: Flow cytometry final analysis for U87MG cells treated with 5.00 mM H_20_2 (positive control) conditions for 24-hours and dual stained with Annexin-V-fluorescein isothiocyanate and propidium iodide, replicate 3.

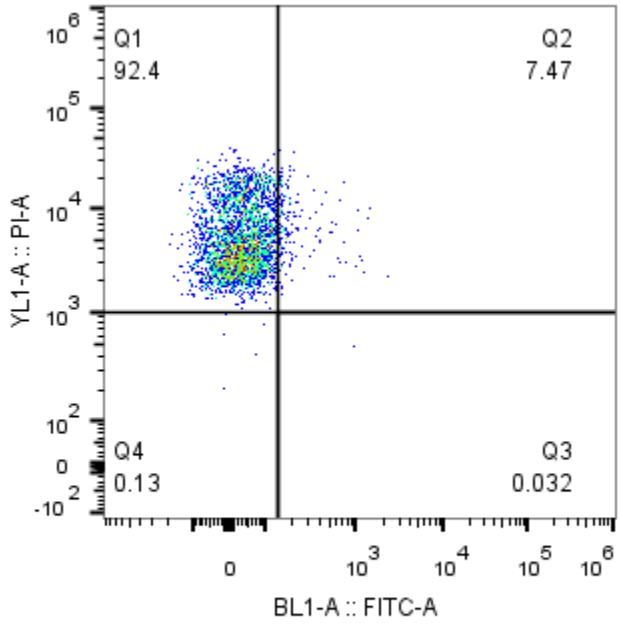


Figure 12.170.: Flow cytometry final analysis for U87MG cells treated with 6.25 µM α-solanine for 24-hours and dual stained with Annexin-V-fluorescein isothiocyanate and propidium iodide, replicate 1.

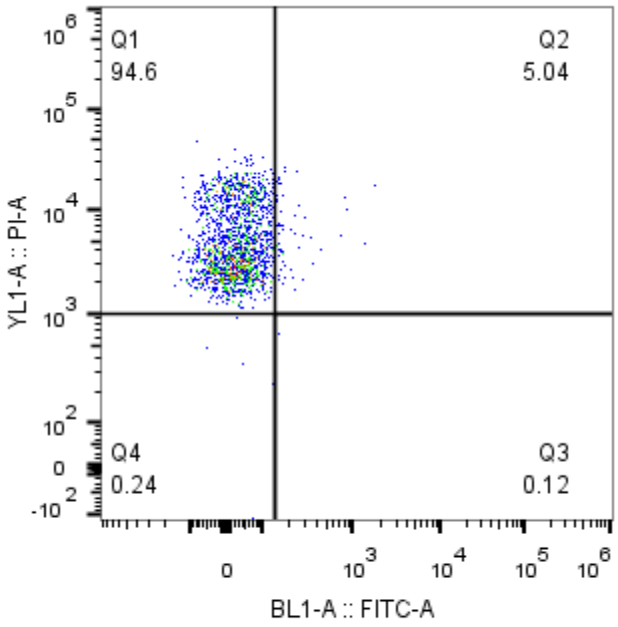


Figure 12.171.: Flow cytometry final analysis for U87MG cells treated with 6.25 µM α-solanine for 24-hours and dual stained with Annexin-V-fluorescein isothiocyanate and propidium iodide, replicate 2.

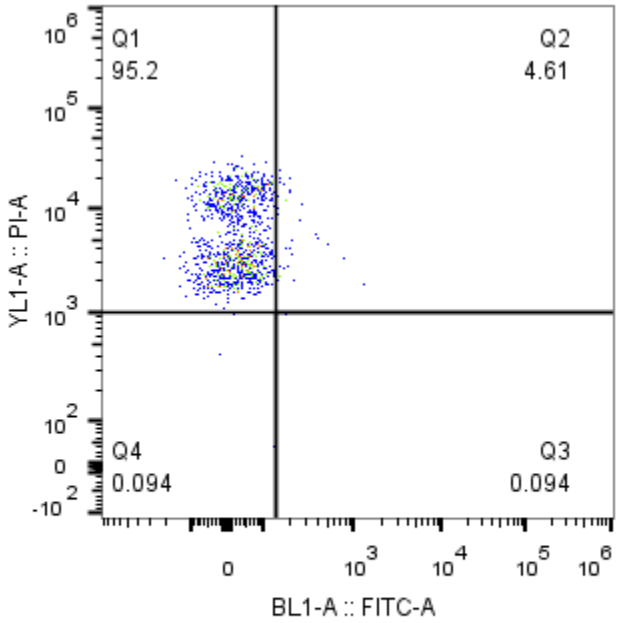


Figure 12.172.: Flow cytometry final analysis for U87MG cells treated with 6.25 µM α-solanine for 24-hours and dual stained with Annexin-V-fluorescein isothiocyanate and propidium iodide, replicate 3.

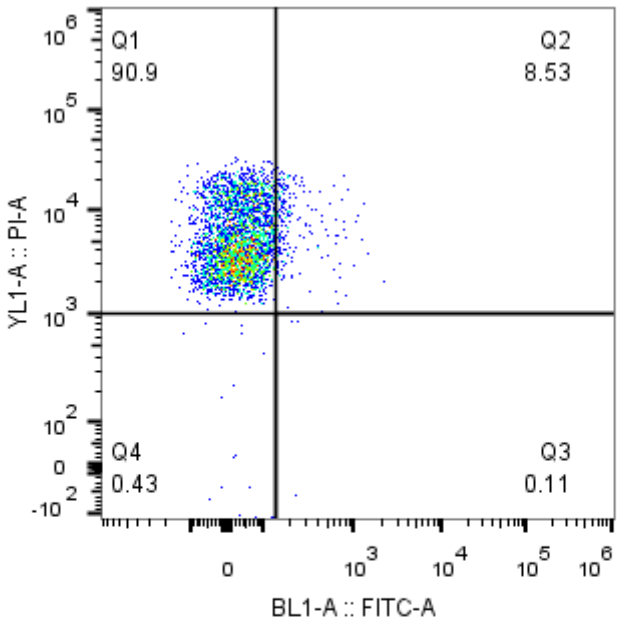


Figure 12.173.: Flow cytometry final analysis for U87MG cells treated with 1200.00 µM temozolomide for 24-hours and dual stained with Annexin-V-fluorescein isothiocyanate and propidium iodide, replicate 1.

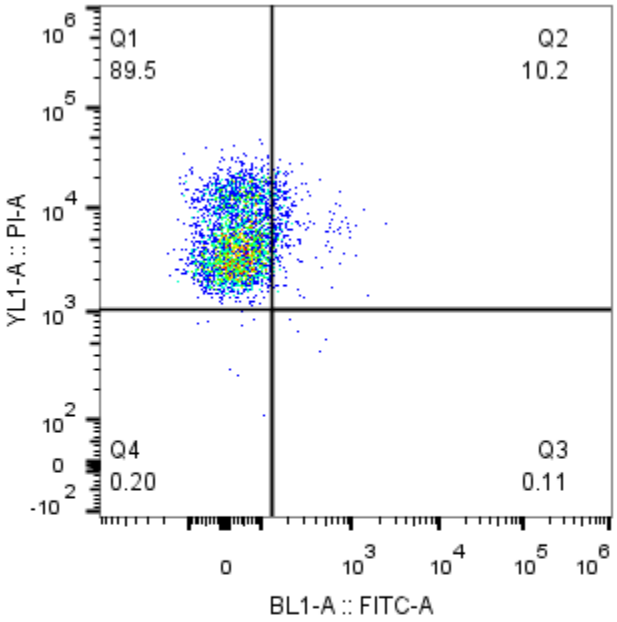


Figure 12.174.: Flow cytometry final analysis for U87MG cells treated with 1200.00 µM temozolomide for 24-hours and dual stained with Annexin-V-fluorescein isothiocyanate and propidium iodide, replicate 2.

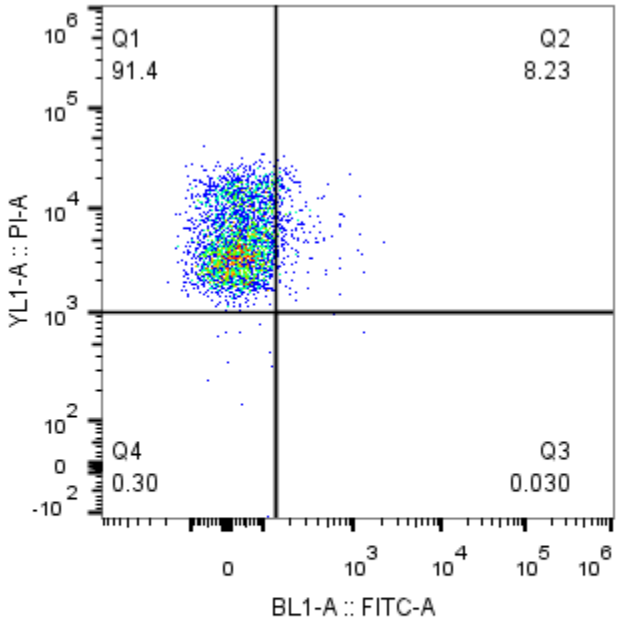


Figure 12.175.: Flow cytometry final analysis for U87MG cells treated with 1200.00 µM temozolomide for 24-hours and dual stained with Annexin-V-fluorescein isothiocyanate and propidium iodide, replicate 3.

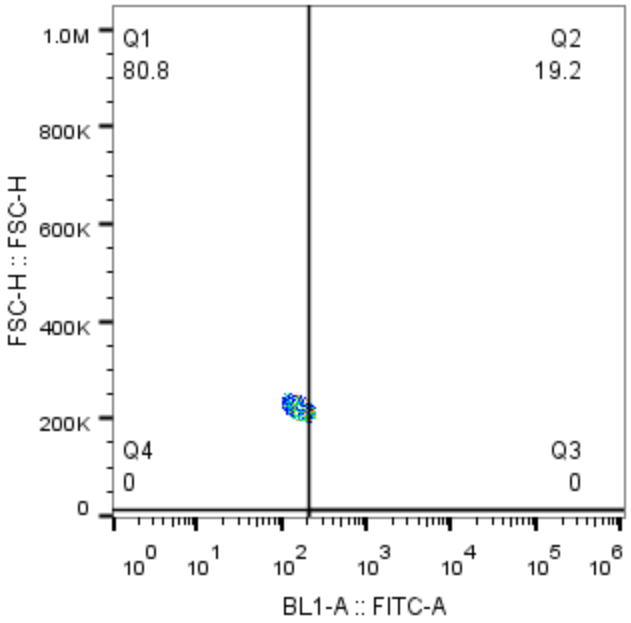


Figure 12.176.: Flow cytometry final analysis for U87MG cells treated with culture (negative control) conditions for 24-hours and dual stained with monodansylcadaverine, replicate 1.

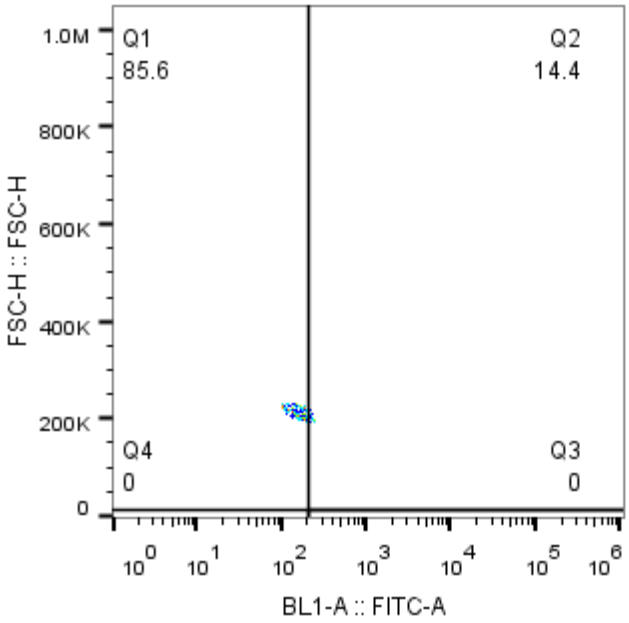


Figure 12.177.: Flow cytometry final analysis for U87MG cells treated with culture (negative control) conditions for 24-hours and dual stained with monodansylcadaverine, replicate 2.

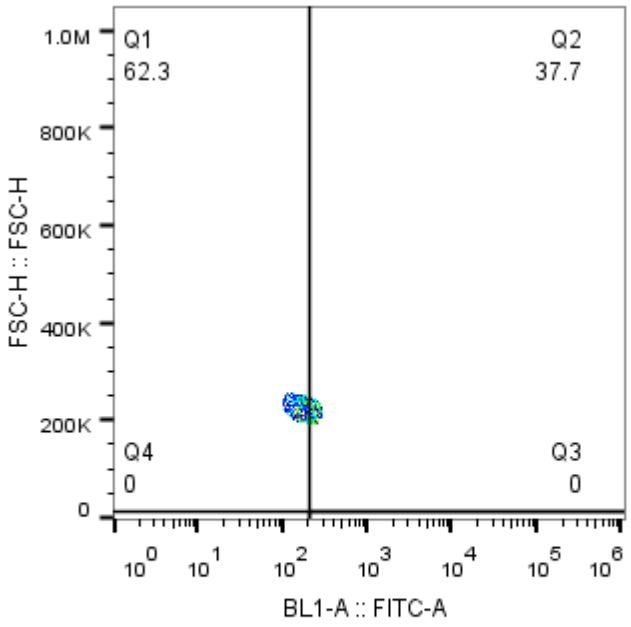


Figure 12.178.: Flow cytometry final analysis for U87MG cells treated with culture (negative control) conditions for 24-hours and dual stained with monodansylcadaverine, replicate 3.

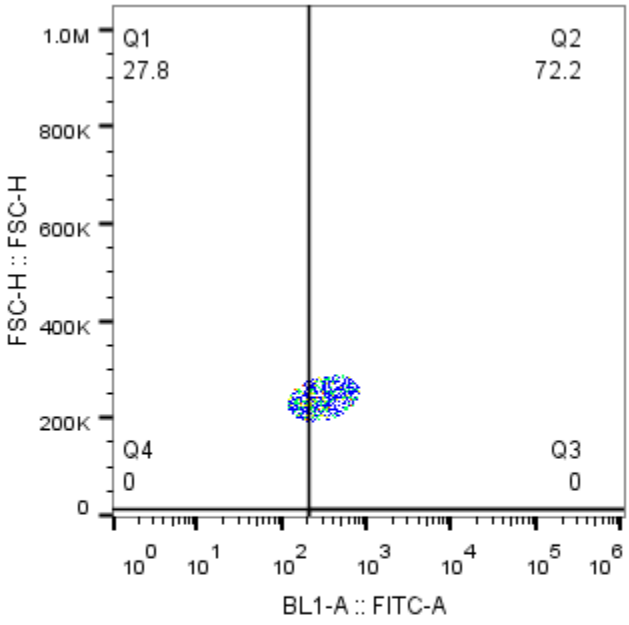


Figure 12.179.: Flow cytometry final analysis for U87MG cells treated with 5.00 mM H_20_2 (positive control) conditions for 24-hours and dual stained with monodansylcadaverine, replicate 1.

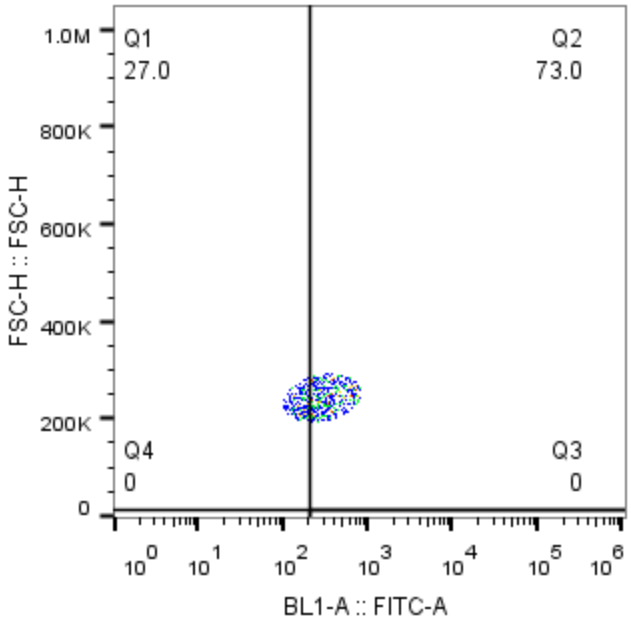


Figure 12.180.: Flow cytometry final analysis for U87MG cells treated with 5.00 mM H_20_2 (positive control) conditions for 24-hours and dual stained with monodansylcadaverine, replicate 2.

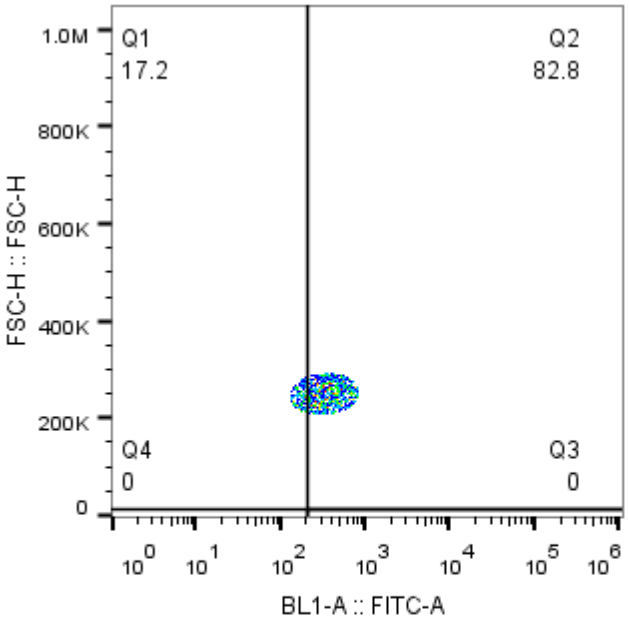


Figure 12.181.: Flow cytometry final analysis for U87MG cells treated with 5.00 mM H_20_2 (positive control) conditions for 24-hours and dual stained with monodansylcadaverine, replicate 3.

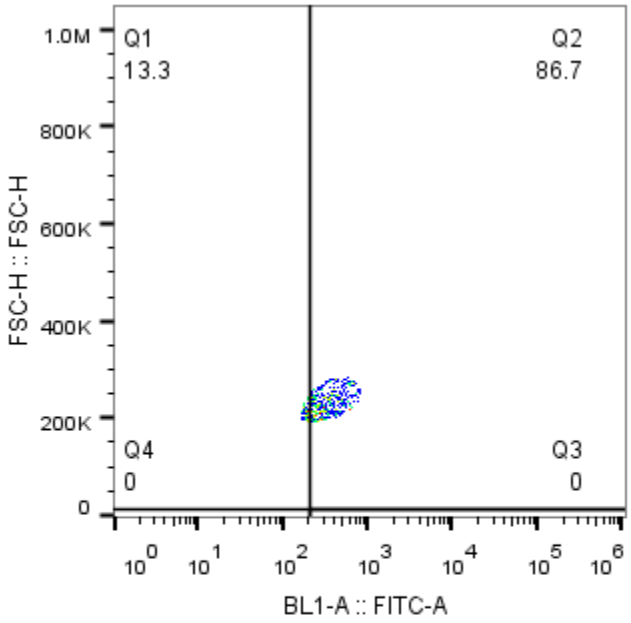


Figure 12.182.: Flow cytometry final analysis for U87MG cells treated with 6.25 µM α-solanine for 24-hours and dual stained with monodansylcadaverine, replicate 1.

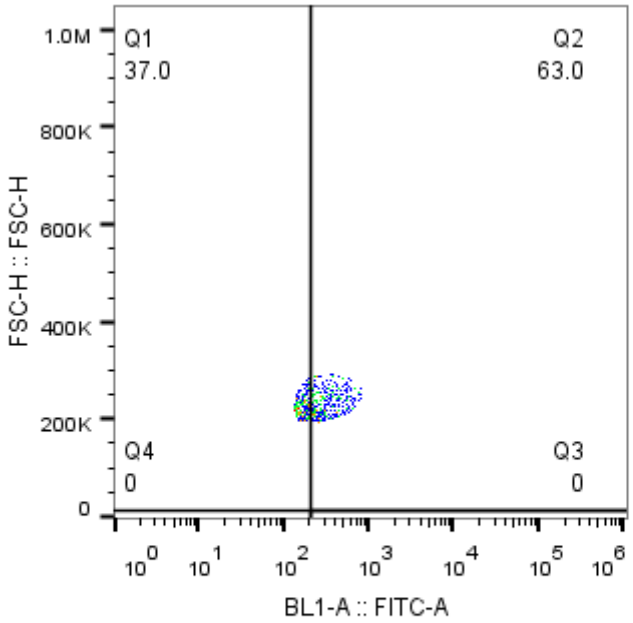


Figure 12.183.: Flow cytometry final analysis for U87MG cells treated with 6.25 µM α-solanine for 24-hours and dual stained with monodansylcadaverine, replicate 2.

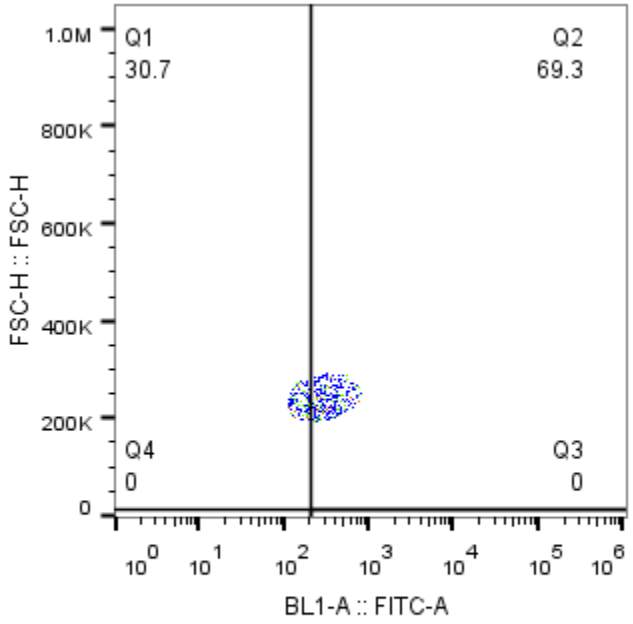


Figure 12.184.: Flow cytometry final analysis for U87MG cells treated with 6.25 µM α-solanine for 24-hours and dual stained with monodansylcadaverine, replicate 3.

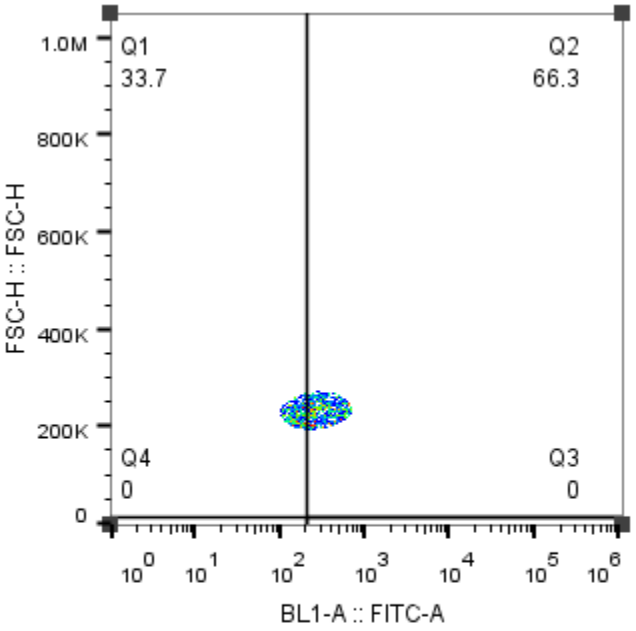


Figure 12.185.: Flow cytometry final analysis for U87MG cells treated with 1200.00 µM temozolomide for 24-hours and dual stained with monodansylcadaverine, replicate 1.

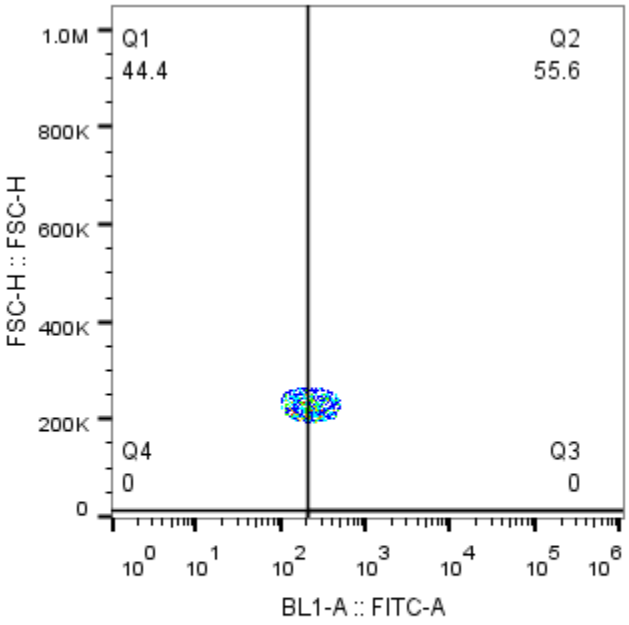


Figure 12.186.: Flow cytometry final analysis for U87MG cells treated with 1200.00 µM temozolomide for 24-hours and dual stained with monodansylcadaverine, replicate 2.

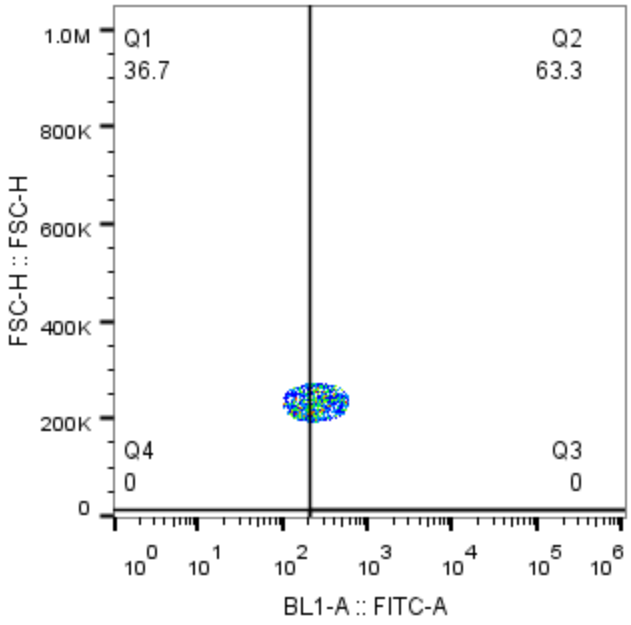


Figure 12.187.: Flow cytometry final analysis for U87MG cells treated with 1200.00 µM temozolomide for 24-hours and dual stained with monodansylcadaverine, replicate 3.

12.7.2. U251 cell flow cytometric analysis pseudo-colour plots

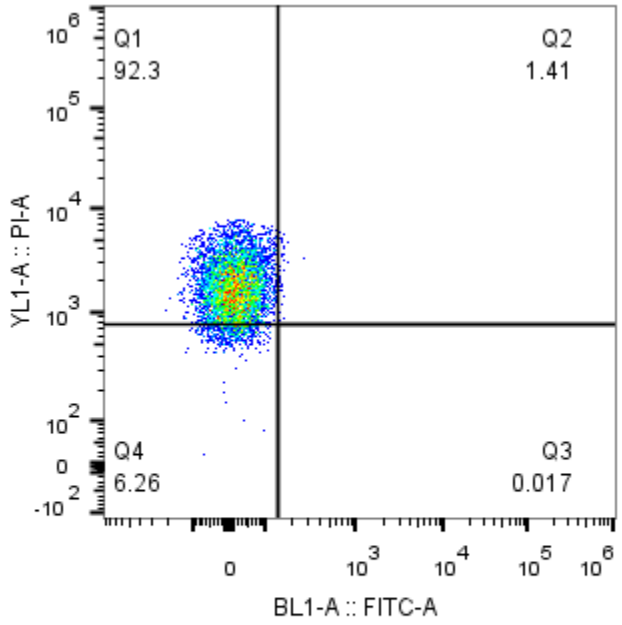


Figure 12.188.: Flow cytometry final analysis for U251 cells treated with culture (negative control) conditions for 24-hours and dual stained with Annexin-V-fluorescein isothiocyanate and propidium iodide, replicate 1.

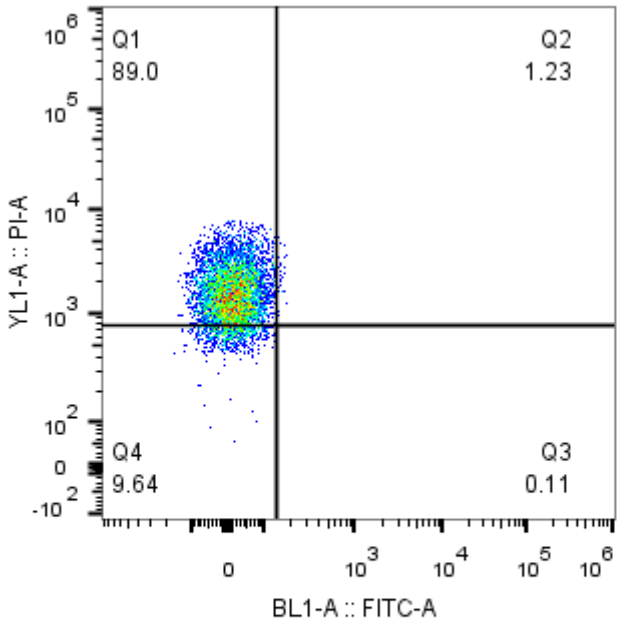


Figure 12.189.: Flow cytometry final analysis for U251 cells treated with culture (negative control) conditions for 24-hours and dual stained with Annexin-V-fluorescein isothiocyanate and propidium iodide, replicate 2.

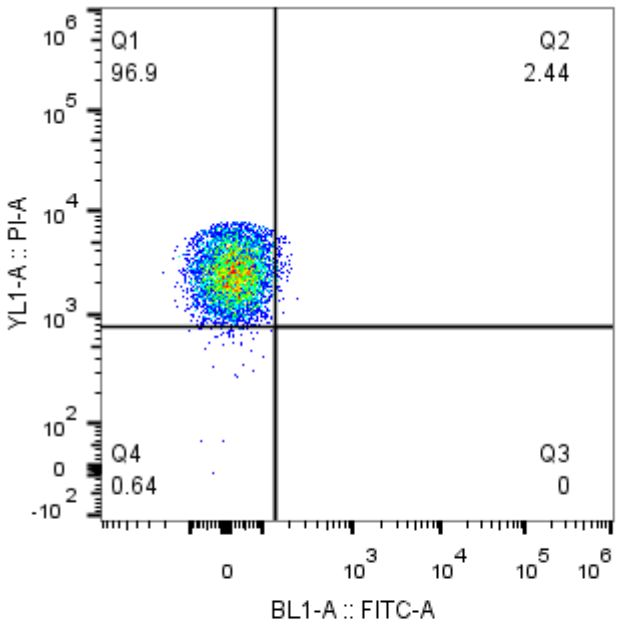


Figure 12.190.: Flow cytometry final analysis for U251 cells treated with culture (negative control) conditions for 24-hours and dual stained with Annexin-V-fluorescein isothiocyanate and propidium iodide, replicate 3.

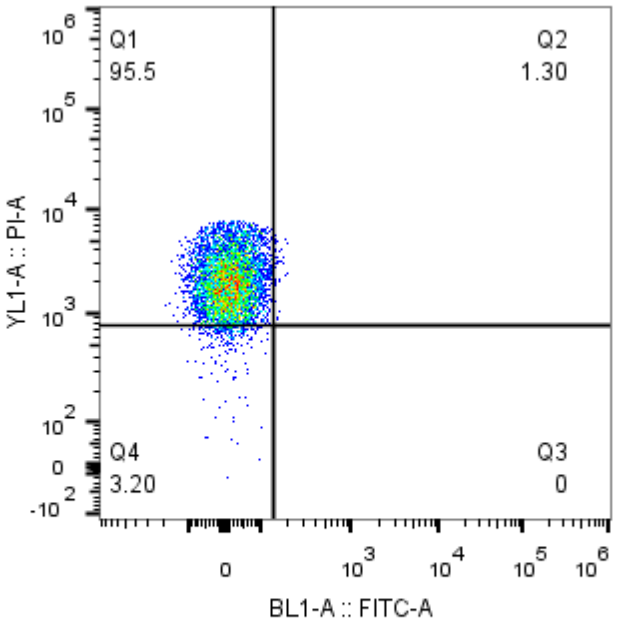


Figure 12.191.: Flow cytometry final analysis for U251 cells treated with 5.00 mM H_2O_2 (positive control) conditions for 24-hours and dual stained with Annexin-V-fluorescein isothiocyanate and propidium iodide, replicate 1.

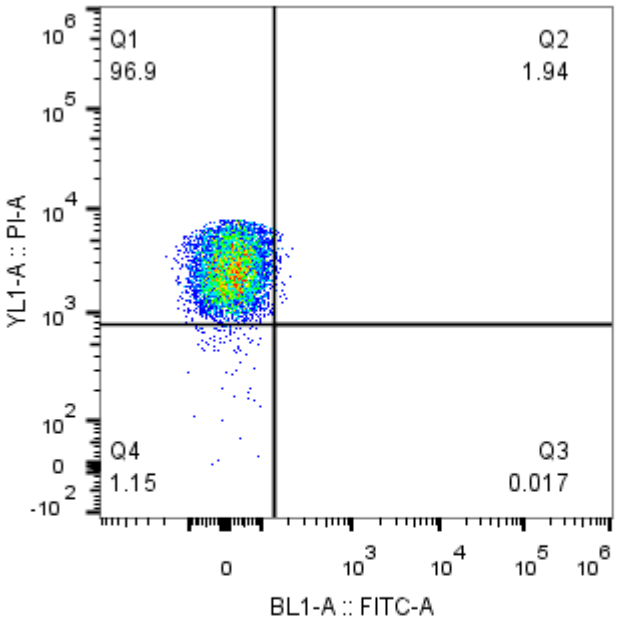


Figure 12.192.: Flow cytometry final analysis for U251 cells treated with 5.00 mM H_20_2 (positive control) conditions for 24-hours and dual stained with Annexin-V-fluorescein isothiocyanate and propidium iodide, replicate 2.

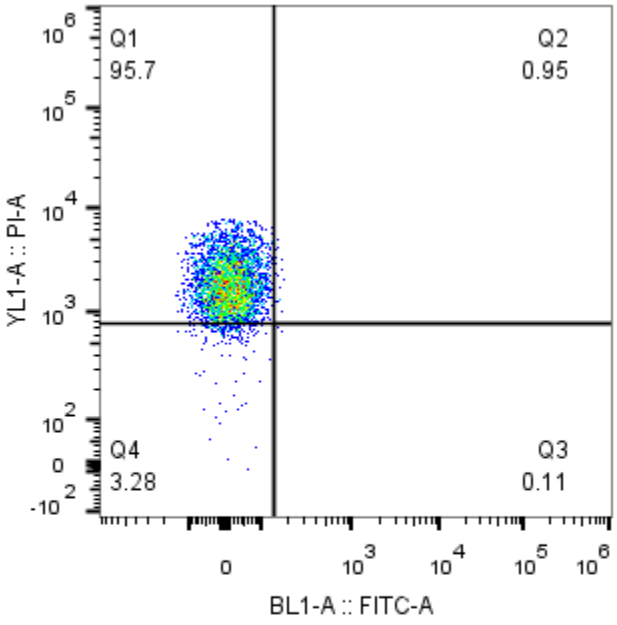


Figure 12.193.: Flow cytometry final analysis for U251 cells treated with 5.00 mM H_20_2 (positive control) conditions for 24-hours and dual stained with Annexin-V-fluorescein isothiocyanate and propidium iodide, replicate 3.

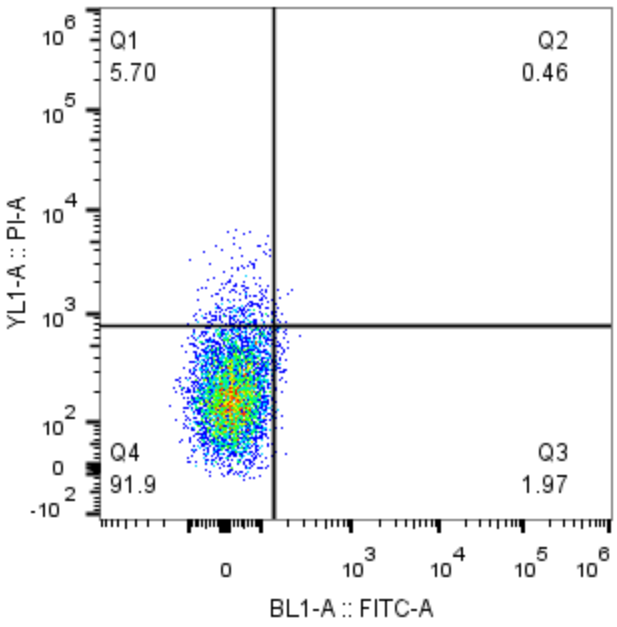


Figure 12.194.: Flow cytometry final analysis for U251 cells treated with 6.25 µM α-solanine for 24-hours and dual stained with Annexin-V-fluorescein isothiocyanate and propidium iodide, replicate 1.

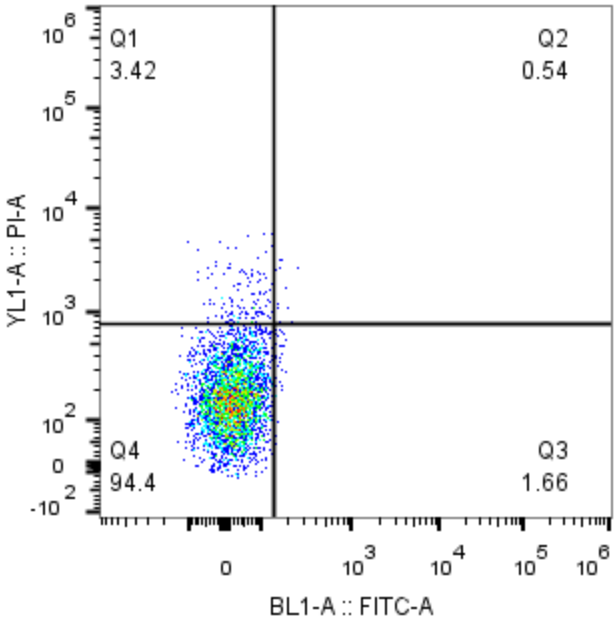


Figure 12.195.: Flow cytometry final analysis for U251 cells treated with 6.25 µM α-solanine for 24-hours and dual stained with Annexin-V-fluorescein isothiocyanate and propidium iodide, replicate 2.

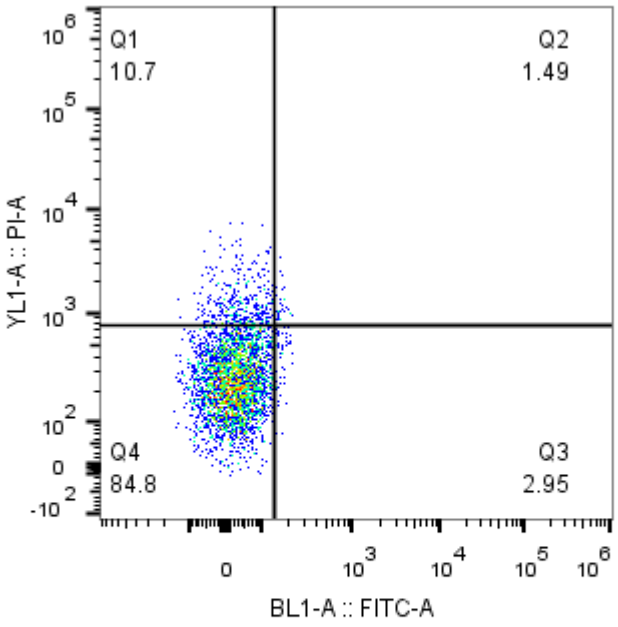


Figure 12.196.: Flow cytometry final analysis for U251 cells treated with 6.25 µM α-solanine for 24-hours and dual stained with Annexin-V-fluorescein isothiocyanate and propidium iodide, replicate 3.

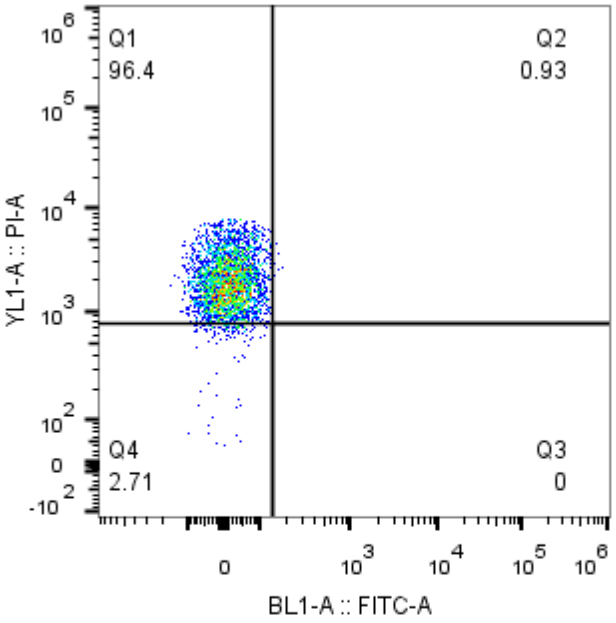


Figure 12.197.: Flow cytometry final analysis for U251 cells treated with 1200.00 µM temozolomide for 24-hours and dual stained with Annexin-V-fluorescein isothiocyanate and propidium iodide, replicate 1.

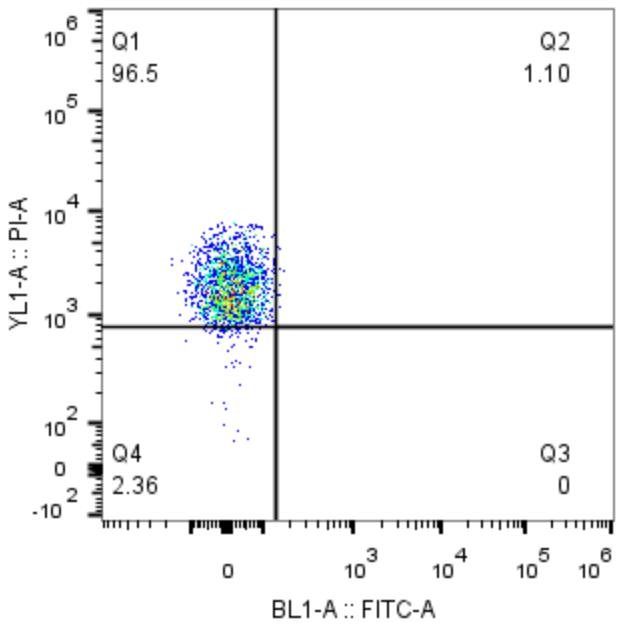


Figure 12.198.: Flow cytometry final analysis for U251 cells treated with 1200.00 µM temozolomide for 24-hours and dual stained with Annexin-V-fluorescein isothiocyanate and propidium iodide, replicate 2.

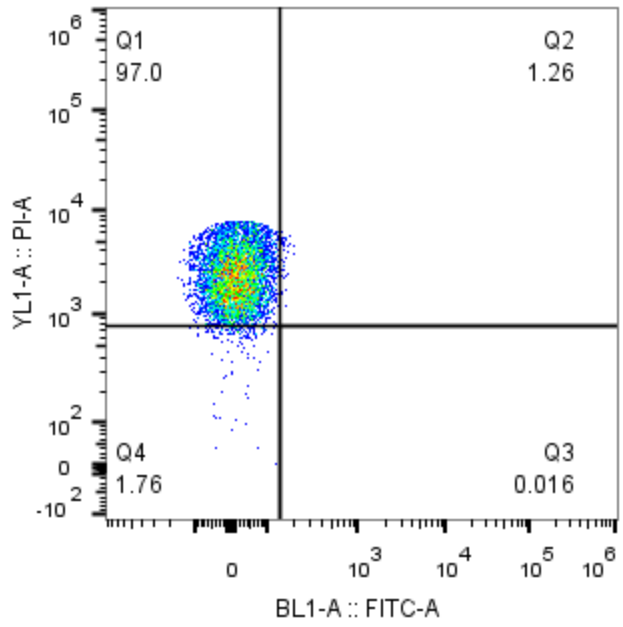


Figure 12.199.: Flow cytometry final analysis for U251 cells treated with 1200.00 µM temozolomide for 24-hours and dual stained with Annexin-V-fluorescein isothiocyanate and propidium iodide, replicate 3.

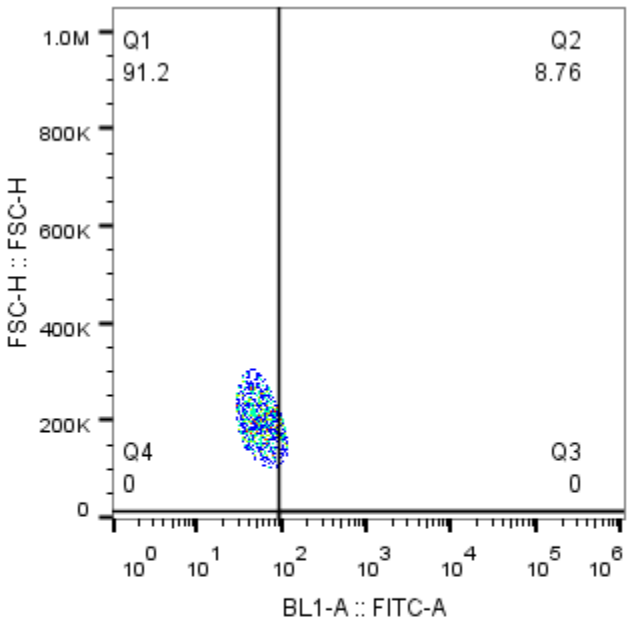


Figure 12.200.: Flow cytometry final analysis for U251 cells treated with culture (negative control) conditions for 24-hours and dual stained with monodansylcadaverine, replicate 1.

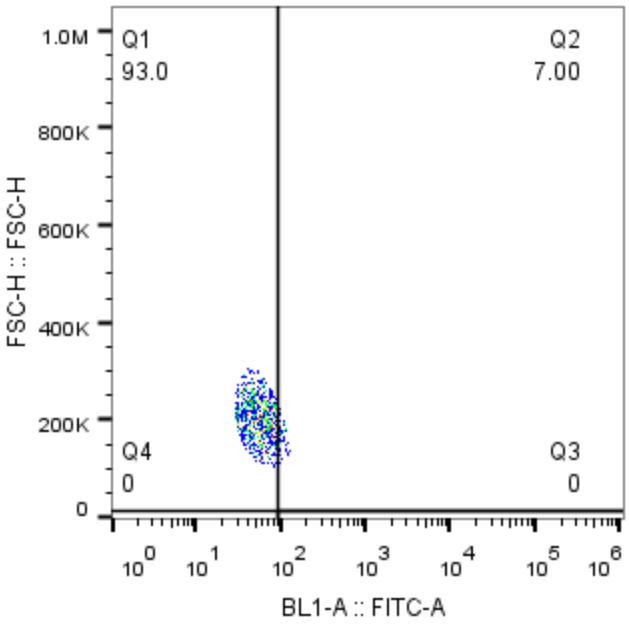


Figure 12.201.: Flow cytometry final analysis for U251 cells treated with culture (negative control) conditions for 24-hours and dual stained with monodansylcadaverine, replicate 2.

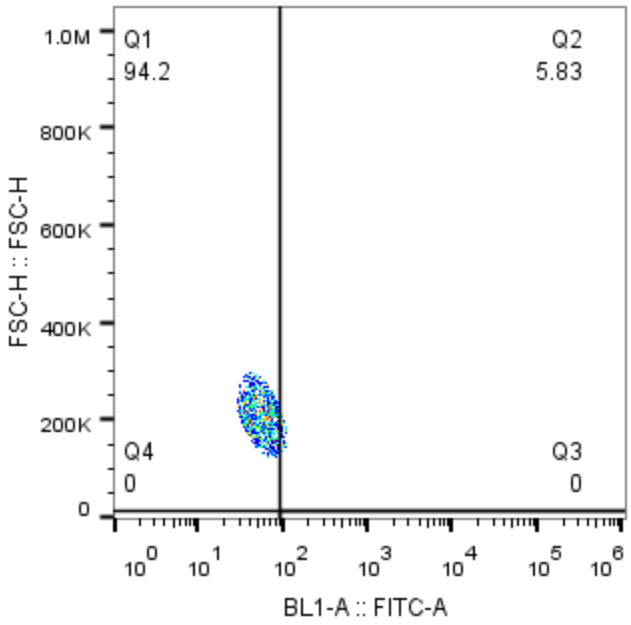


Figure 12.202.: Flow cytometry final analysis for U251 cells treated with culture (negative control) conditions for 24-hours and dual stained with monodansylcadaverine, replicate 3.

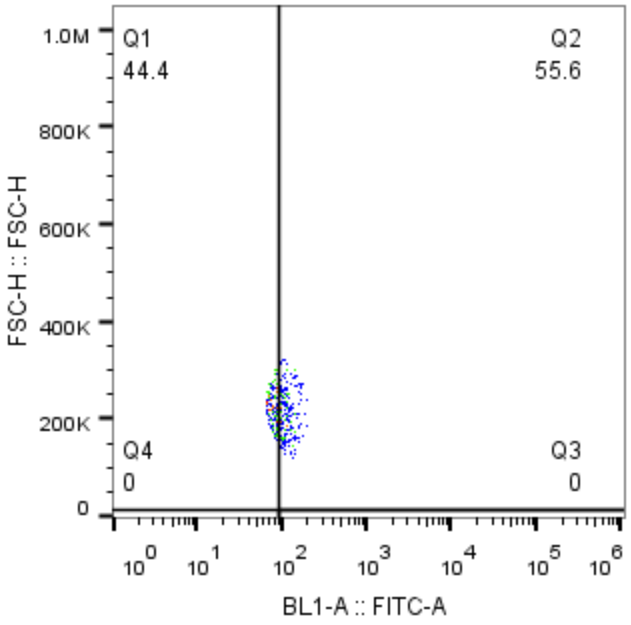


Figure 12.203.: Flow cytometry final analysis for U251 cells treated with 5.00 mM H_20_2 (positive control) conditions for 24-hours and dual stained with monodansylcadaverine, replicate 1.

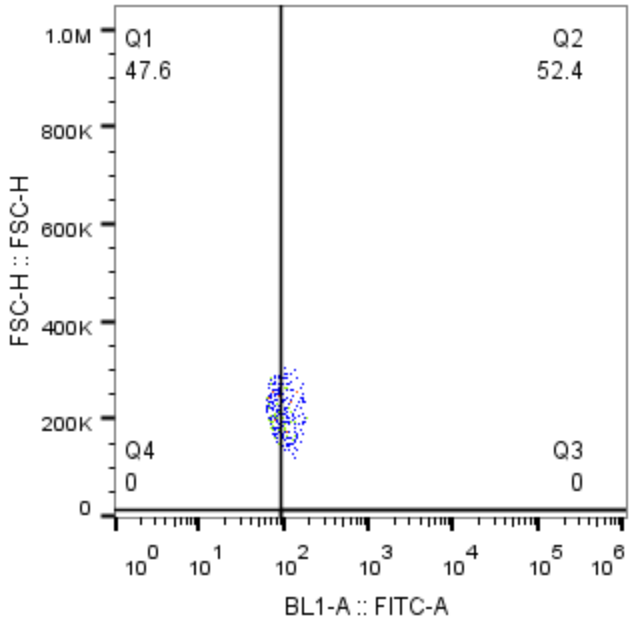


Figure 12.204.: Flow cytometry final analysis for U251 cells treated with 5.00 mM H_20_2 (positive control) conditions for 24-hours and dual stained with monodansylcadaverine, replicate 2.

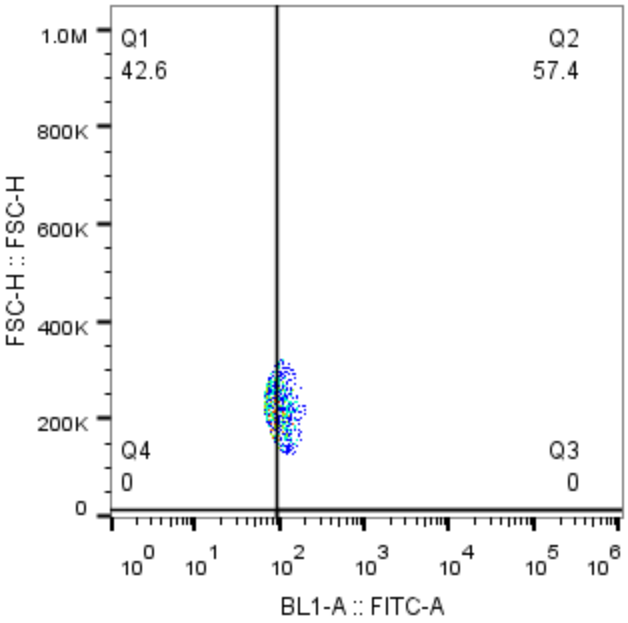


Figure 12.205.: Flow cytometry final analysis for U251 cells treated with 5.00 mM H_20_2 (positive control) conditions for 24-hours and dual stained with monodansylcadaverine, replicate 3.

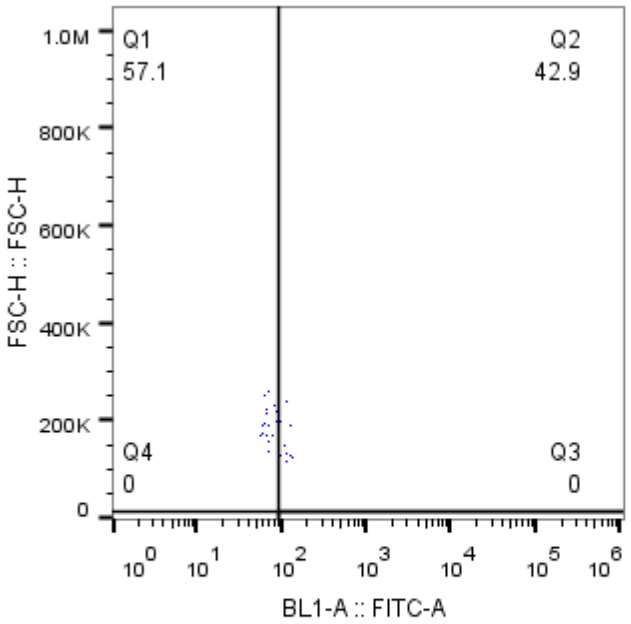


Figure 12.206.: Flow cytometry final analysis for U251 cells treated with 6.25 µM α-solanine for 24-hours and dual stained with monodansylcadaverine, replicate 1.

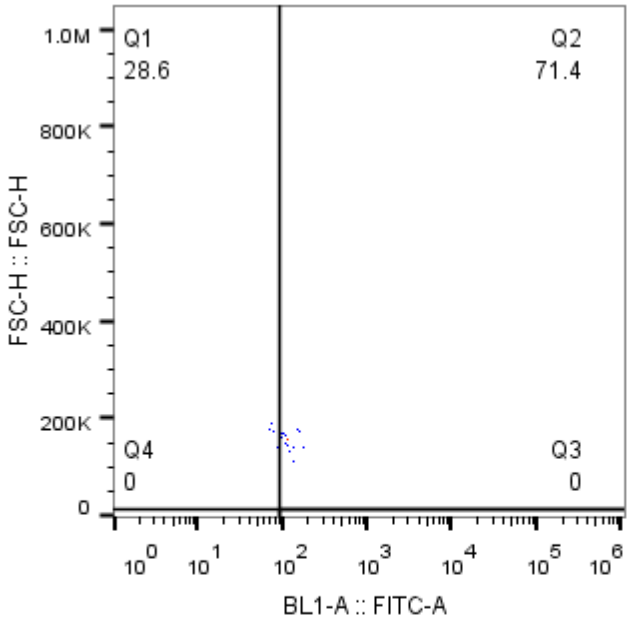


Figure 12.207.: Flow cytometry final analysis for U251 cells treated with 6.25 µM α-solanine for 24-hours and dual stained with monodansylcadaverine, replicate 2.

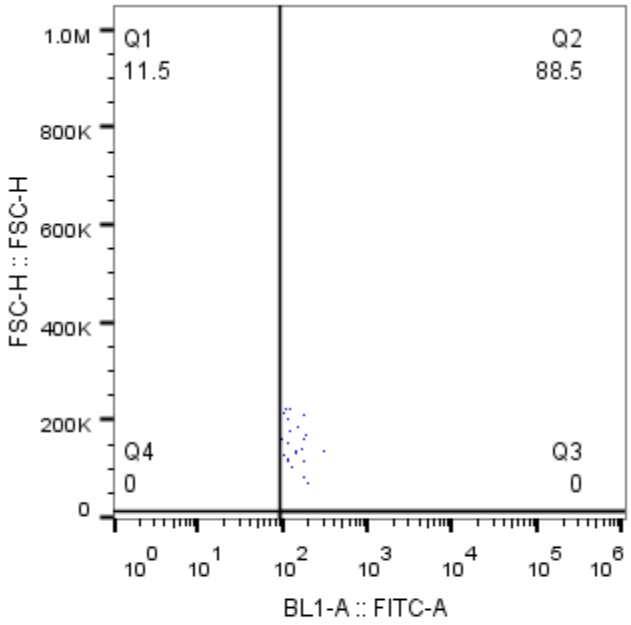


Figure 12.208.: Flow cytometry final analysis for U251 cells treated with 6.25 µM α-solanine for 24-hours and dual stained with monodansylcadaverine, replicate 3.

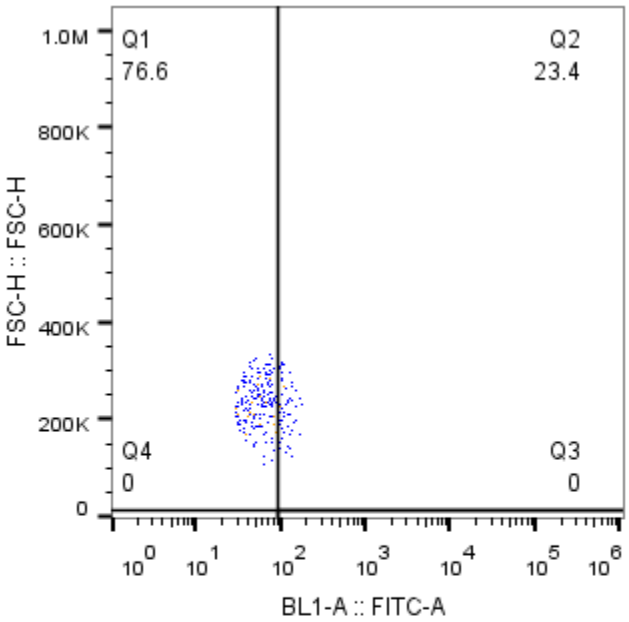


Figure 12.209.: Flow cytometry final analysis for U251 cells treated with 1200.00 µM temozolomide for 24-hours and dual stained with monodansylcadaverine, replicate 1.

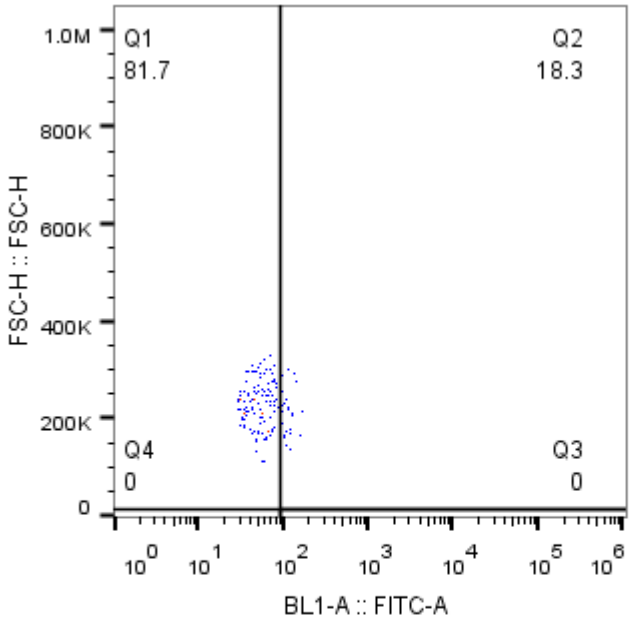


Figure 12.210.: Flow cytometry final analysis for U251 cells treated with 1200.00 µM temozolomide for 24-hours and dual stained with monodansylcadaverine, replicate 2.

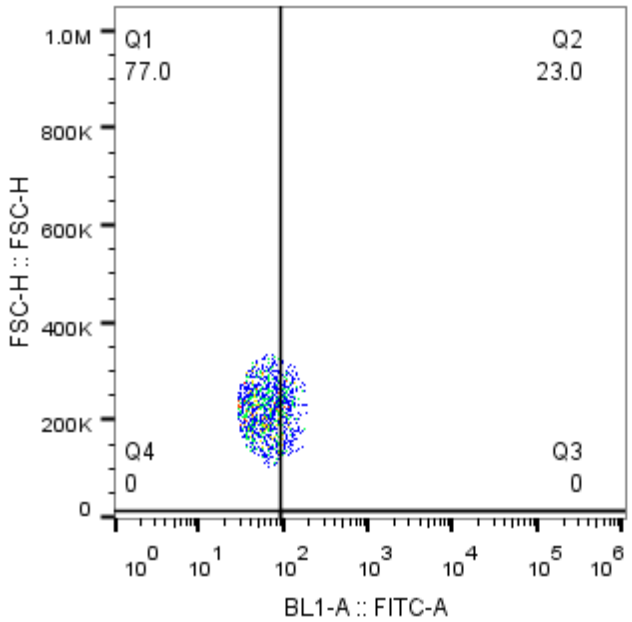


Figure 12.211.: Flow cytometry final analysis for U251 cells treated with 1200.00 µM temozolomide for 24-hours and dual stained with monodansylcadaverine, replicate 3.

12.7.3. T98G cell flow cytometric analysis pseudo-colour plots

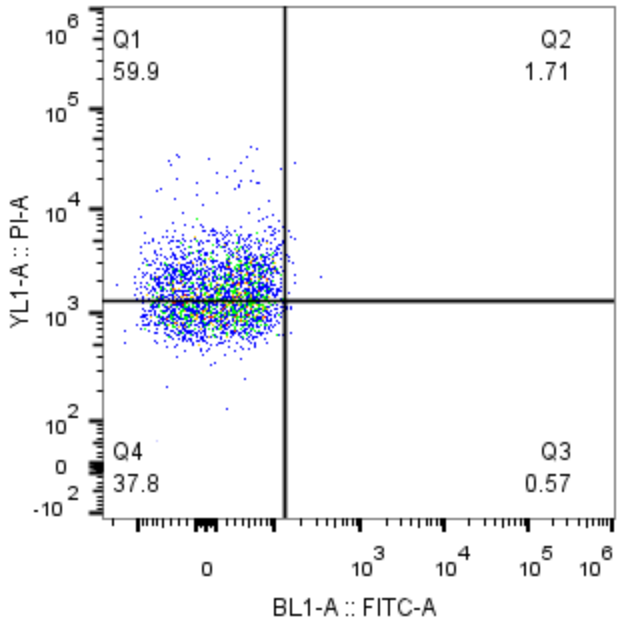


Figure 12.212.: Flow cytometry final analysis for T98G cells treated with culture (negative control) conditions for 24-hours and dual stained with Annexin-V-fluorescein isothiocyanate and propidium iodide, replicate 1.

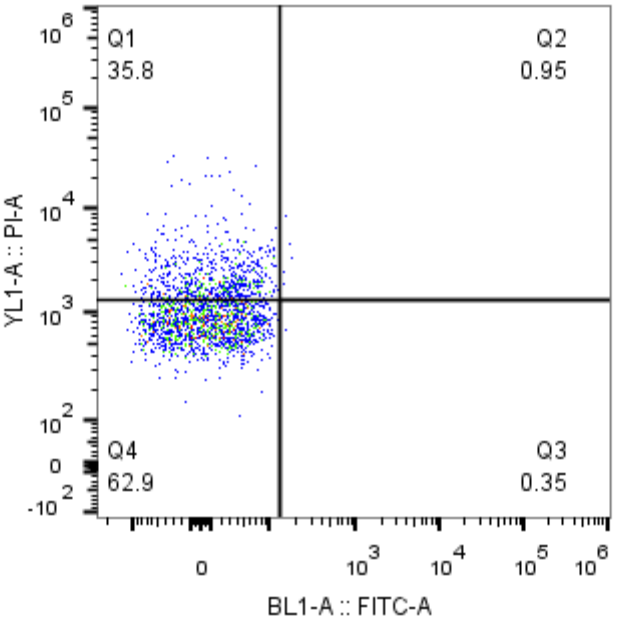


Figure 12.213.: Flow cytometry final analysis for T98G cells treated with culture (negative control) conditions for 24-hours and dual stained with Annexin-V-fluorescein isothiocyanate and propidium iodide, replicate 2.

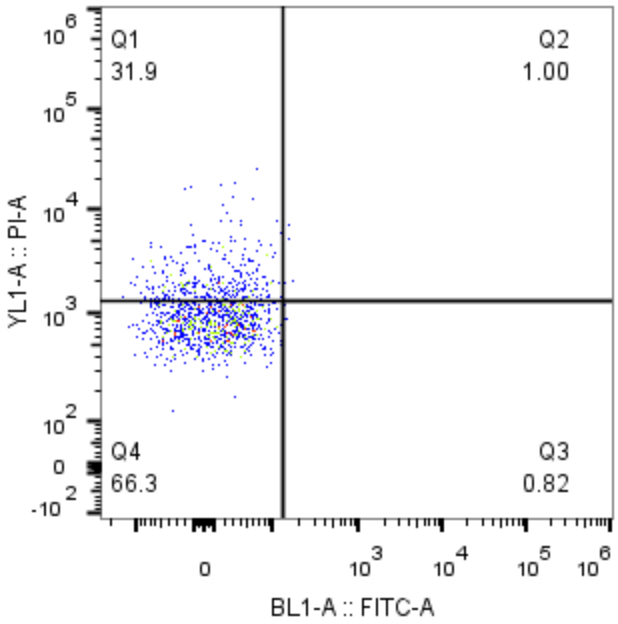


Figure 12.214.: Flow cytometry final analysis for T98G cells treated with culture (negative control) conditions for 24-hours and dual stained with Annexin-V-fluorescein isothiocyanate and propidium iodide, replicate 3.

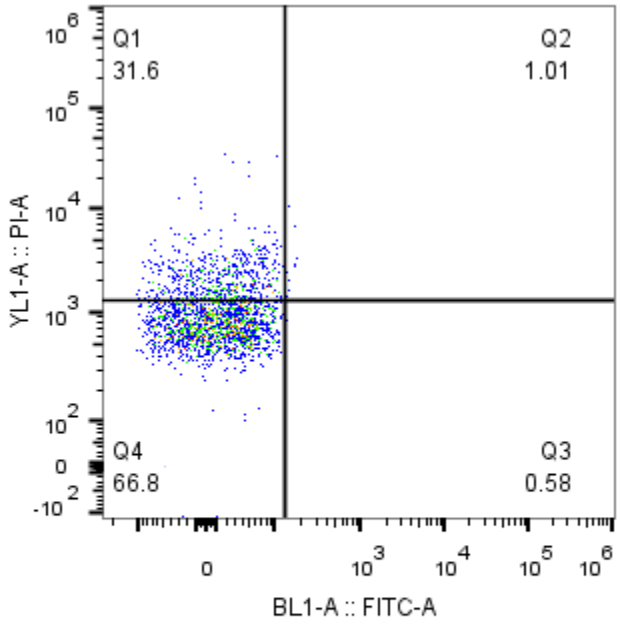


Figure 12.215.: Flow cytometry final analysis for T98G cells treated with 5.00 mM H_20_2 (positive control) conditions for 24-hours and dual stained with Annexin-V-fluorescein isothiocyanate and propidium iodide, replicate 1.

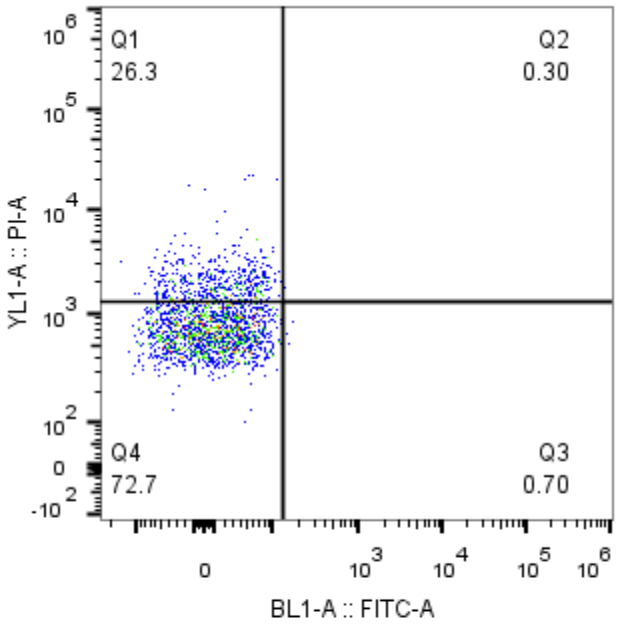


Figure 12.216.: Flow cytometry final analysis for T98G cells treated with 5.00 mM H_20_2 (positive control) conditions for 24-hours and dual stained with Annexin-V-fluorescein isothiocyanate and propidium iodide, replicate 2.

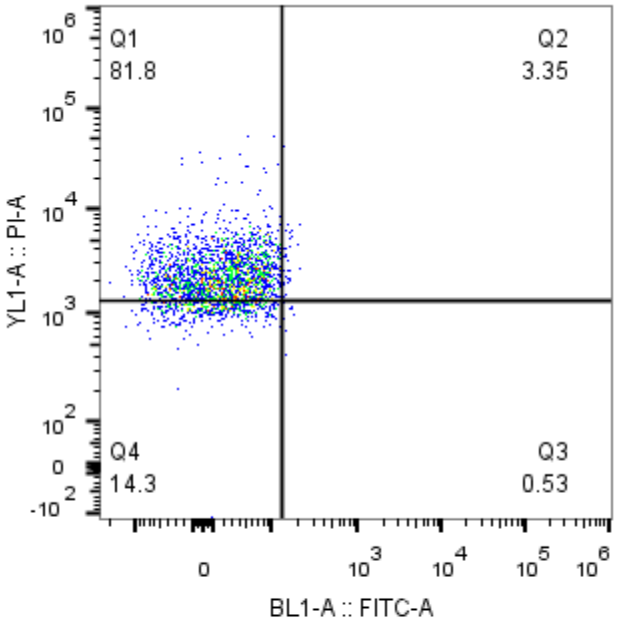


Figure 12.217.: Flow cytometry final analysis for T98G cells treated with 5.00 mM H_20_2 (positive control) conditions for 24-hours and dual stained with Annexin-V-fluorescein isothiocyanate and propidium iodide, replicate 3.

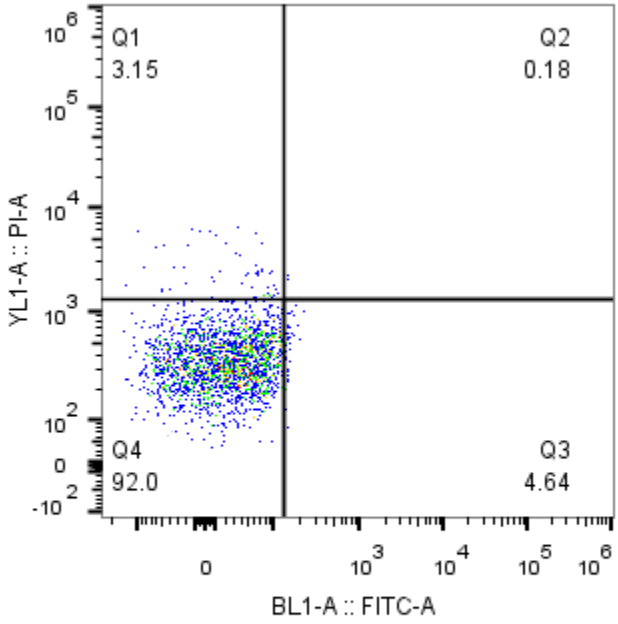


Figure 12.218.: Flow cytometry final analysis for T98G cells treated with 6.25 µM α-solanine for 24-hours and dual stained with Annexin-V-fluorescein isothiocyanate and propidium iodide, replicate 1.

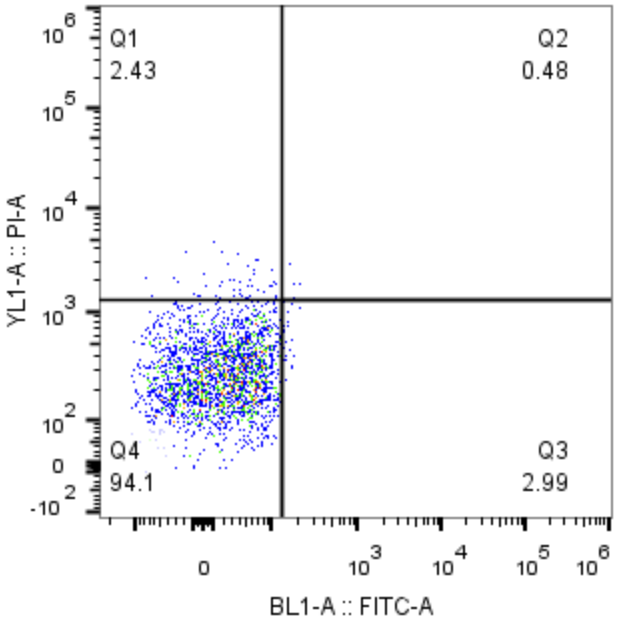


Figure 12.219.: Flow cytometry final analysis for T98G cells treated with 6.25 µM α-solanine for 24-hours and dual stained with Annexin-V-fluorescein isothiocyanate and propidium iodide, replicate 2.

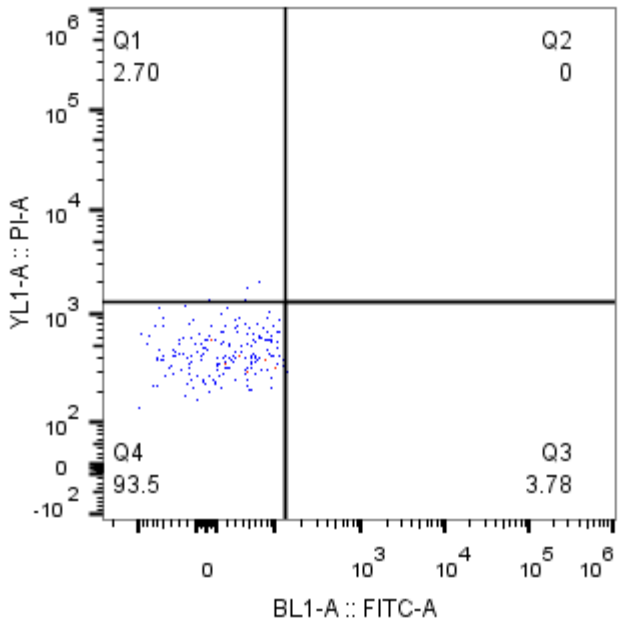


Figure 12.220.: Flow cytometry final analysis for T98G cells treated with 6.25 µM α-solanine for 24-hours and dual stained with Annexin-V-fluorescein isothiocyanate and propidium iodide, replicate 3.

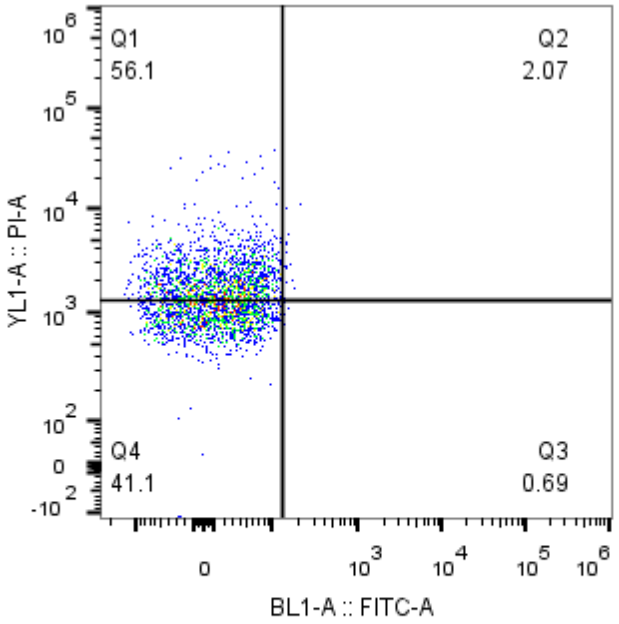


Figure 12.221.: Flow cytometry final analysis for T98G cells treated with 1200.00 µM temozolomide for 24-hours and dual stained with Annexin-V-fluorescein isothiocyanate and propidium iodide, replicate 1.

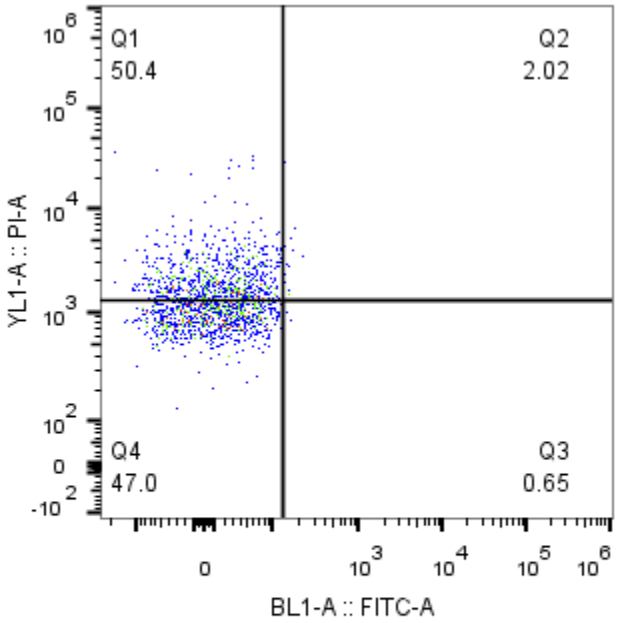


Figure 12.222.: Flow cytometry final analysis for T98G cells treated with 1200.00 µM temozolomide for 24-hours and dual stained with Annexin-V-fluorescein isothiocyanate and propidium iodide, replicate 2.

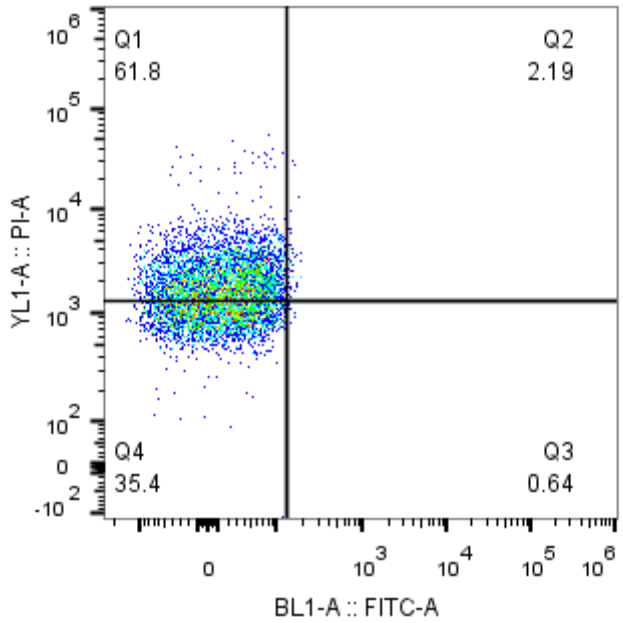


Figure 12.223.: Flow cytometry final analysis for T98G cells treated with 1200.00 µM temozolomide for 24-hours and dual stained with Annexin-V-fluorescein isothiocyanate and propidium iodide, replicate 3.

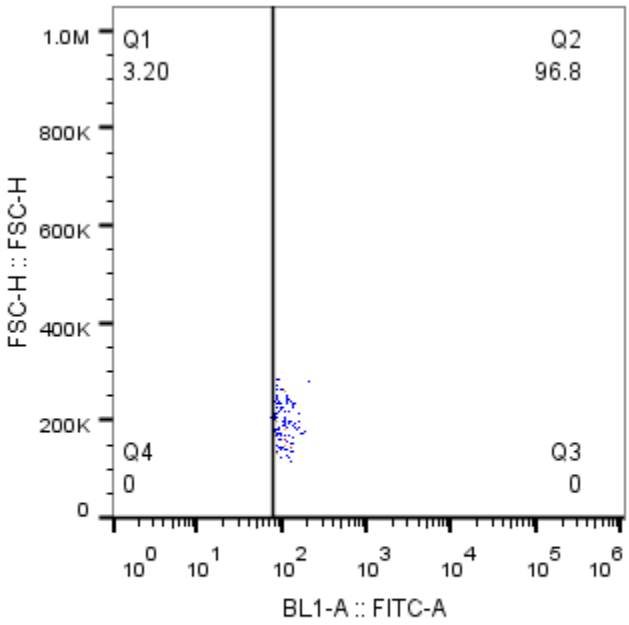


Figure 12.224.: Flow cytometry final analysis for T98G cells treated with culture (negative control) conditions for 24-hours and dual stained with monodansylcadaverine, replicate 1.

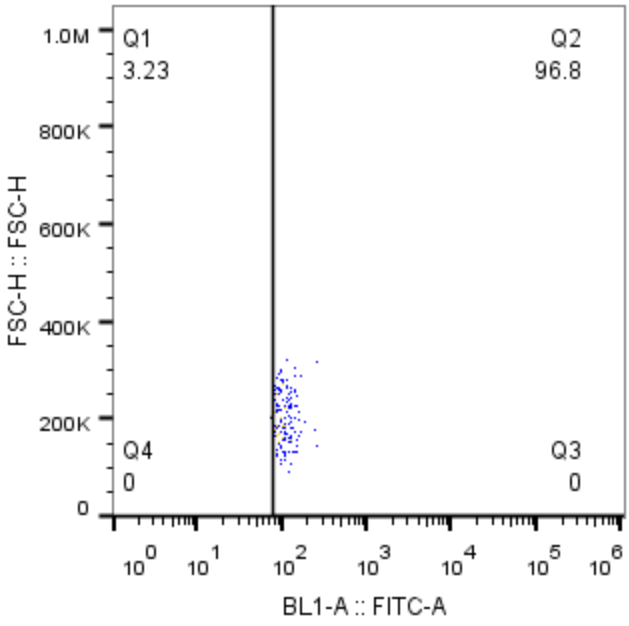


Figure 12.225.: Flow cytometry final analysis for T98G cells treated with culture (negative control) conditions for 24-hours and dual stained with monodansylcadaverine, replicate 2.

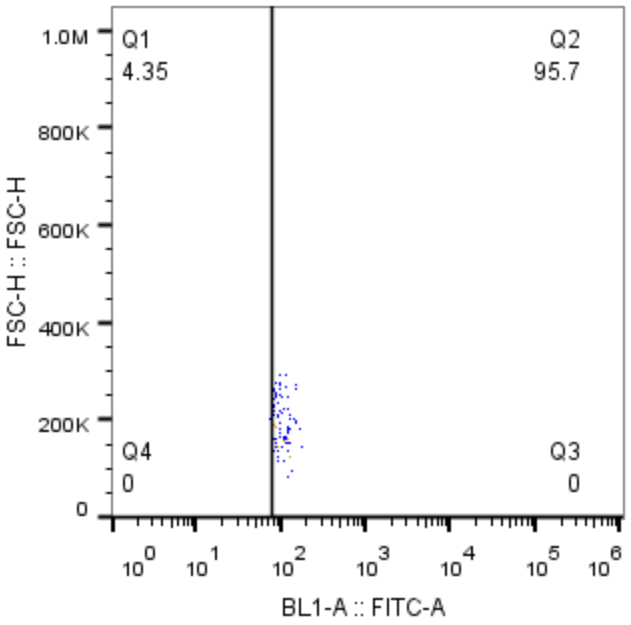


Figure 12.226.: Flow cytometry final analysis for T98G cells treated with culture (negative control) conditions for 24-hours and dual stained with monodansylcadaverine, replicate 3.

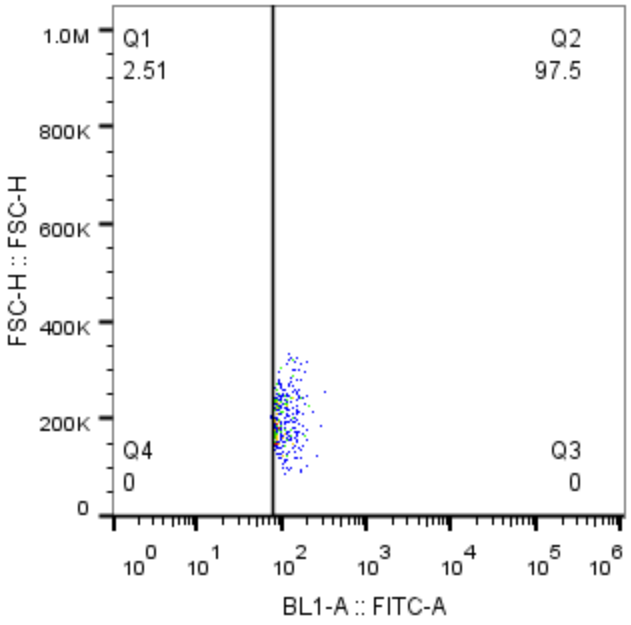


Figure 12.227.: Flow cytometry final analysis for T98G cells treated with 5.00 mM H_2O_2 (positive control) conditions for 24-hours and dual stained with monodansylcadaverine, replicate 1.

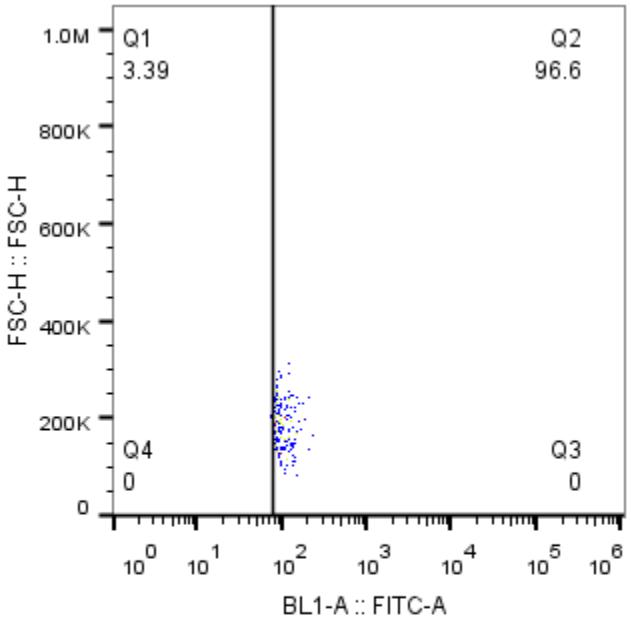


Figure 12.228.: Flow cytometry final analysis for T98G cells treated with 5.00 mM H_2O_2 (positive control) conditions for 24-hours and dual stained with monodansylcadaverine, replicate 2.

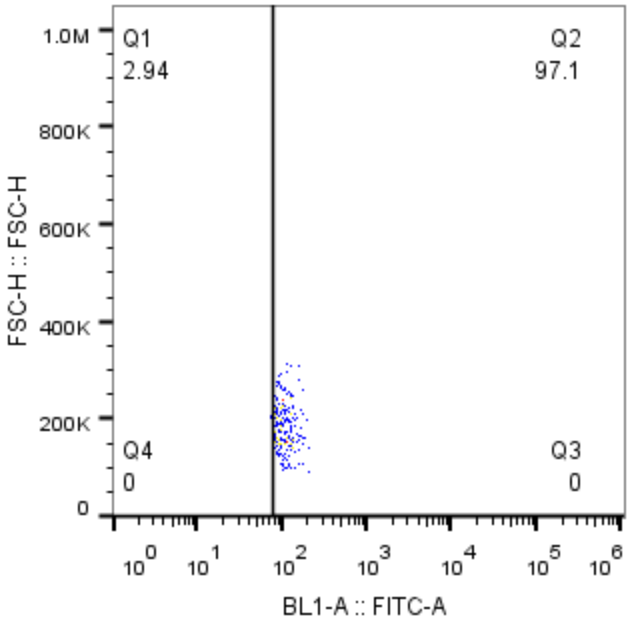


Figure 12.229.: Flow cytometry final analysis for T98G cells treated with 5.00 mM H_2O_2 (positive control) conditions for 24-hours and dual stained with monodansylcadaverine, replicate 3.

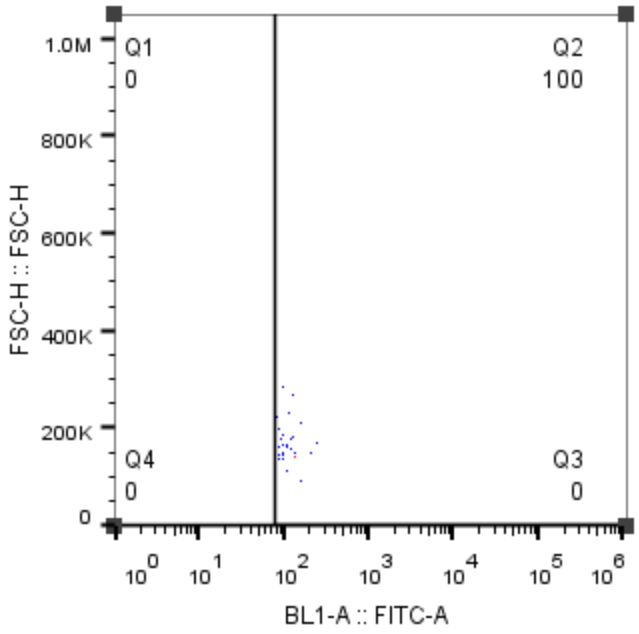


Figure 12.230.: Flow cytometry final analysis for T98G cells treated with 6.25 µM α-solanine for 24-hours and dual stained with monodansylcadaverine, replicate 1.

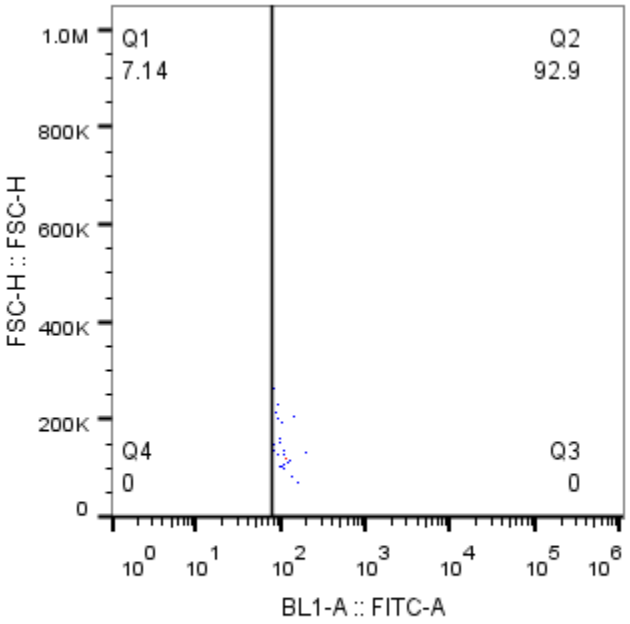


Figure 12.231.: Flow cytometry final analysis for T98G cells treated with 6.25 µM α-solanine for 24-hours and dual stained with monodansylcadaverine, replicate 2.

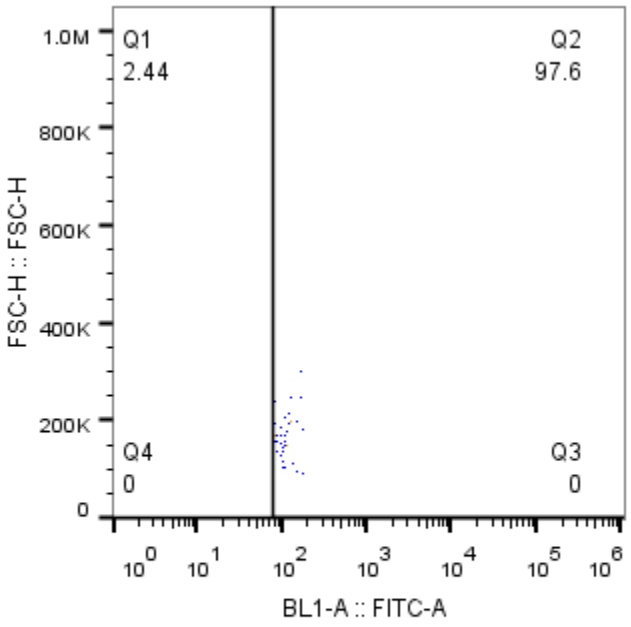


Figure 12.232.: Flow cytometry final analysis for T98G cells treated with 6.25 µM α-solanine for 24-hours and dual stained with monodansylcadaverine, replicate 3.

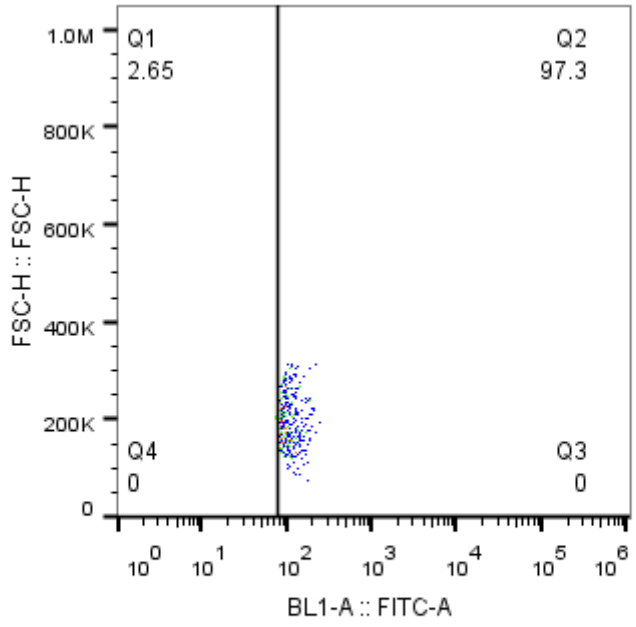


Figure 12.233.: Flow cytometry final analysis for T98G cells treated with 1200.00 µM temozolomide for 24-hours and dual stained with monodansylcadaverine, replicate 1.

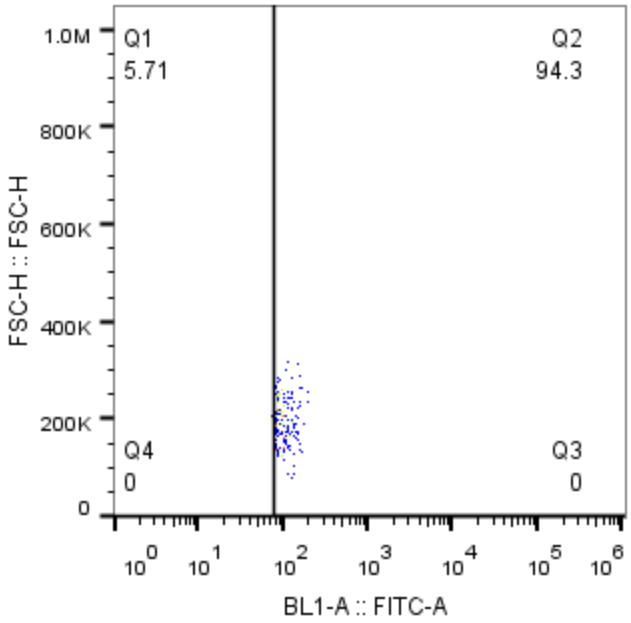


Figure 12.234.: Flow cytometry final analysis for T98G cells treated with 1200.00 µM temozolomide for 24-hours and dual stained with monodansylcadaverine, replicate 2.

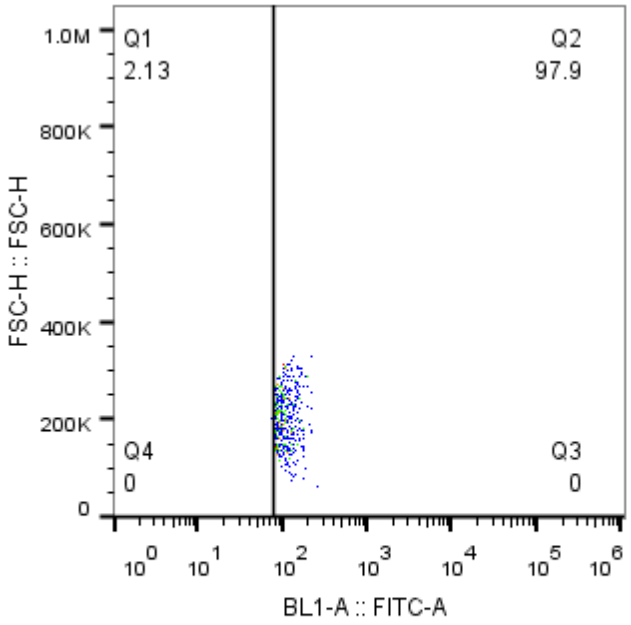


Figure 12.235.: Flow cytometry final analysis for T98G cells treated with 1200.00 µM temozolomide for 24-hours and dual stained with monodansylcadaverine, replicate 3.

12.7.4. Flow cytometry data extracted from final analysis pseudo-colour plots

Table 12.17.: U87MG flow cytometry data

Cell line	Treatment condition	Replicate	Count of gated cells	% Early apoptosis	% Late apoptosis	% Necrotic	% Autophagic vacuoles
U87MG	H2O2	R1	3680	0.16	7.96	90.6	/
	H2O2	R2	3778	0.16	6.8	92.2	/
	H2O2	R3	3668	0.19	7.93	91.1	/
	TMZ	R1	3483	0.11	8.53	90.9	/
	TMZ	R2	3509	0.11	13.4	86.4	/
	Temozolomide	R3	3364	0.03	8.23	91.4	/
	Negative control	R1	4423	0.32	8.95	90.4	/
	Negative control	R2	3808	0.13	7.59	92.2	/
	Negative control	R3	4308	0.12	9.31	90.5	/
	∝-solanine	R1	1666	0.12	5.04	94.6	/
	∝-solanine	R2	1064	0.094	4.61	95.2	/
	∝-solanine	R3	3080	0.032	7.47	92.4	/
	H2O2	R1	637	/	/	/	72.2
	H2O2	R2	541	/	/	/	73
	H2O2	R3	986	/	/	/	82.8
	TMZ	R1	1120	/	/	/	66.3
	TMZ	R2	651	/	/	/	55.6
	TMZ	R3	1014	/	/	/	63.3
	Negative control	R1	364	/	/	/	19.2
	Negative control	R2	167	/	/	/	14.4
	Negative control	R3	626	/	/	/	37.7
	∝-solanine	R1	430	/	/	/	86.7
	∝-solanine	R2	441	/	/	/	63
	∝-solanine	R3	368	/	/	/	69.3

Table 12.18.: U251 flow cytometry data

Cell line	Treatment condition	Replicate	Count of gated cells	% Early apoptosis	% Late apoptosis	% Necrotic	% Autophagic vacuoles
U251	H2O2	R1	5442	0	1.3	95.5	/
	H2O2	R2	3776	0.11	0.95	95.7	/
	H2O2	R3	5837	0.017	1.94	96.9	/
	TMZ	R1	3210	0	0.93	95.4	/
	TMZ	R2	1991	0	1.1	96.5	/
	TMZ	R3	6290	0.016	1.26	97	/
	∝-solanine	R1	5285	1.97	0.46	5.7	/
	∝-solanine	R2	3864	1.66	0.54	3.42	/
	∝-solanine	R3	3421	2.95	1.49	10.7	/
	Negative control	R1	5853	0.017	1.14	92.3	/
	Negative control	R2	5507	0.11	1.23	89	/
	Negative control	R3	5324	0	2.44	96.9	/
	H2O2	R1	349	/	/	/	55.6
	H2O2	R2	273	/	/	/	52.4
	H2O2	R3	702	/	/	/	57.4
	TMZ	R1	231	/	/	/	23.4
	TMZ	R2	131	/	/	/	18.3
	TMZ	R3	1122	/	/	/	23
	∝-solanine	R1	28	/	/	/	42.9
	∝-solanine	R2	21	/	/	/	71.4
	∝-solanine	R3	26	/	/	/	88.5
	Negative control	R1	959	/	/	/	8.76
	Negative control	R2	743	/	/	/	7
	Negative control	R3	977	/	/	/	5.83

Table 12.19.: T98G flow cytometry data

Cell line	Treatment condition	Replicate	Count of gated cells	% Early apoptosis	% Late apoptosis	% Necrotic	% Autophagic vacuoles
T98G	Positive control	R1	2075	0.58	1.01	31.6	/
		R2	1991	0.7	0.3	26.3	/
		R3	2450	0.53	3.35	81.8	/
	Temozolomide	R1	2748	0.69	2.07	56.1	/
		R2	1531	0.65	2.02	50.4	/
		R3	5765	0.64	2.19	61.8	/

	Negative control	R1	2627	0.57	1.71	59.9	/
		R2	1999	0.35	0.95	35.8	/
		R3	1103	0.82	1	31.9	/
	∝-solanine	R1	2221	4.64	0.18	3.15	/
		R2	2305	2.99	0.48	2.43	/
		R3	185	3.78	0	2.7	/
	Positive control	R1	204	/	/	/	97.1
		R2	199	/	/	/	96.6
		R3	399	/	/	/	97.5
	Temozolomide	R1	339	/	/	/	97.3
		R2	175	/	/	/	94.3
		R3	423	/	/	/	97.9
	Negative control	R1	125	/	/	/	96.8
		R2	155	/	/	/	96.8
		R3	92	/	/	/	95.7
	∝-solanine	R1	28	/	/	/	100
		R2	28	/	/	/	9.29
		R3	41	/	/	/	97.6

12.8. Antibody array data

Table 12.20.: Antibody array data for glioblastoma cells treated with 6.25 µM ∝-solanine.

Protein	Corrected mean grey value						Average corrected mean grey value	Fold change
	U87MG R1	U87MG R2	T98G R1	T98G R2	U251 R1	U251 R2		
Bad	66.48	48.00	85.19	69.37	54.27	43.51	61.14	1.50
Bax	21.50	23.80	54.73	38.70	28.81	31.05	33.10	1.31
Bcl-2	93.91	92.94	100.32	84.76	99.20	104.82	95.99	1.54
Bcl-w	96.66	87.61	103.75	94.28	98.92	97.83	96.51	1.47
Bid	62.14	58.92	49.67	52.01	56.00	58.03	56.13	1.64
Bim	57.64	64.67	131.22	117.66	118.26	122.51	101.99	1.74
Casp-3	29.60	39.50	63.09	76.01	42.16	48.79	49.86	1.43
Casp-8	5.56	6.81	7.38	8.89	6.94	8.09	7.28	1.19
TNFRSF5	94.07	105.41	78.64	80.49	54.89	49.57	77.18	1.57
TNFSF5	157.36	173.79	137.97	119.15	97.35	88.94	129.09	1.57
cIAP-2	102.79	123.01	94.81	79.62	78.71	69.80	91.46	1.48
Cyt-C	171.98	208.64	212.98	186.76	149.93	125.85	176.02	1.46
TNFRSF21	12.11	12.28	12.22	14.01	7.29	6.25	10.69	1.18
Fas	72.18	88.13	95.05	149.64	89.16	67.28	93.57	1.67
Fas ligand	98.49	98.74	135.32	202.97	109.61	77.30	120.41	1.73
HSP27	32.16	34.53	49.49	47.84	39.11	34.06	39.53	1.31
HSP60	108.15	130.75	181.93	157.24	137.26	118.60	138.99	1.32
HSP70	70.82	72.30	99.05	89.27	115.40	68.42	85.88	1.09
HTRA2	97.63	101.76	128.21	112.47	68.81	91.62	100.08	1.01
IGF-1	80.51	97.40	171.42	91.00	101.57	116.22	109.69	1.39
IGF-2	88.27	101.92	173.20	94.56	128.81	108.89	115.94	1.47
IGFBP-1	94.84	85.49	69.57	72.11	50.86	57.43	71.72	1.06
IGFBP-2	119.78	97.58	83.43	82.13	58.65	63.59	84.19	1.14
IGFBP-3	121.60	125.68	80.76	80.88	102.35	96.42	101.28	0.99
IGFBP-4	91.95	86.54	83.78	57.96	84.73	79.76	80.79	1.05
IGFBP-5	99.62	76.11	118.09	75.94	70.77	73.77	85.72	1.07
IGFBP-6	82.89	81.18	153.48	156.52	82.75	77.92	105.79	1.39
IGF-1R	70.11	64.31	143.67	141.76	62.38	60.58	90.47	1.71
livin	20.80	19.62	34.33	31.90	17.70	23.00	24.56	1.32
p21	94.25	101.84	138.64	124.33	73.54	101.28	105.65	1.14
p27	98.22	103.83	125.71	117.48	83.33	108.58	106.19	0.98
p53	98.61	109.56	121.29	116.93	92.25	93.22	105.31	1.03
SMAC	27.09	22.12	23.96	17.11	24.23	22.95	22.91	1.00
Survivin	76.48	86.64	72.75	72.64	71.87	80.08	76.74	1.13

TNF RI	68.45	74.78	69.15	72.25	65.27	69.35	69.87	1.08
TNF RII	88.22	101.18	82.85	115.22	58.35	71.47	86.22	1.13
TNF alpha	86.53	106.41	85.35	97.92	57.54	69.05	83.80	1.17
TNF beta	80.91	90.41	54.53	60.64	55.04	64.64	67.70	0.99
TRAIL R1	107.56	121.60	63.28	69.07	76.31	84.39	87.03	0.93
TRAIL R2	103.91	117.87	84.08	70.07	94.11	96.91	94.49	0.90
TRAIL R3	74.93	90.48	90.55	58.71	76.14	79.60	78.40	1.09
TRAIL R 4	100.42	118.56	137.00	128.26	76.54	102.96	110.62	1.20
XIAP	108.28	121.77	125.39	129.42	84.57	101.64	111.84	1.11
ATG3	28.36	30.03	21.09	23.39	19.65	21.78	24.05	0.84
ATG4A	208.84	205.42	197.75	193.81	197.58	191.22	199.10	1.47
ATG4B	153.33	151.99	134.38	153.96	141.82	142.04	146.25	1.46
ATG5	203.82	200.65	201.89	187.82	198.33	213.15	200.94	1.17
ATG7	192.64	198.53	161.99	173.48	163.47	166.39	176.08	1.12
ATG10	118.40	137.40	102.54	106.97	107.10	105.46	112.98	1.09
ATG12	114.02	107.18	93.10	97.02	105.99	116.09	105.57	1.18
ATG13	185.67	194.22	166.49	163.65	184.46	175.28	178.29	1.24
BECN1	194.99	195.02	188.86	192.53	195.40	191.18	193.00	1.46
BNIP3L	136.42	131.69	137.45	164.58	142.66	149.25	143.68	1.54
DDR2	22.76	23.62	25.21	27.07	11.79	12.41	20.48	0.97
GABARAP	125.96	126.95	90.04	95.45	71.32	77.04	97.79	1.20
LAMP1	206.35	198.14	165.82	169.70	167.15	159.34	177.75	1.26
LC3A	152.44	149.54	145.27	153.06	137.94	135.11	145.56	1.46
LC3B	81.80	84.53	84.00	103.99	79.54	79.66	85.59	1.19
NBS1	182.03	180.54	160.69	166.23	174.08	170.31	172.31	1.18
P62	178.26	195.98	137.47	162.88	147.59	163.03	164.20	1.13
Rheb	192.18	196.73	193.75	190.27	174.74	182.51	188.36	1.19
MSK1	118.71	111.18	106.68	110.51	68.93	67.66	97.28	1.06
Alpha-synuclein	201.29	188.59	167.60	179.57	169.90	170.62	179.59	1.21

Table 12.21.: Antibody array data for glioblastoma cells treated with negative control (culture) conditions.

Protein	Corrected mean grey value						Average corrected mean grey value
	U87MG R1	U87MG R2	T98G R1	T98G R2	U251 R1	U251 R2	
Bad	37.14	36.65	36.91	40.98	44.82	47.73	40.70
Bax	20.93	19.99	26.59	26.89	28.14	29.42	25.32
Bcl-2	50.33	50.56	69.54	77.31	63.09	62.43	62.21
Bcl-w	64.11	56.57	68.22	72.10	70.03	64.14	65.86
Bid	31.78	25.86	29.45	42.20	33.90	42.22	34.23
Bim	54.39	55.33	63.99	58.84	56.00	63.47	58.67
Casp-3	32.02	43.64	37.46	37.16	27.86	31.71	34.98
Casp-8	6.01	6.26	5.94	6.60	6.15	5.83	6.13
TNFRSF5	39.66	47.61	50.55	52.20	50.80	54.93	49.29
TNFSF5	79.65	79.86	87.19	79.12	86.15	82.68	82.44
cIAP-2	49.52	73.30	52.91	55.01	59.73	80.63	61.85
Cyt-C	83.14	138.88	101.13	101.91	111.81	188.64	120.92
TNFRSF21	6.37	8.86	8.93	11.57	9.51	9.01	9.04
Fas	53.45	51.55	63.98	58.40	56.11	53.65	56.19
Fas ligand	67.61	61.81	80.22	64.31	82.36	61.18	69.58
HSP27	27.17	25.77	32.82	34.51	31.29	29.27	30.14
HSP60	83.55	82.06	114.49	117.17	125.18	107.06	104.92
HSP70	59.81	58.33	89.24	90.19	86.94	87.22	78.62
HTRA2	110.50	91.70	96.18	95.44	102.74	99.06	99.27
IGF-1	72.33	66.66	89.27	78.85	86.22	80.71	79.01
IGF-2	63.69	73.11	86.37	86.06	82.52	82.25	79.00
IGFBP-1	61.92	61.91	71.74	68.46	71.38	69.81	67.54
IGFBP-2	73.22	63.34	85.43	67.09	79.46	75.29	73.97
IGFBP-3	127.45	116.96	90.02	88.93	93.17	95.78	102.05
IGFBP-4	98.64	93.43	67.81	59.90	69.55	74.35	77.28
IGFBP-5	96.03	92.36	76.55	72.15	68.77	75.06	80.15
IGFBP-6	96.18	92.75	68.80	67.20	67.50	65.74	76.36
IGF-1R	47.73	61.33	57.58	53.46	52.94	44.94	53.00
livin	13.83	16.42	18.43	23.30	18.37	21.32	18.61
p21	73.23	80.44	107.40	120.77	85.54	89.69	92.84
p27	133.24	82.78	114.63	119.49	99.17	97.72	107.84
p53	106.01	91.98	112.41	110.14	96.46	95.84	102.14
SMAC	23.29	19.46	26.55	24.49	25.97	17.89	22.94
Survivin	56.83	62.56	79.85	82.12	67.92	59.31	68.10
TNF RI	66.25	57.14	72.23	69.08	63.02	59.90	64.60
TNF RII	63.58	74.88	78.85	84.48	77.75	78.28	76.30

TNF alpha	58.58	76.14	70.98	84.90	70.40	69.34	71.72
TNF beta	84.54	86.63	53.01	63.20	60.01	61.75	68.19
TRAIL R1	107.63	117.99	78.51	85.77	90.37	81.37	93.60
TRAIL R2	126.47	139.21	93.39	98.82	87.58	84.84	105.05
TRAIL R3	85.44	93.01	62.40	78.30	55.52	56.69	71.89
TRAIL R 4	96.01	121.12	77.65	101.62	60.90	96.41	92.28
XIAP	71.00	131.88	102.75	115.00	96.23	89.65	101.08
ATG3	29.20	31.94	24.57	32.02	25.80	28.58	28.68
ATG4A	133.74	135.25	132.92	139.33	133.56	135.30	135.02
ATG4B	107.22	104.37	83.54	98.73	101.55	105.11	100.09
ATG5	184.90	181.54	154.46	178.37	166.53	163.75	171.59
ATG7	178.38	164.45	154.94	150.94	148.63	143.83	156.86
ATG10	113.52	108.00	115.85	104.65	93.62	88.56	104.03
ATG12	94.17	105.95	91.77	82.31	84.31	78.48	89.50
ATG13	149.01	153.47	139.32	135.83	145.34	143.08	144.34
BECN1	133.96	136.44	131.99	128.83	137.90	125.28	132.40
BNIP3L	95.68	94.92	95.78	88.16	93.17	90.54	93.04
DDR2	27.11	28.16	16.86	15.25	17.75	21.70	21.14
GABARAP	96.33	100.72	69.18	72.37	84.47	66.47	81.59
LAMP1	151.73	155.53	138.92	141.79	129.15	129.90	141.17
LC3A	117.80	129.75	95.91	98.95	83.39	70.50	99.38
LC3B	84.10	91.90	65.80	70.73	62.53	57.16	72.04
NBS1	154.91	158.54	140.17	145.81	135.57	137.56	145.43
P62	151.94	150.89	131.91	147.89	142.00	143.83	144.74
Rheb	172.30	171.98	160.41	152.84	152.15	136.38	157.68
MSK1	95.17	98.30	79.66	79.18	114.44	82.99	91.62
Alpha-synuclein	162.18	156.39	145.69	152.51	135.85	135.10	147.95

12.9. Presto blue® cell viability assay optimisation data

Table 12.22.: Presto blue® cell viability assay optimisation data

Treatment Condition	Concentration	Replicate	Reading	% Viability
DMSO	1 %	R1	0.468	12.82
		R2	0.472	
		R3	0.488	
	10 %	R1	0.467	13.03
		R2	0.474	

		R3	0.471	
α-solanine in DMSO	5 uM	R1	0.434	14.25
		R2	0.446	
		R3	0.452	
	50 uM	R1	0.459	12.68
		R2	0.472	
		R3	0.478	
α-solanine in DMEM	5 uM	R1	0.672	94.73
		R2	0.645	
		R3	0.668	
	50 uM	R1	0.459	12.70
		R2	0.472	
		R3	0.478	

Chapter 13 Appendix VI: Statistical analysis

13.1. Statistical analysis of Presto blue® cell viability assays

13.1.1. Statistical analysis of Presto blue® cell viability data regarding U87MG, U251 and T98G cells following 72 hours treatment with different concentrations of α-temozolomide.

Output 13.1.: Descriptive statistics and normality (Shapiro-Wilk) assumption checking for U87MG, U251 and T98G cell-lines treated with 800.00 µM temozolomide for 72 hours.

Descriptive Statistics

	800 uM TMZ		
	T98G	U251	U87MG
Valid	3	3	3
Missing	0	0	0
Mean	0.611	0.611	0.639
Std. Deviation	0.011	0.011	0.004
Shapiro-Wilk	0.999	0.999	0.942
P-value of Shapiro-Wilk	0.948	0.948	0.537
Minimum	0.600	0.600	0.635
Maximum	0.621	0.621	0.642

Output 13.2.: Equality of Variance (Levene's) assumption checking for U87MG, U251 and T98G cell-lines treated with 800.00 µM temozolomide for 72 hours.

Test for Equality of Variances (Levene's)

F	df1	df2	p
0.831	2.000	6.000	0.480

Output 13.3.: One-way ANOVA testing for U87MG versus U251 versus T98G cells treated cell-lines treated with 800.00 temozolomide µM α-solanine for 72 hours.

ANOVA - 800 uM TMZ

Cases	Sum of Squares	df	Mean Square	F	p
Cell line_9	0.002	2	8.028e −4	10.307	0.011
Residuals	4.673e −4	6	7.789e −5		

Note. Type III Sum of Squares

Output 13.4.: One-way ANOVA post-hoc analysis for U87MG versus U251 versus T98G cells treated cell-lines treated with 800.00 µM α-solanine for 72 hours.

Standard

Post Hoc Comparisons - Cell line_9

		Mean Difference	SE	t	p_{tukey}
T98G	U251	−3.469e −18	0.007	−4.815e −16	1.000
	U87MG	−0.028	0.007	−3.932	0.018
U251	U87MG	−0.028	0.007	−3.932	0.018

Note. P-value adjusted for comparing a family of 3

Output 13.5.: Descriptive statistics and normality (Shapiro-Wilk) assumption checking for U87MG, U251 and T98G cell-lines treated with 1200.00 µM temozolomide for 72 hours.

Descriptive Statistics

	1200 uM TMZ		
	T98G	U251	U87MG
Valid	3	3	3
Missing	0	0	0
Mean	0.636	0.622	0.621
Std. Deviation	0.010	0.011	0.003
Shapiro-Wilk	0.949	0.989	0.964
P-value of Shapiro-Wilk	0.567	0.800	0.637
Minimum	0.627	0.612	0.618
Maximum	0.647	0.634	0.624

Output 13.6.: Equality of Variance (Levene's) assumption checking for U87MG, U251 and T98G cell-lines treated with 1200.00 µM temozolomide for 72 hours.

Test for Equality of Variances (Levene's)

F	df1	df2	p
1.673	2.000	6.000	0.265

Output 13.7.: One-way ANOVA testing for U87MG versus U251 versus T98G cells treated cell-lines treated with 1200.00 temozolomide µM α-solanine for 72 hours.

ANOVA - 1200 uM TMZ

Cases	Sum of Squares	df	Mean Square	F	p
Cell line_11	3.842e −4	2	1.921e −4	2.432	0.168
Residuals	4.740e −4	6	7.900e −5		

Note. Type III Sum of Squares

Output 13.8.: Descriptive statistics and normality (Shapiro-Wilk) assumption checking for U87MG, U251 and T98G cell-lines treated with 1600.00 µM temozolomide for 72 hours.

Descriptive Statistics

	1600 uM TMZ		
	T98G	U251	U87MG
Valid	3	3	3
Missing	0	0	0
Mean	0.646	0.648	0.611
Std. Deviation	0.005	0.009	0.003
Shapiro-Wilk	0.750	0.947	0.987
P-value of Shapiro-Wilk	< .001	0.554	0.780
Minimum	0.643	0.641	0.609
Maximum	0.651	0.658	0.614

Output 13.9.: Equality of Variance (Levene's) assumption checking for U87MG, U251 and T98G cell-lines treated with 1600.00 µM temozolomide for 72 hours.

Test for Equality of Variances (Levene's)

F	df1	df2	p
2.774	2.000	6.000	0.140

Output 13.10.: Kruskal-Wallis testing for U87MG versus U251 versus T98G cells treated cell-lines treated with 1600.00 temozolomide µM α-solanine for 72 hours.

Kruskal-Wallis Test

Factor	Statistic	df	p
Cell line_13	5.468	2	0.065

Output 13.11.: Descriptive statistics and normality (Shapiro-Wilk) assumption checking for U87MG, U251 and T98G cell-lines treated with 2000.00 µM temozolomide for 72 hours.

Descriptive Statistics

	2000 uM TMZ		
	T98G	U251	U87MG
Valid	3	3	3
Missing	0	0	0
Mean	0.656	0.615	0.574
Std. Deviation	0.014	0.020	0.007
Shapiro-Wilk	0.996	0.792	0.807
P-value of Shapiro-Wilk	0.878	0.094	0.132
Minimum	0.643	0.592	0.566
Maximum	0.670	0.628	0.579

Output 13.12.: Equality of Variance (Levene's) assumption checking for U87MG, U251 and T98G cell-lines treated with 2000.00 µM temozolomide for 72 hours.

Test for Equality of Variances (Levene's)

F	df1	df2	p
2.191	2.000	6.000	0.193

Output 13.13.: One-way ANOVA testing for U87MG versus U251 versus T98G cells treated cell-lines treated with 2000.00 temozolomide µM α-solanine for 72 hours.

ANOVA - 2000 uM TMZ

Cases	Sum of Squares	df	Mean Square	F	p
Cell line_15	0.010	2	0.005	23.278	0.001
Residuals	0.001	6	2.149e −4		

Note. Type III Sum of Squares

Output 13.14.: One-way ANOVA post-hoc analysis for U87MG versus U251 versus T98G cells treated cell-lines treated with 2000.00 µM α-solanine for 72 hours.

Standard

Post Hoc Comparisons - Cell line_15

		Mean Difference	SE	t	p_{tukey}
T98G	U251	0.041	0.012	3.398	0.034
	U87MG	0.082	0.012	6.823	0.001
U251	U87MG	0.041	0.012	3.425	0.032

Note. P-value adjusted for comparing a family of 3

Output 13.15.: Descriptive statistics and normality (Shapiro-Wilk) assumption checking for U87MG, U251 and T98G cell-lines treated with 2400.00 µM temozolomide for 72 hours.

Descriptive Statistics

	2400 uM TMZ		
	T98G	U251	U87MG
Valid	3	3	3
Missing	0	0	0
Mean	0.669	0.618	0.492
Std. Deviation	0.014	0.020	0.005
Shapiro-Wilk	0.998	0.865	0.964
P-value of Shapiro-Wilk	0.921	0.281	0.637
Minimum	0.655	0.603	0.487
Maximum	0.683	0.641	0.496

Output 13.16.: Equality of Variance (Levene's) assumption checking for U87MG, U251 and T98G cell-lines treated with 2400.00 µM temozolomide for 72 hours.

Test for Equality of Variances (Levene's)

F	df1	df2	p
2.847	2.000	6.000	0.135

Output 13.17.: One-way ANOVA testing for U87MG versus U251 versus T98G cells treated cell-lines treated with 2400.00 temozolomide µM α-solanine for 72 hours.

ANOVA - 2400 uM TMZ

Cases	Sum of Squares	df	Mean Square	F	p
Cell line_17	0.050	2	0.025	117.956	< .001
Residuals	0.001	6	2.116e −4		

Note. Type III Sum of Squares

Output 13.18.: One-way ANOVA post-hoc analysis for U87MG versus U251 versus T98G cells treated cell-lines treated with 2400.00 µM α-solanine for 72 hours.

Standard

Post Hoc Comparisons - Cell line_17

		Mean Difference	SE	t	p_{tukey}
T98G	U251	0.052	0.012	4.351	0.011
	U87MG	0.177	0.012	14.932	< .001
U251	U87MG	0.126	0.012	10.582	< .001

Note. P-value adjusted for comparing a family of 3

13.1.2. Statistical analysis of Presto blue® cell viability data regarding U87MG, U251 and T98G cells following 72 hours treatment with different concentrations of α-solanine.

Output 13.19.: Descriptive statistics and normality (Shapiro-Wilk) assumption checking for U87MG, U251 and T98G cell-lines treated with 5.00 µM α-solanine for 72 hours.

Descriptive Statistics

	5 uM α-solanine		
	T98G	U251	U87MG
Valid	3	3	3
Missing	0	0	0
Mean	0.662	0.682	0.662
Std. Deviation	0.038	0.007	0.015
Shapiro-Wilk	0.994	0.902	0.858
P-value of Shapiro-Wilk	0.855	0.391	0.263
Minimum	0.626	0.676	0.645
Maximum	0.702	0.690	0.672

Output 13.20.: Equality of Variance (Levene's) assumption checking for U87MG, U251 and T98G cell-lines treated with 5.00 µM α-solanine for 72 hours.

Test for Equality of Variances (Levene's)

F	df1	df2	p
2.402	2.000	6.000	0.171

Output 13.21.: One-way ANOVA testing for U87MG versus U251 versus T98G cells treated cell-lines treated with 5.00 µM α-solanine for 72 hours.

ANOVA - 5 uM α-solanine

Cases	Sum of Squares	df	Mean Square	F	p
Cell line	7.742e −4	2	3.871e −4	0.676	0.544
Residuals	0.003	6	5.730e −4		

Note. Type III Sum of Squares

Output 13.22.: Descriptive statistics and normality (Shapiro-Wilk) assumption checking for U87MG, U251 and T98G cell-lines treated with 25.00 µM α-solanine for 72 hours.

Descriptive Statistics

	25 uM α-solanine		
	T98G	U251	U87MG
Valid	3	3	3
Missing	0	0	0
Mean	0.565	0.551	0.658
Std. Deviation	0.010	0.008	0.030
Shapiro-Wilk	0.832	0.999	0.855
P-value of Shapiro-Wilk	0.194	0.927	0.253
Minimum	0.554	0.544	0.637
Maximum	0.572	0.559	0.693

Output 13.23.: Equality of Variance (Levene's) assumption checking for U87MG, U251 and T98G cell-lines treated with 25.00 µM α-solanine for 72 hours.

Test for Equality of Variances (Levene's)

F	df1	df2	p
5.917	2.000	6.000	0.038

Output 13.24.: Kruskal-Wallis testing for U87MG versus U251 versus T98G cells treated cell-lines treated with 25.00 µM α-solanine for 72 hours.

Kruskal-Wallis Test

Factor	Statistic	df	p
Cell line_3	6.489	2	0.039

Output 13.25.: Kurskal-Wallis post-hoc analysis for U87MG versus U251 versus T98G cells treated cell-lines treated with 25.00 µM α-solanine for 72 hours.

Standard

Post Hoc Comparisons - Cell line_3

		Mean Difference	SE	t	p_{tukey}
T98G	U251	0.014	0.015	0.907	0.656
	U87MG	−0.093	0.015	−6.028	0.002
U251	U87MG	−0.107	0.015	−6.936	0.001

Note. P-value adjusted for comparing a family of 3

Output 13.26.: Descriptive statistics and normality (Shapiro-Wilk) assumption checking for U87MG, U251 and T98G cell-lines treated with 50.00 µM α-solanine for 72 hours.

Descriptive Statistics

	50 uM α-solanine		
	T98G	U251	U87MG
Valid	3	3	3
Missing	0	0	0
Mean	0.555	0.552	0.470
Std. Deviation	0.016	0.019	0.010
Shapiro-Wilk	0.893	0.998	0.957
P-value of Shapiro-Wilk	0.363	0.911	0.600
Minimum	0.537	0.533	0.459
Maximum	0.567	0.570	0.478

Output 13.27.: Equality of Variance (Levene's) assumption checking for U87MG, U251 and T98G cell-lines treated with 50.00 µM α-solanine for 72 hours.

Test for Equality of Variances (Levene's)

F	df1	df2	p
0.528	2.000	6.000	0.615

Output 13.28.: One-way ANOVA testing for U87MG versus U251 versus T98G cells treated cell-lines treated with 50.00 µM α-solanine for 72 hours.

ANOVA – 50 uM α–solanine

Cases	Sum of Squares	df	Mean Square	F	p
Cell line_5	0.014	2	0.007	30.616	< .001
Residuals	0.001	6	2.298e −4		

Note. Type III Sum of Squares

Output 13.29.: One-way ANOVA post-hoc analysis for U87MG versus U251 versus T98G cells treated cell-lines treated with 50.00 µM α-solanine for 72 hours.

Standard

Post Hoc Comparisons – Cell line_5

		Mean Difference	SE	t	p_{tukey}
T98G	U251	0.003	0.012	0.242	0.968
	U87MG	0.085	0.012	6.895	0.001
U251	U87MG	0.082	0.012	6.652	0.001

Note. P–value adjusted for comparing a family of 3

Output 13.30.: Descriptive statistics and normality (Shapiro-Wilk) assumption checking for U87MG, U251 and T98G cell-lines treated with 75.00 µM α-solanine for 72 hours.

Descriptive Statistics

	75 uM α-solanine		
	T98G	U251	U87MG
Valid	3	3	3
Missing	0	0	0
Mean	0.513	0.501	0.458
Std. Deviation	0.011	0.007	0.021
Shapiro-Wilk	0.824	0.993	0.988
P-value of Shapiro-Wilk	0.174	0.843	0.791
Minimum	0.506	0.494	0.438
Maximum	0.526	0.508	0.480

Output 13.31.: Equality of Variance (Levene's) assumption checking for U87MG, U251 and T98G cell-lines treated with 75.00 µM α-solanine for 72 hours.

Test for Equality of Variances (Levene's)

F	df1	df2	p
1.632	2.000	6.000	0.272

Output 13.32.: One-way ANOVA testing for U87MG versus U251 versus T98G cells treated cell-lines treated with 75.00 µM α-solanine for 72 hours.

ANOVA - 75 uM α-solanine

Cases	Sum of Squares	df	Mean Square	F	p
Cell line_7	0.005	2	0.003	12.419	0.007
Residuals	0.001	6	2.057e −4		

Note. Type III Sum of Squares

Output 13.33.: One-way ANOVA post-hoc analysis for U87MG versus U251 versus T98G cells treated cell-lines treated with 75.00 µM α-solanine for 72 hours.

Standard

Post Hoc Comparisons – Cell line_7

		Mean Difference	SE	t	p_{tukey}
T98G	U251	0.013	0.012	1.082	0.558
	U87MG	0.056	0.012	4.754	0.008
U251	U87MG	0.043	0.012	3.672	0.024

Note. P-value adjusted for comparing a family of 3

13.1.3. Generation of IC_{50} α-solanine using AATC BioQuest® IC_{50} calculator

Output 13.34.: U87MG IC_{50} α-solanine

Parameter	Value
IC_{50}	22.9178
Equations	(show alternative)
Equation	$Y = 0.0453 + \frac{1.0002 - 0.0453}{1 + (\frac{X}{22.9178})^{5.5486}}$
Equation Form	$Y = Min + \frac{Max - Min}{1 + (\frac{X}{IC50})^{Hill\ coefficient}}$

Output 13.35.: U251 IC_{50} α-solanine

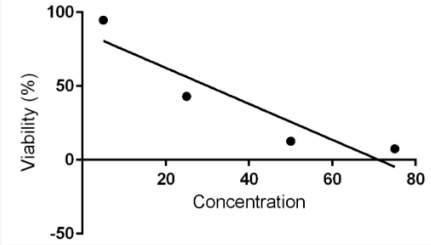
Parameter	Value
IC_{50}	21.3151
Equations	(show alternative)
Equation	$Y = 0.1562 + \frac{1.0002 - 0.1562}{1 + (\frac{X}{21.3151})^{5.7784}}$
Equation Form	$Y = Min + \frac{Max - Min}{1 + (\frac{X}{IC50})^{Hill\ coefficient}}$

Output 13.36.: T98G IC_{50} α-solanine

Parameter	Value
IC_{50}	19.6577
Equations	(show alternative)
Equation	$Y = 0.2879 + \frac{1.0003 - 0.2879}{1 + (\frac{X}{19.6577})^{5.6221}}$
Equation Form	$Y = Min + \frac{Max - Min}{1 + (\frac{X}{IC50})^{Hill\ coefficient}}$

13.1.4. Logistic linear regression of α-solanine and temozolomide cell viability data to determine IC_{75} α-solanine using GraphPad® linear regression calculator.

Output 13.37.: U87MG α-solanine cell viability data linear regression



Best-fit values

Slope	-1.218 ± 0.3538
Y-intercept	86.73 ± 16.57
X-intercept	71.18
1/Slope	-0.8208

95% Confidence Intervals

Slope	-2.741 to 0.3042
Y-intercept	15.41 to 158.0
X-intercept	38.30 to +infinity

Goodness of Fit

R square	0.8557
Sy.x	18.62

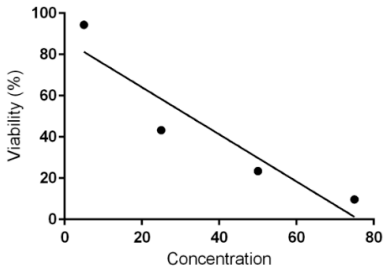
Is slope significantly non-zero?

F	11.86
DFn,DFd	1,2
P Value	0.0750
Deviation from horizontal?	Not Significant

Data

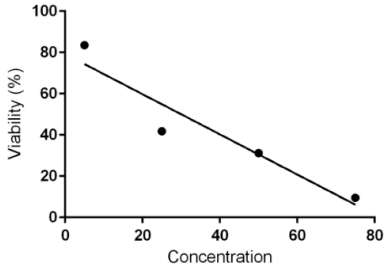
Number of XY pairs	4
Equation	Y = -1.218*X + 86.73

Output 13.38.: U251 α-solanine cell viability data linear regression.



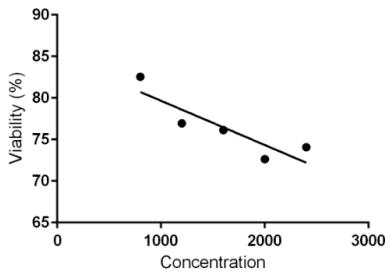
Best-fit values	
Slope	-1.143 ± 0.3042
Y-intercept	86.97 ± 14.25
X-intercept	76.12
1/Slope	-0.8753
95% Confidence Intervals	
Slope	-2.452 to 0.1666
Y-intercept	25.65 to 148.3
X-intercept	45.11 to +infinity
Goodness of Fit	
R square	0.8758
Sy.x	16.01
Is slope significantly non-zero?	
F	14.10
DFn,DFd	1,2
P Value	0.0642
Deviation from horizontal?	Not Significant
Data	
Number of XY pairs	4
Equation	Y = -1.143*X + 86.97

Output 13.39.: T98G α-solanine cell viability data linear regression.



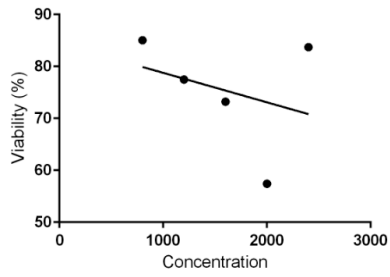
Best-fit values	
Slope	-0.9738 ± 0.2202
Y-intercept	79.27 ± 10.31
X-intercept	81.40
1/Slope	-1.027
95% Confidence Intervals	
Slope	-1.921 to -0.02636
Y-intercept	34.89 to 123.6
X-intercept	52.51 to 1622
Goodness of Fit	
R square	0.9072
Sy.x	11.59
Is slope significantly non-zero?	
F	19.56
DFn,DFd	1,2
P Value	0.0475
Deviation from horizontal?	Significant
Data	
Number of XY pairs	4
Equation	Y = -0.9738*X + 79.27

Output 13.40.: U87MG temozolomide cell viability data linear regression



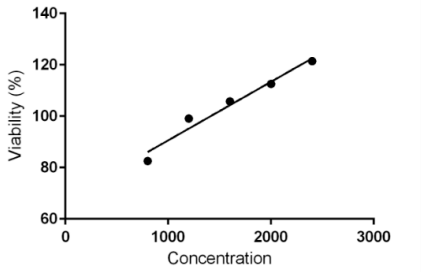
Best-fit values	
Slope	-0.005325 ± 0.001618
Y-intercept	84.99 ± 2.746
X-intercept	15961
1/Slope	-187.8
95% Confidence Intervals	
Slope	-0.01047 to -0.0001769
Y-intercept	76.25 to 93.73
X-intercept	8891 to 433797
Goodness of Fit	
R square	0.7831
Sy.x	2.046
Is slope significantly non-zero?	
F	10.83
DFn,DFd	1,3
P Value	0.0460
Deviation from horizontal?	Significant
Data	
Number of XY pairs	5
Equation	Y = -0.005325*X + 84.99

Output 13.41.: U251 temozolomide cell viability data linear regression



Best-fit values	
Slope	-0.00568 ± 0.009610
Y-intercept	84.46 ± 16.31
X-intercept	14870
1/Slope	-176.1
95% Confidence Intervals	
Slope	-0.03626 to 0.02490
Y-intercept	32.57 to 136.4
X-intercept	3613 to +infinity
Goodness of Fit	
R square	0.1043
Sy.x	12.16
Is slope significantly non-zero?	
F	0.3493
DFn,DFd	1,3
P Value	0.5961
Deviation from horizontal?	Not Significant
Data	
Number of XY pairs	5
Equation	Y = -0.00568*X + 84.46

Output 13.42.: T98G temozolomide cell viability data linear regression



Best-fit values	
Slope	0.02279 ± 0.002575
Y-intercept	67.82 ± 4.370
X-intercept	-2976
1/Slope	43.88
95% Confidence Intervals	
Slope	0.01460 to 0.03098
Y-intercept	53.91 to 81.72
X-intercept	-5557 to -1753
Goodness of Fit	
R square	0.9631
Sy.x	3.257
Is slope significantly non-zero?	
F	78.33
DFn,DFd	1,3
P Value	0.0030
Deviation from horizontal?	Significant
Data	
Number of XY pairs	5
Equation	Y = 0.02279*X + 67.82

13.2. Statistical analysis of scratch migration assays

13.2.1. Statistical analysis of relative scratch assay wound closure (%) data for U87MG versus U251 versus T98G cells treated with 1200.00 µM temozolomide or 6.25 µM α-solanine per duration of incubation.

Output 13.43.: Descriptive statistics and normality (Shapiro-Wilk) assumption checking of U87MG versus U251M versus T98G cells treated with 1200.00 µM temozolomide for 24-hours.

Descriptive Statistics

	Wound closure relative to control at 24hrs (%), Temozolomide		
	T98G	U251	U87MG
Valid	3	3	3
Missing	0	0	0
Mean	77.513	82.323	25.897
Std. Deviation	1.870	1.947	5.155
Shapiro-Wilk	1.000	0.803	0.920
P-value of Shapiro-Wilk	0.994	0.123	0.452
Minimum	75.640	80.080	20.110
Maximum	79.380	83.570	30.000

Note. Excluded 1 rows from the analysis that correspond to the missing values of the split-by variable Cell line

Output 13.44.: Equality of Variance (Levene's) assumption checking of U87MG versus U251M versus T98G cells treated with 1200.00 µM temozolomide for 24-hours.

Test for Equality of Variances (Levene's)

F	df1	df2	p
3.193	2.000	6.000	0.114

Output 13.45.: One-way ANOVA testing for U87MG versus U251 versus T98G cells treated cell-lines treated with 1200.00 µM temozolomide for 24-hours.

ANOVA - Wound closure relative to control at 24hrs (%), Temozolomide

Cases	Sum of Squares	df	Mean Square	F	p
Cell line	5871.385	2	2935.693	260.063	< .001
Residuals	67.730	6	11.288		

Note. Type III Sum of Squares

Output 13.46.: One-way ANOVA post-hoc analysis for U87MG versus U251 versus T98G cells treated cell-lines treated with 1200.00 µM temozolomide for 24-hours.

Standard

Post Hoc Comparisons - Cell line

		Mean Difference	SE	t	p_{tukey}
T98G	U251	−4.810	2.743	−1.753	0.262
	U87MG	51.617	2.743	18.816	< .001
U251	U87MG	56.427	2.743	20.569	< .001

Note. P-value adjusted for comparing a family of 3

Output 13.47.:Descriptive statistics and normality (Shapiro-Wilk) assumption checking of U87MG versus U251M versus T98G cells treated with 1200.00 µM temozolomide for 48 hours.

Descriptive Statistics

	Wound closure relative to control at 48hrs (%), Temozolomide		
	T98G	U251	U87MG
Valid	3	3	3
Missing	0	0	0
Mean	95.293	99.200	83.530
Std. Deviation	6.944	1.027	2.537
Shapiro-Wilk	0.779	0.829	0.998
P-value of Shapiro-Wilk	0.066	0.186	0.915
Minimum	87.280	98.020	81.060
Maximum	99.540	99.890	86.130

Note. Excluded 1 rows from the analysis that correspond to the missing values of the split-by variable Cell line _4

Output 13.48.: Equality of Variance (Levene's) assumption checking of U87MG versus U251M versus T98G cells treated with 1200.00 µM temozolomide for 48 hours.

Test for Equality of Variances (Levene's)

F	df1	df2	p
6.965	2.000	6.000	0.027

Output 13.49.: Kruskal-Wallis testing for U87MG versus U251 versus T98G cells treated cell-lines treated with 1200.00 µM temozolomide for 48 hours.

Kruskal-Wallis Test

Factor	Statistic	df	p
Cell line _4	5.956	2	0.051

Output 13.50.: Kruskal-Wallis post-hoc analysis for U87MG versus U251 versus T98G cells treated cell-lines treated with 1200.00 µM temozolomide for 48 hours.

Post Hoc Comparisons - Cell line _4

		Mean Difference	SE	t	p_{tukey}
T98G	U251	−3.907	3.519	−1.110	0.543
	U87MG	11.763	3.519	3.343	0.036
U251	U87MG	15.670	3.519	4.454	0.010

Note. P-value adjusted for comparing a family of 3

Output 13.51.: Descriptive statistics and normality (Shapiro-Wilk) assumption checking of U87MG versus U251M versus T98G cells treated with 1200.00 µM temozolomide for 72 hours.

Descriptive Statistics

	Wound closure relative to control at 72hrs (%), Temozolomide		
	T98G	U251	U87MG
Valid	3	3	3
Missing	0	0	0
Mean	97.710	93.257	88.883
Std. Deviation	0.998	0.864	6.256
Shapiro-Wilk	0.994	0.784	0.987
P-value of Shapiro-Wilk	0.851	0.077	0.782
Minimum	96.670	92.260	83.080
Maximum	98.660	93.790	95.510

Note. Excluded 1 rows from the analysis that correspond to the missing values of the split-by variable Cell line _6

Output 13.52.: Equality of Variance (Levene's) assumption checking of U87MG versus U251M versus T98G cells treated with 1200.00 µM temozolomide for 72 hours.

Test for Equality of Variances (Levene's)

F	df1	df2	p
4.104	2.000	6.000	0.075

Output 13.53.: One-way ANOVA testing for U87MG versus U251 versus T98G cells treated cell-lines treated with 1200.00 µM temozolomide for 72 hours.

ANOVA – Wound closure relative to control at 72hrs (%), Temozolomide

Cases	Sum of Squares	df	Mean Square	F	p
Cell line _6	116.868	2	58.434	4.289	0.070
Residuals	81.754	6	13.626		

Note. Type III Sum of Squares

Output 13.54.: Descriptive statistics and normality (Shapiro-Wilk) assumption checking of U87MG versus U251M versus T98G cells treated with 6.25 µM α-solanine for 24-hours.

Descriptive Statistics

	Wound closure relative to control at 24hrs (%), α-solanine		
	T98G	U251	U87MG
Valid	3	3	3
Missing	0	0	0
Mean	53.500	60.880	5.537
Std. Deviation	8.554	7.987	1.167
Shapiro-Wilk	0.829	0.968	0.955
P-value of Shapiro-Wilk	0.187	0.659	0.590
Minimum	43.670	52.200	4.540
Maximum	59.250	67.920	6.820

Note. Excluded 1 rows from the analysis that correspond to the missing values of the split-by variable Cell line _8

Output 13.55.: Equality of Variance (Levene's) assumption checking of U87MG versus U251M versus T98G cells treated with 6.25 µM α-solanine for 24-hours.

Test for Equality of Variances (Levene's)

F	df1	df2	p
3.811	2.000	6.000	0.085

Output 13.56.: One-way ANOVA testing for U87MG versus U251 versus T98G cells treated cell-lines treated with 6.25 µM α-solanine for 24-hours.

ANOVA - Wound closure relative to control at 24hrs (%), α-solanine

Cases	Sum of Squares	df	Mean Square	F	p
Cell line _8	5417.830	2	2708.915	58.750	< .001
Residuals	276.654	6	46.109		

Note. Type III Sum of Squares

Output 13.57.: One-way ANOVA post-hoc analysis for U87MG versus U251 versus T98G cells treated cell-lines treated with 6.25 µM α-solanine for 24-hours.

Standard

Post Hoc Comparisons - Cell line _8

		Mean Difference	SE	t	p_{tukey}
T98G	U251	−7.380	5.544	−1.331	0.430
	U87MG	47.963	5.544	8.651	< .001
U251	U87MG	55.343	5.544	9.982	< .001

Note. P-value adjusted for comparing a family of 3

Output 13.58.: Descriptive statistics and normality (Shapiro-Wilk) assumption checking of U87MG versus U251M versus T98G cells treated with 6.25 µM α-solanine for 48 hours.

Descriptive Statistics

	Wound closure relative to control at 48hrs (%), α-solanine		
	T98G	U251	U87MG
Valid	3	3	3
Missing	0	0	0
Mean	68.857	95.320	58.200
Std. Deviation	18.102	2.108	18.448
Shapiro-Wilk	0.995	0.964	0.917
P-value of Shapiro-Wilk	0.870	0.637	0.443
Minimum	51.510	93.480	43.590
Maximum	87.630	97.620	78.930

Note. Excluded 1 rows from the analysis that correspond to the missing values of the split-by variable Cell line _8

Output 13.59.: Equality of Variance (Levene's) assumption checking of U87MG versus U251M versus T98G cells treated with 6.25 µM α-solanine for 48 hours.

Test for Equality of Variances (Levene's)

F	df1	df2	p
2.779	2.000	6.000	0.140

Output 13.60.: One-way ANOVA testing for U87MG versus U251 versus T98G cells treated cell-lines treated with 6.25 µM α-solanine for 48 hours.

ANOVA - Wound closure relative to control at 48hrs (%), α-solanine

Cases	Sum of Squares	df	Mean Square	F	p
Cell line _10	2191.767	2	1095.883	4.889	0.055
Residuals	1344.907	6	224.151		

Note. Type III Sum of Squares

Output 13.61.: Descriptive statistics and normality (Shapiro-Wilk) assumption checking of U87MG versus U251M versus T98G cells treated with 6.25 µM α-solanine for 72 hours.

Descriptive Statistics

	Wound closure relative to control at 72hrs (%), α-solanine		
	T98G	U251	U87MG
Valid	3	3	3
Missing	0	0	0
Mean	89.013	87.687	40.423
Std. Deviation	6.478	5.739	3.940
Shapiro-Wilk	0.806	0.997	1.000
P-value of Shapiro-Wilk	0.128	0.892	0.980
Minimum	81.550	81.770	36.460
Maximum	93.180	93.230	44.340

Note. Excluded 1 rows from the analysis that correspond to the missing values of the split-by variable Cell line _12

Output 13.62.: Equality of Variance (Levene's) assumption checking of U87MG versus U251M versus T98G cells treated with 6.25 µM α-solanine for 72 hours.

Test for Equality of Variances (Levene's)

F	df1	df2	p
0.632	2.000	6.000	0.564

Output 13.63.: One-way ANOVA testing for U87MG versus U251 versus T98G cells treated cell-lines treated with 6.25 µM α-solanine for 72 hours.

ANOVA – Wound closure relative to control at 72hrs (%), α–solanine

Cases	Sum of Squares	df	Mean Square	F	p
Cell line _12	4596.571	2	2298.285	76.247	< .001
Residuals	180.856	6	30.143		

Note. Type III Sum of Squares

Output 13.64.: One-way ANOVA post-hoc analysis for U87MG versus U251 versus T98G cells treated cell-lines treated with 6.25 µM α-solanine for 72 hours.

Post Hoc Comparisons – Cell line _12

		Mean Difference	SE	t	p_{tukey}
T98G	U251	1.327	4.483	0.296	0.953
	U87MG	48.590	4.483	10.839	< .001
U251	U87MG	47.263	4.483	10.543	< .001

Note. P–value adjusted for comparing a family of 3

13.2.2. Statistical analysis of relative scratch assay wound closure (%) data glioblastoma cell lines treated with 1200.00 µM temozolomide or 6.25 µM α-solanine for 24-hours versus 48 hours versus 72 hours duration of incubation, per cell line

Output 13.65.: Descriptive statistics and normality (Shapiro-Wilk) assumption checking of U251 cells incubated for 24-hours versus 48 hours versus 72 hours treated with 1200.00 µM temozolomide.

Descriptive Statistics

	Wound closure relative to control U251 (%), Temozolomide		
	24hrs	48hrs	72hrs
Valid	3	3	3
Missing	0	0	0
Mean	82.323	99.200	93.257
Std. Deviation	1.947	1.027	0.864
Shapiro-Wilk	0.803	0.829	0.784
P-value of Shapiro-Wilk	0.123	0.186	0.077
Minimum	80.080	98.020	92.260
Maximum	83.570	99.890	93.790

Note. Excluded 1 rows from the analysis that correspond to the missing values of the split-by variable Duration of incubation

Output 13.66.: Equality of Variance (Levene's) assumption checking of U251 cells incubated for 24-hours versus 48 hours versus 72 hours treated with 1200.00 µM temozolomide.

Test for Equality of Variances (Levene's)

F	df1	df2	p
2.810	2.000	6.000	0.138

Output 13.67.: One-way ANOVA testing for of U251 cells incubated for 24-hours versus 48 hours versus 72 hours treated with 1200.00 µM temozolomide.

ANOVA - Wound closure relative to control U251 (%), Temozolomide

Cases	Sum of Squares	df	Mean Square	F	p
Duration of incubation	439.683	2	219.841	117.971	< .001
Residuals	11.181	6	1.864		

Note. Type III Sum of Squares

Output 13.68.: One-way ANOVA post-hoc analysis for U251 cells incubated for 24-hours versus 48 hours versus 72 hours treated with 1200.00 µM temozolomide.

Standard

Post Hoc Comparisons - Duration of incubation

		Mean Difference	SE	t	p_{tukey}
24hrs	48hrs	−16.877	1.115	−15.141	< .001
	72hrs	−10.933	1.115	−9.809	< .001
48hrs	72hrs	5.943	1.115	5.332	0.004

Note. P-value adjusted for comparing a family of 3

Output 13.69.: Descriptive statistics and normality (Shapiro-Wilk) assumption checking of T98G cells incubated for 24-hours versus 48 hours versus 72 hours treated with 1200.00 µM temozolomide.

Descriptive Statistics

	Wound closure relative to control T98G (%), Temozolomide		
	24hrs	48hrs	72hrs
Valid	3	3	3
Missing	0	0	0
Mean	77.513	95.293	97.710
Std. Deviation	1.870	6.944	0.998
Shapiro-Wilk	1.000	0.779	0.994
P-value of Shapiro-Wilk	0.994	0.066	0.851
Minimum	75.640	87.280	96.670
Maximum	79.380	99.540	98.660

Note. Excluded 1 rows from the analysis that correspond to the missing values of the split-by variable Duration of incubation _16

Output 13.70.: Equality of Variance (Levene's) assumption checking of T98G cells incubated for 24-hours versus 48 hours versus 72 hours treated with 1200.00 µM temozolomide.

Test for Equality of Variances (Levene's)

F	df1	df2	p
8.480	2.000	6.000	0.018

Output 13.71.: Kruskal-Wallis testing for of T98G cells incubated for 24-hours versus 48 hours versus 72 hours treated with 1200.00 µM temozolomide.

Kruskal-Wallis Test

Factor	Statistic	df	p
Duration of incubation _16	5.600	2	0.061

Output 13.72.: Descriptive statistics and normality (Shapiro-Wilk) assumption checking of U87MG cells incubated for 24-hours versus 48 hours versus 72 hours treated with 1200.00 µM temozolomide.

Descriptive Statistics

	Wound closure relative to control at U87MG (%), α-solanine		
	24hrs	48hrs	72hrs
Valid	3	3	3
Missing	0	0	0
Mean	5.537	58.200	40.423
Std. Deviation	1.167	18.448	3.940
Shapiro-Wilk	0.955	0.917	1.000
P-value of Shapiro-Wilk	0.590	0.443	0.980
Minimum	4.540	43.590	36.460
Maximum	6.820	78.930	44.340

Note. Excluded 1 rows from the analysis that correspond to the missing values of the split-by variable Duration of incubation _18

Output 13.73.: Equality of Variance (Levene's) assumption checking of U87MG cells incubated for 24-hours versus 48 hours versus 72 hours treated with 1200.00 µM temozolomide.

Test for Equality of Variances (Levene's)

F	df1	df2	p
7.512	2.000	6.000	0.023

Output 13.74.: Kruskal-Wallis testing for of U87MG cells incubated for 24-hours versus 48 hours versus 72 hours treated with 1200.00 µM temozolomide.

Kruskal-Wallis Test

Factor	Statistic	df	p
Duration of incubation _18	6.489	2	0.039

Output 13.75.: Kruskal-Wallis post-hoc analysis for U87MG cells incubated for 24-hours versus 48 hours versus 72 hours treated with 1200.00 µM temozolomide.

Output 13.76.: Descriptive statistics and normality (Shapiro-Wilk) assumption checking of U251 cells incubated for 24-hours versus 48 hours versus 72 hours treated with 6.25 µM α-solanine.

Descriptive Statistics

	Wound closure relative to control at U251 (%), α-solanine		
	24hrs	48hrs	72hrs
Valid	3	3	3
Missing	0	0	0
Mean	60.880	95.320	87.687
Std. Deviation	7.987	2.108	5.739
Shapiro-Wilk	0.968	0.964	0.997
P-value of Shapiro-Wilk	0.659	0.637	0.892
Minimum	52.200	93.480	81.770
Maximum	67.920	97.620	93.230

Note. Excluded 1 rows from the analysis that correspond to the missing values of the split-by variable Duration of incubation _20

Output 13.77.: Equality of Variance (Levene's) assumption checking of U251 cells incubated for 24-hours versus 48 hours versus 72 hours treated with 6.25 µM α-solanine.

Test for Equality of Variances (Levene's)

F	df1	df2	p
1.700	2.000	6.000	0.260

Output 13.78.: One-way ANOVA testing for of U251 cells incubated for 24-hours versus 48 hours versus 72 hours treated with 6.25 µM α-solanine.

ANOVA – Wound closure relative to control at U251 (%), α–solanine

Cases	Sum of Squares	df	Mean Square	F	p
Duration of incubation _20	1962.979	2	981.489	29.102	< .001
Residuals	202.356	6	33.726		

Note. Type III Sum of Squares

Output 13.79.: One-way ANOVA post-hoc analysis for U251 cells incubated for 24-hours versus 48 hours versus 72 hours treated with 6.25 µM α-solanine.

Standard

Post Hoc Comparisons – Duration of incubation _20

		Mean Difference	SE	t	p_{tukey}
24hrs	48hrs	−34.440	4.742	−7.263	< .001
	72hrs	−26.807	4.742	−5.653	0.003
48hrs	72hrs	7.633	4.742	1.610	0.312

Note. P–value adjusted for comparing a family of 3

Output 13.80.: Descriptive statistics and normality (Shapiro-Wilk) assumption checking of T98G cells incubated for 24-hours versus 48 hours versus 72 hours treated with 6.25 µM α-solanine.

Descriptive Statistics

	Wound closure relative to control at T98G (%), α–solanine		
	24hrs	48hrs	72hrs
Valid	3	3	3
Missing	0	0	0
Mean	53.500	68.857	89.013
Std. Deviation	8.554	18.102	6.478
Shapiro–Wilk	0.829	0.995	0.806
P–value of Shapiro–Wilk	0.187	0.870	0.128
Minimum	43.670	51.510	81.550
Maximum	59.250	87.630	93.180

Note. Excluded 1 rows from the analysis that correspond to the missing values of the split–by variable Duration of incubation _22

Output 13.81.: Equality of Variance (Levene's) assumption checking of T98G cells incubated for 24-hours versus 48 hours versus 72 hours treated with 6.25 µM α-solanine.

Test for Equality of Variances (Levene's)

F	df1	df2	p
1.339	2.000	6.000	0.331

Output 13.82.: One-way ANOVA testing for of T98G cells incubated for 24-hours versus 48 hours versus 72 hours treated with 6.25 µM α-solanine.

ANOVA – Wound closure relative to control at T98G (%), α−solanine

Cases	Sum of Squares	df	Mean Square	F	p
Duration of incubation _22	1903.315	2	951.658	6.447	0.032
Residuals	885.649	6	147.608		

Note. Type III Sum of Squares

Output 13.83.: One-way ANOVA post-hoc analysis for T98G cells incubated for 24-hours versus 48 hours versus 72 hours treated with 6.25 µM α-solanine.

Standard

Post Hoc Comparisons – Duration of incubation _22

		Mean Difference	SE	t	p_{tukey}
24hrs	48hrs	−15.357	9.920	−1.548	0.336
	72hrs	−35.513	9.920	−3.580	0.027
48hrs	72hrs	−20.157	9.920	−2.032	0.185

Note. P−value adjusted for comparing a family of 3

Output 13.84.: Descriptive statistics and normality (Shapiro-Wilk) assumption checking of U87MG cells incubated for 24-hours versus 48 hours versus 72 hours treated with 6.25 µM α-solanine.

Descriptive Statistics

	Wound closure relative to control at U87MG (%) @ 24 hours		
	24hrs	48hrs	72hrs
Valid	3	3	0
Missing	0	0	3
Mean	25.897	5.537	NaN
Std. Deviation	5.155	1.167	NaN
Shapiro-Wilk	0.920	0.955	NaN[a]
P-value of Shapiro-Wilk	0.452	0.590	NaN[a]
Minimum	20.110	4.540	∞[b]
Maximum	30.000	6.820	-∞[b]

Note. Excluded 1 rows from the analysis that correspond to the missing values of the split-by variable Duration of incubation _24

[a] All values are identical

[b] Infimum (minimum) of an empty set is ∞, supremum (maximum) of an empty set is -∞.

Output 13.85.: Equality of Variance (Levene's) assumption checking of U87MG cells incubated for 24-hours versus 48 hours versus 72 hours treated with 6.25 µM α-solanine.

Test for Equality of Variances (Levene's)

F	df1	df2	p
5.985	1.000	4.000	0.071

Output 13.86.: One-way ANOVA testing for of U87MG cells incubated for 24-hours versus 48 hours versus 72 hours treated with 6.25 µM α-solanine.

ANOVA - Wound closure relative to control at U87MG (%) @ 24 hours

Cases	Sum of Squares	df	Mean Square	F	p
Duration of incubation _24	621.794	1	621.794	44.510	0.003
Residuals	55.879	4	13.970		

Note. Type III Sum of Squares

Output 13.87.: One-way ANOVA post-hoc analysis for U87MG cells incubated for 24-hours versus 48 hours versus 72 hours treated with 6.25 µM α-solanine.

Standard

Post Hoc Comparisons - Duration of incubation _24

		Mean Difference	SE	t	p_{tukey}
24hrs	48hrs	20.360	3.052	6.672	0.003

13.2.3. Statistical analysis comparing relative scratch assay wound closure (%) data of glioblastoma cell lines treated with 1200.00 µM temozolomide versus 6.25 µM α-solanine at 24-hours, 48 hours or 72 hours duration of incubation.

Output 13.88.: Descriptive statistics of U87MG cells treated with 1200.00 µM temozolomide versus with 6.25 µM α-solanine incubated for 24-hours.

Descriptive Statistics

	Wound closure relative to control at U87MG (%) @ 24 hours	
	Temozolomide	α-solanine
Valid	3	3
Missing	0	0
Mean	25.897	5.537
Std. Deviation	5.155	1.167
Minimum	20.110	4.540
Maximum	30.000	6.820

Note. Excluded 4 rows from the analysis that correspond to the missing values of the split-by variable Drug

Output 13.89.: Normality (Shapiro-Wilk) and Equality of Variance (Levene's) assumption checks for pairwise sample testing for U87MG cells treated with 1200.00 µM temozolomide versus with 6.25 µM α-solanine incubated for 24-hours.

Test of Normality (Shapiro-Wilk)

		W	p
Wound closure relative to control at U87MG (%) @ 24 hours	Temozolomide	0.920	0.452
	α-solanine	0.955	0.590

Note. Significant results suggest a deviation from normality.

Test of Equality of Variances (Levene's)

	F	df	p
Wound closure relative to control at U87MG (%) @ 24 hours	5.985	1	0.071

Output 13.90.: Independent sample T-testing for U87MG cells treated with 1200.00 µM temozolomide versus with 6.25 µM α-solanine incubated for 24-hours.

Independent Samples T-Test

	t	df	p
Wound closure relative to control at U87MG (%) @ 24 hours	6.672	4	0.003

Note. Student's t-test.

Output 13.91.: Descriptive statistics of U251 cells treated with 1200.00 µM temozolomide versus with 6.25 µM α-solanine incubated for 24-hours.

Descriptive Statistics

	Wound closure relative to control at U251 (%) @ 24 hours	
	Temozolomide	α-solanine
Valid	3	3
Missing	0	0
Mean	82.323	60.880
Std. Deviation	1.947	7.987
Minimum	80.080	52.200
Maximum	83.570	67.920

Note. Excluded 4 rows from the analysis that correspond to the missing values of the split-by variable Drug _28

Output 13.92.: Normality (Shapiro-Wilk) and Equality of Variance (Levene's) assumption checks for pairwise sample testing for U251 cells treated with 1200.00 µM temozolomide versus with 6.25 µM α-solanine incubated for 24-hours.

Test of Normality (Shapiro-Wilk)

		W	p
Wound closure relative to control at U251 (%) @ 24 hours	Temozolomide	0.803	0.123
	α-solanine	0.968	0.659

Note. Significant results suggest a deviation from normality.

Test of Equality of Variances (Levene's)

	F	df	p
Wound closure relative to control at U251 (%) @ 24 hours	3.945	1	0.118

Output 13.93.: Independent sample T-testing for U251 cells treated with 1200.00 µM temozolomide versus with 6.25 µM α-solanine incubated for 24-hours.

Independent Samples T-Test

	t	df	p
Wound closure relative to control at U251 (%) @ 24 hours	4.518	4	0.011

Note. Student's t-test.

Output 13.94.: Descriptive statistics of T98G cells treated with 1200.00 µM temozolomide versus with 6.25 µM α-solanine incubated for 24-hours.

Descriptive Statistics

	Wound closure relative to control at T98G (%) @ 24 hours	
	Temozolomide	α-solanine
Valid	3	3
Missing	0	0
Mean	77.513	53.500
Std. Deviation	1.870	8.554
Minimum	75.640	43.670
Maximum	79.380	59.250

Note. Excluded 4 rows from the analysis that correspond to the missing values of the split-by variable Drug _30

Output 13.95.: Normality (Shapiro-Wilk) and Equality of Variance (Levene's) assumption checks for pairwise sample testing for T98G cells treated with 1200.00 µM temozolomide versus with 6.25 µM α-solanine incubated for 24-hours.

Test of Normality (Shapiro-Wilk)

		W	p
Wound closure relative to control at T98G (%) @ 24 hours	Temozolomide	1.000	0.994
	α-solanine	0.829	0.187

Note. Significant results suggest a deviation from normality.

Test of Equality of Variances (Levene's)

	F	df	p
Wound closure relative to control at T98G (%) @ 24 hours	8.520	1	0.043

Output 13.96.: Welch T-testing for T98G cells treated with 1200.00 µM temozolomide versus with 6.25 µM α-solanine incubated for 24-hours.

Independent Samples T-Test

	t	df	p
Wound closure relative to control at T98G (%) @ 24 hours	4.750	2.191	0.035

Note. Welch's t-test.

Output 13.97.: Descriptive statistics of U87MG cells treated with 1200.00 µM temozolomide versus with 6.25 µM α-solanine incubated for 48 hours.

Descriptive Statistics

	Wound closure relative to control at U87MG (%) @ 48 hours	
	Temozolomide	α-solanine
Valid	3	3
Missing	0	0
Mean	83.530	58.200
Std. Deviation	2.537	18.448
Minimum	81.060	43.590
Maximum	86.130	78.930

Note. Excluded 4 rows from the analysis that correspond to the missing values of the split-by variable Drug _32

Output 13.98.: Normality (Shapiro-Wilk) and Equality of Variance (Levene's) assumption checks for pairwise sample testing for U87MG cells treated with 1200.00 µM temozolomide versus with 6.25 µM α-solanine incubated for 48 hours.

Test of Normality (Shapiro-Wilk)

		W	p
Wound closure relative to control at U87MG (%) @ 48 hours	Temozolomide	0.998	0.915
	α-solanine	0.917	0.443

Note. Significant results suggest a deviation from normality.

Test of Equality of Variances (Levene's)

	F	df	p
Wound closure relative to control at U87MG (%) @ 48 hours	7.859	1	0.049

Output 13.99.: Welch T-testing for U87MG cells treated with 1200.00 µM temozolomide versus with 6.25 µM α-solanine incubated for 48 hours.

Independent Samples T-Test

	t	df	p
Wound closure relative to control at U87MG (%) @ 48 hours	2.356	2.076	0.138

Note. Welch's t-test.

Output 13.100.: Descriptive statistics of U251 cells treated with 1200.00 µM temozolomide versus with 6.25 µM α-solanine incubated for 48 hours.

Descriptive Statistics

	Wound closure relative to control at U251 (%) @ 48 hours	
	Temozolomide	α-solanine
Valid	3	3
Missing	0	0
Mean	99.200	95.320
Std. Deviation	1.027	2.108
Minimum	98.020	93.480
Maximum	99.890	97.620

Note. Excluded 4 rows from the analysis that correspond to the missing values of the split-by variable Drug _34

Output 13.101.: Normality (Shapiro-Wilk) and Equality of Variance (Levene's) assumption checks for pairwise sample testing for U251 cells treated with 1200.00 µM temozolomide versus with 6.25 µM α-solanine incubated for 48 hours.

Test of Normality (Shapiro-Wilk)

		W	p
Wound closure relative to control at U251 (%) @ 48 hours	Temozolomide	0.829	0.186
	α-solanine	0.964	0.637

Note. Significant results suggest a deviation from normality.

Test of Equality of Variances (Levene's)

	F	df	p
Wound closure relative to control at U251 (%) @ 48 hours	1.604	1	0.274

Output 13.102.: Independent sample T-testing for U251 cells treated with 1200.00 µM temozolomide versus with 6.25 µM α-solanine incubated for 48 hours.

Independent Samples T-Test

	t	df	p
Wound closure relative to control at U251 (%) @ 48 hours	2.866	4	0.046

Note. Student's t-test.

Output 13.103.: Descriptive statistics of T98G cells treated with 1200.00 µM temozolomide versus with 6.25 µM α-solanine incubated for 48 hours.

Descriptive Statistics

	Wound closure relative to control at T98G (%) @ 48 hours	
	Temozolomide	α-solanine
Valid	3	3
Missing	0	0
Mean	95.293	68.857
Std. Deviation	6.944	18.102
Minimum	87.280	51.510
Maximum	99.540	87.630

Note. Excluded 4 rows from the analysis that correspond to the missing values of the split-by variable Drug _36

Output 13.104.: Normality (Shapiro-Wilk) and Equality of Variance (Levene's) assumption checks for pairwise sample testing for T98G cells treated with 1200.00 µM temozolomide versus with 6.25 µM α-solanine incubated for 48 hours.

Test of Normality (Shapiro-Wilk)

		W	p
Wound closure relative to control at T98G (%) @ 48 hours	Temozolomide	0.779	0.066
	α-solanine	0.995	0.870

Note. Significant results suggest a deviation from normality.

Test of Equality of Variances (Levene's)

	F	df	p
Wound closure relative to control at T98G (%) @ 48 hours	1.573	1	0.278

Output 13.105.: Independent sample T-testing for T98G cells treated with 1200.00 µM temozolomide versus with 6.25 µM α-solanine incubated for 48 hours.

Independent Samples T-Test

	t	df	p
Wound closure relative to control at T98G (%) @ 48 hours	2.362	4	0.078

Note. Student's t-test.

Output 13.106.: Descriptive statistics of U87MG cells treated with 1200.00 µM temozolomide versus with 6.25 µM α-solanine incubated for 72 hours.

Descriptive Statistics

	Wound closure relative to control at U87MG (%) @ 72 hours	
	Temozolomide	α-solanine
Valid	3	3
Missing	0	0
Mean	88.883	40.423
Std. Deviation	6.256	3.940
Minimum	83.080	36.460
Maximum	95.510	44.340

Note. Excluded 4 rows from the analysis that correspond to the missing values of the split-by variable Drug _38

Output 13.107.: Normality (Shapiro-Wilk) and Equality of Variance (Levene's) assumption checks for pairwise sample testing for U87MG cells treated with 1200.00 µM temozolomide versus with 6.25 µM α-solanine incubated for 72 hours.

Test of Normality (Shapiro-Wilk)

		W	p
Wound closure relative to control at U87MG (%) @ 72 hours	Temozolomide	0.987	0.782
	α-solanine	1.000	0.980

Note. Significant results suggest a deviation from normality.

Test of Equality of Variances (Levene's)

	F	df	p
Wound closure relative to control at U87MG (%) @ 72 hours	0.634	1	0.470

Output 13.108.: Independent sample T-testing for U87MG cells treated with 1200.00 µM temozolomide versus with 6.25 µM α-solanine incubated for 72 hours.

Independent Samples T-Test

	t	df	p
Wound closure relative to control at U87MG (%) @ 72 hours	11.353	4	< .001

Note. Student's t-test.

Output 13.109.: Descriptive statistics of U251 cells treated with 1200.00 µM temozolomide versus with 6.25 µM α-solanine incubated for 72 hours.

Descriptive Statistics

	Wound closure relative to control at U251 (%) @ 72 hours	
	Temozolomide	α-solanine
Valid	3	3
Missing	0	0
Mean	93.257	87.687
Std. Deviation	0.864	5.739
Minimum	92.260	81.770
Maximum	93.790	93.230

Note. Excluded 4 rows from the analysis that correspond to the missing values of the split-by variable Drug _40

Output 13.110.: Normality (Shapiro-Wilk) and Equality of Variance (Levene's) assumption checks for pairwise sample testing for U251 cells treated with 1200.00 µM temozolomide versus with 6.25 µM α-solanine incubated for 72 hours.

Test of Normality (Shapiro–Wilk)

		W	p
Wound closure relative to control at U251 (%) @ 72 hours	Temozolomide	0.784	0.077
	α–solanine	0.997	0.892

Note. Significant results suggest a deviation from normality.

Test of Equality of Variances (Levene's)

	F	df	p
Wound closure relative to control at U251 (%) @ 72 hours	3.333	1	0.142

Output 13.111.: Independent sample T-testing for U251 cells treated with 1200.00 µM temozolomide versus with 6.25 µM α-solanine incubated for 72 hours.

Independent Samples T–Test

	t	df	p
Wound closure relative to control at U251 (%) @ 72 hours	1.662	4	0.172

Note. Student's t–test.

Output 13.112.: Descriptive statistics of T98G cells treated with 1200.00 µM temozolomide versus with 6.25 µM α-solanine incubated for 72 hours.

Descriptive Statistics

	Wound closure relative to control at T98G (%) @ 72 hours	
	Temozolomide	α–solanine
Valid	3	3
Missing	0	0
Mean	97.710	89.013
Std. Deviation	0.998	6.478
Minimum	96.670	81.550
Maximum	98.660	93.180

Note. Excluded 4 rows from the analysis that correspond to the missing values of the split–by variable Drug _42

Output 13.113.: Normality (Shapiro-Wilk) and Equality of Variance (Levene's) assumption checks for pairwise sample testing for T98G cells treated with 1200.00 µM temozolomide versus with 6.25 µM α-solanine incubated for 72 hours.

Test of Normality (Shapiro-Wilk)

		W	p
Wound closure relative to control at T98G (%) @ 72 hours	Temozolomide	0.994	0.851
	α-solanine	0.806	0.128

Note. Significant results suggest a deviation from normality.

Test of Equality of Variances (Levene's)

	F	df	p
Wound closure relative to control at T98G (%) @ 72 hours	10.774	1	0.030

Output 13.114.: Welch T-testing for T98G cells treated with 1200.00 µM temozolomide versus with 6.25 µM α-solanine incubated for 72 hours.

Independent Samples T-Test

	t	df	p
Wound closure relative to control at T98G (%) @ 72 hours	2.298	2.095	0.143

Note. Welch's t-test.

13.2.4. Statistical analysis of relative rate of scratch assay wound closure (%) data of glioblastoma cell lines treated with 1200.00 µM temozolomide versus 6.25 µM α-solanine

Output 13.115.: Descriptive statistics of relative rate of migration of U87MG cells treated with 1200.00 µM temozolomide versus with 6.25 µM α-solanine.

Descriptive Statistics

	Relative rate of wound closure	
	U87MG TMZ	U87MG ∝-solanine
Valid	3	3
Missing	0	0
Mean	1.312	0.727
Std. Deviation	0.237	0.106
Minimum	1.106	0.618
Maximum	1.571	0.829

Note. Excluded 3 rows from the analysis that correspond to the missing values of the split-by variable Cell line_Treatment condition

Output 13.116.: Normality (Shapiro-Wilk) and Equality of Variance (Levene's) assumption checks for pairwise sample testing for relative rate of migration of U87MG cells treated with 1200.00 µM temozolomide versus with 6.25 µM α-solanine.

Test of Normality (Shapiro-Wilk)

		W	p
Relative rate of wound closure	U87MG TMZ	0.964	0.633
	U87MG ∝-solanine	0.997	0.892

Note. Significant results suggest a deviation from normality.

Test of Equality of Variances (Levene's)

	F	df	p
Relative rate of wound closure	2.010	1	0.229

Output 13.117.: Independent sample T-testing for relative rate of migration of U87MG cells treated with 1200.00 µM temozolomide versus with 6.25 µM α-solanine.

Independent Samples T-Test

	t	df	p
Relative rate of wound closure	3.907	4	0.017

Note. Student's t-test.

Output 13.118.: Descriptive statistics of relative rate of migration of U251 cells treated with 1200.00 µM temozolomide versus with 6.25 µM α-solanine.

Descriptive Statistics

	Relative rate of wound closure_4	
	U251 TMZ	U251 ∝-solanine
Valid	3	3
Missing	0	0
Mean	0.352	0.558
Std. Deviation	0.020	0.240
Minimum	0.336	0.289
Maximum	0.374	0.747

Note. Excluded 3 rows from the analysis that correspond to the missing values of the split-by variable Cell line_Treatment condition_3

Output 13.119.: Normality (Shapiro-Wilk) and Equality of Variance (Levene's) assumption checks for pairwise sample testing for relative rate of migration of U251 cells treated with 1200.00 µM temozolomide versus with 6.25 µM α-solanine.

Test of Normality (Shapiro-Wilk)

		W	p
Relative rate of wound closure_4	U251 TMZ	0.922	0.458
	U251 ∝-solanine	0.914	0.431

Note. Significant results suggest a deviation from normality.

Test of Equality of Variances (Levene's)

	F	df	p
Relative rate of wound closure_4	9.083	1	0.039

Output 13.120.: Independent sample T-testing for relative rate of migration of U251 cells treated with 1200.00 µM temozolomide versus with 6.25 µM α-solanine.

Independent Samples T-Test

	W	df	p
Relative rate of wound closure_4	3.000		0.700

Note. Mann-Whitney U test.

Output 13.121.: Descriptive statistics of relative rate of migration of T98G cells treated with 1200.00 µM temozolomide versus with 6.25 µM α-solanine.

Descriptive Statistics

	Relative rate of wound closure_6	
	T98G TMZ	T98G ∝-solanine
Valid	3	3
Missing	0	0
Mean	0.421	0.320
Std. Deviation	0.054	0.265
Minimum	0.360	0.163
Maximum	0.462	0.626

Note. Excluded 3 rows from the analysis that correspond to the missing values of the split-by variable Cell line_Treatment condition_5

Output 13.122.: Normality (Shapiro-Wilk) and Equality of Variance (Levene's) assumption checks for pairwise sample testing for relative rate of migration of T98G cells treated with 1200.00 µM temozolomide versus with 6.25 µM α-solanine.

Test of Normality (Shapiro-Wilk)

		W	p
Relative rate of wound closure_6	T98G TMZ	0.899	0.382
	T98G ∝-solanine	0.761	0.026

Note. Significant results suggest a deviation from normality.

Test of Equality of Variances (Levene's)

	F	df	p
Relative rate of wound closure_6	9.757	1	0.035

Output 13.123.: Independent sample T-testing for relative rate of migration of T98G cells treated with 1200.00 µM temozolomide versus with 6.25 µM α-solanine.

Independent Samples T-Test

	t	df	p
Relative rate of wound closure_6	0.646	2.163	0.580

Note. Welch's t-test.

Output 13.124.: Descriptive statistics and normality (Shapiro-Wilk) assumption checking of relative rate of migration of U87MG versus U251 versus T98G cells treated with 1200.00 µM temozolomide.

Descriptive Statistics

	Relative rate of wound closure_8		
	T98G TMZ	U251 TMZ	U87MG TMZ
Valid	3	3	3
Missing	0	0	0
Mean	0.421	0.352	1.312
Std. Deviation	0.054	0.020	0.237
Shapiro-Wilk	0.899	0.922	0.964
P-value of Shapiro-Wilk	0.382	0.458	0.633
Minimum	0.360	0.336	1.106
Maximum	0.462	0.374	1.571

Output 13.125.: Equality of Variance (Levene's) assumption checks for one-way ANOVA testing of relative rate of migration of U87MG versus U251 versus T98G cells treated with 1200.00 µM temozolomide.

Test for Equality of Variances (Levene's)

F	df1	df2	p
5.369	2.000	6.000	0.046

Output 13.126.: Kruskal-Wallis testing for relative rate of migration of U87MG versus U251 versus T98G cells treated with 1200.00 µM temozolomide.

Kruskal-Wallis Test

Factor	Statistic	df	p
Cell line_Treatment condition_7	6.489	2	0.039

Output 13.127.: One-way ANOVA post-hoc analysis for relative rate of migration of U87MG versus U251 versus T98G cells treated with 1200.00 µM temozolomide.

Standard

Post Hoc Comparisons - Cell line_Treatment condition_7

		Mean Difference	SE	t	p_{tukey}
T98G TMZ	U251 TMZ	0.069	0.115	0.602	0.824
	U87MG TMZ	−0.891	0.115	−7.762	< .001
U251 TMZ	U87MG TMZ	−0.961	0.115	−8.364	< .001

Note. P-value adjusted for comparing a family of 3

Output 13.128.: Descriptive statistics and normality (Shapiro-Wilk) assumption checking of relative rate of migration of U87MG versus U251 versus T98G cells treated with 6.25 µM α-solanine.

Descriptive Statistics

	Relative rate of wound closure_10		
	T98G ∝-solanine	U251 ∝-solanine	U87MG ∝-solanine
Valid	3	3	3
Missing	0	0	0
Mean	0.320	0.558	0.727
Std. Deviation	0.265	0.240	0.106
Shapiro-Wilk	0.761	0.914	0.997
P-value of Shapiro-Wilk	0.026	0.431	0.892
Minimum	0.163	0.289	0.618
Maximum	0.626	0.747	0.829

Output 13.129.: Equality of Variance (Levene's) assumption checks for one-way ANOVA testing of relative rate of migration of U87MG versus U251 versus T98G cells treated with 6.25 µM α-solanine.

Test for Equality of Variances (Levene's)

F	df1	df2	p
2.190	2.000	6.000	0.193

Output 13.130.: Kruskal-Wallis testing for relative rate of migration of U87MG versus U251 versus T98G cells treated with 6.25 µM α-solanine.

ANOVA – Relative rate of wound closure_10

Cases	Sum of Squares	df	Mean Square	F	p
Cell line_Treatment condition_9	0.251	2	0.125	2.705	0.145
Residuals	0.278	6	0.046		

Note. Type III Sum of Squares

13.3. Statistical analysis of trans-well invasion assays

Output 13.131.: Chi-square analysis for trans-well invasion assay data of U87MG cells treated with α-solanine versus temozolomide for 72 hours.

U87MG α-solanine vs Temozolomide			
Observed			
	α-solanine	**Temozolomide**	**Total**
R1	2	29	31
R2	5	33	38
R3	1	21	22
Totals	8	83	91
Expected			
	α-solanine	**Temozolomide**	
R1	2.725274725	28.27472527	
R2	3.340659341	34.65934066	
R3	1.934065934	20.06593407	
p-value	**0.44711771**		

Output 13.132.: Chi-square analysis for trans-well invasion assay data of U251 cells treated with α-solanine versus Temozolomide for 72 hours.

U251 α-solanine vs Temozolomide			
Observed			
	α-solanine	Temozolomide	Total
R1	5	0	5
R2	6	0	6
R3	6	2	8
Totals	17	2	19
Expected			
	α-solanine	Temozolomide	
R1	4.473684211	0.526315789	
R2	5.368421053	0.631578947	
R3	7.157894737	0.842105263	
p-value	0.215075811		

Output 13.133.: Chi-square analysis for trans-well invasion assay data of T98G cells treated with α-solanine versus Temozolomide for 72 hours.

T98G α-solanine vs Temozolomide			
Observed			
	α-solanine	Temozolomide	Total
R1	21	25	46
R2	15	24	39
R3	10	13	23
Totals	46	62	108
Expected			
	α-solanine	Temozolomide	
R1	19.59259259	26.40740741	
R2	16.61111111	22.38888889	
R3	9.796296296	13.2037037	
p-value	0.79624988		

Output 13.134.:Chi-square analysis for trans-well invasion assay data of U87MG versus U251 versus T98G cells treated with α-solanine for 72 hours.

U87MG vs U251 vs T98G Temozolomide				
Observed				
	U87MG	U251	T98G	Total
R1	29	0	25	29
R2	33	0	24	33
R3	21	2	13	23
Totals	83	2	62	85
Expected				
	U87MG	U251	T98G	
R1	28.3176471	0.6823529	21.152941	
R2	32.2235294	0.7764706	24.070588	
R3	22.4588235	0.5411765	16.776471	
p-value	0.1321739			

Output 13.135.: Chi-square analysis for trans-well invasion assay data of U87MG versus U251 versus T98G cells treated with temozolomide for 72 hours.

U87MG vs U251 vs T98G Temozolomide				
Observed				
	U87MG	U251	T98G	Total
R1	29	0	25	29
R2	33	0	24	33
R3	21	2	13	23
Totals	83	2	62	85
Expected				
	U87MG	U251	T98G	
R1	28.3176471	0.6823529	21.152941	
R2	32.2235294	0.7764706	24.070588	
R3	22.4588235	0.5411765	16.776471	
p-value	0.1321739			

13.4. Statistical analysis of real-time quantitative polymerase chain reaction experiments

Output 13.136.: Descriptive statistics and normality (Shapiro-Wilk) assumption checking of real time quantitative polymerase chain reaction data of fold change in expression of the Bax gene in glioblastoma multiforme cells treated with 1200.00 µM temozolomide versus 6.25 µM α-solanine versus 5.00 mM H_2O_2 incubated for 24-hours.

Descriptive Statistics

	Bax		
	H202	TMZ	solanine
Valid	6	6	6
Missing	0	0	0
Mean	21.257	21.150	24.460
Std. Deviation	0.762	1.049	1.046
Shapiro-Wilk	0.854	0.873	0.748
P-value of Shapiro-Wilk	0.168	0.237	0.019
Minimum	20.100	20.090	23.040
Maximum	21.930	22.650	25.290

Note. Excluded 24 rows from the analysis that correspond to the missing values of the split-by variable treatment condition

Output 13.137.: Equality of Variance (Levene's) assumption checks for one-way ANOVA testing of real time quantitative polymerase chain reaction data of fold change in expression of the Bax gene in glioblastoma multiforme cells treated with 1200.00 µM temozolomide versus 6.25 µM α-solanine versus 5.00 mM H_2O_2 incubated for 24-hours.

Test for Equality of Variances (Levene's)

F	df1	df2	p
0.874	2.000	15.000	0.438

Output 13.138.: Kruskal-Wallis testing for relative rate real time quantitative polymerase chain reaction data of fold change in expression of the Bax gene in glioblastoma multiforme cells treated with 1200.00 µM temozolomide versus 6.25 µM α-solanine versus 5.00 mM H_2O_2 incubated for 24-hours.

Kruskal–Wallis Test

Factor	Statistic	df	p
treatment condition	11.380	2	0.003

Output 13.139.: Kruskal-Wallis post-hoc analysis for relative rate real time quantitative polymerase chain reaction data of fold change in expression of the Bax gene in glioblastoma multiforme cells treated with 1200.00 µM temozolomide versus 6.25 µM α-solanine versus 5.00 mM H_2O_2 incubated for 24-hours.

Standard

Post Hoc Comparisons – treatment condition

		Mean Difference	SE	t	p_{tukey}
H202	TMZ	0.107	0.555	0.192	0.980
	solanine	−3.203	0.555	−5.770	< .001
TMZ	solanine	−3.310	0.555	−5.962	< .001

Note. P–value adjusted for comparing a family of 3

Output 13.140.: Descriptive statistics and normality (Shapiro-Wilk) assumption checking of real time quantitative polymerase chain reaction data of fold change in expression of the BECN1 gene in glioblastoma multiforme cells treated with 1200.00 µM temozolomide versus 6.25 µM α-solanine versus 5.00 mM H_2O_2 incubated for 24-hours.

Descriptive Statistics

	BECN1		
	H202	TMZ	solanine
Valid	6	6	6
Missing	0	0	0
Mean	21.775	21.537	25.480
Std. Deviation	0.696	0.869	0.617
Shapiro-Wilk	0.847	0.820	0.865
P-value of Shapiro-Wilk	0.148	0.089	0.207
Minimum	21.110	20.710	24.740
Maximum	22.820	22.740	26.240

Note. Excluded 24 rows from the analysis that correspond to the missing values of the split-by variable treatment condition

Output 13.141.: Equality of Variance (Levene's) assumption checks for one-way ANOVA testing of real time quantitative polymerase chain reaction data of fold change in expression of the BECN1 gene in glioblastoma multiforme cells treated with 1200.00 µM temozolomide versus 6.25 µM α-solanine versus 5.00 mM H_2O_2 incubated for 24-hours.

Test for Equality of Variances (Levene's)

F	df1	df2	p
0.904	2.000	15.000	0.426

Output 13.142.: One-way ANOVA testing for relative rate real time quantitative polymerase chain reaction data of fold change in expression of the BECN1 gene in glioblastoma multiforme cells treated with 1200.00 µM temozolomide versus 6.25 µM α-solanine versus 5.00 mM H_2O_2 incubated for 24-hours.

ANOVA - BECN1

Cases	Sum of Squares	df	Mean Square	F	p
treatment condition	58.667	2	29.334	54.277	< .001
Residuals	8.107	15	0.540		

Note. Type III Sum of Squares

Output 13.143.: One-way ANOVA post-hoc analysis for relative rate real time quantitative polymerase chain reaction data of fold change in expression of the BECN1 gene in glioblastoma

multiforme cells treated with 1200.00 µM temozolomide versus 6.25 µM α-solanine versus 5.00 mM H_2O_2 incubated for 24-hours.

Standard

Post Hoc Comparisons – treatment condition

		Mean Difference	SE	t	p_{tukey}
H202	TMZ	0.238	0.424	0.562	0.842
	solanine	−3.705	0.424	−8.729	< .001
TMZ	solanine	−3.943	0.424	−9.291	< .001

Note. P-value adjusted for comparing a family of 3

Output 13.144.: Descriptive statistics and normality (Shapiro-Wilk) assumption checking of real time quantitative polymerase chain reaction data of fold change in expression of the Casp-3 gene in glioblastoma multiforme cells treated with 1200.00 µM temozolomide versus 6.25 µM α-solanine versus 5.00 mM H_2O_2 incubated for 24-hours.

Descriptive Statistics

	Casp3		
	H202	TMZ	solanine
Valid	6	6	6
Missing	0	0	0
Mean	35.108	34.973	36.445
Std. Deviation	1.298	0.477	0.797
Shapiro-Wilk	0.937	0.984	0.782
P-value of Shapiro-Wilk	0.634	0.970	0.040
Minimum	33.610	34.300	34.920
Maximum	37.360	35.690	37.030

Note. Excluded 24 rows from the analysis that correspond to the missing values of the split-by variable treatment condition

Output 13.145.: Equality of Variance (Levene's) assumption checks for one-way ANOVA testing of real time quantitative polymerase chain reaction data of fold change in expression of the Casp-3 gene in glioblastoma multiforme cells treated with 1200.00 µM temozolomide versus 6.25 µM α-solanine versus 5.00 mM H_2O_2 incubated for 24-hours.

Assumption Checks

Test for Equality of Variances (Levene's)

F	df1	df2	p
1.755	2.000	15.000	0.207

Output 13.146.: Kruskal-Wallis testing for relative rate real time quantitative polymerase chain reaction data of fold change in expression of the Casp-3 gene in glioblastoma multiforme cells treated with 1200.00 µM temozolomide versus 6.25 µM α-solanine versus 5.00 mM H_2O_2 incubated for 24-hours.

Kruskal-Wallis Test

Factor	Statistic	df	p
treatment condition	5.075	2	0.079

Output 13.147.: Descriptive statistics and normality (Shapiro-Wilk) assumption checking of real time quantitative polymerase chain reaction data of fold change in expression of the PKM2 gene in glioblastoma multiforme cells treated with 1200.00 µM temozolomide versus 6.25 µM α-solanine versus 5.00 mM H_2O_2 incubated for 24-hours.

Descriptive Statistics

	PKM2		
	H202	TMZ	solanine
Valid	6	6	6
Missing	0	0	0
Mean	22.538	15.508	18.750
Std. Deviation	10.485	1.094	1.067
Shapiro-Wilk	0.716	0.741	0.816
P-value of Shapiro-Wilk	0.009	0.016	0.082
Minimum	15.020	14.580	17.340
Maximum	37.360	16.930	19.770

Note. Excluded 24 rows from the analysis that correspond to the missing values of the split-by variable treatment condition

Output 13.148.: Equality of Variance (Levene's) assumption checks for one-way ANOVA testing of real time quantitative polymerase chain reaction data of fold change in expression of the PKM2 gene

in glioblastoma multiforme cells treated with 1200.00 µM temozolomide versus 6.25 µM α-solanine versus 5.00 mM H_2O_2 incubated for 24-hours.

Test for Equality of Variances (Levene's)

F	df1	df2	p
28.828	2.000	15.000	< .001

Output 13.149.: Kruskal-Wallis testing for relative rate real time quantitative polymerase chain reaction data of fold change in expression of the PKM2 gene in glioblastoma multiforme cells treated with 1200.00 µM temozolomide versus 6.25 µM α-solanine versus 5.00 mM H_2O_2 incubated for 24-hours.

Kruskal–Wallis Test

Factor	Statistic	df	p
treatment condition	8.047	2	0.018

Output 13.150.: Kruskal-Wallis post-hoc analysis for relative rate real time quantitative polymerase chain reaction data of fold change in expression of the PKM2 gene in glioblastoma multiforme cells treated with 1200.00 µM temozolomide versus 6.25 µM α-solanine versus 5.00 mM H_2O_2 incubated for 24-hours.

Post Hoc Comparisons – treatment condition

		Mean Difference	SE	t	p_{tukey}
H202	TMZ	7.030	3.532	1.990	0.149
	solanine	3.788	3.532	1.073	0.545
TMZ	solanine	−3.242	3.532	−0.918	0.638

Note. P–value adjusted for comparing a family of 3

Output 13.151.: Descriptive statistics and normality (Shapiro-Wilk) assumption checking of real time quantitative polymerase chain reaction data of fold change in expression of the VEGFA gene in glioblastoma multiforme cells treated with 1200.00 µM temozolomide versus 6.25 µM α-solanine versus 5.00 mM H_2O_2 incubated for 24-hours.

Descriptive Statistics

	VEGFA		
	H202	TMZ	solanine
Valid	6	6	6
Missing	0	0	0
Mean	23.498	23.208	25.188
Std. Deviation	4.075	4.474	4.661
Shapiro-Wilk	0.796	0.754	0.827
P-value of Shapiro-Wilk	0.054	0.022	0.102
Minimum	19.810	19.530	20.580
Maximum	28.630	28.980	30.900

Note. Excluded 24 rows from the analysis that correspond to the missing values of the split-by variable treatment condition

Output 13.152.: Equality of Variance (Levene's) assumption checks for one-way ANOVA testing of real time quantitative polymerase chain reaction data of fold change in expression of the VEGFA gene in glioblastoma multiforme cells treated with 1200.00 µM temozolomide versus 6.25 µM α-solanine versus 5.00 mM H_2O_2 incubated for 24-hours.

Test for Equality of Variances (Levene's)

F	df1	df2	p
0.098	2.000	15.000	0.907

Output 13.153.: Kruskal-Wallis testing for relative rate real time quantitative polymerase chain reaction data of fold change in expression of the VEGFA gene in glioblastoma multiforme cells treated with 1200.00 µM temozolomide versus 6.25 µM α-solanine versus 5.00 mM H_2O_2 incubated for 24-hours.

Kruskal-Wallis Test

Factor	Statistic	df	p
treatment condition	1.310	2	0.519

Output 13.154.: Descriptive statistics and normality (Shapiro-Wilk) assumption checking of real time quantitative polymerase chain reaction data of fold change in expression of the ATF6 gene in glioblastoma multiforme cells treated with 1200.00 µM temozolomide versus 6.25 µM α-solanine versus 5.00 mM H_2O_2 incubated for 24-hours.

Descriptive Statistics

	ATF6		
	H202	TMZ	solanine
Valid	6	6	6
Missing	0	0	0
Mean	24.693	24.670	28.528
Std. Deviation	2.684	2.644	2.429
Shapiro-Wilk	0.857	0.901	0.792
P-value of Shapiro-Wilk	0.180	0.377	0.049
Minimum	21.890	21.950	26.240
Maximum	28.140	28.460	31.650

Note. Excluded 24 rows from the analysis that correspond to the missing values of the split-by variable treatment condition

Output 13.155.: Equality of Variance (Levene's) assumption checks for one-way ANOVA testing of real time quantitative polymerase chain reaction data of fold change in expression of the ATF6 gene in glioblastoma multiforme cells treated with 1200.00 µM temozolomide versus 6.25 µM α-solanine versus 5.00 mM H_2O_2 incubated for 24-hours.

Test for Equality of Variances (Levene's)

F	df1	df2	p
0.023	2.000	15.000	0.978

Output 13.156.: Kruskal-Wallis testing for relative rate real time quantitative polymerase chain reaction data of fold change in expression of the ATF6 gene in glioblastoma multiforme cells treated with 1200.00 µM temozolomide versus 6.25 µM α-solanine versus 5.00 mM H_2O_2 incubated for 24-hours.

Kruskal-Wallis Test

Factor	Statistic	df	p
treatment condition	4.253	2	0.119

Output 13.157.: Descriptive statistics and normality (Shapiro-Wilk) assumption checking of real time quantitative polymerase chain reaction data of fold change in expression of the ATG4B gene

in glioblastoma multiforme cells treated with 1200.00 µM temozolomide versus 6.25 µM α-solanine versus 5.00 mM H_2O_2 incubated for 24-hours.

Descriptive Statistics

	ATG4B		
	H202	TMZ	solanine
Valid	6	6	6
Missing	0	0	0
Mean	30.570	30.387	33.312
Std. Deviation	0.554	0.801	0.546
Shapiro-Wilk	0.872	0.735	0.943
P-value of Shapiro-Wilk	0.233	0.014	0.681
Minimum	29.760	29.730	32.670
Maximum	31.110	31.470	34.120

Note. Excluded 24 rows from the analysis that correspond to the missing values of the split-by variable treatment condition

Output 13.158.: Equality of Variance (Levene's) assumption checks for one-way ANOVA testing of real time quantitative polymerase chain reaction data of fold change in expression of the ATG4B gene in glioblastoma multiforme cells treated with 1200.00 µM temozolomide versus 6.25 µM α-solanine versus 5.00 mM H_2O_2 incubated for 24-hours.

Test for Equality of Variances (Levene's)

F	df1	df2	p
1.689	2.000	15.000	0.218

Output 13.159.: Kruskal-Wallis testing for relative rate real time quantitative polymerase chain reaction data of fold change in expression of the ATG4B gene in glioblastoma multiforme cells treated with 1200.00 µM temozolomide versus 6.25 µM α-solanine versus 5.00 mM H_2O_2 incubated for 24-hours.

Kruskal-Wallis Test

Factor	Statistic	df	p
treatment condition	11.474	2	0.003

Output 13.160.: One-way ANOVA post-hoc analysis for relative rate real time quantitative polymerase chain reaction data of fold change in expression of the ATG4B gene in glioblastoma

multiforme cells treated with 1200.00 µM temozolomide versus 6.25 µM α-solanine versus 5.00 mM H_2O_2 incubated for 24-hours.

Post Hoc Comparisons – treatment condition

		Mean Difference	SE	t	p_{tukey}
H202	TMZ	0.183	0.372	0.493	0.876
	solanine	−2.742	0.372	−7.367	< .001
TMZ	solanine	−2.925	0.372	−7.860	< .001

Note. P-value adjusted for comparing a family of 3

13.5. Statistical analysis of fluorescent imaging experiments

13.5.1. Assessing changes in different staining corrected total cell fluorescence per treatment condition.

Output 13.161.: Descriptive statistics and normality (Shapiro-Wilk) assumption checking of corrected total cell fluorescence data on glioblastoma cells stained with Annexin-V-fluorescein isothiocyanate, propidium iodide or monodansylcadaverine treated with 6.25 µM α-solanine incubated for 24-hours.

Descriptive Statistics

	Solanine		
	Annexin-FITC	Autophagy	PI
Valid	9	9	9
Missing	0	0	0
Mean	1.337e +6	8.087e +6	90526.300
Std. Deviation	2.161e +6	1.108e +7	137344.649
Shapiro-Wilk	0.698	0.625	0.733
P-value of Shapiro-Wilk	0.001	< .001	0.003
Minimum	0.000	1.037e +6	0.000
Maximum	6.481e +6	3.653e +7	408756.647

Output 13.162.: Equality of Variance (Levene's) assumption checks for one-way ANOVA testing of corrected total cell fluorescence data on glioblastoma cells stained with Annexin-V-fluorescein isothiocyanate, propidium iodide or monodansylcadaverine treated with 6.25 µM α-solanine incubated for 24-hours.

Test for Equality of Variances (Levene's)

F	df1	df2	p
4.901	2.000	24.000	0.016

Output 13.163.: Kruskal-Wallis testing for corrected total cell fluorescence data on glioblastoma cells stained with Annexin-V-fluorescein isothiocyanate, propidium iodide or monodansylcadaverine treated with 6.25 µM α-solanine incubated for 24-hours.

Kruskal-Wallis Test

Factor	Statistic	df	p
Stain	16.057	2	< .001

Output 13.164.: Kurskal-Wallis post-hoc analysis for corrected total cell fluorescence data on glioblastoma cells stained with Annexin-V-fluorescein isothiocyanate, propidium iodide or monodansylcadaverine treated with 6.25 µM α-solanine incubated for 24-hours.

Standard

Post Hoc Comparisons - Stain

		Mean Difference	SE	t	p_{tukey}
(Annexin-FITC)	Autophagy	−6.750e +6	3.073e +6	−2.196	0.092
	PI	1.246e +6	3.073e +6	0.405	0.914
Autophagy	PI	7.996e +6	3.073e +6	2.602	0.040

Note. P-value adjusted for comparing a family of 3

Output 13.165.: Descriptive statistics and normality (Shapiro-Wilk) assumption checking of corrected total cell fluorescence data on glioblastoma cells stained with Annexin-V-fluorescein isothiocyanate, propidium iodide or monodansylcadaverine treated with 1200.00 µM temozolomide incubated for 24-hours.

Descriptive Statistics

	Temozolomide		
	Annexin-FITC	Autophagy	PI
Valid	9	9	9
Missing	0	0	0
Mean	61088.090	2.403e +6	12812.780
Std. Deviation	60807.921	1.989e +6	20342.191
Shapiro-Wilk	0.806	0.856	0.665
P-value of Shapiro-Wilk	0.024	0.087	< .001
Minimum	0.000	652867.141	0.000
Maximum	145430.643	6.264e +6	47017.640

Output 13.166.: Equality of Variance (Levene's) assumption checks for one-way ANOVA testing of corrected total cell fluorescence data on glioblastoma cells stained with Annexin-V-fluorescein isothiocyanate, propidium iodide or monodansylcadaverine treated with 1200.00 µM temozolomide incubated for 24-hours.

Test for Equality of Variances (Levene's)

F	df1	df2	p
18.708	2.000	24.000	< .001

Output 13.167.: Kruskal-Wallis testing for corrected total cell fluorescence data on glioblastoma cells stained with Annexin-V-fluorescein isothiocyanate, propidium iodide or monodansylcadaverine treated with 1200.00 µM temozolomide incubated for 24-hours.

Kruskal-Wallis Test

Factor	Statistic	df	p
Stain	19.190	2	< .001

Output 13.168.: Kurskal-Wallis post-hoc analysis for corrected total cell fluorescence data on glioblastoma cells stained with Annexin-V-fluorescein isothiocyanate, propidium iodide or monodansylcadaverine and treated with 1200.00 µM temozolomide incubated for 24-hours.

Standard

Post Hoc Comparisons - Stain

		Mean Difference	SE	t	p_{tukey}
(Annexin-FITC)	Autophagy	−2.342e +6	541729.157	−4.322	< .001
	PI	48275.310	541729.157	0.089	0.996
Autophagy	PI	2.390e +6	541729.157	4.411	< .001

Note. P-value adjusted for comparing a family of 3

Output 13.169.: Descriptive statistics and normality (Shapiro-Wilk) assumption checking of corrected total cell fluorescence data on glioblastoma cells stained with Annexin-V-fluorescein isothiocyanate, propidium iodide or monodansylcadaverine and treated with culture (negative control) conditions incubated for 24-hours.

Descriptive Statistics

	Negative control		
	Annexin-FITC	Autophagy	PI
Valid	9	9	9
Missing	0	0	0
Mean	44979.481	7.126e +6	17957.816
Std. Deviation	45646.952	7.004e +6	27967.745
Shapiro-Wilk	0.885	0.850	0.691
P-value of Shapiro-Wilk	0.177	0.074	0.001
Minimum	0.000	1.063e +6	0.000
Maximum	132724.872	2.144e +7	69073.499

Output 13.170.: Equality of Variance (Levene's) assumption checks for one-way ANOVA testing of corrected total cell fluorescence data on glioblastoma cells stained with Annexin-V-fluorescein isothiocyanate, propidium iodide or monodansylcadaverine and treated with culture (negative control) conditions incubated for 24-hours.

Test for Equality of Variances (Levene's)

F	df1	df2	p
23.175	2.000	24.000	< .001

Output 13.171.: Kruskal-Wallis testing for corrected total cell fluorescence data on glioblastoma cells stained with Annexin-V-fluorescein isothiocyanate, propidium iodide or monodansylcadaverine and treated with culture (negative control) conditions incubated for 24-hours.

Kruskal-Wallis Test

Factor	Statistic	df	p
Stain	18.787	2	< .001

Output 13.172.: Kurskal-Wallis post-hoc analysis for corrected total cell fluorescence data on glioblastoma cells stained with Annexin-V-fluorescein isothiocyanate, propidium iodide or monodansylcadaverine treated with culture (negative control) conditions incubated for 24-hours.

Standard

Post Hoc Comparisons - Stain

		Mean Difference	SE	t	p_{tukey}
(Annexin-FITC)	Autophagy	−7.081e +6	1.906e +6	−3.714	0.003
	PI	27021.665	1.906e +6	0.014	1.000
Autophagy	PI	7.108e +6	1.906e +6	3.728	0.003

Note. P-value adjusted for comparing a family of 3

13.5.2. Assessing the effect of different treatment conditionson stain specific corrected total cell fluorescence.

Output 13.173.: Descriptive statistics and normality (Shapiro-Wilk) assumption checking of corrected total cell fluorescence data on glioblastoma cells stained with propidium iodide treated with 1200.00 µM temozolomide, 6.25 µM α-solanine versus culture (negative control) conditions incubated for 24-hours.

Descriptive Statistics

	PI		
	Negative control	Solanine	Temozolomide
Valid	9	9	9
Missing	0	0	0
Mean	17957.816	90526.300	12812.780
Std. Deviation	27967.745	137344.649	20342.191
Shapiro-Wilk	0.691	0.733	0.665
P-value of Shapiro-Wilk	0.001	0.003	< .001
Minimum	0.000	0.000	0.000
Maximum	69073.499	408756.647	47017.640

Output 13.174.: Equality of Variance (Levene's) assumption checks for one-way ANOVA testing of corrected total cell fluorescence data on glioblastoma cells stained with propidium iodide treated

with 1200.00 µM temozolomide, 6.25 µM α-solanine versus culture (negative control) conditions incubated for 24-hours.

Test for Equality of Variances (Levene's)

F	df1	df2	p
8.931	2.000	24.000	0.001

Output 13.175.: Kruskal-Wallis testing for corrected total cell fluorescence data on glioblastoma cells stained with propidium iodide treated with 1200.00 µM temozolomide, 6.25 µM α-solanine versus culture (negative control) conditions incubated for 24-hours.

Kruskal–Wallis Test

Factor	Statistic	df	p
V1	3.119	2	0.210

Output 13.176.: Descriptive statistics and normality (Shapiro-Wilk) assumption checking of corrected total cell fluorescence data on glioblastoma cells stained with annexin-V conjugated fluorescein isothiocyanate treated with 1200.00 µM temozolomide, 6.25 µM α-solanine versus culture (negative control) conditions incubated for 24-hours.

Descriptive Statistics

	Annexin–FITC		
	Negative control	Solanine	Temozolomide
Valid	9	9	9
Missing	0	0	0
Mean	44979.481	1.337e +6	61088.090
Std. Deviation	45646.952	2.161e +6	60807.921
Shapiro–Wilk	0.885	0.698	0.806
P–value of Shapiro–Wilk	0.177	0.001	0.024
Minimum	0.000	0.000	0.000
Maximum	132724.872	6.481e +6	145430.643

Output 13.177: Equality of Variance (Levene's) assumption checks for one-way ANOVA testing of corrected total cell fluorescence data on glioblastoma cells stained with annexin-V conjugated fluorescein isothiocyanate treated with 1200.00 µM temozolomide, 6.25 µM α-solanine versus culture (negative control) conditions incubated for 24-hours.

Test for Equality of Variances (Levene's)

F	df1	df2	p
10.977	2.000	24.000	< .001

Output 13.178.: Kruskal-Wallis testing for corrected total cell fluorescence data on glioblastoma cells stained with annexin-V conjugated fluorescein isothiocyanate treated with 1200.00 µM temozolomide, 6.25 µM α-solanine versus culture (negative control) conditions incubated for 24-hours.

Kruskal-Wallis Test

Factor	Statistic	df	p
V1	5.017	2	0.081

Output 13.179.: Descriptive statistics and normality (Shapiro-Wilk) assumption checking of corrected total cell fluorescence data on glioblastoma cells stained with monodansylcadaverine treated with 1200.00 µM temozolomide, 6.25 µM α-solanine versus culture (negative control) conditions incubated for 24-hours.

Descriptive Statistics

	Autophagy		
	Negative control	Solanine	Temozolomide
Valid	9	9	9
Missing	0	0	0
Mean	7.126e +6	8.087e +6	2.403e +6
Std. Deviation	7.004e +6	1.108e +7	1.989e +6
Shapiro-Wilk	0.850	0.625	0.856
P-value of Shapiro-Wilk	0.074	< .001	0.087
Minimum	1.063e +6	1.037e +6	652867.141
Maximum	2.144e +7	3.653e +7	6.264e +6

Output 13.180.: Equality of Variance (Levene's) assumption checks for one-way ANOVA testing of corrected total cell fluorescence data on glioblastoma cells stained with monodansylcadaverine treated with 1200.00 µM temozolomide, 6.25 µM α-solanine versus culture (negative control) conditions incubated for 24-hours.

Test for Equality of Variances (Levene's)

F	df1	df2	p
2.558	2.000	24.000	0.098

Output 13.181.: Kruskal-Wallis testing for corrected total cell fluorescence data on glioblastoma cells stained with monodansylcadaverine treated with 1200.00 µM temozolomide, 6.25 µM α-solanine versus culture (negative control) conditions incubated for 24-hours.

Kruskal-Wallis Test

Factor	Statistic	df	p
V1	4.448	2	0.108

13.6. Statistical analysis of flow-cytometry experiments

13.6.1. Assessing mode of cell death between cell lines per treatment condition

Output 13.182.: Descriptive statistics and normality (Shapiro-Wilk) assumption checking of data representing the occurrence of early apoptosis in U87MG versus U251 versus T98G cells treated with 5.00 mM H_2O_2 for 24-hours.

Descriptive Statistics

	Transformed %		
	T98G_positive-control_apoptosis_early apoptosis	U251_positive-control_apoptosis_early apoptosis	U87MG_positive-control_apoptosis_early apoptosis
Valid	3	3	3
Missing	0	0	0
Mean	−5.111	−8.234	−6.379
Std. Deviation	0.143	1.260	0.099
Shapiro-Wilk	0.960	0.906	0.750
P-value of Shapiro-Wilk	0.617	0.405	< .001
Minimum	−5.235	−9.210	−6.436
Maximum	−4.955	−6.811	−6.264

Note. Excluded 31 rows from the analysis that correspond to the missing values of the split-by variable Condition and cell line

Output 13.183.: Equality of Variance (Levene's) assumption checks of of data representing the occurrence of early apoptosis in U87MG versus U251 versus T98G cells treated with 5.00 mM H_2O_2 for 24-hours.

Test for Equality of Variances (Levene's)

F	df1	df2	p
9.048	2.000	6.000	0.015

Output 13.184.: Kruskal-Wallis testing of data representing the occurrence of early apoptosis in U87MG versus U251 versus T98G cells treated with 5.00 mM H2O2 for 24-hours.

Kruskal–Wallis Test

Factor	Statistic	df	p
Condition and cell line	7.261	2	0.027

Output 13.185.: K*rus*kal-Wallis post-hoc analysis of data representing the occurrence of early apoptosis in U87MG versus U251 versus T98G cells treated with 5.00 mM H_2O_2 for 24-hours.

Post Hoc Comparisons - Condition and cell line

		Mean Difference	SE	t	P_{tukey}
(T98G_positive-control_apoptosis_early apoptosis)	(U251_positive-control_apoptosis_early apoptosis)	3.122	0.600	5.207	0.005
	(U87MG_positive-control_apoptosis_early apoptosis)	1.268	0.600	2.114	0.167
(U251_positive-control_apoptosis_early apoptosis)	(U87MG_positive-control_apoptosis_early apoptosis)	−1.855	0.600	−3.093	0.048

Note. P-value adjusted for comparing a family of 3

Output 13.186.: Descriptive statistics and normality (Shapiro-Wilk) assumption checking of data representing the occurrence of late apoptosis in U87MG versus U251 versus T98G cells treated with 5.00 mM H_2O_2 for 24-hours.

Descriptive Statistics

	Transformed %_6		
	T98G_positive-control_apoptosis_late apoptosis	U251_positive-control_apoptosis_late apoptosis	U87MG_positive-control_apoptosis_late apoptosis
Valid	3	3	3
Missing	0	0	0
Mean	−4.584	−4.300	−2.506
Std. Deviation	1.222	0.363	0.097
Shapiro-Wilk	1.000	0.995	0.768
P-value of Shapiro-Wilk	0.999	0.864	0.040
Minimum	−5.806	−4.647	−2.618
Maximum	−3.362	−3.923	−2.448

Note. Excluded 31 rows from the analysis that correspond to the missing values of the split-by variable Condition and cell line_5

Output 13.187.: Equality of Variance (Levene's) assumption checks of of data representing the occurrence of late apoptosis in U87MG versus U251 versus T98G cells treated with 5.00 mM H_2O_2 for 24-hours.

Test for Equality of Variances (Levene's) ▼

F	df1	df2	p
2.513	2.000	6.000	0.161

Output 13.188.: Kruskal-Wallis testing of data representing the occurrence of late apoptosis in U87MG versus U251 versus T98G cells treated with 5.00 mM H_2O_2 for 24-hours.

Kruskal-Wallis Test

Factor	Statistic	df	p
Condition and cell line_5	5.422	2	0.066

Output 13.189.: Descriptive statistics and normality (Shapiro-Wilk) assumption checking of data representing the occurrence of necrosis in U87MG versus U251 versus T98G cells treated with 5.00 mM H_2O_2 for 24-hours.

Descriptive Statistics

	Transformed %_9		
	T98G_positive-control_apoptosis_necrosis	U251_positive-control_apoptosis_necrosis	U87MG_positive-control_apoptosis_necrosis
Valid	3	3	3
Missing	0	0	0
Mean	−0.100	3.200	2.354
Std. Deviation	1.394	0.211	0.105
Shapiro-Wilk	0.826	0.841	0.947
P-value of Shapiro-Wilk	0.177	0.215	0.556
Minimum	−1.030	3.055	2.266
Maximum	1.503	3.442	2.470

Note. Excluded 31 rows from the analysis that correspond to the missing values of the split-by variable Condition and cell line_8

Output 13.190.: Equality of Variance (Levene's) assumption checks of of data representing the occurrence of necrosis in U87MG versus U251 versus T98G cells treated with 5.00 mM H_2O_2 for 24-hours.

Test for Equality of Variances (Levene's)

F	df1	df2	p
11.410	2.000	6.000	0.009

Output 13.191.: Kruskal-Wallis testing of data representing the occurrence of necrosis in U87MG versus U251 versus T98G cells treated with 5.00 mM H_2O_2 for 24-hours.

Kruskal-Wallis Test

Factor	Statistic	df	p
Condition and cell line_8	7.200	2	0.027

Output 13.192.: Kurskal-Wallis post-hoc analysis of data representing the occurrence of necrosis in U87MG versus U251 versus T98G cells treated with 5.00 mM H_2O_2 for 24-hours.

Standard

Post Hoc Comparisons - Condition and cell line_8

		Mean Difference	SE	t	P_{tukey}
(T98G_positive-control_apoptosis_necrosis)	(U251_positive-control_apoptosis_necrosis)	−3.300	0.666	−4.951	0.006
	(U87MG_positive-control_apoptosis_necrosis)	−2.454	0.666	−3.682	0.024
(U251_positive-control_apoptosis_necrosis)	(U87MG_positive-control_apoptosis_necrosis)	0.846	0.666	1.270	0.460

Note. P-value adjusted for comparing a family of 3

Output 13.193.: Descriptive statistics and normality (Shapiro-Wilk) assumption checking of data representing the occurrence of autophagy in U87MG versus U251 versus T98G cells treated with 5.00 mM H_2O_2 for 24-hours.

Descriptive Statistics

	Transformed %_12		
	T98G_positive-control_autophagy	U251_positive-control_autophagy	U87MG_positive-control_autophagy
Valid	3	3	3
Missing	0	0	0
Mean	3.507	0.206	1.174
Std. Deviation	0.158	0.102	0.345
Shapiro-Wilk	1.000	0.975	0.799
P-value of Shapiro-Wilk	0.959	0.699	0.111
Minimum	3.347	0.096	0.954
Maximum	3.664	0.298	1.572

Note. Excluded 31 rows from the analysis that correspond to the missing values of the split-by variable Condition and cell line_11

Output 13.194.: Equality of Variance (Levene's) assumption checks for data representing the occurrence of autophagy in U87MG versus U251 versus T98G cells treated with 5.00 mM H_2O_2 for 24-hours.

Test for Equality of Variances (Levene's)

F	df1	df2	p
3.951	2.000	6.000	0.080

Output 13.195.: One-way ANOVA testing of data representing the occurrence of autophagy in U87MG versus U251 versus T98G cells treated with 5.00 mM H_2O_2 for 24-hours.

ANOVA - Transformed %_12

Cases	Sum of Squares	df	Mean Square	F	p
Condition and cell line_11	17.276	2	8.638	167.429	< .001
Residuals	0.310	6	0.052		

Note. Type III Sum of Squares

Output 13.196.: One-way ANOVA post-hoc analysis of data representing the occurrence of autophagy in U87MG versus U251 versus T98G cells treated with 5.00 mM H_2O_2 for 24-hours.

Standard

Post Hoc Comparisons - Condition and cell line_11

		Mean Difference	SE	t	P_{tukey}
(T98G_positive-control_autophagy)	(U251_positive-control_autophagy)	3.301	0.185	17.798	< .001
	(U87MG_positive-control_autophagy)	2.334	0.185	12.583	< .001
(U251_positive-control_autophagy)	(U87MG_positive-control_autophagy)	−0.967	0.185	−5.215	0.005

Note. P-value adjusted for comparing a family of 3

Output 13.197.: Descriptive statistics and normality (Shapiro-Wilk) assumption checking of data representing the occurrence of early apoptosis in U87MG versus U251 versus T98G cells treated with 6.25 µM α-solanine for 24-hours.

Descriptive Statistics ▼

	Transformed %_24		
	T98G_positive-control_apoptosis_early apoptosis	U251_positive-control_apoptosis_early apoptosis	U87MG_positive-control_apoptosis_early apoptosis
Valid	3	3	3
Missing	0	0	0
Mean	−3.246	−3.827	−7.247
Std. Deviation	0.228	0.302	0.704
Shapiro-Wilk	0.999	0.948	0.883
P-value of Shapiro-Wilk	0.931	0.559	0.333
Minimum	−3.480	−4.082	−8.047
Maximum	−3.023	−3.493	−6.724

Note. Excluded 31 rows from the analysis that correspond to the missing values of the split-by variable Condition and cell line_23

Output 13.198.: Equality of Variance (Levene's) assumption checks of of data representing the occurrence of early apoptosis in U87MG versus U251 versus T98G cells treated with 6.25 µM α-solanine for 24-hours.

Test for Equality of Variances (Levene's)

F	df1	df2	p
3.619	2.000	6.000	0.093

Output 13.199.: One-way ANOVA testing of data representing the occurrence of early apoptosis in U87MG versus U251 versus T98G cells treated with 6.25 µM α-solanine or 24-hours.

ANOVA - Transformed %_24

Cases	Sum of Squares	df	Mean Square	F	p
Condition and cell line_23	28.029	2	14.015	65.825	< .001
Residuals	1.277	6	0.213		

Note. Type III Sum of Squares

Output 13.200.: One-way ANOVA post-hoc analysis of data representing the occurrence of early apoptosis in U87MG versus U251 versus T98G cells treated with 6.25 µM α-solanine for 24-hours.

Standard

Post Hoc Comparisons - Condition and cell line_23

		Mean Difference	SE	t	P_{tukey}
(T98G_positive-control_apoptosis_early apoptosis)	(U251_positive-control_apoptosis_early apoptosis)	0.581	0.377	1.542	0.338
	(U87MG_positive-control_apoptosis_early apoptosis)	4.000	0.377	10.618	< .001
(U251_positive-control_apoptosis_early apoptosis)	(U87MG_positive-control_apoptosis_early apoptosis)	3.419	0.377	9.075	< .001

Note. P-value adjusted for comparing a family of 3

Output 13.201.: Descriptive statistics and normality (Shapiro-Wilk) assumption checking of data representing the occurrence of late apoptosis in U87MG versus U251 versus T98G cells treated with 6.25 µM α-solanine for 24-hours.

Descriptive Statistics

	Transformed %_27		
	T98G_positive-control_apoptosis_late apoptosis	U251_positive-control_apoptosis_late apoptosis	U87MG_positive-control_apoptosis_late apoptosis
Valid	3	3	3
Missing	0	0	0
Mean	−6.954	−4.928	−2.827
Std. Deviation	2.015	0.643	0.273
Shapiro-Wilk	0.925	0.850	0.882
P-value of Shapiro-Wilk	0.471	0.240	0.329
Minimum	−9.210	−5.377	−3.030
Maximum	−5.334	−4.191	−2.517

Note. Excluded 31 rows from the analysis that correspond to the missing values of the split-by variable Condition and cell line_26

Output 13.202.: Equality of Variance (Levene's) assumption checks of of data representing the occurrence of late apoptosis in U87MG versus U251 versus T98G cells treated with 6.25 µM α-solanine for 24-hours.

Test for Equality of Variances (Levene's)

F	df1	df2	p
2.136	2.000	6.000	0.199

Output 13.203.: One-way ANOVA testing of data representing the occurrence of late apoptosis in U87MG versus U251 versus T98G cells treated with 6.25 µM α-solanine for 24-hours.

ANOVA - Transformed %_30

Cases	Sum of Squares	df	Mean Square	F	p
Condition and cell line_29	71.669	2	35.834	235.709	< .001
Residuals	0.912	6	0.152		

Note. Type III Sum of Squares

Output 13.204.: One-way ANOVA post-hoc analysis of data representing the occurrence of late apoptosis in U87MG versus U251 versus T98G cells treated with 6.25 µM α-solanine for 24-hours.

Standard

Post Hoc Comparisons - Condition and cell line_29

		Mean Difference	SE	t	P_{tukey}
(T98G_positive-control_apoptosis_necrosis)	(U251_positive-control_apoptosis_necrosis)	−0.811	0.318	−2.549	0.096
	(U87MG_positive-control_apoptosis_necrosis)	−6.351	0.318	−19.948	< .001
(U251_positive-control_apoptosis_necrosis)	(U87MG_positive-control_apoptosis_necrosis)	−5.539	0.318	−17.399	< .001

Note. P-value adjusted for comparing a family of 3

Output 13.205.: Descriptive statistics and normality (Shapiro-Wilk) assumption checking of data representing the occurrence of necrosis in U87MG versus U251 versus T98G cells treated with 6.25 µM α-solanine for 24-hours.

Descriptive Statistics

	Transformed %_30		
	T98G_positive-control_apoptosis_necrosis	U251_positive-control_apoptosis_necrosis	U87MG_positive-control_apoptosis_necrosis
Valid	3	3	3
Missing	0	0	0
Mean	−3.568	−2.756	2.783
Std. Deviation	0.134	0.611	0.254
Shapiro-Wilk	0.988	0.995	0.925
P-value of Shapiro-Wilk	0.792	0.865	0.471
Minimum	−3.693	−3.341	2.498
Maximum	−3.426	−2.122	2.987

Note. Excluded 31 rows from the analysis that correspond to the missing values of the split-by variable Condition and cell line_29

Output 13.206.:Equality of Variance (Levene's) assumption checks of of data representing the occurrence of necrosis in U87MG versus U251 versus T98G cells treated with 6.25 µM α-solanine for 24-hours.

Test for Equality of Variances (Levene's)

F	df1	df2	p
2.136	2.000	6.000	0.199

Output 13.207.: One-way ANOVA testing of data representing the occurrence of necrosis in U87MG versus U251 versus T98G cells treated with 6.25 µM α-solanine for 24-hours.

ANOVA - Transformed %_30

Cases	Sum of Squares	df	Mean Square	F	p
Condition and cell line_29	71.669	2	35.834	235.709	< .001
Residuals	0.912	6	0.152		

Note. Type III Sum of Squares

Output 13.208.: One-way ANOVA post-hoc analysis of data representing the occurrence of necrosis in U87MG versus U251 versus T98G cells treated with 6.25 µM α-solanine for 24-hours.

Standard

Post Hoc Comparisons - Condition and cell line_29

		Mean Difference	SE	t	P_{tukey}
(T98G_positive-control_apoptosis_necrosis)	(U251_positive-control_apoptosis_necrosis)	−0.811	0.318	−2.549	0.096
	(U87MG_positive-control_apoptosis_necrosis)	−6.351	0.318	−19.948	< .001
(U251_positive-control_apoptosis_necrosis)	(U87MG_positive-control_apoptosis_necrosis)	−5.539	0.318	−17.399	< .001

Note. P-value adjusted for comparing a family of 3

Output 13.209.: Descriptive statistics and normality (Shapiro-Wilk) assumption checking of data representing the occurrence of autophagy in U87MG versus U251 versus T98G cells treated with 6.25 µM α-solanine for 24-hours.

Descriptive Statistics

	Transformed %_33		
	T98G_positive-control_autophagy	U251_positive-control_autophagy	U87MG_positive-control_autophagy
Valid	3	3	3
Missing	0	0	0
Mean	3.546	0.890	1.074
Std. Deviation	5.746	1.163	0.708
Shapiro-Wilk	0.999	1.000	0.899
P-value of Shapiro-Wilk	0.954	0.964	0.383
Minimum	−2.279	−0.286	0.532
Maximum	9.210	2.041	1.875

Note. Excluded 31 rows from the analysis that correspond to the missing values of the split-by variable Condition and cell line_32

Output 13.210.:Equality of Variance (Levene's) assumption checks of of data representing the occurrence of autophagy in U87MG versus U251 versus T98G cells treated with 6.25 µM α-solanine for 24-hours.

Test for Equality of Variances (Levene's)

F	df1	df2	p
2.871	2.000	6.000	0.133

Output 13.211.: One-way ANOVA testing of data representing the occurrence of autophagy in U87MG versus U251 versus T98G cells treated with 6.25 µM α-solanine for 24-hours.

ANOVA - Transformed %_33

Cases	Sum of Squares	df	Mean Square	F	p
Condition and cell line_32	13.197	2	6.599	0.568	0.595
Residuals	69.746	6	11.624		

Note. Type III Sum of Squares

Output 13.212.: Descriptive statistics and normality (Shapiro-Wilk) assumption checking of data representing the occurrence of early apoptosis in U87MG versus U251 versus T98G cells treated with culture (negative control) conditions for 24-hours.

Descriptive Statistics

	Transformed %_45		
	T98G_positive-control_apoptosis_early apoptosis	U251_positive-control_apoptosis_early apoptosis	U87MG_positive-control_apoptosis_early apoptosis
Valid	3	3	3
Missing	0	0	0
Mean	−5.203	−8.234	−6.370
Std. Deviation	0.430	1.260	0.546
Shapiro-Wilk	0.993	0.906	0.811
P-value of Shapiro-Wilk	0.841	0.405	0.140
Minimum	−5.651	−9.210	−6.724
Maximum	−4.795	−6.811	−5.741

Note. Excluded 31 rows from the analysis that correspond to the missing values of the split-by variable Condition and cell line_44

Output 13.213.: Equality of Variance (Levene's) assumption checks of of data representing the occurrence of early apoptosis in U87MG versus U251 versus T98G cells treated with culture (negative control) conditions for 24-hours.

Test for Equality of Variances (Levene's)

F	df1	df2	p
3.316	2.000	6.000	0.107

Output 13.214.: One-way ANOVA testing of data representing the occurrence of early apoptosis in U87MG versus U251 versus T98G cells treated with culture (negative control) conditions for 24-hours.

ANOVA - Transformed %_45

Cases	Sum of Squares	df	Mean Square	F	p
Condition and cell line_44	14.022	2	7.011	10.160	0.012
Residuals	4.140	6	0.690		

Note. Type III Sum of Squares

Output 13.215.: One-way ANOVA post-hoc analysis of data representing the occurrence of early apoptosis in U87MG versus U251 versus T98G cells treated with culture (negative control) conditions for 24-hours.

Standard

Post Hoc Comparisons - Condition and cell line_44

		Mean Difference	SE	t	P_{tukey}
(T98G_positive-control_apoptosis_early apoptosis)	(U251_positive-control_apoptosis_early apoptosis)	3.031	0.678	4.469	0.010
	(U87MG_positive-control_apoptosis_early apoptosis)	1.167	0.678	1.721	0.273
(U251_positive-control_apoptosis_early apoptosis)	(U87MG_positive-control_apoptosis_early apoptosis)	−1.864	0.678	−2.748	0.075

Note. P-value adjusted for comparing a family of 3

Output 13.216.: Descriptive statistics and normality (Shapiro-Wilk) assumption checking of data representing the occurrence of late apoptosis in U87MG versus U251 versus T98G cells treated with culture (negative control) conditions for 24-hours.

Descriptive Statistics

	Transformed %_48		
	T98G_positive-control_apoptosis_late apoptosis	U251_positive-control_apoptosis_late apoptosis	U87MG_positive-control_apoptosis_late apoptosis
Valid	3	3	3
Missing	0	0	0
Mean	−4.431	−4.179	−2.365
Std. Deviation	0.330	0.427	0.118
Shapiro-Wilk	0.815	0.824	0.889
P-value of Shapiro-Wilk	0.150	0.172	0.352
Minimum	−4.647	−4.463	−2.499
Maximum	−4.051	−3.688	−2.276

Note. Excluded 31 rows from the analysis that correspond to the missing values of the split-by variable Condition and cell line_47

Output 13.217.: Equality of Variance (Levene's) assumption checks of of data representing the occurrence of late apoptosis in U87MG versus U251 versus T98G cells treated with culture (negative control) conditions for 24-hours.

Test for Equality of Variances (Levene's)

F	df1	df2	p
3.675	2.000	6.000	0.091

Output 13.218.:One-way ANOVA testing of data representing the occurrence of late apoptosis in U87MG versus U251 versus T98G cells treated with culture (negative control) conditions for 24-hours.

ANOVA - Transformed %_48

Cases	Sum of Squares	df	Mean Square	F	p
Condition and cell line_47	7.622	2	3.811	37.518	< .001
Residuals	0.609	6	0.102		

Note. Type III Sum of Squares

Output 13.219.: One-way ANOVA post-hoc analysis of data representing the occurrence of late apoptosis in U87MG versus U251 versus T98G cells treated with culture (negative control) conditions for 24-hours.

Standard

Post Hoc Comparisons - Condition and cell line_47

		Mean Difference	SE	t	p_{tukey}
(T98G_positive-control_apoptosis_late apoptosis)	(U251_positive-control_apoptosis_late apoptosis)	−0.252	0.260	−0.969	0.621
	(U87MG_positive-control_apoptosis_late apoptosis)	−2.066	0.260	−7.939	< .001
(U251_positive-control_apoptosis_late apoptosis)	(U87MG_positive-control_apoptosis_late apoptosis)	−1.814	0.260	−6.970	0.001

Note. P-value adjusted for comparing a family of 3

Output 13.220.: Descriptive statistics and normality (Shapiro-Wilk) assumption checking of data representing the occurrence of necrosis in U87MG versus U251 versus T98G cells treated with culture (negative control) conditions for 24-hours.

Descriptive Statistics

	Transformed %_51		
	T98G_positive-control_apoptosis_necrosis	U251_positive-control_apoptosis_necrosis	U87MG_positive-control_apoptosis_necrosis
Valid	3	3	3
Missing	0	0	0
Mean	−0.314	2.672	2.322
Std. Deviation	0.625	0.695	0.128
Shapiro-Wilk	0.860	0.945	0.788
P-value of Shapiro-Wilk	0.267	0.547	0.086
Minimum	−0.758	2.091	2.242
Maximum	0.401	3.442	2.470

Note. Excluded 31 rows from the analysis that correspond to the missing values of the split-by variable Condition and cell line_50

Output 13.221.: Equality of Variance (Levene's) assumption checks of of data representing the occurrence of necrosis in U87MG versus U251 versus T98G cells treated with culture (negative control) conditions for 24-hours.

Test for Equality of Variances (Levene's)

F	df1	df2	p
3.389	2.000	6.000	0.104

Output 13.222.: One-way ANOVA testing of data representing the occurrence of necrosis in U87MG versus U251 versus T98G cells treated with culture (negative control) conditions for 24-hours.

ANOVA - Transformed %_51

Cases	Sum of Squares	df	Mean Square	F	p
Condition and cell line_50	15.986	2	7.993	26.921	0.001
Residuals	1.781	6	0.297		

Note. Type III Sum of Squares

Output 13.223.: One-Way ANOVA post-hoc analysis of data representing the occurrence of necrosis in U87MG versus U251 versus T98G cells treated with culture (negative control) conditions for 24-hours.

Standard

Post Hoc Comparisons - Condition and cell line_50

		Mean Difference	SE	t	p_{tukey}
(T98G_positive-control_apoptosis_necrosis)	(U251_positive-control_apoptosis_necrosis)	−2.986	0.445	−6.712	0.001
	(U87MG_positive-control_apoptosis_necrosis)	−2.636	0.445	−5.925	0.002
(U251_positive-control_apoptosis_necrosis)	(U87MG_positive-control_apoptosis_necrosis)	0.350	0.445	0.787	0.724

Note. P-value adjusted for comparing a family of 3

Output 13.224.: Descriptive statistics and normality (Shapiro-Wilk) assumption checking of data representing the occurrence of autophagy in U87MG versus U251 versus T98G cells treated with culture (negative control) conditions for 24-hours.

Descriptive Statistics

	Transformed %_54		
	T98G_positive-control_autophagy	U251_positive-control_autophagy	U87MG_positive-control_autophagy
Valid	3	3	3
Missing	0	0	0
Mean	3.307	−2.571	−1.241
Std. Deviation	0.177	0.220	0.662
Shapiro-Wilk	0.750	0.996	0.934
P-value of Shapiro-Wilk	< .001	0.880	0.504
Minimum	3.103	−2.782	−1.782
Maximum	3.409	−2.343	−0.502

Note. Excluded 31 rows from the analysis that correspond to the missing values of the split-by variable Condition and cell line_53

Output 13.225.: Equality of Variance (Levene's) assumption checks of of data representing the occurrence of autophagy in U87MG versus U251 versus T98G cells treated with culture (negative control) conditions for 24-hours.

Test for Equality of Variances (Levene's)

F	df1	df2	p
3.934	2.000	6.000	0.081

Output 13.226.: Kruskal-Wallis testing of data representing the occurrence of autophagy in U87MG versus U251 versus T98G cells treated with culture (negative control) conditions for 24-hours.

Kruskal-Wallis Test

Factor	Statistic	df	p
Condition and cell line_53	7.261	2	0.027

Output 13.227.: Kurskal-Wallis post-hoc analysis of data representing the occurrence of autophagy in U87MG versus U251 versus T98G cells treated with culture (negative control) conditions for 24-hours.

Standard

Post Hoc Comparisons - Condition and cell line_53

		Mean Difference	SE	t	P_{tukey}
(T98G_positive-control_autophagy)	(U251_positive-control_autophagy)	5.878	0.339	17.318	< .001
	(U87MG_positive-control_autophagy)	4.548	0.339	13.400	< .001
(U251_positive-control_autophagy)	(U87MG_positive-control_autophagy)	−1.330	0.339	−3.919	0.018

Note. P-value adjusted for comparing a family of 3

Output 13.228.: Descriptive statistics and normality (Shapiro-Wilk) assumption checking of data representing the occurrence of early apoptosis in U87MG versus U251 versus T98G cells treated with 1200.00 µM temozolomide for 24-hours.

Descriptive Statistics

	Transformed %_66		
	T98G_positive-control_apoptosis_early apoptosis	U251_positive-control_apoptosis_early apoptosis	U87MG_positive-control_apoptosis_early apoptosis
Valid	3	3	3
Missing	0	0	0
Mean	−5.015	−9.054	−7.245
Std. Deviation	0.040	0.271	0.751
Shapiro-Wilk	0.897	0.750	0.750
P-value of Shapiro-Wilk	0.375	< .001	< .001
Minimum	−5.045	−9.210	−8.111
Maximum	−4.969	−8.740	−6.811

Note. Excluded 31 rows from the analysis that correspond to the missing values of the split-by variable Condition and cell line_65

Output 13.229.: Equality of Variance (Levene's) assumption checks of of data representing the occurrence of early apoptosis in U87MG versus U251 versus T98G cells treated with 1200.00 µM temozolomide for 24-hours.

Test for Equality of Variances (Levene's)

F	df1	df2	p
9.883	2.000	6.000	0.013

Output 13.230.: Kruskal-Wallis testing of data representing the occurrence of early apoptosis in U87MG versus U251 versus T98G cells treated with 1200.00 µM temozolomide or 24-hours.

Kruskal-Wallis Test

Factor	Statistic	df	p
Condition and cell line_65	7.322	2	0.026

Output 13.231.: Kurskal-Wallis post-hoc analysis of data representing the occurrence of early apoptosis in U87MG versus U251 versus T98G cells treated with 1200.00 µM temozolomide for 24-hours.

Standard

Post Hoc Comparisons - Condition and cell line_65

		Mean Difference	SE	t	P_{tukey}
(T98G_positive-control_apoptosis_early apoptosis)	(U251_positive-control_apoptosis_early apoptosis)	4.039	0.377	10.721	< .001
	(U87MG_positive-control_apoptosis_early apoptosis)	2.230	0.377	5.920	0.003
(U251_positive-control_apoptosis_early apoptosis)	(U87MG_positive-control_apoptosis_early apoptosis)	−1.809	0.377	−4.801	0.007

Note. P-value adjusted for comparing a family of 3

Output 13.232.: Descriptive statistics and normality (Shapiro-Wilk) assumption checking of data representing the occurrence of late apoptosis in U87MG versus U251 versus T98G cells treated with 1200.00 µM temozolomide for 24-hours.

Descriptive Statistics

	Transformed %_69		
	T98G_positive-control_apoptosis_late apoptosis	U251_positive-control_apoptosis_late apoptosis	U87MG_positive-control_apoptosis_late apoptosis
Valid	3	3	3
Missing	0	0	0
Mean	−3.846	−4.510	−2.217
Std. Deviation	0.042	0.154	0.304
Shapiro-Wilk	0.951	0.996	0.803
P-value of Shapiro-Wilk	0.572	0.885	0.123
Minimum	−3.882	−4.668	−2.411
Maximum	−3.799	−4.361	−1.866

Note. Excluded 31 rows from the analysis that correspond to the missing values of the split-by variable Condition and cell line_68

Output 13.233.: Equality of Variance (Levene's) assumption checks of data representing the occurrence of late apoptosis in U87MG versus U251 versus T98G cells treated with 1200.00 µM temozolomide for 24-hours.

Test for Equality of Variances (Levene's)

F	df1	df2	p
5.311	2.000	6.000	0.047

Output 13.234.: Kruskal-Wallis testing of data representing the occurrence of late apoptosis in U87MG versus U251 versus T98G cells treated with 1200.00 µM temozolomide for 24-hours.

Kruskal-Wallis Test

Factor	Statistic	df	p
Condition and cell line_68	7.200	2	0.027

Output 13.235.: Kruskal-Wallis post-hoc analysis of data representing the occurrence of late apoptosis in U87MG versus U251 versus T98G cells treated with 1200.00 µM temozolomide for 24-hours.

Standard

Post Hoc Comparisons - Condition and cell line_68

		Mean Difference	SE	t	P_{tukey}
(T98G_positive-control_apoptosis_late apoptosis)	(U251_positive-control_apoptosis_late apoptosis)	0.664	0.162	4.098	0.015
	(U87MG_positive-control_apoptosis_late apoptosis)	−1.629	0.162	−10.060	< .001
(U251_positive-control_apoptosis_late apoptosis)	(U87MG_positive-control_apoptosis_late apoptosis)	−2.293	0.162	−14.158	< .001

Note. P-value adjusted for comparing a family of 3

Output 13.236.: Descriptive statistics and normality (Shapiro-Wilk) assumption checking of data representing the occurrence of necrosis in U87MG versus U251 versus T98G cells treated with 1200.00 µM temozolomide for 24-hours.

Descriptive Statistics

	Transformed %_72		
	T98G_positive-control_apoptosis_necrosis	U251_positive-control_apoptosis_necrosis	U87MG_positive-control_apoptosis_necrosis
Valid	3	3	3
Missing	0	0	0
Mean	0.247	3.275	2.171
Std. Deviation	0.233	0.225	0.281
Shapiro-Wilk	1.000	0.974	0.839
P-value of Shapiro-Wilk	0.984	0.691	0.211
Minimum	0.016	3.032	1.849
Maximum	0.481	3.476	2.363

Note. Excluded 31 rows from the analysis that correspond to the missing values of the split-by variable Condition and cell line_71

Output 13.237.: Equality of Variance (Levene's) assumption checks of of data representing the occurrence of necrosis in U87MG versus U251 versus T98G cells treated with 1200.00 µM temozolomide for 24-hours.

Test for Equality of Variances (Levene's)

F	df1	df2	p
0.247	2.000	6.000	0.789

Output 13.238.: One-way ANOVA testing of data representing the occurrence of necrosis in U87MG versus U251 versus T98G cells treated with 1200.00 µM temozolomide for 24-hours.

ANOVA - Transformed %_72

Cases	Sum of Squares	df	Mean Square	F	p
Condition and cell line_71	14.085	2	7.043	115.080	< .001
Residuals	0.367	6	0.061		

Note. Type III Sum of Squares

Output 13.239.: One-way ANOVA post-hoc analysis of data representing the occurrence of necrosis in U87MG versus U251 versus T98G cells treated with 1200.00 µM temozolomide for 24-hours.

Standard

Post Hoc Comparisons - Condition and cell line_71

		Mean Difference	SE	t	P_{tukey}
(T98G_positive-control_apoptosis_necrosis)	(U251_positive-control_apoptosis_necrosis)	−3.028	0.202	−14.989	< .001
	(U87MG_positive-control_apoptosis_necrosis)	−1.924	0.202	−9.525	< .001
(U251_positive-control_apoptosis_necrosis)	(U87MG_positive-control_apoptosis_necrosis)	1.104	0.202	5.464	0.004

Note. P-value adjusted for comparing a family of 3

Output 13.240.: Descriptive statistics and normality (Shapiro-Wilk) assumption checking of data representing the occurrence of autophagy in U87MG versus U251 versus T98G cells treated with 1200.00 µM temozolomide for 24-hours.

Descriptive Statistics

	Transformed %_75		
	T98G_positive-control_autophagy	U251_positive-control_autophagy	U87MG_positive-control_autophagy
Valid	3	3	3
Missing	0	0	0
Mean	3.411	−1.297	0.482
Std. Deviation	0.539	0.173	0.232
Shapiro-Wilk	0.922	0.804	0.945
P-value of Shapiro-Wilk	0.460	0.124	0.548
Minimum	2.806	−1.496	0.225
Maximum	3.842	−1.186	0.677

Note. Excluded 31 rows from the analysis that correspond to the missing values of the split-by variable Condition and cell line_74

Output 13.241.: Equality of Variance (Levene's) assumption checks of of data representing the occurrence of autophagy in U87MG versus U251 versus T98G cells treated with 1200.00 µM temozolomide for 24-hours.

Test for Equality of Variances (Levene's)

F	df1	df2	p
3.188	2.000	6.000	0.114

Output 13.242.: One-way ANOVA testing of data representing the occurrence of autophagy in U87MG versus U251 versus T98G cells treated with 1200.00 µM temozolomide for 24-hours.

ANOVA - Transformed %_75

Cases	Sum of Squares	df	Mean Square	F	p
Condition and cell line_74	33.903	2	16.952	135.661	< .001
Residuals	0.750	6	0.125		

Note. Type III Sum of Squares

Output 13.243.: One-way ANOVA post-hoc analysis of data representing the occurrence of autophagy in U87MG versus U251 versus T98G cells treated with 1200.00 µM temozolomide for 24-hours.

Standard

Post Hoc Comparisons - Condition and cell line_74

		Mean Difference	SE	t	P_{tukey}
(T98G_positive-control_autophagy)	(U251_positive-control_autophagy)	4.708	0.289	16.311	< .001
	(U87MG_positive-control_autophagy)	2.929	0.289	10.147	< .001
(U251_positive-control_autophagy)	(U87MG_positive-control_autophagy)	−1.779	0.289	−6.164	0.002

Note. P-value adjusted for comparing a family of 3

13.6.2. Assessing differences in the occurrence of different cell death types investigated per cell line and treatment condition.

Output 13.244.: Descriptive statistics and normality (Shapiro-Wilk) assumption checking of data representing the occurrence of early apoptosis versus late apoptosis versus necrosis versus autophagy in U87MG cells treated with 5.00 mM H_2O_2 for 24-hours.

Descriptive Statistics

	Transformed %_15			
	U87MG_positive-control_apoptosis_early apoptosis	U87MG_positive-control_apoptosis_late apoptosis	U87MG_positive-control_apoptosis_necrosis	U87MG_positive-control_autophagy
Valid	3	3	3	2
Missing	0	0	0	0
Mean	−6.379	−2.506	2.354	0.975
Std. Deviation	0.099	0.097	0.105	0.028
Shapiro-Wilk	0.750	0.768	0.947	NaN
P-value of Shapiro-Wilk	< .001	0.040	0.556	NaN
Minimum	−6.436	−2.618	2.266	0.954
Maximum	−6.264	−2.448	2.470	0.995

Note. Excluded 29 rows from the analysis that correspond to the missing values of the split-by variable Condition and cell line_14

Output 13.245.: Equality of Variance (Levene's) assumption checks of data representing the occurrence of early apoptosis versus late apoptosis versus necrosis versus autophagy in U87MG cells treated with 5.00 mM H_2O_2 for 24-hours.

Test for Equality of Variances (Levene's)

F	df1	df2	p
1.441	3.000	7.000	0.310

Output 13.246.: Kruskal-Wallis testing of data representing the occurrence of early apoptosis versus late apoptosis versus necrosis versus autophagy in U87MG cells treated with 5.00 mM H_2O_2 for 24-hours.

Kruskal–Wallis Test

Factor	Statistic	df	p
Condition and cell line_14	9.452	3	0.024

Output 13.247.: Kurskal-Wallis post-hoc analysis of data representing the occurrence of early apoptosis versus late apoptosis versus necrosis versus autophagy in U87MG cells treated with 5.00 mM H_2O_2 for 24-hours.

Standard

Post Hoc Comparisons - Condition and cell line_14

		Mean Difference	SE	t	P_{tukey}
(U87MG_positive-control_apoptosis_early apoptosis)	(U87MG_positive-control_apoptosis_late apoptosis)	−3.873	0.076	−50.654	< .001
	(U87MG_positive-control_apoptosis_necrosis)	−8.733	0.076	−114.213	< .001
	(U87MG_positive-control_autophagy)	−7.353	0.085	−86.020	< .001
(U87MG_positive-control_apoptosis_late apoptosis)	(U87MG_positive-control_apoptosis_necrosis)	−4.860	0.076	−63.559	< .001
	(U87MG_positive-control_autophagy)	−3.480	0.085	−40.714	< .001
(U87MG_positive-control_apoptosis_necrosis)	(U87MG_positive-control_autophagy)	1.379	0.085	16.135	< .001

Note. P-value adjusted for comparing a family of 4

Output 13.248.: Descriptive statistics and normality (Shapiro-Wilk) assumption checking of data representing the occurrence of early apoptosis versus late apoptosis versus necrosis versus autophagy in U251 cells treated with 5.00 mM H_2O_2 for 24-hours.

Descriptive Statistics

	Transformed %_18			
	U251_positive-control_apoptosis_early apoptosis	U251_positive-control_apoptosis_late apoptosis	U251_positive-control_apoptosis_necrosis	U251_positive-control_autophagy
Valid	3	3	3	2
Missing	0	0	0	0
Mean	−8.234	−4.300	3.200	0.161
Std. Deviation	1.260	0.363	0.211	0.091
Shapiro-Wilk	0.906	0.995	0.841	NaN
P-value of Shapiro-Wilk	0.405	0.864	0.215	NaN
Minimum	−9.210	−4.647	3.055	0.096
Maximum	−6.811	−3.923	3.442	0.225

Note. Excluded 29 rows from the analysis that correspond to the missing values of the split-by variable Condition and cell line_17

Output 13.249.: Equality of Variance (Levene's) assumption checks of data representing the occurrence of early apoptosis versus late apoptosis versus necrosis versus autophagy in U251 cells treated with 5.00 mM H_2O_2 for 24-hours.

Test for Equality of Variances (Levene's)

F	df1	df2	p
5.640	3.000	7.000	0.028

Output 13.250.: Kruskal-Wallis testing of data representing the occurrence of early apoptosis versus late apoptosis versus necrosis versus autophagy in U251 cells treated with 5.00 mM H_2O_2 for 24-hours.

Kruskal–Wallis Test

Factor	Statistic	df	p
Condition and cell line_17	9.409	3	0.024

Output 13.251.: K*rus*kal-Wallis post-hoc analysis of data representing the occurrence of early apoptosis versus late apoptosis versus necrosis versus autophagy in U251 cells treated with 5.00 mM H_2O_2 for 24-hours.

Post Hoc Comparisons - Condition and cell line_17

		Mean Difference	SE	t	P_{tukey}
(U251_positive-control_apoptosis_early apoptosis)	(U251_positive-control_apoptosis_late apoptosis)	−3.934	0.580	−6.778	0.001
	(U251_positive-control_apoptosis_necrosis)	−11.434	0.580	−19.701	< .001
	(U251_positive-control_autophagy)	−8.394	0.649	−12.937	< .001
(U251_positive-control_apoptosis_late apoptosis)	(U251_positive-control_apoptosis_necrosis)	−7.500	0.580	−12.923	< .001
	(U251_positive-control_autophagy)	−4.460	0.649	−6.874	0.001
(U251_positive-control_apoptosis_necrosis)	(U251_positive-control_autophagy)	3.039	0.649	4.684	0.009

Note. P-value adjusted for comparing a family of 4

Output 13.252.: Descriptive statistics and normality (Shapiro-Wilk) assumption checking of data representing the occurrence of early apoptosis versus late apoptosis versus necrosis versus autophagy in T98G cells treated with 5.00 mM H_2O_2 for 24-hours.

Descriptive Statistics

	Transformed %_21			
	T98G_positive-control_apoptosis_early apoptosis	T98G_positive-control_apoptosis_late apoptosis	T98G_positive-control_apoptosis_necrosis	T98G_positive-control_autophagy
Valid	3	3	3	2
Missing	0	0	0	0
Mean	−5.111	−4.584	−0.100	3.429
Std. Deviation	0.143	1.222	1.394	0.116
Shapiro-Wilk	0.960	1.000	0.826	NaN
P-value of Shapiro-Wilk	0.617	0.999	0.177	NaN
Minimum	−5.235	−5.806	−1.030	3.347
Maximum	−4.955	−3.362	1.503	3.511

Note. Excluded 29 rows from the analysis that correspond to the missing values of the split-by variable Condition and cell line_20

Output 13.253.: Equality of Variance (Levene's) assumption checks of data representing the occurrence of early apoptosis versus late apoptosis versus necrosis versus autophagy in T98G cells treated with 5.00 mM H_2O_2 for 24-hours.

Test for Equality of Variances (Levene's)

F	df1	df2	p
3.268	3.000	7.000	0.089

Output 13.254.: One-way ANOVA testing of data representing the occurrence of early apoptosis versus late apoptosis versus necrosis versus autophagy in T98G cells treated with 5.00 mM H_2O_2 for 24-hours.

ANOVA - Transformed %_21

Cases	Sum of Squares	df	Mean Square	F	p
Condition and cell line_20	118.829	3	39.610	40.024	< .001
Residuals	6.928	7	0.990		

Note. Type III Sum of Squares

Output 13.255.: One-way ANOVA post-hoc analysis of data representing the occurrence of early apoptosis versus late apoptosis versus necrosis versus autophagy in T98G cells treated with 5.00 mM H_2O_2 for 24-hours.

Post Hoc Comparisons - Condition and cell line_20

		Mean Difference	SE	t	P_{tukey}
(T98G_positive-control_apoptosis_early apoptosis)	(T98G_positive-control_apoptosis_late apoptosis)	−0.527	0.812	−0.649	0.913
	(T98G_positive-control_apoptosis_necrosis)	−5.011	0.812	−6.170	0.002
	(T98G_positive-control_autophagy)	−8.540	0.908	−9.404	< .001
(T98G_positive-control_apoptosis_late apoptosis)	(T98G_positive-control_apoptosis_necrosis)	−4.485	0.812	−5.521	0.004
	(T98G_positive-control_autophagy)	−8.013	0.908	−8.824	< .001
(T98G_positive-control_apoptosis_necrosis)	(T98G_positive-control_autophagy)	−3.529	0.908	−3.886	0.024

Note. P-value adjusted for comparing a family of 4

Output 13.256.: Descriptive statistics and normality (Shapiro-Wilk) assumption checking of data representing the occurrence of early apoptosis versus late apoptosis versus necrosis versus autophagy in U87MG cells treated with 6.25 µM α-solanine for 24-hours.

Descriptive Statistics

	Transformed %_36			
	U87MG_positive-control_apoptosis_early apoptosis	U87MG_positive-control_apoptosis_late apoptosis	U87MG_positive-control_apoptosis_necrosis	U87MG_positive-control_autophagy
Valid	3	3	3	3
Missing	0	0	0	0
Mean	−7.247	−2.827	2.783	1.074
Std. Deviation	0.704	0.273	0.254	0.708
Shapiro-Wilk	0.883	0.882	0.925	0.899
P-value of Shapiro-Wilk	0.333	0.329	0.471	0.383
Minimum	−8.047	−3.030	2.498	0.532
Maximum	−6.724	−2.517	2.987	1.875

Note. Excluded 28 rows from the analysis that correspond to the missing values of the split-by variable Condition and cell line_35

Output 13.257.: Equality of Variance (Levene's) assumption checks of data representing the occurrence of early apoptosis versus late apoptosis versus necrosis versus autophagy in U87MG cells treated with 6.25 µM α-solanine for 24-hours.

Test for Equality of Variances (Levene's)

F	df1	df2	p
2.769	3.000	8.000	0.111

Output 13.258.: One-way ANOVA testing of data representing the occurrence of early apoptosis versus late apoptosis versus necrosis versus autophagy in U87MG cells treated with 6.25 µM α-solanine for 24-hours.

ANOVA - Transformed %_36

Cases	Sum of Squares	df	Mean Square	F	p
Condition and cell line_35	179.222	3	59.741	210.407	< .001
Residuals	2.271	8	0.284		

Note. Type III Sum of Squares

Output 13.259.:One-way ANOVA post-hoc analysis of data representing the occurrence of early apoptosis versus late apoptosis versus necrosis versus autophagy in U87MG cells treated with 6.25 µM α-solanine for 24-hours.

Standard

Post Hoc Comparisons - Condition and cell line_35

		Mean Difference	SE	t	P_{tukey}
(U87MG_positive-control_apoptosis_early apoptosis)	(U87MG_positive-control_apoptosis_late apoptosis)	−4.419	0.435	−10.157	< .001
	(U87MG_positive-control_apoptosis_necrosis)	−10.029	0.435	−23.053	< .001
	(U87MG_positive-control_autophagy)	−8.320	0.435	−19.124	< .001
(U87MG_positive-control_apoptosis_late apoptosis)	(U87MG_positive-control_apoptosis_necrosis)	−5.610	0.435	−12.895	< .001
	(U87MG_positive-control_autophagy)	−3.901	0.435	−8.967	< .001
(U87MG_positive-control_apoptosis_necrosis)	(U87MG_positive-control_autophagy)	1.709	0.435	3.928	0.018

Note. P-value adjusted for comparing a family of 4

Output 13.260.: Descriptive statistics and normality (Shapiro-Wilk) assumption checking of data representing the occurrence of early apoptosis versus late apoptosis versus necrosis versus autophagy in U251 cells treated with 6.25 µM α-solanine for 24-hours.

Descriptive Statistics ▼

	Transformed %_39			
	U251_positive-control_apoptosis_early apoptosis	U251_positive-control_apoptosis_late apoptosis	U251_positive-control_apoptosis_necrosis	U251_positive-control_autophagy
Valid	3	3	3	3
Missing	0	0	0	0
Mean	−3.827	−4.928	−2.756	0.890
Std. Deviation	0.302	0.643	0.611	1.163
Shapiro-Wilk	0.948	0.850	0.995	1.000
P-value of Shapiro-Wilk	0.559	0.240	0.865	0.964
Minimum	−4.082	−5.377	−3.341	−0.286
Maximum	−3.493	−4.191	−2.122	2.041

Note. Excluded 28 rows from the analysis that correspond to the missing values of the split-by variable Condition and cell line_38

Output 13.261.: Equality of Variance (Levene's) assumption checks of data representing the occurrence of early apoptosis versus late apoptosis versus necrosis versus autophagy in U251 cells treated with 6.25 µM α-solanine for 24-hours.

Test for Equality of Variances (Levene's)

F	df1	df2	p
1.069	3.000	8.000	0.415

Output 13.262.: One-way ANOVA testing of data representing the occurrence of early apoptosis versus late apoptosis versus necrosis versus autophagy in U251 cells treated with 6.25 µM α-solanine for 24-hours.

ANOVA - Transformed %_39 ▼

Cases	Sum of Squares	df	Mean Square	F	p
Condition and cell line_38	57.354	3	19.118	34.263	< .001
Residuals	4.464	8	0.558		

Note. Type III Sum of Squares

Output 13.263.: One-way ANOVA post-hoc analysis of data representing the occurrence of early apoptosis versus late apoptosis versus necrosis versus autophagy in U251 cells treated with 6.25 µM α-solanine for 24-hours.

Standard

Post Hoc Comparisons - Condition and cell line_38

		Mean Difference	SE	t	P_{tukey}
(U251_positive-control_apoptosis_early apoptosis)	(U251_positive-control_apoptosis_late apoptosis)	1.101	0.610	1.805	0.338
	(U251_positive-control_apoptosis_necrosis)	−1.071	0.610	−1.756	0.358
	(U251_positive-control_autophagy)	−4.717	0.610	−7.734	< .001
(U251_positive-control_apoptosis_late apoptosis)	(U251_positive-control_apoptosis_necrosis)	−2.172	0.610	−3.561	0.030
	(U251_positive-control_autophagy)	−5.818	0.610	−9.539	< .001
(U251_positive-control_apoptosis_necrosis)	(U251_positive-control_autophagy)	−3.646	0.610	−5.978	0.001

Note. P-value adjusted for comparing a family of 4

Output 13.264.: Descriptive statistics and normality (Shapiro-Wilk) assumption checking of data representing the occurrence of early apoptosis versus late apoptosis versus necrosis versus autophagy in T98G cells treated with 6.25 µM α-solanine for 24-hours.

Descriptive Statistics

	Transformed %_42			
	T98G_positive-control_apoptosis_early apoptosis	T98G_positive-control_apoptosis_late apoptosis	T98G_positive-control_apoptosis_necrosis	T98G_positive-control_autophagy
Valid	3	3	3	3
Missing	0	0	0	0
Mean	−3.246	−6.954	−3.568	3.546
Std. Deviation	0.228	2.015	0.134	5.746
Shapiro-Wilk	0.999	0.925	0.988	0.999
P-value of Shapiro-Wilk	0.931	0.471	0.792	0.954
Minimum	−3.480	−9.210	−3.693	−2.279
Maximum	−3.023	−5.334	−3.426	9.210

Note. Excluded 28 rows from the analysis that correspond to the missing values of the split-by variable Condition and cell line_41

Output 13.265.: Equality of Variance (Levene's) assumption checks of data representing the occurrence of early apoptosis versus late apoptosis versus necrosis versus autophagy in T98G cells treated with 6.25 µM α-solanine for 24-hours.

Test for Equality of Variances (Levene's)

F	df1	df2	p
3.401	3.000	8.000	0.074

Output 13.266.: Kruskal-Wallis testing of data representing the occurrence of early apoptosis versus late apoptosis versus necrosis versus autophagy in T98G cells treated with 6.25 µM α-solanine for 24-hours.

ANOVA - Transformed %_42

Cases	Sum of Squares	df	Mean Square	F	p
Condition and cell line_41	174.224	3	58.075	6.253	0.017
Residuals	74.295	8	9.287		

Note. Type III Sum of Squares

Output 13.267.: Kruskal-Wallis post-hoc analysis of data representing the occurrence of early apoptosis versus late apoptosis versus necrosis versus autophagy in T98G cells treated with 6.25 µM α-solanine for 24-hours.

Standard ▼

Post Hoc Comparisons - Condition and cell line_41 ▼

		Mean Difference	SE	t	P_{tukey}
(T98G_positive-control_apoptosis_early apoptosis)	(T98G_positive-control_apoptosis_late apoptosis)	3.708	2.488	1.490	0.485
	(T98G_positive-control_apoptosis_necrosis)	0.321	2.488	0.129	0.999
	(T98G_positive-control_autophagy)	−6.792	2.488	−2.730	0.097
(T98G_positive-control_apoptosis_late apoptosis)	(T98G_positive-control_apoptosis_necrosis)	−3.387	2.488	−1.361	0.554
	(T98G_positive-control_autophagy)	−10.500	2.488	−4.220	0.012
(T98G_positive-control_apoptosis_necrosis)	(T98G_positive-control_autophagy)	−7.113	2.488	−2.859	0.081

Note. P-value adjusted for comparing a family of 4

Output 13.268.: Descriptive statistics and normality (Shapiro-Wilk) assumption checking of data representing the occurrence of early apoptosis versus late apoptosis versus necrosis versus autophagy in U87MG cells treated with culture (negative control) conditions for 24-hours.

Descriptive Statistics

	Transformed %_57			
	U87MG_positive-control_apoptosis_early apoptosis	U87MG_positive-control_apoptosis_late apoptosis	U87MG_positive-control_apoptosis_necrosis	U87MG_positive-control_autophagy
Valid	3	3	3	3
Missing	0	0	0	0
Mean	−6.370	−2.365	2.322	−1.241
Std. Deviation	0.546	0.118	0.128	0.662
Shapiro-Wilk	0.811	0.889	0.788	0.934
P-value of Shapiro-Wilk	0.140	0.352	0.086	0.504
Minimum	−6.724	−2.499	2.242	−1.782
Maximum	−5.741	−2.276	2.470	−0.502

Note. Excluded 28 rows from the analysis that correspond to the missing values of the split-by variable Condition and cell line_56

Output 13.269.: Equality of Variance (Levene's) assumption checks of data representing the occurrence of early apoptosis versus late apoptosis versus necrosis versus autophagy in U87MG cells treated with culture (negative control) conditions for 24-hours.

Test for Equality of Variances (Levene's)

F	df1	df2	p
4.701	3.000	8.000	0.036

Output 13.270.: Kruskal-Wallis testing of data representing the occurrence of early apoptosis versus late apoptosis versus necrosis versus autophagy in U87MG cells treated with culture (negative control) conditions for 24-hours.

Kruskal-Wallis Test

Factor	Statistic	df	p
Condition and cell line_56	10.385	3	0.016

Output 13.271.: *Kruskal*-Wallis post-hoc analysis of data representing the occurrence of early apoptosis versus late apoptosis versus necrosis versus autophagy in U87MG cells treated with culture (negative control) conditions for 24-hours.

Standard

Post Hoc Comparisons - Condition and cell line_56

		Mean Difference	SE	t	p_{tukey}
(U87MG_positive-control_apoptosis_early apoptosis)	(U87MG_positive-control_apoptosis_late apoptosis)	−4.005	0.358	−11.202	< .001
	(U87MG_positive-control_apoptosis_necrosis)	−8.692	0.358	−24.312	< .001
	(U87MG_positive-control_autophagy)	−5.129	0.358	−14.347	< .001
(U87MG_positive-control_apoptosis_late apoptosis)	(U87MG_positive-control_apoptosis_necrosis)	−4.687	0.358	−13.111	< .001
	(U87MG_positive-control_autophagy)	−1.125	0.358	−3.146	0.054
(U87MG_positive-control_apoptosis_necrosis)	(U87MG_positive-control_autophagy)	3.563	0.358	9.965	< .001

Note. P-value adjusted for comparing a family of 4

Output 13.272.: Descriptive statistics and normality (Shapiro-Wilk) assumption checking of data representing the occurrence of early apoptosis versus late apoptosis versus necrosis versus autophagy in U251 cells treated with culture (negative control) conditions for 24-hours.

Descriptive Statistics

	Transformed %_60			
	U251_positive-control_apoptosis_early apoptosis	U251_positive-control_apoptosis_late apoptosis	U251_positive-control_apoptosis_necrosis	U251_positive-control_autophagy
Valid	3	3	3	3
Missing	0	0	0	0
Mean	−8.234	−4.179	2.672	−2.571
Std. Deviation	1.260	0.427	0.695	0.220
Shapiro-Wilk	0.906	0.824	0.945	0.996
P-value of Shapiro-Wilk	0.405	0.172	0.547	0.880
Minimum	−9.210	−4.463	2.091	−2.782
Maximum	−6.811	−3.688	3.442	−2.343

Note. Excluded 28 rows from the analysis that correspond to the missing values of the split-by variable Condition and cell line_59

Output 13.273.: Equality of Variance (Levene's) assumption checks of data representing the occurrence of early apoptosis versus late apoptosis versus necrosis versus autophagy in U251 cells treated with culture (negative control) conditions for 24-hours.

Test for Equality of Variances (Levene's)

F	df1	df2	p
3.880	3.000	8.000	0.056

Output 13.274.: Kruskal-Wallis testing of data representing the occurrence of early apoptosis versus late apoptosis versus necrosis versus autophagy in U251 cells treated with culture (negative control) conditions for 24-hours.

Kruskal-Wallis Test

Factor	Statistic	df	p
Condition and cell line_59	10.385	3	0.016

Output 13.275.: Kruskal-Wallis post-hoc analysis of data representing the occurrence of early apoptosis versus late apoptosis versus necrosis versus autophagy in U251 cells treated with culture (negative control) conditions for 24-hours.

Standard

Post Hoc Comparisons - Condition and cell line_59

		Mean Difference	SE	t	P_{tukey}
(U251_positive-control_apoptosis_early apoptosis)	(U251_positive-control_apoptosis_late apoptosis)	−4.055	0.619	−6.547	< .001
	(U251_positive-control_apoptosis_necrosis)	−10.906	0.619	−17.610	< .001
	(U251_positive-control_autophagy)	−5.663	0.619	−9.144	< .001
(U251_positive-control_apoptosis_late apoptosis)	(U251_positive-control_apoptosis_necrosis)	−6.851	0.619	−11.063	< .001
	(U251_positive-control_autophagy)	−1.608	0.619	−2.597	0.117
(U251_positive-control_apoptosis_necrosis)	(U251_positive-control_autophagy)	5.243	0.619	8.466	< .001

Note. P-value adjusted for comparing a family of 4

Output 13.276.: Descriptive statistics and normality (Shapiro-Wilk) assumption checking of data representing the occurrence of early apoptosis versus late apoptosis versus necrosis versus autophagy in T98G cells treated with culture (negative control) conditions for 24-hours.

Descriptive Statistics

	Transformed %_63			
	T98G_positive-control_apoptosis_early apoptosis	T98G_positive-control_apoptosis_late apoptosis	T98G_positive-control_apoptosis_necrosis	T98G_positive-control_autophagy
Valid	3	3	3	3
Missing	0	0	0	0
Mean	−5.203	−4.431	−0.314	3.307
Std. Deviation	0.430	0.330	0.625	0.177
Shapiro-Wilk	0.993	0.815	0.860	0.750
P-value of Shapiro-Wilk	0.841	0.150	0.267	< .001
Minimum	−5.651	−4.647	−0.758	3.103
Maximum	−4.795	−4.051	0.401	3.409

Note. Excluded 28 rows from the analysis that correspond to the missing values of the split-by variable Condition and cell line_62

Output 13.277.: Equality of Variance (Levene's) assumption checks of data representing the occurrence of early apoptosis versus late apoptosis versus necrosis versus autophagy in T98G cells treated with culture (negative control) conditions for 24-hours.

Test for Equality of Variances (Levene's)

F	df1	df2	p
2.053	3.000	8.000	0.185

Output 13.278.: One-way ANOVA testing of data representing the occurrence of early apoptosis versus late apoptosis versus necrosis versus autophagy in T98G cells treated with culture (negative control) conditions for 24-hours.

ANOVA - Transformed %_63

Cases	Sum of Squares	df	Mean Square	F	p
Condition and cell line_62	140.149	3	46.716	261.082	< .001
Residuals	1.431	8	0.179		

Note. Type III Sum of Squares

Output 13.279.: One-way ANOVA post-hoc analysis of data representing the occurrence of early apoptosis versus late apoptosis versus necrosis versus autophagy in T98G cells treated with culture (negative control) conditions for 24-hours.

Standard

Post Hoc Comparisons - Condition and cell line_62

		Mean Difference	SE	t	P_{tukey}
(T98G_positive-control_apoptosis_early apoptosis)	(T98G_positive-control_apoptosis_late apoptosis)	−0.772	0.345	−2.234	0.194
	(T98G_positive-control_apoptosis_necrosis)	−4.889	0.345	−14.156	< .001
	(T98G_positive-control_autophagy)	−8.510	0.345	−24.639	< .001
(T98G_positive-control_apoptosis_late apoptosis)	(T98G_positive-control_apoptosis_necrosis)	−4.117	0.345	−11.921	< .001
	(T98G_positive-control_autophagy)	−7.738	0.345	−22.405	< .001
(T98G_positive-control_apoptosis_necrosis)	(T98G_positive-control_autophagy)	−3.621	0.345	−10.484	< .001

Note. P-value adjusted for comparing a family of 4

Output 13.280.: Descriptive statistics and normality (Shapiro-Wilk) assumption checking of data representing the occurrence of early apoptosis versus late apoptosis versus necrosis versus autophagy in U87MG cells treated with 1200.00 µM temozolomide for 24-hours.

Descriptive Statistics

	Transformed %_78			
	U87MG_positive-control_apoptosis_early apoptosis	U87MG_positive-control_apoptosis_late apoptosis	U87MG_positive-control_apoptosis_necrosis	U87MG_positive-control_autophagy
Valid	3	3	3	3
Missing	0	0	0	0
Mean	−7.245	−2.217	2.171	0.482
Std. Deviation	0.751	0.304	0.281	0.232
Shapiro-Wilk	0.750	0.803	0.839	0.945
P-value of Shapiro-Wilk	< .001	0.123	0.211	0.548
Minimum	−8.111	−2.411	1.849	0.225
Maximum	−6.811	−1.866	2.363	0.677

Note. Excluded 28 rows from the analysis that correspond to the missing values of the split-by variable Condition and cell line_77

Output 13.281.: Equality of Variance (Levene's) assumption checks of data representing the occurrence of early apoptosis versus late apoptosis versus necrosis versus autophagy in U87MG cells treated with 1200.00 µM temozolomide for 24-hours.

Test for Equality of Variances (Levene's)

F	df1	df2	p
4.545	3.000	8.000	0.039

Output 13.282.: Kruskal-Wallis testing of data representing the occurrence of early apoptosis versus late apoptosis versus necrosis versus autophagy in U87MG cells treated with 1200.00 µM temozolomide for 24-hours.

Kruskal-Wallis Test

Factor	Statistic	df	p
Condition and cell line_77	10.421	3	0.015

Output 13.283.: Kurskal-Wallis post-hoc analysis of data representing the occurrence of early apoptosis versus late apoptosis versus necrosis versus autophagy in U87MG cells treated with 1200.00 µM temozolomide for 24-hours.

Standard

Post Hoc Comparisons - Condition and cell line_77

		Mean Difference	SE	t	P_{tukey}
(U87MG_positive-control_apoptosis_early apoptosis)	(U87MG_positive-control_apoptosis_late apoptosis)	−5.028	0.363	−13.867	< .001
	(U87MG_positive-control_apoptosis_necrosis)	−9.416	0.363	−25.968	< .001
	(U87MG_positive-control_autophagy)	−7.727	0.363	−21.310	< .001
(U87MG_positive-control_apoptosis_late apoptosis)	(U87MG_positive-control_apoptosis_necrosis)	−4.388	0.363	−12.101	< .001
	(U87MG_positive-control_autophagy)	−2.699	0.363	−7.443	< .001
(U87MG_positive-control_apoptosis_necrosis)	(U87MG_positive-control_autophagy)	1.689	0.363	4.658	0.007

Note. P-value adjusted for comparing a family of 4

Output 13.284.: Descriptive statistics and normality (Shapiro-Wilk) assumption checking of data representing the occurrence of early apoptosis versus late apoptosis versus necrosis versus autophagy in U251 cells treated with 1200.00 µM temozolomide for 24-hours.

Descriptive Statistics

	Transformed %_81			
	U251_positive-control_apoptosis_early apoptosis	U251_positive-control_apoptosis_late apoptosis	U251_positive-control_apoptosis_necrosis	U251_positive-control_autophagy
Valid	3	3	3	3
Missing	0	0	0	0
Mean	−9.054	−4.510	3.275	−1.297
Std. Deviation	0.271	0.154	0.225	0.173
Shapiro-Wilk	0.750	0.996	0.974	0.804
P-value of Shapiro-Wilk	< .001	0.885	0.691	0.124
Minimum	−9.210	−4.668	3.032	−1.496
Maximum	−8.740	−4.361	3.476	−1.186

Note. Excluded 28 rows from the analysis that correspond to the missing values of the split-by variable Condition and cell line_80

Output 13.285.: Equality of Variance (Levene's) assumption checks of data representing the occurrence of early apoptosis versus late apoptosis versus necrosis versus autophagy in U251 cells treated with 1200.00 µM temozolomide for 24-hours.

Test for Equality of Variances (Levene's)

F	df1	df2	p
0.784	3.000	8.000	0.535

Output 13.286.: Kruskal-Wallis testing of data representing the occurrence of early apoptosis versus late apoptosis versus necrosis versus autophagy in U251 cells treated with 1200.00 µM temozolomide for 24-hours.

Kruskal-Wallis Test

Factor	Statistic	df	p
Condition and cell line_80	10.421	3	0.015

Output 13.287.: Kruskal-Wallis post-hoc analysis of data representing the occurrence of early apoptosis versus late apoptosis versus necrosis versus autophagy in U251 cells treated with 1200.00 µM temozolomide for 24-hours.

Standard

Post Hoc Comparisons - Condition and cell line_80

		Mean Difference	SE	t	P_{tukey}
(U251_positive-control_apoptosis_early apoptosis)	(U251_positive-control_apoptosis_late apoptosis)	−4.544	0.172	−26.393	< .001
	(U251_positive-control_apoptosis_necrosis)	−12.329	0.172	−71.606	< .001
	(U251_positive-control_autophagy)	−7.757	0.172	−45.053	< .001
(U251_positive-control_apoptosis_late apoptosis)	(U251_positive-control_apoptosis_necrosis)	−7.784	0.172	−45.214	< .001
	(U251_positive-control_autophagy)	−3.213	0.172	−18.660	< .001
(U251_positive-control_apoptosis_necrosis)	(U251_positive-control_autophagy)	4.572	0.172	26.554	< .001

Note. P-value adjusted for comparing a family of 4

Output 13.288.: Descriptive statistics and normality (Shapiro-Wilk) assumption checking of data representing the occurrence of early apoptosis versus late apoptosis versus necrosis versus autophagy in T98G cells treated with 1200.00 µM temozolomide for 24-hours.

Descriptive Statistics

	Transformed %_84			
	T98G_positive-control_apoptosis_early apoptosis	T98G_positive-control_apoptosis_late apoptosis	T98G_positive-control_apoptosis_necrosis	T98G_positive-control_autophagy
Valid	3	3	3	3
Missing	0	0	0	0
Mean	−5.015	−3.846	0.247	3.411
Std. Deviation	0.040	0.042	0.233	0.539
Shapiro-Wilk	0.897	0.951	1.000	0.922
P-value of Shapiro-Wilk	0.375	0.572	0.984	0.460
Minimum	−5.045	−3.882	0.016	2.806
Maximum	−4.969	−3.799	0.481	3.842

Note. Excluded 28 rows from the analysis that correspond to the missing values of the split-by variable Condition and cell line_83

Output 13.289.: Equality of Variance (Levene's) assumption checks of data representing the occurrence of early apoptosis versus late apoptosis versus necrosis versus autophagy in T98G cells treated with 1200.00 µM temozolomide for 24-hours.

Test for Equality of Variances (Levene's)

F	df1	df2	p
5.667	3.000	8.000	0.022

Output 13.290.: Kruskal-Wallis testing of data representing the occurrence of early apoptosis versus late apoptosis versus necrosis versus autophagy in T98G cells treated with 1200.00 µM temozolomide for 24-hours.

Kruskal–Wallis Test

Factor	Statistic	df	p
Condition and cell line_83	10.385	3	0.016

Output 13.291.: *Kruskal*-Wallis post-hoc analysis of data representing the occurrence of early apoptosis versus late apoptosis versus necrosis versus autophagy in T98G cells treated with 1200.00 µM temozolomide for 24-hours.

Standard

Post Hoc Comparisons - Condition and cell line_83

		Mean Difference	SE	t	P_{tukey}
(T98G_positive-control_apoptosis_early apoptosis)	(T98G_positive-control_apoptosis_late apoptosis)	−1.169	0.241	−4.850	0.006
	(T98G_positive-control_apoptosis_necrosis)	−5.262	0.241	−21.836	< .001
	(T98G_positive-control_autophagy)	−8.425	0.241	−34.964	< .001
(T98G_positive-control_apoptosis_late apoptosis)	(T98G_positive-control_apoptosis_necrosis)	−4.093	0.241	−16.986	< .001
	(T98G_positive-control_autophagy)	−7.257	0.241	−30.114	< .001
(T98G_positive-control_apoptosis_necrosis)	(T98G_positive-control_autophagy)	−3.163	0.241	−13.128	< .001

Note. P-value adjusted for comparing a family of 4

13.6.3. Comparing the effect of treatment conditions on cell death investigated per cell line

Output 13.292.: Descriptive statistics and normality (Shapiro-Wilk) assumption checking of data representing the occurrence of early apoptosis in U87MG cells treated with 6.25 µM α-solanine versus 5.00 mM H_2O_2 versus culture (negative control) conditions versus 1200.00 µM temozolomide for 24-hours.

Descriptive Statistics

	Transformed %_123			
	negative control	positive control	temozolomide	∝-solanine
Valid	3	3	3	3
Missing	0	0	0	0
Mean	−6.370	−6.379	−7.245	−7.247
Std. Deviation	0.546	0.099	0.751	0.704
Shapiro-Wilk	0.811	0.750	0.750	0.883
P-value of Shapiro-Wilk	0.140	< .001	< .001	0.333
Minimum	−6.724	−6.436	−8.111	−8.047
Maximum	−5.741	−6.264	−6.811	−6.724

Note. Excluded 28 rows from the analysis that correspond to the missing values of the split-by variable Condition and cell line_122

Output 13.293.: Equality of Variance (Levene's) assumption checks of data representing the occurrence of early apoptosis in U87MG cells treated with 6.25 µM α-solanine versus 5.00 mM H_2O_2 versus culture (negative control) conditions versus 1200.00 µM temozolomide for 24-hours.

Test for Equality of Variances (Levene's)

F	df1	df2	p
3.710	3.000	8.000	0.061

Output 13.294.: Kruskal-Wallis testing of data representing the occurrence of early apoptosis in U87MG cells treated with 6.25 µM α-solanine versus 5.00 mM H_2O_2 versus culture (negative control) conditions versus 1200.00 µM temozolomide for 24-hours.

Kruskal-Wallis Test

Factor	Statistic	df	p
Condition and cell line_122	8.124	3	0.044

Output 13.295.: Kruskal-Wallis post-hoc analysis of data representing the occurrence of data representing the occurrence of early apoptosis in U87MG cells treated with 6.25 µM α-solanine versus 5.00 mM H_2O_2 versus culture (negative control) conditions versus 1200.00 µM temozolomide for 24-hours.

Standard

Post Hoc Comparisons - Condition and cell line_122

		Mean Difference	SE	t	p_{tukey}
negative control	positive control	0.009	0.477	0.019	1.000
	temozolomide	0.875	0.477	1.833	0.326
	(∝-solanine)	0.877	0.477	1.837	0.325
positive control	temozolomide	0.866	0.477	1.815	0.334
	(∝-solanine)	0.868	0.477	1.819	0.332
temozolomide	(∝-solanine)	0.002	0.477	0.004	1.000

Note. P-value adjusted for comparing a family of 4

Output 13.296.: Descriptive statistics and normality (Shapiro-Wilk) assumption checking of data representing the occurrence of late apoptosis in U87MG cells treated with 6.25 µM α-solanine versus 5.00 mM H_2O_2 versus culture (negative control) conditions versus 1200.00 µM temozolomide for 24-hours.

Descriptive Statistics

	Transformed %_126			
	negative control	positive control	temozolomide	∝-solanine
Valid	3	3	3	3
Missing	0	0	0	0
Mean	−2.365	−2.506	−2.217	−2.827
Std. Deviation	0.118	0.097	0.304	0.273
Shapiro-Wilk	0.889	0.768	0.803	0.882
P-value of Shapiro-Wilk	0.352	0.040	0.123	0.329
Minimum	−2.499	−2.618	−2.411	−3.030
Maximum	−2.276	−2.448	−1.866	−2.517

Note. Excluded 28 rows from the analysis that correspond to the missing values of the split-by variable Condition and cell line_125

Output 13.297.: Equality of Variance (Levene's) assumption checks of data representing the occurrence of late apoptosis in U87MG cells treated with 6.25 µM α-solanine versus 5.00 mM H_2O_2 versus culture (negative control) conditions versus 1200.00 µM temozolomide for 24-hours.

Test for Equality of Variances (Levene's)

F	df1	df2	p
3.284	3.000	8.000	0.079

Output 13.298.: Kruskal-Wallis testing of data representing the occurrence of late apoptosis in U87MG cells treated with 6.25 µM α-solanine versus 5.00 mM H_2O_2 versus culture (negative control) conditions versus 1200.00 µM temozolomide for 24-hours.

Kruskal-Wallis Test

Factor	Statistic	df	p
Condition and cell line_125	7.718	3	0.052

Output 13.299.: Kruskal-Wallis post-hoc analysis of data representing the occurrence of data representing the occurrence of late apoptosis in U87MG cells treated with 6.25 µM α-solanine versus 5.00 mM H_2O_2 versus culture (negative control) conditions versus 1200.00 µM temozolomide for 24-hours.

Standard

Post Hoc Comparisons - Condition and cell line_125

		Mean Difference	SE	t	p_{tukey}
negative control	positive control	0.141	0.178	0.789	0.857
	temozolomide	−0.149	0.178	−0.833	0.838
	(∝-solanine)	0.462	0.178	2.594	0.118
positive control	temozolomide	−0.289	0.178	−1.622	0.419
	(∝-solanine)	0.322	0.178	1.804	0.338
temozolomide	(∝-solanine)	0.611	0.178	3.427	0.037

Note. P-value adjusted for comparing a family of 4

Output 13.300.:Descriptive statistics and normality (Shapiro-Wilk) assumption checking of data representing the occurrence of necrosis in U87MG cells treated with 6.25 µM α-solanine versus 5.00 mM H_2O_2 versus culture (negative control) conditions versus 1200.00 µM temozolomide for 24-hours.

Descriptive Statistics

	Transformed %_129			
	negative control	positive control	temozolomide	∝-solanine
Valid	3	3	3	3
Missing	0	0	0	0
Mean	2.322	2.354	2.171	2.783
Std. Deviation	0.128	0.105	0.281	0.254
Shapiro-Wilk	0.788	0.947	0.839	0.925
P-value of Shapiro-Wilk	0.086	0.556	0.211	0.471
Minimum	2.242	2.266	1.849	2.498
Maximum	2.470	2.470	2.363	2.987

Note. Excluded 28 rows from the analysis that correspond to the missing values of the split-by variable Condition and cell line_128

Output 13.301.: Equality of Variance (Levene's) assumption checks of data representing the occurrence of necrosis in U87MG cells treated with 6.25 µM α-solanine versus 5.00 mM H_2O_2 versus culture (negative control) conditions versus 1200.00 µM temozolomide for 24-hours.

Test for Equality of Variances (Levene's)

F	df1	df2	p
2.264	3.000	8.000	0.158

Output 13.302.: One-way ANOVA testing of data representing the occurrence of necrosis in U87MG cells treated with 6.25 µM α-solanine versus 5.00 mM H_2O_2 versus culture (negative control) conditions versus 1200.00 µM temozolomide for 24-hours.

ANOVA - Transformed %_129

Cases	Sum of Squares	df	Mean Square	F	p
Condition and cell line_128	0.621	3	0.207	4.838	0.033
Residuals	0.342	8	0.043		

Note. Type III Sum of Squares

Output 13.303.: One-way ANOVA post-hoc analysis of data representing the occurrence of data representing the occurrence of necrosis in U87MG cells treated with 6.25 µM α-solanine versus 5.00 mM H_2O_2 versus culture (negative control) conditions versus 1200.00 µM temozolomide for 24-hours.

Standard

Post Hoc Comparisons - Condition and cell line_128

		Mean Difference	SE	t	p_{tukey}
negative control	positive control	−0.032	0.169	−0.188	0.997
	temozolomide	0.151	0.169	0.893	0.809
	(∝-solanine)	−0.461	0.169	−2.729	0.098
positive control	temozolomide	0.183	0.169	1.081	0.710
	(∝-solanine)	−0.429	0.169	−2.541	0.127
temozolomide	(∝-solanine)	−0.612	0.169	−3.622	0.028

Note. P-value adjusted for comparing a family of 4

Output 13.304.: Descriptive statistics and normality (Shapiro-Wilk) assumption checking of data representing the occurrence of autophagy in U87MG cells treated with 6.25 µM α-solanine versus 5.00 mM H_2O_2 versus culture (negative control) conditions versus 1200.00 µM temozolomide for 24-hours.

Descriptive Statistics

	Transformed %_132			
	negative control	positive control	temozolomide	∝-solanine
Valid	3	3	3	3
Missing	0	0	0	0
Mean	0.482	1.174	−1.241	1.074
Std. Deviation	0.232	0.345	0.662	0.708
Shapiro-Wilk	0.945	0.799	0.934	0.899
P-value of Shapiro-Wilk	0.548	0.111	0.504	0.383
Minimum	0.225	0.954	−1.782	0.532
Maximum	0.677	1.572	−0.502	1.875

Note. Excluded 28 rows from the analysis that correspond to the missing values of the split-by variable Condition and cell line_131

Output 13.305.: Equality of Variance (Levene's) assumption checks of data representing the occurrence of autophagy in U87MG cells treated with 6.25 µM α-solanine versus 5.00 mM H_2O_2 versus culture (negative control) conditions versus 1200.00 µM temozolomide for 24-hours.

Test for Equality of Variances (Levene's)

F	df1	df2	p
2.141	3.000	8.000	0.173

Output 13.306.: One-way ANOVA testing of data representing the occurrence of autophagy in U87MG cells treated with 6.25 µM α-solanine versus 5.00 mM H_2O_2 versus culture (negative control) conditions versus 1200.00 µM temozolomide for 24-hours.

ANOVA - Transformed %_132

Cases	Sum of Squares	df	Mean Square	F	p
Condition and cell line_131	11.242	3	3.747	13.469	0.002
Residuals	2.226	8	0.278		

Note. Type III Sum of Squares

Output 13.307.: One-way ANOVA post-hoc analysis of data representing the occurrence of data representing the occurrence of autophagy in U87MG cells treated with 6.25 µM α-solanine versus 5.00 mM H_2O_2 versus culture (negative control) conditions versus 1200.00 µM temozolomide for 24-hours.

Standard

Post Hoc Comparisons - Condition and cell line_131

		Mean Difference	SE	t	p_{tukey}
negative control	positive control	−0.691	0.431	−1.605	0.427
	temozolomide	1.723	0.431	4.000	0.017
	(∝−solanine)	−0.591	0.431	−1.373	0.547
positive control	temozolomide	2.414	0.431	5.605	0.002
	(∝−solanine)	0.100	0.431	0.232	0.995
temozolomide	(∝−solanine)	−2.314	0.431	−5.374	0.003

Note. P-value adjusted for comparing a family of 4

Output 13.308.: Descriptive statistics and normality (Shapiro-Wilk) assumption checking of data representing the occurrence of early apoptosis in U251 cells treated with 6.25 µM α-solanine

versus 5.00 mM H_2O_2 versus culture (negative control) conditions 1200.00 µM versus temozolomide for 24-hours.

Descriptive Statistics

	Transformed %_135			
	negative control	positive control	temozolomide	∝-solanine
Valid	3	3	3	3
Missing	0	0	0	0
Mean	−8.234	−8.234	−9.054	−3.827
Std. Deviation	1.260	1.260	0.271	0.302
Shapiro-Wilk	0.906	0.906	0.750	0.948
P-value of Shapiro-Wilk	0.405	0.405	< .001	0.559
Minimum	−9.210	−9.210	−9.210	−4.082
Maximum	−6.811	−6.811	−8.740	−3.493

Note. Excluded 28 rows from the analysis that correspond to the missing values of the split-by variable Condition and cell line_134

Output 13.309.: Equality of Variance (Levene's) assumption checks of data representing the occurrence of early apoptosis in U251 cells treated with 6.25 µM α-solanine versus 5.00 mM H_2O_2 versus culture (negative control) conditions versus 1200.00 µM temozolomide for 24-hours.

Test for Equality of Variances (Levene's)

F	df1	df2	p
4.266	3.000	8.000	0.045

Output 13.310.:Kruskal-Wallis testing of data representing the occurrence of early apoptosis in U251 cells treated with 6.25 µM α-solanine versus 5.00 mM H_2O_2 versus culture (negative control) conditions versus 1200.00 µM temozolomide for 24-hours.

Kruskal-Wallis Test

Factor	Statistic	df	p
Condition and cell line_134	7.507	3	0.057

Output 13.311.: Descriptive statistics and normality (Shapiro-Wilk) assumption checking of data representing the occurrence of late apoptosis in U251 cells treated with 6.25 µM α-solanine versus 5.00 mM H_2O_2 versus culture (negative control) conditions versus 1200.00 µM temozolomide for 24-hours.

Descriptive Statistics

	Transformed %_138			
	negative control	positive control	temozolomide	∝-solanine
Valid	3	3	3	3
Missing	0	0	0	0
Mean	−4.179	−4.300	−4.510	−4.928
Std. Deviation	0.427	0.363	0.154	0.643
Shapiro-Wilk	0.824	0.995	0.996	0.850
P-value of Shapiro-Wilk	0.172	0.864	0.885	0.240
Minimum	−4.463	−4.647	−4.668	−5.377
Maximum	−3.688	−3.923	−4.361	−4.191

Note. Excluded 28 rows from the analysis that correspond to the missing values of the split-by variable Condition and cell line_137

Output 13.312.: Equality of Variance (Levene's) assumption checks of data representing the occurrence of late apoptosis in U251 cells treated with 6.25 µM α-solanine versus 5.00 mM H_2O_2 versus culture (negative control) conditions versus 1200.00 µM temozolomide for 24-hours.

Test for Equality of Variances (Levene's)

F	df1	df2	p
2.636	3.000	8.000	0.121

Output 13.313.: One-way ANOVA testing of data representing the occurrence of late apoptosis in U251 cells treated with 6.25 µM α-solanine versus 5.00 mM H_2O_2 versus culture (negative control) conditions versus 1200.00 µM temozolomide for 24-hours.

ANOVA - Transformed %_138

Cases	Sum of Squares	df	Mean Square	F	p
Condition and cell line_137	0.974	3	0.325	1.730	0.238
Residuals	1.502	8	0.188		

Note. Type III Sum of Squares

Output 13.314.: Descriptive statistics and normality (Shapiro-Wilk) assumption checking of data representing the occurrence of necrosis in U251 cells treated with 6.25 µM α-solanine versus 5.00 mM H_2O_2 versus culture (negative control) conditions versus 1200.00 µM temozolomide for 24-hours.

Descriptive Statistics

	Transformed %_141			
	negative control	positive control	temozolomide	∝-solanine
Valid	3	3	3	3
Missing	0	0	0	0
Mean	2.672	3.200	3.275	−2.756
Std. Deviation	0.695	0.211	0.225	0.611
Shapiro-Wilk	0.945	0.841	0.974	0.995
P-value of Shapiro-Wilk	0.547	0.215	0.691	0.865
Minimum	2.091	3.055	3.032	−3.341
Maximum	3.442	3.442	3.476	−2.122

Note. Excluded 28 rows from the analysis that correspond to the missing values of the split-by variable Condition and cell line_140

Output 13.315.: Equality of Variance (Levene's) assumption checks of data representing the occurrence of necrosis in U251 cells treated with 6.25 µM α-solanine versus 5.00 mM H_2O_2 versus culture (negative control) conditions versus 1200.00 µM temozolomide for 24-hours.

Test for Equality of Variances (Levene's)

F	df1	df2	p
1.868	3.000	8.000	0.213

Output 13.316.: One-way ANOVA testing of data representing the occurrence of necrosis in U251 cells treated with 6.25 µM α-solanine versus 5.00 mM H_2O_2 versus culture (negative control) conditions versus 1200.00 µM temozolomide for 24-hours.

ANOVA - Transformed %_141

Cases	Sum of Squares	df	Mean Square	F	p
Condition and cell line_140	76.474	3	25.491	107.124	< .001
Residuals	1.904	8	0.238		

Note. Type III Sum of Squares

Output 13.317.: One-way ANOVA post-hoc analysis of data representing the occurrence of data representing the occurrence of necrosis in U251 cells treated with 6.25 µM α-solanine versus 5.00 mM H_2O_2 versus culture (negative control) conditions versus 1200.00 µM temozolomide for 24-hours.

Standard

Post Hoc Comparisons - Condition and cell line_140

		Mean Difference	SE	t	P_{tukey}
negative control	positive control	−0.528	0.398	−1.325	0.574
	temozolomide	−0.603	0.398	−1.513	0.473
	(∝-solanine)	5.428	0.398	13.629	< .001
positive control	temozolomide	−0.075	0.398	−0.188	0.997
	(∝-solanine)	5.956	0.398	14.954	< .001
temozolomide	(∝-solanine)	6.031	0.398	15.142	< .001

Note. P-value adjusted for comparing a family of 4

Output 13.318.: Descriptive statistics and normality (Shapiro-Wilk) assumption checking of data representing the occurrence of autophagy in U251 cells treated with 6.25 µM α-solanine versus 5.00 mM H_2O_2 versus culture (negative control) conditions versus 1200.00 µM temozolomide for 24-hours.

Descriptive Statistics

	Transformed %_144			
	negative control	positive control	temozolomide	∝-solanine
Valid	3	3	3	3
Missing	0	0	0	0
Mean	−2.571	0.206	−1.297	0.890
Std. Deviation	0.220	0.102	0.173	1.163
Shapiro-Wilk	0.996	0.975	0.804	1.000
P-value of Shapiro-Wilk	0.880	0.699	0.124	0.964
Minimum	−2.782	0.096	−1.496	−0.286
Maximum	−2.343	0.298	−1.186	2.041

Note. Excluded 28 rows from the analysis that correspond to the missing values of the split-by variable Condition and cell line_143

Output 13.319.: Equality of Variance (Levene's) assumption checks of data representing the occurrence of autophagy in U251 cells treated with 6.25 µM α-solanine versus 5.00 mM H_2O_2 versus culture (negative control) conditions versus 1200.00 µM temozolomide for 24-hours.

Test for Equality of Variances (Levene's)

F	df1	df2	p
2.962	3.000	8.000	0.098

Output 13.320.: One-way ANOVA testing of data representing the occurrence of autophagy in U251 cells treated with 6.25 µM α-solanine versus 5.00 mM H_2O_2 versus culture (negative control) conditions versus 1200.00 µM temozolomide for 24-hours.

ANOVA - Transformed %_144

Cases	Sum of Squares	df	Mean Square	F	p
Condition and cell line_143	21.614	3	7.205	19.979	< .001
Residuals	2.885	8	0.361		

Note. Type III Sum of Squares

Output 13.321.: One-way ANOVA post-hoc analysis of data representing the occurrence of data representing the occurrence of autophagy in U251 cells treated with 6.25 µM α-solanine versus 5.00 mM H_2O_2 versus culture (negative control) conditions versus 1200.00 µM temozolomide for 24-hours.

Standard

Post Hoc Comparisons - Condition and cell line_143

		Mean Difference	SE	t	p_{tukey}
negative control	positive control	−2.777	0.490	−5.664	0.002
	temozolomide	−1.274	0.490	−2.598	0.117
	(∝-solanine)	−3.461	0.490	−7.058	< .001
positive control	temozolomide	1.503	0.490	3.066	0.061
	(∝-solanine)	−0.683	0.490	−1.394	0.536
temozolomide	(∝-solanine)	−2.187	0.490	−4.460	0.009

Note. P-value adjusted for comparing a family of 4

Output 13.322.: Descriptive statistics and normality (Shapiro-Wilk) assumption checking of data representing the occurrence of early apoptosis in T98G cells treated with 6.25 µM α-solanine versus 5.00 mM H_2O_2 versus culture (negative control) conditions versus 1200.00 µM temozolomide for 24-hours.

Descriptive Statistics

	Transformed %_147			
	negative control	positive control	temozolomide	∝-solanine
Valid	3	3	3	3
Missing	0	0	0	0
Mean	−5.203	−5.111	−5.015	−3.246
Std. Deviation	0.430	0.143	0.040	0.228
Shapiro-Wilk	0.993	0.960	0.897	0.999
P-value of Shapiro-Wilk	0.841	0.617	0.375	0.931
Minimum	−5.651	−5.235	−5.045	−3.480
Maximum	−4.795	−4.955	−4.969	−3.023

Note. Excluded 28 rows from the analysis that correspond to the missing values of the split-by variable Condition and cell line_146

Output 13.323.: Equality of Variance (Levene's) assumption checks of data representing the occurrence of early apoptosis in T98G cells treated with 6.25 µM α-solanine versus 5.00 mM H_2O_2 versus culture (negative control) conditions versus 1200.00 µM temozolomide for 24-hours.

Test for Equality of Variances (Levene's)

F	df1	df2	p
2.192	3.000	8.000	0.167

Output 13.324.: One-way ANOVA of data representing the occurrence of early apoptosis in T98G cells treated with 6.25 µM α-solanine versus 5.00 mM H_2O_2 versus culture (negative control) conditions versus 1200.00 µM temozolomide for 24-hours.

ANOVA - Transformed %_147

Cases	Sum of Squares	df	Mean Square	F	p
Condition and cell line_146	7.863	3	2.621	40.528	< .001
Residuals	0.517	8	0.065		

Note. Type III Sum of Squares

Output 13.325.: One-way ANOVA post-hoc analysis of data representing the occurrence of data representing the occurrence of early apoptosis in T98G cells treated with 6.25 µM α-solanine versus 5.00 mM H_2O_2 versus culture (negative control) conditions versus 1200.00 µM temozolomide for 24-hours.

Standard

Post Hoc Comparisons - Condition and cell line_146

		Mean Difference	SE	t	p_{tukey}
negative control	positive control	−0.092	0.208	−0.441	0.970
	temozolomide	−0.188	0.208	−0.906	0.802
	(∝-solanine)	−1.956	0.208	−9.422	< .001
positive control	temozolomide	−0.097	0.208	−0.465	0.965
	(∝-solanine)	−1.865	0.208	−8.981	< .001
temozolomide	(∝-solanine)	−1.768	0.208	−8.515	< .001

Note. P-value adjusted for comparing a family of 4

Output 13.326.: Descriptive statistics and normality (Shapiro-Wilk) assumption checking of data representing the occurrence of late apoptosis in T98G cells treated with 6.25 µM α-solanine versus

5.00 mM H_2O_2 versus culture (negative control) conditions versus 1200.00 µM temozolomide for 24-hours.

Descriptive Statistics

	Transformed %_150			
	negative control	positive control	temozolomide	∝-solanine
Valid	3	3	3	3
Missing	0	0	0	0
Mean	−4.431	−4.584	−3.846	−6.954
Std. Deviation	0.330	1.222	0.042	2.015
Shapiro-Wilk	0.815	1.000	0.951	0.925
P-value of Shapiro-Wilk	0.150	0.999	0.572	0.471
Minimum	−4.647	−5.806	−3.882	−9.210
Maximum	−4.051	−3.362	−3.799	−5.334

Note. Excluded 28 rows from the analysis that correspond to the missing values of the split-by variable Condition and cell line_149

Output 13.327.: Equality of Variance (Levene's) assumption checks of data representing the occurrence of late apoptosis in T98G cells treated with 6.25 µM α-solanine versus 5.00 mM H_2O_2 versus culture (negative control) conditions versus 1200.00 µM temozolomide for 24-hours.

Test for Equality of Variances (Levene's)

F	df1	df2	p
4.410	3.000	8.000	0.041

Output 13.328.: Kruskal-Wallis testing of data representing the occurrence of late apoptosis in T98G cells treated with 6.25 µM α-solanine versus 5.00 mM H_2O_2 versus culture (negative control) conditions versus 1200.00 µM temozolomide for 24-hours.

Kruskal-Wallis Test

Factor	Statistic	df	p
Condition and cell line_149	7.000	3	0.072

Output 13.329.: Descriptive statistics and normality (Shapiro-Wilk) assumption checking of data representing the occurrence of necrosis in T98G cells treated with 6.25 µM α-solanine versus 5.00 mM H_2O_2 versus culture (negative control) conditions versus 1200.00 µM temozolomide for 24-hours.

Descriptive Statistics

	Transformed %_153			
	negative control	positive control	temozolomide	α-solanine
Valid	3	3	3	3
Missing	0	0	0	0
Mean	−0.314	−0.100	0.247	−3.568
Std. Deviation	0.625	1.394	0.233	0.134
Shapiro-Wilk	0.860	0.826	1.000	0.988
P-value of Shapiro-Wilk	0.267	0.177	0.984	0.792
Minimum	−0.758	−1.030	0.016	−3.693
Maximum	0.401	1.503	0.481	−3.426

Note. Excluded 28 rows from the analysis that correspond to the missing values of the split-by variable Condition and cell line_152

Output 13.330.: Equality of Variance (Levene's) assumption checks of data representing the occurrence of necrosis in T98G cells treated with 6.25 µM α-solanine versus 5.00 mM H_2O_2 versus culture (negative control) conditions versus 1200.00 µM temozolomide for 24-hours.

Test for Equality of Variances (Levene's)

F	df1	df2	p
7.864	3.000	8.000	0.009

Output 13.331.: Kruskal-Wallis testing of data representing the occurrence of necrosis in T98G cells treated with 6.25 µM α-solanine versus 5.00 mM H_2O_2 versus culture (negative control) conditions versus 1200.00 µM temozolomide for 24-hours.

Kruskal-Wallis Test

Factor	Statistic	df	p
Condition and cell line_152	6.897	3	0.075

Output 13.332.: Descriptive statistics and normality (Shapiro-Wilk) assumption checking of data representing the occurrence of autophagy in T98G cells treated with 6.25 µM α-solanine versus 5.00 mM H_2O_2 versus culture (negative control) conditions versus 1200.00 µM temozolomide for 24-hours.

Descriptive Statistics

	Transformed %_156			
	negative control	positive control	temozolomide	α-solanine
Valid	3	3	3	3
Missing	0	0	0	0
Mean	3.307	3.507	3.411	3.546
Std. Deviation	0.177	0.158	0.539	5.746
Shapiro-Wilk	0.750	1.000	0.922	0.999
P-value of Shapiro-Wilk	< .001	0.959	0.460	0.954
Minimum	3.103	3.347	2.806	−2.279
Maximum	3.409	3.664	3.842	9.210

Note. Excluded 28 rows from the analysis that correspond to the missing values of the split-by variable Condition and cell line_155

Output 13.333.: Equality of Variance (Levene's) assumption checks of data representing the occurrence of autophagy in T98G cells treated with 6.25 µM α-solanine versus 5.00 mM H_2O_2 versus culture (negative control) conditions versus 1200.00 µM temozolomide for 24-hours.

Test for Equality of Variances (Levene's)

F	df1	df2	p
3.877	3.000	8.000	0.056

Output 13.334.: Kruskal-Wallis testing of data representing the occurrence of autophagy in T98G cells treated with 6.25 µM α-solanine versus 5.00 mM H_2O_2 versus culture (negative control) conditions versus 1200.00 µM temozolomide for 24-hours.

Kruskal-Wallis Test

Factor	Statistic	df	p
Condition and cell line_155	1.158	3	0.763

13.6.4. Assessing the overall changes in the different forms of cell death under the treatment conditions investigation

Output 13.335.: Descriptive statistics and normality (Shapiro-Wilk) assumption checking of data representing the overall occurrence of early apoptosis versus late apoptosis versus necrosis versus autophagy in glioblastoma multiforme cells treated with 5.00 mM H_2O_2 for 24-hours.

Descriptive Statistics

	Transformed %_159			
	autophagy	early apoptosis	late apoptosis	necrosis
Valid	9	9	9	9
Missing	0	0	0	0
Mean	1.629	−6.575	−3.797	1.818
Std. Deviation	1.483	1.501	1.167	1.644
Shapiro-Wilk	0.833	0.879	0.923	0.822
P-value of Shapiro-Wilk	0.049	0.151	0.419	0.036
Minimum	0.096	−9.210	−5.806	−1.030
Maximum	3.664	−4.955	−2.448	3.442

Note. Excluded 4 rows from the analysis that correspond to the missing values of the split-by variable Condition and cell line_158

Output 13.336.: Equality of Variance (Levene's) assumption checks of data representing the overall occurrence of early apoptosis versus late apoptosis versus necrosis versus autophagy in glioblastoma multiforme cells treated with 5.00 mM H_2O_2 for 24-hours.

Test for Equality of Variances (Levene's)

F	df1	df2	p
0.316	3.000	32.000	0.813

Output 13.337.: Kruskal-Wallis testing of data representing the overall occurrence of early apoptosis versus late apoptosis versus necrosis versus autophagy in glioblastoma multiforme cells treated with 5.00 mM H_2O_2 for 24-hours.

Kruskal-Wallis Test

Factor	Statistic	df	p
Condition and cell line_158	29.094	3	< .001

Output 13.338.: Kruskal-Wallis post-hoc analysis of data representing the overall occurrence of early apoptosis versus late apoptosis versus necrosis versus autophagy in glioblastoma multiforme cells treated with 5.00 mM H_2O_2 for 24-hours.

Standard

Post Hoc Comparisons – Condition and cell line_158

		Mean Difference	SE	t	p_{tukey}
autophagy	early apoptosis	8.204	0.688	11.926	< .001
	late apoptosis	5.426	0.688	7.888	< .001
	necrosis	−0.189	0.688	−0.275	0.993
early apoptosis	late apoptosis	−2.778	0.688	−4.038	0.002
	necrosis	−8.393	0.688	−12.201	< .001
late apoptosis	necrosis	−5.615	0.688	−8.163	< .001

Note. P-value adjusted for comparing a family of 4

Output 13.339.: Descriptive statistics and normality (Shapiro-Wilk) assumption checking of data representing the overall occurrence of early apoptosis versus late apoptosis versus necrosis versus autophagy in glioblastoma multiforme cells treated with 6.25 µM α-solanine for 24-hours.

Descriptive Statistics

	Transformed %_162			
	autophagy	early apoptosis	late apoptosis	necrosis
Valid	9	9	9	9
Missing	0	0	0	0
Mean	1.836	−4.773	−4.903	−1.180
Std. Deviation	3.220	1.914	2.081	3.012
Shapiro-Wilk	0.862	0.808	0.909	0.737
P-value of Shapiro-Wilk	0.102	0.025	0.307	0.004
Minimum	−2.279	−8.047	−9.210	−3.693
Maximum	9.210	−3.023	−2.517	2.987

Note. Excluded 4 rows from the analysis that correspond to the missing values of the split-by variable Condition and cell line_161

Output 13.340.: Equality of Variance (Levene's) assumption checks of data representing the overall occurrence of early apoptosis versus late apoptosis versus necrosis versus autophagy in glioblastoma multiforme cells treated with 6.25 µM α-solanine for 24-hours.

Test for Equality of Variances (Levene's)

F	df1	df2	p
1.025	3.000	32.000	0.394

Output 13.341.: Kruskal-Wallis testing of data representing the overall occurrence of early apoptosis versus late apoptosis versus necrosis versus autophagy in glioblastoma multiforme cells treated with 6.25 µM α-solanine for 24-hours.

Kruskal-Wallis Test

Factor	Statistic	df	p
Condition and cell line_161	20.714	3	< .001

Output 13.342.: *Kruskal*-Wallis post-hoc analysis of data representing the overall occurrence of early apoptosis versus late apoptosis versus necrosis versus autophagy in glioblastoma multiforme cells treated with 6.25 µM α-solanine for 24-hours.

Standard

Post Hoc Comparisons – Condition and cell line_161

		Mean Difference	SE	t	p_{tukey}
autophagy	early apoptosis	6.610	1.235	5.354	< .001
	late apoptosis	6.740	1.235	5.459	< .001
	necrosis	3.017	1.235	2.444	0.089
early apoptosis	late apoptosis	0.130	1.235	0.105	1.000
	necrosis	−3.593	1.235	−2.911	0.031
late apoptosis	necrosis	−3.723	1.235	−3.016	0.024

Note. P-value adjusted for comparing a family of 4

Output 13.343.: Descriptive statistics and normality (Shapiro-Wilk) assumption checking of data representing the overall occurrence of early apoptosis versus late apoptosis versus necrosis versus autophagy in glioblastoma multiforme cells treated with 1200.00 µM temozolomide for 24-hours.

Descriptive Statistics

	Transformed %_165			
	autophagy	early apoptosis	late apoptosis	necrosis
Valid	9	9	9	9
Missing	0	0	0	0
Mean	0.865	−7.104	−3.524	1.898
Std. Deviation	2.081	1.797	1.036	1.344
Shapiro-Wilk	0.883	0.858	0.870	0.890
P-value of Shapiro-Wilk	0.168	0.091	0.123	0.202
Minimum	−1.496	−9.210	−4.668	0.016
Maximum	3.842	−4.969	−1.866	3.476

Note. Excluded 4 rows from the analysis that correspond to the missing values of the split-by variable Condition and cell line_164

Output 13.344.: Equality of Variance (Levene's) assumption checks of data representing the overall occurrence of early apoptosis versus late apoptosis versus necrosis versus autophagy in glioblastoma multiforme cells treated with 1200.00 µM temozolomide for 24-hours.

Test for Equality of Variances (Levene's)

F	df1	df2	p
2.181	3.000	32.000	0.110

Output 13.345.: One-way ANOVA testing of data representing the overall occurrence of early apoptosis versus late apoptosis versus necrosis versus autophagy in glioblastoma multiforme cells treated with 1200.00 µM temozolomide for 24-hours.

ANOVA - Transformed %_165

Cases	Sum of Squares	df	Mean Square	F	p
Condition and cell line_164	465.985	3	155.328	59.506	< .001
Residuals	83.530	32	2.610		

Note. Type III Sum of Squares

Output 13.346.: One-way ANOVA post-hoc analysis of data representing the overall occurrence of early apoptosis versus late apoptosis versus necrosis versus autophagy in glioblastoma multiforme cells treated with 1200.00 µM temozolomide for 24-hours.

Standard

Post Hoc Comparisons - Condition and cell line_164

		Mean Difference	SE	t	p_{tukey}
autophagy	early apoptosis	7.970	0.762	10.464	< .001
	late apoptosis	4.389	0.762	5.763	< .001
	necrosis	−1.032	0.762	−1.356	0.536
early apoptosis	late apoptosis	−3.580	0.762	−4.701	< .001
	necrosis	−9.002	0.762	−11.820	< .001
late apoptosis	necrosis	−5.422	0.762	−7.119	< .001

Note. P-value adjusted for comparing a family of 4

Output 13.347.: Descriptive statistics and normality (Shapiro-Wilk) assumption checking of data representing the overall occurrence of early apoptosis versus late apoptosis versus necrosis versus autophagy in glioblastoma multiforme cells treated with culture (negative control) conditions for 24-hours.

Descriptive Statistics

	Transformed %_168			
	autophagy	early apoptosis	late apoptosis	necrosis
Valid	9	9	9	9
Missing	0	0	0	0
Mean	−0.168	−6.602	−3.658	1.560
Std. Deviation	2.693	1.507	1.014	1.490
Shapiro-Wilk	0.794	0.909	0.814	0.853
P-value of Shapiro-Wilk	0.018	0.308	0.030	0.080
Minimum	−2.782	−9.210	−4.647	−0.758
Maximum	3.409	−4.795	−2.276	3.442

Note. Excluded 4 rows from the analysis that correspond to the missing values of the split-by variable Condition and cell line_167

Output 13.348.: Equality of Variance (Levene's) assumption checks of data representing the overall occurrence of early apoptosis versus late apoptosis versus necrosis versus autophagy in glioblastoma multiforme cells treated with culture (negative control) conditions for 24-hours.

Test for Equality of Variances (Levene's)

F	df1	df2	p
5.413	3.000	32.000	0.004

Output 13.349.: Kruskal-Wallis testing of data representing the overall occurrence of early apoptosis versus late apoptosis versus necrosis versus autophagy in glioblastoma multiforme cells treated with culture (negative control) conditions for 24-hours.

Kruskal-Wallis Test

Factor	Statistic	df	p
Condition and cell line_167	28.393	3	< .001

Output 13.350.: Kruskal-Wallis post-hoc analysis of data representing the overall occurrence of early apoptosis versus late apoptosis versus necrosis versus autophagy in glioblastoma multiforme cells treated with culture (negative control) conditions for 24-hours.

Standard

Post Hoc Comparisons - Condition and cell line_167

		Mean Difference	SE	t	p_{tukey}
autophagy	early apoptosis	6.434	0.842	7.637	< .001
	late apoptosis	3.490	0.842	4.143	0.001
	necrosis	−1.728	0.842	−2.051	0.191
early apoptosis	late apoptosis	−2.944	0.842	−3.494	0.007
	necrosis	−8.162	0.842	−9.689	< .001
late apoptosis	necrosis	−5.219	0.842	−6.195	< .001

Note. P-value adjusted for comparing a family of 4

Output 13.351.: Descriptive statistics and normality (Shapiro-Wilk) assumption checking of data representing the overall occurrence of early apoptosis in glioblastoma multiforme cells treated with 6.25 µM α-solanine versus 5.00 mM H_2O_2 versus culture (negative control) conditions versus 1200.00 µM temozolomide for 24-hours.

Descriptive Statistics

	Transformed %_171			
	negative control	positive control	temozolomide	α-solanine
Valid	9	9	9	9
Missing	0	0	0	0
Mean	−6.602	−6.575	−7.104	−4.773
Std. Deviation	1.507	1.501	1.797	1.914
Shapiro-Wilk	0.909	0.879	0.858	0.808
P-value of Shapiro-Wilk	0.308	0.151	0.091	0.025
Minimum	−9.210	−9.210	−9.210	−8.047
Maximum	−4.795	−4.955	−4.969	−3.023

Note. Excluded 4 rows from the analysis that correspond to the missing values of the split-by variable Condition and cell line_170

Output 13.352.: Equality of Variance (Levene's) assumption checks of data representing the overall occurrence of early apoptosis in glioblastoma multiforme cells treated with 6.25 µM α-solanine versus 5.00 mM H_2O_2 versus culture (negative control) conditions versus 1200.00 µM temozolomide for 24-hours.

Test for Equality of Variances (Levene's)

F	df1	df2	p
0.934	3.000	32.000	0.435

Output 13.353.: One-way ANOVA testing of data representing the overall occurrence of early apoptosis in glioblastoma multiforme cells treated with 6.25 µM α-solanine versus 5.00 mM H_2O_2 versus culture (negative control) conditions versus 1200.00 µM temozolomide for 24-hours.

ANOVA - Transformed %_171

Cases	Sum of Squares	df	Mean Square	F	p
Condition and cell line_170	28.246	3	9.415	3.299	0.033
Residuals	91.339	32	2.854		

Note. Type III Sum of Squares

Output 13.354.: Descriptive statistics and normality (Shapiro-Wilk) assumption checking of data representing the overall occurrence of late apoptosis in glioblastoma multiforme cells treated with 6.25 µM α-solanine versus 5.00 mM H_2O_2 versus culture (negative control) conditions versus 1200.00 µM temozolomide for 24-hours.

Descriptive Statistics

	Transformed %_174			
	negative control	positive control	temozolomide	α-solanine
Valid	9	9	9	9
Missing	0	0	0	0
Mean	−3.658	−3.797	−3.524	−4.903
Std. Deviation	1.014	1.167	1.036	2.081
Shapiro-Wilk	0.814	0.923	0.870	0.909
P-value of Shapiro-Wilk	0.030	0.419	0.123	0.307
Minimum	−4.647	−5.806	−4.668	−9.210
Maximum	−2.276	−2.448	−1.866	−2.517

Note. Excluded 4 rows from the analysis that correspond to the missing values of the split-by variable Condition and cell line_173

Output 13.355.: Equality of Variance (Levene's) assumption checks of data representing the overall occurrence of late apoptosis in glioblastoma multiforme cells treated with 6.25 µM α-solanine versus 5.00 mM H_2O_2 versus culture (negative control) conditions versus 1200.00 µM temozolomide for 24-hours.

Test for Equality of Variances (Levene's)

F	df1	df2	p
1.590	3.000	32.000	0.211

Output 13.356.: Kruskal-Wallis testing of data representing the overall occurrence of late apoptosis in glioblastoma multiforme cells treated with 6.25 µM α-solanine versus 5.00 mM H_2O_2 versus culture (negative control) conditions versus 1200.00 µM temozolomide for 24-hours.

Kruskal-Wallis Test

Factor	Statistic	df	p
Condition and cell line_173	4.086	3	0.252

Output 13.357.: Descriptive statistics and normality (Shapiro-Wilk) assumption checking of data representing the overall occurrence of necrosis in glioblastoma multiforme cells treated with 6.25 µM α-solanine versus 5.00 mM H_2O_2 versus culture (negative control) conditions versus 1200.00 µM temozolomide for 24-hours.

Descriptive Statistics

	Transformed %_177			
	negative control	positive control	temozolomide	α-solanine
Valid	9	9	9	9
Missing	0	0	0	0
Mean	1.560	1.818	1.898	−1.180
Std. Deviation	1.490	1.644	1.344	3.012
Shapiro-Wilk	0.853	0.822	0.890	0.737
P-value of Shapiro-Wilk	0.080	0.036	0.202	0.004
Minimum	−0.758	−1.030	0.016	−3.693
Maximum	3.442	3.442	3.476	2.987

Note. Excluded 4 rows from the analysis that correspond to the missing values of the split-by variable Condition and cell line_176

Output 13.358.: Equality of Variance (Levene's) assumption checks of data representing the overall occurrence of necrosis in glioblastoma multiforme cells treated with 6.25 µM α-solanine versus 5.00 mM H_2O_2 versus culture (negative control) conditions versus 1200.00 µM temozolomide for 24-hours.

Test for Equality of Variances (Levene's)

F	df1	df2	p
6.263	3.000	32.000	0.002

Output 13.359.: Kruskal-Wallis testing of data representing the overall occurrence of necrosis in glioblastoma multiforme cells treated with 6.25 µM α-solanine versus 5.00 mM H_2O_2 versus culture (negative control) conditions versus 1200.00 µM temozolomide for 24-hours.

Kruskal-Wallis Test

Factor	Statistic	df	p
Condition and cell line_176	5.459	3	0.141

Output 13.360.: Descriptive statistics and normality (Shapiro-Wilk) assumption checking of data representing the overall occurrence of autophagy in glioblastoma multiforme cells treated with 6.25 µM α-solanine versus 5.00 mM H_2O_2 versus culture (negative control) conditions versus 1200.00 µM temozolomide for 24-hours.

Descriptive Statistics

	Transformed %_180			
	negative control	positive control	temozolomide	∝-solanine
Valid	9	9	9	9
Missing	0	0	0	0
Mean	0.406	1.629	0.291	1.836
Std. Deviation	2.552	1.483	2.380	3.220
Shapiro-Wilk	0.864	0.833	0.759	0.862
P-value of Shapiro-Wilk	0.107	0.049	0.007	0.102
Minimum	−2.782	0.096	−1.782	−2.279
Maximum	3.409	3.664	3.842	9.210

Note. Excluded 4 rows from the analysis that correspond to the missing values of the split-by variable Condition and cell line_179

Output 13.361.: Equality of Variance (Levene's) assumption checks of data representing the overall occurrence of autophagy in glioblastoma multiforme cells treated with 6.25 µM α-solanine versus 5.00 mM H_2O_2 versus culture (negative control) conditions versus 1200.00 µM temozolomide for 24-hours.

Test for Equality of Variances (Levene's)

F	df1	df2	p
0.714	3.000	32.000	0.551

Output 13.362.: Kruskal-Wallis testing of data representing the overall occurrence of autophagy in glioblastoma multiforme cells treated with 6.25 µM α-solanine versus 5.00 mM H_2O_2 versus culture (negative control) conditions versus 1200.00 µM temozolomide for 24-hours.

Kruskal-Wallis Test

Factor	Statistic	df	p
Condition and cell line_179	3.022	3	0.388

13.7. Statistical analysis of antibody array experiments

Output 13.363.: Descriptive statistics for Bad protein corrected mean grey area data for glioblastoma multiforme cells treated with 6.25 µM α-solanine versus negative control (culture) treatment.

Descriptive Statistics

	Bad	
	Neg control	∝-solanine
Valid	6	6
Missing	0	0
Mean	40.704	61.137
Std. Deviation	4.690	15.525
Minimum	36.645	43.506
Maximum	47.730	85.185

Output 13.364.: Normality (Shapiro-Wilk) and Equality of Variance (Levene's) assumption checks for pairwise sample testing for Bad protein corrected mean grey area data for glioblastoma multiforme cells treated with 6.25 µM α-solanine versus negative control (culture) treatment.

Test of Normality (Shapiro-Wilk)

		W	p
Bad	Neg control	0.853	0.167
	∝-solanine	0.952	0.758

Note. Significant results suggest a deviation from normality.

Test of Equality of Variances (Levene's)

	F	df	p
Bad	8.055	1	0.018

Output 13.365.:Output 13.366.: Welch testing for Bad protein corrected mean grey area data for glioblastoma multiforme cells treated with 6.25 µM α-solanine versus negative control (culture) treatment.

Independent Samples T-Test

	t	df	p
Bad	−3.086	5.905	0.022

Note. Welch's t-test.

Output 13.367.: Descriptive statistics for Bax protein corrected mean grey area data for glioblastoma multiforme cells treated with 6.25 µM α-solanine versus negative control (culture) treatment.

Descriptive Statistics

	Bax	
	Neg control	∝-solanine
Valid	6	6
Missing	0	0
Mean	25.324	33.098
Std. Deviation	3.911	12.189
Minimum	19.986	21.503
Maximum	29.416	54.732

Output 13.368.: Normality (Shapiro-Wilk) and Equality of Variance (Levene's) assumption checks for pairwise sample testing for Bax protein corrected mean grey area data for glioblastoma multiforme cells treated with 6.25 µM α-solanine versus negative control (culture) treatment.

Test of Normality (Shapiro-Wilk)

		W	p
Bax	Neg control	0.860	0.191
	∝-solanine	0.892	0.330

Note. Significant results suggest a deviation from normality.

Test of Equality of Variances (Levene's)

	F	df	p
Bax	3.900	1	0.077

Output 13.369.: Independent sample T-testing for Bax protein corrected mean grey area data for glioblastoma multiforme cells treated with 6.25 µM α-solanine versus negative control (culture) treatment.

Independent Samples T-Test

	t	df	p
Bax	−1.488	10	0.168

Note. Student's t-test.

Output 13.370.: Descriptive statistics for Bcl-2 protein corrected mean grey area data for glioblastoma multiforme cells treated with 6.25 µM α-solanine versus negative control (culture) treatment.

Descriptive Statistics

	Bcl-2	
	Neg control	∝-solanine
Valid	6	6
Missing	0	0
Mean	62.210	95.994
Std. Deviation	10.577	7.027
Minimum	50.326	84.757
Maximum	77.309	104.823

Output 13.371.: Normality (Shapiro-Wilk) and Equality of Variance (Levene's) assumption checks for pairwise sample testing for Bcl-2 protein corrected mean grey area data for glioblastoma multiforme cells treated with 6.25 µM α-solanine versus negative control (culture) treatment.

Test of Normality (Shapiro-Wilk) ▼

		W	p
Bcl-2	Neg control	0.924	0.534
	∝-solanine	0.966	0.861

Note. Significant results suggest a deviation from normality.

Test of Equality of Variances (Levene's)

	F	df	p
Bcl-2	0.661	1	0.435

Output 13.372.: Independent sample T-testing for Bcl-2 protein corrected mean grey area data for glioblastoma multiforme cells treated with 6.25 µM α-solanine versus negative control (culture) treatment.

Independent Samples T-Test

	t	df	p
Bcl-2	−6.517	10	< .001

Note. Student's t-test.

Output 13.373.: Descriptive statistics for Bcl-w protein corrected mean grey area data for glioblastoma multiforme cells treated with 6.25 µM α-solanine versus negative control (culture) treatment.

Descriptive Statistics

	Bcl-w	
	Neg control	∝-solanine
Valid	6	6
Missing	0	0
Mean	65.861	96.508
Std. Deviation	5.554	5.367
Minimum	56.569	87.612
Maximum	72.102	103.746

Output 13.374.: Normality (Shapiro-Wilk) and Equality of Variance (Levene's) assumption checks for pairwise sample testing for Bcl-w protein corrected mean grey area data for glioblastoma multiforme cells treated with 6.25 µM α-solanine versus negative control (culture) treatment.

Independent Samples T-Test

	t	df	p
Bcl-w	−9.720	10	< .001

Note. Student's t-test.

Output 13.375.: Independent sample T-testing for Bcl-w protein corrected mean grey area data for glioblastoma multiforme cells treated with 6.25 µM α-solanine versus negative control (culture) treatment.

Test of Normality (Shapiro-Wilk)

		W	p
Bcl-w	Neg control	0.935	0.618
	∝-solanine	0.963	0.842

Note. Significant results suggest a deviation from normality.

Test of Equality of Variances (Levene's)

	F	df	p
Bcl-w	0.084	1	0.778

Output 13.376.: Descriptive statistics for Bid protein corrected mean grey area data for glioblastoma multiforme cells treated with 6.25 µM α-solanine versus negative control (culture) treatment.

Descriptive Statistics

	Bid	
	Neg control	∝-solanine
Valid	6	6
Missing	0	0
Mean	34.234	56.129
Std. Deviation	6.727	4.611
Minimum	25.861	49.668
Maximum	42.215	62.144

Output 13.377.: Normality (Shapiro-Wilk) and Equality of Variance (Levene's) assumption checks for pairwise sample testing for Bid protein corrected mean grey area data for glioblastoma multiforme cells treated with 6.25 µM α-solanine versus negative control (culture) treatment.

Test of Normality (Shapiro-Wilk)

		W	p
Bid	Neg control	0.901	0.381
	∝-solanine	0.967	0.873

Note. Significant results suggest a deviation from normality.

Test of Equality of Variances (Levene's) ▼

	F	df	p
Bid	1.057	1	0.328

Output 13.378.: Independent sample T-testing for Bid protein corrected mean grey area data for glioblastoma multiforme cells treated with 6.25 µM α-solanine versus negative control (culture) treatment.

Independent Samples T-Test

	t	df	p
Bid	−6.576	10	< .001

Note. Student's t-test.

Output 13.379.: Descriptive statistics for Bim protein corrected mean grey area data for glioblastoma multiforme cells treated with 6.25 µM α-solanine versus negative control (culture) treatment.

Descriptive Statistics ▼

	Bim	
	Neg control	∝-solanine
Valid	6	6
Missing	0	0
Mean	58.669	101.994
Std. Deviation	4.194	32.078
Minimum	54.389	57.642
Maximum	63.989	131.217

Output 13.380.: Normality (Shapiro-Wilk) and Equality of Variance (Levene's) assumption checks for pairwise sample testing for Bim protein corrected mean grey area data for glioblastoma multiforme cells treated with 6.25 µM α-solanine versus negative control (culture) treatment.

Test of Normality (Shapiro-Wilk)

		W	p
Bim	Neg control	0.862	0.196
	∝-solanine	0.786	0.044

Note. Significant results suggest a deviation from normality.

Test of Equality of Variances (Levene's)

	F	df	p
Bim	23.744	1	< .001

Output 13.381.: Independent sample T-testing for Bim protein corrected mean grey area data for glioblastoma multiforme cells treated with 6.25 µM α-solanine versus negative control (culture) treatment.

Independent Samples T-Test

	t	df	p
Bim	−3.280	5.171	0.021

Note. Welch's t-test.

Output 13.382.: Descriptive statistics for Casp-3 protein corrected mean grey area data for glioblastoma multiforme cells treated with 6.25 µM α-solanine versus negative control (culture) treatment.

Descriptive Statistics

	Casp-3	
	Neg control	∝-solanine
Valid	6	6
Missing	0	0
Mean	34.975	49.859
Std. Deviation	5.587	16.955
Minimum	27.864	29.599
Maximum	43.643	76.014

Output 13.383.: Normality (Shapiro-Wilk) and Equality of Variance (Levene's) assumption checks for pairwise sample testing for Casp-3 protein corrected mean grey area data for glioblastoma multiforme cells treated with 6.25 µM α-solanine versus negative control (culture) treatment.

Test of Normality (Shapiro-Wilk)

		W	p
Casp-3	Neg control	0.956	0.787
	∝-solanine	0.955	0.781

Note. Significant results suggest a deviation from normality.

Test of Equality of Variances (Levene's)

	F	df	p
Casp-3	5.133	1	0.047

Output 13.384.: Independent sample T-testing for Casp-3 protein corrected mean grey area data for glioblastoma multiforme cells treated with 6.25 µM α-solanine versus negative control (culture) treatment.

Independent Samples T-Test

	t	df	p
Casp-3	−2.042	6.073	0.087

Note. Welch's t-test.

Output 13.385.: Descriptive statistics for Casp-8 protein corrected mean grey area data for glioblastoma multiforme cells treated with 6.25 µM α-solanine versus negative control (culture) treatment.

Descriptive Statistics

	Casp-8	
	Neg control	∝-solanine
Valid	6	6
Missing	0	0
Mean	6.131	7.278
Std. Deviation	0.276	1.145
Minimum	5.829	5.561
Maximum	6.603	8.893

Output 13.386.: Normality (Shapiro-Wilk) and Equality of Variance (Levene's) assumption checks for pairwise sample testing for Casp-8 protein corrected mean grey area data for glioblastoma multiforme cells treated with 6.25 µM α-solanine versus negative control (culture) treatment.

Test of Normality (Shapiro-Wilk)

		W	p
Casp-8	Neg control	0.940	0.656
	∝-solanine	0.984	0.970

Note. Significant results suggest a deviation from normality.

Test of Equality of Variances (Levene's)

	F	df	p
Casp-8	5.005	1	0.049

Output 13.387.: Independent sample T-testing for Casp-8 protein corrected mean grey area data for glioblastoma multiforme cells treated with 6.25 µM α-solanine versus negative control (culture) treatment.

Independent Samples T-Test

	t	df	p
Casp-8	−2.385	5.579	0.058

Note. Welch's t-test.

Output 13.388.: Descriptive statistics for CD40 protein corrected mean grey area data for glioblastoma multiforme cells treated with 6.25 µM α-solanine versus negative control (culture) treatment.

Descriptive Statistics

	TNFRSF5	
	Neg control	∝-solanine
Valid	6	6
Missing	0	0
Mean	49.294	77.177
Std. Deviation	5.285	21.702
Minimum	39.662	49.565
Maximum	54.926	105.408

Output 13.389.: Normality (Shapiro-Wilk) and Equality of Variance (Levene's) assumption checks for pairwise sample testing for CD40 protein corrected mean grey area data for glioblastoma multiforme cells treated with 6.25 µM α-solanine versus negative control (culture) treatment.

Test of Normality (Shapiro-Wilk)

		W	p
TNFRSF5	Neg control	0.886	0.299
	∝-solanine	0.941	0.666

Note. Significant results suggest a deviation from normality.

Test of Equality of Variances (Levene's)

	F	df	p
TNFRSF5	6.627	1	0.028

Output 13.390.: Welch testing for CD40 protein corrected mean grey area data for glioblastoma multiforme cells treated with 6.25 µM α-solanine versus negative control (culture) treatment.

Independent Samples T-Test

	t	df	p
TNFRSF5	−3.058	5.591	0.024

Note. Welch's t-test.

Output 13.391.: Descriptive statistics for CD40 ligand protein corrected mean grey area data for glioblastoma multiforme cells treated with 6.25 µM α-solanine versus negative control (culture) treatment.

Descriptive Statistics

	TNFSF5	
	Neg control	∝-solanine
Valid	6	6
Missing	0	0
Mean	82.440	129.093
Std. Deviation	3.515	33.450
Minimum	79.123	88.939
Maximum	87.186	173.791

Output 13.392.: Normality (Shapiro-Wilk) and Equality of Variance (Levene's) assumption checks for pairwise sample testing for CD40 ligand protein corrected mean grey area data for glioblastoma multiforme cells treated with 6.25 µM α-solanine versus negative control (culture) treatment.

Test of Normality (Shapiro-Wilk)

		W	p
TNFSF5	Neg control	0.852	0.165
	∝-solanine	0.954	0.774

Note. Significant results suggest a deviation from normality.

Test of Equality of Variances (Levene's)

	F	df	p
TNFSF5	15.634	1	0.003

Output 13.393.: Welch testing for CD40 ligand protein corrected mean grey area data for glioblastoma multiforme cells treated with 6.25 µM α-solanine versus negative control (culture) treatment.

Independent Samples T-Test

	t	df	p
TNFSF5	−3.398	5.110	0.019

Note. Welch's t-test.

Output 13.394.: Descriptive statistics for cIAP-2 protein corrected mean grey area data for glioblastoma multiforme cells treated with 6.25 µM α-solanine versus negative control (culture) treatment.

Descriptive Statistics ▼

	cIAP-2	
	Neg control	∝-solanine
Valid	6	6
Missing	0	0
Mean	61.851	91.457
Std. Deviation	12.387	19.531
Minimum	49.523	69.795
Maximum	80.632	123.013

Output 13.395.: Normality (Shapiro-Wilk) and Equality of Variance (Levene's) assumption checks for pairwise sample testing for cIAP-2 protein corrected mean grey area data for glioblastoma multiforme cells treated with 6.25 µM α-solanine versus negative control (culture) treatment.

Test of Normality (Shapiro-Wilk)

		W	p
cIAP-2	Neg control	0.891	0.324
	∝-solanine	0.939	0.650

Note. Significant results suggest a deviation from normality.

Test of Equality of Variances (Levene's)

	F	df	p
cIAP-2	1.336	1	0.275

Output 13.396.: Independent sample T-testing for cIAP-2 protein corrected mean grey area data for glioblastoma multiforme cells treated with 6.25 µM α-solanine versus negative control (culture) treatment.

Independent Samples T-Test

	t	df	p
cIAP-2	−3.136	10	0.011

Note. Student's t-test.

Output 13.397.: Descriptive statistics for Cyt-C protein corrected mean grey area data for glioblastoma multiforme cells treated with 6.25 µM α-solanine versus negative control (culture) treatment.

Descriptive Statistics

	Cyt-C	
	Neg control	∝-solanine
Valid	6	6
Missing	0	0
Mean	120.918	176.023
Std. Deviation	37.872	33.939
Minimum	83.137	125.849
Maximum	188.635	212.976

Output 13.398.: Normality (Shapiro-Wilk) and Equality of Variance (Levene's) assumption checks for pairwise sample testing for Cyt-C protein corrected mean grey area data for glioblastoma multiforme cells treated with 6.25 µM α-solanine versus negative control (culture) treatment.

Test of Normality (Shapiro-Wilk)

		W	p
Cyt-C	Neg control	0.877	0.255
	∝-solanine	0.946	0.706

Note. Significant results suggest a deviation from normality.

Test of Equality of Variances (Levene's)

	F	df	p
Cyt-C	0.026	1	0.876

Output 13.399.: Independent sample T-testing for Cyt-C protein corrected mean grey area data for glioblastoma multiforme cells treated with 6.25 µM α-solanine versus negative control (culture) treatment.

Independent Samples T-Test

	t	df	p
Cyt-C	−2.654	10	0.024

Note. Student's t-test.

Output 13.400.: Descriptive statistics for TNFRSF21 protein corrected mean grey area data for glioblastoma multiforme cells treated with 6.25 µM α-solanine versus negative control (culture) treatment.

Descriptive Statistics

	TNFRSF21	
	Neg control	∝-solanine
Valid	6	6
Missing	0	0
Mean	9.042	10.694
Std. Deviation	1.663	3.135
Minimum	6.366	6.252
Maximum	11.574	14.009

Output 13.401.: Normality (Shapiro-Wilk) and Equality of Variance (Levene's) assumption checks for pairwise sample testing for TNFRSF21 protein corrected mean grey area data for glioblastoma multiforme cells treated with 6.25 µM α-solanine versus negative control (culture) treatment.

Test of Normality (Shapiro–Wilk)

		W	p
TNFRSF21	Neg control	0.904	0.398
	∝–solanine	0.833	0.113

Note. Significant results suggest a deviation from normality.

Test of Equality of Variances (Levene's)

	F	df	p
TNFRSF21	4.901	1	0.051

Output 13.402.: Independent sample T-testing for TNFRSF21 protein corrected mean grey area data for glioblastoma multiforme cells treated with 6.25 µM α-solanine versus negative control (culture) treatment.

Independent Samples T–Test

	t	df	p
TNFRSF21	−1.140	10	0.281

Note. Student's t–test.

Output 13.403.: Descriptive statistics for Fas protein corrected mean grey area data for glioblastoma multiforme cells treated with 6.25 µM α-solanine versus negative control (culture) treatment.

Descriptive Statistics

	Fas	
	Neg control	∝-solanine
Valid	6	6
Missing	0	0
Mean	56.188	93.573
Std. Deviation	4.495	29.473
Minimum	51.547	67.283
Maximum	63.976	149.635

Output 13.404.: Normality (Shapiro-Wilk) and Equality of Variance (Levene's) assumption checks for pairwise sample testing for Fas protein corrected mean grey area data for glioblastoma multiforme cells treated with 6.25 µM α-solanine versus negative control (culture) treatment.

Test of Normality (Shapiro-Wilk)

		W	p
Fas	Neg control	0.912	0.449
	∝-solanine	0.814	0.078

Note. Significant results suggest a deviation from normality.

Test of Equality of Variances (Levene's)

	F	df	p
Fas	3.472	1	0.092

Output 13.405.: Independent sample T-testing for Fas protein corrected mean grey area data for glioblastoma multiforme cells treated with 6.25 µM α-solanine versus negative control (culture) treatment.

Independent Samples T-Test

	t	df	p
Fas	−3.072	10	0.012

Note. Student's t-test.

Descriptive statistics for Fas ligand protein corrected mean grey area data for glioblastoma multiformOutput 13.406.:e cells treated with 6.25 µM α-solanine versus negative control (culture) treatment.

Descriptive Statistics

	Fas ligand	
	Neg control	∝-solanine
Valid	6	6
Missing	0	0
Mean	69.579	120.405
Std. Deviation	9.370	44.641
Minimum	61.179	77.297
Maximum	82.356	202.970

Output 13.407.: Normality (Shapiro-Wilk) and Equality of Variance (Levene's) assumption checks for pairwise sample testing for Fas ligand protein corrected mean grey area data for glioblastoma multiforme cells treated with 6.25 µM α-solanine versus negative control (culture) treatment.

Test of Normality (Shapiro-Wilk)

		W	p
Fas ligand	Neg control	0.829	0.105
	∝-solanine	0.851	0.161

Note. Significant results suggest a deviation from normality.

Test of Equality of Variances (Levene's)

	F	df	p
Fas ligand	4.939	1	0.050

Output 13.408.: Independent sample T-testing for Fas ligand protein corrected mean grey area data for glioblastoma multiforme cells treated with 6.25 µM α-solanine versus negative control (culture) treatment.

Independent Samples T-Test

	t	df	p
Fas ligand	−2.729	10	0.021

Note. Student's t-test.

Output 13.409.: Descriptive statistics for HSP27 protein corrected mean grey area data for glioblastoma multiforme cells treated with 6.25 µM α-solanine versus negative control (culture) treatment.

Descriptive Statistics

	HSP27	
	Neg control	∝-solanine
Valid	6	6
Missing	0	0
Mean	30.140	39.532
Std. Deviation	3.356	7.451
Minimum	25.774	32.159
Maximum	34.514	49.491

Output 13.410.: Normality (Shapiro-Wilk) and Equality of Variance (Levene's) assumption checks for pairwise sample testing for HSP27 protein corrected mean grey area data for glioblastoma multiforme cells treated with 6.25 µM α-solanine versus negative control (culture) treatment.

Test of Normality (Shapiro-Wilk)

		W	p
HSP27	Neg control	0.969	0.883
	∝-solanine	0.856	0.176

Note. Significant results suggest a deviation from normality.

Test of Equality of Variances (Levene's)

	F	df	p
HSP27	5.056	1	0.048

Output 13.411.: Welch testing for HSP27 protein corrected mean grey area data for glioblastoma multiforme cells treated with 6.25 µM α-solanine versus negative control (culture) treatment.

Independent Samples T-Test

	t	df	p
HSP27	−2.815	6.948	0.026

Note. Welch's t-test.

Output 13.412.: Descriptive statistics for HSP60 protein corrected mean grey area data for glioblastoma multiforme cells treated with 6.25 µM α-solanine versus negative control (culture) treatment.

Descriptive Statistics

	HSP60	
	Neg control	∝-solanine
Valid	6	6
Missing	0	0
Mean	104.919	49.859
Std. Deviation	18.088	16.955
Minimum	82.064	29.599
Maximum	125.177	76.014

Output 13.413.: Normality (Shapiro-Wilk) and Equality of Variance (Levene's) assumption checks for pairwise sample testing for HSP60 protein corrected mean grey area data for glioblastoma multiforme cells treated with 6.25 µM α-solanine versus negative control (culture) treatment.

Test of Normality (Shapiro-Wilk)

		W	p
HSP60	Neg control	0.874	0.243
	∝-solanine	0.955	0.781

Note. Significant results suggest a deviation from normality.

Test of Equality of Variances (Levene's)

	F	df	p
HSP60	0.106	1	0.751

Output 13.414.: Independent sample T-testing for HSP60 protein corrected mean grey area data for glioblastoma multiforme cells treated with 6.25 µM α-solanine versus negative control (culture) treatment.

Independent Samples T-Test

	t	df	p
HSP60	5.440	10	< .001

Note. Student's t-test.

Output 13.415.: Descriptive statistics for HSP70 protein corrected mean grey area data for glioblastoma multiforme cells treated with 6.25 µM α-solanine versus negative control (culture) treatment.

Descriptive Statistics

	HSP70	
	Neg control	∝-solanine
Valid	6	6
Missing	0	0
Mean	78.619	85.876
Std. Deviation	15.200	18.826
Minimum	58.330	68.421
Maximum	90.186	115.396

Output 13.416.: Normality (Shapiro-Wilk) and Equality of Variance (Levene's) assumption checks for pairwise sample testing for HSP70 protein corrected mean grey area data for glioblastoma multiforme cells treated with 6.25 µM α-solanine versus negative control (culture) treatment.

Test of Normality (Shapiro-Wilk)

		W	p
HSP70	Neg control	0.716	0.009
	∝-solanine	0.886	0.298

Note. Significant results suggest a deviation from normality.

Test of Equality of Variances (Levene's)

	F	df	p
HSP70	0.331	1	0.578

Output 13.417.: Independent sample T-testing for HSP70 protein corrected mean grey area data for glioblastoma multiforme cells treated with 6.25 µM α-solanine versus negative control (culture) treatment.

Independent Samples T-Test

	t	df	p
HSP70	−0.735	10	0.479

Note. Student's t-test.

Output 13.418.: Descriptive statistics for HTRA2 protein corrected mean grey area data for glioblastoma multiforme cells treated with 6.25 µM α-solanine versus negative control (culture) treatment.

Descriptive Statistics

	HTRA2	
	Neg control	∝-solanine
Valid	6	6
Missing	0	0
Mean	99.270	100.083
Std. Deviation	6.630	20.014
Minimum	91.699	68.811
Maximum	110.504	128.205

Output 13.419.: Normality (Shapiro-Wilk) and Equality of Variance (Levene's) assumption checks for pairwise sample testing for HTRA2 protein corrected mean grey area data for glioblastoma multiforme cells treated with 6.25 µM α-solanine versus negative control (culture) treatment.

Test of Normality (Shapiro-Wilk)

		W	p
HTRA2	Neg control	0.943	0.680
	∝-solanine	0.985	0.972

Note. Significant results suggest a deviation from normality.

Test of Equality of Variances (Levene's)

	F	df	p
HTRA2	2.824	1	0.124

Output 13.420.: Independent sample T-testing for HTRA2 protein corrected mean grey area data for glioblastoma multiforme cells treated with 6.25 µM α-solanine versus negative control (culture) treatment.

Independent Samples T-Test

	t	df	p
HTRA2	−0.095	10	0.927

Note. Student's t-test.

Output 13.421.: Descriptive statistics for IGF-1 protein corrected mean grey area data for glioblastoma multiforme cells treated with 6.25 µM α-solanine versus negative control (culture) treatment.

Descriptive Statistics

	IGF-1	
	Neg control	∝-solanine
Valid	6	6
Missing	0	0
Mean	79.007	109.687
Std. Deviation	8.455	32.466
Minimum	66.658	80.512
Maximum	89.273	171.415

Output 13.422.: Normality (Shapiro-Wilk) and Equality of Variance (Levene's) assumption checks for pairwise sample testing for IGF-1 protein corrected mean grey area data for glioblastoma multiforme cells treated with 6.25 µM α-solanine versus negative control (culture) treatment.

Independent Samples T-Test

	t	df	p
IGF-1	−2.240	10	0.049

Note. Student's t-test.

Output 13.423.: Independent sample T-testing for IGF-1 protein corrected mean grey area data for glioblastoma multiforme cells treated with 6.25 µM α-solanine versus negative control (culture) treatment.

Test of Normality (Shapiro-Wilk)

		W	p
IGF-1	Neg control	0.968	0.881
	∝-solanine	0.824	0.095

Note. Significant results suggest a deviation from normality.

Test of Equality of Variances (Levene's)

	F	df	p
IGF-1	3.528	1	0.090

Output 13.424.: Descriptive statistics for IGF-2 protein corrected mean grey area data for glioblastoma multiforme cells treated with 6.25 µM α-solanine versus negative control (culture) treatment.

Descriptive Statistics

	IGF-2	
	Neg control	∝-solanine
Valid	6	6
Missing	0	0
Mean	78.999	115.941
Std. Deviation	8.901	31.347
Minimum	63.688	88.270
Maximum	86.365	173.197

Output 13.425.: Normality (Shapiro-Wilk) and Equality of Variance (Levene's) assumption checks for pairwise sample testing for IGF-2 protein corrected mean grey area data for glioblastoma multiforme cells treated with 6.25 µM α-solanine versus negative control (culture) treatment.

Test of Normality (Shapiro-Wilk)

		W	p
IGF-2	Neg control	0.840	0.130
	∝-solanine	0.856	0.175

Note. Significant results suggest a deviation from normality.

Test of Equality of Variances (Levene's)

	F	df	p
IGF-2	4.609	1	0.057

Output 13.426.: Independent sample T-testing for IGF-2 protein corrected mean grey area data for glioblastoma multiforme cells treated with 6.25 µM α-solanine versus negative control (culture) treatment.

Independent Samples T-Test

	t	df	p
IGF-2	−2.777	10	0.020

Note. Student's t-test.

Output 13.427.: Descriptive statistics for IGFBP-1 protein corrected mean grey area data for glioblastoma multiforme cells treated with 6.25 µM α-solanine versus negative control (culture) treatment.

Descriptive Statistics

	IGFBP-1	
	Neg control	∝-solanine
Valid	6	6
Missing	0	0
Mean	67.536	71.716
Std. Deviation	4.510	16.544
Minimum	61.907	50.861
Maximum	71.740	94.844

Output 13.428.: Normality (Shapiro-Wilk) and Equality of Variance (Levene's) assumption checks for pairwise sample testing for IGFBP-1 protein corrected mean grey area data for glioblastoma multiforme cells treated with 6.25 µM α-solanine versus negative control (culture) treatment.

Test of Normality (Shapiro-Wilk)

		W	p
IGFBP-1	Neg control	0.814	0.078
	∝-solanine	0.967	0.873

Note. Significant results suggest a deviation from normality.

Test of Equality of Variances (Levene's)

	F	df	p
IGFBP-1	4.934	1	0.051

Output 13.429.: Independent sample T-testing for IGFBP-1 protein corrected mean grey area data for glioblastoma multiforme cells treated with 6.25 µM α-solanine versus negative control (culture) treatment.

Independent Samples T-Test

	t	df	p
IGFBP-1	−0.597	10	0.564

Note. Student's t-test.

Output 13.430.: Descriptive statistics for IGFBP-2 protein corrected mean grey area data for glioblastoma multiforme cells treated with 6.25 µM α-solanine versus negative control (culture) treatment.

Descriptive Statistics

	IGFBP-2	
	Neg control	∝-solanine
Valid	6	6
Missing	0	0
Mean	73.971	84.194
Std. Deviation	8.050	22.484
Minimum	63.342	58.653
Maximum	85.428	119.784

Output 13.431.: Normality (Shapiro-Wilk) and Equality of Variance (Levene's) assumption checks for pairwise sample testing for IGFBP-2 protein corrected mean grey area data for glioblastoma multiforme cells treated with 6.25 µM α-solanine versus negative control (culture) treatment.

Test of Normality (Shapiro-Wilk)

		W	p
IGFBP-1	Neg control	0.814	0.078
	∝-solanine	0.967	0.873

Note. Significant results suggest a deviation from normality.

Test of Equality of Variances (Levene's)

	F	df	p
IGFBP-1	4.934	1	0.051

Output 13.432.: Independent sample T-testing for IGFBP-2 protein corrected mean grey area data for glioblastoma multiforme cells treated with 6.25 µM α-solanine versus negative control (culture) treatment.

Independent Samples T-Test

	t	df	p
IGFBP-1	−0.597	10	0.564

Note. Student's t-test.

Output 13.433.: Descriptive statistics for IGFBP-3 protein corrected mean grey area data for glioblastoma multiforme cells treated with 6.25 µM α-solanine versus negative control (culture) treatment.

Descriptive Statistics

	IGFBP-3	
	Neg control	∝-solanine
Valid	6	6
Missing	0	0
Mean	102.053	101.281
Std. Deviation	16.140	19.338
Minimum	88.933	80.758
Maximum	127.451	125.675

Output 13.434.: Normality (Shapiro-Wilk) and Equality of Variance (Levene's) assumption checks for pairwise sample testing for IGFBP-3 protein corrected mean grey area data for glioblastoma multiforme cells treated with 6.25 µM α-solanine versus negative control (culture) treatment.

Test of Normality (Shapiro-Wilk)

		W	p
IGFBP-3	Neg control	0.814	0.078
	∝-solanine	0.892	0.327

Note. Significant results suggest a deviation from normality.

Test of Equality of Variances (Levene's)

	F	df	p
IGFBP-3	0.145	1	0.712

Output 13.435.: Independent sample T-testing for IGFBP-3 protein corrected mean grey area data for glioblastoma multiforme cells treated with 6.25 µM α-solanine versus negative control (culture) treatment.

Independent Samples T-Test

	t	df	p
IGFBP-3	0.075	10	0.942

Note. Student's t-test.

Output 13.436.: Descriptive statistics for IGFBP-4 protein corrected mean grey area data for glioblastoma multiforme cells treated with 6.25 µM α-solanine versus negative control (culture) treatment.

Descriptive Statistics

	IGFBP-4	
	Neg control	∝-solanine
Valid	6	6
Missing	0	0
Mean	77.278	80.786
Std. Deviation	15.343	11.870
Minimum	59.900	57.958
Maximum	98.635	91.954

Output 13.437.: Normality (Shapiro-Wilk) and Equality of Variance (Levene's) assumption checks for pairwise sample testing for IGFBP-4 protein corrected mean grey area data for glioblastoma multiforme cells treated with 6.25 µM α-solanine versus negative control (culture) treatment.

Test of Normality (Shapiro-Wilk)

		W	p
IGFBP-4	Neg control	0.899	0.366
	∝-solanine	0.807	0.068

Note. Significant results suggest a deviation from normality.

Test of Equality of Variances (Levene's)

	F	df	p
IGFBP-4	1.102	1	0.319

Output 13.438.: Independent sample T-testing for IGFBP-4 protein corrected mean grey area data for glioblastoma multiforme cells treated with 6.25 µM α-solanine versus negative control (culture) treatment.

Independent Samples T-Test

	t	df	p
IGFBP-4	−0.443	10	0.667

Note. Student's t-test.

Output 13.439.: Descriptive statistics for IGFBP-5 protein corrected mean grey area data for glioblastoma multiforme cells treated with 6.25 µM α-solanine versus negative control (culture) treatment.

Descriptive Statistics

	IGFBP-5	
	Neg control	∝-solanine
Valid	6	6
Missing	0	0
Mean	80.153	85.715
Std. Deviation	11.258	18.949
Minimum	68.768	70.766
Maximum	96.028	118.086

Output 13.440.: Normality (Shapiro-Wilk) and Equality of Variance (Levene's) assumption checks for pairwise sample testing for IGFBP-5 protein corrected mean grey area data for glioblastoma multiforme cells treated with 6.25 µM α-solanine versus negative control (culture) treatment.

Test of Normality (Shapiro-Wilk)

		W	p
IGFBP-5	Neg control	0.859	0.186
	∝-solanine	0.792	0.049

Note. Significant results suggest a deviation from normality.

Test of Equality of Variances (Levene's)

	F	df	p
IGFBP-5	2.320	1	0.159

Output 13.441.: Independent sample T-testing for IGFBP-5 protein corrected mean grey area data for glioblastoma multiforme cells treated with 6.25 µM α-solanine versus negative control (culture) treatment.

Independent Samples T-Test

	t	df	p
IGFBP-5	−0.618	10	0.550

Note. Student's t-test.

Output 13.442.: Descriptive statistics for IGFBP-6 protein corrected mean grey area data for glioblastoma multiforme cells treated with 6.25 µM α-solanine versus negative control (culture) treatment.

Descriptive Statistics

	IGFBP-6	
	Neg control	∝-solanine
Valid	6	6
Missing	0	0
Mean	76.361	105.790
Std. Deviation	14.096	38.173
Minimum	65.740	77.919
Maximum	96.176	156.522

Output 13.443.: Normality (Shapiro-Wilk) and Equality of Variance (Levene's) assumption checks for pairwise sample testing for IGFBP-6 protein corrected mean grey area data for glioblastoma multiforme cells treated with 6.25 µM α-solanine versus negative control (culture) treatment.

Test of Normality (Shapiro–Wilk)

		W	p
IGFBP–6	Neg control	0.726	0.011
	∝–solanine	0.689	0.005

Note. Significant results suggest a deviation from normality.

Test of Equality of Variances (Levene's)

	F	df	p
IGFBP–6	13.618	1	0.004

Output 13.444.: Independent sample T-testing for IGFBP-6 protein corrected mean grey area data for glioblastoma multiforme cells treated with 6.25 µM α-solanine versus negative control (culture) treatment.

Independent Samples T–Test

	t	df	p
IGFBP–6	−1.772	6.339	0.124

Note. Welch's t–test.

Output 13.445.: Descriptive statistics for IGF-1R protein corrected mean grey area data for glioblastoma multiforme cells treated with 6.25 µM α-solanine versus negative control (culture) treatment.

Descriptive Statistics

	IGF-1R	
	Neg control	∝-solanine
Valid	6	6
Missing	0	0
Mean	52.995	90.467
Std. Deviation	6.056	40.600
Minimum	44.937	60.580
Maximum	61.329	143.668

Output 13.446.: Normality (Shapiro-Wilk) and Equality of Variance (Levene's) assumption checks for pairwise sample testing for IGF-1R protein corrected mean grey area data for glioblastoma multiforme cells treated with 6.25 µM α-solanine versus negative control (culture) treatment.

Test of Normality (Shapiro-Wilk)

		W	p
IGF-1	Neg control	0.968	0.881
	∝-solanine	0.824	0.095

Note. Significant results suggest a deviation from normality.

Test of Equality of Variances (Levene's)

	F	df	p
IGF-1	3.528	1	0.090

Output 13.447.: Independent sample T-testing for IGF-1R protein corrected mean grey area data for glioblastoma multiforme cells treated with 6.25 µM α-solanine versus negative control (culture) treatment.

Independent Samples T-Test

	t	df	p
IGF-1	−2.240	10	0.049

Note. Student's t-test.

Output 13.448.: Descriptive statistics for livin protein corrected mean grey area data for glioblastoma multiforme cells treated with 6.25 µM α-solanine versus negative control (culture) treatment.

Descriptive Statistics

	livin	
	Neg control	∝-solanine
Valid	6	6
Missing	0	0
Mean	18.612	24.559
Std. Deviation	3.379	6.890
Minimum	13.833	17.700
Maximum	23.304	34.333

Output 13.449.: Normality (Shapiro-Wilk) and Equality of Variance (Levene's) assumption checks for pairwise sample testing for livin protein corrected mean grey area data for glioblastoma multiforme cells treated with 6.25 µM α-solanine versus negative control (culture) treatment.

Test of Normality (Shapiro-Wilk)

		W	p
livin	Neg control	0.978	0.939
	∝-solanine	0.866	0.210

Note. Significant results suggest a deviation from normality.

Test of Equality of Variances (Levene's)

	F	df	p
livin	5.014	1	0.049

Output 13.450.: Welch testing for livin protein corrected mean grey area data for glioblastoma multiforme cells treated with 6.25 µM α-solanine versus negative control (culture) treatment.

Independent Samples T-Test

	t	df	p
livin	−1.898	7.274	0.098

Note. Welch's t-test.

Output 13.451.:Descriptive statistics for p21 protein corrected mean grey area data for glioblastoma multiforme cells treated with 6.25 µM α-solanine versus negative control (culture) treatment.

Descriptive Statistics

	p21	
	Neg control	∝-solanine
Valid	6	6
Missing	0	0
Mean	92.844	105.647
Std. Deviation	17.852	22.942
Minimum	73.228	73.543
Maximum	120.768	138.640

Output 13.452.: Normality (Shapiro-Wilk) and Equality of Variance (Levene's) assumption checks for pairwise sample testing for p21 protein corrected mean grey area data for glioblastoma multiforme cells treated with 6.25 µM α-solanine versus negative control (culture) treatment.

Test of Normality (Shapiro-Wilk)

		W	p
p21	Neg control	0.930	0.582
	∝-solanine	0.963	0.844

Note. Significant results suggest a deviation from normality.

Test of Equality of Variances (Levene's)

	F	df	p
p21	0.227	1	0.644

Output 13.453.: Independent sample T-testing for p21 protein corrected mean grey area data for glioblastoma multiforme cells treated with 6.25 µM α-solanine versus negative control (culture) treatment.

Independent Samples T-Test			
	t	df	p
p21	−1.079	10	0.306

Note. Student's t-test.

Output 13.454.: Descriptive statistics for p27 protein corrected mean grey area data for glioblastoma multiforme cells treated with 6.25 µM α-solanine versus negative control (culture) treatment.

Descriptive Statistics		
	p27	
	Neg control	∝-solanine
Valid	6	6
Missing	0	0
Mean	107.840	106.193
Std. Deviation	18.068	14.873
Minimum	82.784	83.332
Maximum	133.238	125.711

Output 13.455.: Normality (Shapiro-Wilk) and Equality of Variance (Levene's) assumption checks for pairwise sample testing for p27 protein corrected mean grey area data for glioblastoma multiforme cells treated with 6.25 µM α-solanine versus negative control (culture) treatment.

Test of Normality (Shapiro-Wilk)

		W	p
p27	Neg control	0.976	0.931
	∝-solanine	0.989	0.987

Note. Significant results suggest a deviation from normality.

Test of Equality of Variances (Levene's)

	F	df	p
p27	0.523	1	0.486

Output 13.456.: Independent sample T-testing for p27 protein corrected mean grey area data for glioblastoma multiforme cells treated with 6.25 µM α-solanine versus negative control (culture) treatment.

Independent Samples T-Test

	t	df	p
p27	0.172	10	0.867

Note. Student's t-test.

Output 13.457.: Descriptive statistics for p53 protein corrected mean grey area data for glioblastoma multiforme cells treated with 6.25 µM α-solanine versus negative control (culture) treatment.

Descriptive Statistics

	p53	
	Neg control	∝-solanine
Valid	6	6
Missing	0	0
Mean	102.140	105.308
Std. Deviation	8.481	12.412
Minimum	91.976	92.247
Maximum	112.409	121.286

Output 13.458.: Normality (Shapiro-Wilk) and Equality of Variance (Levene's) assumption checks for pairwise sample testing for p53 protein corrected mean grey area data for glioblastoma multiforme cells treated with 6.25 µM α-solanine versus negative control (culture) treatment.

Test of Normality (Shapiro-Wilk)

		W	p
p53	Neg control	0.900	0.376
	∝-solanine	0.898	0.361

Note. Significant results suggest a deviation from normality.

Test of Equality of Variances (Levene's)

	F	df	p
p53	2.486	1	0.146

Output 13.459.: Independent sample T-testing for p5 protein corrected mean grey area data for glioblastoma multiforme cells treated with 6.25 µM α-solanine versus negative control (culture) treatment.

Independent Samples T-Test

	t	df	p
p53	−0.516	10	0.617

Note. Student's t-test.

Output 13.460.: Descriptive statistics for SMAC protein corrected mean grey area data for glioblastoma multiforme cells treated with 6.25 µM α-solanine versus negative control (culture) treatment.

Descriptive Statistics

	SMAC	
	Neg control	∝-solanine
Valid	6	6
Missing	0	0
Mean	22.939	22.910
Std. Deviation	3.533	3.303
Minimum	17.885	17.111
Maximum	26.545	27.089

Output 13.461.: Normality (Shapiro-Wilk) and Equality of Variance (Levene's) assumption checks for pairwise sample testing for SMAC protein corrected mean grey area data for glioblastoma multiforme cells treated with 6.25 µM α-solanine versus negative control (culture) treatment.

Test of Normality (Shapiro-Wilk)

		W	p
SMAC	Neg control	0.902	0.388
	∝-solanine	0.923	0.528

Note. Significant results suggest a deviation from normality.

Test of Equality of Variances (Levene's)

	F	df	p
SMAC	0.321	1	0.584

Output 13.462.: Independent sample T-testing for SMAC protein corrected mean grey area data for glioblastoma multiforme cells treated with 6.25 µM α-solanine versus negative control (culture) treatment.

Independent Samples T-Test

	t	df	p
SMAC	0.015	10	0.989

Note. Student's t-test.

Output 13.463.: Descriptive statistics for survivin protein corrected mean grey area data for glioblastoma multiforme cells treated with 6.25 µM α-solanine versus negative control (culture) treatment.

Descriptive Statistics

	Survivin	
	Neg control	∝-solanine
Valid	6	6
Missing	0	0
Mean	68.099	76.742
Std. Deviation	10.672	5.758
Minimum	56.829	71.868
Maximum	82.116	86.642

Output 13.464.: Normality (Shapiro-Wilk) and Equality of Variance (Levene's) assumption checks for pairwise sample testing for survivin protein corrected mean grey area data for glioblastoma multiforme cells treated with 6.25 µM α-solanine versus negative control (culture) treatment.

Test of Normality (Shapiro-Wilk)

		W	p
Survivin	Neg control	0.889	0.312
	∝-solanine	0.857	0.179

Note. Significant results suggest a deviation from normality.

Test of Equality of Variances (Levene's)

	F	df	p
Survivin	2.980	1	0.115

Output 13.465.: Independent sample T-testing for survivin protein corrected mean grey area data for glioblastoma multiforme cells treated with 6.25 µM α-solanine versus negative control (culture) treatment.

Independent Samples T-Test

	t	df	p
Survivin	−1.746	10	0.111

Note. Student's t-test.

Output 13.466.: Descriptive statistics for TNF-RI protein corrected mean grey area data for glioblastoma multiforme cells treated with 6.25 µM α-solanine versus negative control (culture) treatment.

Descriptive Statistics

	TNF RI	
	Neg control	∝-solanine
Valid	6	6
Missing	0	0
Mean	64.602	69.875
Std. Deviation	5.680	3.278
Minimum	57.137	65.272
Maximum	72.230	74.782

Output 13.467.: Normality (Shapiro-Wilk) and Equality of Variance (Levene's) assumption checks for pairwise sample testing for TNF-RI protein corrected mean grey area data for glioblastoma multiforme cells treated with 6.25 µM α-solanine versus negative control (culture) treatment.

Test of Normality (Shapiro-Wilk)

		W	p
TNF RI	Neg control	0.979	0.947
	∝-solanine	0.964	0.851

Note. Significant results suggest a deviation from normality.

Test of Equality of Variances (Levene's)

	F	df	p
TNF RI	2.606	1	0.138

Output 13.468.: Independent sample T-testing for TNF-RI protein corrected mean grey area data for glioblastoma multiforme cells treated with 6.25 µM α-solanine versus negative control (culture) treatment.

Independent Samples T-Test

	t	df	p
TNF RI	−1.970	10	0.077

Note. Student's t-test.

Output 13.469.: Descriptive statistics for TNF-RII protein corrected mean grey area data for glioblastoma multiforme cells treated with 6.25 µM α-solanine versus negative control (culture) treatment.

Descriptive Statistics

	TNF RII	
	Neg control	∝-solanine
Valid	6	6
Missing	0	0
Mean	76.303	86.216
Std. Deviation	6.977	20.371
Minimum	63.575	58.349
Maximum	84.480	115.224

Output 13.470.: Normality (Shapiro-Wilk) and Equality of Variance (Levene's) assumption checks for pairwise sample testing for TNF-RII protein corrected mean grey area data for glioblastoma multiforme cells treated with 6.25 µM α-solanine versus negative control (culture) treatment.

Test of Normality (Shapiro-Wilk)

		W	p
TNF RII	Neg control	0.876	0.253
	∝-solanine	0.993	0.995

Note. Significant results suggest a deviation from normality.

Test of Equality of Variances (Levene's)

	F	df	p
TNF RII	4.354	1	0.063

Output 13.471.: Independent sample T-testing for TNF-RII protein corrected mean grey area data for glioblastoma multiforme cells treated with 6.25 µM α-solanine versus negative control (culture) treatment.

Independent Samples T-Test

	t	df	p
TNF RII	−1.128	10	0.286

Note. Student's t-test.

Output 13.472.: Descriptive statistics for TNF-α protein corrected mean grey area data for glioblastoma multiforme cells treated with 6.25 µM α-solanine versus negative control (culture) treatment.

Descriptive Statistics

	TNF alpha	
	Neg control	∝-solanine
Valid	6	6
Missing	0	0
Mean	71.724	83.800
Std. Deviation	8.646	18.040
Minimum	58.584	57.543
Maximum	84.900	106.405

Output 13.473.: Normality (Shapiro-Wilk) and Equality of Variance (Levene's) assumption checks for pairwise sample testing for TNF-α protein corrected mean grey area data for glioblastoma multiforme cells treated with 6.25 µM α-solanine versus negative control (culture) treatment.

Test of Normality (Shapiro-Wilk)

		W	p
TNF alpha	Neg control	0.954	0.771
	∝-solanine	0.965	0.857

Note. Significant results suggest a deviation from normality.

Test of Equality of Variances (Levene's)

	F	df	p
TNF alpha	2.712	1	0.131

Output 13.474.: Independent sample T-testing for TNF-α protein corrected mean grey area data for glioblastoma multiforme cells treated with 6.25 µM α-solanine versus negative control (culture) treatment.

Independent Samples T-Test

	t	df	p
TNF alpha	−1.479	10	0.170

Note. Student's t-test.

Output 13.475.: Descriptive statistics for TNF-β protein corrected mean grey area data for glioblastoma multiforme cells treated with 6.25 µM α-solanine versus negative control (culture) treatment.

Descriptive Statistics

	TNF beta	
	Neg control	∝-solanine
Valid	6	6
Missing	0	0
Mean	68.188	67.696
Std. Deviation	13.939	14.716
Minimum	53.006	54.533
Maximum	86.633	90.408

Output 13.476.: Normality (Shapiro-Wilk) and Equality of Variance (Levene's) assumption checks for pairwise sample testing for TNF-β protein corrected mean grey area data for glioblastoma multiforme cells treated with 6.25 µM α-solanine versus negative control (culture) treatment.

Test of Normality (Shapiro-Wilk)

		W	p
TNF beta	Neg control	0.844	0.141
	∝-solanine	0.869	0.223

Note. Significant results suggest a deviation from normality.

Test of Equality of Variances (Levene's)

	F	df	p
TNF beta	0.011	1	0.919

Output 13.477.: Independent sample T-testing for TNF-β protein corrected mean grey area data for glioblastoma multiforme cells treated with 6.25 µM α-solanine versus negative control (culture) treatment.

Independent Samples T-Test

	t	df	p
TNF beta	0.060	10	0.954

Note. Student's t-test.

Output 13.478.: Descriptive statistics for TRAIL R1 protein corrected mean grey area data for glioblastoma multiforme cells treated with 6.25 µM α-solanine versus negative control (culture) treatment.

Descriptive Statistics

	TRAIL R1	
	Neg control	∝-solanine
Valid	6	6
Missing	0	0
Mean	93.605	87.035
Std. Deviation	15.752	22.916
Minimum	78.511	63.275
Maximum	117.987	121.604

Output 13.479.: Normality (Shapiro-Wilk) and Equality of Variance (Levene's) assumption checks for pairwise sample testing for TRAIL R1 protein corrected mean grey area data for glioblastoma multiforme cells treated with 6.25 µM α-solanine versus negative control (culture) treatment.

Test of Normality (Shapiro-Wilk) ▼

		W	p
TRAIL R1	Neg control	0.886	0.299
	∝-solanine	0.915	0.472

Note. Significant results suggest a deviation from normality.

Test of Equality of Variances (Levene's)

	F	df	p
TRAIL R1	1.081	1	0.323

Output 13.480.: Independent sample T-testing for TRAIL R1 protein corrected mean grey area data for glioblastoma multiforme cells treated with 6.25 µM α-solanine versus negative control (culture) treatment.

Independent Samples T-Test

	t	df	p
TRAIL R1	0.579	10	0.576

Note. Student's t-test.

Output 13.481.: Descriptive statistics for TRAIL R2 protein corrected mean grey area data for glioblastoma multiforme cells treated with 6.25 µM α-solanine versus negative control (culture) treatment.

Descriptive Statistics ▼

	TRAIL R2	
	Neg control	∝-solanine
Valid	6	6
Missing	0	0
Mean	105.051	94.490
Std. Deviation	22.424	16.408
Minimum	84.843	70.065
Maximum	139.209	117.867

Output 13.482.: Normality (Shapiro-Wilk) and Equality of Variance (Levene's) assumption checks for pairwise sample testing for TRAIL R2 protein corrected mean grey area data for glioblastoma multiforme cells treated with 6.25 µM α-solanine versus negative control (culture) treatment.

Test of Normality (Shapiro-Wilk) ▼

		W	p
TRAIL R2	Neg control	0.855	0.171
	∝-solanine	0.992	0.994

Note. Significant results suggest a deviation from normality.

Test of Equality of Variances (Levene's)

	F	df	p
TRAIL R2	1.419	1	0.261

Output 13.483.: Independent sample T-testing for TRAIL R2 protein corrected mean grey area data for glioblastoma multiforme cells treated with 6.25 µM α-solanine versus negative control (culture) treatment.

Independent Samples T-Test

	t	df	p
TRAIL R2	0.931	10	0.374

Note. Student's t-test.

Output 13.484.: Descriptive statistics for TRAIL R3 protein corrected mean grey area data for glioblastoma multiforme cells treated with 6.25 µM α-solanine versus negative control (culture) treatment.

Descriptive Statistics

	TRAIL R3	
	Neg control	∝-solanine
Valid	6	6
Missing	0	0
Mean	71.893	78.398
Std. Deviation	15.872	11.830
Minimum	55.522	58.706
Maximum	93.011	90.546

Output 13.485.: Normality (Shapiro-Wilk) and Equality of Variance (Levene's) assumption checks for pairwise sample testing for TRAIL R3 protein corrected mean grey area data for glioblastoma multiforme cells treated with 6.25 µM α-solanine versus negative control (culture) treatment.

Test of Normality (Shapiro-Wilk)

		W	p
TRAIL R3	Neg control	0.895	0.345
	∝-solanine	0.903	0.393

Note. Significant results suggest a deviation from normality.

Test of Equality of Variances (Levene's)

	F	df	p
TRAIL R3	2.017	1	0.186

Output 13.486.: Independent sample T-testing for TRAIL R3 protein corrected mean grey area data for glioblastoma multiforme cells treated with 6.25 µM α-solanine versus negative control (culture) treatment.

Independent Samples T-Test

	t	df	p
TRAIL R3	−0.805	10	0.440

Note. Student's t-test.

Output 13.487.: Descriptive statistics for TRAIL R4 protein corrected mean grey area data for glioblastoma multiforme cells treated with 6.25 µM α-solanine versus negative control (culture) treatment.

Descriptive Statistics

	TRAIL R 4	
	Neg control	∝-solanine
Valid	6	6
Missing	0	0
Mean	92.284	110.624
Std. Deviation	20.730	21.882
Minimum	60.898	76.541
Maximum	121.117	136.996

Output 13.488.: Normality (Shapiro-Wilk) and Equality of Variance (Levene's) assumption checks for pairwise sample testing for TRAIL R4 protein corrected mean grey area data for glioblastoma multiforme cells treated with 6.25 µM α-solanine versus negative control (culture) treatment.

Test of Normality (Shapiro-Wilk)

		W	p
TRAIL R 4	Neg control	0.963	0.841
	∝-solanine	0.965	0.856

Note. Significant results suggest a deviation from normality.

Test of Equality of Variances (Levene's)

	F	df	p
TRAIL R 4	0.088	1	0.773

Output 13.489.: Independent sample T-testing for TRAIL R4 protein corrected mean grey area data for glioblastoma multiforme cells treated with 6.25 µM α-solanine versus negative control (culture) treatment.

Independent Samples T-Test

	t	df	p
TRAIL R 4	−1.490	10	0.167

Note. Student's t-test.

Output 13.490.: Descriptive statistics for XIAP protein corrected mean grey area data for glioblastoma multiforme cells treated with 6.25 µM α-solanine versus negative control (culture) treatment.

Descriptive Statistics

	XIAP	
	Neg control	∝-solanine
Valid	6	6
Missing	0	0
Mean	101.085	111.844
Std. Deviation	20.998	17.039
Minimum	70.997	84.568
Maximum	131.884	129.422

Output 13.491.: Normality (Shapiro-Wilk) and Equality of Variance (Levene's) assumption checks for pairwise sample testing for XIAP protein corrected mean grey area data for glioblastoma multiforme cells treated with 6.25 µM α-solanine versus negative control (culture) treatment.

Test of Normality (Shapiro-Wilk)

		W	p
XIAP	Neg control	0.995	0.998
	∝-solanine	0.928	0.562

Note. Significant results suggest a deviation from normality.

Test of Equality of Variances (Levene's)

	F	df	p
XIAP	0.086	1	0.775

Output 13.492.: Independent sample T-testing for XIAP protein corrected mean grey area data for glioblastoma multiforme cells treated with 6.25 µM α-solanine versus negative control (culture) treatment.

Independent Samples T-Test

	t	df	p
ATG3	2.183	10	0.054

Note. Student's t-test.

Output 13.493.: Descriptive statistics for ATG3 protein corrected mean grey area data for glioblastoma multiforme cells treated with 6.25 µM α-solanine versus negative control (culture) treatment.

Descriptive Statistics

	ATG3	
	Neg control	∝-solanine
Valid	6	6
Missing	0	0
Mean	28.685	24.049
Std. Deviation	3.074	4.195
Minimum	24.572	19.649
Maximum	32.020	30.026

Output 13.494.: Normality (Shapiro-Wilk) and Equality of Variance (Levene's) assumption checks for pairwise sample testing for ATG3 protein corrected mean grey area data for glioblastoma multiforme cells treated with 6.25 µM α-solanine versus negative control (culture) treatment.

Test of Normality (Shapiro-Wilk)

		W	p
ATG3	Neg control	0.913	0.456
	∝-solanine	0.891	0.324

Note. Significant results suggest a deviation from normality.

Test of Equality of Variances (Levene's)

	F	df	p
ATG3	1.086	1	0.322

Output 13.495.: Independent sample T-testing for ATG3 protein corrected mean grey area data for glioblastoma multiforme cells treated with 6.25 µM α-solanine versus negative control (culture) treatment.

Independent Samples T-Test

	t	df	p
ATG3	2.183	10	0.054

Note. Student's t-test.

Output 13.496.: Descriptive statistics for ATG4A protein corrected mean grey area data for glioblastoma multiforme cells treated with 6.25 µM α-solanine versus negative control (culture) treatment.

Descriptive Statistics

	ATG4A	
	Neg control	∝-solanine
Valid	6	6
Missing	0	0
Mean	135.016	199.103
Std. Deviation	2.320	6.771
Minimum	132.917	191.216
Maximum	139.332	208.843

Output 13.497.: Normality (Shapiro-Wilk) and Equality of Variance (Levene's) assumption checks for pairwise sample testing for ATG4A protein corrected mean grey area data for glioblastoma multiforme cells treated with 6.25 µM α-solanine versus negative control (culture) treatment.

Test of Normality (Shapiro-Wilk)

		W	p
ATG4A	Neg control	0.837	0.122
	∝-solanine	0.931	0.589

Note. Significant results suggest a deviation from normality.

Test of Equality of Variances (Levene's)

	F	df	p
ATG4A	6.123	1	0.033

Output 13.498.: Welch testing for ATG4A protein corrected mean grey area data for glioblastoma multiforme cells treated with 6.25 µM α-solanine versus negative control (culture) treatment.

Independent Samples T-Test

	t	df	p
ATG4A	−21.933	6.158	< .001

Note. Welch's t-test.

Output 13.499.: Descriptive statistics for ATG4B protein corrected mean grey area data for glioblastoma multiforme cells treated with 6.25 µM α-solanine versus negative control (culture) treatment.

Descriptive Statistics

	ATG4B	
	Neg control	∝-solanine
Valid	6	6
Missing	0	0
Mean	100.087	146.253
Std. Deviation	8.629	8.009
Minimum	83.540	134.380
Maximum	107.224	153.962

Output 13.500.: Normality (Shapiro-Wilk) and Equality of Variance (Levene's) assumption checks for pairwise sample testing for ATG4B protein corrected mean grey area data for glioblastoma multiforme cells treated with 6.25 µM α-solanine versus negative control (culture) treatment.

Test of Normality (Shapiro-Wilk)

		W	p
ATG4B	Neg control	0.801	0.060
	∝-solanine	0.869	0.224

Note. Significant results suggest a deviation from normality.

Test of Equality of Variances (Levene's)

	F	df	p
ATG4B	0.114	1	0.742

Output 13.501.: Independent sample T-testing for ATG4B protein corrected mean grey area data for glioblastoma multiforme cells treated with 6.25 µM α-solanine versus negative control (culture) treatment.

Independent Samples T-Test

	t	df	p
ATG4B	−9.606	10	< .001

Note. Student's t-test.

Output 13.502.: Descriptive statistics for ATG5 protein corrected mean grey area data for glioblastoma multiforme cells treated with 6.25 µM α-solanine versus negative control (culture) treatment.

Descriptive Statistics

	ATG5	
	Neg control	∝-solanine
Valid	6	6
Missing	0	0
Mean	171.590	200.941
Std. Deviation	11.852	8.213
Minimum	154.460	187.816
Maximum	184.895	213.146

Output 13.503.: Normality (Shapiro-Wilk) and Equality of Variance (Levene's) assumption checks for pairwise sample testing for ATG5 protein corrected mean grey area data for glioblastoma multiforme cells treated with 6.25 µM α-solanine versus negative control (culture) treatment.

Test of Normality (Shapiro-Wilk)

		W	p
ATG5	Neg control	0.934	0.607
	∝-solanine	0.954	0.770

Note. Significant results suggest a deviation from normality.

Test of Equality of Variances (Levene's)

	F	df	p
ATG5	2.445	1	0.149

Output 13.504.: Independent sample T-testing for ATG5 protein corrected mean grey area data for glioblastoma multiforme cells treated with 6.25 µM α-solanine versus negative control (culture) treatment.

Independent Samples T-Test

	t	df	p
ATG5	−4.986	10	< .001

Note. Student's t-test.

Output 13.505.: Descriptive statistics for ATG7 protein corrected mean grey area data for glioblastoma multiforme cells treated with 6.25 µM α-solanine versus negative control (culture) treatment.

Descriptive Statistics

	ATG7	
	Neg control	∝-solanine
Valid	6	6
Missing	0	0
Mean	156.860	176.085
Std. Deviation	12.626	15.724
Minimum	143.827	161.994
Maximum	178.377	198.531

Output 13.506.: Normality (Shapiro-Wilk) and Equality of Variance (Levene's) assumption checks for pairwise sample testing for ATG7protein corrected mean grey area data for glioblastoma multiforme cells treated with 6.25 µM α-solanine versus negative control (culture) treatment.

Test of Normality (Shapiro-Wilk)

		W	p
ATG7	Neg control	0.915	0.473
	∝-solanine	0.844	0.141

Note. Significant results suggest a deviation from normality.

Test of Equality of Variances (Levene's)

	F	df	p
ATG7	0.718	1	0.417

Output 13.507.: Independent sample T-testing for ATG7 protein corrected mean grey area data for glioblastoma multiforme cells treated with 6.25 µM α-solanine versus negative control (culture) treatment.

Independent Samples T-Test			
	t	df	p
ATG7	−2.335	10	0.042

Note. Student's t-test.

Output 13.508.: Descriptive statistics for ATG10 protein corrected mean grey area data for glioblastoma multiforme cells treated with 6.25 µM α-solanine versus negative control (culture) treatment.

Descriptive Statistics		
	ATG10	
	Neg control	∝-solanine
Valid	6	6
Missing	0	0
Mean	104.031	112.977
Std. Deviation	10.896	13.129
Minimum	88.555	102.535
Maximum	115.847	137.396

Output 13.509.: Normality (Shapiro-Wilk) and Equality of Variance (Levene's) assumption checks for pairwise sample testing for ATG10 protein corrected mean grey area data for glioblastoma multiforme cells treated with 6.25 µM α-solanine versus negative control (culture) treatment.

Test of Normality (Shapiro-Wilk)

		W	p
ATG10	Neg control	0.925	0.540
	∝-solanine	0.788	0.046

Note. Significant results suggest a deviation from normality.

Test of Equality of Variances (Levene's)

	F	df	p
ATG10	0.126	1	0.730

Output 13.510.: Independent sample T-testing for ATG10 protein corrected mean grey area data for glioblastoma multiforme cells treated with 6.25 µM α-solanine versus negative control (culture) treatment.

Independent Samples T-Test

	t	df	p
ATG10	−1.284	10	0.228

Note. Student's t-test.

Output 13.511.: Descriptive statistics for ATG12 protein corrected mean grey area data for glioblastoma multiforme cells treated with 6.25 µM α-solanine versus negative control (culture) treatment.

Descriptive Statistics

	ATG12	
	Neg control	∝-solanine
Valid	6	6
Missing	0	0
Mean	89.498	105.566
Std. Deviation	9.978	9.092
Minimum	78.476	93.102
Maximum	105.949	116.093

Output 13.512.: Normality (Shapiro-Wilk) and Equality of Variance (Levene's) assumption checks for pairwise sample testing for ATG12 protein corrected mean grey area data for glioblastoma multiforme cells treated with 6.25 µM α-solanine versus negative control (culture) treatment.

Test of Normality (Shapiro-Wilk)

		W	p
ATG12	Neg control	0.942	0.675
	∝-solanine	0.935	0.619

Note. Significant results suggest a deviation from normality.

Test of Equality of Variances (Levene's)

	F	df	p
ATG12	0.076	1	0.788

Output 13.513.: Independent sample T-testing for ATG12 protein corrected mean grey area data for glioblastoma multiforme cells treated with 6.25 µM α-solanine versus negative control (culture) treatment.

Independent Samples T-Test

	t	df	p
ATG12	−2.916	10	0.015

Note. Student's t-test.

Output 13.514.: Descriptive statistics for ATG13 protein corrected mean grey area data for glioblastoma multiforme cells treated with 6.25 µM α-solanine versus negative control (culture) treatment.

Descriptive Statistics

	ATG13	
	Neg control	∝-solanine
Valid	6	6
Missing	0	0
Mean	144.342	178.294
Std. Deviation	6.410	11.908
Minimum	135.829	163.645
Maximum	153.471	194.220

Output 13.515.: Normality (Shapiro-Wilk) and Equality of Variance (Levene's) assumption checks for pairwise sample testing for ATG13 protein corrected mean grey area data for glioblastoma multiforme cells treated with 6.25 µM α-solanine versus negative control (culture) treatment.

Test of Normality (Shapiro-Wilk)

		W	p
ATG13	Neg control	0.990	0.990
	∝-solanine	0.943	0.680

Note. Significant results suggest a deviation from normality.

Test of Equality of Variances (Levene's)

	F	df	p
ATG13	3.781	1	0.080

Output 13.516.: Independent sample T-testing for ATG13 protein corrected mean grey area data for glioblastoma multiforme cells treated with 6.25 µM α-solanine versus negative control (culture) treatment.

Independent Samples T-Test

	t	df	p
ATG13	−6.150	10	< .001

Note. Student's t-test.

Output 13.517.: Descriptive statistics for BECN1 protein corrected mean grey area data for glioblastoma multiforme cells treated with 6.25 µM α-solanine versus negative control (culture) treatment.

Descriptive Statistics

	BECN1	
	Neg control	∝-solanine
Valid	6	6
Missing	0	0
Mean	132.398	192.995
Std. Deviation	4.745	2.626
Minimum	125.278	188.860
Maximum	137.898	195.397

Output 13.518.: Normality (Shapiro-Wilk) and Equality of Variance (Levene's) assumption checks for pairwise sample testing for BECN1 protein corrected mean grey area data for glioblastoma multiforme cells treated with 6.25 µM α-solanine versus negative control (culture) treatment.

Test of Normality (Shapiro-Wilk)

		W	p
BECN1	Neg control	0.965	0.857
	∝-solanine	0.877	0.256

Note. Significant results suggest a deviation from normality.

Test of Equality of Variances (Levene's)

	F	df	p
BECN1	1.946	1	0.193

Output 13.519.: Independent sample T-testing for BECN1 protein corrected mean grey area data for glioblastoma multiforme cells treated with 6.25 µM α-solanine versus negative control (culture) treatment.

Independent Samples T-Test

	t	df	p
BECN1	−27.369	10	< .001

Note. Student's t-test.

Output 13.520.: Descriptive statistics for BNIP3L protein corrected mean grey area data for glioblastoma multiforme cells treated with 6.25 µM α-solanine versus negative control (culture) treatment.

Descriptive Statistics

	BNIP3L	
	Neg control	∝-solanine
Valid	6	6
Missing	0	0
Mean	93.040	143.675
Std. Deviation	3.102	11.868
Minimum	88.155	131.685
Maximum	95.777	164.582

Output 13.521.: Normality (Shapiro-Wilk) and Equality of Variance (Levene's) assumption checks for pairwise sample testing for BNIP3L protein corrected mean grey area data for glioblastoma multiforme cells treated with 6.25 µM α-solanine versus negative control (culture) treatment.

Test of Normality (Shapiro-Wilk)

		W	p
BNIP3L	Neg control	0.877	0.258
	∝-solanine	0.903	0.389

Note. Significant results suggest a deviation from normality.

Test of Equality of Variances (Levene's)

	F	df	p
BNIP3L	4.888	1	0.051

Output 13.522.: Independent sample T-testing for BNIP3L protein corrected mean grey area data for glioblastoma multiforme cells treated with 6.25 µM α-solanine versus negative control (culture) treatment.

Independent Samples T-Test

	t	df	p
BNIP3L	−10.111	10	< .001

Note. Student's t-test.

Output 13.523.: Descriptive statistics for DDR2 protein corrected mean grey area data for glioblastoma multiforme cells treated with 6.25 µM α-solanine versus negative control (culture) treatment.

Descriptive Statistics

	DDR2	
	Neg control	∝-solanine
Valid	6	6
Missing	0	0
Mean	21.136	20.476
Std. Deviation	5.474	6.656
Minimum	15.245	11.794
Maximum	28.160	27.071

Output 13.524.: Normality (Shapiro-Wilk) and Equality of Variance (Levene's) assumption checks for pairwise sample testing for DDR2 protein corrected mean grey area data for glioblastoma multiforme cells treated with 6.25 µM α-solanine versus negative control (culture) treatment.

Test of Normality (Shapiro-Wilk)

		W	p
DDR2	Neg control	0.887	0.305
	∝-solanine	0.822	0.092

Note. Significant results suggest a deviation from normality.

Test of Equality of Variances (Levene's)

	F	df	p
DDR2	0.551	1	0.475

Output 13.525.: Independent sample T-testing for DDR2 protein corrected mean grey area data for glioblastoma multiforme cells treated with 6.25 µM α-solanine versus negative control (culture) treatment.

Independent Samples T-Test

	t	df	p
DDR2	0.188	10	0.855

Note. Student's t-test.

Output 13.526.: Descriptive statistics for GABARAP protein corrected mean grey area data for glioblastoma multiforme cells treated with 6.25 µM α-solanine versus negative control (culture) treatment.

Descriptive Statistics

	GABARAP	
	Neg control	∝-solanine
Valid	6	6
Missing	0	0
Mean	81.588	97.793
Std. Deviation	14.555	23.834
Minimum	66.467	71.323
Maximum	100.715	126.949

Output 13.527.: Normality (Shapiro-Wilk) and Equality of Variance (Levene's) assumption checks for pairwise sample testing for GABARAP protein corrected mean grey area data for glioblastoma multiforme cells treated with 6.25 µM α-solanine versus negative control (culture) treatment.

Test of Normality (Shapiro-Wilk)

		W	p
GABARAP	Neg control	0.890	0.320
	∝-solanine	0.879	0.266

Note. Significant results suggest a deviation from normality.

Test of Equality of Variances (Levene's)

	F	df	p
GABARAP	1.744	1	0.216

Output 13.528.: Independent sample T-testing for GABARAP protein corrected mean grey area data for glioblastoma multiforme cells treated with 6.25 µM α-solanine versus negative control (culture) treatment.

Independent Samples T-Test

	t	df	p
GABARAP	−1.421	10	0.186

Note. Student's t-test.

Output 13.529.: Descriptive statistics for LAMP1 protein corrected mean grey area data for glioblastoma multiforme cells treated with 6.25 µM α-solanine versus negative control (culture) treatment.

Descriptive Statistics

	LAMP1	
	Neg control	∝-solanine
Valid	6	6
Missing	0	0
Mean	141.168	177.751
Std. Deviation	10.907	19.453
Minimum	129.146	159.339
Maximum	155.530	206.354

Output 13.530.: Normality (Shapiro-Wilk) and Equality of Variance (Levene's) assumption checks for pairwise sample testing for LAMP1 protein corrected mean grey area data for glioblastoma multiforme cells treated with 6.25 µM α-solanine versus negative control (culture) treatment.

Test of Normality (Shapiro-Wilk)

		W	p
LAMP1	Neg control	0.916	0.479
	∝-solanine	0.826	0.099

Note. Significant results suggest a deviation from normality.

Test of Equality of Variances (Levene's)

	F	df	p
LAMP1	4.053	1	0.072

Output 13.531.: Independent sample T-testing for LAMP1 protein corrected mean grey area data for glioblastoma multiforme cells treated with 6.25 µM α-solanine versus negative control (culture) treatment.

Independent Samples T-Test

	t	df	p
LAMP1	−4.018	10	0.002

Note. Student's t-test.

Output 13.532.: Descriptive statistics for LC3 protein corrected mean grey area data for glioblastoma multiforme cells treated with 6.25 µM α-solanine versus negative control (culture) treatment.

Descriptive Statistics

	LC3A	
	Neg control	∝-solanine
Valid	6	6
Missing	0	0
Mean	99.383	145.561
Std. Deviation	21.743	7.572
Minimum	70.497	135.111
Maximum	129.749	153.062

Output 13.533.: Normality (Shapiro-Wilk) and Equality of Variance (Levene's) assumption checks for pairwise sample testing for LC3A protein corrected mean grey area data for glioblastoma multiforme cells treated with 6.25 µM α-solanine versus negative control (culture) treatment.

Test of Normality (Shapiro-Wilk)

		W	p
LC3A	Neg control	0.976	0.929
	∝-solanine	0.892	0.326

Note. Significant results suggest a deviation from normality.

Test of Equality of Variances (Levene's)

	F	df	p
LC3A	3.678	1	0.084

Output 13.534.: Independent sample T-testing for LC3A protein corrected mean grey area data for glioblastoma multiforme cells treated with 6.25 µM α-solanine versus negative control (culture) treatment.

Independent Samples T-Test

	t	df	p
LC3A	−4.913	10	< .001

Note. Student's t-test.

Output 13.535.: Descriptive statistics for LC3B protein corrected mean grey area data for glioblastoma multiforme cells treated with 6.25 µM α-solanine versus negative control (culture) treatment.

Descriptive Statistics

	LC3B	
	Neg control	∝-solanine
Valid	6	6
Missing	0	0
Mean	72.037	85.586
Std. Deviation	13.361	9.257
Minimum	57.156	79.537
Maximum	91.903	103.992

Output 13.536.: Normality (Shapiro-Wilk) and Equality of Variance (Levene's) assumption checks for pairwise sample testing for LC3B protein corrected mean grey area data for glioblastoma multiforme cells treated with 6.25 µM α-solanine versus negative control (culture) treatment.

Test of Normality (Shapiro-Wilk)

		W	p
LC3B	Neg control	0.931	0.590
	∝-solanine	0.697	0.006

Note. Significant results suggest a deviation from normality.

Test of Equality of Variances (Levene's)

	F	df	p
LC3B	1.467	1	0.254

Output 13.537.: Independent sample T-testing for LC3B protein corrected mean grey area data for glioblastoma multiforme cells treated with 6.25 µM α-solanine versus negative control (culture) treatment.

Independent Samples T-Test

	t	df	p
LC3B	−2.042	10	0.068

Note. Student's t-test.

Output 13.538.: Descriptive statistics for NBS1 protein corrected mean grey area data for glioblastoma multiforme cells treated with 6.25 µM α-solanine versus negative control (culture) treatment.

Descriptive Statistics

	NBS1	
	Neg control	∝-solanine
Valid	6	6
Missing	0	0
Mean	145.426	172.311
Std. Deviation	9.473	8.265
Minimum	135.566	160.687
Maximum	158.539	182.031

Output 13.539.: Normality (Shapiro-Wilk) and Equality of Variance (Levene's) assumption checks for pairwise sample testing for NBS1 protein corrected mean grey area data for glioblastoma multiforme cells treated with 6.25 µM α-solanine versus negative control (culture) treatment.

Test of Normality (Shapiro–Wilk)

		W	p
NBS1	Neg control	0.904	0.397
	∝–solanine	0.957	0.793

Note. Significant results suggest a deviation from normality.

Test of Equality of Variances (Levene's)

	F	df	p
NBS1	0.198	1	0.666

Output 13.540.: Independent sample T-testing for NBS1 protein corrected mean grey area data for glioblastoma multiforme cells treated with 6.25 µM α-solanine versus negative control (culture) treatment.

Independent Samples T–Test

	t	df	p
NBS1	−5.238	10	< .001

Note. Student's t–test.

Output 13.541.: Descriptive statistics for p62 protein corrected mean grey area data for glioblastoma multiforme cells treated with 6.25 µM α-solanine versus negative control (culture) treatment.

Descriptive Statistics

	P62	
	Neg control	∝-solanine
Valid	6	6
Missing	0	0
Mean	144.743	164.202
Std. Deviation	7.383	20.982
Minimum	131.910	137.474
Maximum	151.943	195.982

Output 13.542.: Normality (Shapiro-Wilk) and Equality of Variance (Levene's) assumption checks for pairwise sample testing for p62 protein corrected mean grey area data for glioblastoma multiforme cells treated with 6.25 µM α-solanine versus negative control (culture) treatment.

Test of Normality (Shapiro-Wilk)

		W	p
P62	Neg control	0.908	0.426
	∝-solanine	0.971	0.902

Note. Significant results suggest a deviation from normality.

Test of Equality of Variances (Levene's)

	F	df	p
P62	3.220	1	0.103

Output 13.543.: Independent sample T-testing for p62 protein corrected mean grey area data for glioblastoma multiforme cells treated with 6.25 µM α-solanine versus negative control (culture) treatment.

Independent Samples T-Test

	t	df	p
P62	−2.143	10	0.058

Note. Student's t-test.

Output 13.544.: Descriptive statistics for Rheb protein corrected mean grey area data for glioblastoma multiforme cells treated with 6.25 µM α-solanine versus negative control (culture) treatment.

Descriptive Statistics

	Rheb	
	Neg control	∝-solanine
Valid	6	6
Missing	0	0
Mean	157.677	188.363
Std. Deviation	13.664	8.211
Minimum	136.378	174.741
Maximum	172.298	196.732

Output 13.545.: Normality (Shapiro-Wilk) and Equality of Variance (Levene's) assumption checks for pairwise sample testing for Rheb protein corrected mean grey area data for glioblastoma multiforme cells treated with 6.25 µM α-solanine versus negative control (culture) treatment.

Test of Normality (Shapiro-Wilk)

		W	p
Rheb	Neg control	0.922	0.517
	∝-solanine	0.905	0.403

Note. Significant results suggest a deviation from normality.

Test of Equality of Variances (Levene's)

	F	df	p
Rheb	1.416	1	0.262

Output 13.546.: Independent sample T-testing for Rheb protein corrected mean grey area data for glioblastoma multiforme cells treated with 6.25 µM α-solanine versus negative control (culture) treatment.

Independent Samples T-Test

	t	df	p
Rheb	−4.715	10	< .001

Note. Student's t-test.

Output 13.547.: Descriptive statistics for MSK1 protein corrected mean grey area data for glioblastoma multiforme cells treated with 6.25 µM α-solanine versus negative control (culture) treatment.

Descriptive Statistics

	MSK1	
	Neg control	∝-solanine
Valid	6	6
Missing	0	0
Mean	91.623	97.280
Std. Deviation	13.785	22.789
Minimum	79.175	67.664
Maximum	114.438	118.714

Output 13.548.: Normality (Shapiro-Wilk) and Equality of Variance (Levene's) assumption checks for pairwise sample testing for MSK1 protein corrected mean grey area data for glioblastoma multiforme cells treated with 6.25 µM α-solanine versus negative control (culture) treatment.

Test of Normality (Shapiro-Wilk)

		W	p
MSK1	Neg control	0.884	0.287
	∝-solanine	0.781	0.039

Note. Significant results suggest a deviation from normality.

Test of Equality of Variances (Levene's)

	F	df	p
MSK1	3.575	1	0.088

Output 13.549.: Independent sample T-testing for MSK1 protein corrected mean grey area data for glioblastoma multiforme cells treated with 6.25 µM α-solanine versus negative control (culture) treatment.

Independent Samples T-Test

	t	df	p
MSK1	−0.520	10	0.614

Note. Student's t-test.

Output 13.550.: Descriptive statistics for alpha-synuclein protein corrected mean grey area data for glioblastoma multiforme cells treated with 6.25 µM α-solanine versus negative control (culture) treatment.

Descriptive Statistics

	Alpha-synuclein	
	Neg control	∝-solanine
Valid	6	6
Missing	0	0
Mean	147.955	179.593
Std. Deviation	11.056	13.192
Minimum	135.100	167.598
Maximum	162.183	201.291

Output 13.551.: Normality (Shapiro-Wilk) and Equality of Variance (Levene's) assumption checks for pairwise sample testing for alpha-synuclein protein corrected mean grey area data for glioblastoma multiforme cells treated with 6.25 µM α-solanine versus negative control (culture) treatment.

Independent Samples T-Test

	t	df	p
Alpha-synuclein	−4.502	10	0.001

Note. Student's t-test.

Output 13.552.: Independent sample T-testing for alpha-synuclein protein corrected mean grey area data for glioblastoma multiforme cells treated with 6.25 µM α-solanine versus negative control (culture) treatment.

Test of Normality (Shapiro-Wilk)

		W	p
Alpha-synuclein	Neg control	0.925	0.544
	∝-solanine	0.882	0.277

Note. Significant results suggest a deviation from normality.

Test of Equality of Variances (Levene's)

	F	df	p
Alpha-synuclein	0.112	1	0.745

13.8. Statistical analysis of Presto blue® cell viability assay optimisation

Output 13.553.: Descriptive statistics for U87MG cells treated with 1.00 % DMSO versus 10.00 % DMSO at 72 hours.

Descriptive Statistics

	Value	
	1 % DMSO	10 % DMSO
Valid	3	3
Missing	0	0
Mean	0.476	0.471
Std. Deviation	0.011	0.004
Minimum	0.468	0.467
Maximum	0.488	0.474

Output 13.554.: Normality (Shapiro-Wilk) and Equality of Variance (Levene's) assumption checks for pairwise sample testing for U87MG cells treated with 1.00 % DMSO versus 10.00 % DMSO at 72 hours.

Test of Normality (Shapiro-Wilk)

		W	p
Value	1 % DMSO	0.893	0.363
	10 % DMSO	0.993	0.843

Note. Significant results suggest a deviation from normality.

Test of Equality of Variances (Levene's)

	F	df	p
Value	4.780	1	0.094

Output 13.555.: Independent sample T-testing for U87MG cells treated with 1.00 % DMSO versus 10.00 % DMSO at 72 hours.

Independent Samples T-Test

					95% CI for Cohen's d	
	t	df	p	Cohen's d	Lower	Upper
Value	0.828	4	0.454	0.676	−1.024	2.302

Note. Student's t-test.

Output 13.556.: Descriptive statistics for U87MG cells treated with with 5.00 µM α-solanine versus 50.00 µM α-solanine dissolved in DMSO at 72 hours.

Descriptive Statistics

	Value_4	
	5 uM α-solanine in DMSO	50 uM α-solanine in DMSO
Valid	3	3
Missing	0	0
Mean	0.464	0.471
Std. Deviation	0.026	0.004
Minimum	0.446	0.467
Maximum	0.494	0.474

Output 13.557.: Normality (Shapiro-Wilk) and Equality of Variance (Levene's) assumption checks for pairwise sample testing for U87MG cells treated with 5.00 µM α-solanine versus 50.00 µM α-solanine dissolved in DMSO at 72 hours.

Test of Normality (Shapiro-Wilk)

		W	p
Value_4	5 uM α-solanine in DMSO	0.842	0.220
	50 uM α-solanine in DMSO	0.993	0.843

Note. Significant results suggest a deviation from normality.

Test of Equality of Variances (Levene's)

	F	df	p
Value_4	10.582	1	0.031

Output 13.558.: Welch testing for U87MG cells treated with with 5.00 µM α-solanine versus 50.00 µM α-solanine dissolved in DMSO at 72 hours.

Independent Samples T-Test

					95% CI for Cohen's d	
	t	df	p	Cohen's d	Lower	Upper
Value_4	−0.438	2.072	0.703	−0.357	−1.952	1.312

Note. Welch's t-test.

Output 13.559.: Descriptive statistics for U87MG cells treated with with 5.00 µM α-solanine versus 50.00 µM α-solanine dissolved in DMEM/F12 medium at 72 hours.

Descriptive Statistics

	Value_6	
	5 uM α-solanine in DMEM	50 uM α-solanine in DMEM
Valid	3	3
Missing	0	0
Mean	0.662	0.470
Std. Deviation	0.015	0.010
Minimum	0.645	0.459
Maximum	0.672	0.478

Output 13.560.: Normality (Shapiro-Wilk) and Equality of Variance (Levene's) assumption checks for pairwise sample testing for U87MG cells treated with 5.00 µM α-solanine versus 50.00 µM α-solanine dissolved in DMEM/F12 medium at 72 hours.

Test of Normality (Shapiro-Wilk)

		W	p
Value_6	5 uM α-solanine in DMEM	0.858	0.263
	50 uM α-solanine in DMEM	0.957	0.600

Note. Significant results suggest a deviation from normality.

Test of Equality of Variances (Levene's)

	F	df	p
Value_6	1.052	1	0.363

Output 13.561.: Independent sample T-testing for U87MG cells treated with 5.00 µM α-solanine versus 50.00 µM α-solanine dissolved in DMEM/F12 medium for 72 hours.

Independent Samples T-Test

					95% CI for Cohen's d	
	t	df	p	Cohen's d	Lower	Upper
Value_6	18.990	4	< .001	15.505	5.242	25.984

Note. Student's t-test.

Output 13.562.: Descriptive statistics for U87MG cells treated with 1.00 % DMSO versus 5.00 α-solanine dissolved in DMSO for 72 hours.

Descriptive Statistics

	Value_8	
	1 % DMSO	5 uM α-solanine in DMSO
Valid	3	3
Missing	0	0
Mean	0.476	0.464
Std. Deviation	0.011	0.026
Minimum	0.468	0.446
Maximum	0.488	0.494

Output 13.563.: Normality (Shapiro-Wilk) and Equality of Variance (Levene's) assumption checks for pairwise sample testing for U87MG cells treated with 1.00 % DMSO versus 5.00 µM α-solanine dissolved in DMSO for 72 hours.

Test of Normality (Shapiro-Wilk)

		W	p
Value_8	1 % DMSO	0.893	0.363
	5 uM α-solanine in DMSO	0.842	0.220

Note. Significant results suggest a deviation from normality.

Test of Equality of Variances (Levene's)

	F	df	p
Value_8	4.320	1	0.106

Output 13.564.: Independent sample T-testing for U87MG cells treated with 1.00 % DMSO versus 5.00 µM α-solanine dissolved in DMSO for 72 hours.

Independent Samples T-Test

					95% CI for Cohen's d	
	t	df	p	Cohen's d	Lower	Upper
Value_8	0.737	4	0.502	0.602	−1.082	2.218

Note. Student's t-test.

Output 13.565.: Descriptive statistics for U87MG cells treated with 10.00 % DMSO versus 50.00 µM α-solanine dissolved in DMSO for 72 hours.

Descriptive Statistics

	Value_10	
	10 % DMSO	50 uM α-solanine in DMSO
Valid	3	3
Missing	0	0
Mean	0.471	0.471
Std. Deviation	0.004	0.004
Minimum	0.467	0.467
Maximum	0.474	0.474

Output 13.566.: Normality (Shapiro-Wilk) and Equality of Variance (Levene's) assumption checks for pairwise sample testing for U87MG cells treated with 10.00 % DMSO versus 50.00 µM α-solanine dissolved in DMSO for 72 hours.

Test of Normality (Shapiro-Wilk)

		W	p
Value_10	10 % DMSO	0.993	0.843
	50 uM α-solanine in DMSO	0.993	0.843

Note. Significant results suggest a deviation from normality.

Test of Equality of Variances (Levene's)

	F	df	p
Value_10	0.000	1	1.000

Output 13.567.: Independent sample T-testing for U87MG cells treated with 10.00 % DMSO versus 50.00 µM α-solanine dissolved in DMSO for 72 hours.

Independent Samples T-Test

	t	df	p	Cohen's d
Value_10	0.000	4	1.000	0.000

Note. Student's t-test.

Output 13.568.: Descriptive statistics for U87MG cells treated with 5.00 µM α-solanine dissolved in DMSO versus 5.00 µM α-solanine dissolved in DMEM/F12 medium for 72 hours

Descriptive Statistics

	Value_12	
	5 uM α-solanine in DMEM	5 uM α-solanine in DMSO
Valid	3	3
Missing	0	0
Mean	0.662	0.464
Std. Deviation	0.015	0.026
Minimum	0.645	0.446
Maximum	0.672	0.494

Output 13.569.: Normality (Shapiro-Wilk) and Equality of Variance (Levene's) assumption checks for pairwise sample testing for U87MG cells treated with 5.00 µM α-solanine dissolved in DMSO versus 5.00 µM α-solanine dissolved in DMEM/F12 medium for 72 hours.

Test of Normality (Shapiro-Wilk)

		W	p
Value_12	5 uM α-solanine in DMEM	0.858	0.263
	5 uM α-solanine in DMSO	0.842	0.220

Note. Significant results suggest a deviation from normality.

Test of Equality of Variances (Levene's)

	F	df	p
Value_12	2.133	1	0.218

Output 13.570.: Independent sample T-testing for U87MG cells treated with 5.00 µM α-solanine dissolved in DMSO versus 5.00 µM α-solanine dissolved in DMEM/F12 medium for 72 hours.

Independent Samples T-Test

					95% CI for Cohen's d	
	t	df	p	Cohen's d	Lower	Upper
Value_12	11.436	4	< .001	9.337	2.996	15.757

Note. Student's t-test.

Output 13.571.: Descriptive statistics for U87MG cells treated with 50 µM α-solanine dissolved in DMSO versus 50 µM α-solanine dissolved in DMEM/F12 medium for 72 hours.

Descriptive Statistics

	Value_14	
	50 uM α-solanine in DMEM	50 uM α-solanine in DMSO
Valid	3	3
Missing	0	0
Mean	0.470	0.471
Std. Deviation	0.010	0.004
Minimum	0.459	0.467
Maximum	0.478	0.474

Output 13.572.: Normality (Shapiro-Wilk) and Equality of Variance (Levene's) assumption checks for pairwise sample testing for U87MG cells treated with 50.00 µM α-solanine dissolved in DMSO versus 50.00 µM α-solanine dissolved in DMEM/F12 medium for 72 hours.

Test of Normality (Shapiro-Wilk)

		W	p
Value_14	50 uM α-solanine in DMEM	0.957	0.600
	50 uM α-solanine in DMSO	0.993	0.843

Note. Significant results suggest a deviation from normality.

Test of Equality of Variances (Levene's)

	F	df	p
Value_14	2.990	1	0.159

Output 13.573.: Independent sample T-testing for U87MG cells treated with 05 µM α-solanine dissolved in DMSO versus 50 µM α-solanine dissolved in DMEM/F12 medium for 72 hours.

Independent Samples T-Test

	t	df	p	Cohen's d
Value_14	−0.168	4	0.875	−0.137

Note. Student's t-test.

Chapter 14 Published and submitted manuscripts; conference presentations and science communication articles